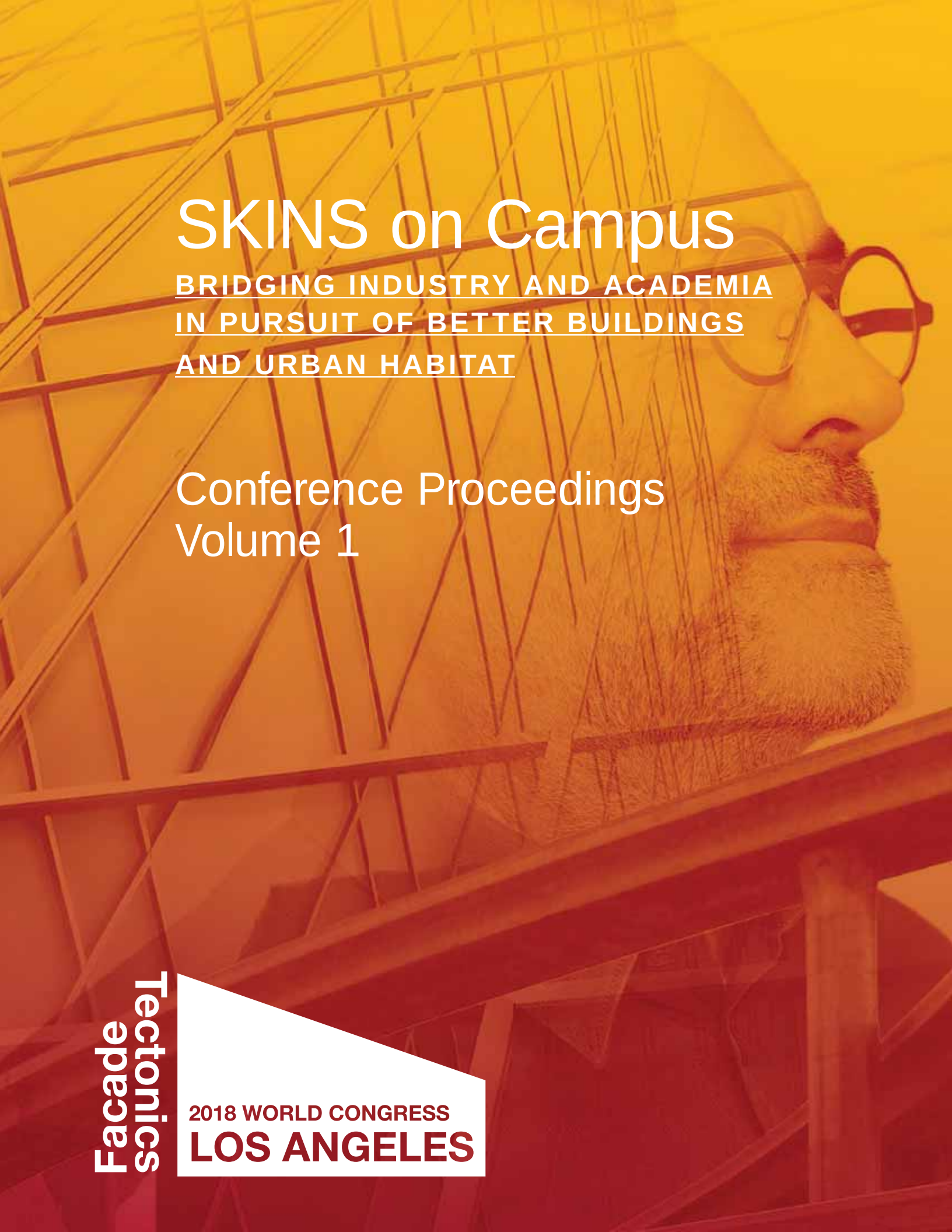


SKINS on Campus

BRIDGING INDUSTRY AND ACADEMIA IN PURSUIT OF BETTER BUILDINGS AND URBAN HABITAT

Conference Proceedings
Volume 1

Facade Tectonics

2018 WORLD CONGRESS
LOS ANGELES

FACADE TECTONICS

2018 World Congress | Los Angeles
Conference Proceedings
Volume 1

Edited by

Douglas Noble, FAIA, Ph.D.
Managing Director of the Facade Tectonics Institute
Director of the Chase L. Leavitt Graduate Building Science Program
Chair of the Ph.D. Program
USC, School of Architecture

Karen Kensek, LEED AP (BD+C)
Executive Director, Facade Tectonics Institute
Associate Professor of the Practice of Architecture
USC, School of Architecture

Matt Elder
Communications Coordinator

Copyright © 2018 by Facade Tectonics Institute

Published by Tectonic Press, Los Angeles

Edited by Douglas Noble, Karen M. Kensek and Matt Elder

Graphic Design by Katie Gould

No part of this publication may be reproduced, stored in a retrieval system, or transmitted in any form or by any means, electronic, mechanical, photocopying, recording, scanning, or otherwise, except as permitted under Section 107 or 108 of the 1976 United States Copyright Act, without either the prior written permission of the Publisher, or authorization through payment of the appropriate per-copy fee to Copyright Clearance Center, Inc., 222 Rosewood Drive, Danvers, MA 01923, 978-750-8400, fax 978-646-8600, or on the web at www.copyright.com. Requests to the Publisher for permission should be submitted online at http://www.FacadeTectonics.org.

Limit of Liability/Disclaimer of Warranty: While the Publisher and authors have used their best efforts in preparing this book, they make no representations or warranties with respect to the accuracy or completeness of the contents of this book and specifically disclaim any implied warranties of merchantability or fitness for a particular purpose. No warranty may be created or extended by sales representatives or written sales materials. The advice and strategies contained herein may not be suitable for your situation. You should consult with a professional where appropriate. Neither the Publisher nor authors shall be liable for any loss of profit or any other commercial damages, including but not limited to special, incidental, consequential, or other damages.

For general information on our other products and services or technical support, please contact us online at http://www.FacadeTectonics.org.

Tectonic Press also publishes its books in a variety of electronic formats. Some content that appears in print may not be available in electronic books.

For more information about Tectonic Press products, visit our website at http://www.FacadeTectonics.org

ISBN 978-1882352463

Printed in the United States of America

9 7 8 1 8 8 2 3 5 2 4 6 3

Contents

The Façade Tectonics Institute……V

Introduction……VII

Energy <> Sustainability

Data-Driven Shading Systems: Application for Freeform Glass Facades……3

EUI of Building Clusters: Integrating Envelope Performance with Urban Design……15

Form as Energy: The Building Envelope as an Expression of Energy……23

Integrated Energy Analysis: Leveraging an Integrated Energy Modeling Process……35

Orbit Tower: Proposal for a Hybrid Structural-Façade System Featuring a Self-Adaptive Solar Shading Device……47

Xilinx Case Study: Accelerating Replicable ZNE Retrofits Through High Performance Facade Optimization……65

Facade <> Material

Architectural Ceramic Assemblies: A Collaborative Research Model for Industry Engagement……79

Ceramic Precast Composite Panels: High Performance Structural and Architectural Building Enclosures……87

Design Considerations and the Complex Facade: Kolon Future Research Park……99

Hybrid Timber: Performative, Biophilic and Beautiful……115

Hydrophobic Stainless Steel Surfaces: Low Maintenance, Energy Efficient Facades……121

Silicone Spandrel Glass Opacifiers: Mitigating Glass Breakage Risk From Thermal and Other Stresses……129

Specifying Commercial Aluminum Finishes……139

Stainless Steel 101: High Performance Alloys for Architecture……149

Terracotta 1912 to 2018: Center Three Case Study……159

Thermoelectric Materials in Exterior Walls: Experimental Study on Using Smart Facades for Heating and Cooling in High-Performance Buildings……171

Transitions Between Diverse Envelope Systems: Facade Joints at Lucile Packard Children's Hospital……181

Vintage Vinyl: Lock-Strip Gasket Replacement and Remediation Strategies……195

Glass <> Material

Design Considerations: Heat Strengthened Glass with Ceramic Enamel Frit……209

Designing Structural Laminated Glass: How the Interlayer Properties Affect Post Breakage Performance……217

Glass Strength Under Point Loading: Parametric Determination of Probability of Breakage for Typical Panel Dimensions…225

Let Thin Glass in the Facade Move……233

Translucent Pre-Fabricated Structural Cast Glass: A New Unitized U-Channel Assembly……245

Transparent Generator: Tapping the Gap……261

Heritage <> Facades

Challenges of Tall Iconic Building Retrofit: Skin, Bones and Internal Systems……273

Contextual Envelopes: Using Modern Methods to Address Heritage in Urban Sites……287

Historical Evolution of Responsive Facades: Factors Affecting the Design and Development……297

Mies Van Der Rohe, Gropius, Le Corbusier: A Comparative Analysis……309

Paul Rudolph's Christian Science Building: The Concrete Facade of a Forgotten Brutalist Masterpiece……321

Renewing Two Saarinen Icons: The 1955 MIT Chapel Window Wall and Kresge Curtainwall……329

Retrofit Options for Historic Facades: Analysis and Design of Coil Drapery Catcher Systems……345

Transformation as Movement: A Roman Baroque Church Facade Case Study……359

Vertical Louvered Solar Control: Richard Neutra and System Development to 1968……365

Integration <> Adaptation

Adaptable Glazing Shields: Pushing the Envelope of Facade and Window Retrofits……375

Adaptive Facades: Towards Responsive Building Structures and Envelopes……397

Algorithmic Patterns for Facade Design: Merging Design Exploration, Optimization, and Rationalization……413

Exo-Skins: Self-Actuating, Thermally-Responsive, Laminated Bio-Composites for Retrofits……423

Heat-Actuated Auxetic Facades……435

Kinetic Shading Systems: A Parametric Approach to Optimizing Daylighting Performance……447

Kinematic Structural Glass: 111 Main Case Study, Accommodating Extreme Building Movements……461

Kinetics in Building Facades: Development of Taxonomy of Kinetics in Climatic Building Envelopes……473

Patchwork: Textile Techniques and their Influence on Space, Form, and Structure in the Digital Age……..481

Structuring Skin: Patterns of Integrating Cladding and Structure……..497

Unitized Curtain Wall: Case Studies in Performance Optimization and Design Variation……..519

Multi-Layer <> Facades

A Compact, Unitized Double Skin Facade: Thermal Performance Comparison in US Climates……..539

Differentiated Building Skin: An Experimental Case for AM Structural Components……..555

The Double Skin Facade: Enhancing Air Quality……..563

Multi-Layer Design Technique in the Metal Facades……..569

Multi-Layer Facades: A Modern Take on the Challenges and Balances……..581

The ‘Thermal Blanket’ Concept: An Active Double Skin Facade at the Manhattan Beach Public Library……..587

Process <> Design

Emulating Nature’s Structured Randomness in Facade Design: Using Parametric Modeling Tools……..601

Performance Criteria for Museum Design……..613

Safety <> Structure

Ballistic and Blast Integrated Design……..623

Blast Performance of TSSA: Testing of Point Fixed Assemblies……..635

Fire Safety in High Rise Exterior Facades: Mineral Wool Design Strategies for ASTM E 2307 and NFPA 285 Compliance…647

Hardened Facades Effects on Structural Systems: Analytical Study and Test of Blast-Resistant Facades Effects on Structural Braced Frames……..661

Lightning Protection as Building Envelope……..677

When Facades Kill: A Problem of Extreme Flammability……..687

Conference Sponsors……..703

Organizational Members……..705

Scientific Review Committee……..707

The Facade Tectonics Institute

PRESIDENT

Helen Sanders

PAST PRESIDENT

Mic Patterson

SECRETARY

Valerie Block

TREASURER

Attila Arian

BOARD OF DIRECTORS

Ana Bertuna
Keith Boswell
James Doerfler
Jeff Haber
Jeff Heymann
Stacey Hooper
Erik Olsen
Mic Patterson
Stephen Selkowitz
Chris Stutzki
Peter Weismantle
Roger Fricke

COMMUNICATIONS COORDINATOR

Matt Elder

EVENTS COORDINATOR

Katie Gould

DIRECTOR SCIENTIFIC & TECHNICAL REVIEW COMMITTEE

Karen Kensek

ANNUAL CONFERENCE DIRECTOR

Douglas Noble

Introduction

NOTHING IN ARCHITECTURE COMBINES ISSUES OF APPEARANCE AND PERFORMANCE LIKE THE BUILDING SKIN

The Facade Tectonics Institute is an international member organization with the mission of carrying out progressive and broad-based research in building facade technology. The intent is to catalyze and foster a deep dialogue of collaborative research activity that bridges the fragmented market segments of the building industry, pairing industry, government, academia, the profession, and ownership.

Facade Tectonics started in 2007 at the USC School of Architecture with considerable efforts in ongoing conferences, research initiatives and publications related to the building envelope. In 2015, we saw the coalescence of these efforts in the formation of the Facade Tectonics Institute. The dialogue we started together in 2007, along with the assets and activities we have accumulated along the way, now have a permanent home at the Institute. However, the Institute is not merely a string of conferences; we are a building facade focused research institute that produces events as educational and collaborative outreach, bridging the fragmentation that characterizes our industry, ultimately bringing together industry, the profession, academia, government, owners, and others. In addition, we are expanding our publication programs, launching new research initiatives, developing educational programs, pursuing research grant opportunities, and forming working groups to address key areas of building facade science and technology at this very moment. In addition to the 2018 World Congress in Los Angeles, we have hosted smaller regional focus forums and roundtable events, with many more planned in upcoming years.

The 2018 Annual Conference and World Congress focused on issues of facades for both professionals and academics while featuring blind peer reviewed papers with both new research and case studies. It combined the art, science, and technology of the building skin with an unparalleled networking opportunity from the domestic and international building community. This year we moved the conference to Spring, March 12-13, and returned to our roots, bringing the conference back to the University of Southern California campus where it all started over a decade ago.

The presentations and conference proceedings of the Facade Tectonics Annual Conference is a curated speaker program that includes diverse voices in the creation of advanced building facade systems that showcase new perspectives on the opportunities for innovation in the design and delivery of the building skin. Multiple emergent drivers are forcing a step change in the performance demands on buildings, and most particularly on the facade system. These demands mandate an innovative response to issues ranging from systems and materials to design and delivery strategies. A stellar line-up of authors wrote papers sorted into multiple tracks: facades+material, energy+sustainability, integration+adaption, heritage +facades, process+design, glass+material, multi-layer+facades, safety+structure, collaboration+design, facades+fabrication, process+delivery, education+facades, light+air, consulting+commissioning, and more. Although the discussions and dialogues were only for those in attendance, the papers are contained herein.

Please visit our website, get on our mailing list and join the conversation, and consider becoming a member of the Façade Tectonics Institute at www.facadetectonics.org.

Sincerely,

Helen Sanders, Ph.D.
President
Facade Tectonics Institute
Strategic Business Development
Technoform Glass Insulation NA, Inc.
hsanders@technoform.us

Karen Kensek, LEED AP (BD+C)
Director Scientific & Technical Review Committee
Facade Tectonics Institute
USC School of Architecture
kensek@facadetectonics.org

Douglas E. Noble, FAIA, Ph.D.
Conference Director
Facade Tectonics Institute
Director of the Chase L. Leavitt Graduate Building Science Program
USC School of Architecture
dnoble@usc.edu

Energy <> Sustainability

DATA-DRIVEN SHADING SYSTEMS

Application for freeform glass facades



Simon Schleicher
University of California, Berkeley
simon_s@berkeley.edu



Luis Santos
University of California, Berkeley
luis_sds82@berkeley.edu



Luisa Caldas
University of California, Berkeley
lcaldas@berkeley.edu

ABSTRACT

Analyzing the energy performance of complex building envelopes, determining the need for sun protection, and assessing the effectiveness of shading devices is a difficult problem. Modeling the complex geometry of facades and shading systems is very cumbersome and usually leads to computationally expensive energy simulations that cannot easily be integrated during the early stages of the design process.

Aiming to improve the workflow of modeling and energy simulation, this paper presents a new approach that couples parametric design with Building Energy Models (BEMs). The proposed method integrates different abstraction and data simplification processes that convert geometrical parameters of shading systems into thermal and optical glazing properties and thus accelerate building energy simulations. This way, it becomes possible to use results from energy simulations at early design phases and compare, for example, different shading devices or customize solutions to specific facade constraints. To illustrate the potential of this approach, the paper will briefly summarize the general challenges related to shading freeform facades and discuss an exemplary envelope in more detail. By mapping incident solar radiation, the authors will show that each facade panel is not only irregular in shape but also unique regarding its solar exposure and resulting shading requirements. This information can be used to assign custom panel properties and inform the shape, orientation, and distribution of common shading devices like glass frits or externally mounted louvers. Finally, by comparing multiple shading solutions, the paper will show how this design process can significantly reduce the facade's cooling demands.

KEYWORDS

façade, energy efficiency, shading systems, building energy models (BEMs), parametric workflows

INTRODUCTION

The fact that the building sector is responsible for nearly half (44.6%) of U.S. CO^2 emissions, calls for immediate and sustained action (EIA, 2012). Thus, transforming the way buildings are designed, built, and operated is a primary concern nowadays. One of the most effective ways to reduce CO^2 emissions in buildings is reducing the need for artificial heating, cooling and lighting. In the case of freeform glass facades, the problem of overheating that leads to high cooling demands is particularly acute, especially in temperate and hot climates. With the rise of computational tools, complex building envelopes have become increasingly popular and are used, for example, in airports, museums, and mixed-use high-rise buildings.

Protecting a freeform glass facade from the sun, however, is a particularly challenging task for various reasons: On the one hand, due to its irregular geometry, one cannot easily apply standard off-the-shelf shading devices but relies on highly customized tailored solutions. On the other hand, the complex panelization makes it very difficult to determine a facade's demand for shading and to assess the efficiency of shades. Thus, it is not uncommon that developers try to avoid high acquisition costs and plan freeform facades either without any sun protection or with only a rudimentary knowledge about their effectiveness. However, neither strategy offers a real solution, since a total lack or inefficient sun protection results in user-unfriendly buildings, which constantly require energy-intensive artificial cooling. Motivated by this problem, the goal for this paper is to improve the energy efficiency of freeform glass facades by investigating a new approach for the design and evaluation of data-driven static shading systems.

BACKGROUND

One of the current limits in the design of shading systems for freeform facades is the difficulty to assess their energy performance. Digital simulations must consider not only the location of the building, its orientation, and sun exposure, but also need to incorporate the envelope's complex and irregular panelization. Additionally, describing the geometry of the shading device and the effects created by it makes this task even more challenging. All aspects together quickly result in time-consuming modeling tasks and in computationally intensive simulations. As a result, the slow energy simulations are unfortunately often moved to a post-design stage where they have less influence on the building design. Since the goal for this paper is to integrate energy simulations in early design stages, new streamlined workflows need to be developed that by abstracting and simplifying data inputs accelerate simulations and deliver useful information to steer the design process in its early development.

To achieve this goal, the authors propose a combination of parametric modeling tools with BEM in a mutually beneficial approach. More precisely, the aim is to improve the data exchange between Grasshopper and Rhinoceros with EnergyPlus (E+), Radiance, and WINDOW 7.5 (Coakley et al. 2014, Ward and Rubinstein 1988, Huizenga et al. 2017). While each of these tools is very powerful, their combination can unleash additional synergy effects. To combine these tools, it is worth having a closer look at some individual strengths and weaknesses. For example, although E+ is a state-of-the-art building energy simulation software, its actual modeling features are very limited in comparison to those provided in Rhinoceros and Grasshopper. Being able to control geometrical parameters and meshing strategies, however, is a very important prerequisite for a successful simulation in E+, especially since this software relies so heavily on mesh planarity. While simple triangulation can help to overcome these limitations, it may also lead to follow-up problems. For instance, mesh triangulation typically results in very dense meshes that exponentially increase simulation time. Such geometrical limitations usually force the designer to manually oversimplify a facade's geometry whenever an energy simulation is needed. Although, experts have streamlined the manual simplification of model geometry in the past, there are inevitable consequences of this approach: the mismatch between BEM and CAD models; the loss of accuracy, which is particularly relevant for facades that use passive solar design strategies and have a significant amount of self-shaded surface area. It is precisely here where E+ can greatly benefit from the advanced surface modeling and planarization tools offered by Rhinoceros/Grasshopper namely in modeling automation for BEM. Another major advantage of these tools is their parametric modeling capability, which comprises the potential for automatic geometry changes and the creation and comparison of multiple design solutions.

METHOD

To illustrate the potential of the proposed workflow, the methodology will be applied on a concrete example: a prototypical freeform glass facade on which different shading systems are deployed. The method consists of five steps: firstly, defining a building envelope in Rhinoceros 5.0 and panelizing it in Grasshopper (build 0.9.0076). Secondly, using Radiance to conduct an annual solar radiation analysis and determine the shading needs of each facade panel. Thirdly, using WINDOW 7.5 to convert the geometry of different shading devices like louvers and glass frits into thermal and optical glazing panel properties. The resulting dataset is then used to assign different thermal and optical glazing properties to the individual panels in the façade based on the incident solar radiation already mapped in the building envelope. In the fourth step, E+ (version 8.4) is used to simulate the energy consumption for heating, cooling, and lighting of the thermal zone defined by the enclosed envelope and to compare the energy performance of the different shading systems. Finally, the fifth step takes the data of the energy simulation to re-create the actual geometry of the shading devices back into Rhinoceros/Grasshopper for visual feedback and possible design alterations. Figure 1 illustrates in a flow chart the adopted method. To validate the accuracy of this approach, the team compared the energy performance of two re-created energy models, with detailed shading geometry, and their simplified counterparts. Each step will be described in more detail in the following sections.

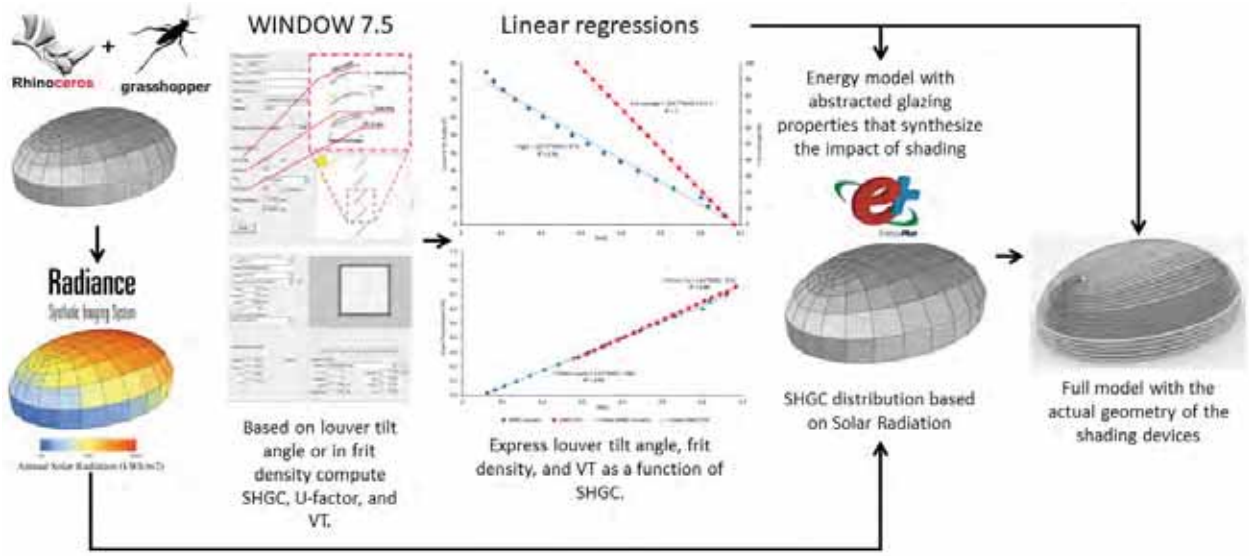


Figure 1: Flow-chart of the method used in this research.

FORM-GENERATION AND PANELIZATION

To test the proposed method, the team chose an ellipsoidal building as a geometrically challenging case study. This form is interesting because it features deviating surface curvature while being defined by only three parameters. For the meshing, a conformal mapping approach was applied (Sechelmann et al. 2013). This panelization strategy enables a subdivision of the surface into planar mesh faces of different sizes, but similar in shape and angles. The process followed a series of steps: the team began by modeling an ellipsoid of 25x18x7 meters and then generated a net on the surface using the lines of curvature. Afterwards, a quadrilateral mesh was obtained based on the intersection points of these lines. The resulting mesh consists of completely planar quads, illustrated by the touching inner circles of the mesh faces in Figure 2. The here-achieved mesh planarity is a very important prerequisite for the subsequent energy simulations.

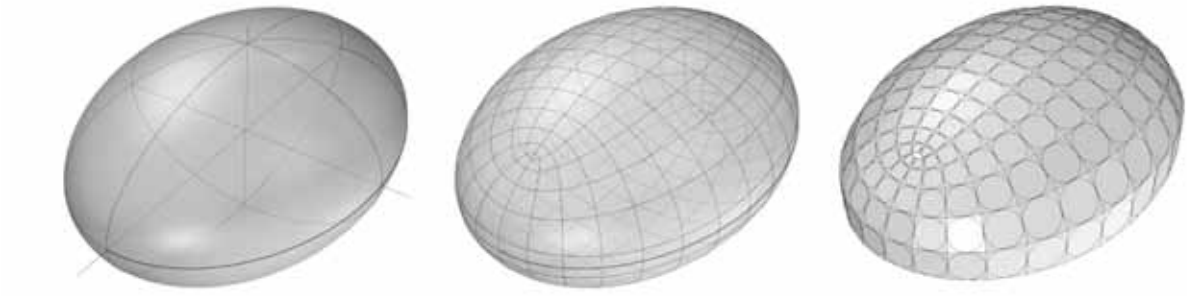


Figure 2: Conformal mapping of an ellipsoidal test body creates a mesh with planar quadrilateral panels.

MAPPING ANNUAL SOLAR RADIATION

Los Angeles (LA) is the location of the building and its main axis is aligned with the north-south axis. Because the main concern of this paper is to assess the impact of shading in the overall energy performance, the dry warm climate of LA (climate Zone 3B according to ASHRAE) is suitable to conduct this study. Using the typical meteorological year (TMY3) LA file, Radiance is able to calculate the cumulative annual solar radiation (Fig. 3). As expected, the solar exposure of the

individual panels varies over the entire facade, which questions a uniform treatment of the facade and instead supports the argument for locally adapted shading solutions. The color gradient shows the annual solar irradiance ranging from 100 to 2000 kWh/m^2.

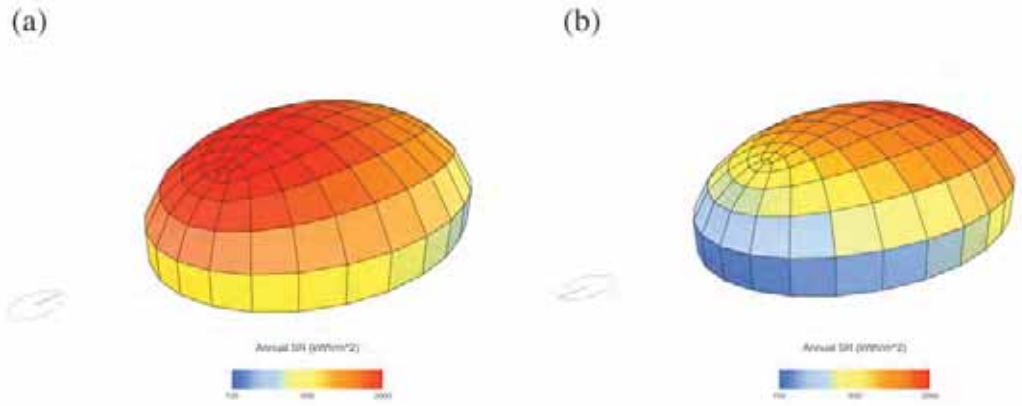


Figure 3: Based on the LA TMY file, the software Radiance determines the annual solar radiation of the facade as seen from south-east (a) and north-west perspective (b).

CONVERSION OF SHADING GEOMETRY INTO THERMAL/OPTICAL GLAZING PROPERTIES

In BEM a glazed facade panel can be modeled using two different procedures: either (i) detailed by specifying each layer of the window or (ii) simplified by describing the glazing assembly through conductivity (U-factor [W/m^{2}K]), Solar Heat Gain Coefficient (SHGC), and Visual Transmittance (VT). Although the detailed modeling of windows delivers more precise results, the simplified description of a glazing system is accurate enough to inform early design stages. Because the goal of this work is to simplify the geometrical features of louver-based shading devices and glass frits, this study adopts the simplified modeling approach. To assess the impact that these shading systems may have on U-factor, SHGC, and VT of a standard glazing assembly, the team used WINDOW 7.5 (Fig. 4). The standard glazing assembly consists of two 6 mm clear glass panes (the same substrate used in WINDOW 7.5 for glass frit calculations) with an air gap of 12 mm. The SHGC for this setup is 0.68, U-factor 2.83 W/m^{2}K, and VT of 0.76 (76%). The louvers are white colored metal and the frit ceramic cover is white with specular and diffuse light distribution data measured in Lawrence Berkeley National Laboratory (LBNL). For the case of the louver-based shading system the ratio between slat spacing and slat width is 1:1 and kept as a constant. By preserving this ratio, it is possible to generate louvers in different size and geometry while keeping the same profile angle and thus the same overall performance.



Figure 4: WINDOW 7.5 interface. Left: louver editor with slat width, louver spacing, blind tilt angle key parameters highlighted. Center: glazing assembly editor. Right: Window assembly editor with glazing and total window optical and thermal properties.

To compare different shading systems in a systematic way, two types of modifications were investigated in more detail. The louver-based system was tested for various tilt angles in steps of 5º in relation to the axis parallel to the glass plane. The frit-based system was analyzed for different densities in steps of 5% coverage. By post-processing the resulting data it is possible to express the slat tilt angle, frit coverage, and VT as functions of SHGC. Regarding the U-factor the authors observed that the different shading variations did not produce a relevant impact. The only significant change in U-factor was

when a louver shading system was added to the standard glazing unit in the first place. With louvers, the U-factor dropped from 2.83 to 2.5 W/m^{2}K. After this all variations of the tilted louvers had a negligible impact. The adding of frit to the standard glazing system did not change its U-factor. Thus, the U-factor of all louver shading variations is 2.5 W/m^{2}K while the U-factor of the frit based assemblies is 2.83 W/m^{2}K. Figure 5 and 6 show the linear regression models obtained for the louver- and frit-based shading systems. In both cases the high R^2 values indicate a strong correlation between the variables. Thus, these linear models can be used to map SHGC and VT as a function of solar radiation as well as to generate the respective louver and/or frit geometry in relation to a specific SHGC value.

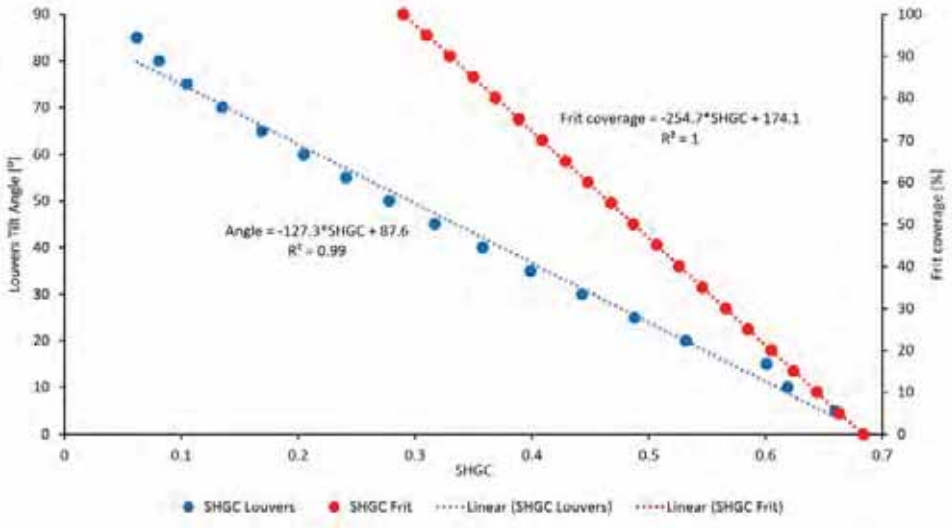


Figure 5: Linear regression models for the louver- and frit-based shading systems. In blue, the tilt angle of the individual louvers as a function of SHGC. In red the glass frit coverage percentage as a function of SHGC

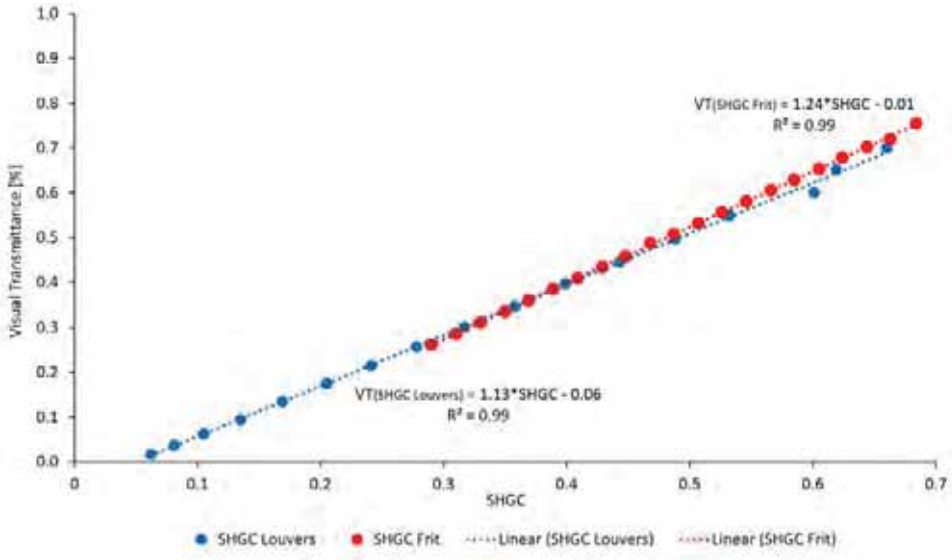


Figure 6: Visual transmittance as a function of SHGC for louver- (blue) and frit-based (red) shading systems.

ENERGY SIMULATION

This work used E+ to simulate the annual hourly energy consumption for heating, cooling, and lighting of the hemiellipsoid building envelope in LA. The team tested seven different shading conditions (Fig. 7-8):

A. Base Case - No shading and standard glazing.

B. Perpendicular Louvers - all louvers are perpendicular to the glass panel, which corresponds to a tilt angle of 0°.

C. 45° tilted Louvers - the glass panels have louvers with a tilt angle of 45°.

D. SR based Gradient Louvers - previous studies by Santos et al. (2017) showed that applying a shading density gradient that follows the distribution of Solar Radiation (SR) on the envelope yields significant reduction in cooling energy demands. Thus, for each panel this solution remaps the incident SR to a SHGC value and corresponding tilt angle of the louver. This remapping is based on a linear interpolation, where the highest SR value relates to the lowest SHGC that the louver-based shading system can reach (0.06), and vice versa. In this way, the louvers of the panels with high SR will be more closed than the ones with low SR.

E. 25% Frit Coverage - the envelope has a homogeneous frit coverage of 25%.

F. 50% Frit Coverage - all panels have a frit coverage of 50%.

G. SR based Gradient Frit - the same logic of SR based Gradient Louvers but applied to the frit-based shading system where the range of SHGC only goes from 0.3 to 0.68.

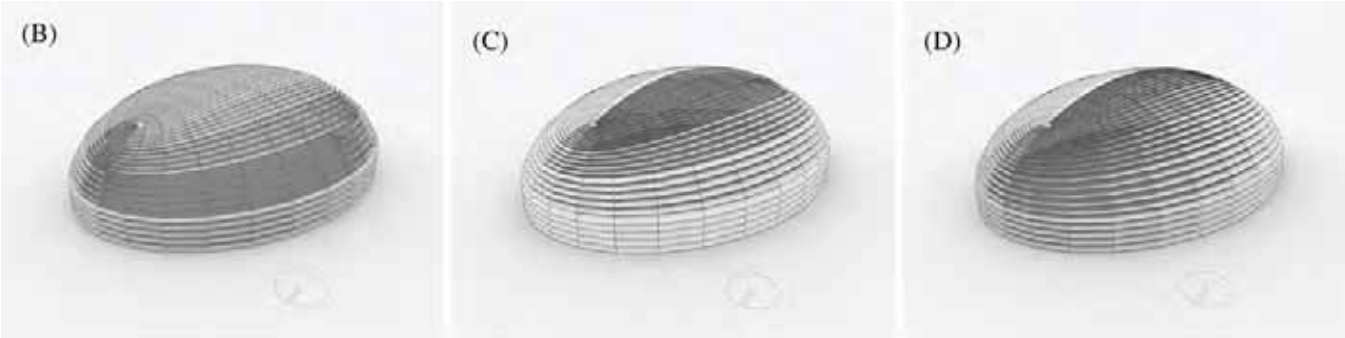


Figure 7: Freeform facade with different louver configurations: perpendicular louvers (B), 45° tilted louvers (C), and SR based gradient louvers (D).

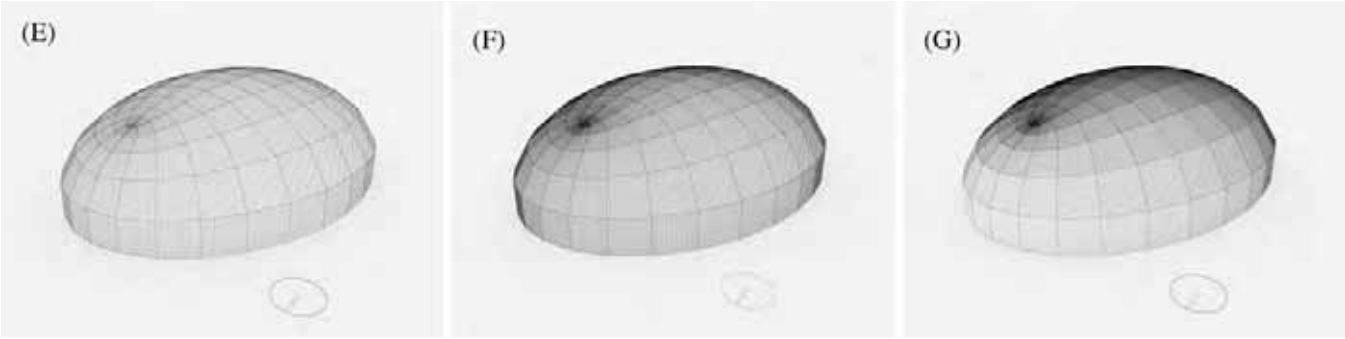


Figure 8: Freeform facade with different frit configurations: 25% frit coverage (E), 50% frit coverage (F), and SR based gradient frits (G).

The building was simulated as a single zone energy model with a floor composed of a 200 mm concrete slab plus and a 120 mm XPS insulation board covered with a cement screed resulting in a combined U-factor of 0.28 W/m^2K. Table 1 describes the input parameters. The schedules for occupancy, light, and equipment are typical office schedules as provided by ARCHSIM E+ front-end library.

Input parameter	*Value and unit*
Heating set point	20 °C
Cooling set point	26 °C
People Density	0.2 p/m²
Equipment Power Density	12 W/m²
Light Power Density	12 W/m²
Illuminance target for Continuous Dimmable Light system	300 lux

Table 1: Fixed input parameters for E+ simulations.

The results of the energy simulation are expressed in annual energy consumption (kWh) per end-use and in Energy Use Intensity (EUI), which normalizes energy consumption per unit area (kWh/m^2). In this study, total energy consumption is considered the sum of heating, cooling, and lighting energy. Since the study focuses on the energy performance of the shading systems, other factors like plug loads or fan energy are not included in the total energy calculation. Finally, to compare the performance of the different shading conditions, the % of improvement in total EUI is calculated as described in (ASHRAE 2013):

% of improvement = 100 x (Base Case EUI - Alternative EUI) / Base Case EUI

RE-CREATING THE GEOMETRY OF THE SHADING SYSTEM

Once a correlation between abstracted geometry and glazing properties is established, the process of converting data can also be used in reverse to re-create the three-dimensional features of a shading devices in Grasshopper. The SHGC of each panel can inform, for example, the modeling of a louver-based shading system with specified tilt angles or a frit-based shading system with defined frit coverage. This visual feedback is helpful for the further development of the facade design and allows, for instance, to compare the solutions for their optical effect or to fine-tune design alternatives parametrically (Fig. 9).

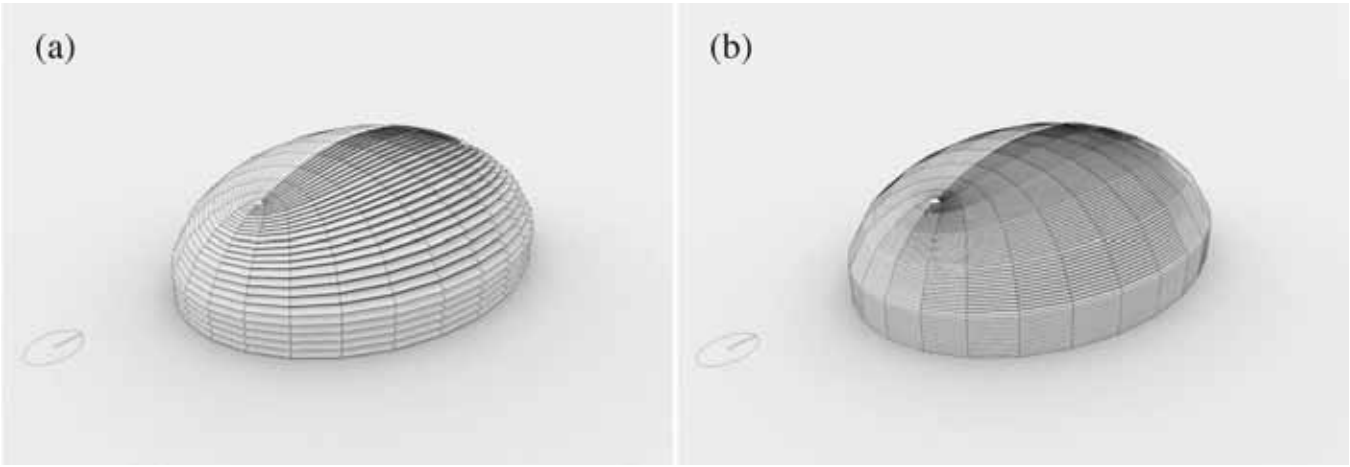


Figure 9: The workflow allows to parametrically modify the geometrical features of a selected shading device, for example from 8 (a) to 14 louvers per panel (b), without affecting the predefined glazing properties of the panels.

VALIDATION

To assess the accuracy of the proposed simplification method, the team compared the energy simulations of two fully detailed re-created solutions with their simplified counterparts. The louver-based shading system was tested in configuration (C), while the frit-based system was tested for solution (F). The validation process is based on three statistical metrics used in energy simulation calibration (Coakley et al. 2014): (i) the Coefficient of Variation of the Root Mean Squared Error (CV RMSE), (ii) the Mean Bias Error (MBE), and (iii) % of error. CV RMSE and MBE use hourly data either for each energy end use or total energy. This paper applied % of error only to assess the deviation in total EUI. The acceptance criteria of CV RMSE and MBE are set out by ASHRAE Guideline 14 (2002) which are 30% and - or + 10% respectively. The acceptance threshold for % of error is 10%. Finally, to assess the cost-benefit of the proposed method the study compares the time of each simulation.

DATA

Table 2, shows the summary results of the E+ simulations for all shading alternatives. Figure 10-12 plot the results of the annual energy performance for each individual shading solution. The chart of Figure 10 compares in detail the annual cumulative energy consumption per end-use of all solutions. Due to the cooling outliers, the values are mapped in $\log_{10}$ scale. Through the analysis of Table 2 and Figure 10, it is possible to assess the weight of each energy end-use in the overall energy performance.

	Annual Energy Consumption				EUI			
	Heating [kWh]	Cooling [kWh]	Lighting [kWh]	Total [kWh]	Heating [kWh/m²]	Cooling [kWh/m²]	Lighting [kWh/m²]	Total [kWh/m²]
Base Case	99.1	148,289.4	1,066.3	149,454.8	0.3	418.1	3	421.4
Perpendicular Louvers	55.2	143,128.8	1,066.5	144,250.5	0.2	403.6	3	406.8
45° tilted Louvers	755.7	53,975.3	1,072.5	55,803.5	2.1	152.2	3	157.4
SR-based Gradient Louvers	1,039.7	42,502.1	1,083	44,624.8	2.9	119.9	3	125.8
25% Frit Coverage	205.4	113,307.9	1,066.7	114,580	0.6	319.5	3	323.1
50% Frit Coverage	360	93,684.1	1,067.4	95,111.5	1	264.2	3	268.2
SR-based Frit Coverage	627.6	71,130.3	1,069.3	72,287.2	1.8	200.6	3	205.4

Table 2: Energy simulation results summary table per shading design solution.

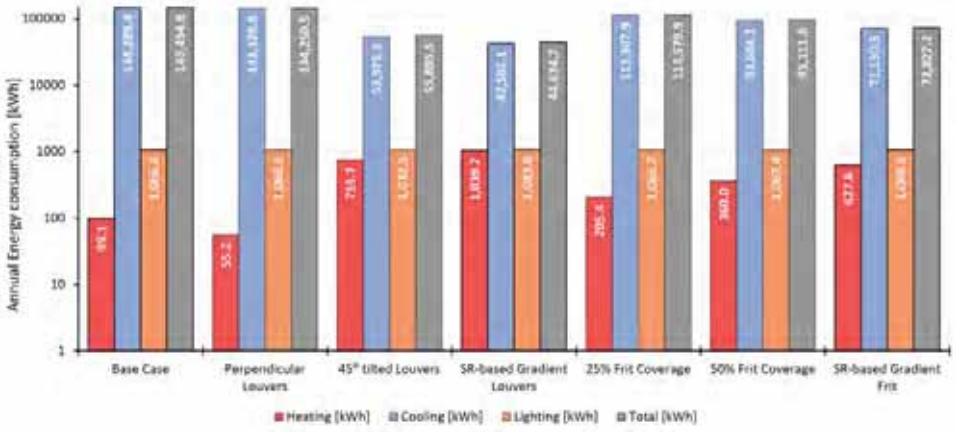


Figure 10: Bar chart of annual energy consumption (kWh) for each shading system.

Figure 11 shows the total EUI (kWh/m^2) per shading solution while Figure 12 the percentage of improvement in total EUI of each shading solution when compared with the EUI of the base case.

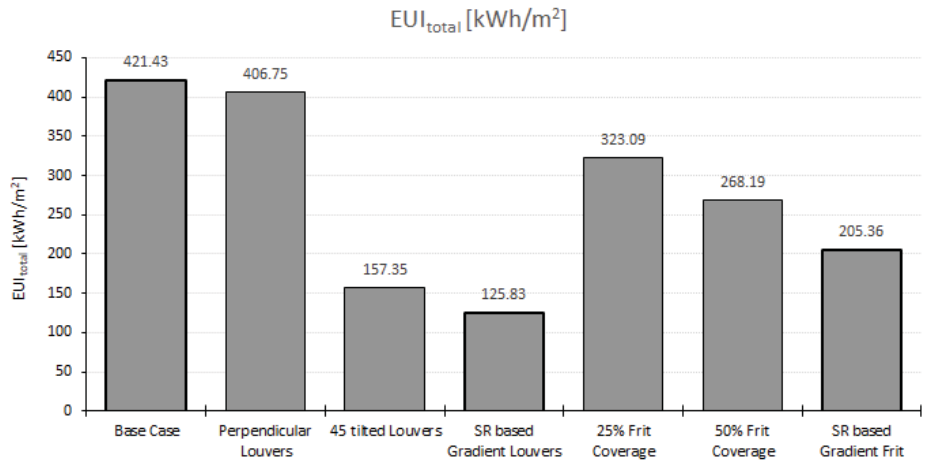


Figure 11: Total Energy Use Intensity (EUI) per design alternative.

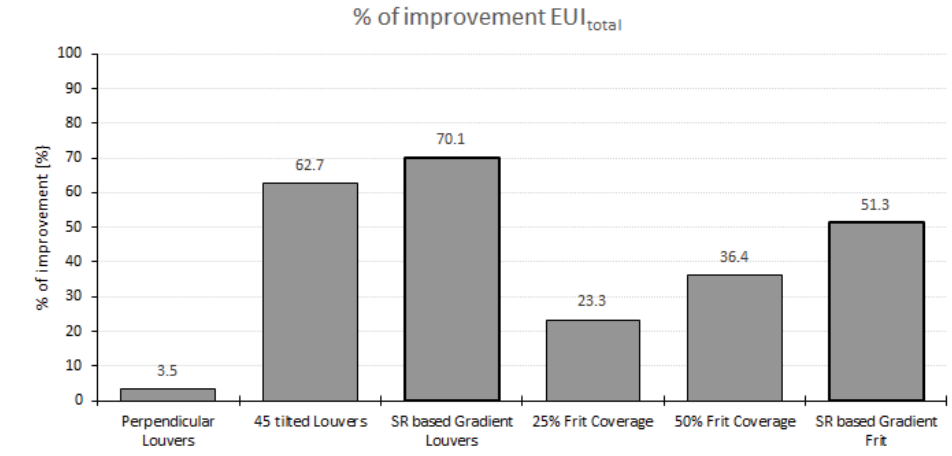


Figure 12: Percentage of improvement of each shading design alternative when compared with the Base Case.

Figure 13 and 14 show the validation results. Figure 13 maps out the deviation error of the simplified selected models in terms of CV RMSE and MBE. Figure 14 shows the % of error in total EUI and compares the simulation time of the fully detailed energy models with the simplified ones.

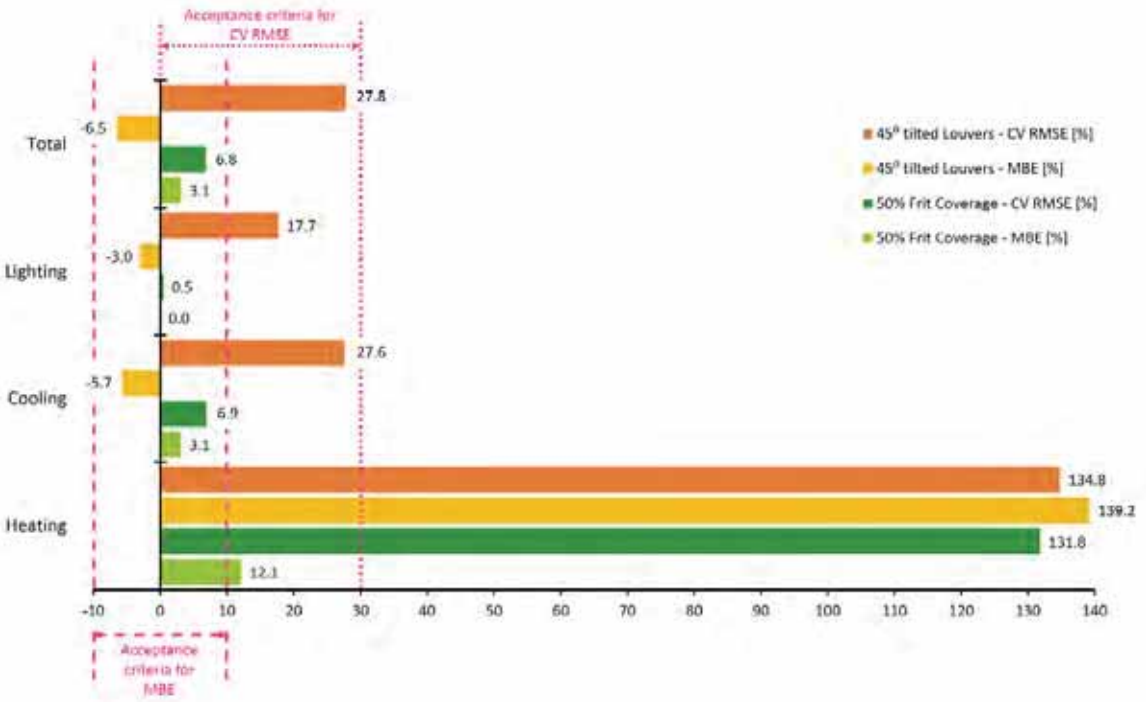


Figure 13: Assessment of the error metrics CV RMSE and MBE. The deviation of the proposed simplification for the 45° tilted Louvers and 50% Frit Coverage simplified solutions is measured against their fully modeled counterparts.

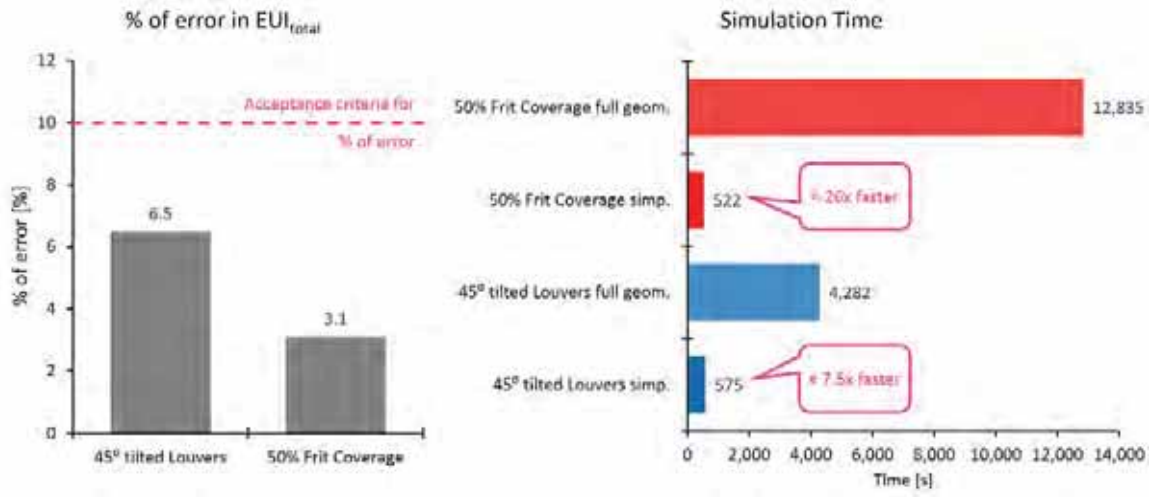


Figure 14: Left: percentage of error in total EUI between the simplified (simp.) and detailed modeled versions (full geom.) of solutions 45° tilted louvers and 50% frit coverage. Right: comparison of E+ simulation time for the same solutions.

EXPLANATION

Table 2 and Figure 10 show that cooling is the most relevant energy end-use. Even in the best performing case (D), cooling still represents more than 95% of the overall energy consumption. The weight of cooling loads in the energy performance of all cases indicates that it is possible to analyze the energy benefits of shading by analyzing the total energy consumption or the total EUI. As expected, the base case has the worst energy performance due to the overwhelming amount of cooling required to ensure thermal comfort. The adding of perpendicular shades to each panel produces a marginal improvement of only 3.5% (Fig. 12). This is related to the small impact that this shading solution has on the SHGC of the standard glazing unit. In comparison, a relative small percentage of frit coverage produces a bigger impact: an improvement of 23.3% for 25% of frit coverage (Fig. 12). Figure 10 and 11 show that either increasing the louver tilt angle or the frit coverage yields a positive impact in energy performance. Nevertheless, the impact of incrementally closing the louvers by changing their tilt has a bigger impact in decreasing cooling loads than increasing frit coverage would achieve. A closer look at Figure 5 explains this

phenomenon: the slope of the linear regression in the louver system is more pronounced than in the frit system, meaning that the tilt angle is more effective in reducing SHGC than frit coverage.

The adaptive shading schemes based on solar radiation present the best results in each shading type, following the pattern observed by Santos et al. (2017). The SR based Gradient Frit (G) improves the energy performance of the base case in 51.3% while the SR based Gradient Louvers (D) yield an outstanding 70.1% improvement, lowering the total EUI from 421.4 kWh/m^2 to a reasonable 125.8 kWh/m^2. In sum, the louver-based shading systems have the highest potential of reducing cooling loads in fully glazed envelopes. The gradient louvers that were informed by solar radiation values are the most effective in reducing cooling loads at minimal expense of heating and lighting loads.

The validation results show that the proposed simplification of shading geometry is very effective in accelerate energy simulations with a low impact in accuracy. Figure 13 error results are within the acceptable criteria both in the total energy and in all the energy end-uses except for heating. However, heating is of little relevance in the error assessment due to its small weight in the overall energy performance: 1.4% and 0.38% for the louver and frit cases respectively. The % of error in total EUI is also comfortably below the acceptance threshold. The simplified energy models can run 7.5 to 26x faster than the detailed models (Fig. 14) improving the usefulness of energy simulation for complex building geometry in early design phases. Finally, the wide range of simulation acceleration (7.5 to 26x) demonstrates how sensitive numerical energy simulations are to the number of faces of the energy model.

CONCLUSION AND FUTURE WORK

This work is a first successful step in improving the design and energy performance evaluation of freeform glass facades with data-driven shading systems. By combining parametric modeling with building energy simulations, the authors presented a streamlined workflow that is fast and accurate enough to inform early design phases. The key innovation of this work is based on the idea to abstract and simplify the geometrical features of the respective shading systems into thermal and optical glazing properties. The application of the proposed method in the design and simulation of louver- and frit-based shading systems for a fully glazed hemiellipsoid delivered accurate results in useful time. Simulating different variations of two shading systems showed that assigning a specific louver tilt or frit coverage to facade panels based on annual incident solar radiation is the most effective strategy to improve the energy performance of fully glazed envelopes with static shading devices. The work also indicates that a more refined study, which would include hourly variation of solar radiation, may have the potential to inform the design and operation of dynamic shading devices that most likely outperform static shading solutions. This particularly true for buildings with continuous envelopes that simultaneously face different orientations, as was the case for the hemiellipsoid used in this study. Finally, future work should also include the study of more complex shading and/or macroscopic light-redirecting fenestration systems and a refined assessment of annual daylight performance that can complement the energy simulations performed here.

ACKNOWLEDGMENTS

Work presented in this paper was partially financed by the Portuguese Science and Technology Foundation (FCT) through the PhD scholarship SFRH/BD/98658/2013. The authors like to thank Constantina Tsiara and Tanya Makker for their help in producing rendered images.

REFERENCES

ASHRAE. 2002. “Guideline 14-2002, Measurement of Energy and Demand Savings.” American Society of Heating, Ventilating, and Air Conditioning Engineers, Atlanta, Georgia.

ASHRAE. 2013. ASHRAE Standard 90.1-2013 Determination of Energy Savings: Quantitative Analysis.

Coakley, Daniel, Paul Raftery, and Marcus Keane. 2014. “A Review of Methods to Match Building Energy Simulation Models to Measured Data.” Renewable and Sustainable Energy Reviews 37: 123–141.

Crawley, Drury B., Linda K. Lawrie, Frederick C. Winkelmann, Walter F. Buhl, Y. Joe Huang, Curtis O. Pedersen, Richard K. Strand et al. "EnergyPlus: creating a new-generation building energy simulation program." *Energy and buildings* 33, no. 4 (2001): 319-331.

Energy Information Administration (US), ed. *Annual Energy Outlook 2012: With Projections to 2035*. Government Printing Office, 2012.

Huizenga, Charlie, Dariush Arasteh, Charlie Curcija, Joe Klems, Christian Kohler, Robin Mitchell, Tiefeng Yu, et al. 2017. *WINDOW 7.5.* Lawrence Berkeley National Laboratory.

Santos, Luis, Simon Schleicher, and Luisa Caldas. "Automation of CAD models to BEM models for performance based goal-oriented design methods." *Building and Environment* 112 (2017): 144-158.

Sechelmann, Stefan, Thilo Rörig, and Alexander I. Bobenko. "Quasiisothermic mesh layout." In *Advances in Architectural Geometry 2012*, pp. 243-258. Springer, Vienna, 2013.

Ward, Gregory J., and Francis M. Rubinstein. "A new technique for computer simulation of illuminated spaces." *Journal of the Illuminating Engineering Society* 17, no. 1 (1988): 80-91.

All images by the authors.

EUI OF BUILDING CLUSTERS

Integrating envelope performance with urban design



Srinivas M. Rao, AIA, AICP, LEED AP
KRITZINGER+RAO
srao@krdesigninc.com

ABSTRACT

Large master planned developments such as Battery Park City in Manhattan, Mission Bay in San Francisco, and Playa Vista in Los Angeles were built over several decades and were guided by urban design guidelines that focus on built form, architectural styles, and elements of the public realm. These guidelines were generally written by architect-planners and urban designers. Envelope performance is governed by building codes and client goals. The goals are often focused on getting certified by a reputed rating agency such as the US Green Building Council. While more holistic rating systems for large developments such as the Ecodistricts Protocol and Star Communities exist, the adherence to multiple regulatory or appraisal systems can get very complex. Thus, there is an increasing need for urban design guidelines to step up and include sophisticated building envelope performance criteria while controlling built form and the public realm.

A Master Plan for a 230-acre mixed-use urban redevelopment in New Delhi, India was prepared along with Urban Design Guidelines (UDG). In addition to conventional development guidelines, performance standards were included as part of the Urban Design Guidelines. One of the key criteria was energy performance. Computer analysis of buildings as clusters rather than discrete structures showed over 6% reduction in Energy Use Intensity (EUI). A 9.8% reduction in EUI was achieved when radiant heat gain was reduced using interventions at the cluster level such as a strategically place canopy over a space between buildings. Preliminary modeling showed a 21.9% reduction in EUI when 4-storied bridges were added between pairs of buildings. Results showed strong evidence that clustered approach to energy modelling can influence building planning and development strategy to achieve EUI goals.

KEYWORDS

design optimization; energy efficiency; urban design; codes - standards - rating systems; design processes; performance standards; urban habitat and the building facade

INTRODUCTION

Planning and Urban Design shape the fabric of cities by establishing block sizes, land use, densities and streets. Urban Design Guidelines are intended to shape the public realm by controlling development parameters such as density distribution, height, streetwall, bulk, streetfront articulation, corner conditions, curb cuts, etc. These controls are intended to shape urban form, encourage a healthy lifestyle by providing access to services and promoting walkability, provide easy access to open space and improve air quality, and promote the overall wellbeing of citizens. Various studies have shown a strong correlation between densities, energy consumption(Güneralpa et. al., 2016) and greenhouse gas emissions (Sanders, 2014).

Human habitats are complex systems that are interdependent and interconnected, and in the ideal world, should be analyzed collectively rather than as isolated systems. While the unpredictability of a constantly changing urban landscape may make it difficult to implement, newly planned communities and urban redevelopments that establish their own development controls as “Planned Unit Developments” or “Specific Plans” could consider Title 24 energy compliance at a building cluster level. Currently, in any project involving a cluster of buildings, California Energy Code requires that each building comply with Title 24 separately even if they are planned to be constructed at the same time.

BACKGROUND

A master plan and urban design guidelines were prepared for a 230-acre mixed-use urban redevelopment in New Delhi, India. The urban design guidelines relating to physical form and design were separated into public and private realms (Fig. 1). Public realm includes streetscape and dedicated public open space. Private realm includes all commercial development, private open spaces, through-block alleys, and other site improvements within private ownership of developable property.

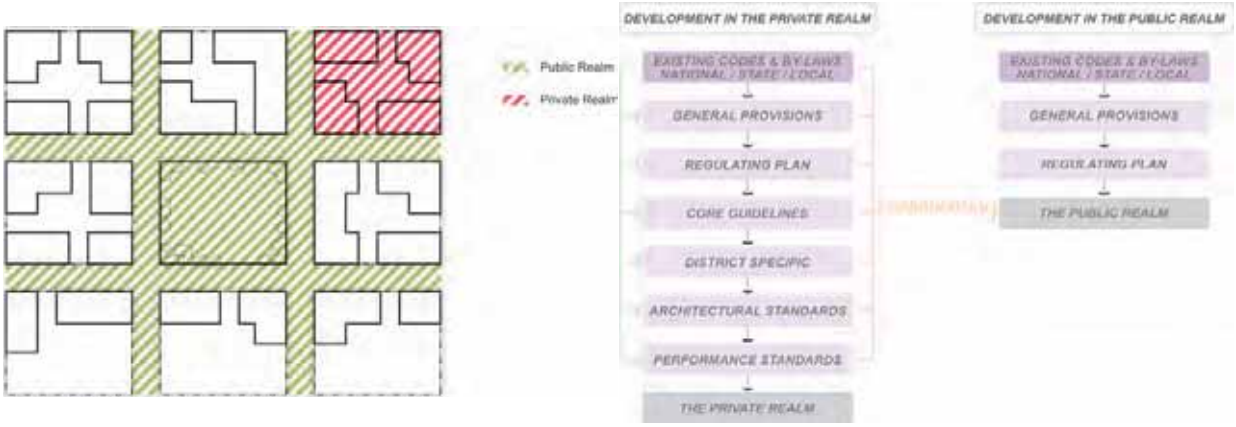


Figure 1: Typical public and private realms. Flow diagram illustrating use of document.

The urban design guidelines:

- strongly address the physical form of building and development. Instead of relying purely on conventional zoning where development is primarily based on use and density, it uses a mixed-use zoning framework on a flexible development block with robust guidelines that control form and performance that can achieve predictable outcomes without compromising architectural creativity.
- promote cohesive, sustainable development, sense of community, transit options, walkable and mixed-use neighborhoods, civic vitality, and a vibrant public realm.
- prevent a car-oriented, hostile public realm, and a disjointed, resource-intensive development.
- implement the project's fair share of the voluntary commitment made by the Indian Government at the Paris Climate Summit. This commitment included three broad goals:
    1. To reduce the emissions intensity of its GDP by 33 to 35 percent by 2030 from 2005 level;
    2. To achieve about 40 percent cumulative electric power installed capacity from non-fossil fuel based energy resources by 2030 with the help of transfer of technology and low cost international finance including from Green Climate Fund (GCF);
    3. To create an additional carbon sink of 2.5 to 3 billion tons of CO_2 equivalent through additional forest and tree cover by 2030.

The guidelines influence the overall performance of the buildings through:

- elements that *directly* affect the building envelope and its performance. These elements provide guidelines on the physical form, massing and other attributes of the building skin.
- elements that *indirectly* affect the building envelope and its performance. These elements affect the micro-climate of the development and thereby reduce (or increase) the energy loads on the buildings.

Design Guideline Elements	Potentially influences the building envelope directly	Potentially influences the building performance indirectly
Streetwall	✓	✓
Though-Block Pedestrian Connections		✓
Architectural Form and Massing	✓	✓
Building Orientation & Entries	✓	
Encroachment & Projections	✓	✓
Landscape & Trees		✓
Hardscape		✓
Roof Performance	✓	
Tree Canopy Density		✓
Water Conservation		✓
Block Typology/ Clustering (Fig. 3)		✓

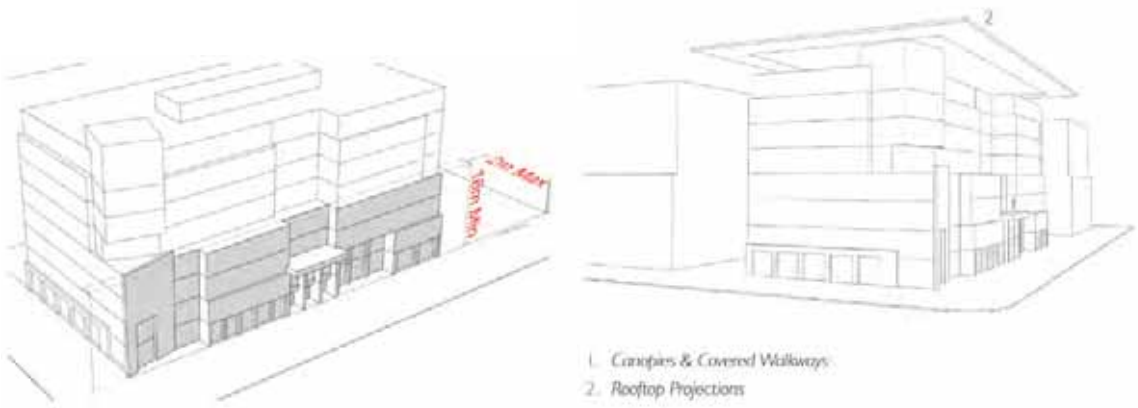


Figure 2: Streetwall, rooftop projects and canopies.

For example, the design guidelines define the Streetwall as the continuous facade of buildings generally built along the Setback line facing a street or open space. It extends up to a minimum height of 16m. Facade modulation within the 16m height is permitted within 2m of the setback line such that the perception of building edge from the street is along the setback line. Streetwall requirements do not apply above the 16m height (Fig. 2).

Roof top projections over public rights-of-way are permitted up to six meters. This not only reduces radiant heat gain but the increased roof areas (up to 37% larger) also provide greater and better opportunities for rainwater harvesting, photo-voltaics, and green roofs (Fig. 2).

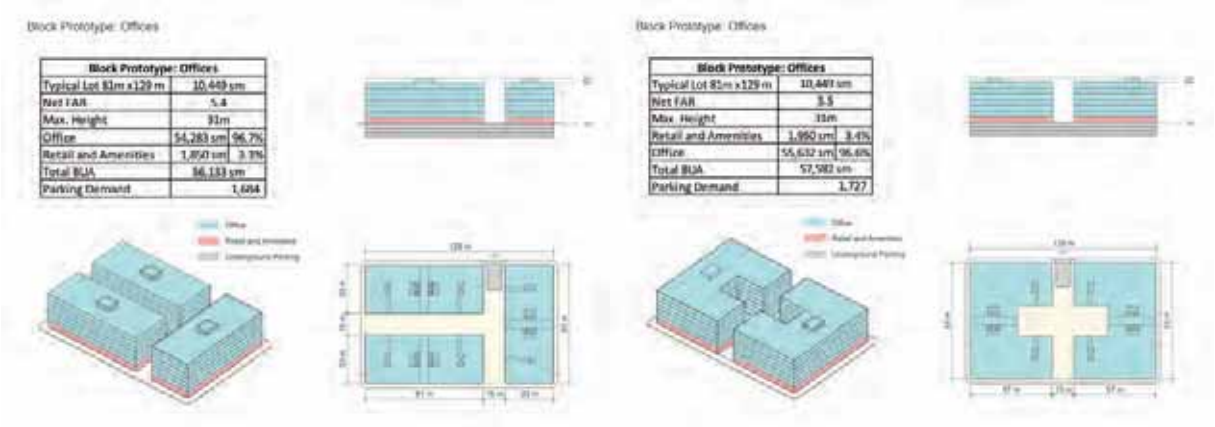


Figure 3: Block typologies are examples of building clustering that illustrate ways in which the development program and design guidelines can be met.

All buildings are required to meet minimum EUI target as set forth in the design guidelines. Energy performance may be demonstrated by modelling buildings individually or as a cluster. Any group of buildings may be modelled together provided that all buildings in the cluster are built at the same time. The EUI targets were formulated using a combination of computer modeling and benchmarking of high performance buildings in Delhi. Additionally, the guidelines also mandate on-site power generation using photovoltaics, roof gardens, and rain water harvesting.

Computer modelling demonstrated that substantial improvements in performance can be achieved by modelling buildings as a cluster. It was also observed that such an approach influenced the building planning and architecture in ways that are not possible using conventional modelling of individual buildings.

METHOD

The computer modeling of buildings and clusters were performed using the following tools and criteria:

- 8 storied buildings with 33m x 68m floor plate, and 4m floor-to-floor height.
- Buildings were built as 32m high single masses with fifty percent glazing on all facades, and modeled as offices.
- Building mass was built with Autodesk Revit 2017, and energy modeling & analysis was performed using Insight 360.
- Weather data of New Delhi, India (28° 33' N, 77° 6' E) was used.
- The first phase of the project consisting of 6 buildings was used for the analysis.

DATA

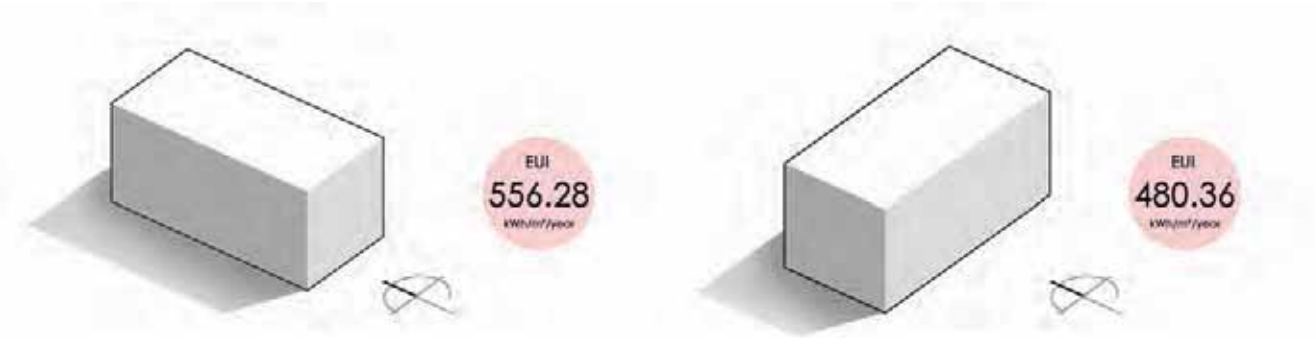


Figure 4: Effect of orientation on EUI of building mass with unprotected openings.

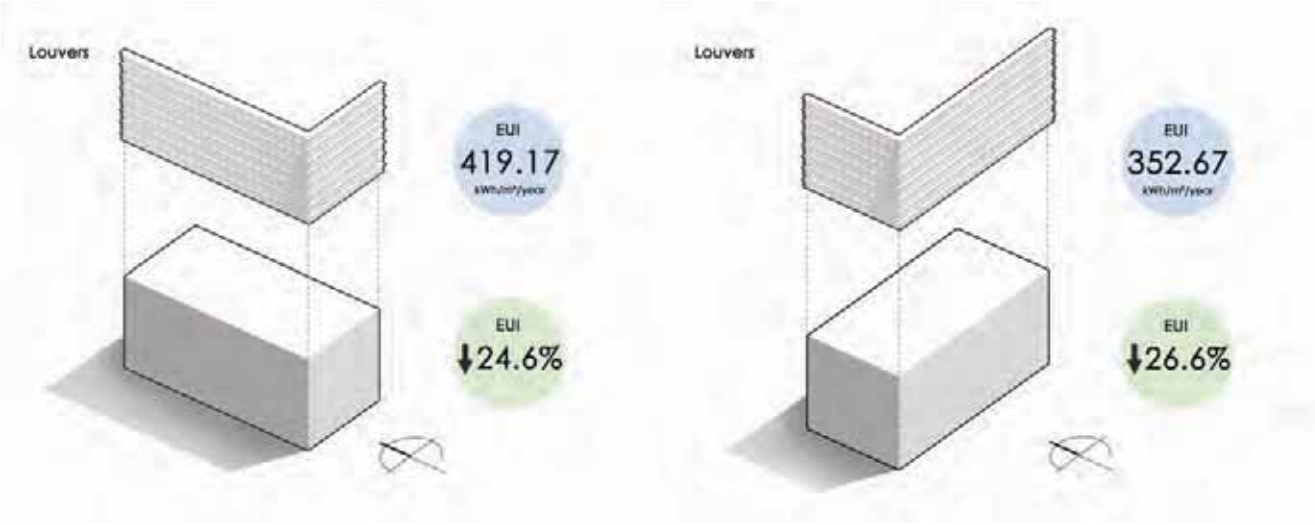


Figure 5: Effect of orientation on EUI of building mass with protected openings on west and south faces.



Figure 6: Effect of modeling buildings as a cluster on EUI of building mass(es) with unprotected openings. Rendering shows first phase development.



Figure 7: Effect of modeling buildings as a cluster on EUI of building mass(es) with protected openings on west and south faces. Rendering shows protected openings at a concept level.



Figure 8: Effect of modeling buildings as a cluster on EUI of building mass(es) with canopy and protected openings on west and south faces. Rendering shows canopy at a concept level.

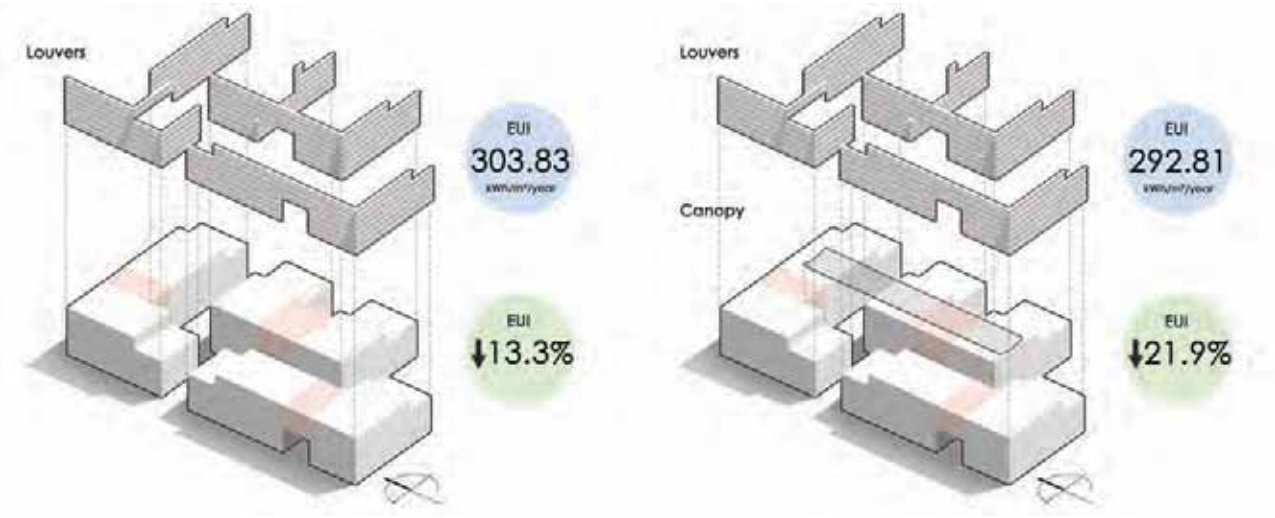


Figure 9: Effect of modeling buildings as a reconfigured cluster on EUI of building mass(es) with canopy and protected openings on west and south faces.

DATA & EXPLANATION

All EUIs are exaggerated since the buildings were modelled as single masses without floors. Relative performances of various conditions were used for analysis.

The building mass was analyzed in two orientations with unprotected glazing (Fig. 4). The EUI of the east-west (E-W) oriented building was found to be 13.65% lower than the building oriented in the north-south (N-S) direction. Addition of louvers to the west and south facades resulted in significant improvements in both orientations. The EUIs reduced by 24.6% and 26.6% on the buildings in the N-S and E-W directions respectively (Fig. 5).

SIMULATION OF BUILDING CLUSTER

The first phase of the master plan included 6 buildings (Fig. 6). The 6 buildings with unprotected opening were analyzed as a cluster. There was no significant improvement (0.6% reduction) in the performance of the cluster as compared to their individual EUIs. It was clear that for this configuration, cluster modelling had little improvement in buildings with unprotected openings.

EUIs of the buildings were analyzed as a cluster and compared with the baseline case where the average EUI (374.83 kWh/m^2/year) was computed using the individual EUIs of the 6 buildings (Fig. 7 “Discrete”). The “Discrete” method EUI was computed using individual EUI’s of 2 N-S and 4 E-W louvred buildings and dividing their sum by 6. The analysis showed a reduction of 6.5% in the EUI merely by analyzing the six buildings as a cluster (Fig. 7 “Cluster”).

IMPROVEMENTS AT CLUSTER LEVEL

Louvers are interventions at the building level that directly affect the energy efficiency of a building by limiting radiant heat gains. If the buildings are treated as one cluster, it was hypothesized that strategically placed canopies and covering walkways may improve the performance of the cluster further. A canopy was added along the north-south alley between the buildings. A 9.8% reduction in the EUI of the cluster was observed as compared to the baseline (Fig. 8).

INFORMED ARCHITECTURE

The above results showed that a clustered approach can have a substantial influence on how buildings are designed. Based on these results the six buildings were reconfigured as pair of two buildings connected with a four-storied bridge. The ends of the buildings were stepped to ensure that the buildings mass (and the development area) was not affected. Louvers were added to the southern and western faces. This reconfigured cluster showed a 13.3% reduction in the EUI compared to the baseline (Fig 9 – Left). Addition of a covered walkway reduced it further by 8% resulting in a 21.9% reduction in the EUI as compared to the baseline condition (Fig 9 – Right).

CONCLUSION AND FUTURE WORK

The California Energy Code treats each building as though it exists in a climate zone with nothing around it. Since each building owner has little control on how the City around will change in the future, taking context into account for Title 24 energy compliance can become quite cumbersome. Preliminary analyses show that significant improvements in energy performance can be achieved by modelling buildings as clusters. Energy codes therefore, should consider this option within Planned Unit Developments(PUDs) where: (a) buildings in the cluster are built in the same development phase, or (b) urban design guidelines specifically incorporate the performance criteria using the clustered approach. This can provide powerful new ways in which performance can be improved through building planning, massing, cluster-oriented improvements in the envelope and use of exterior canopies. The New Delhi Commercial Development Project will be a testing ground for energy compliance using the cluster approach.

As part of the cluster modelling approach, impact of improvements in the micro-climate on building performance need to be studied. Due to availability of advanced computing platforms, simulations using Computational Fluid Dynamics (CFD) are being successfully used to assess urban microclimate (Toparlar et. al., 2014). Energy modelling softwares currently rely on general climate data of a region. It would be a giant leap in simulating real world conditions if data from CFD modelling could be used for energy compliance of buildings and building clusters. The New Delhi project proposes several strategies for improving the micro-climate such as tree canopy density requirements, ground water recharge and habitat restoration, mandatory green roofs, native vegetation, and several strategies for air quality improvements. A micro-climate simulation is likely to more accurately represent the improvements in ambient conditions than the standard climate data. This will be the scope of future work on the project.

ACKNOWLEDGMENTS

The author wishes to acknowledge the following persons for contributing to the project in various capacities:
Yinan Wu, Kritzinger+Rao
David Wang, Kritzinger+Rao

REFERENCES

Burak Güneralpa, Yuyu Zhouc, Diana Ürge-Vorsatzd, Mukesh Guptad, Sha Yue, Pralit L. Patele, Michail Fragkiasf, Xiaoma Lic,g,h, and Karen C. Setog, “Global scenarios of urban density and its impacts on building energy use through 2050” http://www.pnas.org/content/114/34/8945.full (accessed September 2017).

Robert Sander, “Suburban sprawl cancels carbon-footprint savings of dense urban cores” http://news.berkeley.edu/2014/01/06/suburban-sprawl-cancels-carbon-footprint-savings-of-dense-urban-cores/ (accessed September 2017).

Toparlar, Y & Blocken, B & Vos, P & van Heijst, GJF & Janssen, WD & Hooff, Twan & Montazeri, Hamid & Timmermans, HJP. “CFD simulation and validation of urban microclimate: A case study for Bergpolder Zuid, Rotterdam. Building and Environment.” 201.

FORM AS ENERGY

The building envelope as an expression of energy



Matthew Fineout
Smart Architecture
matt@smart-arch.com

ABSTRACT

All too often, high-performance building envelopes are considered in terms of new materials and technologies that push specific systems to improve energy savings, without questioning the underlying geometry of the building, as if it is an a prior condition without recourse to examination. Material advances that offer occupant benefits while decreasing energy consumption are of a positive development but typically embed additional energy demands throughout their manufacturing processes. Triple silver coated glass provides enhanced performance over double coated silver glass but there is an obvious price to pay for this increased performance both in terms of energy consumption and the environment. It was Buckminster Fuller that said, 'Do More with Less' (Lopez-Perez, Daniel; Allen, Stan; *R. Buckminster Fuller World Man*; Princeton Architectural Press, 2014). This statement in its broadest sense extends to the constituent principles underlying a buildings form which directly translates to energy consumption.

The geometry of a buildings' form has a critical impact on energy consumption, both in terms of embedded and operational energy. The reduction in the surface area of a building envelope inherently reduces the embedded energy of the project. It also serves to reduce operational energy required for human comfort by minimizing the building skin contact area between inclement exterior conditions and regulated interior conditions. Unfortunately, contemporary manufacturing techniques are at odds with environmentally sensitive forms, specifically forms that aim to reduce energy usage. Today's manufacturing techniques are characterized by straight runs of steel or flat panes of glass; they are based on straight linear procedures that result in a built environment of orthogonal geometries, least favorable to environmental conditions. For a building envelope to strike a resonating chord with the environment and reduce energy consumption, a reassessment of its constituent underlying geometries in light of manufacturing techniques is required.

A case study of the Nuevo Aeropuerto Internacional de la Ciudad de Mexico, (NAICM), or Mexico City New International Airport, a joint venture between Foster Partners and FR-EE, will be offered as a vehicle to explore this issue in greater detail. This project is a seminal example of rethinking the manifold criteria that goes into the determination of an energy efficient form and its enclosing skin. The project presents a tabula rasa of sorts reexamining the underlying principles that constitute the building form and enclosing structure.

KEYWORDS

envelope, geometry, energy, environment, symmetry, asymmetry

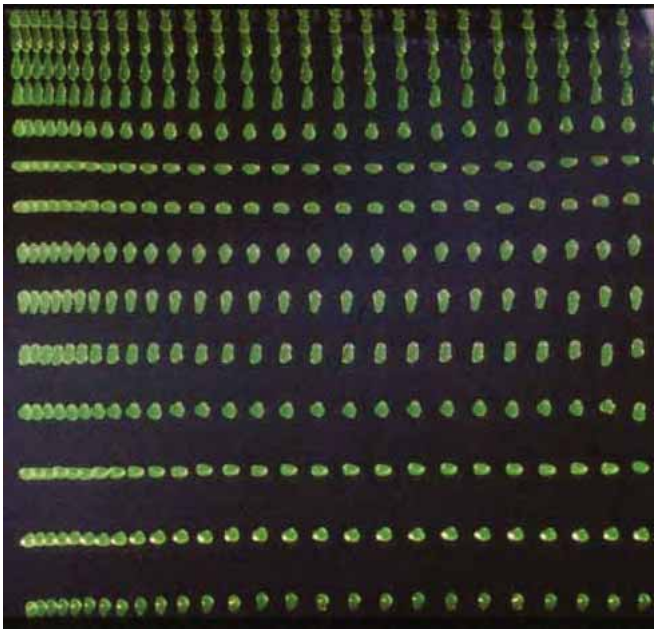
PUTTING IT IN CONTEXT

NATURE IS ASYMMETRICAL | NATURE IS NUANCED

As we know from our earliest childhood experiences, continuing in our day to day experiences, nature is not symmetrical. Although the surface tension of a water droplet favors a symmetrical spherical geometry, as seen in photographs of water droplets aboard the international space station (Fig. 1) water droplets, subjected to the natural environment, twist and turn in response to surrounding forces (Fig. 2). Rain droplets are asymmetrical; their form is a result of the acceleration of earth's gravity, lateral accelerations of the wind, pressure, and temperature differentials, as well as other forces that act upon the water droplet.



Figure 1: Water droplet aboard the International Space Station. Photo by NASA.



1:

Figure 2: Time elapsed photograph of water droplets. Photo by Edgerton Digital Collections.

These forces that shape the asymmetrical form of water droplets, extend into the patterns and motions of nature. The path of the sun throughout the year as seen from the earth is also asymmetrical. The solar analemma takes the shape of an unbalanced figure eight due to the elliptical orbit of the earth and the tilt of its axis around an off-centered sun (Fig. 3). In response to the dynamic forces that surround us, nature establishes micro and macro ecologies; systems that respond to the environmental factors they are placed within. If nature twists and contorts to adapt to ever changing phenomena why are the buildings we build of such a rigid geometric order? Although, it may be premature to fashion self-organizing skins in response to the environment, it is not premature to conceive of buildings with geometries that offer a sensitivity to their surroundings.



Figure 3: Solar analemma Photo by NASA.

As we know, our built environment consists primarily of orthogonal geometries; geometries which are foreign in nature and which inherently do not respond to the nuanced variations of natural systems. To account for the performance disadvantages of the square, remedial solutions are developed and deployed in the form of system add-ons that exacerbate energy consumption of the originating geometries. Shading louvers and similar devices attempt to mitigate or minimize adverse effects of prior decisions made in the design process that may not have taken into account orientation or other environmentally sensitive issues. Although, these 'Band-Aids', so to speak, may help reduce operational energy, they increase energy consumption throughout the building's overall life span, through embodied energy; energy related to the mining of ores and their transformation into the final product which is shipped and installed, not to mention the recycling efforts required at the building's end of life.

It takes 14,200MJ or 13.5MMBtu of energy to produce one metric ton of metallurgical alumina, the base material for virgin aluminum metal. In addition, 1.91 tons of alumina is required to produce 1 ton of primary aluminum, or 27,122MJ, 25.785MMBtu's. This does not include energy related to mining and shipping; just the process to convert bauxite ores to alumina, and alumina to primary aluminum (The Aluminum Association; *North American Aluminum Industry Sustainability Report;* September 2011; PP 22). As this illustrates, there is an abundance of energy embodied in these materials. Adding systems and materials to address performance inadequacies originating from the form of the building as it relates to its environment only adds to the overall energy consumption of the project over its entire life span. These mitigation techniques do not address the systemic underlying cause of the failure, they only put a Band-Aid on an inadequately considered holistic system that begins with building geometry. As stated above, nature is nuanced in all its forms, patterns and movements, so why shouldn't our buildings be the same to more closely align with their surroundings.

ORTHOGONAL CONSTRUCTION | MANUFACTURING TECHNIQUES

The built environment consists primarily of orthogonal forms. There are many reasons that can be attributed to this which are beyond the scope of this paper, but one primary driver is manufacturing techniques. Although, it is easily overlooked and seemingly over simplistic, building products, or better materials and their manufactured forms are the result of processes undergone in their making. Most manufacturing techniques involve the mixture of raw materials in a liquefied state, then taking this malleable mixture and rolling it over a conveyer belt or rollers to create a long orthogonal ribbon of material that creates a plane in its final state (Fig. 4-5). This then, sets up the conditions for these originating orthogonal geometries to be carried downstream through progressive sequences of the construction process. As benign as the processes may seem, they establish the conditions for the final form of the building, to maintain the residue of the originating geometries. After all, it is more work to create a spherical structure with a rectangular piece of material.

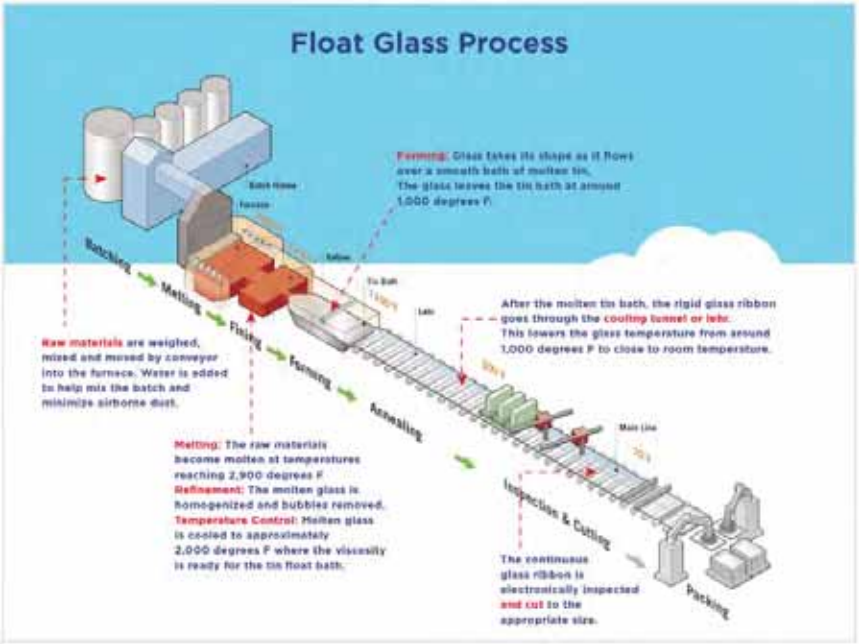


Figure 4: Float glass manufacturing process. Photo by Vitro Architectural Glass.



Figure 5: Glass tempering process Image by United Plate Glass.

Like all industrial methods, these manufacturing processes will be overthrown when printing technologies mature, allowing much more freedom to the building form but for now we are stuck with flat planes of material. Until printing technologies offer these possibilities, one is faced with the challenge of creating buildings that respond to their environment and local ecologies while employing standard manufactured materials that favor rectangular forms. What this requires then, is a reassessment of building systems, including structural and enclosure systems and construction techniques, that favor forms adaptably suited to their environment in light of these manufacturing techniques.

STRUCTURE RECONSIDERED | BUCKMINSTER FULLER

It was Buckminster Fuller that said, 'Do More with Less' (Lopez-Perez, Daniel, Allen, Stan; *R. Buckminster Fuller World Man*; Princeton Architectural Press, 2014). Fuller, the visionary, realized in the early 50's and 60's that we could not sustain our way of living and our consequential built environment. The geodesic dome was the physical manifestation of his mantra 'Do More with Less' and the direct expression of his central tenets: (A) 'Spherical structures enclose the greatest volume with the least surface', (B) 'Geodesic spherical structures, which are inherently omnitriangularly framed entirely of great-circle chords, give the strongest structure per weight of materials employed' (Fuller, Buckminster R.; *Critical Path;* St. Martin's Press, 1981). The structures he created were revolutionary. They deployed the lightest materials following pure geometrical forms. But herein lies the challenge, although the domes were remarkable for their reconsideration of structure and formal typologies their geometry adheres to strict platonic forms. Their greatest use is in military installations, radar housings and similar functions but their formal ability to meet the needs of people, urban issues, and a sense of civic and public architecture met mixed results. If the principles developed by Buckminster Fuller break free from their rigid geometric orders and attune themselves to the finely nuanced conditions that respond to the greater ecologies of the environment and how people negotiate their daily lives, an architecture arises that is embedded within its conditions and therefore provides an overarching integrated sustainable approach.

NUEVO AEROPUERTO INTERNACIONAL DE LA CIUDAD DE MEXICO

FORM AND GEOMETRY

The Mexico City New International Airport is a joint venture between Fernando Romeo EnterprisE (FR-EE) and Foster Partners (F+P) (Fig. 6). It is an entirely new airport, located to the north-east of the existing airport, on a dry lake bed. The passenger terminal building for the airport will be the single largest terminal building in the world, serving 68 million passengers annually, when complete, projected for 2020. The design of the terminal building is very unique, and in plan, forms an X, optimizing passenger flows and connectivity. The building envelope departs from conventional airport design and offers the most innovative aspect of the project. Sir Norman Foster and Fernando Romero proposed the building envelope to be one system; to do away with conventional walls, roofs, clerestories and their associated structural elements and ancillary systems but to consider the envelope as one unifying system. This offered a tabula rasa of sorts to reconsider the building envelope from the ground up.

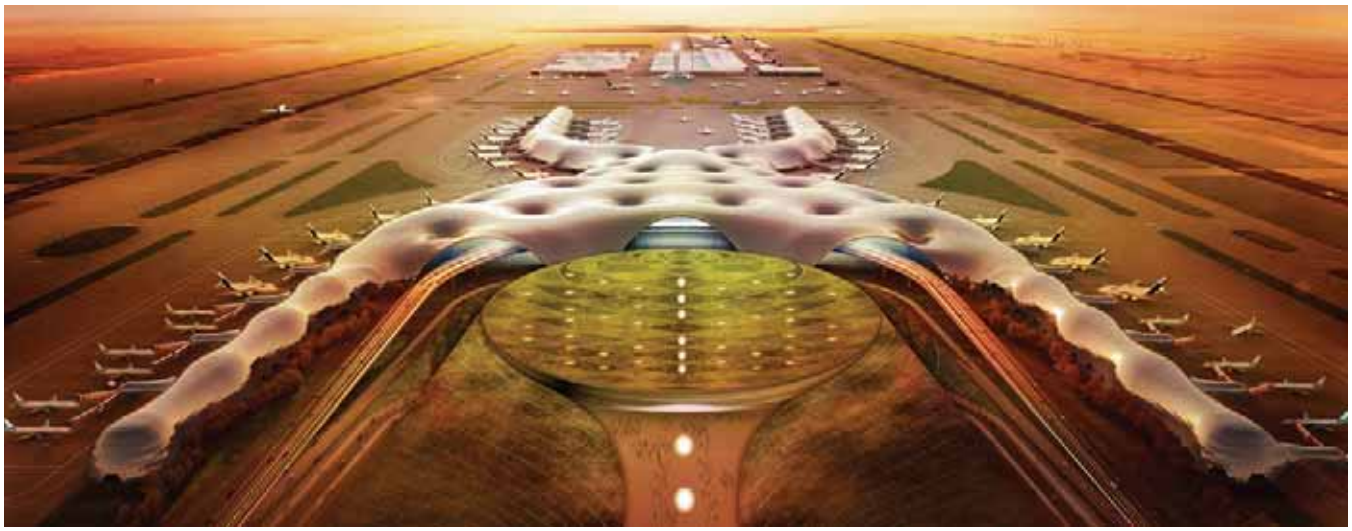


Figure 6: The Mexico City New International Airport (NAICM). Image by FR-EE|F+P|JV.

The building envelope for the Mexico City New International Airport terminal is approximately five million square feet. It is a stand-alone system that is detached from the terminal superstructure that supports floor slabs, mechanical systems, and elements specific to the functioning of the airport. In essence, the building envelope acts as a single membrane that spans great distances to enclose the programmatic areas and functions of the terminal, protecting the interior environment from the exterior conditions or, better said, creating a symbiotic relationship between the two (Fig. 7).

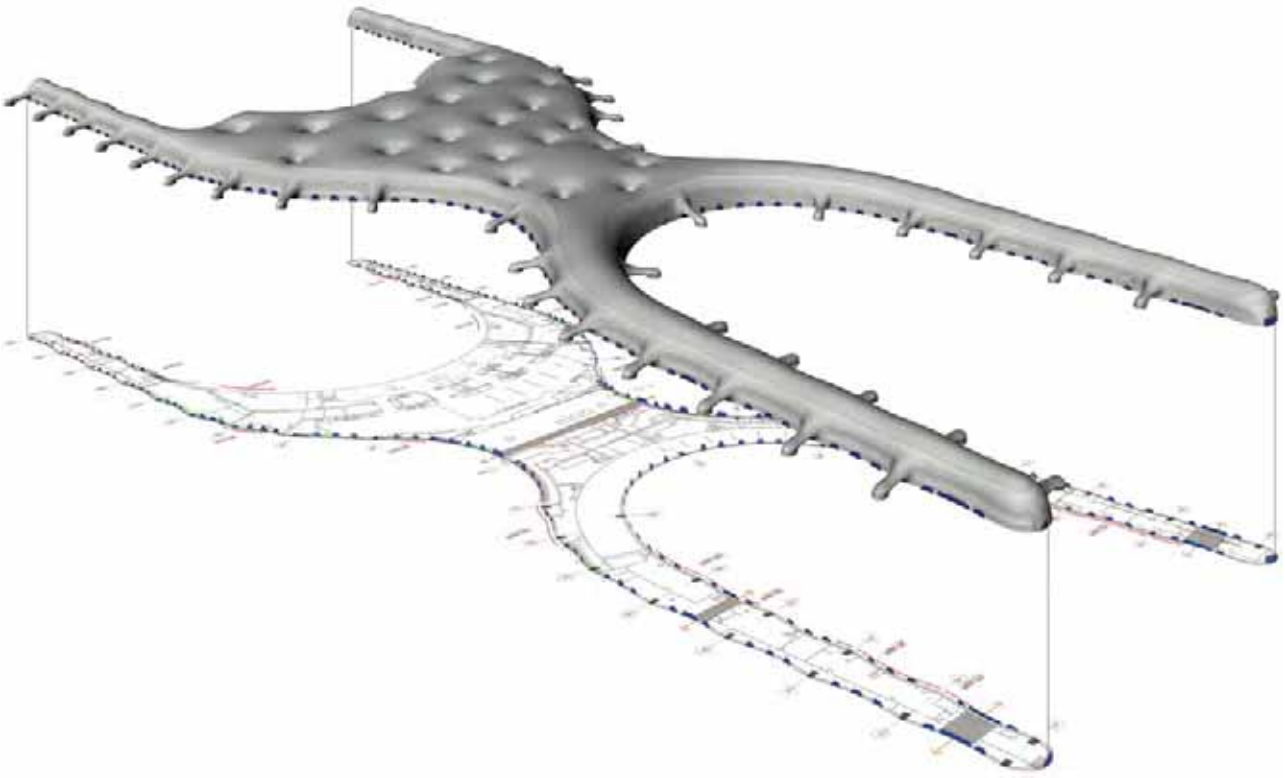


Figure 7: NAICM envelope to program fit. Image by FR-EE|F+P|JV.

The building skin is very closely choreographed to the inner workings of the airport and as well to airside constraints and environmental conditions. To that end, the envelope mediates numerous conditions responding to and fostering each. To achieve a single unifying system Norman Foster and Fernando Romero along with Arup proposed a shell structure (Fig. 8). Shell structures provide the benefit of highly efficient structural systems; the least amount of mass and weight required to

accommodate structural forces. Shell or form-active structures, do this by optimizing loads axial to the structural member there-by minimizing bending, torque and shear within the member that requires additional material to overcome these forces (Macdonald, Angus; *Structure & Architecture;* Taylor Francis Group; 2001). In addition, the building skin is a direct expression of the structure, thereby eliminating miscellaneous assemblies that mediate between dissimilar assemblies. The cohesive structural logic of the Mexico City Airport is differentiated into three framing techniques based upon programmatic requirements and load bearing functions. The vast majority of the envelope is supported by a tetrahedral, double layer space frame structure. At the boarding gates, this double layer system merges into a single geodesic layer, mechanical, nodal system. At the central portion of the terminal, the space frame converges into twenty-one vertical supporting elements called funnels, that consist of a single, welded, layer frame (Fig. 9).

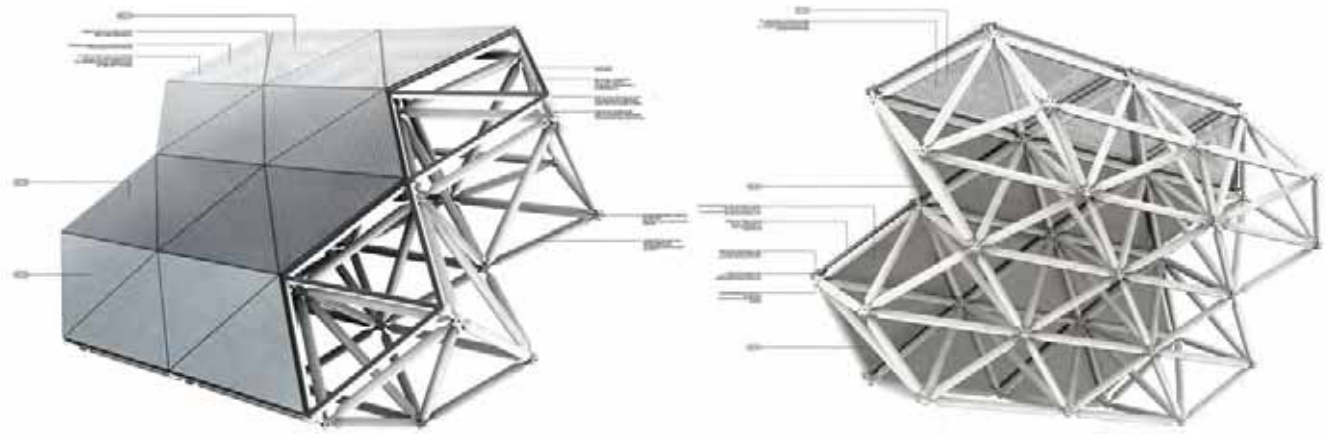


Figure 8: NAICM envelope assembly, cladding & space frame. Image by FR-EE|F+P|JV.

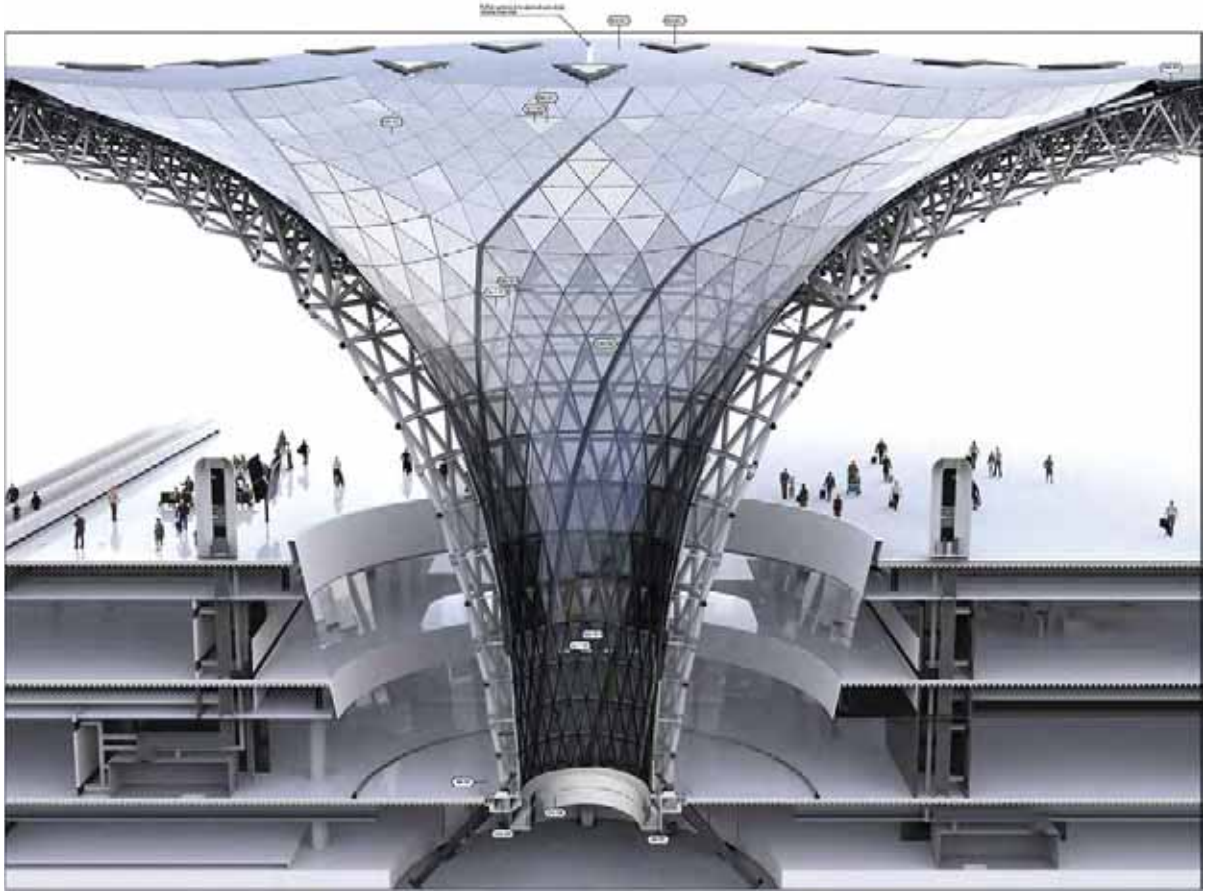


Figure 9: NAICM funnels. Image by FR-EE|F+P|JV.

FORM FITTING

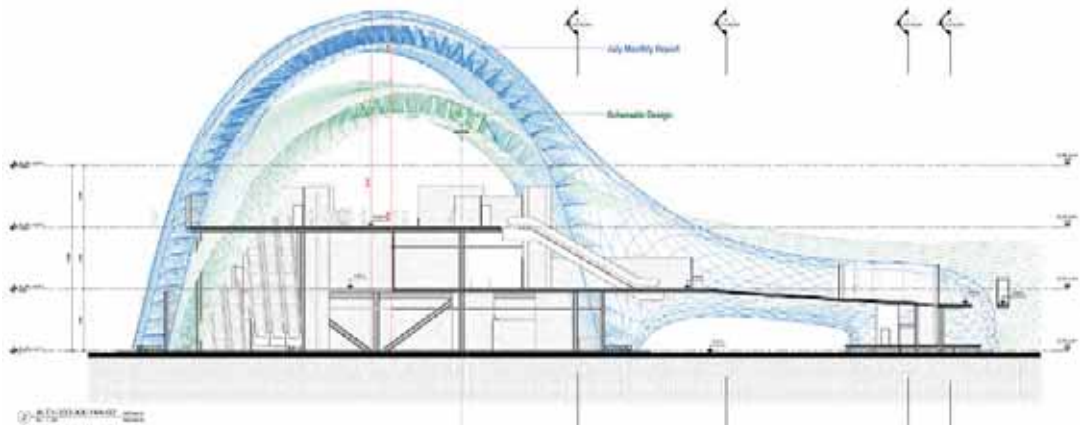


Figure 10: Comparison of iterative building envelope geometries. Image by FR-EE|F+P|JV.

The geometry of the building envelope is the result of a year and a half long form fitting process that took into account several different and often times competing criteria and conditions. The resulting form is a balancing of these constraints and conditions. First and foremost, the envelope provides shelter for the terminals program and various functions. The center of the 'X', surrounded by seven funnels that project to form a dome, provides a generously scaled atrium with shops and other amenities that provide rest and respite for travelers. The central dome, also known as the '*Heart'* of the project, feeds into four terminal arms, lined with boarding gates, that provide access to aircraft beyond. Clearance requirements for such pragmatic elements as elevator shaft overruns were carefully studied to minimize faulting and associated surface area of the space frame over these elements. The terminal arms are not just linear extrusions of a concourse but gently swell and contract in relation to the boardinggates (Fig. 11-12). This subtle modulation of the form not only provides ample area and visual ques for the boarding gates but, between gates, reduces the footprint, volume and related surface area of the building skin. This yields tremendous savings in both operational and embodied energy. A ten percent variation in a five million square foot building envelope equals five hundred thousand square feet, which is significant. Tuning the envelope to recognize these nuances is paramount in its final design and energy savings.

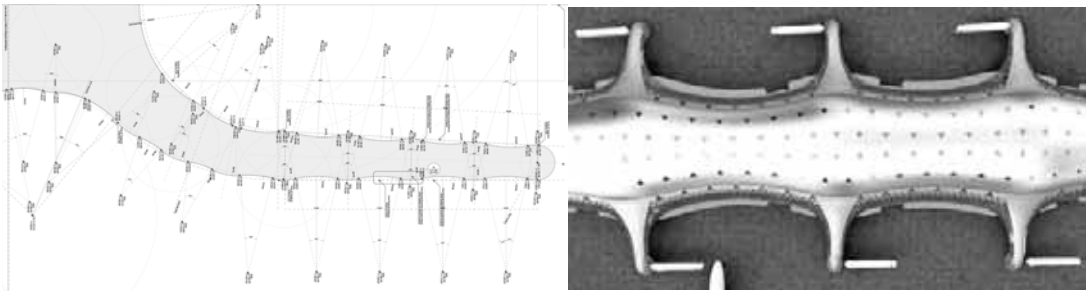


Figure 11-12: NAICM terminal arm setting out drawing; terminal arm digital model visualization. Image by FR-EE|F+P|JV.

It also bears mentioning that the terminal, although in its overall form appears symmetrical, in fact is not symmetrical. Small localized deviations in response to internal functional requirements occur throughout the terminal that prevents any symmetrical reading of the project especially as it relates to construction, which precludes the possibility of mirroring elements. For instance, the forty-six boarding gates that ring the perimeter are not evenly distributed but are located in response to operations and aircraft types. Domestic versus international gates, associated aircraft and other operational functions set the location of the boarding gates also known as the "*fixed link bridges*". The geodesic mesh of the fixed link bridges merge into the overriding space frame shell of the terminal but localized adjustments are made to accommodate their unique locations. Great lengths were taken to minimize disparities and their effect on the terminal shell that would distract from a cohesive structure, not only to simplify construction but create an intuitive environment for passengers. This speaks clearly of a form adaptive structural system that can act upon localized conditions within a broader overarching geometry and form. This approach moves beyond the rigid platonic geometries of Buckminster Fuller, not mentioning the strict prescribed orthogonal geometries of manufacturing techniques, to an open-end system receptive to balancing form and function.

Beyond spatial criteria, the envelope was also developed in response to functional and performative criteria. In order for a shell structure to work certain geometries must be maintained; an arch has a limit to its flatness. Airside constraints limited the height of the building to forty-one meters above the runway apron while internal programmatic requirements called for generously scaled volumes. The positioning of the supporting funnels and the arching capability of the space frame mediates these two opposing constraints, reaching clear spans of up to 178 meters at the dome. Seismic and volcanic events play a critical role in the development of the building envelope. The light weight structural space frame was designed to reduce the 'table-top' mass that exacerbates forces in a seismic event. Detailed rain water flow analyses were performed to insure the 'slipperiness' of the envelope during rain and hail storms to maintain balanced flow and drainage. Proper minimum slopes are maintained that prevent ponding even under deflection of volcanic ash events from the nearby Popocatepetl volcano (Fig. 12-13). The project will be certified LEED Platinum when completed, the first LEED platinum airport in the world. To this end, extraordinary time and effort was devoted to the study and analysis of thermal and daylighting performance, which is subject for another paper.

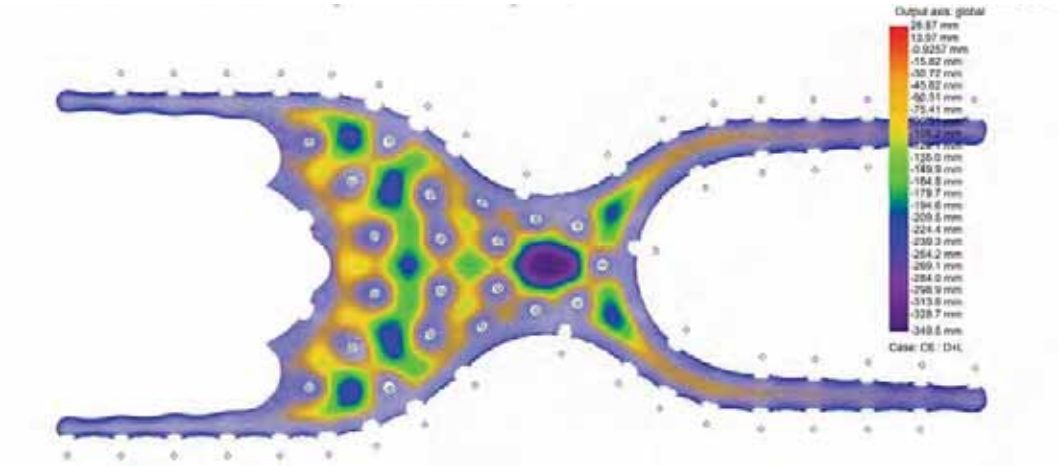


Figure 13: NAICM structural deflection mapping. Image by FR-EE|F+P|JV.

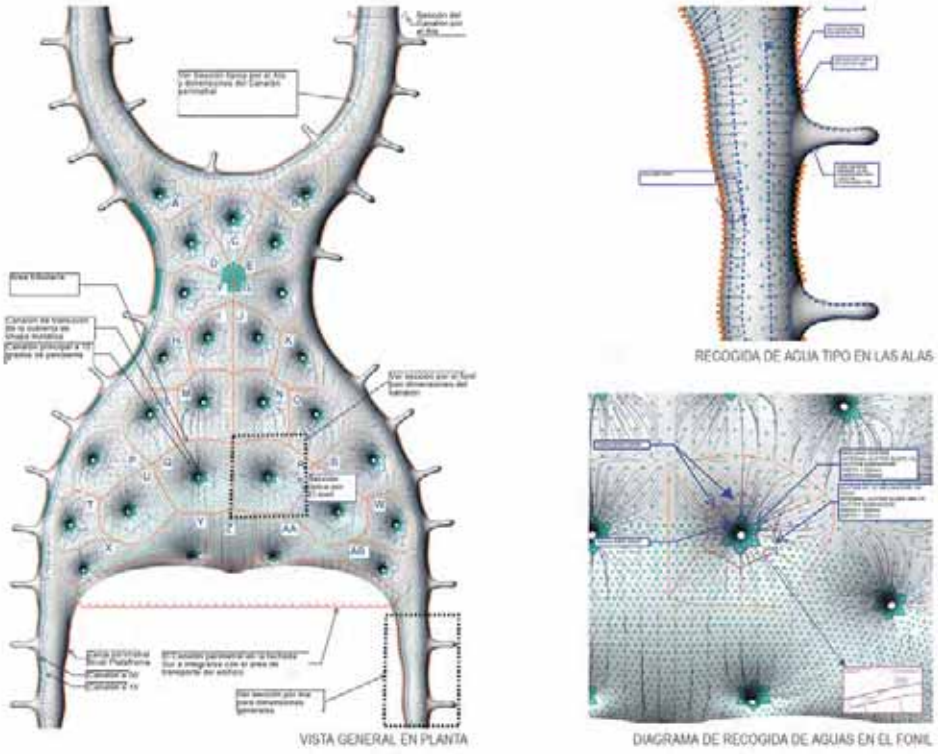


Figure 14: NAICM rain water flow analysis. Image by FR-EE|F+P|JV.

KIT OF PARTS

To develop an envelope, that avoids orthogonal geometries originating from manufacturing techniques, and is more akin to a highly organized chrysalis, required the reconsideration of its components as a highly integrated kit-of-parts (Fig. 15-16). There is a strong correlation between the members that form the kit of parts; structural members to cladding elements. The triangular mesh pattern of the kit-of parts was determined by the triangulated tetrahedral spaceframe. The size of the triangular modules was determined by the size of a tempering oven for a piece of glass which is not to exceed 2.5M. A fully glazed IGU, without internal divisions, can face an entire triangular module. The triangulated mesh and module size were ideally suited to approximate the continuous curvatures of the envelope; similar to differential calculus, where the measurement of a free-form is broken into progressively smaller parts to approximate that shape. The fine granularity of the module size afforded the skin its adaptable ability to reconcile various and diverse conditions. As mentioned previously, the skin is a direct expression of the structure thereby eliminating miscellaneous assemblies required to negotiate between dissimilar systems; another weight savings advantage. There are various permutations of triangular modules but great lengths went into standardizing modules for economies in production. The terminal arms employ a repetitive geometry between terminal boarding gates that employ repetitive family clusters of elements; cladding panels and structural members (Fig. 17). In addition, the 46 fixed link bridges that connect terminal arm to jet ways are all identical

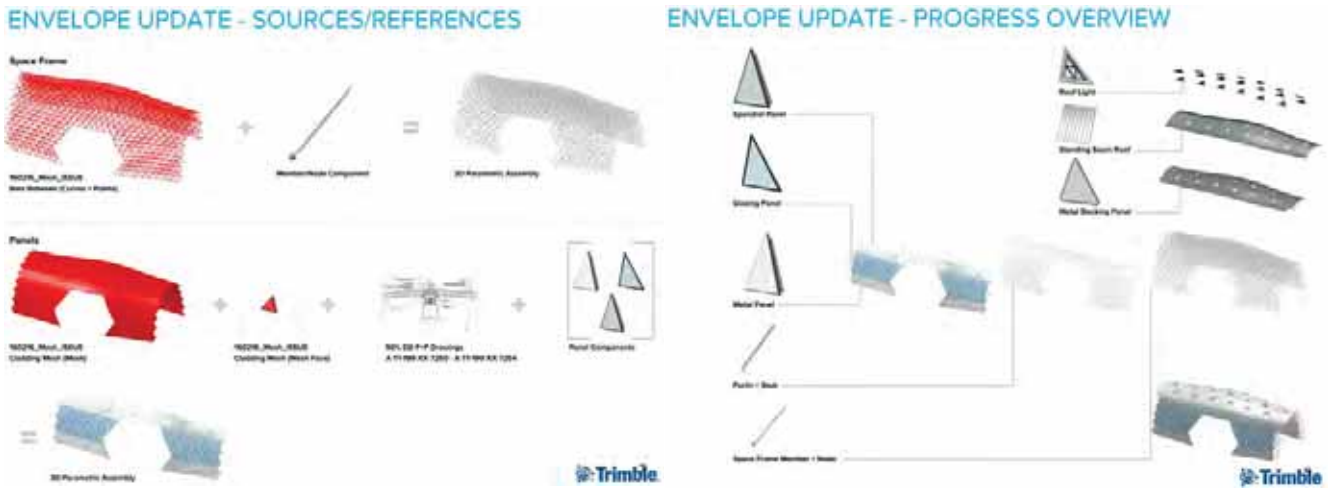


Figure 15-16: NAICM building envelope space frame & components. Image by Trimble & FR-EE|F+P|JV.

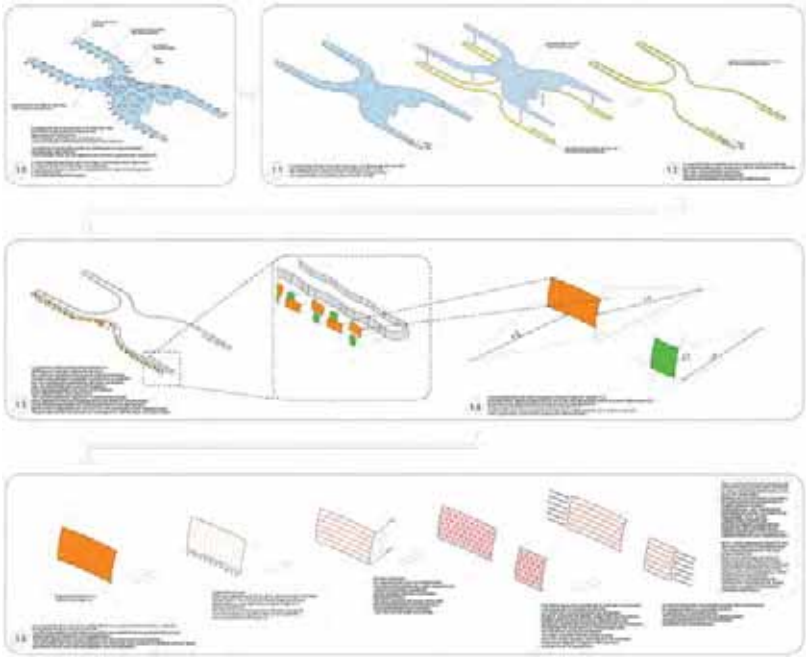


Figure 17: NAICM building envelope setting out logic. Image by Trimble & FR-EE|F+P|JV.

LESS IS MORE

A cursory study will help illustrate the potential these strategies, related to the reconsideration of constituent geometries and systems, can offer in terms of increased energy savings. Figures 18A-18C represent three versions of the building envelope. Figure A represents the envelope as designed with exterior openings or an unclosed volume. Figure B represents the envelope as designed with these exterior openings closed, providing an enclosed volume and Figure C is an orthogonal extrusion of the terminal footprint as designed. The height of the extrusion is based on an average height between the terminal arms and the dome of the airport. In reality, this average height would be inadequate to house the various programmatic functions and would require a stepped roof with all its inherent complications in lieu of the sinuously smooth geometry of the current design.



Figure 18A: Envelope mesh figure.



Figure 18B: Closed envelope mesh figure.



Figure 18C: Orthogonally extruded footprint.

In Figure 18B, the surface area of the enclosed mesh equals 472,506.362M^2. The surface area of the building envelope in Figure 18C, the orthogonally extruded footprint, equals 526,273.445M^2 This represents an increase in surface area of over ten percent. This is significant for a building of this scale, costing an additional 53,767.083M^2 of material.

To illustrate how this additional material translates into energy consumption, apply the energy values related to the production of aluminum noted earlier. Hypothetically, one square meter of aluminum sheet equal five kilograms. Following the equations below, there is over a seven million Mega Joule increase in energy consumption for the orthogonal geometry, and as mentioned, this does not even take into consideration energy related to mining, shipping and installation.

$$1\ Ton\ Virgin\ Aluminum\ Metal = 27{,}122MJ\ or 25.785MBtu$$

$$1\ Ton = 1{,}000Kg = 27{,}122MJ\ or\ 25.785MBtu$$

$$1Kg = 27.122MJ\ or\ 0.025785MBtu$$

$$1\text{M}^2 = 5Kg = 135.61MJ\ or\ 0.128925MBtu$$

Embodied Energy Increase: $53{,}767.083\text{M}^2\ x\ 135.61MJ\ =\ 7{,}291{,}354.13MJ$

CONCLUSION

In summary, the Mexico City New International Airport presents a new paradigm in the relation of architecture to its environment. Substantial reductions in energy consumption can be realized in challenging a priori forms borne from orthogonal geometries embedded in the manufacturing process. This, coupled with form active, highly efficient structures, further reduces weight and material and the associated embodied energies of each. The formal approach in defining the mesh also discards the shackles of a straitjacket geometry that is unforgiving to local conditions. Instead this geometric strategy enables the ability of the form to adapt to localized conditions. As always architecture is an art, it is not strictly scientific. There is always an art in balancing quantitative facts with qualitative conditions. Architecture, first and foremost inspires the human condition but at the same time must be vigilantly conscious of the costs for its realization. Perhaps the most interesting aspect of the Mexico City New International Airport is that it provides a malleable enclosure within a comprehensive logic that allows the freedom for nuanced behavior while respecting the responsibility of energy conscious forms.

We have new tools at our disposal and a variety of manufacturing techniques that are quickly evolving. We also have the capacity to analyze big data, related to various phenomena, hitherto unavailable before. By the year 2030, three and a half times the existing building stock of the United States, including infrastructure, will be built worldwide, primarily in Asia (Architecture 2030, UN Habitat, *State of the World's Cities 2010/2011*; McKinsey Global Institute). In light of these conditions, in which we now find ourselves, a paradigm shift is required; The Nuevo Aeropuerto Internacional de la Ciudad de Mexico points in this new direction.

REFERENCES

Lopez-Perez, Daniel; Allen, Stan; *R. Buckminster Fuller World Man*; Princeton Architectural Press, 2014.
Fuller, Buckminster R.; *Critical Path;* St. Martin's Press, 1981.
The Aluminum Association; *North American Aluminum Industry Sustainability Report;* September 2011.
Macdonald, Angus; *Structure & Architecture;* Taylor Francis Group; 2001.

INTEGRATED ENERGY ANALYSIS

Leveraging energy modeling to improve the conceptual level decision making process



Greg Verabian
HKS
gverabian@hksinc.com



Saurabh Shrestha
HKS
sshrestha@hksinc.com



Laure Michelon
Glumac
lmichelon@glumac.com

ABSTRACT

Energy codes across the country are progressively getting stricter and increasing the threshold for a baseline building's energy performance. California's Title 24 Energy Code is pushing towards net-zero energy for all new construction residential buildings by 2020, and all new construction commercial buildings by 2030. This makes it increasingly important for architects and engineers to collaborate to ensure that the architectural intent of a building can be maintained while meeting energy code.

Typically, architects create models early on to orient the building massing and layout. Once the general building design has been solidified, engineers and energy analysts will be brought on board to assess more detailed design options. While these energy models can impact the HVAC system design, glazing selections, and window performance, it is often too late to improve upon or adjust the overall building massing or envelope design. This can lead to missed opportunities to optimize the overall building design.

Using Hollywood & Gower, a high rise residential project, as an example, this paper discusses how architects and engineers can work together in the conceptual and entitlement phases (a pre-development phase whereby The City grants development rights to a specific parcel) to optimize a building's design and ensure the design intent can meet California's strict energy code. The architects, began by running a parametric energy analysis for various external shading options. This helped to understand the effectiveness of various shading devices to reduce solar heat gains. Energy analysts then used the architectural geometry to build an energy compliance model to assess the impacts of the shading strategies compared to Title 24 energy code. This process allowed for the team to understand the effect of design decisions on Title 24 energy code compliance.

This paper will showcase the Hollywood & Gower integrated work flow, how this dynamic can be applied to other projects, how design can be as aesthetically sophisticated as it is performative and how it can be expanded in the future.

KEYWORDS

building information modeling (BIM), design optimization, energy efficiency, external shading, integrated design process, code compliance, parametric workflows

INTRODUCTION

Green building design is continuously evolving to require a more holistic approach, especially with ever escalating concerns about Climate Change, rising CO2 levels, and progressive energy code cycles. California's Title 24 Energy Code is moving towards net-zero energy for all new construction commercial buildings by 2030. This push in sustainability and efficiency makes it increasingly important for architects and engineers to collaborate early in design to ensure that the architectural intent of a building can be maintained while effectively meeting energy code with the project's sustainability goals.



Figure 1: Hollywood & Gower. Rendering courtesy of HKS.

BACKGROUND

The Hollywood & Gower high rise residential project is currently in the entitlement phase of its project life. HKS started the design process with conceptual ideas that maximized views and efficiency while minimizing costs. The team needed to understand how the various shading designs would reduce solar gains in the units, ensure a comfortable environment with a high window-to-wall ratio, and identify if the design would pass energy code. The intent of this analysis was to understand the quantitative benefit to designing external shading for a building. We attempted to understand first how design decisions impact sustainability and compliance of the project. Then, through the lens of the energy model, we wanted to help inform future design decisions for the project.

METHOD

Using Hollywood & Gower, a **HIGH-RISE** residential project, as an example, this paper discusses how architects and engineers should work together in the conceptual and entitlement phases to optimize a building's design and ensure the design intent can meet energy code. In a more traditional approach to analyzing the energy in building, the architect brings on the energy analyst in the beginning of the schematic design phase, or once the project design requires compliance documentation for city approval. The former option carries less risk than the latter as there is still an opportunity to influence the design to increase efficiency earlier in the process. In the Hollywood & Gower scenario, the architect and energy modeler worked hand in hand to analyze different envelope options. The following stages detail the design processes and analysis phases from the initial ideas to preliminary compliance modeling results.

STAGE 1 – DESIGN IDEAS

This proposed 22-story residential/mixed-use tower, located at the intersection of Hollywood and Gower, is generally regarded as being at the eastern gateway to the Hollywood Walk of Fame, where Lucille Ball's star is at its front door. Its next-door neighbor, The Henry Fonda Theater, is a historically significant building and has hosted numerous high profile live events. The tower, which contains 220 apartments, is designed for the young entrepreneur, or soon to be famous, stylish and hip-society type.

The tower has been positioned on a north south axis to maximize views both to the north and the south for all units. To the north is a direct view to the Hollywood Sign and to the south the Los Angeles city basin. On a clear day (yes we have them), the Pacific coastline and Catalina Island can be seen. The orientation of the building also creates an opportunity for a sun-filled open space which acts as a "massing buffer" from the adjacent Fonda Theater and maximizes daylight entering the resident's amenity space.

Several elevational/skin concepts were developed using Maya, a modeling, simulation and rendering software, for its ability to rapid-prototype concepts, each with an approach to creating a sustainable and performative skin that would preserve views and daylight but also protect against solar heat gain and glare.

- Scheme 1 was developed with the notion of connecting the building to the larger street-grid, scaffold supports and intense shading blurring the boundaries of the building edges.
- Scheme 2 took a far more measured approach and created a thin veil of metal tubes running horizontally, like venetian blinds only to be pierced by balcony openings. The second skin would extend beyond the footprint of the tower to emphasize the "superficial" nature and clearly identify the shading technique. In Scheme 1 and 2 the Tower façade concept extended down to the podium levels tow rap and conceal parking and other uses.
- Scheme 3 utilized a series of horizontal "trays". Between each floor tray is a fluctuating ribbon of vision glass, patterned glass and metal panel, creating a digitized pattern. Vision glass is located to maximize exposure into living spaces, while bedrooms were primarily glazed with patterned or screened glass.
- Scheme 4 established a series of shingled/angled glass panels in an attempt to create a skin resembling elements found in nature. Glass angles were set to maximize views and minimize solar heat gain. Panels on upper floors shaded the floor below and balconies could be added into each "cell" by removing glass selectively.



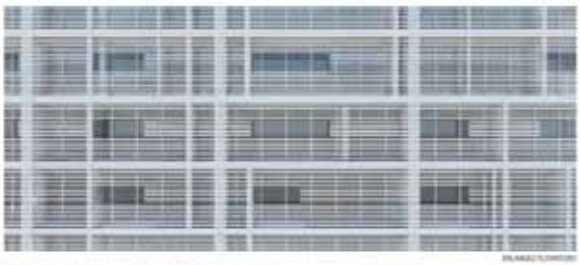






HOLLYWOOD / GOWER - RESIDENTIAL TOWER

1









HOLLYWOOD / GOWER - RESIDENTIAL TOWER

2





HOLLYWOOD / GOWER - RESIDENTIAL TOWER

3





HOLLYWOOD / GOWER - RESIDENTIAL TOWER

4

Figures 2-5: Hollywood & Gower exterior shading scheme. Renderings courtesy of HKS.

Probably the most striking feature of the tower will be its performative exo-skeletal bris-solei. Wrapped in a prefinished white aluminum panel, it was designed in hopes that it would:

- Maximize vision glazing around the building
- Create a foil that organizes the otherwise randomness of the “diving board” balconies. The skin is offset four feet, to create usable but structurally achievable platforms from the main structure in front of clear vision glass and dark metal mullions/ panels. In a sense, the bris-solei becomes art and recalls the history of billboards, scaffolds and the structure of the iconic Hollywood Sign.

Full-length south-facing terrace balconies provide ample shading while not compromising views from the units. The roof-top features a full indoor prep kitchen, indoor activity room and landscaped terrace with outstanding views.

STAGE 2 – PRELIMINARY ENERGY MODELING – ARCHITECT

As described in the preceding section, the basic massing of the building and the options for shading structure - exo-skeletal bris-solei, were narrowed down based on various site parameters and restrictions, including view preservation strategies and aesthetics. Although it was obvious that any type of shading structure would have some positive impact on the energy consumption of the building, it had not been quantified to help in the decision-making process. It was also important to determine how it would compare against a code-baseline building to make sure that it would meet code.

As a first step, the architects went through a rudimentary energy modeling exercise to quantify the comparative benefits of the selected shading strategies compared to a code-baseline building with no shading device. Additionally, this exercise informed the sensitivity of the window to wall ratio (WWR) to the performance of the building. The goal of the exercise was to identify a window to wall ratio for the design case combined with the shading structure that would meet the performance of a code-baseline building with no shading device and a 40% WWR.

The representative floor method was used to run energy simulations for the purpose of this exercise. A total of three floors were modeled, however only the results of the middle floor was used for calculations as the floors on the top and the bottom were only modeled to capture the boundary conditions, as would be the case in a typical floor in the residential tower. The model was created in Rhinoceros 3D and Honeybee for Grasshopper was used to run the energy simulations. Honeybee uses Energy Plus as its simulation engine. Although most of the geometry was created in Rhinoceros 3D, the windows were generated through Honeybee, which made it possible to control the WWR parametrically as a variable input.

The program of a mid-rise apartment was used to generate the default Honeybee model inputs for the simulations. The envelope parameters that were used are listed below:

- Roof insulation: R-27
- Wall insulation: R-8.7
- Window: U value 0.42; SHGC 0.28

Three sets of iterations were run, each with three variations. The first set was with no shading devices with a window to wall ratio of 78%, 60% and 40%. A 78% WWR was chosen as a maximum allowable and a 40% WWR is the ASHRAE 90.1 and Title-24 code baseline percentage that all energy models are compared against. The second set included horizontal shading devices with the same variations in WWR. The third set had the external frames as shading structure with the same variations in WWR.

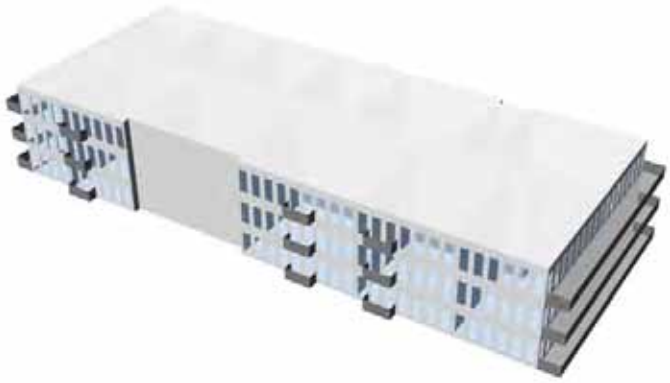


Figure 6: Three floor sectional representation with no shading device. Image courtesy of HKS.



Figure 7: Three floor sectional representation with exterior frames as balconies. Image courtesy of HKS.

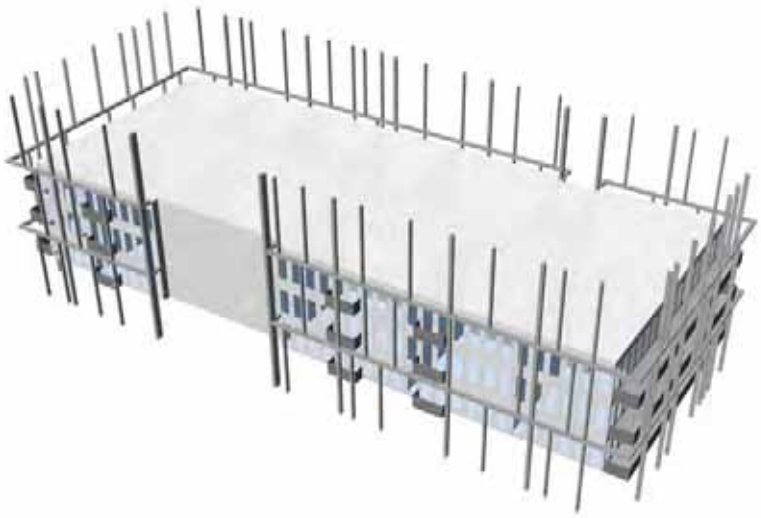


Figure 8: Three floor sectional representation with exterior frames as shading structure. Image courtesy of HKS.

As the inputs for the electric light and equipment were kept constant, the results for those end uses show no change. The climate in Los Angeles (ASHRAE Climate Zone 3B, Title 24 Climate Zone 9) at the project site is cooling dominated and requires very little heating over the year. Thus, the load that the shading devices and the windows can impact the most is the cooling energy.

Isolating the cooling energy numbers, as shown in Figure 9, the option with frames as shading devices at a WWR of 40% performs the best among the nine options, whereas the option with no shading at a WWR of 78% performs the worst.

The option with no shading device at a WWR of 40% was established as the baseline. With both horizontal shades and the frames as shading devices, the building could increase the WWR to about 60% and still perform better than the baseline (a % savings of 1.7% and 3.5% in Table 1). However, the option using frames as a shading device would perform better among the two. As the building is elongated north-south, and the east and west facades have maximum exposure, vertical shading elements of the frames at regular intervals proved beneficial to block solar radiation.

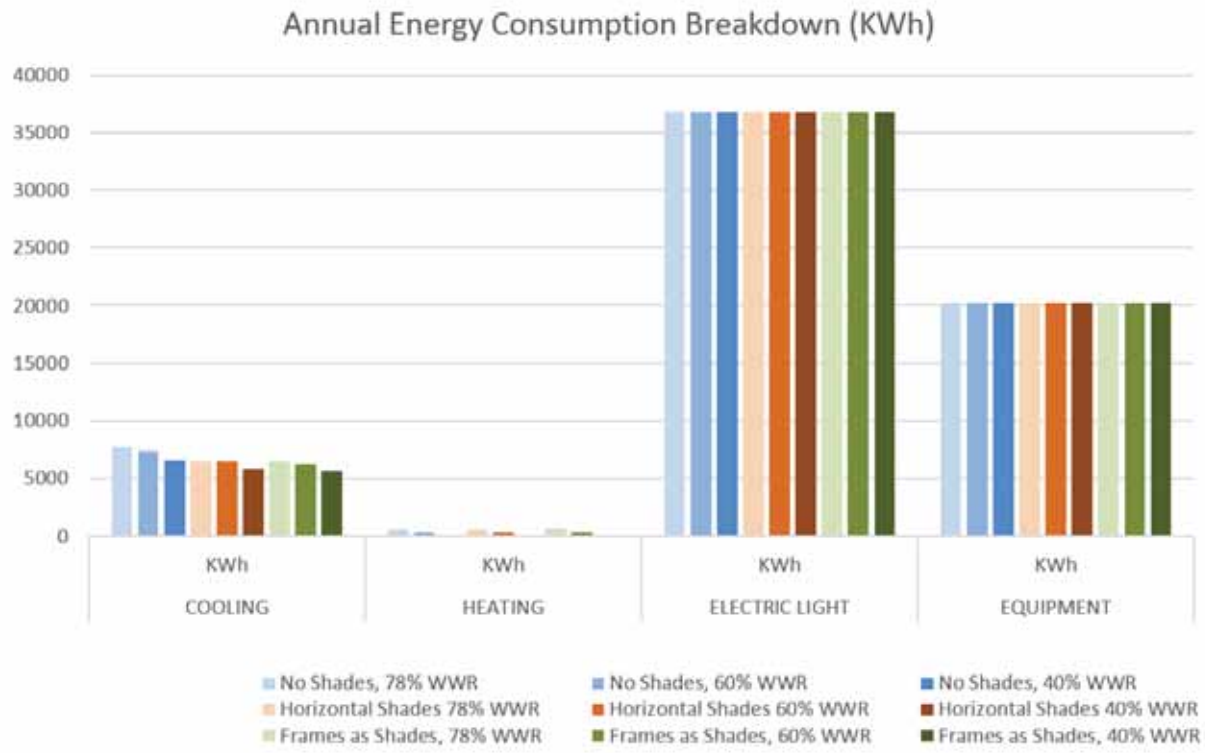


Figure 9: Comparison of cooling energy from Honeybee (kWh) and percentage savings. Image courtesy of HKS.

	WWR 78%	% Savings	WWR 60%	% Savings	WWR 40%	% Savings
No shading device	7777.9	-18.8%	7380.4	-12.7%	6547.2	0.0%
Horizontal shading device	7893.4	1.4%	7283.4	1.7%	6321.4	10.7%
Frame as shading device	6510.4	0.6%	6321.2	3.5%	5657.5	13.6%

Table 1: Percentage Savings from Honeybee. Image courtesy of HKS.

STAGE 3 – DETAILED ENERGY COMPLIANCE MODELING – ENGINEER

After the initial modeling effort, the team needed to see how the building was expected to comply with California Title-24 energy code. The idea being to analyze how the energy compliance margin was affected by different window to wall ratios and differing levels of exterior shading in the compliance model.

The project team modeled a three-floor representative section of the building. Using multipliers for a standard floor plate the energy performance of the entire residential portion of the building can be accurately extrapolated. The energy model was initially created in Revit to capture the full 3D geometry of the building. This was imported into CBECC-Com, the official state approved Title 24 compliance software. Based on previous experience with high-rise residential projects in Los Angeles, the team recommended that the representative residential portion of the building should have a compliance margin of at least 3% better than code baseline.

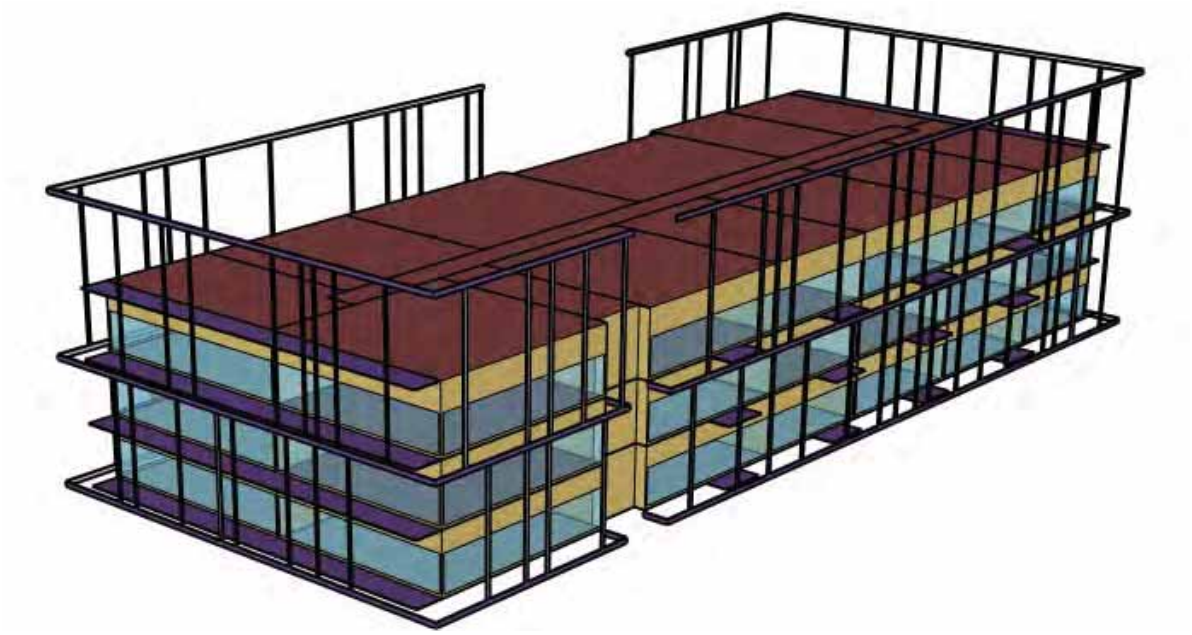


Figure 10: CBECC-Com detailed model in Sketchup 2016. Images courtesy of Glumac.

The project team assessed the shading structure with various window-to-wall ratios in order to determine its effect on the energy code compliance. Three different window-to-wall ratios were analyzed, 40%, 60%, and 78% to match the preliminary energy modeling analysis. Each WWR was analyzed both with and without the shading structure for comparison and to see its effect on compliance. This assessment aims to determine how impactful the structure and WWR are on energy code compliance.

The following outlines all assumptions that were assumed as part of the basis of design for the Hollywood & Gower. These parameters were based on past project experience with high-rise residential towers in Los Angeles.

Envelope

- Exterior Walls U-factor of 0.122
- Roof insulation of R-30 insulation with cool roof finish (SRI 0.9)
- Window SHGC of 0.25 and U-factor of 0.42 (thermally broken frames)

HVAC

- HVAC was comprised of central condenser water loop with water source heat pumps (WSHPs)
- Condensing boilers: 93% efficiency
- Closed loop fluid cooler with a 10F degree approach
- Dedicated outside air corridor ventilation unit (DOAS)
- Condensing DHW water heaters with 96% efficiency
- The residential unit WSHPs (17 EER, 5 COP) and ECM fan motors

The building was also assessed for three shading options: no balconies or cage, with only balconies, and with both the balconies and the cage. The Revit geometry models of each are shown in Figures 11-13, and the compliance results of these simulations are shown below in Table 2.

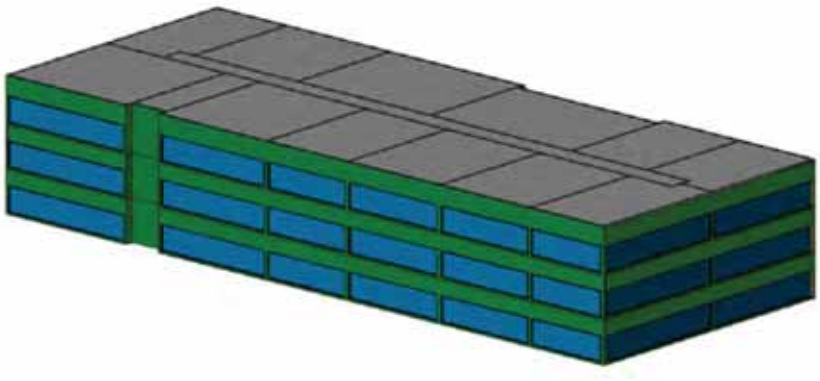


Figure 11: Revit 2016 model of building no external shading. Images courtesy of Glumac.

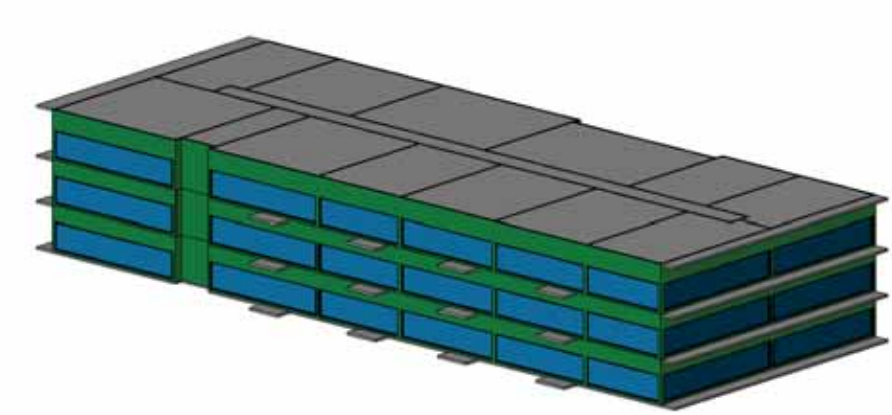


Figure 12: Revit 2016 model of building with balconies only. Images courtesy of Glumac.

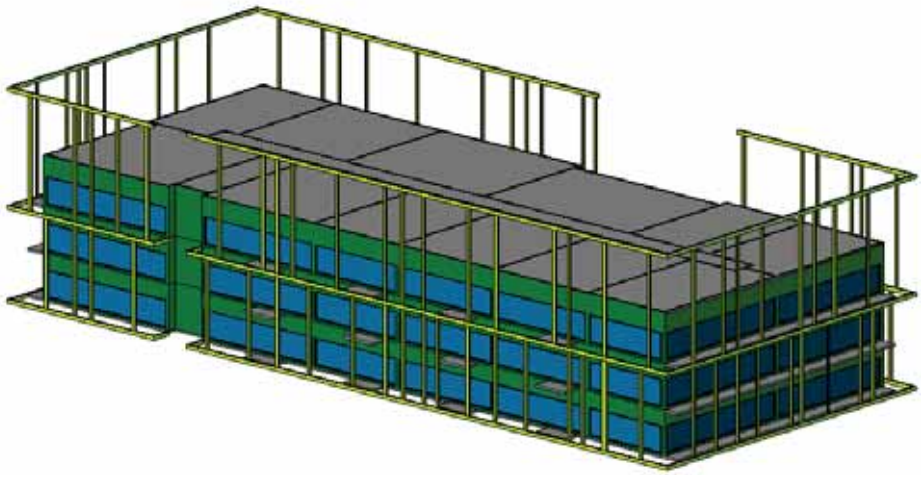


Figure 13: Revit 2016 model of building external shading. Images courtesy of Glumac.

It was determined that that both the shading options and WWR had a significant effect on complying with Title-24. The 60% WWR with both balconies and the cage exceeded code by 1.2%, and would only require minor design changes to meet the recommended compliance margin.

	NO & NO SHADING		BALCONIES ONLY		BALCONIES & SHADING	
WWR	Title 24 Compliance	Change in Compliance	Title 24 Compliance	Change in Compliance	Title 24 Compliance	Change in Compliance
40%	2.4%	-	3.2%	0.8%	3.8%	0.6%
60%	-0.9%	-3.3%	0.1%	1.0%	1.2%	1.1%
78%	-4.4%	-6.8%	-2.8%	1.6%	-1.5%	1.3%

Table 2: Compliance margins. Images courtesy of Glumac.

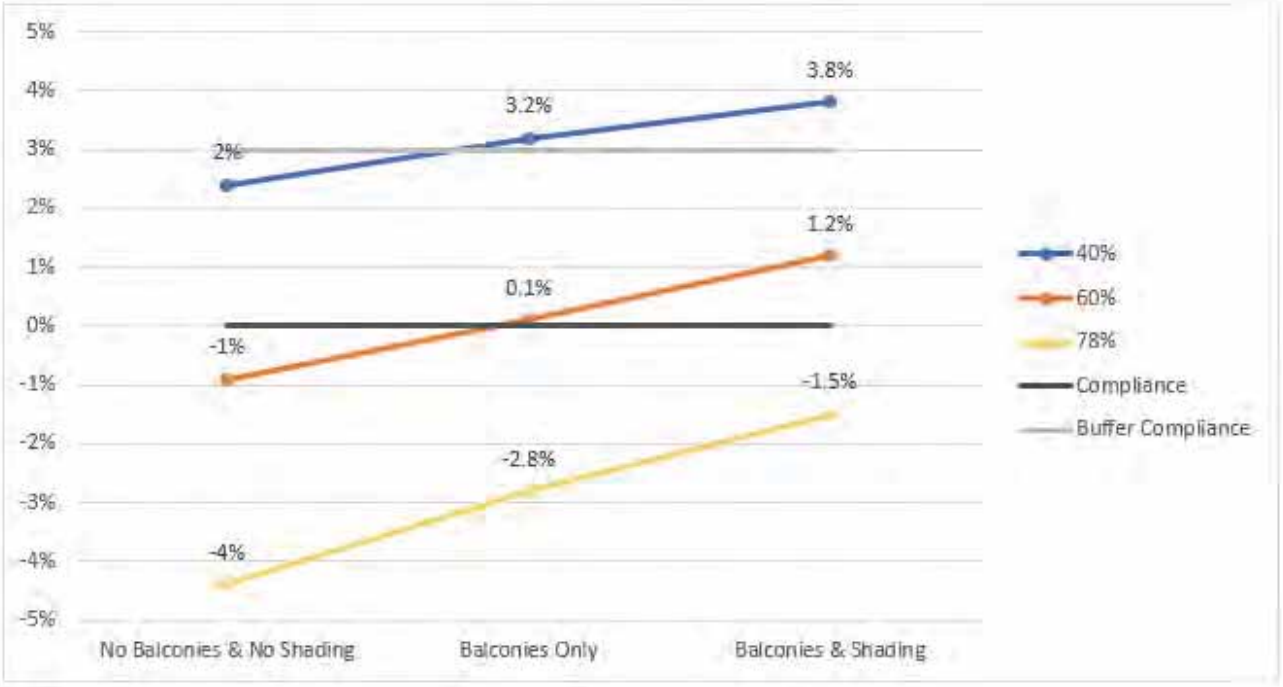


Figure 14: Graph of compliance margins in relation to compliance requirement. Images courtesy of Glumac.

The 78% WWR design took a more significant compliance penalty of -6.8% relative to a baseline 40% WWR design. The balconies and cage shading structures were very helpful in reducing cooling-related loads and improved the compliance margin by 2.9%. This however did not make up for the overall penalty and additional energy efficiency upgrades would be required to offset the increase in WWR, so additional energy efficiency measures are required in order to obtain the 3% target margin for a mixed use residential building. These energy efficiency measures could include high performance glazing, premium efficiency HVAC equipment, or solar hot water system to offset the domestic hot water load.

EXPLANATION

The Honeybee and CBECC-Com models both show the same narrative, that an increase in window-to-wall ratio has a decrease in performance due to the increase in cooling loads. From this analysis, we can deduce that through energy modeling the exterior shading of the building, the energy impact can be quantified and implications can be ascertained. By designing and modeling detailed exterior shading early in design one is more flexible to create a more interesting building with a lower cooling load and larger windows. External shading design works best when it is validated both architecturally and by the design engineer in order to create an integrated design that adds to the building aesthetically as well as for energy performance. Without the integrated process, the systems will not be optimized for efficiency and could potentially add cost

with minimal performance benefit. This type of early collaboration is critical to meeting sustainability goals such as Architecture 2030 or Title-24 Net Zero Energy.

CONCLUSION AND FUTURE WORK

Because the architect worked hand in hand with both the initial energy modeler and the compliance energy modeler every step of the external shading structure was analyzed. Performing these iterative energy analyses in the entitlement phase is critical. The entitlement phase sets a precedent for the project and creates some design constraints for the project moving forward. If the building design is floor to floor glazing in the entitlement phase, when the building goes through compliance the HVAC system will need to be able to mitigate the harsh solar loads and will end up increasing the cost of the building's HVAC system.

The design of a 21st century building requires a holistic design approach. Architectural and structural elements influence the mitigation loads required by HVAC (possibly saving on first cost) and can potentially lessen the energy requirements of the building. These up-front analyses help integrate different disciplines and assist in understanding the impact of design decisions early on. While this specific CBECC-Com analysis will resonate most specifically with people in California, the results and understanding span globally.

Moving forward, green building will continuously evolve to include a holistic approach to design. With ever escalating concerns about Climate Change and CO2 levels in the environment, it is becoming evidently clear that even the highest standards of construction performance used today are not progressive enough. In order to hit Architecture 2030, it will not be enough to decrease the solar loads through the use of external shading; more passive strategies will need to be incorporated such as natural ventilation and maximized daylighting.

	Baseline EUI (kBTU/sf-yr)	Goal EUI (Architecture 2015)
AIA 2030 Commitment Set Use Types	US National Site EUI	Architecture 2030 Challenge Site EUI
Residential Mid-High Rise	78.8	23.6

Table 3: EUI associated with Architecture 2030.

More passive, energy efficient strategies will need to be implemented in order to reach Architecture 2030 goals. These strategies include natural ventilation, night pre-cooling strategies, daylighting, solar tubes, designing with thermal mass, using perennial plants as shade walls, and optimizing solar penetration into the building for heating/cooling mitigation. By optimizing the building for the climate that it resides in, the project can take advantage of "free" heating or cooling. These strategies can allow for reduced HVAC loads and can decrease first cost on HVAC systems and savings on utility costs throughout the projects life. By tailoring the envelope and building design to incorporate natural lighting through daylighting or solar tubes, the project can decrease the amount of energy required to light the space while also providing a better environment for the tenant.

ACKNOWLEDGMENTS

Thank you to Brian Stern and Jacob Chan for their help with the analysis and report.

REFERENCES

The American Institute of Architects. "The Carbon Neutral Design Project: What is Carbon Neutral Design?" http://www.tboake.com/carbon-aia/carbon_definition.html (accessed August 25, 2017).

Architecture 2030. "The 2030 Challenge" http://architecture2030.org/2030_challenges/2030-challenge/ (accessed August 12, 2017).

Ladybug Tools www.ladybug.tools

ORBIT TOWER

Proposal for a hybrid structural-facade system featuring a self-adaptive solar shading device



Enrica Oliva
Werner Sobek New York
enrica.oliva@wernersobek.com



Michele Andaloro
Werner Sobek Stuttgart
michele.andaloro@wernersobek.com



Werner Sobek
Werner Sobek Group
werner.sobek @wernersobek.com

ABSTRACT

While most of high-rise buildings feature a core surrounded by a spatial frame defining the volume, one could envision a column-free plan where the perimeter structure is constituted of steel cables, working in tension to suspend the floor plates and transferring the loads to the core by means of story-high trusses located along the perimeter, as well as diagonally across the floor, at the mechanical levels.

The steel cables feature custom fittings to support the fully-glazed skin and allow for an optimized redistribution of the loads between the supporting members. The resulting hybrid scheme has beneficial impacts from a structural, sustainability, and indoor environmental quality standpoint.

The abundant natural light, penetrating through the fully-glazed skin, is controlled by an adaptive shading system, integrated with the IGU, consisting of perforated steel sheets woven together by two-way shape-memory alloy hinges that enable the component to work like an origami, opening and folding automatically according to the exterior environmental conditions: in the summer, the unfolded geometry creates an external overhang that varies with each panel exposure and alleviates the energy demand required for cooling; in the winter, the folded shape allows for a higher solar heat gain, thus lowering the heating energy demand. Therefore, the self-adaptive skin designed allows for unobstructed views throughout the envelope, as well as for an optimized control of the light, both in terms of energy and of daylighting comfort, thus mastering a Class A metropolitan office space.

Ultimately, the proposed hybrid scheme, fostering an optimized behavior of the load bearing members and an absolute minimization of the facade elements, has led to significant improvements: 11% less steel, 6% less concrete, 35% less embodied energy are required, when compared to a standard high-rise construction with identical geometry and featuring steel columns around the perimeter and an aluminum curtain wall facade.

KEYWORDS

adaptive - kinetic - dynamic, daylighting - glare - shading, energy and carbon, parametric workflows, cable facade, shape-memory alloy, hybrid structure-skin.

INTRODUCTION

There are several ways to improve the energy performance of a building; however a certain level of compromise in terms of aesthetics, natural daylight and organization of the interior spaces is often required with the currently available solutions. In an effort to guarantee high energy efficiency, abundant natural light and column-free spaces in a metropolitan office building, a system that acts at the same time as skin and structure is proposed. In this office building there is no interior column, and the natural light can reach the entire footprint thanks to the 10 ft ceilings and its unique adaptive facade. The energy consumption of the building is highly reduced, compared to a standard office building, thanks to the origami-like shading system made of shape-memory alloy elements: the system is triggered by certain temperature values and therefore adapts throughout the seasons and folds according to the Sun exposure, thus reducing the risk of glare, overheating of the space and need for artificial lighting in the working spaces.

The absence of columns in the 30-50 ft spans is possible thanks to a system of steel cables hung from cantilever trusses at each mechanical level, which are strategically placed at quarter points along the building elevation.

Above these levels, where story-high trusses are suspended off of the cast-in-place concrete core, 24 ft high “outdoor garden” levels offer amenity spaces and opportunities to enjoy the views of the city. In fact, several wind tunnel tests on buildings of similar size in New York City have highlighted that the wind speed on such floors would generate discomfort in the occupants only 1 or 2 days per year, and could be occupied as public amenity spaces for the remainder of the time.

The result of such an optimized structural system is that the facade does not require a separate frame (often aluminum) and the foundation system can cover a much smaller footprint (essentially, the layout of the core only), when compared to a standard office building with steel columns and aluminum curtain wall.

A direct comparison between the proposed building and an identical building with a standard structural and facade system has highlighted the following:

- 11% less steel required;
- 6% less concrete required;
- no aluminum needed for the facade (100% reduction);
- 35% less embodied energy in the building with the self-adaptive facade;
- 25% reduction in carbon footprint in the proposed solution.

BACKGROUND

Smart Materials are capable of automatically and inherently sensing or detecting changes in their environment and responding to those changes with some kind of actuation or action (Lelieveld, 2013). These materials are the inspiration for the shading system on an office building, such that the response of the material to the outside temperature conditions can trigger action in the shading device without the need for energy input. A component can therefore bend to a specific angle and recover completely when the temperature rises above a defined threshold. This type of thermal activation allows for optimization of the natural daylight without causing overheating in the office spaces, and at the same time reducing the risk of glare.

The fabrication of such shading system is at one time cost-effective and rather straightforward in its geometry, thus making these kinds of systems an optimal solution to be further developed and more widely implemented.

METHOD

OVERVIEW

An innovative cable-suspended structural skin replaces the typical aluminum-and-glass curtain wall in a 44-story office building in the heart of Manhattan, New York, significantly reducing its embodied energy and carbon emissions, allowing more access to the natural light and also reducing the heating and cooling demand of the building.



Figure 1: Rendering of the building. Image courtesy of Werner Sobek and ODA.

The project is designed using advanced technologies: parametric models to generate and optimize shape and modular components of the tower, and analytical software to optimize its structure.

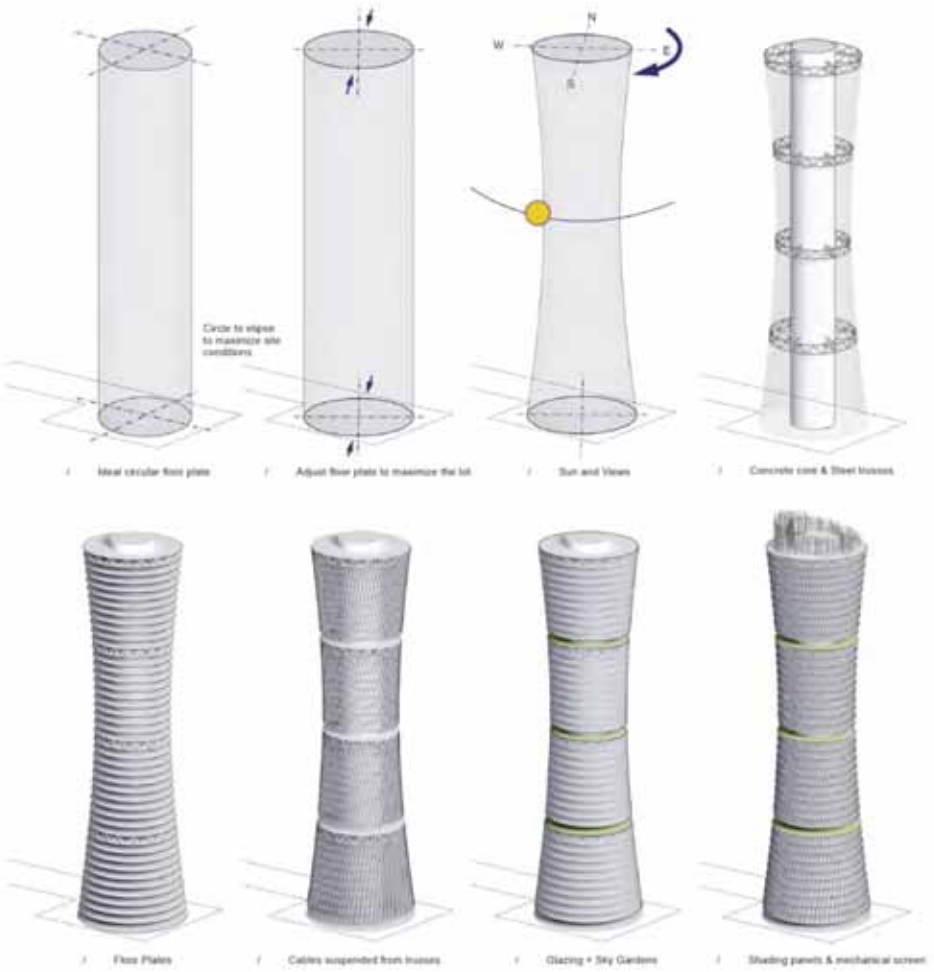


Figure 2: Shape development diagrams. Image courtesy of Werner Sobek and ODA.

The plan outline is the answer to the challenge of optimizing the enclosure: the ideal circle becomes an ellipse as it fits the specific site configuration. Rising from the street grid, the volume gently twists, sunflower-like, to adjust to a cardinal orientation, thereby increasing the surface area exposed to daylight.

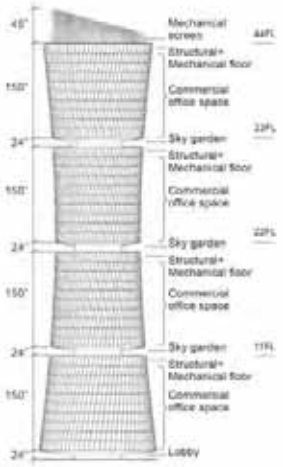


Figure 3: Tower elevation. Image courtesy of Werner Sobek and ODA.

The abundant natural light, combined with 10 feet-high ceilings, a raised access floor with unobtrusive service distribution and exceptional views through a clear glazed facade, provides for an outstanding interior environment. The high-performance facade optimizes solar heat gain through an innovative dynamic shading system, unfolding and closing as solar conditions demand. Daylight harvesting helps significantly reduce lighting and cooling energy demand.

The building's dynamic shading system works like an origami that automatically opens and folds itself according to the exterior temperature.

The shape has been designed to embed two different configurations and, therefore, two optimized behaviors. In the summer, the unfolded geometry creates an overhang - differentiated according to each panel exposure - that reduces the amount of solar radiation hitting the facade and alleviates the energy demand required for cooling; in the winter, the folded shape allows for solar heat gain, thus lowering the heating energy demand.

The results, obtained through a comprehensive daylighting study, show that glazing and shading, working together, create a comfortable environment: they grant both good penetration of natural light, even at wider floor plans, and an effective protection from excessive exposure and glare issues.

Furthermore, the application of highly efficient triple glazing, together with the absolute minimization of thermally weak points, provides a top-grade thermal comfort in the interior spaces and a significant reduction of the energy demand.

Column-free spaces and the enhanced optical quality of glazed surfaces allow for quality views throughout the interior spaces, while the elliptical floor configuration gives an optimized ratio between the envelope surface and the occupied floor area.

The proposed tower can be divided into 4 "blocks", 10 stories each, defined by a truss level (mechanical) at the top and 9 office floors below it. Between two consecutive "blocks" there is an additional "open" level, which will serve as an amenity space. The building therefore consists of 44 stories, with a typical story height of 15 ft at the office and mechanical levels, and 24 ft at the amenity floors, for a total height of 715 ft above ground.



Figure 4: Rendering of a typical office floor. Image courtesy of Werner Sobek and ODA.

PARAMETRIC WORKFLOW

The proposed geometry was defined and analyzed via a Grasshopper 3D (Rutten and McNeel, 2014) script within Rhinoceros (McNeel, 2011).

Several optimization steps were taken between the architect's team and the engineer's team, in order to attain a tower geometry and a facade panelization that would allow for a cost-effective fabrication of the glazing and its connections, more efficient connection details, and a high level of repetition. The panel size was kept below the standard sizes, so as not to trigger the demand for expensive jumbo sheets and the glass panes require a small enough curvature that they can easily be cold-bent on site. This process, for such curvatures, is extremely more cost-effective than the hot bending, and does not require special equipment, nor does it add lead time to the fabrication of the glass.

LOAD PATH

The structure's lateral system consists of cast-in-place concrete core walls, while the gravity loads are taken by a composite steel floor framing system with slab on metal deck at each floor plate and delivered to the core walls on one end, and to steel cables all around the perimeter. The cables then carry the floor loads up to the trusses at the top of each block, and from there the loads can reach the core and be carried down to the foundations. This allows for a fully open floor plan at each typical level, and the only floors where the steel members extend across the plate are the mechanical spaces; careful coordination with the MEP engineers allows for this arrangement to be successful and efficient.

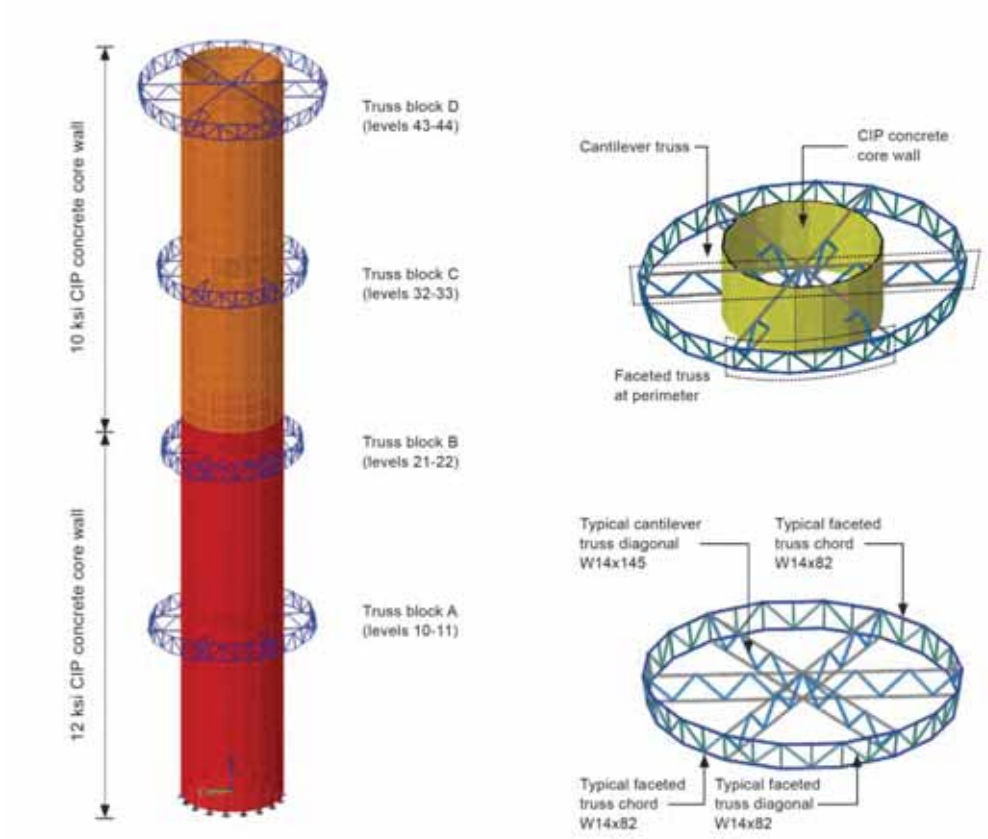


Figure 5: 3D view of the structural analysis model (ETABS by CSI) (left), top steel truss and concrete walls, colored by member cross-section (ETABS by CSI) (top right), truss block D colored by member cross-section (ETABS by CSI) (bottom right). Images by the authors.

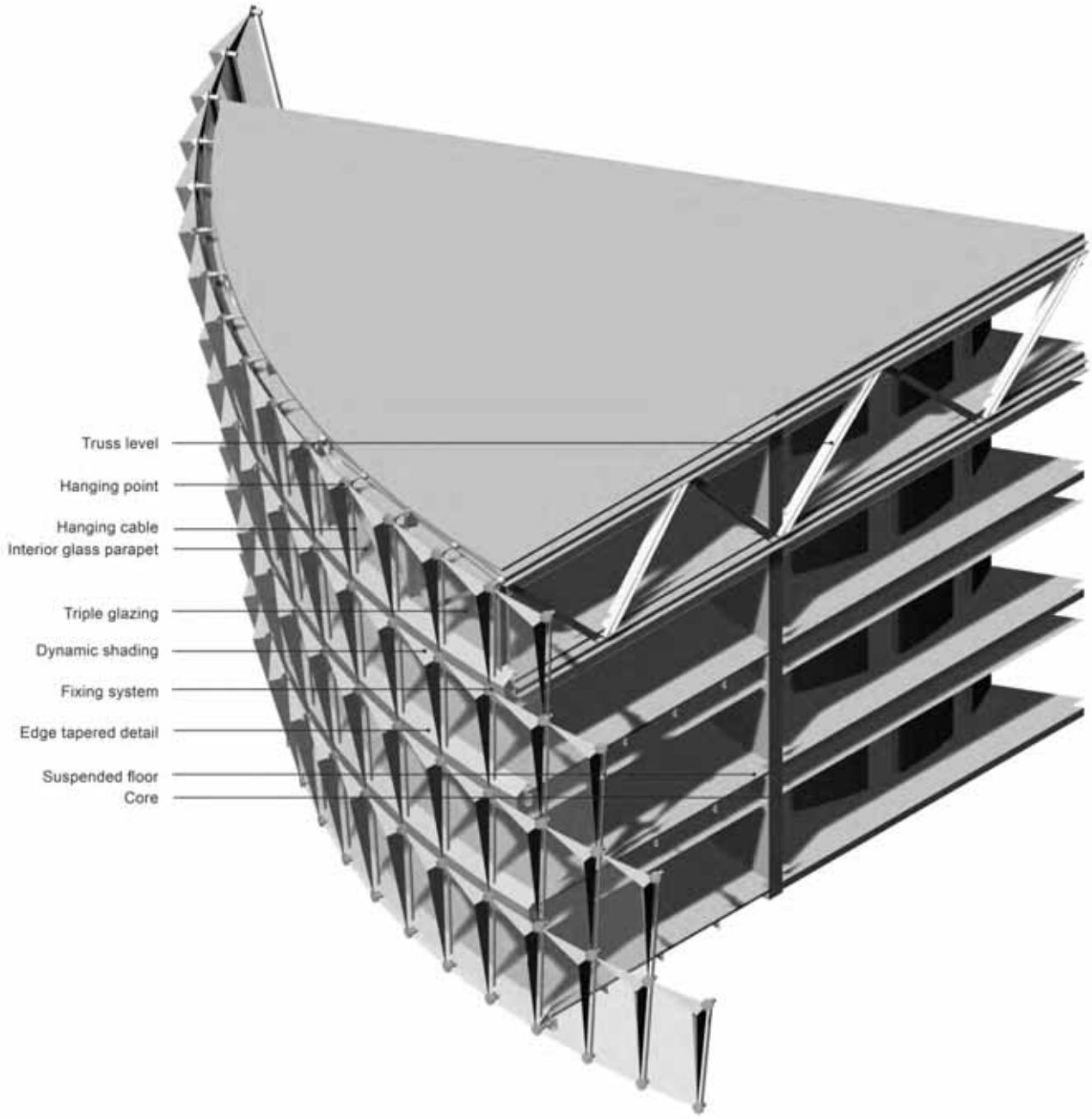


Figure 6: 3D view of the proposed integrated structural-facade system. Image by the authors.

MECHANICAL LEVELS: TRUSSES

Each mechanical level features six main cantilever trusses, evenly distributed and intersecting at the very center of the core, as well as faceted edge trusses at the perimeter that support the hung cables and deliver their loads to the main cantilever trusses at each end. All the trusses are story-high and the layout of the core has been coordinated not to conflict with the truss members. Due to the varying dimensions of the floor plates, the cantilever length of the main trusses also varies, ranging between 30 and 50 ft. For this reason, each one of the four truss blocks along the elevation has been optimized to reduce the tonnage associated to its members to a minimum, while the faceted trusses remain identical by virtue of the unvaried geometry and loading conditions on them.

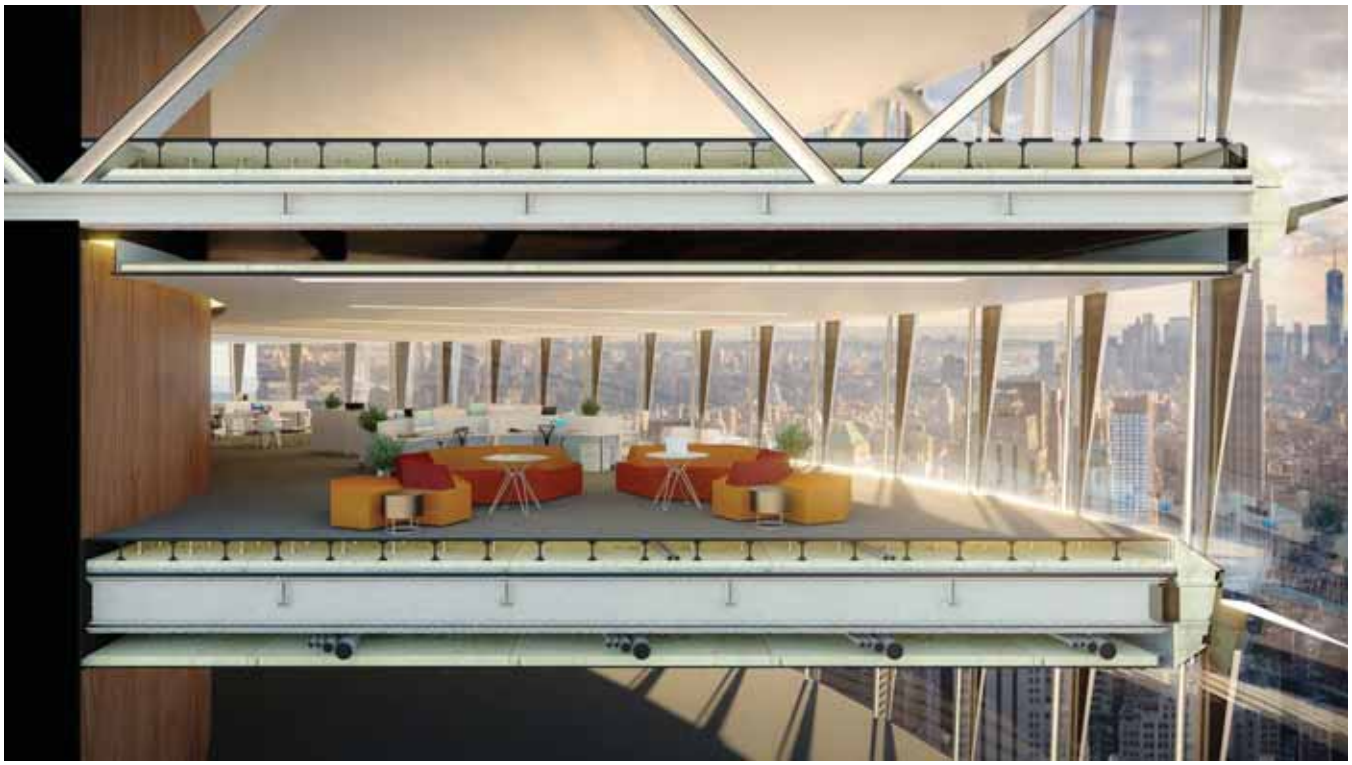


Figure 7: Rendering showing the hybrid system at the transition between a typical floor and the mechanical level featuring cantilever trusses. Image courtesy of Werner Sobek and ODA.

FOUNDATIONS

Based on geotechnical reports issued for several buildings in the immediate surroundings of the selected location, the foundation for the structure can reasonably consist of a mat slab, 15 inches thick with a 5 ksi concrete. In order to minimize the volume of concrete (and the rebar) involved in the pouring of the mat slab, its shape is assumed to mimic the shape of the core, and is represented by a hollowed circular shape with internal diameter of 65 ft and external diameter of 115 ft.

INTEGRATED FACADE AND STRUCTURE

The custom suspension system designed for this project provides an integrated facade-structure scheme made up of a bundle of steel cables that wraps the building defining the panelization pattern and collecting the loads from both the slabs and the facade. The resulting envelope features a frameless system that has a beneficial impact both from an energy and a sustainability point of view. This system consists of two main elements: the cables and the joint component. The cables deliver the vertical loads from the facade and - given the absence of perimeter columns - from the slab to the trusses, and ultimately to the core.

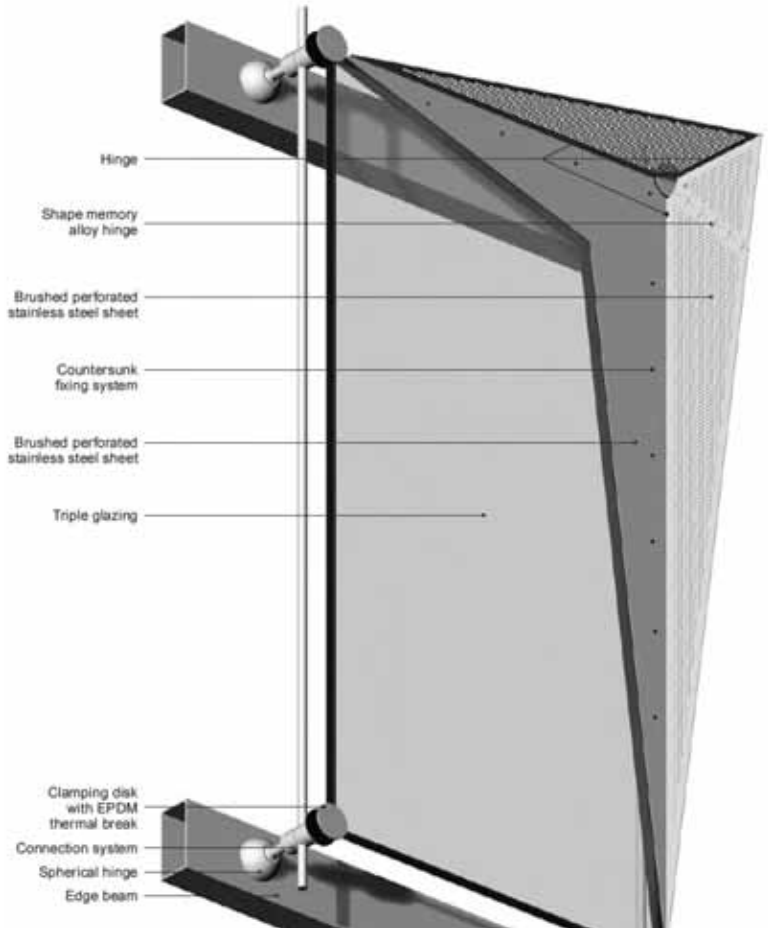


Figure 8: 3D view of the hybrid facade-structure system. Image by the authors.

The connection between the cables and the edge beam is created by the joint component, which is made of three elements:

- The joint detail features a spherical hinge that has a triple function: it connects the cables to the edge beam with no moment transfer, it accommodates the movements of the facade and it allows creating the facade curved geometry.
- The glass fixing detail consists of two 8''-diameter steel clamping discs kept together by a central bolt. Two EPDM interlayers located between the discs and the glass enable the joints to accommodate the different panel orientations and redistribute the stress from the facade to the fixing detail. This component has also an EPDM core that wraps the central bolt and allows to thermally break the connection.
- The connection detail, keeping the clamp and the spherical hinge together, is made of two coupled cylindrical elements bolted together to clasp the cable and channel the vertical loads.

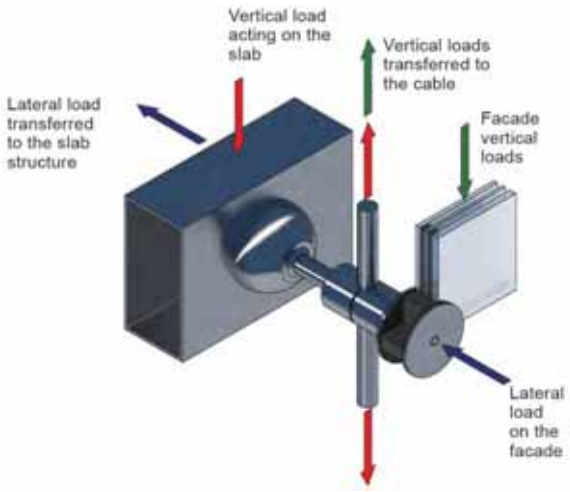


Figure 9: Suspension system diagram. Figure courtesy of Werner Sobek and ODA.

The glass build-up has been engineered to resist the design loads and to accommodate the stresses generated as a consequence of the on-site cold bending process.

The panel shape has been optimized to feature a single curved surface with straight edges thus making production and installation faster and more efficient.

The laminated inner and outer panels enable for a better redistribution of the stresses between the glass and the clamps and they give more stiffness to the build-up, thus reducing the overall defection of each panel (max deflection: 11/16’’).

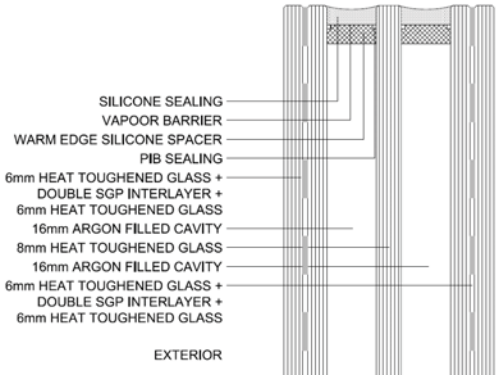


Figure 10: Glass build-up. Figure by the authors.

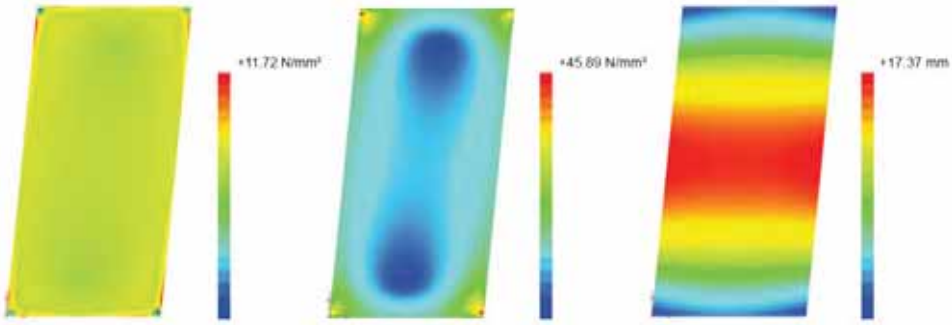


Figure 11: Stresses- top side - exterior pane (MEPLA) (left), stresses- bottom side - exterior pane (MEPLA) (center), displacements - exterior pane (MEPLA) (right). Image by the authors.

Each panel has only four corner supports and this, together with the panel size, has led to the design decision of specifying heat toughened glass, which can resist higher stress, especially at the edges. Furthermore the IGU features silicon spacers that enhance the thermal performance of the panel.

The fire stopping detail consists of two perimeter rings of fire-expanding tabs, attached to the tapered slab edge, that create a barrier only in case of fire, without compromising the thermal performance of the interface during normal service use.

Furthermore, according to the building category, structural members shall be 3-hour rated. In order to achieve this performance, the slab elements have been fireproofing sprayed, while the facade elements, given their nature and the need to be accessible for maintenance, have been covered with a 0.25 inch-thick fireproofing paint.

With respect to the acoustical performance, envelope, partitions and interface details offer acoustic insulation at different wavelengths together with protection against flanking transmission at transitions.

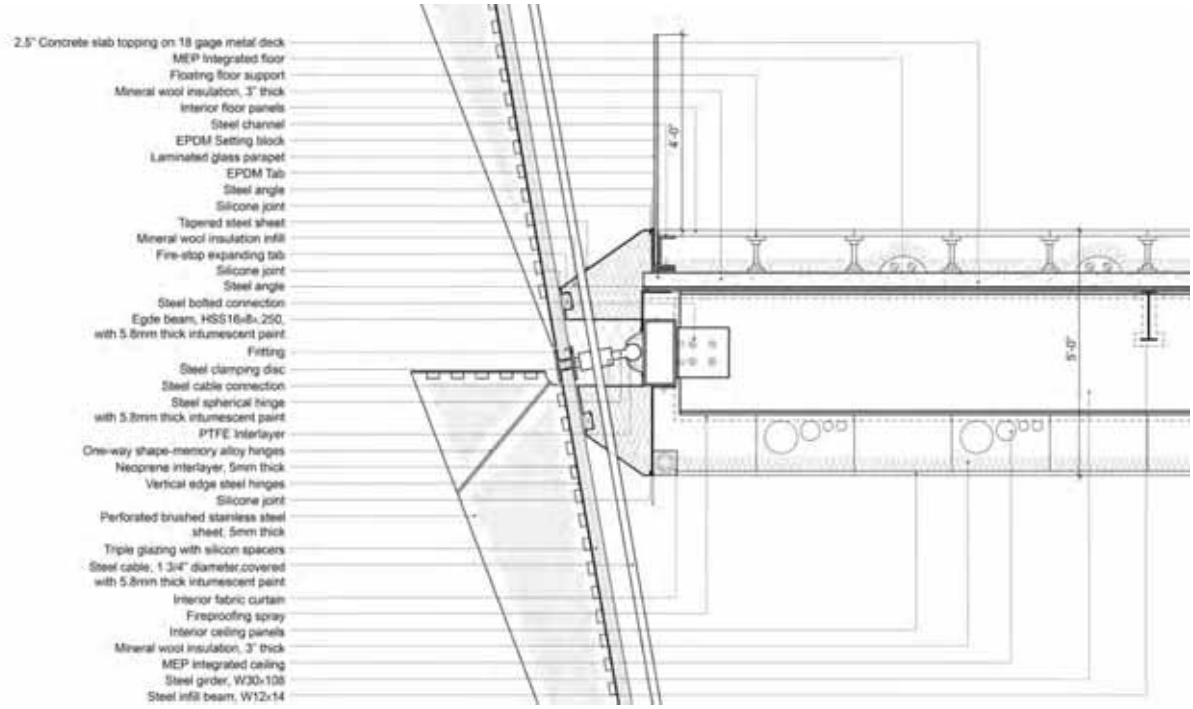


Figure 12: Typical section detail. Image by the authors.



Figure 13: Thermal analysis diagram (THERM). Image by the authors.

SHADING SYSTEM

The dynamic shading device designed for this project consists of brushed perforated stainless steel sheets woven together by a four-hinge system. The hinge dividing the vertical overhang is made of a custom shape-memory alloy that enables the component to work like an origami that automatically opens and folds itself according to the exterior temperature.

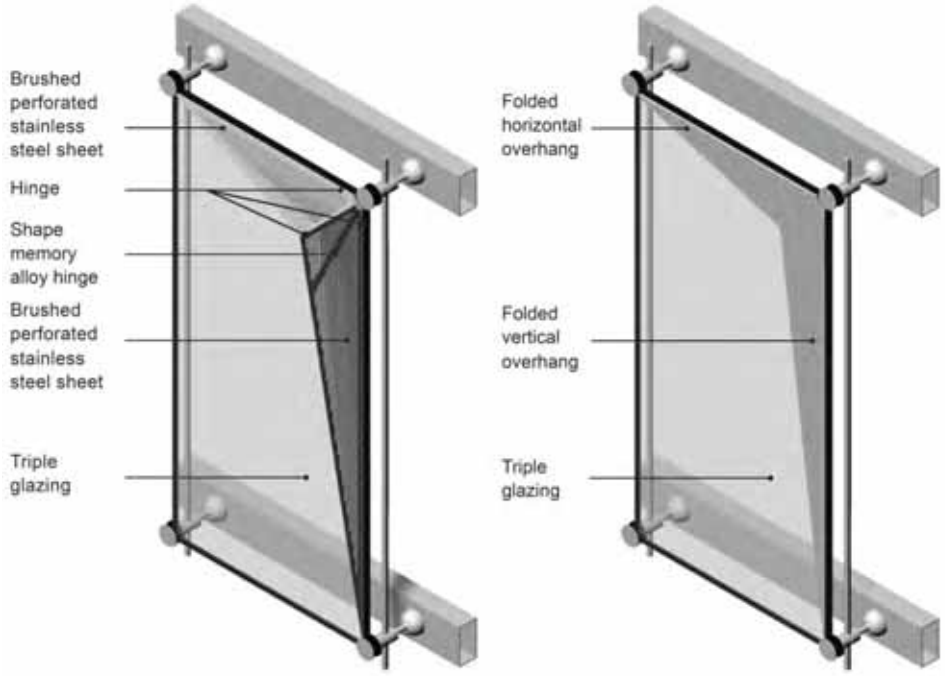


Figure 14: 3D view facade system – open configuration (left), 3D view facade system – folded configuration (right). Image by the authors.

The shape has been designed to embed two different configurations and, therefore, two optimized behaviors.

In the summer, when solar radiation weighs on the overall energy demand for cooling, the shading system enables to cut the solar radiation by 21.5%, when compared to the un-shaded configuration.

On the other hand, the winter “folded” shape does not prevent solar rays from hitting the facade, thus allowing the natural energy source to reduce the heating energy demand.

In order to foster an optimized behavior, each shading element features a different overhang length ranging from 0 to 3 feet, from North to South, governed by the sun-path.

Furthermore, the shape consists of two overhangs: the vertical one works for the East/West exposure when the Sun is lower on the horizon; the horizontal one works the southern exposure when the Sun in higher.



Figure 15: Examples of facade shading diagrams at different Sun positions. Figure courtesy of Werner Sobek and ODA.

FABRICATION

The fabrication process for the shading system envisions contemporary cutting edge techniques, such as numerically controlled machines and robot, which enable for a flexible and efficient management of mass-customized products in the construction field.

PERFORMANCE OPTIMIZATION

Another crucial feature of the metal sheets is the perforation pattern that is beneficial from multiple points of view:

- From a structural standpoint, it cuts the selfweight of the component by 50%;
- Acoustically, it helps preventing whistling noises;
- From a light penetration stand point, it empowers diffuse daylight components, while reducing the direct one, with beneficial contribution for both natural light penetration and glare protection.

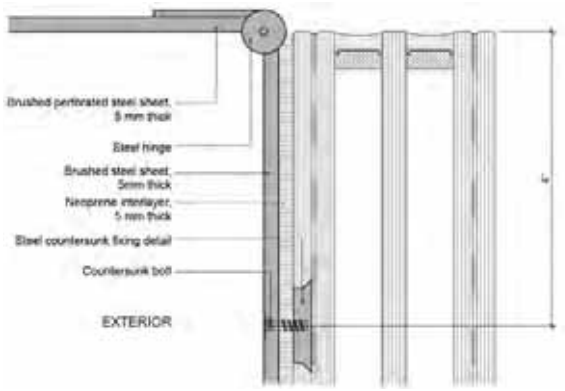


Figure 16: Shading fixing detail. Image by the authors.

The fixing detail has been designed in order to allow for ease in both installation and removal: the brushed stainless steel sheet is fixed to a steel cylinder, countersunk in the exterior laminated glass. Between the glass and the metal sheet there is a neoprene interlayer that preserves the thermal properties of the facade.

Finally, by virtue of the mechanical connection between glass and sheets, the breakage of one of these elements allows for the other to be reused in the replaced configuration, thus minimizing material waste and costs of maintenance.

DATA

DAYLIGHTING

The daylighting study has included five parameters in order to validate the performance of the proposed design in terms of natural light utilization and comfort for the users. The analysis encompasses all of the 36 office levels and the results represent the average values. The diagrams, shown above, picture a sample office floor and the parameter's trend.

CDA – Continuous Daylight Autonomy parameter indicates the percentage of typical office hours (from 9AM to 5PM) when the illuminance is higher than 300 lux. It also considers the contribution under the threshold value in linear fashion. Continuous Daylight Autonomy is 79.34%.

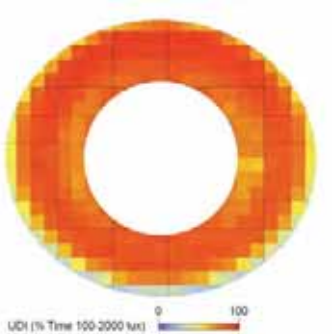


Figure 17: Continuous Daylight Autonomy diagram of a typical floor (DIVA-for-Rhino). Image by the authors.

UDI - Useful Daylight Illuminance represents the percentage of typical office hours (9AM – 5PM) when the illuminance value is between 100 and 2000 lux. This offers a measure of the contribution of natural light. Useful Daylight Illuminance is 87.64%.

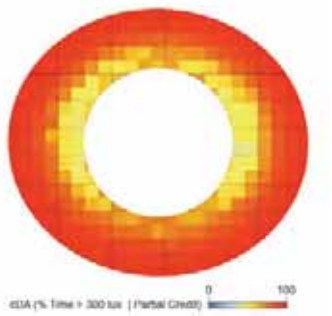


Figure 18: Useful Daylight Illuminance diagram of a typical floor (DIVA-for-Rhino). Image by the authors.

DF - Daylight Factor is a daylighting parameter that gives the ratio of the illuminance level of a control point in an indoor space to the illuminance level, in the same time and space conditions, on a horizontal plane from an unobstructed hemisphere of overcast sky. Values under 2% represent under-lit zones, while values over 5% are over-lit ones. Daylight Factor is 4.35%.

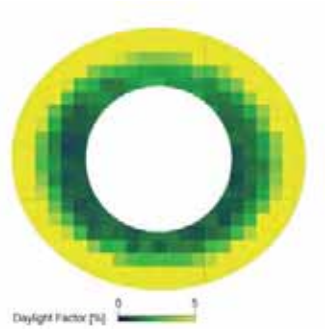


Figure 19: Daylight Factor diagram of a typical floor (DIVA-for-Rhino). Image by the authors.

LEED V4

The daylighting study has also embraced LEED v4 parameters to forecast the credits the proposed design would be eligible for, in the “Indoor Environmental Quality – Daylight“ section.

- Spatial Daylight Autonomy is 82.55%.
- Annual Sunlight Exposure is 9.18%.

SDA – Spatial Daylight Autonomy represents the percentage of area where there is a minimum illuminance value of 300 lux for at least 50% of occupied time (from 9 AM to 5 PM.) If this value is higher than 55% LEED v4 attributes 2 credits, while if it is greater than 75% 3 credits are assigned.

ASE - Annual Sunlight Exposure is the percentage of the analysis area where illuminance is higher than 1,000 lux for more than 250 hours per year. This metric gives an indication of over-lit areas where there might be glaring issues. In order to be eligible for daylighting credits a project shall not exceed an Annual Sunlight Exposure value of 10%.

EXPLANATION

The analysis shows that the proposed design has a good daylighting behavior: the floor plan is well lit and the natural light plays a key role in mastering the interior environment. The interior conditions are well distributed throughout the floor plan and, therefore, there is a uniform comfort level for the users.

The over-lit areas are limited to the immediate perimeter, which is not accessible due to the presence of the glass parapet. Furthermore the interior rolling curtains provide a good control device in case of over exposition and glare.

Finally, the dynamic shading system in the winter allows for good penetration of natural light, while in the summer it helps - thanks to its shape - to protect from direct light at multiple Zenith/Azimuth combinations.

The application of highly efficient triple glazing, glass U-value is 1.6 W/m·K, together with the absolute minimization of thermally weak points, overall U-value is 1.8 W/m·K, provides a top-grade thermal comfort in the interior spaces and a significant reduction of the energy demand, for both cooling and heating.

The facade detail, together with fostering an energy efficient behavior, also acts in terms of fire safety and acoustic insulation.



Figure 20: Rendering of the building. Image courtesy of Werner Sobek and ODA.

CONCLUSION AND FUTURE WORK

The following assumptions have been made for a "conventional" office building with identical geometry, as a means of comparison with the proposed solution:

Geometry and program	Identical to the proposed building
Lateral system	Cast-in-place concrete core
Gravity system	Concrete core and sloped steel columns (18 columns total)
Floor framing	Slab on metal deck, identical to the proposed building, and composite steel beams, with sizes identical to the proposed building
Foundations	15 in thick cast-in-place mat foundation under the core, 50 ft long 18 in diameter caissons under the columns (a 30-in thick 2-pile pile cap has been assumed under each column, based on design parameters provided for projects in the surrounding areas and column load take down values)
Facade system	Aluminum frame supporting the glazing units consisting of triple insulated glass units (IGU), built-up thickness 2 5/8 in
Shading system	None

The comparison between the conventional building and the proposed building highlights a few crucial aspects:

- The steel tonnage and the cubic yards of concrete associated with the two buildings are comparable (the proposed building is 11% higher in steel and 6% higher in concrete, respectively). On the other hand, the conventional building requires a large amount of aluminum for the framing of the facade glazing, which is not required in the proposed design. For this reason, the overall weight of the two buildings (including all the materials) is comparable (only 3% more in the proposed building).
- The embodied energy associated with the proposed design is however a striking 35% less than the one of the standard building, mainly due to the high embodied energy value of the aluminum curtain wall framing (155 MJ/kg, compared to 2.12 for concrete or 25.4 for structural steel).

COMPETITION PROPOSAL	WEIGHT tons	WEIGHT +12.5% tons	EMBODIED ENERGY MJ/kg	TOTAL MJ	EMBODIED CARBON kg CO_2/kg	TOTAL kg CO_2
STEEL	4,171.80	4,693.28	-	123,786,810.00	-	8,993,142.00
CORE REINFORCEMENT	146.00	164.25	25.40	4,171,950.00	1.78	292,365.00
SLAB STRUCTURE	1,526.80	1,717.65	25.40	43,628,310.00	1.78	3,057,417.00
TRUSS	800.00	900.00	25.40	22,860,000.00	1.78	1,602,000.00
CABLE	154.00	173.25	25.40	4,400,550.00	1.78	308,385.00
CABLE ACCESSORIES	370.00	416.25	25.40	10,572,750.00	1.78	740,925.00
SHADING	130.00	146.25	56.70	8,292,375.00	6.15	899,437.50
FOUNDATION	1,045.00	1,175.63	25.40	29,860,875.00	1.78	2,092,612.50
MISCELLANOUS	0.00	0.00	25.40	0.00	1.78	0.00
CONCRETE	24,168.00	27,189.00	-	57,640,680.00	-	6,552,549.00
CORE	15,250.00	17,156.25	2.12	36,371,250.00	0.24	4,134,656.25
CORE SLAB	178.00	200.25	2.12	424,530.00	0.24	48,260.25
DECK	425.00	478.13	2.12	1,013,625.00	0.24	115,228.13
FOUNDATION	8,315.00	9,354.38	2.12	19,831,275.00	0.24	2,254,404.38
GLASS	2,554.00	2,873.25	-	67,521,375.00	-	3,649,027.50
FACADE	2,160.00	2,430.00	23.50	57,105,000.00	1.27	3,086,100.00
PARAPET	244.00	274.50	23.50	6,450,750.00	1.27	348,615.00
SPECIAL LEVEL	150.00	168.75	23.50	3,965,625.00	1.27	214,312.50
INSULATION	486.00	546.75	-	9,076,050.00	-	656,100.00
MINERAL WOOL	486.00	546.75	16.60	9,076,050.00	1.20	656,100.00
BUILDING	**31,379.80**	**35,302.28**	**-**	**258,024,915.00**	**-**	**19,850,818.50**

Figure 21: Embodied energy and embodied carbon recap table for the proposed building. Figure by the authors.

COMPARABLE STANDARD BUILDING	WEIGHT tons	WEIGHT +12.5% tons	EMBODIED ENERGY MJ/kg	TOTAL MJ	EMBODIED CARBON kg CO_2/kg	TOTAL kg CO_2
STEEL	3,885.80	4,371.53	-	115,614,360.00	-	8,420,427.00
CORE REINFORCEMENT	116.00	130.50	25.40	3,314,700.00	1.78	232,290.00
SLAB STRUCTURE	1,526.80	1,717.65	25.40	43,628,310.00	1.78	3,057,417.00
COLUMN	941.00	1,058.63	25.40	26,889,075.00	1.78	1,884,352.50
SHADING	130.00	146.25	56.70	8,292,375.00	6.15	899,437.50
FOUNDATION	1,172.00	1,318.50	25.40	33,489,900.00	1.78	2,346,930.00
MISCELLANOUS	0.00	0.00	25.40	0.00	1.78	0.00
CONCRETE	22,773.00	25,619.63	-	54,313,605.00	-	6,174,329.63
CORE	15,250.00	17,156.25	2.12	36,371,250.00	0.24	4,134,656.25
CORE SLAB	178.00	200.25	2.12	424,530.00	0.24	48,260.25
DECK	425.00	478.13	2.12	1,013,625.00	0.24	115,228.13
FOUNDATION	6,920.00	7,785.00	2.12	16,504,200.00	0.24	1,876,185.00
GLASS	2,554.00	2,873.25	-	67,521,375.00	-	3,649,027.50
FACADE	2,160.00	2,430.00	23.50	57,105,000.00	1.27	3,086,100.00
PARAPET	244.00	274.50	23.50	6,450,750.00	1.27	348,615.00
SPECIAL LEVEL	150.00	168.75	23.50	3,965,625.00	1.27	214,312.50
ALUMINUM	920.00	1,035.00	-	160,425,000.00	-	8,528,400.00
CURTAIN WALL FRAMING	920.00	1,035.00	155.00	160,425,000.00	8.24	8,528,400.00
INSULATION	486.00	546.75	-	9,076,050.00	-	656,100.00
MINERAL WOOL	486.00	546.75	16.60	9,076,050.00	1.20	656,100.00
BUILDING	**30,618.80**	**34,446.15**		**406,950,390.00**		**27,428,284.13**

Figure 22: Embodied energy and embodied carbon recap table for the comparison building. Figure by the authors.

As highlighted in the Shading System Overview section of this report, the conventional building does not feature any shading devices, thus weighing on its solar gain and performance in the summer months.

Should the shading device be included in this design, the total embodied energy would go up to being 37% higher than the proposed building.

Consequently, the embodied carbon value of the proposed building, which is the parameter that best describes the impact of a structure on the environment, is only 75% of the value associated with a standard office building of identical size and geometry.

Alternative geometries and configurations for the shading system are under investigation for this specific case study as well as for different applications in order to further demonstrate the potential of adaptive skin concepts in terms of daylight and energy optimization. With regard to the shape-memory-alloys, additional researches will be carried out to study the feasibility of the application of these new generation materials in the building industry and to test their durability, their aging behavior, and their phase transition when exploited for exterior application in urban environments. In terms of the design workflow, additional strategies to integrate the structural analyses within the developed integrated parametric environment, where the architectural design and the daylighting/energy studies have been performed, will be investigated and validated in terms of results' reliability and operability between the design stakeholders. Ultimately, the hybrid structural/facade scheme introduced will be implemented on different architectural typologies and results in terms of structural performance and embodied energy savings will be compared to widespread construction.

ACKNOWLEDGEMENTS

ODA New York – architectural design credit
Metals in Construction magazine 2017 Design Challenge – entry was awarded 1st prize
Maritime Museum – structural and facade engineering concept by Werner Sobek

REFERENCES

Lelieveld, C.M.J.L. “Smart Materials for the Realization of an Adaptive Building Component” Doctoral Thesis TU Delft (2013).
Pesenti, M., Masera, G., Fiorito, F., Sauchellia, M. “Kinetic Solar Skin: a Responsive Folding Technique” Energy Procedia Volume 70 (2015): 661-672.
Pesenti, M., Masera, G., Fiorito, F. “Shaping an Origami shading device through visual and thermal simulations” Energy Procedia 78 (2015): 346-351.
Scuderi, G. “Self-adaptive membrane for the building envelope of the future” Platea Magazine (2016).
Beer, B. “Glazed cable facades and special structures - Focus on complex geometries and warping deflections of insulating glass units” Glass Performance Days 2009 (2009).
Addington, M., Kienzl, N., and Schodek, D. “Smart Materials and Technologies in Architecture” Harvard Design School Design and Technology Report Series 2(2002).
Schwartz, M. *The Encyclopedia of Smart Materials*. John Wiley and Sons, 2002.
Addington, M., Schodek, D. *Smart materials and new technologies for the architecture and design professions*. Architectural Press, 2005.
Antonelli, P. *Mutant Materials in Contemporary Design*. MoMA, 1995.
Yamauchi, K., Ohkata, I., Tsuchiya, K., Miyazaki, S. *Shape Memory and Superelastic Alloys*. Woodhead Publishing, 2011.
Chamilothori, K., Kampitaki, A.M., Oungrinis, K.A. “Climate-Responsive Shading Systems with Integrated Shape Memory Alloys (SMA)” Conference proceedings of the 8th ENERGY FORUM 2013 on Advanced Building Skins (2013).
Fiorito, F., Sauchelli, M., Arroyo, D., Pesenti, M., Imperadori, M., Masera, G., Ranzi, G. (2016). “Shape morphing solar shadings: a Review” Renewable and Sustainable Energy Reviews 55 (2016): 863-884.
Schumacher, M., Schaeffer, O., Vogt, M.M. *Move architecture in motion – dynamic components and elements*. Birkhäuser, 2010.
Loonen, R.C.G.M., Trčka, M., Cóstola, D., Hensen, J.L.M. “Climate adaptive building shells: State-of-the-art and future challenges” Renewable and Sustainable Energy Reviews (2013): 483-93.
Wigginton, M., Harris, J. *Intelligent Skins*. Oxford: Butterworth-Heinemann, 2002.

XILINX CASE STUDY

Accelerating replicable ZNE retrofits through high performance façade optimization



Michael Martinez, LEED AP
Integral Group
mmartinez@integralgroup.com



Stet Sanborn, AIA, LEED AP, CPHC
Integral Group
ssanborn@integralgroup.com

ABSTRACT

The transformation of a dark and inhumane 1970s tilt-up concrete office building into a high performance, light-filled modern workplace was enabled by a thoughtful retrofit of the existing envelope. By sculpting the existing building skin into a healthy, high performing filter of light, heat, and air, the resultant building aims for net zero energy cost and also achieved substantial carbon savings through reuse of the existing, high-footprint building.

Adding new daylight apertures, carefully crafted shading elements, and a new thermal enclosure of rigid mineral wool insulation around the existing concrete walls offered the primary tools for design transformation. When executed together, this design enabled low energy mechanical solutions and ultimately an estimated EUI that is fully offset by rooftop and building-integrated photovoltaics.

The existing concrete walls were insulated to isolate the thermal mass from the exterior and reduced both the heating and cooling energy by 50% over the existing building energy use. Additionally, light wells were punched through strategic locations to maximize daylight distribution, which paired with new LED lighting, properly specified high performance glazing, and finely tuned external shades made of BIPV panels that control direct sun and balance daylight levels, reduced the lighting energy use by some 80%.

A local utility incentive program is validating the modeled results through a yearlong study, comparing submetered building energy use to modeled end use predictions. The program offers controls assistance and optimization during the first year of occupancy to meet anticipated performance goals. While initially seen as individual efficiency measures, the design team discovered the interdependent relationships between seemingly disparate energy saving design measures and optimized the cascading set of decisions that enabled this design transformation.

KEYWORDS

retrofit, energy and carbon, daylighting - glare – shading, net zero - net plus, ventilation, sustainability – holistic, BIPV

INTRODUCTION

In the United States, nearly half of all commercial buildings were constructed prior to 1980 (CBECS, 2017). Construction of these buildings predated rigorous updates to state and national building codes addressing energy conservation required by the OPEC oil embargo. The approximately 6 billion square feet of new office buildings constructed each year in the United State is dwarfed by the square footage of existing office building stock, more than 300 billion square feet.



Figure 1: Low-rise tilt up commercial buildings built in the 1970's dominate the landscape in Santa Clara, California. Image courtesy of Google Earth.

While constructing efficient new buildings is important, the time-value of carbon reductions (the impact of carbon savings relative to their ability to alter current climate change projections) indicate that reducing the 2.2 billion metric tons of operating CO_2 from existing buildings is more critical than the current industry focus on new buildings alone (Sullens, et al, 2015).

In addition to operating carbon savings associated with deep energy retrofits, additional embodied carbon savings are achieved through the reuse of existing building stock and avoidance of new construction and associated Scope 3 emissions. These total life cycle embodied carbon savings can be as high as 70% (Sullens, et al, 2015). Those savings are significant, as they are immediate carbon savings not accumulated over time.

The corporate headquarters of Xilinx, located in San Jose, California is a prototypical office park developed in the mid-1970s. A retrofit of one campus building provides the context for achieving net zero energy performance and massive carbon savings through the careful design and retrofit of an ordinary tilt-up concrete building skin. The existing two-story building provided approximately 90,000 square feet of office space, primarily supporting software engineers.



Figure 2: Xilinx Building 3, existing conditions. Image courtesy of Google Earth.

METHOD

The transformation of this building was catalyzed by well-tuned modifications to the building skin. An integrated design team advised on optimization strategies related to opaque wall thermal performance, daylight apertures, glazing specifications, shading strategies and their implications for whole building system options and energy performance.

Through the design process, the façade evolved to admit abundant amounts of daylight into the occupied spaces, turned the existing concrete tilt-up walls into thermal mass through strategic exterior insulation and cladding strategies, and integrated exterior shading strategies into the on-site renewable energy production system.

DAYLIGHTING

Daylighting analysis documented how the existing façade admitted daylight, calibrated a simulation model using High Dynamic Range (HDR) analytical photography, and studied the transformative impact of daylight-focused envelope design measures.

The existing façade featured ribbon windows with single pane, dark tinted glass. The existing visible light transmittance (VLT) was measured to be less than 25%, and in addition to overheating the perimeter due to metal framed, single pane glass with a 0.90 SHGC, the windows also provided negligible daylight to the interior space. Site HDR photography verified that the space was primarily lit by electric lighting during all occupied hours and provided a reference point to calibrate a daylighting model built in Radiance. From this preliminary analysis, simple design measures such as removing the dropped ceiling and replacing the windows with new high performance glazing revealed a dramatic opportunity for daylight in the building.

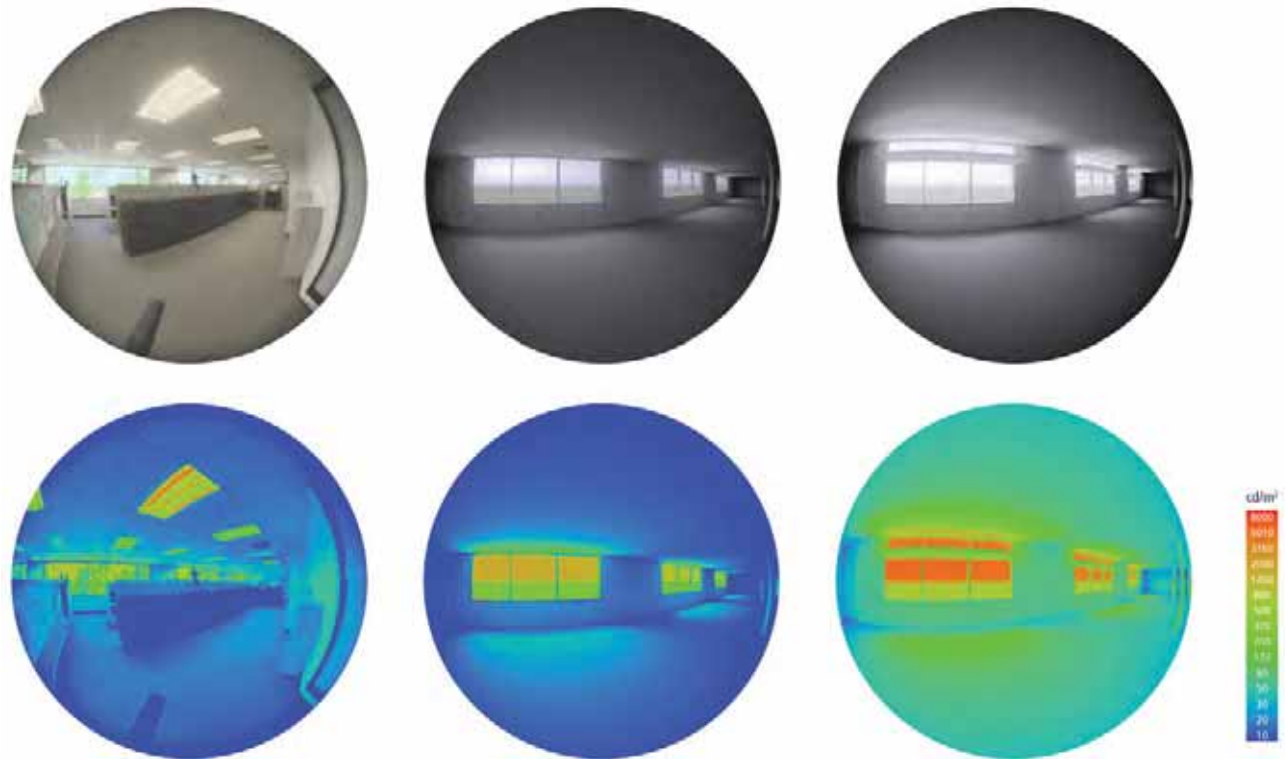


Figure 3: 180-degree fisheye view HDR photography and falsecolor luminance maps of existing interior space (left), calibrated model of existing conditions (center), schematic model with improved glazing and higher ceiling (right). Images by the authors.

Improved glazing proved critical for both visual and thermal comfort. Spectrally selective glass on a low-iron substrate maximized visible light transmitted through the perimeter while providing crucial control of unwanted solar gains. The low-iron substrate offered an 11% increase in VLT over a normative code-minimum low-e glass, and also an ultra-clear aesthetic valued by the design team. The final glazing featured thermally broken aluminum frames, with center-of-glass values SHGC of 0.30 and VLT of 0.71.



Figure 4: Sample of normative code minimum low-e glass (left), and high performance glass on low iron substrate (right). Photographs by the authors.

Further analysis of the building skin highlighted the impact of modifications to the roof plane. Beyond implications as a daylight aperture, the roof provided strategic points to introduce light and air wells through the center of the deep 100 foot wide existing floor plate. These anchored public and collaborative spaces provided vertical circulation and connectivity and created a pathway for night-purge air movement. Daylighting studies resulted in full structural bays dedicated to light and air wells, offering balancing daylight to the back of open office areas and daylight autonomous collaboration spaces.

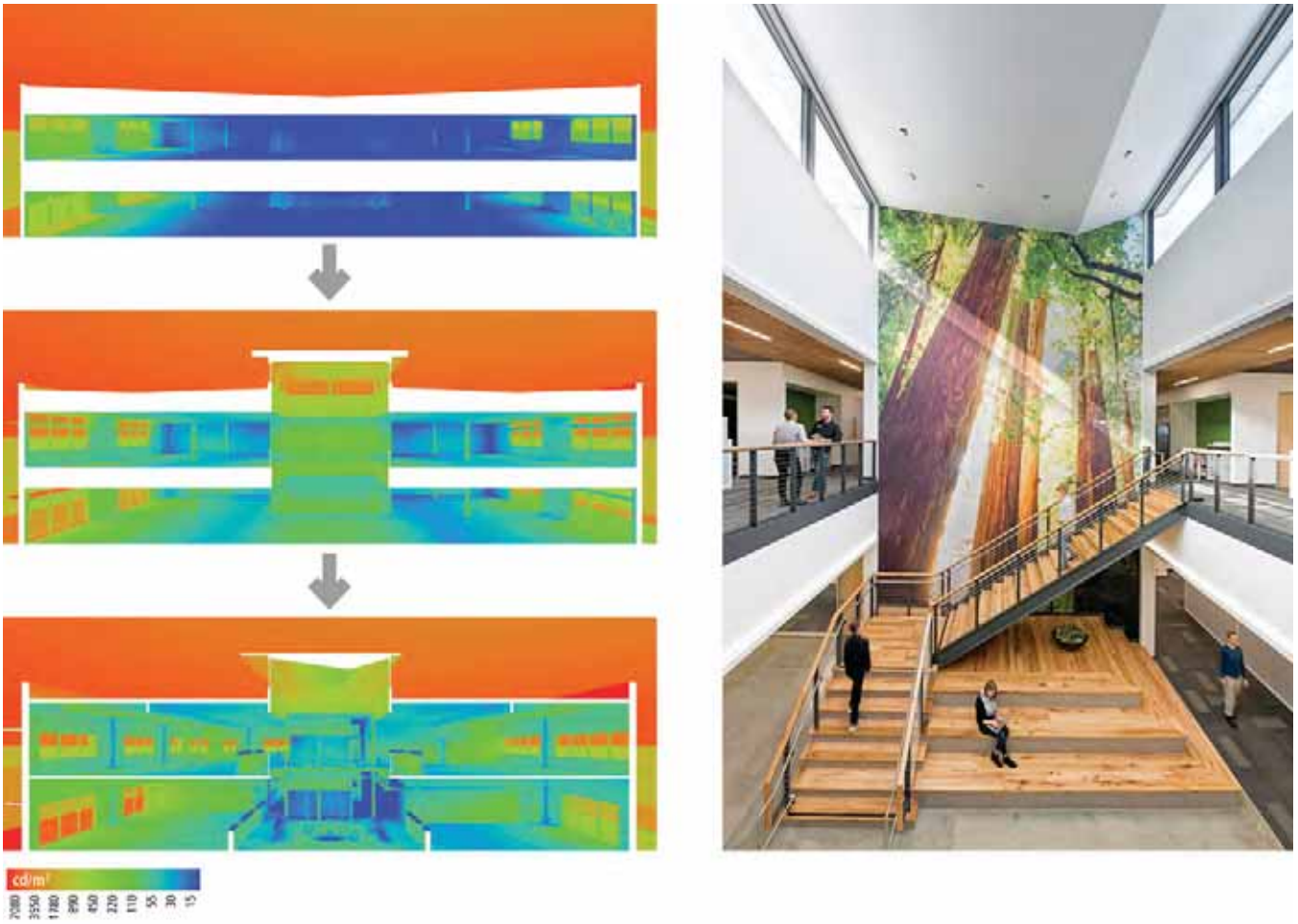


Figure 5: Iterations of daylight model luminance analysis (left) and completed light well (right). Analysis images by the authors, photograph by Jasper Sanidad.

Roof monitors were deployed over single-story zones of the building where data center program elements interrupted the potential path of a full building light well. These spaces created vertical spatial release from the compression of the surrounding open office areas and anchored working groups with collaboration spaces connected to the sky. What was once the darkest and most inhumane zone of the existing building was transformed into a biophilic retreat.



Figure 6 Collaboration space below a rooftop daylight monitor. Photograph by Jasper Sanidad.

The overall façade modifications of improved glazing and rooftop aperture design introduced abundant daylight to a previously cavernous box. The energy savings associated with reduced electric lighting energy correspond directly with the modeled spatial daylight autonomy results. More than 75% of the regularly occupied office spaces are expected to meet their illumination target of 30 footcandles by daylight alone, for more than 50% of annual occupied hours.

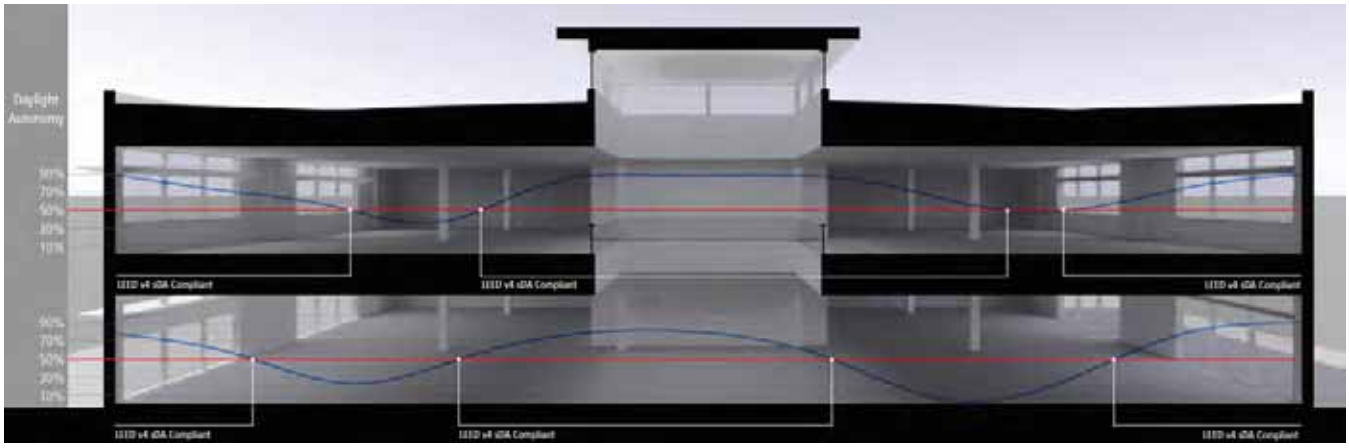


Figure 7: Spatial daylight autonomy simulation results, section view. Image by the authors.

FAÇADE RETROFIT- INSULATION

The façade insulation retrofit analysis included three characteristic parameters to balance against cost: annual energy cost savings, HVAC peak load reductions and associated plant size reduction, and long term material durability. In order to reduce annual energy use and reduce HVAC peak loads, the design team focused on retrofitting the walls and roof to include continuous insulation at a reasonable cost.

Through parametric modeling, the engineering design team was able to show the benefits of locating the insulation outside the existing tilt-up concrete walls. This provided two benefits: It reduced annual energy use by reducing U-value and turned the existing concrete walls into a significant, useful thermal mass. The thermal mass benefits of the walls reduced peak loads on the HVAC system, allowing for a reduced equipment tonnage. In addition, the dedicated outdoor air system (DOAS) could take advantage of the thermal mass for a night-purge economizer cycle, further reducing the hours of each day requiring compressor-based cooling.



Figure 8: Installation of exterior rigid wool insulation and cladding system. Left photograph by the authors. Right photograph courtesy of Grigg Systems.

Thermally broken fiberglass z-girts were used to support the new rain-screen cladding, minimizing thermal bridging between the existing tilt-up concrete structure and the new cladding system. The fiberglass z-girts allow the design team to maximize the effective R-value of the continuous exterior insulation. Rigid mineral wool insulation boards were used for the continuous insulation due to its moderately high R-value, excellent drainability and vapor-open characteristics, and non-combustibility.

SHADING RETROFIT AND PV DESIGN

To balance daylighting and visual comfort, horizontal overhangs were deployed over the ribbon window openings. A key aspect of the daylighting strategy was to maximize shadow cast on the façade glass, allowing interior shades to remain open for as many hours as possible. The building massing featured a long south exposure, well suited for large amounts of horizontal shading.

With the goal of achieving Net Zero performance and a relatively large three-story building, the roof alone was an insufficient area to offset the cost of energy used by the building annually. The horizontal overhang surfaces provided critical supplemental PV area, allowing for a pathway to Net Zero by transforming overhang elements into energy-producing surfaces. In addition, the top surfaces of the light well pop-up geometry were capped with PV arrays, as was the entirety of the available roof surface. To maximize the production of the flat packed PV array on the roof, a novel, positively attached A-frame racking system was developed in partnership with the solar subcontractor.



Figure 9: Rooftop and lightwell pop-ups covered by the PV array (left), exterior horizontal overhang PV modules as facade shading devices (right). Images by the authors.

DATA

Historic energy bills revealed baseline energy use. A detailed site energy audit augmented this data, which documented plug loads, equipment types, equipment efficiency, existing HVAC systems, existing lighting systems and schedules, and data center energy use. Energy models were then calibrated against the historic data to form baseline energy models, used to test EEM measures.

Through parametric modeling and input from a cost estimator, the design team settled on a series of 10 energy efficiency measures. Six dealt directly with the façade. The table below indicates the final package of both façade and non-façade upgrades.

Description	Detail	Category
Roof Monitors	Daylight Autonomy ~75%	Lighting
LED Lighting	High Efficacy Fixtures	Lighting
Exterior Wall Insulation	3" Rigid R-19 Insulation	Heating/Cooling
Exterior Roof Insulation	6" Rigid R-39 Insulation	Heating/Cooling
Thermally Insulated Windows	Solarban 72 on Starphire with thermally broken frames	Heating/Cooling
Exterior Window Shading	Shading on the E,W,S Facades	Heating/Cooling
Thermodynamic A/C Unit Zoning	Assign A/C units specific to zonal needs; avoid "re-heat" energy	Heating/Cooling
Night Flush Controls	Ventilate building with cold night air during unoccupied hours, "pre-cool" building	Heating/Cooling
Ceiling Fans	32 "Big Ass-Fans" installed throughout open office area	Heating/Cooling
Plug Load Control	Install occupancy control on selected plug loads; eliminate off-hour consumption	Plug Loads

Table 1: Final energy efficiency measures.

The six façade measures noted above include daylighting roof monitors, exterior wall insulation, exterior roof insulation, insulated glazing units, exterior window shading, and night-flush controls enabled by the externally insulated thermally-active concrete structure. The impacts of the efficiency measures impacted heating, cooling and lighting loads.

The combined strategies enabled each other, and also resulted in 80% lighting predicted energy savings (includes LED retrofit), 50% reduction in predicted heating energy use, and 50% reduction in predicted cooling energy use. The façade retrofit measures, in addition to plug load controls, ceiling fans, and improved HVAC system results in a 60% total predicted energy use reduction. The building Energy Use Intensity (EUI, kBtu/sf-yr) is reduced from 80 kBtu/sf-yr to 34 kBtu/sf-yr, resulting in a predicted savings of $165,000 annually.

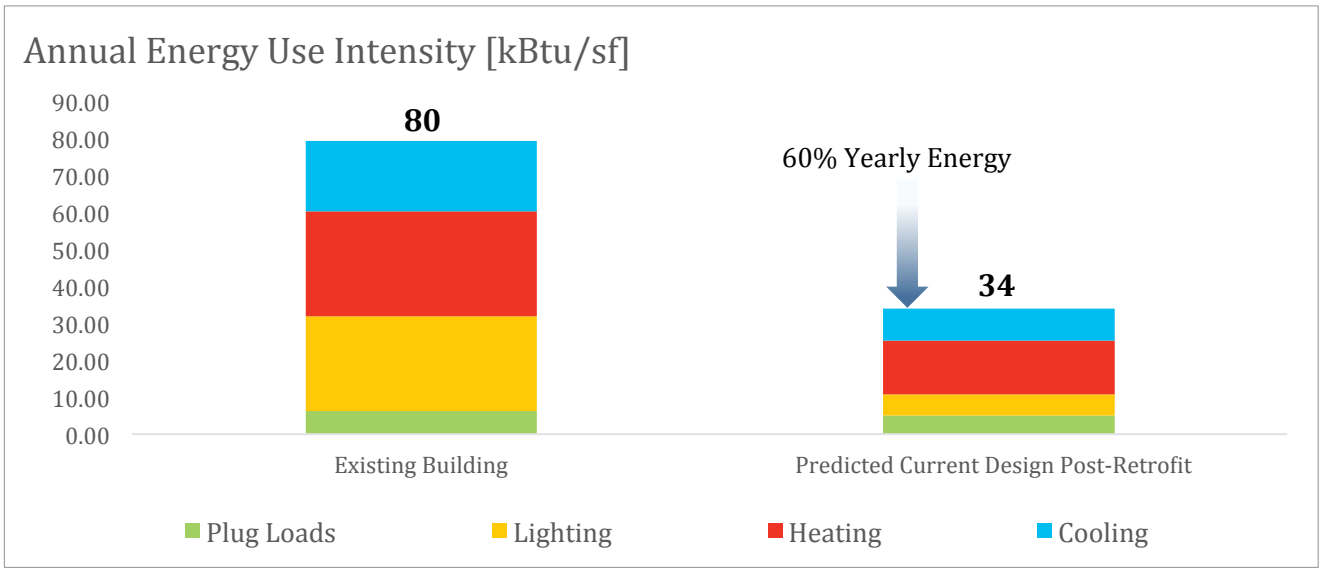


Figure 10: Existing energy use vs. predicted.

	Existing Building		Post-Renovation		Savings		
	Energy Consumption (kBtu/yr)	Cost Per Year ($/yr)	Energy Consumption (kBtu/yr)	Cost Per Year ($/yr)	Energy Consumption (kBtu/yr)	Cost Per Year ($/yr)	% Energy Savings from Existing
Plug Loads	688,000	$ 30,000	553,000	$ 25,000	135,000	$ 5,000	20%
Lighting	2,791,000	$ 123,000	621,000	$ 27,000	2,170,000	$ 96,000	80%
Heating	3,098,000	$ 31,000	1,578,000	$ 16,000	1,520,000	$ 15,000	50%
Cooling	2,072,000	$ 91,000	946,000	$ 42,000	1,126,000	$ 49,000	50%
Totals	8,649,000	$ 275,000	3,698,000	$ 110,000	4,951,000	$ 165,000	60%

Figure 11: Energy savings associated with each end-use.

EXPLANATION

The individual design measures to retrofit this building were relatively modest in isolation. But when used together, small, good design decisions cascaded to the next, enabling radically better performance. Daylighting strategies led to shading and load reduction strategies, which in turn revealed the value of continuous exterior insulation, creating internal thermal mass and enabling low energy mechanical strategies, resulting in a comfortable and beautiful space powered by on-site renewable energy.

Each item didn't "pay for itself" through the direct reductions in energy use, and isolating the EUI reduction of façade-only design moves tells an incomplete story of energy use reduction. Rather, the cumulative effects of each move enabled lower and lower energy strategies at each level of design and decision making, resulting in a remarkable transformation of California's worst building type into its best. To rejuvenate these high carbon footprint, heavy mass, poorly insulated, and energy intensive structures, holistic design processes that reveal systemic interdependences are crucial.

CONCLUSION AND FUTURE WORK

This project highlights the potential mistake of considering design as a list of efficiency measures. Particularly when focused on the building skin, high performance buildings are possible when the interdependencies of design moves are understood both for their own merits, and for what they unlock in tangential elements. In the life of design projects, this way of thinking is often in conflict with budgeting decisions, where cost implications are held in isolation of each component, regardless of chain-reaction implications on building performance. But when design teams understand the totality of performance related systems, from the skin to the service systems, focused modeling and analysis can equip them to demonstrate the holistic value of design decisions, unlocking exceptional performance from the most unlikely of starting points.

The performance of this project will be subject to scrutiny in the coming year. To ensure performance goals are met, the owner has engaged the local utility in an operational performance incentive program: PG&E's *Savings by Building Operations and Performance*, a demonstration program aimed to ensure energy-efficient buildings perform as well as, or better than, designed. The demonstration program provides support during design, construction, and post-occupancy to assist with the successful implementation of submetering to measure energy end uses during occupancy. The submetered trend data is used to compare actual energy use and profiles to those values predicted during design modeling, identify potential areas of improvement, and implement controls changes. The program goes beyond standard commissioning to provide controls assistance and optimization during the first year of building occupancy. Colleagues from the author's consulting firm have been engaged as consultants to run the project through this incentive program, with the first month of data collected September 2017.

ACKNOWLEDGMENTS

Thanks to the project design team: Noll and Tam – Architecture, Integral Group – MEP, KPFF – Structural, BFS – Landscape, Charles M Salter Assoc. – A/V and Telecom. Most importantly to our colleagues at Integral Group, this project was successful due to the skilled contributions of Laura Fedoruk, Emily Jacobson, Willy Stober, Shannon Allison, John Andary, and Dylan Connelly.

REFERENCES

CBECS. “A Look at the U.S. Commercial Building Stock: Results from EIA's 2012 Commercial Buildings Energy Consumption Survey.” https://www.eia.gov/consumption/commercial/reports/2012/buildstock/. Accessed September 20, 2017.

Sullens, et al; *The Total Carbon Study*, November 13, 2015.

Facade <> Material

ARCHITECTURAL CERAMIC ASSEMBLIES

A collaborative research model for industry engagement



Omar Khan
University at Buffalo (SUNY)
omarkhan@buffalo.edu



Bill Pottle
Boston Valley Terra Cotta
Billp@Bostonvalley.com



Mitchell Bring
University at Buffalo (SUNY)
mbring@buffalo.edu

ABSTRACT

This paper documents a six year academia/industry collaboration between researchers at the Department of Architecture, University at Buffalo (SUNY) and the Boston Valley Terra Cotta Company. For the company, it was an essential undertaking to be able to meet the design challenges in a globally competitive marketplace. For the Department of Architecture, it meant fulfilling the three core tenets of its mission: professional education, advancing the profession through significant research and outreach, and economic development by growing the number and quality of jobs available in Western New York.

The engagement involved faculty and students developing new tools and work flows to facilitate better responses to Boston Valley's architectural clients. They assisted with the design development phase as well as improving the manufacturing processes that resulted in several award winning building projects. While the faculty taught classes to company employees and set technology agendas with senior management, the students themselves became the real change agents. The factory floor became the proving ground for the introduction of 3D scanning, parametric modeling, digital modeling, 5 axis CNC milling, 3 axis wire cutting, computational fluid dynamics for extrusion die design, post extrusion ruled surface cutting, and numerous CAD/CAM innovations.

Furthermore, the collaboration has expanded beyond specific projects into the annual Architectural Ceramic Assemblies Workshop (ACAW); a forum for a worldwide collective of architects, façade engineers, ceramic artists, architectural manufacturers, university faculty and students to develop bio-climatically responsive façades and surfaces. This week-long eworkshop's goal is to educate the architectural profession about ceramics, test the state of the art in terra cotta manufacturing and develop new research agendas that can be undertaken through professional, manufacturing and academic partnership.

KEYWORDS

parametric workflows, academia/industry partnerships, digital fabrication, terra cotta, project delivery-design assist, heritage conservation-preservation-restoration, rain screen

INTRODUCTION

Western New York has a unique history in ceramic manufacturing and retains vestiges of a substantial industrial cluster. Building on this regional capacity, we have begun to build a nexus of expertise in architectural ceramics that involves faculty and researchers at the University at Buffalo's Sustainable Manufacturing and Robotic Technologies (SMART) Community of Excellence, faculty from Alfred University's College of Ceramics and Boston Valley Terra Cotta, the foremost North American manufacturer of architectural terra cotta. This triad's collaboration has resulted in a unique annual workshop- Architectural Ceramic Assemblies Workshop (ACAW) - that brings professional architecture and engineering practices into collaborative research with academia and manufacturing. The road to the workshop was paved by collaborative research between the University at Buffalo, Department of Architecture's faculty and Boston Valley Terra Cotta. By establishing an embedded research unit in the company, the collaboration demonstrated that design research could be implemented as part of daily practice. These lessons have formed the basis for ACAW that looks to expand this approach to include architecture and engineering firms and other manufacturers.

EMBEDDED RESEARCH- BOSTON VALLEY TERRA COTTA AND THE UNIVERSITY AT BUFFALO, DEPARTMENT OF ARCHITECTURE

Boston Valley Terra (BVTC), originally named Boston Valley Pottery was established as a brick producer in the 1880's. In the 1980's, it was purchased by the Krouse family and rebranded to do architectural terra cotta restoration. Its first significant project was the restoration of Buffalo's landmark Louis Sullivan's Guaranty Building. The company rapidly grew to meet the needs of the architectural restoration community, becoming one of two US companies doing such work nationally. Alfred University graduate John Krouse led the company in the mid 2000's to become the first and still only western hemisphere producer of terra cotta rain screen. This opened them to the market for contemporary architectural design. The company gained a reputation for doing projects that needed unique panel profiles and extraordinary glazes. Increasingly it found itself competing against highly capitalized European multinationals. The company succeeded in part because it combined both the traditional handcrafted ways of making product with the latest computer technology in drier and kiln operation. However, further progress required better CAD documentation, model and mold production on the historic side of the business. For the new construction side of the business the company needed greater CAD integration with their architectural clients especially during the design development part of innovative projects, as well as advanced quality control assurance during manufacture of its one of kind products.

It is during this period (2012) that BVTC began engagement with the University at Buffalo's Department of Architecture (UB). Together BVTC and UB evolved a unique strategy to address the challenge of introducing the best digital practices into an ongoing architectural production line. The shop floor became a classroom laboratory for both UB students, faculty and BVTC craftspeople. An ad-hoc room was constructed on the factory floor and called the "Mesh-Lab" to house the embedded UB/BVTC researchers. From here they would collaboratively develop techniques and technologies and see if they could replace existing practices. The intention was to expand digital competency in the workplace and see how manual craft and digital craft could collaborate. Below are three cases that demonstrate this process.

CASE 1- PHOTOGRAMMETRY: A TECHNOLOGY FOR ENABLING DIGITAL CRAFT

BVTC's standard practice for restoration projects involved the removal of the original historic ornament from the building, block by block. Some of these pieces would be considerably damaged and broke apart on removal. Others could weigh up to 400lbs, making removal difficult and costly. These were trucked to Buffalo, where their profiles were measured and drawn in a 2D CAD package. A sculptural modeler would use the profiles and the original pieces (sometimes in tatters) to reconstruct the ornament in clay. From these plaster molds were developed and new parts in terra cotta produced. The entire process took months, was very expensive and prone to mistakes.

The Meshlab had been experimenting with photogrammetry[1] as process to scan architectural ornaments and develop digital models that were dimensionally accurate. These meshes could be rescaled to accommodate the clay shrinkage when dried and fired, and outputted to a CNC router. The issue was precision and a workflow that could be easily adopted by the staff. After about a year of developing the techniques and technologies the Meshlab's hybrid digital/analogue process was put to the test to replace four two-story tall caryatids standing atop a 20 story building in downtown New York City. 150 Nassau

[1] A process pervasively used in animation that extracts geometry from images.

Street was one of the first steel frame buildings in the city, and the original terra cotta was improperly installed allowing water to seep through the retaining hardware, saturating the clay and becoming structurally unstable.

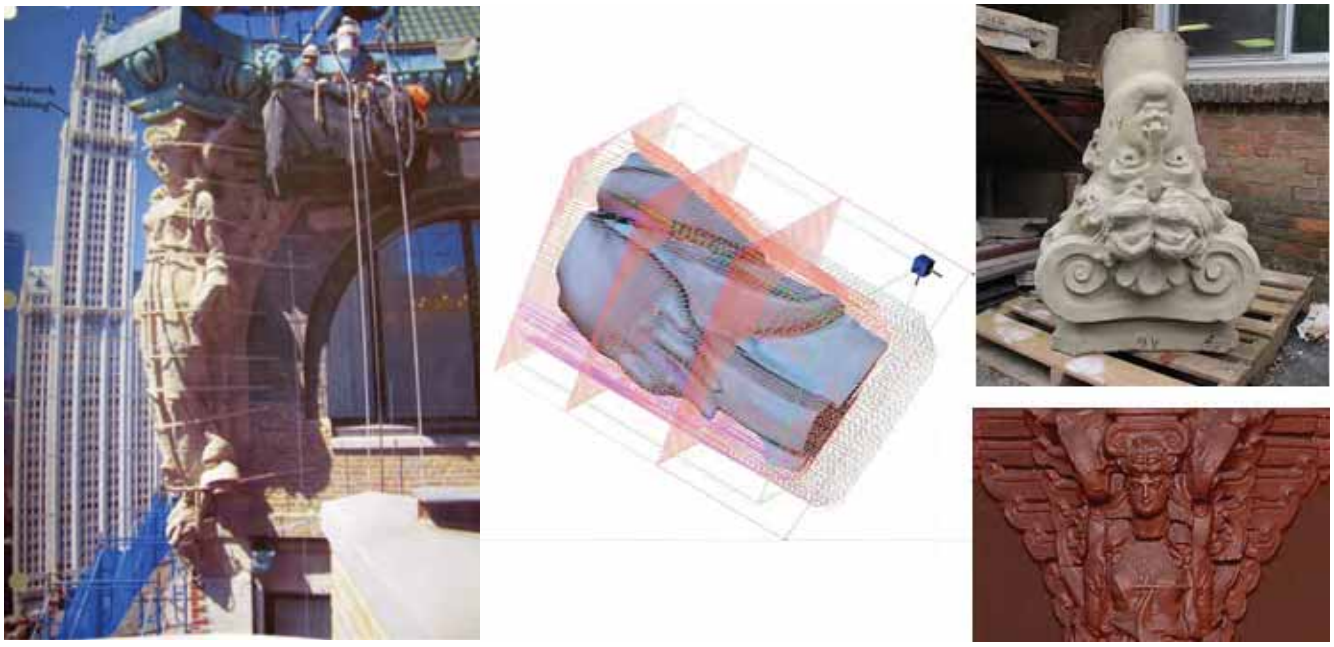


Figure 1: (Clockwise from left) One of four caryatids atop 150 Nassau Street in New York City, strapped to the façade as it had become structurally unstable. Photogrammetrically scanning each block and the resultant mesh. The original head. The scanned sculpture being cleaned up in Zbrush.

The caryatid(s) were removed from the building and one complete statue, nicknamed “Dorothy”, consisting of 55 blocks, weighing 11 tons was sent to Buffalo for replication. Each block was scanned using both laser and photogrammetric methods to develop a complete digital documentation. The workflow adopted and now standard at BVTC involved extracting 3D models from photographs in Agisoft PhotoScan Pro, repairing and refining the models in Zbrush, and then exporting the mesh to Rhino where the measured documentation is completed. The Rhino models can be inverted to develop the molds which can be cut in plater on a CNC (Fig.1).

Dorothy was a major step towards implementing a digital workflow into actual practice. It proved both the scale and accuracy of the digital replacement model and became with two more years of refinement BVTC’s standard practice for historical restoration. It also demonstrated that the steps between documentation and replication could be reduced. Photogrammetry as opposed to other 3D scanning methods became the technique of choice as it could be adapted to work on scaffolding using nothing more than an iPhone. It also captured data like color and textures which provided a way to archive these historical pieces without having to keep the damaged part.

CASE 2- DIGITAL WORKFLOW: DESIGN DEVELOPMENT WITH MANUFACTURING

The architects at Machado Silvetti were exploring a complex tiled surface for the Asian Art Study Center at the Ringling Museum of Art. They had already investigated other cladding materials and found that either they could not get the desired effect or the unique form and color were impossible within budget. Having never worked with terra cotta they recognized they needed BVTC’s assistance early in the project if they were to achieve the design intent of the project.

The Meshlab team had been already training the drafting department in using Rhino as the CAD platform and moving slowly away from a 2D AutoCAD environment. Upon receiving the drawings they recognized the complex forms of the façade had been parametrically derived, most likely using Rhino and Grasshopper. They also were aware that the design needed considerable “rationalization” in that the size, variety and façade profiles needed simplification so that manufacturing and installation of the tiles could follow their best practices (Fig. 2).

A productive collaboration during design development ensued where the design was refined and prototypes were developed and glazing colors explored. Central to this productive conversation was the digital workflow that was already set in place, which reduced the steps from representation to production. By incorporating the designer's tools- Rhino and Grasshopper- into their internal workflow the Meshlab created a new capacity in the company such that it could influence the design early enough in the process where it mattered (Fig. 2).



Figure 2: Grasshopper script developed to rationalize the types of tiles. The Ringling Museum's Asian Art Study Center under construction.

CASE 3- INVENTING NEW TOOLS: CNC CERAMIC WIRE CUTTER

Graduate student Peter Schmidt was one of the student researchers on the team in the Meshlab. When it came to doing his Master of Architecture thesis, he identified a technological need at BVTC that could make many projects they were working on easier to implement. Extruded panels are the basis of most rain screen design. These are produced by forcing terra cotta through a die that is shaped the appropriate profile. Since the die's shape is fixed any reshaping or texturing of the panel must be done post extrusion and most commonly by hand. Small runs are not a problem but with the more common large runs being able to maintain consistency becomes an issue. Peter conceived that a wire cutter that could integrated into the extrusion process could allow for customized paneling. The thesis involved designing a four-axis CNC wire cutter, its interface for running the machine and prototyping some of its parts (Fig. 3). It was awarded the ARCC King Prize and will being prototyped and tested in the new SMART lab that will come online in 2018.



Figure 3: Peter Schmidt's Terra Cotta Extrusion Wire Cutter as it would be incorporated into the existing factory machinery.

ARCHITECTURAL CERAMIC ASSEMBLIES WORKSHOP (ACAW)

The Meshlab has been absorbed into BVTC's corporate structure, with many of the students that worked in it now employed by the company and leading its digital modeling and fabrication department. In economic development parlance, a cluster is a regional concentration or network of specialty manufacturers, suppliers, subcontractors, and ancillary support services, which together give that region a competitive advantage. Higher education often serves to recruit talent and its retention within such clusters has been shown to be a major factor in a region's economic growth. Our experience has shown this to be the case with BVTC that now attracts a number of our graduates who would have otherwise left the region in search of work.

In 2015, UB's Provost funded the establishment of a Community of Excellence in Advanced Manufacturing. A joint effort between the School of Architecture and Planning, the School of Engineering and the School of Management, the Sustainable Manufacturing and Robotic Technologies (SMART) community became the ideal vehicle to continue the industry engagement already begun between UB and BVTC. A new laboratory is being constructed as part of SMART that will support full scale ceramic prototyping and testing. It will host several newly purchased industrial digital prototyping machines, salvaged ceramic manufacturing equipment, and some exceptional student designed and built digital machines.

In response to the establishment of SMART and in anticipation of the new lab, Boston Valley Terra Cotta and UB's Department of Architecture have initiated an annual workshop/symposium; the Architectural Ceramic Assemblies Workshop (ACAW). ACAW's mission is twofold: to educate architectural and engineering practice about ceramics and to develop collaborative research agendas across academia, industry and practice focusing on architectural ceramic design. ACAW follows an interdisciplinary workshop model where participants from architecture, engineering, manufacturing and academia work collaboratively on directed projects. These focus on ceramic's unique material properties, the way that they are manufactured and their potential for bioclimatic design.

The first workshop was held on August 8-12, 2016 at the Boston Valley Terra Cotta factory and the University at Buffalo, School of Architecture and Planning. It included 9 architects, 3 engineers, 5 artists, 8 academics (architecture, ceramic art and engineering), 7 manufacturers and 11 graduate students. These were broken up into four interdisciplinary teams tasked with developing ideas for "bioclimatic" applications for ceramics in architecture. The bioclimatic focus allowed material properties to be central components in the design, such that ceramic's hydrological, thermal and structural properties became the driving force for conceiving a performative and responsive architecture.

There were four distinct approaches taken by the teams that spanned from engineered responses at one end to perceptual affects at the other. Clay's material affordances suggest a variety of passive environmental control applications. The teams explored these through architectural applications like walls, structures, panels, and facades. Group 1 developed a heat exchange panel that sits as part of a façade system and allows for fluids to move through ceramics to modulate interior temperature. Group 2 explores a cooling system that also becomes a self-supporting structure. Group 3 developed a humidity mitigating wall and a digital fabrication system to produce it. While Group 4 explored the design of a sandwich panel whose different layers can be exposed to address different performances- form heat absorption to water channeling (Fig. 4).

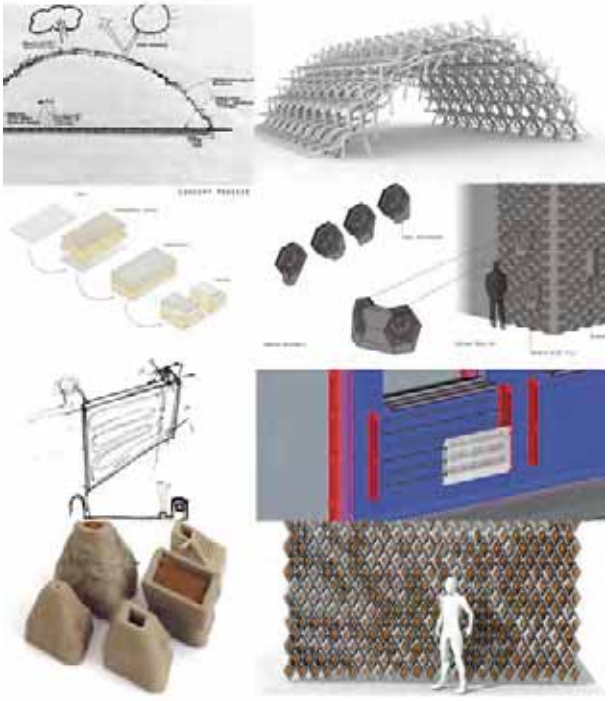


Figure 4: ACAW 2016 ideation - Different performances of ceramics from structural, hydrological, and thermal considered in the design of enclosures.

What all of these propositions demonstrate is a reconsideration of how we construct shelter in response to climate change. Reyner Banham in his seminal book the Well-Tempered Environment, articulated two alternative ways that humans create shelter, either by erecting structures or by burning materials to release their energy. Our modern architectural heritage would

suggest that we have become overly reliant on the latter. Access to cheap energy has led to an excessive reliance on air-conditioning systems to temper our environment. This has impoverished our thinking about structures and materials since they have been tasked to do little more than keep the water and wind out. These propositions redress this shortcoming and suggest an expanded set of performances for materials and structures that include environmental mitigation in addition to other architectural concerns.

The second ACAW took place on August 14-17, 2017 at the Boston Valley Terra Cotta factory and the School of Architecture and Planning's fabrication shop. The focus this year was on developing some of the ideas from the previous workshop into preliminary prototypes. Team leaders were identified from the first year and asked invite other participants from their professional networks to help develop their design. Four teams, led by AECOM, Morphosis, Walter P. Moore and UB/Alfred engaged Boston Valley over the summer to develop prototypes that would be assembled during the workshop and studied for their performance.

What resulted was a participant list that included 15 architects, 10 engineers, 2 artists, 9 academics (architecture, ceramic art and engineering), 11 manufacturers and 9 graduate students. Where last year focused on ideation and representation, this year the emphasis was on prototyping and assembly. This shift resulted in a more nuanced approach to the problem of performance oriented design. While material properties remained the driving force, issues like formal complexity, manufacturing constraints, assembly systems and quality controls played a significant role in the design refinement process. Also, performance testing, like heat retention and luminescence, could be initiated on the prototypes. This hands on approach, while pervasive in studio teaching and academic research, is difficult to entertain in all but the best financed practices. The workshop' aims to develop a more inclusive structure where different types and sizes of practices can partake in the research and use the opportunity to expand their understanding of ceramics (Fig. 5).



Figure 5: ACAW 2017 prototyping - Fired and glazed prototypes prepared prior to the workshop were assembled and tested during the workshop.

CONCLUSION AND FUTURE DIRECTIONS

Our engagement with Boston Valley Terra Cotta has had at its center a desire to affect manufacturing by narrowing the gap between ideation and production. Adoption of digital technologies for design and production has accelerated the workflow and develop better channels of communication between practice and manufacturing. As we look forward to a third installment of the Architectural Ceramic Assemblies Workshop, we are keen to bring more manufacturers into the mix. This stems from the reality that ceramics are just a part of the complex assemblies that go into making a high performance façade. Manufacturers that deal with the structure, waterproofing, glazing and unitization of the assemblies need to be in the mix for us to be able to improve the process and the design. Likewise, there is an opportunity to better build the ceramic nexus between UB/SMART, Boston Valley Terra Cotta and Alfred University. This nexus is the basis for developing innovative faculty research and new curricular offerings that would be unique in the US.

ACKNOWLEDGMENTS

Boston Valley Terra Cotta, Sustainable Manufacturing and Advanced Robotic Technologies (SMART)

REFERENCES

Banham, R. The Architecture of the Well-Tempered Environment. The University of Chicago Press; 2nd edition, 1984.

Cortright, Joseph. "Making Sense of Clusters: Regional Competitiveness and Economic Development." https://www.brookings.edu/research/making-sense-of-clusters-regional-competitiveness-and-economic-development/ (accessed September 28, 2017).

CERAMIC PRECAST COMPOSITE PANELS

High performance structural and architectural building enclosures



Edward Rubio
American Craftsmen Inc.
er@americancraftsmeninc.com



Edward J. Rubio
American Craftsmen Inc.
ejr@americancraftsmeninc.com



Gregory Lucier, Ph.D.
North Carolina State University
gwlucier@ncsu.edu



Brian Moskow, PE
Red Engineering and Design
bmoskow@redengineering.com



Sami H. Rizkalla, Ph.D., FACI, FASCE, FEIC, FCSCE, FIIFC, FPCI
North Carolina State University
sami_rizkalla@ncsu.edu

ABSTRACT

An innovative lightweight ceramic precast composite panel is introduced in this paper that offers the unique benefits of prefabricated off-site construction. The panel system enables broad application by providing structural strength, thermal efficiency, and a sustainable modular construction solution. Ceramic composite panel technology offers improved public safety over some traditional building systems, and may be an attractive choice for energy-efficient developments. The patented system features excellent fire ratings (ASTM-E119-12) and high thermal insulation values. The thin ceramic concrete shell is lightweight, while still providing structural performance at a significantly high strength to weight ratio. The composite panel provides a high-performance technology at a low-cost due to efficient product manufacturing methods, allowing the technology to be economically competitive with current building systems. In addition, the prefabricated panels can be used as wall, floor, and/or roof assemblies that interface to create a complete enclosure and structural system. The composite building system is designed to meet and exceed the requirements set forth by the International Building Codes. This paper introduces the system, reviews laboratory test results, and presents two projects recently completed in central North Carolina. In these case studies, the ceramic precast panels were successfully implemented after the technology was

selected by the architect, reviewed by a 3rd party engineer who developed engineered shop drawings, and was approved for construction by local city building officials and the North Carolina Department of Insurance.

KEYWORDS

ceramic precast, fire resistant, energy efficient, lightweight modular panels, case study, pre-fabrication, ASTM-E119-12

INTRODUCTION

The construction industry faces challenges attributed to building methods, safety both during construction and during occupancy, energy consumption, fire resistance, and costs. Out-dated building methods continue to persist in the industry, and argue for a transition to new advanced modular technologies that can be used to create durable and efficient structures with a reduced carbon footprint. Specific challenges that the proposed ceramic precast panel system can help to address include:

- Building fires, including life safety and asset protection
- Construction schedule / time
- Resistance to natural disasters and storms
- Moisture and mold intrusion
- Thermal efficiency
- Indoor air quality (VOCS)
- Sustainability
- Labor shortages and safety burdens, particularly on site

The commercial feasibility of lightweight precast composites is a key element to advancing construction technology and providing fire-rated, insulated, water-tight, mold-free structures. The new ceramic precast composite panels are described below, followed by laboratory testing data, and case studies demonstrating successful field implementation.

BACKGROUND

The proposed system is shown in cross-section in Figure 1. The system consists of conventional cold-rolled steel framing (studs and track, track not shown) encapsulated in a sheet of rigid foam insulation. Critically, slots the shape of studs are pre-cut in the rigid insulation at the desired stud spacing, enabling one flange of each stud to be completely encapsulated inside the foam. Studs are installed into the foam as the panel is being assembled. Pin connectors are then installed into the encapsulated flange, through the foam, to enable a connection between stud and concrete face. In the orientation shown, the rigid foam serves as the bottom surface of a form used to cast a thin shell of reinforced ceramic concrete that serves as the exterior surface of the structure. Panels of this type have been used for wall, floor, and roof systems, as will be shown in more detail later. The system is lightweight, 20 lbs. per square foot (or less), and facilitates rapid construction. It also offers a 3-hour ASTM E119 fire rating in a structural panel 8" thick.

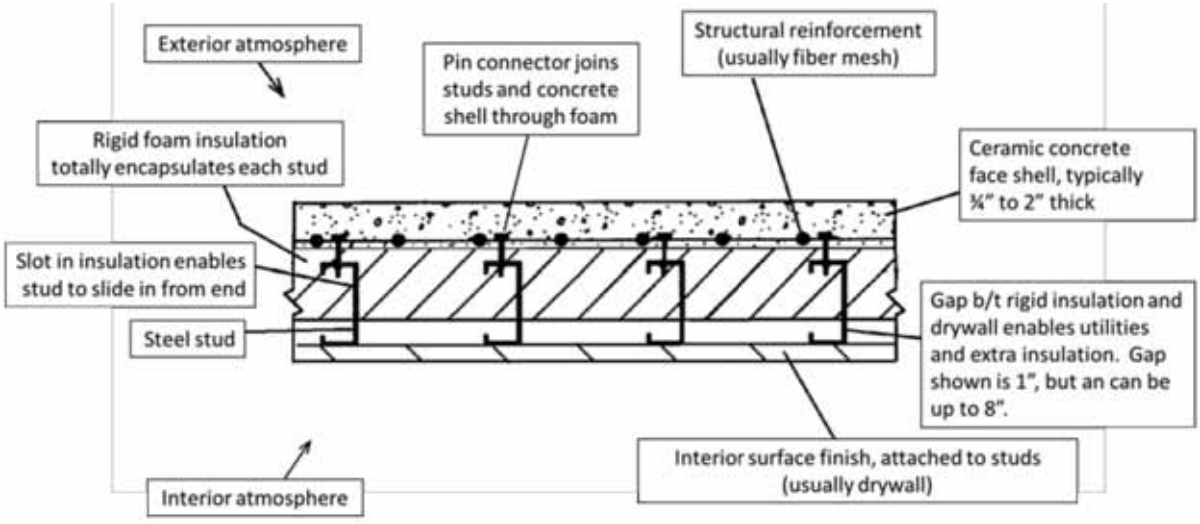


Figure 1: The cross-section of a typical panel. Image courtesy of American Craftsmen, Inc.

The components of the system are described in more detail as follows:

STEEL

Standard recycled cold-formed steel profiles make up the structural core of the panel system. Any depth and thickness stud can be used, as required by the project specifications and determined by the architect and engineer. Deeper studs are used to create thicker panels, which may be necessary to meet thermal or structural requirements. Stud depths of 8" or more are commonly available. Cold-formed framing is commonly designed per SSMA guidelines, and steel products are available from a variety of traditional sources and suppliers. Steel mill certificates provided by stud manufacturers can be used as part of a quality assurance program, and cold-formed steel members often contain a high recycled content. The stud finish is galvanized for durability, and studs are connected together within the panel at their ends using common galvanized stud track. Lateral bracing for the panel is provided by the concrete face shell (and sometimes by interior finished surfaces like fire-rated drywall), but can also be supplemented as required by steel straps included within the panel. Internal bracing can be attached to the stud flange(s) either under the drywall or within the ceramic concrete shell.

INSULATION

The insulation incorporated into the system consists of rigid EPS foam, used to totally encapsulate the steel framing. This encapsulation creates a continuous thermal break between the inside and outside surfaces of the wall system that greatly reduces the flow of heat through the wall cavity, as compared to traditional steel stud construction. In addition to this continuous envelope, high insulation values are provided by the ceramic concrete itself. Rigid insulation of varying thickness can be used to fabricate panels, so, panels can be manufactured and shipped with high R-values directly from the factory. Alternatively, panels can be manufactured with only enough rigid foam to encapsulate the exterior stud flange (a 1"-2" thickness), leaving a mostly-empty stud cavity. The depth of this empty cavity can be controlled by the designer through selection of the stud depth. Providing panels to the jobsite with mostly-empty cavities enables utilities and additional insulation to be added on-site, as is typically done for traditional construction. Empty cavities having a depth of 6"-8" or more are easily obtainable, so walls of R-50 or greater can be achieved in structural panels with a modest depth (12" or less).

MOISTURE AND VAPOR BARRIER

Panels can be configured to offer an integrated moisture and vapor barrier. A vapor barrier can be provided on the surface of the foam insulation, and the ceramic concrete itself provides excellent resistance to moisture and vapor ingress. Joints between panels must be caulked during assembly to prevent leakage.

REINFORCING MESH

Fiber reinforcement is incorporated into the ceramic concrete shell to further enhance the structural capacity of the panel. The exterior concrete shell acts as the exterior sheathing of a building (as a wall or roof), or the subfloor (as a floor), and must be reinforced to span between studs. Non-metallic fiber mesh is strong, lightweight, and does not corrode or degrade. Using non-metallic reinforcement allows for a reduction in face-shell concrete thickness since corrosion of internal steel reinforcement is not a concern and concrete cover requirements for corrosion protection are not relevant.

CERAMIC CONCRETE FACE

The ceramic concrete mixture used to cast the face shell of the panels is one of the unique elements of the system, and it is this material that enables a thin shell of concrete material to be effective. The cementitious ceramic material is similar to Portland cement in that water is mixed with a dry powder to create a flowable slurry that hardens, however, the ceramic concrete offers many unique features over traditional Portland cement concrete. The ceramic concrete is a magnesium-based material that does not harden via the traditional hydration reaction of Portland cement concrete. Rather, water triggers a reaction between the inorganic elements of the concrete, and the flowable slurry created sets quickly into a hard shell. Working time for the material is about 15 minutes, and strengths of several thousand psi can be achieved in only a few hours. The ultimate compressive strength of the ceramic concrete used in the panels is between 5,000 and 8,000 psi, depending on the design requirements. The ceramic concrete shell is non-toxic, does not corrode or dissolve, and offers excellent bonding strength to the rigid foam insulation and to the steel connecting pins. Most importantly, the material has excellent thermal resistance, will not burn, and can withstand temperatures of close to 2000°F without cracking. The wet concrete is highly flowable, reducing the labor required for casting. The material does not shrink when curing, so microcracking common to Portland cement concrete does not develop. Thus, the ceramic concrete face provides a good barrier to air and water, and

can serve as an exterior finished surface. Alternatively, paint, stucco, or other treatments can be applied. Architectural colors or finishes can also be cast into the surface at the time of production.

METHOD

The design and production process for the panels is outlined in this section. Design of the panelized structure and of the panel assemblies themselves is completed with custom-tailored BIM software that provides modeling, engineering, and estimating tools. The software generates shop drawings for the individual panel components, as well as precise budgetary values for materials, labor, profit, and overhead on a particular job. Panels can be designed for loadbearing and non-loadbearing applications for wall, floor, and/or roof applications. Shop drawings are generated for panels and connections, which are designed and engineered per architectural specifications. The shop drawings are produced in a BIM-compatible format, allowing designers to 3D model all members and materials implemented in the fabrication process. The detailed modeling software provides a high level of confidence, as well as a transparent design process with architects, engineers, general contractors, erectors, and fabricators. Panel shop drawings for construction are usually sealed by a Professional Engineer and approved by the Project Architect prior to the start of panel fabrication. As panels will be fabricated in a factory, trucked to the site, and then erected to form the building, additional attention must be spent on specifying the lifting, handling, and bracing details. Temporary construction bracing must be designed so that the building can be safely erected, and any clips or attachment points needed to connect other parts of the building (mechanical systems, etc.) to the panels can ideally be included in the design process. Panel size is limited only by what can be transported to the jobsite, and, with early coordination, features such as electrical conduits and outlet boxes can be cast right into the panel. Since all panels have a small cavity space, additional furring is not required even if utilities are added on-site. The building system supports a variety of wall heights and accommodates myriad openings for custom doors and windows.

The benefits of panel prefabrication are numerous and significantly reduce trade overlap problems on the jobsite, bringing down projects costs associated with the simultaneous management of multiple materials and trades. Field labor costs are reduced, as installations can be completed simply by rigging finished panels into place, bracing and connecting, pulling wires, running piping, and installing fixtures. The cavity space provided allows for easy installation of electrical and plumbing mechanicals before drywall and interior finishes are applied. The prefabricated modular panels speed up project schedules, allow for structures to be dried-in more quickly, and provide savings on construction management and labor costs.

PANEL ASSEMBLY

A complete building system can be manufactured and assembled per project-specific engineered drawings and specifications. The precast panel manufacturer cuts materials to size from rough stock and assembles the steel stud wall and encapsulating insulation as shown in Figure 2. Steel framing components should have proper mill certificates and ATSM/code certifications. Engineer-sealed shop drawings should be followed for proper member sizing and placement. With the foam in place, special pin connectors are installed into the encapsulated flange of the steel stud. Reinforcing mesh is installed, the temporatry form walls are positioned, and ceramic concrete is cast on the panel face, as shown in Figure 3. An exterior finish can be applied to the panel at the fabrication plant, either in the wet concrete (via pigment, texture, or both), or to the cured surface (via paint, stucco, etc.). Panels are cured (less than 1 hour of curing is required for ceramic concrete), stored to the fabrication yard, and transported to the jobsite when needed.



Figure 2: A panel with studs slipped into the foam and connected together with tracks. Note the marks on the foam for installing pin connectors through foam into flanges. Photo courtesy of American Craftsmen, Inc.



Figure 3: A typical panel with a freshly cast ceramic concrete face. Photo courtesy of American Craftsmen, Inc.



Figure 4: The lightweight panels are easy to load, unload, and handle. Photo courtesy of American Craftsmen, Inc.

LABORATORY TESTS AND DATA

A series of tests have been completed on typical panels, including structural tests at North Carolina State University in Raleigh, North Carolina, where flexural, racking, and concentrated load tests were completed. Fire resistance tests, hose stream tests, and thermal performance tests have been completed at Fenestration Testing Laboratory in Medley, Florida.

STRUCTURAL TESTS

A flexure test was conducted on a typical prefabricated panel that measured 12’ long by 4’ wide by 8” thick and contained (4) 16ga studs. The panel was tested on a simple span (pin and roller supports) in four point bending. Supports were centered 11’-6” apart and load points were centered 11.5” apart about the midspan. The panel face was a ¾” thick layer of ceramic

concrete with an average compressive strength of about 6,500 psi. Load was applied to the panel using a hydraulic actuator at a rate of 0.25" per minute. The widths of the supports and loading pads were all 6" wide. The applied load and panel vertical deflection were measured and recorded.

Panel failure was ultimately governed by local buckling of an outer steel stud near one panel support at total applied load of 5,750 lbs. with a corresponding midspan vertical deflection of 1.3". The applied load at failure was equivalent to an applied distributed pressure of about 120 PSF. No cracking or crushing was observed in the top ceramic concrete surface, prior to or after failure. The panel after failure and the measured load-deflection data are shown in Figure 5.

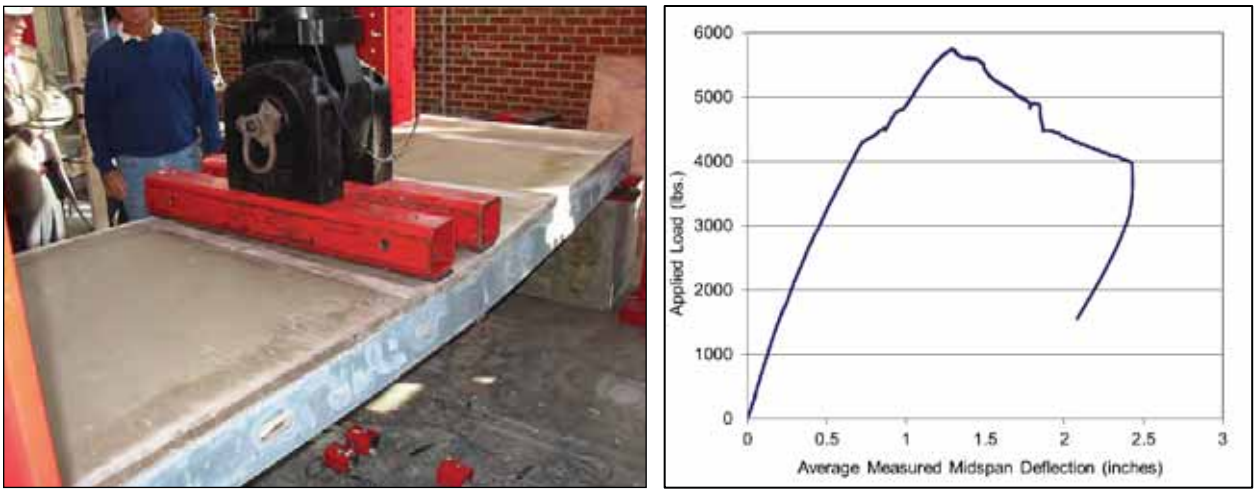


Figure 5: Photograph of the deformed panel after a flexure test (left) next to the measured load-deflection data (right). Photo and chart courtesy of North Carolina State University.

Two concentrated load tests were performed on 4' square prefabricated panels that were approximately 8" thick, including a ¾" thick ceramic concrete face shell. Each panel was supported on a 42" span, and each was loaded with a concentrated force on the panel face, placed between the internal studs. The first panel was loaded to failure using a 4" x 4" steel plate, and the second panel was loaded to failure with a 2.5" x 19.5" steel tube (oriented parallel to the internal studs). A hydraulic actuator was used to apply vertical loads to each of the platens, and the relative deflection of the ceramic concrete face spanning between adjacent internal studs was measured. Both tests are shown in Figure 6.

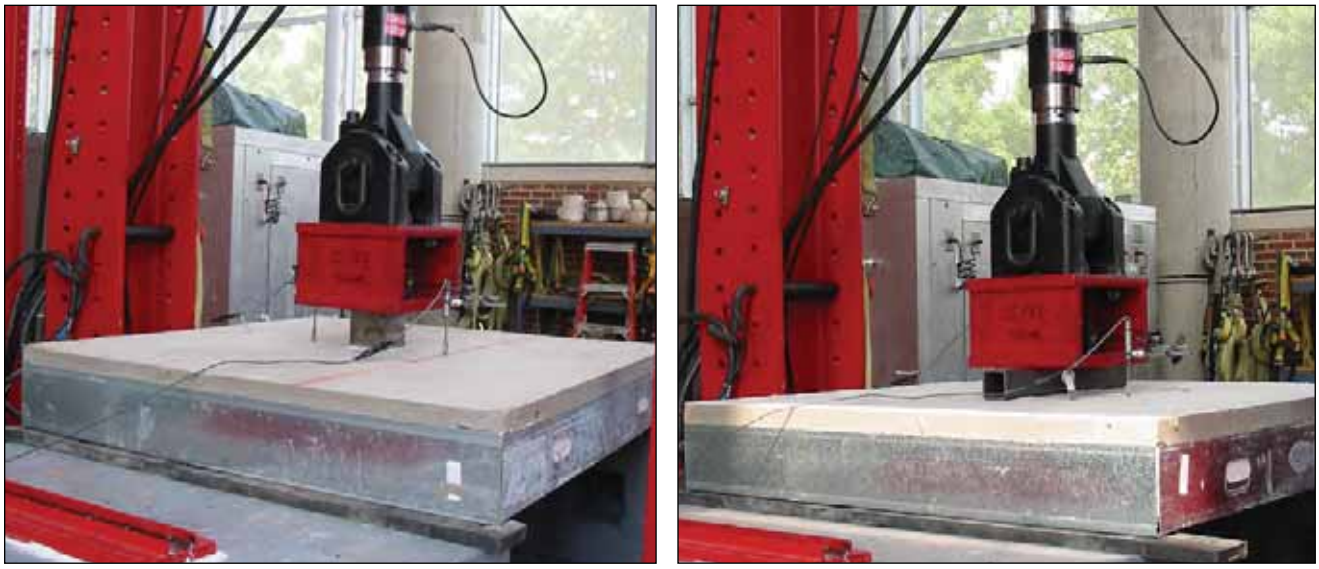


Figure 6: Photographs of concentrated load tests with a 4"x4" loading platen (left) and a 2.5"x19.5" loading platen (right). Photos courtesy of North Carolina State University.

Both concentrated load tests produced failure modes of localized punching through the ceramic concrete surface, as shown in Figure 7. The peak load for the 4" x 4" platen was 3,590 lbs. and the peak load for the 2.5" x 19.5" platen was 4,130 lbs.



Figure 7: Photographs of concentrated test failure modes, 4"x4" platen (left) and 2.5"x19.5" platen (right). Photos courtesy of North Carolina State University.

A racking shear test was completed on a 12' x 4' x 8" thick prefabricated panel, including a ¾" thick ceramic concrete face shell. The panel was tested in racking shear in a sideways orientation by supporting the panel base on a rigid steel column. In this orientation, the panel was turned 90-degrees from its typical orientation in a building. Thus, loads that would normally act laterally were applied vertically. The base of the panel was supported to resist the applied load by bearing against a steel angle. Normally, this supporting reaction would be provided by bolts or clips connecting the panel to the foundation. The panel was also anchored to the supporting column with steel cables configured to prevent uplift due to the applied load. Normally, this tie-down supporting reaction would be provided by a combination of gravity forces acting on the panel from applied loads, and connection bolts and clips holding the panel to the foundation. The test setup is shown in Figure 11. The panel sustained a peak racking load of 3,660 lbs. before failing due to local concrete shell spalling at the load point and support. This level of racking load is equivalent to 915 lbs. per linear foot.

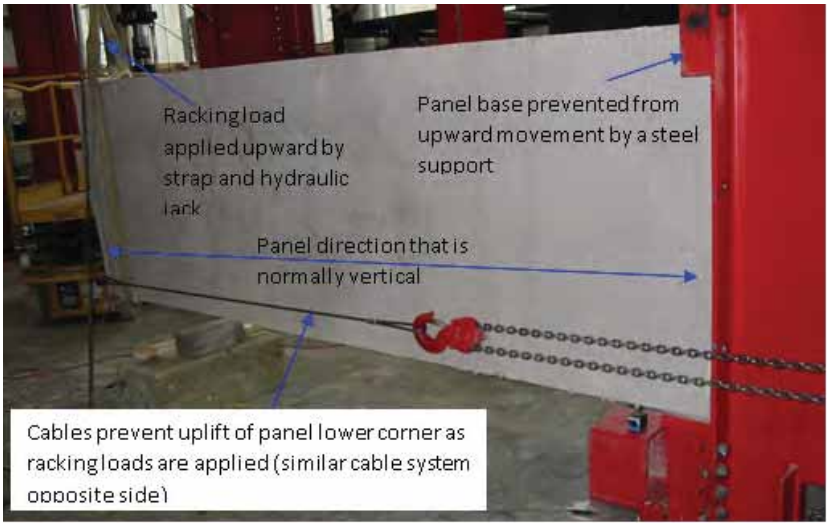


Figure 8: Photograph of the racking shear test setup. Photo courtesy of NC State University.

FIRE RESISTANCE TEST

An ASTM E119 three-hour fire test was performed on a pair of prefabricated panels, configured to form a 10' x 10' x 8" thick wall. A 7/8" thick ceramic concrete face shell was orientated towards the fire (exposed face), and the interior (unexposed) face of the panels was configured with three layers of 5/8" thick fire-rated drywall. This panel configuration was intended to simulate what might be specified for the walls of fire-resistance-rated areas such as a high-rise building envelope. The ASTM E119 fire test proceeds by subjecting the exposed side of the panel to rapidly increasing temperature, exceeding 1,000°F

after 6 minutes, exceeding 1,500°F after 30 minutes, and approaching 2,000°F after 3 hours. Importantly, as these were loadbearing panels, a vertical live load of 2,600 lbs. per linear foot of wall (26,000 lbs. total) was continuously maintained on the top surface of the wall during the fire test. Temperatures on the unexposed wall surface are measured, and are not allowed to exceed 325°F per the ASTM Standard. For the tested panels, unexposed surface temperatures only reached 100°F at 3 hours, far below the 325°F allowed by the standard. No visible changes in the panel had occurred when the test was terminated after 3 hour of exposure, and no passage of flame or hot gas was observed. The test panels in the furnace are shown near the end of the 3-hour exposure period in Figure 9.



Figure 9: The unexposed surface of the test panels stabilized at 100°F while the exposed surface inside the furnace was subjected to nearly 2,000°F at the end of a 3 hour fire test. Photo courtesy of American Craftsmen, Inc.

Immediately after the fire exposure test, the panel assembly was withdrawn from the furnace and subjected to the impact and cooling effects of a standard hose stream test. In this test, water is sprayed at pressure onto the hot exposed surface. The nozzle pressure was 30 psi, the distance between nozzle and wall surface was 20 feet, and water was applied for a total period of 1 minute based on a total exposed area of 100 square feet and duration of 0.6 seconds per square foot. The wall assembly withstood the fire and hose stream test without passage of water from one side of the wall to the other. No opening developed between the exposed and unexposed surface. Some surface cracking was observed on the exposed face of the tested panels, however, no spalling or structural cracking was observed.



Figure 10: Photographs of the hot exposed surface of test panels during (left) and after (right) a hose-stream test. Note that the difference in color between panels is due to two different architectural finishes. Photos courtesy of American Craftsmen, Inc.

SOUND AND THERMAL TRANSMISSION

Prefabricated panels were tested for sound transmission and received an STC rating of 47. This rating indicates that the panels blocked 47dB of sound across an average spectrum from passing to the inside face of the panel from the outside face. While an STC rating of 47 is impressive, it is important to note that the tested panel included only a ¾" thick layer of ceramic concrete and a 1" thick layer of integral rigid foam insulation along with a single interior layer of 5/8" thick gypsum board. The wall cavity of the tested walls was empty. Additional insulation that would be added to the cavity in the field after utility installation (up to 8" of insulation depending on wall thickness) and would likely increase the STC score further.

The same panels were tested for thermal transmission via ASTM C1363, Standard Method for Thermal Performance of Building Materials and Envelope Assemblies by Means of a Hot Box Apparatus. With an empty wall cavity, the panels were measured to have a thermal resistance (R-value) of 5. As with the sound resistance test, insulation that will typically be included in the field will dramatically increase thermal performance. If a 6" wall cavity were provided (by using a panel thickness of 8"), then insulating this cavity could bring the R-value of the wall system to a level in excess of R40.

CASE STUDIES

Two case studies are presented in the following sections. Both projects were recently completed in the Raleigh-Durham, North Carolina area.

HILTON GARDEN INN

One of the earliest field applications of the ceramic concrete precast panels was the renovation of a seven-level Hilton Garden Inn in Durham, North Carolina. The hotel was being upgraded to add new exterior mechanical chases and parapets, along with other upgrades. The project architect and owner accepted the panelized design as a change order from an original steel frame stick-built design after hearing of the benefits provided by ceramic precast composite panels. An aggressive schedule of 6 months on-site, while maintaining full operation of the hotel at all times, was made possible by the prefabricated construction. Precast ceramic composite panels were successfully implemented on the project to panelize exterior cantilever roof parapet around the perimeter of structure, to enclose a new exterior mechanical chase, to provide HVAC mechanical fencing, to enclose dumpsters, to serve as a pool fence, and to frame in a new storage room. Elements of the project are shown during construction and at completion in Figure 11 and Figure 12.

The prefabricated panels enabled the original 6-month schedule to be completed in only 3 months, at a lower cost than stick-built. No scaffolding was needed, and only a small crane and boom lift were required. The minimal equipment improved job safety, and kept the jobsite clean and clear which was important to the hotel operator. Panels were cast on the jobsite in a remote corner of the parking lot in lengths of up to 30'. The project demonstrated accelerated completion and substantial cost savings, installing over 18,000 square feet of panels in under three months without interrupting hotel operations.



Figure 11: Lightweight panels are used to clad exterior mechanical chases and screen equipment. Panel installation on a chase (left), and the completed project (right).

Photos courtesy of American Craftsmen, Inc.



Figure 12: Lightweight panels are used to fabricate a new parapet. Panels installation on a chase (left), and the completed project (right).

Photos courtesy of American Craftsmen, Inc.

THE MAO RESIDENCE

Master Chef Khi David Mao owns a local restaurant in Raleigh, North Carolina. Mr. Mao was inspired to build a home using ceramic concrete prefabricated panels knowing that it would be the first of its kind in the world. It was appealing to Mr. Mao to inhabit a home with premium indoor air quality, excellent thermal efficiency, superior fire resistance, a high degree of sustainability, and security. Mr. Mao hired Ted Van Dyk, AIA and Brian Moskow, P.E. to design and engineer a large, modern structure on a small, urban lot. The project and panelized building system were approved by the City of Raleigh Building Inspections Department as well as by the North Carolina Department of Insurance.

The Mao Residence features walls, floors, and roof made from prefabricated modular ceramic concrete panels, as shown in Figure 13. Exterior surfaces of the structure, including the roof, were either raw ceramic concrete, textured stucco, or tile. A tight urban site of 7000 square feet (0.16 acres) with 50' of road frontage made construction of a 4356 square foot, 2-level home a challenge. Approximately 13,000 square feet of panels were fabricated off-site, delivered in sequence, and installed using a small crane. The lightweight panels facilitated work on the small site, and streamlined shipping, unloading, and placement.

The building features net zero sustainable design by incorporating geothermal and PV solar with a highly efficient thermal envelope to virtually eliminate dependence on fossil fuels. The energy-efficient panels provided a quiet and thermally-efficient space. All panels (walls, roofs, and floors) were fabricated with a ¾" thick ceramic concrete face. Wall panels generally used 6" deep studs and roof and floors generally used 10" deep studs. Finished floors (manufactured hardwood) were able to be installed directly over top of the ceramic concrete floor face without leveling compound. Exterior panel joints were sealed with backer rod and caulk (walls) or ceramic concrete (clean roof). The flexibility of the precast panels was demonstrated on-site when the owner decided to add window openings in certain locations after panels were installed. Openings were cut out and stud ends were framed together with steel track. The finished structure is shown in Figure 14, and recently won the U.S. Green Building Council *Local Leader Category for Most Innovative Residential Building*.



Figure 13: Installation of a prefabricated wall panel (left) and a prefabricated roof panel (right). Photos courtesy of American Craftsmen, Inc.



Figure 14: Photographs of the finished Mao Residence, outside (left) and inside (right). Photos courtesy of American Craftsmen, Inc.

CONCLUSION AND FUTURE WORK

An innovative prefabricated panel system has been develop and was presented here. The practicality and feasibility of this system was demonstrated through laboratory testing and successfully completed field projects. The new panel system offers structural performance, thermal performance, energy efficiency, light transport weights, and excellent fire resistance. Additional research and testing are being pursued to further facilitate broad acceptance of this system in the marketplace.

ACKNOWLEDGMENTS

The authors would like to thank American Craftsmen, Inc. of Raleigh, North Carolina for sponsoring the tests presented here. In addition, the authors would like to acknowledge Ted Van Dyk, AIA and his team at New City Design Group in Raleigh, North Carolina for their work on the Mao Residence along with officials from the City of Raleigh and the North Carolina Department of Insurance. Finally, many thanks are due to Khi David Mao for his continued support of this innovative technology.

REFERENCES

ASTM Standard E119-16a, 2016, "Standard Test Methods for Fire Tests of Building Construction and Materials," ASTM International, West Conshohocken, PA.

Rubio, Edward. Concrete Composite Wall Panel. U.S. Patent 7,681,368 B1. Filed August 21, 2007, and issued March 23, 2010.

Report 15-5699. Fire Exposure Test on ACI Smartwall System: Evaluation of 3 Hours Fire Endurance. Fenestration Testing Laboratory, Medley, FL. 4/13/2015.

Lucier, G., “Concentrated Load Tests on American Craftsmen Patented Smartwall Panel”, Technical Report IS-11-14, submitted to American Craftsmen by the North Carolina State University Department of Civil, Construction, and Environmental Engineering, Constructed Facilities Laboratory (CFL), Raleigh, North Carolina, August, 2011.

Lucier, G., “Racking Shear Test of Smartwall Panel”, Technical Report IS-10-18, submitted to American Craftsmen, Inc. by the North Carolina State University Department of Civil, Construction, and Environmental Engineering, Constructed Facilities Laboratory (CFL), Raleigh, North Carolina, December, 2010.

Lucier, G., “Flexure Testing of Smartwall Panel”, Technical Report IS-10-16, submitted to American Craftsmen, Inc. by the North Carolina State University Department of Civil, Construction, and Environmental Engineering, Constructed Facilities Laboratory (CFL), Raleigh, North Carolina, November, 2010.

DESIGN CONSIDERATIONS AND THE COMPLEX FAÇADE

Kolon Future Research Park



Stan Su
Morphosis Architects
s.su@morphosis.net

ABSTRACT

The design of complex, high-performance facades involves balancing attention towards principles of material selection, thermal and moisture protection, structural integrity, and durability. When these demands are coupled with the desire to create aesthetically interesting and “beautiful” skins, design teams may find themselves tasked with reconciling conflicting formal and performative drivers in the creation of an exterior envelope. The formal vision of a complex façade skin, for example, may not be appropriate for the climatic and site-specific realities of a given project location; material properties, compatibility, and interface will also often pose issues of concern. Technical designers will typically negotiate these challenges within the detailing of a given system. However, through the research and interrogation of given systems earlier in the design process, disparities between design considerations and technical drivers can lead to unexpected and innovative solutions.

This paper will present design and fabrication processes employed in the development of a high-performance complex façade for Kolon Future Research Park, a research laboratory building in Seoul, South Korea. The main facade of the building has been designed with the intention to serve as visually-striking, exemplary construct demonstrating the client’s commitment to innovation, technology, and sustainability. To achieve this design, a second skin of composite construction was developed using parametric design workflows and building performance analysis. Fiber reinforced polymer (FRP) was selected as the final material for the external sunshades, given the material’s durability, structural characteristics, and potential for plasticity in form. A monocoque sunshade assembly that challenges conventional formal notions of solar shading was developed for the project. The resultant body of the continuous outer skin is reflected in the glazed wall behind, to create visual complexity and tension amplified by the sense of weightlessness that the minimal support structure affords.

KEYWORDS

design process, stick curtainwall, sustainability – holistic, daylighting - glare – shading, finite element analysis (FEA), parametric workflows, composites, sunshades, FRP

INTRODUCTION

Kolon Future Research Park (Fig. 1) represents an investigation into the use of FRP in a bespoke, high-performance façade of complex geometry. The formal exploration and design of a bespoke glazed wall with FRP sunshades was accomplished utilizing virtual design and construction processes and performance analysis at a holistic level.

Key performance and sustainable design strategies employed include:

- The development of building mass and orientation to respond to the solar path.
- Incorporating solar shading to minimize cooling loads and glare.
- Daylighting to reduce energy used for artificial lighting and for visual amenity.
- Providing natural ventilation to reduce cooling loads and improve thermal comfort.

The above strategies were balanced with the design drivers to arrive at solutions that not only satisfy the design intent but also work to strengthen the design's performance. Formal design drivers, project requirements, building performance analysis, and structural analysis on the main facade served to inform parametric workflows in the design of a complex, glazed wall with external sunshades.

The development of the building's main facade involved addressing the fundamental issues of thermal and moisture control, compatibility, constructability, and durability. However, the overarching driver at a project-wide level was innovation in system design. The design team was encouraged to reach beyond conventional systems, to consider the form and performance potential of fabric, aluminum plate, and FRP for an external sunshade material. Each material's benefits and disadvantages were evaluated with regards to aesthetic qualities, structural performance, constructability, durability, and cost (both initial and life-cycle).



Figure 1: View from Northwest to the Kolon Future Research Park building.

BACKGROUND

Kolon Future Research Park is the new 76,300 m^2 R&D laboratory building for the Kolon Group, a leading textile manufacturer in South Korea. The corporation's name, "Kolon," is an amalgamation of "Korea" and "nylon," the original product produced by the company. Today, Kolon's activities cover research, primary material manufacture, fashion design, and product construction, spread amongst the group's 38 divisions. This is a unique configuration that enables the company to capitalize on its own resources and advances, and to forge innovative collaborations between divisions. Supporting this collaborative model was a primary goal behind the design of Kolon Future Research Park, which brings together researchers, leadership, and designers in one location. The program of the building combines flexible laboratory facilities and executive offices with active social spaces that encourage greater interaction and exchange across the company.

The headquarters is in Seoul's Magok district, an emerging hub for technology and light industry that is revitalizing the Han-River area in south-eastern Seoul. The Magok district has been fostered by the Seoul Metropolitan Government. The district is conceived to function as an "industrial ecosystem" where a range of technology companies will co-locate to spawn new intersecting markets. Kolon is one of the first firms moving their R & D operations to Magok, and the new building will set the standard for performance and design in the district. The four-acre project site sits adjacent to Magok's central park – a prominent location for what will be the district's first major completed building (Fig. 2).

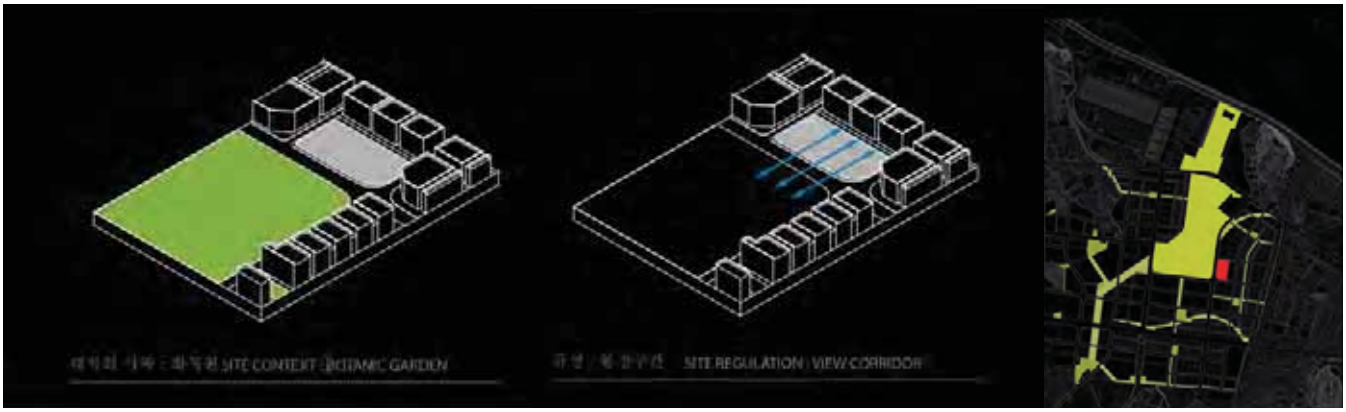


Figure 2: (From left to right) Park diagram, View corridor requirement diagram, Magok District site plan with project site in "red."

The building's west façade faces the park and serves as the main facade of the building. Bridging the three extending laboratory wings, this folding volume contains conference rooms and social spaces, augmented by exhibition galleries at the street level to communicate the company's vision to the public. The design strategy for the building's functional spaces is pervasive to the formal expression of the building. This includes the design of the building's façade systems. There is a consistent functional response of the skins to the spaces they define beyond, and a further interconnectedness provided by the interplay of spaces (Fig. 3). The relationship between the west façade's glazed wall and sunshades is non-hierarchical. The FRP sunshades create bodies beyond the face of glass, which work to dissolve the materiality of the façade with the convergence of mass, negative space, and reflections.

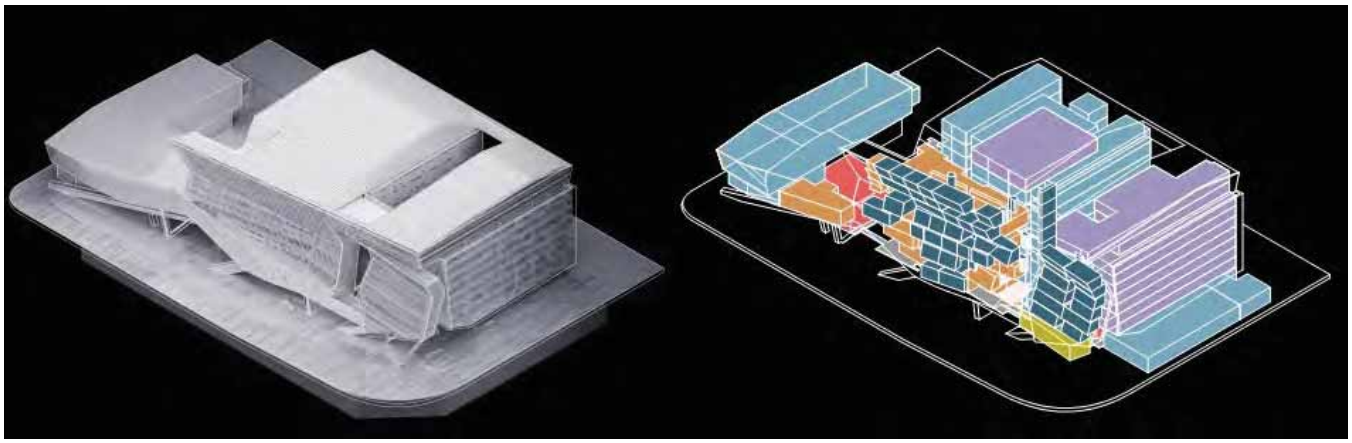


Figure 3: Programmatic massing diagram.

Local projects that incorporated FRP in cladding solutions were studied early in the design process. Two of the projects identified for investigation were fabricated by the same FRP subcontractor. The Yeosu Pavilion is a kinetic FRP façade with large FRP panels that can be deformed to enable passive ventilation of the façade. Initial research in kinetic facades led the team's investigations into this project, and the project team recognized the potential for large-scale façade units. The Dior flagship store in Seoul is another example of an FRP exterior wall assembly utilizing megapanels. Each of the 11 megapanels span the full height of the 4-story building with roof terrace; the largest panel measures ca. 20M x 7M (Design Base, nd). Investigations into the design and construction of the two facades provided beneficial information regarding local fabrication expertise, connection detailing, material fit and finish, as well as the ability of materials to create self-supporting structures with concealed reinforcement. Further discussions with FRP specialty contractors from the industrial, aerospace, and automotive industries helped to formulate an understanding of local preference for fabrication.

METHOD

The design of the building was approached holistically with sustainability as a primary driver. Along with goals for LEED (Leadership in Energy and Environmental Design) Gold from the U.S. and Korean Green Building Councils, the project

focuses on the quality of the work environment through roof terraces, courtyards, and other measures that increase access to natural light and air for employees. Other sustainable measures include a green roof, use of recycled materials, and utilization of a bubble deck slab that reduced the amount of concrete used by 30%. The sunshade system on the west façade is both a performative and symbolic feature of the building, with the FRP sunshade units shaped to balance design drivers based on solar shading and view requirements. The building's siting, spatial qualities, and technological innovations strive to express Kolon’s investment in and commitment to sustainability.

Large view corridors punch through the lab blocks at east, through to the west façade facing Magok Park. These view corridors are a project requirement for all buildings bordering the park and are intended to maintain open lines of sight in the parks surrounding fabric. This requirement is also meant to encourage daylighting of the buildings within the park masterplan, which supports the desire for energy conservation and improved human comfort. As such, the west façade curtainwall system was designed to respond to these view requirements, whilst achieving performance targets. Continuous lines of sight afforded from the rear courtyards to the west façade can be seen in a diagram of the building’s skin, atrium liners, and circulation spine (Fig. 4). Views onto the landscape beyond are afforded to all occupants within the social space’s meeting, cafeteria, and breakout rooms along the west façade.

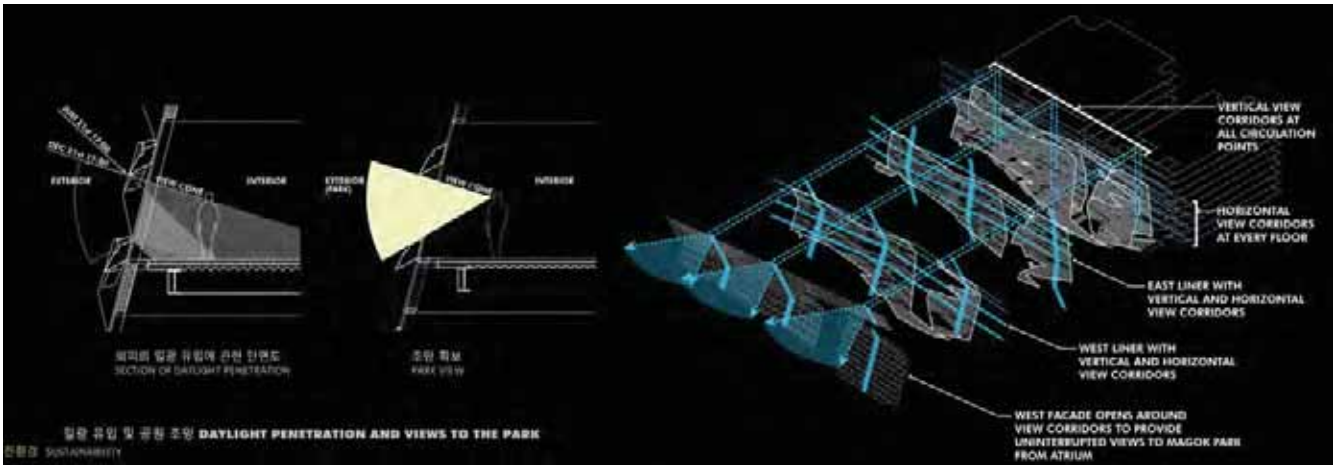


Figure 4: Daylight penetration and view diagrams depicting the successive layers of exterior and interior skins.

The concept of weaving became the underlying formal concept for the design of the west façade. This idea is a reference to the client group’s research in textiles, as well as a symbol of collaboration between the company’s many departments. The analogy of a woven fabric was used as a reference for the interconnected array of sunshades that form the monolithic, outer skin (Fig. 5).

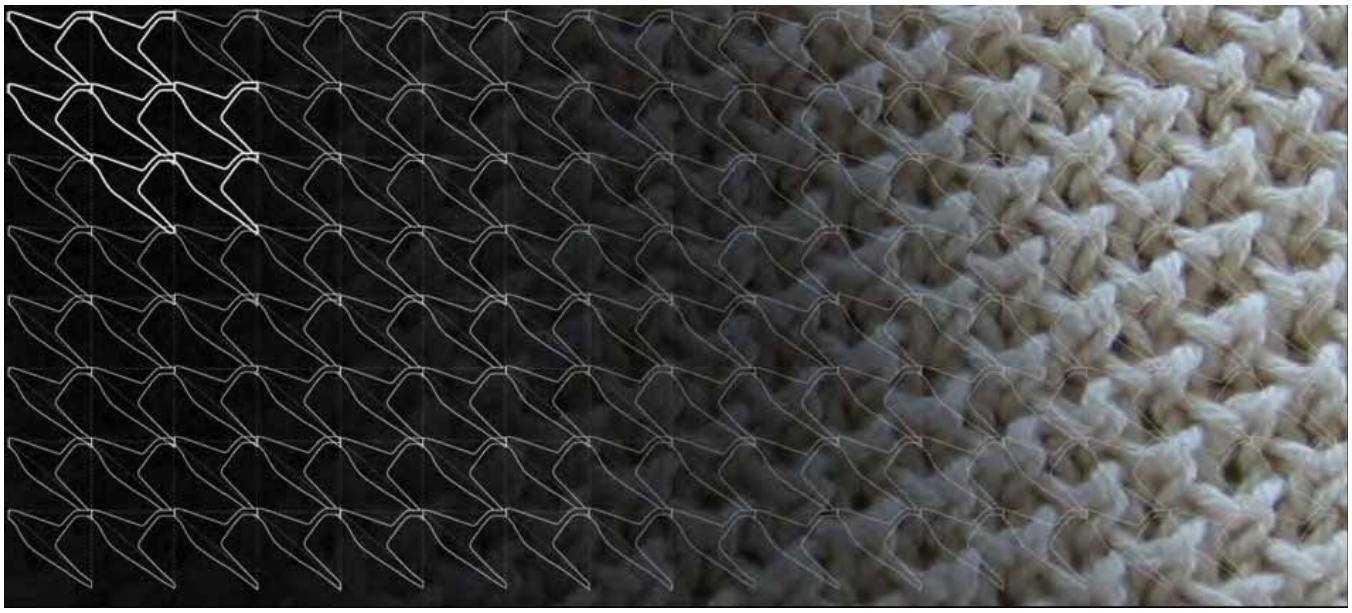


Figure 5: Conceptual diagram of the sunshade pattern.

A BIM project model, developed using Bentley MicroStation / Version 8 - S6 (Bentley 2016) was the vehicle for design geometry, drawing production, 3D visualization, and final fabrication. Organizational drawings with regards to panel types diagrams, geometry drawings, and detailing were important to convey the design in coordination with the project 3D model and specifications. The use of rapid prototyping for physical model studies and in-house visual mockups allowed the design team to quickly assess the visual characteristics of various assemblies and interfaces (Fig. 6). The use of various 3D modeling software platforms was required for the shaping of components as well as the parametric design of the façade panel patterns. Each software was chosen for its ultimate utility for the given task in the design process. Rhinoceros 3D / Release 5 (Robert McNeel & Associates 2012), in conjunction with Grasshopper visual programming language was used for optimization and propogation of the sunshade units.



Figure 6: Digitally printed physical models in varying scales.

CATIA V5 / Digital Project (Dassault Systemes, Gehry Technologies 2012) was used for geometry and workpoint coordination during design, and later during construction administration with specialty contractors (Fig. 7). Ultimately the 3D project

design geometry was used to drive CNC (computer numeric control) tooling of the sunshade mold positives. The use of virtual design and constuction (VDC) methodology enabled effective collaboration on design iterations amongst the design, engineering, fabrication, and contractor teams.

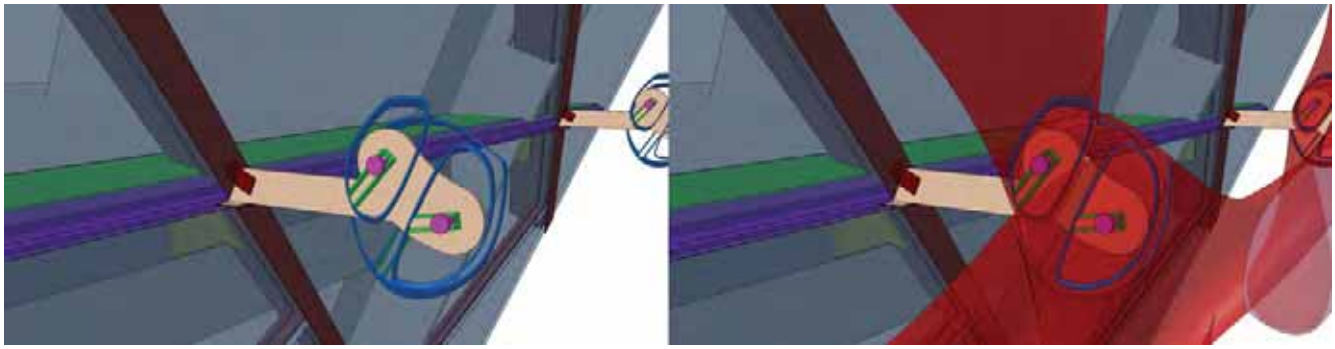


Figure 7: Views of the 3D parametric façade model, with and without sunshade bodies.

DATA

The west façade glazing system is a stick-built, floor-to-floor curtain wall, with insulating glass unit cassettes and external sunshades. The decision to proceed with a stick-built system was predicated upon the need for the system to accommodate a variety of unique and complex geometrical conditions. This was underscored by the regional preference for non-unitized systems, and an expertise in complex steel fabrication. The mullions on the west façade curtain wall were required to be steel based on structural requirements for wind loads. As such, the design team proceeded to develop a bespoke curtainwall system comprised of steel mullions with extruded aluminum closures, cassette insulating glass unit panels, and external FRP sunshades. The final design of the envelope systems on the building are the result of investigations serving to balance design drivers, code requirements, local building methods, and cost.

The design team researched materials which in form and materiality would serve as an expressive and high-performance component of the façade. Materials research and investigations into local built precedents yielded examples in FRP that embodied formal potentials and efficiencies in production. The structural performance of the material is unique, with a high strength-to-weight ratio (Kreysler 2017). These characteristics can be further improved by creating shelled or monocoque assemblies. Exploiting the material characteristics of FRP allowed the design team to explore sculptural solutions, which challenged the conventional approach to sunshade design utilizing planar, one-sided constructs, with exposed support structure.

A key characteristic of the west facade is that much of the upper wall is self-shaded due to the building's folded geometry in section, and its orientation relative to the sun. This inherent feature of the social space massing greatly reduces the amount of solar heat gain on the façade's glazed layer. This was a beneficial feature established early in the design process. The external sunshade system provides additional solar shading and is the expressive, second skin of the façade. By reducing the surface area of exposed glazing, the overall solar heat gain at this façade is greatly reduced (Fig. 8). The percentage of shaded glazing was optimized with information from daylighting and solar shading analyses to optimize performance throughout the year.

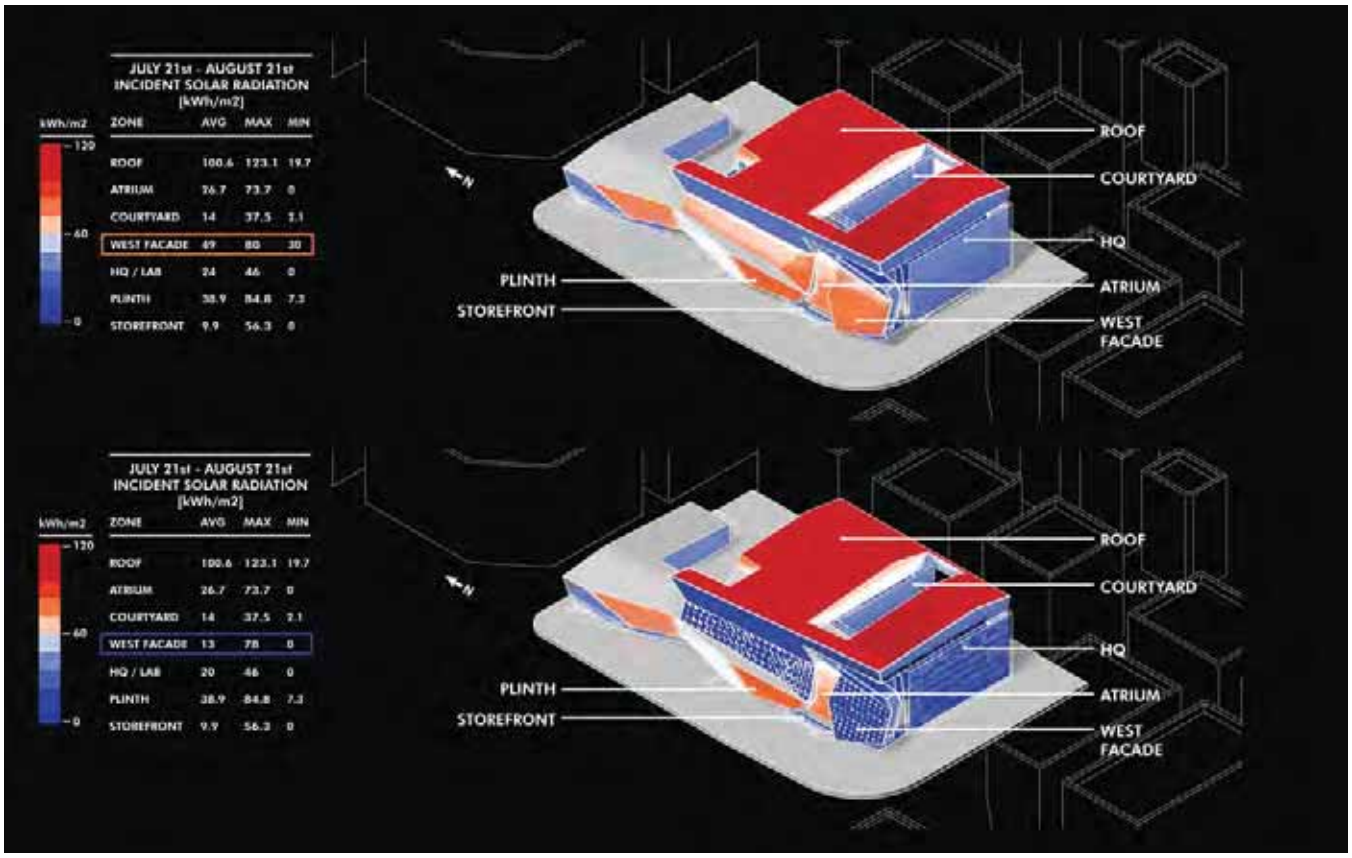


Figure 8: Solar radiation comparison of the façade system, with and without external sunshades. Images by Arup Facades.

At a percentage of 33% open, the cooling system demand is greatly reduced (Fig. 9). The sunshade forms were initially modeled with planar and folded geometry. Daylighting analysis was conducted to confirm if useful daylighting levels were being provided throughout the year. Useful daylight defined as penetrating sunlight at 100-2000 lux. Insufficient daylighting may lead to more lighting consumption, while excessive daylight would lead to glare. It was determined through daylighting analysis that the meeting rooms within the west façade would receive direct sunlight starting at 5pm in the summer, when interior blinds would be employed (Fig. 10).

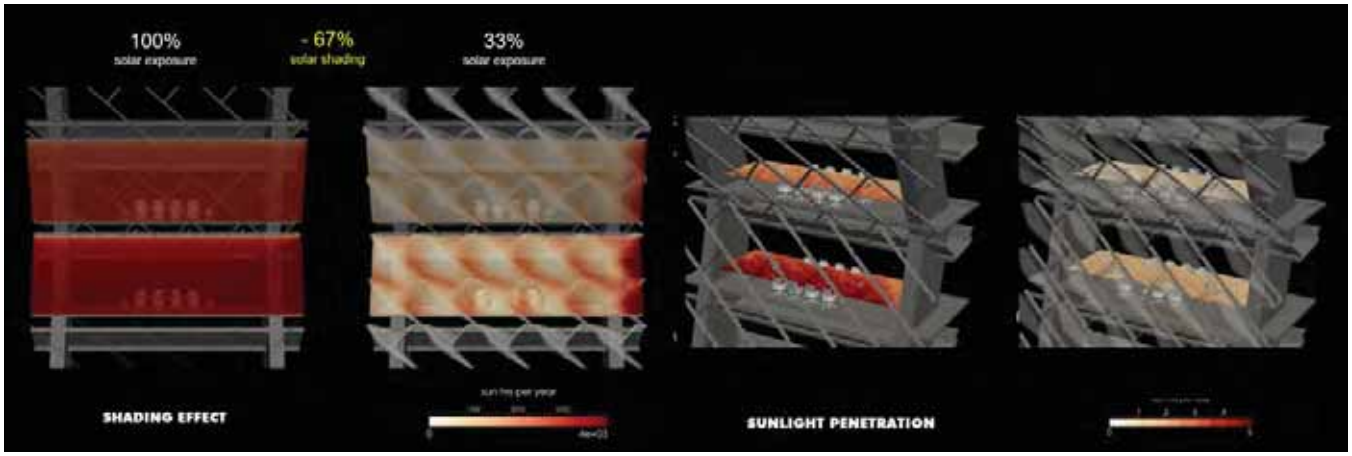


Figure 9: Shading and sunlight penetration analysis images, with and without external sunshades. Images by Arup Lighting.

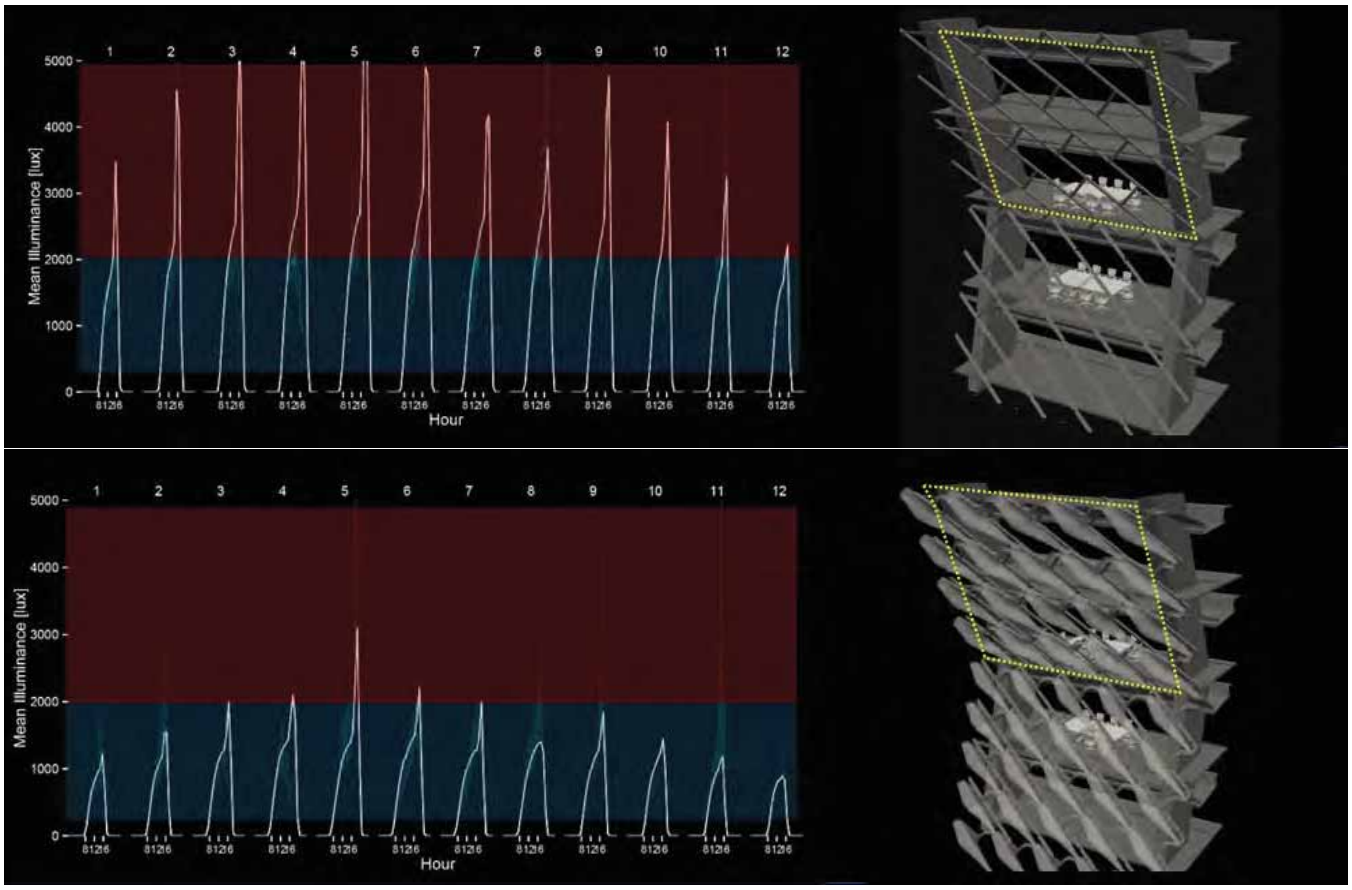


Figure 10: Useful daylight penetration analysis images, with and without external sunshades. Images by Arup Lighting.

The forms were derived using solar path diagrams to identify angles of solar incidence coupled with the interior view angles required. Surfaces oriented perpendicular to the angle of solar incidence for the longest and shortest days of the year were the basis for the key surfaces in the sunshade forms (Fig. 11). These shapes were developed into planar forms and then propagated using scripts and 3D parametric software. The geometry of the sunshades was continually shaped and analyzed to optimize the forms to solar shading and daylighting criteria, while preserving views from within the building (Fig. 12).

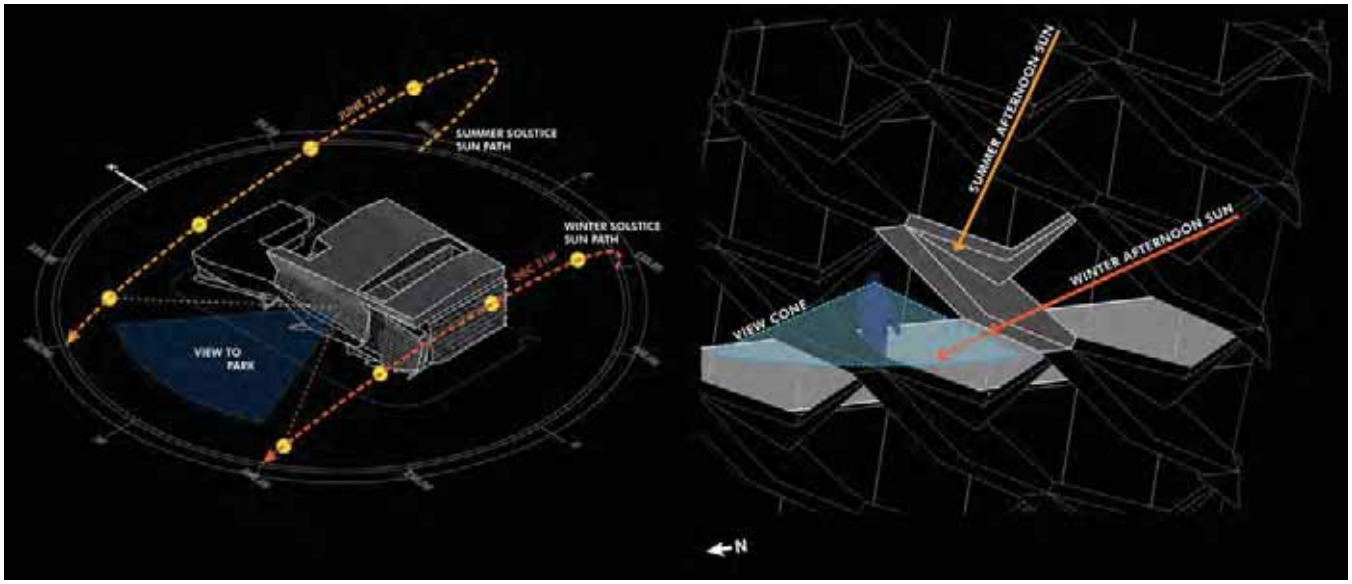


Figure 11: Sun path diagram and early sunshade geometry diagram.



Figure 12: Views of various stages of the sunshade form development, from initial planar geometry to the final form.

Concurrent with the solar optimization of the sunshades, Arup performed structural finite element analysis (FEA) to ensure that the formal iterations were performing within stress and deflection limits (Fig. 13). Indicative member sizing and preliminary connection design was also performed by the façade engineer. A key focus was with the attachment methodology for the sunshades. Complex conditions required focused development and analysis by the design and engineering teams.

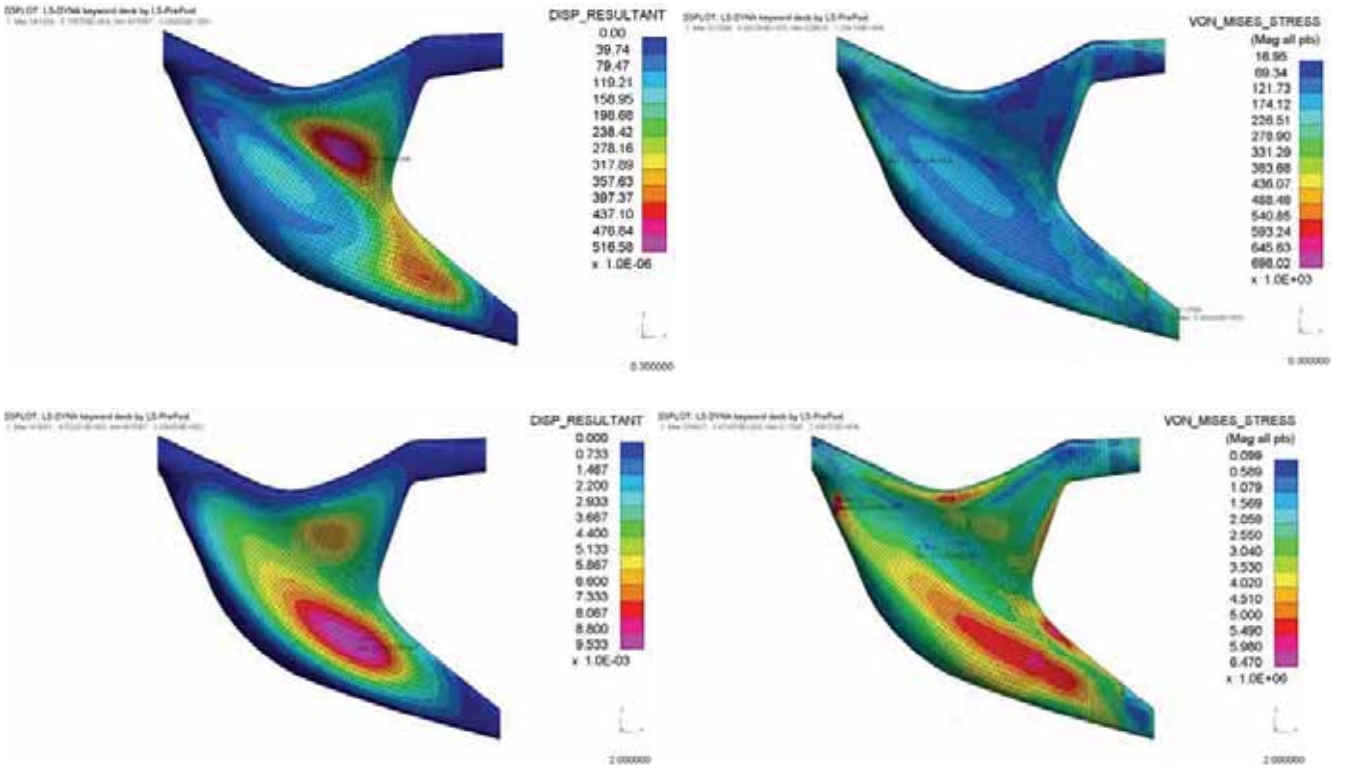


Figure 13: FEA Analysis Images. (Top left to right) Displacement and stress under gravity load. (Bottom left to right) Displacement and stress under wind load. Images by Arup Facades.

A passive ventilation strategy was developed for the building with natural ventilation provided at the lab, headquarter offices, atrium, and social spaces at the west façade. In the case of the glazed facades, operable windows were introduced to provide improved occupant comfort. At the west façade, operable panels were designed to operate by physically offsetting the glazed panel from the face of glass design position. This type of operable panel was necessary to avoid clashes with the sunshades and the bracket arms when in an open position.

EXPLANATION

Investigations and documentation early in the design process was initiated for the specialty glazing systems, fiber-reinforced concrete (FRC) cladding systems, and fiber-reinforced polymer (FRP) sunshades. The local process, with regards to the development of design documents does not typically involve the participation of specialty facade consultants prior to award of the project to the general contractor. Facade engineering support typically comes from the subcontractor or supplier after the general contractor has come on board. The design team's early investigations served to fill this gap in system development. The west facade glazing system continued to be refined during the construction documentation phase in response to costing exercises and system optimization. However, major revisions impacting the design intent were greatly reduced, due to the team's efforts in the design development phase.

The design team investigated fabric, metal, and FRC material sunshade options before the final determination to proceed with FRP. Potential materials for each of the façade systems were evaluated based on the ability to satisfy the design intent when considering material characteristics, form & finish potential, cost, and carbon footprint. Life-cycle studies on the embodied carbon footprint of FRP showed that materials such as glass-fiber reinforced concrete consume much more energy in their production in comparison to FRP (Stanford 2009). Durability of FRP is long-proven with examples in boat construction and exterior construction maintaining structural integrity after 50+ years of exposure to the elements (Kreysler Interview 2017). Life expectancy of exterior FRP constructions using modern resins and woven fibers are conceivably 75-100 years without the benefit of having built examples to analyze.

A primary reason for choosing FRP was the material's high strength to weight ratio, and its ability to be formed into plastic, doubly-curved surfaces. The structural performance of the material can be further improved by creating folded, shelled, or monocoque assemblies. Exploiting the material characteristics of FRP allowed the design team to explore sculptural and self-supporting solutions, which challenged conventional approaches to sunshade design. The stick-built glazing system was installed first to complete the envelope of the building as early as possible. This was to allow the interior fit-out to commence as soon as possible, and a response to lead time for the FRP components. Vertical, stainless-steel mullions were affixed to the floor slab edges, insulating glass unit cassettes affixed, and then the sunshade brackets were installed and left awaiting the installation of the sunshade units (Fig. 14).



Figure 14: (From left to right) Installation of insulating glass units cassettes and operable panels. View of stainless steel mullions and sunshade brackets at fold.

A reflective, solar-control, low-e coating was specified for the insulating glass units to achieve the target solar heat gain coefficient, and to create visual interest with the reflections of the sunshades. The bracket design is comprised of a stainless-steel knife plate bracket that is connected to the vertical mullions, through the vertical glazing joints. Stainless steel mounting plates with mounting studs were mechanically-fixed and bonded to the arms of the sunshades, which engage into hooks cut into the brackets (Fig. 15). These connections were either slotted or fixed to allow for racking of the curtain wall units, as well as slab deflections. The connections also accommodate the removal of any single sunshade unit for glass replacement without the need to demount adjacent units. The west façade glazing system and sunshades were developed and vetted from a feasibility standpoint by the design and engineering team early in design development. Typical details were identified

and studied in all phases of the project with attention to member sizing and movements about connections (Fig. 16). Details were tested at all interfaces to study the continuity of thermal and weather lines, as well as compatibility in materials and system componentry.

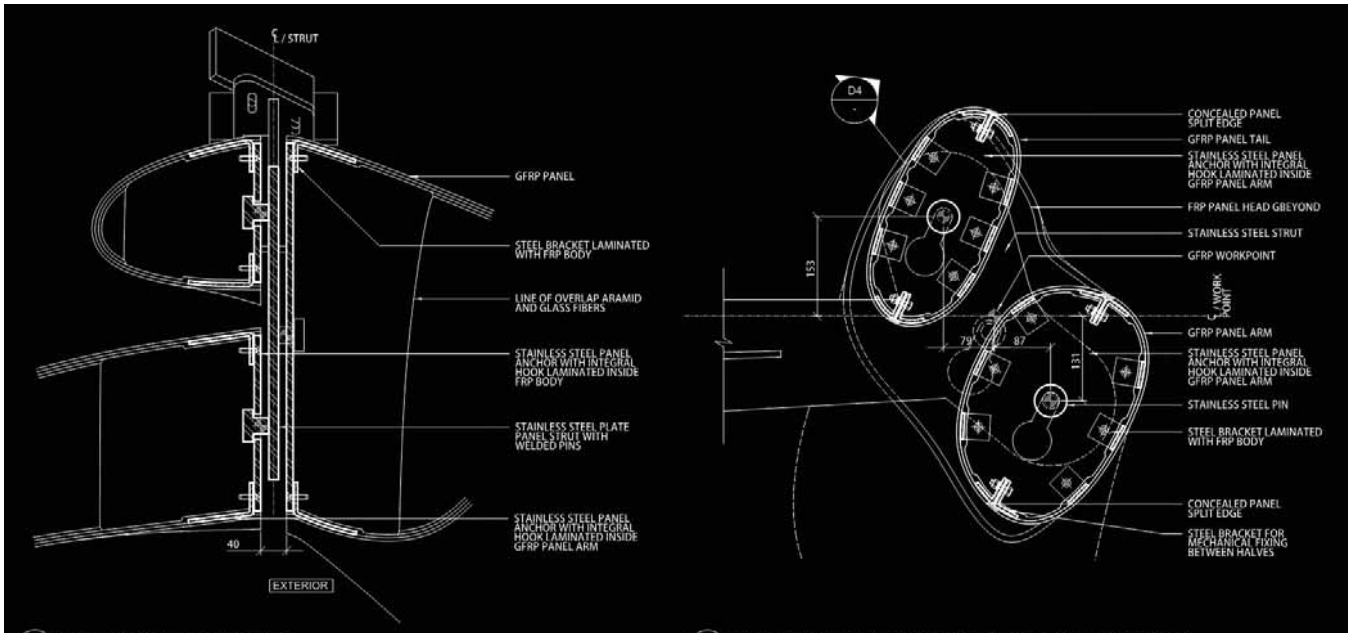


Figure 15: Design Development details. (Left) Plan view through the bracket arm connection. (Right) Section view of sunshade arms at bracket.

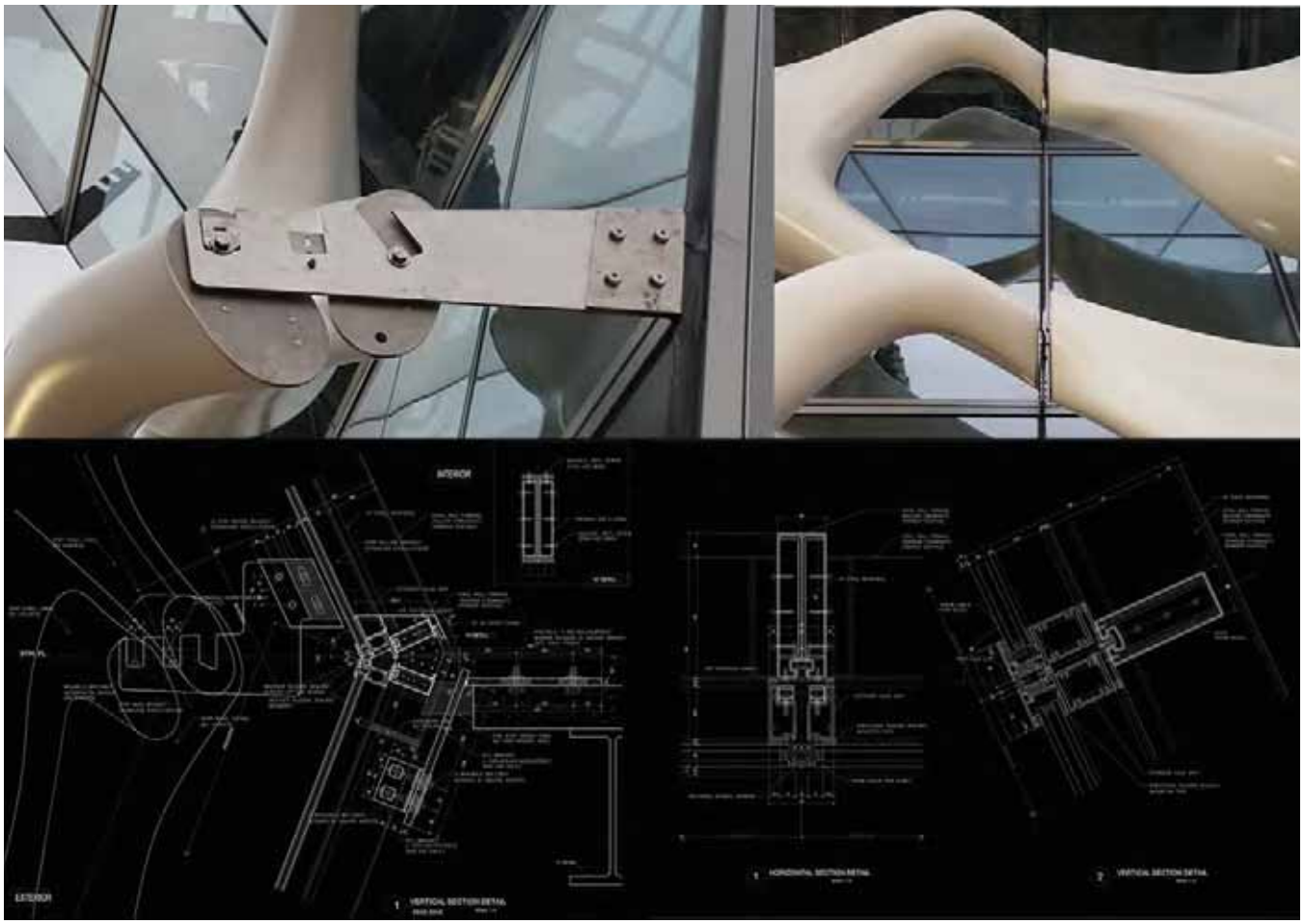


Figure 16: (Top) Views of the final sunshade installation. (Bottom) Shop drawing details of the typical slab edge and typical mullion. Drawings by POSCO.

Special attention was given to the FRP components early on in understanding local fire code requirements. The Korean building code does not allow the use of FRP exterior wall assemblies for buildings over six stories in height. Although the Kolon Future Research Park exceeds this height, the sunshades are categorized as ornamental facade elements which are not subject to this height limitation. Fire testing was conducted for both the typical matrix and aramid-reinforced matrix Korea per test methods 14CFR Part 25.853 ("Title 14, Code of Federal Regulations ("Ecfr - Code Of Federal Regulations" 2018) and DOT/FAA/AR-012 ("Aircraft Materials Fire Test Handbook" 2000).

A typical composite buildup is comprised of a polymer matrix and fiber reinforcement. A surface coating layer which is compatible with the matrix resin can also be utilized in the molding process. This is the gel-coat, which eliminates the need for painting the component once it is cured. There are many resins available on the market, and the main driver in selection is processability in consideration of the fabrication process being used. Strength of the matrix is primarily a function of the type of fiber reinforcement used, as well as the pattern by which the fibers are oriented in the mold (Fig. 17). A common strategy in pattern design incorporates non-crimping fabric (NCF) over traditional woven fabrics. Plies in a woven fabric are crimped about one another in the weaving process, which compromises strength. NCF's are comprised of plies of unidirectional reinforcement fibers, which are layered upon one another and then stitched together.

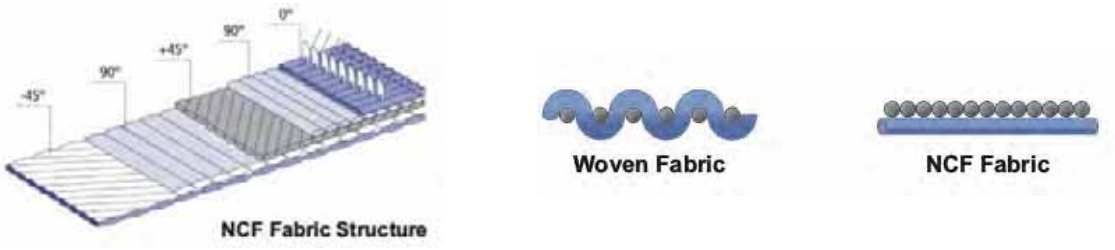


Figure 17: Diagrams courtesy of Poliya ("Poliya Polyester Composites Resins, Polyester Resins, Vinyl Ester, Polymers, Gelcoats and More" 2018).

There are two techniques used in the fabrication of FRP components. The first technique is hand lay-up whereby reinforcement fabrics are placed in a negative mold, with the manual application of resin using rollers, brushes, or other means. The second technique is the Vacuum Infusion Process. This is a process like hand lay-up, but with the added step of utilizing a vacuum bag to draw the resin in and then draw out the excess. This leads to a better distribution ratio fiber-to-resin and less wasted resin.

A local FRP fabricator with experience in the automotive and aerospace industries was awarded the sunshade fabrication scope. The fabrication method proposed by the fabricator team was the vacuum infusion process, but with the monocoque sunshade body being produced in two halves and later joined. The contractor created plugs (positive form in mold making) for the fabrication molds using wood, foam, and modeling putty. The plugs were first CNC-milled out of foam and modeling putty to create the rough form. A final hand-finished putty layer was then applied to ensure a smooth and uniform surface. The plugs were used to create negative molds out of FRP, based on the advantage of being able to re-use the molds for multiple sunshade units. A front and back mold for the each of the sunshade types was created. A gel-coat and reinforcement layers were hand-laid in the mold. Resin was then introduced via vacuum infusion process (Fig. 18). The typical wall thickness of the panels is 13mm. In areas of concentrated stress about the bracket connections, the thickness was increased. Aramid fiber meshes are produced worldwide by three manufacturers, one of which is Kolon Industries. Kolon's Heracron aramid fiber reinforcement was utilized in areas about the connection brackets requiring reinforcement to meet the structural requirements of the design (Fig. 19).



Figure 18: (Left to right) Technician conducting QA/QC survey check of clay plug, view of a finished FRP Mold, vacuum infusion of resin after lay-up of fiber reinforcement.

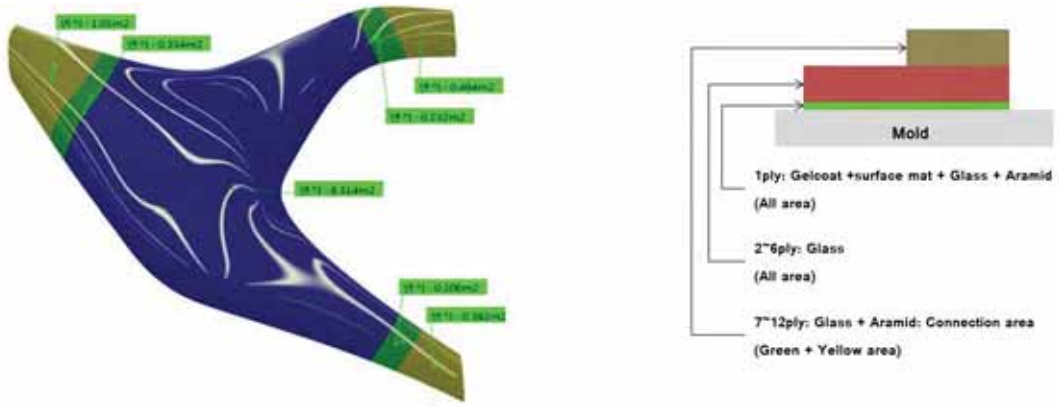


Figure 19: FRP sunshade final buildup diagrams. Diagram courtesy of Hankuk Carbon.

The two halves of the sunshades were joined using a jig to ensure proper registration of the halves. Additional layers of aramid reinforcement were introduced to the ends of the sunshade arms during this joining process (Fig. 19). After the joined halves had cured, they were finished on the racks used for handling within the shop and transportation to site. There is a total of 441 FRP panels, and out of these a total of 14 typical sunshade types. The number of new molds required for atypical panels at the perimeter of the façade, was greatly reduced by blocking-off pre-existing molds for the typical panel types. At 200kg each and at a typical size of 3.0M x 3.25M, consideration regarding the handling and transportation of the FRP sunshade units was important. Lifting points, and steel cradles were required to be carefully designed with regards to transportation between staging and work areas within the fabrication shops. These same steel cradles and lifting points were utilized for transportation to the project site, and installation onto the façade.



Figure 19: (Clockwise from upper left) Storage of cured halves of sunshade forms; View of steel cradle and bonding frame; View of joined front and back panels of sunshade; Joined halves of sunshade with parting seam rough finished; Workers employing a jig to position and fix the stainless steel mounting endplates; Stainless steel endplate with rivets from bonding process visible, and threaded hole for anchor pin during final installation (lifting ring during shop handling and transportation).

The lack of a visible support structure is perhaps the most important feature of the west façade glazed wall design. The result is an outward view from the interior space which is clear of secondary structure (Fig. 20). The reflections of the sunshades at the surface of the glass further adds to the complexity of the sunshade bodies. Visual connections from the exterior to

interior spaces are strengthened due to this design feature. The individual monocoque sunshades together form a 3-dimensional and continuous second skin, which seemingly floats outside the glazed main façade (Fig. 21).



Figure 20: Progress construction photo looking out from the interior of the social space.



Figure 21: View of the west façade performance mockup.

CONCLUSION AND FUTURE WORK

The design of the Kolon Future Research Park, was an investigation into the use of FRP in a bespoke, high-performance façade of complex geometry. A formal exploration into the design of large-scale FRP sunshades was informed through the development of workflows utilizing virtual design and construction processes and performance targets derived through analysis at a holistic level. By fully-vetting the solutions proposed, design teams can successfully balance design intent, project requirements, material limitations, and construction methodology throughout the design and construction administration phases of a project. In this way, the realization of a project may be kept in alignment with the underlying intent of the design. Through an interrogative design process, design teams can reconcile formal and performative drivers to arrive at innovative solutions for complex facades. The west façade of the Kolon Future Research Park serves as a successful demonstration of the Kolon company's culture and commitment to innovation, technology, and sustainability.

ACKNOWLEDGEMENTS

Sung-Soo Lim, Project Architect, Morphosis Architects
Nicole Meyer, Business Development & Communications, Morphosis Architects
Kerenza Harris, Director of Design Technology, Morphosis Architects
Atsushi Sugiuchi, Advanced Technology Group, Morphosis Architects
Neil Smith, Technical Support Manager, Composites One
Irene Martin, Senior Engineer, Arup Facade Engineering + Building Physics
Galen Burrell, Senior Engineer, Arup Lighting
Ian Bruce, Associate, Arup Advanced Technology + Research
Felix Weber, Associate, Arup Facade Engineering + Material Consultants
Guglielmo Carra, Senior Engineer, Arup Materials Consulting
Sung-Min Shin, Hankuk Carbon | Hankuk Advanced Materials

REFERENCES

Bentley Microstation (Version 8 Series 6). 2016. Bentley Systems.
Rhinoceros 3D (Release 5). 2012. Robert McNeel & Associates.
Catia V5 / Digital Project V1 (Release 5). 2013. Dassault Systemes / Gehry Technologies.
"Title 14, Code of Federal Regulations (14 CFR) Part 25.853". 2017.Office of the Federal Register https://www.ecfr.gov/cgi-bin/text-.idx?SID=b753d263ccaa7f9a69bf8009fac72d83&mc=true&node=ap14.1.25_11801.f&rgn=div9.
"DOT/FAA/AR-00/12 Aircraft Materials Fire Test Handbook". 2000. Washington D.C.: Office of Aviation Research.
Stanford University. 2009. "Architectural Facades for the Heydar Aliyev Cultural Center." Life Cycle Assessment, Stanford.
Kreysler, Bill. 2016, "FRP Composites | Using FRP on high-rise buildings." Façade Tectonics The Building Envelope 17.
Team meeting with Bill Kreysler, 2016.
Team meeting with Design Base Corporation LTD, 2014.
Poliya n.d. "Poliya | Products > Auxiliary Materials > Reinforcement Materials". 2018. Accessed 11/16/2017 https://www.poliya.com/en/products/materials/reinforcement_materials/.

HYBRID TIMBER

Performative, biophilic and beautiful



Stacey Hooper, AIA, LEED BD+C
NBBJ
shooper@nbbj.com

ABSTRACT

This case study provides an overview of building hybrid curtain wall system and future opportunities for the use of timber. It will also review the benefits and hurdles inherent in conceiving and constructing a fully timber curtain wall in an industry where the standard practice is organized around the use of glass, aluminum and steel.

Pairing the use of timber with curtain wall construction provides many benefits and several challenges relative to navigating a silo-ed construction industry. Wood is higher performing compared to the thermal characteristics of aluminum and steel, and it provides significant environmental benefits. While interior product transparency declaration is becoming mainstream, the building envelope industry has done little to advance chemical transparency or reduce the use of toxic products and chemicals. These include poly vinyl chloride (PVC), used for thermal breaks and the use of heavy metals in products such as Low E coatings on glass, both known to be harmful to human health and the environment. In addition, aluminum processing carries a high embodied energy and chemical paint coating process, despite its end of life recycled potential.

In contrast, technological advancement and digital fabrication drive an impassioned and motivated timber industry towards the use of sustainable wood products within the marketplace, notably building with mass timber. The benefits of sustainable forestry are numerous, including carbon offsets and capture, reduction in waste, low-embodied energy, water based coatings, biophilic outcomes, and sustained strength and re-use.

This case study will stitch together an opportunity for cross-industry advancement and expertise to drive innovation towards higher performance, reductions in our carbon footprint, less harmful chemical dependency and beautiful biophilic outcomes.

KEYWORDS

curtain wall, hybrid timber, biophilia, sustainable forestry

PERFORMANCE VS. PLANET

We are in an age of revolutionary technology and digital fabrication. This revolution propels innovation and imaginative partnerships to realize more complex, efficient and high-performance buildings, built faster than ever before. However, for every successful high performance, innovation/ transformative built solution, we still fall far short of our industry goals relative to energy reduction and environmentally friendly/ do-no-harm building materials. This is especially true in looking at exterior envelope materials and systems, which compared to interior materials, face added challenges of longevity and risk relative to weather ability. In many cases, envelope materials and systems end up with opposing benefit to harm. As an example, high-performance Low E coatings support maximized areas of glass, which mitigate heat gain and support high visible light and views. The trade-off is that many of these products render the glass itself, an otherwise highly recyclable product, not recyclable. And the metals used in these coatings are not environmentally friendly. The list of products within envelope systems having similar trade-offs is ubiquitous. Product declarations for interior products have pushed significant innovations that help achieve higher Indoor Air Quality and use fewer chemicals, but the envelope industry has not been evolving at a similar pace. And there are good reasons for these trade-offs and challenges. Envelope systems hold the highest risk in construction holding the highest incidence of litigation for moisture related defects.

The 2030 Challenge tracks committed firms towards a collective goal of carbon neutrality by 2030. Incremental improvement has been made over the past several years, primarily due to more stringent energy codes. Many states, such as California, are implementing increasingly stringent regulatory requirements for carbon neutrality and low-energy buildings, which outpace advancements in construction practices and innovation needed to achieve these goals. Good building design should always be the first step in achieving high performance design that supports the human experience and well-being as well as our collective environmental obligations. Equivalent products that support higher thermal performance, better daylight and views and are not riddled with hazardous chemicals should be made available, thereby not offsetting the full advancement of sustainable strategy.

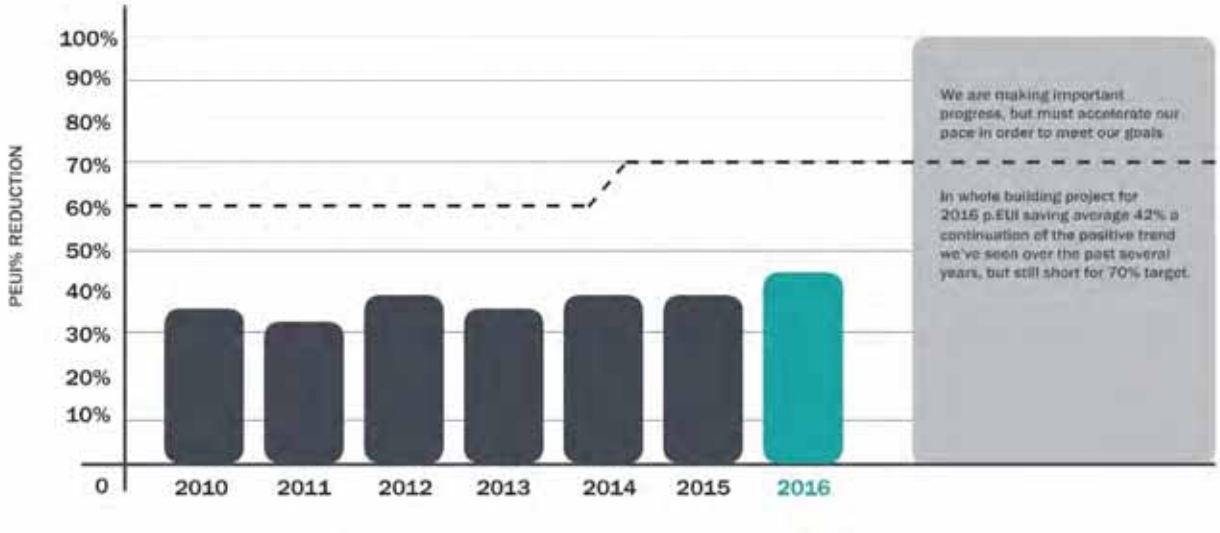


Figure 1: Annual pEUI Reduction compared to the Architecture 2030 target. AIA 2030 Commitment 2016 Progress Report.

Imaginative industry partnerships with shared goals towards environmental stewardships are key to allowing critical and cost-effective innovation to happen. Stephen E. Selkowitz, senior advisor for building science at the Lawrence Berkeley National Laboratory, has aptly drawn the comparison, “We have self-driving cars, why is it we can’t figure out how to cost effectively put exterior operable shading on a building?”

The best projects I’ve worked on within the industry are defined by great teams with shared goals and an undying shared commitment to achieving those goals. I recently attended the Kaiser Southern California Symposium. Kaiser has a goal to reach carbon positive construction by the year 2025. Similarly, the UC system has a goal to be carbon neutral by 2025. Kaiser has undertaken impressive construction partnerships by supporting established companies and some start-up companies manufacturing prefabricated structural systems and envelope systems and products such as dynamic solar control glazing. They see the strong relationship between technology and innovation as a cornerstone of their success in propelling these investments forward. Large-scale investment and a willingness to challenge long-held construction practices and beliefs are what we need to move forward as an industry. The industry is also propelled forward by aspiration and a shared commitment to doing something unusual or has meaning beyond the typical systems on the market. Beyond any individual project aspiration exists a collective aspiration and call to action for supporting a healthy life within our buildings, our communities and our planet.

APPLIED RESEARCH AND EXPERIENCE

The use of wood in curtain wall construction is an emerging trend, and an increasing number of examples can be referenced industry wide. I have worked on several integrated aluminum and wood systems and am inspired to build upon these experiences towards an entirely wood-supported building in the future. What is striking about comparing these experiences is the similarities both in challenges and beautiful outcomes.

A typical approach to long span exterior curtain wall is an aluminum curtain wall framing with secondary steel support. We are increasingly looking through the lens of well-being and routinely benchmarking our project work towards the WELL Building Standard which includes criteria for supporting a healthy state-of-mind. The use of wood supports these connection by reinforcing biophilic connections within the building. The use of wood challenges the convention of metal and glass by evaluating the use of wood as the primary structural support of the glazing. Given the industry's unfamiliarity incorporating wood within typical curtain wall assemblies, this proves to be a challenge for several reasons:

- Interest in bidding: The curtain wall market has been busy making it difficult to draw interest in bidding, especially for smaller scale work.
- A-typical: The use of wood is not familiar to most large-scale builders.
- Cost: The prior two variables drive cost upwards, even though the cost of glu-laminated timber is more cost effective than steel at similar spans.
- Engineering: Wood does not possess the same properties as steel, and in fact its strength varies by species.

TEAM AND PROCESS

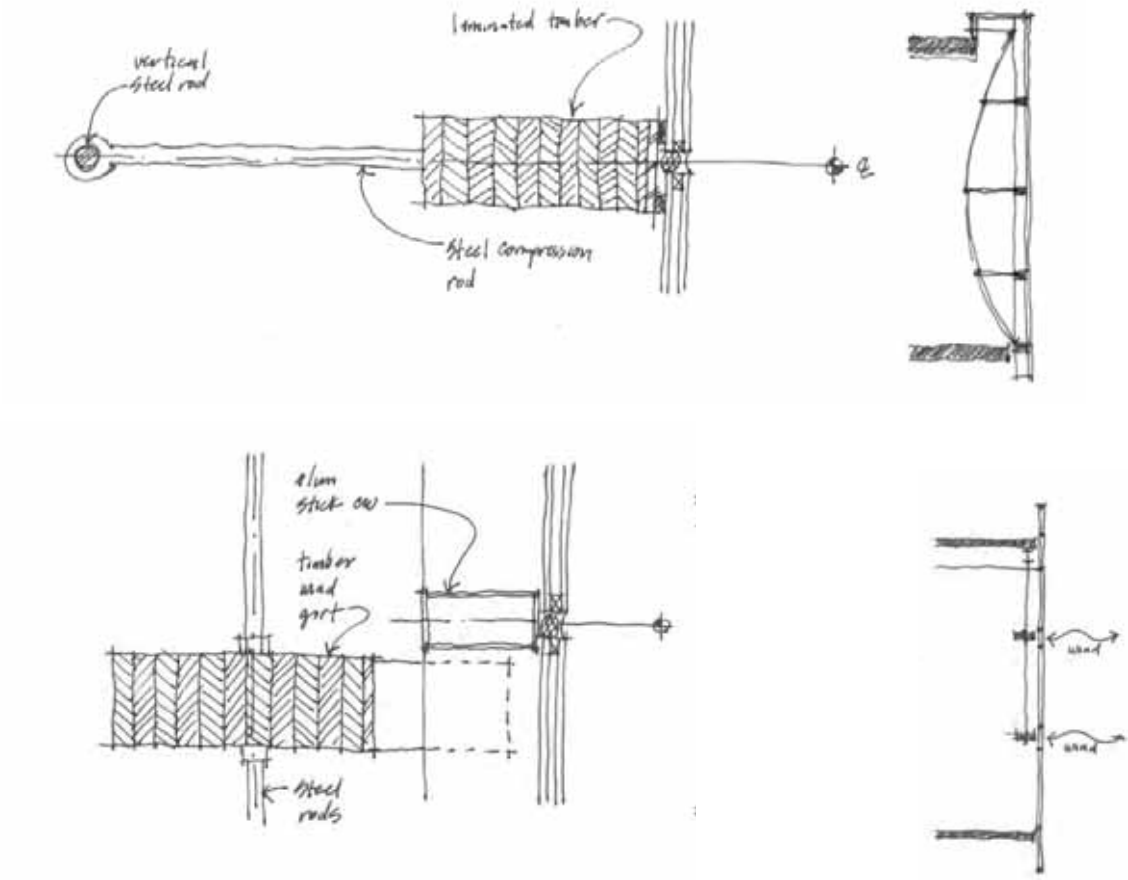
Challenges which I encountered after working on several hybrid wood systems include connecting markets and suppliers and building consensus between them, defining engineering roles and responsibilities, and effectively addressing fire and combustibility concerns. Building a proper team with supportive and knowledgeable industry partnerships is paramount in being able to meet these challenges with clarity. Therefore, it is critical to partner with both an experienced timber/ curtain wall engineer and forestry partners that have an in-depth knowledge of the process and the fluency to ask the right questions at the right time to support success and mitigate risk.

NBBJ teams with a number of qualified façade engineers to support these design efforts evaluating the firm's familiarity in supporting the specific application and goal. NBBJ has also partnered with GR Plume, an architectural millwork firm known for their deep experience within the timber industry. This specific relationship enables our engagement with the forestry industry to understand the timeline of local resources, the chain of custody for timber as it travels from the forest to the plant, and the availability of resources to support a design that is in alignment with those resources. GR Plume has also become a go-to resources for proper water-based and UV resistant finish options to support the longevity and beauty of the material.

Once the design team has been established, we work closely with the curtain wall subcontractor to vet engineering challenges and support the success of the installed and final design.

We evaluate several design options through the lens of the timber's strengths and weaknesses. Most of the curtain wall solutions to date involve some type of hybrid solution. A mix of timber, steel and aluminum is then vetted against all-timber solutions in evaluating appropriate system solutions for the space. This approach allows us to understand the characteristics and strengths of each building material and leverage it to its fullest potential in support of the most cost effective and innovative timber solution that can be delivered within the schedule constraints.

The appropriate application of wood is not a matter of "all or nothing", and it's important to embrace all options moving through the design process. The variables of lateral, seismic and clear span loading of the glass relative to the aesthetic intent begins to define the best application for how and where the wood is most effective. This includes sight lines, available clear dimension within the space, such as adjacent design elements such as stairs, and overall scale of the elements within the space. Hybrid options using wood as the lateral supporting system or as a dead load support combined with more conventional aluminum systems or semi-unitized curtain wall system can yield a more conventional and familiar system design, making the wall a more viable option for cost and schedule.



The wood is an integrated part of the engineered curtain wall system. In one example, the curtain wall subcontractor provides the engineering of the curtain wall and attachments to the glue-laminated timber and the structural engineer of record provides the engineering of glue-laminated timber and its attachment to the primary structure of the building, similar to the use of a more conventional secondary steel system. In another example, the curtain wall subcontractor provided the entire engineering of the composite system, including the wood dead load supports, which transfer the window system loads to the primary structure. With both of these options, the curtain wall consultants worked closely with the full engineering team as the point of intersection and peer review for the system as a whole. Wood suppliers provided design information on the wood and glue-laminated timbers available, and communicated their unique strength characteristics by species to the design team. The availability of wood and species is also a design consideration. Douglas Fir is the standard species used in architectural glue laminated timbers, but there are a range of options available from Cedar to Pine, each species possessing its own characteristics and color, which contributes to the overall palette of materials and aesthetic.

PERFORMANCE CHARACTERISTICS

As in all curtain wall applications, assessing the visual and thermal characteristics of the glazing and shading systems in support of programmatic requirements of the space is another measure for the overall success of a project. Working closely with our mechanical and integrated building system management partners helps support integrated and operable shading control systems. There are many options relative to sensors and controls. Light (clear sky) sensors can be located on the roof, or systems can be regulated from pre-programmable interface with building management systems. The most optimal shading control strategies are exterior shade controls to prevent the heat from getting into the building and control peak cooling loads. Shade technology has been advancing allowing each shade to have its own addressable motor, which maximizes the owner's flexibility in programing the system and gives owners the option of remote programming and software adjustment. In addition to optimizing performance this allows maximum flexibility to control shades relative to orientation and visual control, including the ganging of shades. The electrical coordination of shading systems through curtain wall systems remains a challenge, and is a current silo of responsibilities, making this seemingly simple coordination a challenge on every project. How can our industry better accommodate the increasing availability and development of technology, but

more easily and cost effectively integrate? I've often thought how wonderful it would be to have the option for plug and play electrical systems in off the shelf curtain wall systems.

ADDITIONAL CHALLENGES

Use of timber within Type 1 non-combustible construction within the United States can be challenging from a code perspective, depending on jurisdictions and familiarity with the use of timber within this construction type. Often, fire protection, seismic properties and in certain regions, hurricane force wind resistance are in question. Fire is the easiest to address. Timber is fire resistant. When timber is exposed to fire and heat, the outside will char. The structural engineer takes this char depth into account as they are sizing members. It is also recommended to partner with local fire authorities early in the process, onboarding them to the use of timber prior to permit submission.

In addition to code challenges, the integrated use of timber products within exterior wall systems is equally challenged by lack of familiarity. The glazing industry is built upon glass, aluminum and steel. Introducing unfamiliar materials into the equation drives cost and the perception of risk upwards, which can be managed with the right partners and the right experience.

WHY TIMBER?

The increased use of timber in construction is a growing and robust opportunity. The International Mass Timber Conference was held March 2017 in Portland, Oregon. The event was characterized as "uplifting, passionate and motivated". The use of wood evokes deep passion and motivation within our industry, but why? For one, it's exciting to have technological and structural advancement within an industry that has been fairly constant since wood balloon framing was invented. In addition, the prospect of managing our forests sustainably is the future. It supports the use of wood while avoiding the use of old growth species, instead using young saplings or beetle kill forests. In addition, it creates sustained carbon capture by circumventing the carbon release that occurs at the end of a tree's life through decomposition, thereby reducing greenhouse gas emissions.

Other benefits include:

- Low embodied energy
- Low Thermal Conductivity compared to aluminum or steel
- Support better IAQ
- Support biophilic connections supporting a sense of well-being and health
- Outperforms other building materials Cradle to Cradle

DRIVERS OF TIMBER INNOVATION

Technological advancements now pave the way for cost effective building practices surrounding timber construction. CNC machines and computer technology are meshing and revolutionizing production, which further enables timber products to be produced with smaller diameter/ lesser grade raw materials. This reduces waste and optimizes the quality of milled timber products.

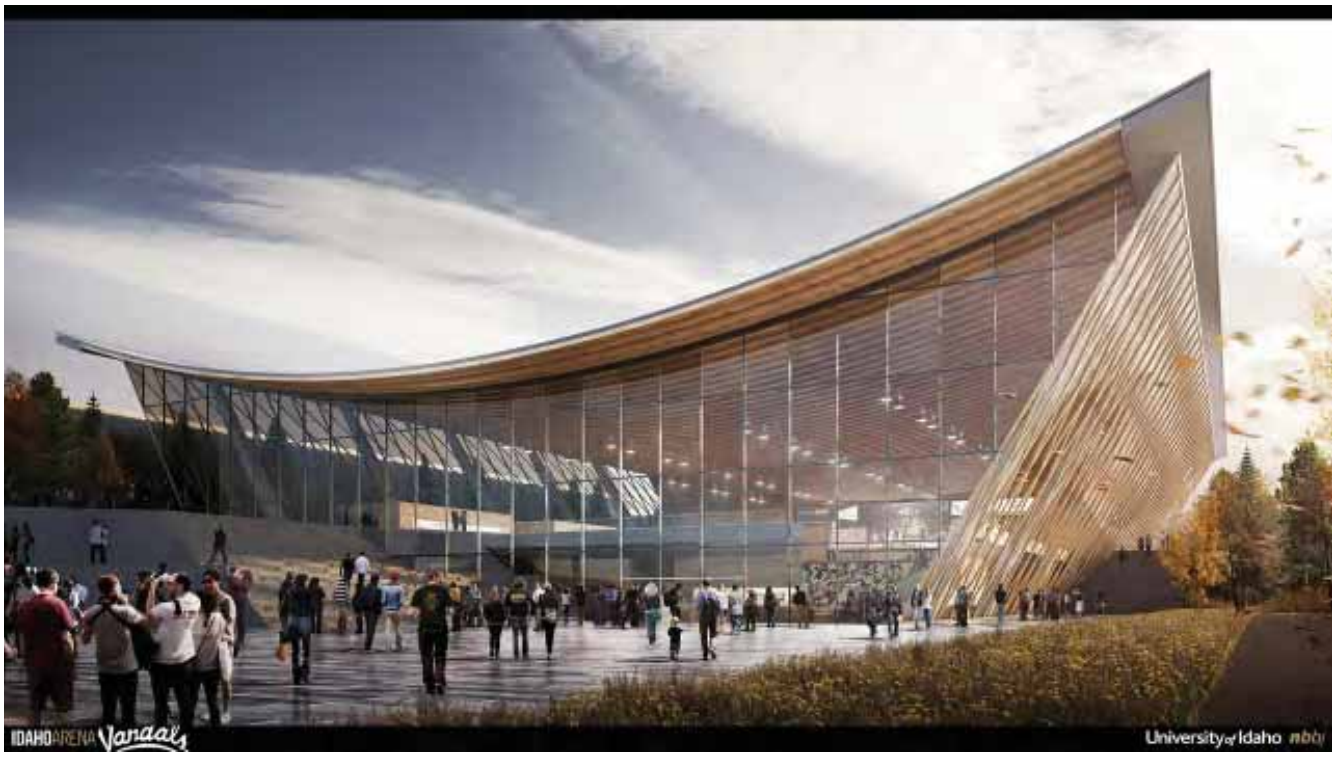
Cross Laminated Timber (CLT) is one example of mass timber. Whereas traditional decking materials spanned in one direction and relied upon nailed planks laid side by side, CLTs provide structural performance in two directions. This increases structural possibilities, reducing the need for beams and creating flat plate structural properties, similar to concrete. Both CLT plants within the US can use fiber should the project go in this direction.

Engineered laminated beams (Glu-lams) are a more traditional timber approach and provide excellent structural/ architectural solutions. Newer veneered solutions on less expensive glu-lam cores maximize yield while supporting the responsible use of beautiful wood. In addition, curved gluing allows the use of a single timber to be sliced into lamination, kept in sequence and re-glued in a curve, so it appears to be one single and seamless member.

Radio Frequency Vacuum Kiln Drying processes make use of microwaves in a near total vacuum to dry timber from the inside out, versus traditional kiln drying methods which dry surface-to-center. This results in a higher quality timber products with reduced tolerances by reducing checking or twisting, and a low moisture content of 12-15 percent.

FUTURE OPPORTUNITY

It's an exciting time to be in practice with the advancement of technology and the prospect of using our natural resources sustainability at a large scale. We had the opportunity to propose on the University of Idaho arena in Moscow Idaho. The campus has a legacy of both teaching and building with timber on campus, giving them a unique perspective and commitment for this construction type. Although not selected for this project, we are able to leverage these past experiences and our in-house research looking forward to our next opportunity and future partnerships towards a fully integrated sustainable timber solution.



Our ability to make informed and sustainable material choices within our exterior wall assemblies is critical to supporting resilient built environments that support a healthy life. The choice to explore wood for these small projects is a calculated decision, not only based upon these specific design parameters, but also a commitment to advance and expand our thinking towards the use of more resilient materials. Our hope it to create a ripple effect for the imperative change needed at a larger, industry-wide scale. Similar to code related energy requirements, only larger scale demand will propel cross-industry advancement and expertise. This will drive innovation towards higher performance, reductions in our carbon footprint, less harmful chemical dependency and beautiful biophilic outcomes. The ultimate outcome will enhance our human experience with respect for our planet.

REFERENCES

2020 By the Numbers: The 2016 Summary of the AIA 2030 Commitmnt, The American Institute of Architects, Web. July 2017, http://aiad8.prod.acquia-sites.com/sites/default/files/2017-07/2016BytheNumbers-AIA2030CommitmentFinal_0.pdf.

Woodworks Wood Product Council, "Why Wood," http://www.woodworks.org/why-wood.

The G.R. Plume Company, "Sustainability," http://www.grplume.com/sustainability.

HYDROPHOBIC STAINLESS STEEL SURFACES

For low maintenance, energy efficient facades



Fred Deuschle
Rigidized Metals Corporation
fdeuschle@rigidized.com



Jim Halliday
Rigidized Metals Corporation
jhalliday@rigidized.com



Mike McGuire
McGuire & Associates, Metallurgical Consulting
mfm304@gmail.com

ABSTRACT

There is no doubting the longevity of stainless steel building facades. The Chrysler Building and numerous buildings that followed have stood the test of time in providing durable facades that can be readily cleaned to restore their original appearance. Cleaning a stainless steel façade can be done with mild detergent solutions.

Stainless steel has impressive solar reflectance, which is roughly equivalent to high performance white paint when measured in accordance with ASTM E1980, alternate method. There is one important difference; unlike paint coatings, as well as aluminum and titanium, stainless steel does not oxidize over time. It therefore provides sustainably superior solar reflectance in the form of a permanent radiant barrier based upon aged SRI data.

The best performance of all comes from the use of hydrophobic stainless steel surfaces that resist the accumulation of dirt, maximizing solar reflectance and minimizing the need to clean the façade. Accumulated surface soil absorbs more solar radiation than it reflects. It is therefore important to keep the stainless steel clean in order to maintain maximum solar reflection. The use of a hydrophobic surface will delay, if not eliminate the need to clean the building's surface. Three stainless steel building roofs installed at least 10 years prior with a hydrophobic surface finish showed no degradation of solar reflectance when SRI measurements were taken.

A hydrophobic surface, as defined by the angle of incidence of droplets, repels water and has low surface tension, which tends not to attract contaminants and rinses cleanly. A permanent hydrophobic surface is achieved in stainless steel by micro-texturing the surface of a mill-finished coil with a surface pattern that has features smaller than the diameter of a human hair. There are several such hydrophobic stainless steel finishes available ranging from dull to bright.

This investigation concludes that maximum solar reflectance of a building façade can be achieved through the use of hydrophobic stainless steel surfaces.

KEYWORDS

energy efficiency, durability, energy and carbon, metal, aesthetics, self-cleaning, low maintenance

INTRODUCTION

It is first important to understand how stainless steel as a building material relates to solar energy, global warming, heat islands, cool roofs and SRI (solar reflectance index). Issues relating to high reflectance roof energy and insulation value were explored in the first phase of the study. The fact is a stainless steel roof has major advantages in both warm climates and cold. A stainless roof provides a degree of insulation value in and of itself, thereby enhancing the performance of insulating systems or even reducing the extent to which the building must be insulated. This allows the designer to make an informed decision to determine the optimal balance of construction versus operating costs.

The investigation centered on roofing surfaces given their ease of access and propensity to accumulate dirt. The translation to façade applications is no less relevant. Solar heat gain is a valid issue in façade applications and solar radiation comes in contact with façade surfaces nearly as much as in the case of roofing.

Stainless steel also has a distinct advantage in that its surface does not degrade. Unlike other metals, including their painted versions, all of which will oxidize, the only degradation of solar reflectance that can affect stainless steel (provided corrosion resistance is suitably matched to the environment) is the accumulation of dirt. Further, hydrophobic finishes of stainless steel are more dirt resistant than others, creating opportunity for minimal degradation of solar reflectance over an extended period of time, which is demonstrated by SRI data collected on hydrophobic stainless steel roofs that are at least 10 years old.

Characteristics of a given stainless steel surface weigh heavily in the solar reflectance equation. Particular attention is paid to hydrophobic stainless steel finishes, which were designed for building envelope applications. While the original objective in developing the first product of this type was to create a uniform low glare finish that would not produce unwanted environmental glare when used in large surface areas, the energy investigation we have undertaken has shown distinct advantages of this finish as it relates to energy performance.

The team investigated the David Lawrence convention center in Pittsburgh, Pennsylvania, which had a hydrophobic stainless steel installed on its roof. Since its construction in 2002, the owner has enjoyed less than expected energy costs in order to heat and cool the building. Data collected from the convention center roof support the notion that the stainless steel roof is a contributor to the building's low operating costs.

The data collected in Pittsburgh indicated there was no degradation of solar reflectance over time. It was surmised that there were not sufficient surface contaminants present to interfere with solar reflection. Since dirt on the surface is the sole means of degradation of solar reflectance in a stainless steel surface of sufficient alloy not to oxidize in a given environment, there could be no other explanation. Admittedly, it would have been interesting to test dirty stainless steel surfaces for comparison, but the presence of dirt on a typical stainless steel surface is an accepted reality and dirt is a widely accepted solar absorber. Incidentally, other stainless steel features on the building, which had a conventional surface polish, showed distinct soiling.

The cleanliness of the roof tested here is what led to the discovery of the hydrophobic property of the tested surface. The lack of dirt on the aged roof's surface was a surprise to the team and an additional investigation was conducted to understand why. To be sure Pittsburgh was not an anomaly, it became important to investigate other sites to collect data. Investigations of roofs at least 10 years of age that had never been cleaned were conducted in Scottsdale, AZ and Bristol, RI. Similar results were obtained.

With a clear indication of three different environments facilitating sustainably clean surfaces, for at least a decade in the three roofs examined, investigators set about understanding why the product, which had been installed on those roofs, stayed so surprisingly clean. Surface characterization and general reading on self-cleaning surfaces quickly revealed the hydrophobic property of the finish in question. Originally designed to be low glare and uniform in appearance, the micro-scale texture actually repels water, achieving a hydrophobic surface similar to that of a lotus leaf. Since stainless steel's chromium oxide layer has rather low surface tension in the first place, the hydrophobic surface (one which limits the degree to which water fully wets the depressions in its surface) effectively reduces the resultant surface tension by nearly half, which causes contaminants to prefer to attach to water droplets than the surface of the metal.

BACKGROUND

Stainless steel, unlike every other outdoor metal people have day-to-day experience with, doesn't get burning hot in the sun. This is counter-intuitive. People are used to metals which oxidize and the oxide coatings have high absorption of solar energy (low solar reflectivity, or low SRI). Stainless steel doesn't behave like normal metal. Its passive film being stable and only angstroms thick, it is not an oxide in the traditional sense, so its surface behaves like a bare metal and reflects incoming electromagnetic energy, including sunlight. This property of stainless steel as it relates to buildings was first recognized on top of the Doha airport roof during the inspection the installation of roof panels made from stainless steel. A representative of the company which produced it was able to place his hand comfortably on the metal surface on a sunny 118°F day. That phenomenon suggested there was more to the story of stainless steel as a building material. As a result of that day, the company initiated a study to understand the thermal properties of stainless steel, and how they relate to energy efficiency, as well as the heat island effect. This effort demonstrates how stainless steel building envelopes save energy and help reduce urban atmospheric temperatures.

The accepted measure of solar reflectance quality of a building material is SRI, solar reflectance index. It differs very little from ordinary reflectance. Because of the preceding analysis on “Cool Roofs,” SRI placed too much value on emissivity, whereas pure solar reflectance is probably a better criterion. Nonetheless the SRI formula is dominated by the solar reflectance factor, so it does no harm. The simple fact is that the less energy absorbed by a roof, and therefore the more reflected, represents the value of the material to global warming, as well as the local environment. Reflected solar radiation escapes to space. Absorbed solar radiation stays within the atmosphere, increasing the temperature of the environment. Increased use of reflective materials will reduce atmospheric temperature.

Self-cleaning surfaces theoretically can achieve their propensity to shed soil in two different ways; either by super- efficient wettability (sheeting action) or by hydrophobicity (repelling water and contaminants). It is the latter phenomenon we discuss here as it relates to micro textured stainless steel surfaces. The claims of self-cleaning for hydrophilic (water sheeting) surfaces have not been demonstrated and must be regarded as dubious, since all other foreign materials would also be attracted to such a surface.

METHODS

SOLAR REFLECTANCE DATA

ASTM E 1980, alternate method for bare metals.

HYDROPHOBICITY

Sessile drop testing.

DATA

10 Year Aged SRI Measurements (ASTM E1980, alternate method).

Stainless steel with hydrophobic surface that was installed in a roofing application for at least 10 years at the sites below were tested in several locations at each site and compared to a clean standard sample of the same product, which had never been put in service, which was also measured for SRI at each site.

Site	Aged Roof SRI	Clean Standard SRI
Pittsburgh, PA	111.6	111.7
Scottsdale, AZ	113.8	114.0
Bristol, RI	113.5	114.0

EXPLANATION

When metals oxidize, i.e. corrode, their surfaces take on the physical properties of the oxide. Oxides have low reflectance and high emissivity. Thus, as metals corrode, their initial superior performance, in terms of SRI, degrades. This can happen quickly. Steel rusts in hours, copper oxidizes in days, aluminum in months. The first stainless steel used in buildings has been there for nearly 100 years with no sign of degradation. Non-metallic materials have their own problems with aging. Coatings are organic chemicals. They are degraded by light (UV, primarily), temperature, abrasion, and chemicals in the environment.

These are aggregated in the term weathering. When materials weather, their SRI and appearance change and not for the better. That is the reason initial SRI values must be accompanied by field tested SRI values after at least three years of weathering.

SRI weathering data have been published on over 1400 commercial coatings. Selected results are in the table below.

Material	**Initial SRI**	**3 Year SRI**
#209 white paint	103	102
#418 white paint	111	105
#425 white paint	109	101
#981 white paint	117	110
#982 white paint	108	102
304 stainless InvariMatte	112	112

Table 1: From www.facilitize.com/.../AdditionalRoofingProducts-w-SRI-Values.xls.

The aged stainless data point is not three year weathering; it is 10 year, taken from the 140,000 square meter roof of the David L Lawrence Convention Center in Pittsburgh. It is clear that even the very best coatings degrade, by an average of 5% over three years. There is no reason to expect that to decelerate. Thus, for a building with a 30-year lifespan a degradation of 50% cannot be ruled out; indeed it should be expected for coatings. Stainless steel changes only as much as the dirt that lands on it and isn't removed by wind and rain.

The insulation savings of high SRI materials can't be justifiably credited to a material, which only saves insulation initially, so an architect must design the HVAC system to account for such degradation.

There are many types of stainless steel based on chemical composition and then there are many surface finishes for each. Both of these factors determine the corrosion resistance and the resistance to soiling in service. The most common stainless steel for architecture is type 304. It fully resists corrosion in non-marine climates. In marine climates, 316, which has 2% molybdenum, an expensive ingredient, is used. In even more severe environments 2003 or 2205 may be used. These latter two have more molybdenum and are harder to form into shapes, but have been used successfully on buildings in the extremely inhospitable climate of the Arabian Peninsula. The selection of the correct stainless is important but not difficult for the many available expert sources.

STAYING CLEAN

Among the high SRI finishes the ability to stay clean varies a lot. Coatings are organic; so, is most dirt. The polarity of organic molecules attracts other polar molecules. Metals have no polarity because of their dispersed electron cloud bonding. This eliminates one type of soiling for metals and accounts for some of the differences from coatings in terms of soiling. The second factor is mechanical damage. Metals are much, much harder than any organic coating so particles of dirt cannot embed in stainless steel when driven by wind and rain.

The last factor is trapping. This is controlled by surface configuration on a micro scale. Most coatings are quite smooth, at least initially, so in this regard they are okay.

MAINTENANCE

Facades can be high maintenance parts of a building, especially as they age. One of the great, unanticipated benefits of the stainless roof on the DLCC is that it has required absolutely no maintenance in its lifetime. It probably never will. This building received a Platinum award from LEED for maintenance and operations. Its management is happy that the roof has never been a source of difficulty. Interestingly, the same 304 stainless with an abraded finish on exterior wall panels has soiled sufficiently that expensive hand cleaning was required for the hosting of the G20 meetings there several years ago.

THE UNIQUE BENEFITS OF HYDROPHOBIC STAINLESS STEEL

Among stainless steels there are important differences with regard to micro-finish and therefore the ability to stay clean. Abraded surfaces are rather jagged on the microscopic scale. They can snag and hold debris. It is preferable to have a rolled surface wherein variations are controlled. The surface the team investigated is 75% planar in the as cold rolled, as-pickled condition. The other 25% consists of smooth depressions spaced to scatter, but not absorb visible light. The depressions are sufficiently shallow and rounded so that they cannot entrap the vast majority of atmospheric dust, soot, ash, etc. Some surfaces rolled to coarser finishes, as in the case of the “Linen” finish, have low energy and small pockets. They don’t have the same avoidance of dirt and precipitates.

In order to understand how this works, we need to accept that molecules like to stick to other molecules. If a surface has very highly-bonded molecules it has a lower tendency to attract other molecules. Surfaces with high molecular stability have low surface energy. The PTFE (Teflon) surface has the very low energy of 18 mJ/m^2. Water has high energy (82 mJ/m^2.) so it minimizes its contact with the surface by beading at a contact angle above 90 degrees when resting on PTFE (Fig. 1).



Figure 1.

The contact angle between the drop and the surface is proportional to the difference in surface energy (Fig. 2). If we want to know the energy of a surface we measure the contact angle of a number of known surface energy liquids on its surface and make a Zisman plot (Fig. 3).

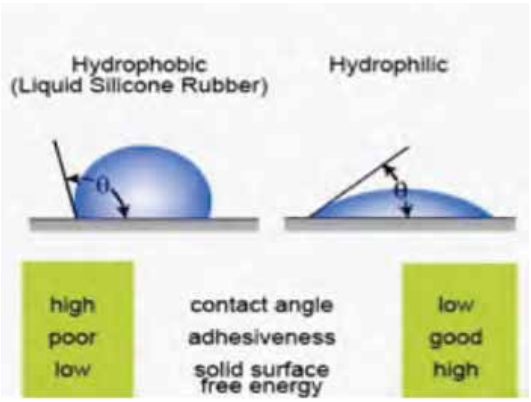


Figure 2.



Figure 3.

The concept here is that a liquid, which spreads on a substrate surface, has the same or lower surface energy of that surface and it will wet it. If a pollutant or soiling agent has lower surface energy than the surface in question, it will tend to stick to that surface. Non-soiling surfaces are low energy surfaces. In terms of stainless steel, water will bead on a common 2B mill finish at an angle of 50 degrees, which equates to a surface energy of 30 mJ/m^2 (Fig. 4).



Figure 4.

Common soils have energy above 30 mJ/m^2, which is why dirt resistant surfaces need to be below that level. Paints have energies above 35 mJ/m^2. Metals do as well. Glass is 83, about the same as water. While the 2B stainless steel finish is respectable enough at 30 mJ/m^2, the popular #4 finish is much worse at 40 to 50, exemplified by a water droplet angle of 35 degrees (Fig. 5).

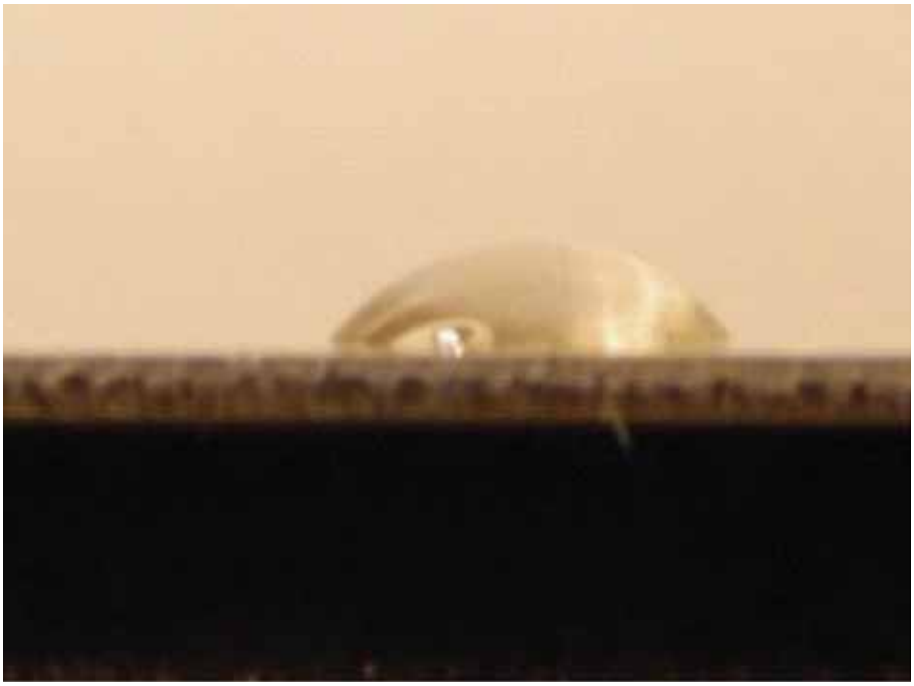


Figure 5.

Surface irregularities can help by preventing contact between foreign liquids or solids and the surface. Grosser irregularities such as #4 polish and Linen finish stainless steel provide varying angles to help increase wetting, which is undesirable.

A hydrophobic surface has a higher contact angle than typical stainless steel surfaces like smooth 2B, #4 or Linen. A water droplet on the stainless steel finish investigated measures at a contact angle of 60 to 70 degrees (Fig. 6). Note the internal reflection of air trapped at the steel/water interface. This hydrophobic surface consists of a high density of micron-sized indentations covering an otherwise very smooth surface. Since drops and dirt can't reach the bottoms of the indentations, they can't stick. Even soot and smoke, which are large enough to settle, are too large to get in. The diameter of a human hair is twice the size on the indentations in this surface.

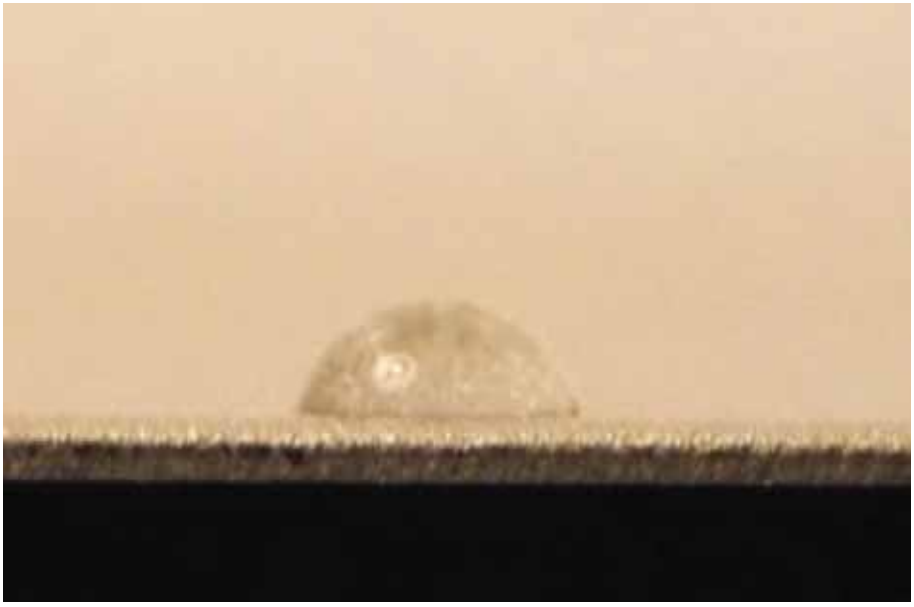


Figure 6.

In contrast, the popular Linen stainless steel finish is readily soiled. Its large, visible texture is more easily soiled than even smooth surfaces with a contact angle of 30 degrees (Fig. 7).

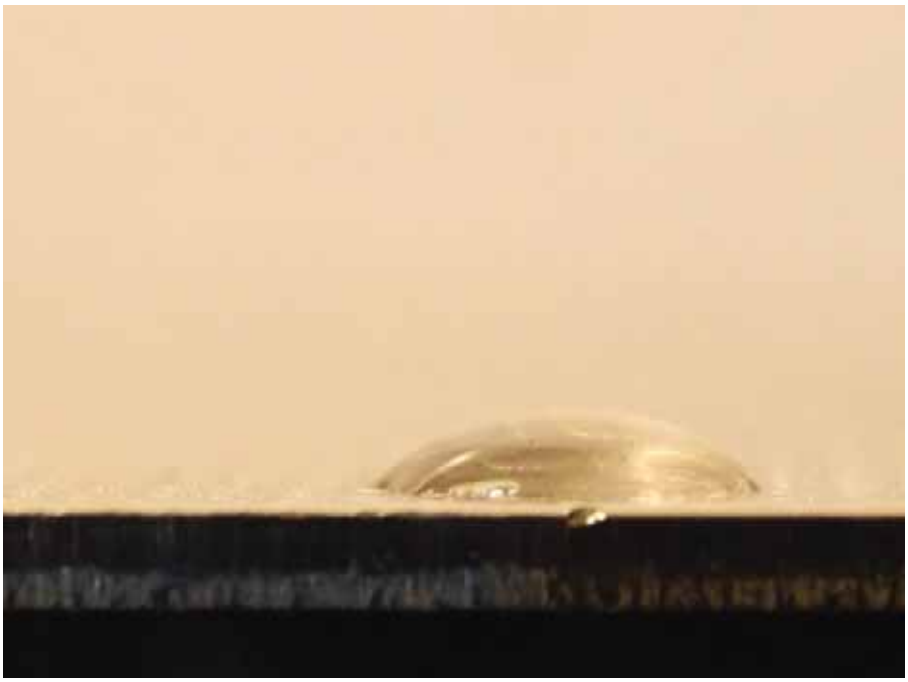


Figure 7.

CONCLUSION AND FUTURE WORK

It is apparent from this investigation that it is possible to build facades that sustain themselves as self-cleaning, energy efficient surfaces that do not degrade over time. Future efforts will focus on aged building envelope surfaces of other types to measure their solar reflectance.

All photos provided by the authors.

SILICONE SPANDREL GLASS OPACIFIERS

Mitigating glass breakage risk from thermal and other stresses



Scott Norville
Texas Tech University
scott.norville@ttu.edu



Chris Barry
chrisbarryglassconsultant@gmail.com



Samir Blanchet
Texas Tech University
s.blanchet@ttu.edu



Lawrence Carbary
Dow Corning Corporation
l.carbary@dowcorning.com



George Torok
Morrison Hershfield
gtorok@morrisonhershfield.com



Stephane Hoffman
Morrison Hershfield
shoffman@morrisonhershfield.com



Kris Vockler
ICD High Performance Coatings
kris.vockler@icdcoatings.com



Timothy Krytenberg
ICD High Performance Coatings
tim.krytenberg@icdcoatings.com



John Swanson
ICD High Performance Coatings
john.swanson@icdcoatings.com



Chris Fronsoe
ICD High Performance Coatings
chris.fronsoe@icdcoatings.com

ABSTRACT

Curtain wall design commonly uses insulating glass units for vision and spandrel glazing to provide better visual harmonization of building façade glass. Risks with this design approach include higher thermal stresses, especially when low-emissivity coatings are used on insulating glass units in spandrel areas. Ceramic enamel frit – commonly used to opacify spandrel glass – is known to induce a bending strength reduction of up to 50 percent. The ability of ceramic enamel frit coated glass to resist thermal stress is similarly reduced. Multiple incidences of thermal stress related fracture have occurred with heat-strengthened, ceramic enamel frit opacified spandrel glass. An increased chance of spontaneous breakage, by nickel sulfide inclusions, may occur if ceramic enamel frit opacified spandrel glass is fully-tempered to withstand the thermal stresses that it is exposed to.

Silicone spandrel glass coatings have been examined as a solution to prevent the strength reduction in heat-treated glass when ceramic enamel frit is applied as an opacifier. Four-point bending tests were used to investigate the flexural strength of coated heat-strengthened and fully-tempered glass. Ball drop testing was used to investigate the impact resistance of coated fully-tempered glass. Silicone coatings have no adverse effect on the flexural strength or impact resistance of the substrate and, in some instances, improve it. Therefore, silicone opacifiers do not reduce the resistance to thermal stress of heat-treated glass. These coatings also provide fallout protection in accordance with ASTM C1048 (ASTM, 2012). This suggests using a silicone opacifier on heat-treated spandrel glass could greatly reduce the risk of fracture resulting from thermally induced tensile stress, flexural stress, and impact related glass breakage in addition to reducing risk of injury from fallout if breakage occurs.

KEYWORDS

Glass strength, silicone opacifiers, ceramic frit, glass performance, architectural glass, design process, codes – standards – ratings systems

INTRODUCTION & BACKGROUND

In the world of façade glass, there are two types of glass: vision, and spandrel. Vision glass is transparent to provide viewing areas for occupants and daylight for the interior. Spandrel glass areas, where slab ends, vents, and mechanical elements reside, are opaque. Since the 1990's, the amount of spandrel glass on a building has fluctuated between 15 and 30 percent of a building's total glass area, as dictated by design trends. Recent energy codes, where the baseline building is governed by lower glazing ratios, have resulted in increased spandrel areas of glazed facades. As a sizable area of a building's exterior, spandrel glass not only contributes to visual appeal, but a building's energy use, since insulating glass (IG) units improve the energy performance of the spandrel area.

Insulating glass units have been used in commercial and residential high-rise construction for many years to increase HVAC energy efficiency, and more recently, in the case of spandrel areas, to provide greater color and visual harmonization between vision and spandrel areas. As vision glass improves – greater light transmission with lower reflectance, plus increased energy performance – with the use of low emissivity (low-e) coatings it can become difficult to visually harmonize façade glass unless the spandrel areas use the same glass configuration.

However, there is a risk associated with using IG units in a closed spandrel area. Most importantly, known to the industry, is thermal stress will increase, particularly in the opacified inboard glass lite. This is primarily due to heat gain that accumulates in the center of the inboard lite as the sun's rays strike it. The increased heat differential between the inboard glass center and its edges, often exacerbated with the use of low-e coatings or by dark colors in a spandrel cavity (Mognato and Barbieri, 2013), leads to thermal stresses which can result in fracture. The accepted rule is that 0.34 MPa (50 psi) hoop stress is created around the edge of a lite of glass for every 0.56°C (1°F) increase in temperature of the exposed area (NSG Group, 2013). Therefore, a center-to-edge temperature difference (ΔT) of 56°C (100°F) will create 34.5 MPa (5,000 psi) thermal stress.

Issues from thermal stress are further aggravated by the use of ceramic enamel frit as a spandrel opacifier. In recent years, there has been increased awareness in the industry that ceramic enamel frit, used as a spandrel coating, lowers the flexural strength of both heat-strengthened (HS) and fully-tempered (FT) glass. The degree of weakening depends on glass coverage, the colors used, and even the formulation of the ceramic enamel frit itself (Maniatis and Elstner, 2016). There are several newly published works that discuss the weakness of various heat-treated (HT) products with an applied ceramic enamel frit opacifier; "full coverage black ceramic enamel…reduced the load resistance (LR) of FT glass and HS glass by approximately factors of 2.0" (Natividad et al., in press) and 37.5% reduction of strength (Krampe, 2014).

In summary: laboratory tests have shown significant flexural strength reductions in both new and artificially weathered glass, in both HS and FT glass, when fully covered with a ceramic enamel frit opacifier. Strength reductions, of approximately 50 to 20 percent have been measured in mean strength and in the 8 per 1000 probability of breakage strength, respectively. Bergers, et al. (2016) attributed the difference between mean strength values and design strength values to the fact that samples with ceramic enamel frit opacifiers have a much lower coefficient of variation (CoV) than clear samples. A lower CoV signifies the difference between values for design load resistance is less than the differences between mean load resistance. It can also be said a lower CoV means there is less spread in the range of results when strength tested.

European product standards EN 12150-1 (2015) & EN 1863-2 (2004) address reductions in flexural strength of HT – HT referring to either HS and/or FT – glasses resulting from the application of ceramic enamel frit. These standards reduce the minimum surface flexural strengths of HT glass from 120 N/mm2 (17400 psi) to 75 N/mm2 (10900 psi) and from 70 N/mm2 (10200 psi) to 45 N/mm2 (6500 psi) for FT and HS glass with ceramic enamel frit, respectively.

The American standard, ASTM E 1300 “Standard Practice for Determining Load Resistance of Glass in Buildings,” uses conservative 2X and 4X multiplying factors for the strength of HS and FT glass, when compared to annealed glass (ASTM, 2016). Since no field-breakage has been reported from flexural stress in enameled HT glass, there has been little immediate incentive to change the published uniform load strength values in ASTM E 1300-16 (2016). Currently, there is no standard available to determine the resistance of glass to thermal loads in insulating glass units.

However, there have been a significant number of thermal stress breakages in HS IG spandrel units with ceramic enamel frit (Barry and Norville, 2015). In all the reported cases, the fracture origin is typically located 13 mm (0.5”) to 25 mm (1”) in from the cut-edge of the glass (Fig. 1). Fracture origins away from the cut-edge are significant because it eliminates glass cut-edge quality as a factor in explaining the strength reduction when heat treated glass is enameled. Significantly, the fracture origin has always occurred on the glass surface in contact with the ceramic enamel frit and *never* on the uncoated glass surface (Fig. 2). This clearly indicates a relatively large reduction of the tensile strength of HS, in-service, glass with an application of ceramic enamel frit.

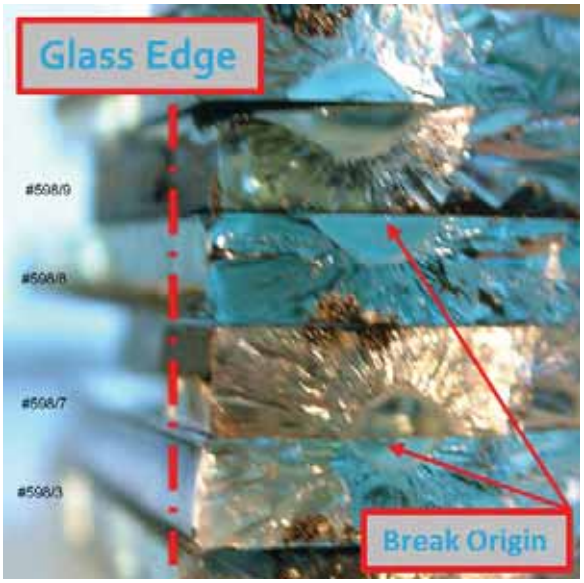


Figure 1: Ceramic enamel frit opacifiers on spandrel glass with thermal stress fractures beginning away from the glass edge.

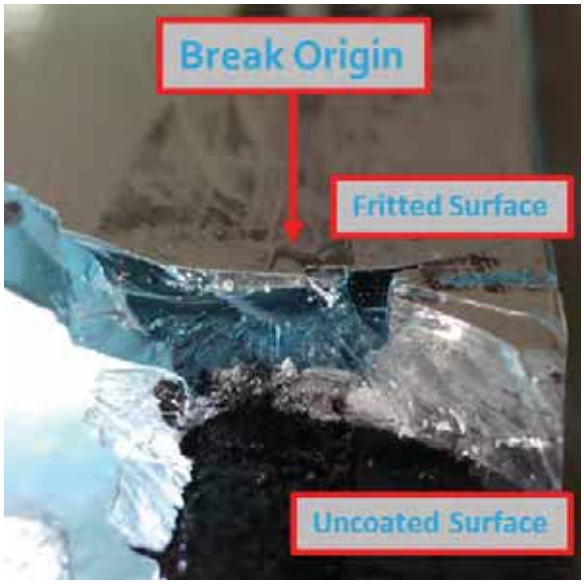


Figure 2: Ceramic enamel frit opacifier on spandrel glass with thermal stress fracture located where frit material interfaces with glass.

In response to the thermal stress failures in the field, FT glass lites have been used in spandrel areas to mitigate thermally induced breakage. However, this mitigation strategy increases the risk of spontaneous breakage from nickel sulfide inclusions in FT glass, unless the glass is heat soaked, with a consequent cost increase. Also, if a FT inboard lite of an IG unit breaks and goes unnoticed, the LR of the IG unit decreases to where additional fracture may occur allowing glass shards to fall from the spandrel cavity. An IG unit inboard spandrel light fracture is often not readily obvious and poses a risk if unnoticed.

As such, there is an increasing need for a spandrel opacifier that does not weaken the glass, but ideally, increases its strength and offers fallout protection. Silicone coatings were examined as a solution to the strength reduction issue created by applying ceramic enamel frit to HT glass as a spandrel opacifier. Investigations were performed using four-point bending and ball drop test methods.

EXPERIMENTAL METHOD

Study and procedure details about the two different experiment methods are defined below – what tools, software or models were implemented, how results were measured, etc.

FOUR-POINT BENDING TEST

Six samples of HS and six samples of FT 102 x 305 x 6 mm (4 x 12 x ¼ in.) flat glass beams were obtained, with each sample comprised of at least 30 specimens (Fig. 3). Heat-treated glass, of thickness 6 mm (1/4 in.), is used because it is by far the most common spandrel glass thickness in current constructions.

SAMPLE	SAMPLE SIZE	GLASS TYPE	COATING
1	34	HS	CLEAR (UNCOATED)
2	33	HS	OPACI-COAT-300®
3	30	HS	OPACI-COAT-500®
4	33	FT	CLEAR (UNCOATED)
5	33	FT	OPACI-COAT-300®
6	30	FT	OPACI-COAT-500®

Figure 3: Samples tested via four-point bending.

Specimens were coated using OPACI-COAT-300®, a water borne silicone elastomer, or with OPACI-COAT-500®, a 100% solids silicone elastomer. All coatings were applied to the air side of the specimen – the side most commonly coated with opacifiers in spandrel glass fabrication. A total of 193 specimens were tested. All coatings were black. OPACI-COAT-300® was applied via spray gun to 330 µm (13 mils) wet film thickness (WFT). OPACI-COAT-500® was applied via roll coat to 150 µm (6 mils) WFT.

Specimens were tested in four-point bending using an MTS machine to provide load at a uniformly increasing rate as per ASTM C 1161-13 (ASTM, 2013). The MTS machine was certified by the American Association for Laboratory Accreditation (ASLA Cert. No. 11455.01) for the basis of the ISO/IEC 17025 international standards for calibration laboratories. During loading, a data acquisition (DAQ) system captured the load-time history from inception of loading to fracture for each specimen. Traditional beam theory was used to convert load-time histories to stress-time histories. Next, using equation 1 (Beason, 1980), each stress-time history was converted to a three-second equivalent fracture stress (σ_3). Finally, each value of (σ_3), was used to determine values for equivalent fracture load (P_3) from traditional beam theory.

$$\sigma_3 = \left[\frac{\int_0^{t_f} (\sigma(t) - RCSS)^{16} dt}{3\ sec}\right]^{1/16} + RCSS \qquad \text{[Equation 1]}$$

Where,

- $\boldsymbol{\sigma_3}$ denotes the 3-second equivalent fracture stress
- t_f denotes the time of fracture
- σ(t) denotes stress at time, t
- RCSS denotes the minimum observed residual compressive surface stress in a sample

All specimens were installed in the four-point testing mechanism with the float glass air side (coated side) facing down (Fig. 4). This orientation induces tensile stresses in the float glass air side and compressive stresses in the float glass tin side during testing. Glass will break under excessive tensile stress. This is true whether glass is stressed mechanically or thermally. The loading supports spanned 254 mm (10 in.) where each glass beam specimen was placed center to center (c-c) allowing 63.5 mm (2.5 in.) between each support and loading point. The four-point bending creates uniform stresses between the inside loading supports' 127mm (5 in.) span.

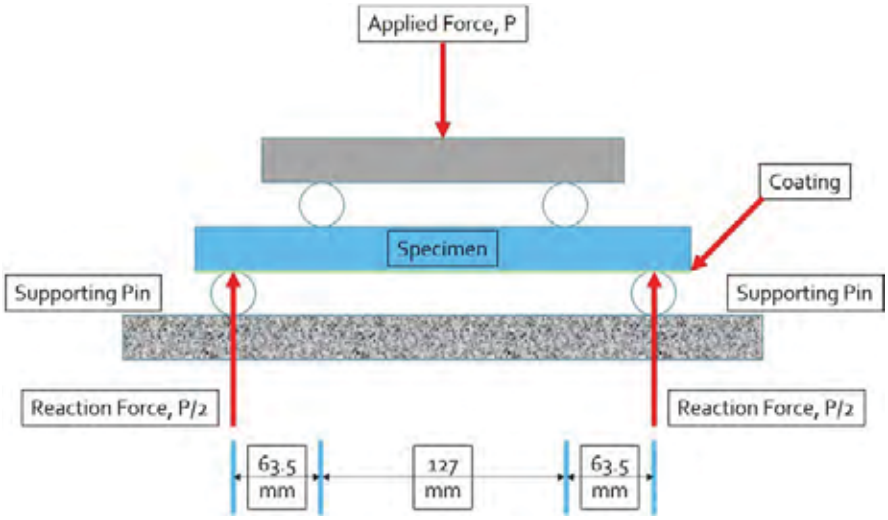


Figure 4: Schematic diagram of four-point bending test.

Once installed each test consisted of loading a beam specimen at a rate of 2.54 mm per min (0.1 inches per min), an equivalent loading rate of 445 N per min (100 lbs per min), while the DAQ system recorded the load and time histories at a sampling rate of 10 Hz. Each test concluded with the fracture of the beam specimen, followed by inspection and measurement.

Using the Maximum Likelihood Estimation (MLE), the σ_3 values were used to fit a three parameter Weibull distribution to obtain cumulative distribution functions (CDFs) for the P_3 using equation 2:

$$P_f = 1 - \exp(-B) \qquad \text{[Equation 2]}$$
$$B = kS_m$$
$$S_m = {\sigma_3}^m A_{surface}$$

Where,

- m, k denote statistical parameters
- B denotes a risk function,
- $\boldsymbol{S_m}$ denotes an equivalent plate area that depends on the magnitude of the tensile stress and the Weibull parameter m
- $\boldsymbol{A_{surface}}$ denotes the surface area

The CDF's allow direct comparison concerning the LR of clear (uncoated) and coated beam specimens of the same glass type. In this work, LR for the glass beams is defined as the constant applied force with 3-second duration that leads to a probability of breakage equal to or less than 8 per 1000. Work by others (Bergers, et al., 2016) has indicated a reasonable correspondence between results from four-point bending tests and full-scale test of rectangular lites.

BALL DROP TEST

Four samples of FT 305 x 305 x 3 mm (12 x 12 x 1/8 in.) flat glass beams were obtained, with each sample comprised of at least 30 specimens (Fig. 5).

SAMPLE	SAMPLE SIZE	GLASS TYPE	COATING
1	34	FT	CLEAR (UNCOATED)
2	34	FT	OPACI-COAT-300®
3	31	FT	OPACI-COAT-500®
4	33	FT	CERAMIC ENAMEL FRIT

Figure 5: Samples tested via ball drop.

Specimens were coated using OPACI-COAT-300®, a water-borne silicone elastomer, OPACI-COAT-500®, a 100% solids silicone elastomer, and with a ceramic enamel frit. All coatings were applied to the air side of the specimen. A total of 132 specimens were tested. All coatings were black. OPACI-COAT-300® was applied via spray gun to 330 µm (13 mils) WFT. OPACI-COAT-500® was applied via roll coat to 150 µm (6 mils) WFT. Ceramic enamel frit was applied via screen print to 38 µm (1.5 mils) WFT.

Specimens were tested in a ball drop impact test frame following the parameters from a GANA Specification (GANA 76-12-10a, 2008), using a 50 mm (2 in.) diameter steel ball with 535 g mass weighing approximately 5.25 N (1.18 lbs).

Samples were loaded into the test frame, float glass air side (coated side) facing down. Impact height was increased until fracture occurred, at which point drop height was recorded and the specimen inspected.

DATA & EXPALNATION

FOUR-POINT BENDING TEST

All specimen fracture origins lay between the load points on the beam specimens, that is, within the area of constant bending moment and flexural stress. No fracture origin was located on the edge of a specimen.

Below is a summary of the statistical results for the samples. Researchers used the minimum RCSS for each sample in calculations described (Fig. 6).

SAMPLE	MEAN P_3 (kN)	STD DEV (kN)	CoV (%)	MINIMUM RCSS (MPa)
1	2.19	0.23	10.5	50.2
2	2.35	0.16	6.67	52.0
3	2.36	0.17	7.26	52.9
4	2.75	0.15	5.48	104
5	2.74	0.16	5.76	104
6	2.77	0.11	3.81	82.6

Figure 6: Sample statistics displaying mean P_3, standard deviation, coefficient of variation (CoV), and minimal residual compressive surface stress of all samples.

The CoVs for samples of HS glass beams coated with OPACI-COAT-300® and OPACI-COAT-500® were relatively small. The small values of CoV led to large and similar values of the statistical parameter m = 17 and m = 18 for Sample 2 and

Sample 3, respectively, which were significantly larger than m = 10 for Sample 1. One can make a similar observation concerning values of m and the CoVs for Samples 4, 5, and 6.

Figures 7 and 8 display the empirical values and CDFs for the P_3 values for HS and FT samples respectively while Figures 9 and 10 present the lower portion of the CDFs for HS and FT samples respectively. The solid blue curved lines in each graph represent the strength expected from HT glass when bought from a typical glass fabricator. Orange and red perforated, curved lines in each graph represents HT glass strength when coated with the OPACI-COAT-300®, and OPACI-COAT-500® silicone opacifiers.

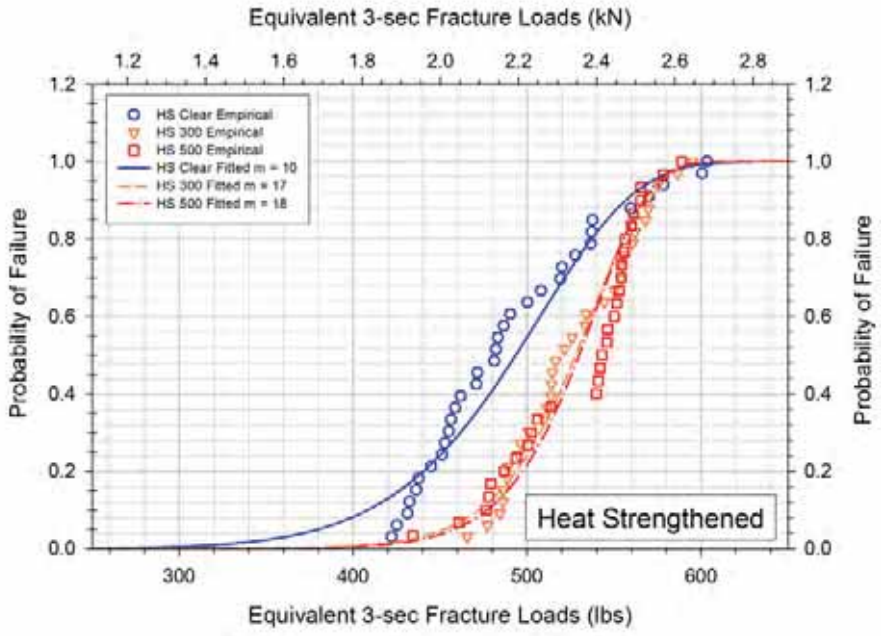


Figure 7: Cumulative distribution function for the probability of failure for clear HS, OPACI-COAT-300®, and OPACI-COAT-500® specimens.

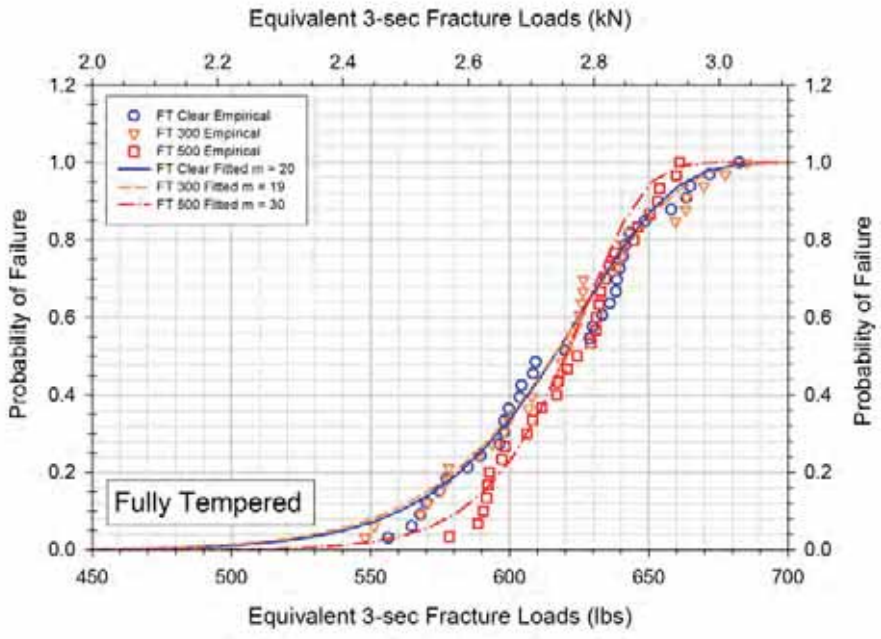


Figure 8: Cumulative distribution function for the probability of failure for clear FT, OPACI-COAT-300®, and OPACI-COAT-500® specimens.

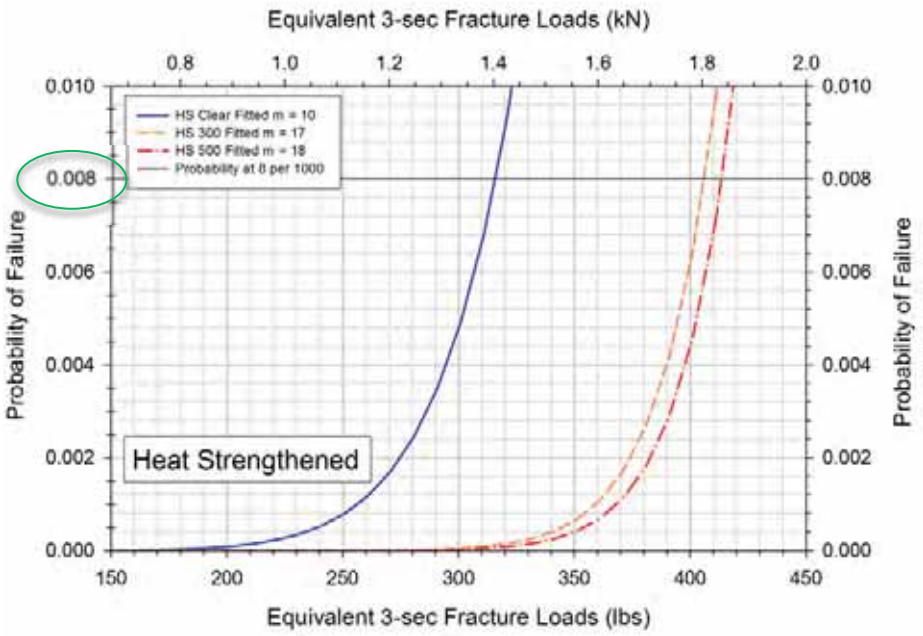


Figure 9: Fitted cumulative distribution function for the probabilities of failure less than or equal to 10 per 1000 for clear HS, OPACI-COAT-300®, and OPACI-COAT-500® specimens.

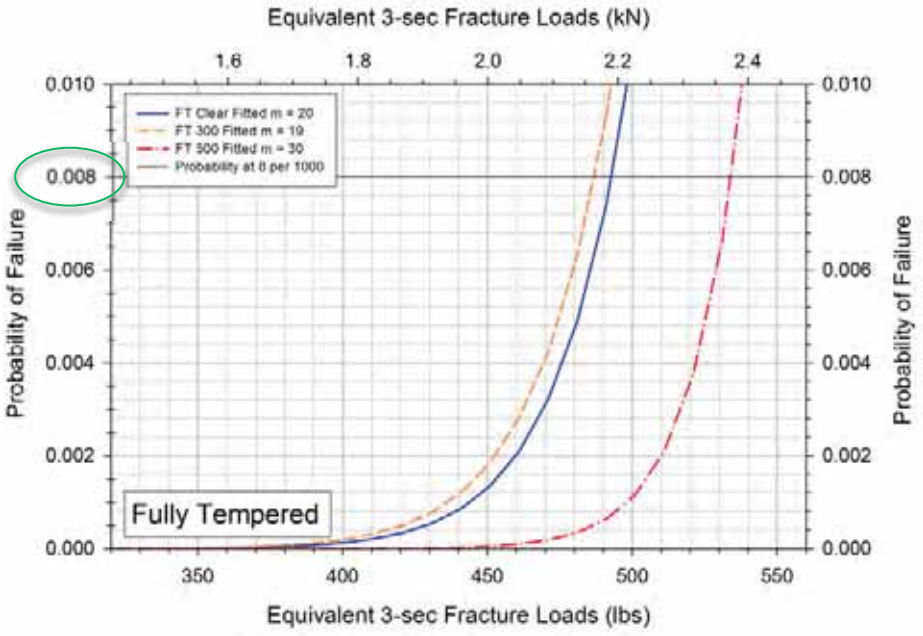


Figure 10: Fitted cumulative distribution function for the probabilities of failure less than or equal to 10 per 1000 for clear FT, OPACI-COAT-300®, and OPACI-COAT-500® specimens.

The CDFs in Figures 7 and 9 indicate that both OPACI-COAT-300® and OPACI-COAT-500® increased the strength of HS glass a statistically significant amount. This is demonstrated in mean P_3 values and most prominently at a probability of breakage less than or equal to 8 per 1000. This data is summarized in Figure 11.

In Figure 11, Samples 2 and 3 are HS specimens coated with OPACI-COAT-300®, and OPACI-COAT-500® respectively, while samples 5 and 6 are FT specimens coated with OPACI-COAT-300®, and OPACI-COAT-500® respectively.

SAMPLE	Δ P_3(%)	Δ LR (%)
2	7.28	28.50
3	7.66	30.90
5	-0.16	-1.20
6	0.75	8.36

Figure 11: Change in P_3 and load resistance (LR) relative to the associated clear samples.

Fully-tempered specimens coated with OPACI-COAT® coatings however do not demonstrate a statistically significant change in either P_3 or load resistance relative to uncoated specimens.

BALL DROP TEST

Figure 12 summarizes the statistical results for the samples while Figure 13 displays the mean fracture height of all samples. Figure 14 shows the statistical values associated with mean fracture heights relative to those of uncoated Sample 1. Figure 15 displays the percent change in fracture height of the sample means relative to that of uncoated Sample 1.

SAMPLE	MEAN HEIGHT		STD DEV		CoV
	(m)	(ft)	(m)	(ft)	(%)
1	1.42	4.65	0.36	1.17	25.3
2	2.13	7.00	0.72	2.36	33.7
3	2.06	6.76	0.84	2.74	40.6
4	0.44	1.43	0.05	0.17	11.8

Figure 12: Sample statistics displaying mean fracture height, standard deviation, and coefficient of variation of all samples.

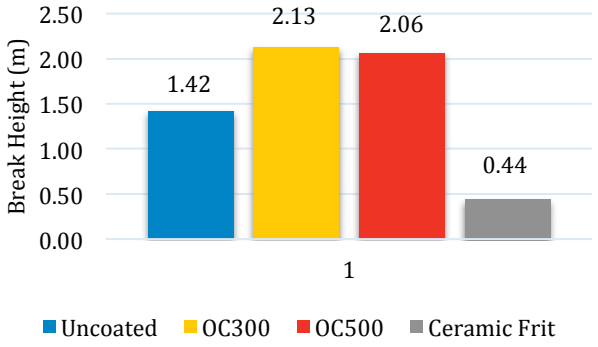


Figure 13: Mean fracture height of coated and uncoated specimens.

SAMPLE	Δ HEIGHT		Δ HEIGHT	P-VALUE
	(m)	(ft)	(%)	
2	0.72	2.35	50.6	$7.9(10^{-5})$
3	0.64	2.11	45.5	$22.2(10^{-5})$
4	-0.98	-3.21	-69.2	$6.1(10^{-14})$

Figure 14: Sample statistics displaying change in mean fracture height relative to uncoated Sample 1, and associated P-value.

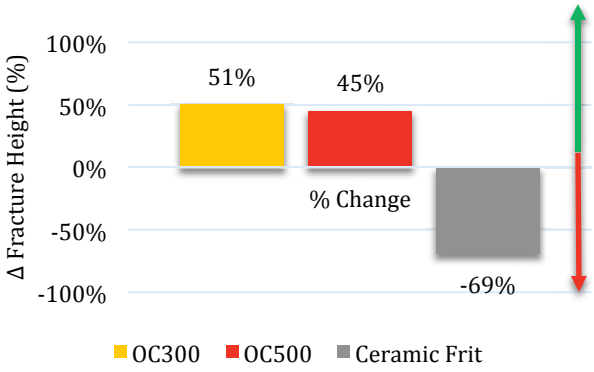


Figure 15: Percent change in fracture height of coated specimens relative to uncoated glass specimens.

Specimens coated with OPACI-COAT-300® demonstrated a mean increase in fracture height of 0.72 m (2.35 ft.) compared to uncoated glass, while specimens coated with OPACI-COAT-500® displayed a similar mean increase in fracture height of 0.64 m (2.11 ft.). This corresponds to increases of 50.6% and 45.5% respectively. Specimens coated with ceramic frit demonstrated a reduction in break height of 0.98 m (3.2 ft.), or -69.2% compared to uncoated glass.

CONCLUSION AND FUTURE WORK

Four-point bending test results indicate OPACI-COAT® coatings have a positive impact on the flexural strength of HS glass, and have little to no impact on the strength of FT glass. Furthermore, ball drop tests displayed a large increase in impact resistance for OPACI-COAT® coated FT glass. Since four-point bending is generally considered a more precise flexural strength testing methodology those results should be given greater weight.

It is clear silicone opacifiers, such as OPACI-COAT® coatings, certainly do not decrease the LR or thermal stress control capability of HT glass, unlike ceramic enamel frit. As such, silicone opacifiers should be considered instead of ceramic enamel frit as a spandrel opacifier when glass breakage from thermal or bending induced tensile stresses, or from impact loads, is a concern.

Further testing should be conducted to explore the applications where increased load resistance and/or impact resistance of silicone opacified HS glass compared to uncoated glass may be important.

REFERENCES

ASTM “Standard Specification for Heat Strengthened and Fully Tempered Flat Glass.” ASTM C 1048-12e1, West Conshohocken, PA, (2012).

ASTM “Standard Test Method for Flexural Strengths of Advanced Ceramics at Ambient Temperature.” ASTM C 1161-13, West Conshohocken, PA, (2013).

ASTM “Standard Practice for Determining the Load Resistance of Glass in Buildings.” ASTM E 1300-16, West Conshohocken, PA, (2016).

Barry, Chris, Norville, H. Scott, “Unexpected Breakage in Ceramic Enameled (Frit) HS IG Spandrels.” IGMA Winter Conference, FL, (Feb 5, 2015).

Beason, William L., “A Failure Prediction Model for Window Glass.” Institute for Disaster Research, Texas Tech University, Lubbock, (NTIS Accession No. PB81-148421), (May, 1980).

Bergers, Matt, Natividad, Kayla, Morse, Stephen M., Norville, H. Scott, “Full Scale Tests of Heat Strengthened Glass with Ceramic Frit.” Glass Structures & Engineering; Springer: Switzerland, Vol. 1, Issue 1, (2016): p. 261.

EN 1863-2 “Glass in Building – Heat Strengthened Soda Lime Silicate Glass – Part 2: Evaluation of Conformity/Product Standard.” BSI, Brussels, (2004).

EN 12150-1 “Glass in Building – Thermally Toughened Soda Lime Silicate Safety Glass.” BSI, Brussels, (2015).

GANA 76-12-10a “Fully Tempered Glass Uses Requiring Strength and Resistance to Temperature – Rev #1.” Topeka, KS, (2008).

Krampe, Philipp. “The Strength of Enamelled Glass.” In Challenging Glass 4 & COST Action TU0905 Final Conference; Louter, C., Ed.; Taylor & Francis: London, (2014): p. 691.

Maniatis, Iris, and Elstner, Michael. “Investigation on the Mechanical Strength of Enamelled Glass.” Glass Structures & Engineering; Springer: Switzerland, Vol. 1, Issue 1, (2016): p. 277.

Mognato, Ennio, and Barbieri, Alessandra. “The Breakage of Glass – Thermal Shock and Nickel Sulfide Inclusion.” COST Action TU0905, Mid-term Conference on Structural Glass; Mocibob, D. Louter, C., Ed.; CRC Press: Boca Raton, (2013): p. 155.

Natividad, Kayla, Morse, Stephen M., and Norville, H. Scott. “Tests of Heat Treated Glass with Full Coverage Ceramic Frit.” J. of Architectural Engineering, ASCE, (In Press).

NSG Group “Properties of Soda-lime Silica Float Glass.” NSG Technical Bulletin #129: http://www.pilkington.com/resources/ats129propertiesofglass20130114.pdf, (January 2013): p. 1.

SPECIFYING COMMERCIAL ALUMINUM FINISHES



Ben Mitchell, MBA
AkzoNobel
Ben.Mitchell@AkzoNobel.com

ABSTRACT

Many factors will influence coating selection, but to achieve the desired performance level for a given situation, coatings must be specified based upon their resin and pigment chemistries. Fluoropolymer resins—which include Polyvinylidene fluoride (PVDF) and Fluoroethylene vinyl ether (FEVE)—are high performers and are the most widely known resin types available to the fenestration industry for both liquid-applied and powder-applied coatings.

The American Architectural Manufacturers Association (AAMA) is the leading trade association representing residential and commercial fenestration. AAMA standards 2603 (for good performance), 2604 (for high performance), and 2605 (for superior performance) are the most commonly referenced coating standards worldwide for painted fenestration products. The AAMA standards describe test procedures and performance requirements for organic coatings applied to aluminum extrusions and panels. The performance tests that are of most concern to end users are adhesion, film integrity and weatherability, particularly UV resistance. Tests that are specific to weatherability measure a coating's color retention, chalk resistance, gloss retention, and corrosion resistance.

Just as coating chemistries are always being improved, testing and assessment methods are continually being evaluated and improved. Task groups will continue to prioritize research into:

- Accelerated testing methods, which include intensifying the amount of natural sunlight on test panels, in order to more quickly deliver useful and accurate weathering data for coatings.
- Best practices in terms of scientific color standards.
- Corrosion definition and testing, with a goal of better correlating real-world coating performance with test results.

KEYWORDS

codes - standards - rating systems, component performance, material science, physical testing - mockups, durability, extreme environments, aluminum

INTRODUCTION

Commercial aluminum wall, window, and roof systems have undergone improvements in recent decades, making them technologically sufficient to meet contemporary standards for sustainability and durability. The performance of these structural systems could, however, be compromised by suboptimal performance of constituents such as the building finish. Coatings used should meet the highest standards established by third-party quality organizations in the fenestration industry—most commonly AAMA.

Designers need to understand basic paint chemistry and the difference between powder and liquid coating application methods. Many factors will influence coating selection, but to achieve the desired performance level for a given situation, coatings must be specified based upon their resin and pigment chemistries. It is also important to understand standard methods of testing coatings and how those tests inform the three levels of performance: standard, super-durable, and hyper-durable (these correspond to AAMA 2603, 2604, and 2605, respectively).

The performance tests that are of most concern to end users are adhesion, film integrity and weatherability, particularly UV resistance. Tests that are specific to weatherability measure a coating's color retention, chalk resistance, gloss retention, and corrosion resistance.

BACKGROUND: AN OVERVIEW OF COATING CHEMISTRY

Whether liquid or powder, coatings are comprised of two principal ingredients: resin and pigment. The most important part of a coating is its resin. A resin binds the coating to the substrate, providing weather resistance and durability. Resin also provides the coating's resistance to abrasion, scratching, and dirt accumulation. Resins used to define paint include:

- Fluoropolymers (PVDF & FEVE)
- Silicone-modified polyesters
- Super durable polyesters
- Polyesters
- Acrylics

Additionally, urethanes and epoxies can be used in primers for adhesion and to improve corrosion resistance.

Fluoropolymer resins are the most widely known resin types available to the fenestration industry for both liquid-applied and powder-applied coatings. They are high performers for exterior weatherability and UV stability. Types of fluoropolymers include:

- Polyvinylidene fluoride (PVDF)
- Fluoroethylene vinyl ether (FEVE)

The resin system is the primary determining factor in many of the performance properties of paint. Different resins contribute to different performance characteristics of the coating (Table 1).

Coating Performance*				
Resin Type	**Acrylics**	**Polyesters**	**Silicone-modified polyesters/ Super durable polyesters**	**Fluoropolymers**
Chemical Resistance	5	4	7	10
Exterior Durability (including color and gloss retention)	4	4	8	10
Hardness	10	8	8	5
Flexibility	4	7	7	9
Mar Resistance	9	7	8	5
***On a scale of 1-10, with 10 being the best**				

Table 1. Coating Performance Attributable to Resin. Image by AkzoNobel.

The second most important part of a coating is its pigment. Pigments are generally organic (with carbon-containing molecules) or inorganic (e.g., ceramic and silica). They provide color and coverage as well as enhance certain physical properties of the coating. Each has particular qualities. Organic pigments are bright, for example; ceramic ones are durable and silica is glossy.

Inorganics, made from metal oxides, have superior color stability and chemical resistance. They are not, however, available in all colors, and sometimes both pigment types are used to achieve a certain color. The selection of pigments is done on the basis of physical needs, durability, gloss, color fastness, and chemical exposure.

TEST METHODS

The American Architectural Manufacturers Association (AAMA) is the leading trade association representing residential and commercial fenestration. AAMA standards 2603, 2604, and 2605 are the most commonly referenced coating standards worldwide for painted fenestration products. The AAMA standards describe test procedures and performance requirements

for organic coatings applied to aluminum extrusions and panels. (They apply to factory-applied organic coatings only.) As defined by AAMA:

- AAMA 2603, "Voluntary Specification, Performance Requirements and Test Procedures for Pigmented Organic Coatings on Aluminum Extrusions and Panels," identifies pigmented organic coatings that will provide a good level of performance in terms of film integrity, exterior weatherability, and general appearance (AAMA 2013).
- AAMA 2604, "Voluntary Specification, Performance Requirements and Test Procedures for High Performance Organic Coatings on Aluminum Extrusions and Panels," focuses on high-performance organic coatings that will provide and maintain a high level of performance in terms of film integrity, exterior weatherability, and general appearance (AAMA 2013).
- AAMA 2605, "Voluntary Specification, Performance Requirements and Test Procedures for Superior Performing Organic Coatings on Aluminum Extrusions and Panels," focuses on organic coatings that will provide and maintain a *superior* level of performance in terms of film integrity, exterior weatherability, and general appearance (AAMA 2013).

AAMA testing procedures include both mechanical tests—for example, the application of loads or abrasive forces—and exposure testing. Some issues, such as coverage, fall within the purview of quality control and are therefore *not* within the scope of AAMA testing.

A few of the many tests required during a coating's research and development include:

- Impact resistance
- Adhesion to multiple substrates
- Multiple pretreatment systems in regional conditions
- Humidity resistance
- Mortar resistance
- Acid resistance

But the most significant factor influencing a coating's performance is its weatherability, particularly its UV resistance. AAMA tests that are specific to weatherability measure a coating's color retention, chalk resistance, gloss retention, and corrosion resistance.

Laboratory tests of painted panels, conducted within cabinets using an artificial light source to simulate sunlight, can provide some measure of a coating's UV resistance. The most complete results, however, are obtained in natural environments that provide exposure to the full spectrum of light in combination with other factors such as condensation, biological growth, and physical erosion that are not recreated in a laboratory cabinet.

AAMA 2603 specifies that weathering testing involve exposing "six samples representing typical products on an exposure rack for one year in Southern Florida at a 45-degree angle facing South . . . . [The] exposure site should be inland at least 3.2 km" (AAMA 2603). AAMA 2604 further specifies that Florida exposure must be south of latitude 27 degrees North and that the panel must be in position for a minimum of five years (AAMA 2604); AAMA 2605 requires the same latitude and specifies that the panel must be in position for a minimum of ten years (AAMA 2605).

Data from weather testing performed in South Florida is considered to be the global "gold standard" of testing data. The subtropical climate in that region provides natural, realistic exposure to product specimens, yet results can be achieved on an accelerated timeline because one year of Florida's sunshine and moisture can equate to several years of exposure on other parts of the globe. The 45-degree south-facing exposure also makes the exposure more severe. The state offers high annual UV, high year-round temperatures, abundant rainfall, and very high humidity. South Florida exposure data are mandatory by AAMA.

Coatings manufacturers typically work directly with a testing lab, conducting a series of tests that will provide the most complete set of data for a given product. Specimens are usually sent to the testing lab directly from the manufacturer's R&D group; the testing lab then conducts the exposures and issues progress reports to the manufacturer. All testing is "blind" so there is no bias in the data from the testing lab. Manufacturers then provide customers with the AAMA test data.

ACCELERATED TESTING

While current standards rely upon Florida data to provide benchmark numbers, in an effort to collect even more data—and collect it faster—testing facilities are branching into different locations and different types of testing. For example, Q-Lab Arizona is a desert exposure facility which offers about 20% more sunlight, higher annual temperatures, and lower humidity than is typical in Florida (Q-Lab 2017). The increased UV and the extreme dry heat make Arizona the ideal location for testing highly durable materials that are intended for use in the drier desert areas of the western regions.

To accelerate the weathering process even beyond what would naturally occur in the intense Arizona climate, Q-Lab uses its Q-TRAC Natural Sunlight Concentrator. Q-TRAC's array of ten mirrors reflects and concentrates full spectrum sunlight onto test specimens. The Q-TRAC system automatically tracks the sun throughout the day in both azimuth and elevation. The combination of mirrors and tracking maximizes the amount of UV exposure that a test specimen receives; data show that the radiation received by test samples, measured in megajoules per square meter (MJ/m2), can be several times greater (on average) in Arizona's Q-TRAC facility than in rack-mounted Florida specimens, depending upon the season and monthly average of sunny days. This results in approximately a two-thirds reduction in the amount of time required for equivalent results. (For example, an extrapolation of data collected during one recent month showed that the amount of radiation achieved in three years of direct 45-degree South Florida exposure was reached in approximately eight months on the Q-TRAC.) This makes Q-TRAC results excellent predicters of a coating's long-term durability (Q-Lab 2017).

COLOR STANDARDS

Two color scales, which exist in order to communicate color values and form the basis for a common measurement of color, are in wide use in many industries: Hunter L, a, b and CIE 1976 L*a*b* (CIELAB). Hunterlab founder Richard Hunter published the Hunter L,a,b color theory in 1938 and the Hunter L, a, b color scale has been in use since 1966 (Hunterlab 2017). The CIELAB color scale was created in 1976 by the Commission Internationale de l´Eclairage (CIE), also known as The International Commission on Illumination. The CIE is an independent, non-profit organization that serves member countries on a voluntary basis and is recognized by ISO as an international standardization body (International Commission on Illumination 2017).

The letters L, a, and b represent pairs of opposites that describe how receptors in the human eye perceive color, as set forth in the Opponent-Color Theory (Hunterlab 2012):

- L scale: Light vs. dark where a low number (0-50) indicates dark and a high number (51-100) indicates light.
- a scale: Red vs. green where a positive number indicates red and a negative number indicates green.
- b scale: Yellow vs. blue where a positive number indicates yellow and a negative number indicates blue.

Together, these three values describe a given color. Colors are numerically mapped on a rectangular coordinate system (Fig. 1).

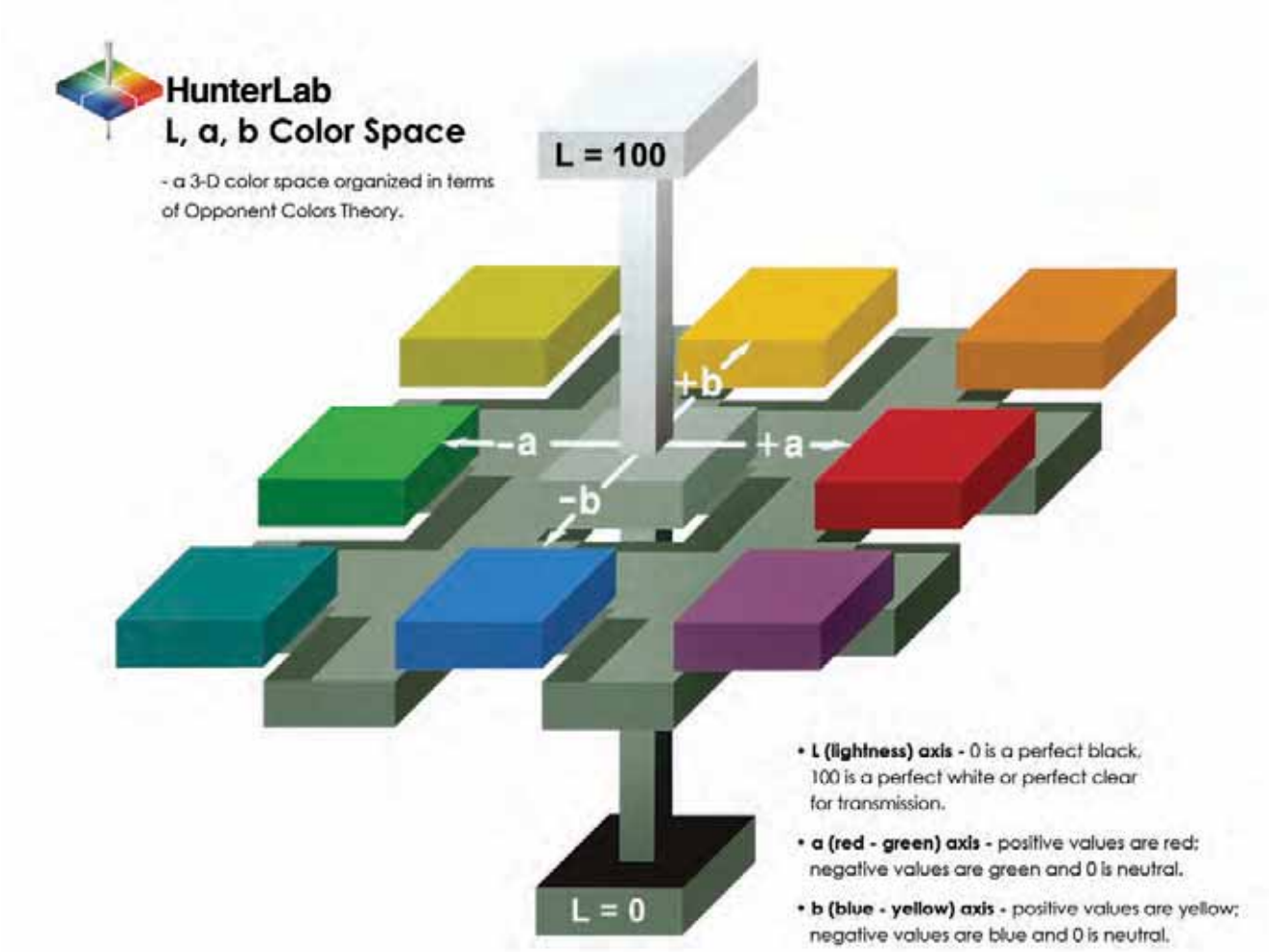


Figure 1: L a b Color Space. Image by Hunterlab.

Whereas L, a, and b values are absolute, being defined by their position on the coordinate system, real-world deviations from a color's absolute value are designated as ΔL, Δa, and Δb. According to Hunterlab, "ΔL, Δa, and Δb values are often used for quality control or formula adjustment. Tolerances may be set for the delta values. Delta values that are out of tolerance indicate that there is too much difference between the standard and the sample" (Hunterlab 2012).

In addition to assessing a color sample for its deviation from a standard lightness (ΔL), standard redness/greenness (Δa), and standard yellowness/blueness (Δb), the sample's overall deviation can be captured in a single value: ΔE. Representing the total color difference, ΔE is calculated based on delta L, a, b color differences and “represents the distance of a line between the sample and standard" (Hunterlab 2016). ΔE provides a single value against which a color sample can be measured for tolerance and one unit is the smallest degree of color change perceivable by the naked eye.

The CIELAB color space—officially written as CIE L*a*b*, with asterisks to differentiate it from the Hunter L, a, b, scale—was created in response to the fact that equal distances plotted along X,Y,Z axes in rectangular coordinates do not correspond to equal differences in perceptual color. CIELAB's coordinates are nonlinear functions of X, Y, and Z, which correspond to the nonlinear functions of the human eye. CIELAB is calculated using cube roots of CIE XYZ and Hunterlab uses square roots (Hunterlab 2012).

The intent of the CIELAB scale was to create a situation in which changes from point to point within the color space exactly corresponded to changes in perceived color. Such uniformity proved elusive, however, since human perception of color is

subjective, varying from person to person based on physiology and psychology. Moreover, each scale performs better in some color conditions than others. "The Hunter L, a, b scale contracts in the yellow region of color space and expands in the blue region. The CIELAB scale expands in the yellow region and this is more obvious when a sample's CIE Z value is less than one. The CIELAB scale generally gives better approximation to visual evaluation of color difference for very dark colors" (Hunterlab 2016). Consequently, Hunterlab measures blues more effectively than yellows, whereas the CIELAB scale measures yellows more effectively than blues and dark colors. This makes it challenging to choose a scale for the standardization of color in the building materials industry.

Given the complexities of creating color standards that closely approximate human perception across the entire color spectrum, multiple color scales are in use industrywide. AAMA began recommending that use of the Hunter scale be discontinued except for legacy users and instead favored CIELAB, referencing ASTM D2244 "Standard Practice for Calculation of Color Tolerances and Color Differences from Instrumentally Measured Color Coordinates." As recently as July 2017, however, a Color Space Task Group assembled by AAMA announced that "per the results of the visual assessment study conducted at the 2016 Fall Conference, members agreed to recommend that Hunter (vs. CIELAB) should remain the color space used in AAMA finish standards and the parameters within that color space should remain at the discretion of [AAMA's substrate-specific] Material Councils" (American Architectural Manufacturers Association 2017).

In general, to ensure color uniformity, AAMA specifies that random samples be visually checked from multiple angles under a uniform light source. AAMA 2505 and 2604 also specify that instrumental methods be used. While buyer and seller are responsible for agreeing upon an acceptable color range for the product, AAMA 2605 and 2604 suggest a maximum deviation of 2ΔE per ASTM D2244, Appendix X1.1. It is also noted that a coating's final, factory-produced appearance may vary from lab samples due to differences in line conditions, for example, so production line samples should be used for all color uniformity tests.

Many gray and silver paints contain mica flakes, which bend light, and/or metallic flakes, which reflect light. Some coating application methods can shear or break the mica/metallic particles. The method of application also influences the orientation of the flakes within the coating layer. Differences in flake size and orientation can cause a paint to appear lighter or darker by several units, making precise color uniformity impractical for those types of paint (AAMA 2605 2011). However, mica/metallic coatings are typically used to mimic anodized metal with its natural variation in appearance; therefore, these coatings are not held to the same standard as a solid paint color. It is recommended that close technical oversight be maintained when applying mica/metallic paints and that architectural components be color matched (rather than running an entire paint order in a single batch) to ensure a consistent appearance between building elements.

Lack of color retention, or "fade," is caused by gradual breakdown of the pigment and can be affected by the loss of gloss. Fade is measured according to Hunterlab or CIELAB color standard scales. A maximum of 5ΔE Hunter units is allowable after the minimum ten-year 45 degree South Florida exposure required for AAMA 2605 and after the minimum five-year exposure test required for AAMA 2604. In terms of real-world performance, uniform fading of four or five units across a surface is not usually an issue because it is difficult for viewers to detect. However, a non-uniform fade is noticeable and unacceptable.

CHALK RESISTANCE

Chalking is the appearance of a powdery substance on the paint surface; it occurs when ultraviolet light breaks down the resin. Chalking will not only cause a lower gloss but make the color appear faded when the pigment may still be durable and performing well. This fact underscores the importance of having the correct durable pigment combined with the correct resin for optimal coating performance. AAMA 2605 refers to ASTM D4214, "Standard Test Methods for Evaluating the Degree of Chalking of Exterior Paint Films," and specifies testing a coated sample panel, which has experienced ten years of South Florida exposure, in accordance with Method A. Also known as the Cloth Tape Method, Method A testing involves using a fabric such as wool or velvet, wrapping it around the index fingertip, then making a 50- to 75-mm (2- to 3-inch) stroke with medium pressure on the coating. When removed, the fabric should be compared with ASTM's Photographic Reference Standard No. 1.

Chalk testing results are rated on a scale of 10 to 1, with 10 being no measurable degradation. A chalk rating of 9 is not noticeable, while a rating of 7 or below can be conspicuous. To comply with AAMA 2605 and 2604 standards, chalking should be no more than a number 8 rating for colors.

SPECULAR GLOSS AND GLOSS RETENTION

The term "gloss" refers to the ability of a surface to reflect, or mirror, light. AAMA refers to ASTM D523, "Standard Test Method for Specular Gloss," which specifies testing using a 60-degree gloss meter. The specular gloss of a new coating should be within +/- five units of the manufacturer's specification.

Gloss loss occurs as a result of resin breakdown, similar to the effect of chalking, and is measured by a percentage of gloss reflectance. Tests should be conducted on both exposed and unexposed areas of panels after weathering testing is complete. To comply with AAMA 2605, the solar reflectance index should maintain a minimum of 50% original gloss after ten years and for AAMA 2604, gloss retention should be 30% after five years.

CORROSION RESISTANCE

To comply with AAMA 2605, humidity resistance is tested by exposing the sample in a controlled heat and humidity cabinet for 4,000 hours at 38°C (100°F) and 100% relative humidity with the cabinet operated in accordance with ASTM D2247 ("Standard Practice for Testing Water Resistance of Coatings in 100% Relative Humidity"), or ASTM D4585 ("Standard Practice for Testing Water Resistance of Coatings Using Controlled Condensation”). Both ASTM D2247 and ASTM D4585 rely on condensation to create humid conditions. However, ASTM D2247 requires the entire specimen to be within the exposure area, allowing condensation to form on all surfaces, whereas the apparatus used for ASTM D4585 involves exposing only one side of the test sample to condensation. Practices outlined in ASTM D2247 are therefore the most common for testing coated architectural components such as panels and extrusions that have complex three-dimensional geometries.

The sample must demonstrate minimal blistering, as shown in Figure No. 4 of ASTM D714, "Standard Test Method for Evaluating Degree of Blistering of Paints." AAMA 2604 requires exposing the sample for 3,000 hours at 38°C (100°F) at 100% relative humidity, and performance measurements are the same as for 2605. AAMA 2603 specifies exposing the sample to 1,500 hours at 38°C (100°F) and 100% relative humidity, with the same performance measures.

Cyclic corrosion testing is conducted in accordance with ASTM G85 Annex A5, "Standard Practice for Modified Salt Spray (Fog) Testing," for AAMA 2605, which specifies scoring the film deeply enough to expose the base metal, then exposing the sample to 2000 hours of dilute electrolyte cyclic fog and drying. To measure corrosion, tape is applied at a width of 20 mm (3/4 inch) over the scored area. When the tape is pulled away, corrosion must rate a minimum of 7 on scribe or cut edges and achieve a minimum blister rating of 8 within the test specimen field in accordance with the following Creepage tables (Tables 2 and 3).

Representative Mean Creepage From Scribe		
Millimeters	Inches (Approx.)	Rating Number
Zero	0	10
Over 0 to 0.5	0 to 1/64	9
Over 0.5 to 1.0	1/64 to 1/32	8
Over 1.0 to 2.0	1/32 to 1/16	7
Over 2.0 to 3.0	1/16 to 1/8	6
Over 3.0 to 5.0	1/8 to 3/16	5
Over 5.0 to 7.0	3/16 to 1/4	4
Over 7.0 to 10.0	1/4 to 3/8	3
Over 10.0 to 13.0	3/8 to 1/2	2
Over 13.0 to 16.0	1/2 to 5/8	1
Over 16.0	Over 5/8	0

Table 2. Rating of Failure at Scribe (Procedure A). Image by AAMA.

Area Failed, %	Rating Number
No Failure	10
0 to 1	9
2 to 3	8
4 to 6	7
7 to 10	6
11 to 20	5
21 to 30	4
31 to 40	3
41 to 55	2
56 to 75	1
Over 75	0

Table 3. Rating of Unscribed Areas (Procedure B). Image by AAMA.

AAMA 2604 and 2603 still test for salt spray resistance in accordance with ASTM B117, "Standard Practice for Operating Salt Spray (Fog) Apparatus." The film is scored as above and then exposed in a closed chamber to an atomized 5% salt solution spray for 3000 hours (to meet 2604 standards) or 1,500 hours (to meet 2603 standards). After the sample is removed from the chamber and wiped dry, a 20 mm- (3/4 inch-) wide tape is applied over the scored area and pulled away. A minimum of 7 on scribe or cut edges and a minimum blister rating of 8 within the test specimen field is required in accordance with the above tables.

Corrosion testing and measurement have been subject to debate and process changes in recent years. The service life of many coatings was found to correlate poorly to salt spray test results, thus the AAMA 2605 switch from salt spray testing to cyclic testing. (ASTM G85 and its annexes represent modifications to ASTM B117.) Furthermore, there is some disagreement regarding which geographic zones qualify as corrosive. Even inland regions sometimes have a high chlorine ion content (as a result of frequent road salt use, for example). Those environments can be corrosive even though they are not coastal, although historic corrosion exemptions in paint warranties have been limited to a distance of 1000 meters from mean high tide.

Task groups are evaluating differences between corrosive testing methods and intend to recommend a replacement to ASTM standards. AAMA 2604 G85 methods are currently being compared to tests conducted by Battelle at its Florida Materials Research Facility, a commercial ocean-front facility for subtropical exposure studies. Classified as “Humid Subtropical” by NOAA, the oceanfront location also has a high concentration of atmospheric chlorine. Test panels are mounted on exposure racks for seventeen months, with sheltered under-eave mounting at 90 degrees east-facing as well as unsheltered (no eave)

mounting at 90 degrees east-facing (Battelle 2017). Tests conducted to date show that sheltered panels, which don't get rinsed by rain, experience more corrosion. These tests are valuable indicators of real-world coating performance; applications that mimic the Florida Materials Research Facility testing apparatus include high-end coastal hotels that both face the oceanfront and feature large protective canopy coverings.

CONCLUSION AND FUTURE WORK

Just as coating chemistries are always being improved, testing and assessment methods are continually being evaluated and improved. Task groups will continue to prioritize research into:

- Accelerated testing methods, which include intensifying the amount of natural sunlight on test panels in order to more quickly deliver useful and accurate weathering data for coatings.
- Color spaces used in finish standards. Determining color uniformity has proven to be an art as well as a science, therefore the Hunter color standard will continue to be used and parameters within that color space will remain discretionary.
- Corrosion definition and testing, with a goal of better correlating real-world coating performance with test results.

ACKNOWLEDGMENTS

AkzoNobel would like to thank the American Architectural Manufacturers Association for their support and diligence in investigating the best procedures for testing the performance characteristics of coatings.

REFERENCES

American Architectural Manufacturers Association. "AAMA 2603: Voluntary Specification, Performance Requirements and Test Procedures for Pigmented Organic Coatings on Aluminum Extrusions and Panels," Schaumburg, IL: American Architectural Manufacturers Association, 2013.

American Architectural Manufacturers Association. "AAMA 2604: Voluntary Specification, Performance Requirements and Test Procedures for High Performance Organic Coatings on Aluminum Extrusions and Panels." Schaumburg, IL: American Architectural Manufacturers Association, 2013.

American Architectural Manufacturers Association. "AAMA 2605: Voluntary Specification, Performance Requirements and Test Procedures for Superior Performing Organic Coatings on Aluminum Extrusions and Panels," Schaumburg, IL: American Architectural Manufacturers Association, 2013.

American Architectural Manufacturers Association. "Visual Assessment Study Finds Hunter Color Space Acceptable." http://aamanet.org/news/amc-conforms-long-and-short-term-objectives-more-at-summer-conference (accessed August 4, 2017).

Battelle.org. "Florida Materials Research Facility." https://www.battelle.org/commercial-offerings/industry-solutions/advanced-materials/florida-materials-research-facility (accessed August 14, 2017).

Hunterlab. 2012. "Measuring Color using Hunter L, a, b versus CIE 1976 L*a*b." Reston, VA: Hunter Associates Laboratory.

Hunterlab. "Brief Explanation of delta E or delta E*." https://support.hunterlab.com/hc/en-us/articles/203023559-Brief-Explanation-of-delta-E-or-delta-E- (accessed August 4, 2017).

Hunterlab. "About Us." https://www.hunterlab.com/about-us.html (accessed August 4, 2017).

Q-Lab. "Arizona Outdoor Exposure Testing." http://www.q-lab.com/test-services/arizona.aspx (accessed August 14, 2017).

Q-Lab. "Q-Trac Sunlight Concentrator Testing." http://www.q-lab.com/test-services/natural-sunlight.aspx (accessed August 14, 2017).

STAINLESS STEEL 101

High performance alloys for architecture



Michael Mulhern
TriPyramid Structures, Inc.
mcm@tripyramid.com

ABSTRACT

This paper presents a summary of the industry advances beyond T304 and T316 austenitic stainless steels. The greater availability of precipitation hardening and duplex stainless steels has increased the material pallet for designers and engineers. However, these materials vary widely in price and applicable fabrication practices. A working knowledge of stainless steel characteristics is required for the successful use of these materials.

The successful integration of stainless steel for architectural elements is challenging. There are well documented cost savings in maintenance with corrosion resistant materials when looked at over a building's full lifecycle. High performance stainless steel alloys afford greater strength than traditional building materials. This results in aesthetic advantages to the designer, however the higher costs and difficulties in fabrication present challenges for the building team. New stainless alloys have been developed for use in other industries. Some of these alloys have advanced material properties that make them applicable in the construction marketplace. In order for these materials to be properly utilized, it is important to understand their benefits and drawbacks.

Building construction is not a primary consumer of stainless steel in the global marketplace. The metallurgical innovation going on today can be broadly classified as follows: the transportation sector desires stainless steel materials with higher strength at lower prices. The development of light, more fuel-efficient vehicles is responsible for innovations such as lean duplex stainless steels (high strength, lower cost). The oil and gas industry continues to press for materials that are extremely corrosion resistant for sour wells. The aerospace sector requires alloys that maintain their strength and corrosion resistance at very high temperatures. Our goal is to provide the reader with a better understanding of how to benefit from these innovations and illustrate the pitfalls/inefficiencies of simply specifying "stainless steel" in bidding documentation.

KEYWORDS

metal, material, new, innovation, façade, unique structure, Stainless steel, life cycle analysis

INTRODUCTION

In 1928 when the Chrysler building was built Krupp Steel in Germany had just begun to produce small amounts of non-rusting stainless steel they called "Nirosta." The steel was developed using empirical methods and a great deal of trial and error (Cobb, 2010). Ninety years later huge advances have been made in both the metallurgy of stainless steels and in the range of alloys available to the user.

Take a walk in most any seaside urban area or in a region where de-icing salts are used and you are likely to see corrosion like that seen in Figure 1. It can be argued that each of these would be in much better shape had the paint and galvanizing been done properly. However, had these been made in readily available stainless steel a failure in craftsmanship would lead to staining, not structural failure. A vast improvement would not require super alloys or being on the cutting edge of stainless steel fabrication.



Figure 1: These painted and galvanized steel guardrails and bollards are past the point of reasonable remediation. Would the owner have been better served had the initial installation been made in stainless steel? Note that the base plate on the left is simple mill finish stainless steel and has held up very well next to the East River in New York City. Photos by the author.

In 2017, there are many applications that benefit from the use of more advanced alloys and sophisticated fabrication techniques. The move from readily available annealed stainless steels to more advanced alloys is generally made for either reasons of increased strength to reduce section area or improved corrosion resistance.

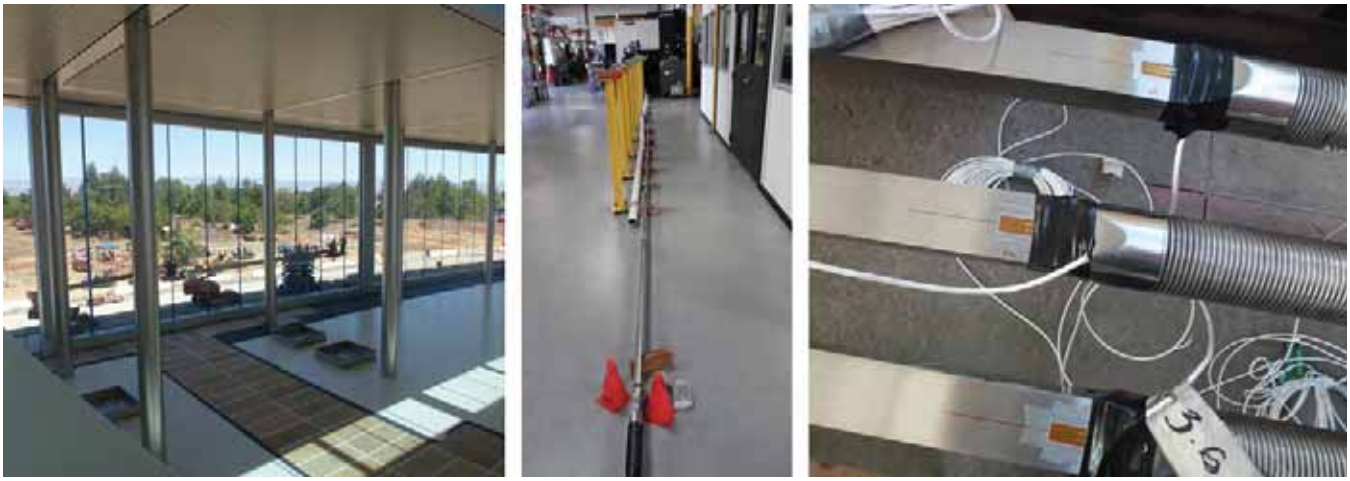


Figure 2: This application would not have been possible without the use of high strength stainless steel. These 40' tall glass panels are stiffened with 17-4PH welded bars in the vertical seams. There was extensive R&D required both for the welding procedures and for the manufacturing technique. Photos by the author.

Our job as designers and engineers is to understand both what is possible and what is practical. There are hundreds of stainless steel alloys listed by steel manufacturers. A large percentage of them have only limited availability or are not suitable for use in commercial and residential construction. While there are a handful of specialty stainless steel that are fruitfully used in architectural applications, there are many applications where the best stainless steel choices are still T304/304L and T316/316L alloys. To understand the proper application of advanced alloys it is essential to have a basic understanding of the nature of stainless steel and the properties associated with the various types.

SECTION 1: STAINLESS STEEL BASICS

Stainless steels are a mixture of iron and alloying materials such as carbon, nickel, chrome, molybdenum, copper, nitrogen etc. The ratio of these alloying elements changes the properties and the cost of the final material. Broadly speaking, the greater percentage of alloying element (except carbon) the higher the costs. Steel alloys with a chromium content greater than 12% are generally classified as stainless steels (Outokump HSS, 2013).

The addition of alloying elements changes the properties of steel at an atomic level. There are a number of complex transformations that occur as the molten alloy is cooled to a solid. In the elevated temperature state the metal goes through phase transformations that yields the grain structure we see in the final material. These transformations are a function of time, temperature, and carbon content. They are different for every alloy. The resulting grain structure is what determines the physical properties of the stainless. These physical properties include strength, strength at high and low temperatures, various types of corrosion resistance, ductility, thermal coefficient of expansion, magnetic permeability, formability,

machinability, etc. Metallography techniques have evolved to the point where we can see the grain structures of metals at a sub-micron level (see Figure 3).

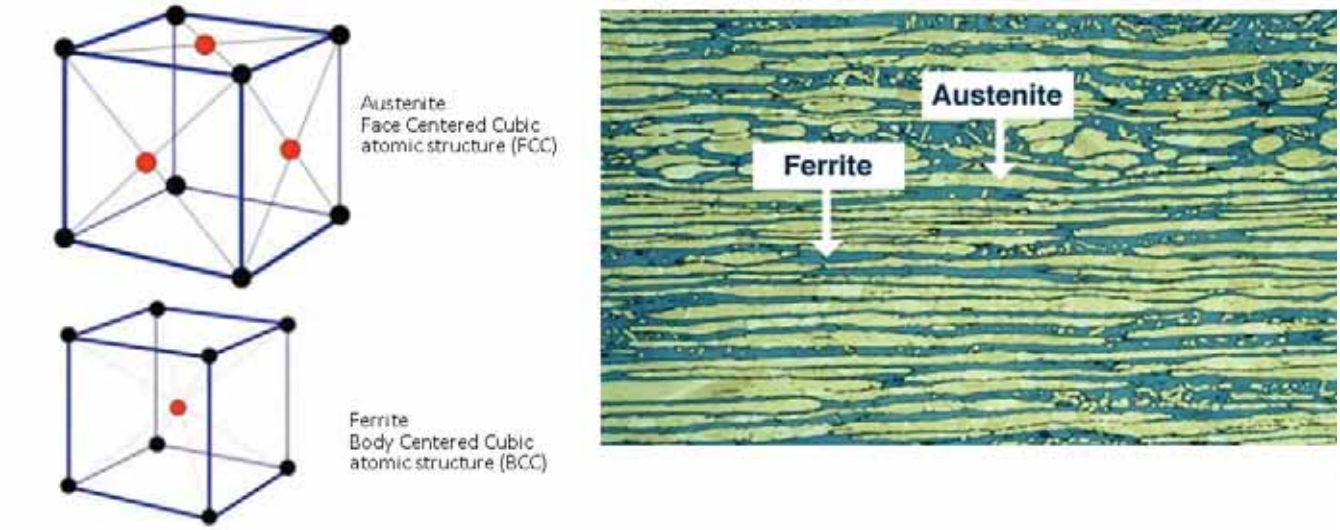


Figure 3: The atomic building blocks of steel alloys are referred to as "phases". The atomic structure of Austenite and Ferrite are shown. The image identifies the crystals of these phases. The technology exists today to predict the structure of alloys without trial and error and to verify the existence and extent of those structures with sub-micron image resolution.

While the specifics of the phases of steel and their atomic structures need not be fully understood by the practitioner, it is important to understand that these different atomic structures determine the material's properties and capabilities. The types of stainless steel are differentiated by their crystalline, or phase, structure. As an example, in Figure 3 you will note that the Ferritic phase is characterized by what is known as a Body Centered Cubic (BCC) structure. Likewise, the Austenitic phase has a Face Centered Cubic (FCC) atomic structure. The nature of the FCC lattice is that it is nonmagnetic. A BCC iron lattice (i.e. the Ferrite phase) is magnetic. Thus, if an alloy is being developed and specified for an application that requires zero magnetic permeability (e.g. use in a super collider) then it is critical that the alloy be designed and processed in a way that precludes the growth of the ferritic phase (Bhadeshia, 2008).

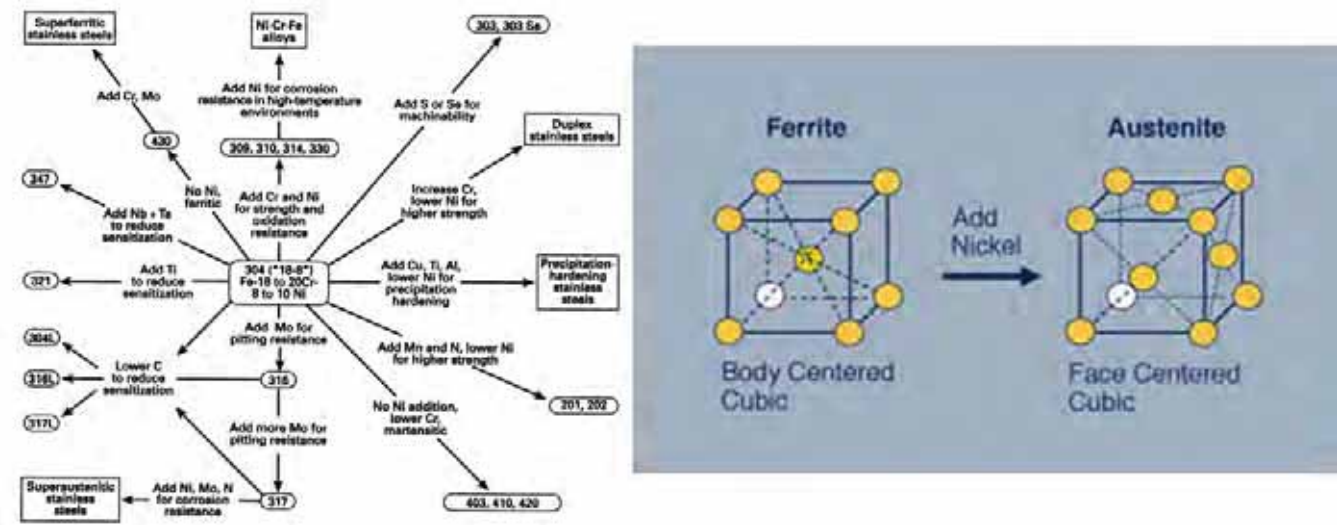


Figure 4: Using the ubiquitous type 304ss as a baseline, we can build a family tree for the various types of stainless steel commonly seen. The addition and subtraction of the alloying metals gives us the diversity of materials available today.

The principal classifications of stainless steels are Austenitic, Duplex, Ferritic and Martensitic. Precipitation Hardening stainless steels are a type of Martensitic so we generally refer to this type as "Martensitic and Precipitation Hardening steels"(Outokumpu HSS, 2013). The grain structure and properties of stainless steel are effected by the time and temperature as the metal solidifies. At elevated temperatures, the martensite phase that characterizes martensitic stainless steels does

not exist in equilibrium state. However, if the material is cooled rapidly from a high temperature the transformation of austenite to ferrite is not completed and martensite is formed. This martensitic grain structure is hard, compact, and has sharp points. This phase degrades the ductility in a stainless steel alloy but it is a very close packed structure which increases the strength of the alloy (Bhadeshia, 2008). Trade-offs such as balancing strength and ductility are the essence of stainless steel development. Each of the four classes of SS have inherently different behaviors. Just as a ferritic stainless steel would be inappropriate for an application requiring no magnetic permeability, the common austenitic stainless steels are highly susceptible to stress corrosion cracking and can be dangerous in high chloride environments such as the support structure in the enclosure for a swimming pool using chlorine as a bactericide.

SECTION 2: PROPERTIES AND PROCESSES DIFFERNENTIATE THE STAINLESS GRADES

A. Corrosion resistance: Stainless steels gain their corrosion resistance from a passive film that develops in an oxidizing environment. This film develops quickly after the stainless steel has been cut or finished. A passivation treatment is not required for the generation of this film. The elements required for corrosion are a disruption of this film, an electrolytic solution, heat, and a lack of free oxygen to redevelop a disturbed passive layer. In architectural applications the electrolyte is usually a chloride in suspension like seawater, deicing salts in slush and spray, or chlorine in industrial and cleaning processes. The higher the nickel and chrome content in a stainless steel the more robust the passive film and the more robust is the healing of the film if it is disturbed (Outokumpu, OCH, 2010).

The types of corrosion commonly seen in architectural applications are as follows:

- Pitting failure/crevice corrosion: These constitute the majority of stainless corrosion problems in this marketplace. The mechanism is that a pit or crevice in the material makes a pocket to capture the electrolyte. The solution is entrained on the surface due to the crevice. The chloride rich solution both breaks down the passive film and inhibits the flow of oxygen over the surface. Without the oxygen for re-generating the passive film the corrosion can accelerate. There are 2 ways to mitigate the chances of pitting and crevice corrosion. The first is to have a pit free finish. The second is to move to a stainless steel alloy with higher nickel and/or chrome content (Houska, 2014) (Honess et al, 2005).
- Stress corrosion cracking: Chloride stress corrosion cracking has been seen in buildings such as swimming pool enclosures. This requires chlorides in relatively high concentrations and components that are highly stressed. Stress corrosion cracking in T304 and T316 can occur at relatively low temperatures, sometimes as low as 30° C (Outokumpu, HSS 2010). The failure is catastrophic. Either more highly alloyed Austenitic stainless steels or Duplex stainless steels should be chosen.
- Galvanic corrosion: Galvanic corrosion occurs when dissimilar metals are in close proximity with heat and an electrolyte. Stainless steel is more noble than all other construction materials thus it is not susceptible to degradation by this mechanism. However, when stainless steel is used in combination with less noble materials such as copper alloys, AL, and plain steel it may be advisable to use an electrical barrier between the materials.

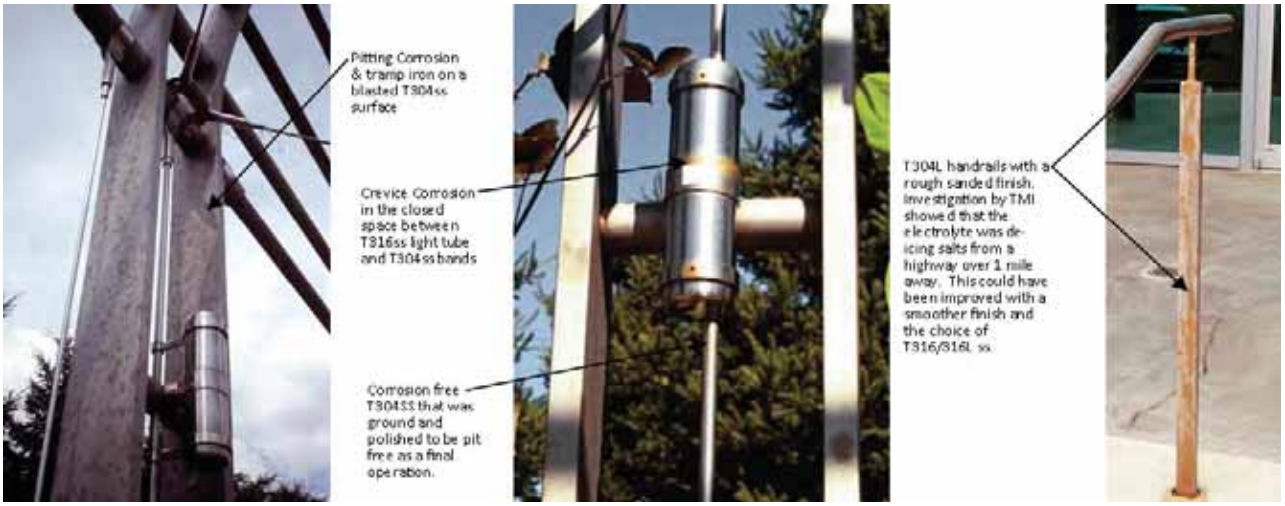


Figure 5: Several types of surface corrosion are shown. Note how critical both the surface finish and avoiding crevices is to the prevention of surface rust. Both T304 & T316 stainless steels are shown and when the conditions are conducive to corrosion each will stain. Photos courtesy of C. Houska @ TMI and the author.

B. Heat and Heat Treatment: As described above, the grain structure (and thus properties) can be altered by time at elevated temperature. For some types, a heat treatment process can be done to purposefully to alter a steel's properties. The addition of heat in processing, either by welding or other means, can have a negative effect on the metal's properties if proper precautions are not followed (Baduuri et al, 1995).

C. Annealing (or solution heat treating): This is the most common heat treatment process. It is a part of the production process for just about all stainless steel grades. After casting and processing most raw steel does not have a homogeneous grain structure. Annealing is a process that re-organizes the grain structure and removes the phases that are not useful to the material's final properties.

D. Tempering and stress relieving: These processes are heat treatments designed to increase ductility and formability in stainless steels. The process varies greatly between alloy types. Typically, they are done at temperatures below the annealing temperature and the heat cycle is followed by rapid cooling (BSSA, 2017).

E. Aging & hardening: These heat treatment cycles increase the strength of a material by precipitating a martensitic phase. This is done in martensitic and precipitation hardening stainless steels. Austenitic stainless steel cannot be strengthened by heat treatment (Outokumpu, HSS 2010).

SECTION 3: STAINLESS TYPES

There are many references available to find the chemical and mechanical properties of all stainless steels. One good guide is the Outokumpu Handbook of Stainless Steel. However most of the alloys listed are not readily available in less than mill run quantities and are not available in a wide range of forms (i.e sheet metal, plate, solid bars, pipes etc). These guides do not give guidance as to what processes may or may not be appropriate for a specific material. Herein is an overview of the defining characteristics of these types and the alloys appropriate for the architectural marketplace.

AUSTENITIC STAINLESS STEEL

The austenitic alloys are the workhorse in the architectural marketplace. Types 304 and 316 stainless steels are the most commonly used and can be found in all forms. The unique properties of this class of alloys are:

- They are generally non-magnetic and very corrosion resistant
- The 200 and 300 grades of stainless steel are both classified as austenitic stainless steels. Although inexpensive, due to low ductility and corrosion resistance the 200 series is not commonly used except for some interior applications like appliances.
- In their annealed state austenitics have relatively low yield strength (206 MPa) but have great ductility. The standard alloys can be readily formed, sheared and punched.
- The austenitic stainless steels cannot be hardened with a heat-treating cycle. However, most can be strengthened with a process called cold work. As the name implies, they can be rolled, drawn, or squished to make a smaller section while the material is cold (i.e. without first heating it). This plastic deformation of the material produces high heat, pressures, and internal stresses in the material. The cold work causes a reordering of the grain structure into a tightly packed austenitic phase and some "strain induced" martensite is produced (BSSA, 2017). The cold worked material will have increased strength and decreased ductility. Due to the formation of the martensitic phase, cold worked austenitic stainless steels can have increased magnetic permeability and decreased corrosion resistance.
    - Note: Some austenitic alloys can be purchased with their strength increased by cold work. In working with "high strength" austenitic stainless steels, welding and hot forming should be avoided. The addition of heat can locally stress relieve or anneal the material. That is, the strain induced matensitic phase returns to an austenitic phase. The result is that the advantages of the cold work may be lost in these zones.
- The standard austenitic stainless steels are susceptible to both crevice corrosion cracking and stress corrosion cracking. For structural elements that will be in a chloride rich environment great care should be used and a switch to a Super Austenitic or Duplex alloy should be considered (Houska, 2014).
- Some of the austenitic alloys are highly susceptible to galling. This is the tearing of material in close bearing contact (see Figure 7).



Figure 6: Austenitic types T304L & T316L used for 50' tall façade mullions. The application was not stress limited so the low strength austenitics were a good choice for these weldments. Note the curl on the upper right image. These plates were pre-cambered to mitigate the effect of the heat induced deformations from welding. To avoid any surface tarnishing the stock was milled and then finished to a fine grain to remove all pits and potential crevices in the skin of the raw plate material. Photos by the author.

A PRACTICAL GUIDE TO AUSTENITIC ALLOYS IN BUILDINGS

Alloy	General usage and Availability	Corrosion resistance	Strength and Strengthening mechanism	Forming and fabricating	Welding	Other Factors
Type 304 and 304L S30400 & S30403 EN 1.4301 & EN 1.4307	This is the workhorse of stainless steels. It is readily available in all forms.	304 will stain in marine and other salty environments. It will keep its luster in most interior applications. 304 is highly susceptible to stress corrosion cracking and crevice corrosion.	The most common condition for this material is annealed with a yield strength of 206 MPA. It can be bought in cold worked conditions with strengths up to 750 MPA.	304 has very good ductility. It draws, bends, punches and shears well when starting with annealed stock.	304 welds well and has many pre-qualified welds. It has a low heat transfer rate which means that heat deformation in welds can be a serious problem.	Cheapest of the commonly used austenitic stainless steels The "L" in 304L indicates that it has very low carbon. When properly welded T304L precipitates very few carbides and does not need to be annealed after weld.
Type 316 and 316L S31600 & S31603 EN 1.4436 & EN 1.4432	Similar to 304 except more chrome and nickel. Available in all forms.	Better than 304 and the recommended alloy for most low strength outdoor applications. It will stain and pit in severe marine environments such as Saudi Arabia and the UAE.	Same as T304	Similar to T304. The increased alloy content means that it machines more slowly than T304.	Same as T304	The increased alloying increases the cost of both the raw material and some forming & fabricating applications. As with T304/304L, the low carbon T316L is a better choice for welded components.
Advanced Alloys						
Nitronic-50 (XM-19) UNS S20910 EN 1.3964	The N-50 is a super austenitic that has twice the strength of T304 both annealed and after cold work. It is available in round bar but most other forms are mill run.	N-50 performs better than T316 in all regards. It is not susceptible to crevice corrosion or stress corrosion cracking in architectural applications.	N-50 has a yield strength of 380 MPa when annealed and up to 1,240 MPa in the cold worked condition. This material is non-magnetic after cold work.	With its high yield strength, this material takes a lot of horsepower to form, but it has good ductility and forms well. It machines more slowly than T316ss.	The alloy can be welded. It has he potential to lose it's cold work when welded and there re few pre-qualified welds or qualified welders. It is not welded often.	N-50 is expensive due to the high amounts of nickel, manganese, and molybdenum. It is a very good tie rod material.
N-60 UNS S21800	N-60 is a specialty super austenitic with very good anti-galling properties. It is available mostly as a round bar product.	For generalized corrosion resistance, this alloy falls between T304 & T316ss.	The N-60 alloy is generally used in the annealed condition with a yield strength of 345 MPa.	N-60 machines at the same rate as T304ss.	Not generally welded.	The primary use for this material is for high strength ss threaded components. 2205 Duplex is sometimes used in place of N-60 since the 2205 is usually cheaper.



Figure 7: Galling of threads is a problem for many stainless steels, especially T304 & T316. Here the super austenitic Nitronic-60 may have been a better choice. This T316ss part suffered a galling failure as it was being installed. This alloy is soft and tears relatively easily. Small bits of dirt or surface roughness can cause mating threads to become bound. When this happens and the installer applies more torque, the thread tears and a curl of torn away material jams in the thread interface and locks the thread (galling). The N-60 alloy was formulated to reduce this behavior in stainless steel. Photos by the author.

MARTENSITIC & PRECIPITATION HARDENING STAINLESS STEELS

The Martensitic and Precipitation Hardening stainless steels depend upon an aging heat treatment to achieve their final properties. For the most part pure martensitic stainless steels are not used in building structures since they do not form well and do not weld well. When properly heat treated, precipitation hardening stainless steels undergo a transformation of the hard and sharp crystals of martensite into structures called pearlite and bainite (Bhadeshia, 2008). By altering the temperature of the aging cycles a range of material properties can be achieved. For instance, in the 17-4PH alloy an aging temp of 480° C (H900) has a very high strength (1,172 MPa) but poor corrosion resistance, poor ductility, and low toughness even at room temperature. In that temper it is only appropriate for a narrow range of industrial purposes and is inappropriate for use in buildings. When it is aged to 620° C (H1150) it has lower strength (758 MPa) but vastly improved ductility, toughness, and corrosion resistance. It is useful in the building marketplace in this condition (Armco, 17-4PH, 1986).



Figure 8: The process development and testing procedure required for welds in heat treated 17-4PH can be complex. In the case of the long tie rods shown earlier in Figure 2, these welds needed to be qualified for both their strength and corrosion resistance properties. Note the heavy corrosion on the exterior surface of the bar after 72-hour salt spray testing. After machining the flats the core of the bar had no hint of corrosion in the HAZ.. Photos by the author.

GUIDE: PRECIPITATION HARDENING STAINLESS STEELS

Alloy	General usage and Availability	Corrosion resistance	Strength and Strengthening mechanism	Forming and fabricating	Welding	Other Factors
17-4PH S17400 EN 1.4542	17-4PH is generally used for component parts of a fitting system that requires decent corrosion resistance and high strength.	For general corrosion 17-4PH performs better than T304ss in the H1150 heat treated condition.	The H1150 heat treat condition is most commonly specified in building applications as it has reasonable corrosion resistance with very good strength. The yield strength in this condition is 725 MPa.	The material can be formed cold (i.e. without pre-heating). It can be softened with a special heat treat before forming if the forming requires large deformations. Formed parts are generally solution treated and aged after the cold work.	17-4Ph can be successfully welded but the welding procedures need to be rigorously developed and tested. Care needs to be taken to maintain ductility and corrosion resistance in the heat affected zone.	The raw material costs for 17-4PH are in the range of T316 ss. However, the costs in fabrication and heat treating can make finished components expensive from this alloy.

FERRITIC STAINLESS STEELS

In the US engineering community, these are referred to as the 400 series stainless steels. These steels do not weld well and in general do not have enough corrosion resistance to be appropriate for use in buildings. These alloys are seen in appliances, cutlery and other non-structural applications.

DUPLEX STAINLESS STEELS

These alloys are stronger than annealed T304 & T316 austenitic stainless steels. They have good corrosion resistance. Many of them have very good ductility and toughness. While the Precipitation Hardening stainless steels are a ferritic-martensitic phase mixture, these alloys are a ferritic-austenitic phase mixture. High quantitates of chromium and molybdenum are added to the iron base in order to achieve this phase mixture (BSSA [DSG] 2017). These alloys require nitrogen as part of the alloying process. The recent development of duplex alloys is due to the increased use of closed induction furnaces in specialty mills instead of the older open furnaces. Controlling the alloying of gaseous elements was very difficult in older furnaces.

Most of the common Duplex alloys are low in nickel content. This lack of nickel divorces the price of the duplexes from the volatility of the nickel market. They machine well and are dimensionally stable as they are heated during welding. When heated, these alloys have a sensitization temperature at which deleterious carbides can develop in the matrix. Thus, care must be taken in welding in order to avoid too much time in this sensitization zone. In general, thin sections can be welded without concern, but multi-pass welds must be planned and carefully monitored. Since these alloys are relatively new, there are not pre-approved welds and most shops are not qualified to weld it without testing and certification. Structural welds must be qualified and special care must be made to keep the interpass temperatures low by means of rapid cooling techniques and careful monitoring (IMOA, 2009). This can be a drawback to the use of these alloys.

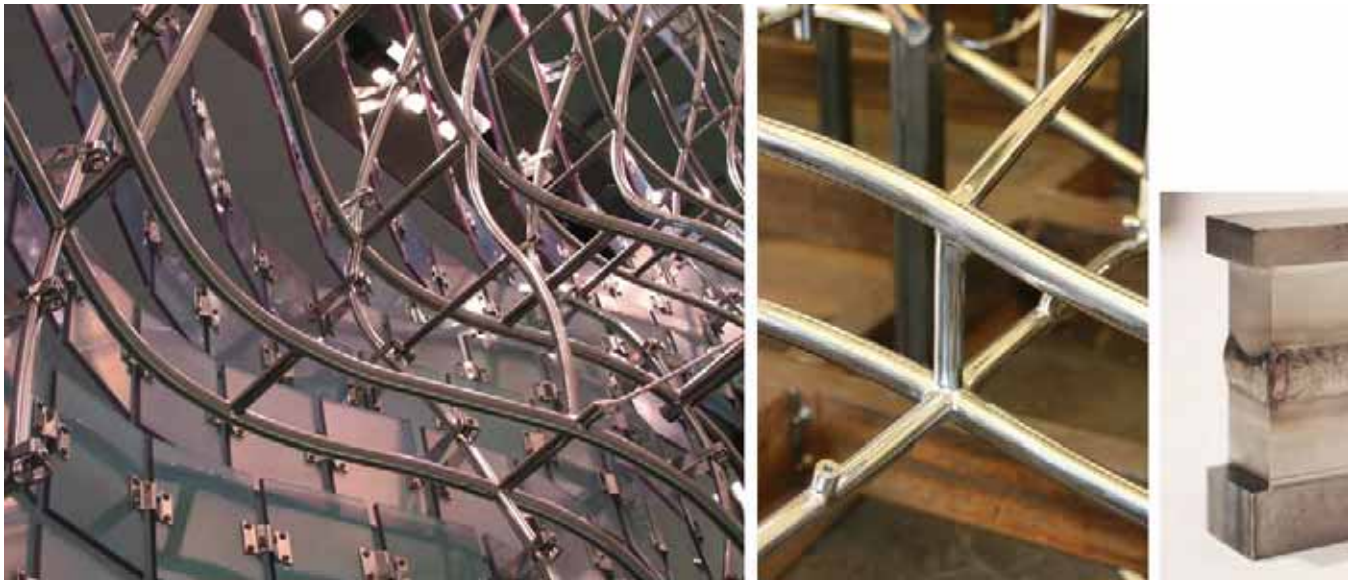


Figure 9: This sculptural frame was produced from 2205 & 2101 LDX Duplex stainless steels to reduce the member sizes.

The welding required testing and monitoring to avoid carbide precipitates and test coupons for all welders. Photos by the author.

GUIDE: DUPLEX STAINLESS STEELS

Alloy	General usage and Availability	Corrosion resistance	Strength and Strengthening mechanism	Forming and fabricating	Welding	Other Factors
2205 Duplex S32205 EN 1.4462	2205 is the most common of the duplex alloys. As of 2017 it is widely available in Europe. Most common sizes of bar up to 4" diameter and plate up to 2" can be found in the USA. Sheet and pipe products are generally hard to find in any quantity but can be ordered in mill runs.	2205 has better corrosion resistance than T316ss. It has been used successfully in hot marine climates like the Saudi and UAE coastal cities. Unlike austenitic stainless steels it is not susceptible to stress corrosion cracking.	2205 Duplex has a yield strength of 435MPA. This is approximately twice that ot T316 in the annealed state.	2205 has reasonably good ductility and forms well. However, there is a lot of spring back in forming so over bending is required.	2205 can be successfully welded but heed must be paid to keep the heat input low and avoiding the sensitization zone for any significant time. Multi pass welds require careful planning and test welds should b checked for reduced ductility in the HAZ due to the formation of carbides. The alloy's very high thermal transfer rate means that deformation during welding is quite small. This is very helpful in close tolerance work.	In the USA this alloy is generally substantially more expensive than T316ss. In Europe, the difference is not near as large so there is some hope that the delta may close here. Some of the increased cost can be offset by the higher yield strength. For strength, limited applications the section area required can be reduced as strength increases.
2101LDX S21010 EN 1.4162	This is a "lean" alloy developed by Outokumpu. It was developed with aim of low alloying content and thus reduced price.	2101LDX has general corrosion resistance similar to that of T304SS. Like 2205, it is not susceptible to stress corrosion cracking.	Same as 2205.	Similar to 2205	Like 2205, 2101LDX can be welded but the weld and the welders must both be qualified and attention must be paid to time in the sensitization zone (Grazinio, 2015).	This alloy is still proprietary to Outokumpu and thus availability can be a challenge. When available it is more expensive that T316SS but not nearly as expensive as 2205.
2507 Duplex S32750 EN 1.4410	This is a "super Duplex" with superior strength and corrosion resistance to that of 2205. It is available in most common bar sizes under 3" and in some plate thicknesses.	Extremely good in all building applications.	The yield strength of 2507 is 550 MPa (2.5 x the YLD of T316ss).	As with the super austenitics, 2507 has good formability but relatively large forces are required to form it due to its high yield strength.	Like 2205, 2507 welds well and is dimensionally stable in the HAZ. As will all duplex alloys, carbide formation should be avoided by keeping interpass temps below the sensitization zone.	2507 is expensive to buy and expensive to fabricate.

CONCLUSION

The demand for stainless steel in global industry has led to the development of new alloys. While most of these are not widely seen in the building arena, some of the new alloys have been designed to be less expensive than the super-austenitic alloys that have been available for many decades. The choice of alloys is complex in that those with the most appealing properties are generally price prohibitive.

Building components in stainless steel will always have a higher upfront cost than those in painted or galvanized steel. Most successful implementations of stainless steels for architectural purposes are justified either by their inherent aesthetic appeal or a life cycle expense analysis. For those designers seeking to use the material, it is imperative to understand what differentiates the various alloys and how to be able to confidently use materials that will serve their purpose over the full life of the project with a minimum of care.

REFERENCES

Cobb, Harold. *The History of Stainless Steel*. ASM International, 2010.

Outokumpu. “Handbook of Stainless Steel.” [HSS], 2013.

Bhadeshia, H.K. “Interpretation of the Microstructure of Steels.” University of Cambridge, 2008.

Outokumpu. “The Outokumpu Corrosion Handbook” [OCH], 2010.

Houska, Catherine. “Stainless Steels in Architecture, Building and Construction: Guidelines for corrosion protection.” Nickel Institute Reference Book Series No 11.024, 2014.

Bhaduri, A.K, S. Sujith, G.Srinivasan, T.P.S. Gill, S.L. Mann. “Optimized Postweld Heat Treatment Procedures for 17-4PH Stainless Steels.” Welding Research Supplement, 1995.

Honess, Colin, Alan Harris. “Importance of Surface Finish in the Design of Stainless Steel.” Stainless Steel Industry, 2005.

BSSA. “Stress relieving heat treatments for austenitic stainless steels.” [AST] http://www.bssa.org.uk/topics.php?article=76 / (accessed 9/30/2017)

Armco Steel. “17-4PH Product Data Bulletin.” BS-82. 1986

BSSA. “Duplex Stainless Steels- A simplified Guide.” [DSG] http://www.bssa.org.uk/topics.php?article=7668 / (accessed 9/30/2017)

IMOA. “Practical Guidelines for fabrication of Duplex Stainless Steels.” International Molybdenum Association, 2009.

Grazinio, Ubertalli, Dinato Firrao, Gianmarco Tiveri. “Characterizationof Welded Joints (MIG and SAW) on LDX 2101.” Procedia Engineering, Volume 109, 2015.

TERRACOTTA 1912 TO 2018

Center Three case study



Carol Loewenson, FAIA, LEED AP
Mitchell | Giurgola Architects, LLP
loewenson@mitchellgiurgola.com



Stephen Dietz, AIA, LEED AP
Mitchell | Giurgola Architects, LLP
dietz@mitchellgiurgola.com

with Heidi Sadler, AIA, LEED AP, and Catherine Vera, RA.

ABSTRACT

Center Three is a 100-year-old, one million square-foot building in Long Island City, New York that was constructed over the course of one year. It was built with concrete frame construction and clad with hand-set, glazed terracotta blocks and large wood-frame windows. The building was erected for the Loose-Wiles Biscuit Company and was known as both the Sunshine Biscuit Factory and The Thousand Window Bakery. It remained a bakery until 1965 when the plant relocated to New Jersey. Between the mid 60's and mid 90's the building was used for storage, back office needs, and an emerging local Community College. In the 1990's the building was purchased by the state of New York and the primary tenant became LaGuardia Community College.

Years of neglect, patching, inadequate and sometimes damaging repairs contributed to exterior wall failures including chunks of terracotta falling from the building. A sidewalk shed to protect pedestrians from falling objects surrounded the building for over a decade while potential solutions were considered. Tear the building down? Replace the façade? If so, with what material? Replacing the entire building was not an option since there was no swing space, nor was there a budget for a new million square foot building.

The decision to select unitized terracotta curtainwall emerged as a response to the unique conditions of the building. The goal was to design a new envelope that respected the long history of terracotta use on the façade, but to employ terracotta using contemporary technology represented by a unitized curtainwall system. The appearance, logistical and detail challenges that arose were significant. Today, standardized panel sizes are mounted to the face of the concrete structure. Installation has been done by crane and monorail with six phases of construction over a 2.5-year period. Over fifty unique glazed terracotta extrusions are integrated with aluminum sunshades and ceramic-fritted insulated glazing to create a high performance sustainable façade that should last another 100 years.

KEYWORDS

curtainwall, unitized curtainwall, sustainability, adaptability, terracotta, case study

INTRODUCTION

The replacement of the exterior cladding of a one-million square-foot building in Long Island City Queens touches on three stories at once: the underlying importance of reinventing 100+ year-old structures in the search for sustainable solutions in the built environment; the remarkable resilience of old buildings and the creativity it takes to re-purpose them over time; and the technical success of using contemporary terracotta as a cladding material in a new way. The project and this paper are at the intersection of these three stories.



Figure 1: Façade undergoing replacement as seen from northeast corner. Photo courtesy of Ashok Sinha.

BACKGROUND

The Sunshine Biscuit Factory was built rapidly, over the course of one year, with completion in December of 1913. Located at the nexus of rail and water transit in Long Island City, Queens, New York, this 1,000,000 square-foot building was part of an emerging economy of large scale manufacturing and transport. Turner Construction, still one of the major players in the construction industry today, was responsible for the construction of this novel reinforced concrete building. The reinforced concrete frame allowed for the speed and incredible breadth of the project (Fig. 2). A relatively new construction method at the time, the reinforced concrete was not built to today's dimensional tolerances or allowances.



Figure 2: Sunshine Biscuit Factory concrete frame under construction in 1912 (left) and at completion in 1913 (right). Photos courtesy of Turner Construction.

Fortunately, the original enclosure and cladding system was forgiving and the large dimensional deviations could be accommodated. Nicknamed the "thousand window bakery," the many large wood framed windows were surrounded by white glazed terracotta blocks, ranging from 4" to 16" high x 24" wide, which were fully mortared and tied directly to the concrete structural frame and masonry infill beyond.

A large electrified sign sat on top of the building and faced north and west. This sign was 35 feet tall and could be seen from as far away as Manhattan. Additional lights were installed within the terracotta wall beneath each window, turning the whole building façade and sign above into a giant billboard. Thousands of people worked in this building and Sunshine biscuits were shipped to and known by people far beyond the borders of New York City.

By the 1950's, the demand for large scale manufacturing buildings was beginning to wane. The Sunshine Biscuit factory gave way to the Executone Systems Building, the sign changed, the façade lights wore out, and eventually Executone was gone as well. Long Island City was no longer a center of manufacturing but rather became a place for large scale and back office storage. With minimal mechanical, electrical, or plumbing infrastructure or vertical circulation, the building was considered a white elephant. On the other hand, it was close to public transit and was close to the nearby immigrant communities of Astoria and Hunter's Point. In the early 1980's the City of New York tried to jump start the creation of a design community in Long Island City by transforming several buildings into the International Design Center (IDC). The rooftop of the Sunshine Building sported the 40' tall IDCNY sign and the entire building next door was transformed into showrooms and meeting places for designers. Unfortunately, the IDC never achieved desired success in the building next door and the only notable transformation at the Sunshine Building was the sign.

In 1971, LaGuardia Community College was founded in Long Island City. Committed to serving its local immigrant community, the school grew rapidly and became a major tenant in the building. The New York State Dormitory Authority took ownership of the building in 1998 and did its best to maintain the original structure and façade that had been largely neglected for nearly 80 years. Large portions of glazed terracotta were chipping, and the wood framed windows were beginning to fail (Fig. 3). Some windows were replaced, and the façade was coated with a sealer that simply accelerated the terracotta failure.

At that moment, the building was at a tipping point. Was it time to tear down the tired, failing vestige of another era, or could it/should it be saved?



Figure 3: Deterioration of original terracotta façade. Photos by Mitchell Giurgola.

A Master Plan study was commissioned in 2010 that showed how the interior could be transformed to a contemporary, state of the art, education facility. Further, a façade replacement study showed that there were several viable options for the exterior. The fact that the building was a key part of a community in transition justified not tearing it down, but equally compelling was the argument for a sustainable solution. Instead of demolishing the massive structure, the embodied energy of the existing building could be re-used. Thus, the new Center Three was born.

METHOD

Once it was decided that the building would remain and be re-clad, discussions began regarding what this new façade should be. Major issues included:

- Material – Should glass, metal and terracotta be the palate or something altogether new and different?
- Design – Should the appearance of the large white highly articulated building be maintained?
- Energy Efficiency – How to make the new façade as energy efficient as possible?
- Construction Method – Should the building be contemporary unitized, handset, or stick built?
- Standardization – How could components be developed that could be repeated across a highly variable façade?
- Phasing – How could the building be kept fully operational throughout the exterior wall replacement process?

After looking at many material recladding options, the design team and client all agreed that terracotta and glass was the right solution. After additional consideration, including consulting with the construction manager who aided in the pre-construction buildability process, the design team and client also agreed that a unitized curtainwall system would be the basis of the re-cladding strategy. By embracing the material of terracotta, the design would evoke the past, but by utilizing contemporary curtainwall panels the design would also engage state-of-the-art technology. Even more importantly, it was agreed that a façade of varying depths, setbacks, and overhangs would be designed to provide the play of light and shadows that made the original facade so visually successful at both the large, urban scale and the more intimate, human scale. These decisions, to install contemporary terracotta panels on a unitized curtainwall to achieve maximum depth and variation, established key design challenges for the team.

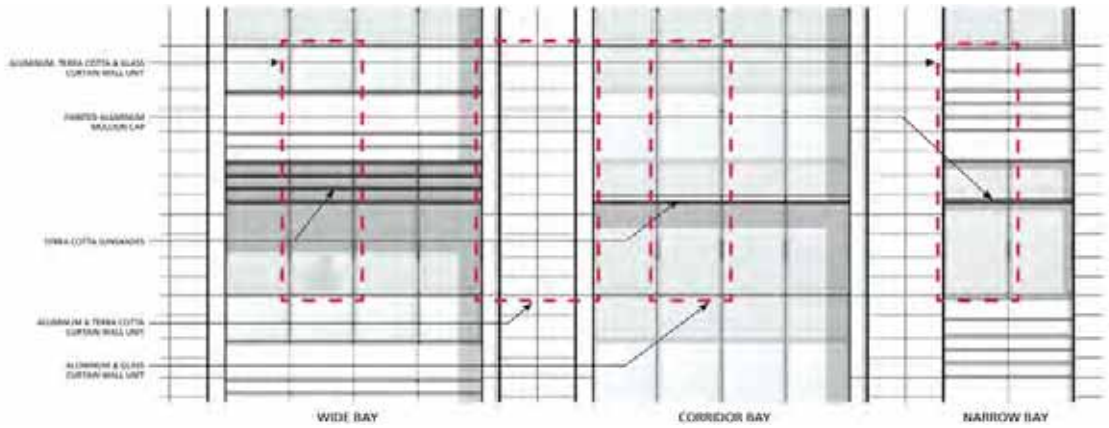


Figure 4: Façade bay types. Diagrams by Mitchell Giurgola.

First, the irregular structural bays of the original design combined with the speed with which the building had been erected, produced literally thousands of inconsistencies in dimensional relationships between the existing components (Fig. 4). Despite the complexity of the existing conditions, the allure of a fully engineered and factory sealed system that could be brought to the site and quickly and easily assembled proved too great to resist. Since the College is extremely active year-round, it was also highly desirable to keep on-site work to an absolute minimum. With this understood, the design team began developing highly-engineered, high-performance, standardized curtainwall units that could easily align over the top of the various existing conditions.

Second, contemporary terracotta is most commonly used and assembled in relatively flat, uniform panels that are edged-captured in metal. The three-dimensional qualities of the building's original hand-set terracotta with deviations of over 18 inches simply weren't replicated in typical contemporary applications. The design team, in concert with the façade consultant, terracotta manufacturer, and curtainwall manufacturer, worked together to develop new shapes and assemblies that could be used to create a dynamic and complex façade which emphasized depth and shadow.

Additionally, large tolerances of the existing concrete frame conditions had to be reconciled with the precision of factory assembly. And while variation and articulation in the façade was desired at multiple scales, it was crucial to establish repetition to enable standardization of both the curtainwall units and individual terracotta panels.

Finally, an approach to standardized panel recladding was developed to ensure that the building could remain fully operational throughout the construction process. This required careful sequencing of façade removal, temporary wall enclosure, new panel installation, and temporary wall removal (Fig. 5).

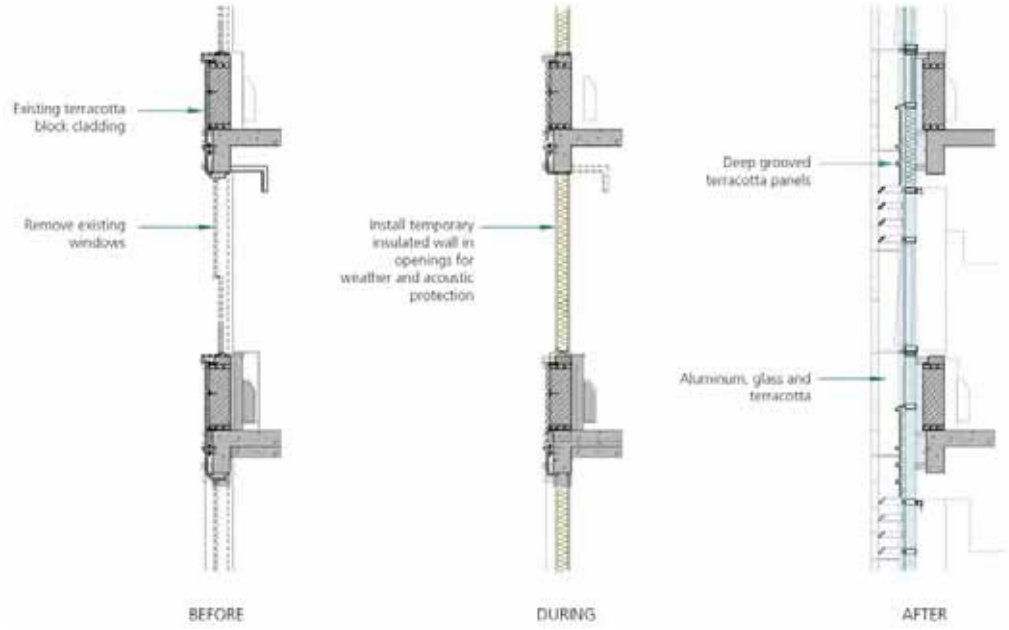


Figure 5: Process for recladding: before, during and after installation. Diagrams by Mitchell Giurgola.

DATA

The design team developed a fully engineered 6” deep aluminum curtainwall system that could support an open-jointed rain-screen installation of terracotta panels. Based on the overall façade composition and interior programmatic requirements, six different curtainwall unit types were established as the basis of the cladding solution. Each unit type roughly correlates in size to a full floor height (approximately 14 feet), and what became a typical panel width of approximately four feet. As shown, these curtainwall unit types have a range of opacity. Some units are entirely glass and shadowbox, while other units are entirely terracotta (Fig. 6). As the design developed, the typical dimensions of these units were standardized to accommodate the various dimensional changes of the existing conditions. The adaptation and standardization of the units addressed the unique existing conditions while also reducing the number of unique curtainwall types the design team, and later the contractor, needed to organize.

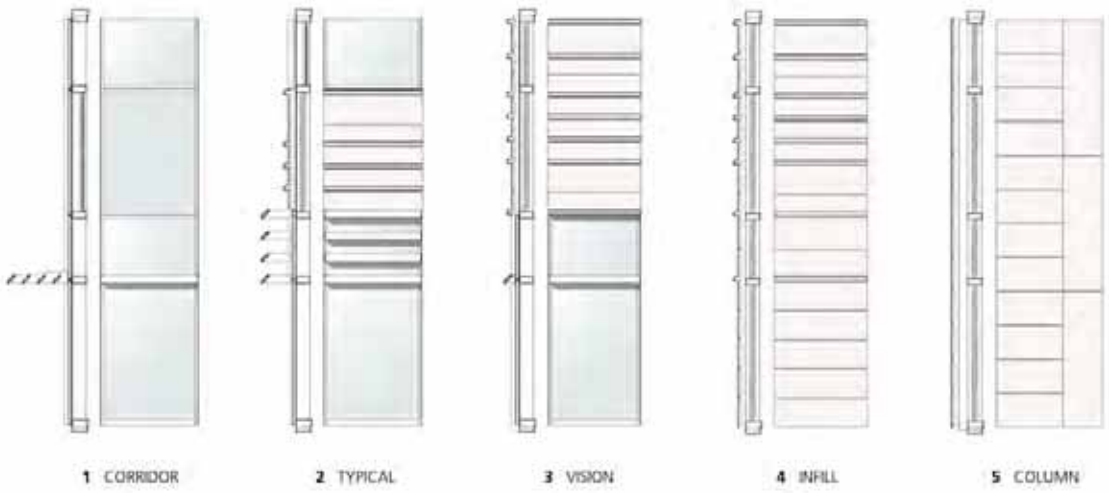


Figure 6: Sections and elevations of wall panel types, ranging from transparent to opaque. Diagrams by Mitchell Giurgola.

At the next level of detail, the team set out to design and standardize the terracotta units themselves. Starting with the standard terracotta depth of 1.5”, the design team worked with the terracotta manufacturer to determine that it was possible to vary the depth of the material to 3” over a short amount of height. This proved very important in the development of the terracotta design as it provided the team with an opportunity to create custom, deep grooved, profiles for use across the façade (Fig. 7). These custom profiles were combined with other standard horizontal and vertical format panels to create a standardized set of terracotta panels (Fig 8). When projected across the entire façade, the various combinations of relatively simple panel types create shadow, depth, and complexity at a fine-grained scale.



Figure 7: Individual terracotta tiles. Photo by Mitchell Giurgola.

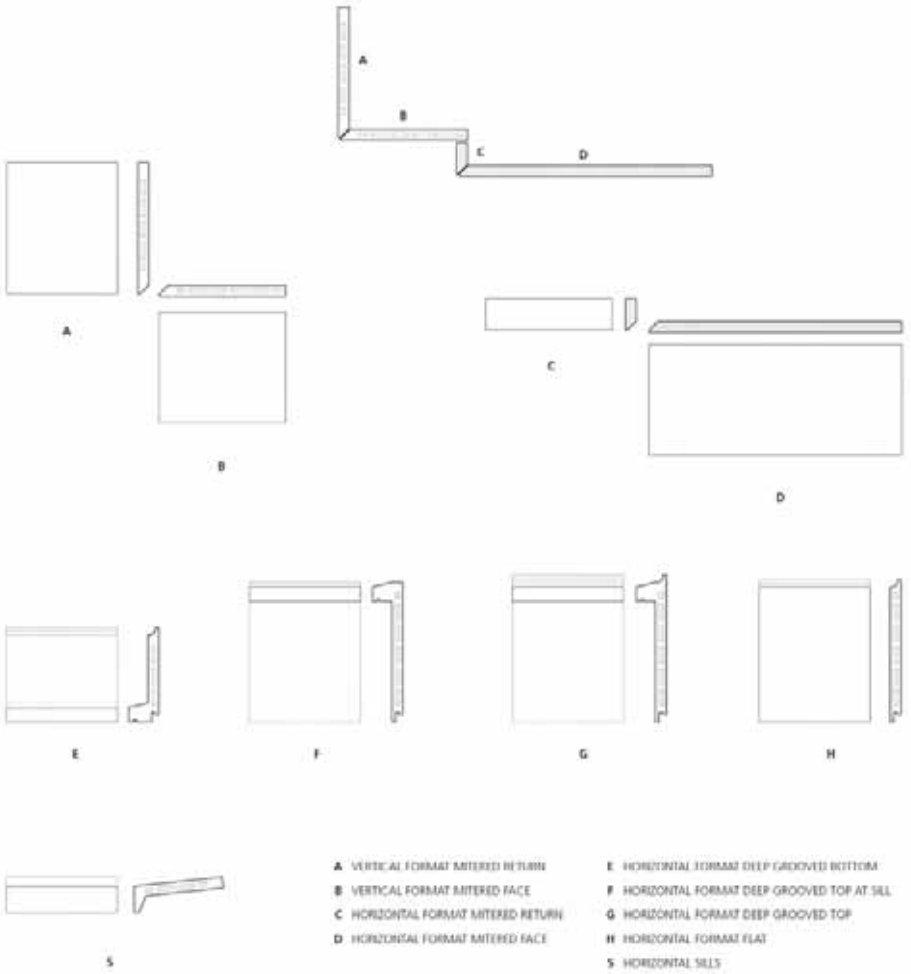


Figure 8: Sections and elevations of terracotta panel types. Diagrams by Mitchell Giurgola.

A clear example of that fine-grained complexity can be seen in the bays of solid terracotta infill. These windowless bays reflect the location of core components (stairs, elevators, and toilets) along the perimeter of the building. The design team used the deep-grooved panels to make a rhythmic pattern of terracotta which activate the surface. This texture stands in contrast to the very regular expression of the columns on either side (Fig. 9).



Figure 9: Solid infill terracotta reflect the location of core components (stairs, elevators and toilets). Photo by Mitchell Giurgola.

Depth was further emphasized through the development of corner curtainwall units to wrap the existing concrete structural frame (Fig. 10). These units allow for continuous vertical expression at the existing columns while also emphasizing the depth created in the original façade. The design team implemented additional aluminum sub-framing at these corner units to further project the face of the terracotta and develop an appearance of monumental piers. The curtainwall units themselves add 12” of depth to the façade while the sub-framing contributes another 3”-7.”

To create depth in the facade with relatively flat terracotta panels, the design team focused heavily on the treatment of corners and intersections. Two solutions to this challenge were developed: vertical format open mitered corners and horizontal format bonded mitered corners (Fig. 10). With the vertical format terracotta, the mitered shape was built into the profile design so that the extrusion would create a consistent mitered edge. This open mitered corner detail did produce an open vertical joint at the corner, but it also allowed for deep returns which were invaluable to the façade design. It allowed the terracotta panels to be manufactured as individual pieces which produced increased reliability in the baking, finishing, and assembly process. These corners were used to express the deep return face of the columns at the recessed structural bays. The other solution, a horizontal format bonded mitered corner, produced a much tighter corner condition, but had to be fabricated in the shop. Horizontal terracotta panels were individually cut and bonded together, and a very slight white-colored finish bead was added at the miter itself to complete the corner condition. The result was a single terracotta panel which appeared to be nearly 4” deep. These corners were used to express every column across the façade.

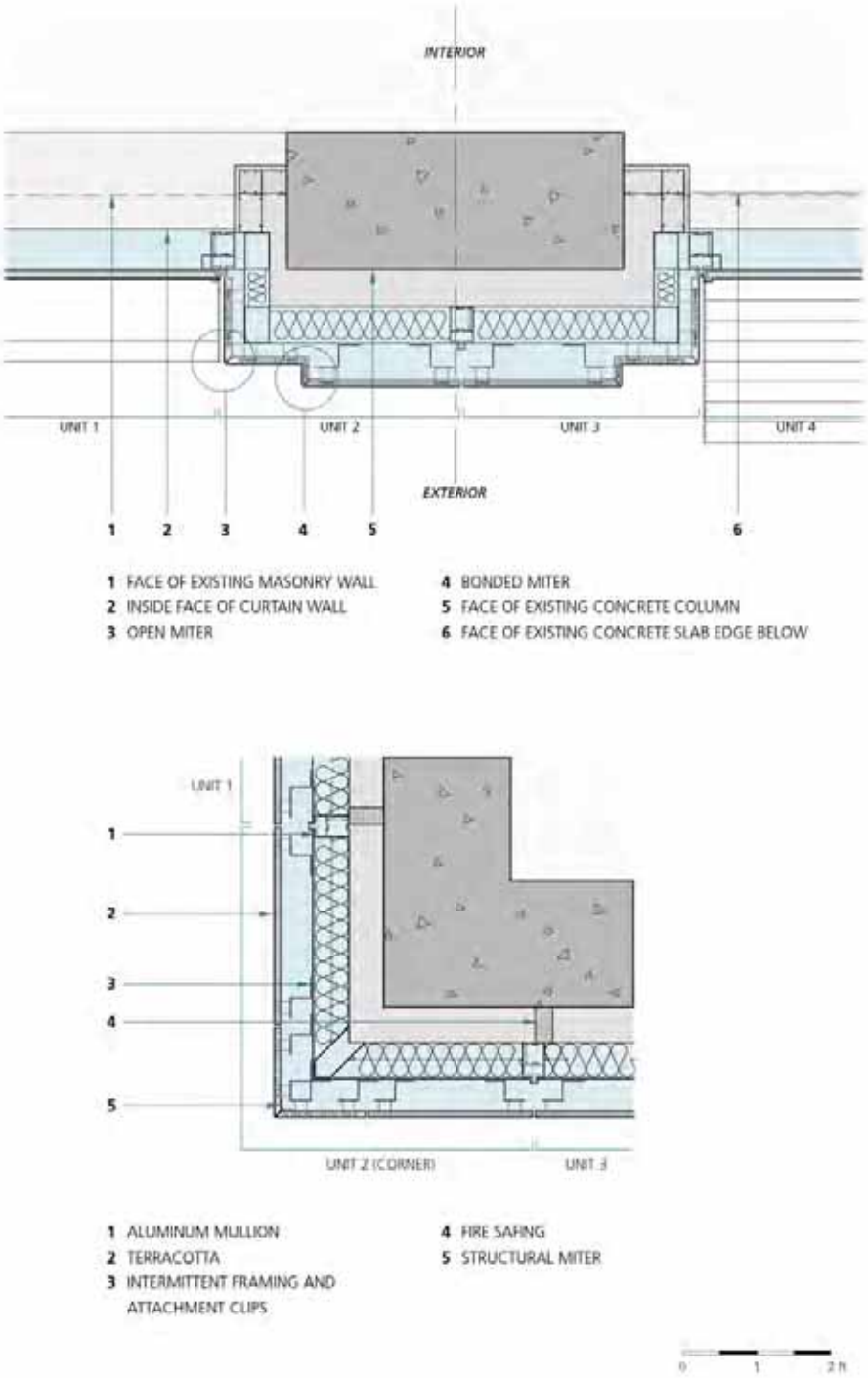


Figure 10: Column plan detail (above), corner plan detail (below). Diagrams by Mitchell Giurgola.

In addition to major vertical expression across the façade, it was also necessary to develop a method for accentuating important horizontal elements. Again, both curtainwall unit modifications and additional aluminum sub-framing were used to highlight ‘belt’ courses at the 3rd and 9th floors (Fig. 11). At the 3rd floor, aluminum sub-framing helps support a horizontal band of terracotta panels that are projected nearly two feet from the face of the curtainwall. At the 9th floor, existing projecting brick arches required that the curtainwall change plane by one foot, and aluminum sub-framing creates nearly another foot of projection of the terracotta panels. These elements successfully established the larger rhythms of the façade.

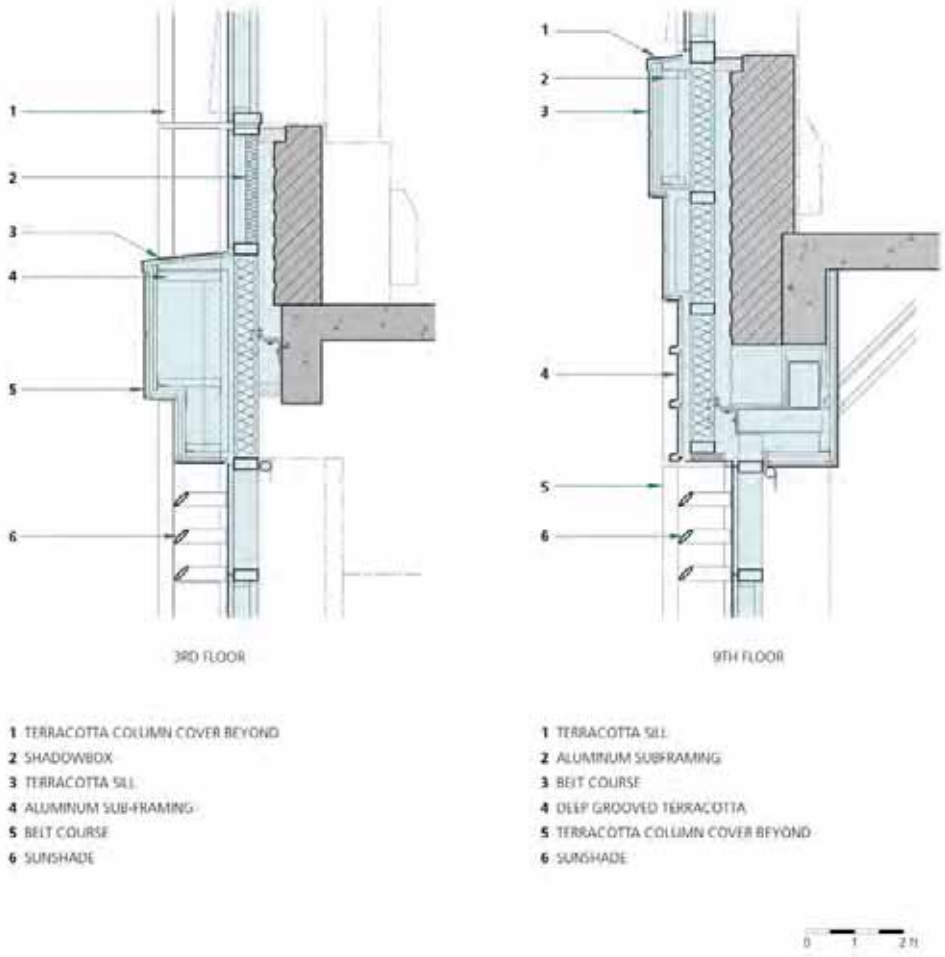


Figure 11: Belt courses wall sections. Diagrams by Mitchell Giurgola.

EXPLANATION

The final product, as evidenced in the attached photographs of the current on-going installation, is a new outcome for the use of contemporary terracotta (Fig. 12-13). The intensity of shape, depth, form, and texture is unique. The complexity and variation within this design strategy is what makes the design sing and it also connects the new building to its original condition.

Remarkably, the installation has shown no significant misalignment between the curtainwall units and the existing structure. This is a testament to the amount of tolerance built into the curtainwall unit sizes, as well as the significant tolerance the design team allowed for in the development of the curtainwall anchoring system. The anchoring system was designed to handle 2”-6” of assumed variation in the location of the concrete structural system. The final anchor design, as further developed with the curtainwall contractor has been able to accommodate variation from 1”-9”.



Figure 12: Wall unit being lifted during construction (left), façade in progress (right). Photos by Mitchell Giurgola.

In some instances, the curtainwall unit standardization did produce some less than optimal conditions on the interior of the building. The variation in exact location of the final window sill, for example, has been more significant than anticipated. In some cases, the sill ends up 2”-4” higher than the design anticipated; and in other instances, the jamb location in relation to the masonry rough opening is not ideal. But the fact that there have been no major discrepancies in misalignment attests to the successful tolerance that was built into the units.

Another challenging issue has been the ability to keep the terracotta panels straight with consistent joints from fabrication through transportation and installation. The cladding design is based on a stack-joint pattern, which depends on the vertical joints to line up properly. The clip that holds the terracotta unit onto the aluminum sub-framing is connected to the back of the terracotta unit in such a way that it allows for very slight movement to accommodate minimal natural expansion and contraction. Unfortunately, this produced units with terracotta that became misaligned in transit from the fabrication site. A jig was developed in the shop to assure the largest, vertical open joints remained consistent, and additional caulk was added to the connection detail to minimize the movement of the panels themselves. This has solved the movement issue and the joints have developed a consistent visual appearance.



Figure 13: Progress shot from southeast corner. Photo by Mitchell Giurgola.

Finally, the client also commissioned a full Energy Modeling Report of the new cladding system to further demonstrate the benefits of this building re-clad project. The analysis compared the existing cladding system to the new unitized fully insulated wall system. Per the chart below (Fig. 14), the Overall Thermal Transfer Value (OTTV – a measure of energy consumption of a building envelope) of the new façade provides a 64% improvement in comparison to the existing cladding; and a 55% improvement to the overall U-Value of the envelope. This translated to a 7% reduction in energy costs to the client on an annual basis, which further justified the work.

Simulation Results by Model						
	Building Envelope		*Whole-building System*			
	OTTV		Energy Consumption		Energy Cost	
	kBtu/hr	% Improve	kBtu/SF-yr	% Improve	$/yr	% Savings
Baseline Model – Existing Building	4,672.93	-	107.7	-	$5,142,423	-
Proposed Model – w/ New Facade	1,665.58	64.36%	95.5	11.33%	$4,794,604	6.76%

Figure 14: Energy modeling simulation results.

CONCLUSION AND FUTURE WORK

Transforming a building intended for manufacturing into a major center for teaching and learning is not necessarily a natural fit. Deciding to replace a 100+ year old façade of a building that is fully occupied is awkward and challenging. But the Center Three Project accomplishes both and does so while using terracotta in a contemporary and new way. The result is a visually active and complex façade that will inspire new approaches to the use of the cladding material in the built environment. It also provides a new skin for an old building, that reduces energy consumption, and that will last for another 100+ years.



Figure 15: Detail of terracotta façade. Photo courtesy of Sinziana Velicescu & Shildan, Inc.

ACKNOWLEDGMENTS

Architect: Mitchell | Giurgola Architects, LLP - Paul Broches, Partner; Carol Loewenson, Partner; Stephen Dietz, Partner; Heidi Sadler, Associate; Catherine Vera; Andrew Thomas; Cristina Greavu; and Andrea Kirk
Curtainwall Consultant: Heintges & Associates - Areta Pawlynsky, AIA, Partner
MEP Engineer: Joseph R. Loring & Associates
Structural Engineer: Ysrael A. Seinuk, P.C.
Clients: Dormitory Authority of the State of New York; The City University of New York; La Guardia Community College
Construction Manager: TDX Construction Corp.
Curtainwall Manufacturer + Installer: Enclos
Terracotta Manufacturer: Shildan, Inc.

REFERENCES

Burrows, Edwin G., and Mike Wallace. *Gotham: A History of New York City to 1898*. Oxford University Press, 1999.

Comstock, WM Phillips. “The Loose-Wiles Building: A Reinforced Concrete Building in New York City.” *Architecture and Building: A Magazine Devoted to Contemporary Architectural Construction*, Vol. XLVI, No. 1, The William T. Comstock Company, 1914, pp. 142–147.

“Industrial Plants Costing Millions of Dollars Within Few Blocks of Queensboro Bridge Plaza.” *The New York Times*, 28 June 1914.

Morrone, Francis. “The Gems of Dumbo.” *The New York Sun*, The New York Sun, 18 Oct. 2007, www.nysun.com/arts/gems-of/dumbo/64838.

Rinaldi, T.E. “Long Island City.” *New York Neon*, New York Neon, 27 Sept. 2012, nyneon.blogspot.com/2012/09/long-island-city.html.

Slesin, Suzanne. “Queens Site to Be Converted Into International Design Center.” *The New York Times*, 10 Mar. 1983.

THERMOELECTRIC MATERIALS IN EXTERIOR WALLS

Experimental study on using smart facades for heating and cooling in high-performance buildings



Ajla Aksamija, Ph.D.
University of Massachusetts Amherst
aaksamija@umass.edu



Zlatan Aksamija, Ph.D.
University of Massachusetts Amherst
zlatana@engin.umass.edu



Chris Counihan
University of Massachusetts Amherst
chris.counihan@gmail.com



Dylan Brown
University of Massachusetts Amherst
dtdylanb@gmail.com



Meenakshi Upadhyaya
University of Massachusetts Amherst
mupadhyaya@umass.edu

ABSTRACT

This article discusses design, prototype development and an experimental study of facade-integrated thermoelectric (TE) materials. TEs are smart materials that have the ability to produce a temperature gradient when electricity is applied, exploiting the Peltier effect, or to generate a voltage when exposed to a temperature gradient, utilizing the Seebeck effect. TEs can be used for heating, cooling, or power generation. In this research, heating and cooling potentials of these novel systems were explored. Initially, two low fidelity prototypes were designed and constructed, where one prototype was used to study integration of TE modules (TEM) as stand-alone elements in the facade, and one prototype was used to explore integration of TEMs and heat sinks in facade assemblies. Both prototypes were tested, in ambient conditions and within a thermal chamber. The thermal chamber was used to represent four different exterior environmental conditions (0°F, 30°F, 60°F and 90°F), while the interior conditions were kept constant at room temperature. The supplied voltage to facade-integrated TEMs varied from 1 to 8 V. Temperature outputs of TEMs for all investigated thermal conditions were measured using thermal imaging, which are discussed in detail in this article. The results indicate that while stand-alone facade-integrated TEMs are not stable, addition of heat sinks improves their performance drastically. Facade-integrated TEMs with

heatsinks showed that they would operate well in heating and cooling modes under varying exterior environmental conditions.

KEYWORDS

facade, intelligent, physical testing – mockups, fabrication prototypes, smart materials, heating and cooling, experimental, thermal imaging

INTRODUCTION

Buildings consume 40% of energy in the United States, and influence greenhouse gas emissions. High demand for energy used for lighting, heating, ventilation, and air conditioning leads to significant amount of carbon dioxide emissions. According to the U.S. Department of Energy, 15% of global electricity is consumed by various refrigeration and air-conditioning processes, and 46% of the energy used in household and commercial buildings is attributed to heating, ventilation and air-conditioning (HVAC) systems in 2011 (DOE, 2011). Given the high energy usage and inefficiencies found in conventional HVAC systems, new heating and cooling sources are needed in order to reduce buildings' carbon footprint. Moreover, integration of different building systems, particularly building envelope and HVAC, are essential for high-performance buildings. Thermoelectrics (TEs) are one example of a promising technology with potential architectural applications. Research and development has largely focused on thermoelectric modules (TEMs) that convert heat energy into electrical energy (Montecucco et al., 2012; Yilmazoglu, 2016) and novel TE materials that offer higher energy efficiency through nanoscale engineering (Snyder and Toberer, 2008). Heating and cooling modes can be switched by reversing the current direction (Fig. 1). TEMs can offer low cost electricity without the use of mechanical parts or production of toxic wastes (Seetawan et al., 2014). The optimal performance of TEMs depends on many factors, ranging from material selection to operation strategy (Twaha et al., 2016).

TEMs can be used for heating, cooling, or power generation (Fig. 2). TEMs consist of arrays of N and P type semiconductors. When a heat source is applied on one side of the semiconductor and the other side is exposed to a cooler temperature, electric power is produced (and can be generated in reverse). Electricity supply can actively provide cooling or heating by reversing the current direction (Zheng et al., 2014).

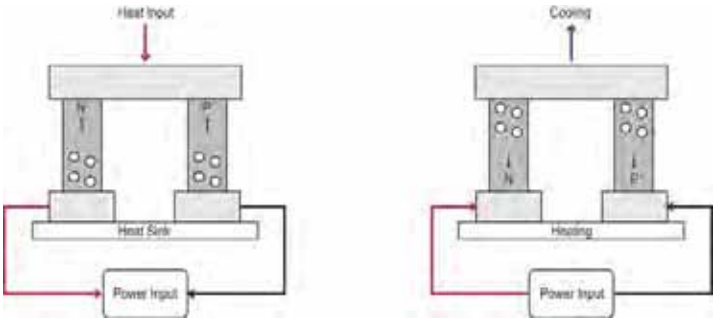


Figure 1: Thermoelectric materials produce electricity when exposed to thermal gradient, and cooling/heating when voltage is applied. Image by the authors.

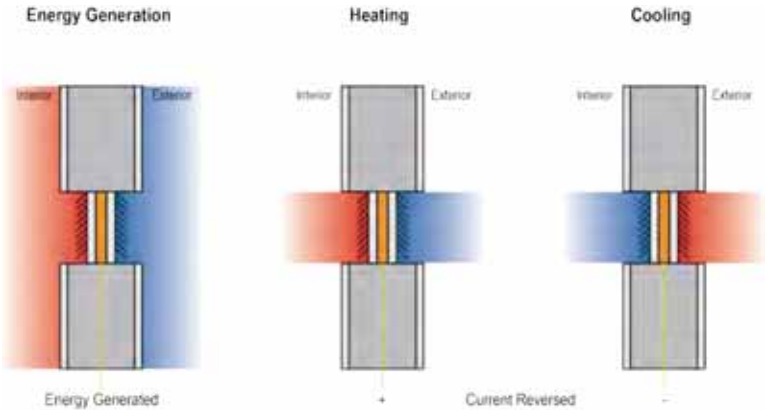


Figure 2: Potential use of TE materials in exterior walls for energy generation, heating and cooling Image by the authors.

More recently, research on TE applications has gained momentum (Twaha et al., 2016; Zhao and Tan, 2014). A promising, but not widely researched area, includes use of TE applications for heating and cooling, as well as energy generation.

BACKGROUND

In the past 15 years, significant growth of research into thermoelectric energy conversion is reflected in the increase in related annual publications, increasing from 500 to 2500 (Bell, 2008). TEMs have been used for cooling and heating applications in the military and aerospace fields, and for electronic instruments (Kraemer et al., 2011). Since TEMs do not contain any moving parts, their operation is quite reliable and stable. This greatly reduces maintenance costs when compared to other types of air conditioning systems (Shen et al., 2013). It is possible to use TEMs as an alternative to HVAC applications with properly designed heat exchangers (Yilmazoglu, 2016).

Research TEs began with Thomass J. Seebeck's 1821 discovery of the eponymous effect at a junction between two metals. In the 1950's, Ioffe and Goldsmid authored seminal works outlining the criteria for materials selection and optimization in TE modules. As a technology, TEs have a five-decades-long history dating back to early NASA deep-space probes, where they were used in conjunction with radioisotope heat sources to power satellites ranging from Pioneer 10 to Cassini as well as the Mars Rover (Ritz and Peterson, 2004). However, modest conversion efficiency (around 6-8%) limited the use of TEs to niche applications where robustness and reliability were more important than efficiency. In the past decade, global need for sustainable and renewable energy, coupled with advances in materials theory, simulation, and synthesis, have fueled a resurgence of interest in both materials discovery of more efficient TEMs and commercial applications in a variety of markets (Dresselhaus et al., 2007; Kanatzidis, 2010). Recent examples range from wearables such as the Matrix smart watch powered entirely by body heat to waste heat scavenging from car exhaust systems.

Thermoelectric heating and cooling has several advantages over conventional counterparts. The compact size, light weight, reliability, lack of mechanical parts and elimination of the need for chlorofluorocarbons make them environmentally friendly and appealing. But, applying thermoelectric systems for space heating and cooling remains much more challenging and has not been explored beyond small scale applications and in theoretical proposals (Zhao and Tan, 2014).

Few applications of TEMs in facade assemblies have been researched, proposed, or constructed. This has created a significant gap in knowledge in the potential architectural applications of TEMs. Some researchers, however, have proposed architectural applications with promising preliminary results. Liu et al. proposed a facade assembly that integrates TEM with a heat sink for heating and cooling needs. Results indicate that the total input power required to operate a TEM decreases as the distribution density of the TEMs increase. The thermal resistance of the heat sink plays an important role in determining the number of TE coolers optimizing all potential design configurations (Liu et al., 2015). This study proposed a window composed of four parts: a passive window, a PV module, thermoelectric cooling units, and heat sinks. A semi-transparent PV module is integrated into the front pane of a passive double-pane window and it is used to power TEMs integrated into the window frame. Finned heat sinks are placed in contact with the TE units to control the heat transfer between the TEMs and the ambient environment. The PV unit converts solar radiation into electrical energy, while the TEMs change this electrical energy into thermal energy. The TEMs can heat or a cool, depending on the direction of the current supplied by the PV unit.

This would allow the building envelope to be used in both heating and cooling applications (Liu et al., 2015).

While the scientific principles and properties that govern TEs were discovered over one hundred years ago, the applications in facade systems have not been widely explored. This research addresses this gap in knowledge by investigating integration of TEMs into building facades for heating and cooling.

METHOD

The research questions that were addressed include:

- How can TEMs be integrated into architectural facade assemblies?
- How do TEMs behave in typical thermal conditions in various climates?
- How is TEM's thermal performance affected by varying voltages, climatic conditions and assembly construction?
- How is TEM performance affected by different configuration of heat sinks?

Two low fidelity TEM facade prototypes were designed and assembled for the purposes of this study. These were tested in ambient and thermally controlled conditions to measure temperature gradients, heating and cooling potential. Materials for these assemblies were selected for their commercial availability, as well as their specifications. Two heat sink types were chosen to provide a comparison in heat transfer performance values.

The dimensions of TEM modules are 40mm x 40mm, drawing up to 12V, with operating conditions from -22°F to 181°F. Small heat sinks of 40mm x 40mm x 11mm, composed of aluminum cooling fins, were used to provide direct heat sinks for a flat heat sink assembly. These were fixed to the TEMs using 0.5mm silicone based thermal pads. The second prototype included larger heat sinks. Two 120mm heat sinks were used, with four direct heat copper pipes for heat dissipation. Thermal paste provided a thermal connection to the TEM module.

Five configurations were considered when constructing prototypes for testing (Fig. 3). A direct contact TEM facade module would provide the simplest assembly, applying heat sinks directly to the TEM. This assembly, however, poses the greatest potential for thermal bridging and gaps in the facade assembly. A sink transfer assembly expands upon the direct contact assembly, but relies on conductors to transfer heat from the TEM to heat sinks. Location shift assemblies are similar to sink transfer assemblies, but allow for flexibility in regards to heat sink location in relation to the TEM. Stacked TEMs provide the opportunity to increase the temperature differences between the hot and cold sides beyond what is possible with a single TEM across multiple modules. Floor mounted assemblies consider integrating TEMs, conductors, and heat sinks into the floor plate and facade. This assembly is the most complicated application, but provides benefits that include natural convection and heat sink concealment.

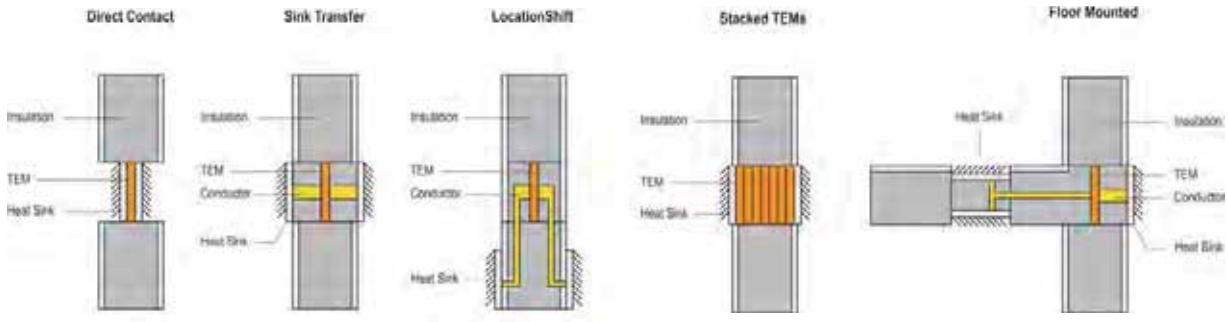


Figure 3: Schematic representation of possible configuration and placement of TEMs in facades. Image by the authors.

For the purposes of this research, direct contact and sink transfer TEM facade assemblies were selected, for their simplicity and broad applicability. Each assembly was constructed using 2, 1" foam insulation panels with an R-value of 5, providing each assembly with an R-value of 10. Thin board (1/8") was glued to face the foam insulation and provided a housing within the assembly for the TEM modules and heat sinks. Heat sinks were inserted into the assembly and connected to the TEM using thermal paste or thermal pads. The flat assembly did not rely on any fasteners to connect the TEMs to the heat sinks, instead thermal pads provided the adhesion. The large heat sink assembly required an assembly composed of nuts, bolts,

and washers to sandwich the TEM, foam, and board assembly together. Spray foam insulation was applied to the larger heat sink assembly to prevent any thermal breaks that may have developed through use of metal hardware and fasteners. These assemblies can be seen in Figures 4 and 5.

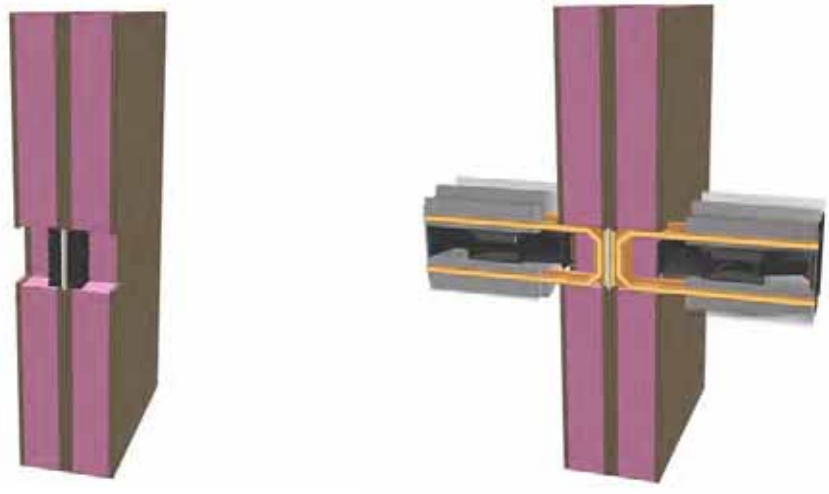


Figure 4: *Architectural TEM proof of concept assembly model sections. Image by the authors.*

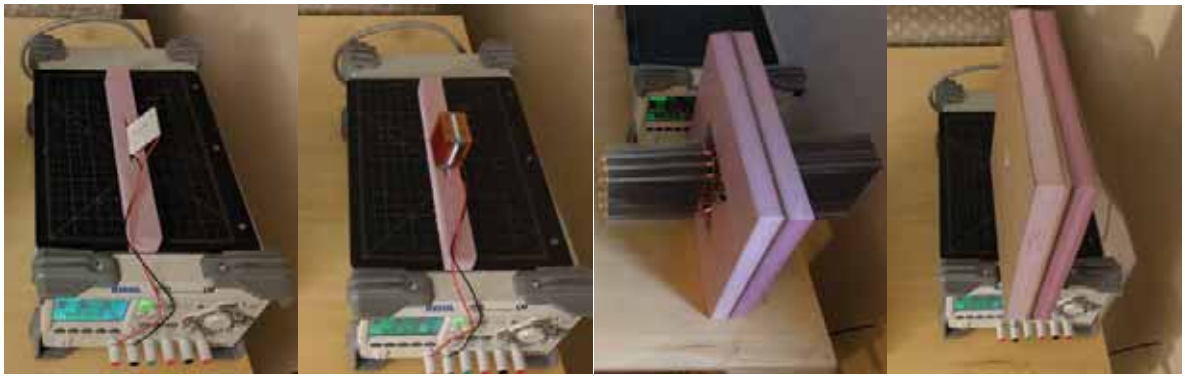


Figure 5: TEM proof of concept mockups. Image by the authors.

To understand how facade-integrated TEMs behave, these prototypes were first tested in ambient room conditions (temperature of 72°F). An independent module without a heat sink, a module with a flat heat sink, as well as the assembly mockups were tested with applied voltage of 1V increments. Results were measured using thermal imaging camera, as well as a power supply. Thermal images were taken at one volt increments up to 8V, and temperatures were recorded using thermal camera.

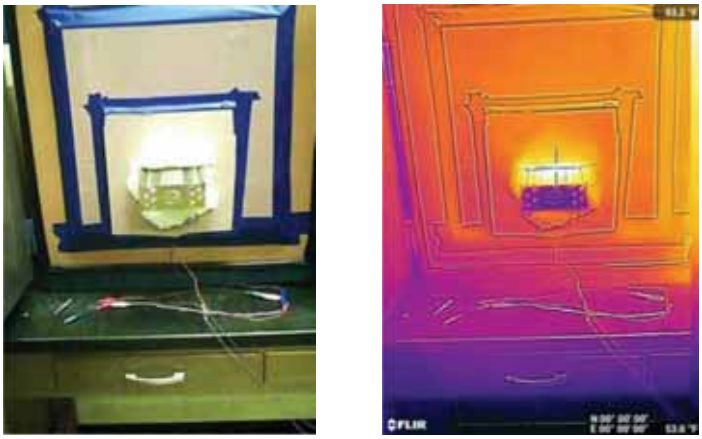


Figure 6: TEM assembly testing in thermal chamber with thermal imaging. Image by the authors.

Further testing involved the use of a temperature controlled thermal chamber. The thermal chamber's 16.5" x 16.5" opening was sealed using 1" of insulating foam with tape applied to provide a relatively air tight seal for the testing. Assemblies were inserted into a 10"x10" void and were taped again (Fig. 6). The 10"x10" void allowed for easy insertion and removal of the prototypes. The chamber was set to 0°, 30°, 60°, and 90°F to represent different exterior temperatures (winter, summer and intermediate seasons). This method of testing simulated typical exterior temperatures found in most climates while allowing for temperature data to be collected in a controlled setting. The thermal chamber was allowed time to stabilize (1 hr) before each testing session, and 20 minute breaks were taken in between each observation. The ambient temperature of the room was kept relatively stable at 73°F. Voltage was applied in 1 V increments in both heating and cooling modes. Temperature measurements on the exterior surface of the prototypes were recorded using a thermal camera.

RESULTS

AMBIENT TESTING RESULTS

Results were collected, tabulated, and graphed for analysis. The temperatures observed in ambient testing ranged from 48.8°F to 258.3°F in both cooling and heating modes. The maximum temperature observed occurred on the hot side of the flat heat sink at 8V. The independent TEM approached this value, reaching 238.2°F at 6V before module failure. Heating side maximums exceeded 200°F in all ambient assembly tests, except for the large heat sink (measured temperature for of this assembly was 98.3°F at 8V). All heating side temperatures show positive temperature trends (Fig. 7).

Cooling temperatures displayed inconsistent data. Temperatures ranged from 48.8°F to 181.1°F. Cold side temperatures elevate significantly on the independent TEM, flat heat sink, and flat heat sink assembly above 4V. The cold side temperatures of these testing modules exceed 100°F at or around 4V. The large heat sink shows temperatures ranging from 59.5°F to 48.8°F. The temperature difference and average temperature values were the lowest for this assembly.

Modules without heat sinks were stressed by high temperature difference values, often times exceeding those suggested by the manufacturer. Average temperatures show similar stresses, and can reach or exceed 200°F. TEM failures occurred on several occasions, most notably when TEMs were not paired with heat sinks, or if voltages exceeded 8V. Only the large heat sink maintained a stable average temperature, stressing the importance of incorporating a heat sink for the proper functioning of facade-integrated TEMs.

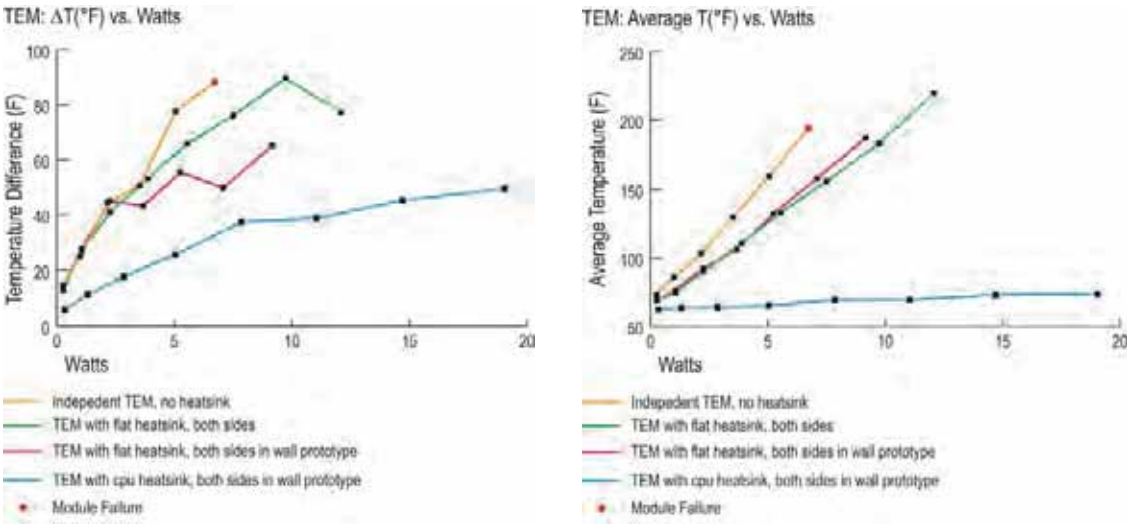


Figure 7: Temperature difference and average temperature results in ambient conditions. Image by the authors.

Temperature difference data indicates that a threshold of failure exists within the TEM module, occurring around 80°F, 15°F above the manufacturer's stated value. When plotted against power, the data show performance in line with observations, indicating that the temperature differentials were directly influenced by the presence of a heat sink. Data also shows that heat sinks allow a higher power input without leading to extreme temperature differentials.

THERMAL CHAMBER TESTING RESULTS: HEATING

Results of the thermal chamber testing indicate that the temperature values increase as higher voltages are applied, regardless of the assembly type or tested temperature (Fig. 8). The results for the prototype with a large heat sink show that temperatures range from 56.4°F to 97.1°F when applied in 1V increments. Tested temperature of 0°F yields a heating temperature range of 66.9°F to 80.1°F. Observed values start at 66.9°F due to the ambient temperatures of the testing room. Values always remained above 0°F temperature. 30°F ambient temperature data show values rising from 56.4°F to 81.6°F from 1V to 5V respectively. At 6V, a decline in temperature to 75.8 was observed. At 60°F ambient temperature, heat sink values ranged from 73.8°F to 97.1°F. Temperatures rose relatively consistently at this tested temperature.

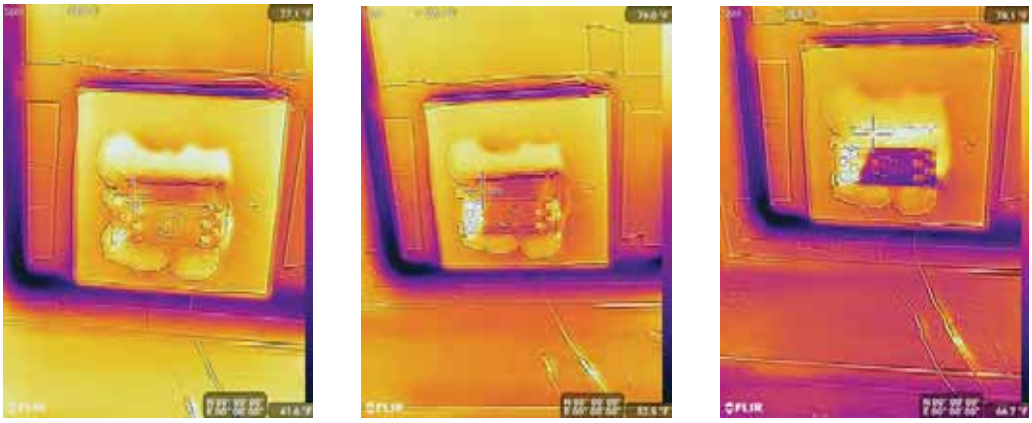


Figure 8: Assembly heating at 0, 30, 60°F with 3V applied.

Heating performance of the assembly with flat heat sink shows temperatures ranging from 28.8°F to 177°F. The heating from this assembly always exhibits a positive trend with increasing voltage. At 0°F temperature, heating temperatures range between 28.8°F to 80.6°F. Observed values without applied voltage start at 26.6°F. At 30°F temperature, results show values rising from 49.6°F to 159.8°F from 1V to 6V respectively. At 60°F temperature, values ranged from 70.5°F to 177°F. Heat sink temperatures at this temperature exceeded 100°F when 3V is applied.

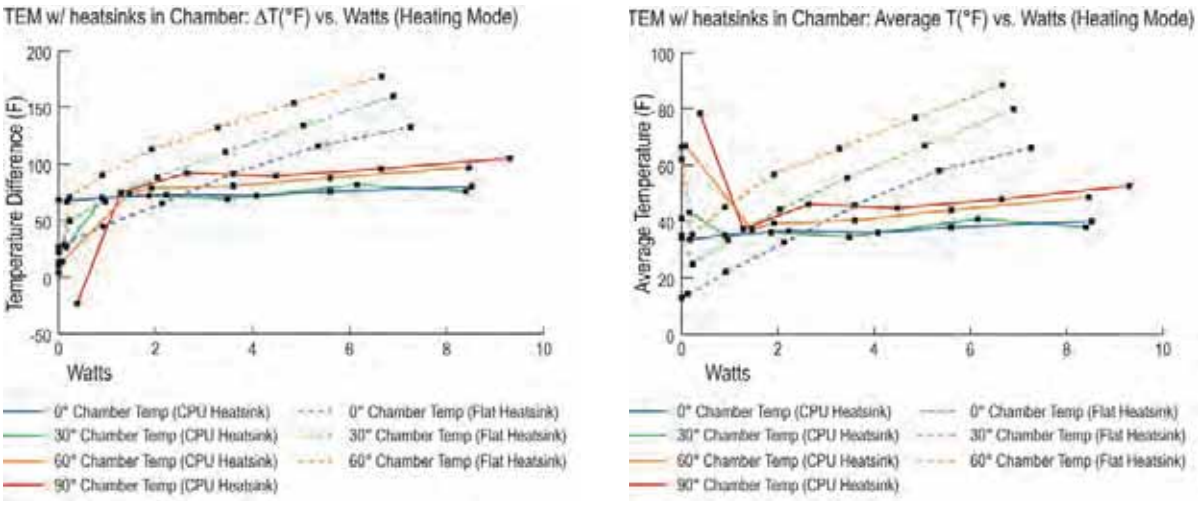


Figure 9: ΔT vs Watts and average temperature vs Watts in heating mode. Image by the authors.

Temperature difference data in the heating mode indicates that heating performance behaves consistently despite thermal chamber temperatures (Fig. 9). Higher thermal chamber temperatures lead to higher temperature differences with increasing power being applied. This was observed in both assemblies; however, the flat heat sink showed positive trends, while the large heat sink showed relatively constant temperature differences with increasing power. The temperature differences observed in the flat heat sink greatly exceeded the manufacturer stated maximum of 65°F, leading to failure at 7W. The large heat sink assembly displayed a relatively constant difference of 65-70°F, even as power input increases.

THERMAL CHAMBER TESTING RESULTS: COOLING

TEM cooling data shows temperature values that are dependent on TEM assembly. The large heat sink data show that at a 60°F ambient temperature, cooling ranges from 71.6°F to 46.1°F when voltage is applied in 1V increments. However, cooling does not occur linearly. The minimum temperature was observed when 4V was applied to the large heat sink, while 5V and 6V values were slightly higher, at 53.7°F and 49.5°F respectively. Cooling performance was more effective at 60°F. Temperatures observed at 1-3V were higher than 60°F temperature (due to testing room temperature), but lowered significantly when higher voltages were applied. At 90° temperature, TEM performance is relatively uniform. Measured temperatures ranged from 57.2°F to 66.8°F.

The flat heat sink assembly showed results ranging from 43.3°F to 93.9°F. Observed temperatures were lower when operated at a 60°F temperature, and remained below the ambient temperature through 4V. Temperatures observed at 90°F ranged from 72.8°F to 93.9°F. Temperatures remained below the ambient temperature up to 5V, but temperatures observed would not provide adequate cooling for occupant thermal comfort.

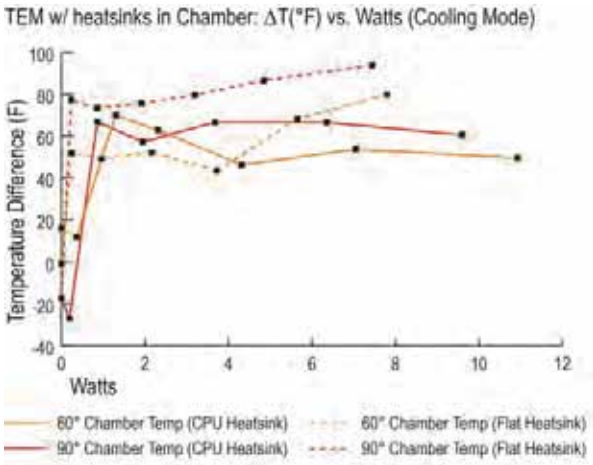


Figure 10: ΔT vs Watts and average temperature vs Watts in cooling Mode. Image by the authors.

Results for the cooling mode indicates that higher temperature differences arise as power inputs increases within the assemblies (Fig. 10). This was observed in both assemblies; however, the flat heat sink showed positive trends, while the large sink showed a slightly negative trend or constant temperature difference trend.

DISCUSSION

The results show that TEMs operate at effective heating and cooling temperatures even when exposed to variable exterior temperatures, represented by the thermal chamber. They are most effective when paired with a larger heat sink, especially for cooling. Results also show that TEMs, when integrated into facade prototypes, operate effectively in heating and cooling modes.

Data shows that the TEMs are more effective for heating and cooling applications when paired with heat sinks. Data also shows that when TEMs are paired with a larger heat sink, the cooling side operates more efficiently, and is affected to a lesser extent by temperatures generated within the TEM and any thermal bridging that may be occurring across the TEM.

The heating and cooling functions of TEMs appear to be most effective and efficient for cooling operations when 2-4V are applied to the module. This effect is more evident in the small heat sink assembly, whereas the larger heat sink assembly maintains a more consistent temperature as voltage above 3V is applied.

TEM modules operating without a heat sink or with a small heat sink are inefficient or ineffective. Without a means to transport and dissipate heat, TEM modules overheat due to the thermal transport involved at the molecular level. Thermal bridging may also contribute to high cold side temperatures.

CONCLUSION AND FUTURE WORK

Results of this study show promising opportunities for integrating TEMs in facade systems, since these smart materials can be used for heating and cooling of interior spaces. The performance of facade-integrated TEMs is most useful when paired with a larger heat sink, especially for the purposes of heating. This assures adequate heat dissipation from these advanced materials. TEM modules operating without a heat sink or with a small heat sink are inefficient. Results indicate that stand-alone facade-integrated TEMs are not stable, and are not promising for architectural heating and cooling needs. Without a means to transport heat, TEM modules overheat due to the molecular thermal transport within the modules. However, facade integrated TEMs paired with heat sinks displayed effective heating and cooling operation under varying exterior environmental conditions.

Integrated TEM facades offer many potential benefits. The mechanical equipment required for HVAC can be reduced, leading to lower maintenance requirements and operational cost reductions. TEMs can be integrated and paired with radiant panels to cause less disruption to interior spaces than traditional HVAC equipment. Finally, TEMs do not require moving parts or refrigerants for heating and cooling, thus improving environmental impact of HVAC systems.

Next steps for this research will include investigation of thermal transport in several different exterior wall types (computational and experimental), used for commercial and residential applications. Actual wall assemblies will be investigated, including rainscreen applications, light-wood framed walls and curtain walls. Also, efficiencies and impact on energy consumption will be studied, and the results will be reported in future publications.

REFERENCES

Bell, L. “Cooling, heating, generating power, and recovering waste heat with thermoelectric systems.” Science 321 (2008): 57–61.

Department of Energy. “Building Energy Data Book 2011.” https://openei.org/doe-opendata/dataset/buildings-energy-data-book (accessed March 30, 2017).

Dresselhaus, M., Chen, G., Tang, M., Yang, R., Lee, H., Wang, D., Ren, Z., Fleurial, J., and Gogna, P. "New directions for low-dimensional thermoelectric materials." Advanced Materials 19 (2007):1043–1053

Kanatzidis, M. G. "Nanostructured thermoelectrics: the new paradigm?" Chemistry of Materials 22 (2010): 648–659.

Kraemer, D., Poudel, B., Feng, H., Caylor, J., Yu, B., Yan, X., Ma, Y., Wang, X., Wang, D., Muto, A., McEnnaney, K., Chiesa, M., Ren, Z., and Chen, G. “High-performance flat-panel solar thermoelectric generators with high thermal concentration.” Nature Materials 10 (2011): 532-538.

Liu, Z. B., Zhang, L., Gong, G., and Luo, Y. “Evaluation of a prototype active solar thermoelectric radiant wall system in winter conditions.” Applied Thermal Engineering 89 (2015): 36-43.

Montecucco, A., Buckle, J. R., and Knox, A. R., “Solution to the 1-D unsteady heat conduction equation with internal Joule heat generation for thermoelectric devices.” Applied Thermal Engineering 35 (2012): 177–184.

Ritz, F. and Peterson, C. "Multi-mission radioisotope thermoelectric generator (MMRTG) program overview." Proceedings of the 2004 IEEE Aerospace Conference (2004): 2950-2957.

Seetawan, T., Singsoog, K., and Srichai, K. “Thermoelectric energy conversion of p-Ca3Co4O9/n-CaMnO3 module.” Proceedings of the 6th International Conference on Applied Energy (2014): 2–5.

Shen, L., Xiao, F., Chen, H., and Wang, S. “Investigation of a novel thermoelectric radiant air-conditioning system.” Energy and Buildings 59 (2013): 123-132.

Snyder, G.. and Toberer, E. “Complex thermoelectric materials.” Nature Materials 7 (2008): 105-114.

Twaha, S., Zhu, J., Yan, Y., and Li, B. “A comprehensive review of thermoelectric technology: Materials, applications, modelling and performance improvement.” Renewable and Sustainable Energy Reviews 65 (2016): 698-726.Yilmazoglu, M. “Experimental and numerical investigation of a prototype thermoelectric heating and cooling unit.” Energy and Buildings 113 (2016): 51-60.

Zheng, X.F., Liu, C. X., Yan, Y. Y., and Wang, Q. “A review of thermoelectrics research - recent developments and potentials for sustainable and renewable energy applications.” Renewable Sustainable Energy 32 (2014): 486–503.

Zhao D., and Tan G. “A review of thermoelectric cooling: Materials, modeling and applications.” Applied Thermal Engineering 66 (2014): 15-24.

TRANSITIONS BETWEEN DIVERSE ENVELOPE SYSTEMS

Façade joints at Lucile Packard Children's Hospital



Kristian Fosholt, LEED AP BD+C
John Maniscalco Architecture
kristian.fosholt@gmail.com



Megan Koehler, AIA, LEED AP BD+C
Perkins+Will
megan.koehler@perkinswill.com



Andrew Tsay Jacobs, AIA, EIT, LEED AP BD+C
Perkins+Will
andrew.tsayjacobs@perkinswill.com

ABSTRACT

The Lucile Packard Children's Hospital at Stanford University in Palo Alto, California features an extremely diverse set of façade systems within one continuous building envelope. Systems used include: shading devices including gratings, fins, and louvers; rain screen elements including natural stone, GFRC, precast concrete, sheet metal and insulated metal panels; and glazing systems including point supported, punched window, structural silicone, storefront and curtain wall. The variety of systems used and their interfaces with one another required a wide range of joint detailing solutions. Designing and building the interface between myriad systems became one of the largest challenges for the design and construction teams. Joint systems for seismic joints, thermal expansion joints, system transition joints, penetration joints and anchorage joints all presented unique challenges. Designers and builders, working together through the Design Assist/Design Build delivery method, successfully tied many disparate systems together to a complete envelope using a variety of joints including: proprietary break away panels, sliding joint covers, double sealant joints, single sealant joints with concealed air and water barrier (AWB), foam infill joints, sacrificial crumple panel with concealed AWB, slotted/sheathed metal panel, single sealant and flashing covering waterproofing transition to gasket, single sealant and flashing covering waterproofing transition to AWB, chicken-head gasketing, rubber isolation gaskets and plastic separation shims.

KEYWORDS

GFRC, unitized curtainwall, precast façade, project delivery, pre-fabrication, case study, thermal break, structure and seismic, storefront façade, point supported glazing, adhesives, sealants, laminated glass, structural silicone glazing, physical testing, mockups

INTRODUCTION

Many of the assemblies used on the Lucile Packard Children's Hospital are common assemblies: unitized curtain wall, storefront, point supported glass, GFRC on metal frame, punched windows, catwalks, insulated metal panel, louvers, plaster, precast cladding, aluminum shading grilles, laminated glass shade fins. The unique aspect of the Lucile Packard Children's Hospital project is the inclusion of all these and more systems deployed together on a hospital in a high seismic zone. To successfully tie the many façade systems together required many unique jointing solutions. Thermal expansion joints and seismic joints between the assemblies varied based on the materials being adjoined. Panel to panel joints of different systems called for unique detailing solutions that could accommodate the movement, geometry and unique material compatibility requirements of each system. Penetration joints and structural anchorage joints for the various, visually exposed façade elements each required custom solutions. Using 'typical details' was not an option because of the extreme diversity of the façade system interfaces and the rigorous seismic requirements for a California hospital. The array of solutions developed and implemented by the design and construction teams represents a library of examples of how building elements come together to express a unified exterior envelope.





Figures 1 and 2: Images of LPCH showing the variety of façade systems and assemblies.

BACKGROUND

A primary challenge for the design and construction teams was to tie a variety of dissimilar systems together into a cohesive whole. The diversity of façade systems on the project necessitated coordination between numerous trades and organizations. Each interface between systems required evaluation of transition materials compatible with both adjoining façade systems - accommodating and responding to their respective movements, moisture management strategies, colors, textures, anchorage and geometries. This evaluation was carried out through a Design Assist / Design Build (DA/DB) Process. Representatives from the various sub-contracted façade builders became stakeholders in the design process, recommending joint detailing that supported their own fabrication and erection process while maintain consistency with the design intent and adjacent trade requirements.

To achieve the design intent, several of the designs developed were non-standard and required the design team and DA/DB teams to work with the authority having jurisdiction to gain approval through alternate methods of compliance (AMCs). The reviewing agency for LPCH was California's Office of Statewide Health and Planning and Development (OSHPD), which has jurisdiction over all hospitals in California. The review process for OSHPD projects is thorough and rigorous to ensure the safety of the occupants and to ensure that hospitals remain operational after catastrophic events. For each non-standard

assembly, the AMC process required the development of an initial design with a supporting engineering approach, selection of test criteria to support the design, and identification of applicable tests for review and approval by OSHPD. After approval of the approach, tests were conducted on a mockup and results were provided to OSPHD for approval. Upon approval of the test results, final design of the façade was submitted to OSHPD for approval prior to construction. The façade systems that underwent this process include: 4-sided silicone glazing, point-supported glazing, glass fins, and curtain wall anchorage.

The many façade material variations of Lucile Packard Children's Hospital derive from their relationship to the programs they are enclosing (Fig. 3-4). Each envelope type is correlated to interior programmatic functions. The primary types are as follows:

1. Patient bed tower façades are clad with pre-fabricated, steel-framed GFRC wall panels and an outrigger system supporting shading and planted catwalks.
2. Public waiting rooms are clad with 4-sided structural silicone glazed curtain wall with integrated frit patterns and alcove planters.
3. Mechanical back of house areas are clad with insulated metal panel systems, plaster systems or louvers.
4. Public entrance and lobby areas are clad with stone and point supported glass.
5. Pharmacy and public corridors are clad with GFRC, Precast and ribbon windows.
6. Stairs are clad with insulated metal panel and 4-sided structural silicone glazed curtain wall.
7. Meditation Pavilion is clad with stone and storefront glazing.
8. Dining facilities and garden access areas are clad with storefront glazing and precast concrete.
9. Building Entrance Billboard features Point Supported Glass.
10. Roofs at Ground and First floor are Garden Roofs.
11. Garden area feature walls, cladding and copings are precast concrete.

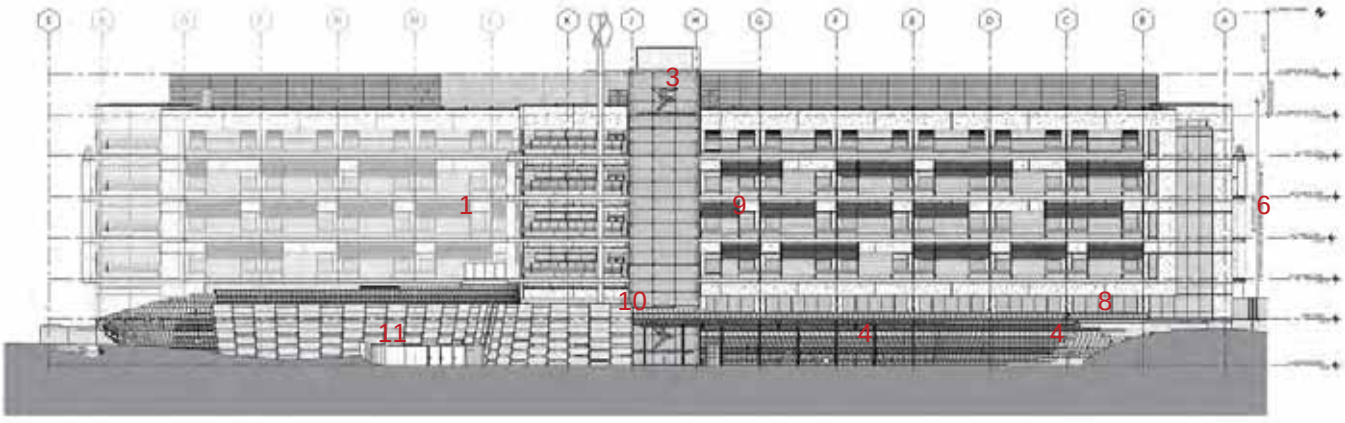


Figure 3: North Elevation with envelope types identified.

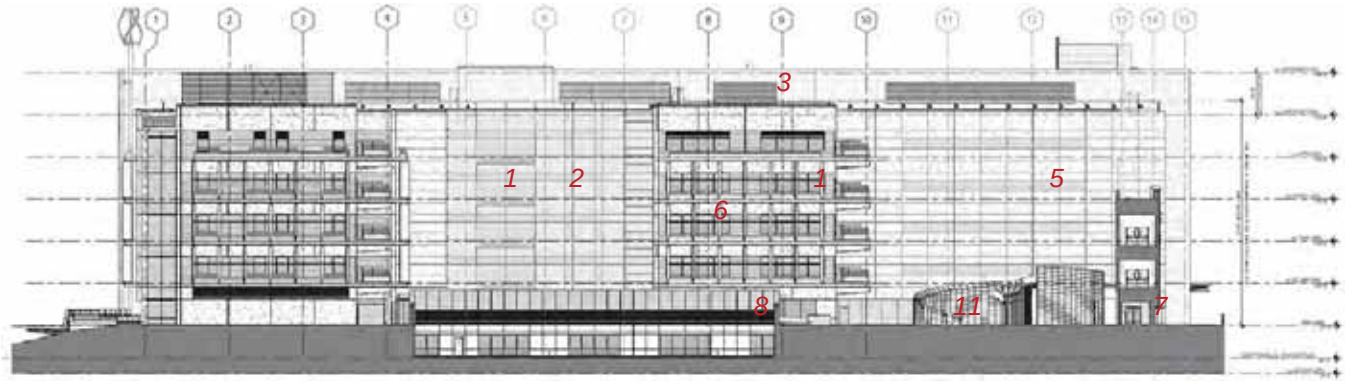


Figure 4: West Elevation with envelope types identified.

JOINT TYPES

Five joint types between disparate materials encountered on the project are considered: 1) Seismic Joints, 2) Expansion Joints, 3) Material Transition Joints, 4) Penetration Joints and 5) Anchorage Joints.

1) SEISMIC JOINTS

- GFRC to EIFS (proprietary break away panel with concealed, flexible sheet membrane)
- GFRC to Insulated metal panel (foam infill)
- GFRC to GFRC (foam infill)
- Precast cladding to storefront glazing (foam infill)
- Precast cladding to waterproofed roof garden (sliding metal joint cover with concealed, flexible sheet membrane)
- Insulated metal panel to waterproofed roof garden (sliding metal joint cover with concealed flexible sheet membrane)
- Stone wall to gypsum board soffit (sacrificial crumple panel and concealed air and water barrier [AWB])

2) EXPANSION JOINTS

- GFRC to curtain wall (foam infill)
- GFRC to insulated metal panel (foam infill)
- Insulated metal panel to precast cladding (foam infill)
- Storefront to point supported glass (slotted/sheathed metal panel)

3) SYSTEM TRANSITION JOINTS

- Storefront glazing to GFRC (double sealant)
- Storefront glazing to precast cladding (double sealant)
- Curtain wall to GFRC (double sealant)
- Curtain wall to storefront glazing (double sealant)
- GFRC to louvers (double sealant)
- GFRC to garden roof (single sealant and flashing covering roof waterproofing membrane transition to gasket)
- Stone to storefront glazing (single sealant and concealed AWB)
- Stone to precast cladding (single sealant and concealed AWB)
- Precast cladding to gypsum soffit (single sealant and concealed AWB)
- Precast to garden roof (single sealant and flashing covering roof waterproofing membrane transition to AWB)
- Precast coping to plaster (single sealant and flashing covering roof waterproofing membrane transition to AWB)
- Metal panel to insulated metal panel (single sealant and concealed AWB)
- Metal panel to curtain wall (single sealant and concealed AWB)
- Plaster to louvers (single sealant and concealed AWB)
- Point Supported Glazing to waterproofed roof garden (single sealant and flashing covering transition from roof waterproofing membrane to gasket)

4) PENETRATION JOINTS

- Painted steel outrigger through GFRC (double sealant)
- Painted steel outrigger through Curtain Wall (single sealant)
- Metal Clad outrigger through Stone (single sealant)
- Galvanized steel outrigger through spandrel metal panel (double sealant)
- Painted steel outrigger through metal panel (single sealant)
- Punched window within GFRC (double sealant at jambs and head; chicken-head gasketing at sill)
- Ribbon window within GFRC (double sealant at jambs and head; chicken-head gasketing at sill)

5) ANCHORAGE JOINTS

- Fiberglass grating to Painted steel outrigger (plastic isolation shim, anchor clip with friction weld pins)
- Aluminum shading shelf to Laminated Glass fin (stainless steel point support with rubber isolation gaskets)
- Laminated Glass fin to Painted steel outrigger (aluminum shoe with isolation pad bolted to steel outrigger)
- Point supported glazing to Painted steel outrigger (stainless steel point support with rubber isolation gaskets)
- Point supported glazing to Painted steel column (stainless steel point support with rubber isolation gaskets)

METHOD

JOINT STRATEGIES

Descriptions below explain the challenges associated with the design of each of the various joint types.

SEISMIC JOINTS

Seismic joints on the project were typically between disparate materials. The solutions varied greatly based on the amount of movement expected, the materials being joined by the joint and the visibility of the joint.

In areas with expected displacements of 10” or more, proprietary break-away covers were used, such as at the connection between the project building and the existing hospital building. In this instance, the joint cover system was anchored to steel framing on both sides of the joint, connecting GFRC on the new building to the exterior insulation and finish system (EIFS) on the existing building. Because these joints required significant seismic movement, the team selected a break-away cover painted to match the adjacent GFRC and EIFS. To maintain a continuous functional weather barrier, the assembly uses an oversized silicone sheet lapped in at both sides of the joint.

Wall to roof seismic joints were typically served by proprietary L-shaped metal joint covers. These were used to shed bulk water and required a continuous, flexible waterproof sheet membrane connecting the wall moisture management system to the roof waterproofing. Applications included: precast coping to waterproofed roof garden, insulated metal panel to waterproofed roof garden.

In areas where minimizing the visible width of the joint was a priority, sacrificial crumple panels were used. Sacrificial crumple panels afforded the most versatility for connecting disparate façade systems due to their light weight, simple geometry and straightforward anchorage with screws. Sacrificial panels were used at entry area seismic joints between stone and gypsum soffits. AWBs were maintained at support structures behind these façade systems, allowing for a continuous system with a flexible joint behind the sacrificial panels.

Self-adhesive foam infill joints were used for movements up to 3” (corresponding to joint widths up to 6”) where adjacent materials were able to provide an adhesion surface for the foam to attach to and where the joint material needed to provide multiple benefits: color matching to adjacent materials, moisture management, thermal resistance, geometric flexibility to follow changing façade profile. The versatility of the foam infill made it an ideal candidate for the following seismic joint interfaces: GFRC to curtain wall, precast cladding to storefront glazing, and GFRC to insulated metal panel.

EXPANSION JOINTS

Inter-story drift on the project necessitated the use of expansion joints to accommodate up to 2.5” of movement between panels. In the plane of the wall, GFRC panels are horizontally restrained at their base and are unrestrained at the top of the panels. This movement was accounted for with a horizontal inter-story drift joint between panels using highly resilient silicone sealants. Curtain wall panels, on the other hand, are horizontally restrained at the top and are un-restrained at the base. Thus, at GFRC to curtain wall panel transitions, careful consideration of relative movements was required to avoid conflicts during seismic events inducing inter-story drift. At inside and outside corners, similar considerations were required to avoid panel to panel conflicts in drift events. To eliminate these conflicts, foam infill was used at all reentrant GFRC corners (Fig. 6).

Where movement was expected between façade elements exposed to view on all sides, a slotted metal panel joint was used to elegantly tie the façade systems together. This occurred where entries’ storefront glass walls teed into the by-passing point supported glass lobby wall. The slotted metal panel provided a weather tight seal that was aesthetically consistent with the aluminum storefront and the tube steel structure supporting the point supported glass wall (Fig. 5).





Figure 5: Slotted/Sheathed Expansion Joint between Pointsupported Facade and Storefront Façade Figure 6: Foam Infill Joint Tracking Vertically

SYSTEM TRANSITION JOINTS

Transitions between façade systems that did not have any significant relative displacement were of two primary types: double sealant and rain screen over an AWB over substrate.

Double sealant joints were used on transitions between curtain walls, storefront walls, GFRC walls and some precast cladding panels. The outer sealant line was provided to shed water and included weeps to let water between the two lines of sealant to escape. The inner sealant provided the weather barrier tying the two façade systems together into an airtight envelope. The use of the double sealant solution required adjoining façade systems to provide 4” return surfaces to which the sealant lines could be applied.

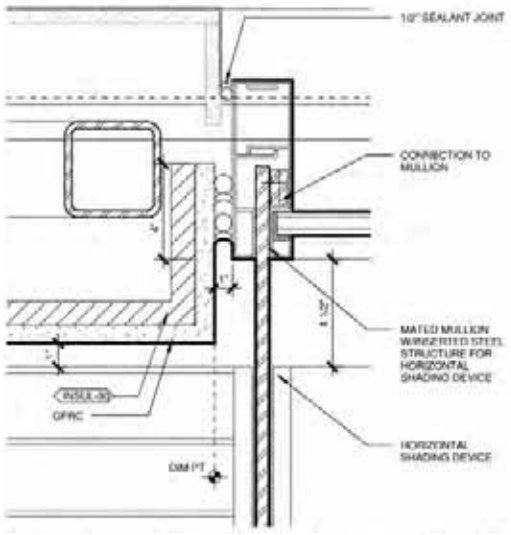


Figure 7: Double sealant joint between GFRC and Curtain wall mullion.

For façade systems having an AWB over a substrate, such as at stone walls, some precast cladding, metal panel, and insulated metal panel façades, the AWB was continuous behind cladding joints and a single line of sealant, or a gasket was used to provide a rain screen between elements.

In addition to the two above mentioned transition joint types, metal panel was also used to bridge the gap between façade systems that were separated by large distances due to building geometry and a desire to contain tectonic expressions without clashing visual effects. This strategy was used at curtain wall to insulated metal panel transitions, where the internal datum lines of the curtain wall were not aligned with the panel-to-panel joints of the insulated metal panel. The bridging metal panel was used to separate the two façade systems while tying the envelope together. Both ends of the metal panel were sealed to the adjacent façade systems and an AWB ran behind the metal panel.

Where façade systems having an AWB intersected with systems having no AWB (GFRC and curtain wall), the AWB was extended to the system having no membrane, where it was sealed to that system to maintain moisture management continuity and air-tightness using a flexible silicone sealant. This occurred at the following transitions: stone to storefront; stone to precast; insulated metal panel to GFRC, storefront, curtain wall, or precast; and gypsum board soffit to GFRC or precast.

At intersections of façade elements with waterproofed garden roofs and walls, stainless steel flashing was used to transition from the façade system to the roof system. Typically, the flashing was installed over a curb and below the façade system and acted as a rain screen and UV-protection for the transition between the roof waterproofing and the façade system AWB or inner sealant/gasket.

PENETRATION JOINTS

Façade systems were penetrated by architecturally exposed structural steel (AESS) outriggers throughout the project. The typical joint between the façade systems and the steel outriggers was double lines of sealant. This occurred at: painted steel outrigger through GFRC, painted steel outrigger through curtain wall, and galvanized steel outrigger through insulated spandrel metal panel. At the hospital entrance, painted steel outriggers penetrate metal panel that bridges between curtain wall and insulated metal panel façades. Single sealant is used at the penetration because an AWB over substrate runs behind the metal panel, connecting the AWB of the insulated metal panels to the curtain wall system.

Punched windows and ribbon windows also constituted penetrations through the GFRC envelope. Double sealant joints were used at jambs and window head, while a chicken-head base plate with gaskets was used below the sill mullion. Weeps at the base of the jambs allowed water to escape while the chicken-head base plate allowed ease of installation and alignment while still providing a continuous weather barrier.





Figures 8 and 9: Penetration Joints at Metal Panel (left) and Stone (right, prior to metal panel cladding on steel beams).

ANCHORAGE JOINTS

The Lucile Packard Children's Hospital façade features catwalks with vegetative planters and multiple shading devices outboard of the main façade cladding. The structural connections tying the many catwalk elements together presented various challenges as the design and construction teams sought to execute elegant and efficient 'anchorage joints'. While not necessarily seam-like, these joints are connection points and interfaces between disparate materials that presented various compatibility questions and challenges.

The first anchorage joint is the thermal break joint between the interior, fireproofed steel framing and the painted exterior outrigger beams. At the location of the thermal insulation behind the GFRC, the steel to steel connection plates are separated by a thermal break plate. This design minimizes the thermal impact of cantilevering steel beams through the façade to the exterior.

Anodized aluminum shoes supporting laminated glass fins were attached to painted steel outriggers. This anchorage joint required selection of materially-compatible fasteners as well as neoprene interface plates to physically separate the materials while joining them together structurally. Predrilled, pre-painted holes in the outriggers provided anchor locations while protecting the steel outriggers from corrosion.

The laminated glass fins, which act as shading devices, support two other types of shading devices. Louvers mounted on aluminum plates were attached to the laminated glass fins by means of four point supports (Fig. 11). Aluminum grating 'shelves' were similarly attached to the laminated glass fins via point supports (Fig. 10).





Figure 10: Glass Fins and Horizontal Aluminum Shading Shelves. *Figure 11: Painted Steel Outriggers Supporting Catwalks, Glass Fins and Airfoil Louvers.*

Fiberglass grating catwalks were secured to the outriggers and miscellaneous painted steel members via 'clips' that were shot-pin friction welded to the painted steel (Fig. 12). However, to prevent the grating from wearing on the painted steel supports, plastic shims below the grating separate it from the steel framing.

Point supported glass anchorage joints are found in a variety of configurations in the public spaces. The six-story laminated glass signage element at the building entry features point supported glass anchored to the painted steel outrigger beams, utilized as a decorative element held proud of the building envelope proper. At the main lobby facade, point supports connect the laminated, insulated glass units of the lobby to painted steel interior columns, creating a canted and undulating feature wall (Fig. 13).





Figure 12: Clip and shot pin securing grating to steel outrigger over circular plastic shim. *Figure 13: Point Supported Glass Anchorage Joint.*

ANALYSIS THROUGH PERFORMANCE TESTING

PERFORMANCE TEST OF PATIENT BED TOWER AND PUBLIC WAITING ROOM FAÇADES

In order to verify that the joint solutions developed by the design team and DA/DB sub-contractors would perform as predicted, performance tests of mockups were executed.

Mockups for the patient bed tower façade and the public waiting room façade (the 'Treehouse') were erected at CCL West, in Ontario California.

The GFRC bed tower did not initially pass the dynamic wind and rain test (AAMA 501.1). Differential pressures were pushing water up over the punched window sill chicken-head profile through a tiny gap between the end of the chicken-head gasket and the end dam at the jamb. Application of sealant at this location resolved the infiltration issue and the façade was retested and passed the AAMA 501.1 test. The bed tower easily passed the drift test (AAMA 501.4). The double sealant at the drift joint was able to stretch exceptionally well and accommodated double the in-plane horizontal displacement required by the test.

The Treehouse curtain wall assembly also had water infiltration during initial dynamic wind and rain testing (AAMA 501.1). By adding more weeps for the water and adjusting pressure equalization measures to let water drain, the Treehouse curtain wall passed the test.

With an understanding that these systems were able to achieve performance targets, the focus was placed on tying these and other façade systems together with pre-tested assemblies or materials such as foam infill, proprietary seismic joints, AWBs, sealant, etc.





Figures 14 and 15: Mockups of public waiting area unitized curtain wall façade (left) and GFRC patient bed tower façade with catwalk assemblies (right) in testing apparatus at CCL West.

CHALLENGES AND SOLUTIONS DURING CONSTRUCTION

TOLERANCES AND ALIGNMENT METHODS OF MULTIPLE SYSTEMS

Fitting the prefabricated GFRC and unitized curtain wall systems onto site-fabricated steel assemblies resulted in alignment challenges at panel joints and penetration joints due to misalignment of the steel. The challenges were most keenly felt at the double-sealant joints, where little erection tolerance (+/- ¼") was specified for the 3/4" joints. The double sealant joints that passed the mockup tests had widths of 3/4", compatible with the contract documents. The field conditions, however, yielded some very large (2") and some very small (1/4") joint widths between panels and at outrigger penetrations (Fig. 16). Because the joint widths were not consistent with the mockup test conditions, the sealant manufacturer was engaged to verify that the field joint widths were acceptable based on the anticipated drifts and movement between panels over the life of the product. In retrospect, engaging the steel fabricator in the DA/DB process would have reduced the risk of misalignment between site-built structures and pre-fabricated façade systems. In addition, joint widths sized to accommodate realistic steel erection tolerances would have reduced the variation in site joint widths between façade systems.

The alignment challenges on the project were compounded by the effects of telegraphing through the multiple layers of façade elements and interior elements. Adjusting one panel to conform to required joint widths at one outrigger penetration required the adjustment of other adjacent panels as well. Interior alignments of adjacent walls needed to be adjusted to match slightly offset punched window locations within the GFRC panels.

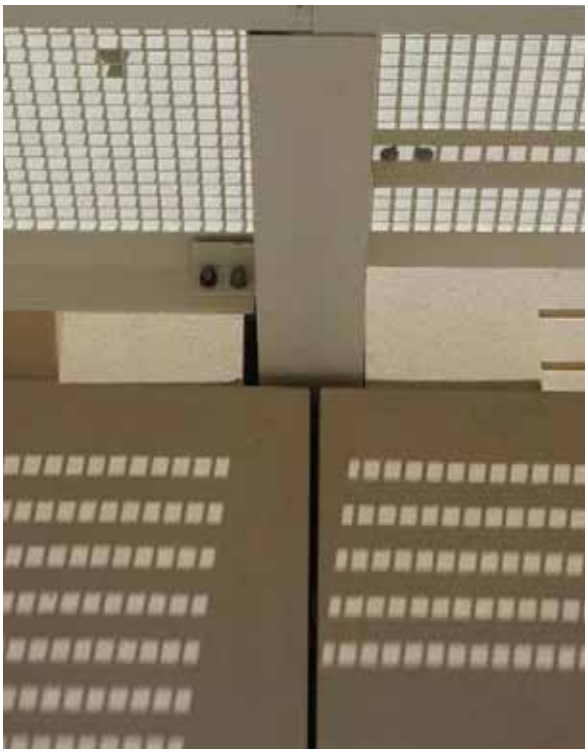




Figure 16: Outrigger and GFRC misalignment. *Figure 17: Complexity of facade geometry compounded alignment challenges and joint installation sequencing.*

DAMAGE AND REPAIR PROCEDURES

The GFRC of the patient bed towers acted as the weather barrier. Some panels experienced cracking during transportation to the site and during installation. Some cracks were located at joints with other materials. To eliminate the potential for water infiltration at the cracks, extensive crack identification and sealing was performed. Panels were retested to ensure that they were impervious to water infiltration.

The project featured several applications of AESS, utilized at the outriggers, as well as at features at the entry approach and lobby wall. The drawings and specifications heavily detailed the level of finishing required throughout, which left very little up to interpretation during installation. The installation was further bolstered by the client's decision to hire a third party paint inspector, who was regularly involved in reviewing the process starting with shop preparation and priming through final in-field patchwork.

AESS elements that were shop painted and shipped to the site generally look quite good upon arrival. Unfortunately, due to installation and adjacent trades, the surfaces were often nicked and marred. At some penetration joint locations, however, the shop priming did not extend far enough into the joint and the AESS needed to be sanded, primed and painted prior to installation of the sealant and overburdens (catwalk grating, planters, glass fins and shading devices). In rare cases, sealant was prematurely installed over un-painted steel. It was then removed for painting of the steel and then re-installed after painting was complete. Though shop-priming and painting proved effective at protecting the majority of the steel during transit and installation, the inevitability of the need to field-repair the paint begged the question whether the schedule would have been better served by a different paint application strategy, such as shop-priming and field painting.

SEISMIC AND EXPANSION JOINT COMPLICATIONS

Seismic joints are complex design and construction challenges. The project geometry required seismic joints not only at the connections to the existing hospital but between elements within the new hospital. The garden landscape on top of the lobby roof introduced significant mass to the structure. The lateral restraints for this mass occur at the ground level and second floor, but not the first floor. Hence, seismic separation from the first floor was carefully considered to allow the roof to laterally

displace without damaging surrounding assemblies. Unfortunately, the building geometry at the surrounding façades was very intricate and had great variation in façade systems adjacent to the joint.

At the east end of the lobby roof, the structure of the roof is adjacent to a precast amphitheater, GFRC cladding and a storefront wall below. At the west end of the lobby roof, the structure of the garden roof is adjacent to an insulated metal panel enclosure, GFRC walls, a precast coping, glass coping, stone walls and gypsum soffits below (Fig. 18-19). Each interface between materials on opposing sides of the joints required careful consideration of the expected movement, and evaluation of whether a visible seismic joint cover was needed (for aesthetic or rain-shedding reasons) or if a simple gap between materials was adequate (at interior and rain-protected areas).

The permutations and variations of the seismic joints that accommodated the movement at these façade interfaces were very challenging to coordinate in the field. Proprietary joint covers were useful in locations where joint size was not of critical aesthetic importance. Custom solutions using crumple panels or foam joints were also used where aesthetics were a driver or where multiple façade systems involved were compatible with these solutions. To reduce the design and construction challenges associated with these joints, two measures considered early in the design process would have facilitated easier project execution: 1. Structural and architectural coordination to ensure that the entire new structure moves together without the need for seismic joints between its constituent parts. Where this is not possible, 2. Simplify the building geometry at the seismic joint location into straight lines with identical façade systems on either side of seismic joints.

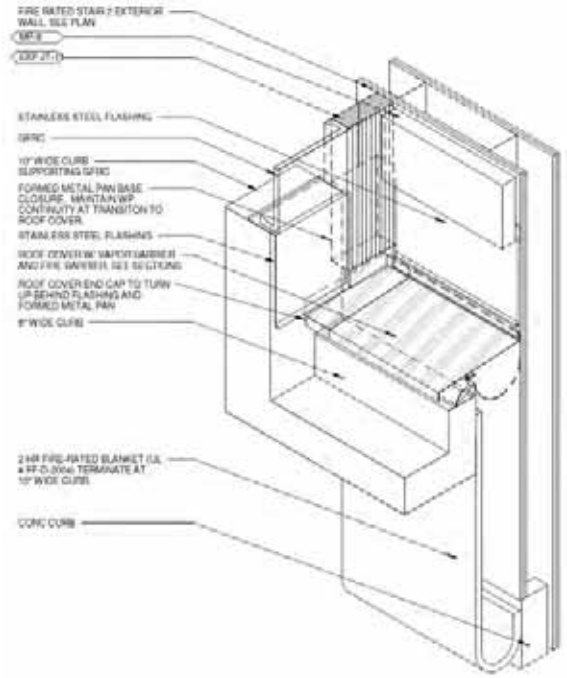


Figure 18. Seismic Joint at Horizontal Garden Roof Deck to Exterior Walls of various types.

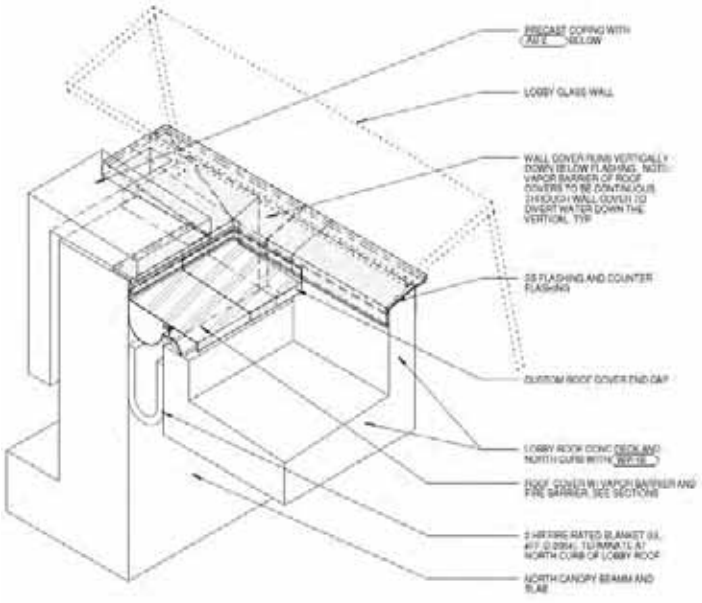


Figure 19. Seismic Joint at Horizontal Garden Roof Deck to Precast and Glass Copings.

FOAM INFILL SUCCESSES

The foam infill used at expansion joints and seismic joints proved very successful for the project for a number of reasons. Firstly, as a self-adhering product with a one-and-done installation, it was a time effective. Secondly, as a foam product, its flexibility accepted minor misalignments between panels without any modifications to the panels or the foam. Thirdly, it provided integral color matching of the rubberized exterior surface. Unlike painted materials which become chipped and marred or metal panel joints and flashing which become dented and bent, the rubberized surface withstands jobsite incidents without requiring any touchup or re-finishing during the punch process.

CONCLUSION

The diversity of façade systems on the Lucile Packard Children's Hospital required the design and DA/DB teams to develop a wide array of joint designs for several joint types: seismic, expansion, system transition, penetration and anchorage joints. Joint designs reflected the relative influence of many factors: geometry of the materials being joined, expected movements, aesthetic importance based on visibility, thermal requirements, material compatibility/corrosion, and water management systems of the façade systems being joined. The DA/DB delivery method helped to ensure that each façade system's requirements were met and that the joints could be constructed as designed. Challenges with joint performance were identified through the mockup process as well as the field observation process. The joints that were designed and built tie together many façade systems and assemblies into a cohesive whole that expresses the programmatic variation behind the façades while maintaining a high-performance envelope at the transitions.

ACKNOWLEDGMENTS

Andy would like to thank: Hajime Ishikawa, Chris Swigert, Chase Rongé, Rob Goodwin, Tom Silva, Tony Tan, Melvin Toddy, Anuj Bansal, Dima Franchuk, Mark Pasveer, and lastly, Kushagra Mittal – your commitment to coordination was second to none.

All photos by Perkins+Will.

VINTAGE VINYL

Lock-strip gasket replacement & remediation strategies



Michael S. Plewacki
Morrison Hershfield
mplewacki@morrisonhershfield.com

ABSTRACT

Mid-century through 1980's buildings with lock-strip or "zipper-gasket" glazing systems are an ever present part of the urban landscape in many cities across North America. Although these systems are considered outdated by many and seldom used in new construction, the systems have performance attributes that should merit respect.

For many in the façade community, lock-strip gasket facades are often dismissed as a system to be removed and replaced with modern aluminum curtain wall. While this may be practical in certain situations, it is far from the only option available and not always the right option for the owner's budget or maintaining the original architecture of a building.

Lock-strip facades continue to endure but age has taken its toll on the functionality of what was once a revolutionary glazing system. By maintaining the lock-strip gasket façade and upgrading glazing when possible, building performance can be restored or even increased as retrofit technology improves.

Remedial options are available for a lock-strip gasket façades that focus on preserving and maintaining the primary elements and appearance of the system from simple remediation efforts such as the installation of exterior "wet-seals" to limit air and water infiltration, to complete replacement and reglazing.

Improved curtain wall performance (reduced air infiltration, lowered solar heat gain and improved acoustical performance) are achieved by introducing modern insulating glass with a low-e coating and emerging technologies, such as vacuum insulating glass (VIG), present possibilities for replacement of an original monolithic glazed system for increased energy performance. Reglazing also provides the opportunity to increase spandrel insulation, or change the aesthetic of the façade by introducing (or removing) existing spandrel panels.

While the benefits of the above are appealing, lock-strip gasket replacement projects are not immune to challenges. As with most remediation projects there are technical considerations to address.

KEYWORDS

lock-strip, gasket, curtainwall, remediation, air infiltration, glass performance, standards, manufacturing tolerance, energy efficiency, fabrication, installation

INTRODUCTION

One of the first large scale lock-strip gasket glazing projects was completed in 1952 at the General Motors Technical Center in Warren, Michigan by Architect Eero Saarinen & Associates (Fig. 1). In 2000 the building was listed on the National Register of Historic Places and in 2014 it was designated a National Historic Landmark.



Figure 1: General Motors Technical Center in Warren, Michigan. Photo by Batthazar Korab, courtesy of the Michigan State Historic Preservation Office.

In 1974 C.J. Parise made mention of this building's façade system in his paper "Evaluation and Test of Lock-Strip Gasket Glazing Systems" in the American Society for Testing and Materials (ASTM) Special Technical Publications 552 where he concluded:

"*There have been many successful (lock-strip) installations in the past 20 years which are still providing satisfactory service. Lock-strip gasket glazing is an excellent glazing system, but as true of any building system, there are certain precautions which must be observed for optimal performance (Parise et.al, 1974*)."

Although he did not live to see the GM Tech Center become a National Historic Landmark, his conclusion on this topic is as true today as it was in 1974 and concisely summarizes the wide range of challenges associated with working with lock-strip gasket glazing systems.

Since this article in 1974, the technology of the lock-strip gasket has largely remained the same. Modern lock-strip gasket designs have however improved based upon early research and testing as well as improvements in manufacturing technology. As state of the industry processes and body of technical knowledge have evolved so have the standards governing the properties, installation and glazing of these systems.

Technical standards are well documented and are a readily accessible resource to gain perspective where the “experience factor” of someone who has specific working knowledge of these systems, such as C.J. Parise in the 1970’s and those like him of that era, becomes less available.

To effectively remediate and replace lock-strip gasket systems, a team must understand not only the applicable standards but also the lessons learned and documented by product manufacturers and those with experience if lock-strip glazed buildings are to stay relevant in our time.

BACKGROUND

Lock-strip gaskets or “zipper gaskets” are generally described as a two-part neoprene gasket assembly consisting of a main body gasket which is used to capture and support the glazed infill, and a lock-strip or “zipper” that is inserted into a receiving channel on the main body gasket to provide compression between the main body gasket, glazing infill and framing. Lock-strip gaskets provide a complete thermal break from the frame of the building and glass to assist in providing an efficient envelope. With no exposed metal the systems provide exceptional condensation control as well as exceptional vibration and noise dampening (Griffith Rubber Mills, 2010).

Remediation of a lock-strip gasket curtain wall system, including removal and replacement of the lock-strip gasket curtain wall and glazing is an option for consideration in many cases where preservation of the building façade is desired.

In such cases, it is likely the lock-strip gasket will require full replacement due to the existing condition of the gasket material. This is highly dependent on the age and exposure of the materials, but the majority of projects considering reglazing have aged to the point where replacement is a prerequisite. There are however times when this may not be necessary and a waterproofing remediation can be undertaken.

During a reglaze and gasket replacement project there is an opportunity for the existing aluminum framing system seals (internal/perimeter) as well as coatings to be restored and the system structurally modified to accept modern high performance glass.

Improvements may include, dual paned insulating glazing unit (IGU) as infill, as well as increased spandrel insulation. The aesthetic of the façade can be altered by introducing (or removing) metal spandrel panels. As the technology becomes more commercially viable, there is the opportunity to reglaze with vacuum insulating glass (VIG) for projects where the modification of monolithic glazed system is prohibitive and increased energy performance is desired.

Introducing a new lock-strip gasket system to an aged façade with modern low-e coated, insulating glass can provide additional visible light transmittance, lower solar heat gain, improved sound transmittance (OITC and STC) performance, all which translates to an increased interior occupant comfort and safety as well as energy savings.

LOCK-STRIP GASKET REPLACEMENT

When replacing gaskets it is critical to understand that RMA (Rubber Manufacturers Association) tolerance for the production of rubber products including lock-strip gaskets are not the same as the tolerances used in the production of glass and insulating glazing units. Tolerance in rubber product production is based on the degree of reproducibility of given dimension and there are many factors that affect molded rubber products and these differ from that generally seen in glass production.

RMA has developed tolerance tables with ranges to provide communication between user and provider across a wide range of industries. RMA standard cross-sectional tolerances are established for measurement of outside diameters, inside diameters, walls, width, height and general cross-sectional dimensions of extrusions. Tolerance for each class of material is generally outlined in table format by RMA. As gasket size in each category increase so do acceptable tolerance ranges.

ASTM C542 “Standard Specification for Lock-Strip Gaskets” establishes minimum dimension for thickness and cross-sectional tolerance of lock-strip gaskets. The basis measurements are derived from reference to RMA Class 2 tolerance. Likewise, standards established by the IGMA (Insulating Glass Manufacturers Association) such as those outlined in TR-1200 “Sigma Voluntary Guidelines for Commercial Insulating Glass Dimensional Tolerances” as well as ASTM C1036 “Standard

Specification for Flat Glass" are often referenced in glass manufacturing. Additional more stringent tolerance requirements may be held by the IGU manufacturer and these can vary.

The disparity between the glass and rubber tolerance can be an issue during gasket replacement and reglazing. It is recommended that the design of the gasket system be coordinated to accommodate these tolerances so that the system will be able to achieve specified performance within the dimensional range.

Issues of tolerance are not however limited to production. Rubber gaskets are susceptible to distortion, shrinkage and environmental factors so it is critical that consideration be made for these factors early in a project. It is important to have conversations with supplier regarding production tolerance and to review gasket shipping and storage as part of the preconstruction process.

Although gasket design tolerance may be adequate, quality control protocols must be established to ensure the permissible tolerances for the gasket physical properties and dimensions. Critical dimensions such as channel width and depth should be verified prior to gasket installation to ensure glass bite, edge clearance, and lip pressure will be maintained (Fig. 2).



Figure 2: Caliper measurement of lock-strip gasket profiles. Photos by Michael Plewacki.

Installation procedures for lock strip gaskets are outlined in ASTM C716 "Standard Specification for Installing Lock-Strip Gaskets and Infill Glazing Materials" This specification includes detailed descriptions of the installation of the system including inspection, preparation and conditioning of gaskets, use of tools, lubricants and sealants, as well as the installation of the gasket in various configurations and glass installation.

The lock-strip receiving channel and lock-strip gasket are continuous at the perimeter of the main gasket. Depending on the gasket profile the lock-strip can be either interior or exterior of the glazing. The mechanical engagement of the lock-strip to the main body gasket is achieved by the marrying of the strip and receiver profile and the difference in durometer Shore A hardness of the two materials.

The lock-strip of harder durometer is forced into the grove in the lower durometer gasket body. This results in a compressive force transfer to the gasket lip, which applies pressure to the glass and frame. Per ASTM C542 a lip pressure of 4lbs/ln.ft. is required for lock-strip gasket glazing. The lip pressure provides the weather seal between the glass and gasket (Fig. 3).



Figure 3: Laboratory and field testing of lock-strip gasket lip pressure by load cell and digital sensor. Photos by Michael Plewacki.

ASTM C 542 “Standard Specification for Lock-Strip Gaskets” outlines the physical requirements of the assembly. Lock-strip gasket main body gaskets are specified to have a Shore A durometer hardness of 75 plus or minus 5 points, however the footnote on Table 1 of this standard allows for a hardness of 80 plus or minus 5 durometer if a separate stock is used for the locking strip. This statement should not be interpreted as suggesting that the lock-strip should be 80 durometer plus or minus 5 points. At that range the gasket and lock-strip may be of similar durometer are unlikely to provide the required lip pressure.

ASTM C964 “Standard Guide for Lock-Strip Glazing” Should be referenced for glazing requirements. Section 8.1.3 of this standard specifies a separate lock-strip of 10 points harder durometer than the gasket as the additional hardness of the lock-strip resists deformation under compression and maintains the designated lip pressure for longer periods than would a lock-strip of equal size of lower durometer (Fig. 4).

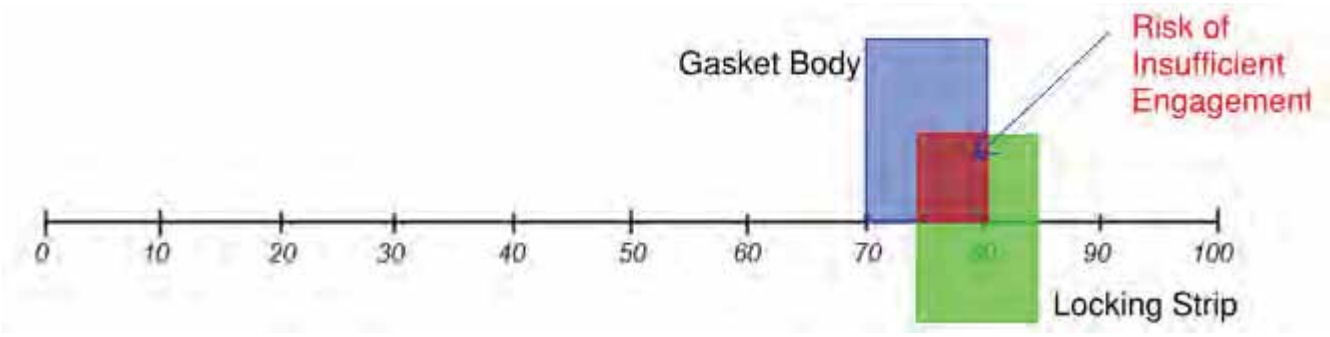


Figure 4: Durometer Range for Main Gasket Body & Locking Strip. Figure by Michael Plewacki.

The proper installation of the lock-strip gasket system should result in a system that meets specified performance considerations of air and water infiltration as well as provide structural integrity to meet ASTM E283, ASTM E330, and ASTM E331 test methods.

REGLAZING WITH IGU

Assuming that the original glazing of the lock-strip gasket system being remediated included monolithic glass, there are additional considerations to be aware of when replacing this glazing with dual-pane insulating glass.

From a structural perspective, review of the existing glazing systems should be performed by a qualified professional engineer to determine if the lock-strip gasket curtain wall system may be remedially engineered and modified to accept standard one inch nominal insulating glass units. This is critical since the addition of the IGU may require modification of the existing aluminum framing and system anchorage. Generally, the introduction of an IGU in a lock-strip glazing system will require additional support of the gasket body to accommodate the increased profile depth and weight of the glass (Fig. 5).

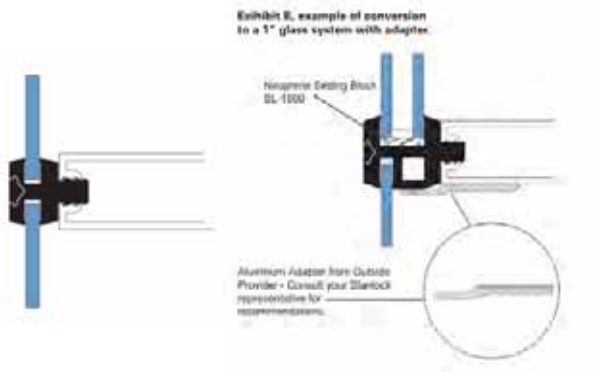


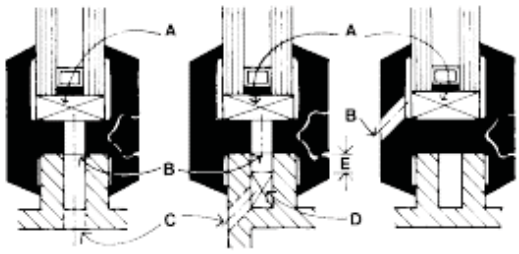
Figure 5: Lock-strip gasket support for IGU glazing. Image courtesy of Griffith Rubber Mills, Stanlock Catalog 2010.

The remedial designer should also determine if the depth of the existing aluminum framing members will meet current code and load requirements. Depending on the significance of the elements of the system to remain or be changed, the project may or may not be subjected to the same code requirements as a full façade replacement. Code and engineering reviews/evaluations should be performed to determine these requirements during the remedial project design phase.

With the introduction of insulating glass, the rubber and glass tolerance becomes of critical importance to the performance of the new glazing system. Care in specifying the design dimensions of the gasket system must be taken to ensure not only lip pressure for air and water penetration resistance, but also main body dimensions for structural performance such as roll off resistance.

Another critical consideration to anticipate is that IGU glazing in lock-strip gasket systems require the gasket system to weep moisture from the glazing pocket to the exterior. This is not always the case when monolithic glass is used. The introduction of weeps to the original glazing rough opening conditions may prove problematic depending on the surrounding conditions.

The preferred method of weeping lock-strip gaskets, in accordance with ASTM C964, is though the bottom of gasket glazing pocket into weepholes at the metal perimeter frame below. This location is often where existing perimeter weather seal joints or other interfaces with adjacent air and weather barriers are located. The standard does allow for weeping of the gasket through the vertical flange, however, this method is not preferable since the weeps are not protected and can conceivably allow water to enter from the exterior under conditions of pressure differential (Fig. 6).



A	Setting blocks at ¼ points
B	Weepholes not covered by setting blocks (center between and on each side of blocks near jambs)
C	Weepholes in frame
D	Open-cell polyurethane pad behind each weephole in frame
E	6.4 mm (¼ in.) minimum clearance when pad is in line with weephole above

Figure 6: Weep strategies for lock-strip gasket with insulating glass. Diagram courtesy of ASTM C 964.

REGLAZING WITH VIG

As discussed, the introduction of an insulating glass unit as part of a lock-strip gasket replacement and reglazing project for a building previously equipped with monolithic glass has distinct benefits and challenges. The challenges faced by modification of the system to accommodate the increased weight of the IGU and new gasket profile to accept the IGU are one of the major disadvantages of engaging in this sort of remedial project and they have the potential to greatly increase the cost of the project.

Advancements in the technology of vacuum insulating glass (VIG) offer a promising solution to the IGU reglazing challenges and the product offers to provide superior energy performance over traditional dual pane insulating glass units.

VIG has a weight and glass thickness similar to monolithic glass of the same thickness. This is a considerable advantage for lock-strip gasket systems. With VIG the remedial project may be able to employ a new gasket similar to the original project lock-strip gasket die as well as avoid modification of the system structurally.



Figure 7: Vacuum insulating glass (VIG) and comparison to traditional 1" IGU. Photo and diagram courtesy of Pilkington North America.

The benefits of employing a VIG system should be evaluated as part of the overall remedial project. While VIG offer increased performance over IGU and may alleviate some need for engineering and system modification, the cost of VIG may be prohibitive to the project. Although the technology is not new, there has only been limited use of VIG in commercial glazing applications. As the VIG technology becomes more commercially available and accepted, the products should become more viable as a solution.

LOCK-STRIP GASKET REMEDIATION

As previously mentioned, remediation of a lock-strip glazing system should include an evaluation of the current physical condition for structural performance, as well as an evaluation air and water infiltration. Depending on the findings of this evaluation, a remediation of the existing lock-strip gaskets could be considered to maintain the serviceability and of the facade.

There are several elements of a lock-strip gasket system remediation that may be considered to extend the serviceability of the existing glazing system. Generally, a remedial program will employ a strategy of mechanical stabilization and preservation of the existing gasket as well as a means of reducing air and water infiltration.

REINFORCEMENT CLIPS

To provide structural support of the existing system, a remediation may include installation of retaining clips at exterior horizontal and vertical lock-strip gaskets. The addition of mechanically attached retaining clips will help to ensure structural performance of system as deteriorated gaskets may not exhibit the same performance characteristics as originally designed. This is especially important at corner zones and locations anticipated to have significant wind exposure (Fig. 8).

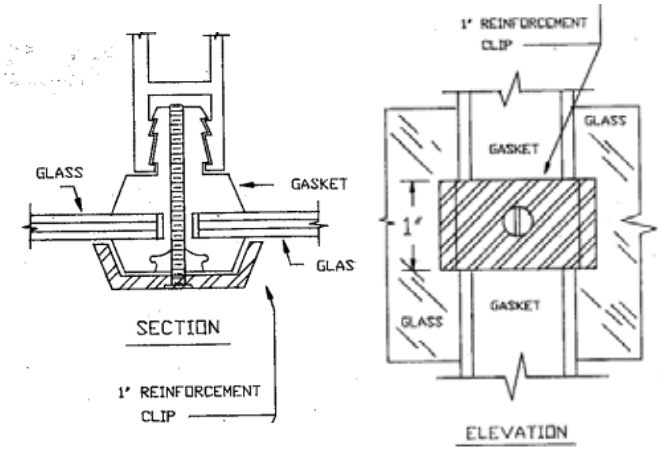


Figure 7: Retaining clips for lock-strip gasket. Diagram courtesy of Image, courtesy of Griffith Rubber Mills.

The use of reinforcement clips results in an increase in the resistance of the gasket to roll off the frame. The use of one clip per side provides substantially higher load capacity and still greater capacity is obtained using two clips per side.

Depending on the gasket and frame profile, several reinforcement clip options are available. The majority of applications require an exterior installation but interior clips are used for some systems to augment exterior clips.

The project specific reinforcement requirements for the lock-strip gasket system should be designed by a professional engineer with experience in façade engineering evaluations. The engineer will be able to determine the number of clips and spacing requirements as well as evaluate the profile of the clip to ensure glass to metal contact is avoided. The clip design strategy can then be coordinated with any remedial waterproofing work.

SEALANTS

To provide reduced air infiltration and increased water penetration resistance an aged lock-strip gasket system may be sealed along the exterior of the gasket. This work generally includes installation of new silicone “wet seals” between the lock-strip gasket and the exterior glass at all perimeters and “bridge seals” at gasket splices and at transitions such as the welded corners of the extrusion.

Typical wet seals consist of a bead of neutral cure silicone sealant tooled between the gasket and the exterior surface of the glass. These joints are tooled to a triangular fillet profile to seal the gasket to the glass. Typical bridge seal work at gaskets splices and transitions is intended to seal voids and cracks at the exterior of the gasket. These seals are generally tooled silicone sealant installed with at a profile of ½” – 1” of sealant adhesion surface and a flat thickness of ¼”. Generally black neutral cure sealants are used in these applications due to potential staining of the sealant from contact with the aged gasket and to mask the repairs.

COATINGS AND COVERS

Along with installation of remedial sealants the exterior lock-strip gasket system may be coated with silicone elastomeric coating or covered with extruded silicone sheet to lessen the exposure of the gasket rubber to additional weathering.

Silicone sealant manufacturers whose products are generally used for wet seal and bridge sealant work offer silicone elastomeric coatings generally used for painting opaque exterior walls. These coatings have been used with success on

exterior lock-strip gasket applications. Coating the gaskets with a silicone elastomeric provide benefits such as encapsulating the gasket to reduce carbon black and other contaminants from staining glass and adjacent finishes, as well as protection from UV to slow the degradation of the rubber (Fig. 9).



Figure 8: Silicone elastomeric and silicone wet seal. Photos by Michael Plewacki.

Another option in covering existing lock-strip gaskets is to use preformed extruded silicone sheet membrane. Silicone sealant manufacturers have developed products specialized for this application and include shape profiles that accommodate wet seal installation at glass perimeters and gasket corner conditions. Silicone sheet covering of the gasket system is generally more costly than coating with silicone elastomeric but there are additional benefits to take into consideration (Fig. 10).

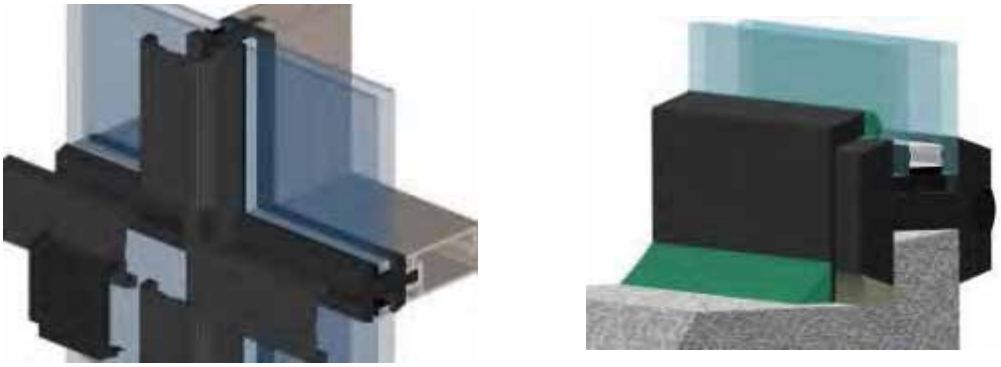


Figure 10: Silicone sheet overlay and wet seal accessories. Diagram courtesy of Tremco Commercial Sealants.

The silicone sheet membrane is advantageous from a long-term performance and durability perspective, and since the product is available in various colors this gives the building owner the ability to change the aesthetic of the façade. In addition, the profile of the extrusion makes it possible to encapsulate gasket reinforcement clips to improve the appearance of the façade.

Other options available include the addition of new aluminum trim color caps installed as part of a lock-strip gasket wet seal remediation. These would be similar to the silicone sheet products in the resulting aesthetics however they are generally attached by mechanical means using a retaining clip system similar to that used to secure the system but with a modified profile that would accept an aluminum cover cap.

CONCLUSION

Mid-century lock-strip façade buildings can continue to function and even perform better with retrofit technology. By maintaining the lock-strip gaskets and upgrading glazing when possible, building performance can be increased and the service life of the building façade can be extended.

There are several options available to achieve a broad range of remediation goals that can be fit to any project or budget. With consideration to available products and emerging technology, lock-strip gasket system architecture can be preserved as a functional façade system well into the future.

Although there are challenges to these projects, the base of knowledge relating to lock-strip gasket glazing is large and well established. The ASTM standards C542, C716, and C964 are a valuable resource for anyone undertaking a lock-strip gasket remediation. These should be referenced and understood alongside of manufacturer's technical documentation and the applicable IGMA and RMA standards to ensure a successful project.

REFERENCES

Michigan State Historic Preservation Office. Michigan Modern. "General Motors Technical Center" http://www.michiganmodern.org/buildings/general-motors-technical-center (accessed July 27, 2017).

Parise C.J. "Evaluation and Test of "Gasket Glazing Systems", Window and Wall Testing ASTM STP 552. American Society of Testing and Materials, 1974, pp. 46-66.

Pilkington North America, NSG Group. Vacuum Glazing, Pilkington Spacia Catalog, 2017.

"SIGMA Voluntary Guidelines for Commercial Insulating Glass Dimensional Tolerances", TR-1200-83, Sealed Insulating Glass Manufacturers Association.

"Standard Specification for Lock-Strip Gaskets", ASTM C542-05, American Society of Testing and Materials, Annual Book of ASTM Standards vol. 4.07.

"Standard Specification for Lock-Strip Gaskets", ASTM C716-06, American Society of Testing and Materials, Annual Book of ASTM Standards vol. 4.07.

"Standard Specification for Lock-Strip Gaskets", ASTM C964-07, American Society of Testing and Materials, Annual Book of ASTM Standards vol. 4.07.

"Stanlock Architectural Gasket Systems Catalog", Griffith Rubber Mills, 2010.

Tremco Commercial Sealants & Waterproofing Structural Lock-Strip Façade Restoration Solutions Catalog, Tremco Commercial Sealants, 2016.

Glass <> Material

DESIGN CONSIDERATIONS

Heat strengthened glass with ceramic enamel frit



Stephen M. Morse, Ph.D.
Michigan Tech University
smmorse@mtu.edu



Kayla Natividad, Ph.D.
Pilkington North America
kayla.natividad@nsg.com



H. Scott Norville, P.E., Ph.D.
Texas Tech University
scott.norville@ttu.edu

ABSTRACT

Window glass design using ASTM E 1300 entails determining glass thickness(es) and types so that the window glass construction load resistance magnitude equals or exceeds the design load magnitude over a specified time interval. A typical spandrel glass configuration consists of an insulating glass unit with an interior heat strengthened lite that has a full flood ceramic enamel frit application. Numerous thermally induced fractures in heat strengthened lites with full flood coverage ceramic enamel frit in spandrel glass configurations have occurred in the recent past. These thermally induced fractures led to investigations concerning the load resistance of heat treated (both heat strengthened and fully tempered) glass with and without ceramic enamel frit. The authors conducted initial investigations using small beam specimens in four-point bending. Following that, they tested full size heat strengthened glass lites with and without ceramic enamel frit.

The investigations have indicated that a full flood application of ceramic enamel frit can reduce the load resistance of heat strengthened glass by as much as 40%-50%. ASTM E 1300 provides no guidance to determine the load resistance of heat strengthened glass that has a surface treatment that reduces its load resistance. In fact, a literal reading of its scope indicates that ASTM E 1300 cannot be used to facilitate thickness selection of glass with a surface treatment that reduces its load resistance. This would include a full flood application of ceramic enamel frit. Based upon their work in investigating heat strengthened glass load resistance, the authors advance recommended reductions to design values of glass load resistance for heat strengthened glass lites with ceramic enamel frit.

KEYWORDS

architectural glass, glass performance, durability, heat strengthened glass, ceramic enamel frit, design processes, load resistance

INTRODUCTION

ASTM E 1300-16 (2016) defines load resistance (LR) as the magnitude of the constant uniform load acting on a glass lite for a duration of 3 seconds that will result nominally in a probability of breakage less than or equal to 8 lites per 1000 at its first occurrence. ASTM E 1300-16 gives users methodologies to determine the LR of monolithic glass types with varying support conditions, laminated glass types with varying support conditions, and insulating glass simply supported along all four edges. ASTM E 1300-16 currently recommends a type factor of 2 to relate the LR of heat strengthened (HS) glass to that of annealed (AN) glass having the same geometry. The authors know of no basis in the literature to support the use of this type factor for HS glass. In addition, ASTM E 1300-16 offers an alternative methodology based upon residual compressive surface stress (RCSS) to determine LR for heat treated (HT) glass. The alternative methodology, termed the “analytical method”, stems from work reported by Morse and Norville (2011). The analytical method results in typically larger magnitudes of LR for HT glass than does the current chart-based approach, now termed the “simplified method.”

Because the LR of HS glass is larger than that of AN glass, designers can use HS glass to resist higher wind loads, for example. Typically, though, under higher loads, deflection considerations will result in specification of thicker glass with or without heat treatment. One very common reason to use HS glass instead of AN glass is to reduce the risk of thermal breakage occurring. This is particularly true in spandrel glass where ceramic enamel frit is frequently used as an opacifier.

An application of ceramic enamel frit to AN glass which is subsequently HT has been shown to alter its LR (Bergers, et al., 2016; Maniatis and Elstner, 2016). Generally, but not always, an application of ceramic enamel frit lowers LR. Based upon insights gained from four-point bending tests (Natividad, et al., 2017) coupled with failure data from full scale tests (Bergers et al., 2016), the authors recommend designers consider applying reduction factors to LR for HS glass with ceramic enamel frit as recommended below in lieu of frit manufacturers providing test data that indicates the LR of HS glass with ceramic enamel frit.

BACKGROUND

An application of ceramic enamel frit alters the LR of HS glass. The change in LR associated with ceramic enamel frit depends on many factors including but not limited to: the frit application method (full flood, silk screen, or ink jet printing), the frit thickness, and even the frit color (Bergers, et al., 2016; Maniatis and Elstner, 2016). New HS and FT glass lites with full flood coverage ceramic enamel frit have been shown to have significantly lower LR than new HS and FT glass without ceramic enamel frit (Bergers, et al., 2016, Natividad, et al., 2017). European glass design recommendations, EN 1863-2 (2004) and others, prescribe a significant reduction in values of allowable stress when sizing HT glass with ceramic enamel frit. Krohn et al. (2002) reported that an applied enamel coating has a negative effect on the strength and fatigue characteristics of heat treated float glass, due to defects in the enamel.

In response to thermal fractures of spandrel glass in a large building in the eastern US, Natividad et al. (2017) conducted four-point bending tests of HT glass beams with a full flood application of black ceramic enamel frit loaded to place the surface with the ceramic enamel frit in tension. They determined that the full flood application of ceramic enamel frit reduced the mean LR of HT glass beams by nearly 50%. In other words, the mean LR of the HS glass beams with a full flood application of ceramic enamel frit displayed LR nearly equal to the mean LR of clear AN glass.

Bergers et al. (2016) reported tests of new full-scale HS glass lites with and without frit. Specifically, they tested five new HS glass samples. Sample 1 consisted of clear HS glass, that is, no ceramic frit. Samples 2, 3, and 4 had ceramic frit patterns with increasing coverage areas applied with a silk screen. Sample 5 had a full flood coverage of ceramic enamel frit. Figure 1 shows the patterns for samples 2, 3, and 4. The ceramic enamel frit on all specimens was grey.



Sample 2: Dots	Sample 3: Lines	Sample 4: Holes
Dot Diameter: 3mm	Line Width: 3mm	Hole Diameter: 3mm
40% Coverage	50% Coverage	60% Coverage

Figure 1. Frit Patterns on Samples 2, 3, and 4.

GLASS STRENGTH DISTRIBUTIONS

ASTM E 1300-16 defines glass LR in terms of a lateral load with constant magnitude over a 3 second duration, P_3, that corresponds to a probability of breakage of 8 lites per 1000 at the first occurrence of the loading. Analysis of the failure load data from Bergers et al. (2016) produced surface flaw parameters that describe the distribution of 3-second equivalent failure loads, P_3. Both Bergers et al. (2016) and Natividad et al. (2017) describe the analysis. Table 1 presents the surface flaw parameters, m and k, along with the minimum RCSS value for the samples in Bergers et al. (2016).

Sample Number	m	k {[meter$^{m/2}$][Newton^{-m}]}	Minimum RCSS Value (MPa)
1	6.60	6.81(10^{-53})	42.9
2	8.40	3.63(10^{-64})	41.1
3	12.0	1.18(10^{-91})	40.1
4	9.40	2.40(10^{-73})	42.3
5	6.60	1.82(10^{-53})	45.7

Table 1. Surface Flaw Parameters (m, k, and Minimum RCSS) for the Cumulative Distribution Functions.

Figure 2 presents the associated cumulative distribution functions (CDF) for the five samples reported by Bergers et al. (2016). It suffices to point out that the CDF to the far right represents the probability of breakage versus P_3 for new clear HS glass; the CDF to the far left, new HS glass with full flood coverage ceramic enamel frit; and those in the middle, new HS glass with ceramic enamel frit patterns.

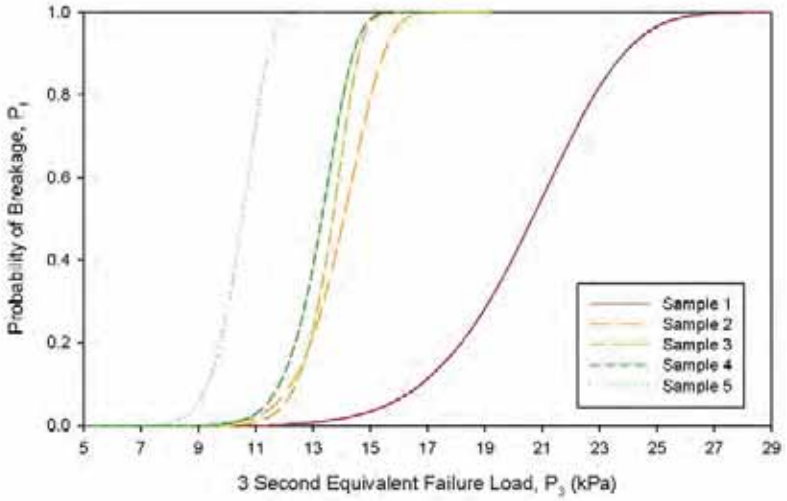


Figure 2: Cumulative distribution functions of P_3 derived from samples reported by Bergers et al. (2016).

COMPARISONS OF EXPERIMENTALLY DETERMINED NEW HS GLASS LOAD RESISTANCE WITH ASTM E 1300 DESIGN LOAD RESISTANCE DETERMINED BY THE SIMPLIFIED METHOD

The surface flaw parameters facilitate the construction of LR charts based upon the experimental failure data. Figure 3 presents a chart similar to non-factored load (NFL) charts in ASTM E 1300-16. This chart presents experimental LR for new HS glass based on Sample 1, the sample with no frit. The broad blue load lines with numerical values printed where they intersect with the sloping aspect ratio 1 (AR1) line represent LR values for nominal 6 mm thick new, clear HS glass based upon the surface flaw parameters and RCSS values from Table 1. The red contour lines show the ratio of the LR in this chart to design values from the simplified method in ASTM E 1300-16, nominally 2 x NFL. As expected, the red contour lines indicate that the new, clear, HS samples have LR at least 1.2 times the design values and as much as 2.4 times the design

values ASTM E 1300-16. This is reassuring in that design values should be safe even if some small degree of in-service weathering occurs.

Figures 4 through 6 present LR charts for new HS samples with ceramic enamel frit patterns based on the surface flaw parameters reported by Bergers et al. (2016). The charts represent LR for nominal 6 mm thick rectangular glass lites simply supported along all four edges. The ceramic frit was applied to the glass using a silk screen. Figure 4 presents load resistance for new HS glass with a ceramic frit pattern covering 40% of the glass surface area. Figure 5 presents load resistance for new HS glass with a ceramic frit pattern covering 50% of the glass surface area. Figure 6 presents load resistance for new HS glass with a ceramic frit pattern covering 60% of the glass surface area.

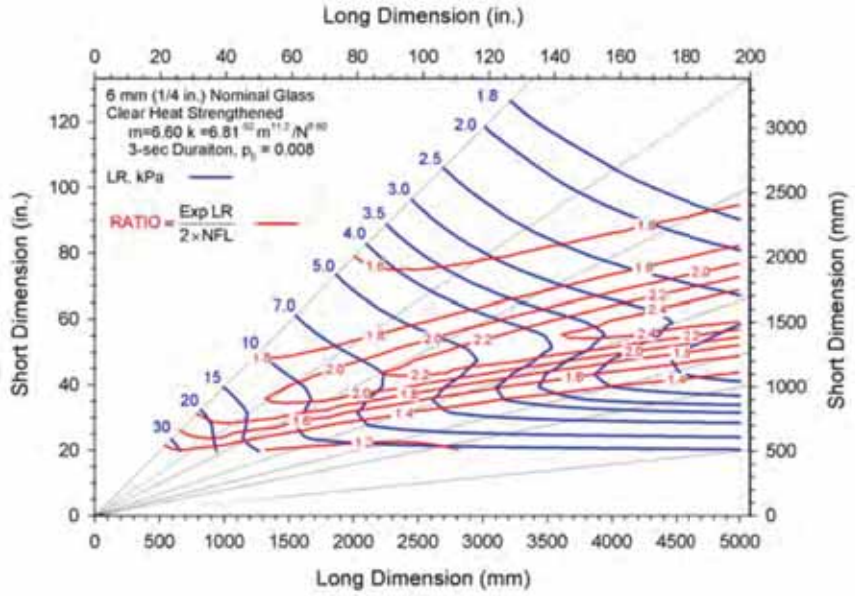


Figure 3: Experiment LR of nominal 6 mm thick new, clear HS glass compared to design values from the simplified method in ASTM E 1300-16.

In general, the LR for the HS glass with ceramic frit patterns has lower magnitude than that for clear HS glass. Only the pattern in Figure 6 (60% ceramic enamel frit coverage) results in LR generally higher than the design LR for HS glass from ASTM E 1300-16.

Figure 7 presents experimentally determined LR for nominal 6 mm thick, new HS glass with a full flood coverage of ceramic enamel frit along with contour lines that relate its LR to design values from ASTM E 1300-16. Full flood ceramic enamel frit coverage results in the most reduction of the magnitude of LR for HS glass. The contour lines indicate that the experimental LR falls as much as 30% below the design values of load resistance from ASTM E 1300-16.

DESIGN EXAMPLE: LR OF A SPANDREL INSULATING GLASS UNIT BY THE SIMPLIFIED METHOD

Consider an IG unit with rectangular dimensions 965 mm x 1930 mm. The design wind load (3-second duration) that the IG unit must resist is 7.00 kPa. We would like to use glass plies with nominal 6 mm thickness. Using ASTM E 1300-16, we find that using HS glass plies gives the IG unit 7.16 kPa LR predicated on the assumption that both lites have full HS load resistance. Since this is a spandrel unit, though, let's put a full flood coat of ceramic enamel frit on the innermost surface of the IG unit. From Figure 7, we find the LR of the inner lite as 3.60 kPa. Because this is an IG unit, we must apply a factor of 0.9 that reduces the LR of the inner lite to 3.24 kPa. The load share factor is 1/0.5 or 2.00 and the LR of the spandrel IG unit is then 6.48 kPa, which falls below the design wind load. This gives an overall reduction of nearly 10% for the IG unit.

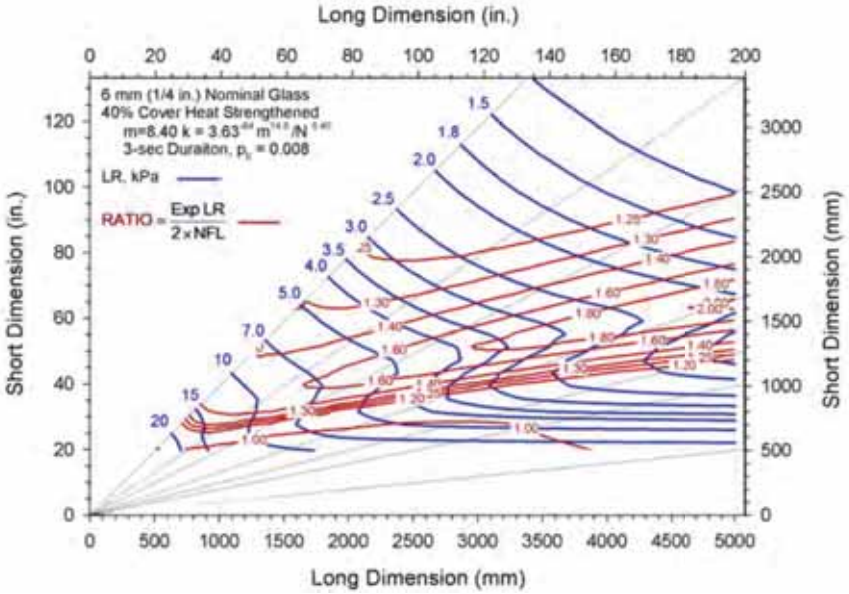


Figure 4: Experiment LR of nominal 6 mm thick new HS glass with 40% coverage ceramic enamel frit pattern compared to design values from the simplified method in ASTM E 1300-16.

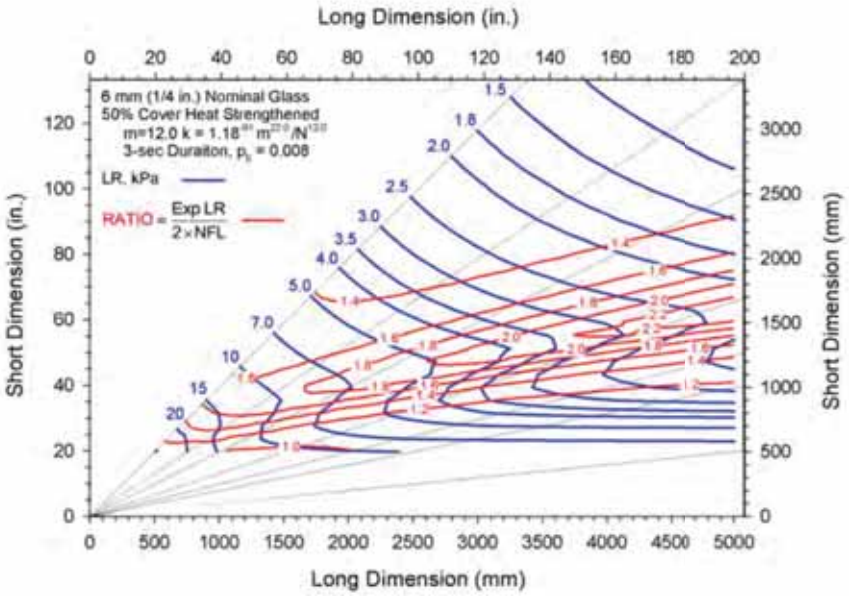


Figure 5: Experiment LR of nominal 6 mm thick new HS glass with 50% coverage ceramic enamel frit pattern compared to design values from the simplified method in ASTM E 1300-16.

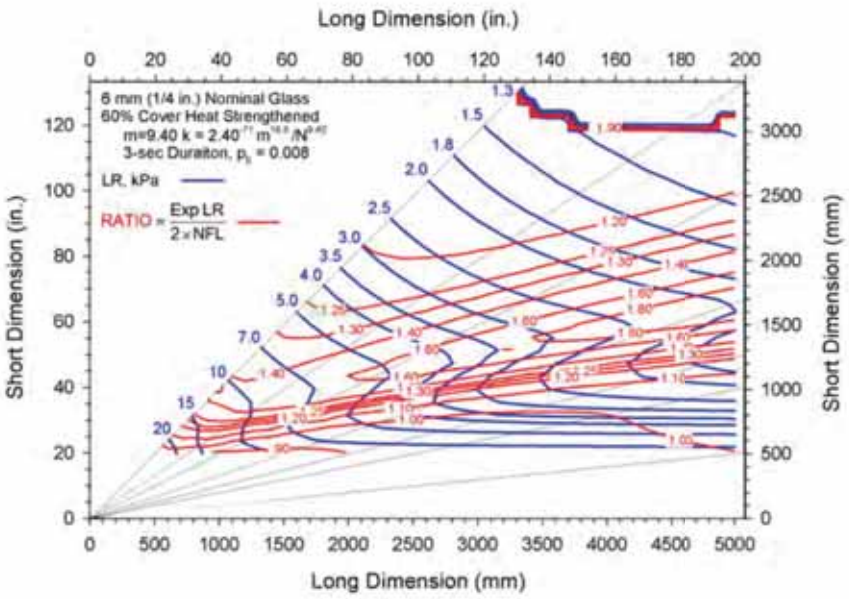


Figure 6: Experiment LR of nominal 6 mm thick new HS glass with 60% coverage ceramic enamel frit pattern compared to design values from the simplified method in ASTM E 1300-16.

This result does not mean that the IG unit will fracture should the design wind load occur. What it means is that the probability of breakage for the unit with full flood ceramic enamel frit on the inner lite will exceed 0.008 at the occurrence of the design wind load if we compute the design load based on LR for clear HS glass. In other words, the overall risk increases.

DESIGN RECOMMENDATIONS

These recommendations may seem draconian but limited data exist concerning the LR of HS glass with ceramic enamel frits. The charts in Figures 4-7 concern one color of frit from one manufacturer applied in two different manners: full flood and silk screen. So, the recommendations go as follows. If using the ceramic enamel frits and patterns used to develop the charts in this paper on which Bergers, et al. (2016) provide additional information. Simply refer to the charts. Other cases are listed below:

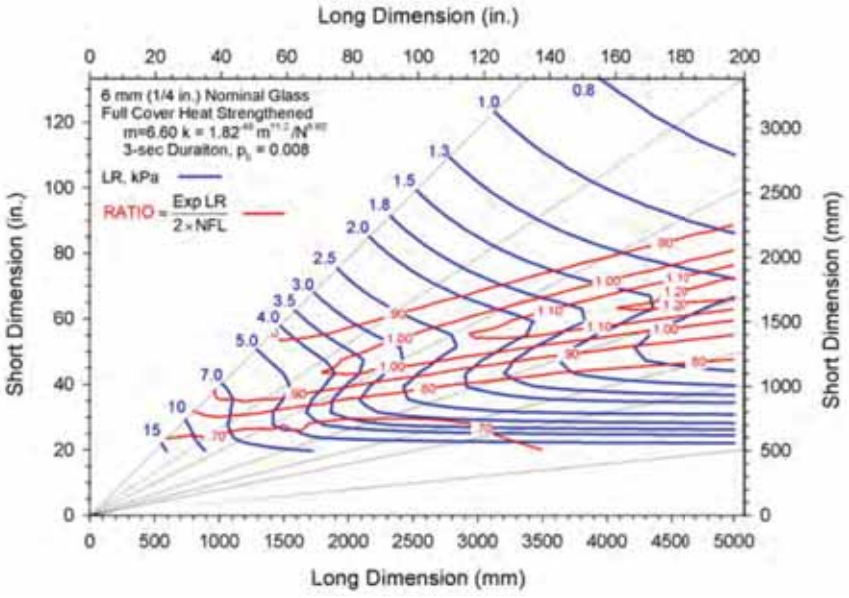


Figure 7: Experiment LR of nominal 6 mm thick new HS glass with full flood coverage ceramic enamel frit pattern compared to design values from the simplified method in ASTM E 1300-16.

FULL FLOOD COVERAGE

If the ceramic enamel frit manufacturer or the glass supplier provides no data, or if they provide comparative data from four-point bending tests in which the mean value of P_3 for the HS glass with ceramic enamel frit is less than or equal to 0.50 of the mean value of P_3 for HS glass with no frit, then reduce the LR of the HS with ceramic enamel frit downward by 30% from the LR of clear HS glass determined from the simplified method in ASTM E 1300-16. In other words, multiply the LR for clear HS glass determined from ASTM E 1300-16 by 0.7. If the ceramic enamel frit manufacturer or the glass supplier can provide a chart similar to that in Figures 7, use it in lieu of this recommendation.

SILK SCREEN APPLIED PATTERNS

If the ceramic enamel frit manufacturer or the glass supplier provides no data, or if they provide comparative data from four-point bending tests in which the mean value of P_3 for the HS glass with ceramic enamel frit is less than or equal to 10% of the mean value of P_3 for HS glass with no frit, then reduce the LR of the HS with ceramic enamel frit downward by 10% from the LR of clear HS glass determined from the simplified method in ASTM E 1300-16. In other words, multiply the LR for clear HS glass determined from ASTM E 1300-16 by 0.9. If the ceramic enamel frit manufacturer or the glass supplier can provide charts similar to those in Figures 4-6 use them in lieu of this recommendation.

INK JET APPLIED PATTERNS

The work herein has not addressed this method of application directly. Understanding that but erring on the side of caution, the authors recommend a reduction of 5% from the LR of HS glass with no frit in the absence of any data that support either a smaller no reduction.

The authors further recommend development of a standard test method to facilitate frit manufacturers to develop test data that they can use to reduce the magnitude of the reduction factor, as appropriate.

DISCUSSION AND CONCLUSIONS

Glass, whether AN, HS, or FT, fractures under the action of tensile stress in combination with other factors. This is true whether the tensile stress is induced by temperature variations and or shade lines over the glass as in ‘thermal” stress or whether it is induced mechanically by lateral loads. Limited research exists concerning the impact of ceramic enamel frit on HS glass LR. Another problem involved in this issue is that, as mentioned above, several factors affect that impact including but not limited to frit application method, frit composition, frit thickness, and frit color.

In future editions, ASTM E 1300 must recognize that ceramic enamel frit reduces the LR of HT glass. More than simply recognizing that established fact, ASTM E 1300 must include factors to account for that reduction such as those suggested above. If those factors become too harsh for ceramic enamel frit manufacturers and HT glass producers, then it becomes incumbent on them to provide guidance concerning their particular ceramic enamel frit compositions in conjunction with the application methods that support either no reduction factors or, at least, lower ones. Following this procedure ensures that the use of ceramic enamel frit will not increase the risk associated with window glass failure under wind load.

REFERENCES

ASTM. “Standard Practice for Determining the Load Resistance of Glass in Buildings.” *ASTM E 1300-16*, West Conshohocken, PA (2016).

Bergers, M., Natividad, K., Morse, S.M., and Norville, H.S. “Full scale tests of heat strengthened glass with ceramic frit,” *Glass Structures and Engineering,* Springer, (2016). 1(1): 261-276.

EN 1863-2. “Glass in Building – Heat Strengthened Soda Lime Silicate Glass – Part 2: Evaluation of Conformity/Product Standard” BSI, Brussels, BE (2004).

Krohn, M., Hellmann, J., Shelleman, D., Pantano, C., and Sakoske, G. “Effect of enameling on the strength and dynamic fatigue of soda-lime-silica float glass,” Journal of the American Ceramic Society, (2002). 85(10): 2507-2514.

Maniatis, I., and Elstner, M. “Investigation on the mechanical strength of enamelled glass.” In Glass Structures & Engineering; Springer: Switzerland, (2016). Vol. 1, Issue 1, p. 277.

Morse, S. M. and Norville, H.S. "An analytical method for determining window glass strength," *Proceedings,* Glass Performance Days 2011. Tampere, Finland. June 18-20.

Natividad, K., Morse, S.M., and Norville, H.S. “Tests of heat treated glass with full coverage ceramic frit,” *Journal of Architectural Engineering, ASCE*, 23(3), (2017). 8 pp.

DESIGNING STRUCTURAL LAMINATED GLASS

How the interlayer properties affect post breakage performance



Vaughn Schauss
Kuraray, Trosifol
Vaughn.schauss@kuraray.com

ABSTRACT

Laminated glass with standard PVB has long been used for safety and security due to its ability to adhere the broken glass fragments together. As the boundaries of glass design keep growing, especially in structural applications, a new classification of stiff interlayers has been developed. With higher shear modulus values, these stiff interlayers provide greater coupling of the glass lites, allowing for stronger and sometimes even thinner laminates. However, these interlayers are viscoelastic in nature, and temperature and load duration play a vital part in their performance. When designing with structural laminates, it is critical that the proper shear modulus values be used to calculate glass strength using tools such as the effective thickness method or finite element method software, at least for pre-breakage conditions. This becomes complicated when considering post breakage strength. Currently, destructive testing is the only reliable method to test for post-breakage strength. To investigate the role of interlayer, two overhead applications were tested. The first testing was performed on laminated glass skylights that were point supported. The laminates were conditioned to 50℃ and then impacted with a 100 Kg soft bodied impactor. Different interlayers were tested; however, only the laminate with the Ionoplast interlayer passed the test. In addition to the skylight testing, another test program was initiated to study the effect temperature has on the interlayer's post breakage strength. Point supported laminated glass canopies were tested with three different interlayers: standard PVB, stiff PVB, and Ionoplast. The samples were conditioned to three different temperatures, -20℃, +21℃, and 50℃. After the top lite of glass was broken, 100 Kg blocks were loaded onto the canopy. At 50℃, only the Ionoplast laminate could sustain the 100 Kg load. In addition to the canopy testing, laminates made with stiff interlayers were subjected to wind load testing at different pressures. The laminate deflection was measured, and then the samples were impacted and subjected again to the same wind load pressures. Before the laminates were impacted, the deflection measurements were essentially identical. However, after impact, a large difference in deflection measurements was observed, with the stiff PVB laminate deflecting more than the Ionoplast laminate, even at 28℃.

KEYWORDS

laminated glass, structural glass, glass engineering, glass interlayers, glass performance, glass

INTRODUCTION

Laminated glass has a significant advantage over monolithic glass. When monolithic annealed or heat-strengthened glass breaks, the glass will shatter into large, dangerously sharp pieces. The pieces may fall out of the supports, and could pose a dangerous cutting hazard to bystanders. In specific areas of concern, such as doors and shower enclosures, Consumer Product Safety Commission, CPSC 16 CFR 1201, requires the use of safety glazing. Historically, this has meant the use of tempered monolithic glass. Since tempered glass breaks into small pieces, the potential for cuts and lacerations is much lower than with annealed or heat-strengthened glass. However, in the event of breakage, tempered monolithic glass, as well as annealed or heat-strengthened monolithic glass, will fall out of the supports creating an opening in the building envelope. This is where laminated glass has an advantage. After breakage, the glass fragments will remain adhered to the interlayer. The glass pieces will lock together so that a certain residual structural capacity is maintained. The remaining structural capacity is dependent on the size of the glass fragments, and increases with increasing fragment size. A laminate made with

annealed or heat-strengthened glass will have a larger post-breakage structural capacity than one made with tempered glass. Another factor in post-breakage structural capacity is the type of interlayer. The most common interlayer is PVB, which is soft at room temperature. With some minimally supported glazing designs, tempered laminates made with PVB will experience the wet blanket effect, meaning the laminate will simply fold over when breakage occurs. Switching to stiffer interlayers, such as Ionoplast (also known as Ionomer) and stiff PVB, can lessen and even eliminate the wet blanket effect. However, stiff PVB, still has some limitations.

INTERLAYER PROPERTIES

When designing laminated glass, there are a few tools to verify the laminate will meet the required loads. One of these tools is ASTM E1300 Standard Practice for Determining Load Resistance of Glass in Buildings. This standard presents the effective thickness approach for determining the strength of laminated glass in Appendix X9. To calculate the effective thickness of a laminate, the shear transfer coefficient is first calculated using the thickness and shear modulus, *G*, values of the interlayer, properties of the glass, and length of the smallest in-plane dimension of bending of the laminate. The shear transfer coefficient is a measure of the transfer of the shear stresses across the interlayer. This value is then used to determine the effective thickness of the laminate for bending and stress, separately. The resulting effective thicknesses may be used as monolithic glass with the load charts in the standard, in standard engineering formulas, or with finite element method (FEM) software. FEM software is another tool for the design of laminated glass. FEM software, such as SJ Mepla, can model the laminated glass as a composite material by incorporating the Young's modulus, *E*, of the interlayer and the glass. Like the shear modulus, the Young's modulus is time and temperature dependent. The values may be measured via dynamic mechanical analysis, and if one value is known, can be calculated using the following equation.

$$E = 2G(1 + \mu)$$

Where:

E = Young's modulus

G= Shear Storage modulus

μ = Poisson's ratio, typically 0.5 for PVB

All polymer interlayers are viscoelastic in nature and their modulus data is temperature and time dependent. As the temperature increases, the polymers become softer. The same effect happens as the load duration increases. Table 1 below shows the shear modulus, G, values for standard PVB, stiff PVB, and Ionoplast interlayers.

		Load Duration										
Temp	Product	3 sec	30 sec	1 min	5 min	30 min	1 hour	1 day	5 days	3 weeks	1 month	1 year
	Standard PVB	8.0		1.6			0.8	0.5			0.4	0.3
20°C	Stiff PVB	342.0	230.0	196.0	122.0	55.0	37.0	5.3	2.8	2.0	1.9	1.6
	Ionoplast	211.0	206.0	195.0	188.0	175.0	169.0	146.0	130.0	115.0	112.0	96.5
	Standard PVB	1.0		0.8			0.4	0.3			0.1	0.1
30°C	Stiff PVB	58.0	14.0	9.2	4.0	2.3	2.0	1.6	1.6	1.5	1.5	1.5
	Ionoplast	141.0	119.0	110.0	82.8	66.1	60.0	49.7	24.7	12.9	11.6	6.8
	Standard PVB	0.6		0.5			0.2	0.2			0.1	0.1
40°C	Stiff PVB	3.4	1.9	1.8	1.6	1.6	1.6	1.5	1.5		1.5	
	Ionoplast	63.0	36.6	30.7	19.4	11.4	9.3	4.5	3.6	3.4	3.3	3.1
	Standard PVB	0.4		0.3			0.1	0.1			0.1	0.1
50°C	Stiff PVB	1.7	1.6	1.6	1.5	1.5						
	Ionoplast	26.4	13.5	11.3	7.3	4.9	4.2	2.8	2.4	2.2	2.2	2.1
	Standard PVB											
60°C	Stiff PVB	1.6	1.5	1.5								
	Ionoplast	8.2	4.3	3.7	2.6	1.9	1.7	1.3	1.2	1.2	1.1	1.0

Table 1: Shear Modulus, G (MPa), for standard PVB, Stiff PVB, and Ionomer interlayers at different temperatures and load durations.

Figure 1 below is a graphical view of the previous data comparing the shear modulus of standard PVB, stiff PVB, and Ionomer interlayers at increasing temperatures and three second load. Although stiff PVB closely matches the performance of the Ionomer at colder temperatures, after 30°C the difference becomes clear.

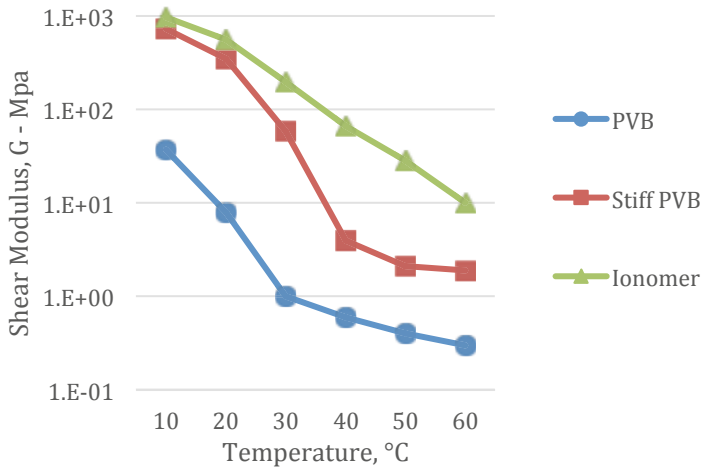


Figure 1: Shear Modulus comparisons for PVB, Stiff PVB, and Ionomer interlayers.

Using the shear modulus data in table 1 at varying temperatures and 3-second load duration, the effective thickness for deflection was calculated according to the formulas in ASTM E1300, see Figure 2. The effective thickness is compared to nominal 12mm monolithic glass. At room temperature, laminated glass with standard PVB has an effective thickness of almost 75% of the monolithic glass. Laminates made with stiff PVB stays close to the monolithic glass up to 30°C, and then dramatically decreases, while the effective thickness of the laminates with the Ionomer interlayer remains close up to 60°C. Since the laminates have a higher effective thickness, it may be possible to meet the load requirements using thinner glass laminates.

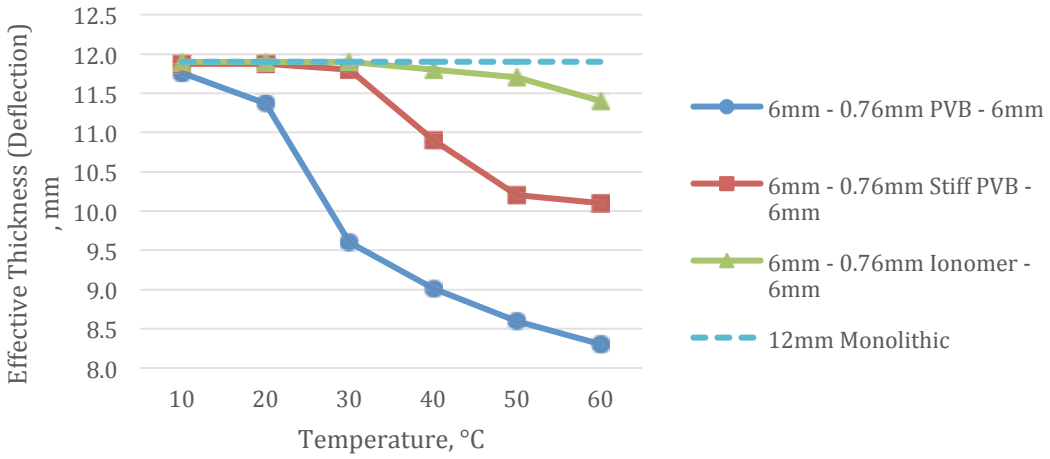


Figure 2: ASTM E1300 effective thickness based on interlayer shear modulus at different temperatures.

POST-BREAKAGE PERFORMANCE

In addition to allowing for designs with thinner glass, stiffer interlayers also provide improved structural performance in the event of accidental glass breakage. This is especially important when considering minimally supported glass, such as point supported or cantilevered balustrades and canopies. Post breakage strength may be categorized into two groups; immediate post breakage strength and medium duration post breakage strength.

SKYLIGHT IMPACT STUDY

Immediate post breakage strength is the result of a quick impact of the glass, such as a swing bag test. It measures the ability of the laminated glass to provide fall through resistance when the glass is impacted. In the last five years, there have been 54 recorded fatalities of employees falling through skylights while on the job (OSHA). This does not even consider the number of instances where non-employees, such as homeowners, have fallen through skylights. To investigate the fall through protection of laminated glass, a test program was initiated. Laminated glass samples made with different interlayers were impacted by dropping a soft bag weighing 100 Kg from a height of 1.2 meters, Figure 3. The laminates were supported using four point supports, one in each corner, Figure 4. The interlayers tested were Ionoplast, stiff PVB, standard PVB, and EVA, and the samples were conditioned for one hour at a temperature of 50°C immediately prior to testing. Upon impact, the laminates made with EVA, PVB, and stiff PVB, Figures 5, 6, and 7 respectively, all tore away from the point supports, offering zero fall through protection. Only the Ionomer laminate remained in place, figure 8. Even though the glass was broken, the laminate did not tear away from the supports. The stiffness of the interlayer even provided enough post breakage structural capacity to support the 100 Kg weight for 15 minutes after breakage. The weight was then removed, and no tears were observed around the point supports.

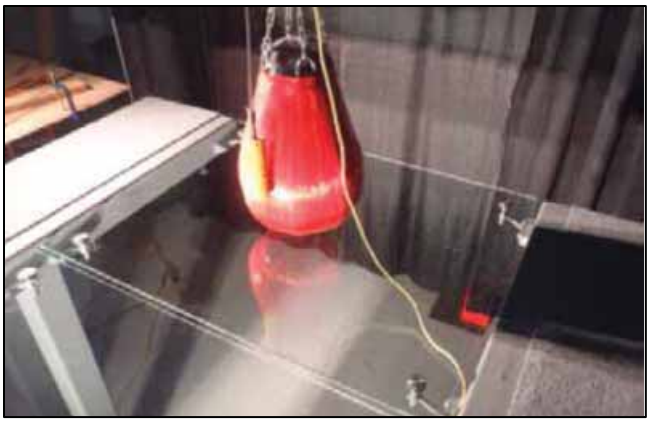


Figure 3: 100Kg soft bag impactor and frameless glass.

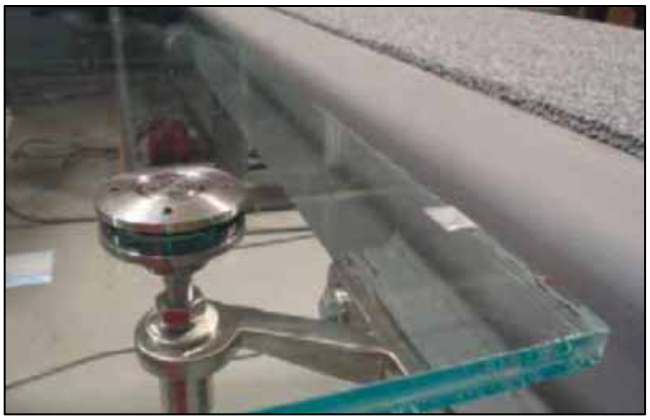


Figure 4: Point supports

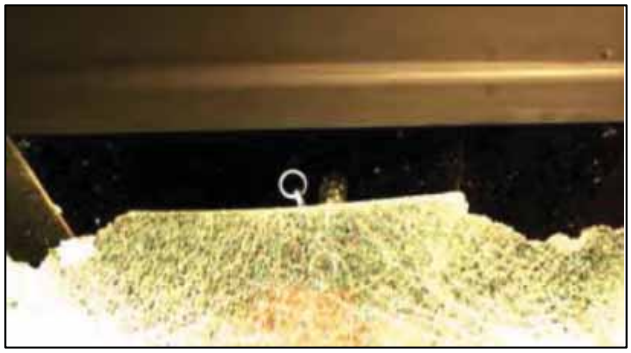


Figure 5: EVA laminate provided NO fall through protection.



Figure 6: Standard PVB laminate provided NO fall through protection.

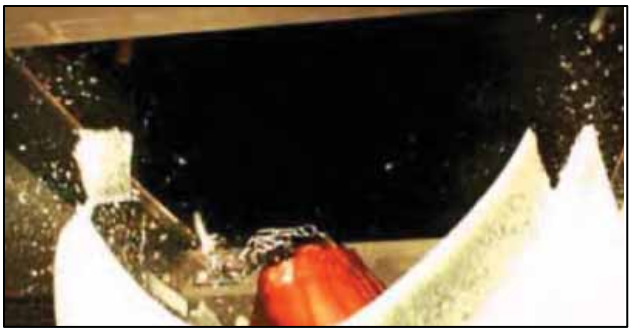


Figure 7: Stiff PVB laminate provided NO fall through protection.



Figure 8: Ionomer laminate provided fall through protection.

CANOPY IMPACT STUDY

Medium duration post breakage strength is the ability of the broken laminate to withstand a load for a longer duration, such as ten or thirty minutes. When calculating the post breakage strength of glass floors, ASTM E2751 Standard Practice for Design and Performance of Supported Laminated Glass Walkways requires an allowable glass stress for ten minutes duration be used. In addition to walkways, overhead glazing also has requirements for medium duration post breakage strength. The German Standard, pr DIN 18008-6 Glass in building – Design and construction rules – Part 6: Additional requirements for walk-on glazing in case of maintenance procedures, requires the laminate to sustain a weight of 100 Kg for at least 30 minutes after the top layer of glass is broken. The laminate is first subjected to an impact with a twin tyre impactor with a weight of 50 Kg and dropped from a height of 900 mm to break the top lite. Next, a 100 Kg load is applied to the laminate over an area of 200mm by 200mm. With the top lite broken, the laminate must support the load for at least 30 minutes. The test is successful if the laminate does not slide out from the supports, the impact does not penetrate the laminate, and no dangerous glass fragments fall down (Haldimann et. al. 2008).

A test program was started to investigate how the temperature influenced the post breakage performance of point-supported canopies using the pr DIN 18008-6 standard. A total of nine laminated glass samples for each interlayer were produced. The interlayers chosen were PVB, stiff PVB, and Ionoplast. The dimensions of the laminated samples were 1.5 m x 2.0 m, and they were point supported in each corner. The testing was conducted at three different temperatures, -20°C, +21°C, and +50°C. Three samples for each interlayer were tested per temperature, and the samples were allowed to condition for 3 hours at each temperature immediately prior to testing. The first objective of the testing was to determine which interlayer would pass the requirements of pr DIN 18008-6 at the different temperatures. The second objective was to determine the maximum weight the point supported laminates could sustain. However, the test apparatus was limited to a maximum of 400 Kg. After the initial breakage, the first 100 Kg weight was placed on the laminate and allowed to remain for 30 minutes or until failure. After the 30 minutes, another 100 Kg weight was added. The additional weights were added in 15-minute intervals until a total of 400 Kg was on the laminate or until failure.

At the coldest temperature, -20°C, standard PVB, stiff PVB, and the Ionoplast interlayers easily passed the 30 minute hold duration with 100 Kg load. In addition, they all supported 400 Kg without any tearing or pulling away from the supports, Figure 19. The test chamber was then heated to +21°C, and after conditioning the new samples, the testing was repeated. This time, when the 100 Kg was added, standard PVB immediately pulled away from the point supports and fell onto the

chamber floor. Stiff PVB and the Ionoplast both passed the 100 Kg load, and both supported 400 Kg, Figure 10. At 50°C, both standard and stiff PVBs failed the initial 100 Kg load. The laminates tore at the point supports and fell on the chamber floor. The 0.89mm and the 1.52 mm Ionoplast passed the initial 100 Kg load. At 200 Kg, the 0.89 Ionoplast tore at one corner, and the laminate deflected enough to allow the weight to touch the floor. The 1.52mm Ionoplast passed the 200 Kg load, but then failed in the same manner at the 300 Kg load, Figure 11.



Figure 9: Post breakage canopy testing at -20°C, from left to right, standard PVB, stiff PVB, Ionomer.



Figure 10: Post breakage canopy testing at +21°C, from left to right, standard PVB, stiff PVB, Ionomer.

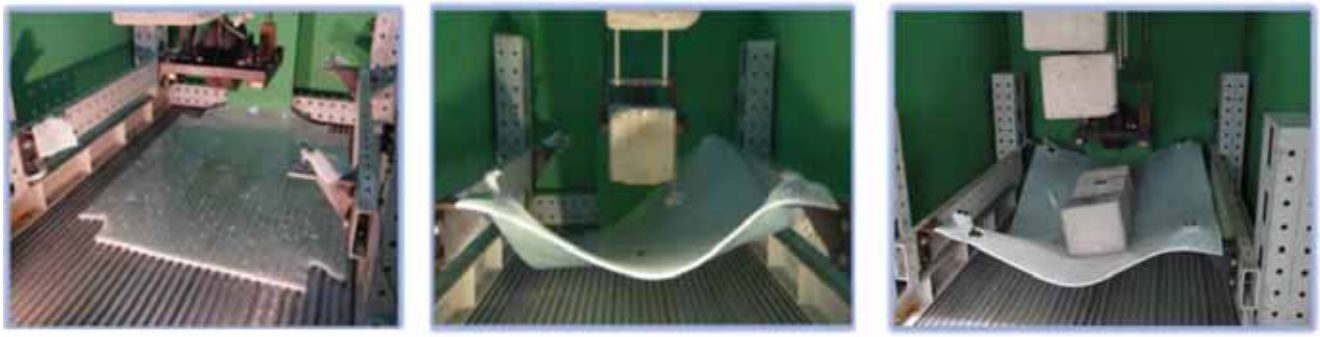


Figure 11: Post breakage canopy testing at +50°C, from left to right, standard PVB, stiff PVB, Ionomer.

WIND LOAD STUDY

In hurricane prone regions, such as Florida's high velocity hurricane zone (HVHZ), laminated glass is designed to protect the building envelope before and after the glass breaks. Before breakage, the laminated glass must meet the required design pressure. However, during a hurricane, flying debris may impact and break the glass, leaving the broken laminate to hold up to the high winds in order to protect the opening. Test methods such as ASTM E1886 and E1996, and Florida Building Code TAS 201, 202, and 203, try to replicate what a window might go through during a hurricane. The window is first impacted to simulate wind borne debris. There are different levels of debris ranging from 2 g steel balls shot at 39.62 m/s to a 2x4 inch lumber weighing 4100 g fired at 24.38 m/s. After the impact, the broken laminate is subjected to positive and negative pressure cycles. To pass, the samples must resist the impact and not pull out of the frame during cycling. A majority of the time, a sample fails during the cycling phase because the deflection becomes too large, and the laminate begins to pull out of the edge supports. To investigate how the properties of the interlayer can impact this failure mechanism, a test program was initiated. The testing was designed to measure the deflection of laminated glass units before and after glass breakage at

different pressure levels. For ease of installation, a dry glaze curtain wall frame was selected that would hold three test panels with dimensions of 1219mm x 1829mm. The laminated panels were made with two lites of 6mm heat strengthened glass with an interlayer thickness of 2.28mm. It was decided to only test the Ionomer and stiff PVB interlayers since standard PVB was not expected to perform well in dry glazed systems. The glass was installed in the frame, and the system was connected to a pressure cycling wall. Before any glass was impacted, the test panels were subjected to 10 second wind loads, and the deflections were recorded under pressures of 50, 75, 100, and 125 psf. The temperature in the lab was controlled, and the test specimens had a recorded temperature of 27.8℃. As expected, the stiff PVB and the Ionoplast samples performed very well, and the deflections were almost identical. In addition, the deflections were also modeled with SJ Mepla FEM software using simply supported conditions and shear modulus, G, values for 30℃ and 3 second load duration for the interlayers. The calculated deflections compared favorably to the actual values. The measured and modeled deflections are depicted in the graph below, Figure 12. The samples were then impacted according to ASTM E1886. A 2x4 inch lumber weighing 4145 g was fired at the glass with a velocity ranging from 15.15 to 15.33 m/sec. Each sample was impacted twice, one in the center and then one in a corner. After the impact, the glass was inspected for punctures and other nonconformities. Both samples passed the impact portion of the test. With the glass broken, the specimens were again subjected to the wind loads. Unlike the pre-breakage deflection measurements, the stiff PVB experienced much larger deflections than the Ionomer laminates, Figure 13. At 100 psf, the Ionomer laminate had a deflection of only 1.5 inches while the stiff PVB experienced a deflection of 4.3 inches. For this reason, it was decided not to proceed with testing at 125 psf.

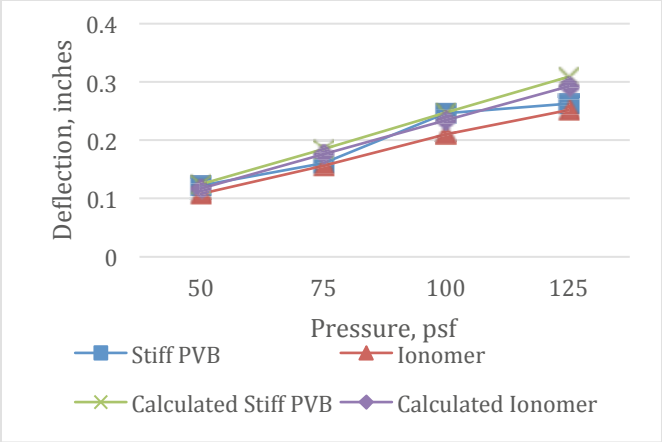


Figure 12: Deflection of glass pre breakage.

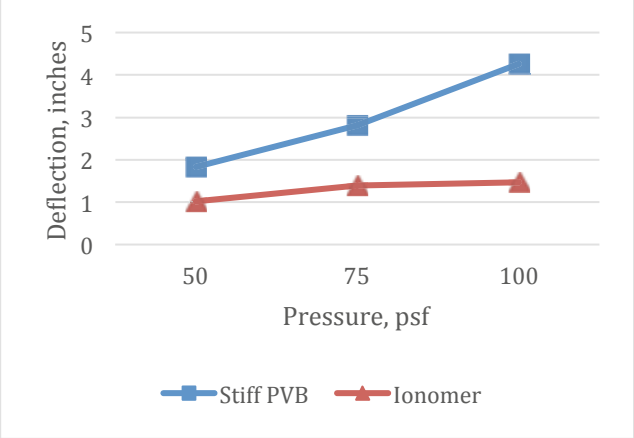


Figure 13: Deflection of glass post breakage.

CONCLUSIONS

At lower temperatures like -20℃, standard PVB was stiff enough to hold the 400 Kg, even after the laminate was broken. However, as the temperature increased, the structural properties of standard PVB diminished, and it could not even hold the 100 Kg weight. Stiff interlayers, such as stiff PVB and Ionomer, provide added strength when temperatures increase. However, above 30℃, stiff PVB begins to soften while the Ionomer interlayer still provides structural capacity up to 50℃. In addition to temperature, the load duration also influences the properties of the interlayer. Longer load times will also diminish the structural properties of the interlayer. In the post breakage wind load test, the laminate made with stiff PVB experienced large deflections, while the Ionomer laminate did not. When designing laminated glass for structural applications, it is important to understand the role the interlayer plays in the performance of the laminate, especially in post breakage performance. Since the interlayers are affected by temperature and load duration, the correct shear modulus should be used when modeling the strength of laminated glass.

REFERENCES

Consumer Products Safety Commission, CPSC 16 CFR 1201. "Safety Standard for Architectural Glazing Materials," 2012.

ASTM E1300-16, "Standard Practice for Determining Load Resistance of Glass in Buildings," ASTM International, West Conshohocken, PA, 2016, www.astm.org.

OSHA https://www.osha.gov/pls/imis/AccidentSearch.search?p_logger=1&acc_description=skylight&acc_Abstract=&acc_keyword=&Fatal=fatal&sic=&naics=&Office=All&officetype=All&endmonth=09&endday=11&endyear=2012&startmonth=09&startday=11&startyear=2017&InspNr= (Accessed September 11, 2017).

Haldimann, Matthias, Andreas Luible, Mauro Overend. "*Structural Use of Glass, Volume 10 of Structural Engineering Documents*." IABSE, 2008.

pr DIN 18008-6:2015-02 (D), "Glass in building - Design and construction rules - Part 6: Additional requirements for walk-on glazing in case of maintenance procedures," German Institute for Standardization, 2015.

ASTM E1886-13a, "Standard Test Method for Performance of Exterior Windows, Curtain Walls, Doors, and Impact Protective Systems Impacted by Missile(s) and Exposed to Cyclic Pressure Differentials," ASTM International, West Conshohocken, PA, 2013, www.astm.org.

ASTM E1996-14a, "Standard Specification for Performance of Exterior Windows, Curtain Walls, Doors, and Impact Protective Systems Impacted by Windborne Debris in Hurricanes," ASTM International, West Conshohocken, PA, 2014, www.astm.org.

The Florida Building Code, TAS 201-94, "Impact Test Procedures," 2014.

The Florida Building Code, TAS 202-94, "Criteria for Testing Impact & Nonimpact Resistant Building Envelope Components Using Uniform Static Air Pressure," 2014.

The Florida Building Code, TAS 203-94, "Criteria for Testing Products Subject to Cyclic Wind Pressure Loading," 2014.

ASTM E2751 / E2751M-17a, "Standard Practice for Design and Performance of Supported Laminated Glass Walkways," ASTM International, West Conshohocken, PA, 2017, www.astm.org.

GLASS STRENGTH UNDER POINT LOADING

Parametric determination of probability of breakage for typical panel dimensions



Joshua Schultz, Ph.D, P.E., LEED AP, ENV SP
Gonzaga University
schultzj@gonzaga.edu



John Knowles, PE SE
Stutzki Engineering
john.knowles@stutzkiengineering.com



Kedar Malusare
Stutzki Engineering
kedar.malusare@stutzkiengineering.com

ABSTRACT

Structural glass is used in a range of building applications, and while the ASTM E1300 has recently been updated to provide a design method to account for probabilistic failure models for a range of geometries under uniform loads, there does not exist detailed design information for point loads. While, ASTM E2751 provides an allowable stress based on a theoretical probability of breakage (POB) of 8/1000 from the appendix of ASTM E1300, these allowable stresses have only a loose correlation to POB and are not accurate for all glass configurations. To address this, the authors explore the effect of point loads on glass strength using the glass failure prediction model (GFPM) from E1300 to determines the allowable stress (or allowable load) for common glass lite geometry based on a POB of 8/1000 and 1/1000. Results allow practitioners to benchmark designs for monolithic and PVB laminated glass based on various point-support boundary conditions.

The parametric study investigates the maximum principle stresses and stress concentrations of specimen types subjected to out-of-plane bending due to a point load over 26 cm^2 (4 in^2).The maximum point load is found for various 4-side supported glass lites at a POB of 8/1000 and 1/1000.

KEYWORDS

structural glass, glass engineering, component performance, structural design, experiment, point load

INTRODUCTION

Structural glass applications, particularly façade and canopy elements, continue to grow in ubiquity as transparency and daylighting remain significant motivators of architectural design. However, current design procedures (i.e., elasticity and plate theories) and US design standards (e.g. ASTM E1300, 2016) are not directly applicable to structural glass with concentrated point loading. While ASTM E2751 (2017) does address point loads as design considerations it lacks a clear approach to determining strength, instead referencing ASTM E1300. The lack of clear design criteria for glass applications with point loading has resulted in designers relying on stress distributions and single largest maximum principle tensile stress (SLMPTS)

as a guide for acceptable behavior which is often either unconservative or over-conservative – even when using low ultimate stress values to dictate design thicknesses. Development of the most recent ASTM E1300 has changed the approach to a range of structural glass applications due to the probabilistic-based failure prediction method explicitly presented in Annex A2, coupled with the acceptance of numerical modeling to obtain stresses and stress distributions. While the current ASTM E1300-16 still only contains non-factored load (NFL) charts for uniformly distributed loads, it is possible to establish a set of plots similar to those found in Annex A1 using the methodology presented in Annex A2. In an effort to provide meaningful design criteria to engineers and architects alike, a statistical glass failure prediction model (GFPM) is applied finite element analysis (FEA) data to provide design strength results for annealed and heat-strengthened (HS) specimens under point loading that provide a probability of breakage (POB) of 1 in 1,000 and 8 in 1,000, respectively. GFPM results are intended to 1) allow practitioners to benchmark designs for Annealed and HS monolithic glass based on various geometric conditions 2) provide strength of annealed and HS specimens for POB of 1/1000 and 8/1000 and 3) serve as a baseline methodology for more comprehensive, on-going efforts to create complete tables for designers. Additionally, a detailed description of the GFPM is provided with background information in order to assist designers with understanding of the necessity of a rigorous POB-based design approach compared to sole reliance on the SLMPTS.

The growth of glass as a façade component includes applications of skylights, glass floors and curtain walls. The industry trend is to produce larger glass lites to increase transparency and by extension the natural lite and sight lines inside the building. As the need for larger glass is desired, loads from human impact have greater consequences than in the traditional applications of smaller glass panels. Impact loads can come from accidental impact from nearby pedestrians or impact while cleaning. For example, the Virginia Tech curtain wall (Fig. 1A), University of Baltimore curtain wall (Fig. 1B) which is subject to regular cleaning, University of Chicago Biomedical School glass wall with floor to ceiling glass (Fig. 1C) and the large line-supported glass panels of the American Girl Doll Store (Fig. 1D) each have considerable design differences, but all required consideration of an applied point load due to the large areas of glass which increase probability of breakage (POB).



(A) *(B)* *(C)* *(D)*

Figure 1: Projects are increasingly using large panels of glass which neccesitate evaluation of point loads, (A) Virginia Tech curtain wall, (B) University of Baltimore curtain wall (C) University of Chicago Biomedical School glass wall, and (D) large line-supported glass panels of the American Girl Doll Store. Photos courtesy of Stutzki Engineering.

A more obvious example would be the skylight glass used on the roof of the Aspen Art Museum, which also is designed for pedestrian traffic (Fig. 2). This skylight needs to consider the concentrated point loads specified in ASTM E2751 (Standard Practice for Design and Performance of Supported Glass Walkways) and references ASTM E1300 for calculation guidance, but the design charts in ASTM E1300 (Standard Practice for Determining Load Resistance of Glass in Buildings) are for uniform loads only.



Figure 2: The Aspen Art Museum in Aspen, Colorado is a typical application of line–supported, rectangular glass lites subjected to point loading in addition to uniformly distributed loads. Photo courtesy of Stutzki Engineering.

In order to address this design gap, the GFPM is applied to two common glass types (annealed and HS glass) and a range of aspect ratios using the same considerations as the provisions in the commonly referenced ASTM E1300 standard, but focuses on the unique results for point-loading as described in ASTM E2751. This method incorporates the relevant parameters (stress concentration due to Griffith surface flaws, load-duration effects, humidity, residual compressive surface stress, etc.,) on the principle stresses in order to provide designers with design strengths for specific POB for glass panels with point loads.

LITERATURE REVIEW ON PROBABILISTIC GLASS FAILURE

In the United States, most structural glass is currently designed either directly or indirectly according to ASTM E1300 (2016). The nonfactored load (NFL) design charts in Annex A1 of E1300 allow for quick selection of minimum thickness for given panel geometry and desired load resistance of annealed glass. Design thicknesses for other glass types (heat strengthened (HS), fully tempered (FT), laminated glass (LG), insulating glass (IG), wired, and etched) are readily achieved by application of modification factors to the annealed selection. While this procedure appears straightforward, it is essential that designers understand the assumptions and limitations of the method. For example, the design charts in Annex A1 of ASTM E1300 are specifically for determination of the minimum thickness of window glass and are explicitly limited to rectangular geometries with a uniform load that are simply supported along at least one edge. Additionally, Appendix X6 offers “conservative” allowable stresses for use with finite element analysis for atypical glass geometries. However, the source of these “conservative” values is unknown, and there is only a loose correlation between these allowable stresses and actual POB of the glass lite. Since this limitation extends only to the charts in Annex A1 and not the procedure of Annex A2 it is important for designers to understand both the theory behind the design charts and methodology presented in ASTM E1300. The glass failure prediction model (GFPM) that serves as the basis for the NFL charts is used in this research to develop design strengths for POB of 1 in 1,000 and 8 in 1,000 for annealed and HS rectangular lites exposed to point loads. The efficient design of a brittle material with statistical failure behavior (i.e., glass) requires an accurate determination of a multitude of factors: SLMPTS, stress distributions, surface flaw characterization, residual compressive surface stress (RCSS), load-duration, temperature and humidity effects, etc (Schultz et al., 2017). In order to accurately use the ASTM E1300 design method it is important to understand each term and how it has been integrated into the procedure over time.

The brittle and probabilistic nature of glass as a material means that it often fails under stresses significantly lower than the ultimate stress. As early as 1920, it was hypothesized that this was a result of microscopic surface flaws that created stress concentrations which promoted crack growth (Griffith, 1920). Evidence of this behavior was readily observed in failures of all glass types, as the initiation of the failure was often not coincident with the SLMPTS (Natividad et al., 2015). The distribution and orientation of these surface flaws was modeled using the statistical multiple parameter fitting method presented by Weibull (1939). In addition to surface flaws, subsequent research attributed the apparent reduction in annealed glass strength to load duration and presence of humidity (Charles 1958). Many experimental initiatives tested annealed and HS glass specimens to failure in an effort to quantify this behavior (Orr, 1957; Bowles and Sugarman, 1962). The results of these tests combined with successful empirical designs formed the basis for a series of design guidelines developed by the glass industry for window glass in the early to mid-1960s.

A significant change in glass design occurred when Beason and Morgan (1984) combined the effects of surface flaws (orientation and distribution) and humidity into a single glass failure prediction method (GFPM) using a two parameter Weibull distribution and determination of SLMPTS based on the work of Vallabhan et al., (1985, 1987). This research reframed glass strength fully in terms of probability of breakage (POB) rather than ultimate strengths (which were readily mistaken for a type of allowable stress design). The method developed by Beason and Morgan assumes that the glass strength is 1) governed by tensile stress failure and 2) independent of load duration (not necessarily an accurate assumption for all types of glass, i.e., laminated glass). This methodology served (and continues to serve) as the fundamental design approach for glass design procedures and charts in every ASTM E1300 standard from 1989 to 2016. However, subsequent research by Morse and Norville (2011, 2012) has relaxed assumptions of glass type (annealed, HS and FT) and geometry used in the ASTM E1300 charts by creating more general forms of the GFPM equation. In fact, Morse and Norville (2012) presented the explicit form of the risk function, B, not found in ASTM E1300, used by Walker and Muir (1984) for consideration of edge flaws in annealed glass fins. More recently, Afolabi, Norville and Morse (2016) provided a detailed experimental study of HS line supported glass with discussion of RCSS and equivalent failure load (EFL). However, none of these studies focused on point-loads. There has been some research into the aapplication of the GFPM to non-traditional applications like point-supported glass (PSG) was addressed by Cervenka et al., (2016). That research focused on experimental stresses and stress distribution near holes in monolithic and laminated FT glass to determine influence of stress concentrations. The work was extended by Schultz et al., (2017) to create 3-second failure load curves and determination of best-fit m- and k-values for PSG.

METHOD

A series of parametric finite element models were run using Abaqus FEA software (Abaqus, 2017) to obtain the maximum principle stresses and stress distributions. The modeling approach followed the methods outlined by Schultz et al. (2012) and Cervenka et al., (2016), both of which were benchmarked to experimental data to determine accuracy of numerical results. The models were line-supported, rectangular panels modeled with quarter panel symmetry. Out-of-plane displacement of the glass edges were fixed and the other BCs were addressed through the symmetry conditions. Due to the importance of boundary conditions (Schultz et al., 2012), contact interactions were evaluated BC's with multiple materials and found to have a negligible impact on the stress results; consequently, the models were created with BC's applied directly to the edge of the glass. Both annealed and HS panels were modeled as industry-standard linear elastic material with Young's modulus, E, of 72 GPa and Poisson's ratio, v, as 0.22 for a range of aspect rations (Fig. 3).

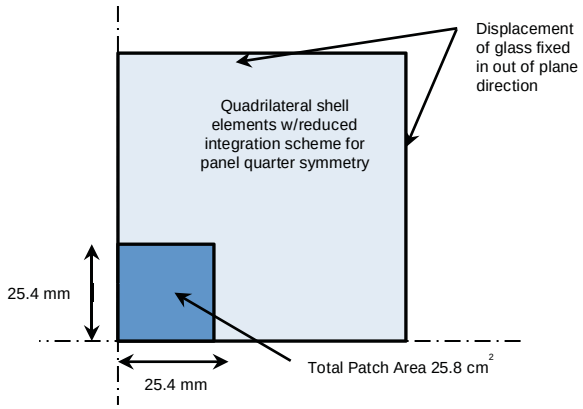


Figure 3: Modeling geometry and options are shown for the parametric study.

A geometrically non-linear analysis was used to account for displacements that are large with respect to the thickness. A quadrilateral shell element with reduced integration scheme, hourglass control, finite membrane strains (Abaqus: S4R) was used as recommended by industry best-practices and previous research (Cervenka et al., 2016, Schultz et al., 2012). Point loads were applied via a 1"x 1" sub-meshed area that was subjected to uniform pressure load.

Once the SMPLTS and stress distributions were obtained from the FEA, the GFPM described by Morse and Norville (2011) was used to determine the POB for annealed and HS glass lites for POB of 8/1000 and 1/1000, respectively. The probability of breakage of a glass specimen using the GFPM is given as:

$$P_b = 1 - e^{-B} \#(1)$$

where, B for a 3-sec EFL is defined in numerical form as:

$$B = k \cdot \sum_{i=1}^{N} \left(\left(c_i \cdot \left(\frac{t_d}{3s} \right)^{\frac{1}{n}} \cdot \sigma_{max} - RCSS \right)^{m} \cdot L_i \right) \#(2)$$

with N as the numbers of nodes in the numerical model, c$_i$ as the biaxial correction factor (in terms of r, σ_{max}, σ_{min}), σ_{max} representing the maximum principal stress, L is the tributary length of the element, n = 16 and m and k are surface flaw parameters are based on a 60s duration (per ASTM E1300-16 A2).

DATA

Maximum, deflections, U, principle stresses, S1, and stress distributions were found for the rectangular panels of varying aspect ratios (Figs 4-6). The stress distributions and deflected shapes of the panels follow symmetric patterns that are expected both from the symmetric BC's as well as from classical plate theory. Representative values of stress and deflection are shown for the loads at failure.

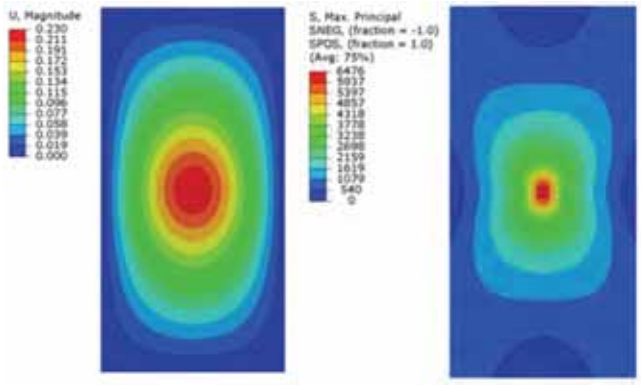


Figure 4: Representative (a) deflections and (b) maximum principle stresses are shown for 75 cm x 150 cm panels.

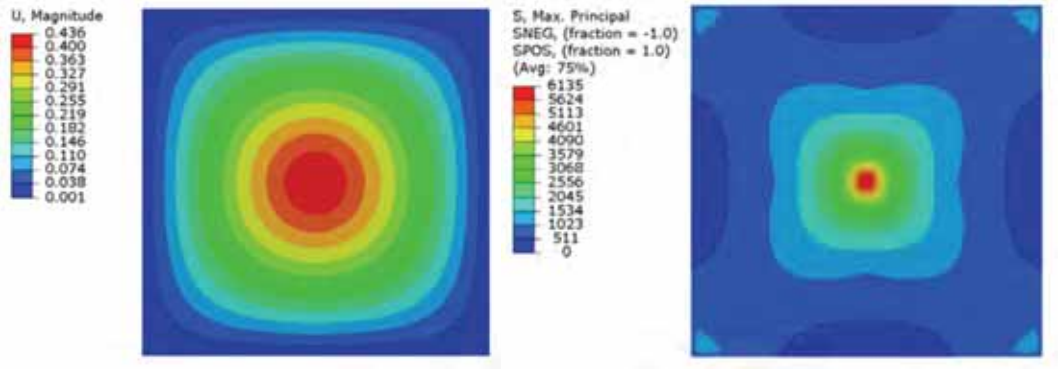


Figure 5: Representative (a) deflections and (b) maximum principle stresses are shown for 150 cm x 150 cm panels.

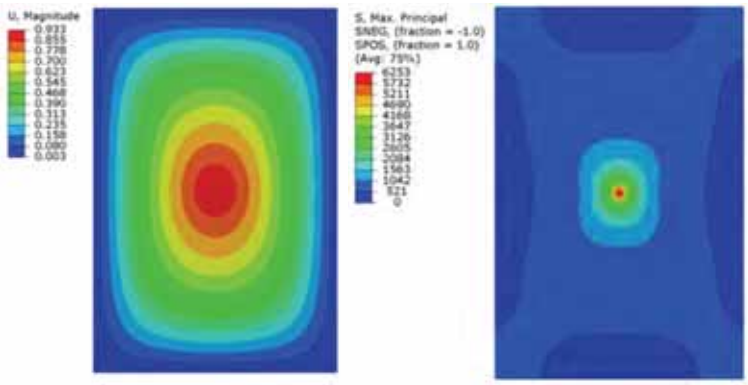


Figure 6: Representative (a) deflections and (b) maximum principle stresses are shown for 245 cm x 370 cm panels.

The stress results were used in combination with the GFPM described by Eqns (1) and (2) to obtain design stresses for POB of 8/1000 (Fig. 7) and 1/1000 (Fig. 8) for annealed glass and HS glass (Fig. 9-10) for a 3-second load duration.

Aspect	Dimensions (m)		Area (m^2)	Load (kN)	Stress (MPa)	POB	Def (mm)
	X	Y					
1	3.05	3.05	9.29	0.83	42.94	0.008	23.37
1	2.16	2.16	4.65	0.81	42.57	0.008	16.38
1	1.52	1.52	2.32	0.78	42.30	0.008	11.07
1	1.08	1.08	1.16	0.76	42.35	0.008	7.14
1.5	2.49	3.73	9.29	0.81	43.11	0.008	23.70
1.5	1.76	2.64	4.65	0.78	43.04	0.008	16.31
1.5	1.24	1.87	2.32	0.75	43.17	0.008	10.72
1.5	0.88	1.32	1.16	0.75	43.69	0.008	6.71
2	2.16	4.31	9.29	0.77	43.68	0.008	23.62
2	1.52	3.05	4.65	0.74	43.68	0.008	15.49
2	1.08	2.16	2.32	0.72	43.63	0.008	9.63
2	0.76	1.52	1.16	0.75	44.65	0.008	5.84

Figure 7: Load and stress results at POB of 8/1000 shown for 6 mm thick annealed glass lites.

Aspect	Dimensions (m)		Area (m^2)	Load (kN)	Stress (MPa)	POB	Def (mm)
	X	Y					
1	3.05	3.05	9.29	0.56	31.16	0.001	19.28
1	2.16	2.16	4.65	0.54	30.79	0.001	13.26
1	1.52	1.52	2.32	0.52	30.60	0.001	8.74
1	1.08	1.08	1.16	0.53	30.73	0.001	5.46
1.5	2.49	3.73	9.29	0.54	31.26	0.001	19.35
1.5	1.76	2.64	4.65	0.52	31.16	0.001	13.00
1.5	1.24	1.87	2.32	0.51	31.34	0.001	8.31
1.5	0.88	1.32	1.16	0.52	31.77	0.001	5.05
2	2.16	4.31	9.29	0.52	31.61	0.001	18.85
2	1.52	3.05	4.65	0.50	31.74	0.001	12.07
2	1.08	2.16	2.32	0.50	31.98	0.001	7.37
2	0.76	1.52	1.16	0.53	32.52	0.001	4.34

Figure 8: Load and stress results at POB of 1/1000 shown for 6 mm thick annealed glass lites.

Aspect	Dimensions (m)		Area (m^2)	Load (kN)	Stress (MPa)	POB	Def (mm)
	X	Y					
1	3.05	3.05	9.29	1.61	72.46	0.008	31.93
1	2.16	2.16	4.65	1.59	72.35	0.008	22.78
1	1.52	1.52	2.32	1.54	72.17	0.008	15.95
1	1.08	1.08	1.16	1.48	71.91	0.008	10.74
1.5	2.49	3.73	9.29	1.57	73.07	0.008	32.69
1.5	1.76	2.64	4.65	1.54	73.15	0.008	23.11
1.5	1.24	1.87	2.32	1.48	73.26	0.008	15.82
1.5	0.88	1.32	1.16	1.42	73.42	0.008	10.31
2	2.16	4.31	9.29	1.52	74.06	0.008	33.40
2	1.52	3.05	4.65	1.47	74.44	0.008	22.94
2	1.08	2.16	2.32	1.40	74.42	0.008	14.94
2	0.76	1.52	1.16	1.37	74.81	0.008	9.25

Figure 9: Load and stress results at POB of 8/000 shown for 6 mm thick HS glass lites.

Aspect	Dimensions (m)		Area (m^2)	Load (kN)	Stress (MPa)	POB	Def (mm)
	X	Y					
1	3.05	3.05	9.29	1.28	60.52	0.001	28.68
1	2.16	2.16	4.65	1.26	60.27	0.001	20.37
1	1.52	1.52	2.32	1.22	60.16	0.001	14.12
1	1.08	1.08	1.16	1.17	59.89	0.001	9.37
1.5	2.49	3.73	9.29	1.25	60.85	0.001	29.26
1.5	1.76	2.64	4.65	1.22	61.00	0.001	20.55
1.5	1.24	1.87	2.32	1.17	61.07	0.001	13.89
1.5	0.88	1.32	1.16	1.13	61.35	0.001	8.92
2	2.16	4.31	9.29	1.21	61.93	0.001	29.77
2	1.52	3.05	4.65	1.16	61.91	0.001	20.09
2	1.08	2.16	2.32	1.12	62.21	0.001	12.93
2	0.76	1.52	1.16	1.10	62.48	0.001	7.90

Figure 10: Load and stress results at POB of 1/1000 shown for 6 mm thick HS glass lites.

EXPLANATION

The design loads and related stresses presented in Figs 7-10, provide designers a simple reference for selection of geometries to meet desired POB for annealed and HS lites of 5.56 mm according to the GFPM used in accordance with the procedure in ASTM E1300 Annex 2 for point loads. For the four side supported 5.56 mm thick specimens, there was relatively weak dependence of loads/stresses on panel dimensions with a maximum observed change of about 5% in breaking load from the aspect ratio of 1:1 to 1:2.

The design values presented far exceed commonly used (i.e., standard) industry values but still fall within the limits of 8/1000 and 1/1000 POB, respectively. The FEA analysis shows significant membrane action due to the four side supports, and it is expected that results may be significantly lower for three and two side supports. Comparing the results to E1300 appendix values shows that ASTM E1300 has conservative design loads.

CONCLUSION AND FUTURE WORK

The results presented are for four side supported, 6 mm thick, annealed and HS glass types. Ongoing studies are being completed to build out a series of design tables for point loads for a range of common thicknesses (6 – 12 mm), glass types (annealed, HS and FT) as well as support types (2, 3, and 4 side support).

ACKNOWLEDGMENTS

The authors gratefully acknowledge Stutzki Engineering for the use of images.

REFERENCES

ABAQUS: Multi-Purpose Finite Element Analysis Software, Dassault Systems. 2017

Afolabi, Bolaji, H. Scott Norville, and Stephen M. Morse. "Experimental study of weathered tempered glass plates from the Northeastern United States." *Journal of Architectural Engineering* 22, no. 3 (2016): 04016010.

ASTM International. ASTM E1300-16 *Standard practice for determining load resistance of glass in buildings.* West Conshohocken, Pennsylvania, USA. ASTM; 2016. www.astm.org p. 1-62.

ASTM International. ASTM E2751-17a. *Standard Practice for Design and Performance of Supported Glass Walkways.* West Conshohocken, Pennsylvania, USA. ASTM; 2017. www.astm.org p. 1-8.

Beason, W. Lynn, and James R. Morgan. "Glass failure prediction model." *Journal of Structural Engineering* 110, no. 2 (1984): 197-212.

Bowles, R., and B. Sugarman. "The strength and deflection characteristics of large rectangular glass panels under uniform pressure." *Glass Technology* 3, no. 5 (1962): 156-170.

Cervenka, J., Schultz, J.A., Stahl, D., and Knowles, J. “Strength of point-supported glass.” In *Proceedings of the 1st Façade Tectonics World Congress*; *Tectonics Press Publications.,* pp. 381-389. 2016.

Charles, R. J. "Static fatigue of glass. I and II." *Journal of Applied Physics* 29, no. 11 (1958): 1549-1553.

Griffith, Alan A. "The phenomena of rupture and flow in solids." *Philosophical transactions of the royal society of london. Series A, containing papers of a mathematical or physical character* 221 (1921): 163-198.

Morse, S. and Norville, H. “An analytical method for determining window glass strength.” In *Proceedings of Glass Performance Days 2011*; *GPD Press 9*; pp. 480-482. 2011.

Morse, Stephen M., and H. Scott Norville. "Design methodology for determining the load resistance of heat-treated window glass." *Journal of Architectural Engineering* 18, no. 1 (2011): 42-51.

Natividad, Kayla, Stephen M. Morse, and H. Scott Norville. "Fracture Origins and Maximum Principal Stresses in Rectangular Glass Lites." *Journal of Architectural Engineering* 22, no. 2 (2015): 04015014.

Orr, Leighton. "Engineering properties of glass." *Publication* 478 (1957): 51-61. Bowles and Sugarman, 1962;

Schultz, J.A., Knowles, J., and Morse, S., “Glass Failure Prediction Model for Out-of-Plane Bending of Waterjet-Drilled Holes,” In *Proceedings of the 39th IABSE Symposium, International Associated of Bridge and Structural Engineers*, Vancouver, Canada. 2017.

Schultz, Joshua, Douglas Stahl, and Christian Stutzki. "Experimental investigation of numerical design method for point-supported glass." *Journal of Architectural Engineering* 18, no. 3 (2012): 223-232.

Vallabhan, CV Girija, Bob Yao-Ting Wang, Gee David Chou, and Joseph E. Minor. "Thin glass plates on elastic supports." *Journal of Structural Engineering* 111, no. 11 (1985): 2416-2426.

Vallabhan, CV Girija, Joseph E. Minor, and Sesha R. Nagalla. "Stresses in layered glass units and monolithic glass plates." *Journal of structural Engineering* 113, no. 1 (1987): 36-43.

Walker, G. R., and L. H. Muir. "Investigation of the Bending Strength of Glass Louvre Blades." In *Ninth Australasian Conference on the Mechanics of Structures and Materials, ACMSM 9.*, pp. 122-126. 1984.

Weibull, Waloddi. "A statistical theory of the strength of materials." *Ingeniors Vetenskaps Akademien* (1939).

LET THIN GLASS IN THE FAÇADE MOVE

Thin glass - new possibilities for glass in the facade



Prof. DI Dr. Jürgen Neugebauer
FH-Joanneum
juergen.neugebauer@fh-joanneum.at



DI Dr. Markus Wallner-Novak
FH-Joanneum
markus.wallner-novak@fh-joanneum.at

ABSTRACT

Façades play an important role in the control of energy flow and energy consumption in buildings as they represent the interface between the outdoor environment and the occupied indoor space. New approaches to sustainable building solutions lead to the option of regulating internal and external conditions being of great relevance. Studies on climate adaptive façades show a very high potential for improved indoor environmental quality conditions and energy savings using moveable façades. A number of movable façades have been realized in the past, but the use of thin glass with a thickness of 0.5 mm to 3 mm opens a brand-new area that makes it possible to play with the geometry of the outer skin and provides an opportunity to make it adaptive by movement.

Thin glass requires curved surfaces in order to gain structural stiffness in static use. In kinetic façades the high flexibility of thin glass allows for new possibilities concerning changes in size and position by bending the elements rather than using hinges in a system of foldable rigid panels. The geometry is based on the known theory of developable surfaces for keeping a low stress-level during movement. This allows for façades made from cold bent thin glass or curved laminated safety glass (produced by the laminating of thin glass plies), a greater simplicity in construction, robustness and durability of moveable components. These movable systems also may be actuated autonomously.

By applying the principles of conventional moveable façades to bendable geometries, a new toolset for the design process by architects may be provided. Some approaches based on the previously mentioned theories were created to both clarify some concepts and discuss their principles and applicability.

KEYWORDS

thin glass, movable systems, adaptive systems, laminated safety glass, chemical pre-stressing

INTRODUCTION

Last year a research center, “Josef Ressel Center for Thin Glass Technology for Structural Glass Applications”, was launched and deals, for example, with the topics of the determination of the ultimate bending strength of thin glass, explores new fields of applications for thin glass or creates new design possibilities for architects. Another aim of this research center is to systematically gather existing knowledge about general moveable structures in buildings and apply this expertise to façades made from thin glass as climate adaptive building shells. Based on experiences with prototypes both at model scale and real size, computer models were carried out and tested in terms of kinematics of bending using Rhinoceros 3D with Grasshopper and other plugins from the Rhino environment.

As a key point the real size model of a movable canopy presented at the Glasstec 2014 in Düsseldorf, Germany (Fig. 1) was an excellent demonstrator for the potential that lies in the utilization of thin glass in moveable structures. This canopy was also the initial point for the application for the research project mentioned above. Several prototype models were first studied in computer models to evaluate their feasibility and subsequently built as cardboard-models to gradually optimize the system to finally build the real-life application.

The basic idea comes from a paper lantern, which can be found at the most birthday celebrations for children. One can buy such a lantern as a piece of flat, folded paper and it can be opened. In the open position the flat paper is forced to a conical geometry. The same principle was used for the canopy, but instead of paper, thin glass was used. In addition, instead of a whole circle only half of a circle was designed. With this, a static system of an arch was achieved. The flat laminated safety glass consists of two0.7 mm chemically pre-stressed glass forced into a conical geometry, which is a stable structure (Neugebauer, 2015).



Figure 1: Skin folding canopy at Glasstec 2014 in Düsseldorf.

Benefits of using thin glass are sustainability as materials are saved in these significantly lighter constructions and as there is the potential of adapting to environmental boundary conditions by movement.

WHAT IS THIN GLASS?

The differentiation between “thin” and “regular” glass requires more than just the definition of a thickness limit, e.g. “everything below 3 mm is thin glass”. It usually depends on the application and mechanical properties of the whole system. For example, a 5 mm glass pane spanning over an area of 3 m by 3 m is seen as thin glass, whereas a microscope slide less than 1 mm thick might be regarded as being “regular” glass.

A glass pane will usually be considered “thin” when its mechanical behavior becomes significantly different from that of an ideal plate, thus complicating the prediction, calculation or simulation of its characteristics. This can comprise effects such as large deflections, local or global buckling and sensitivity to vibrations.

For products intended to be used in the construction industry, which usually have dimensions to the order of one or more meters, the thickness limit between thin and regular glass can be narrowed down to a range of around 3 millimeters.

Thin glass often allows for applications that would not be possible with thick glass panes. One of these applications is (significant) cold bending. This means bending the glass without heating it up to the softening point. The glass is then held in the desired shape for the rest of the final product's lifetime by lamination of several glass layers or by clamping.

Improved material properties and production methods also allow for modern thin glass to be exposed to much higher surface stresses than standard thermally toughened float glass products. One example for a new process is chemical pre-stressing, which results in very high compression forces near the glass surface, much higher than that which can be achieved through thermal pre-stressing.

PRODUCTS

Besides “regular” float glass for window panes, which can also be produced in thicknesses far below (and above) the standard thickness of 4 to 12mm, a wide variety of specialized thin glass products is currently available on the market. Most of them were developed for the consumer electronics industry. The great demand for new high-performance products has boosted glass research within the last decade. Products such as Corning Gorilla® glass (introduced in 2007), which according to the manufacturer can now be found on ¾ of all smartphones, have revolutionized the glass industry. Common applications for thin glass are scratch-resistant display covers, optical conductors and semiconductor substrates. It is also used in biology, chemistry and medicine. The following table contains a small fraction of currently available high-tech thin glass and its applications:

products	thickness t [mm]	max. size [mm]	properties	application
AS 87 eco	0.07 to 0.35	500 x 400	suitable for chemical strengthening	screen protector, fingerprint sensor
Large Cover Gorilla®	0.55 to 2.0	2020 x 1365 (84“)	chemical pre-stressing up to 650MPa	large-format displays, whiteboards
Dragontrail™		3000 x 3000	float glass	smartphones, tablets, LCD displays

Table 1: Small fraction of currently available thin glass (Peters, 2017).

PRODUCTION OF THIN GLASS

For the production of thin the following processes such as float glass, both down-draw and up-draw or the overflow fusing process can be found on the market (Neugebauer, 2016).

FLOAT GLASS PROCESS

Float glass is a sheet of glass made by floating molten glass on a bed of molten tin. After a controlled cooling process, the glass is cut into certain sizes, mainly jumbo size. This method gives the sheet a uniform thickness and plane-parallel surfaces.

DOWN-DRAW PROCESS

The molten glass flows through a small gap at the bottom of the melting tank down and is cooled to ambient temperature by annealing furnaces. After this controlled cooling process, the glass is cut into specific sizes.

UP-DRAW PROCESS

This method is based on the historical “Fourcault” glass producing process from the early 1900s. It is an example of a "vertical draw" process, in that the glass is drawn against gravity in an upward direction. The glass is cooled to ambient temperature by annealing furnaces. After this controlled cooling, the glass is cut into specific sizes.

OVERFLOW FUSING PROCESS

The molten glass is poured into an overflow gutter. From this gutter the molten glass flows down both sides and fuses at the bottom of the gutter. After a cooling phase the glass is cut into panels of specific sizes.

In many cases, for example, for safety issues, the glass must be pre-stressed. Two processes, namely thermal and chemical treatments, are the most used techniques (Neugebauer, 2016).

THERMAL TREATMENT

Thermal treatment is a typical process of pre-stressing, according to EN 12150 (EN 15150), of glass in which the glass is moved forward on rollers into the heating zone and is heated up above the transition point. After this phase of heating, the glass is blown with air. During the phase of cooling to ambient temperature, glass is permanently moved forwards and backwards on rollers in the furnace. The thinner the glass, the greater the so-called roller waves can occur.

For this reason, the Austrian company LISEC has investigated a new process in which the glass is transported on an air cushion. This technique gives the possibility of pre-stressing thinner glass using thermal treatment without roller waves (Neugebauer, 2015).

CHEMICAL TREATMENT

Another possibility to pre-stress the glass is chemical treatment according to EN 12337 (EN 12337). The glass is immerged into molten potassium nitrate. At a temperature of approx. 370 - 450°C the effect of ionic exchange takes place. The smaller sodium ions diffuse from the glass into the liquid potassium nitrate and the larger potassium ions penetrate the glass matrix. Due to the larger ionic diameter of potassium ions, compressive stresses in the close-up range of the surface result. The depth of penetration is around 50 – 100 μm.

BENDING STRENGTH OF THIN GLASS

One approach is to determine the stress using equations (1) and (2). The bending moment can be calculated with equation (1) based on the differential equation of bending theory and with the section modulus the stress can be computed easily with equation (2). This approach neglects the influence of the Poisson's ratio.

$$EIw'' = M;\ EI\kappa = M \qquad \text{(equation 1)}$$

$$\sigma = M/W \qquad \text{(equation 2)}$$

E	Young's modulus
I	modulus of inertia
w''	curvature κ
M	bending moment
W	section modulus

With the characteristic value given for chemically pre-stressed glass as σ=150 MPa (EN 12337), the minimum radius depending on the thickness of the glass can be determined, as shown in Table 2 below.

thickness of glass [mm]	minimum radius [mm]
0.5	116
1	233
2	466
3	700

Table 2: Minimum radii depending on thickness of glass.

METHOD

Kinetics in façades is sometimes dismissed as irrelevant owing to experiences with very complex and consequently fault-prone façade-systems. However, simulations show that the energy consumption of a Central-European office building may be reduced by 85 percent with an adaptive kinetic façade. Even semi-adaptive shading, manually adapted on a monthly basis, improved the indoor environmental quality conditions and helped save energy by 18 percent (Kasinalis, et al. 79 (2014)).

The layout and design process of moveable façades involves the following steps: firstly, the sole geometry of movement – the kinematics – is to be considered in order to obtain a geometrically feasible solution. Secondly, mechanical components have to be implemented for actuation along a guided movement that may be locked in certain positions. Guided movement is possible in structures with one degree of freedom by releasing one constraint of a kinematically determined structure.

Based on these principles, the applicability of basic knowledge of thin glass elements is studied. The topic of kinematics meets the scientific field of developable surfaces and some autonomous actuators are discussed.

GEOMETRY OF MOVEMENT

In the design process, the geometry of movement of structural elements is generally aimed at leading to the lowest degree of complexity for simple and, therefore, robust and durable constructions. The movement of the geometry of thin glass may be realized one-dimensional by shifting along a line or a curve in plane or in space, two-dimensional by rotating around one axis or translation along two or more curves or three-dimensional by a combination of translation and rotation.

In façade elements, common types of movement are linear translation or rotation about one axis. Linear translation of elements is found either in a horizontal direction as in sash windows and sliding doors or in a vertical direction as in lifting panels and lifting façades. Rotation of elements is generally about a vertical axis, as in side-hung windows and conventional doors, or about a horizontal axis, as is the case in top-hung windows and pivot windows. These common types of movement are used for rigid elements. In the case of flexible or foldable façade parts the same types of movement are found with the additional task of storage by either rolling (roller shutters), gathering (venetian blinds) or folding (bi-fold hangar doors). More complex types of movement are rarely found in façades today. Examples of these are the Arabic Institute in Paris by Jean Nouvel with moveable metal sheets as sunshields in the form of an enlarged camera aperture guided by cranks and mechanical actuation and the façade of the Al Bahr Towers by Aedas with a stationary responsive screen system of star-like modules. Each of the modules is built out of six rigid triangular elements, which are around three axes foldable (rotatable) arranged (Fig. 2).



Figure 2: Built kinematic façades: Arabic Institute (Winstanley, 2010) and Al Bahr Towers (Wikiarquitectura, 2014).

In the design of thin-glass-façades the full potential of structural behavior may be obtained by curved geometries, which are generally built from one or more developable surfaces. However, the bending of such curved surfaces leads to more complex kinematics.

The general design process of moveable structures can be split into the following four steps displayed in Figure 3: starting from a kinematically determined structure, one constraint is released (a), rails, hinges or other mechanical elements are then used to guide the movement so that the position of all elements is determined at any time (b), actuators are used to propagate the movement (c). Finally, when a desired position is reached, the structure is again constrained by the means of locks in order to withstand loads (d).

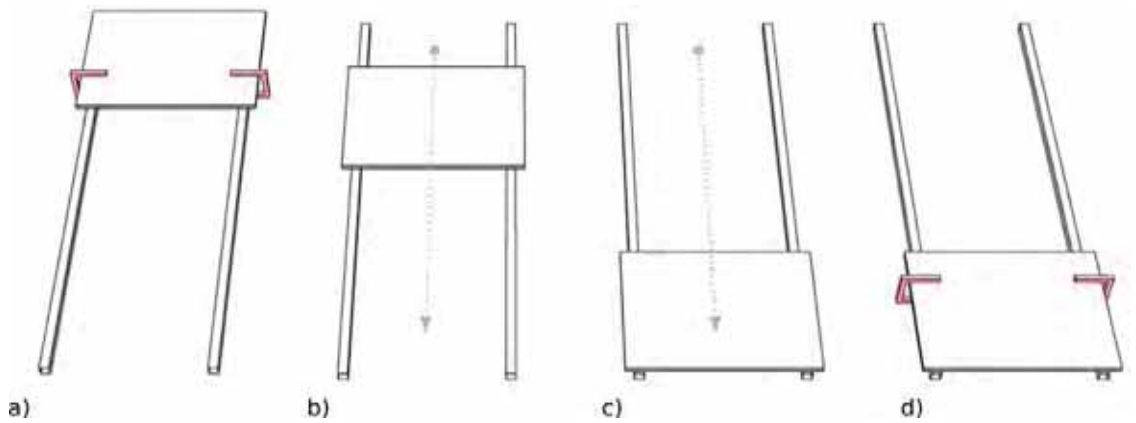


Figure 3: Steps of a moving structure.

The initial design process of moveable elements in architecture usually involves the sole geometry of movement – kinematics. Figure 4 shows the construction of element positions of a bi-fold door during movement as well as the movement lines.

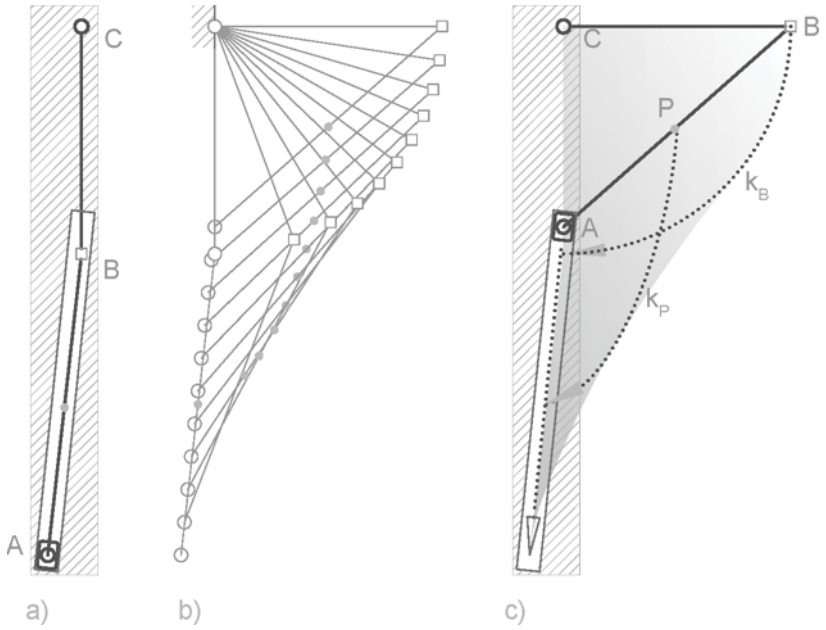


Figure 4: Kinematics of a bi-fold door a) closed position, b) construction of folding geometry, c) open position with envelope and movement paths of two points.

With thin glass involved, kinematics become more complex as the basic geometry in resting positions is already curved. In order to build curved surfaces with cold bending, developable geometry is preferred. Surfaces are developable if at any point one of the two Gaussian curvatures vanish. Examples for developable surfaces are cones and cylinders.
Starting from a developable geometry, deviations from developable shapes during movement may be allowed only to a certain extent. The magnitude is governed by the stresses in the glass panels and may be higher for thin glass elements.

MECHANICAL COMPONENTS

Mechanical components for guide and actuation may be chosen from a library of seven types: pressure driven gears, tension gears, wheel gears, screw gears, crank mechanisms, curve gears and locks (Fig. 5).

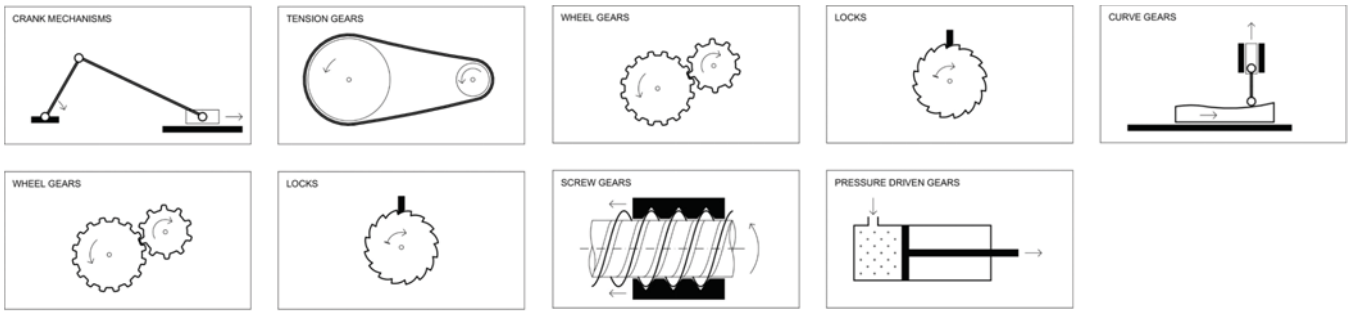


Figure 5: Gear library.

In current moveable façades tension gears in the form of ropes and chains for manual actuation are in use, chains and wheel gears are usually used for electrical actuation. Sometimes screw gears are used in façades in the form of jackscrews or toothed racks and cog wheels. More rarely, crank mechanisms are also applied in façades.

Current applications are based on actuation that is carried out either manually or mechanically either by a system of electric switches and or, as is increasingly the case, by sensors. This system of actuators may be referred to as active actuators as they require a control system in contrast to passive actuators that act autonomously. Passive actuators support the concept of simplicity in building solutions and are more durable and robust and therefore recommended for façades. Examples for such actuators are hoist cylinders filled with expansion materials that elongate when the temperature changes, composites of bi-layered wood or similar hygromorphic composite that bend when there is a change in moisture level or bi-metals that also bend when there is a change in temperature. Another temperature sensitive element is an artificial muscle from a fishing line. While the hub of common temperature sensitive cylinders is limited to 25 mm, the elongation capacity of the artificial muscle elements made of woven fishing line is relatively high as is the tension capacity. This is due to the fact that the actuation elements are tension elements.

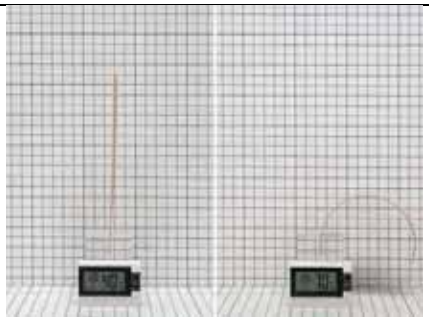
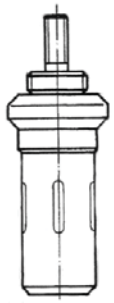
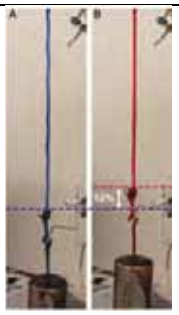
			
a) example of a natural hygromorphic cone (Holstov, Farmer und Bridgens 9 (2017))	b) bi-layered wood composite (Holstov, Farmer und Bridgens 9 (2017))	c) thermos fluid actuator (ACS, Thermo Fluid Control)	d) artificial muscle made of fishing line (Carter S. Haines 343, 868 (2014))

Figure 6: Passive actuators.

DATA

Several models were created using the visual programming language of the generative modelling interface of Rhinoceros 3D by McNeill Associates (Fig. 8). The authors picked out three applications of different scales: a sun shade, an air flow control and a moveable façade.

SUN SHADED TESSILATION

The idea behind this model is a ring-shaped hexagon with a central hole that may be opened and closed like in an enlarged camera aperture. In the example shown, the opening area in a closed state measures about 40% of the one in an open state.

The kinematics involved are translations about concentric lines. The thin glass elements are bent from lower to higher curvature keeping their conical shape (Fig. 7).

Simple linear rails and slotted links may be used as a guide. As active actuators, gears on a tooth rail may be used or as an alternative, a passive temperature sensitive actuator may be involved.

The hexagonal grid may be used as a basic tessellation element in larger structures (Fig. 9).

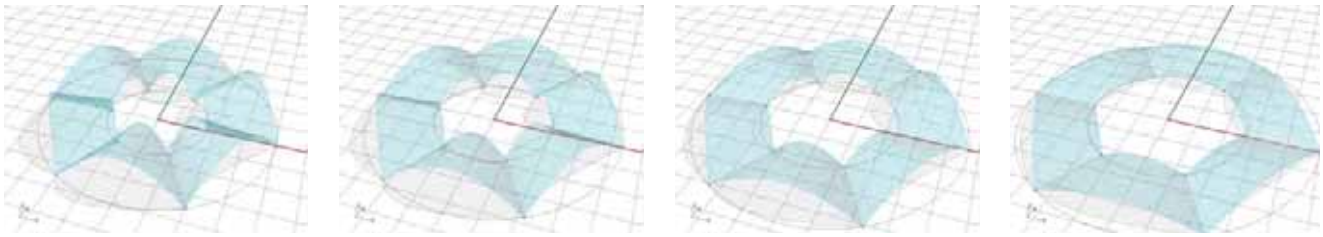


Figure 7: Light shades.

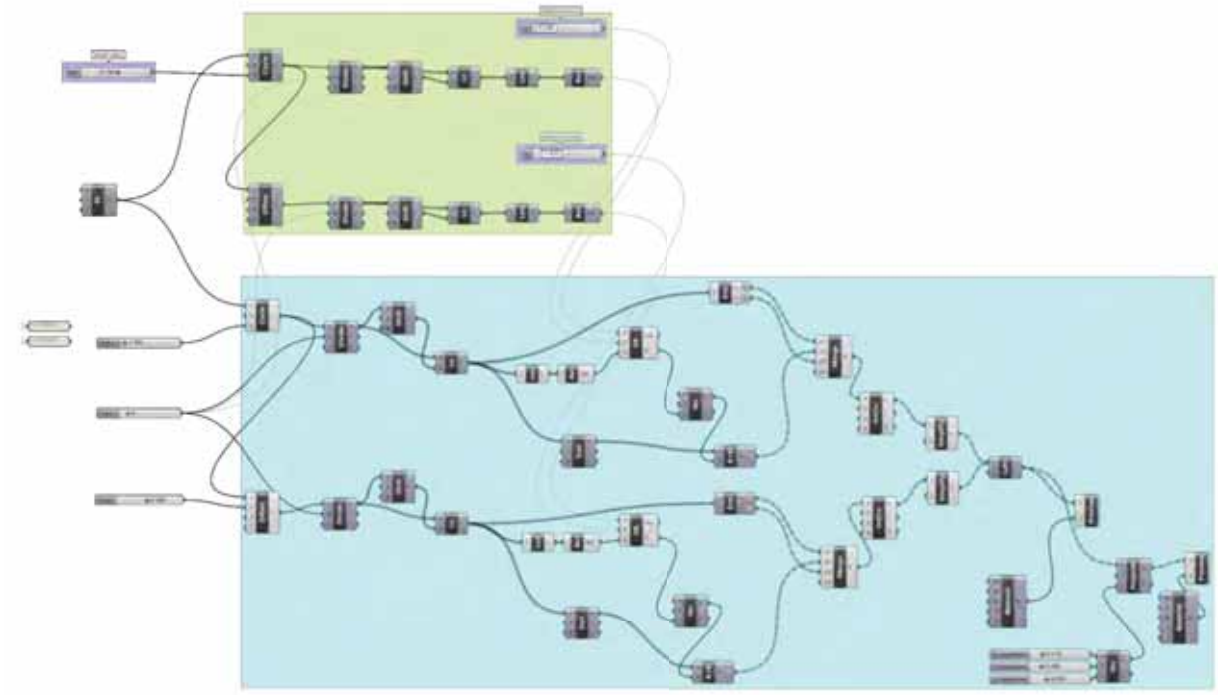


Figure 8: Grasshopper 3D-representation of the kinematic model.

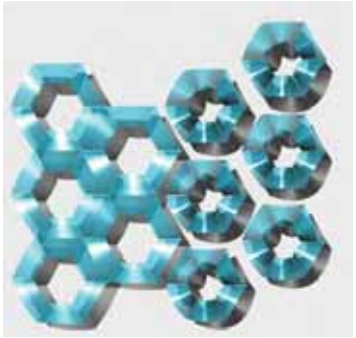


Figure 9: Rendered view of open and closed shades.

OPENING ELEMENTS

In variant A, vertical conical elements overlap like pantiles of a roof. By moving the end points of the lower base curve of any of the truncated cones closer together, the rise of the curve is increased (Fig. 10). This leads to an opening in the horizontal plane. Kinematically, the endpoints move along a straight line. The glass surfaces stay conical during their movement. As a guide small rails at the curve ends may be used. Either two synchronized active actuators such as motorized jackscrews may be used for each cone base as an actuator or passive actuators with crank mechanisms may be employed.

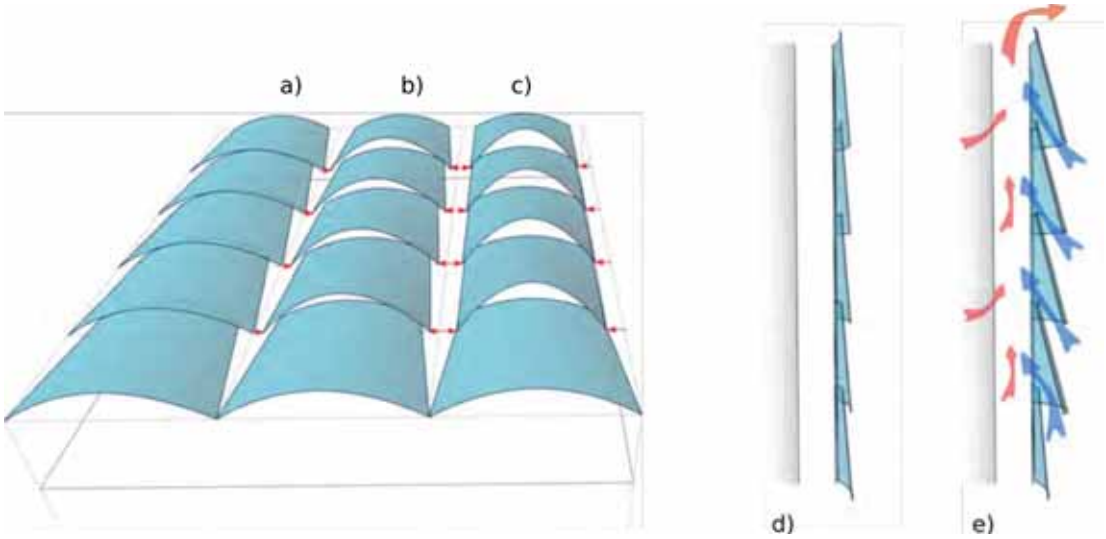


Figure 10: Double layer façade with overlaying conical glass-panels

a) and d) closed b) half open c) open positions e) possible air-flow in opened skin.

In Variant B, two vertical cylindrical elements of parabolic base have a common generating straight line. By rotating this straight line, the two cylinders change shape to form two conical surfaces with base curves of a different rise (Fig. 11). This principle may be used to open the façade and control the air flow. The guide is done by a pin support at midpoint of the profile along the common generating straight line. Actuation may be carried out either actively by pneumatic jacks or a passively using a rotational spring made of bi-metal.

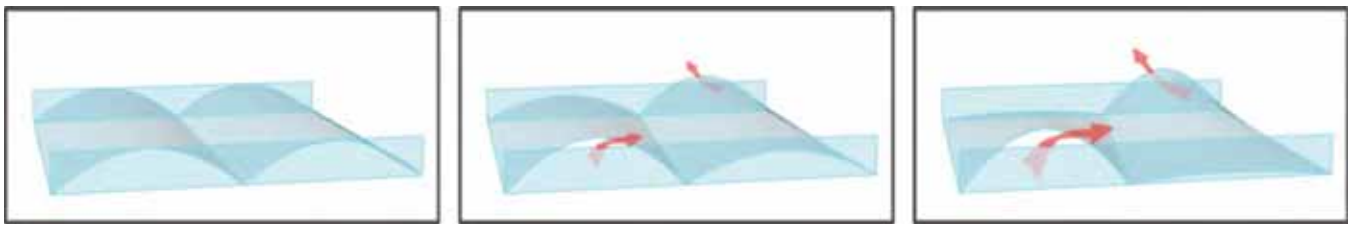


Figure 11: Opening of a cylindrical element.

FOLDING FAÇADE

Another example is a flexible façade based on the principle of curved folding. Thin glass is cut along curved lines (curved folds) into different elements and these elements are assembled together rotatable along these curved lines. This concept shows a movement and deformation of the glass elements both inwards and outwards of the façade level, due to an in-plane, such as, for example, pressure driven gear. Figure 12 shows a visualization of a parametric study with the help of Rhino 3D together with Grasshopper 3D.

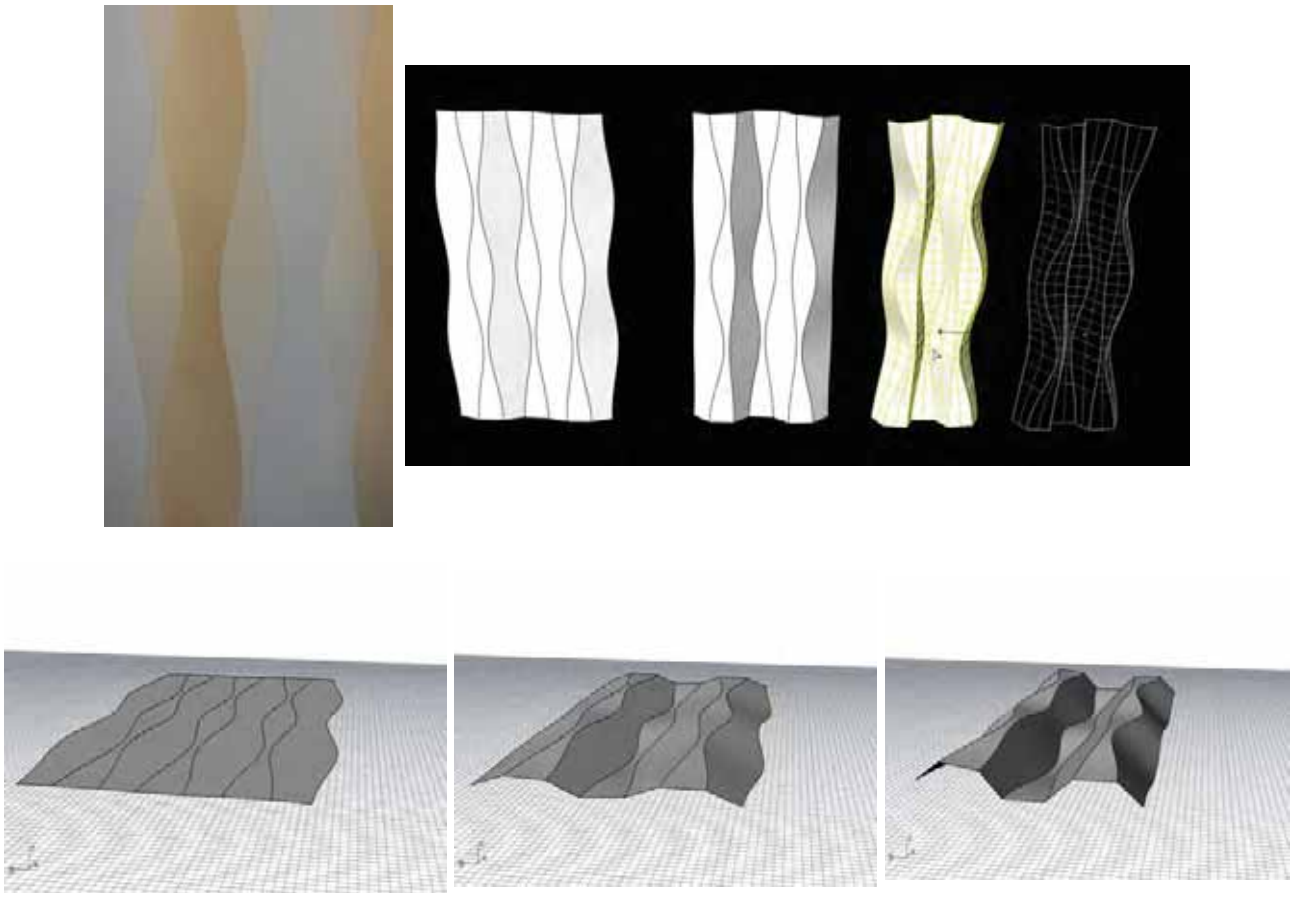


Figure 12: Folded façade.

CONCLUSION AND FUTURE WORK

The aim of this research work is to find new fields of application for thin glass in buildings. One kind of new application is the field of movable and adaptive systems. Due to the high flexibility of thin glass, new design options for example of facades become feasible in comparison to regular thicknesses of glass. Based on the known theory of developable surface new kinds of “organic” facades can be designed. With cold bend glass or curved laminated safety glass produced by laminating glass plies, very interesting elements in the facades can be achieved. Possibilities of movement, with the meaning of a permanent bending of thin glass, for example for elements of the façade which can be opened and closed, creates new tools for the design process of architects.

The research work in future will explore new fields of application for thin glass. These new applications should be categorized according to their concept, for example, the theory of developable surfaces or curved folding. Based on the two basic types of movement - translation and rotation and their combination – new “lively” systems of thin glass structures will be developed.

ACKNOWLEDGMENTS

This paper is the result of a project by the research center named the “Josef Ressel Center for Thin Glass Technology for Structural for Structural Glass Applications” funded by the Austrian “Christin Doppler Research Association” and is supported by industry partners SFL technologies GmbH and LISEC Austria GmbH.

REFERENCES

Carter S. Haines, Márcio D. Lima, Na Li, Geoffrey M. Spinks, Javad Foroughi. “Artificial Muscles from Fishing Line.” *Science*, 343, 868 (2014).

Holstov, Artem, Graham Farmer, and Ben Bridgens. “Sustainable Materialisation of Responsive Architecture.” *Sustainability*, 9 (2017): 435.

Kasinalis, C., R.C.G.M. Loonen, D. Cóstola, and J.L.M. Hensen. “Framework for assessing the performance potential of seasonally adaptable facades using multi-objective optimization.” *Energy & Buildings*, 79 (2014): 106-113.

Moloney, Jules. *Designing Kinetics for Architectural Facades.* Oxon: Routledge, 2011.

wikiarquitectura. *Al Bahar Towers.* 2 10 2014. https://en.wikiarquitectura.com/building/Al-Bahar-Towers/ (accessed 9 5, 2017).

Winstanley, Tim. *AD Classics: Institut du Monde Arabe / Enrique Jan + Jean Nouvel + Architecture-Studio.* 2 10 2010. http://www.archdaily.com/162101/ad-classics-institut-du-monde-arabe-jean-nouvel (accessed 9 5, 2017).

TRANSLUCENT PRE-FABRICATED STRUCTURAL CAST GLASS

A new unitized u-channel assembly



Ian Ritchie
Ian Ritchie Architects Limited
iritchie@ianritchiearchitects.co.uk

ABSTRACT

A new type of translucent pre-fabricated structural cast glass assembly with high thermal performance, good light transmission and acoustic rating.

The cast glass assembly is made from project-specific 404mm wide low-iron u-channel cast glass which is enamelled on the inner faces. Two u-channels are unitized into a ‘flange-to-flange’ arrangement and are bonded together with 2-part structural silicone in a bespoke polyamide extrusion. The cast glass assembly can span in excess of 4.2m without intermediate support or vertical mullions, and the overall thickness of the façade is only 144mm.

The void between the u-channels is filled with optically white translucent glass-fiber insulation, which is hung and held in slight compression. This provides the thermal performance of the assembly and light transmission levels which provide a quality of diffused ‘white’ natural light for the well-being and comfort of the users. The translucent envelope also offers users privacy, with none of the overlooking issues associated with the inner city. The assembly structurally supports openable triple-glazed windows and openings with no additional vertical support, and the unitized system is adaptable to include additional layers of security to protect against intrusion (hard body impact resistance).

The assembly represents an innovation in large unitized u-channel cast glass elements that have been fabricated and sealed off-site and installed on-site in modules, thus maintaining the quality of workmanship while facilitating a faster on-site installation than any previous u-channel cast glass façade.

The contents of this paper set out the design and detail of a new width, size and assembly of u-channel cast glass which makes the material suitable for large-scale and quick installations, which protect against on site contaminants, while also providing superior thermal performance and increased structural performance.

KEYWORDS

façade, unitized curtain wall, double-skin, innovative or unique, cast glass, structural glass, translucency, case study

INTRODUCTION

Rolled cast glass was first produced in 1832[1], and channel glass in Germany since the 1970s. U-channel cast glass is a low-cost cladding material which has been available on the market for over four decades. These u-channels come in a set number of profiles and widths which are broadly homogenous across the four major manufacturers world-wide (Fig.1). Widths available are generally circa 232mm, 262mm and 330mm. The flange depth is generally 60mm. As a general principle, the wider the u-channel the less vertical distance it can span. During the last decade, various manufacturers have advanced and improved the toughening (tempering) process, removing the need to incorporate metal wire mesh into the cast glass channels to improve strength and safety. This has also allowed toughened u-channel glass to be installed at high level because it can break safely.



Figure1: Various cast glass samples from various manufacturers worldwide. Line-up on Architect's terrace. Photo by the author.

HISTORICAL PERSPECTIVE

Ever since glass was placed into openings in walls, to let in light and to keep out wind and rain, there has been an interesting dialogue between transparency and privacy. The need for privacy can be met with opacity or translucency through treatment of the glass itself, and with clear glass by adding a curtain or blind. Light can still enter, but in reduced quantity. However, the other fundamental joy of the glazed window is the view out; if privacy is not an issue then clear glass always wins.

The need for dielectric (insulating) properties of glass in buildings first surfaced in the early part of the 20th century. Examples of double façades using two layers of single glazing to theoretically increase the thermal performance of a transparent glass skin seem to have first appeared in Russia during the 1920s. The Zuyev Workers Club in Moscow is an example.

Le Corbusier no doubt copied this idea with his Centrosoyuz Building, also in Moscow, constructed in 1933. However, in both these early examples there is a failure to understand that glass has virtually no dielectric properties. Hence the single outer window will quickly reach the same temperature as outside.

[1] Chance Brothers, England





Figures 3 and 4: The Zuyev Workers Club in Moscow, completed by Ilia Golosov in 1929. (Left) Photo by Florstein / Wikimedia Commons. (Right) Photo by the author in 2005.



Figure 5: Centrosoyuz Building in Moscow, completed by Le Corbusier in 1933. Photo by the author in 2005.

At approximately the same time, the idea of having a sealed unit of two skins of glass separated by air was put forward, and the first product was manufactured by the Libbey-Owens-Ford Glass Company in 1944 using a welded glass spacer. A double wall with the outer wall double glazed does make better sense. However, cost starts rising dramatically. This, coupled with the need for access between the panes, further complicates the façade construction and begins to reduce the useable floor area of the building.

Today, thermal performance of triple glazed insulated glass units can achieve insulating properties with U Value of 0.8 W/m2K. But the cost of production and the weight of the unit, typically 12mm glass +16mm air +6mm glass+ 16mm air + 6mm glass, preclude much use of it. And ultimately with all insulated glazed units the boundary seals fail over time.

Glass façades were used when little thermal insulation was required and this led to the development of structural glazing in the early 1980s. The system designed by Rice Francis Ritchie[2] for the Bioclimatic Façades at the Cité des Sciences, La Villette, France, relies upon an innovative articulated stainless steel ball-joint fixing through a machined countersunk hole in the glass and separated by pure aluminum washers. The articulation avoids bending stresses in the glass and the fixing can carry up to 4 tonnes (40kN). A similar system, but with much less loading capacity (c.0.7tonnes: 7 kN), is Pilkington Planar formed of float toughened glass panels held by fixed bolts – a "point-fixed" system to create a structural glass "wall". The continued appeal of such systems among architects focuses on the transparency of the assembly and a seemingly "frameless" structure.



Figure 6: Float glass "wall" at La Villette, completed in 1986. Photo by Alain Guisdard.

U-CHANNEL CAST GLASS

In contrast, u-channel cast glass requires a series of support channels connected by movement joints instead of struts or trusses. U-channels can be installed in a variety of ways depending on requirements: vertically or horizontally, in single profile or an "interlocked" double profile. When installing u-channel cast glass as a thermo-acoustic external envelope, one must use the u-channels in a double-glazed arrangement. The additional introduction of spun fiberglass between double profile channels provides further thermal insulation.

As with all glazing solutions, the "interlocking" double profile has its limitations but will continue to be developed and adapted. The contents of this paper set out the design and detail of a new width, size and assembly of u-channel cast glass which makes the material suitable for large-scale and quick installations, which protect against on site contaminants, while also providing superior thermal performance and increased structural performance.

---

[2] Ritchie

COMPONENT PROPERTIES

The toughening of u-channel cast glass is not quite as straightforward as toughening float glass. There is a different distribution of stresses between the flat and the vertical flanges. It needs careful management of the process.

The quality control after toughening involves the “fragmentation test” which determines whether the glass breaks in the manner prescribed for a thermally toughened soda lime silicate safety glass. In fragmentation test EN 12150-1 (July 2005) the defined dimensions of the glass samples for this test do not really relate to 4.2m x 4mm wide cast glass channels, but it is the only prescribed EN standard and the basis of the tests.







Figures 7–9: Lamberts toughened glass channel breakage size test result 128 pieces less than 6-7mm. A minimum of 40 is required with an area of 5cm x 5cm.



Figure 10: Record sheet during tests.



Figure 11: Maximum permitted length of “shard” 100mm.

Although ‘interlocked’ assembly is still widely used, a number of factors were taken into account when comparing this assembly with a possible modularized assembly:

VERTICAL SPANS: Using a typical wind load requirement of 1.5KN/m2 the ‘interlocked’ arrangement achieves a vertical span of 3.27m with 262mm wide toughened u-channels or 2.94m with 330mm wide toughened u-channels compared to a vertical span in excess of 7m for a modularized arrangement (Lamberts Linit).

WIND SUCTION: ‘Interlocked’ assembly is supported by top and bottom horizontal carriers. Additional wind anchors or intermediate support to the vertical spans can be used but these are limited, especially if the ‘interlocked’ system is to be used in areas of high wind loads or at significant height, as the mid-span is held in place only by the weathering silicone joints.



Figure 12: 20 year old 'interlocked' assembly. Mould and dead insect contamination inside assembly due to condensation. Photo by J Braker. IRAL.

THERMAL LIMITATIONS: The lack of thermal breaks/separation with 'interlocking' assembly in addition to the requirement for horizontal and vertical carriers, makes the channels susceptible to condensation. By providing weep holes in the carrier to drain condensation, there is a risk of insect penetration (Fig.12) and no access to clean the interior.

SOFT BODY IMPACT: The edges of the u-channels are, like most glass (and especially toughened), the most susceptible to damage which results in total failure. The 'interlocked' system provides no protection in the case of an impact as the deflection causes glass to glass edge contact and failure.

PROPORTIONS: As a general principle an architecturally 'delightful' proportion (classical columns) can be achieved with a ratio of 1:10 (width:height) and this is possible in u-channel units. Therefore, when the requirement is for a vertical span of 4.2m (floor to floor), a 262mm or 330mm wide u-channel is not as aesthetically pleasing (proportion). Furthermore, by increasing the width of the u-channel the number of vertical silicone joints between u-channels of the whole façade is reduced.

TRANSLUCENCY: Cast glass is not optically clear, but when spun glass fiber insulation is pressed against the inner face of a u-channel it can become highly visible. For an even light-diffusing finish, manufacturers offer a choice of finishes (i.e. sandblasting) that can be applied to the inside face of the u-channels. Unfortunately, some of these finishes weaken the strength of the glass.

GEOMETRY AND WINDOW UNITS: The nature of the 'interlocked' and other assemblies limit the geometry that can be achieved with a u-channel envelope. Generally the assemblies work fine in a linear arrangement or on a single curve with limited radius, but the manual nature of the installation and the interlocked arrangement are not suited for windows and openings if they are not structurally independent from the u-channels. They have always required vertical framing to bridge the gap between the two systems (Fig.13).

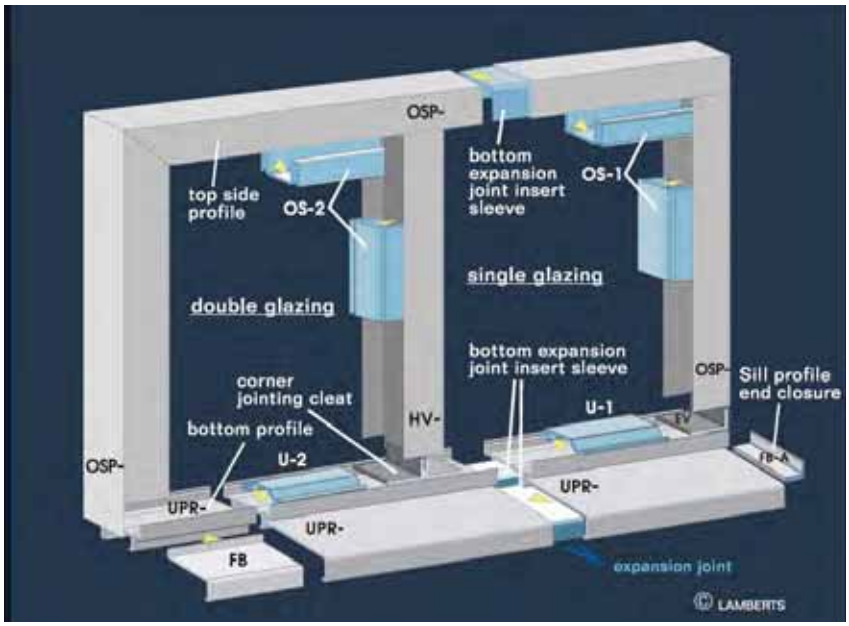


Figure 13: Typical aluminum frame system (both vertically and horizontally) for 'interlocked' assembly. Diagram courtesy of Lamberts Glasfabrik.

INSTALLATION: On-site installation of u-channels is a slow and usually a manual process which involves hand-held suckers and a slide-in procedure of offering the u-channel up into an oversized horizontal top frame and then lowering into a bottom horizontal carrier – and then siliconing to provide the weather seal (Fig.14). This manual installation is incompatible with large scale installations or when installing at high level, and where labor cost is high. It can also result in limited overall thermal performance caused by the installation tolerance voids in the top frame, which must be maintained for glass replacement. The manual handling/installation of the u-channels and the amount of on-site siliconing makes the system susceptible to construction site and insect contamination, as well as irregular workmanship and quality issues.

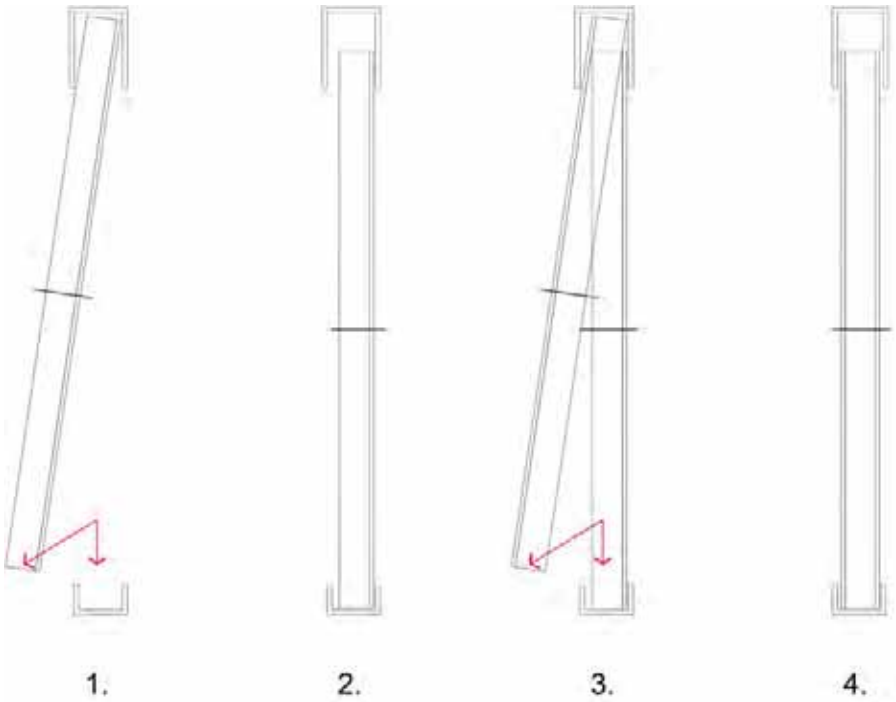


Figure 14: Slide-in procedure for 'interlocked' assembly. Diagram by the author.

METHOD

All these issues described can be addressed by producing a unitized and modularized system.

CAST GLASS UNITS

By taking two u-channels and placing them in a flange-to-flange arrangement and bonding them together one can create a cast glass unit (Fig.15). The two u-channels are unitized by bonding the flanges with a 2-part structural silicone (Dow Corning 993 Structural Glazing sealant) into a double-sided bespoke polyamide extrusion. Care must be taken when selecting the color of the polyamide extrusion and structural silicone, as the color is refracted through the flange of the u-channel profile. The insulation is installed at the same time as the flanges are bonded together. By doing this off-site the amount of contamination during the encapsulation process is minimized. The top and bottom edges of the unit are then sealed with purpose made caps to complete the unit. The bottom cap contains a weep hole, with an interior insect mesh, to provide an outlet for condensation run-off and pressure equalization of the unit.

The overall unit depth is 144mm which significantly increases the vertical span of the u-channel because two u-channels are structurally bonded and act in unison. With a typical wind load requirement of 1.5KN/m^2 the cast glass unit will achieve a vertical span in excess of 7m with 262mm wide toughened u-channels. 7m is generally the longest length of u-channel manufactured within acceptable tolerances; therefore the designer has more freedom with the width of u-channel (the deeper the u-channel assembled unit, the longer the span*). The cast glass unit that was tested for the 4.2m vertical span was made up of two flange-to-flange 404mm wide toughened u-channels. This resulted in cast glass units that were able to be used with a wind load criterion in excess of 2.5KN/m^2.* The moment of inertia was improved and confirmed by a combination of empirical testing and calculations. It significantly increased as a result of fully bonding the two glass sections together with the specific Dow silicone and the resultant development of compound action between the two cast glass modules.

This removes the need for any vertical framing and thus only horizontal carriers are required. This is partially beneficial at intersections with windows and door openings. Previously the window was structurally independent with a soft joint silicone connection to the u-channel. Now a cast glass unit is able to carry the load of a 2000mm x 808mm triple glazed window unit without any additional support; making it an integrated cladding element.

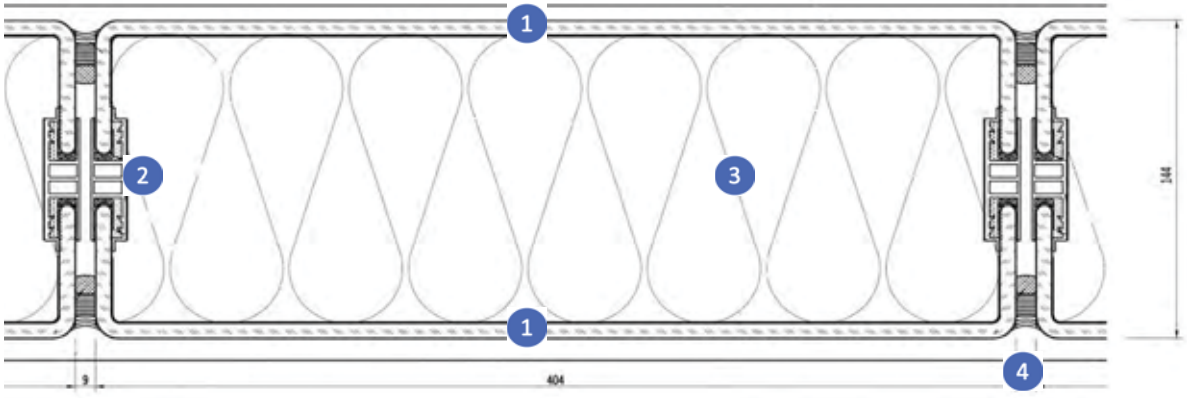


Figure 15: Plan of cast glass unit. Detail by the author.

1. Lamberts Linit 404mm wide 8mm thick low-iron toughened heat-soak tested cast glass with enameled frit to inside face. ‘Cord’ profile to outside face, and selected to reduce maintenance – cleaning requirements (the crest of the profile always remains clean while atmospheric pollution is driven by wind into the valley and rain cleans out the valley.) ‘Solar’ profile to inside face (chosen to allow scientists to use it as whiteboards).
2. Polyamide thermal extrusion. Cast glass flange is bonded into place with Dow Corning 993 white structural silicone.
3. Wacotech TIMax GL translucent glass-fiber insulation
4. Nominal 9mm (variable geometry) weather silicone joints between cast glass assemblies. Joints can vary between 5mm and 25mm to enable curved geometry.

MODULARIZATION

To achieve modularized assemblies one must move entirely away from the conventional slide-in installation procedure and the typical aluminum framing elements. A new thermally-broken extruded aluminum profile with a removable front capping plate (Fig.16) was designed to act as the horizontal carrier. The relevance of the capping plate means individual u-channels and cast glass units do not need to be slid into the top carrier and then dropped into the bottom carrier; they can be offered horizontally, thus removing the need for a large void in the head carrier.

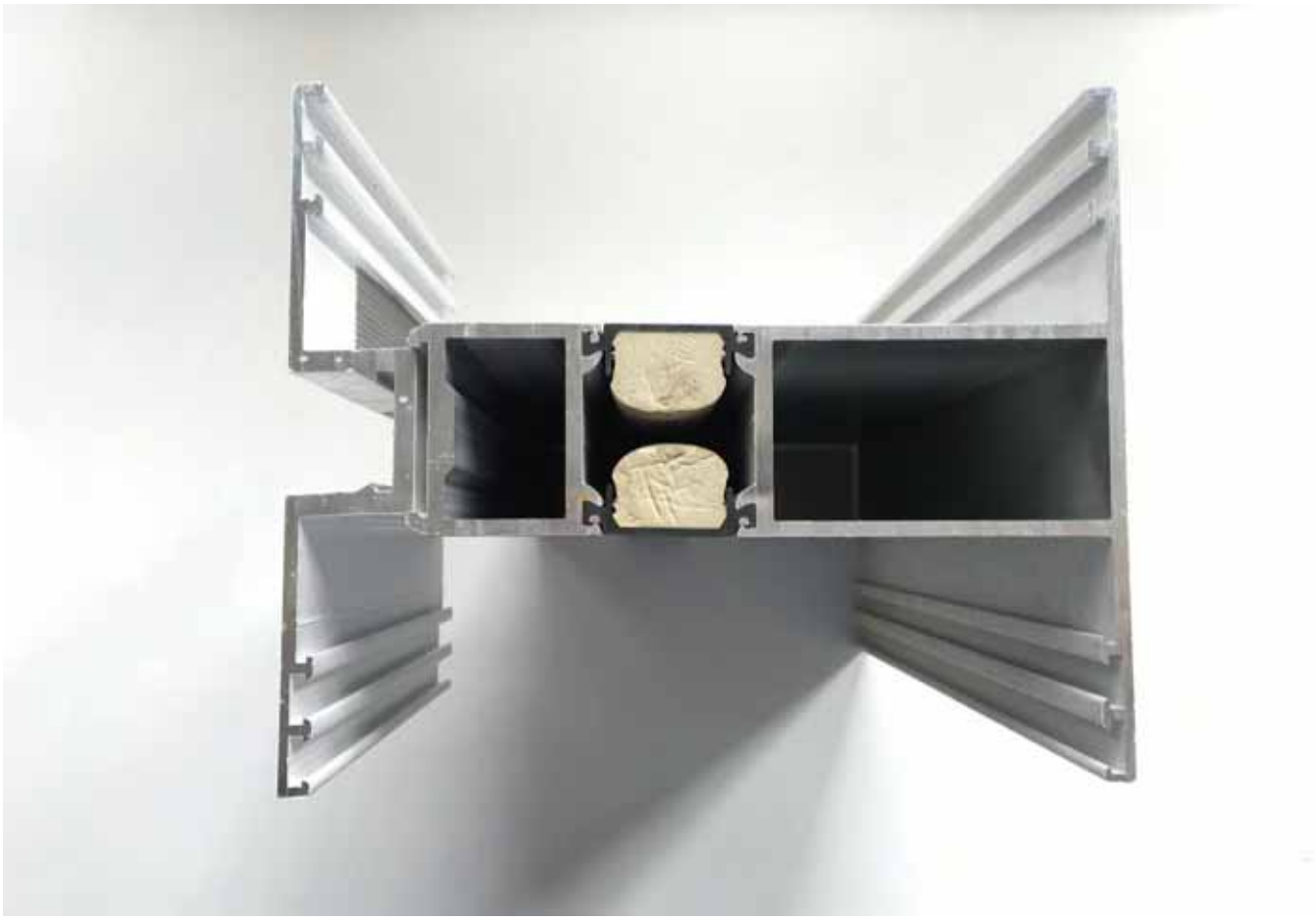


Figure 16: Horizontal aluminum support profile with removable front cap. Photo by the author.

With the front-loading carrier system designed, pre-panelized assembly off-site was conventional. The individual cast glass units were pre-fabricated and then four cast glass units were assembled together into a module (total module size 1.7 x 4.2m) including all the vertical weathering silicone joints. This was also extremely useful when it came to windows and other openings. These were also installed, sealed and wired (building management system window contacts and power to control external motorized louvers) into the module (Fig.17). The modularized assembly represents the first time large unitized u-channel cast glass elements have been fabricated and sealed off-site and installed on-site in modules, maintaining the quality of workmanship and facilitating a rate of installation faster than any previous u-channel cast glass façade (Fig.18 and 19).



Figure17: Modularized curved units with triple glazed windows inset. Photo by the author.

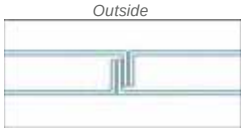
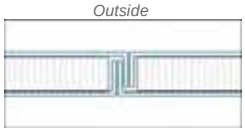
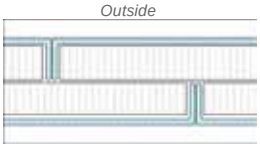
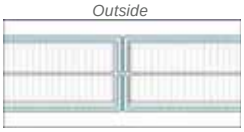




Figures 8 and 19: Lifting arm and site installation of modules at height of 30m above ground. Photos by the author.

DATA

Using data available on the various assemblies and systems the table below compares conventional systems with the new cast glass unit assemblies. The comparison assumes one particular insulation material and one type (and width) of u-channel glass.

	Interlocked [no insulation]	*Interlocked + insulation*	*Independent two track + insulation*	*Flange to flange insulated glass class units*
	Outside  *Inside*	*Outside*  *Inside*	*Outside*  *Inside*	*Outside*  *Inside*
Profile	*262/60/7*	*262/60/7*	*262/60/7*	*262/60/7*
Overall unit depth [mm]	*70*	*70*	*164*	*144*
Plan Arrangement	*60mm Cavity*	*60mm Cavity*	*152mm Cavity*	*128mm Cavity*
Vertical span [m] without immediate support (based on 1.5KN/m^2 wind load)	*3.27*	*3.27*	*2.32*	*>7*
Translucent Thermal Insulation Manufacturer	*-*	*Wacotech - Fiberglass and Sun Protection Insert*	*Wacotech - Fiberglass*	*Wacotech - Fiberglass*
Type	*-*	*TIMax GL and TIMax LT*	*TIMax GL [2no. Layers]*	*TIMax GL [2no. Layers]*
Thickness – Uncompressed [mm]	*-*	*71*	*142*	*142*
Overall U-Value[W/m^2K]	*2.8* *Tested by Fraunhofer Institute ISE, IFT – testing house Rosenheim, Germany*	*1.35* *Tested by Fraunhofer Institut ISE, IFT – testing house Rosenheim, Germany*	*0.80* *Tested by HFB Engineering – testing house Leipzig, Germany*	*0.92* *Tested by Fraunhofer Institute ISE, IFT – testing house Rosenheim, Germany*
G-Value –Direct [0<>1]	*0.82*	*0.27*	*0.19*	*0.23*
Light Transmittance [0<>1]	*0.9 [approx]*	*0.37*	*0.1*	*0.11*

List of cladding testing specified by the architects (authors). Testing and construction managed by Frener & Reifer.

Test	*Result*	*Testing Body*	*Date*
Acoustic Rating	*R_w=39dB*	*ift Rosenheim*	*12.01.12*
U-value test	*U=0.92 W/(m^2K)*	*ift Rosenheim*	*20.01.12*
G-value test	*g=0.23*	*ift Rosenheim*	*24.01.12*
Light Transmission	*τ_v=0.11*	*ift Rosenheim*	*24.01.12*
Light Reflection	*ρ_v=0.45*	*ift Rosenheim*	*24.01.12*
Hard body (Manual Attack) to BS EN 356	*P1A - Pass*	*ift Rosenheim*	*30.04.12*
Soft body impact to BS EN 14019	*Class I4 / E2 - Pass*	*ift Rosenheim*	*30.04.12*
Safe breakage of cast glass to BS EN 12600	*Pass*	*ift Rosenheim*	*30.04.12*
Air Permeability to EN 12153	*Pass*	*gbd LAB*	*12.06.12*
Watertightness to EN 12155	*Pass*	*gbd LAB*	*12.06.12*
Resistance to Wind Load to EN 12211	*Pass*	*gbd LAB*	*12.06.12*



Figure 20: Watertightness to EN 12155 at gbd Lab. Later assembled on site as north façade prototype. Photo by the author.




Figures 21 and 22: Soft body impact testing to BS EN 14019 at F&R's factory. Photo by the author.



Figure 23: Safe breakage testing of toughened cast glass to BS EN 12600 at F&R's factory. Photo by the author.



Figure 24: Hard body (manual attack) impact testing to BS EN 356 at F&R's factory. Photograph by the author.

It was necessary to conduct all these tests as a result of the change in the u-channel width. This is because the u-channel flanges, silicone joints and center pane values are all directly affected by the width of the u-channel as part of an overall assembly.

CONCLUSION AND FUTURE WORK

Understanding the required light level, the degree of transparency versus view, the degree of privacy, the thermal and acoustic performance and balancing these to achieve an economic, safe, long-life and technically performing installed product requires thought and analysis. To compound the environmental design performance of the façade, the scientists advising the architects wanted to have opening windows as well as controlled environmental conditions. There is great joy in synthesizing these parameters into an architectural aesthetic.

The issues inherent in working with u-channel cast glass have been broadly addressed by unitizing and modularizing the envelope. This has been made possible due to the strength found by structurally bonding the u-channels together with a purpose-made polyamide thermal break, resulting in the ability to achieve 7m high structural spans.

All test results for the 404mm u-channel cast glass units show that the thermal performance of the building envelope - its ability to transfer daylight and avoid non-beneficial solar gains - are critical to helping a building achieve compliance with current UK regulations. They also mean that thermal comfort for building users is achieved in close proximity to the building envelope without requiring perimeter heating (statement based on United Kingdom climate).

The façade's light transmission at 11% provides a wonderful quality of diffused 'white' natural illumination to the interior (300 lux overcast sky 4m back from the façade) and removes all glare for the well-being and comfort of the building users, particularly in relation to computer screens. The translucent envelope offers privacy with none of the overlooking issues associated with inner city building proximities.

Further research will explore what improvements could be made to the polyamide profile to increase resistance to deflection and wind suction. This could potentially lead to even greater widths of u-channel cast glass spanning vertically. It would also be of benefit to explore/test other types of thermal insulation within these modular cast glass units (e.g. Aerogel) to achieve even better thermal performance and to explore alternative aesthetics.

ACKNOWLEDGMENTS

The cladding of the Sainsbury Wellcome Centre described in this paper was funded by the Gatsby Charitable Foundation and the Wellcome Trust, and the building is for University College London.

The author would like to thank Frener & Reifer, Reba, Lamberts Glasfabrik, Linit-UK, Wacotech and Schüco.

REFERENCES

Ritchie, Ian, "Science Building, University College London" Intelligent Glass Solutions, (Summer 2015): 25-31.

TRANSPARENT GENERATOR

Tapping the gap



Eric Carbonnier, Ph.D.
University of Oregon / HMC Architects
eric.carbonnier@hmcarchitects.com



G.Z. Brown
University of Oregon
gzbrown@uoregon.edu

ABSTRACT

Windows reduce heat loss and heat gain by resisting conduction, convection, and radiation using thermal breaks, low-emissivity films, and window gaps. Contrary to advancing these resistive qualities, a highly conductive gap medium using Al_2O_3 nanoparticles dispersed in deionized water was used to enhance thermal conductivity. The solution harnessed the photothermal properties of Al_2O_3 nanofluids to trap, store, and transport thermally charged fluids to heat exchangers to preheat air and water, and to generate electricity forming a transparent generator—the Nanowindow.

Seven Nanowindow prototypes with varying orders of air and fluid columns were fabricated and tested using distilled water (H_2Owindows) to establish a baseline of performance, and then replaced with Al_2O_3 nanofluids. A solar simulator was built to avoid environmental radiant flux irregularities providing a uniform test condition averaging 750–850 W/m2. All Nanowindows were tested in a calibrated hot box determined to have a ±4% degree of accuracy based on four laboratory samples establishing a framework to conduct U-factor and solar heat gain coefficient (SHGC) measurements.

Four heat exchange experiments and standardized window performance metrics (U-factor, SHGC, and visible transmission) where conducted on seven H_2Owindows. The top performers were then tested using Al_2O_3 nanofluids. Nanowindows were coupled with thermoelectric generators generating a rated voltage of 0.31VDC/0.075ADC per 12in^2 Nanowindow, an improvement of 38% over baseline. Standardized window performance metrics confirmed Nanowindow U-factors ranging from 0.23 to 0.54, SHGC from 0.43 to 0.67, and visible transmittance coefficient (VT) ranging from 0.27 to 0.38.

The proof of concept experiment shifts window gaps from resisting energy to harnessing solar energy. The Nanowindow thus presents a unique opportunity to turn vast glass facades into transparent generators to offset energy demand, and reduce greenhouse gases.

INTRODUCTION

Windows aim to resist solar heat gain, infiltration, and limit energy transfer while maintaining high levels of visible transmittance, but rarely has a window achieved this balancing act and generated electricity. In Los Angeles, the last five high-rise buildings resulted in two million square feet of exterior glazing, and 1.3 million square feet with access to peak sun hours. With 1.3 million square feet of vertical real estate available for renewable generation not one development offered on-site renewable energy despite solar access and surface area availability.

The five developments resulted in a window-to-wall ratio of approximately 90%, and yet windows continue to be widely applied as a fenestration material of preference that offers aesthetic delight and transparency despite being directly attributed to energy consumption and carbon emissions (Aasteh & Selkiwitz, 1989). As window area increases so does the energy demand to heat and cool buildings. 22-32% of the building energy demand is attributed to poor window performance and results in 2 quads a year in energy or $20 billion dollars. This results in an uptake in carbon emissions and greenhouse gases, and knowingly so, our affinity with glass continues to dominate the built environment.

Window performance is paramount in making a substantial impact on energy conservation measures, but some theorize that windows have reached their theoretical limit of performance (Johnson, 1991), yet the building industry continues to disregard these findings. Analyzing window performance through the lens of conduction, convection, and radiation illustrates that modern windows resist these energy flows in the gap between panes, and it is within the gap that a divergent ideology emerges.

If windows have reached their theoretical performance limit, then what opportunities exist to expand a window's capabilities? What if 1.3 million square feet of windows generated electricity without compromising solar heat gain, infiltration, and heat transfer while offering a high degree of visible transmittance? The physics of the window-sun relationship and the gap between panes was essential to answering these questions.

BACKGROUND

The gap between panes was central to the experiment and resulted in a complex choreography of energy transfer considerations. To activate the gap's electrical generation potential each energy domain was explored. It was theorized that the medium occupying the gap must retain high kinematic viscosity and low thermal conductivity (k) to maintain high insulating values (Johnson, 1991, p. 38). Heat transfer fluid were explored and naturally this increased convective traffic, and raised heat transfer across the glass panes. To offset this conductive transmission to the ambient, an air column was added to resist energy transfer between the fluid column and the ambient air. Conductivity (k) was largely dependent on the buoyancy flow of natural convection, the Rayleigh number[1], and higher conductivity values were beneficial to enhancing thermal exchange. Radiant energy was another opportunity to harness solar radiation. A low-e film was suspended in the gap to trap radiant energy rather than reflected to the ambient or to the surface of the glass (Fig. 1). Collectively these strategies turned the gap in to an energy trap.

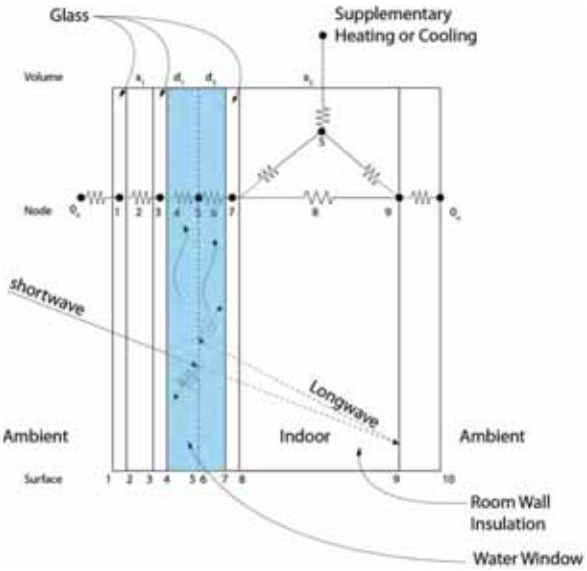


Figure 1: Energy schematic.

Nanofluids exhibited superior properties relative to those not only of conventional heat transfer fluids, but also of fluids containing micrometer-sized metallic particles (Choi, Zhang, Yu, Lockwood, & Grulke, 2001, p. 718). Thus the specific heat of water based fluids can be augmented by adding nanoparticles (Shin & Banerjee, 2011, p. 1), and that corresponding thermal conductivity can increase between 35%-45% (Shin & Banerjee, 2015, p. 898). Water based Al_2O_3 nanofluid's specific heat decreases gradually as the nanoparticle volume fraction Ø increases from 0.0% to 21.7% (Zhou & Ni, 2008, p. 92). The results indicated that the effective heat flow was influenced by volume fraction Ø. Base fluids containing small amounts of nanoparticles resulted in increased thermal conductivity (Murshed, 2005, p. 372).

Öğüt (2009) investigated natural convection heat transfer of Cu, Ag, CuO, Al_2O_3, and TiO_2 water based nanofluids across a variable incline enclosure ranging from 0° to 90°. The test specimen was heated on one side with a constant heat flux, while

[1] Rayleigh number describes a fluids property when heat transfer occurs by conduction or convection.

the opposite was cooled, and all other sides adiabatic. Although the experiment focused on electronics and aerospace cooling solutions that require miniaturized solutions, the research draws parallels application to window environments. Similar to Timofeeva et. al., heat transfer rates increased with water based nanofluids, and as the solid volume faction increases so does the conductive strength. This supports Timofeeva et. al. when mentioning that the 90nm particle was the highest thermally conducting performer. Additionally, the Rayleigh number (Ra) appears to exceed 1000 indicating that convection has started, and an excellent indicator that fluids will move by natural convection, and can be used to circulate nanofluids through heat exchangers. Öğüt concludes that aluminum and copper are the most effective heat transfer nanofluids.

METHODS

Engineer a series of windows with fluid and air columns in varying configurations, and the ability to displace fluids to a heat exchanger and thermoelectric generator. Three factory tested windows (single pane, double pane, and triple pane) were acquired with accompanying window performance criteria. Seven Nanowindows with alternating fluid column, air gap, and suspended heat mirror in double pane, triple pane, and quad pane configurations were designed, fabricated, and tested for rate of heat loss (U-factor), visible transmittance (VT), and solar heat gain (SHGC), and electrical generation. A custom-built 0.5" window spacer fabricated from thermoplastic polycarbonate was engineered to accommodate sensors, fluid inlet/outlet, filling ports, expansion reservoir, and water tightness when fused with glass panes (Fig. 2). The vision area of each window was 76% clear (Finlayson, Arasteh, Huizenga, Rubin, & Reilly, 1993, p. 3), and a fluid capacity of 0.94-liter (0.24-gallons). Two liters of Al_2O_3 nanofluids[2] with article size mean of 10 nm ±5 nm in a concentration of 1% by weight in deionized water, and particle purity (metals basis) of 99.95+% was procured.

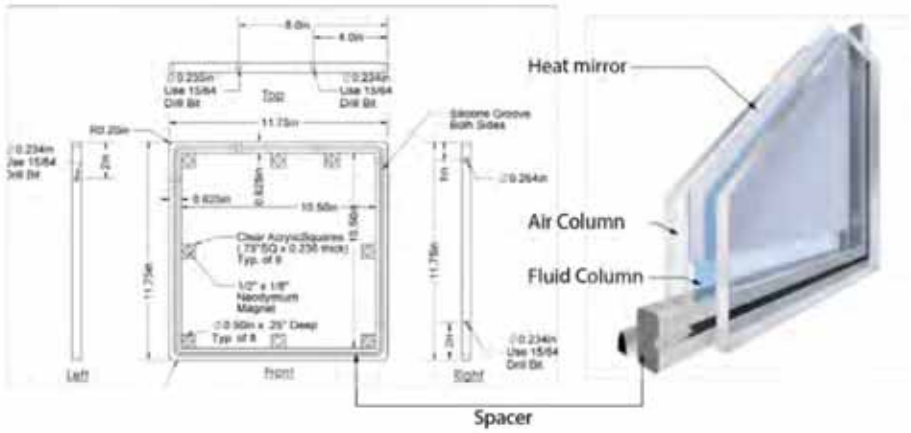
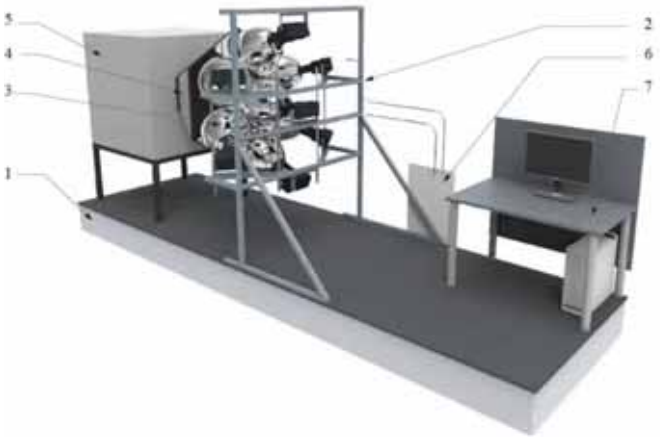


Figure 2: Window spacer and Nanowindow #7 (only 1 of 7 illustrated).

A Solar Lab was built exclusively for testing the Nanowindow, which offered uniform test conditions to limit variability between iterative experiments (Fig. 3). The Solar Lab comprised of a low-cost solar simulator and a calibrated hot box (CHB) coupled with a data acquisition center using a Campbell Scientific equipment capable of sensor measurement, timekeeping, data reduction, programming, and actuation of fans, lights, heating & cooling system, and pumps.

[2] Nanofluids provided by Meliorum Technologies, Inc.



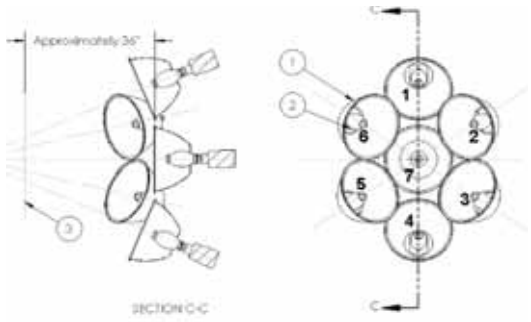


Figure 3: Solar Lab (1. Lab Platform, 2. Array Rack, 3. Luminaires & Lamps 4. Concentrator, 5. Calibrated Hot Box, 6. Load Center, 7. Data Acquisition Center).

Figure 4: Array Geometry (1. Aluminum Spun Ellipsoidal Reflectors, 2. Metal Arc Lamps, 3. Test Plane).

Using a parametric based solid modeler, the solar simulator was engineered to solve for maximum flux output based on various geometric positions to provide one sun at the test plane (Fig. 4). Seven 400 watt MH400/U luminaires were selected and equipped with a SS VertX spun aluminum ellipsoidal 19-inch reflectors, and placed in a hexagonal concentrator fabricated from pre-mirror stainless steel to concentrate flux energy at the test surface.

A 4-foot cube (64ft^3) Calibrated Hot Box (CHB) with a minimum sample area of 1ft^2 was fabricated according to ASTM's Standard Test Method for the Thermal Performance of Building Assemblies by Means of a Hot Box Apparatus (ASTM C1363-11). The CHB was composed of a climate chamber (proximal to the solar simulator), and meter chamber equipped with a heat source and a cooling system respectively.

EXPERIMENT

Three heat exchange experiments coupled nanofluids with air, water, and a thermoelectric generator (TEG[3]). Only the TEG experiment along with SHGC, U-Factor, and VT are reported here. Nanofluids were circulated from the Nanowindow to a 4 in^2 water block attached to a 3.88 in^2 TEG. The TEG was connected to a multimeter and measured electric potential (voltage) and Current (I) in direct voltage (DC) over the course of 4-hours. Tests compared water-based Nanowindows to Al_2O_3 Nanowindows.

Test 1: Thermoelectric Generator Only (H_2O only)
Test 2: Thermoelectric Generator + Heat Sink (H_2O only)
Test 3: Thermoelectric Generator Only (Al_2O_3 only)
Test 4: Thermoelectric Generator + Air Circulation, No Heat Sink (Al_2O_3 only)
Test 5: Thermoelectric Generator + Heat Sink, No Air Circulation (Al_2O_3 only)
Test 6: Thermoelectric Generator + Heat Sink + Air Circulation (Al_2O_3 only)

CALIBRATION

Solar simulator calibration was evaluated using Standard Specification for Solar Simulation for Photovoltaic Testing (ASTM E927-10) and International Electrotechnical Commission (IEC) standards. An Ocean Optics USB2000+VIS-NIR[4] spectroradiometer compared the simulator's ultraviolet (UV), visible light (VIS), and near infrared (NIR) to ASTM G173 Terrestrial Reference Spectra. The calibration evaluated 100nm intervals from 350 to 1100nm wavelengths and resulted in a 2.3% temporal instability (ATSM Class B designation); Irradiance non-uniformity of <2% (ASTM Class B); and a spectral match 18% out of range of ASTM E927 criteria, but corrected using spectra specific filters to lower mismatch.

Heat transfer, flanking loss, and infiltration of the CHB was evaluated to characterize heat flow paths, and time to achieve steady state conditions. Three calibration exercises were performed and concluded that steady state was achieved in 2

[3] Custom Thermoelectric Generator model 28711-5M31-12CW was procured. I_{max}(Amps)12.0, Q_{Max}(Watts)255.3, V_{max}(Volts34.4)
[4] USB2000+VIS-NIR is equipped with a silicon Sony ILX511B detector, 2048 pixels, pixel size of 14 µm x 200 µm, and pixel depth of ~62,500 electrons.

hours with a 0.62°C differential swing in the climate chamber and a 0.79°C differential in the metering chamber which is less than the ±1°C allowed by ASTM and ISO standards. The hot box provided a climate chamber and metering chamber (Fig. 5) capable of heating to 60°C and cooling to 10°C respectively. This condition offered the required differential between chambers of 22 °C (40 °F) which is the desired temperature differential for resistance testing (ISO 12567-1, 2010, p. 14).

To evaluate sample accuracy tested in the CHB three know samples (#0-polyiso, #1-single pane, #2-double pane, #3- triple pane glass) with laboratory certification for SHGC, VT, and U-Factor were tested. U-factor for the polyiso was 8% less compared to the certified value; single pane was 10% less; double pane was 4%, and triple pane was 3% more than the certified value. While the results averaged below 6%, a guarded hot box would have been desirable along with a slight suction in the climate chamber to prevent cold air from infiltrating into the meter chamber and impacting the overall energy balance (Burch, Licitra, & Zarr, 1990, p. 36).

The Solar Lab was equipped with sensors specific to understanding heat transfer, spectroscopy, and energy generation (Fig. 5). An Apogee UV sensor SU100 was used to measure the light intensity from 250nm to 400nm; a hemispherical Hukseflux LP02 Solar Radiation Pyranometer[5] was selected for its compatibility with measuring lamp based solar simulator in-situ experiments; Ocean Optics USB2000+VIS-NIR to measure ultraviolet, visible, and near infrared (UV-Vis-NIR) wavelengths from 350 to 1100 nm; and thermistor ambient temperature sensors, probe temperature sensors, and surface sensors.

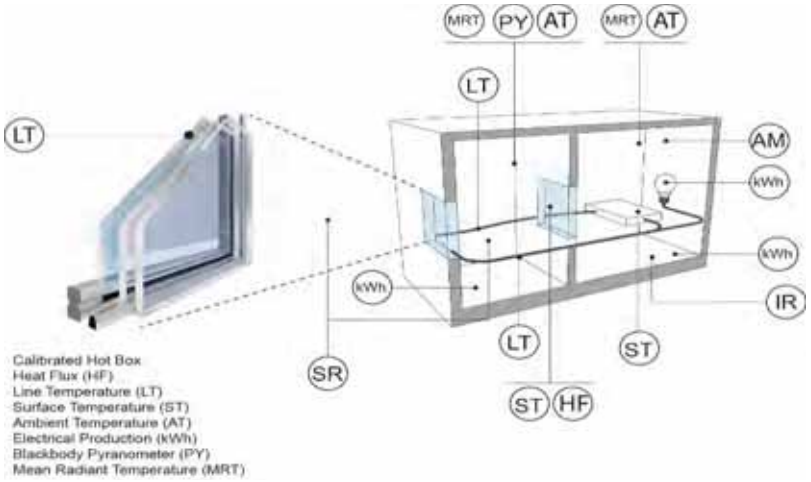


Figure 5: Calibrated hot box and sensor type and placement.

RESULTS

U-factor, VT, SHGC, and electrical generation of seven H_2O Nanowindow and Al_2O_3 Nanowindows were compared. Three factory built baseline windows (single pane, double pane, and triple pane) were also included in the analysis to compare known high performance windows to the Nanowindows.

U-factor for H_2O Nanowindows 7, 8, 9, and 10 offered promising results compared to factory double pane and triple pane windows (Fig. 6) using Equation 1. The U-factor for Nanowindow 7 and H_2Owindow 7 were within ±0.013 Btu/(hr) (ft2)(°F) of each other, and Nanowindow 8 and H_2Owindow 8 were ±0.009 Btu/(hr) (ft2)(°F) of each other. Based on the CHB's accuracy it was deemed that Al_2O_3 Nanowindowshad little to no impact on thermal resistance and nearly equal to H_2O Nanowindows.

[5] Hukseflux LP02 Pyranometer is a hemispherical solar radiation sensor with calibration uncertainty $\pm 0.21 \times 10^{-6}$ v/(W/m^2).

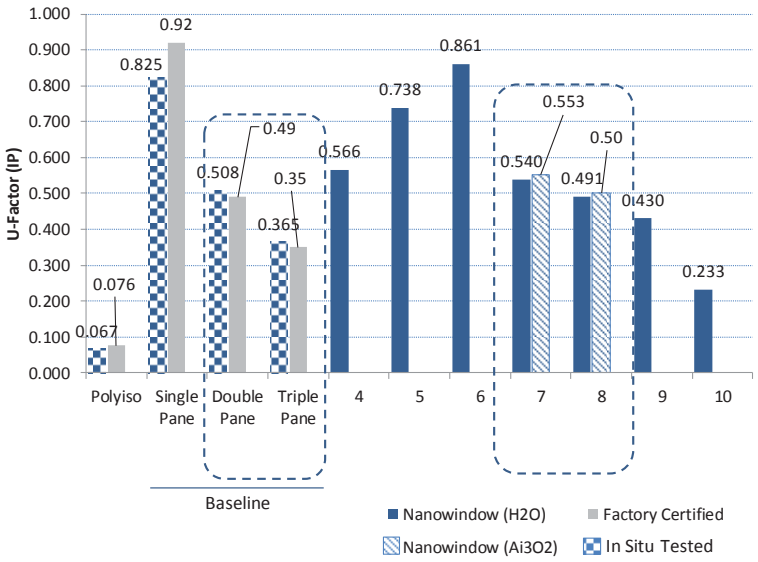


Figure 6: H_2Owindow U-factor results.

Visible Transmittance was calculated using ANSI/NFRC 200-2014 standards to establish a relative baseline of comparison, and it was determined that H_2O Nanowindow 7 and 8 were above the minimum criteria with a VT of 0.47 and 0.51 respectively, both of which are well above the 0.42(42%) VT code compliance for fixed windows. Nanowindow 7 and 8 resulted in 0.27 and 0.23 respectively which is below International Energy Conservation Code compliance (Fig. 7).

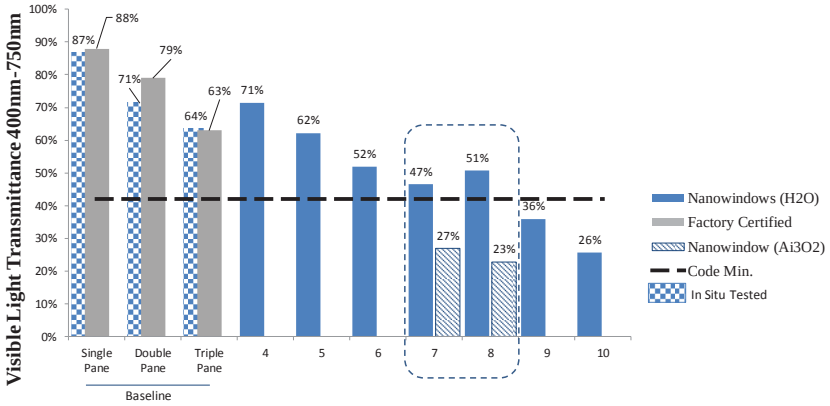


Figure 7: Nanowindow VT results.

H_2O Nanowindows 7,8, 9 and 10 Solar Heat Gain Coefficient (SHGC) yielded favorable results (Fig. 8), but H_2O Nanowindows 7 and 8 resulted in comparable results to double pane and triple pane windows while H_2O Nanowindows 9 and 10 outperformed all the baseline windows. Nanowindow 7 was within ±0.007 (1% difference) of baseline window 7, and the SHGC for Nanowindow 8 was surprisingly 0.049 or 7% more than baseline window 8 (Fig. 8). This raised concerns that a testing error may had occurred as the rate of heat transfer between baseline window 8 and Nanowindow 8 should be similar. After closer examination of the data it was determined that the Climate Chamber had cooled beyond its set-point by 5°C reaching a low of 10°C compared to other test conditions that ran at a steady state of ±15°C.

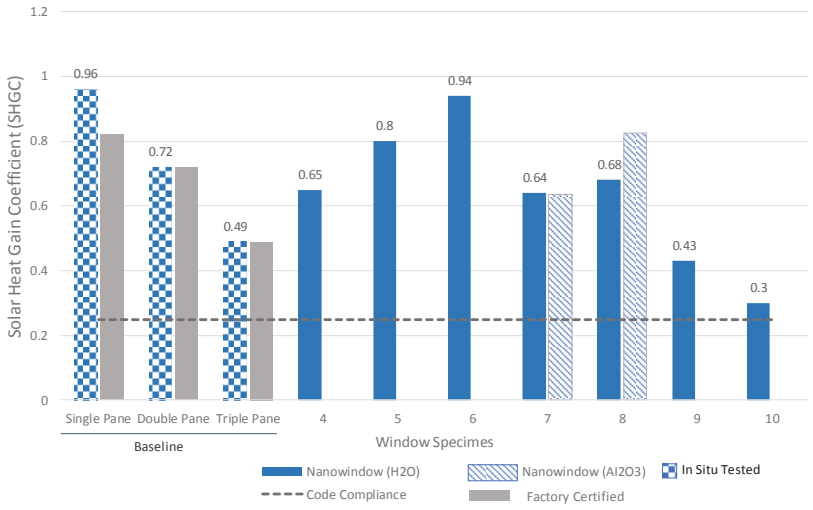


Figure 8: SHGC results.

Al_2O_3 Nanowindows 7 and 8 illustrated the most favorable results so the thermoelectric generator (TEG) experiment focused on these two Nanowindows, and applied six tests. Test 1, the ambient temperature in climate chamber was unregulated for the first half of the experiment, and then cooled to 22°C to simulate a workplace environment. As expected, when the temperature differential across the thermoelectric generator (TEG) was increased so did the power and current output. Test 1 resulted on average ~0.022 vdc. System Size Factor (SSF) was used to determine system size relative to the desired voltage output to the actual voltage output to determine scaling efficiencies. The lower the SSF the more efficient the system regarding heat transfer and energy generation. This resulted in a SSF of 545 (12 vdc/.022 vdc) which was then applied to the TEG area and Nanowindow recognizing that transmission loss and individual system efficiencies where not taken into consideration at this stage.

Based on a 545 SSF to achieve a 12 vdc system would require 2,114 in^2 (14.6ft^2) TEG coupled with 545ft^2 of water based Nanowindows. Test 2 increased the temperature delta between the TEG and the water block using an aluminum heat sink. The power output increased significantly to 0.036 volts and resulted in a system size factor of 333 which was 38% better than Test 1. Thus a 12 vdc system would need 1,292 in^2 of TEG coupled with 333ft^2 of nanowindow.

Tests 3-6 shifted to Al_2O_3 nanoparticles and resulted in increased voltage outputs as a function of larger temperature differential across the TEG as a function of the nanofluids. Test 3 resulted in 0.047volts - a 113% improvement over Test 1.

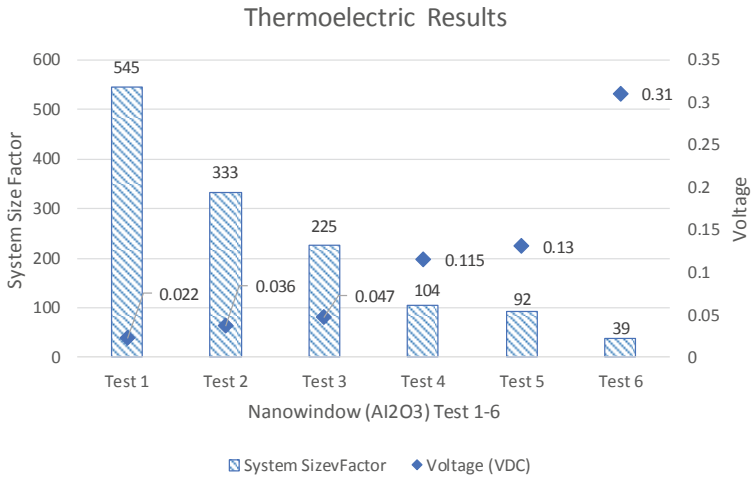


Figure 9: TEG results.

Test 6 generated 0.31volts and a rated current of 0.075Adc. This resulted in a System Size Factor (SSF) of 39 which was significantly better compared to all other water-based and nanoparticle Nanowindows (Fig. 9, Test 6). Thus 151 in^2 (1.04ft^2) of thermoelectric generator is required for every 39ft^2 of nanowindow system based on a system size factor of 39.

CONCLUSION

The gaps between seven prototype windows were filled with aluminum oxide (Al_2O_3) nanofluids. The nanofluids were circulated to a thermoelectric generator to determine the electrical production potential, and evaluated U-factor, VT, SHGC. U-factor performance diminished as a function of increase in conductivity, but on its own was an advantage that had to be balanced with power production. Visible transmission (VT) was less than favorable because of the nanoparticle weight to volume of concentration. Further nanotechnology investigation is required to determine appropriate concentration and sonication to agitate nanoparticle dispersion in the distilled water to improve optical clarity. SHGC of the H_2O Nanofluid and Al_2O_3 Nanofluid performed equally less than baseline, but during trail experiments it appeared that sensible heat gains in the meter chamber was absorbed by the Nanowindow when couple with a larger heat exchanger. This resulted in a cooling effect previously not observef1d.

The Nanowindow was scaled to have meaningful impact as a renewable technology. Applying Ohm's Law derived that 1.3 million sqft of Nanowindows coupled with 33,800sqft of thermoelectric generators results in 18,100 W (18 kW)[6] of electricity, service 14 homes, take 2.4 cars off the street, and eliminates 13 tons of CO_2. While the impact may not be as significant as photovoltaics it illustrates that Nanowindow possess the potential to be considered as a renewable technology alternative with viable beginnings no different than the first silicon cells of Bell Labs. The potential for window gap technology to shift from resisting energy to harnessing solar energy presented a unique opportunity to turn windows into energy brokers, and advance zero net energy goals. Glass skyscrapers may have one more renewable option to turn vertical real estate into energy generators without degrading visible transmittance and offering multiple energy offsets for heating, cooling, and energy generation. The emerging technology established a durable foundation to continue evaluating optical clarity and high-performance characteristics of nanofluids.

FUTURE WORK

It was observed that circulating nanofluids reduced transmitted irradiance levels compared to nanofluids fluids at rest. The absorption of water was a fundamental property that influenced the passage of light through the water column (Pegau & Zaneveld, 1993, p. 188), and that the absorption spectrum of the water column in the Nanowindows changes with an increase in temperature (Collins, 1925, p. 772). The cause of this resided within the microscopic changes in water structure that occurred as the temperature increased (Langford, McKinley, & Quickenden, 2001, p. 8921) causing covalent bonds of the water molecule to produce vibrations that absorbed spectral radiation at varying wavelengths. While this was not the focus of the research, it offered unique advantages that a nanofluid column may have on limiting various portions of the solar spectrum to protect indoor occupants from harmful wavelengths. Future experiments may explore the ultra violet protection offered by nanofluids.

Larger heat exchangers coupled with Nanowindows illustrated an unforeseen benefit that offered cooing potential. It was noted that the climate chamber's ambient temperature dropped as a function of the increased size of the heat exchanger. It is assumed that the Nanowindow can reduce the amount of incoming solar thermal energy entering the adjacent space, and absorb sensible heat in that space as a ratio of heat exchanger-to-Nanowinow size.

ACKNOWLEDGMENTS

Sincere gratitude goes out to G.Z. Brown, Director of the Energy Studies in Buildings Laboratory at the University of Oregon; Dr. Ihab Elzeyadi; Dr. Pablo La Roche; and Dr. Kelly Sutherland for their support in the preparation of this manuscript. Special thanks to Frank Smith with the Lighting Lab at California State University, Pomona, Rich Wipfler at Eastman Chemical Company, Leif Ortegren at Pilkington BPNA, Nicholas Peak at Viracon, Walt Lutzke at Tubelite, Howard Eckstein at MCD Electronics Inc, David Conroy at NASA Jet Propulsion Laboratory, and Dr. Jason Rama at Meliorum Technologies, Inc.

[6] Based on PVWatts the tilt angle was adjusted to 90-degrees to simulate a vertical solar panel. It was determining that there is a 40% degradation in energy production compared to 34-degrees. 18 kW takes into consideration 90-degree tilt.

EQUATIONS

1 $$U = \frac{Q}{(T_{MC} - T_{CC})}$$

Where:

U = thermal transimttance (W/m^2K)

Q = heat flow through the specimen (W/m^2)

T_{MC} = Meter chamber ambient temperature (C^o)

T_{CC} = Climate chamber ambient temperature (C^o)

2 $$VT = \frac{\left(\sum ti_{eog} + \sum ti_{cog}\right) x\ 0.5}{\sum ii_{ss}}$$

Where:

$\sum ti_{eog}$ = sum of transmitted illuminace between 400nm - 750nm at the edge-of-glass

$\sum ti_{cog}$ = sum of transmitted illuminace between 400nm - 750nm at the center-of-glass

Σii_{ss} = sum of incident illumiance between 400nm - 750nm as tested in Part 2

3 $$SHGC = \frac{Q_{hf} - Q_{U-factor}}{A_{specimen} ii}$$

$SHGC$ = Solar Heat Gain Coefficient

Q_{hf} = Heat Flux (W/m2) as defined in Chapter IV

$Q_{U-factor}$ = Specimen U-factor as defined in Chapter II

ii = incident illumiance (W/m2) as defined in Chapter II

4 $$\frac{Vd}{Va} = Nano_{Assembly}$$

Where:

$Vd_{(dc)}$ = Voltage Desired (vdc)

$Va_{(dc)}$ = Voltage Actual (vdc/sqft)

$Nano_{Assembly}$ = Nanowindow Assembly Size (sqft)

REFERENCES

Aasteh, D., & Selkiwitz, J. (1989). The Design and Testing of a Highly Insulating Glazing System for use with Conventional Window System. *ASME, Journal of Solar Engineering*, *III*.

Burch, D. M., Licitra, B. A., & Zarr, R. R. (1990). A COMPARISON OF 2 TEST METHODS FOR DETERMINING TRANSFER-FUNCTION COEFFICIENTS FOR A WALL USING A CALIBRATED HOT BOX. *Journal of Heat Transfer*, *112*(1), 35–42.

Choi, S. U. S. (1998). *Nanofluid Technology: Current Status and Future Research.*

Choi, S. U. S., Zhang, Z. G., Yu, W., Lockwood, F. E., & Grulke, E. A. (2001). Anomalous thermal conductivity enhancement in nanotube suspensions. *Applied Physics Letters*, *79*(14), 2252. https://doi.org/10.1063/1.1408272

Collins, J. R. (1925). Change in the infra-red absorption spectrum of water with temperature. *Physical Review*, *26*(6), 771.

Finlayson, E. U., Arasteh, D. K., Huizenga, C., Rubin, M. D., & Reilly, M. S. (1993, July). WINDOW 4.0: Documentation of Calculation Procedures. LBNL Energy and Environment Division.

ISO 12567-1. (2010). Thermal performance of windows and doors -- Determination of thermal transmittance by the hot-box method -- Part 1: Complete windows and doors. ISO.

Johnson, T. E. (1991). *Low-E glazing design guide*. Boston: Butterworth Architecture.

Langford, V. S., McKinley, A. J., & Quickenden, T. I. (2001). Temperature Dependence of the Visible-Near-Infrared Absorption Spectrum of Liquid Water. *The Journal of Physical Chemistry A*, *105*(39), 8916–8921. https://doi.org/10.1021/jp010093m

Murshed, S. M. S. (2005). Enhanced thermal conductivity of TiO2 - water based nanofluids. *International Journal of Thermal Sciences*, *44*(4).

Pegau, W. S., & Zaneveld, J. R. (1993). Temperature-dependent absorption of water in the red and near-infrared portions of the spectrum. Retrieved from http://ir.library.oregonstate.edu/xmlui/handle/1957/17038

Shin, D., & Banerjee, D. (2011). Enhanced Specific Heat of Silica Nanofluid. *Journal of Heat Transfer*, *133*(2), 024501. https://doi.org/10.1115/1.4002600

Shin, D., & Banerjee, D. (2015). Enhanced thermal properties of SiO2 nanocomposite for solar thermal energy storage applications. *International Journal of Heat and Mass Transfer*, *84*, 898–902. https://doi.org/10.1016/j.ijheatmasstransfer.2015.01.100

Zhou, S.-Q., & Ni, R. (2008). Measurement of the specific heat capacity of water-based Al[sub 2]O[sub 3] nanofluid. *Applied Physics Letters*, *92*(9), 093123. https://doi.org/10.1063/1.2890431

Heritage <> Facades

CHALLENGES OF TALL ICONIC BUILDING RETROFIT

Skin, bones and internal systems



Hamid Vossoughi, P.E., P. Eng.
WSP Canada Inc.
Hamid.Vossoughi@wsp.com

ABSTRACT

Change happens, for better or for worse, to all living and physical matter. In order to thrive and achieve longevity, we constantly need to adapt to our ever changing environment. For individuals, this means taking actions to reduce and manage physical and mental health risks while achieving positive impacts for our family and community. However regardless of corrective measures throughout one's life, mortality is a given. For tall iconic buildings, demolition is not an acceptable or practical option given their scale and significance. Façade or component renewal to maintain durable enclosure is necessary to extend the useful life of iconic tall towers.

Further, climate change has been at the center of public and policy discussions, and building energy consumption has been identified as a key contributor to the problem. The key to solving this problem lies in how the building envelope and mechanical / electrical systems perform, preferably not in isolation, but as part of an overall renewal plan. Energy conservation measures through retro-commissioning can make a substantial impact in large buildings. Façade and retro-commissioning work can be carried out as independent project. Tower Renewal Guide (Kesik, and Saleff 2009) and Roadmap for Retrofits (Chisholm 2016) of large buildings have been developed to guide property owners and stakeholders to plan and take the necessary corrective actions.

This paper highlights retrofit of three tall iconic towers in downtown Toronto (Fig. 1) with various degrees of renewal, ranging from spandrel/vision re-glazing to coating finish renewal, coupled with internal system retro-commissioning to complete to over-cladding of the exterior envelope. The business drivers for change ranged from risk management of an aged façade to image renewal to compete with newly built towers in a competitive market. Primary challenges with the retrofits were the required upfront due diligence and the unforeseen conditions, design limitations regarding the character defining façade elements, managing the existing de-construction and re-construction of an occupied building, project scale, and finally public safety as it relates to execution of work in tight/confined downtown area.



Figure 1: 100 King St. prior to and rendering of façade retrofit, 77 King St. W. (right hand side of photo), and 401 Bay St. prior to and rendering of façade retrofit.

KEYWORDS

retrofit, case study, façade, tall buildings, durability, energy, process

INTRODUCTION

Buildings are major assets that reflect the image of cities through their height, shape, form, and function. Façade plays a key role in portraying that image. Poor performance of a building facade, either through aged appearance, deterioration posing public risk, and/or other factors (such as leakage), can easily stain the image of a building. Anticipated service life (CSA S478-95) of most high-rise (office, commercial, and residential) buildings ranges from 50 to 99 years. For iconic tall buildings, the anticipated service life is over 100 years, or preferably "forever" (Patterson 2016) and as long as we want them and need them." This duration is defined as the period of time that building and or components should perform without unforeseen costs or disruption for maintenance and repair. Meanwhile how frequently does one see such a plan, and let alone, accounting for a façade retrofit! Awareness of such needs has become ever growing in the past few years (University of Southern California 2016).

Developing a durability plan anticipating the lifespan and interventions, and implementation of quality through commissioning (CSA-Z320-11) is essential to establish the path to quality and how to operate, maintain and extend the useful life of building and its components during the service life. This is most common for the building's mechanical, electrical, and life safety systems, but not as much for the building façade. Façade ordinances (Wiss 2016) in various cities, some successfully and some not, have attempted to force the need for planned inspections to address unsafe conditions on an on-going basis. Further, component replacement such as insulating glass units, sealant, localized repair or cladding replacement addressing non-performance are generally deferred as much as possible due to finances. When the severity of the non-performance problem is escalated due to life safety and business risks, the need and cost of façade retrofit, either through recladding or over-cladding, raises the question of return on investment in contrast to the value of the asset. This raises the issue and difficult ethical question (Timberlake 2016) on what to do with the aging building stocks. For existing tall iconic buildings, some form of a façade retrofit will be necessary at least once if not twice during its service life. Given the accelerating advancement of façade materials and system design, new construction should seize the opportunity to implement the best technically viable solutions and minimize such potential needs when possible to arrive at a sustainable durable construction for use by the future generations.

BACKGROUND

Buildings as shelter can be perceived as living structure reacting to environmental and internal loads, resembling human body; façade as skin (hair, nail, teeth, etc.), structure as skeleton, and the MEP system as internal digestive system. Human body is an integrated system and one feels every change imposed, physically and or mentally. It is over the past 10 to 15 years that buildings are perceived as an integrated system, and inter-relation between the façade and mechanical/electrical system, as it impacts energy, realized.

At the time of construction of exiting tall iconic buildings now reaching or exceeding 50 years of age, energy was not a primary factor and consideration in design/operation of building. The building façade was designed as an environmental separator, and independent of the mechanical and electrical systems. Building sciences design and construction relied on state of the art technological advancement, made available through the National Research Council of Canada's publications (Construction Building Digests and Construction Technology Updates). These publications established the best in class practice for durable buildings. Performance based hierarchy of needs (Fig. 2) of building envelope was established and examined by NRC.

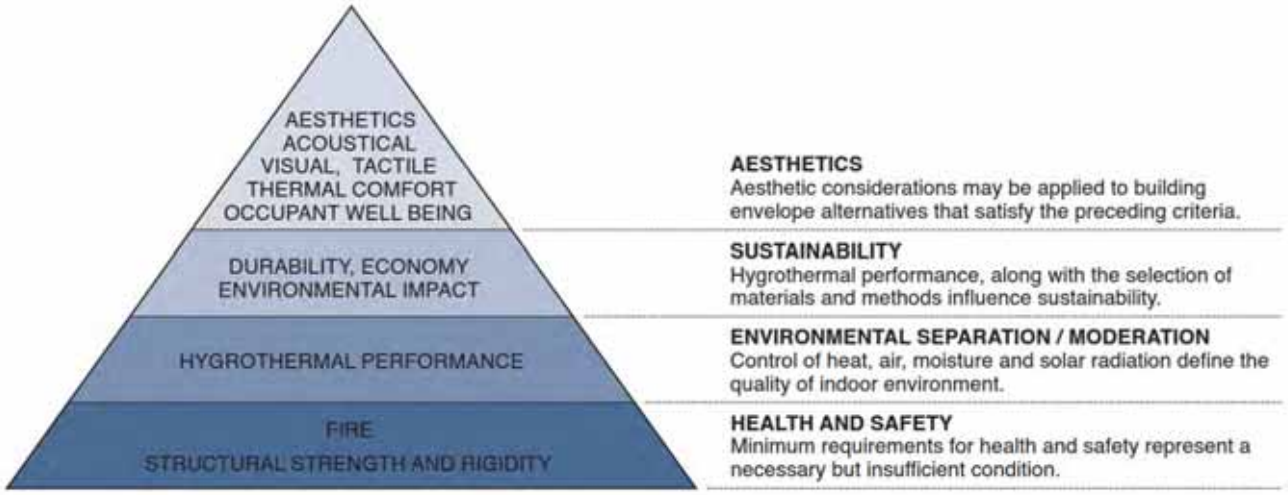


Figure 2: Building envelope performance hierarchy (Kesik 2009).

Circle of life cycle (Fig. 3) depicts an overview of design, construction, repair, restoration and renewal process. The timeline between each stage is varied and not linear as shown. The estimated time lapse per stage, from initial construction to the first retrofit/renewal, can take about 30 to 40 years following the original construction. Business planning and anticipating change, maintenance and repair, based on façade performance and building needs, is essential on an on-going basis. Following the discovery of the issues and decision to proceed with retrofit or renewal, extensive feasibility study, requiring detailed investigation and options analysis, is necessary to set the design direction. Identifying potential risks and mitigating the challenges of existing construction, is the primary challenge during the feasibility study of the project. The first three stage of the process noted below (Fig. 4) may take a minimum of 3 to 5 years, prior to start of the construction stage. During the construction phase, the project challenges shifts to constructability imposed by the existing construction and interface between the existing and new.



Figure 3: Building envelope circle of life.



Figure 4: Façade renewal stages.

CASE STUDIES

The importance of the three subject buildings and what makes them iconic is the fact that they are respectively the tallest building in Canada, a modernist design by Mies van der Rohe, and tallest precast concrete clad office in downtown Toronto. The general relevant high level information of the buildings are as follows (Fig. 5).

BUILDING DATA	First Canadian Place (100 King Street W., Toronto, ON)	Royal Trust Tower (77 King Street W., Toronto, ON)	Simpson Tower (401 Bay Street, Toronto, ON)
Year built	1975	1969	1968
Height (ft.)	978	600	472
No. Floors	72	46	33
Typical Floor Plan (sf)	52,000	23,000	15,000
Structure	Steel frame	Steel frame	Concrete frame
Façade	Marble	Steel	Precast Concrete
Glazing	Thermally broken double glazed windows	Non thermally broken single glazed windows	Non thermally broken single glazed windows
Window to wall ratio	33%	66%	40%
Design Architect	Edward Durrell Stone and Bregman + Hamann Architects	Mies van der Rohe, John B. Parkin Associates and Bregman + Haman Architects	John B. Parkin Associates and Bregman + Hamann Architects
Special Features	Frame tube structure (8 feet deep steel liner per floor), providing later load retinae to the structure, and also backup/liner to the marble façade cladding.	Part of the TD center complex, designed by Mies van der Rohe, and of significance to the heritage defining character of the city skylines.	Part of the modernist architecture, with projected ribbed column covers, extending outboard of the floor plan, encasing high velocity air duct supplying from 10th and 34th level to each floor.

Figure 5: Building descriptions.

PRIMARY DRIVERS

Arriving at solutions to any retrofit project is a balance between the competing business and technical needs. This requires ongoing dialogue and communication with Client, understanding priorities, responding to project challenges, providing option analysis and solutions, and risk management. Improved safety and renewed durability, performance (air, water, and thermal), aesthetics, constructability, consideration of future maintenance / repair, schedule, and economics are essential to project success. Below is the list of (Fig. 6) primary concerns which led to façade retrofit.

DRIVERS	First Canadian Place (100 King Street W., Toronto, ON)	Royal Trust Tower (77 King Street W., Toronto, ON)	Simpson Tower (401 Bay Street, Toronto, ON)
Façade	Deteriorating marble replacement about 1%/yr. Aged appearance	Steel façade not thermally efficient Exterior finish fading	Deteriorating precast concrete Aged appearance
Glazing	IGUs reaching service life	Single glazed, tenant comfort	Single glazed, tenant comfort
Energy	Sustainability (LEED targets demanding energy reduction	Sustainability (LEED) targets demanding energy reduction	Not deemed as a current priority

Figure 6: Primary performance concerns.

CHALLENGES AND SOLUTIONS

The most critical challenge with the subject case studies was their scale, the need to minimize disruption to the occupants, and overall safety. This was achieved through construction logistics and planning, but driven and enabled by design, understanding that solutions have to be relatively simple, practical, and repeatable to achieve efficiencies. Extensive feasibility study, detailed investigation and options analysis, followed by mockup and trial repairs/retrofit with trusted qualified glazing and construction specialist, was key in making the projects a success.

100 KING STREET WEST

The project plan was to achieve a renewed updated image for the building (Fig. 7), while respecting the original architectural design. Typical spandrel façade was made of eight Carrera marble panels (about 80 sf surface area) which looked uniform and non-interrupted façade (Fig. 8) in a clean non-stained state. As a result of age and weathering, in the deteriorated state, panels looked like large stained tiles, and bowed to varying degree. Glass as a modern façade construction material was selected over stone, which as a traditional solid façade construction material, symbolized strength, wealth, and stability representing the financial institutions owning the property. The new replacement façade was a white fritted laminated (white and clear interlayer) triple glazing to create new vibrant appearance and departure to the marble. With the deteriorated marble, that was no longer the case and use of stone was thus deemed unfit. Spandrel panels were structurally glazed to unitized aluminum frames. In order to accommodate installation and also future potential removal needs, design incorporated horizontal aluminum trim covers, acting as access panels, at top and bottom of the spandrel (Fig 9.). Panels were supported on new lateral gravity anchors, attached to the steel existing tube frame liner and close to the building column lines, for direct load transfer to the structure (Fig. 9). The new design introduced bronze corners laminated spandrel glazing, enhancing verticality of the primary elevations. Transition between the primary elevation and bronze corners was differentiated by fly-by white metal panels.

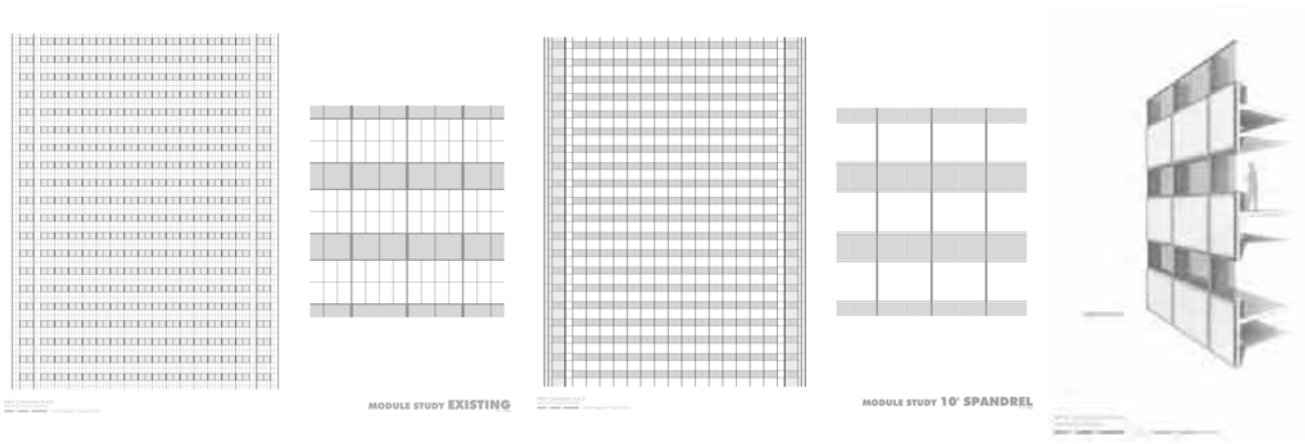


Figure 7: Existing and proposed design by Moed de Armas & Shannon Architects.



Figure 8: Mockup of support (left) and new glass spandrels (right).

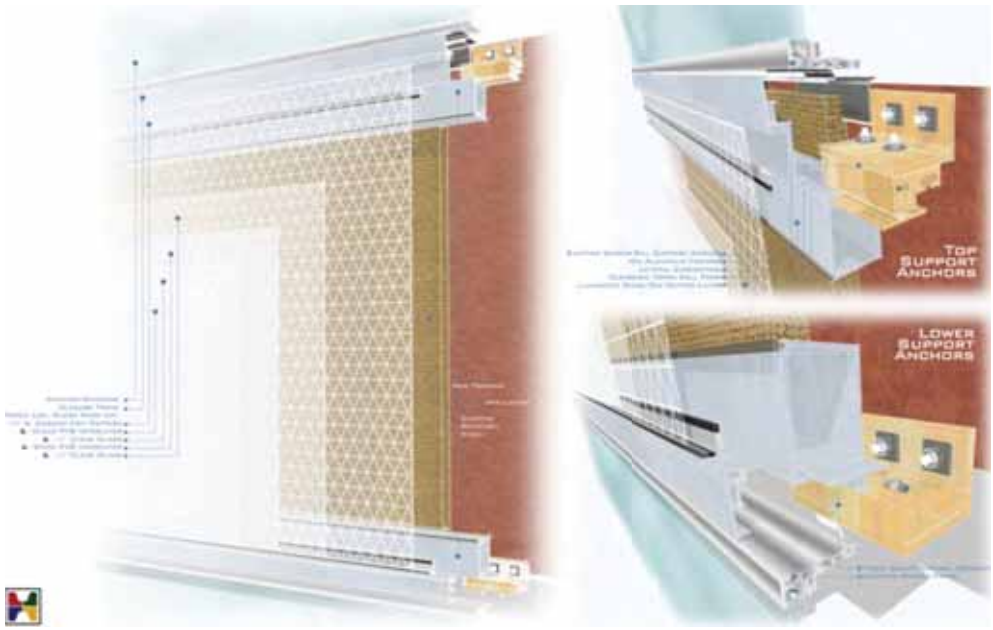


Figure 9: Schematic of spandrel glass, frame, and support design.

An extensive evaluation plan was developed to examine the existing construction of the exiting facade. Large openings on the exterior and from interior of the buildings were made to assess the as constructed façade details and their conditions. The existing construction was robust, and closely resembled the detailed design drawings. There was relatively minimal distress in the building envelope components, but renewal of seals, addressing localized corrosion, addition of cavity

compartment closures, supplementing the existing windows to their respective anchorage, and replacement of the window washing tracks, were completed to extend the useful life of the building for another 40 to 60 years. Extensive mockup was conducted to test and assess remedial measures, to plan and specify the most suitable products/remedial solutions, so the work could proceed throughout the year. Insulating glass unit (IGU) replacement protocol was developed, and these were replaced during tenant turn over as the space became available as a separate project. The objective was to minimize disruption to the building occupants, and also pay for the costs through operations rather than as a capital expenditure.

The logistic challenge of the retrofit was accomplished through innovative design of a three story suspended access platform (Fig. 10), guided through the window washing tracks, and locked into place at the steel tube frame liner at column lines, while stationary and work completed. The platform was divided into four quarters, wrapping the full perimeter of the building, and supplies were provided by two mast climber hoists. Work was completed from top down.



Figure 10: Three story suspended platform.

The building has a low glazing-to-wall ratio and low enclosure-to-floor area ratio. The enclosure's role is largely comfort-related in the perimeter zones. Energy use was above average, and the core loads, heating/ cooling and distributing ventilation air dominated energy consumption (Fig. 11). Modeling concluded that recladding had no impact on energy consumption of the building. Other energy conservation measures however were evaluated. Opportunities were identified in lighting, cooling, plug loads, and ventilation fans, and energy saving measures by optimizing building systems. Projects included mechanical retrofits, sub-metering, retro-commissioning, operational schedule optimization and energy performance tracking. Through analysis and modeling of building systems, the implemented strategy resulted in 26% electricity consumption reduction. The building's score card in 2008 fell below the minimum 68 point requirements per LEED EAp2. Following completed work, in 2011, LEED EB's energy targets were exceeded (Fig. 12).

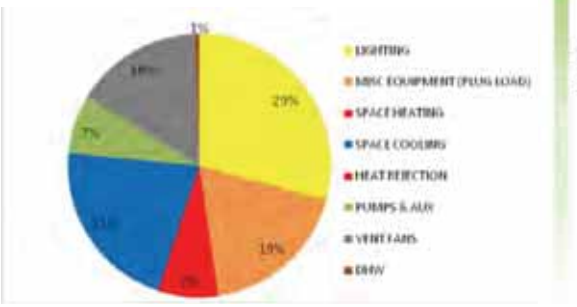


Figure 11: Energy usage breakdown.

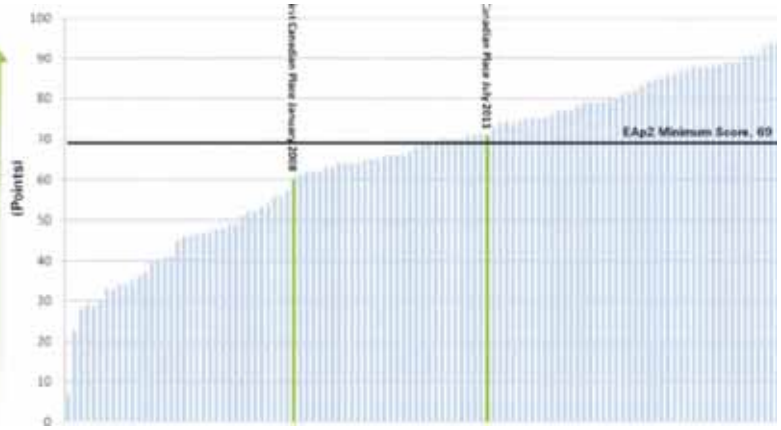


Figure 12: Minimum energy requirements scorecard prior to and after retrofit.

77 KING STREET WEST

The Toronto Dominion (TD) Center complex is comprised of 6 buildings, constructed between 1967 and 1991. Three of the buildings were designed by Mies van der Rohe, are a heritage monument to the city based on the Ontario Heritage Act. Any restoration and renewal of façade had to preserve and not deviate from the original design.

The exterior façade was constructed as a unitized two story tall and 30 to 40 ft. wide steel frame. The façade is highlighted by the exposed steel column mullions (Fig. 13) between the full height singled glazed vision units, and narrow band of steel spandrel. Façade coating was fading, and the existing single glazing was non-thermally broken and inefficient. In order to achieve the Client's objective to promote the property as a leader in energy efficiency, renewal at the property included combination of façade and long-term internal system upgrade projects.

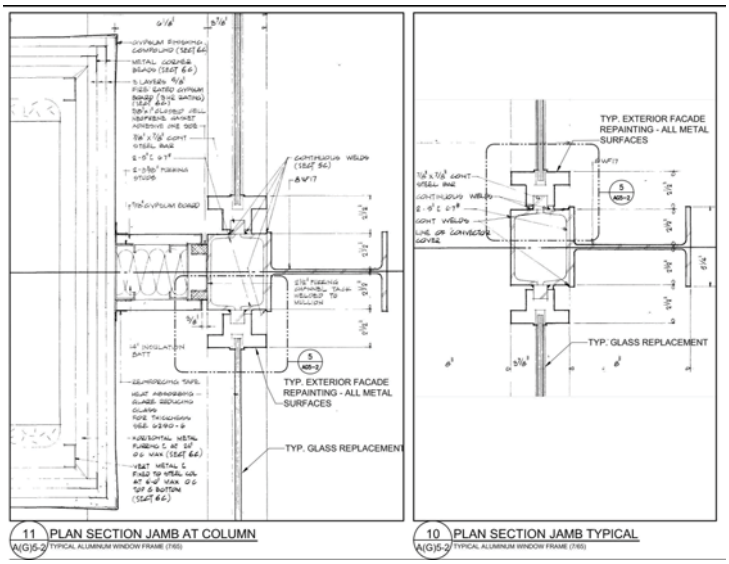


Figure 13: Original construction proposed renewal plan details.



Figure 14: Completed glazing/coating.

On the exterior, the only option was to repair deteriorated steel frame connections, renew the exterior seals, and recoat the spandrels and columns (Fig. 14). This required strict review and approval of mockups by the City preservation authorities. Existing evaluation identified that removal of exterior portion of the window frames was not feasible.

New unitized window insert was added from building interior to upgrade the system from single to double glazed vision unit (Fig. 15). This work was supplemented by addition of rollers shades, and relocation of the induction units from the floor level into the ceiling space at window head. This resulted in a 50% reduction of thermal heat loss when compared to the original design construction. Another proposed solution was to thermally insulating/cladding the mullions from interior; this has been set aside as a future potential project.

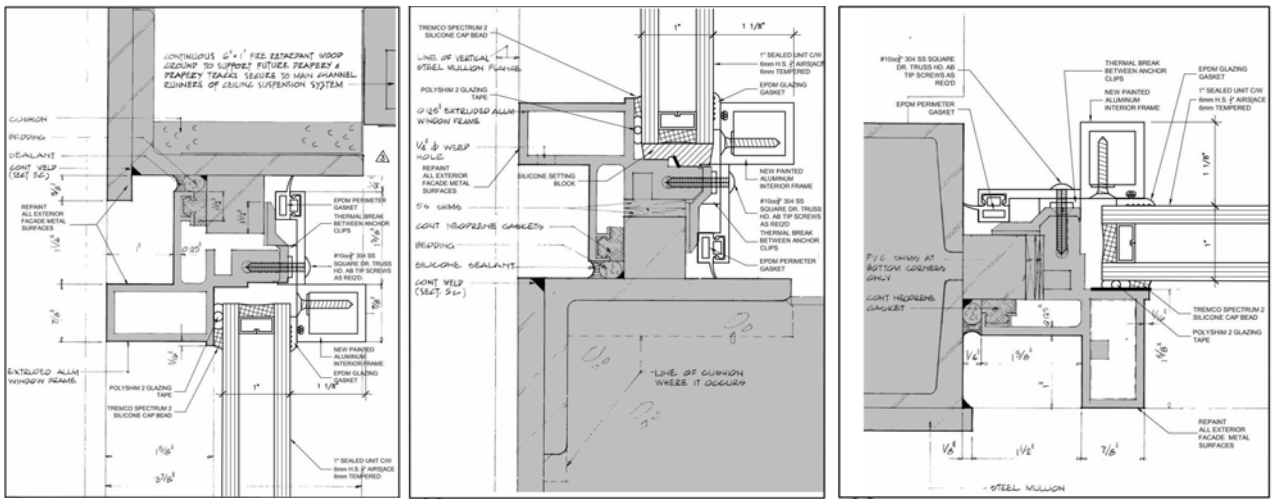


Figure 15: New interior window frame and IGU.

One lost opportunity at 77 King St. W., in contrast to its sister building (100 Wellington St. W) in the same complex, was that as constructed, the exterior portion of the window frame could not be replaced. Therefore, window renewal could not integrate a thermal break into the assembly (Fig. 16). At 100 Wellington, removal and replacement of the entire exiting window frame was feasible, a new thermally broken window was part of the façade renewal and matching the profile of the existing window (Fig. 16).

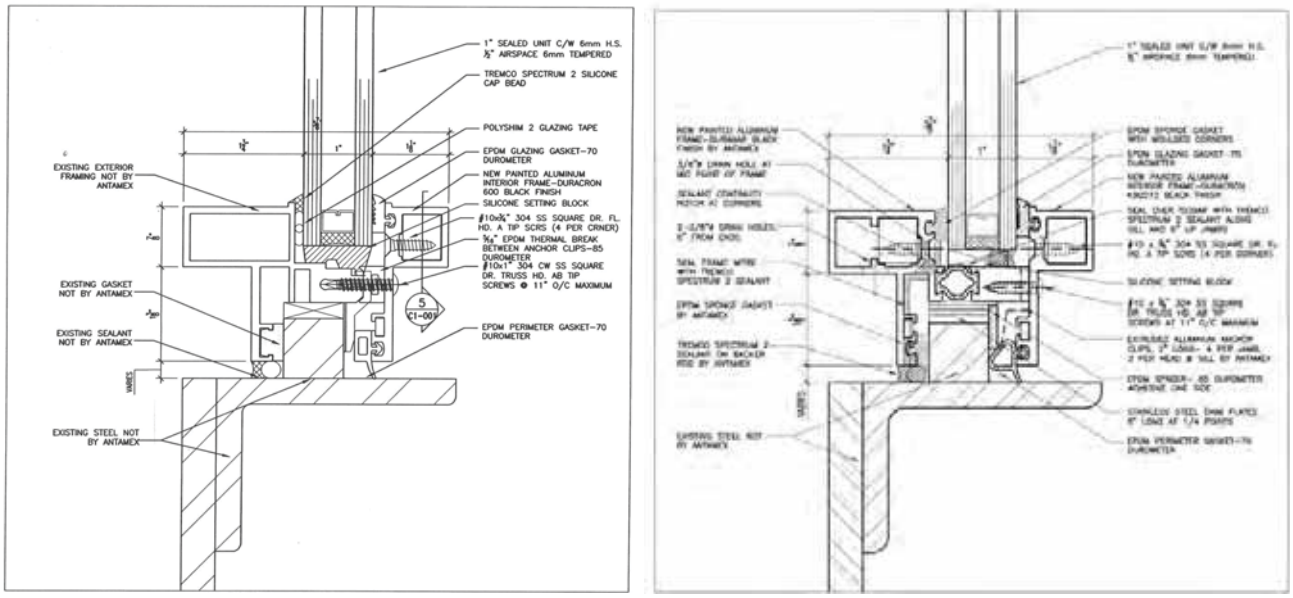


Figure 16: Sill detail of new window insert at 77 King St. W. (left) and new window frame at 100 Wellington St W. (right).

The client's objective was to promote the property as a leader in energy efficiency, and align themselves with industry standards and guidelines. As such, the purpose of study was to evaluate building's energy use (Fig. 17) and identify energy conservation measures (ECM's) to improve performance and achieve the ultimate goal of 18 ekWH/sf/yr., which was a lofty short term goal. A combination of 27 ECM recommendations were presented for consideration, most of which were implemented. Three of the ECM's were related to the exterior façade renewal, and the balance is associated with the building's internal system, as part of capital and operation plans, including retro-commissioning. Now the building has the best performance (i.e. lowest energy use intensity of 27 ekWH/sf in 2011) amongst the 6 TD Center buildings (Fig. 18). 2016 energy audit of the property indicates that the EUI of the property has dropped down to 25 ekWH/sf.

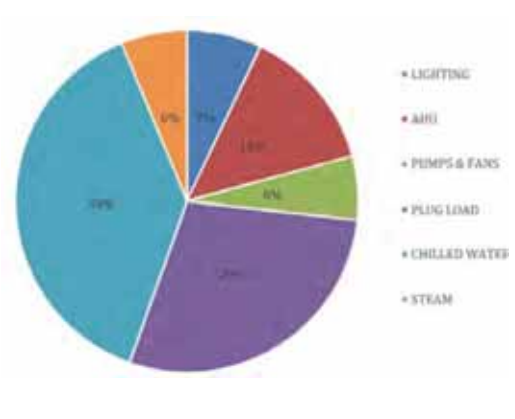


Figure 17: Energy use breakdown.

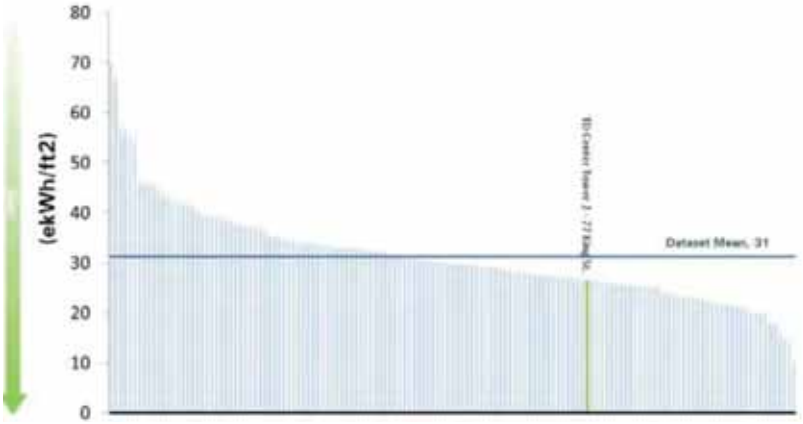


Figure 18: Minimum energy requirements scorecard prior to retrofit.

401 BAY STREET

The existing exterior cladding consists of vertically and horizontally aligned precast panel assemblies, full height glazing on the lower floors and horizontal window bands on the typical floors (Fig. 19). Existing façade is highlighted by column covers, projecting out from the glazed surfaces. Column covers are hung from and enclose the structural columns, which are varied in cross section through the height (Fig. 23). Precast columns had galvanized reinforcement, but evaluation confirmed that about 15% exhibited localized cracking and/or spalling. After 50 years of service, the building appearance was aged, and the Client did not want to continue with future maintenance and repair of the panels. Extensive evaluation, modeling, and option analysis studies were completed. Re-cladding and removal of the panels were ruled out due to financial, scope, and logistics concerns. Over-cladding was selected as the preferred façade renewal option. This work is currently in progress (Fig. 20) and anticipated to be completed in late 2018.



Figure 19: Typical floor façade elevation.



Figure 20: Glazed assembly over-cladding work in progress.

The design concept included installation of a new galvanized external steel framing outboard of the existing precast façade. The new framing was designed to support not only the new cladding, but also supporting and stabilizing the precast column covers (Figs. 21 and 22). The intent was to make the existing precast connections to the structure redundant. Direct load transfer of the new steel framing to the existing structures was accomplished using custom made cementitious grouted sock anchors (Fig. 23). This was made possible due to the deep concrete perimeter beams at each floor. Precast panels and concrete beams had to be cored to accommodate anchor installation. Design accounted for the need for adjustability, site variations, and constructability needs. Preplanning, and developing detail variations, simplified the design solution and made them more economical. As part of construction, horizontal and vertical variation of existing façade from plumb, and cavity width variation to structure had to be measured to determine the required adjustability in connections. Site full scale mock-up was completed to install and test the grout anchors in a typical bay, and resolve constructability of the steel framing assembly. Irrespective of advanced design detailing and mockups, interfaces between the new façade control layers and the existing, and working around the structural framing required several revisions and testing, prior to being finalized. Following the exterior over-cladding (Figs. 24 and 20), interior window frames will be removed and new finishes restored.

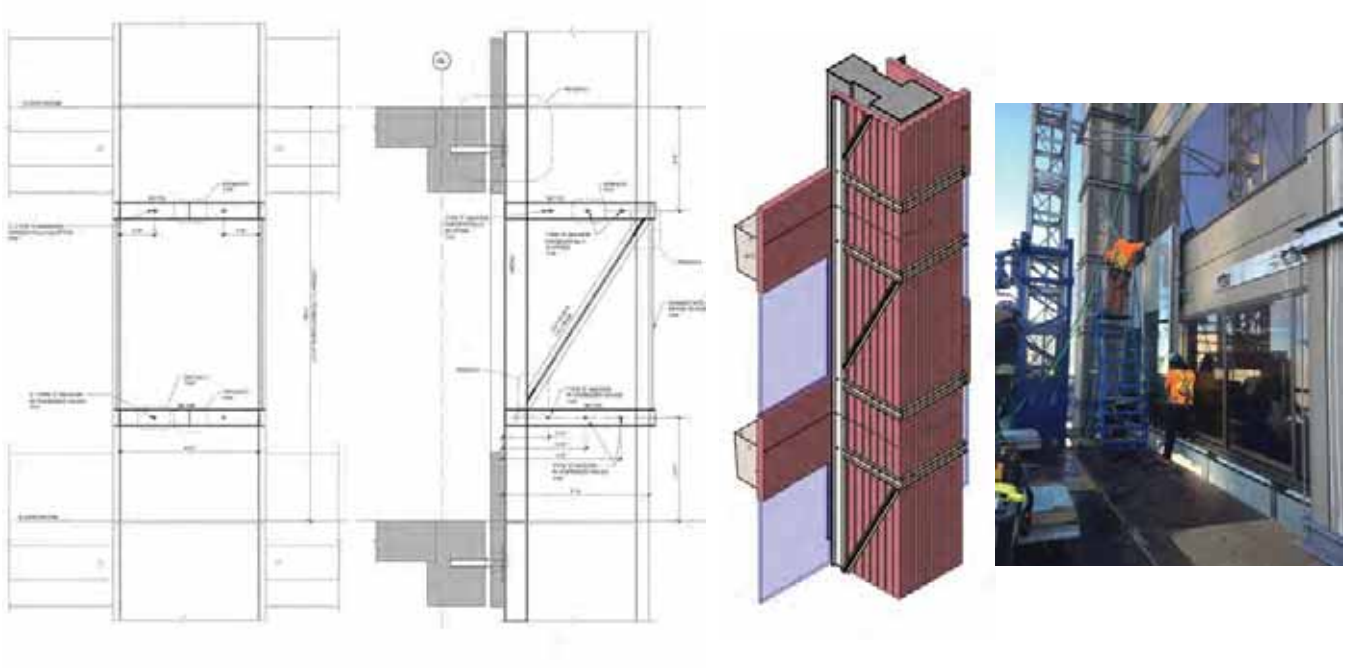


Figure 21: New steel framing support elevations at column covers (left), and work in progress (right).



Figure 22: New steel framing support section and elevation at spandrel (left), and work in progress (right).

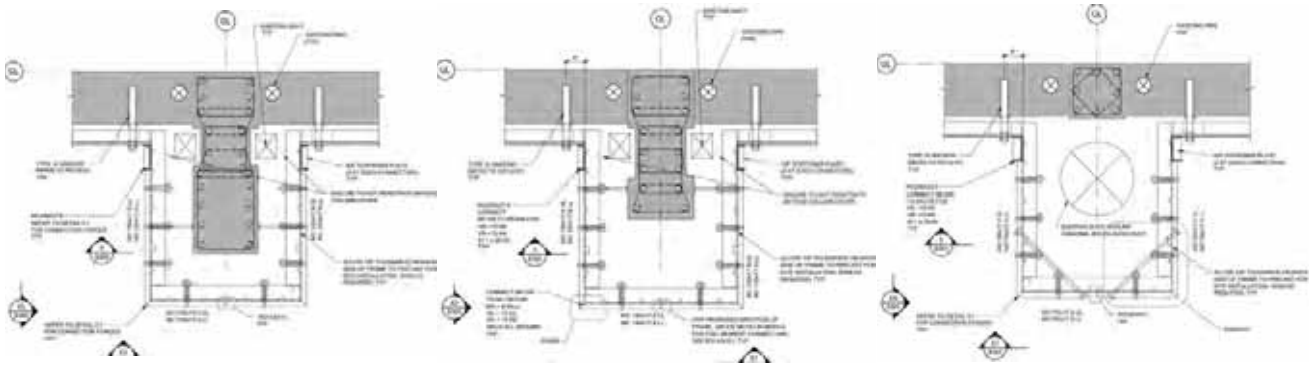


Figure 23: New steel framing support anchorage and existing structural column variation through building height.

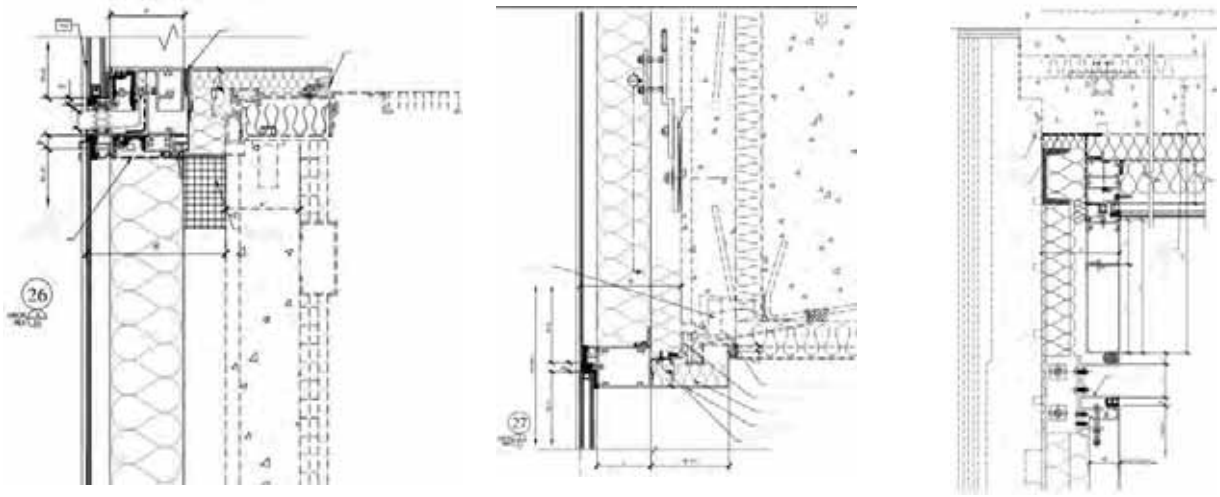


Figure 24: Typical details of new glazed over-cladding (sections at top and bottom of PC spandrel and jamb plan detail at PC spandrel/column cover).

The existing envelope had a non-thermally broken single pane glazing and thermal bridge. Thermographic scan also indicated air leakage at transitions between glazing and precast envelope. Further, the induction units were evaluated, and found to be performing below original design intent levels. At Client's request, testing, adjustment, and rebalancing of the induction units (or their replacement), in conjunction with mechanical system retro-commissioning is expected to be completed as a separate independent project at a later time. We completed a preliminary energy study, assessing potential energy savings following the façade renewal in the future.

Available data indicated that steam heating is the building's major energy end use (Fig. 25), and primarily in the winter months. This is reflective of the original mechanical system type/performance, and potential influence of existing poor performance singles glazed framing. Total energy intensity of the building (excluding atypical space and retail space) is about 63 ekWH/sf., which per Figure 18, is a poor performing for comparable commercial properties. Preliminary analysis indicates that the energy usage is expected to drop down to 22 ekWH/sf following the façade renewal. It is given that added thermal insulation to the opaque walls, and replacement of non-thermally broken glazing with new, should make much improvement to the overall energy usage. However, the results of the analysis seem to be very optimistic, and requires further study, verification of the data, assumptions, and detailed analysis.

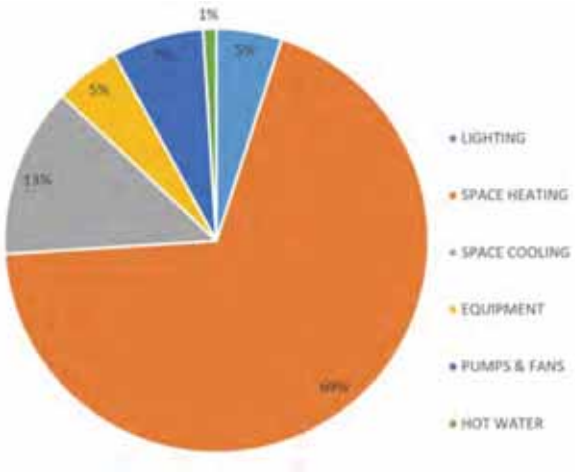


Figure 25: Energy use breakdown.

CONCLUSION AND FUTURE WORK

Façade retrofit and outward transformation of building appearance can be visually dramatic. This takes years of planning and preparation, site assessment of the existing conditions, need for managing existing construction challenges and unforeseen conditions. This process requires extensive collaboration between the client, design and construction team members, and time. The need for such retrofit is on the rise as the number of tall (and iconic) buildings built in the 1960's and 70's are reaching mid-point of their service life. Some of the key questions and need for further consideration regarding such retrofits, and also lessons learned from existing construction for new construction, are as follows:

- Pre-planning and importance of existing construction verifications and feasibility studies/mock-ups are significantly heightened in retrofit projects. Are we spending enough time to do so, and how do we overcome the overwhelming pressures and competing demands of our clients?
- Precedents through exemplar projects, and sharing lessons learned can support to advance knowledge and improved approach in delivery of future projects.
- Benchmarking and monitoring of retrofit performance is highly recommended, but requires approval and building owner's willingness to include this in their operation planning/program.
- New design and construction are becoming more complex with respect to building shape, geometry, and new product/system technologies. Are we designing and constructing with future maintenance, repair, and/or replacement in mind?

ACKNOWLEDGMENTS

The author would like to thank and acknowledge the various teams involved in these projects including but not limited to; Brookfield Properties, Cadillac Fairview, Hudson's Bay Company, Bregman + Hamann Architects, Moed de Armas & Shannon Architects, Highland Associates, Ellis Don Corporation, PCL Constructors Canada Inc., D.F. Pray International, Antamex (Oldcastle Building Envelope), Sota Glazing, Flynn Canada and WSP (Building Sciences, Structures, Energy & Sustainability).

REFERENCES

B+H Architects, “The Second Life of Tall Buildings.” https://www.bharchitects.com/wp-content/uploads/2017/08/The-Second-Life-of-Tall-Bldgs-ENGLISH.pdf (accessed October 30, 2016).

Campbell, Mark. “A Unique Approach to rejuvenating a High Rise Building with Deteriorating Precast Cladding.” Proceedings of 39th IABSE Symposium – Engineering the Future, Vancouver, Canada, September 2017.

Canadian Standards Association, CSA S478-95 (R2007) - Guideline on Durability in Buildings

Canadian Standards Association, CSA-Z320-11 (R2016) - Building Commissioning Standard

Chisholm, Eric. “A Roadmap for Retrofits in Canada - Charting the path forward for large building” https://www.cagbc.org/cagbcdocs/advocacy/CaGBC_Roadmap_for_Retrofits_in_Canada_2017_EN_web.pdf (accessed October 30, 2016).

DeRose, David and Deveau, Adrien. “Rejuvenating a Landmark: Giving First Canadian Place a Look and New Way of Operating.” Ontario Building Envelope Council, Spring 2013.

Kesik, Ted and Saleff, Ivan. *Tower Renewal Guidelines*, University of Toronto, 2009.

Patterson, Mic. “Skinning the Tall Buildings: Framing the Future of Building façade Technology” CTBUH, February 2016

Timberlake, James, “Should We Save Mid-Century Modern Icons that Hurt the Environment?” https://www.fastcodesign.com/3054647/should-we-save-mid-century-modern-icons-that-hurt-the-environment (accessed October 30, 2016).

University of Southern California School of Architecture and Advanced technology Studio of Enclos. http://www.facaderetrofit.org/ (accessed October 30, 2016).

Vossoughi, Hamid and Maleev, Vladimir. “Pushing the Limits with Glass Design – Challenges and Solutions.” 13th Canadian Conference on Building Science and Technology, Winnipeg, Canada, May 2011.

Wiss, Janney, Elstner Associates, Inc., http://www.facadeordinance.com/ (accessed October 30, 2016).

CONTEXTUAL ENVELOPES

Using modern methods to address heritage in urban sites



Zoltan Neville
Coldefy & Associés Architectes Urbanistes (CAAU)
zneville@caau.fr

ABSTRACT

Aesthetic and technical capabilities of façade design have become seemingly endless as building technologies progress. While the capacity to address complexity improves, the fundamental roles of the building envelope must not be overlooked. In urban environments, one of its essential roles is the ability to dialogue and connect with its surroundings. A building's skin is what is perceived from the outside, and thus communicates its presence to the surrounding context, the neighborhood and its inhabitants.

Contextual integration in architectural design, notably in a historical setting, may seem in contradiction with the advancement of contemporary technology and methods. However, it is possible to take advantage of new techniques to strengthen the connection between contemporary architecture and sensitive urban and social context. Three case-studies are used to demonstrate this phenomenon. Two examples are taken from historically charged, fine-grained neighborhoods in France, while the third is taken from a large-scaled, modern neighborhood in China. Their juxtaposition shows that a critical and innovative approach that embraces new techniques can help address contextual design challenges.

In conclusion, these three projects demonstrate the ability to foster historical connection using modern methods in three ways: physically, digitally, and symbolically. Therefore, by carefully considering physical, historical, and cultural conditions, modern technology in façade design can help contribute to the cohesion of built environments and the creation of community at a neighborhood and city scale, in continuously complex urban contexts.

KEYWORDS

curtainwall, masonry façade, innovative or unique, glass, metal, masonry, concrete, case study, fabrication prototypes, aesthetics, urban habitat and the building façade

INTRODUCTION

The advancement of design and building technology has given way to a new generation of architectural possibilities. Architects, engineers, and builders can now achieve results that were previously unthinkable in terms of formal complexity and performance capacity. Material research also pushes the boundary of what was historically a relatively limited palette for façade design, relying on locally sourced materials and natural strategies for thermal comfort (Alexander 1977).

However, the conversation regarding the advancement of façades can be considered introverted, concentrating on the envelope itself in terms of isolated parameters such as formal complexity and technical performance. In contrast, façade technology can be argued to be an equally crucial factor in considering urban issues. No matter how thick or thin the envelope may be, it remains the primary element of a building that communicates with its environment. It is the face of the project to the users and to the community.

Architects building in urban neighborhoods are constantly faced with the question of integration. This challenge is confronted more blatantly in certain contexts than others. Architects in western European cities with dense, historic, urban centers, are especially called upon to mediate between sensitive contextual issues and contemporary design agendas.

Although the theme of innovative technology is often isolated from urban design issues, these developments arguably provide new tools for designers and builders to solve these challenges. By integrating this parameter into the architectural design process, façade technology contributes to contemporary architecture's ability to dialogue with its environment.

The following three case studies display the possibility of assimilating material and technological innovation into the envelope design to connect the projects with their respective contexts, while remaining distinctive in terms of contemporary design. Two projects are in France, where design review of contextual integration is essential to the issuance of building permits, and one project is in China, where the recent construction boom has political leaders calling for a more coherent approach to city-making (Abkowitz 2014).

CASE STUDY 1: LAND'ART, LILLE-MOULINS, FRANCE

The project "Land'art," is in the Moulins neighborhood of Lille, a city in the north of France. The developer asked for the redevelopment of almost an entire city block to include a mix of housing types and parking. Characteristic of developer driven projects in the region, the budget was restrictive yet the objective in terms of product quality remained high. Furthermore, a contemporary architect was chosen for their style and approach. By adding a fashionable touch, the development would aim to attract new buyers and residents into a fatigued and historically working-class neighborhood.



Figure 1: (Left) The city center of Lille, surrounded by intricate brick and stone façades, indicating the patchwork of colors and repetitive rhythm. Photograph by author. (Right) Brick row houses in shades of red on Valenciennes Street in the Lille-Moulins neighborhood. Photograph by VVVCFFrance, distributed under a CC BY-SA 4.0 license.

The northern region of France is characterized historically by its brick and stone construction, both decorative and industrial. The neighborhood of Lille-Moulins was an industrial neighborhood, with small gritty streets, and simple brick-lined façades. It has recently been engaged in a gradual transformation and new developments due to its proximity to the historic city center and relatively low prices.

The architects faced the challenge of creating a contemporary feeling project in a homogenous, historic context, with little budget. The combination of developer housing requirements and urban-planning restrictions limited the possibility to implement any unconventional massing or form. Therefore, the design opportunity lay in the envelope. Using less than 40cm thickness, the project needed to simultaneously fit in with the gritty brick context, while communicating its identity as a fresh, new, contemporary place.

The solution lay in the innovative application of a typical material, concrete. Generally, local construction methods and building regulations call for a poured concrete wall structure, with rockwool insulation, and exterior waterproofing and cladding layers. Due to a restrictive budget, it was not feasible to use any type of brick or a similar quality cladding for the envelope.

Instead, the architect opted to insulate the building from the interior with thermal breaks between the façade and the floors, allowing the poured concrete structure to double as the façade finish. To connect with the surrounding neighborhood, several tints of concrete would be used, extracted from the tones of the surrounding brick context.



Figure 2: A study model of the project shows the massing: volumes in scale and rhythm with the surrounding row houses completing the perimeter of the block. Photograph courtesy of Coldefy & Associés Architectes Urbanistes (CAAU).

The intention was to leave a contemporary, clean and raw finish that lasts over time. Typical processes use a gray concrete to which a colored surface finish is added. However, this solution was inappropriate as the desired colors could not be attained and important color maintenance is required over time. After a series of tests, a specific formula was developed for each color, allowing the pigment of the concrete to be colored in its mass for three colors: “Chocolate,” “Light-gray,” and “Anthracite-gray.”

These three colors were abstracted from the variety of brickwork in the surrounding neighborhood, and applied in a vertical rhythm like the traditional houses of the neighborhood, creating variation the length of the street. This means that every five meters the walls would be poured a distinct color. Of 3,500 cubic meters of concrete used in the construction site, 1,700 were colored, and the assorted colors had to be poured simultaneously with careful attention paid to avoid variations in color, finish, and problems in the removal of formwork due to climatic conditions.



Figure 3: (Left) The exposed structure was poured directly in three colors. Photograph courtesy of Photothèque CEMEX. (Right) Insulated from the inside, the exposed colored concrete becomes the finished façade, a contemporary interpretation of the historic row houses of the neighborhood. Photograph by Julien Lanoo.

Finally, the architectural project was able to meet the objective of fitting into the specific neighborhood context of traditional brick row houses, while presenting a contemporary fresh look that contributes to the rejuvenation of the neighborhood and the attractiveness of the new housing development. The special attention paid to the envelope itself transformed the impact of the project from its individual development goals into an integrated project with an urban impact. Using technological applications available in a typical building material like concrete, the architect was able to adapt to a historical context in a contemporary way.

CASE STUDY 2: LUCIE AUBRAC SECONDARY SCHOOL, TOURCOING, FRANCE

Collège Lucie Aubrac is a secondary school in the city of Tourcoing, a historically industrial city in France near the border of Belgium. The project was launched as a public competition, the program calling for an innovative and sustainable building, representing the “educational facility of tomorrow.” In addition to its role as an educational institution, the public project was to be strategically located on a site that was expected to play an important role in the urban regeneration of a rough neighborhood.

Strict programmatic requirements and urban massing regulations left the architect with little room for derogation in terms of site planning and form. The historic neighborhood and planning requirements encouraged the use of brick as a main material, and the rough character of neighborhood required protection and security. Nevertheless, the architect was challenged to render the project an innovative and open addition to the new community.



Figure 4: (Left) The train station of Tourcoing, with brick façades and a large hardscaped forecourt. Photography by Velvet, distributed under a CC BY-SA 3.0 license. (Right) The city hall of Tourcoing shows off an intricate light stone façade, and a hardscaped plaza. Photography by Velvet, distributed under a CC BY-SA 3.0 license.

This challenge was addressed comprehensively in the architectural planning and technical approach, but the project’s visual identity - in terms of character in relation with the surrounding neighborhood and attractivity for future users - lay largely in the treatment of the envelope. The architect addressed this challenge through primary and secondary façade designs.

The technical program required the project to adhere to strict environmental standards in terms of thermal performance and cost effective construction and maintenance. The exterior wall would be composed with a poured concrete wall structure, insulated on the exterior by a 20 centimeter layer of rockwool to minimize thermal bridges, and covered with waterproofing and cladding layers.



Figure 5: (Left) Early massing model shows the project’s site planning, creating a protected interior courtyard. Photograph courtesy of CAAU. (Right) The main entry features the primary façades, with open-joint, light colored, brickwork and mashrabiya walls. Photograph by Julien Lanoo.

The primary façades were designed in brick in order to connect with the surrounding urban fabric. However, an open, fresh feeling was created by using a more contemporary color and *mise-en-oeuvre* of the material. In contrast with traditional red

or gray tone bricks, a cream color was chosen that creates a lighter atmosphere and relates to the stone color of some major civic architecture of the city center.

Taking advantage of the construction system which supports the brick cladding by directly attaching it back to the concrete structure, a geometric maninuplation was able to be applied, lifting the edge of the skin from the ground to lighten the feeling of the material and achieve a more modern aesthetic. Furthermore, the design allows for increased daylight within and visual continuity with the exterior, fullfilling the programmatic requirements and distinguishing the project from the typical heavy nature of the city's historic masonry buildings.

Additionally, instead of a traditional mortar system the bricks were layed *à joints vifs*. This method mimics historic mortar-less constructions typically used with natural stone. The mortar is recessed out of view, and the bricks are layed with a controlled variation in depth, avoiding vertically-flush alignment. The technique allows the brick cladding to achieve a vibrancy that evokes a more lively, open spirit as wished for the future nighborhood.

Finally, mashrabiya brick walls were created in certain areas around exterior spaces, piercing the typically heavy envelope and allowing light to filter through into the volumes. These applications provide a modern twist on a traditional method to create urban cohesion with the historic nieghborhood while evoking a contemporary identity.



Figure 6: The secondary façade, as seen from the protected courtyard, features a pattern of perforated metal rain screen above a colored waterproofing, integrating QR codes at different scales to be scanned from close or afar. Photograph by Julien Lanoo.

The secondary façade was designed to treat the challenge in a different but complementary way. The architect looked to digital technology for a different means to connect with the neighborhood. Although the spirit of the project was that of an open, connected environment, security concerns required the facility's public spaces to be completely enclosed. Therefore, the architects installed QR codes into the façade cladding. Integrated at different scales, these codes allow students, teachers, or community members to scan the façade with their mobile devices from close or afar, creating the opportunity for connection via the digital community, a way to strenghten the link between the neighborhood and the new institution.

The façade was created using a perforated metal cladding placed over a colored waterproof membrane. Two different colors were used for the membrane in order to underline the playful nature of the school, and contrast with the more sober brick façades. The perforated pattern was based on the codes' geometric language, allowing the scannable areas to blend almost seamlessly into the composition.

Using the envelope, the architects were able to link the project with the urban community in two ways, physically and digitally. The envelope in brick connects the project to the heritage of the area. The contemporary twist on its installation creates a feeling of openness and innovation, that the institution wanted to portray. This feeling is enhanced with the secondary façades, which are not only aesthetically more contemporary but create a digital link to the surrounding community.

The treatment reaches beyond the stylistic and performance criteria of the envelope, achieving a tangible effect on the urban community and contextualizing the project in the past and future of the neighborhood.

CASE STUDY 3: BAO'AN PUBLIC ART CENTER, SHENZHEN, CHINA

The third and final case study selected is a project in a different context in order to demonstrate the capacity of urban contextualization in a more abstract way. The Bao'an public art center is part of a new district in one of the youngest modern cities in the world, Shenzhen. The program called for a cultural center composed of three exhibition-oriented programs in one building.



Figure 7: (Left) Photograph showing the landscape of new construction in the Nanshan district of Shenzhen. Photograph by Wishva de Silva, distributed under a CC BY-SA 4.0 license..

(Right) A main street in the Bao'an District of Shenzhen, showing the high-rise residential construction. Photograph by author.

The development is a part of a larger national effort to create major cultural facilities in the different districts of the city, emphasizing their iconic and public nature. The context of the neighborhood, in contrast to the two preceding examples, is that of glassy commercial centers and high rise housing; a mix-match of modern constructions without a common thread. The challenge for the architects is thus inversed from the previous case studies. How to create an iconic building that represents sophisticated history and culture within a noisy, heterogenous urban fabric?

While the development is intended to create a sense of place, culture, and community, those elements are lacking visibly from the surroundings and make it difficult for the architect to take a stance as an iconic yet inviting building in a meaningful way. In this case, the architect chose to look beyond the physical community immediately surrounding the project, and rather towards a global community, using cultural symbolism to communicate its purpose.

Since Greek civilization, marble has stood as a timeless symbol and representation of culture and refined tastes. The architects thus turned to this imagery to help connect the project with a larger context and its representation. However, due to the local humid climate and large building size – over 90 meters tall – a stone façade was technically difficult to achieve.

In this case, the architects opted for a glass curtain wall façade that was more appropriate for the building typology, and more comfortable for local technical and construction teams. However, by using newly developed large-scale high definition printing techniques, a marble pattern could be achieved to deliver the desired affect.



Figure 8: (Left) Marble was used in early western artworks such as "The creation of man by Prometheus," now featured in the Louvre Museum in Paris. (Right) The white geometric cuts of Naxos marble mining, Greece. Photograph by Heiko Gorski, distributed under a GNU free documentation license.

Furthermore, this method allows for additional control over the finished aspect. The color and pattern of the stone and the grain can be fully controlled by the designers with little impact on the budget. Light transmission, too, can be controlled, allowing different parts of the façade to take on either opaque or translucent nature.

Traditional stone panels, constrained by the weight of the cladding and limited panel size, would be difficult to recognize on a volume of this scale. The sublety of the grain gets lost from afar, becoming a light colored mosaic. By using glass, the size and pattern of the grain can be controlled specifically for the scale of the building, printing a custom designed texture across multiple panels, allowing the façade to be read from a greater distance.



Figure 9: Images of printed-glass samples from early in the project development process show the different stone textures and opacities. Photographs courtesy of CAAU.

Although this example does not connect the building directly to its urban surroundings as it would in a historic environment, the envelope was the means through which the architect could create a sense of place and community through cultural iconography. In this contemporary context, the advancements in technology allowed for a hybridization of traditional and contemporary elements, allowing the building to relate to historical ideas and elements.



Figure 10: Renderings of the project in context show the volume wrapped in a subtle white marble textured façade, scaled to be visible at a distance. Images courtesy of CAAU.

CONCLUSION

These three examples of architectural projects display an approach to façade design that goes beyond isolated aesthetic or technical intentions. The envelope is treated as a connecting piece to the neighborhood, and allows the project to have an impact outside of itself.

Each of the projects treats this differently: physically through the color or texture of concrete and brick, as in Land'art; digitally, through the integration of numeric tools to link users to a social or information network, as in the Lucie Aubrac Secondary School; and culturally, through the reference of historic symbols that would otherwise be lost in the given context, as in the Bao'an Public Art Center.

The approach integrates a wholesome reflection in the envelope design, embracing modern evolutions in technical capacity to achieve works that links to their context. Thus, at this point in the advancement of building technology, it remains important for architects and designers to look beyond the ability of the technology itself, but continue to use it as a tool to develop design solutions that contribute to the built environment in a cohesive and thoughtful way.

REFERENCES

Abkowitz, Alyssa. “Xi Jinping Isn’t a Fan of Weird Architecture in China.” https://blogs.wsj.com/chinarealtime/2014/10/17/xi-jinping-isnt-a-fan-of-weird-architecture-in-china/ (accessed December 15, 2017).

Acha, Carlos, Julio Comendador, Antonio Garcia, Begona Guirao, and Maria Eugenia Lopez. “New QR Survey Methodologies to Analyze User Perception of Service Quality in Public Transport: The Experience of Madrid.” Journal of Public Transportation Vol. 18, No. 3 (2015): 71-88. http://scholarcommons.usf.edu/jpt/vol18/iss3/5/ (accessed October 06, 2017).

Alexander, Christopher. A pattern language: towns, buildings, construction. Oxford University press, 1977.

Collective. Lille métropole: Un siècle d'architecture et d'urbanisme, 1890-1993. Le Moniteur Editions, 1993.

Carré, Dominique. Ville3000: Imaginer de nouveaux quartiers à vivre à Lille. Collectif Olivia Barbet-Massin Dominique Carré, 2010.

Da Silva, Wishva. “One Shenzhen Bay and China Resources Headquarters.” Photograph. 2016. https://commons.wikimedia.org/wiki/File:One_Shenzhen_Bay_and_China_Resources_Headquarters.jpg (accessed October 06, 2017).

Fonseca, David, and Janina Puig. “QR-Codes Applied to Architecture Data and Teaching.” The 7th International Conference on Social and Organizational Informatics and Cybernetics: SOIC 2011. http://www.iiis.org/CDs2011/CD2011SCI/SOIC_2011/PapersPdf/WA768TC.pdf (accessed December 15, 2017).

France. Ministère chargé de l’urbanisme. Récépissé de dépôt d’une demande de permis de construire une maison individuelle et/ou ses annexes - Cerfa n°13406*06. https://www.service-public.fr/particuliers/vosdroits/F1986 (accessed December 15, 2017)

France. Ministère de la transition écologique et solidaire, Ministère de la cohésion des territoires. “Présentation.” Les économies d'énergie dans le bâtiment. http://www.rt-batiment.fr/batiments-neufs/reglementation-thermique-2012/presentation.html (accessed December 15, 2017).

Gorski, Heiko. “Naxos Marble.” Photograph. 2003. https://commons.wikimedia.org/wiki/File:Naxos_Marble.JPG (accessed October 06, 2017).

Hospodarova, Viola, Jozef Junak, and Nadezda Stevulova. “Color Pigments in Concrete and their Properties.” Pollack Periodica Vol. 10, No. 3 (2015): 143-151. https://www.researchgate.net/publication/283276683_Color_pigments_in_concrete_and_their_properties (accessed October 06, 2017).

Lee, Christopher C. Common Frameworks - Rethinking the Developmental City in China. Harvard University Press, 2016.

Moussavi, Farshid. The Function of Style. Actar D, 2016.

Unknown artist. “The creation of man by Prometheus.” Italy, 3rd Century CE. Marble relief. Paris, Louvre Museum. https://commons.wikimedia.org/wiki/File:Creation_Prometheus_Louvre_Ma445.jpg (accessed October 06, 2017).

Van Domelen, Sarah K. “The Choice is Yours: Considerations & Methods for the Evaluation & Selection of Substitute Materials for Historic Preservation.” M.S. Thesis, University of Pennsylvania, 2009. http://repository.upenn.edu/hp_theses/119 (accessed December 15, 2017)

Velvet. “Tourcoing gare.” Photograph. 2011. https://commons.wikimedia.org/wiki/File:Tourcoing_gare.jpg (accessed October 06, 2017).

Velvet. “Tourcoing hotel ville 3-4.” Photograph. 2011. https://commons.wikimedia.org/wiki/File:Tourcoing_hotel_ville_3-4.JPG (accessed October 06, 2017).

VVVCFFrance. “Rue de Valenciennes 73 85.” Photograph. 2017. https://commons.wikimedia.org/wiki/File:Rue_de_Valenciennes_73_85.jpg (accessed October 06, 2017).

HISTORICAL EVOLUTION OF RESPONSIVE FACADES

Factors affecting the design and development



Negar Heidari Matin, Ph.D. Candidate, LEED GA
Eastern Michigan University
nheidari@emich.edu



Ali Eydgahi, Ph.D.
Eastern Michigan University
aeydgahi@emich.edu



Shimming Shyu, Ph.D., RA, LEED AP BD+C
Eastern Michigan University
sshyu@emich.edu



Payam H. Matin, Ph.D.
University of Maryland Eastern Shore
phmatin@umes.edu

ABSTRACT

Responsive façade system is considered a major component of high-performance building envelope that is capable of responding to environmental stimuli and aims to improve occupants' comforts and lower energy consumption. While building design-related articles have frequently addressed the technical and design aspects of responsive facades, very limited historical studies have been conducted to shed light on the evolution of such systems. The paper is the result of a comprehensive study placing emphasis on exploring historical factors that initiated and affected the development of responsive facades. The objective is to examine and classify the factors explored in a chronological manner and present a graphical timeline to address the evolution of design and development. A comprehensive literature review has been conducted on evolution of design and development of responsive facades in historical contexts to explore the influential factors. It turns out that the influential factors can be classified into a set of sociocultural, technological, political/economic, and environmental factors originating from revolutionary changes in art, technology and building construction since late 19th century. The factors are presented in chronological manner. A graphical timeline that explains the evolution of design and development is also presented. The historical timeline developed is intended to serve as a helpful resource for researchers and educators in their research and teaching activities. The timeline formulated can be utilized to track the pattern of current developments and predict what might be expected in the future. While the focus of the paper is on individual architecture scale, the trend of the recent developments presented in the timeline suggests that responsive facades will be possibly implemented for urban-scaled development of smart neighborhoods or cities in the future.

KEYWORDS

facade, responsive active facade, historical evolution of facades, future smart cities

INTRODUCTION

A façade system is one of the most significant contributors to the energy consumption and the occupants' comfort of buildings (Aksamija 2016), due to the fact that 20 to 60 % of annual energy consumption of a building is attributed to the design and construction of façade system (International Energy Agency 2013). A traditional façade, as a static system, is not capable of adjusting its own performance over time in response to climatic conditions. Such static facades feature design variables such as window-to-wall ratio, glazing type, shading shape, and insulation with limited reactions to various dynamic climatic conditions (Shan 2016). To overcome the limitations of traditional façade systems, various types of high-performance façade systems have been proposed. During past decades, responsive façade systems have attracted increasing attentions in both construction industry and academia as high-performance façade systems, which utilize active strategies for achieving higher level of sustainability (Basarir, and Altun, 2017). The recent studies on the existing responsive façades indicated the influential role of such systems in lowing carbon emission and increasing saving in energy consumption. Under such systems, a reduction of 20% in carbon emission and a saving of 50% in energy consumption can be achieved (Karanouh, and Kerber, 2015). This paper conducts a comprehensive literature review of several journal articles, conference papers, theses, and dissertations available on the area of responsive facades. The previous studies have covered many aspects of responsive facades. For instance, some authors have focused more on energy performance and design aspects of responsive facades. Others have investigated such systems from geometrical, material, structural, and technological point of view. Some authors have studied social and historical aspects of responsive facades. While the majority of the previous studies have covered technical and design aspects of responsive facades, very limited historical studies have been conducted.

The objective of this paper is to conduct a historical study that explores historical factors that originated and influenced responsive facades in different time periods. The factors to be explored are presented in chronological manner. A graphical timeline associated with the chronological discussion is created to depict the historical sequence of the factors affecting the design and development of responsive facades. The factors are classified into different categories and presented pictorially in a diagram. It will be attempted that the current trend of advancements depicted in the timeline is used to predict what advancements may to come with respect to responsive facades in the future.

INITIATION AND EVOLUTION OF CONCEPT OF MOTION IN ARCHITECTURE

The concept of motion in art first appeared in artistic movements during the 19th century when impressionist painters portrayed the motions existed in nature including those of human bodies in realistic scenes of life (Jenkins, and Quick, 1989). During the revolutionary advancement in technology and associated industrial booming, the artistic concept of motion was further evolved by modernism when the concept was affected by the industrial life in modern cities emerging in the beginning of the 20th century. As motion became an integral part of machines during the industrial revolution, art was affected by the technology. Futurism, as a social and artistic movement in art and architecture, preliminarily envisioned and portrayed machines by their specific features such as motion, speed, time, and the associated technologies in the artistic works from 1910 to 1930 (Perrone, and Buchler, 2005). During this era, since machines were viewed as tools of perfection with specific features, an architecture tended to be considered, viewed and designed as a machine (Corbusier 1923). Such consideration led to the idea of "house-machine" and "city-machine" concepts that would supposedly improve both the efficiencies of buildings and comfortability of occupants (Corbusier 1923; Perrone, and Buchler, 2005).

Affected by socialism philosophy, the constructivism movement branched out from Russian futurism to serve communism in art and architectural domains (Chen, Lin, and Fan, 2015). To this end, a Constructivism artist, Yakov Chernikhov, pioneered the first perspectives of moving architectures and their kinetic components in 2-dimensional context in 1933 (Khmelnitsky 2013). The concept of motion was further integrated in artistic works in 3-dimensional forms as kinetic sculptures that featured motions were first made. The kinetic movement was originated from dada art and affected by Russian constructivism philosophy in 1955. The kinetic movement rejected the aestheticism of modern capitalistic societies to promote its political dependence on communism. In this movement, the beauty of art was redefined in mechanical motions featured in the sculptures. The motions featured in the sculptures were generated by a mechanism that was driven by either mechanical or electromechanical actuators, or stimuli of natural resources such as water, wind, or gravity (Chen, Lin, and Fan, 2015).

Envisioning the future, being fascinated about motions in the context of technological advancements or scientific achievements was not limited to artistic movements but it was also reflected in literature or even media where the futuristic

utopian cities and lifestyles were predictively described. For instance, in 1962, the idea of a “responsive house-machine” was introduced by a British novelist, James Graham, who described a “psychotropic house” as a live, mood-sensitive, and shape-adapting house, which responded to its occupants’ preferences and requirements (Kolarevic, and Parlac, 2015). That was a turning point where the motions featured in architectures were implemented for functional purpose rather than artistic one. Furthermore, the science fiction television series and films such as The Jetsons, Barbarella, and 2001 A Space Odyssey predicted futuristic cities inspired by moving machines and advanced technologies in late 1960s and early 1970s (Veliko, and Thun, 2013; Kolarevic, and Parlac, 2015; Caplescu 2015).

CYBERNETICS IN RESPONSIVE ARCHITECTURES

Paralleled by the cold-war politics and military practices, new disciplines emerged such as cybernetics, information theory, and general system theory in the 1940s. In 1947, machines were interpreted anthropologically as extensions of human intelligent systems. This biological interpretation of machines and technologies established a new science of cybernetics in 1948. Subsequently, the science of automatics control systems and communications were implemented in mechanisms. Basic principles of cybernetic theory were formulated by synthesizing information theory, communication theory, and theory of machine control during various Macy conferences held between 1942 and 1965 (Yiannoudes 2016).

Cybernetic theory of design was proposed by Gorden Pask to apply the concept of cybernetics to architecture in an article titled “The Architectural Relevance of Cybernetics.” Considering a building as a machine, the cybernetic theory of design was originated from functionalism and mutualism theories of architecture. Based on this theory, architecture and its components have reciprocal interactions with building occupants to manage, control, and adapt the performance of the building based on occupants’ preferences and needs. So, buildings are required to be designed as dynamic entities rather than static ones (Pask 1969; Yiannoudes 2016).

The term responsive architecture was first introduced by Nicholas Negroponte during the late 1960s (Kolarevic, and Parlac, 2015). The concept of responsive architecture was formed based on the theory of interaction, the theory of conversation, and the adaptive-conditional theory, which defined a building as a self-adjusted system operated by the feedback from both the occupants and the environment (Matin, Eydgahi, and Shyu, 2017). Responsive architectures featured the use of dynamic entities in components of the architecture such as the building envelopes offering wide interactions between humans and the environment.

The first architectural group that employed cybernetic concepts such as indeterminacy, information feedback, self-regulation, and adaptation in their hypothetical designs was Archigram. This group formed as a neo-futuristic, anti-heroic and pro-consumerist firm in London 1960 (Sadler 2005). Archigram published British architect Ron Herron hypothetical “Walking City” project in 1964. The walking city idea was imagined as a massive, transformable and mobile structure with its own intelligence that could interconnect with other walking cities to form “walking metropolises” (Khmelnitsky 2016). In 1969, Reyner Banham implemented the cybernetic feedback mechanisms in several conceptual design projects to dynamically engage buildings with environmental changes. Banham’s responsive projects such as “Transportable Standard-of-living Package”, “Environmental Bubble” “Anatomy of Dwelling” were published in a book titled “A Home is not a House” (Yiannoudes 2016).

As another representation of responsive architecture, the “Fun Palace” was designed by Cedric Price in the early 1960s using the emerging fields of information technology and cybernetics as the socio-political changes in the post second-world-war Britain promoted public optimism and enthusiasm (Kolarevic, and Parlac, 2015; Veliko, and Thun, 2013). With implementation of sensors, actuators, transducers, and processor technologies, the cybernetic system in the “Fun Palace” were capable of collecting and analyzing information about preferences and activities of individuals. The data collected were processed to determine how the architecture were transformed. The “Fun Palace” was capable of learning behavioral patterns to plan future activities (Yiannoudes 2016).

In 1969, during the post war socio-economic environment, the emerging communication and information technologies were utilized to design a floating mega-structure city called “Electronic Urbanism” (Baraona, Karanastasi, and Skoutelis, 2013). This system embedded communications technologies that allowed wide-ranging connections such as tele-work, tele-management, tele-medicine, and tele- education between people and social groups (Yiannoudes 2016). Such idea may initiate the emerging concepts of smart cities.

ENVIRONMENTAL AND POLITICAL EVENTS AFFECTING ARCHITECTURES

Following the technological advancements, the environmental movement and energy crisis during the 1960s and 1970s along with concerns for availability of natural resources increased the cost of fossil fuel energy and created a growing public awareness about crucial environmental issues such as ecological balance, green culture, and sustainable strategic planning (Veliko, and Thun, 2013). In 1960, the worldwide levels of carbon dioxide climbed. The environmental movement was initiated by Silent Spring in 1963. The book claimed how technological advancements could disrupt the natural systems (Griswold 2012).

The environmental movement triggered the passage of the Clean Air Act in 1963, and the Water Quality and Motor Vehicle Air Pollution Control Acts in 1965. Also, the OPEC oil export embargo affected by ongoing Israel and Arab conflict, the Islamic revolution of Iran and the Iran hostage crisis caused energy crises in the 1970s and the early 1980s. In 1989, the environmental movement, energy crisis, and its subsequent consequences caused the American Institute of Architects (AIA) to form a Committee on energy and environment to focus and promote passive and active technological approaches on the design of buildings' components such as active responsive building envelopes (United States Environmental Protection Agency 2016). In 1990, the Building Research Establishment Environmental Assessment Method (BREEAM) was launched by the Building Research Establishment in the United Kingdom as the first method to assess, rate and certify sustainability of buildings (Veliko, and Thun, 2013). After eight years, in 1998, the United States Green Building Council (USGBC) developed a US rating system called Leadership in Energy and Environmental Design (LEED) for the design, construction, and operation of high-performance green buildings. The LEED certifications specifies the standards related to the design and construction of the high-performance building envelopes (including responsive facade systems) which affects indoor environmental quality in a stand-alone chapter.

TECHNOLOGY IMPLEMENTATION IN RESPONSIVE ARCHITECTURES

Technologies of sensing, actuating, and switching control in buildings first published by Popular Science Magazine with the application in remote control of garage door opener in 1931(Veliko, and Thun, 2013). Control of building mechanisms such as responsive facades was advanced due to the availability of electrical components and control systems in the 1960s (Ahmed, Abdel-Rahman, Bady, Mahrous, and Suzuki, 2016). The Kaufmann's hand-operated facade was the basis for the development of motorized mechanism blinds that were used in the Los Angeles County Hall of Records in 1962. The facade mechanism was equipped to a switch control technique to adjust pivotal actuators based on a preset algorithm (Matin, Eydgahi, and Shyu, 2017). Furthermore, advances in computer engineering introduced a new possibility in central controlling of facade systems. The advancement of computer engineering provided the access to many digital systems such as mainframe computers, primitive microprocessors, desktop microcomputer, home computer and personal computer since 1960s to early 1980s (Veliko, and Thun, 2013). In 1967, Buckminster Fuller designed a futuristic responsive façade for the united State Pavilion at Montreal Expo 67. The technology used in this responsive facade was a soft self-regulated shading system with structural cables, which operated using a roller blind mechanism (Khoo 2013).

Different responsive facade systems were designed since 1989 to 2011. These systems are different in geometry, mechanism, sensing technology (featuring different sensors such as light, temperature, and touch sensors) and actuating technology (featuring different actuators such as motor-based, pneumatic, and hydraulic actuators). Although, in the earlier design of responsive facades, switches were used for control purposes, they were replaced by the central computerized system in newer more advanced design. The central control system is still the most reliable technology implemented in the design of responsive facade systems. The central control system was utilized in the responsive facades of some well-known buildings including Council House 2 Building in 2006, Showroom Kiefer Technic in 2007, Q1 Headquarters Building in 2010, Al-Bahar Towers 2012 and One Ocean Pavilion in 2012 (Matin, Eydgahi, and Shyu, 2017). In 2007, optimization techniques were implemented to improve occupants' comfort extending capabilities of responsive facade systems in the Showroom Kiefer Technic designed by Ernst Giselbrecht (Khoo 2013).

Various groups, labs and institutions have been established to advance design and construction of responsive facades. These groups included MIT Architecture Machine group established in 1968, MIT Media Lab established in 1980, Intelligent Building Institute established in 1986, Hoberman Associate founded in 1990 And MIT Adaptive Building Initiative (AIP) established in 2008 (Veliko, and Thun, 2013). The mission of MIT AIP is to create the products, systems, and tools that achieve new levels of sustainable performance. AIP customized design, engineering and analysis, prototyping, sourcing, control system integration, manufacturing and installation oversight in several individual projects (Hoberman Transformable Design 2017). Tessellate in 2008, Strata in 2009, and Adaptive Fritting 2009 were the projects that have been managed by

Hoberman association and their partners. In these projects, the facade systems equipped with motor-based actuators are controlled centrally using electro-mechanical technologies (Matin, Eydgahi, and Shyu, 2017). Information technology has changed the way control systems are implemented (Decker, and Zarzycki, 2013). The idea of a distributed control system is implemented in responsive facades to control the interconnected panels by microcontrollers in 2011 (Grobman, and Yekutiel, 2013). The local sensors collected data and provided them to microcontrollers that processed the data and subsequently triggered actuators for the intended functions (Yekutiel, and Grobman, 2014).

Through 2010s, advanced materials such as shape memory alloys, shape memory polymers, electro-active polymers, and phase-changing materials were applied in design of responsive facade systems in very small scale (Sharaidin 2014). These smart materials were invented between 1940s to1980s and used as actuators, sensors or control systems in the structure of responsive systems (Decker, and Zarzycki, 2013). Mechanical and electro-mechanical actuations could be replaced by material-based actuations in years to come (Kolarevic, and Parlac, 2015).

INTEGRATION OF SOCIO-CULTURAL CONCEPTS IN RESPONSIVE ARCHITECTURES

In order to address the problem of uniformity existed in modernist style, post-modern architecture proposed incorporating historical and cultural references in façade design from the 1980s to the 1990s. While modernist slogans such as “ornament is crime” and “a house is a machine for living” led to dominance of technological culture in architectural design, post-modernism accepted technology when integrated in conjunction with socio-cultural values, local or regional identities. Historical motifs manifested in building ornaments represented national cultures (Loos 1908). In the post-modern era, advanced technologies are integrated along with socio-cultural values while complying with environmental principles in design of responsive facade systems (Sandi 2014). So, responsive facade systems could feature aesthetic desires, socio-cultural values as well as technical functionalities simultaneously. The implementation of the historical motifs as socio-cultural values in facade design can be considered as a convergence of technology and culture (Mossavi 2006).

In Middle Eastern culture, geometric pattern design is one of the most prominent visual arts widely used for decoration and ornamentation purposes in regional architecture (Broug 2013). Depiction of anthropomorphic forms and their incorporation in architecture are prohibited based on religious beliefs. So, the art of Islamic ornamentation has been developed mainly in the form of geometric pattern generation. As a result, a praised, elegant, and complex set of geometric patterns has been introduced and developed (Abas, and Salman, 1992). In 1989, such geometric patterns were integrated in the design of the responsive facade installed in the Arab Institute building in Paris manifesting Middle Eastern cultural symbols in the western world. This façade was geometrically designed and built in a form of a traditional Middle Eastern sunscreen called mashrabiyas, which was equipped with photo-sensing technology to control the natural light. In 2012, a similar approach was adopted in the design of the Al-Bahar Towers’ responsive facade systems in which five-folded geometric patterns were implemented as underlying geometry (Wilkinson 2012; Broug 2013).

TIMELINE REPRESENTING HISTORICAL EVOLUTION OF RESPONSIVE SYSTEMS

Based on the discussions presented in the previous sections, Figure 1 has been prepared as a timeline that depicts the historical evolution of responsive facades. In this timeline, the vertical line shows the continuity of the events as they proceed with respect to time. The circles are indicative of milestones associated with the events discussed. The horizontal lines in each row are originated from the milestones and pointed toward the descriptions of the events outlined in the timeline. It has been attempted that the events to be linked to the relevant illustrations brought in the timeline.

CLASSIFICATION OF INFLUENTIAL FACTORS

Based on the discussion presented in the previous sections, the influential factors affecting the development of responsive facades have been summarized pictorially in Figure 2. The influential factors are categorized into four different group factors presented as follows:

- Socio-cultural factors were defined based on different artistic and social movements established during the 20th century. These artistic and social movements such as impressionism, futurism, constructivism, Dadaism, modernism and post-modernism affected social sciences, philosophical viewpoints of artists, aesthetic definitions of art, and the value of socio-cultural motifs. These factors affected the motion, form and geometry of responsive facade systems.
- Ecopolitical factors were defined based on various political and economic events such as wars, revolutions, sanctions, and energy crises, which encouraged designers to implement sustainable strategies in design, material selection and structural systems. These factors affected the energy efficiency and optimization strategies in responsive facade designs.
- Environmental factors were defined based on different environmental regulation and acts that became mandatory subsequent to the environmental disasters of the 20th century. The disasters raised awareness about crucial environmental issues such as ecological balances, public green culture and sustainable strategies planning.
- Technological factors were defined based on the advancements in science and technologies such as cybernetics, information technology, control systems, materials science, world-wide web, smartphones, the internet of things and so on.

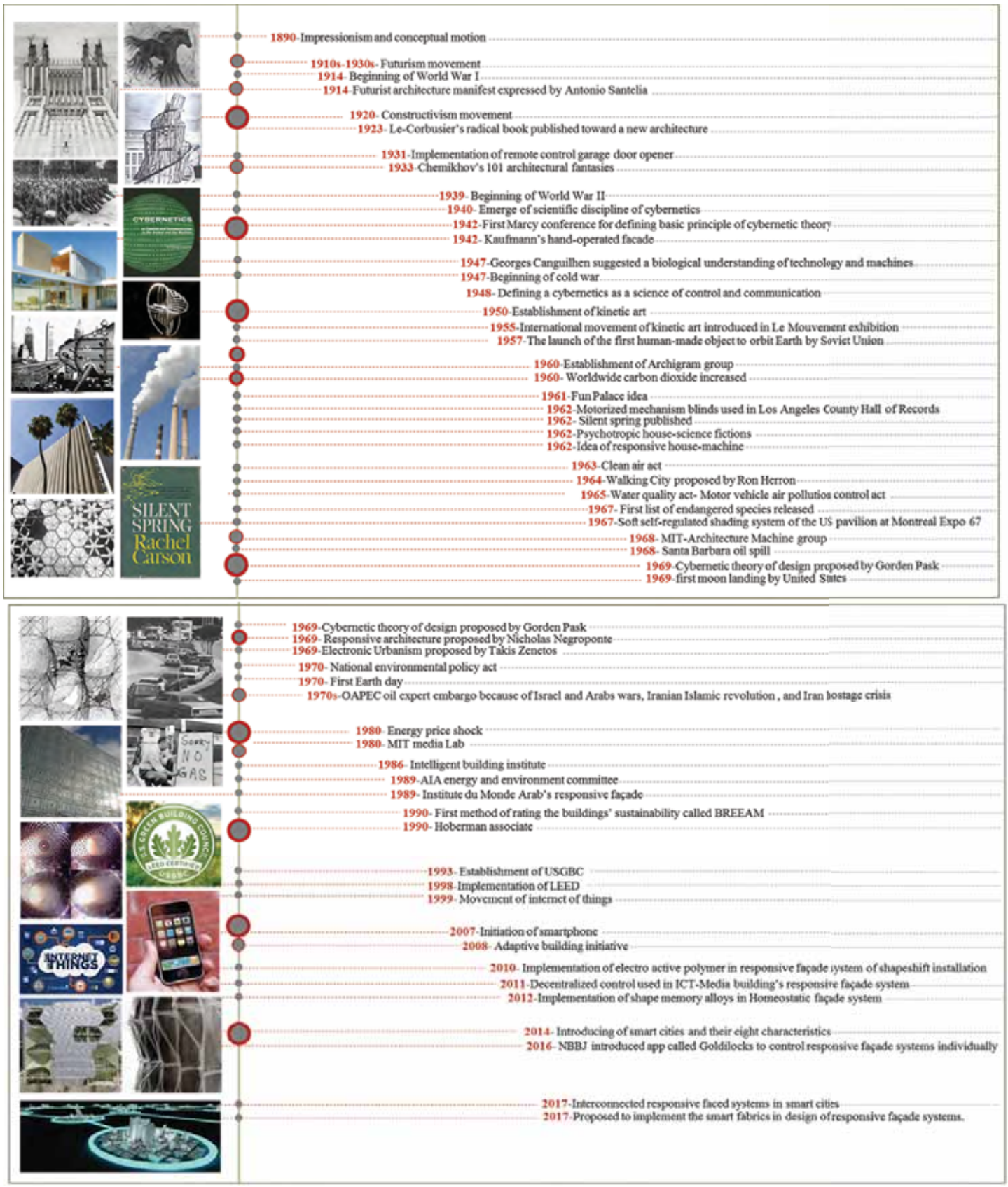


Figure 1: Timeline representing historical evolution of responsive facade systems.

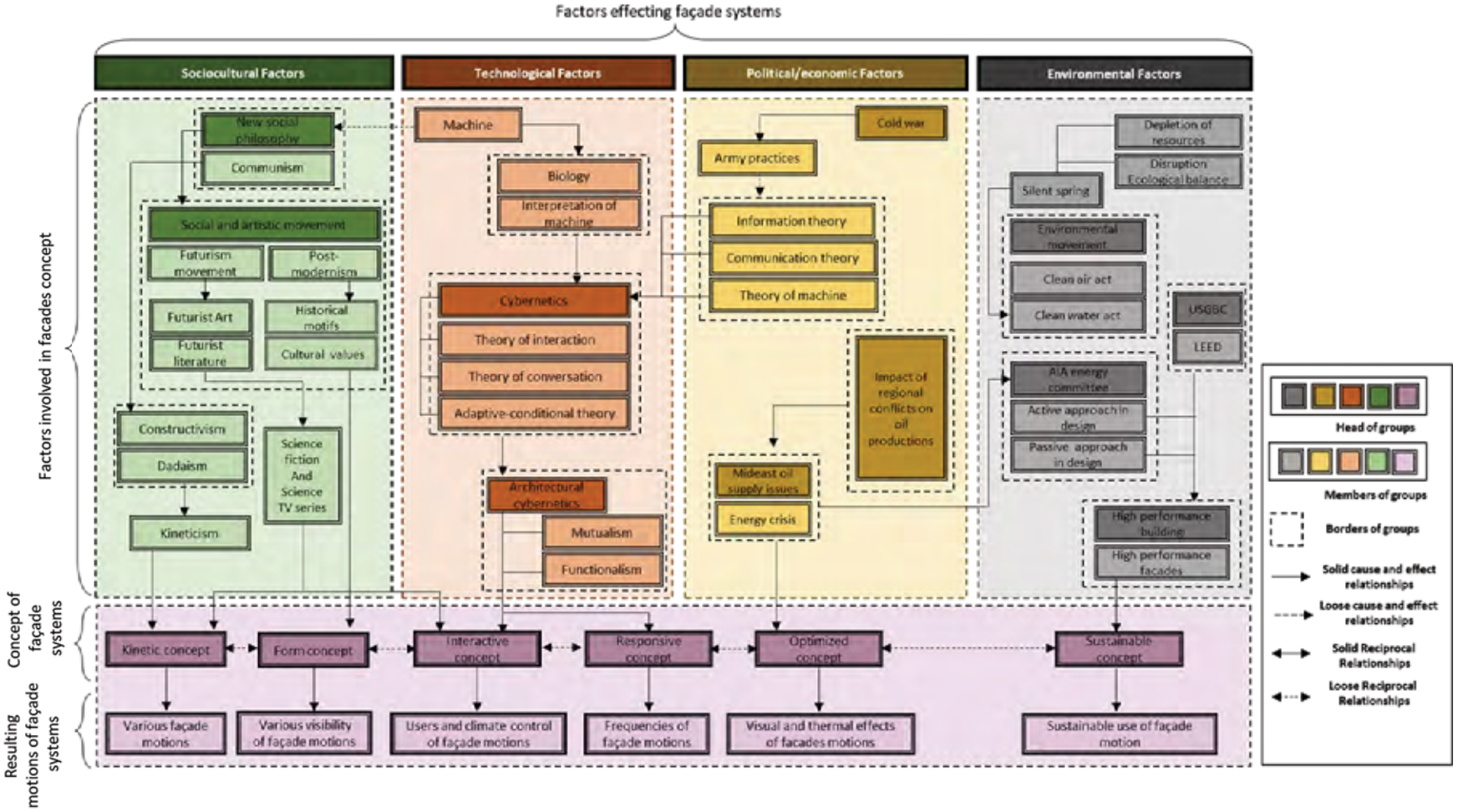


Figure 2: Influential factors affecting the development of responsive facade systems.

These advancements affected motions, controls, interactions, and selections of materials and structures in responsive facade designs.

FUTURE ADVANCEMENT IN RESPONSIVE FAÇADE SYSTEMS

The current trend of advancements depicted in the timeline presented in Figure 1 is used to predict what advancements may to come with respect to responsive facades in future. Some of these potential advancements are discussed in the following sections.

INTERNET OF THINGS IN RESPONSIVE FACADE SYSTEMS

The recent advancement in new internet technologies featuring cloud-based services, the internet of things (IoT), real-world user/machine interactions, smart phones and smart-meters, and sensors networks provide opportunities for responsive facade systems to be potentially integrated as elements of smart cities. Networks of sensors embedded in facade systems collect real-time data related to temperature, humidity, light, wind, and behavioral patterns of occupants. Collected data are stored in a cloud that provides information to control systems. These control systems communicate with façade actuators for optimized performance to improve efficiencies.

The movement of internet of things (IoT) was initiated in 1999 and developed the sensor and control industries globally (Konis, and Selkowit, 2017). Networks of sensors embedded in responsive facade systems could be linked by software-based connectivity to enable the system to not only collect climate data but also exchange data among other building systems called agents. These agents could be located at different zones of a building or at different buildings of a neighborhood. Technology of internet of things (IoT) is based on four critical elements, which are created initially by the smart phone industry. These elements include low-cost distributed sensors with embedded computing, wireless communications, cloud-based data storage, and shared inter-operable protocols (Konis, and Selkowit, 2017). These elements can be incorporated in responsive facades.

SMARTPHONES-BASED CONTROLLABLE RESPONSIVE FACADE SYSTEMS

Since 2007, the introduction of smartphones and wide usage of smartphone apps have provided a possibility of smartphone-based controllable responsive facade systems. The capability of decentralized systems and local sensors allow individual facade panels to be controlled by smartphone apps. In 2016, the NBBJ architectural company developed an app called Goldilocks that employed real-time data to provide occupants with the option of setting a desired interior environment. The desired interior environment is achieved by a control system working in conjunction with a sensors network gathering different data on acoustical conditions, temperature, day light, and users' activities within the interior environments (Stoughton 2017).

INTERCONNECTED RESPONSIVE FACADE SYSTEMS

Integration of information technology, communication technology, and internet of things (IoT) introduced the concept of a smart city, which was promoted as future urban development in the late 2000s. According to International Data Corporation (IDC), a smart building is considered as a key aspect of smart cities that would utilize advanced automation to measure, monitor, control, and optimize operation and maintenance. As an element of a smart building, a responsive facade is a self-adjusted system operated by real-time data from the environment and feedback from occupants. Responsive facades are potentially capable of controlling, managing and adjusting the light level, glare discomfort, light energy efficiency, thermal resistance value, solar heat gain co-efficiency, heat energy efficiency, response to solar patterns, occupant comfort level, and passive ventilation (Matin, Eydgahi, and Shyu, 2017).

In smart cities, the concept of control in responsive facade systems could be replaced from the individual control by users to global control by a master. Distributed control systems can promote the concept of interconnected facade systems, which link various building facades in smart cities. In this concept, independent microcontrollers embedded in individual facade panels are connected to each other to exchange local real-time data. At a higher level, a set of individual panels of a building is connected to various facade systems in a smart neighborhood or a smart city to transfer information globally. A master is designed to control these interconnected facade systems in a smart city. At local level, microcontrollers are embedded in the facade panels or groups of panels working in conjunction with local sensors that are triggered by internal or external stimuli. So, actuations occur based on the program logic of the local agents. Motion starts in the panels, which can affect the adjacent panels and create a chain of motions in a building facade. At the global level, each building with its set of

microcontrollers in a neighborhood is considered a slave that is registered to a master microcontroller. The master measures, monitors, and analyzes real-time environmental data along with users' feedback to control and optimize facade automations. Synchronization among interconnected facade systems in a smart neighborhood or a smart city can provide smart shading for pedestrians, adjust natural light intensity and reflection in urban spaces, control natural ventilation in urban paths and pedestrians, decrease annual energy consumed for urban services purposes, prevent environmental noises, and represent aesthetic desires and socio-cultural values. Thus, interconnected facade systems can improve the quality of life for citizens in future.

CONCLUSION

Historical evidence shows how the design and development of responsive facades have been affected from sociocultural, technological, political/economic, and environmental factors. In response, to the lack of comparative chronological analysis of responsive facade systems, a historical study was presented graphically. The influential factors involved in design and development of responsive facades were identified and discussed. In addition, a new idea of interconnected responsive facades in smart neighborhood or smart city was proposed. The advantages of implementation of such innovative system were described.

REFERENCES

Abas & Salman.1992a. "Geometric and Group-Theoretic Methods for Computer Graphic studies of Islamic Symmetric Patterns". Computer Graphic Form, 11(1), 43-53.

Ahmed, Mostafa, Abdel-Rahman, Ali, Bady, Mohmoud, Mahrous, Essam & Suzuki, Mahrous. 2016. "Optimum energy consumption by using kinetic shading system for residential buildings in hot arid areas". International Journal of Smart Grid and Clean Energy, 5.

Baraona, Ethel, Karanastasi, Elina, & Skoutelis, Nikos. 2013. "Takis Zenetos: Unbuilt Tropes". http://www.mascontext.com/issues/18-improbable-summer-13/takis-zenetos-unbuilt-tropes/

Broug, Eric. 2013a. "Islamic geometric design. New York: Thames & Hudson Ltd.

Caplescu, Onna Andreea. 2015. "Architecture in Science Fiction Movies". Romania.

Chen, Guang-Dah, & Lin, Chih-Wei, & Fan, His-Wen. 2015a." The History and Evolution of Kinetic Art." International Journal of Social Science and Humanity.15, 922-930.

Corbusier, Le.1923a. "Toward a New Architecture". London: John Rodker Publisher.

Decker, Martina & Zarzycki, Andrzej .2013. "Designing Resilient Building with Emergent Materials". eCAADe, 32,179–184.

Griswold, Eliza. 2012. "How 'Silent Spring' Ignited the Environmental Movement." http://www.nytimes.com/2012/09/23/magazine/how-silent-spring-ignited-the-environmental-movement.html

Grobman, Jacob Yasha & Yekutiel, Tatyana Pankratov .2013. "Autonomous Movement of Kinetic Cladding Components in Building Facades". Presented at the Int. Conf. on Research into Design (ICoRD'13), Indian Institute of Technology Madras, Chennai.https://www.researchgate.net/publication/287644074_Autonomous_Movement_of_Kinetic_Cladding_Components_in_Building_Facades.

Hoberman Transformable Design. 2017. "Adaptable Building Initiative". http://www.hoberman.com/abi.html

Jenkins, Jim & Quick, Dave. 1989a. "Motion Motion Kinetic Art". Gibbs Smith Publisher.

Khoo, Chin Koi. 2013. "Morphing Architecture: with responsive material system". https://researchbank.rmit.edu.au/view/rmit:160591

Khoo, Chin Koi & Salim, Flora Dilys. 2013. "Lumina: A Soft Kinetic Material for Morphing Architectural Skins and Organic User Interfaces". International conference on pervasive and ubiquitous computing, Zurich, Switzerland.

Khmelnitsky, Dmitry. 2013a. "Yakov Chernikhov: Architectural Fantasies in Russian Constructivism". DOM Publishers.

Kolarevic, Branko, & Parlac, Vera. 2015. "Building Dynamics: Exploring Architecture of Change". New York, US.: Routledge Press.

Konis, Kyle & Selkowit, Stephen. 2017. "Effective Daylighting with High-Performance Facades, Emerging Design Practices". Springer International Publishing, Switzerland.

Loos, Adolf.1908a. "Ornament and Crime".

Mossavi, Farshid, & Kubo, Michael. 2006a. "The Function of Ornaments". Harvard University Graduate School of Design.

Matin, Negar, Eydgahi, Ali & Shyu, Shimming. "Comparative Analysis of Technologies Used in Responsive Building Facades". 124th Conf. American society of engineering education, Colombus, Ohio, 2017.

Mondia 2014. "Adaptive building envelopes." http://publications.lib.chalmers.se/records/fulltext/214574/214574.pdf

Pask, Gorden. 1969. "The Architectural Relevance of Cybernetics." http://workgroups.clemson.edu/AAH0503_ANIMATED_ARCH/879Readings/GordonPask_Architectural%20Relevance%20of%20Cybernetics.pdf

Perrone, R. & Buchler. 2005. "An investigation futurist architectural design"

Sadler, Simon. 2005. "Archigram: Architecture without Architecture". MIT Press.

Sendi, Mona. 2014a. “The Effect of Technology to Integrate Aesthetic Desire of Contemporary Architecture with Environmental Principles in Facade Design”. International Scientific, Journal Architecture and Engineering, 2(1).
Sharaidin, Kamil. 2014. “Kinetic Facades: towards design for environmental performance”. School of Architecture, RMIT University, Australia.
Stoughton, John .2017. “A smartphone-controlled responsive shading system prototype”. https://archpaper.com/2017/06/seattle-based-nbbjs-sunshade-prototype/#gallery-0-slide-2
United States Environmental Protection Agency.2016. Green Building. https://archive.epa.gov/greenbuilding/web/html/about.html?__hstc=23243621.f6d8d83307931013c2035c870506d914.1469468270039.1469468270039.1469468270039.1&__hssc=23243621.1.1469468270039&__hsfp=3935260784
Velikov, K. & Thun, G. 2013. “Responsive Building Envelopes: Characteristics and evolving paradigms in Design and Construction of High Performance Homes”. London, UK: Routledge Press.
Wilkinson, Ch., & Wood, A. 2013. “Al Bahar Towers: External Automated Shading System,” Jury statement of CTBUH Innovation Award.
Yiannoudes, Socrates.2016. “Architecture and Adaptation: From Cybernetics to Tangible Computing”. New York: Routledge.
Yekutiel, Tatyana Pankratov & Grobman, Jacob Yasha. 2014. Controlling kinetic cladding components in building facades: A case for autonomous movement. Presented at the 19th Int. Conf. of the Association of Computer-Aided Architectural Design Research in Asia CAADRIA, Hong Kong. http://grobman.net.technion.ac.il/files/2014/05/CAADRIA-2014-autonemous-movement.pdf.

MIES VAN DER ROHE, GROPIUS AND LE CORBUSIER

A comparative analysis



Edgar Stach, Dipl.-Ing. AIA/IA
Thomas Jefferson University / Oak Ridge National Laboratory
stache@philau.edu



Barbara Klinkhammer, Dipl.-Ing.
Thomas Jefferson University
klinkhammerb@philau.edu

ABSTRACT

"When technology reaches its true fulfillment, it transcends into architecture."[1]
Mies van der Rohe

Ludwig Mies van der Rohe (1886-1969)[2], Walter Gropius (1907-10)[3], both German-born architects and educators, and Le Corbusier (1887 –1965)[4], a Swiss-French architect, designer and painter, are widely acknowledged as the 20th century's most influential architects. This paper focuses on the development of complex building envelopes in the key works of Mies', Gropius' and Le Corbusier's extensive oeuvres, spanning from the 1920s to the end of the 1960s. In a comparative analysis, this paper unlocks the architects' approach and development of complex building envelopes over a span of 50 years, and places their design and construction methods into a historical context.

KEYWORDS

Ludwig Mies van der Rohe, Walter Gropius, Le Corbusier, building envelopes, early modernism, mid-century modernism, construction methods, history of facades

INTRODUCTION

At the beginning of his career, Mies worked in Peter Behrens' architecture office (1908–19) in Berlin, where he also met his later contemporaries Walter Gropius (1907–1910) and Le Corbusier (1910–1911). Behrens was one of the most influential architects and industrial designers in Europe at the beginning of the 20th century and played an important role in the development of modern architecture. Among other things, he was co-founder of the Deutsche Werkbund and gained international recognition for his AEG Turbine Factory built in 1909 in Berlin. His buildings combined architecture, industrial design and art in a pared-back architectural language and represented a first step away from the decorative tendencies of Art Nouveau and towards modernism, which his protégés would later embrace. In Mies' early villas in Berlin built between 1908 (Riehl House) and 1926 (Mosler House), the influence of Schinkel and Behrens is clearly visible in the abstract and reductive use of Schinkel's classicist formal elements and Behrens' approach to ornament and structure.[5]

In contrast to Gropius and Le Corbusier, however, mass production and standardization was not a primary concern for Mies. Despite recurring patterns in his design concepts, details and materials, all his buildings are unique. Mies' conception of space differs in key respects from that of Le Corbusier. Mies defined space as continuous, flowing space, and later as universal space bounded only by a transparent skin and defined by a few carefully placed walls (Fig. 1 and 2). For Le Corbusier, space is a walk-through sculpture based on the principle of the "rectangle élastique",[6] in which the free plan[7] is

experienced through passage along a “promenade architecturale”,[8] additionally modulated by color[9] and structured by his “five points of architecture”.[10]

For Mies, public space was above all an aesthetic space without a strong social component. For Le Corbusier, by contrast, public space was always a place for social interaction and communal use. This is especially evident in his concepts for high-rise complexes such as the Unité d’Habitation in Marseilles (1952), which was conceived as a fully functional vertical city. Unlike Mies, Le Corbusier was less interested in new forms of construction and materials. His architectural virtuosity is most evident in his spatial creations and less in architectural detailing.[11] The relationship between architectural detail and the building as a whole is for Le Corbusier mostly a product of standardization of the building process whereas for Louis Kahn, Mies van der Rohe, Alvar Aalto and Walter Gropius the quality of the detail was an integral part of the design concept.

MIES, GROPIUS AND LE CORBUISER – USE OF MATERIALS

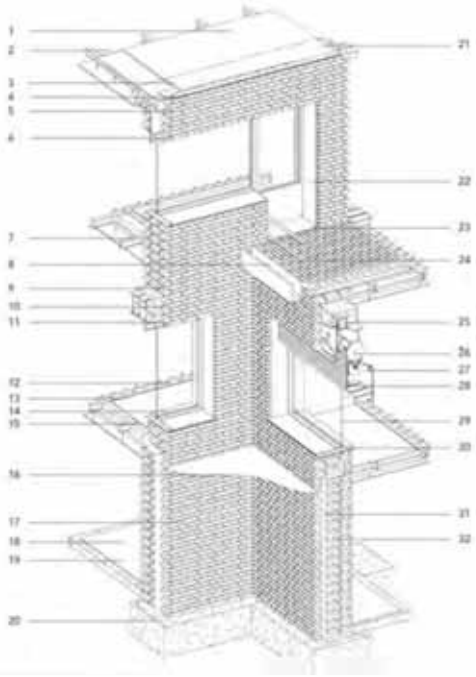
Mies’ declaration that “each material is only what we make of it”[12] describes his fundamental approach to materials. Because his buildings are so rigorously geometric and unadorned, their appearance is much more dependent on the careful choice of materials, balanced proportions and meticulously precise detailing. “Each material has its specific characteristics which we must understand if we want to use it”.[13] For him, this applies equally to craftsmanship as it does to industrialized technologies, and to combinations of natural materials, such as marble, onyx and travertine, and industrially produced products such as chrome, glass, steel and aluminum.



Figure 1: Garden facade, west corner, exterior. Drawing by Edgar Stach.

Figure 2: House Lange, exterior view looking at back porch, garden façade.

Photo: Doehne Volker, Kunstmuseum Krefeld.



1 Waterproof membrane
2 Steel reinforcement bars
3 Asphalt roofing
4 Cant strip
5 Steel plate
6 Steel angle bar
7 Drop ceiling
8 Planter box
9 Concrete
10 Steel retaining bolt
11 Steel C-channel
12 Concrete floor blocks
13 Steel beams
14 Hardwood floor
15 Steel retaining bolt
16 Ground plane
17 Steel moisture barrier
18 Masonry tiles
19 Concrete floor slabs
20 Concrete footing
21 Lead flashing
22 Door
23 Door frame
24 Steel railing
25 Steel reinforcement bars
26 Gears
27 Rope
28 Shutter
29 Glass window
30 Concrete sill
31 Steel moisture barrier
32 Load-bearing brick basement wall

Le Corbusier preferred the raw simplicity of materials such as exposed timber-shuttered concrete, simple wood, and glass. His spaces from the early 1920s have a sculptural quality in which the building material is secondary, often covered with plaster to create the required spatial geometry. From the Villa Savoye (1931) onwards, he began to use industrially produced materials and developed an interest in standardization and industrial prefabrication. Le Corbusier’s approach to materials and detailing is therefore characterized by his interest in industrialized and standardized construction systems, and in the industrialization of the construction industry following the model of automation in automobile and aircraft manufacturing (Fig. 3). This can be seen in his use of new materials and construction methods for the development of new wall constructions for the Swiss pavilion.

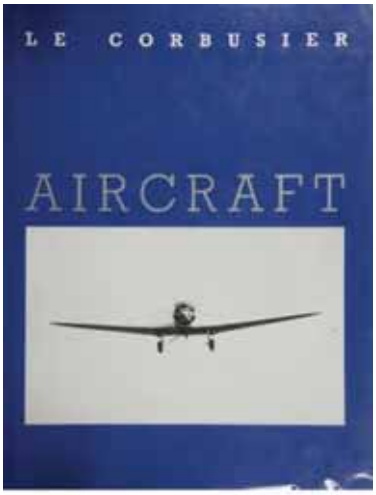






Figure 3: Le Corbusier, 1935 Aircraft.

Figure 4: Le Corbusier, Maison Citrohan, 1922. Photo: FLC.

Figure 5: Le Corbusier, Houses at Weissenhofsiedlung, Stuttgart, Germany, 1927. Photo: FLC.

Like Le Corbusier, Mies van der Rohe met Walter Gropius, three years his senior, in the office of Peter Behrens. As an architect and industrial designer, Gropius was responsible for the AEG turbine factory in Berlin (completed in 1909). After leaving the architect's office of Peter Behrens, he founded his own office with Adolf Meyer. His first project, the 1911 completed Fagus Werke in Alfeld on the Leine, are a built manifesto of modernism and laid the foundation for his later fame as an architect. The industrial building is designed without any ornamentation and was built in Ferro-cement construction with a three-story curtain wall made of steel. This is evidence of Gropius' groundbreaking attitude in using materials from industry without considerations of hitherto valid building traditions. Unlike Mies, who was a representative of classicism until the early 1920s, Gropius fully represented rationalism and functionalism even before the Great War.





Figure 6: Walter Gropius, Houses at Weissenhofsiedlung, Stuttgart, Germany, 1927. Photo: Harvard Art Museums/Busch-Reisinger Museum, Gift of Ise Gropius. BRGA.23.36.

Figure 7: Prefabricated modular system for the Houses at Weissenhofsiedlung. The image shows a box-shaped building and some of the panel connections.

The panel system was limited and only rectangular, linear object could be achieved.14 Photo: www.arthistory.upenn.edu.

Mies van der Rohe was far from being so radical and progressive. In his *5 Studien* (Fig. 13) (5 studies), Mies began to deal with a new architectural language in the early twenties, but it was not until the second half of the twenties that he translated his visions of a new, modern architecture into actual buildings.

Similar to Mies van der Rohe later at IIT in Chicago, Gropius had the opportunity to implement his architectural philosophy as a campus planner, architect and educator. With a completely new educational approach of bringing architecture, art and design together, Gropius founded the Staatliches Bauhaus in Weimar (1919-1925)[15] and later in Dessau (1925-1932)[16]. The Bauhaus building (Fig. 9 and 10) designed by Gropius in Dessau with its glass curtain wall[17], its revolutionary reinforced concrete skeleton and functional floor plan anticipates Mies van der Rohe's objectivity of the IIT campus buildings (Fig. 8).







Figure 8: Exterior view from the south at night, showing pedestal, the four columns and horizontal roof line. Photo: Chicago History Museum, Hedrich-Blessing Collection: HB-18691-D.

Figure 9: Bauhaus Building Dessau Germany, 1925-1926, Walter Gropius with Carl Fieger, Ernst Neufert, and others, Unidentified Artist.

Figure 10: Bauhaus Building, The main entrance on opening day, 4 December 1926, Harvard Art Museums/Busch-Reisinger Museum, Gift of Ise Gropius, BRGA.20.57.2.

More fundamentally than Mies, Gropius experimented with the mechanization of building and industrial fabrication methods[18]. Thus, the urban layout of the settlement Dessau-Törten (1926) (Fig. 11 and 12) is the result of an efficient rail track of the crane system and an innovative assembly-line production. The stereotypical stringing together of seemingly endless rows of houses was received quite critical19. During the Werkbund exhibition in Stuttgart in 1927 led by Mies van der Rohe, Gropius demonstrated solutions for modern construction assembly. He developed a single-family house in dry construction with industrially manufactured elements based on steel frame construction, cork insulation and asbestos-cement for the outer skin. Floor plans, high construction costs and design errors were generally criticized negatively. Mies reflected on this at the opening of the exhibition: "Rationalization and typification are only means, but must never be the goal."20





Figures 11-12: Bauhaussiedlung Dessau–Törten von Walter Gropius (1926–28). Photo: www.bauhaus-dessau.de/de/architektur/bauhausbauten/siedlung-dessau-toerten.html.

BUILDING ENVELOPES: CONSTRUCTION – SPACE - DETAIL

The importance of glass as a material for Mies can already be seen in his idealized designs for an office high-rise on the Friedrichstraße (Fig. 13) and glass skyscraper at the beginning of the 1920s. Its novel construction concept shows the column grid set back from the front plane of the facade and a completely glazed facade membrane. The 'window' as a link to the surroundings and indicator of human scale was replaced by a facade that responds universally to its surroundings and became generalized as an expression of the International Style. "My experiments with a glass model help me along the way and I soon recognized that by employing glass, it is not an effect of light and shadow one wants to achieve but a rich interplay of light reflections."[21] The dematerialization of the wall and unhindered connection between the interior and the natural surroundings was first realized most convincingly in the Barcelona Pavilion and taken to perfection in the Farnsworth House. The material glass and transparent building skin are an essential part of Mies' architecture (Fig. 14 and 15).





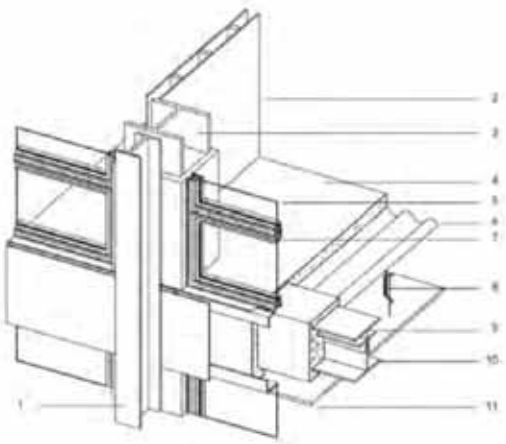


Figure 13: Model for a glass skyscraper at Friedrichstrasse, Berlin (unrealized). Print, 1921: bpk Bildagentur, Staatsbibliothek zu Berlin, Stiftung Preussischer Kulturbesitz / Art Resource, NY / C 2017 Artists Rights Society, (ARS), NY / VG Bild Kunst, Bonn: Dietmar Katz.

Figure 14: Apartment building at 860–880 Lake Shore Drive under construction. The photo shows the structural columns and the non-load-bearing I-beams. Photo: Chicago History Museum, Hedrich-Blessing Collection.

Figure 15: Window facade structural column and decorative I-beam exterior/core. 1. Wide flange decorative element, 2. Partition wall, 3. Wide flange column, 4. Concrete floor slab, 5. Glazing, 6. Corrugated metal, 7. Steel mullion, 8. Drop ceiling hanger, 9. Steel angle, 10. Steel wide flange beam, 11. Drop ceiling. Drawing by Edgar Stach.

Le Corbusier embraced modern environmental solutions for climate control and lighting more holistically then Mies and Gropius and developed five building-physic concepts: 1. natural ventilation (*aération naturelle*), 2. natural lighting (*éclairage solaire*), 3. solar control (*brise-soleil*), 4. thermally active facade in opaque or glazed walls (*mur neutralisant*), 5. internal air

conditioning (*respiration exacte*). These concepts are an essential part of Le Corbusiers' "modern techniques" (*les techniques modernes*). Also, many of these concepts failed in practice, they advanced the knowledge in building technologies and envelope design greatly. He was especially interested in double skin façades.

Rosa Urbano Gutierrez describes in the publication 'Le pan de verre scientifique: Le Corbusier and the Saint-Gobain glass laboratory experiments (1931–32)'[22] Le Corbusier's interest in the development of new facade technologies. 'Le Corbusier's fascination with light and glass formed a continuing thread throughout his career. After his maxim 'architecture is lighted floors[23], came passionate discourses to defend the building's openness, first with his *fenêtre en longueur*, the ribbon window, and ultimately with his emblematic *pan de verre*, the glass wall that would not only provide sunlight-flooded interiors but would also most significantly contribute to shape the Modernist imagery. Despite the profuse explorations invested in this concept, Le Corbusier would always lament his failure to execute his '*pan de verre* 100%' in the way he would have desired: 'as a *mur neutralisant (Fig. 16 and 17)* constituted by a double glass-wall with an internal cavity through which conditioned air would circulate, hot in winter, cold in summer.'[24]



Figure 16. Double-glazed sliding window in Anticorodal, manufactured by Ernst Koller, 1928–9. FLC 29855. © FLC/ ADAGP, Paris and DACS, London 2012.

Figure 17. Implementation of the principles of aération ponctuelle and the murs neutralisants in the Centrosoyuz building, 3 January 1930. FLC 15720.

© FLC/ ADAGP, Paris and DACS, London 1 2012.

Appropriating technology, not inventing it, Le Corbusier and Pierre Jeanneret's proposal was to combine a double-skin structure with an air conditioning unit in order to regulate the environment of the usable space independently of the exterior environment. But their idea never brought satisfactory results due to two fundamental factors: the negative insulating capacity of a cavity with air in movement, and the exclusion of a heating system in the internal space adjacent to the façades. This demonstrates a misunderstanding of the physical principles involved in the proposal, which were issues beyond Le Corbusier and Pierre Jeanneret's expertise. What is difficult to understand is why, during all the years devoted to this system, they were not very much engaged in the aspect of the invention that is within the competence of the architect: namely the design of the façade. It is particularly surprising that they did not reflect on the critical role of joints and frames in the *mur neutralisant*, not only in its architectural dimension but also in the physical requirements of a façade container that is intended to encapsulate air.[25]

TRANSPARENCY VERSUS LIGHT AND SHADOW – AUTOMATION / PREFABRICATION

Mies van der Rohe interpreted transparency[26] in two respects: in the direct sense as a property of light- and air-permeable materials and in a figurative sense as a means of spatial arrangement in which several different spaces can be seen at once. The most lasting influence on the architecture of offices and workplaces was without doubt the development of the curtain wall, first seen in the buildings on Lake Shore Drive and Lake View. The breakthrough for this new suspended facade system, however, came with the Seagram Building in New York (1958). Mies succeeded in applying the highly efficient facade unit as an internal organizational system. The system of grid-based modular façade panels was used as an ordering principle for the adaptive spatial planning, at the time a revolutionary new concept for flexible workspaces.





Figure19: Mies van der Rohe corner detail and roof detail. Drawing by Edgar Stach.

1 Steel reinforcement bar
2 Gravel roof
3 Water-tight membrane
4 Double E-paned glass
5 Aluminum
6 Ornamental aluminum I-beam
7 Aluminum

Figure 18: Lake View Drive, Chicago, curtain wall. Photo: Chicago History Museum, Hedrich-Blessing Collection.

This also made it possible to incorporate modular installation elements within the building skin, for example office partitions and lighting and ventilation systems. The curtain wall (Fig. 18 and 19) became the new uniform face of the modern city and not only corresponded to the new modern age but also created the conditions for efficiently organizing staff in the universal workplace. Through standardization and categorization, the curtain wall was replicated endlessly, ultimately undermining the role of the designing architect and Mies' idea that each building is unique and site-specific.[27]





Figure 20. Dominican Monastery Sainte Marie de la Tourette, Éveux (near Lyon), Rhône-Alpes, France, 1953-1960, Le Corbusier & Iannis Xenakis.

Figure 21. Room showing fixed window door to balcony and on left side of the façade the operable wood shutter for ventilation.

Le Corbusier preferred the raw simplicity of materials such as exposed timber-shuttered concrete, simple wood and glass (Fig. 20 and 21). His spaces from the early 1920s have a sculptural quality in which the building material is secondary, often covered with plaster to create the required spatial geometry. From the Villa Savoye (1931) onwards, he began to use industrially produced materials and developed an interest in standardization and industrial prefabrication. Le Corbusier's approach to materials and detailing is therefore characterized by his interest in industrialized and standardized construction systems and in the industrialization of the construction industry following the model of automation in automobile and aircraft manufacturing.[28] This can be seen in his use of new materials and construction methods for the development of new wall constructions.

At the beginning of the nineteen twenties, Le Corbusier started experimenting with novel construction methods as shown in the Monol houses (1919) where he used two layers of 6 mm asbestos plates with an airspace for thermal insulation.

Elsewhere, he experimented with shotcrete (Citrohan House 1922, Fig. 4) again with an air-conducting layer between the walls. Facing major thermal and constructional problems in his executed buildings, Le Corbusier abandoned around 1930 the development of multi-layered wall constructions as a mass-produced product and resumed to monolithic walls.

The Swiss Pavilion at the Cité Universitaire in Paris (1932) (Fig. 22-27) with its steel frame and curtain wall represents a clear break from the previously used concept of reinforced concrete paired with standardized building parts. The building shows a complex range of materials and a new conceptual relationship between the closed and glazed wall surface made possible by a structural steel frame. The building is based on two separate support systems: a reinforced concrete slab supported by pilotis, which forms the second floor, and a steel structure with concrete floor slabs for the floors above. The steel structure dictates the spatial grid on the upper floors and as well as the layout of the well-detailed curtain wall. The clear steel structure is reminiscent of the steel frame of House Tugendhat.





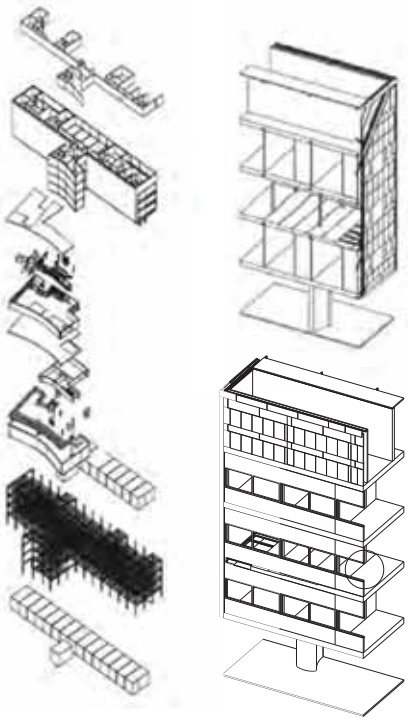
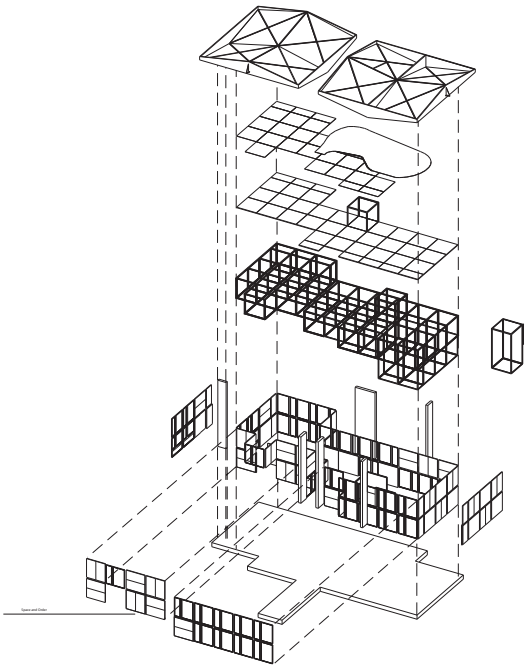


Figure 22-23: Photo: Le Corbusier, Swiss Pavillon, Paris, France. The structural system consists of a reinforced concrete slab supported by pilotis and a steel skeleton. The clear steel construction is reminiscent of the steel structure of Tugendhat House. 1930–1932. Photo: FLC / ADAGP, Paris / C 2017 Artists Rights Society (ARS), NY.

Figure 24: Exploded axonometric drawing: The structural system consists of a reinforced concrete slab supported by pilotis and a steel skeleton. The clear steel construction is reminiscent of the steel structure of house Tugendhat. Drawing by Edgar Stach.

Figure 25-27: Axonometric drawing of building corner: Le Pavillon Suisse, Le Corbusier, 1930- 1932, Paris France, front entry façade, curtain wall façade. Drawing by Edgar Stach.

Le Corbusier's Heidi Weber Pavilion (1960 -1967) (Fig. 28-31) is a completely prefabricated building assembled in a park setting at Lake Zürich in Zürich, Switzerland. The most prominent architectural element, the roof, consists of two square parts and consisting of welded metal sheets and having a weight of 40 tons. The prefabricated roof was transported in units to the building site and assembled on the ground. The two finally welded parts of the roof were then lifted to their final height by a crane and fixed on the pillars. The two-floor tall modular building was prefabricated and consists of cubes 2.26 x 2.26 meter (7.4 ft). Walls, windows, ceilings and floors were then screwed onto the steel frame. The walls consist of enameled panels and placed according to a particular rhythmic system. Only the concrete floor slab was built on site. In total, more than 20,000 bolts were used to assemble the pavilion.







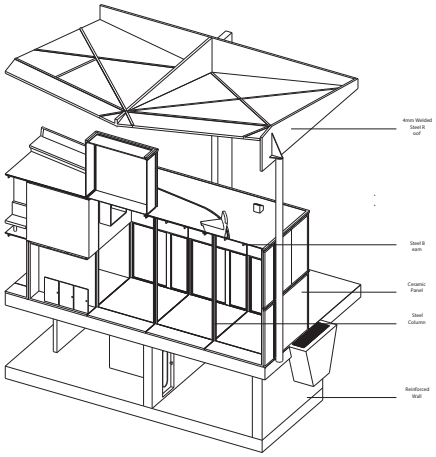


Figure 28: Exploded axonometric drawing showing the free spanning roof, modular room container and façade system. Drawing by Edgar Stach.

Figure 29-30: Steel façade with glass and colored enameled panels measuring 1.13 meter (3.7 ft) x 2.26 meter (7.4 ft).

Figure 31: Detail axonometric drawing: steel roof, consists of two square parts, 12 x 12 meter (39 ft). Drawing by Edgar Stach.

CONCLUSION

Exemplary for a whole generation of architects influenced by Mies is Gordon Bunshaft[28]. An employee since 1946, Bunshaft later partnered with the New York office of Skidmore, Owings and Merrill (SOM). The Lever House (1951)[29], designed by Bunshaft, is an office tower near Mies van der Rohe's Seagram Building in New York City. With its blue-green glass and stainless steel columns, it represents one of the first skyscrapers built in the international style in the US. The building consists of two intersecting volumes with balanced proportions but contrasting shapes, a two-story raised horizontal podium with an underlying plaza and a 21-story tower.

The Inland Steel Building (1957)[30] in Chicago designed by SOM (architects Walter Netsch and Bruce Graham), is an ideal demonstration of Mies' spatial concept of a pillar-free universal space for an office building. This spatial concept was new at the time of completion and unsurpassed in its flexibility. The placement of all columns along the facade and the consolidation of elevators and other service functions in a separate tower allowed a highly flexible and column-free spatial layout.

In 1946, Gropius founded the young architects' association, The Architects' Collaborative (TAC) in Cambridge, USA. TAC's architecture in the 50[31] and 60[32] was following the International Style, created by Gropius and his colleagues at the Bauhaus (Fig. 33). Starting in the 1970s, TAC's style largely shifted from modernism to postmodernism. Gropius and TEC were mainly interested in the standardization of the design processes and construction methods, some of the projects were problematic urbanistic, aesthetically and socially. For example, the *Pan Am Building* (MetLife Building) (Fig. 34) was unpopular from its 1963 origins do to its bulky massing, uninspiring façade, the placing in the middle of the city at the southern end of Park Avenue and blocking the view of Grand Central Terminal. The social housing development Gropius Stadt in Berlin 1960 is prime example for social segregation and a failed brutalist city panning.

Le Corbusier was an early adapter of prefabricated industrialized products and experimented with prefabricated building systems and complex facade assemblies. He developed early on new concepts for double-skin facades, including multi-layered façade systems, *brise-soleils*, and integrated ventilation systems. His use of “raw” concrete – *béton brut*, as shown in the 1952 Unite d’habitation in Marseille and the 1953 Secretariat Building (Palace of Assembly) in Chandigarh, India -

is maybe the strongest legacy of Le Corbusier apart from impacting the development of modern cities with his urban planning and social agendas. Later coined “brutalism”, the architectural style gained considerable momentum in Europe, Asia and the United States in the 1950s and 1960s as a low-cost construction method for mass housing projects and large government buildings.

Mies van der Rohe had a decisive influence on the design and fabric of American cities in the second half of the twentieth century. He changed the way skyscrapers were constructed and transformed the American office landscape. In their objectivity, his designs became the prototype of the modern American skyscraper and model for countless replications. However, this success ultimately led to a monotonous uniformity of office buildings and was the reason for the departure from the International Style towards a new style emerging in the mid-seventies, Postmodernism[2].





Figure 32: Interbau, International Building Exhibit Berlin housing development July 1957.

Figure 34: Pan Am Building, (MetLife Building) 1963.





Figure 35: Cite de Refuge, Salvation Army, Paris, mur neutralisant: double wall system with cool or warm air circulating between layers, tried in a couple of residential buildings prior (Glass and Interactive Building Envelopes – Michel Crisinel, page 29).

Image 36: Usine Duval, St. Dié, 1946 (brise-soleils).

REFERENCES

---

[1] Cited in: James Baker (ed.), Perspecta 3. The Yale Architectural Journal, published by School of Art and Architecture at Yale University. New Haven and London, 1955.
[2] March 27, 1886 in Aachen – August 17, 1969 in Chicago.
[3] May 18, 1883 – Juy 5, 1969.
[4] October 6, 1887 – August 27, 1965.
[5] Stanford Anderson. *Peter Behrens and a New Architecture for the Twentieth Century*. MIT Press, Cambridge (Mass.), 2002.
[6] The term "rectangle élastique" was coined by the French artist Fernand Léger.
[7] Le Corbusier first used the term "plan libre" in 1914 in the schematic construction for the Dom-ino House.
[8] Corbusier describes the "promenade architecturale" as a path through a built space through which a sequence of images unfolds for the visitor. See also: Flora Samuel. *Le Corbusier and the Architectural Promenade*. Birkhäuser, 2010.
[9] Le Corbusier developed his color theory "Polychromie Architecturale" in 1931. For him the color scheme of a building was a crucial aspect as important as the plan and section. Published in: Arthur Rüegg. *Le Corbusier. Polychromie architecturale*. *Les Claviers de couleurs de 1931 et de 1959*. Birkhäuser, 2015 (3rd Edition).
[10] Le Corbusier defined the principles of his new architecture in 1927 in *Les cinq points de l'architecture moderne* written by himself and his cousin Pierre Jeanneret.
[11] Eduard R. Ford. *Das Detail in der Architektur der Moderne*. Birkhäuser, 1994.
[12] Cited in: Fritz Neumeyer. *Mies van der Rohe – The Artless Word*, MIT Press, 1991. Neumeyer provides a comprehensive interpretation of the philosophical basis of the architect's thoughts and writings and includes a commentary of nearly all Mies' writings, from published articles to handwritten notes.
[13] Recorded in Werner Blaser's notes of conversations with the architect during his period in Chicago between 1951 and 1953.
[14] http://weimararchitecture.weebly.com/weissenhof-siedlung.html.
[15] Grand-Ducal Saxon School of Arts and Crafts.
[16] Professors at the Bauhaus: Paul Klee, Johannes Itten, Josef Albers, Herbert Bayer, László Moholy-Nagy, Otto Bartning and Wassily Kandinsky.
[17] A curtain wall is understood as a construction method with a non-load-bearing external wall attached to a framed structure,in which the facades only carry their own weight and no other static loads.
[18] Maybe, the most impresssive example of his interest in industrial buildings ist the Metall Prototype House (1926-1927) developped in collaboration with the Hugo Junkers Flugzeug Werke in Dessau.
[19] Alfred Gellhorn. *Rationalismus und Kunst*. Die Baugilde 1927.
[20] In report oft the Reichsforschungsgesellschaft: "Der konstruktivistische Doktrinarismus des Bauhauses gibt den Häusern einen eigentümlich trockenen pedantischen Zug und zugleich etwas provisorisch barackenmässiges".
[21] Ludwig Mies van der Rohe. "Hochhäuser", Frühlicht 1, Vol. 4, (1922): 124. Translated in Fritz Neumeyer. *The Artless Word: Mies van der Rohe on the Building Art*. MIT Press, 1991, p. 240.
[22] Gutiérrez, Rosa Urbano. "Le pan de verre scientifique: Le Corbusier and the Saint-Gobain glass laboratory experiments (1931-32)". Architectural Research Quarterly. Cambridge17.1 (Mar 2013): 63-72.
[23] See for example Le Corbusier. *Précisions sur un état présent de l'architecture et de l'urbanisme*. Editions Crès, 1930, p. 41: 'Je vais dire une énormité fondamentale, tant pis: "l'architecture, c'est des planchers éclairés".'
[24] Jules Alazardet, Jean-Pierre Hébert. „De la fenêtre au pan de verre dans l'oeuvre de Le Corbusier". Étude conçue et rédigée avec l'accord de Le Corbusier. P.V.P.,1961, p. 19.
[25] Gutiérrez, Rosa Urbano. "Le pan de verre scientifique: Le Corbusier and the Saint-Gobain glass laboratory experiments (1931-32)". Architectural Research Quarterly. Cambridge17.1 (Mar 2013): 63-72.
[26] Colin Rowe and Robert Slutzky. *Transparency*. Birkhäuser, 1997. Interior Crown Hall, IIT, Chicago 1950s Crown Hall under construction, IIT, Chicago 1955.
[27] The British architecture journal Architectural Review published a special edition entitled "Machine – Made America" in May 1957 (vol. 121) dedicated to the curtain wall, including an ironic commentary on the role of the architect in the design as being fettered by the catalog of general technical details.
[28] In Aircraft (1935), Le Corbusier celebrates the aircraft as the pinnacle of human technological achievement.

[29] Thomas E. Luebke, ed., *Civic Art: A Centennial History of the U.S. Commission of Fine Arts* (Washington, D.C.: U.S. Commission of Fine Arts, 2013): Appendix B, p. 541.
[30] www.som.com/projects/lever_house.
[31] http://www.som.com/projects/inland_steel_building.
[32] Postmodernism as a style of architecture is seen as a critical response to the crisis of modern architecture with its functionalized everyday architecture of the post-war period. Based on the theoretical debate at the end of the sixties, Postmodernism finds its practical application in western industrial nations especially in the seventies and eighties of the twentieth century.

PAUL RUDOLPH'S CHRISTIAN SCIENCE BUILDING

The concrete façade of a forgotten Brutalist masterpiece



Scott Murray
University of Illinois at Urbana-Champaign
scmurray@illinois.edu

ABSTRACT

This paper presents new historical research on the concrete façade of an important but relatively unknown and now demolished building by the American modernist architect Paul Rudolph (1918-1997). Today Rudolph is best known as a proponent of Brutalism and for designing a series of projects built of concrete in the 1960s, exemplified by the Yale Art & Architecture Building (1963). Closely related in materiality and form to the famous Yale building was Rudolph's design for the Christian Science Building (1965) in Champaign, Illinois, a smaller and lesser known but still remarkable concrete building. However, in contrast to the Yale building, which was recently carefully restored and renamed as "Rudolph Hall" to honor its architect, the Christian Science Building was demolished in 1986 after only 20 years of use. One of the factors cited for the building's abandonment was the poor performance of its concrete façades. Archival drawings reveal that during the design process Rudolph initially proposed using custom CMU blocks to form cavity walls with continuous insulation. However, due to cost concerns cited by the builder, the walls were instead constructed of monolithic cast-in-place concrete with no added thermal insulation. This decision had significant impacts on the subsequent energy performance of the envelope; eventually the cost of heating and maintaining the building was cited as a major reason for its abandonment and demolition. This research reveals the potentially significant impact that façade construction techniques may have on the future preservation or destruction of twentieth-century modernist architecture.

KEYWORDS

history of façades, modern architecture, concrete, masonry, heritage conservation - preservation - restoration, Paul Rudolph

INTRODUCTION

In the 1960s, Paul Rudolph was among the most prominent and prolific of American architects. Robert A.M. Stern described Rudolph as "the greatest talent of his generation of American architects" who achieved a "meteoric rise to the top of the profession in the years following World War II (Rudolph 2008). After establishing his practice in the late 1940s and 50s in Florida, where he designed a number of iconic modernist houses, Rudolph was appointed chairman of the Department of Architecture at Yale University in 1958, a position that he would hold for the next seven years. During this period, Rudolph rose to national renown, completing a number of large-scale institutional commissions that included the Blue Cross and Blue Shield Building (1960) in Boston and the Temple Street Parking Garage (1963) and Yale Art & Architecture Building (1963) in New Haven, Connecticut. Rudolph's work at this time was characterized by a sense of monumentality bolstered by the predominant use of concrete and a design aesthetic aligned with the rising trend toward Brutalism in modern architecture. Although the Art & Architecture Building has had a turbulent history (including a devastating fire in 1969 and a comprehensive $126 million restoration in 2008), it is the work most positively associated with Rudolph today. The historian Timothy Rohan has called it "Rudolph's true masterpiece" (Rohan 2014).

During this same highly productive period in the early 1960s, Rudolph also designed a building in Champaign, Illinois, for a Christian Science student organization at the University of Illinois (Fig. 1). Although relatively small in scale at just 5,630 square feet in comparison to 114,000 at the Art & Architecture Building, the two buildings share several defining

characteristics: facades of a rough corrugated concrete, fortress-like tower elements, a pinwheel plan-form, a focus on natural light, and complex interior spatial volumes. Rudolph's Christian Science Building was an embodiment of many of the architect's priorities at the height of his career and is historically important as it represents a critical link between the architect's engagement with the monumental scale of his 1960s institutional buildings and the more intimate scale of his earlier residential work. However, the building was used for only two decades before its original owners moved out and sold it to a local developer, who in 1986 demolished it to build an unremarkable apartment complex in its place. The Christian Science Building is nearly forgotten today, even amidst a resurgence of interest in Brutalism in general and Paul Rudolph in particular. The building does not appear, for example, in the most recent monograph on Rudolph, Timothy Rohan's The Architecture of Paul Rudolph, published in 2014. But had it survived, the building would likely be considered today on par with the Art & Architecture Building as a prime example of the architecture Rudolph designed at the peak of his career.

Now, more than 50 years after its construction and 30 years since its demolition, the Christian Science Building remains essentially unknown among architects and historians. It deserves more recognition, not only as an illustration of its designer's skill and development, but also as a cautionary tale about the potential loss of key examples of 20th-century modern buildings, as many of them now reach a critical point in their useful lifespan where either restoration, adaptation, or demolition are deemed necessary. This research addresses the questions: Why was the Christian Science Building demolished after such a short time period? And what role did the design and construction of the building's façade play in the untimely abandonment and eventual destruction of the building?



Figures 1 and 2: At left, a view looking west toward the Christian Science Building in Champaign, Illinois, designed by Paul Rudolph. Construction was completed in 1965. Photo credit: HB-29509-A, Chicago History Museum, Hedrich-Blessing Collection. At right, a photograph taken during the building's demolition in 1986. Photo credit: Myra Kaha.

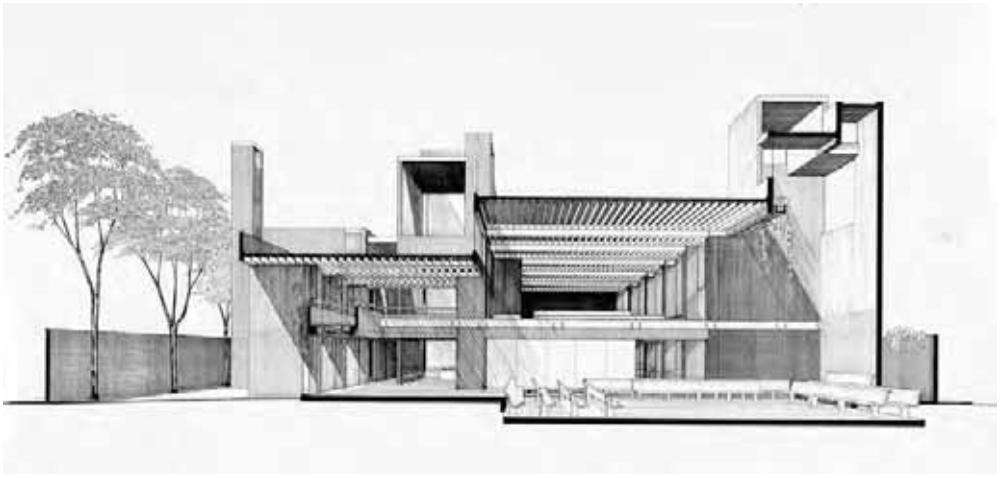
BACKGROUND

Built in 1965 on a corner lot on the campus of the University of Illinois at Urbana-Champaign, the two-story Christian Science Building contained spaces for religious services, study, and meetings for a Christian Science organization of approximately 150 students. Even within a compact volume, there was great variety in the scale and composition of the interior spaces: ceiling heights ranged from just over 7 feet up to 42 feet, and movable partitions allowed spaces to be combined in different arrangements for different purposes. Three "tower" forms topped by clerestory windows and skylights provided natural light and contributed to the building's distinctive profile (Fig. 3).

The walls and foundations were built of cast-in-place reinforced concrete, which supported floors and roofs of plywood over exposed wood beams and joists. In addition to providing the primary structure, the load-bearing concrete walls were an important aesthetic feature: they established the massive, monumental presence of the building and, with their ornamental surface treatment, contributed an expressive quality to the facades. Exposed inside and out, the textured surfaces of the concrete walls were corrugated with vertical ridges that animated the façade with changing patterns of light and shadow throughout the day (Fig. 4). The walls were conventionally poured, with corrugated formwork, but then after removal of the

forms, the resulting ridges of concrete were bush-hammered by hand to knock away the sharp edges and expose the aggregate. This type of corrugated concrete, which Rudolph had first used two years earlier at the Art & Architecture Building, became a signature feature of his 1960s work. Rudolph wrote poetically of the effects of bush-hammered corrugated concrete: “Light was fractured in a thousand different ways and the sense of depth was increased. As the light changed the walls seemingly quivered, dematerialized, took on additional solidity” (Rudolph 1977).

Upon its completion, Rudolph’s Christian Science Building was praised by architectural critics. *Inland Architect* called the building “daring” and “positively inspired,” designed with “imagination and sensitivity, a considerable addition to Urbana’s campus” (Miller 1973). *Architectural Record* declared the building a demonstration of Rudolph’s “virtuosity” in creating “an architecture strongly manipulated in space and scale” (1967). Despite initially receiving such positive reviews, by the 1980s the building faced a crisis of ownership. Student membership in the Christian Science Organization at the University had declined and the remaining members found it increasingly difficult to fund the maintenance and operation of their now over-sized building. The excessive cost of heating the building during winter, in particular, was cited as a primary problem, and eventually forced the group to close the building during the winter months (Soo, and Ousterhout 1986). The building was ultimately sold to a local developer who planned to demolish it and build a large apartment complex on its prominent site. Facing protests from preservationists as well as students and faculty at the School of Architecture, the developer offered to sell the property to the University; however, University administrators declined, and the demolition was carried out in March of 1986 (Fig. 2). The destruction of the building echoed the decline of Rudolph’s professional influence; by the 1980s a Postmodernist critique of Rudolph’s brand of modernism had taken hold, and Rudolph virtually disappeared from architectural discourse (Rohan 2014).





Figures 3 and 4: The Meeting Room, which was the primary assembly space of the Christian Science Building, is shown in a section perspective drawing and interior photo, both from the Paul Rudolph Archive (public domain), Library of Congress, Prints & Photographs Division.

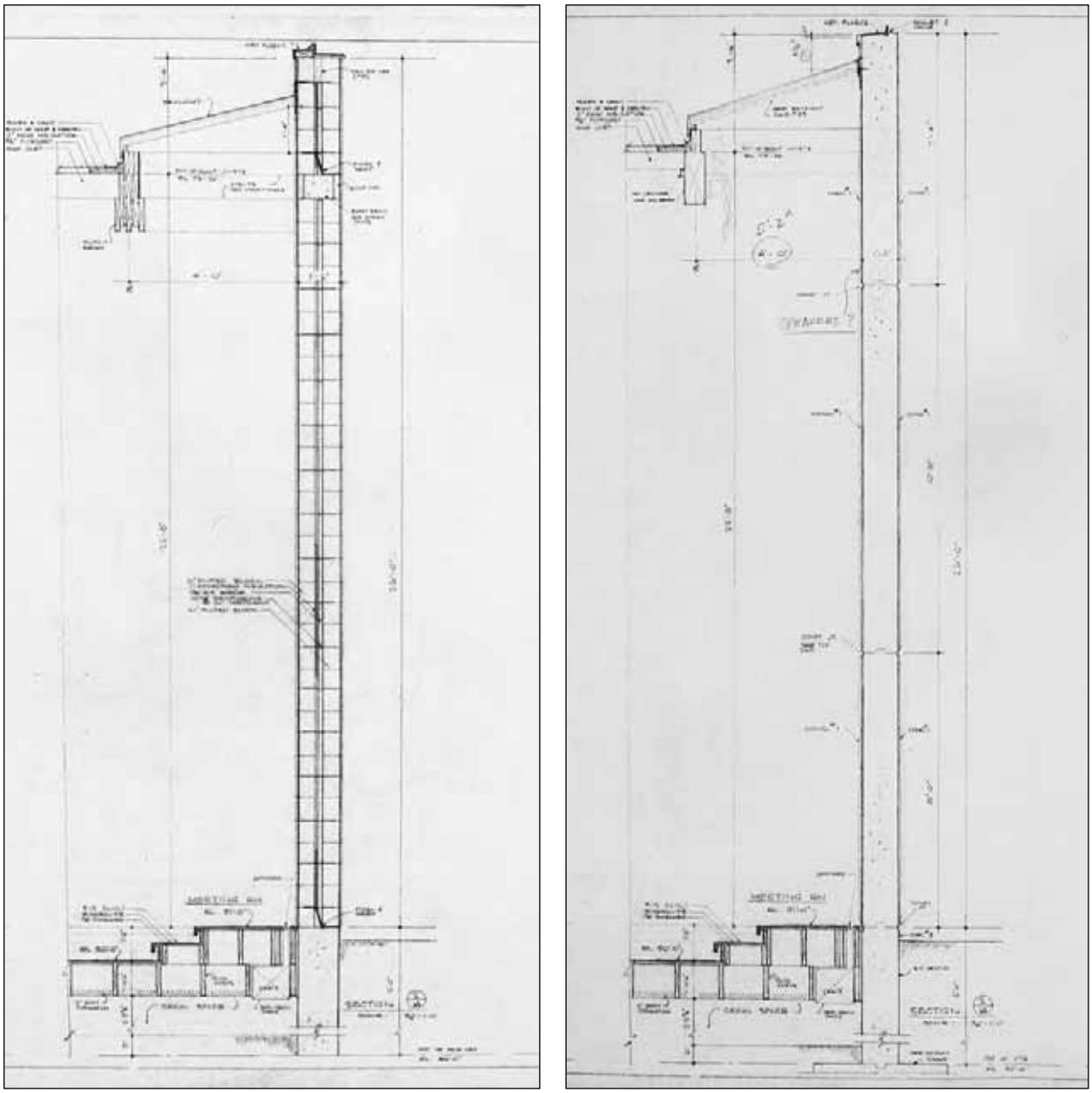
METHOD

In order to examine the role that the concrete facades of the Christian Science Building played in its ultimate destruction, two primary sources were consulted: (1) an extensive interview of Paul Rudolph conducted in 1986 by Robert Bruegmann under the auspices of the Chicago Architects Oral History Project for the Art Institute of Chicago, and (2) the project drawings and photographs included in the Paul Rudolph Archive at the Library of Congress in Washington, DC.

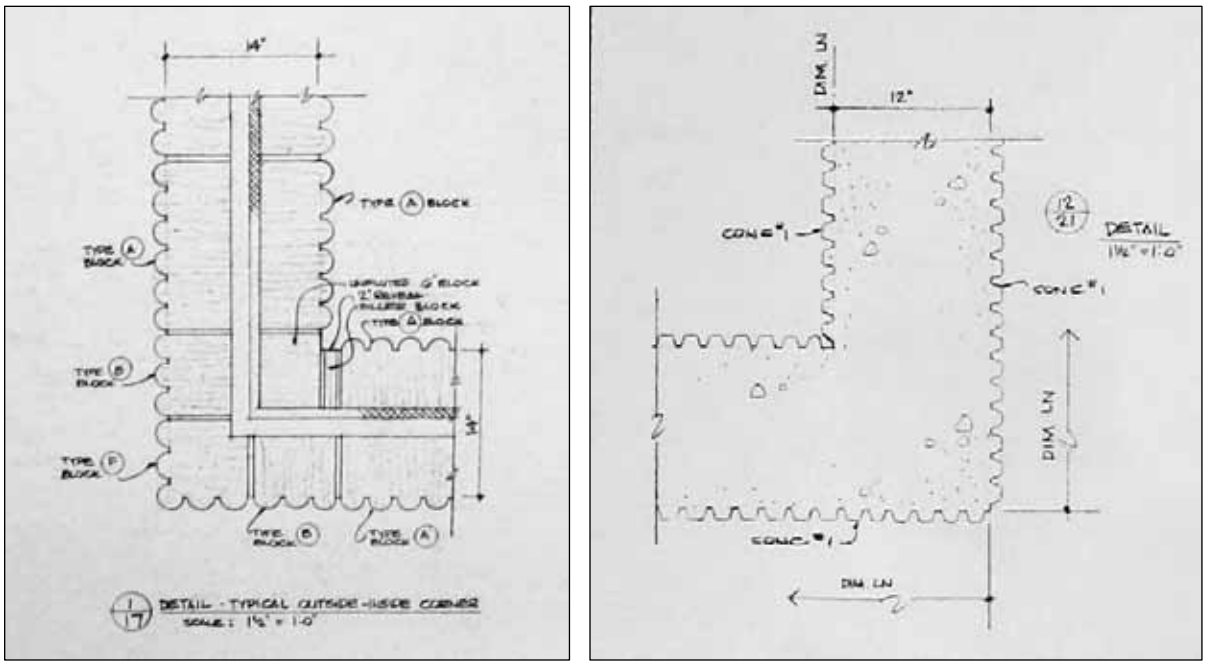
In the interview conducted at Rudolph’s New York office in February 1986—just one month before the Christian Science Building was demolished—Bruegmann reported to Rudolph that it appeared the demolition would soon go forward and asked him about the project. In addition to discussing the client and the design process, Rudolph stated his belief that the Christian Science Building was “one of the more successful of my buildings” and that “I will be unhappy if it’s demolished, but I’m not in control of that” (Bruegmann 1986). Rudolph also revealed that he had initially proposed to build the walls with concrete block, rather than poured concrete. Rudolph believed that using blocks would be less expensive than cast-in-place concrete, but the builders disagreed with him, saying that the block walls would be more costly to build. Through a process that would today fall under the euphemism of “value engineering,” the drawings were changed accordingly and the project

was built with poured concrete. There was apparently no discussion about the value of thermal insulation and which construction type would provide a better thermal envelope for the building.

Among its voluminous holdings, the Paul Rudolph Archive at the Library of Congress contains prints of several drawing sets produced by Rudolph's office (in association with local architect of record Delbert R. Smith) for the Christian Science Building. These drawings confirm Rudolph's recollection that the initial design specified walls of concrete block: in fact, early issues of the drawings (dated June 15, 1964) show the exterior walls consisting of two wythes of custom-formed concrete blocks with an interstitial air cavity and a layer of foam insulation (14 inches total wall thickness), while a subsequent revision (dated Nov. 11, 1964) changed the walls to monolithic cast-in-place reinforced concrete with no added insulation (12 inches total wall thickness). The different wall types are clearly evident in floor plans, building sections, wall sections, and detail drawings (Figs. 5 and 6). In either case, however, the same corrugated effect would be achieved: Rudolph's office had designed a set of custom-shaped corrugated blocks with rounded ridges, including typical field blocks and special corner blocks (Fig. 9) that would produce the desired vertical striations achieved by the bush-hammered cast-in-place walls described above.



Figures 5 and 6: Wall section drawings show the original design of cavity wall with custom fluted CMU and insulation (left) and revised design of monolithic cast-in-place reinforced concrete without insulation (right). Drawings from Paul Rudolph Archive (public domain), Library of Congress, Prints & Photographs Division.



Figures 7 and 8: Corner plan details show the original design of cavity wall with custom fluted CMU and insulation (left) and revised design of monolithic cast-in-place reinforced concrete without insulation (right). Drawings from Paul Rudolph Archive (public domain), Library of Congress, Prints & Photographs Division.

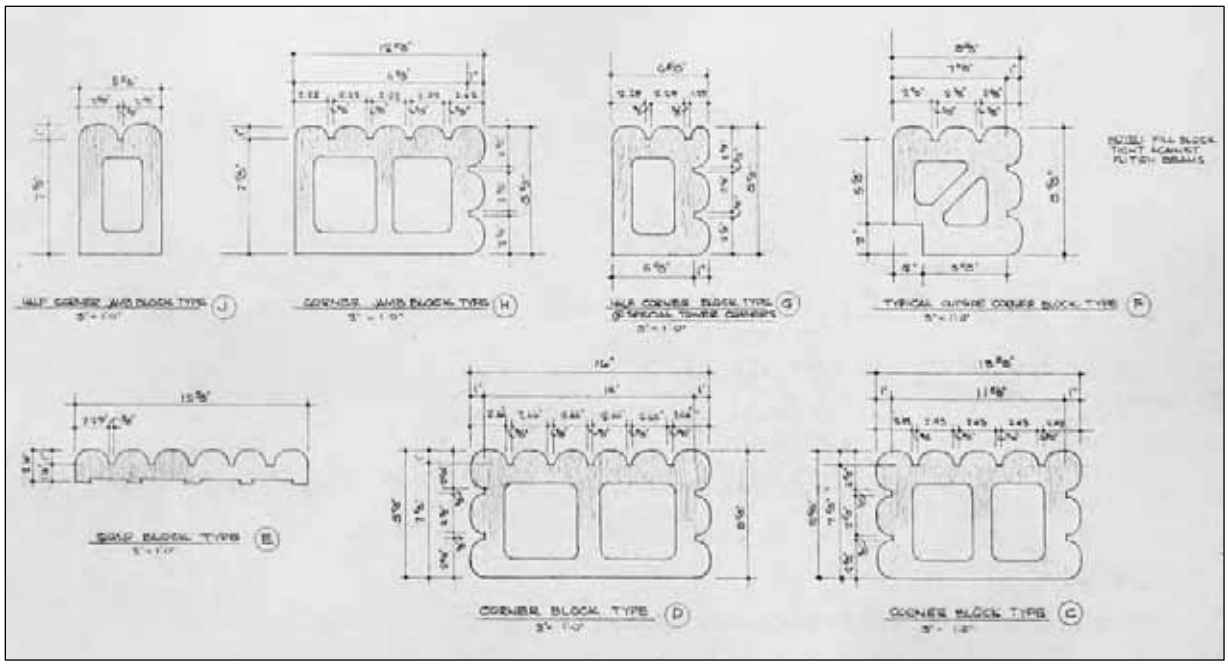


Figure 9: CMU block types from initial drawing set by Paul Rudolph Architect; later revisions replaced CMU walls with cast-in-place concrete. Drawings from Paul Rudolph Archive (public domain), Library of Congress, Prints & Photographs Division.

In any construction project, competing forces of initial construction cost vs. future operating costs can complicate the design process and may have unforeseen ramifications. Given that the cost of heating the building was cited as one of the major reasons for its eventual abandonment by the original owners, the decisions about how to construct the envelope of the Christian Science Building take on major significance in retrospect. For context, it is useful to consider the expected thermal performance of the Christian Science Building's concrete walls *as built* in comparison with Rudolph's original plan to utilize CMU cavity-wall construction and in comparison with today's energy code requirements. While it is unrealistic to expect that an architect working in the 1960s would design facades that meet today's standards for energy performance (and there was no energy code in effect at the time), such comparisons are instructive in assessing the building's purportedly poor thermal performance.

If it were built today, Rudolph's Christian Science Building would be subject to the requirements of the Illinois Energy Conservation Code, which currently adopts a slightly modified version of the 2015 International Energy Conservation Code (IECC). For Champaign's climate zone (5A), the minimum required R-value for a mass wall is R-11.4ci (IECC Table C402.1.3). As built, the 12-inch thick cast-in-place concrete walls of the Christian Science Building contained no insulation material; the concrete alone would have achieved approximately R-1.3 to 1.5. The CMU cavity walls indicated in early issues of Rudolph's construction drawings indicate two wythes of custom-fluted 6" concrete blocks with a 1-3/4" air space and 1"-thick foam-board insulation. The insulation alone would have an R-value of approximately R-5, and the overall assembly would reach approximately R-8. While a singular focus on thermal resistance and isolation as a measure of energy performance has been criticized (Moe 2014), it provides one lens through which to understand the relative performance of the Christian Science Building's concrete façade. This analysis shows that Rudolph's original plan to use a CMU cavity wall would not meet today's energy-performance standards but would have performed much better in the Illinois climate than the as-built "value-engineered" wall did, achieving a nearly seven-fold increase in R-value. Thermal-gradient analysis using THERM software further demonstrates the relative heat loss of the two wall systems as well as the increased risk of interior-surface condensation during winter conditions for the as-built monolithic concrete wall (Fig. 10). It is also notable that Rudolph's construction drawings indicate 2 inches of rigid insulation located above the plywood roof deck, which would also fall significantly below the IECC minimum of R-30ci for roofs in zone 5A.

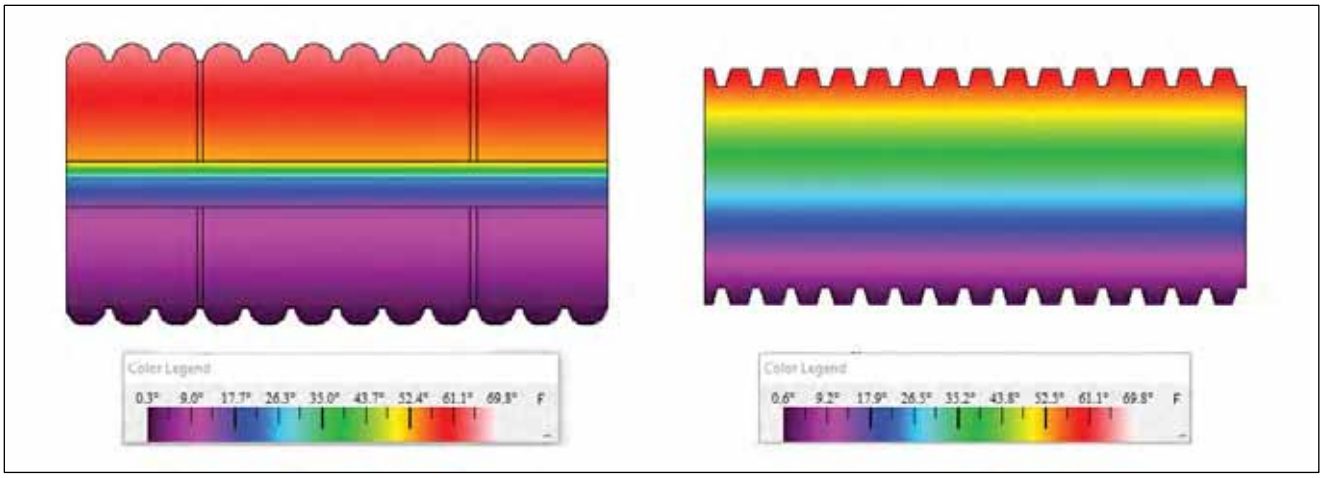


Figure 10: Thermal analysis demonstrates temperature gradients based on 70° F interior and 0° F exterior conditions in winter for the original design of cavity wall with custom fluted CMU and insulation (left) vs. revised design of monolithic cast-in-place reinforced concrete (right). Drawings by the author.

CONCLUSION

It is clear that Rudolph's original intent to use an insulated cavity wall would have provided more robust thermal insulation than the as-built cast-in-place wall. Would such a difference have impacted the building's longevity? It is of course impossible to know with certainty, but such an outcome seems at least possible considering that heating costs were cited as the building's fatal flaw. Of the two main components of the building envelope—roof and walls—the roof's lack of sufficient insulation could have most easily been remediated with additional layers of rigid foam. The single-pane glazing used throughout the building could have been replaced by insulating glass, albeit at significant cost. Technically, it would have been possible to consider various retrofit options for the concrete facades as well that could have improved the overall thermal performance of the envelope. These range from the extreme and expensive (removing and reconstructing the concrete walls with internal insulation, for example) to more realistic options such as adding an internal layer of insulation to the existing concrete walls, covered by a new interior finish of gypsum board or other material. However, while such an approach would improve the R-value, it would have destroyed the architectural integrity of Rudolph's building, which placed such emphasis on the materiality of corrugated concrete forming nearly all of the interior and exterior surfaces. There is no evidence that any such retrofit options were seriously considered by the owners of the building, which suggests that its fate was sealed by other factors such as the loss of population in the student organization and the value of the land for other development purposes.

The history of the Christian Science Building presents a cautionary tale about the importance of thermal performance of building envelopes, the consideration of construction vs. operating costs, and the potential issues facing the preservation of 20th-century modern architecture. As expectations for energy performance continue to rise, strategies for mitigating the

inherent deficiencies of decades-old building-envelope technologies will continue to be a challenge for owners, architects, and preservationists.

REFERENCES

2015 International Energy Conservation Code (IECC). International Code Council, 2014.

"An Architecture Strongly Manipulated in Space and Scale." Architectural Record 141:2 (1967): 137-142.

Bruegmann, Robert. "Interview with Paul Rudolph." Compiled under the auspices of the Chicago Architects Oral History Project, Department of Architecture, The Art Institute of Chicago, 1986.

Futagawa, Yukio, ed. Paul Rudolph: Architectural Drawings. Architectural Book Publishing, 1972.

Miller, Nory. "Rudolph's Rich Molding of Space." Inland Architect 17:9 (1973): 18-19.

Moe, Kiel. Insulating Modernism: Isolated and Non-Isolated Thermodynamics in Architecture. Birkhauser, 2014.

Rohan, Timothy. The Architecture of Paul Rudolph. Yale University, 2014.

Rudolph, Paul. The Architecture of Paul Rudolph. Intro. by Sibyl Moholy-Nagy, captions by Gerhard Schwab. Praeger, 1970.

Rudolph, Paul. "Enigmas of Architecture," in Toshio Nakamura, ed., 100 by Paul Rudolph: 1946-74. A+U Publishing, 1977.

Rudolph, Paul. Writings on Architecture. Yale School of Architecture, 2008.

Soo, Lydia M., and Robert Ousterhout. "Has Functionalism Triumphed? The Destruction of Paul Rudolph's Christian Science Building." Reflections 4:1 (Fall 1986): 40-45.

RENEWING TWO SAARINEN ICONS

The 1955 MIT Chapel window wall and Kresge curtainwall



David N. Fixler, FAIA
David Fixler Architecture Planning Preservation
david@davidfixler.com



Gary Tondorf-Dick, AIA, LEED AP
Massachusetts Institute Of Technology
gtd@mit.edu



Katherine S. Wissink, PE
Simpson Gumpertz & Heger, Inc.
kswissink@sgh.com



Matthew B. Bronski, PE
Simpson Gumpertz & Heger, Inc.
mbbronski@sgh.com

ABSTRACT

Kresge Auditorium and the MIT Chapel, designed by Eero Saarinen and built in 1955, are both world renowned works of architecture and powerful symbols of MIT's commitment in the post-war era to the creation of a humanistic campus community to complement and enhance their status as one of the world's great technical universities. Conceived as simple, powerful and expressive geometric forms, Kresge and the Chapel each feature an unusual, custom-designed curtainwall (Kresge) and window wall (Chapel) that are character-defining features of these iconic works of mid-century modernist architecture.

In planning a comprehensive renewal of the two landmark buildings, MIT sought to preserve and maintain the iconic Saarinen designs, while also addressing deterioration, fundamental shortcomings, and improving performance. While the comprehensive renewal project included many interior and exterior materials and systems, this paper focuses on the curtainwall and window wall. The success of the project was due in large part to the highly collaborative, integrated design assist process with MIT, the general contractor, four curtainwall/ glazing/stained glass subcontractors, architect, structural, envelope and MEP FP engineers all collaborating from early mock-ups, prototypes, and testing, through final design, shop drawings, construction, and punchlisting.

Both designs retained key components of the original fabric, such as the steel support structure at Kresge and the original German art glass at Chapel, while replacing worn and deteriorated aluminum or steel components sections with laser welded stainless steel. On Kresge, our design optimized both performance and historic appearance by replacing annealed monolithic glazing with high-performing laminated glass with a low e coating, while on the Chapel our design laminated the German art glass to improve its resistance to breakage (a recurrent problem), and also improve life safety. Overall, our

collaborative design and construction process developed an optimal solution through sympathetic, technical improvements to solve original problems, as well as evolutionary upgrades that balanced the demands of historic preservation and high-performance design.

KEYWORDS

curtainwall, case study, glass, modernist, restoration, structure

INTRODUCTION

Kresge Auditorium and the MIT Chapel, designed by Eero Saarinen and built in 1955, are both world renowned works of architecture and powerful symbols of MIT's commitment in the post-war era to the creation of a humanistic campus community to complement and enhance their status as one of the world's great technical universities. Conceived as simple, powerful and expressive geometric forms, Kresge and the Chapel are significant both as prominent milestones in the development of Saarinen's illustrious career, and further evidence of MIT's embrace of modern architecture at the highest level – complementing Alvar Aalto's adjacent Baker House, completed in 1949. They are also critical components in the daily life of MIT and create, through the nature of their programs, strong connections to the metropolitan community and the world at large.

Saarinen was fundamentally an expressionist, constantly testing and expanding the parameters of modern architecture, eschewing formulas, and seeking innovative, program and site-specific design solutions to a given problem. For MIT, he imagined a dynamic play of the primal geometries that impart a crisp, minimal nature to both the two buildings and their precinct. The Kresge Auditorium structure pushes the capabilities of an uninterrupted thin-shelled concrete design in the form of 1/8ᵗʰ of a sphere, resting only on three point supports, to the limits of available technology. The three resultant facades are clad entirely in metal and glass curtainwall scribed in plan and section to the arc of the dome, which is clad in a copper standing seam roof that though not original, has nonetheless become an important (and effective) character defining element of the design. The structural supports also define the circle of the surrounding plaza, and the brick pavers extend directly into the lobby. The form of the rising auditorium is expressed in the walls of the lobby. The interior of the hall is lined with vertical finely spaced natural finish oak slats in the contemporary Scandinavian manner, with only an acoustic cloud overhead partially concealing the exposed shell above.

The curtainwall members have a unique profile that was both innovative and problematic, and they had reached the end of their service life. However, as they are arguably the most important character defining features of the building, developing the best possible rehabilitation scenario – that maintains the appearance of the iconic original design, yet mitigates its problems – was of paramount importance to the success of the renovation.

The Chapel is a windowless brick cylinder set over an undulating concrete base. It is entered through a low, single-story entry lobby fully glazed with leaded German art glass that is both textured and "seeded" (includes seed-sized air bubbles) set in a steel window wall system. The floor is travertine in an elongated diamond pattern and the ceiling is the painted concrete structural slab, with a shallow wood slat cloud containing downlights. The floor continues into the cylindrical Sanctuary, whose walls are the same water-struck brick articulated with protruding clinker brick as the exterior but built in an undulating pattern designed to control reverberation in the hall, and to allow for horizontal glazing strips to infill the gaps between the inner and outer walls, washing the walls with reflected light from the moat below. The ceiling is acoustic plaster with an aluminum egg-crate grill screening the skylight over the altar.

The delicacy and quality of light imparted by the art glass in the steel frames in the Chapel lobby is essential in creating the transition between the outside world and the otherworldly space of the sanctuary. After 60 years MIT's charge was to address the deterioration of the system in a manner that would enhance and protect the quality and durability of the glass and the entire assembly.



Figure 1: Early view of the Kresge Auditorium (left) and MIT Chapel (right). Archival photo taken shortly after completion of the original construction c. 1955.

OVERALL APPROACH TO AND OBJECTIVES FOR THE PROJECT

OVERVIEW

MIT has undertaken an intensive Capital Renewal Campaign and Program that began in 1996 with the rehabilitation of Alvar Aalto's Baker House, in which many iconic campus buildings have been or are in process of significant restoration in conjunction with programmatic upgrades, including renovation of the original 1916 Campus Main Group Buildings, as well as restoration of the MIT's significant modern buildings. From 2013-2016, MIT undertook a renovation of both Kresge Auditorium and the MIT Chapel to address sixty years of weathering and deterioration. The rehabilitation of these structures are important examples of this renewal process in which 21st Century design and construction craft and technologies are being utilized to restore and enhance these important mid-20th century buildings.

KRESGE AUDITORIUM

The scope of work for Kresge Auditorium, a venue for events, classes, and performances, included a curtainwall renewal, concrete and steel repairs, repairs to and partial replacement of the standing seam copper roofing, and mechanical upgrades.

Challenging technical issues and procurement procedures were addressed in the renewal, and a Design Assist process was implemented to fit within a larger, collaboratively developed stewardship plan designed to restore and enhance Saarinen's vision. As MIT discovered in implementing the restoration of the 1916 MIT Main Group buildings, the traditional Design-Bid-Build process was not seen as appropriate for the restoration of unique structures built in a very different time, with components and details uncommon today. The successful restoration of Kresge and the MIT Chapel could not have been

achieved without the forging of this successful process for working in a collaborative, integrated design assist process with MIT, the general contractor, two curtainwall/glass/glazing subcontractors, architect, structural, envelope and MEP FP engineers.

This resulted in a seamless team approach to undertake the renovation and restoration of these two technologically unique, significant buildings while protecting their architectural and structural integrity and achieving desired performance goals. This is in line with MIT's Capital Renewal goals and objectives, which mandate that renovations to all Campus buildings must achieve both performance enhancement and program goals beyond those that might normally be expected in a traditional "white-glove" restoration.

Of particular interest are the glazing solutions for both buildings. Each step of the process involved meticulous planning and multiple, iterative design exercises. The team's goal in renewing the Kresge curtainwall was to maintain and restore the original appearance, but with an improvement in the durability, detailing and performance of the system. The team developed a structural and building enclosure renewal scheme for the curtainwall of Kresge Auditorium that improves life safety issues, durability, and energy efficiency, while respecting the original design and profiles, as further described below.

MIT CHAPEL

The scope of work for the Chapel, a nondenominational space for worship and gathering, included masonry repairs, reconstruction of the leaded glass window wall, roofing replacement, skylight refurbishment, restoration of the aluminum spire, fall protection, moat replacement, and mechanical upgrades.

The scope of work for the Chapel's failed and leaking concrete moat included reconstructing the structural slab-on-grade, installing a waterproof liner (where one had been included in the original design, but never constructed), and constructing a topping slab to recreate the original configuration, texture and exposed aggregate concrete finish of the original moat. A new filtration system was installed to provide minimal movement for the water, preventing stagnation and organic growth. This work restored the beauty and function of the moat, which reflects a soft secondary light up through concealed glazing slots to rake and dapple the interior brick walls of the sanctuary with subtle, indirect natural light.

During the renewal, the Chapel's stained-glass window walls were rebuilt with a new frame, while conserving and strengthening the original art glass. The project team worked carefully with design and fabrication specialists, including glass restoration artisans, to restore the full material palette of the building. On the window wall, this meant a careful reconstruction of the original window wall framing in painted stainless steel to match the original design, and a refurbished glazing scheme that married hand blown restoration glass from Leipzig, Germany to the original German art glass.

RENEWAL AND RESTORATION

Renewal and restoration of both of these iconic buildings required collaborative teamwork between architects, engineers, contractors, fabricators, installers and artists. In the end MIT received updated facilities with almost no perceptible difference in appearance – except to correct unsympathetic later interventions – but with substantial upgrades in material durability and performance.

ASSESSMENT OF EXISTING CONDITIONS

KRESGE AUDITORIUM CURTAINWALL

The original curtainwall construction consisted of an interior steel frame supporting an exterior glazing system of aluminum and glass (Fig. 2). The glazing frame was constructed primarily of thin aluminum members resulting in narrow sight lines. The tee-shaped horizontal glazing frame members (Fig. 3), transferred wind and gravity loads from the glass to the aluminum vertical glazing frame members which transferred the loads to the interior steel frame. The vertical glazing frame members were originally constructed of two Z-shaped pieces held to the interior steel frame with an exposed steel pressure bar (Fig. 4). The original glazing was 1/8 in. thick annealed glass.

The interior steel frame originally supported both the wind and gravity loads of the exterior glazing system. The interior steel frame was constructed of vertical bar mullions located at each vertical glazing frame member. These vertical mullions connect to horizontal wind girts. The wind girts, in turn, span between vertical wind posts which carry the wind loads to the shell and to a bottom channel member that was integral with the floor slab. Diagonal rods brace the weak axis of the vertical

wind posts (Fig. 5). During the original construction, three steel “crutch” posts, each with a rectangular cross section, were added near the center of each of the facades, during construction, as permanent shoring to limit unexpected deflections of the shell observed when the formwork was removed during the original construction.

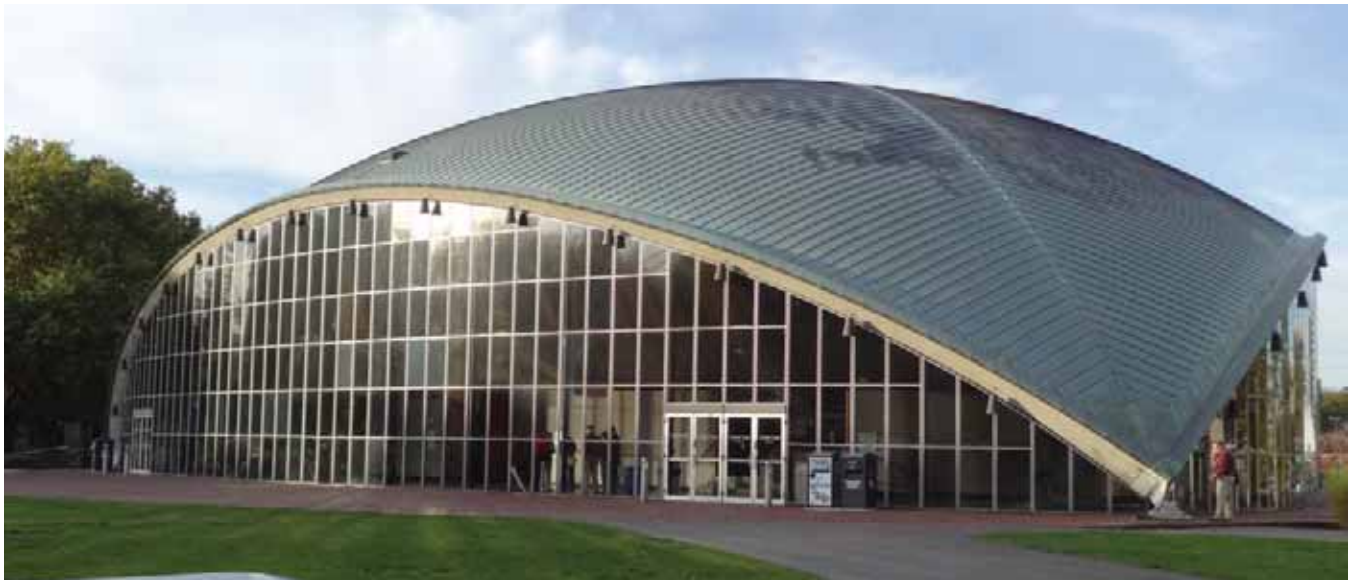


Figure 2: Kresge Auditorium prior to renewal.

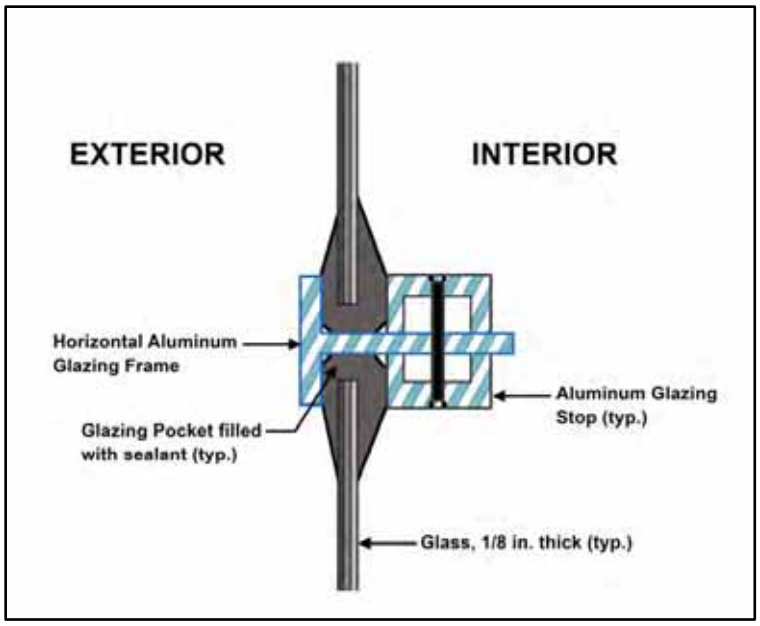


Figure 3: Kresge Auditorium’s horizontal glazing frame members, with terminology adopted by the restoration design team.

Figure generated from Kresge Auditorium original construction drawings and built condition.

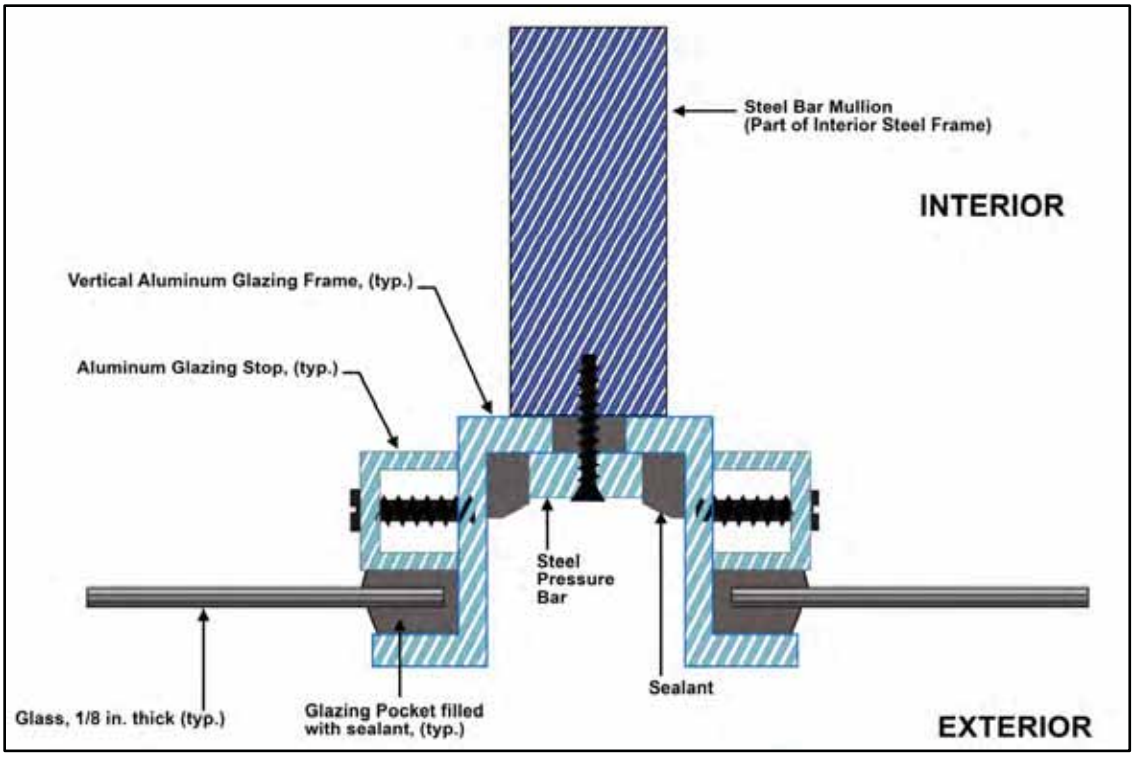


Figure 4: Kresge Auditorium's vertical glazing frame members, with terminology adopted by the restoration design team. Figure generated from Kresge Auditorium original construction drawings and built conditions. Note that the bar mullion is part of the interior steel frame and not the exterior glazing frame.

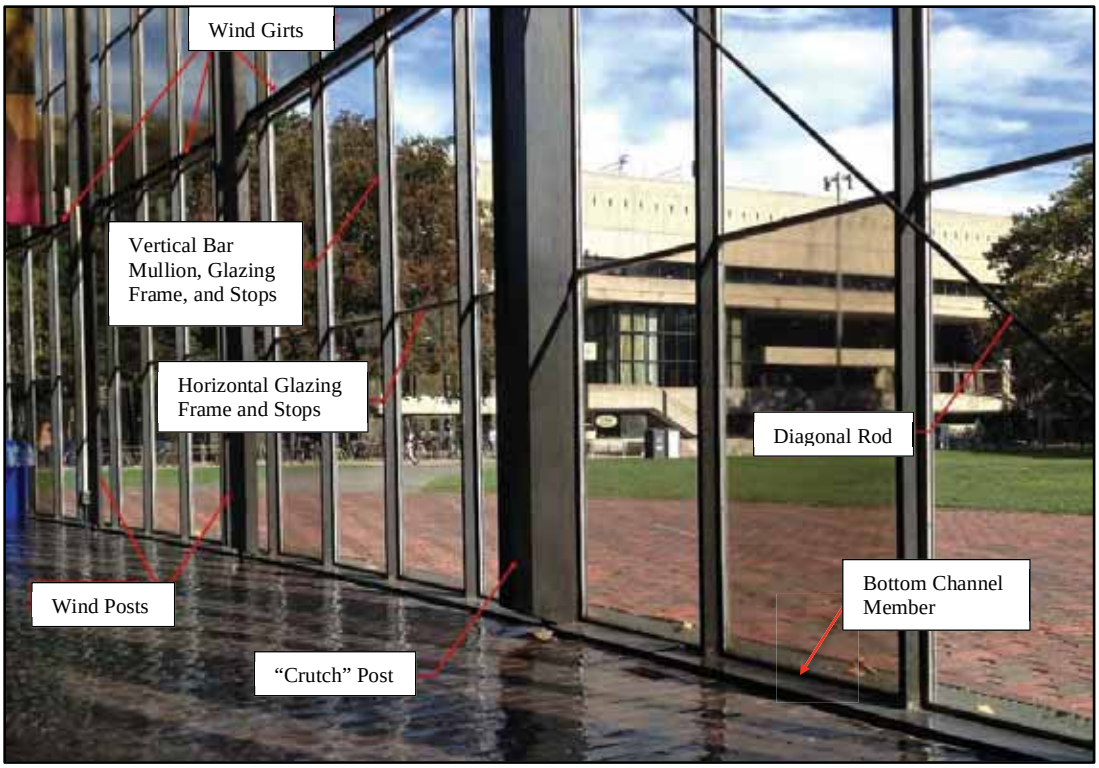


Figure 5: Terminology used by the Kresge Auditorium's restoration design team for the interior steel frame.

The original exterior glazing system was a source of chronic leakage, with the most prominent leakage path being between the two Z-shaped pieces that made up the vertical glazing frame (Fig. 3). Saarinen's original design details showed copious amounts of sealant at this location, bulging out from the pressure bar, nevertheless, leakage persisted. Subsequent attempts

at re-sealing or over-sealing the curtainwall with were also unsuccessful at stopping the leakage. As a result of the continued leakage, over time the interior steel frame exhibited localized areas of corrosion, mostly at the bottom channel member, and mostly superficial. Unrelated to leakage, the bottom channel member at and near doors exhibited more significant corrosion and section loss from sixty years of deicing salts. Also unrelated to leakage, the exterior trench drain at the base of the curtainwall was severely corroded and deteriorated with displaced and missing grates, and with heavy rust on the exposed steel member below the curtainwall that supported the grates.

The main structure of the Kresge Auditorium consists of a thin concrete shell that is only 3-1/2 inches over most of the shell, with the outer 4-foot wide strip along each of the three shell edges thickened to 5-1/2 inches, and with an integral 20-inch deep by 10-1/2-inch wide edge beam along each shell edge. The shell is approximately triangular in plan and is supported at grade by three massive concrete buttresses, one at each corner, that are mostly below grade, but extend slightly above grade to connect to the corner of the shell (Fig. 2). Differential movement between the concrete shell and the exterior glazing system from live loads, snow loads, and thermal expansion/contraction was accommodated in the original design by the installation of two continuous, nested steel angles running between the top of the curtainwall and the underside of the concrete edge beam. The top steel angle is installed tight to the concrete; the lower angle is at the top of the curtainwall. The angles are connected with bolts in vertically slotted holes that allow vertical movement but restrict lateral movement. While this detail appears to have performed as intended structurally, we identified the gap between the two angles as a source of leakage, particularly at discontinuities in the angles where straight sections were butted to approximate the curve of the thin shell concrete roof directly above.

MIT CHAPEL WINDOW WALL

The original window wall consisted of a painted steel frame with single pane leaded glass (aka “stained glass”) (Fig. 6). The leaded glass was originally set in glazing putty in the glazing pocket of the steel frame (Fig. 7). The original window wall suffered from chronic leakage through the glazing putty in the glazing pocket. As a result, the steel window wall members exhibited heavy corrosion in some areas, particularly at the sill, which had caused some members to buckle or displace. Additionally, the window wall frame appeared to be deformed in plan in a zig-zag manner, similar to an accordion, the result of unaccommodated, restrained, in-plane thermal expansion of the metal window wall. The original designers had thoughtfully provided a narrow vertical expansion joint concealed behind each vertical mullion to accommodate in-plane thermal expansion, but the detail appears not to have been effective because the screws that penetrated through the narrow expansion joint were threaded for their full length, “biting” (engaging) the steel on each side of the expansion joint – thus the screws prevented the joint from either opening or closing with thermal movement. The bottom sub-sill member of the window wall is a concealed Z-shaped sub-sill support piece that extends below the edge of the interior travertine floor tile and was secured to the concrete floor slab with relatively few widely spaced fasteners. Consequently, in the approximately 3-foot long spaces between fasteners, this lower leg of this sub-sill member had rotated upward and caused the overlying travertine floor tile directly above to crack.



Figure 6: MIT Chapel window wall prior to renewal.

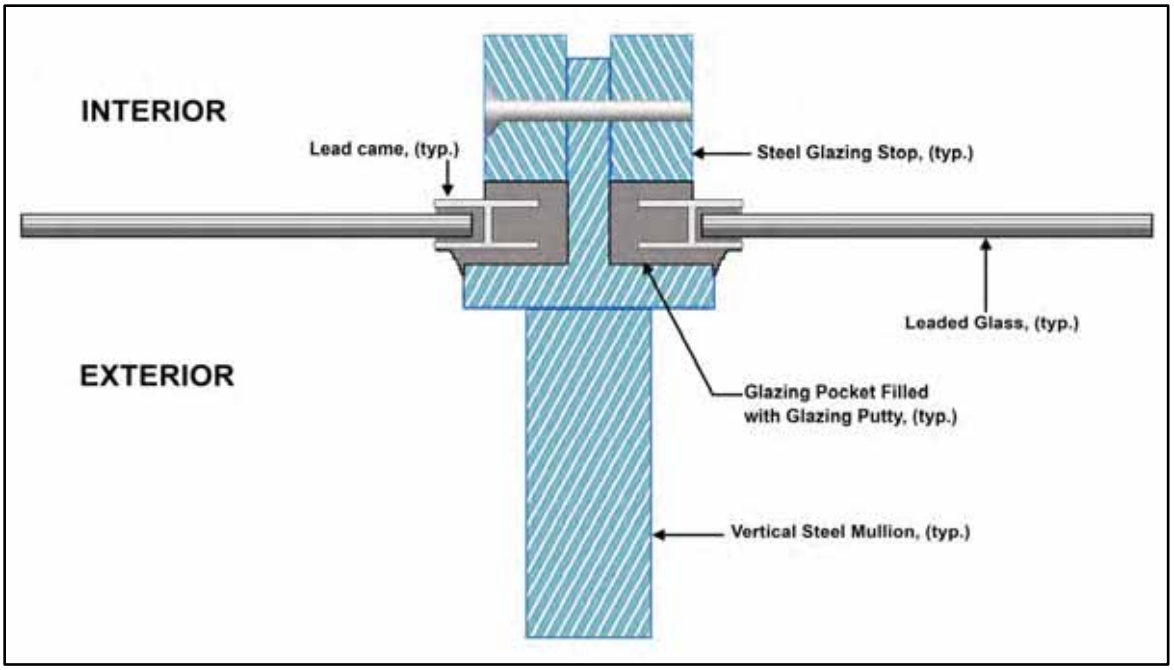


Figure 7: MIT Chapel's vertical members of the window wall frame. Figure generated from MIT Chapel original construction drawings and built condition.

DESIGN

KRESGE AUDITORIUM CURTAINWALL

Evaluation of the existing curtainwall was based on the following considerations to determine if it could be repaired in-kind, or if it had to be replaced in its entirety, or if the best approach was something between these options.

- **Occupant and Public Safety:** The original glass in the curtainwall consisted of 1/8 in. thick annealed (non-safety) glass. This presented risks to public safety as a potential falling object hazard from broken glass caused by activities such as students playing Frisbee and ball games in the grass field in front of the building. In addition, this presented a risk to public safety as a potential fall-through hazard as the non-safety glass extended to grade. The lack of laminated glass also posed both a security concern and a climate control concern when accidental breaks did occur.
- **Air and water leakage:** The curtainwall suffered from chronic water leakage for years caused by deteriorated sealant joints in the surface-sealed system and vulnerabilities in the design of the glazing attachment. Despite the deteriorated sealant joints, air leakage through the curtainwall was a less pressing issue since all the lites are fixed and sealed.
- **Occupant Comfort/Thermal Efficiency**: The original curtainwall felt cold in the winter, and the clear glass allowed excessive solar heat gain in the summer. In an effort to reduce the solar heat gain, a previous retrofit added a film to the interior of the glass lites above eye level. In addition, at some time after the original construction, the glass at the backstage areas was replaced with metal panels to better control undesired and distracting backlighting of the backstage area in the auditorium during performances.
- **Structural Adequacy**: We did not observe any apparent structural deficiency of the interior steel frame of the curtainwall. The supporting interior steel frame had some surface rusting but was overall in good condition. One exception was the more extensive corrosion of the bottom channel member at and near doorways, attributable to the winter use of deicing salts.
- **Material degradation**: The aluminum components of the exterior glazing system were generally in fair condition except for some pitting of the aluminum, especially near grade. Sealants in the exterior glazing system were typically failed. The exterior steel pressure bar, and the grate and supporting angle at the perimeter trench drain along the exterior base of the curtainwall were rusted and in disrepair.

Based on these considerations, the restoration design team determined that the existing interior steel frame had minimal corrosion or deterioration and could be reused and rehabilitated in-place, that the exterior glazing frame components would need to be replaced to address pitting and deterioration, and that the interior and exterior seals and gaskets would need to be replaced to address water leakage issues. Furthermore, it was obvious that the replacement system should include laminated safety glass to address the occupant and public safety concerns noted above. The laminated glass also allowed

for the inclusion of a low-e coating on the #2 surface of the laminated surface of the glass which would help improve thermal efficiency. However, the change of the glass from 1/8 in. thick monolithic annealed glass to thicker, laminated glass more than doubled the weight of the glass, triggering a code-mandated structural review of the system as a whole.

A structural analysis model was created of the existing interior steel frame with the higher dead loads (from the proposed thicker laminated glass) and current code-prescribed wind loads. The increase in the dead loads triggered provisions of the International Existing Building Code which required evaluating the retrofitted system with the wind loads of the current building code for new construction. The 36 psf wind pressures of the current code were more than triple the 10 psf pressures used in the original design. Not surprisingly, the structural analysis revealed that many of the existing interior steel framing members (specifically the wind girts and wind posts) were overstressed under the new loads (Fig. 8). The overstressed wind posts were acting as beam-columns that carried both the vertical gravity loads of the exterior glazing system, as well as the lateral loads from wind. A common solution to solve this overstress problem but generally maintain the appearance of the structure would have been to strengthen the existing structural steel members by extending (e.g., making deeper) their existing rectangular cross sections. This is typically done by welding the required steel extensions to the posts and girts, then grinding smooth and painting the welded joints to conceal the alteration. While such an approach is often considered aesthetically acceptable, we thought the resulting deeper, bulkier members would have compromised the aesthetic of the visual lightness and slenderness of the original steel frame and marred the way light and views were experienced from the inside and the outside of the lobby. To prevent such an outcome, the structural scheme and load paths of the curtainwall was creatively changed by engaging the replacement vertical glazing frame to work as a mini column. The column consisted of the hat-shaped glazing frame supporting the gravity loads of the glass and transferring them down to the bottom channel member and floor slab. The proportions of the new column cross section were verified for their structural adequacy; its slenderness was limited by laterally bracing the column back to the steel frame with details that transfer only wind loads to the steel frame. To ensure that gravity loads were not transferred to the interior steel frame, the new vertical glazing frame was designed to connect to the bar mullion of the interior steel frame with vertically slotted holes at the fasteners. Removing the gravity loads from the interior steel frame not only eliminated the code triggers that would have required enlarging the cross sections of the steel, but also, without altering the original interior steel structure, increased the wind loads that the frame can resist, thereby providing a structural performance upgrade, albeit not to the full load that would have required by the current code had it been in effect.

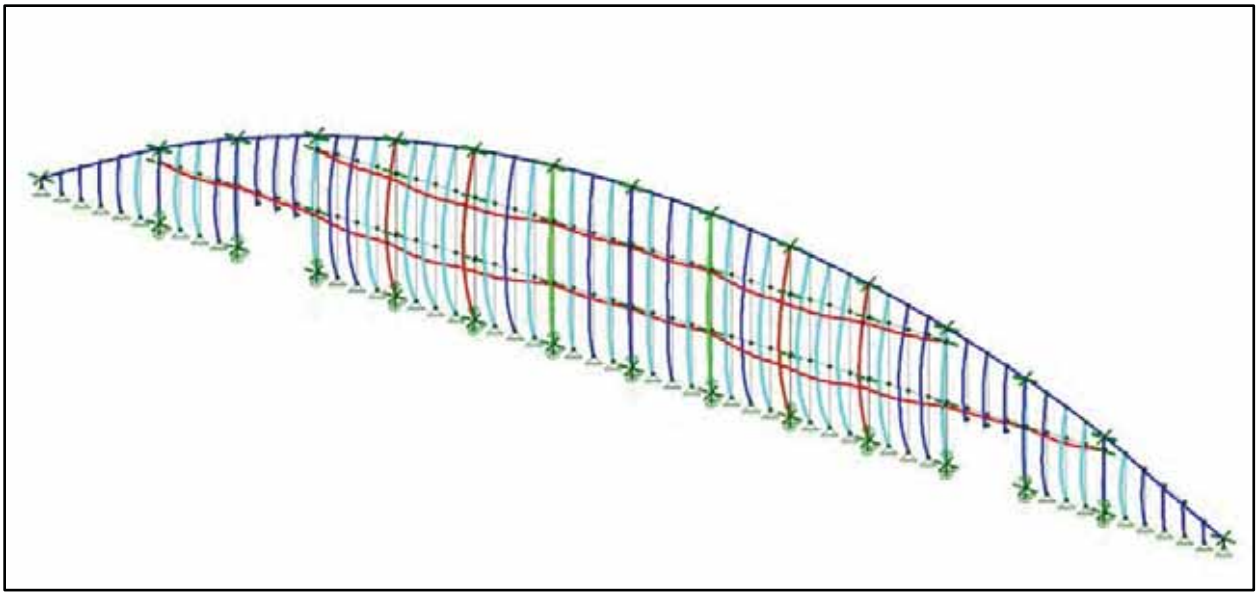


Figure 8: Structural analysis model image of the Kresge Auditorium's existing interior steel frame at the curtainwall with increased glazing dead load and current code-prescribed wind loads applied, but without the change to the gravity load path. Note the red members in the model, which indicate the members that would be overstressed.

To carry the gravity loads, the vertical glazing frame was changed from two adjacent L-shaped aluminum pieces to a single hat-shaped stainless steel piece, for greater strength and stiffness, which was needed to support the gravity loads, and also to eliminate the dissimilar metals "sandwich" of steel, aluminum, steel (exterior pressure bar, exterior vertical glazing frame,

interior frame) in the original design. An added benefit was that the lower thermal conductivity of stainless steel also helped improve the overall thermal performance of the envelope.

Another benefit of the one-piece vertical glazing frame member over the two-piece members of the original construction was better resistance to water leakage (one fewer joint at each vertical glazing frame member). Sealant was originally used between the two Z-shaped pieces, and the sealant lacked backer rod or release tape and was installed without optimal geometry for successful performance of the sealant joint. Hence, this sealant failed and was a primary leakage path. The pressure bar in the new glazing system is shaped like a small channel (instead of being a solid bar) to conceal the fasteners securing the vertical glazing frame members and is fastened to the vertical glazing frame members with separate offset fasteners. To help prevent water from penetrating below the pressure bar, the design included an adhered silicone sheet gasket between the pressure bar and the vertical glazing frame members (Fig. 9), which further increased the resistance to leakage at the vertical glazing frame members. The clamping action on the silicone sheet by the channel edges, creating compressed gasket edges, further enhances the waterproofing reliability of this joint and detail, the most significant source of leakage in the original system. The horizontal glazing members were stiffened to support the increased weight of the laminated glass by making the upper interior stop integral and monolithic with the horizontal glazing member (Fig. 10).

Like the original system, the new glazing system is surface sealed, and still relies on sealant between metal and glass to maintain air and water tightness. This was determined to be acceptable by the design team on this particular project because the interior materials and finishes adjacent to the curtainwall consist of painted rolled steel sections, and brick paving over a concrete floor slab, which are highly resistant to damage from incidental leakage or moisture. No highly moisture sensitive materials, such as gypsum board, batt insulation, or carpeting, occur at or near the curtainwall. In addition, even as the sealants age and weather, the improvements to the detailing and seals on the curtainwall, especially to the Achilles heel detail as described above, will significantly reduce the propensity for leakage that the curtainwall experienced for decades before the renewal, without adverse consequences to the interior materials or finishes.

In addition to the historic preservation, architectural, sustainability, and structural benefits; this solution also had cost and schedule benefits.

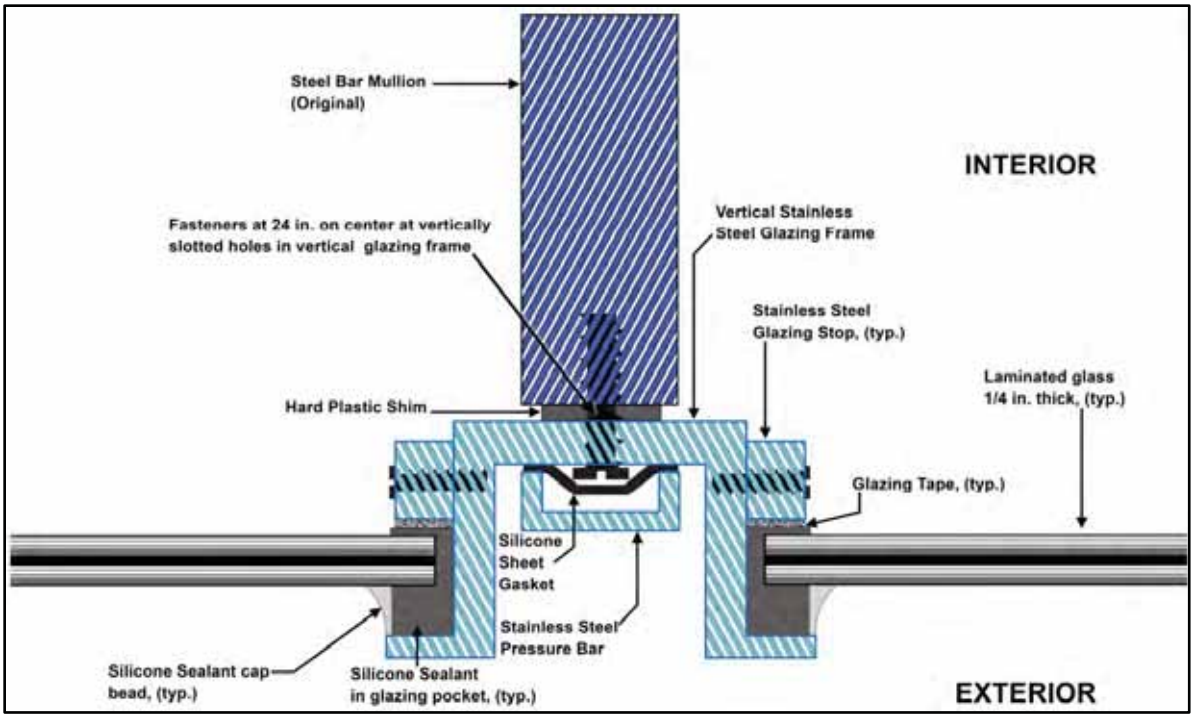


Figure 9: Kresge Auditorium's curtainwall vertical glazing member. Figure generated from Kresge Auditorium curtainwall renewal shop drawings.

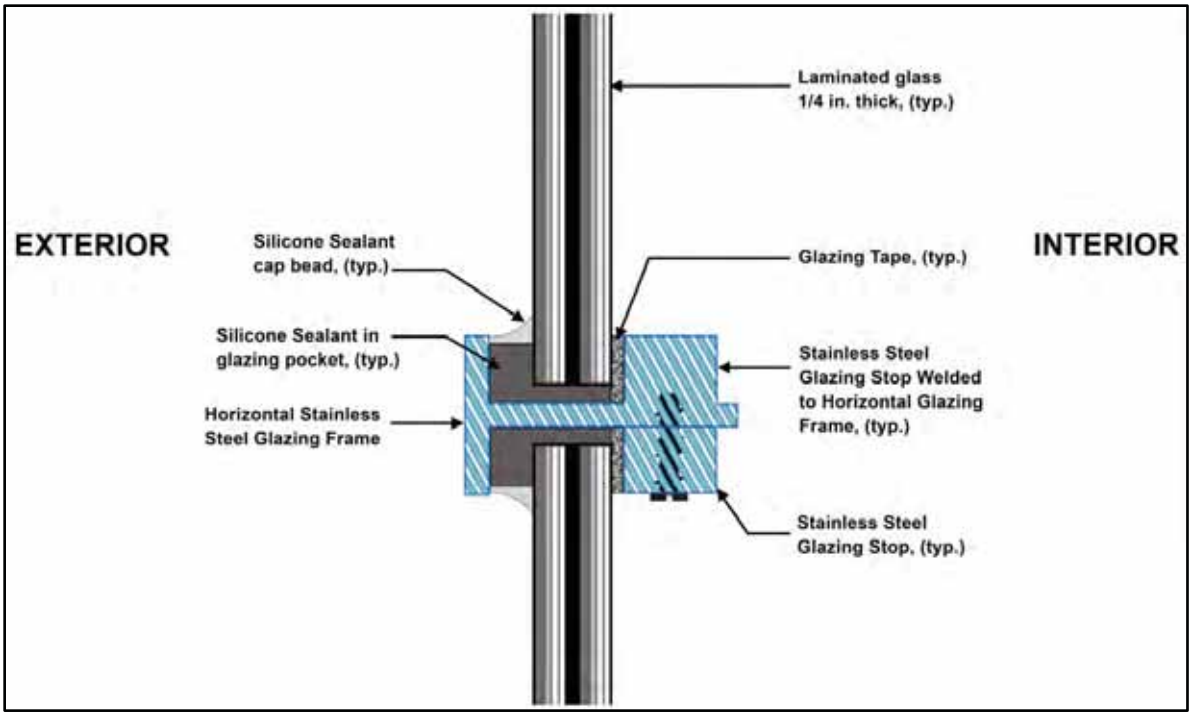


Figure 10: Kresge Auditorium's curtainwall horizontal glazing member. Figure generated from Kresge Auditorium curtainwall renewal shop drawings.

The design also addressed degraded materials at the base of the curtainwall by localized repair of corroded areas of the steel bottom channel near doors, and replacement of the exterior steel angle and grates at the exterior trench drain at the base of the curtainwall. The glazing system sill piece and the trench drain grates were originally constructed out of two separate pieces, however, we integrated these into a single stainless-steel piece that did the job of both. Finally, to mitigate leakage between the two angles at the top of the curtainwall and bottom of the concrete perimeter beam, a wept dual sealant joint was added (with a continuous inner seal and periodic sealant end dams and an outer seal with weeps upslope of the end dams).

MIT CHAPEL WINDOW WALL

The window wall frame was replaced with a new frame constructed of painted stainless steel. The new frame was constructed to closely replicate the appearance of the original frame, but the depth of the frame was increased slightly to accommodate thicker glass (Fig. 11). The original "seeded" German art glass was reused in the new window wall frame, but was laminated to clear seeded art glass, also from Germany, to improve safety and resistance to breakage from impact, which had been an ongoing problem give the floor to ceiling height of the window wall, the lack of a safety rail, and the frequent use of wheeled coat racks and folding tables in the space.

Like the curtainwall at the Kresge Auditorium, the window wall at the Chapel also is a surface-sealed system that, like the original, relies on surface seals for watertightness. Like the auditorium, the Chapel interior also has robust materials (painted rolled steel, travertine, and concrete) highly sensitive to moisture or incidental leakage, along the base of the window wall. Thus, the team accepted the inherent limitations of a surface-sealed system in this particular case, and sought performance improvements where possible, such as improved resistance to breakage as discussed above, and improved resistance to leakage and accommodation of thermal movement, as discussed below. To address the leakage path in the glazing pocket, the leaded glass panes were set in silicone sealant in the glazing pocket, and cap beads of silicone were installed between the leaded glass panels and the steel frames. To address the previous problems with unaccommodated in-plane thermal expansion, the design revision to the original narrow vertical expansion detail was relatively simple – the screws that crossed the joint were changed to a half-threaded screw that engaged the threads on only one side of the expansion joint, so that the expansion joint could open and close as designed, sliding past the smooth shank portion of the screw, without being restrained from moving by a fully threaded screw engaged on both sides of the joint, as had occurred in the original construction.

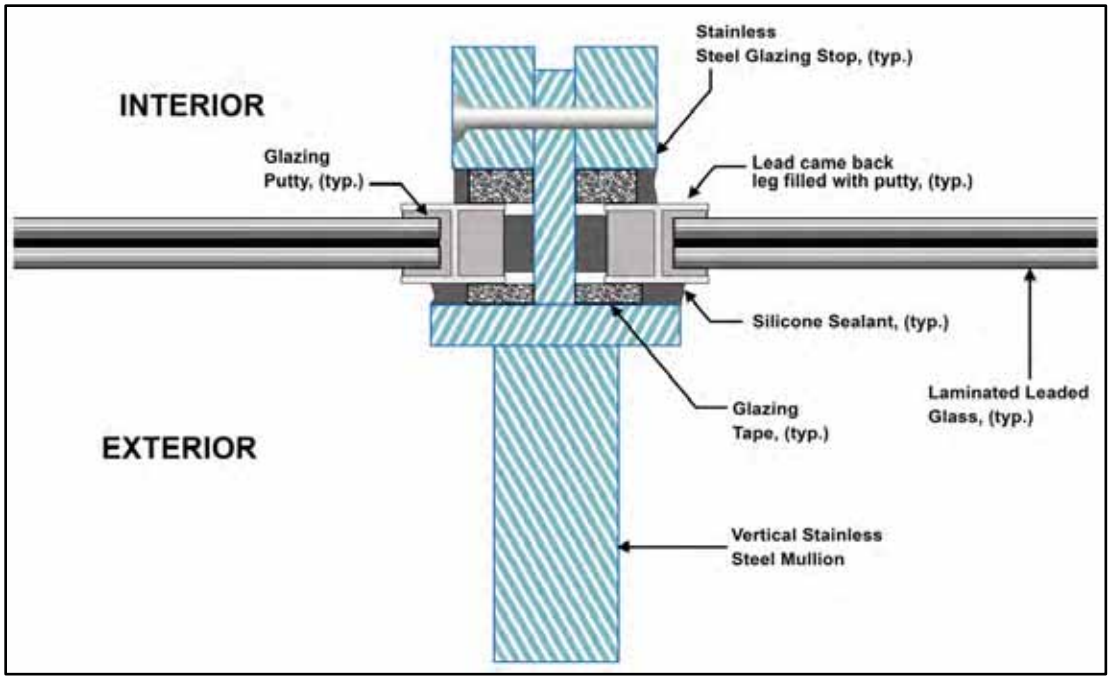


Figure 11: MIT Chapel's horizontal section through a vertical member of the window wall frame. Figure generated from MIT Chapel window wall renewal shop drawings.

FABRICATION AND CONSTRUCTION

KRESGE AUDITORIUM CURTAINWALL

As with most 50+ year old buildings, the individual as-built dimensions varied from those shown on the original drawings, which created a measurement, fabrication, and construction tolerance challenge in terms of replacing all of the glazing and some of the framing components, while retaining the main structural members to which they would need to be fitted in the field. The Contractor did a detailed laser survey of the entire curtain wall, including every lite and framing element on every elevation, prior to creating shop drawings. As a strategy for providing some regularized "knowns" to speed fabrication and erection, while also allowing for tolerance at each vertical bay to meet the existing dimensions at connections to the internal structural frame, the contractor rather cleverly decided to pre-assemble and pre-glaze every other vertical "ladder" section of the glazing system in the shop which helped maintain tighter control of the quality of the installation and reduced the contractor's time on site. The site-built vertical sections between the prefabricated sections provided the tolerance to meet the existing conditions and accommodate the existing variations in dimensions.

During the construction phase of the project, the contractor built a freestanding mockup of the replacement exterior glazing system, on which we performed air and water leakage testing. From the results of this testing, we identified the metal-to-metal joint between the horizontal and vertical glazing system members as a leakage path (Fig. 12). The design team discussed options for improving watertightness of this metal-to-metal joint. The contractor provided an aesthetic mockup of each of the options discussed. In the end, the restoration design team agreed that a concealed continuity seal would be added at the joint between the horizontal and vertical glazing frame members to help seal small gaps in the metal-to-metal joint. The horizontal glazing frame members were notched at the ends to accommodate the continuity seal that was installed after the exterior glazing frame was assembled.

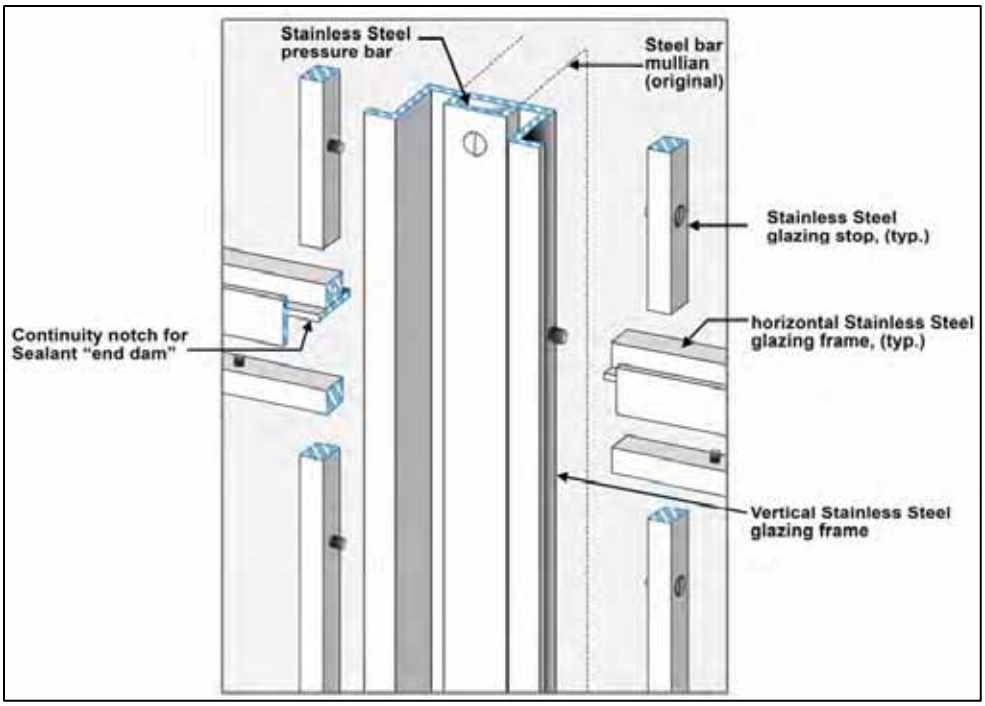


Figure 12: Exploded, exterior isometric view of the Kresge Auditorium's juncture between the vertical glazing frame and the horizontal glazing frame. Detail generated from Kresge Auditorium curtainwall renewal shop drawings.

The stainless-steel members of the new exterior glazing system were specially fabricated out of bar stock material and laser welded together to create the unique shapes required and to provide sharp corners and crisp edges to replicate the original extruded aluminum sections. A finishing technique was selected for the stainless steel, through samples and mock-ups, to replicate the duller metallic sheen of the original aluminum sections. While construction was still in progress, but after much of the new exterior glazing system was fully installed, we observed leakage at the exterior glazing system following a severe rain event. Through targeted water testing in the area of observed leakage, we identified the following sources of leaks:

- Deficiencies in the wet-seals (between the glass and the exterior glazing frame)
- Deficiencies in the continuity seals
- Deficiencies in the dual sealant joint between the double angles at the top of the curtainwall
- Field-drilled fastener holes for attachment of the interior glazing stops that inadvertently penetrated all the way through the vertical glazing frame member (rather than part way through, as called for on the design and shop drawings).

At the request of MIT, we performed water testing on 100% of the installed curtainwall to identify and punch list all leaks so that they could be repaired by the contractor. After the contractor repaired each leak, we retested each area to make sure leakage was stopped. After multiple rounds of water testing and punch listing, the team collectively turned over a curtainwall to MIT that was tested over 100% of the exterior surface and had no leaks.



Figure 13: View of Kresge Auditorium after completion of the renewal project, with the exterior wall and moat of the MIT Chapel in the left foreground.

MIT CHAPEL WINDOW WALL

Similarly, the new stainless-steel frame at the chapel window wall was constructed to replicate the appearance of the original mild steel frame. Sections of the stainless-steel frame were assembled in the contractor's shop and installed in the field with joints between the frame sections designed to accommodate thermal expansion of the frame members. After the frame was installed, the leaded glass panels containing newly laminated original seeded German art glass were installed in the frame (Fig. 14). The window wall system, similar to the exterior glazing system at Kresge Auditorium, relies on surface seals between the leaded glass and the stainless-steel frame to be water tight. In addition, it relies on the continuity and bond of the glazing putty at the leaded glass to be water tight. Following a severe rain event, we observed leakage on the floor below

the window wall. Through water testing of 100% of the installed window wall, we identified several locations where water penetrated the glazing putty of the leaded glass and leaked to the interior. To mitigate this leakage path, a cap bead of clear silicone sealant was added between the lead cames and the glass.

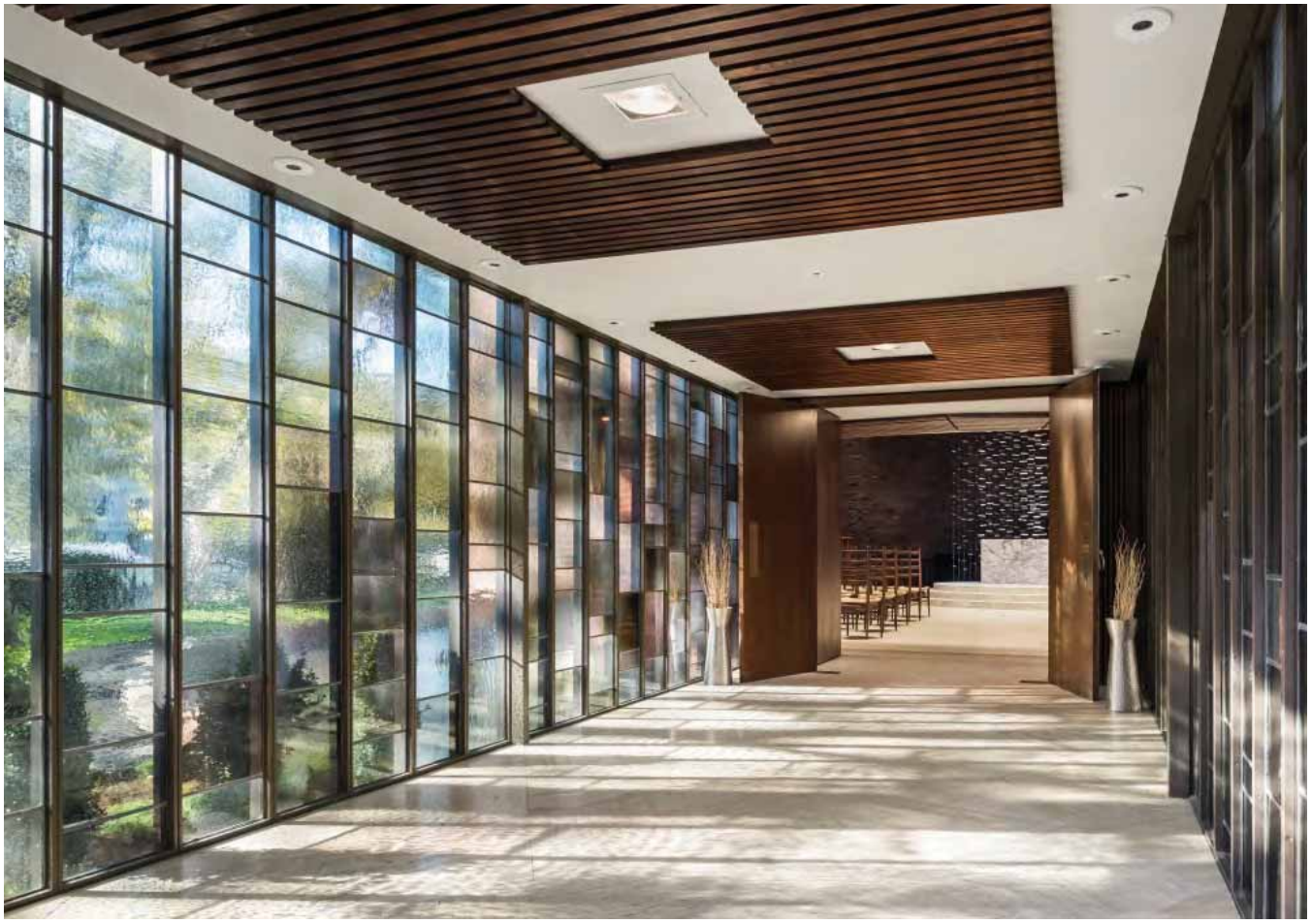


Figure 14: Interior view of the MIT Chapel window wall after renewal, in the narthex space that bridges over the moat, with the Chapel's sanctuary visible through the doors in the background.

CONCLUSION AND FUTURE WORK

The project addresses many of the issues that confront working with mid-century modern structures. Although our project was extremely exacting, and the profiles and materials highly unusual, the general challenges we faced regarding the need to balance historic considerations and respect for the original design and appearance with the bona fide need to mitigate chronic problems and improve deficient performance are universal to almost any rehabilitation or renewal of a historically significant curtain wall, window wall, or fenestration system. Thus, rather than being viewed as an esoteric anomaly of a case study, instead our project should be viewed as evidence that a good balance can be achieved between these two realms (historic respect, and improved performance), in even the most unusual and challenging cases.

The renewal of both the Kresge curtainwall and the Chapel narthex window wall build upon tested developments in enhancing the durability and performance of the curtain and window wall systems that were used in important modern buildings of the 1950 and early '60s. These have increasingly included the use of high performance laminated glass as a reasonable way to improve performance within the depth of existing glazing pockets, without the added bulk or depth of insulating glass units. It is hoped that further development of the interlayers in laminated glass can further enhance its performance and enable its future use in a broader range of applications.

More broadly, it is important to understand that these are heavily used "workhorse" structures still serving their original functions, not museums, and that the charge was to stabilize and enhance performance and functionality, with virtually no

visual change to their historic appearance. While these buildings are in many ways unique, the work does speak to and illustrate success with the more general necessity to balance conservation of original materials and systems with performance enhancement. The interventions to achieve this renewal - include retaining some original elements where prudent, in combination with replacing other original elements where critical – provide a paradigm for ensuring the continued vitality and viability of allegedly “technically outdated” mid-century modernist buildings and fenestration systems. In doing so, it is necessary to carefully design, prototype, mock-up and test proposed solutions to ensure that they meet team expectations for both performance and appearance. Perhaps therein lies our greatest assertion – significant improvements to building performance are possible, even with highly unusual or “outdated” mid-century modernist fenestration systems, without altering the historic character of a building. The success of our project underscores as well the significant mandate that historic structures, and indeed any existing building, share with new construction for improving energy performance in the 21st century.

ACKNOWLEDGMENTS

Renewal and restoration of both iconic buildings required collaborative teamwork between the owner, architects, engineers, contractors, fabricators, installers and artists. In the end MIT received updated facilities with almost no perceptible difference in appearance – except to correct unsympathetic later interventions – which in this case is exactly what was desired.

MIT would like to credit and acknowledge the excellence of the entire Kresge Auditorium and Chapel Project teams.

Design (for both Kresge Auditorium and MIT Chapel)
Architect, MEP & Fire Protection Engineer: EYP Architecture and Engineering, Inc.
Structural and Envelope Engineers: Simpson Gumpertz & Heger, Inc.
Landscape Architect: Reed Hildebrand, Inc.
Civil Engineers: Vanesse Hangen Brustlin, Inc.
Acoustic Consultant: Acentech, Inc.

Construction (as listed):
General Contractor, Kresge Auditorium and MIT Chapel: Lee Kennedy Company, Inc.
Glazing Contractor, Kresge Auditorium: Salem Glass Company
Curtainwall Engineering and Fabrication, Kresge Auditorium: Bellwether Design Technologies
Glazing Contractor, MIT Chapel: Karas & Karas Glass Company, Inc.
Stained Glass Restoration, MIT Chapel: Lynn Hovey Stained Glass Studio

REFERENCES

For a more detailed discussion of a similar process to evaluate and select a performance-enhancing replacement glazing system for an historic modernist curtainwall or window wall system, see:

Fixler, David, and Davis, Aaron. “Louis Kahn’s Stainless Steel Glazing System; Performance Upgrades in the Richards Building.” Proceedings of the Façade Tectonics Institute World Congress, 2016.

RETROFIT OPTIONS FOR HISTORIC FACADES

Analysis and design of coil drapery catcher systems



Carrie Davis, P.E., LEED Green Assoc.
Protection Engineering Consultants
cdavis@protection-consultants.com



George Kantrales, Ph.D.
Protection Engineering Associates
gkantrales@protection-consultants.com



Matt Barsotti
Protection Engineering Associates
mbarsotti@protection-consultants.com



Andrew Schoenheit
Cascade Coil Drapery
andrew@cascadecoil.com

Ty Vandergriff
Cascade Coil Drapery
ty@cascadecoil.com

ABSTRACT

Building design criteria requires that government buildings be designed for a variety of extreme loads including blast, hurricane, and impact conditions. The main goal of blast-resistant window and wall design is to minimize hazardous debris to prevent human injury and minimize the response of load-bearing members to prevent progressive collapse and human fatalities. New buildings can utilize hardened façade systems designed for extreme loads. However, retrofit design of existing buildings can be more challenging—especially when historic buildings are involved. Retrofit of historic buildings requires that original facades remain as much as possible. Therefore, interior retrofits must be utilized that provide the required thermal and energy efficiency, in addition to resistance to extreme loads.

Retrofit options for windows include anti-shatter films, storm windows with laminated glass, (fabric) blast curtains, and glazing cable or bar catcher systems. Another option is use of a heavy-duty curtain as a façade catcher system. A Cascade Coil Drapery product was designed for use as a catcher retrofit for a curtainwall system. Shock tube tests had been conducted and were used to validate modeling techniques employed to represent material-level and structural-level response modes of the woven coil drapery. After validation, finite element models (using LS-DYNA) were utilized to create

resistance functions for different Cascade Coil products in this application. Variables included: coil orientation, coil gauge, coil pitch, connection type, and span. The resistance functions (or load vs deflection curves) were used in the Single-degree-of-freedom Blast Effects Spreadsheet (SBEDS) distributed by the US Army Corps of Engineers Protective Design Center (USACE PDC). The fast running models allowed for quick evaluation of all retrofits subjected to all applicable blast loads for a “mock” entry curtainwall in a representative 1930’s to early 1940’s government building. Connection design to existing structural systems was also considered during the design process. An explanation of the model validation and selected Cascade Coil drapery system for this application is provided.

KEYWORDS

glass, facade, retrofit, anti-terrorism, blast-resistant design, security, finite element analysis

INTRODUCTION

Unlike conventional loads, extreme loads, particularly blast-induced loads, generate structural demands that are difficult to resist through elastic response alone. Consequently, with the exception of critical government facilities, most structures designed to resist extreme loads provide an acceptable level of protection by allowing a level of damage concordant with the value and function of the facility. For new structures, blast-resistant façades are incorporated into the overall design process during schematic design with review through construction to provide an efficient (structural, environmental, and economical) solution while maintaining the intended architectural aesthetic. These facades typically utilize insulated glass units (IGUs) with laminated glass supported by adequate structural systems (i.e., ranging from continuous aluminum mullions with steel inserts to cables attached at point-supports). However, for retrofit of existing structures, it is costly to completely replace an existing façade with blast-resistant alternatives and sometimes not allowed in historic buildings where the original façade must remain. Consequently, viable structural retrofit measures are preferred whenever they are shown to be cost-effective. In both cases, considerations must be made to ensure the existing structure can sufficiently support the new façade or façade retrofit option and to address any specified energy improvements.

The focus of the present study is a structural retrofit option consisting of novel interwoven coil mesh curtains that serve as a façade catcher system. The development of material-level and structural-level models for this system are described in the sections that follow along with a mock design exercise demonstrating the viability of the proposed approach.

BACKGROUND

As an alternative to a new hardened façade, catcher systems are capable of protecting building occupants from hazardous debris by arresting failed façade components before they penetrate too far into the protected space. Catcher systems can be more cost-effective than recladding a façade, but can be more difficult to design and detail depending on the opening geometry and supporting structure conditions. One of the most common types of catcher systems consists of a series of vertically-oriented cables anchored to the main structure at each end. While such systems are capable of preventing filmed monolithic or laminated glass units from threatening a protected space, a sufficiently think film or interlayer must be used and the systems tend to generate high localized forces at cable connection locations. Consequently, when connections concerns to the existing structure are of great importance, a closer cable spacing to a continuous system, such as a coil mesh curtain, can prove to be a viable alternative.

Coil mesh curtains have been utilized in industry for a variety of purposes, including as functional catcher systems and purely aesthetic drapes or sunshades (Fig. 1a). Two coil orientations may be used: horizontal and vertical (Fig. 1b&c). The primary functional differences between horizontal and vertical orientations are related to system stiffness and end connection schemes. For ease of reference, a coil mesh curtain is typically designated by a nominal opening size and wire gauge (e.g., 3/8 in.-16 ga. weave). Common coil materials vary depending on the intended application, but most structural applications require steel. Due to the inherent ductility and flexible of interlocking coils, they possess a notable capacity to absorb energy. Consequently, coil mesh curtains are a promising alternative to currently-employed façade catcher systems.



(a) (b) (c)

Figure 1: An architectural mesh system (a), a horizontally-oriented coil swatch (b), and a vertically-oriented coil swatch (c). Photo courtesy of the authors.

OBJECTIVE

To demonstrate the viability of coil mesh curtains as curtainwall catcher systems, a mock design was performed in the present study considering several coil mesh alternatives. The selected sample building was intended to be representative of a typical 1930's to 1940's style government building, with a glazed curtainwall entry, a reinforced concrete frame, and a masonry façade (Fig. 2a). For simplicity, a single catcher system was designed for a 17.5-ft x 20-ft curtainwall panel, with four mesh curtains needed to catch the entire glazed entry (Fig. 2b). The glazed entry consisted of 1/4-in. annealed glass lites (no film or interlayer) within 7.5-in. deep aluminum mullions spanning between the first and second floor reinforced concrete structural diaphragms. Design blast loads were derived from an unscreened vehicle-borne improvised explosive device (VBIED) detonated 40 ft from the entry. The curtainwall was prohibited from advancing more than 10 ft into the building (i.e., allowable response limit) in-line with a 'low hazard' rating as specified in UFC 4-010-01 (U.S. Department of Defense 2013) and quantified in ASTM F1642 (ASTM 2017).

METHODOLOGY

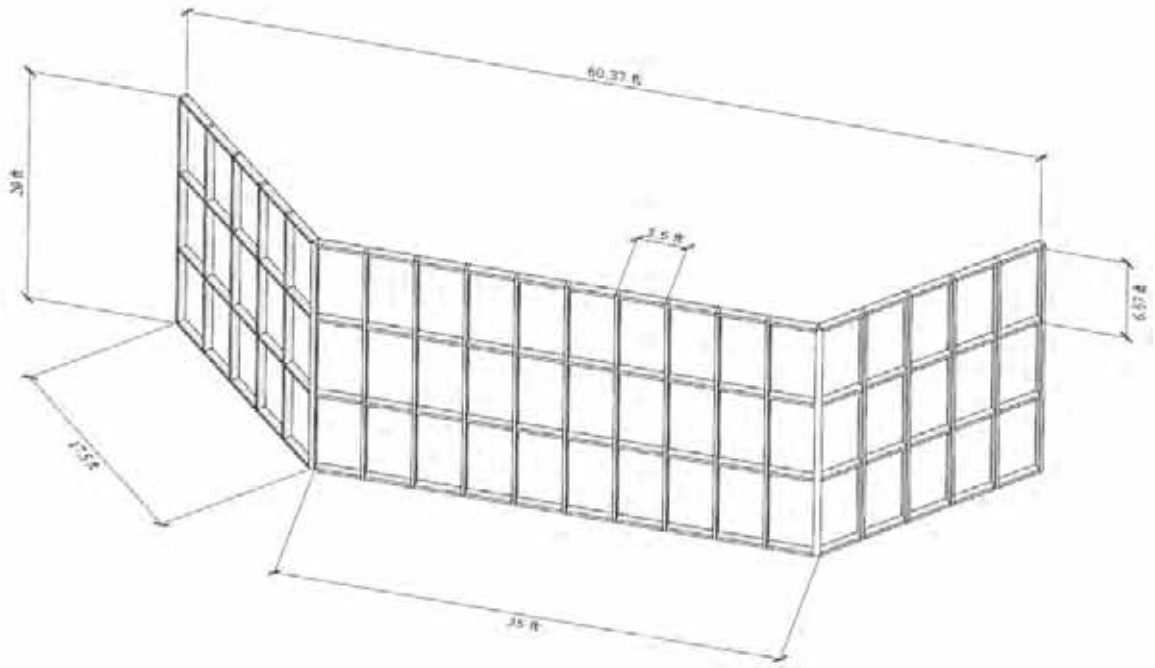
A woven coil mesh curtain is a relatively novel material for a façade catcher system. Consequently, little information is available in published literature regarding performance characteristics and important structural response modes associated with coil mesh curtains subjected to blast-induced loads. Therefore, to rigorously evaluate the efficacy of such systems in the present study, a multi-phase methodology was employed leveraging both computational and experimental aspects. In the initial phases, high-fidelity numerical modeling techniques were utilized to generate material-level and structural-level models of formed coils and coil mesh systems. Importantly, material models were calibrated using available test data and structural modeling techniques were validated through a comparison between analytical predictions and shock tube test data. In the latter phases, the validated modeling approach was used to develop simplified models and resistance functions for various coil mesh configurations. Single degree of freedom (SDOF) analyses for each configuration were then conducted using the Single-degree-of-freedom Blast Effects Spreadsheet (SBEDS) and the Single-degree-of-freedom Blast Effects Spreadsheet for Windows (SBEDS-W) to produce a conceptual design of a window catcher system for comparison against more conventional retrofit options.

MODEL DEVELOPMENT

As described previously, the first phase of the present study involved the development of a high-fidelity finite element model of a Cascade Coil Drapery system. Accordingly, detailed material models for the formed coils were developed as a part of this effort. To assess the validity of the material models, available uniaxial tensile test data obtained from experiments were compared against results from a simulated uniaxial tension test with reasonable agreement observed (Fig. 3).



(a)



(b)

Figure 2: Mock government building (a) and glazed entry (b).

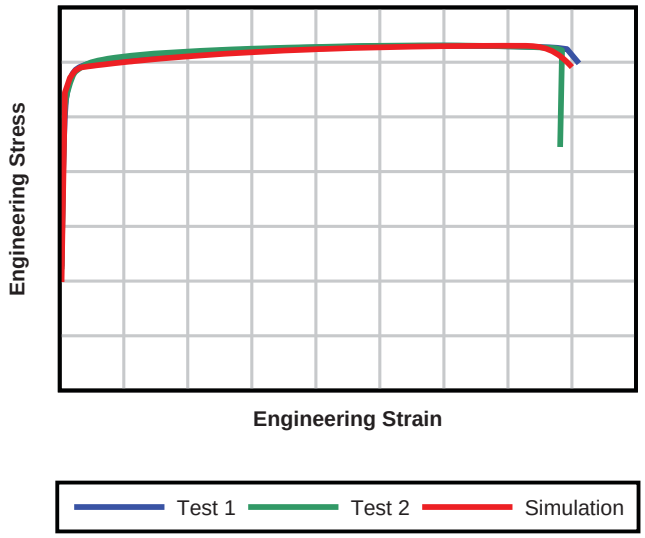


Figure 3: A comparison of results between uniaxial tension test data and analytical predictions for a steel material model.

Following development, each material model was subsequently adapted for use with beam elements in order to allow for the utilization of a computationally-efficient modelling approach whereby coils were meshed with cross-section integrated beams to capture through-thickness plasticity instead of solid elements. While this adaptation reduced simulation times considerably, care needed to be taken to ensure that the resolution of the beam element mesh was sufficient to accurately represent the nonlinear stiffness of the interwoven coils. Consequently, a series of mesh convergence studies were conducted using individual coils and 6-in. x 6-in. coil mesh swatches. Response modes of interest included: vertical extension of individual coils, longitudinal (along the coil axis) stiffness of interlocking coils, and lateral (orthogonal to the coil axis) stiffness of interlocking coils (Fig. 4).

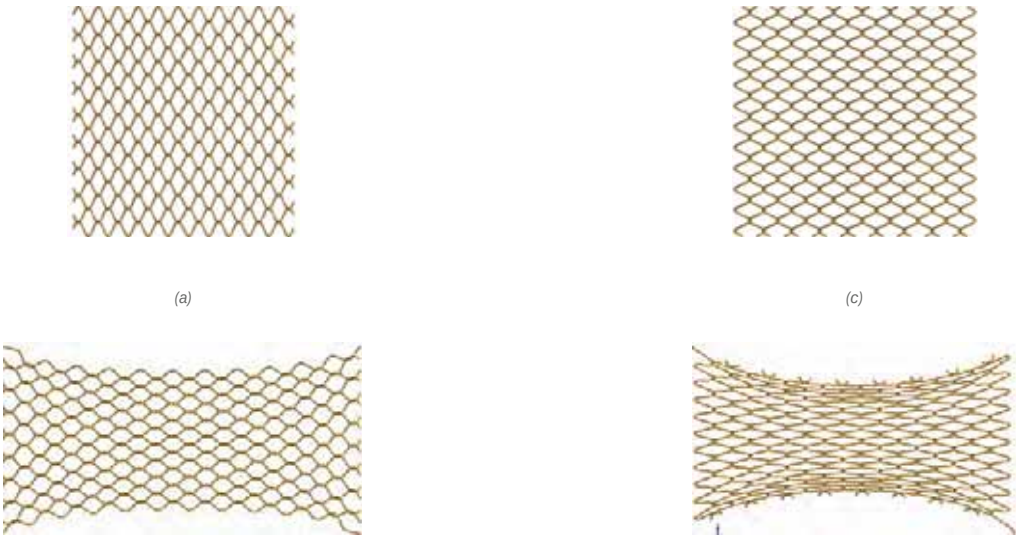


Figure 4: Un-deformed and deformed configurations associated with longitudinal (a-b), and lateral (c-d) pull simulations.

MODEL VALIDATION

Modeling techniques refined using the approach described above were used to develop a full-scale model of a Cascade Coil Drapery catcher system that was previously tested at the University of Ottawa (Castonguay, Jacques and Saatcioglu 2015). The Ottawa shock tube test was performed on a 44-in. x 44-in. punched window with aluminum frame mounted to a steel test frame along all four sides (Fig. 5a). The 1-in IGU layup consisted of a 1/4-in. annealed glass outer lite (assumed building exterior), a 1/2-in. air gap, and a 1/4-in. annealed glass inner lite with a 5-mil security film attached on all four sides with structural silicone (assumed building interior). The glazing utilized a 1/2-in. dry bite on all four sides.

During the test, the IGU fractured after being subjected to shock loading, came out of the frame, and was arrested by a Cascade Coil catcher system that was nominally 7-ft x 6.5-ft. The coil system employed for this test consisted of an array of vertically-oriented interlocking coils placed behind the window (Fig. 5b).



(a) *(b)*

Figure 5: Ottawa University shock tube tests highlighting the punched window and supporting frame (a) and the position of the vertically-orientated coil mesh curtain (b) (Castonguay, Jacques and Saatcioglu 2015).

To replicate the shock tube test setup analytically, the coil mesh was modeled using beam elements and was attached to an explicitly modeled wheel-and-track connection system (Fig. 6). The punched window was modeled with a previously-validated approach to represent glass fracture and breakup of the laminated glass lites (Marchand, K., et al. 2017), while rigid shell elements were used to model the frame. Importantly, the glass used in the Ottawa shock tube tests was mostly held together by the overlaid film. This continuity was represented in the analytical replication of the tests through the use of a thin polyvinyl butyral (PVB) layer.

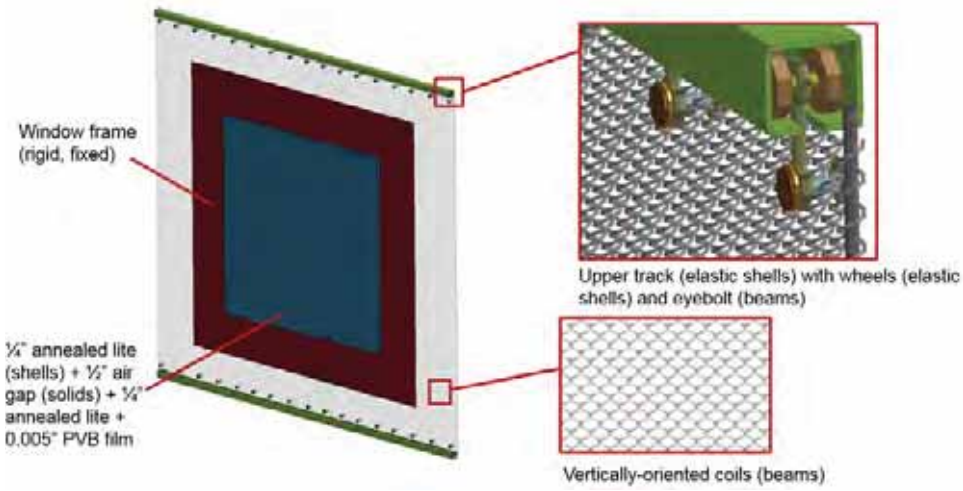


Figure 6: The model employed to replicate the Ottawa shock tube test.

During the simulation, as in the test, the IGU fractured from the applied blast loads. The fractured glass was held together by the attached film (acting as a membrane) and arrested by the Cascade Coil catcher system (Fig. 7a). The center-point deflection of the coil mesh was tracked through time and compared against a peak deflection obtained from the Ottawa test report with reasonable agreement noted (Fig. 7b). Although coil mesh strain data associated with the Ottawa test was not available, localized deformations of the coil mesh at connection points appeared visually-similar to post-test photos (Fig. 8).

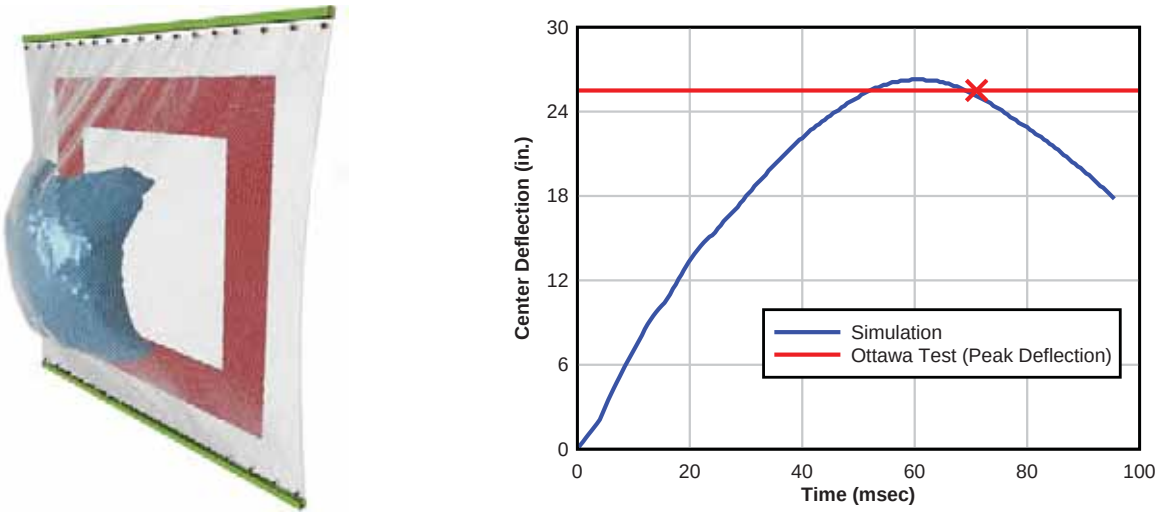
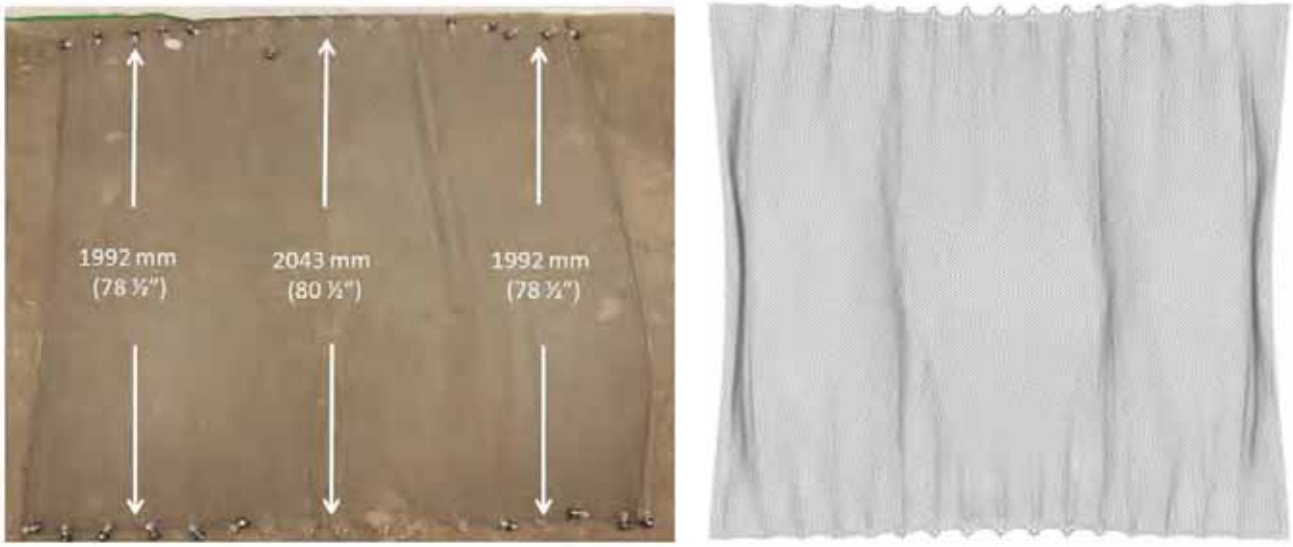


Figure 7: The peak model deflection (a) and deflection time-history (b) associated with the Ottawa shock tube test simulations.



(a) (b)

Figure 8: A comparison of the final deflected states of the coil mesh following testing (Castonguay, Jacques and Saatcioglu 2015) (a) and simulation (b).

RETROFIT DESIGN

Following development and validation of high-fidelity numerical techniques for modeling coil mesh systems subjected to blast-induced loading, such techniques were simplified and adapted to develop general-purpose resistance functions. These resistance functions were then used in a series of SDOF analyses to evaluate the viability of using a coil mesh system to catch the failed building façade discussed previously.

STATIC RESISTANCE FUNCTION DEVELOPMENT

Due to the significant time-cost associated with explicitly modeling and simulating coil mesh systems using high-fidelity finite element analysis techniques, a simplified and readily adaptable modeling approach was employed to quantify resistance functions. This process consisted of three distinct stages In the first, three-dimensional (6-in. x 6-in.) coil swatch models with varying characteristics (Table 1) were subjected to longitudinal and lateral extension simulations similar to what was done previously in the mesh convergence study (Fig. 4). However, in this case, edge contractions were restrained to mimic the behavior of interlocking coils that are away from an edge condition.

Weave Size	Wire Gauge	Material	Coil Orientation
3/8-in.	16	Steel	Horizontal
			Vertical
1/4-in.	19	Steel	Horizontal
			Vertical

Table 1: Characteristics for the coil mesh weaves considered in the present study.

The outcome of these simulations were nonlinear coil swatch stiffness curves unique to each coil weave. Coil swatch stiffness curves were then employed as element axial stiffness definitions in a two-dimensional beam element model representative of a strip of coil mesh panel. The overall length of the equivalent beam element model employed in this stage was 20-ft to be nominally representative of the height of a typical façade catcher system. Importantly, the length of each beam element was 6 in. to match the length of the swatch models used to produce the element stiffness curves. This beam element model was then subjected to a gradually-increasing lateral body force load and a center-point deflection time-history was recorded until the onset of failure. The resulting force-deflection relationship obtained was representative of a coil mesh

strip. To adapt each curve to be representative of a full coil mesh *panel*, the strip force-deflection curves were scaled using the relative widths of the panel and the swatch model (Equation 1):

$$SF = \frac{W_{panel}}{W_{swatch}} \tag{1}$$

Where, *SF* was the scale factor applied to the strip force-deflection curves, W_{panel} was the panel width, and W_{swatch} was the width of the swatch model (6 in.) The scaled force-deflection curves (Fig. 9) were used as input static resistance functions for subsequently conducted SDOF analyses.

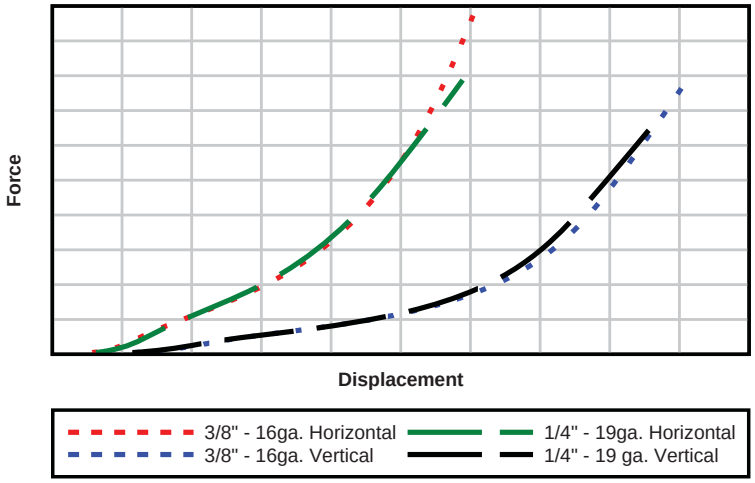


Figure 9: Mesh panel resistance functions employed in the present study.

QUANTIFICATION OF DYNAMIC INCREASE FACTOR

Blast-induced loads typically generate very high strain rates in affected structural components. Thus, effective material-level capacities are greater for most common structural materials (U.S. Department of Defense 2014). This effect can significantly influence the overall capacities of structural components and should be accounted for in blast-resistant design and analysis methodologies. This is frequently accomplished in steel design through the use of dynamic increase factors (DIFs) applied to yield and ultimate strengths. In the finite element method, one common way of capturing the rate-dependence of ductile metals is through employing the Cowper-Symonds scaling method (Cowper and Symonds 1958). To quantify DIFs for the coil material considered in the present study, the Cowper-Symonds method was implemented into the swatch model employed for static resistance function development. The swatch model was then rapidly extended at an overall strain rate of 1 s^{-1} and the total resisting force was recorded. A dynamic increase factor was then determined by comparing an equivalent static curve with the resulting dynamic curve and noting the approximate difference in magnitudes (Fig. 9).

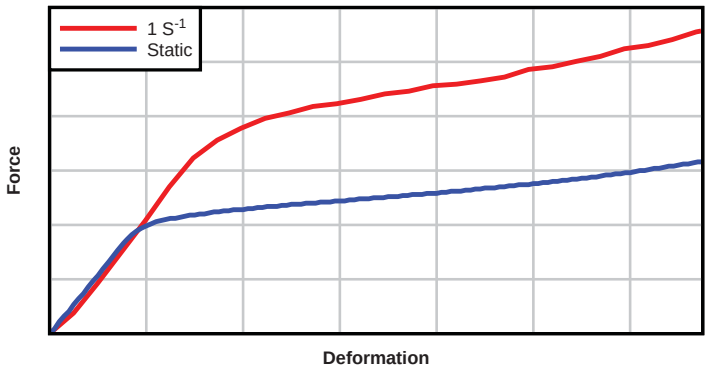


Figure 10: A comparison between static and high-rate force-deformation curves from swatch pull simulations.

SDOF ANALYSES

Employing the resistance functions and DIF described previously, a series of SDOF analyses were conducted with SBEDS to rapidly evaluate the suitability of several coil mesh systems for catching the failed building curtainwall using ASTM F1642 (ASTM 2017) hazard levels as a metric. The momentum of the failed curtainwall due to the design blast load, as determined through preliminary SDOF calculations in SBEDS-W, was used as load input. Peak mesh deflections and connection reaction forces associated with each analysis were recorded and used to compare the performance of the various systems (Table 2).

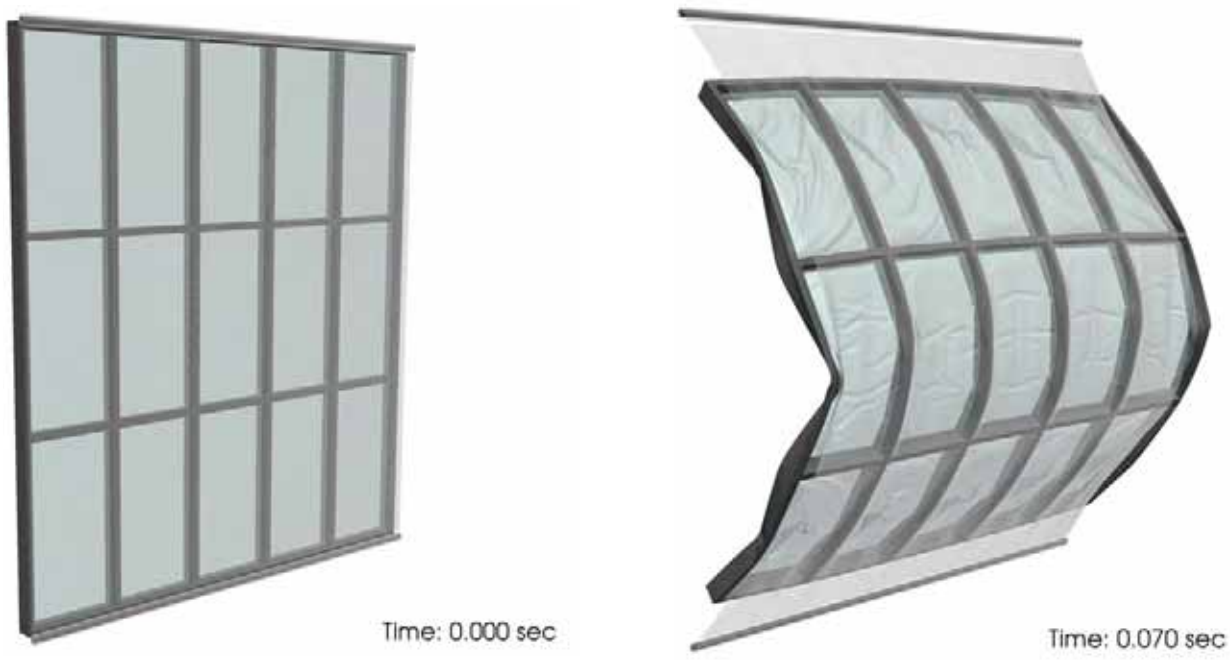
Weave Size	Wire Gauge	Material	Coil Orientation	Maximum Deflection	Performance Notes
3/8-in.	16	Steel	Horizontal	8.6 ft	No failure observed; meets deflection criteria
			Vertical	13.4 ft	No failure observed; does not meet deflection criteria
1/4-in.	19	Steel	Horizontal	8.4 ft	No failure observed; meets deflection criteria
			Vertical	13.1 ft	No failure observed; does not meet deflection criteria

Table 2: A performance comparison between coil mesh curtain wall catcher systems.

Overall, the performance levels of the 3/8-in. mesh curtains were similar to analogous 1/4-in. variants. However, vertically-oriented coil mesh curtains required significantly more deflection to arrest the momentum of the failed façade. This is a direct result of the difference in stiffness between vertical and horizontal coil orientations. When oriented vertically, coil mesh stiffness is predominantly controlled by coil elongation. In contrast, when oriented horizontally, coil-coil interlock dominates response. Resultantly, only horizontally-oriented coil mesh panels were able to fully arrest the failed façade prior to reaching the 10-ft deflection limit associated with a low hazard rating specified for the mock design. However, in all cases considerable residual mesh capacity remained.

HIGH-FIDELITY ANALYSIS OF SELECTED SYSTEM

After determining that horizontally-orientated coil mesh curtains performed suitably when subjected to impact from the failed building curtainwall, a high-fidelity model of the 3/8-in. horizontally-oriented catcher system was constructed to further demonstrate the viability of the SDOF approach. This model featured a single 17.5-ft x 20-ft curtainwall panel that was subjected to blast loads from the VBIED threat discussed previously. The momentum of the failed curtainwall was arrested by a similarly-sized Cascade Coil mesh panel (Fig. 11). Since the selected mesh system was horizontally-oriented, a common pipe wrap anchorage scheme was employed at the top and bottom of the mesh (Fig. 12). Importantly, the coil mesh was able to arrest the façade without nearing ultimate capacity—a finding which is congruous with the SDOF study.



(a) (b)

Figure 11: Initial (a) and final (b) states of deflection are shown for the high-resolution curtainwall catcher simulation.

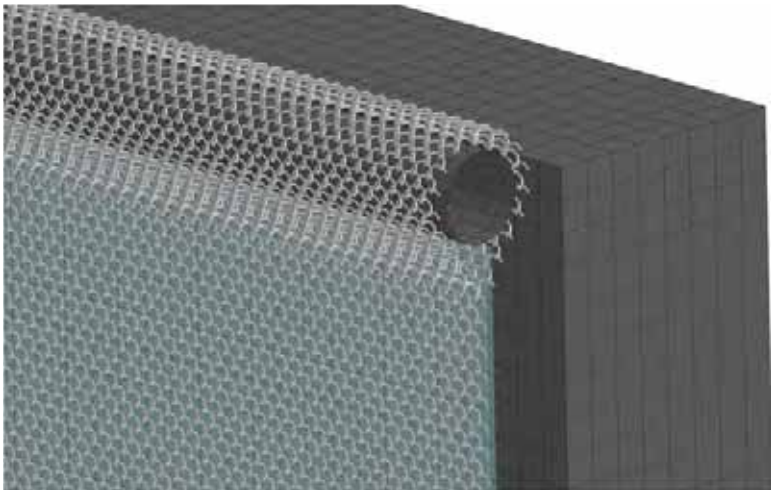


Figure 12: The pipe wrap anchorage scheme used in the high-resolution curtainwall catcher simulation.

CONNECTION DESIGN CONSIDERATIONS

In order for any coil mesh design to perform well when subjected to blast-induced loads, connections to supporting structural elements must engage the coil mesh in such a way that excessive stress localization is inhibited. To accomplish this, discrete connections (e.g., through-bolts) must be spaced close enough to ensure proper load distribution. Conversely, a continuous connection scheme, such as a pipe wrap, can also be employed (Fig. 12). Importantly, connections must be designed for both lateral and transverse loading to ensure proper development of catenary response mechanisms in the coil mesh. If applied loads to the existing supporting structural elements are still too high, then energy absorbing anchors should be explored to further reduce loads to the existing building diaphragms.

PERFORMANCE ADVANTAGES COMPARED TO CONVENTIONAL SYSTEMS

In addition to coil mesh catcher systems, conventional retrofit options for historic curtainwall facades include façade replacement, a secondary window wall system with laminated glass, and glazing cable catcher systems with anti-shatter security films. Replacing the façade in its entirety, is an expensive option as it must match the aesthetic of original historic

system but an adequate structural and environmental system can be designed. A secondary window wall behind the historic system provides minimal visual impedance and some energy performance benefits by creating an air gap for insulation, however it will cost similar to a façade replacement. Lastly cable catcher systems require the installation of anti-shatter security film on the existing façade. Energy performance improvements are solely based on the selected film performance. Cost-wise, less materials are needed for cable catcher systems over façade replacements and secondary window walls, however installation costs could be significant depending on the anchorage conditions and need for energy absorbing connectors to mitigate high localized reaction loads.

When compared to more conventional cable catcher systems, coil mesh curtains possess a variety of advantages. Foremost among these is the increased ability to retain fragmented glass. Cable catcher systems, due to their discrete nature, require anti-shatter security film keep the glass debris together to arrest the entire lite. In contrast, coil mesh curtains cover more surface area, thereby providing an increase in fragment retention without the need for security film. Importantly, glass shards smaller than the selected mesh opening will be able to pass through relatively unimpeded. However, shards less than 1-in. in any united dimension are defined by ASTM F1642 (ASTM 2017) as glazing dust and slivers and present much less of a threat to building occupants thus are not included in hazard rating determinations. A second advantage afforded to coil mesh curtains is related to connection design. Since a coil mesh is continuous in nature, connection forces may be distributed more evenly into the structure through an appropriate connection design. In addition, unlike cables, coil mesh curtains are capable of sustaining plastic deformations. These mechanisms allow for lower local connection demands relative to cable catcher systems and reduce the need to use energy absorbing connectors to reduce connection loads. Such specialized details can be costly when utilized for large facades and should be used sparingly. Moreover, interwoven coils possess a greater inelastic range than cables, which tend to rupture at relatively low levels of inelastic deformation. Because inelastic deformation dissipates energy, coil mesh systems will send less overall load into the structure relative to cable systems and will tend to fail in a much more progressive and less brittle manner. Lastly, coil mesh curtains reduce glare and internal heat gains into the protected space, however additional energy improvements are not inherent to this retrofit option.

SUMMARY AND CONCLUSIONS

In the present study, a conceptual coil mesh catcher system was developed for a mock structure to arrest a failed façade subjected to blast loads. To form the basis for the conceptual design, high-fidelity numerical modeling techniques were used to develop material-level and structural-level models for the coil mesh panels. These techniques were then validated through an analytical reproduction of a full-scale shock tube test. Subsequent to the validation effort, simplified numerical models and SDOF resistance functions for various coil mesh panels were developed and used to explore the efficacy of each alternative. Overall, horizontally-oriented coil panels were able to arrest the façade within 10 ft of the exterior façade (per a low hazard rating in ASTM F1642 (ASTM 2017)) while vertically-oriented variants did not meet the response limit. However, all coil mesh catcher systems were able to successfully prevent significant intrusion of the failed components into the protected space, which prevents human injury due to hazardous debris (following the design intent of most blast-resistant design criteria).

Because of the ductile nature of interwoven coils and the continuous layout of coil mesh panels, they possess a variety of advantages over traditional cable catcher systems, which can be difficult to detail. Furthermore, as demonstrated in the present study, coil mesh panels can be analyzed and designed using cost-effective SDOF methods. The associated connection details will experience lower overall load levels relative to cable catcher systems, but still require proper detailing. The internal retrofit option is ideal for historic facades, however energy performance is not fully addressed with a coil mesh panel.

ACKNOWLEDGMENTS

The authors would like to acknowledge Cascade Coil Drapery for sponsoring the present study.

REFERENCES

ASTM. 2017. F1642/F1642M-17, Standard Test Method for Glazing and Glazing Systems Subject to Airblast Loadings. West Conshohocken, PA: ASTM International.

Castonguay, S., E. Jacques, and M. Saatcioglu. 2015. Blast Testing of GuardianCoil as a Protection System. Ottawa, Ontario, Canada: University of Ottawa.

Cowper, G.R., and P.S. Symonds. 1958. Strain Hardening and Strain Rate Effects in the Impact Loading of Cantilever Beams. Brown University, Applied Mathematics Report.

Marchand, K., Davis, C., Sammarco, E., and Bui, J. 2017. "Extending Glass Facade Performance Predictions for Natural and Man-made Hazards Using Accesible High-Fidelity Formulations." 39th IABSE Symposium. Vancouver, Canada.

U.S. Department of Defense. 2013. "DoD Minimum Antiterrorism Standards for Buildings (UFC 4-010-01)."

U.S. Department of Defense. 2014. "Structures to Resist the Effects of Accidental Explosions (UFC 3-340-02)."

TRANSFORMATION AS MOVEMENT

A Roman Baroque church façade case study



Vytenis Gureckas
The Catholic University of America
gureckas@cua.edu

ABSTRACT

In 1888 the art historian Heinrich Wölfflin proposed the notion that the primary characteristic of baroque architecture is the illusion of movement. Captivating as this suggestion may be he was not very clear about how movement manifests itself. In the case of buildings utilizing curved forms such as San Carlo alla Quatro Fontane one might surmise that the sweeping lines suggest movement and the bulging exterior is a result of the pressure the oval space inside seems to exert on the façade. But how is movement to be understood in the case of so many baroque buildings that have no curved forms? In this formal analysis of a baroque façade it is asserted that the illusion of movement is achieved through various operations that can be described through a series of transformation diagrams from an initial condition of complete flatness to an end condition that accounts for the full depth of the façade. Using one of the first Baroque examples in Rome as a case study – the façade of Santa Susanna by Carlo Maderno – a set of transformation diagrams is presented here which imply movement in much the same way that consecutive still frames make up a motion picture (Fig. 4.1 – 4.6). This makes explicit what is implied when dynamic words such as ‘stepping’ is used to describe the massing or ‘multiplying’ is used to describe the elements of a façade.

KEYWORDS

façade, masonry façade, stone, case study, history, formal analysis

INTRODUCTION

Much of classical architecture involves pilasters, columns, entablatures, pediments, etc. that are integrated with the wall and are not structural. It is a type of ornament that represents a trabeated tectonic governed by the rules of the Orders. Hence it is a representational tectonic and can be said to be a fictive structure or fictive frame. This study is an examination of the fictive frame of Santa Susanna in Rome. It is a study that might be of interest to several audiences, namely the historian, the classical architect practicing today, and a broader audience of architects interested in the appreciation of architecture.

Santa Susanna stood on the Quirinal hill in Rome from very early times. In the late cinquecento it was renovated and a new façade was designed by Carlo Maderno. The work was completed in 1603 (Blunt 1982). It was inspired by the façade of the Gesù also in Rome and is one of the earliest examples of Baroque architecture.





Figures 1-3: Façade of Santa Susanna; façade of Santa Susanna from Insignium Romae Templorum Prospectus by Giovanni Giacomo Rossi in Rome (1683); detail of Santa Susanna façade.

BACKGROUND

A full enumeration of the characteristics of Baroque architecture is a complex matter and beyond the scope of this paper. Since the focus here is on the illusion of movement, of interest is the writing on this subject by Heinrich Wölfflin. He draws a distinction between Renaissance and Baroque architecture. To Renaissance architecture he attributes clarity of elements, purity, calm, balance, and solidity of structure. He calls this the 'linear style' or the 'severe style'. Of the Baroque he says:

> "If the beauty of a building is judged by the enticing effects of moving masses, the restless jumping forms or violently swaying ones which seem constantly on the point of change, and not by balance and solidity of structure, then the strictly architectonic [Renaissance] conception of architecture is depreciated. In short, the [Renaissance] severe style of architecture makes its effect by what it *is*, that is, by its corporeal substance, while the [Baroque] painterly architecture acts through what it *appears* to be, that is, an illusion of movement" (Wölfflin 1964).

He goes on to discuss how movement is incorporated in painting but unfortunately never explicitly describes how movement works in the architecture of church façades. Paolo Portoghesi is a bit more specific when he writes about the façade of Santa Susanna saying it "…springs forward from the wall surface of the street, acquiring volumetric consistency, and gradually, through progressive transformations from its outer edges towards its center, takes on plastic tension and chiaroscural vibration" (Portoghesi 1970).

METHOD

The methodology employed here does not concern itself with the construction of the façade but rather involves the formal analysis of the front façade of Santa Susanna. The method used here involves a series of analytical transformational diagrams. These diagrams show the development of the façade from the most minimal state – a blank wall – to incrementally more complex conditions until the final configuration is reached (Fig. 4.1 – 4.6). The diagrams are not a reconstruction of the design process taken by the architect. This is not known and in all likelihood involved a less linear development. Nor is it an attempt to make a historical outline from simpler Renaissance façades to Mannerist ones even though several precedents could be cited for the design at different stages in the transformation. Instead the intention of the diagrams is to make explicit the incremental application of operations on the fictive frame and wall such as stepping, duplicating, layering etc. which are implicit in the final design. For example where there is a pairing of pilasters or columns in the final façade the condition of singularity can be derived and it can be said that such a condition precedes the condition of pairing. In this manner the diagrams are derivatives one of the other in incremental stages when read from the last to the first diagram. Read in the order given, each stage is one of synthesis and articulation leading to ever greater levels of complexity and in the words of Heinrich Wölfflin from a ‘linear style’ of repose to a ‘painterly style’ of movement.

EXPLANATION

The first condition is simply a blank wall (Fig. 4.1). It can be designated as the zero datum surface relative to which the other layers of the façade are positioned. It is not however undifferentiated. It is shown with lower flanks topped with scrolls which correspond to the side-chapels beyond and a taller center topped with a gable which corresponds to the nave and associated roof. From a purely practical performance point of view, it is all that is necessary to provide enclosure to the building.

The second diagram shows a layer in front of the datum wall which is a fictive frame composed of pilasters, pedestals, entablatures and a pediment (Fig. 4.2) The three bays over five composition is the basic form that will be retained in the final existing condition, but at this point it is shown flat. For the Renaissance architect this stage would suffice and an example of it deployed is the façade for Santo Spirito in Sassia, Rome (Fig. 5). Here is the ‘linear style’ that Heinrich Wölfflin speaks of. There is no duplication or pairing of pilasters so that the lines or edges between bays is crystal clear. The lower and upper entablatures do not step forward or backward thus allowing the horizontal lines to continue unbroken which contributes to the sense of repose and clarity attributable to the Renaissance. Since this diagram is presented as a stage in the derivation of the final design, it can be said that this baroque building carries the DNA of a Renaissance church façade. It substantiates the fact that the baroque style derived from the Renaissance and is indebted to it for much of its affect. That is to say that the one is understood in terms of the other

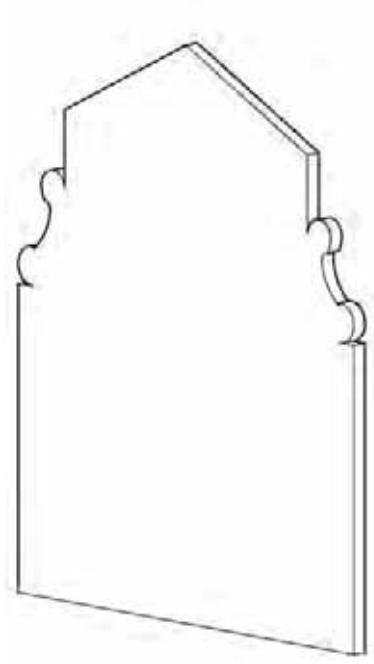


Figure 4.1: Santa Susanna façade diagram (Stage 1).

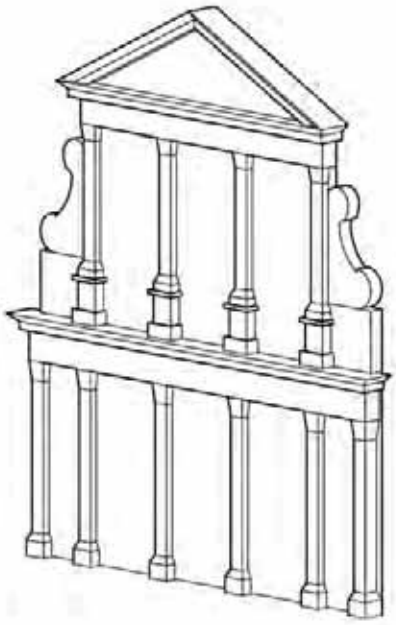


Figure 4.2: Santa Susanna façade diagram (Stage 2).

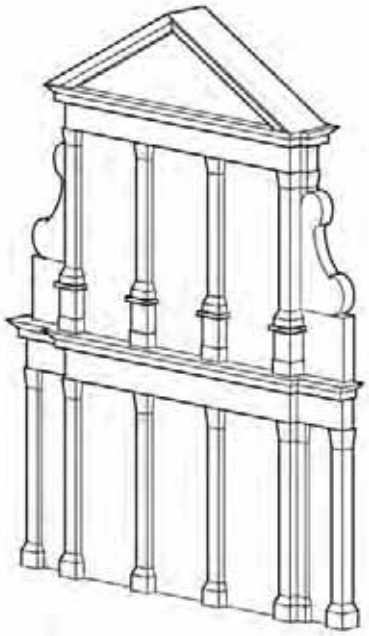


Figure 4.3: Santa Susanna façade diagram (Stage 3).

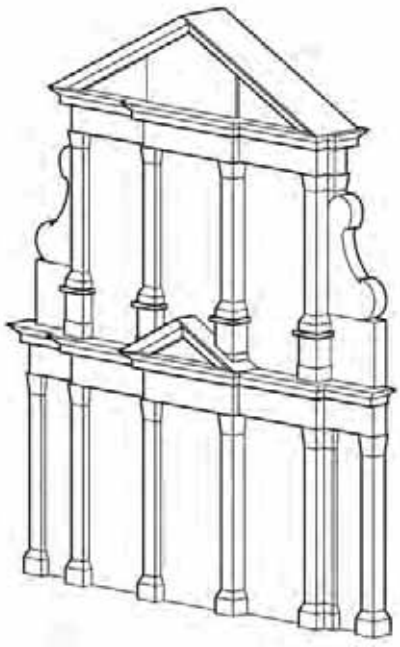


Figure 4.4: Santa Susanna façade diagram (Stage 4).

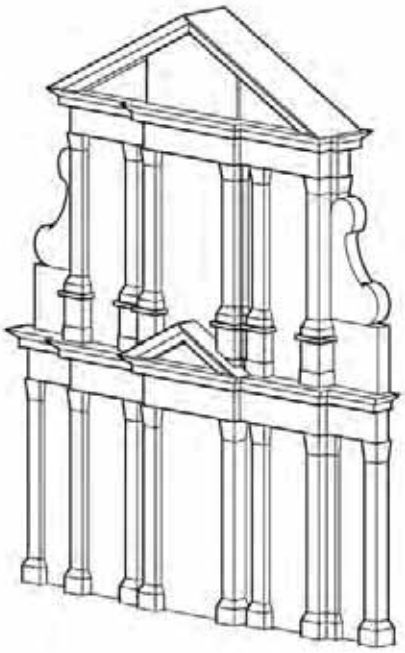


Figure 4.5: Santa Susanna façade diagram (Stage 5).

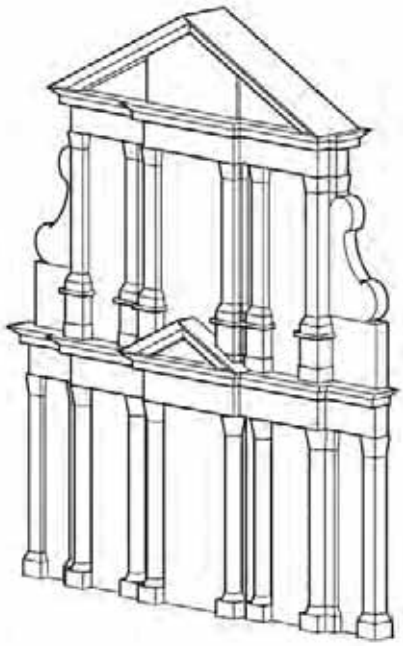


Figure 4.6: Santa Susanna façade diagram (Stage 6).



Figure 5: Santo Spirito in Sassia, Rome.

In the third diagram the flanking bays on each side are made to step back, a portion of a pilaster is added in the resulting inside corner on the lower level, and a top portion of a pilaster is added on top of the scroll (Fig. 4.3). This stepping of the wall and entablature back necessitates a mitering of the entablature which creates a vertical line and a separation of the entablature into three parts – center and two flanks. It articulates the relationship of the central three bays in the lower level in relation to the central three bays on the upper level. The temple front is made clear. But why were the partial pilasters added? In the case of the ones on the lower level one could conjecture that without it the short segment of the entablature would be in a sense visually unsupported and therefore not satisfactory in the classical language of architecture. But why not a full pilaster? It seems that it was desirable to tuck the pilaster behind the one in front as if a bas-relief technique to indicate it stands behind the front pilaster. If the pilaster in the inside corner had been placed directly behind the pilaster in front it would have virtually disappeared. The other partial pilaster on the second level sits on top of the scroll and serves an entirely different function. It is full in width but turned 90˚ relative to the façade. Since that portion of the façade does not come in contact with the adjoining building the pilaster turns the corner. Nevertheless it is a bit strange in that it is undercut by the scroll.

In the fourth diagram the central bay steps forward and a small pediment the width of the central bay is added at the lower entablature (Fig. 4.4). Again, as a result of the stepping the entablatures are mitered. There is also a corresponding stepping of the tympanum above.

The fifth diagram shows the duplication of pilasters where the central bay steps forward (Fig. 4.5). The pilasters can be read as a pair with the stepping between them or alternatively as a pair framing each bay separately. In this case the new pilasters are full width and not tucked behind the pilasters of the central bay. In fact there is a clear gap between the paired pilasters. However, if one examines this location closely, there is another partial pilaster tucked in the inside corner, but only on the upper level. Why this detail appears only in the upper level is not exactly clear.

The last diagram shows the six round columns which were deployed instead of pilasters on the lower level (Fig. 4.6). Of particular interest is the fact that the column shafts do not touch the wall. There is a pocket or miniature niche within which the column stands. Such a detail is referred to as an immured column and the source of this detail can be found in the loggias of the two facing palazzi by Michelangelo at the Campidoglio (see the plan of the façade in Fig. 2).

So far the diagrams and accompanying text describe the configuration and the stages of transformation. But what is the emotive effect? The transformations which include the operations of stepping, folding, layering, pairing, etc. all serve to

evoke movement and dynamism. The transformation diagrams could be thought of as stills of a motion picture. It is a way to explain the movement that is ascribed to baroque architecture and, in this case study, achieved without the use of curves. The stepping also has the effect of creating vertical lines which along with the multiplicity of pilasters and columns carry the eye upwards. In tandem with the horizontal moldings of the entablatures a complex matrix of lines is created which come to life in the presence of light. Strong shadows and highlights are created. There are other effects as well which lend great beauty to the façade but which are not in and of themselves associated with movement. One worth mentioning is the plastic effect created by the immured column detail. The column is free of the wall and hence it reaches its full sculptural potential. Likewise the wall is strengthened and its thickness is revealed

CONCLUSION AND FUTURE WORK

The illusion of movement in Baroque architecture is perceivable to the attune observer even without access to the transformation diagrams presented here. Layers that advance or recede imply movement and are readily detectable. However the transformation diagrams make explicit what is implicit and hopefully add to the appreciation of the building. Further investigation could be conducted by applying the method to other Baroque church façades.

REFERENCES

Blunt, Anthony. Guide to Baroque Rome. Philadelphia: Harper & Row, 1982.
Portoghesi, Paolo. *Roma Barocca: The History of an Architectonic Culture*. Cambridge: MIT Press, 1970.
Wölfflin, Heinrich. Translated by Kathrin Simon. *Renaissance and Baroque*. New York: Cornell University Press, 1964.

ILLUSTRATION CREDITS

Façade etching from Rossi, Giovanni Giacomo. *Insignium Romae Templorum Prospectus*. Roma: 1683.
All other images and diagrams by the author.

VERTICAL LOUVERED SOLAR CONTROL

Richard Neutra and system development to 1968



Clifton Fordham, RA, LEED AP
Temple University
clifton.fordham@temple.edu

ABSTRACT

Exterior shading devices, when typically used, are horizontal planes that are most effective at the south face of buildings in the northern hemisphere. Horizontal devices are less effective on the eastern and western exposures of buildings due to lower solar altitude in the morning and evening. An iconic response to the limitations of horizontal shading is the brise-soleil, propelled into the lexicon of modern architecture by Le Corbusier. The vertical extrusions of the waffle like device are better suited for eastern and western exposures, especially if the vertical extrusions are not oriented directly on an east-west axis.

Less iconic is a movable vertical louver shading system, which appeared in Brazil and was introduced to the United States by Richard Neutra in the late 1940's. Neutra's advancement of the system culminated in an automated system that satisfied shortcomings in the brise-soleil, and provided an additional aesthetic for modern architects. A kinetic system addressed the difficult challenge of shading western and eastern exposures during the cooling season, while allowing for daylighting when heat gain is less of a liability. Neutra's use of the system countered a horizontal emphasis in mid-century architecture and conveyed order like Mies van der Rohe's exterior curtain wall extrusions. Neutra's order, unlike Mies's, integrated poetry with performance.

Use of exterior solar-breaks in the United States receded in the 1960's, and returned with limited use after the energy crisis of the 1970's. However, many applications are less integrated then earlier iterations. Moveable exterior vertical louvers have reappeared in Europe, and in only one recent project by a notable architect in the United States. This paper traces the development of the mechanized vertical louvers system and contextualizes its disappearance. Relatively low-tech by today's standards, the system represents a viable contemporary solar control solution.

KEYWORDS

louvers, solar control, automated, kinetic, history of facades, façade theory, aesthetics

INTRODUCTION

Solar control features have long been associated with western and non-western building construction including the ancient civilizations of the Mediterranean. Most often, they have merged into traditional architectural languages to create vernacular forms in which the performance of specific elements is not overt and easily extracted. The modern movement, a movement in which Richard Neutra was a key contributor, broke from traditions including those of vernacular form, material usage, and ornament. His design for the Lowell Health House featured in the seminal 1932 Museum of Modern Art exhibit on the International Style, helped to define an aesthetic of stark white finishes and abstract form. The impetus to forge new architectural responses to the times contributed to a culture of invention that Neutra participated in throughout his career until his death in 1970.

An innovation with significance to the current era of solutions to environmental problems was a dynamic exterior vertical louver system that controlled natural light penetration from low sun angles while allowing views when control was less vital. An important characteristic of the system was that it was architectural, and not supplemental like interior window treatments. The system disappeared in the United States after a brief life, almost exclusively in buildings Neutra designed in a style that is

characteristic of post-war architecture. Building elements that address solar control warrant contemporary consideration in light of the need for architecture that speaks to its functionality.

BACKGROUND

SOLAR CONTROL AND EARLY ERA MODERN ARCHITECTURE

Early modern residential architecture incorporated extensive overhangs including houses by Greene and Greene who practiced in Pasadena, California, and Bernard Maybeck who practiced in Berkeley, California. They became signature elements in Frank Lloyd Wright's buildings including the Robie House (1910) in Chicago with sweeping horizontal elements recalling the flat expanses of the American Mid-west. Wright also introduced the exploded floor plan where room definition was fluid and the exteriors extended out toward the landscape, with interior and exterior spaces blurring. Neutra, who apprenticed with Wright from 1924 to 1925, adopted a similar formal approach and orientation toward recognizing the relationship of natural features and buildings. Rudolph Schindler another architect Neutra worked for before gaining the Lowell commission, incorporated overhangs into a distinctly modern aesthetic (Hines 2005).

Without the motivating force of extreme climate, vertical shading planes were less appealing than horizontal planes since horizontal planes obstructed fewer views and served more functions including protection from precipitation. The first appearances of vertical shading and devising planes in contemporary American buildings, as opposed to recesses in volumes, appeared in buildings by recent emigres, most notably Walter Gropius and Richard Neutra. Their vertical screens provided some privacy, shading, permitted breezes, and helped accentuate horizontal movement. Gropius's home in Lincoln, Massachusetts (1938) incorporated a vertical screen wall composed of wood slats on the western side of the house. The earliest appearance of a similar element in a Neutra building was the Davey House (1939). Vertical devices in these projects were peripheral to their overall expression, escaping notice in historical accounts.

BRISE-SOLEIL AND SOUTH AMERICA

In the absence of other accounts, vertical shading devices in modern architecture has been tied to Le Corbusier and his brise-soleil, an egg-crate extension from the face of a building that matched horizontal shading planes with integral and similarly proportioned vertical planes. Vertical planes offered protection from the sun that horizontal projections effectively could not during the late hours when the sun is low on the horizon, particularly on the western and eastern orientations of buildings. Inspiration for the strategy likely came from North Africa where Corbusier would have observed geometric screens at window openings with small apertures that permitted airflow while mediating undesired solar heat gain. By enlarging the apertures, and increasing the depth of the screen to compensate for larger apertures, Le Corbusier developed a new vocabulary that was functional and memorable. Le Corbusier's system found few early adopters except in tropical countries eager to demonstrate technological solutions tied to novel aesthetics. The earliest example designed by Lucio DeCosta and Oscar Niemeyer, with Corbusier operating as a consultant, was the Ministry of Education Building (1936-43) located in Rio de Jeneiro and completed in 1943 (Curtis 1994). It contained manually locally adjustable horizontal louvers in the cells (Fig. 1).



Figure 1: Ministry of Education in Rio by DeCosta and Niemeyer. Photo courtesy of Enviado Pel.

The first examples of a movable vertical louver system can be found in Niemeyer's Yacht Club (1940-43) and Casino (1940-43) in Pampultha, Brazil. Discrete sections of the louvers are hand operated similar to the Ministry of Education Building.

Richard Neutra brought a wide range of solar control strategies in South America to the attention of an American audience in a 1946 *Progressive Architecture* article he authored based on a trip to the continent earlier that year. In the article, he remarks that his own design experiments with vertical louvers predated the Niemeyer projects although they were unrealized. These experiments were consistent with Neutra's interest in vertical devices during the 1930's.



Figure 2: Kaufmann Desert House. Photo courtesy of Thom Watson.

EARLY WORKS IN THE UNITED STATES

KAUFMANN DESERT HOUSE

Competing objectives including providing privacy, shading, permitting views, and defining outdoor spaces were the primary benefits sought when Richard Neutra created the first rotating vertical louver system in the United States for a house commissioned by the Kaufmann family in Palm Springs, California (1948). The Kaufmann Desert House presented challenges due to local building height restrictions, which prevented Neutra from adding an enclosed second floor to the extensive pinwheel shaped ground floor plan that extended into the landscape, and would have otherwise been resulted flat. This prompted the construction of a covered outdoor room above the first floor not unlike the outdoor space on top of Gropius's house. The Kaufmann roof space (Fig. 2) is open on two sides except for the western and northern faces, shielded by a closable louvered wall providing greater privacy, and protection from windswept sand and radiant heat. The aluminum louvers, of which the longest chain shielded a walkway on the first floor, were linked so that each louver in a section opened simultaneously, relieving the operators of the need to maneuver large extents of stats individually by hand.



Figure 3: Northwestern Mutual Insurance Building. Photo by author.



Figure 4: Close-up of Northwestern Mutual Insurance. Photo by author.

NORTHWESTERN MUTUAL FIRE ASSOCIATION BUILDING

Vertical exterior louvers proved versatile in the Kaufmann House and contributed to a novel aesthetic that allowed Neutra to introduce prominent vertical elements along with his signature spider-leg outrigging. The spider-legs were essentially decorative although Neutra's inspiration in Rotterdam was functional, supporting fabric awnings (Hines 2005). With Neutra's Northwestern Mutual Fire Insurance Building (1950) in Los Angeles, rotating vertical louvers primarily served as solar and glare protection, the role vertical louvers systems played throughout the remainder of his career. Built as local offices for an insurance company, he applied different solar control strategies for different exposures of the building. The operable vertical

louver system was located on the most prominent façade, an eastern exposure facing the street (Figs. 3 & 4). Storefront windows were located on the ground floor and louvers framed by a projection covered the second floor glass and spandrel. The effect was to provide an elongated brise-soleil effect with the louvers open. Louvers on the eastern face complemented horizontal awnings on the south face of the building that faced an open lot at the time the building opened.

In 1949, Richard Neutra and Robert Alexander started collaborating and soon after formed a partnership that allowed Neutra access to larger projects while continuing to design small projects and residences from his home office (Hines 2005). Northwestern Mutual and San Bernardino Medical Center (1953) both contained similar louvers designed before the partnership solidified. Alexander brought his own sensitivity to solar design to the practice contributing to continuity of development of Neutra's earlier work. The first building to contain the louver system under the partnership was the Amalgamated Clothing Workers of America (1956) in Los Angeles. The louvers in the building retained the same profile as Northwestern and Medical Center buildings with a motorized louver wall oriented to the east adjacent to the main entry. All other western and eastern exposures had few openings, with office glazing oriented north and south.

AUTOMATION

OTHER AMERICAN ARCHITECTS

Designed to house a cylindrical painting, the Gettysburg Cyclorama (1959) was the next Neutra commission to include an automated vertical louver system, this time with light sensors. Two non-Nuetra commissions represented progressions with the louvers system prior to Gettysburg. The Raleigh News and Observer Building (1954) in North Carolina had a timed control system by the same Southern California concern, the Lemlar Manufacturing Company, which manufactured the louvers for Neutra's previous louver systems. (Lemlar entered the manufacture of aluminum louvers two decades earlier for residential use and developed a novel system with horizontal rotating louver elements.) The louvers were located across the southern and western faces of the top two stories. A building for the American Association for the Advancement of Science in Washington, DC (1956) had similar controls. Louvers in the latter building were located on the eastern, western, and southern face of the building. A shortcoming of both of the buildings was the use of vertical louvers on the southern façade that are less effective than horizontal louvers.

The Reynolds American Headquarters Building in Richmond, Virginia (1958) contained controls with sensors similar to the Gettysburg building, planned during the same period. Designed by Gordon Bunshaft of Skidmore, Owens & Merrill, the offices surround a central courtyard with the top two floors above first floor set back so that they appear to float. Louvers cover the windows on the top floors on all east and west exposures (AIEE. 909). Most SOM buildings prior to, and after, the Reynolds building did not conform to immediate environmental conditions, or change façade treatments on different orientations including reduced extent of curtain wall. In the case of the Reynolds headquarters, which was a showcase for aluminum, the interior courtyard louvers were largely superfluous during the hottest portion of the year when the sun is lowest on the horizon. The slab extensions on the southern faces provide limited solar protection, but are not optimized for the path of the sun.



Figure 5: Gettysburg Cyclorama prior to demolition (Photo courtesy of Leslie Johnson).

GETTYSBURG CYCLORAMA

The first Neutra & Alexander building completed with louvers operated by an automated solar control system was the Cyclorama in Gettysburg, Pennsylvania (Fig. 5). The design included a low-slung long mechanically operated louver wall on the east façade with a profile similar to Neutra's earlier systems. Neutra and Alexander proposed an automated system in lieu of a manually operated one for greater responsiveness to natural conditions and the likelihood that the louvers would remain fixed if not self-adjusting. Initially the National Park Service was reluctant to follow the advice until reassured with cost-benefit analysis factoring heat loss and gain, and controls incorporating a manual override (Allaback 2000). Like the Gettysburg Cyclorama (1959), the Los Angeles County Hall of Records (1961) and Dunn Library at Simpson College in Iowa (1963) incorporated automated solar control systems that rotated the louvers according to the time of day with over-rides for extreme light conditions. The latter two buildings incorporated more robust aluminum louvers streamlined to resemble the profile of airplane wings, contributing to their structural stability and resistance to displacement from wind.



Figure 6: Façade of Los Angeles County Hall of Records (Photo by author).

LOS ANGELES COUNTY HALL OF RECORDS

The most accessible example of the Neutra louver system is located in the Los Angeles Civic Center on a thirteen-story building designed to house municipal offices and archives. Once operable, the Hall of Record's southwest facing louver wall includes 120-foot high louvers, now fixed at different orientations that obscure the glazing behind (Fig. 6). The fins pivoted on a rear-biased axis allowing for maximum coverage per louver extent and heat induced expansion was anticipated at design, and the interior of the robust louver section designed to induce natural airflow, thus cooling the fins. Text associated with preliminary diagrammatic studies for the louver used to demonstrate the efficacy of the system to the clients compares the louvers to Corbusier's brise-soleil. Especially observant is the difficulty of shielding sun late in the day, even with fixed vertical shading elements. A fixed system at an angle appropriate for late evening sun would obstruct views toward the open mall. Neutra related the vertical fins to classical columns and monumentality worthy of a civic building recognizing a need to adapt solutions to cultural as well as environmental contexts (Boesiger 1966).

SIMPSON COLLEGE LIBRARY

Located approximately fifteen miles south of central Des Moines, Dunn Library is a two story rectangular structure with an open mezzanine above the second level planned for expansion of the book stacks. A two-story high louver system is located on the western face of the building above the main entrance punctuated by a cantilevered awning above the doors (Fig. 7). With the exception of a narrow vertical strip window, the remainder of the western end of the structure does not have glazing. This contrasts with a southern exposure of extensive glazing covered by a horizontal awning constructed of wood slats. Access to the roof permitted the author a close look at louvers now fixed so that the fins are perpendicular to the building, and to the system controls housed in the roof penthouse. The symmetrical louvers pivot on a central axis connected by a small channel at the top and bottom (Fig. 8) that are fused to steel tubes running perpendicular to the building, contributing to the effect that the louvers are floating. A metal bar with a small cross section links the louvers and connects to the motor that facilitated motion.



Figure 7: West façade of Dunn Library. Photo by author.



Figure 8: Close-up of louvers at Dunn Library. Photo by author.

The original control interface (Fig. 9) is still intact despite over twenty years of louver inactivity. Instructions inside the control box outline three operating modes for the louvers. The default mode is a clock function designed to situate the louvers in the optimal position during the day determined by the programmers. Seasonal variation necessitated replacing a clock wheel at specified dates throughout the year. The complication of accessing the penthouse and changing the wheel presented an obstacle in the way of optimal operation of the louvers. Another option connected the control to a photocell, that when triggered that would override the clock function if the lighting levels were significantly different from those anticipated by the programmers. The final mode is a completely manual permitting an individual to open and close the louvers as desired, a function complicated by the need to access the roof penthouse by crossing the roof from the stair tower. The directions inside the circuit panel were intricate enough to discourage use of the full range of options by facility personnel and library staff.



Figure 9: Control at Dunn Library. Photo by author.

LATE CAREER BUILDINGS

After the Kaufmann House, all of Richard Neutra's louver systems were in non-residential buildings until he rebuilt his Los Angeles home after a fire decimated it in 1963. The VDL House II (1964) incorporated a louver system with a similar profile to the larger buildings on the west elevation provide a functioning unifying element for the elevation otherwise dominated by horizontal banding. The last building to include the movable louver system was the Orange County Courthouse in Santa Ana, California (1968) designed in partnership with a local firm Ramberg & Lowrey (Fig. 10). The louvers were similar to those found in the Los Angeles County Hall of Records, encompassing the south facing façade of the tower and western exposure of a lower wing.

CONCLUSION

Reasons why few architects adopted an automated vertical louvers system during Neutra's lifetime relate to timing, lack of knowledge of the benefits of the system relative to costs, and difficulties designing for the sun. By the 1960's, air-conditioning was a standard feature in new office construction in the United States, regardless of climate. Air-conditioning

distanced the control of the internal environment from the user and placed it in the hands of engineers operating under national design standards that determined air-quality and comfort levels for facilities with centrally operated plants. The standards were consistent with developers' goals to reduce costs in buildings since operable windows cost more that fixed windows and effective cross breezes required shallow floor plates, and less enclosure relative to floor area (Cooper. 152-164). Standardization of building services coincided with an aesthetic of mass-produced curtain walls with similar surfaces at different building exposures amplifying a unified appearance of repetitive wall patterns. Interior blinds provided privacy and protection from glare consistent with this aesthetic. Exterior and interior façade treatments that did not acknowledge local environmental conditions were antithetical to the manner in which Neutra designed throughout his career, even when he utilized a monochromatic material pallet during the inter-war years.



Figure 10: Orange County Court House. Photo courtesy of Chris Jepson.

Unlike the brise-soleil, there were fewer opportunities to learn about the system, and it did not benefit from inclusion in theoretical treatises or exhibitions. Outside of personally experiencing a system, exposure was limited to architectural trade journals that did not describe the functioning of the louvers and sporadic advertisements by Lemlar and another company in Miami. Concerns of extra cost compounded notions of unreliability since there were few examples to foster confidence. In the United States, energy shortages during the seventies did not spawn exterior solar control devices in lieu of available glass treatments that reduced direct heat gain but limited heat gain when desirable. Europeans remained more open to solar control strategies due to stringent building codes and less access to fossil fuels. Today, the Colt Group, a European company that specializes in industrial ventilation markets a system that resembles the one fostered by Neutra offering promise that the system will return to the United States where rotating louvers feature prominently in a recent building at Princeton University.

REFERENCES

Allaback, Sarah. *Mission 66 Visitor Centers*, National Park Service Online Books, Government Printing Office, 2000.

American Institute of Electrical Engineers, "Automatic Sun Louver Features of Aluminum Showcase", *Electrical Engineering*, New York, Volume: 77, October 1958.

Boesiger, W. *Neutra, Building and Projects Volume 2*, Frederick A. Praeger, New York, 1966.

Cooper, Gail. *Air-conditioning America: Engineers and the Controlled Environment, 1900-1960*, Johns Hopkins, Baltimore, 1998.

Curtis, William. *Le Corbusier: Ideas and Forms*, Phadion Press, London, 1994

Hines, Thomas. *Richard Neutra: And the Search for Modern Architecture*, Rizzoli, New York, 2005.

Integration <> Adaptation

ADAPTABLE GLAZING SHIELDS

Pushing the envelope of facade and window retrofits



Anas Al Kassas, Assoc. AIA
Inovues
anas@inovues.com

ABSTRACT

Today, about 40% of all buildings in the U.S. still have single-pane windows, and ~70% of the existing building stock is estimated to suffer from under-performing facades. Experts project that 20-40% of the total energy savings in buildings—the #1 end users of energy—to be from windows and building envelopes. Thus, the demand for energy-efficiency facade and window retrofits/upgrades is estimated to grow rapidly over the coming years due to the rapid adoption of energy-efficiency regulations for existing buildings, which in turn, are influencing the real-estate market.

The problem is that window replacement is a highly intrusive and costly solution that is often carried out only when the windows reach the end of their service-life and must be replaced. Additionally, most glazing systems—including the current ones—are designed with little consideration (if any) given to their inevitable retrofit during the service-life of the building. Thus, most facade and window retrofit practices are often considered not feasible as well due to the associated complexity, building and business disruption, and long payback period.

This paper presents the concept of Inovues' patent-pending, external window upgrade system and non-intrusive facade retrofit method. The technology provides a cost-effective and sustainable solution for upgrading the old/inefficient, single- or double-glazed curtainwalls to high-performing double- or triple-glazed systems without requiring any replacement or causing building or business disruption. A case study using Lever House in NYC is presented, which is one of several performed to analyze the visual impact, thermal performance, payback, and ROI. The results showed an improvement of over 50% in the total system U-Factor; over 250% increase in condensation resistance; ~15% improvement in thermal comfort in the perimeter areas; nearly 20% energy savings; and ~85% shorter payback period (compared to replacement) with ~300% ROI over the estimated 20-25-year service-life of the system.

KEYWORDS

facade, curtainwall, glass, retrofit, energy efficiency, adaptability, case study

INTRODUCTION

In the United States—the second largest energy consumer and greenhouse gas emitter in the world after China—most GHG emissions come from energy consumption and production (84% in 2014), and carbon dioxide makes up the majority of these emissions (92% in 2014) (Enerdata 2016; EIA 2016). According to Architecture 2030 (2013), the building sector alone is responsible for almost half of all energy consumption (47.6%) and CO2 emissions (44.6%), outperforming both industry and transportation. Globally, similar percentages (40%) were found in both developed and developing countries (UNEP 2009).

Today, 30+ U.S. cities have set bold emissions reduction targets of 80% or higher by the year 2050 or earlier (WWF 2015). Many of them have started issuing stringent mandates and ambitious action plans that target the energy efficiency of the existing building stock. The reason is that most existing buildings would need to become nearly 40% more energy efficient for cities to achieve their overall 80% reduction target (Long 2011). Meeting this goal means many existing buildings would require deep energy retrofits over the coming years with measures that address all building systems, including the building envelope. Some experts estimate that nearly half of the existing building stock in the U.S., about 150 billion ft², will need to be renovated over the next 30 years (Holness 2008). Currently, the majority of the commercial building stock is ready for retrofit due to being over 20 years old (ESB 2009; EIA 2015).

Taking that into consideration, several reports have highlighted that 20-40% of the total energy savings in buildings is projected to be from windows and building envelopes (IEA 2013; Habibzadeh 2015; Apte and Arasteh 2006). Up until the 1980s, windows and curtainwalls were mainly single-glazed with frameworks that had no thermal breaks, leading to a significant heat loss in the winter and heat gain in the summer, and as a result, higher energy consumption. Today, about 40% of all commercial and multifamily residential buildings in the U.S. still have single-pane windows, and most of the remaining 60% have early/low-performing double-pane window systems that lack significantly in performance compared to the current glazing technologies and building and energy code requirements (DOE 2017; EIA 2016; Schiff 2014; Apte and Arasteh 2006). Some estimates indicate that about 70% of the existing building stock suffer from underperforming facades (Fig. 1) (Enclos 2013).

Therefore, the demand for energy-efficiency façade and window retrofits/upgrades is estimated to grow rapidly over the coming years due to the rapid adoption of energy-efficiency regulations for existing buildings, which in turn, are impacting and influencing the real estate market. For example, New York City highlighted in the recent “One city: Built to Last” action plan that all single-pane windows will need to be replaced, and they announced that they are going to invest $1 billion to retrofit 3,000 city-owned buildings to lead by example (NYC 2016b; NYC 2016c). According to Navigant Research, the building envelope energy-efficiency market in the U.S. has been showing an impressive growth with 60% increase since 2011, reaching $15 billion in 2016 (Navigant 2016).

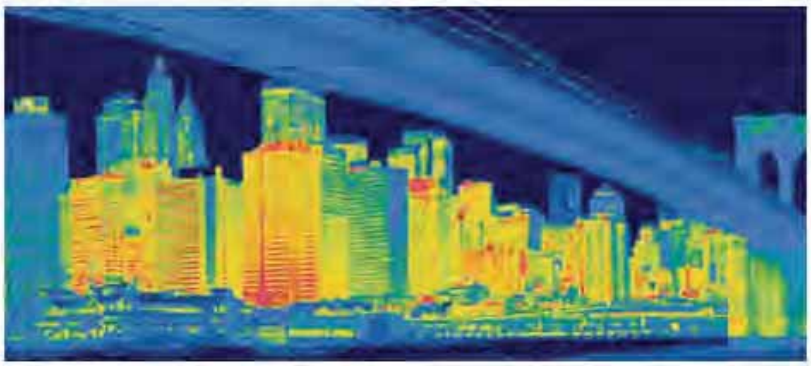


Figure 1: A thermal infrared image showing the heat loss from New York City buildings. Photo by Tyrone Turner, National Geographic (Chambers 2009).

BACKGROUND

Despite the steady and fast growth over the past few years and the projected increase in demand in the future, the building envelope energy-efficiency market is still considered a largely untapped segment with a huge gap between its profitable potential and the reality (UNEP FI 2014). Facade retrofit activities in general and window replacement, in particular, are widely considered a major undertaking that is most likely carried out only when the component is due for replacement—i.e., not earlier as a pure energy saving measure (IEA 2015). One of the main reasons behind such perception is the extended payback periods (50-100 years) that are much longer than the average 3.6 years associated with typical energy efficiency retrofits, like indoor lighting, which render investments in the building envelope as too risky (McGraw-Hill 2011).

Most facade and window retrofit solutions available today include intrusive measures that require the disruption of building uses and business operations for extended periods of time, which increases the overall cost dramatically, and in turn, the payback period. Thus, current retrofit practices are often considered not feasible by most owners and tenants. In many cases, all or major parts of the existing facade and glazing systems would need to be ripped off and replaced with new ones simply because upgrading the critical and under-performing parts, like the glass infill panels or the seals, is just too complex (Fig. 2) (Patterson 2012). In addition, given the destructive nature of these practices, they normally result in a significant amount of construction-related waste and unused materials that need to be shipped to landfills, which increases shipping and labor costs, and in turn, results in a longer payback period. Further, most retrofit solutions utilize complex systems that are associated with complex installation methods. They often require an entirely new and customized system-design for each building, which in turn limits scalability and increases upfront costs.

Therefore, most conventional retrofit methods are considered unsustainable practices—economically and environmentally. Building owners often ignore them due to the associated complexity, building and business disruption, and long payback period. However, given that the service life of most glazing systems is far shorter than that of the whole building (20-30 vs.

50-100 yrs.), retrofitting building windows and curtainwalls—something that is not deliberately considered in their original design, including the current systems—is an inevitable event during the much longer service life of the building.

Recently, a few low-cost and less disruptive window-retrofit practices have been developed and showed some gain in energy efficiency, including interior supplemental vision panels, low-e window films, and low-e storm windows. However, many drawbacks prevent them from being widely adopted by most buildings. Storm windows, which are the only exterior retrofit option available, are a temporary and impractical solution that generally do not work with curtainwalls and cannot be used on high-rise buildings. They are more suitable for single windows in punched openings, particularly for houses and low-rise residential. Moreover, they typically change the appearance of the original window and interfere with its operation, which in turn, limits their adoption.

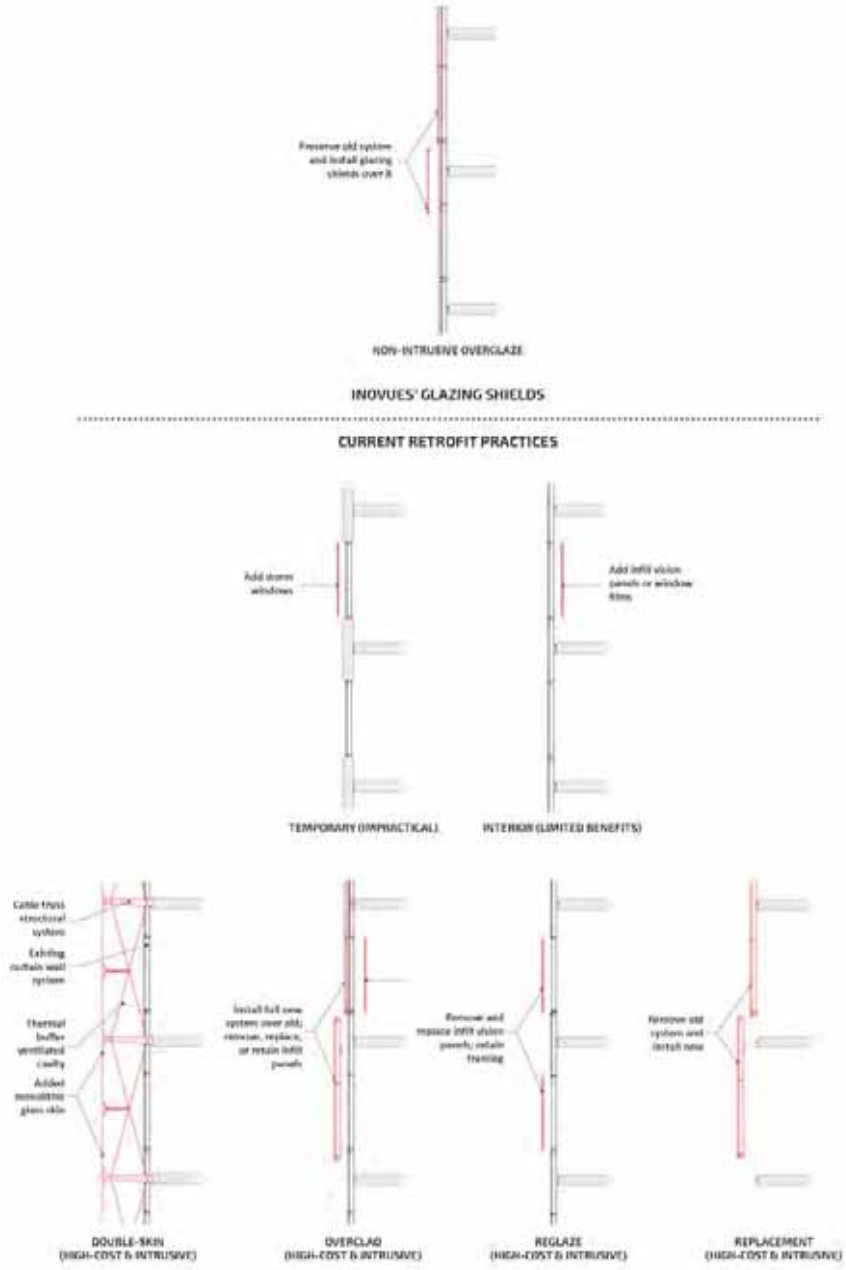


Figure 2: Wall section diagrams comparing Inovues' non-disruptive retrofit method to other conventional facade and glazing retrofit practices. Diagram by the author. (Enclos 2012).

The interior supplemental vision panels, on the other hand, also interfere with operable windows; they are not compatible with some glazing systems; and they often fail to alleviate the performance deficiencies and thermal bridging in the frames, particularly in curtainwalls. In addition, there is a risk when they are installed behind tinted glass, particularly if not heat-strengthened, that the original glass could overheat and break (thermal stress breakage) due to having the newly-formed air gap and the low-e glass of the new panel on the inside and not on the outside. Also, if the existing glazing system is not weather tight, air and moisture may leak through the original seals into the newly-formed air gap, in some applications, and increase the risk of condensation.

Another interior application is the use of low-e window films, which also do not address the performance deficiencies and thermal bridging in the frames—they mainly improve the thermal transmittance (U-Factor) of the glazing infill panels only. Thus, they do not improve the overall thermal performance of the original window system as much as other solutions. Also, they are generally prone to scratches, have a relatively short warranty period, and are only effective on windows without condensation (Wright 2014). There are also applications that significantly alter the optical properties of the glazing infill panels to a point that makes them unpractical as vision panels. Other Retrofit options compromise the historic characteristics or the architectural identity of the building, which prevents them from being adopted by a significant number of properties, particularly those designated as historic landmarks.

Further, it is worth noting that all interior applications do not provide the benefits typically associated with an exterior retrofit—they only offer interior, energy-related benefits. For example, they cannot protect the original glazing systems, address the performance deficiencies that are related to their seals, or extend their service life to delay/avoid their replacement. Also, they cannot offer features to enhance the exterior image of the building if the owner is interested in a facade retrofit for aesthetic purposes. In fact, aesthetic improvement (image update) and performance/failure remediation (durability) were found to be the 1st and 3rd drivers respectively for façade and window interventions according to a market survey by researchers at the University of Southern California (Martinez and Patterson 2013). That is why interior retrofit solutions often face the "split-incentive" barrier with building owners—an issue that is impacting the adoption rate of many energy retrofit solutions and slowing the overall impact of energy efficiency on the existing building stock. The reason for the split incentive barrier is in part because most energy-efficiency retrofit solutions often fail to provide significant economic benefits to building owners who are typically responsible for the upfront costs of energy retrofits, while the tenants—who often pay the energy bills—end up capturing the energy savings.

Therefore, there is a growing need in the largely untapped building envelope energy-efficiency market for next-generation window and curtainwall retrofit solutions that are not only cost-effective and non-disruptive but also able to offer several economic, energy and non-energy related benefits to both owners and tenants—which is necessary to allow new technologies to reach a high level of market penetration, and in turn, promote a faster transformation into a sustainable future.

ADAPTABLE GLAZING SHIELDS

An external window-upgrade system “glazing shield” and a non-intrusive facade retrofit method are being developed. The objective is to provide a cost-effect and sustainable solution for upgrading the inefficient single- or double-pane windows and curtainwalls to high-performing double- or triple-pane systems without having to replace or alter any of their original parts and without causing disruption to the building or the occupants. The glazing shield system comprises a support spacer and a unitized panel (Fig. 3). The anchor-like support spacer is made up of smaller assemblies (individual sides) and is mounted directly on the existing glazing system in a non-intrusive and non-destructive installation method using structural adhesives. The unitized panel is mounted on the support spacer, trapping a volume of air between the infill panel of the original glazing system and the unitized panel of the glazing shield.

The adaptable design and highly compact and lightweight nature of the glazing shield (<1” thk., ~3.5lb/ft) allows it to work with most old and current, framed or frameless-looking glazing systems as an exterior or interior attachment. When used as an exterior retrofit solution, the system results in a new insulating weather barrier that preserves the original window/curtainwall and improves its thermal insulation properties between 40-55% (simulations), sound insulation properties by about 50% (10+ STC pts, 4+ OITC pts, estimates), and condensation resistance by over 240% (simulations). The new weather barrier would also alleviate most of the performance deficiencies in the original window/curtainwall system without compromising its structural integrity. By utilizing a very minimal frame—compared to a full window/curtainwall—the average

weight of the glazing shield with a ¼” laminated glass would be almost half the weight of a typical 1" IGU with two ¼” glass lites (6.5lb/ft).

It is worth noting that in most old and current windows and curtainwalls, the metal frame members often maintain their structural integrity beyond the standard service life of the overall system. Additionally, most glazing systems are typically designed with relatively high safety factors for static and dynamic loads, which is due in part to the limitation in structural simulations with regards to accurately determining the behavior of materials in real life conditions while accounting for any non-factored loads or shortcomings during construction. Moreover, most systems often end up being specified with standard size structural parts and fasteners that are likely to be higher than what is required by the structural calculations. Thus, most glazing systems end up being inefficient with excessive structural capacity beyond needed, making it feasible for the original window or curtainwall to carry the additional light load of the glazing shield. Taking that into consideration, the glazing shields would use only a fraction of the remaining structural capacity in the existing system, which could be determined by a structural field test. A similar application that takes advantage of the excessive structural capacity and is already being used with curtainwalls is the addition of an interior supplemental vision panel (monolithic and IGUs), which is typically supported by the horizontal frame member only.

In terms of performance, the glazing shield system utilizes a thermally-broken attachment that helps create a highly-insulating weather barrier, which significantly improves the overall performance of the original window. The system also incorporates multiple air, water, and moisture barriers that prevent any leakage to the newly-formed, non-permanently sealed air gap. The new seals also cover the existing ones that might not be performing well, which helps mitigate the deficiencies in the performance of the original framework. Additionally, the panel of the glazing shield utilizes multiple desiccant elements, permanent and removable, including a silicone foam with desiccant pre-fill. These desiccant elements would help remove any residual moisture in the air and reduce the risk of condensation and volatile fogging that might form on the surfaces adjacent to the newly-formed air gap.

Further, the glazing shield utilizes a unique locking mechanism that retains the panel in place without requiring any drilling or mechanical fasteners. In addition, the flexible weather-tight joints provide enough tolerance for installation and allow the glazing shields to adapt easily to movements in curtainwall panels—which tend to be very minimal in the glazing shields because they are directly attached to the original infill panels, and thus, they already move together with them as the panels move. Also, the glazing shield system incorporates a flexible rubber gasket around the perimeter of each unit. The gasket would provide a flexible joint between the adjacent units, allowing them to adapt individually to the movement of their associated original infill panels.

The installation is typically performed in two stages. After the original glass is cleaned, the four pre-assembled sides of the support spacer are individually attached to the original glazing infill panel using structural adhesives—a proven material in the glazing industry for similar applications since the 1980s. The second stage is mounting the pre-fabricated unitized panel on the support spacer after the original glass is re-cleaned, creating an insulated air gap between the original glazing system and the glazing shield.

In addition to the lightweight nature of the system, splitting the glazing shield into two separate components allows for a relatively easier and manageable method of installation on site. In many cases, the lightweight glazing shields could be installed using the existing window cleaning platforms or facade access systems (BMUs) without the need for additional scaffolds or custom installation platforms. The split system also makes it feasible to utilize structural adhesives in the field. So, by attaching the 1.5” wide individual sides of the support spacer first, the adhesive will be allowed to fully cure before it is stressed with the load of the panels.

Further, it is worth noting that separating the unitized panel from the support spacer allows it to be non-permanently fixed to the existing glazing system, which makes it easily replaceable/upgradeable if needed. This feature enables building facades and windows to become resilient by allowing them to be easily retrofitted when the need arises. Moreover, given the relatively short payback period of this retrofit, existing buildings will be able to continuously incorporate the latest technologies without the need to rip off all or parts of their original facades or glazing systems every time. For example, cutting-edge technologies like vacuum insulated glazing, dynamic glazing, vision photovoltaic, and media facades would be available for existing buildings by incorporating these technologies in a self-sufficient, mount-and-play panel that replaces the old one without the need for an entirely new facade or window system.

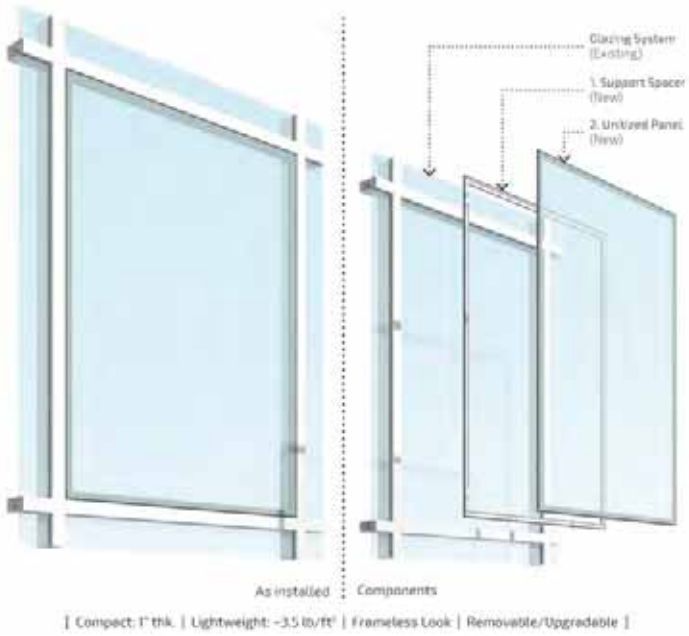


Figure 3: A 3D image showing the primary components and the split structure of the glazing shield system. Image by the author.

METHOD

Several before-and-after system-based and building-based analysis studies were performed on different glazing systems and existing buildings to analyze the overall impact and feasibility of the glazing shields. This includes visual impact, thermal performance, energy savings, and simple payback and return on investment (ROI).

SYSTEM-BASED STUDIES

Before-and-after thermal analysis studies were performed on the following types of glazing systems, which represent a wide range of existing buildings:

- Case 1: Stick Curtainwall System (Fig. 12, 15, and 16)
  Single glazed using 6mm (¼") monolithic clear glass panels. The aluminum framing utilizes a dry seal with pressure plates and cover caps, and the system is not thermally broken.
- Case 2: Unitized Curtainwall System (Fig. 13)
  A 4-sided structural silicone glazing system (SSG) using 25.4mm (1") insulated glass units (IGU) with two 6mm (¼") monolithic clear glass.
- Case 3: Single Fixed Window System (Punched Opening) (Fig. 14)
  Single glazed using 6mm (¼") monolithic clear glass panels. The aluminum framing utilizes a dry seal with pressure plates and cover caps, and the system is not thermally broken.

The following intervention scenarios were simulated and compared against a baseline model to show the difference in performance (Fig. 4):

- Baseline Model: Existing system
- Opt 1: Existing + glazing shield with aluminum profiles.
- Opt 1a: Existing + glazing shield with ~75% uPVC profiles.
- Opt 2: Existing + glazing shield with ~75% uPVC profiles + 2 coats (7mm) of clear thermal insulation paint on caps.
- Opt 3: Existing + glazing shield with uPVC profiles + 12.5mm deep, additional 1.2mm thk. aluminum tube (fake cap) with a double sided structural adhesive tape.

The simulations were performed per the standards of the National Fenestration Rating Council (NFRC) for certifying glazing products using THERM 7.5 and Window 7.5 by Lawrence Berkley National Laboratory (LBNL). By using the NFRC guidelines, the results can be compared against other NFRC certified glazing systems. Also, the percentage of improvement can be

used as a reference or a starting point to estimate the improvement in thermal performance of similar glazing systems that fall under the same family of the ones that were simulated.

Note: The glazing shields simulated in these studies utilized a monolithic laminated glass with a pyrolytic low-e coating (hard coat) on surface #2 of the laminate (Fig. 15).

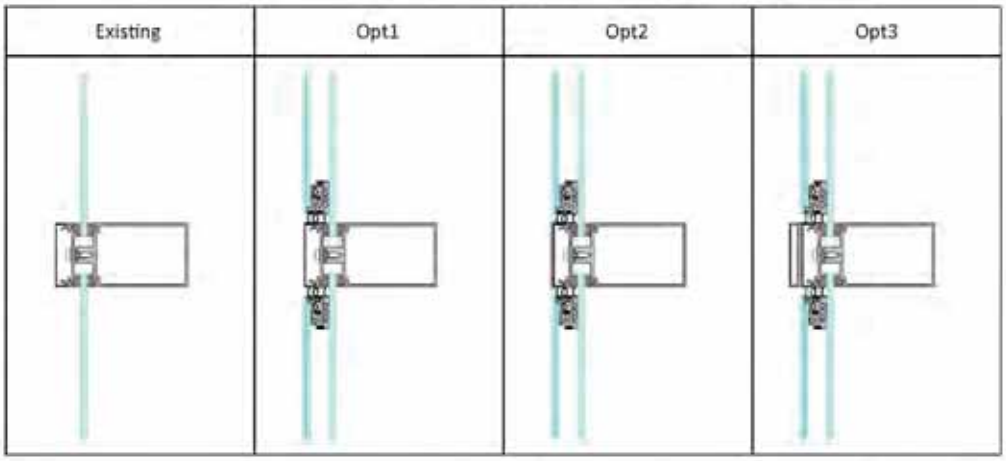


Figure 4: Case 1 stick curtainwall details at a typical horizontal meeting rail showing the existing and the proposed intervention scenarios with glazing shields—early concept. Image by the author.

PARTIAL BUILDING-BASED STUDIES

Partial, building-based analysis studies were performed to examine the impact of the glazing shields on a 5-meter deep perimeter zone (16.4 ft) at several buildings in both heating and cooling dominated climates. The studies analyzed the impact of the shields from several aspects, including energy consumption, indoor environmental quality, and cost and payback. Comfen 5 by (LBNL) was used to model and simulate the scenarios, which were repeated for the four elevations of each building to highlight the differences in impact each scenario has relative to the orientation.

In addition to simulating a baseline model, the primary intervention scenarios outlined above in the system-based studies were simulated twice with curtainwall systems. One set was simulated with the glazing shields applied to the vision and spandrel panels, and the other set with them applied only to the vision panels.

Notes Regarding the Simulation Process:

- Input values in Comfen that are related to the characteristics and the performance of the curtainwall as a system were derived from the results of the system-based case studies outlined above.
- The maximum allowable U-Factor for frame members in Comfen is 6.2 W/m2-K (1.1 Btu/h-ft2-F). Thus, all frame U-Factor values above the maximum value were normalized to align the baseline value of the system with the maximum allowable value in Comfen. However, this does not impact the outcome because it is a comparative and benchmarking process.
- Comfen's location-based labor and material cost adjustment factor was neglected to achieve neutral results (Fig. 17).
- Given that this is a benchmarking and a relative comparison process against a baseline model, Comfen generic values with regards to the HVAC and lighting systems were used for all scenarios.
- It is worth noting that there is no context input in Comfen, so the results do not take into consideration the impact of context shading on solar irradiation.
- Given that energy modeling in Comfen represents only a 5-meter deep perimeter area, the percentage of the total building energy savings will be smaller—estimated to be no less than 1/3 of perimeter savings (Curcija et al. 2017).
- The following are the estimated individual unit costs that represent each intervention option as shown in Figure 17:
    - Opt 1: $20/ft^2
    - Opt 1a: $20.19/ft^2
    - Opt 2: $20.6/ft^2
    - Opt 3: $21.5/ft^2

FULL BUILDING-BASED STUDIES

Full, building-based analysis studies were also performed to examine the impact of glazing shields on the whole building. Parametric energy models were built for each building to simulate a baseline scenario that resembles the current conditions of the facades and the primary intervention scenarios highlighted above. The simulation results of the intervention options were then benchmarked against the results of the baseline scenario to calculate the total estimated percentage of reduction in energy consumption. The percentage of energy reduction was then used with the actual reported source energy use intensity (EUI) to calculate the total estimated energy savings and simple payback period and ROI as shown in Fig. 19 for example.

In addition to simulating a baseline model, the primary intervention scenarios outlined above in the system-based studies were simulated twice with curtainwall systems (similar to the partial building-based studies). One set was simulated with the glazing shields applied to the vision and spandrel panels, and the other set with them applied only to the vision panels.

The parametric energy model was built using Rhinoceros 3d along with the Honeybee plug-in for Grasshopper, and the simulations were performed using the EnergyPlus engine by the U.S. Department of Energy (DOE). To ensure the results were accurate, each scenario model was simulated twice; once directly through the Honeybee plug-in in Rhino 3D, and once through the OpenStudio platform, which is developed by the National Renewable Energy Lab (NREL). The results between the two platforms were almost identical (only about 0.3% off).

The purpose of the full building-based studies was to simulate the impact of the facades on the total energy consumption of the building. Thus, the parameters that were considered variables between the scenarios were only those related to the characteristics of the facade and glazing systems. Taking that into consideration and given that this is a comparative/benchmarking process against a baseline scenario, the energy model focused primarily on the attributes of the building envelope to simplify the process. Therefore, a standard HVAC system was used in all scenarios and each floor was modeled as a single zone except for the mechanical floors. Context shading was taken into consideration in these studies by modeling the primary adjacent buildings that were more likely to drop shadows on the buildings throughout the day as shown in Figure 18 for example.

LEVER HOUSE – CASE STUDY

KEY ATTRIBUTES

- Designed by Gordon Bunshaft of SOM and built in 1952 (Fig. 5).
- 2nd curtainwall building in New York City.
- Designated as a New York City landmark in 1982 and was added to the National Register of Historic Places in 1983.
- The building went through a facade retrofit, also by SOM, between 1998-2001.
- The curtainwall system is till single-glazed.
- The property features a roof-top window-washing gondola.
- The energy use intensity (EUI) of this building is more than 94% of similar properties (Fig. 7).

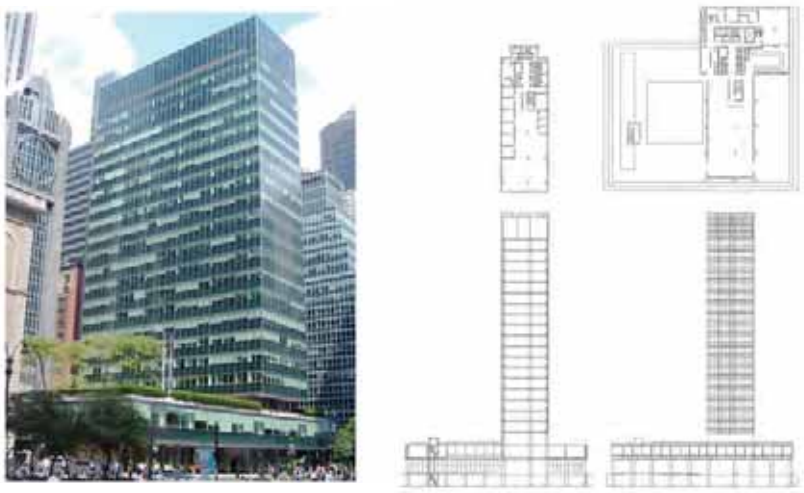


Figure 5: Lever House in NYC (left), image by Beyond My Ken / Wikimedia Commons. Lever House building plans and sections (right), image by www.quondam.com/21/217ki01.gif.

FACADE TYPOLOGY

An early type of metal stick curtainwall system with expressed horizontal and vertical frames that are not thermally broken. The curtainwall is made up of vision and spandrel panels that are single glazed (clear ¼" heat strengthened glass) (Fig. 6).

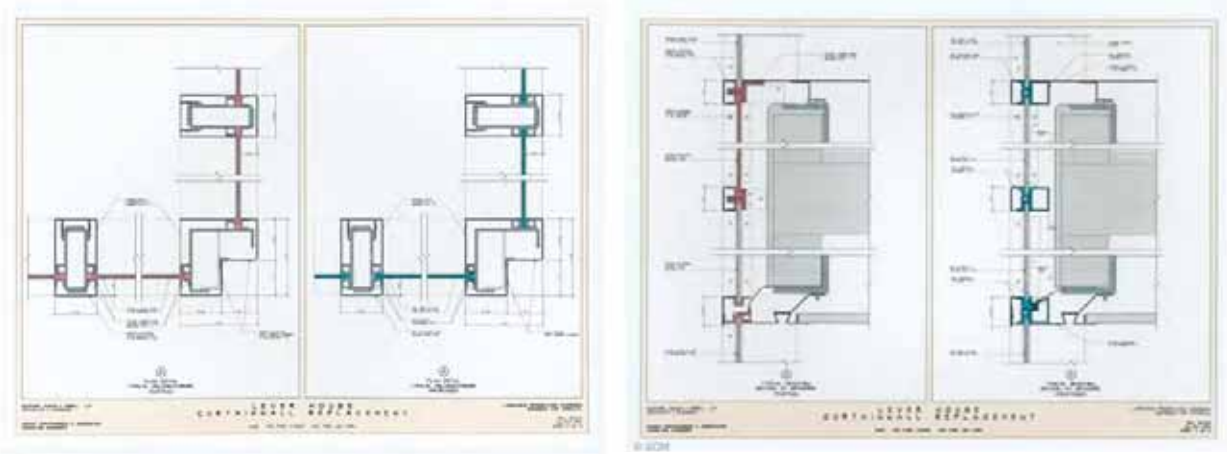


Figure 6: Lever House curtainwall details before and after the restoration job by SOM—horizontal details of typical mullions (left) and vertical details of typical horizontal meeting rails (right). Image courtesy of SOM.

THE POTENTIAL OF REQUIRING A FACADE RETROFIT IN THE NEAR FUTURE

According to New York City Energy & Water Performance Map, the energy use intensity of the building is more than 94% of other properties of similar type, and the greenhouse gas intensity is more than 93% of similar properties. In 2013, the building's source EUI was 345.8 kBtu/ft^2 and in 2014 was 349.9 kBtu/ft^2 (Fig. 7) (NYC 2016). Thus, it is projected that the building will be required to perform an energy efficiency retrofit in the near future to improve its performance by about 40%. This due to the new energy consumption and carbon emissions reduction targets that were introduced in the 2014 action plan "One City: Built to Last" by the mayor's office and its associated energy efficiency laws and regulations that target the existing building stock. To achieve this, the building envelope, in particular, needs to be addressed due to the significant impact of the single-glazed and non-thermally broken curtainwall on the energy consumption of this all-glass building.

Further, although Lever House is designated as a historic landmark—a status that used to allow a building in New York City to be exempt from complying with energy conservation codes and requirements—it was clear that the new action plan will target all existing buildings, including those designated as historic (NYC 2016b). Thus, retrofitting historic building facades is likely to become even more challenging because it needs to meet the stringent requirements of the continuously improving energy codes while complying with preservation guidelines.

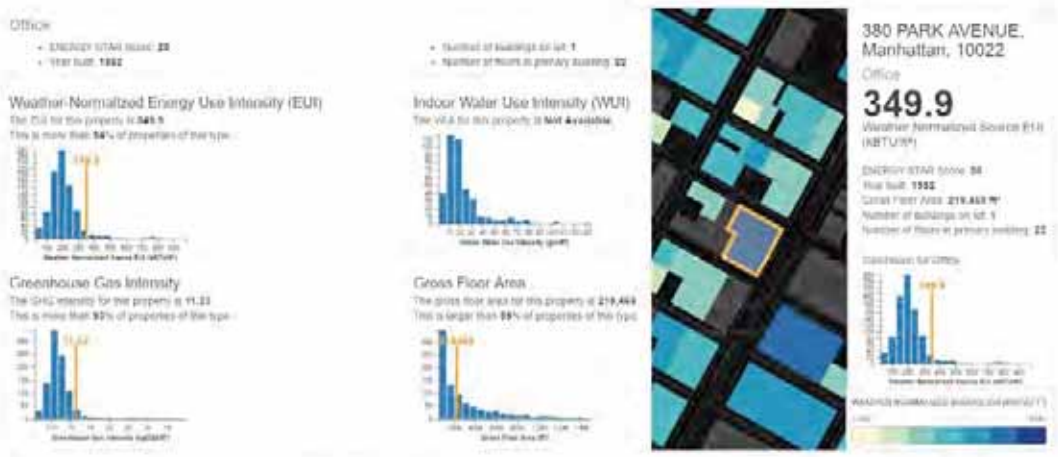


Figure 7: The energy use intensity of Lever House in 2014 as reported in the NYC Energy & Water Benchmarking Map. Image by the author, data by NYC 2016.

RETROFITTING LEVER HOUSE WITH GLAZING SHIELDS

One of the objectives of this case study is to illustrate the limited impact of glazing shields on the architectural identity of Lever House (Fig. 8, 9, 10, and 11). This retrofit method can preserve the historic characteristics of the building, unlike the intrusive and destructive facade retrofit solutions. Another objective is to show that this economically feasible and environmentally friendly retrofit method can significantly improve the performance of the original facade and the overall energy efficiency of the building, offering comparative performance results to new replacement systems. Also, it is worth noting that the window-washing gondola of this 1952 building, which operates around the parapet wall on tracks, could make it possible to install the glazing shields without the need for additional scaffolds or custom installation platforms due to the lightweight nature of the panels. This in turn could result in a shorter payback period and a better ROI.

Note: Given that this is a before-and-after comparative process, and in order to take advantage of this case study and use it as a starting point or a benchmark for other buildings with similar façade systems, the curtainwall analyzed in this case study is not an exact replica of the one at Lever House. Instead, the curtainwall illustrated in Case 1 in the system-based studies above was used, which shares the primary attributes of the curtainwall system at Lever House.

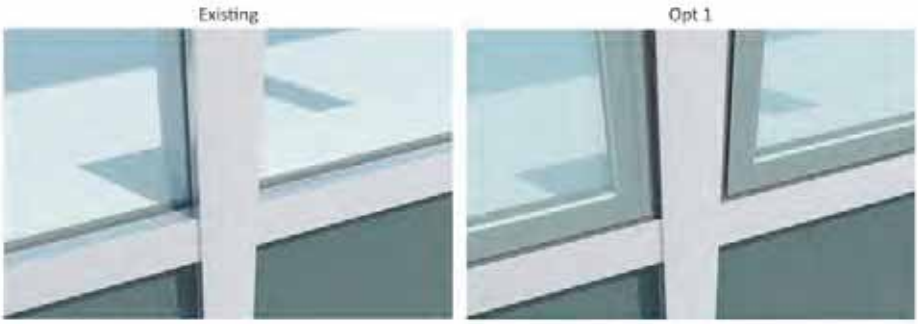


Figure 8: Close-up 3D images of a typical curtainwall joint at Lever House showing the existing and the proposed option 1 scenario with glazing shields on the vision panels only. Image by the author.

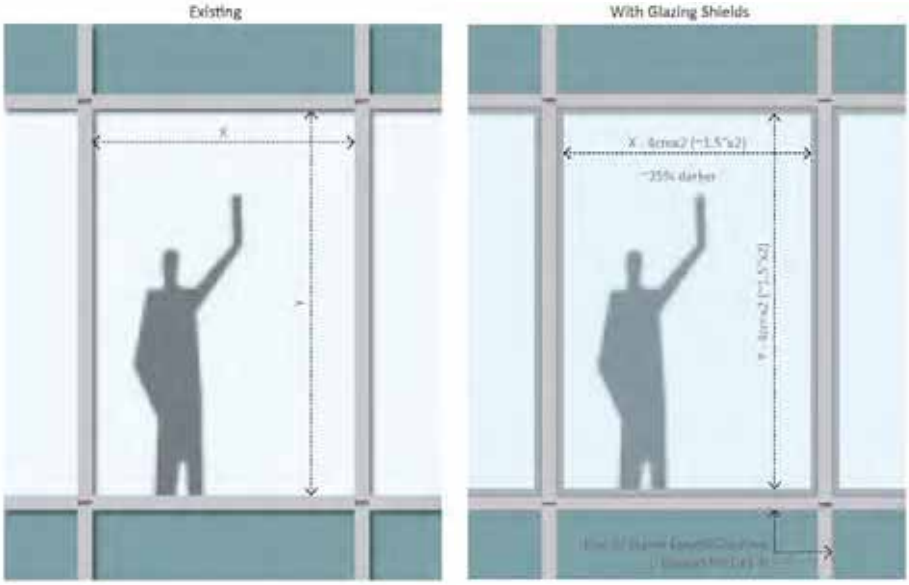


Figure 9: 2D elevation diagrams showing the visual impact of the glazing shields on a curtainwall system with exposed frames similar to the one at Lever House. Image by the author.



Figure 10: 3D rendered views of a partial facade at Lever House showing the existing and the proposed scenarios with glazing shields. Image by the author.



Figure 11: A partial facade view of Lever House showing the existing curtainwall (left) and Opt 1 intervention scenario (right). Image courtesy of SOM, edited by the author.

DATA

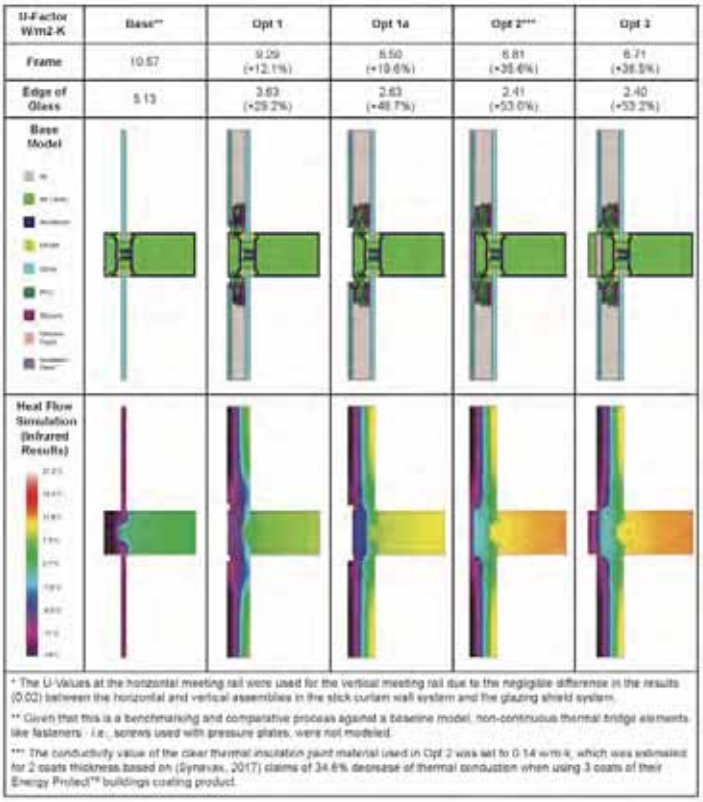


Figure 12: Thermal simulations at the horizontal meeting rail of Case 1 system showing the impact of each intervention scenario on the frame and edge of the glass U-Factor. Image by the author.

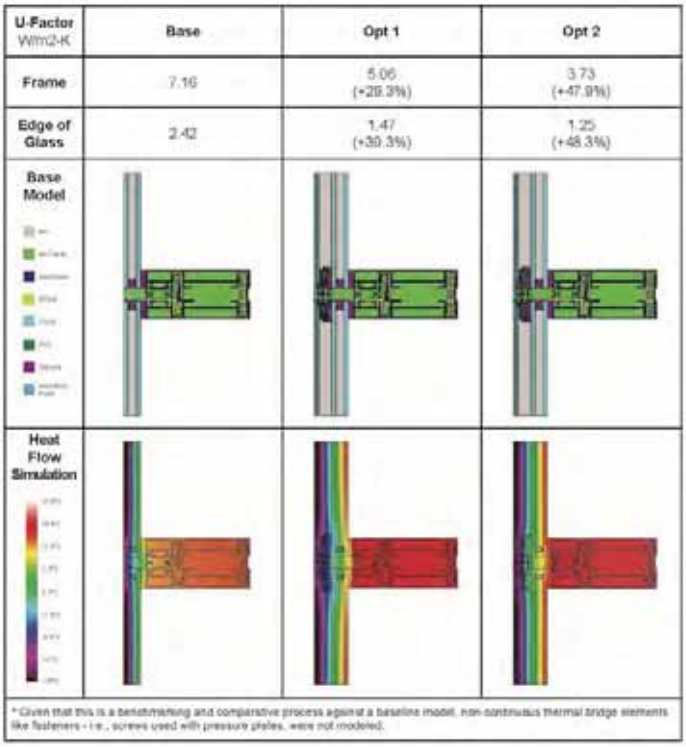


Figure 13: Thermal simulations at the horizontal meeting rail of Case 2 system showing the impact of each intervention scenario on the frame and edge of the glass U-Factor. Image by the author.

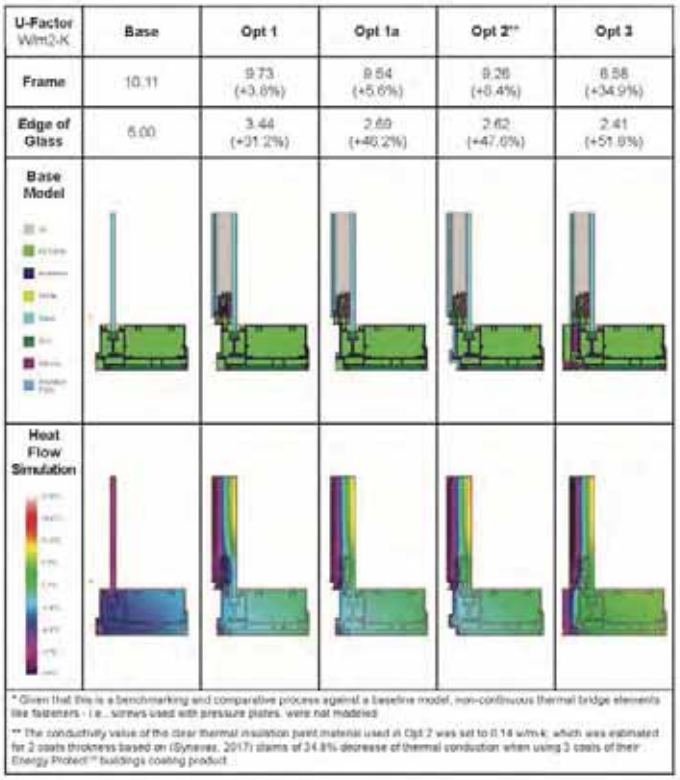


Figure 14: Thermal simulations at the horizontal meeting rail of Case 3 system showing the impact of each intervention scenario on the frame and edge of the glass U-Factor. Image by the author.

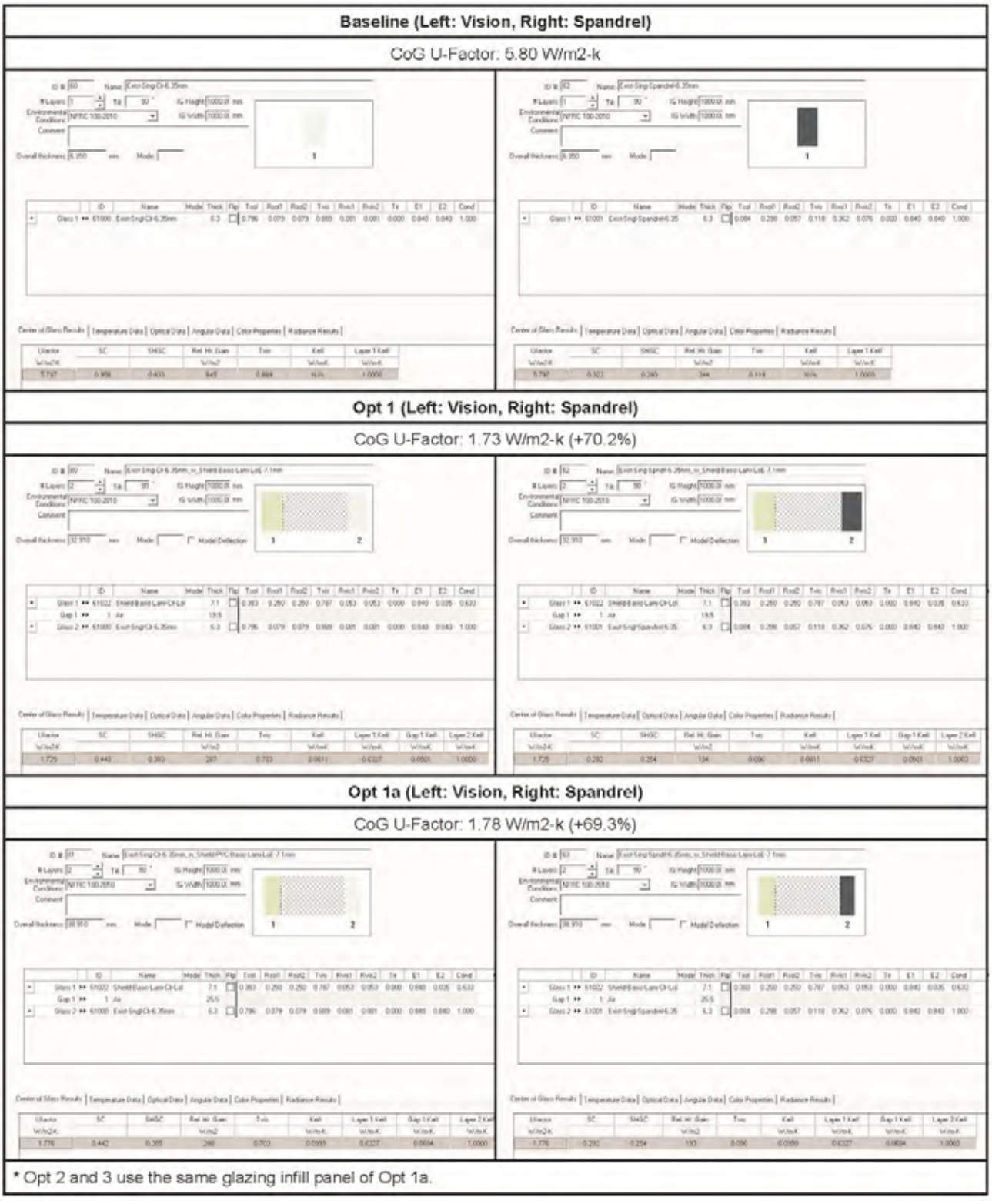


Figure 15: Glazing infill panel and center of glass (CoG) performance for Case 1 intervention scenarios. Image by the author.

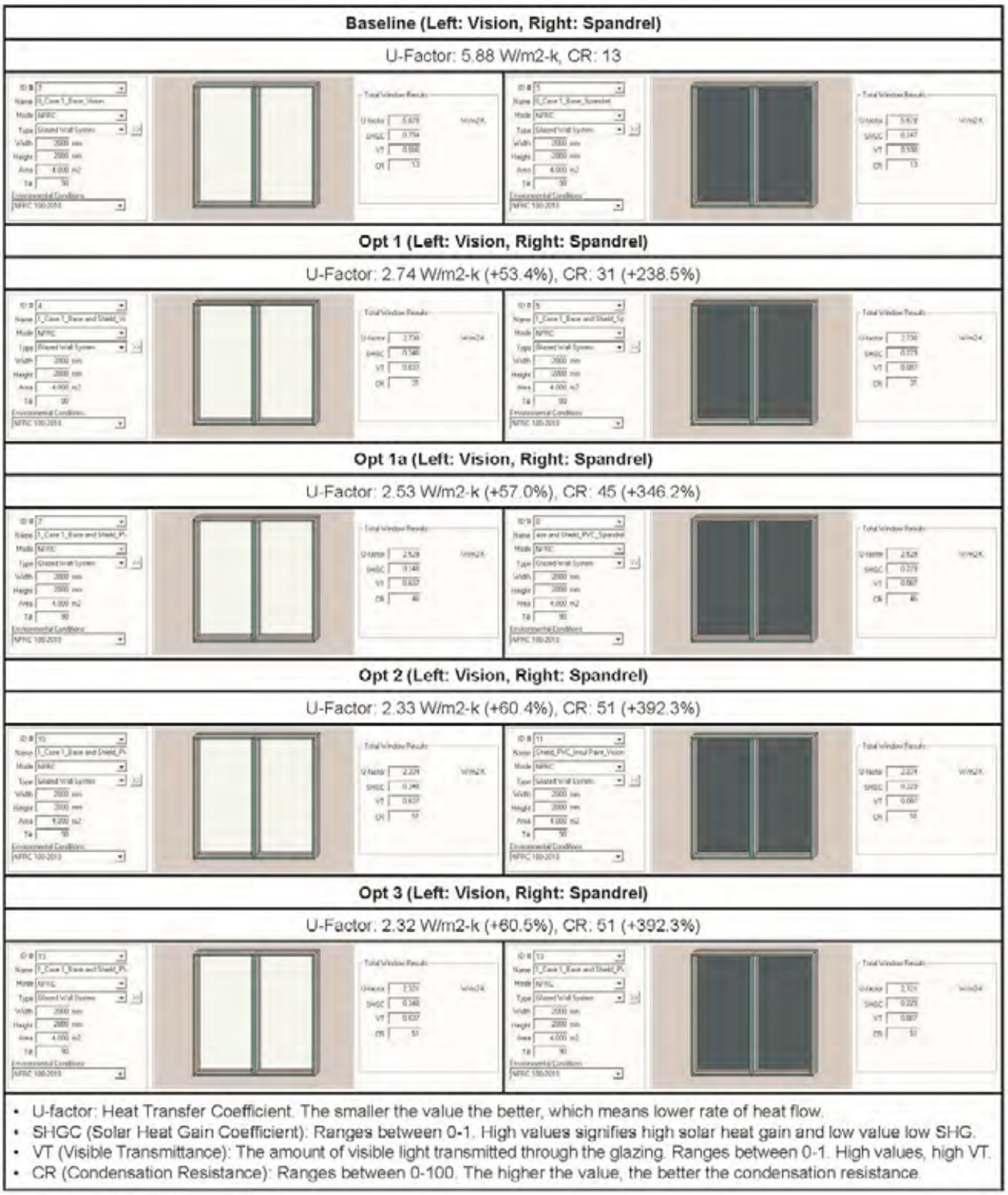


Figure 16: Total thermal performance of Case 1 glazing system for each intervention scenario. Image by the author.



Figure 17: Overview of the basic input values in Comfen and the simulation results of all the intervention scenarios for each elevation of Lever House. Image by the author.

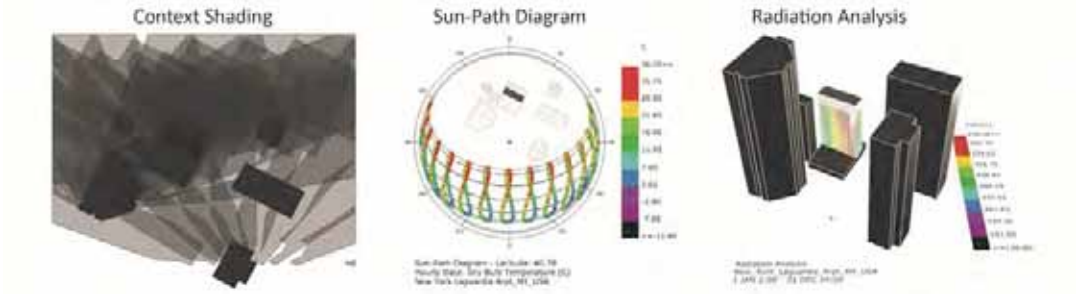


Figure 18: Context shading, sun path, and radiation analysis diagrams for Lever House, which were simulated as part of the energy model. Image by the author.

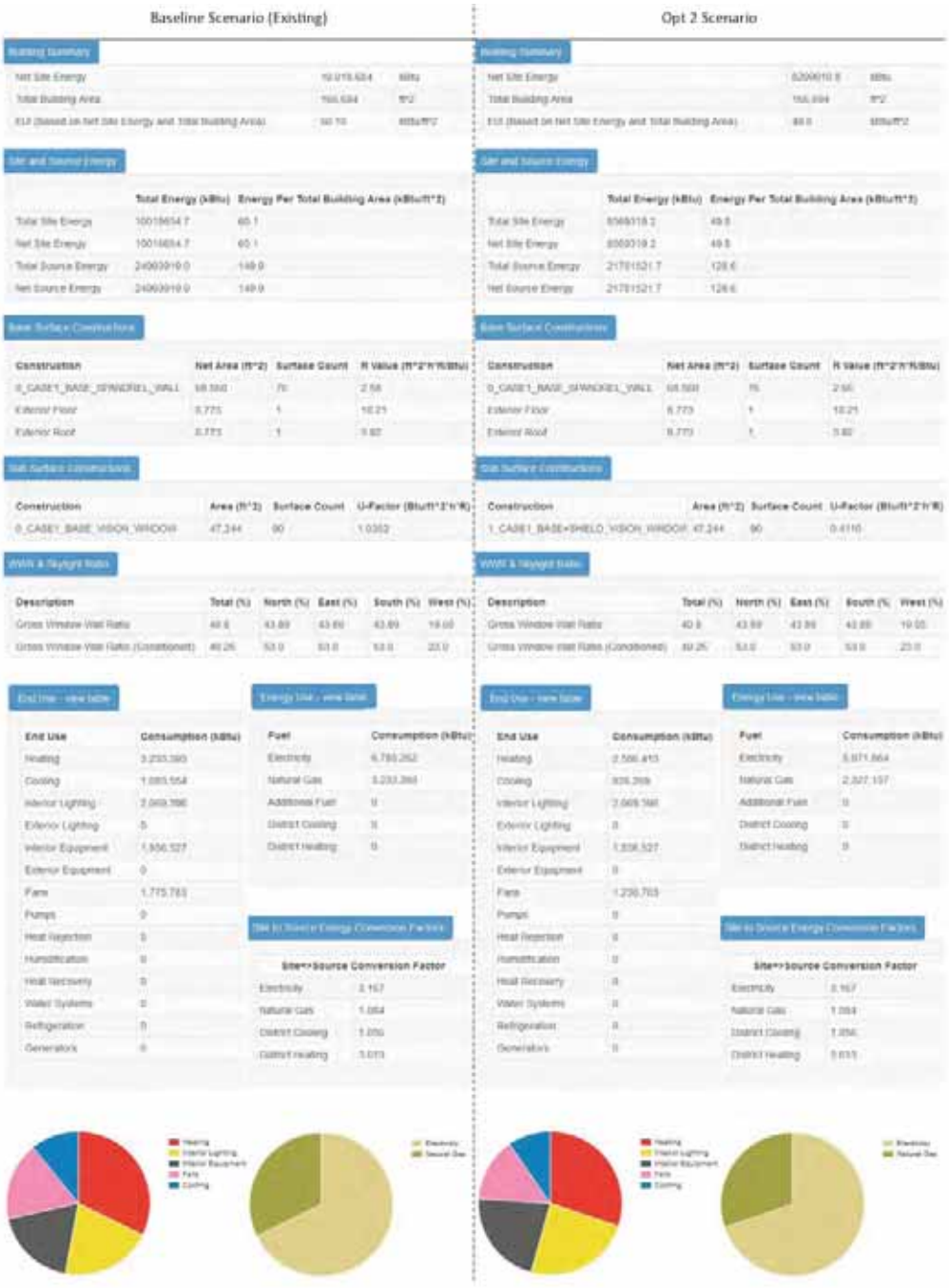


Figure 19: OpenStudio energy model simulation results for Lever House—baseline scenario (left) and Opt 2 intervention scenario (right).

EXPLANATION

SUMMARY OF THE SYSTEM-BASED SIMULATION RESULTS AT LEVER HOUSE

- Opt 1 improved the thermal transmittance (U-Factor) of the curtainwall system by 53.4% and the condensation resistance (CR) by 238.5%.
- Opt 1a improved the thermal transmittance (U-Factor) of the curtainwall system by 57% and the condensation resistance (CR) by 346.2%.
- Opt 2 improved the thermal transmittance (U-Factor) of the curtainwall system by 60.4% and the condensation resistance (CR) by 392.3%.
- Opt 3 improved the thermal transmittance (U-Factor) of the curtainwall system by 60.5% and the condensation resistance (CR) by 392.3%.

SUMMARY OF THE PARTIAL BUILDING-BASED SIMULATION RESULTS AT LEVER HOUSE

- All intervention scenarios reduced the total energy consumption and Co2 emissions at the perimeter area zones by more than one-third and energy costs by around 30%.
- All intervention scenarios reduced peak electricity and natural gas demand between 23-34%.
- All intervention scenarios improved thermal comfort between 9-14% and reduced average glare discomfort by nearly 10%.
- All intervention scenarios provided more than 100% ROI (from energy savings only) by the end of the estimated 20-25-year service life of the glazing shields.
- All scenarios reduced the average daylight illuminance levels by about 25%. However, even on the north side of the building, which normally receives less daylight in the Northern hemisphere, the average levels remained around 450 lux, which is within the recommended range (300-500 lux) for detailed office work (FIG. 17).

SUMMARY OF THE FULL BUILDING-BASED SIMULATION RESULTS AT LEVER HOUSE

The total energy savings, simple payback period, and ROI results shown in this section are related to the Opt 2 scenario with the glazing shields installed on the vision panels only.

By comparing the simulation results of this scenario to the simulation results of the baseline scenario (Fig. 19), the following percentages were found:

- Total site energy use intensity (EUI) was reduced by 17.1%
- Electricity consumption was reduced by 12%
- Natural gas consumption was reduced by 28%

By using the site-to-source conversion rates in (Fig. 19), the actual site EUI and energy uses were calculated based on the reported source EUI for Lever House in 2014 (Fig. 7), which is 350 kBtu/ft^2/yr as follows:

{X * 3.167} + {Y * 1.084} = 350 kBtu/ft2/yr
where:
X: electricity
Y: natural gas
Percentage of electricity use to the total energy consumption in the baseline scenario = 67.73%
Percentage of natural gas use to the total energy consumption in the baseline scenario = 32.27%
=> X = 2.1 Y
=> {2.1 Y * 3.167} + {Y * 1.084} = 350
=> Y = 45.25 kBtu/ft2/yr
=> X = 95.03 kBtu/ft2/yr
=> Actual site EUI = 140.28 kBtu/ft^2/yr

=> Actual estimated reduction in electricity consumption = 95.03 * 12% = 11.4 kBtu/ft^2/yr
=> Actual estimated reduction in natural gas consumption = 45.25 * 28% = 12.67 kBtu/ft^2/yr
=> Actual estimated reduction in site EUI = 24.07 kBtu/ft^2/yr

=> Total building energy reduction annually for the tower portion is:
24.07 kBtu/ft^2/yr * 166,694 ft^2 (total floor area - Fig. 19) = 4,012,325 kBtu

=> Electricity (47.36%) = 1,900,237 kBtu / 3.412 (conversion rate) = 556,928 kWh
=> Natural Gas (52.64%) = 2,112,088 kBtu / 100 (conversion rate) = 21,121 therms

According to the U.S. Bureau of Labor Statistics (BLS 2017):
The average price of 1 kWh of electricity in NYC in 2017 = 19.4 cents
The average price of 1 therm of utility (piped) gas in NYC in 2017 = $1.130
=> Annual savings on Electricity = $108,044
=> Annual savings on Natural Gas = $23,867
=> Total Estimated Annual Energy Savings = $131,911

Simple Payback Period & ROI:
Total vision panels area = 47,244 ft^2
Total frame area = 10,422 ft^2 (47,244 vision + 68,560 spandrel = 115,804 ft2 * 0.09 ft^2 exposed frame area per 1 ft^2 of Lever House CW).
=> The total initial cost = $960,109 {$953,856 (glazing shields on vision panels only = 47,244 * $20.19) + $6,253 (thermal insulation paint on all frames = 10,422 ft2 * $0.6)}
=> The simple payback period from energy savings only = $960,109 / $131,911 = 7.3 years
=> The estimated return on investment over the typical 20-25 year service life of glazing shields:
Over 20 years: 20 / 7.3 = 274%
Over 25 years: 25 / 7.3 = 343%

CONCLUSION AND FUTURE WORK

The purpose of this paper is to present the concept of a patent-pending, external window upgrade system and non-intrusive facade retrofit method. The technology would work with most types of windows and curtainwalls and provides a cost-effective solution to be adopted by the majority of the existing building stock. The paper analyzed the impact of the glazing shields on the thermal performance of different glazing systems, and a case study using Lever House in New York City illustrated their impact on the visual appearance and overall energy performance of the building. The study also analyzed the economic feasibility of this facade retrofit solution by calculating the estimated energy savings, simple payback period, and ROI.

The system-based simulation results showed that using the glazing shields can improve the insulation properties (total system U-Factor) of single-pane window systems by over 50% and improve their condensation resistance by over 240%. The building-based simulation results for Lever House in New York City showed that adding the glazing shields to the exterior of the vision panels only along with 2 coats of thermal insulation paint on caps can reduce heating energy consumption by about 28% and cooling energy consumption by about 12%. As a result, savings on energy bills is estimated to be nearly 20% per year and the simple payback period is projected to be ~85% shorter than that in window replacement, offering ~300% ROI over the estimated 20-25 year service life of the glazing shields.

With regards to future work, we are currently in the process of building a number of prototypes and mockups to validate the performance of the glazing shields per industry standards at an independent testing facility. We plan to test the glazing shields for condensation resistance through accelerated weathering; air, water, and structural performance; and dynamic water penetration under a 130mph wind pressure, which in turn, will allow us to test how effective is the locking mechanism in keeping the panels in place under high wind pressures. Some of the standard tests that we will conduct include the ASTM E 2190 Standard Specification for Insulating Glass Unit Performance and Evaluation, the ASTM E 283 Air Infiltration Test, the ASTM E 331 Static Water Penetration Test, the ASTM E 330 Structural Performance Test, and the AAMA 501.1 Dynamic Water Penetration Test.

The performance mockups will also help us analyze the visual impact in the real world and test the installation method in the field. This in turn will enable us to determine the required installation time and the ideal cleaning process to ensure both the original and new glass surfaces that will be adjacent to the newly formed air gap are clean when the panels are installed.

Future work also includes validating the concept of the second generation—the adaptive glazing shields—which would support 3rd party active/smart window technologies like electrochromic/dynamic glazing in a self-sufficient manner for the first time using the latest clear photovoltaic (vision PV) coating technologies. The future mount-and-play, cleantech panels would

make it economically feasible for existing buildings to enjoy many further benefits through automation and in an environmentally sustainable manner.

REFERENCES

Apte, Joshua S., and Dariush K. Arasteh. 2006. “Window-Related Energy Consumption in the US Residential and Commercial Building Stock”. Lawrence Berkeley National Laboratory. LBNL-60146. Retrieved November 21, 2016. https://facades.lbl.gov/publications/window-related-energy-consumption-us.

Architecture 2030. 2013. “WHY THE BUILDING SECTOR?”. Accessed November 12, 2016. http://architecture2030.org/buildings_problem_why/.

BLS. 2017. “Average Energy Prices, New York-Northern New Jersey-Long Island – February 2017”. U.S. Bureau of Labor Statistics, Mar 17, 2017. Accessed May 06, 2017. https://www.bls.gov/regions/new-york-new-jersey/news-release/averageenergyprices_newyorkarea.htm.

Chambers, Neil. 2009. “New York City and Energy Code Changes”. Treehugger, 26 Oct 2009. Accessed December 11, 2016. http://www.treehugger.com/sustainable-product-design/new-york-city-and-energy-code-changes.html.

Curcija, Charlie, Howdy Goudey, Robin Mitchell. 2017. “Low-e Applied Film Window Retrofit for Insulation and Solar Control”. Prepared by the Lawrence Berkeley National Lab (LBNL) for the U.S. General Services Administration (GSA), Feb 2017. Retrieved April 9, 2017. https://gsa.gov/portal/getMediaData?mediaId=155930.

DOE. 2017. “Building Performance Database”. U.S. Department of Energy (DOE). Accessed March 31, 2017. https://energy.gov/eere/buildings/building-performance-database.

EIA. 2016. “What are greenhouse gases and how much are emitted by the United States?”. U.S. Energy Information Administration (EIA), 20 January 2016. Accessed November 12, 2016. https://www.eia.gov/energy_in_brief/article/greenhouse_gas.cfm.

——. 2015. “A Look at the U.S. Commercial Building Stock: Results from EIA’s 2012 Commercial Buildings Energy Consumption Survey (CBECS)”. U.S. Energy Information Administration (EIA), 04 March 2015. Accessed December 2, 2016. https://www.eia.gov/consumption/commercial/reports/2012/buildstock/.

Enclos. 2013. “New Skins, Old Bones: Facade Retrofits for Tall Curtainwall Buildings”. Enclos corp, 08 August 2013. Accessed November 12, 2016. http://www.enclos.com/site-info/news/enclos-presents-new-skins-old-bones-facade-retrofits-for-tall-curtainwall-b.

——. 2012. “ENCLOS - New Skins for Old Bones: Facade Retrofits for Tall Curtainwall Buildings”. Presented by Mic Patterson at the Metals in Construction Facades Conference, 16 February 2012. Retrieved February 08, 2016. https://issuu.com/archpaper/docs/_2_enclos_patterson_final.

Enerdata. 2016. “Global Energy StatisticalYearbook 2016.” Accessed November 12, 2016. https://yearbook.enerdata.net/.

ESB. 2009. “Empire State Building Case Study”. Empire State Building, 2009. Retrieved December 2, 2016. http://www.esbnyc.com/sites/default/files/ESBOverviewDeck.pdf.

Habibzadeh, Bahman. 2015. “WINDOWS AND BUILDING ENVELOPE OVERVIEW - 2015 BTO PEER REVIEW”. U.S. Department of Energy (DOE), 2015. Retrieved November 17, 2016. http://energy.gov/eere/buildings/downloads/windows-and-building-envelope-overview-2015-bto-peer-review.

Holness, Gordon V.R. 2008. “Improving energy efficiency in existing buildings.” ASHRAE Journal, vol. 50, no. 1, 2008, p. 12+. Academic OneFile, Accessed November 19, 2016. https://search.proquest.com/openview/75ae4dd6272be4362fb0ccaf9b58580a/1?pq-origsite=gscholar&cbl=41118.

IEA. 2013. “Technology Roadmap: Energy Efficient Building Envelope”. International Energy Agency (IEA), Dec 2013. Retrieved November 17, 2016. https://www.iea.org/publications/freepublications/publication/technology-roadmap-energy-efficient-building-envelopes.html.

Long, Jane C. S. 2011. “California’s Energy Future - The View to 2050”. California Council on Science and Technology, May 2011. Retrieved November 20, 2016. http://ccst.us/publications/2011/2011energy.pdf.

Martinez, Andrea, and Mic Patterson. 2013. “Existing Building Retrofit Survey Report”. University of Southern California, September 2013. Retrieved July 29, 2017. http://www.enclos.com/library-pdfviewer/USC_Existing%20Buildings%20Retrofit%20Survey%20Results.pdf?enclos.com/library-pdfviewer/USC_Existing%20Buildings%20Retrofit%20Survey%20Results.pdf.

McGraw-Hill. 2011. “Business Case for Energy Efficient Building Retrofit and Renovation”. McGraw-Hill Construction, Smart Market Report, 2011. Retrieved December 20, 2016. https://energy.gov/sites/prod/files/2013/12/f5/business_case_for_energy_efficiency_retrofit_renovation_smr_2011.pdf

Navigant. 2016. “ADVANCED ENERGY NOW 2016 MARKET REPORT: Global and U.S. Markets by Revenue 2011-2015 and Key Trends in Advanced Energy Growth”. Prepared by Navigant Research for Advanced Energy Economy (AEE), March 2016. Retrieved March 31, 2017. http://info.aee.net/hubfs/PDF/AEN-2016-Market-Report.pdf?t=1464027401576.

NYC. 2016. “New York City Energy & Water Performance Map”. The Mayor’s Office of Sustainability and New York University’s Center for Urban Science and Progress. Accessed November 02, 2016. https://serv.cusp.nyu.edu/projects/evt/.

——. 2016b. “One City: Built to Last, Technical Working Group Report”. The Official Website of the City of New York, Apr 2016. This report lays out the Mayor’s plan for how to reduce citywide carbon emissions 80 percent by 2050 by improving energy efficiency in New York City’s buidlings, 2nd Edition. Retrieved November 20, 2016.

http://www1.nyc.gov/assets/sustainability/downloads/pdf/publications/TWGreport_04212016.pdf.
——.2016c. “Mayor Announces Major New Steps to Dramatically Reduce NYC Buildings’ Greenhouse Gas Emissions.” The Official Website of the City of New York, 22 Apr 2016. Accessed December 07, 2016. http://www1.nyc.gov/office-of-the-mayor/news/386-16/onenyc-mayor-de-blasio-major-new-steps-dramatically-reduce-nyc-buildings-greenhouse.
Patterson, Mic. 2012. “CTBUH 9th World Congress concludes in Shanghai”. Enclos corp, 22 September 2012. Accessed November 26, 2016. http://www.enclos.com/site-info/news/ctbuh-9th-world-congress-concludes-in-shanghai.
Schiff, Eric. 2014. “Single-pane Window Efficiency”. Advanced Research Projects Agency-Energy (ARPA-E), 07 November 2014. Retrieved July 20, 2017. https://arpa-e.energy.gov/sites/default/files/02%20-%20Schiff%20-%20Single%20Pane%20Window%20Opportunity%20-%20FINAL.pdf.
Synavax. 2017. “Energy Protect™ Clear Insulation and Protective Coating for Homes & Buildings”. Synavax. Accessed March 23, 2017. http://www.synavax.com/product/energy-protect/.
UNEP. 2009. “Buildings and Climate Change - Summary for Decision-Makers”. United Nations Environment Program (UNEP) 2009. Retrieved November 12, 2016. http://staging.unep.org/SBCI/pdfs/SBCI-BCCSummary.pdf.
UNEP FI. 2014. “COMMERCIAL REAL ESTATE: UNLOCKING THE ENERGY EFFICIENCY RETROFIT INVESTMENT OPPORTUNITY”. The United Nations Environment Program Finance Initiative (UNEP FI), Feb 2014. Retrieved December 20, 2016. http://www.unepfi.org/publications/investment-publications/property-publications/commercial-real-estate-unlocking-the-energy-efficiency-retrofit-investment-opportunity/.
Wright, J.L. 2014. “The Use of Indoor Surface Low-e Coatings: The Implications Regarding Condensation Resistance”. Presented at the ARPA-E Workshop on Single-pane Window Efficiency, November 2014. Retrieved March 03, 2017. https://arpa-e.energy.gov/sites/default/files/04%20-%20Wright%20ARPA-E-2014_r2%20-%20FINAL.pdf.
WWF. 2015. “Biggest US Cities Setting Unprecedented Emissions Reductions Goals to Fight Climate Change”. World Wildlife Fund (WWF) and ICLEI-Local Governments for Sustainability, 06 August 2015. Retrieved December 10, 2016. https://www.worldwildlife.org/press-releases/biggest-us-cities-setting-unprecedented-emissions-reductions-goals-to-fight-climate-change.

ADAPTIVE FACADES

Towards responsive building structures and envelopes



Walter Haase
ILEK, University of Stuttgart
walter.haase@ilek.uni-stuttgart.de



Werner Sobek
ILEK, University of Stuttgart
werner.sobek@ilek.uni-stuttgart.de



Enrica Oliva
Werner Sobek New York
enrica.oliva@wernersobek.com



Michele Andaloro
Werner Sobek Stuttgart
michele.andaloro@wernersobek.com

ABSTRACT

Facade engineering aims at appropriately balancing the demands imposed by the context and the capabilities inherent to the materials, the geometries and the systems that are implemented. Traditionally, systems are designed for the worst case conditions, thus leading to static designs that are over-dimensioned for most of their service life. Therefore, if a system - just like a living body - is able to adapt itself to the external conditions by changing its properties, then it would bring about a new design paradigm that can lead to substantial savings and that can enhance the performance of the building.

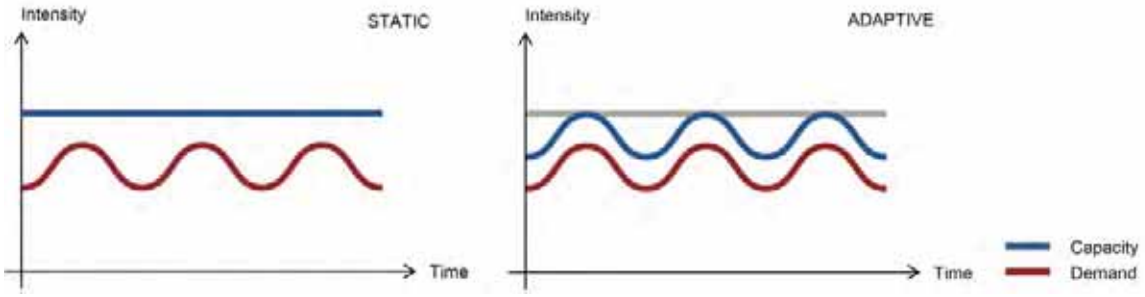


Figure 1: Demand/capacity diagrams. Figure courtesy of the authors.

Numerous researches, prototypes, and components have been carried out so far, and projects, both speculative and realized, are imagining the application of such systems on an architectural scale, in order to exploit their viable potential and redefine the premises on which the development of the built environment is set.

In this light, examples like the visionary proposal for house R129 (Sobek, 2001), where the transparent shell complemented with an electrochromatic foil enables the building to dynamically respond to the changing conditions of its context, or the Cité du Design in St. Etienne (Geipel and Andi, 2004), where the skin adapts to the interior requirements, have shaped this novel approach to envelope design and fueled the dialogue around the concept of adaptivity.

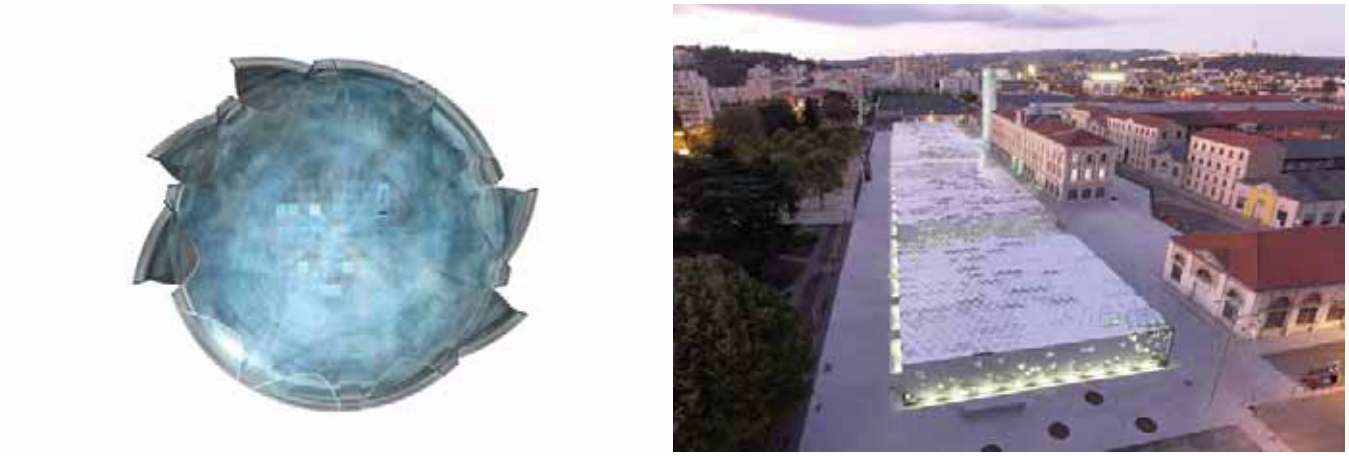


Figure 2: R129 (left), Cité du Design, St. Etienne (right). Figure courtesy of Sobek W. and Kunze J.O.

In this process, research institutions play a crucial role; indeed, through the promotion of studies and researches, innovative systems and methodologies are developed, thus fostering a continuous progress in the building sector, from a design as well as a manufacturing standpoint.

Among the researches currently carried out, this paper aims at presenting in particular two prototypes, developed at the Institute for Lightweight Structures and Conceptual Design (ILEK) in Stuttgart, which address the concept of adaptability with regards to two crucial performances and that introduce two influential references for the design and engineering of future transparent skins.

The first prototype, Research Project A, involves an adaptive glazed facade with vertically prestressed cables, where, by means of actuators, the active components, weaving together the double cables and changing their reciprocal distance, modulate the prestress forces and the curvature of the cables, according to the present loading condition measured by sensors, and optimize the structural behavior of the facade. The results show that - compared to a standard cable construction - the adaptive cables system can lead to a striking minimization of the members sizes and, as a consequence, of the material usage.

Research project A has been carried out by Christine Flaig (ILEK - University of Stuttgart), Dr. Walter Haase (ILEK - University of Stuttgart) and Michael Heidingsfeld (ISYS - University of Stuttgart) within the framework of the Research Group 981 (HIKE) funded by the German Research Foundation (DFG).

The second project, Research Project B, consists of a switchable glazing unit with adjustable light and energy transmission properties. While current switchable glass technologies feature long respond times and rough subdivision of the glazing area, the prototype developed enables substructured control and grey scale states, thus allowing a precise modulation of the daylighting and energy performances, without compromising the visual comfort. Ultimately, by linking together the data from the sun and the test room, an initial automated and dynamic control strategy has been implemented.

Research project B has been realized by Marzena Husser (ILEK - University of Stuttgart) and Dr. Walter Haase (ILEK - University of Stuttgart), supported by the Federal Institute for Research on Building, Urban Affairs and Spatial Development within the Federal Office for Building and Regional Planning, Germany (research projects: “Adaptive glazing systems”, “TN technology for architectural applications”) and by Baden-Württemberg Stiftung GmbH, Germany (research project: “i³: intelligent, interactive, integrative solar control glazing”).

KEYWORDS

adaptive**,** daylighting - glare - shading, structure and seismic, component performance, glass performance, glass engineering, electro-chromic glass

RESEARCH PROJECT A

INTRODUCTION

Suspended facades with prestressed cables have enabled engineers and designers to build highly transparent envelopes, endowed with a highly efficient load-bearing behavior that have deeply influenced the architectural language and broadened the spectrum of the design possibilities. Projects such as the Bremen University (Störmer, 1997), the Lufthansa Aviation Center (Ingenhoven, 2000) or the Sony Center (Jahn, 1995) constitute pivotal references in this field and have triggered the development of numerous projects and researches about super-transparent skins.



Figure 3: Sony Center, Berlin (top left), Bremen University, Bremen (bottom left), and Lufthansa Aviation Center, Düsseldorf (right). Figure courtesy of Esch H.G. and Keller A.

Since building systems are designed to support the maximum loads that are expected to occur during the building service life, most of the material used is functional to a relatively short period of time; in particular, with regards to cable facades, this results in a significant increase of the cables' cross sections that are needed to control the horizontal deflections and the glass panes' warping.

This, together with the fact that the construction industry has a significant contribution on the shortage of energy and material resources, leads to the conclusion that it is fundamental to develop innovative design practices that can meet the highest performance standards while making the most profitable use of the resources implemented in the building's construction and service.

The proposed adaptive glass facade with vertically prestressed cables substitutes the additional material, needed in extraordinary loading conditions, with energy that feeds a dedicated system, constituted by sensors, a control software and actuators, designed to modify the load-bearing behavior of the structure according to the present demand.

BACKGROUND

In the framework of previous research on adaptive shell structures, innovative active supporting systems have been implemented in order to reduce and homogenize stresses and, therefore, minimize the structure's deformation. Nevertheless, with respect to cable facades, due to the virtually non-existing bending stiffness of the cables, prestressed cable systems will show an increase in deflection when stresses are reduced, thus urging the development of an innovative concept of adaptive glass facade with vertically prestressed cables. In particular, Dr. Eng. Walter Haase first introduced the idea of an active deflection-manipulation in 2012.

METHOD

ADAPTIVITY CONCEPT

The objectives of the developed adaptivity concept are to reduce the prestressing forces in the cables and to minimize the horizontal deflections.

In order to address these issues, two strategies have been identified:

- an active system working parallel to the cable axis, able to modulate the prestressing forces according to the loading conditions;
- an active system working perpendicular to the cable axis, that helps reduce the cables' horizontal deflections, thus avoiding high prestressing force demands.

The adaptivity concept envisions both a parallel and a perpendicular adaptivity, and three modes can be recognized:

- mode A, where the prototype has been designed for low gust speeds with a high probability of occurrence;
- mode B, characterized by higher gust speeds with a smaller probability of occurrence, where active struts work in perpendicular directions to minimize the cables' horizontal deflections;
- mode C, where active components work in parallel directions to ensure the stability of the structure in case of extraordinarily high wind loads (larger deflections will be accepted in this state).

This paper focuses on the implementation of mode B.

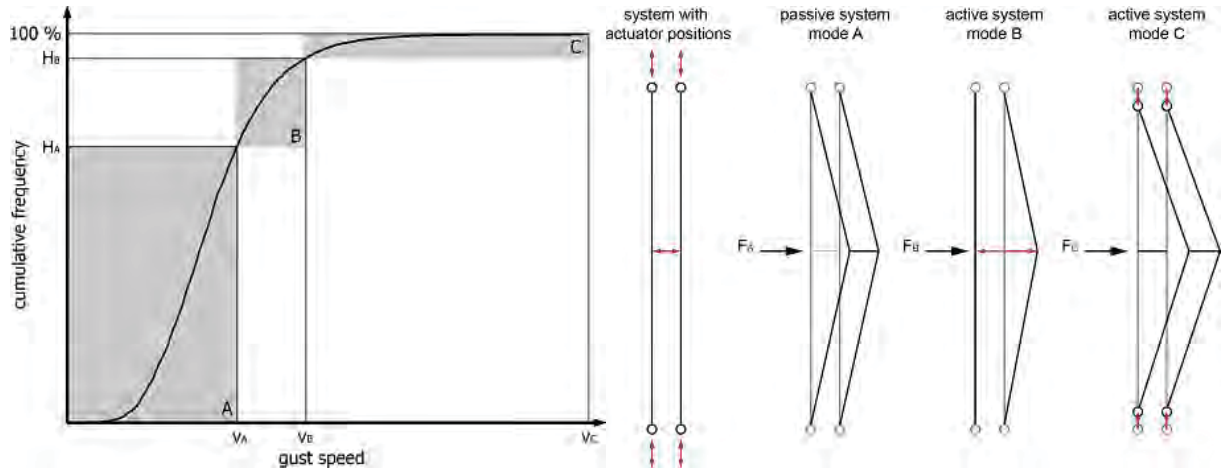


Figure 4: Modes diagram and representation of the active components functionality. Figure courtesy of Flaig, C., Haase, W., Heidingsfeld, M., Sobek, W.

PROTOTYPE

The prototype analyzed, 3.4 m wide and 4.9 m high, is constituted by six 8 mm thick toughened glass panes, measuring 1.5 m by 1.5 m, divided in three rows.

The glass panes are clamped at the edges by means of stainless steel holders with EPDM pads and pinned to the front cables, while the double cables are spiral strands with a 6.1 mm diameter and a 22 mm^2 cross section.



Figure 5: Prototype rendering. Figure courtesy of Flaig, C., Haase, W., Heidingsfeld, M., Sobek, W.

ACTIVE STRUTS

The double cables are connected by means of active struts, designed to extend and contract between the cables' fittings, perpendicular to the facade, in order to adapt the load-bearing behavior of the prototype to the loading conditions.



Figure 6: Active struts. Figure courtesy of Flaig, C., Haase, W., Heidingsfeld, M., Sobek, W.

The active struts have a scissor configuration, whose opening is controlled via pneumatic cylinders with a high reaction rate that work for both dynamic and static deflection control.

Two different sensors oversee the demand and capacity states of the prototype:

- strain gauges at the cable fittings, that monitor the forces in the cables;
- angle transmitters at the actuators, that measure the current extension of the struts.

The data, continuously collected by the sensors, feed the control software, developed by ISYS, that determine the point-in-time optimized configuration of the active struts and actuate the pneumatic cylinders for static and dynamic deflection control.

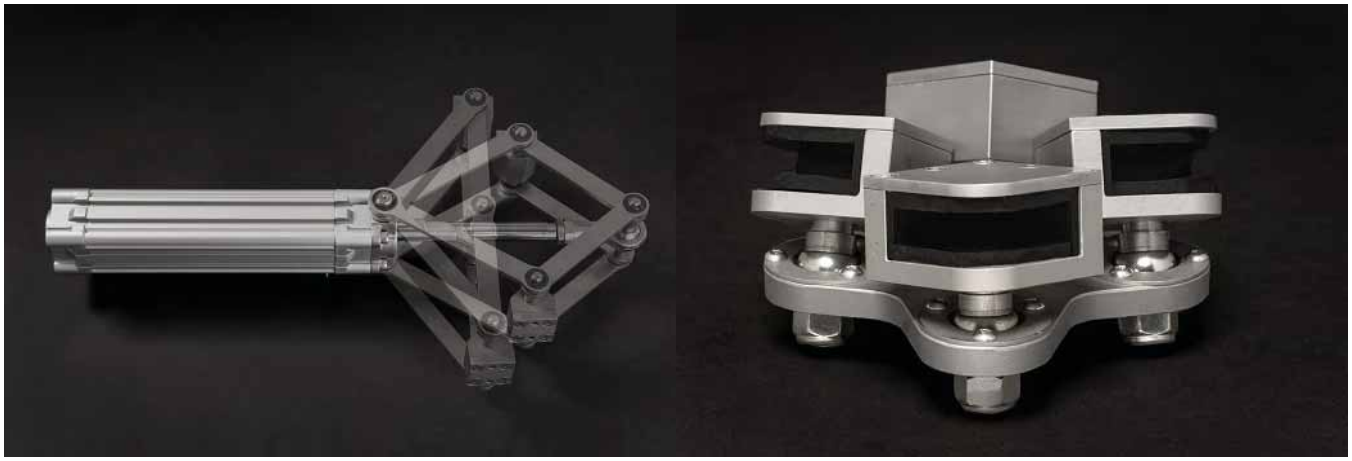


Figure 7: Actuator with pneumatic cylinder and scissor in two positions (left), glass fitting (right). Figure courtesy of Flaig, C., Haase, W., Heidingsfeld, M., Sobek, W.

ANALYSIS

Non-linear numerical simulations have been performed with the FEM software ANSYS – Mechanical APDL.

The design of the prototype has been carried out for USL, without considering the deflection limits per SLS.

For system dimensioning purposes, the following components have been considered:

- dead load applied as point loads at the connecting nodes of the cables;
- wind load, 925 N/m² pressure according to Eurocode 1, applied as point loads at the connecting nodes of the cables;
- prestressing force, induced in the model by a temperature load, to avoid slacking of the cables due to dead loads in the passive state (1.5 kN in the front cables and 0.2 in the back cables).

In the passive state the maximum horizontal deflection is 0.23 m (≈L/20) under a wind pressure of 925 N/m², therefore, the active struts have been designed to perform a maximum extension of 0.23 m.

DATA

Compared to a traditional glass facade with vertically prestressed cables (INACTIVE) featuring the same configuration and subject to the same loading conditions (wind loads), the numerical simulations showed that the developed adaptive glass facade (mode B) with vertically prestressed cables (ACTIVE) is able to reduce the horizontal deflection to nearly zero. Furthermore, when subject to wind load, the maximum forces in the cables are equal to 11.5 kN in the INACTIVE scheme and 15.9 kN in the ACTIVE one.

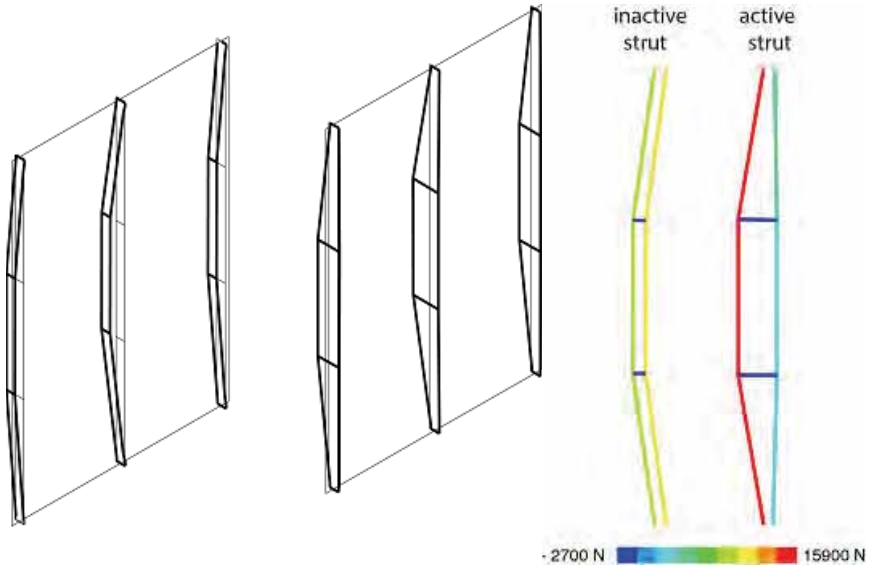


Figure 8: Deformation plot in passive state (left), deformation plot in active state (center), cable forces in the inactive and active struts (right).

Figure courtesy of Flaig, C., Haase, W., Heidingsfeld, M., Sobek, W.

System mode	Maximum cable force	Maximum deflection of the front chord
ACTIVE	15.9 kN	≈ 0 m
INACTIVE	11.5 kN	0.23 m

Ultimately, the proposed system has led to the following reductions:

- 87% of the prestressing force constraint of maximum horizontal deflection of L/50 (SLS);
- 42% of the cables' cross section;
- 57% of the maximum reaction force.

Facade	Maximum prestressing force	Maximum cable force	Cross section of cables
ACTIVE	1.5 kN	13.0 kN	22 mm^2
INACTIVE	11.5 kN	18.9 kN	38 mm^2

CONCLUSION AND FUTURE WORK

The results show that the proposed adaptive glass facade with vertically prestressed cables has led to a significant reduction of the prestressing forces in the cables and, therefore, of the cross section needed to withstand the design loads, thus introducing a possible alternative approach to cable facades' design, where material is substituted with energy, and allowing for material savings (up to 42% in weight for the current prototype).

Furthermore, as demonstrated by means of the non-linear numerical simulations, the absolute minimization of the front cable's deflection, which is not achievable with a passive facade system, allows warping of the glass panes to be neglected in the design, thus leading to thinner and lighter glass build-ups.

Future developments will study the deformability behavior of the prototype, and the comparison of the data with the results of the numerical simulations, as well as the amount of energy required to operate the adaptive system.

RESEARCH PROJECT B

INTRODUCTION

The dynamic nature of light and energy urges for innovative facade designs able to master the indoor environmental quality of a space, together with the thermal performance of the entire building.

Furthermore, the pursuance of a thermally efficient envelope together with an optimal daylighting comfort is crucial from an environmental standpoint as well, since the implementation of advanced strategies would contribute to the building energy demand minimization.

Exterior shading systems, both static and dynamic, have proven themselves to be effective in the facade engineering practice; however it is fundamental to implement alternative strategies, in particular with regard to high-rises or buildings featuring severe loading conditions, where traditional solar control devices might not be used.

To address these issues, a prototype for a substructured adaptive switchable glazing system with integrated sun and glare protection features has been developed.

BACKGROUND

The innovative switchable glass introduced consists of a thin substructured switchable cell, manufactured by BMG MIS GmbH Luminator Technology Group, inserted in an insulating glazing unit, provided by Okalux GmbH. The switchable cell, named 'twisted nematic cell' (TN-cell), is made up of a nematic liquid crystal layer embedded between two thin glass

substrates and complemented with additional conductive and polarizing layers; the system is based on the technology used for liquid crystal displays (LCD) (Collings, 2002; Haase, 2004; Chen, 2011).



Figure 9: TN-cell. Figure courtesy of Husser, M., Haase, W., Hoß, P., Sobek, W.

Through a laser or photolithographic process, the conductive layer of the TN-cell can be subdivided into independent switchable pixels, thus allowing for a substructured control, and, applying a different voltage, the alignment of the rod-shaped liquid crystal molecules can be modulated, enabling grey-scale states with differing transmittance values.

In the presented prototype, pixels measure approximately 14.7 mm x 16.3 mm and are connected by means of transparent wiring that creates a 1.6 mm gap in-between the pixels.

TN-cells have a maximum light transmittance of about 37%, in the clear state, and a minimum light transmittance of about 1%, in the dark state. In the system in object, considering the contribution of the transparent gap between adjacent pixels, the equivalent maximum and minimum light transmittance values are, respectively, 37% and 5%.

Ultimately, the state transition takes a few milliseconds and the system consumes less than 1 W/m^2.



Figure 10: Prototype of the structured switchable glazing in a facade test facility. Figure courtesy of Rettig J.

METHOD

The objectives of the following analyses are to study the potentials of the developed substructured switchable glazing, from an energy and daylighting standpoint, and constitute the basis for further implementations, testing and prototyping of the newly introduced technology.

BOUNDARY CONDITIONS

The test room dimensions are 2.00 m x 4.20 m x 2.70 m (W x D x H), with a fully glazed south-facing side. The characteristics of the model are comparable to the ones of the test rooms of the facade testing facility at the University of Stuttgart, where the prototype is being tested as well.

Four different locations have been considered:

- Stuttgart (48° 46' N, 9° 10' O), Germany;
- Helsinki (60° 10′ N, 24° 56′ O), Finland;
- Valencia (39° 29′ N, 0° 2′ W), Spain;
- Accra (5° 03′ N, 0° 13′ W), Ghana.

SIMULATION METHOD

In order to simultaneously analyze multiple parameters and to simulate the adaptive behavior of the system, a specific integrated method, illustrated in the diagram here below, has been developed.

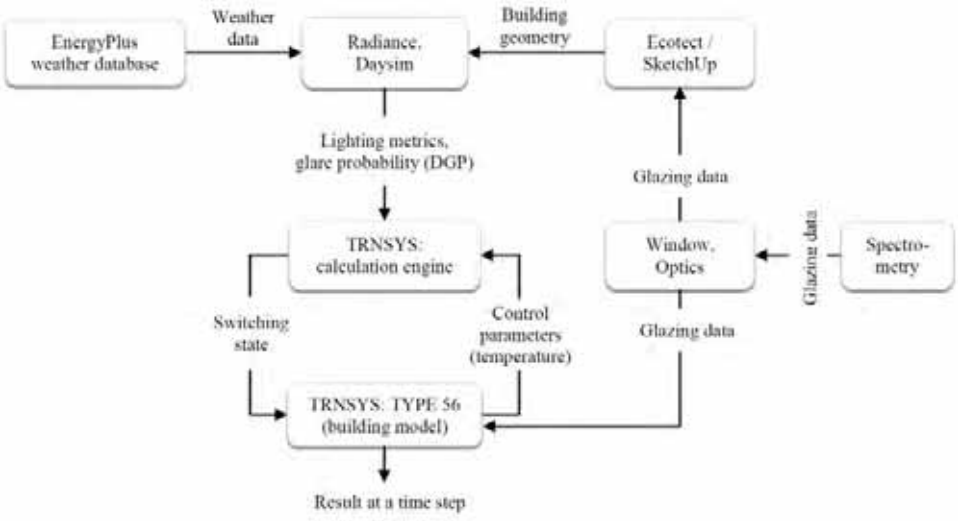


Figure 11: Simulation method diagram. Figure courtesy of Husser, M., Haase, W., Hoß, P., Sobek, W.

In specific, the tools implemented in the method and their objectives are:

- TRNSYS 5.3.0.0 (What, 2015), to simulate the adaptive behavior of the systems;
- TRNSYS: TYPE 56, to model the test room;
- Optics 5.0 and Window 6.3 (Mitchell et al., 2013), to model the glazing systems based on spectral analysis of the glazing components;
- Radiance (Fuller 2015), to simulate daylighting metrics based on local climate and sun position;
- Daysim (Daysim 2015), to perform annual daylighting analyses, glare discomfort predictions, and energy demands calculations for artificial lighting;
- Autodesk Ecotect Analysis (Autodesk, 2015) or Google SketchUp (SketchUp, 2015), to create the building model for Radiance and Daysim;
- EnergyPlus weather database (Weather, 2013), to acquire the climate data for the simulation scenes.

GLAZING SYSTEMS

Together with the developed TN-glazing, two additional highly efficient glazing systems have been taken into account in the analyses in order to carry out a comparison; the compositions of the build-ups considered are presented here below.

A – Glazing with a low-e coating: 6 mm white glass | 16 mm air gap | 4 mm white glass | 16 mm air gap | 6 mm white glass with a low-e coating on face 5.

B – Glazing with a low-e coating and venetian blinds: venetian blinds | 6 mm white glass | 16 mm air gap | 4 mm white glass | 16 mm air gap | 6 mm white glass with a low-e coating on face 5.

C – TN-glazing: 6 mm white glass with a selective coating on position 2 | 2.6 mm TN-cell, fixed on the outer pane with approximately 5 mm air gap | 41 mm air gap | 6 mm white glass with a low-e coating on face 5.

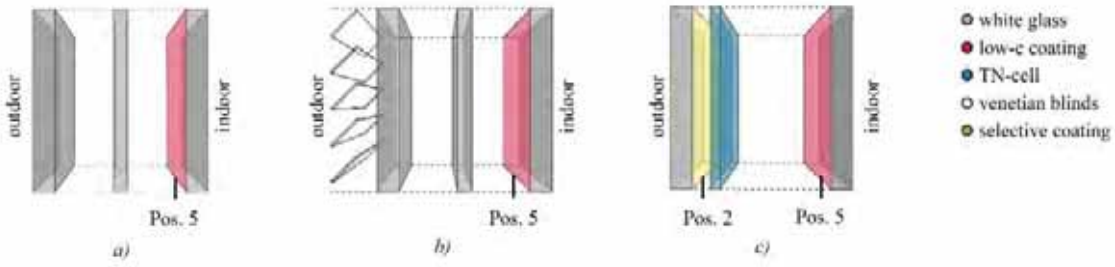


Figure 12: Glazing systems diagrams. Figure courtesy of Husser, M., Haase, W., Hoß, P., Sobek, W.

CONTROL STRATEGIES

In order to fully employ the potentials of the newly introduced switchable glazing, it is fundamental to develop specific control strategies capable of optimizing the response of the adaptive system according to the environmental conditions.

The presented initial strategy, suitable for office buildings, envisions the glazing area as divided into two independently controlled zones that fulfill different requirements.

The glare protection zone (GP-zone) controls the glare effects by linking together the sun parameter with the occupant's expected behavior. Specifically, this zone is as small as possible (0.25 m x 0.25 m) and it is automatically placed at the intersection between the sunbeam and the occupant's viewing direction (view point considered almost 1 m behind the glazed facade). The analysis is based on keeping the Daylight Glare Probability (DGP) factor (Wienold et al., 2006) below a crucial value.

The temperature control zone (TC-zone) controls the indoor thermal comfort, by stepwise modulating the light transmittance of the glazed facade when the interior temperature is between 20 °C and 26 °C. Below the 20 °C threshold the heating system is turned on, while above 26 °C the cooling systems starts working.



Figure 13: control zones diagram. Figure courtesy of Husser, M., Haase, W., Hoß, P., Sobek, W.

DATA

The following diagrams, showing the analysis results in terms of energy demand, demonstrate that the TN-glazing is comparable to a triple insulating glazing with an external shading system (the present analysis does not include the energy demand for the shading device control included in glazing system B) and that the initial control strategy implemented - though simple, open to further developments, and applied to highly different environments - can lead to significant energy savings.

In particular, in heating-dominated regions, the heating energy demand, as a consequence of the control strategy considered, is slightly higher but the cooling as well as the overall energy demand decrease. The savings in terms of cooling energy demand are even more apparent in hot climates, where the proposed TN-glazing, even in darker states, does not introduce a visual obstruction where conventional solar control systems might.

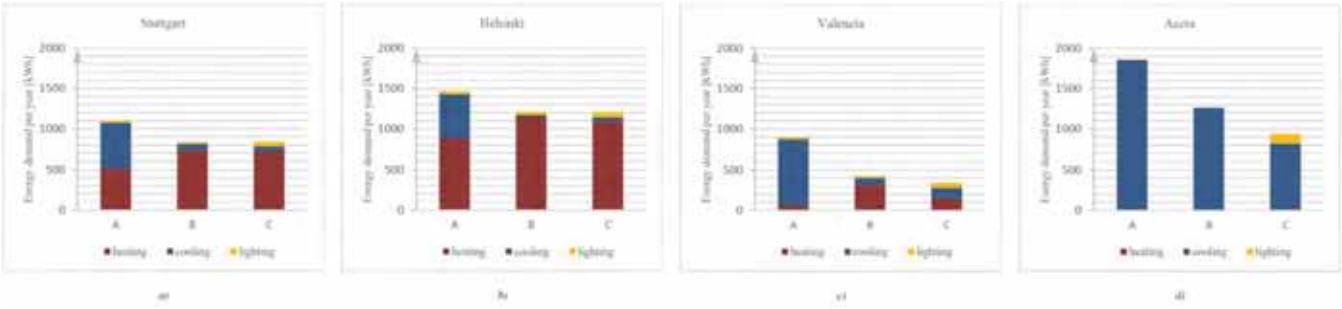


Figure 14: Energy performance diagrams in Stuttgart (a), Helsinki (b), Valencia (a) and Accra (d). Figure courtesy of Husser, M., Haase, W., Hoß, P., Sobek, W.

Further analyses have been performed for a changeable spring day in Stuttgart as, in these conditions, the variability of the direct solar radiation requires a high flexibility in the shading systems and, therefore, the adaptivity of the system can be exploited and demonstrated.

As apparent from the results presented here below, while in the early morning the heating system has to be switched on in order to provide a minimal indoor temperature of 20°C, the rest of the day is efficiently managed by the TN-glazing system that guarantees the thermal comfort as well as glare protection (DGP < 0.45).

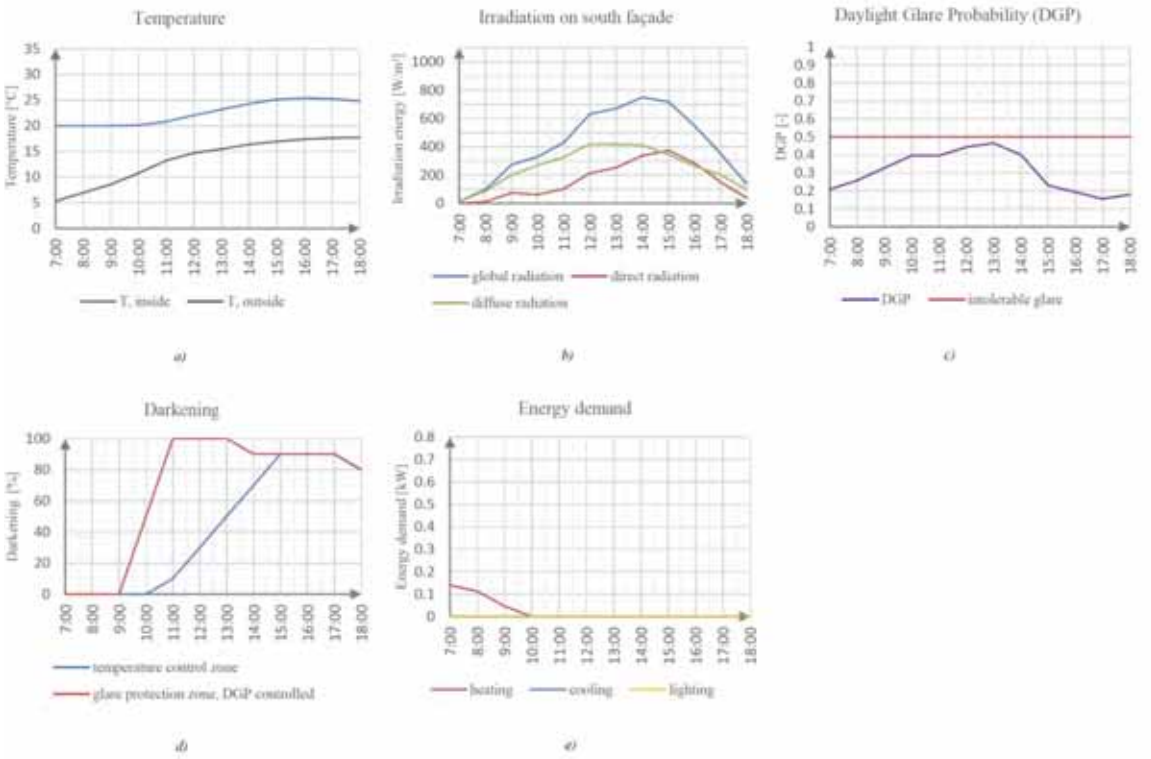


Figure 15: Diagrams of the Temperature (a), the irradiation on South facade (b), the DGP (c), the darkening (d) and the energy demand (e) on changeable spring day in Stuttgart. Figure courtesy of Husser, M., Haase, W., Hoß, P., Sobek, W.

CONCLUSION AND FUTURE WORK

The results show the potential of the developed substructured adaptive switchable glazing system in enabling to design for project-specific control strategies that dynamically optimize the energy performance of the facade and the indoor daylighting comfort, while guaranteeing an effective glare protection.

Further control strategies are under investigation in order to create more climate-specific scenarios and take into consideration further daylighting and energy parameters. An automatic occupant's position detection system will be developed as well, in order to enable a precise and adaptive glare control. In terms of embodied energy, the achievable savings will be evaluated comparing the introduced technology with traditional facade systems having comparable performance. Ultimately, the integration of the switchable system into the building automation system will be researched.

FUTURE SCENARIOS

Over the last decade, advances in engineering, design, and manufacturing have unveiled a high potential perspective for the construction field; indeed, if on the one hand, innovative design practices, in which efficiency and sustainability are conjugated in the definition of active architectural bodies, on the other hand, the evolution of the building technologies is allowing the application of such concepts on a large scale, tackling the crucial challenges the built environment is facing.

Examples like house B10 in Stuttgart (Sobek, 2014), through its sophisticated energy concept and self-learning building control system, show how future buildings can be actively inserted in their own environment: sustainably exploiting the resources of the context and producing more energy, from renewable sources, than what they actually need, thus making them capable to serve further endogenous and exogenous energy demands. In this scenario, part of the surplus of energy produced can be employed to “activate” the building components, making them react and adapt to the changing conditions they are exposed to. Therefore, as the prototypes presented in this paper demonstrate, the energy invested in the activation of the components can result in extremely efficient and lightweight designs endowed, in the light of the overall life cycle assessment, with a lighter environmental impact.

ACNKOWLEDGEMENTS

The authors would like to express their gratitude to the researchers at the Institute for Lightweight Structures and Conceptual Design (ILEK) that developed the presented prototypes as well as the institutions and the industrial partners that supported the projects.

Research project A - Christine Flaig (ILEK - University of Stuttgart), Dr. Walter Haase (ILEK - University of Stuttgart), and Michael Heidingsfeld (ISYS - University of Stuttgart).

Research project B - Marzena Husser (ILEK - University of Stuttgart) and Dr. Walter Haase (ILEK - University of Stuttgart).

REFERENCES

Flaig, C., Haase, W., Heidingsfeld, M., Sobek, W. “Prototype of an adaptive glass facade with vertically prestressed cables.” Engineered Transparency 2016: Glass in architecture and structural engineering (2016): 213-222.

Sobek, W., Rehle, N. “Beispiele fuer verglaste Vertikalseilfassaden. Herrn Prof.Dr.-Ing. Udo Peil zur Vollendung des 60. Lebensjahres gewidmet.” Stahlbau vol. 73 no. 4 (2004): 224-229.

Neuhaeuser, S., Weickgenannt, M., Haase, W., Sawodny, O. “Adaptive Tragwerke - Aktuelle Forschungen im Ultraleichtbau: Stahlbau” Stahlbau vol. 82 no. 6 (2013): 428-437.

Neuhaeuser, S., Weickgenannt, M., Witte, C., Haase, W., Sawodny, O., Sobek, W. “Stuttgart SmartShell – a full scale prototype of an adaptive shell structure.” Journal of the International Association for Shell and Spatial Structures vol. 54 no. 4 (2013): 259-270.

Flaig, C. “Untersuchung verglaster, adaptiver, vorgespannter Seilfassaden.” Institut für Leichtbau Entwerfen und Konstruieren, Universität Stuttgart, Stuttgart.

Haase, W., Husser, M., Sobek, W. “Adaptive Glazing Systems - Survey of Systems” AIM 2017 IEEE International Conference on Advanced Intelligent Mechatronics. Munich, 2017.

Husser, M., Haase, W., Hoß, P., Sobek, W. “New Possibilities of Sun and Glare Protection with a Structured Switchable Glazing” Challenging Glass 5. Ghent, 2016.

Chen, R. H. *Liquid crystal displays: fundamental physics and technology*. Wiley-Blackwell, 2011.

Fehringer, A. *Vergleichende Analyse unterschiedlicher Regelungsstrategien schaltbarer Verglasungen unter besonderer Berücksichtigng der Einflussparameter Strahlung und Temperatur.* University of Stuttgart, 2016.

Haase, W. *Adaptive Strahlungstransmission von Verglasungen mit Flüssigkristallen.* University of Stuttgart, 2004.

Haase, W., Husser, M. *Schaltbare Verglasung auf der Basis von lyotropen und nematischen Flüssigkristallen.* University of Stuttgart, 2014

Haase, W., Husser, M., Sobek, W. “Potentiale strukturierter, schaltbarer Verglasungen.” in Weller, B., Tasche, S., *Glasbau*, Ernst & Sohn GmbH & Co. KG, 2016.

Haase, W., Husser, M., Sobek, W., Kurz, E., Rau, L., Frühauf, N. “Flüssigkristall-basierte Verglasung zur Regelung des Licht- und Energieeintrags in Gebäude.” in Weller, B., Tasche, S., *Glasbau*, Ernst & Sohn GmbH & Co. KG, 2016.

Haase, W., Prskalo, M., Królak, M., Sobek, W., Kurz, E., Rau, L., Frühauf, N. “Switchable Glazing for Architectural Applications based on Liquid Crystal Technology.” Glass Performance Days, Tampere, 2011.

Hoß, P. *Simulation des Einflusses verschiedener klimatischer Randbedingungen auf die Regelungsstrategie schaltbarer Verglasungen und den Gebäudeenergiebedarf.* University of Stuttgart, 2015.

Husser, M., Haase, W., Sobek, W., Kurz, E., Rau, L., Frühauf, N. (2014). “Structured sun protection glazing. Engineered transparency.” International Conference at Glasstec, Düsseldorf, 2014

Lichtmeß, M. *Aktivierung von Blend- und Sonnenschutzsystemen.* Universität Wuppertal, 2008.

Reinhart, C. “Daysim, advanced daylight simulation software.” http://daysim.ning.com/ (accessed November 24, 2015).

The Board of Regents of the University of Wisconsin System. “TRNSYS” http://sel.me.wisc.edu/trnsys/ (accessed November 24, 2015).

U.S. Department of Energy. “Weather Data” http://apps1.eere.energy.gov/buildings/energyplus/ weatherdata_about.cfm (accessed in 2013).

Wienold, J. “Dynamic daylight glare evaluation.” Building Simulation (2009): 944-951.

Wienold, J., Christofferen, J. “Evaluation methods and development of a new glare prediction model for daylight environments with the use of CCD cameras.” Energy and buildings Vol.38 no.7 (2006): 743-757.

ALGORITHMIC PATTERNS FOR FAÇADE DESIGN

Merging design exploration, optimization and rationalization



Inês Caetano
INESC-ID/IST-University of Lisbon
ines.caetano@tecnico.ulisboa.pt



António Leitão
INESC-ID/IST-University of Lisbon
antonio.menezes.leitao@ist.utl.pt

ABSTRACT

Recently, building envelopes have been exhibiting complex shapes and patterns, a trend supported by current digital technologies. Likewise, the design exploration of these envelopes has been combined with analysis and optimization processes, with the aim of achieving better performing solutions. Nevertheless, the exploration of architectural skins still poses some limitation to architects when using new design approaches, such as algorithmic design, simulation, and optimization strategies, as they require specialized expertise. Furthermore, the integration of design analysis and optimization processes in the algorithmic design workflow has shortcomings, such as the fragmentation resulting from the use of multiples models and tools, a process that is error-prone, time-consuming, and hard-working.

In this paper, we discuss a framework developed to ease the mathematical description of algorithmic façade designs, which intends to integrate the most used analysis and optimization processes in a continuous design exploration workflow. To this end, a classification of façades was developed, based on computationally relevant categorical dimensions, that integrates a set of fundamental algorithms and strategies for each dimension. The result is a library of algorithms available in different programming languages, and a set of guidelines that help architects select and combine the most useful algorithms for a given façade design. The algorithmic structure of the developed solutions is flexible, hence, suitable to connect with the chosen analysis and optimization processes, allowing their inclusion in a continuous workflow.

KEYWORDS

design processes, parametric workflows, generative design, design optimization

INTRODUCTION

Architecture has always explored the latest technological advances in terms of building technology, as well as architectural production and representation. Nowadays, the new digital tools play a relevant role in the conception, analysis, and production of architecture. Computation-based design approaches promoted design exploration and the emergence of complex shapes and patterns, which would be difficult and costly to produce without them (Moneo 2001). Within the architectural domain, these approaches had, and still have, great application in the development of building' façades due to the aesthetical and environmental relevance of the latter ones, since these mediate the inside and the outside of a building. Computational approaches also potentiate the design optimization of buildings (Alfaris and Merello 2008). Using optimization

algorithms and one or more performance criteria, it is possible to automatically explore a substantial design space in the search for solutions with an improved performance. Finally, computer-aided manufacture enabled the fabrication of such solutions by allowing the conversion of virtual models into physical ones (Gibson, Rosen, and Stucker 2010), which has been changing the relation between conception and production (Kolarevic 2003).

Despite these advances, computation-based approaches are not yet widespread, mainly due to their complexity and the specialized knowledge required, especially the algorithmic approaches, which require architects to learn programming. Furthermore, it still takes time for the designer to gain enough experience to deal with more advanced algorithmic problems. This means the designer often ends up spending more time with the scripting task than with the design exploration task, thus limiting his creativity. The challenge, then, is to make such approaches, including algorithmic design, design optimization, and digital fabrication, accessible to architects. The aim of this work is to explore the application of these approaches in the design process of a building, more specifically, in the development of its envelope. The focus on the envelope results from the specialized knowledge and work that is usually required for its development, mainly when the goal is meeting several requirements, namely, aesthetical, structural, and environmental ones.

To minimize the existing limitations when using algorithmic approaches, a computational framework is proposed, aiming to reduce the initial time investment required for the scripting task, specifically in the production of building skins. This architectural-oriented framework systematizes and structures the algorithmic generation of façade solutions, embracing both the variety of different scenarios and the different analysis and optimization strategies that are now part of the design process. The framework includes a library of predefined algorithms based on previous design experiences and known façade design strategies, assisting architects in the exploration of a façade solution by suggesting the most suitable strategies and algorithms for each specific situation. Therefore, it decreases the time needed to explore the desired idea, while promoting a better and more appropriate use of the different algorithmic strategies; an important milestone for the subsequent analysis and optimization stages.

BACKGROUND

ALGORITHMIC DESIGN

Algorithmic Design (AD) is a design approach that describes a design through a set of rules and algorithms (Alfaris and Merello 2008), allowing the designer to transcend “the factory-set limitations of current 3D software” (Terzidis 2004). Nevertheless, to take advantage of AD, architects need to learn new skills, such as programming, which is far from trivial. To promote the integration of AD in architecture, some programming languages (PL) were developed to facilitate the learning process to those without previous programming experience. Some PLs are textual (TPL), namely *Processing, Racket,* and *Python*, but the most popular ones are visual (VPL), such as *GenerativeComponents, Dynamo,* and *Grasshopper*, which allow the creation of AD programs through the manipulation of graphical elements instead of using text (Janssen 2014). Their popularity derives from (1) their intuitiveness, a crucial asset for beginners as they require less abstraction; (2) their ability to produce results more easily, without almost having to learn programming (Zboinska 2015); (3) the integration of important features to aid architects with the programming task, namely traceability (i.e. the relationship between parts of the program and those of the generated model), important for the comprehension, maintenance, and debugging of AD programs (Leitão, Lopes, and Santos 2014), and (4) the real-time feedback, e.g., the use of sliders to represent parameters is relevant for immediately understanding the effects of changes in the programs.

Unfortunately, VPLs still present several limitations, mainly when projects get more complex: (1) the lack of scalability - the program gets incomprehensible and, thus, difficult to change (Leitão, Santos, and Lopes 2012b; Janssen 2014); (2) confining the user to the predefined modules and components available in each VPL, a limitation accentuated when the solutions being explored need more advanced features (Zboinska 2015); and, finally, (3) the loss of capacity to support real-time feedback when programs get more complex, due to the software’s performance decrease (Leitão, Lopes, and Santos 2014). To overcome these limitations when dealing with more intricate solutions, architects usually need to replace VPLs with TPLs (Leitão, Santos, and Lopes 2012a), as these are more powerful than the former. Unfortunately, mastering a TPL takes time and, when the programming expertise is still limited, architects often spend more time with the scripting task than with design exploration. Moreover, when facing unanticipated changes in their design process, the parametric model sometimes does not contain the adequate parameters to modify the model in the desired way (Davis, Burry, and Burry 2011). As a result, the model’s programming structure is typically redrawn, a time-consuming process described by Woodbury as “erase, edit, relate and repair” (2010).

ALGORITHMIC PATTERNS

To promote the integration of algorithmic approaches in architecture, the use of algorithmic design patterns is currently in development. Qian (2009) defined *pattern* as a generic solution to a well-defined problem, while Alexander et al. (1977) and Qian et al. (2008) described *design patterns* as known strategies or solutions that can be reused to solve design problems. The main goal for developing algorithmic patterns is taking advantage of previously used knowledge and solutions in the search of new ones. As a result, this avoids repeated reinvention, while reducing the development time of algorithmic solutions (Khwaja and Alshayeb 2013) and anticipating unexpected design changes during the design process (Woodbury, Aish, and Kilian 2007). Some works based on this issue have been developed (Woodbury, Aish, and Kilian 2007; Zhenyu Cheryl Qian 2009; Yu and Gero 2015; Woodbury 2010; Chien, Su, and Huang 2015; Hudson 2010). Regarding the field of façade design, Su & Chien (2016) developed a set of algorithmic patterns to support the development of architectural skins at an initial stage using *Grasshopper* for *Rhino 3D*. Nevertheless, most of these studies (I) simply focus on the modularization of VPLs definitions, therefore also suffering from their inherent shortcomings; (II) do not support the integration of other types of algorithms, such as optimization algorithms, neither connecting them to the multiple analysis and simulation tools; and (III) do not address the application of algorithmic patterns in the exploration of buildings' façades.

On the other hand, tools like *Paneling Tools* for *Rhino* and *Grasshopper*, *Lunch Box* to *Grasshopper*, and *ParaCloud Gem*, also attempt to solve the mentioned limitations by addressing and simplifying typical modelling procedures applied in façade design – point-grids generation, mapping of elements in different ways, application of *attractors* to control element sizes, rotation, etc. Unfortunately, (1) its use is entirely manual (i.e. by interacting directly with the software environment instead of using algorithms), promoting iterative user-driven processes that can be tiresome and error-prone; (2) they resort to VPLs and, once more, suffer from the typical limitations they possess; and (3) they are mostly used for generic panelization, subdivision, and population of surfaces, thus, being unable to directly address relevant concepts in façade design, such as materiality or the tectonic relation between elements.

To sum up, architects are limited by the specificity of existing tools – to extend their capabilities, they need either to build from scratch the necessary functionalities or to use a mix of different tools that, most of the time, are not compatible. For this reason, it is important to systematize and structure the algorithmic generation of façade solutions in a process that considers the variety of different scenarios and the set of different analysis and optimization strategies. The aim of the DrAFT framework is to create a library of predefined algorithms based on the notion of design patterns – i.e., by integrating design processes and known façade design strategies – to support architects in the exploration of an intended façade solution by suggesting the most suitable strategies and algorithms for each specific situation. It therefore reduces the time needed to explore the desired idea, while promoting a better and more appropriate use of the different algorithmic strategies; an important milestone for the subsequent stages – analysis, optimization, and fabrication.

FAÇADE RATIONALIZATION FOR FABRICATION

The design freedom achieved by the latest technologies is limited by physical constraints usually linked to structural performance and fabrication. One of the current concerns of designers is the ease of manufacturing of the complex solutions being developed, a process named as *geometric optimization* (Mesnil et al. 2015), that includes *rationalization*, i.e., the adjustment of a geometrically complex design towards a feasible and affordable way of production. As an example, the fabrication of large-scale free-form structures can be quite challenging, since the designed surface needs to be rationalized through a process named *panelling* (Fu and Cohen-or 2010; Eigensatz, Deuss, et al. 2010; Son et al. 2017; Andrade, Harada, and Shimada 2017; Eigensatz, Kilian, et al. 2010; Flöry and Pottmann 2010), which corresponds to the segmentation of the surface into simpler elements that can be manufactured at a reasonable cost, while preserving the design intent (Eigensatz, Kilian, et al. 2010).

However, most of these works only focus on simple patterning, i.e. triangular, quadrangular, and hexagonal meshes, whereas more complex geometric patterns are not considered, even though they have been applied to several architectural façades. It is therefore important to also consider the complex types of geometric patterning by providing an algorithmic framework of coherent mathematical definitions to facilitate the exploration and subsequent rationalization of these patterns.

METHOD

DRAFT FRAMEWORK

Architectural practice is highly dependent on the specific circumstances of the design brief and, thus, it is unlikely that the exact same approach can be used in a different project. Nevertheless, modular programming techniques allow designers to adapt and reuse ideas in different projects. This implies that the systematic application of these techniques reduces, at least partially, the initial investment required, as they would not have to rewrite all the algorithms from scratch every time they started a new design, decreasing the time and effort spent with the programming task. Furthermore, the use of design patterns would also benefit from the integration of different analysis and optimization processes in a continuous workflow, in which the traditionally detached design stages – design exploration, analysis and optimization – are now merged into a single process. As a result, the obtained solutions (1) are less exposed to errors, (2) respond more easily to the creative needs of the architect, and (3) achieve better performing behaviors.

Draft Algorithmic Façades Tool (DrAFT) is a framework based on a classification of façades according to different dimensions where, for each one, several algorithms were developed, covering a wide variety of design solutions (Caetano, Santos, and Leitão 2015; Caetano and Leitão 2016). The classification is based on four main categorical dimensions that are further subdivided to deal with the specific details of each design stage: A) *Façade Geometry* defines the façade's surface geometry; B) *Elements* generates the façade's elements; C) *Distribution* makes the elements distribution along the façade's surface; and D) *Articulation* gives a final appearance to the façade by relating the previous dimensions. The DrAFT framework guides the designer in the identification of the most suitable algorithms for his design intent, promoting further design exploration and easier adaptation to the ever-changing design process conditions.

With the aim of empowering the architects' design exploration process, the DrAFT framework also provides a growing set of random optimization algorithms, including, e.g., Monte Carlo and Latin Hypercube sampling methods, to help users improve their design solutions. These depend on a fitness function and on the specification of the permitted variations, allowing the search for the closest solution to that criterion, while simultaneously maintaining the initial design concept imposed by the architect. These algorithms were designed to be combined with the algorithms responsible for the geometric exploration, which are adapted during this stage, following a continuous integration of optimization processes throughout the design exploration workflow. Moreover, they allow a direct and automated connection with the analysis tools required for each type of analysis.

Finally, as the DrAFT framework gives a high level of flexibility to its user in terms of geometric exploration, it is important to ensure the obtained solutions are then possible to manufacture in terms of its assembly process and cost of fabrication. The DrAFT framework takes this into consideration by providing algorithms that allow the designer to control the maximum number of different elements that composes his design solution. This is done by discretizing a given parameter of the façade solution, e.g., a length, into *n* different values, where *n* can be specified by the designer, producing as a result *n* different sets of identical façade elements, thus enabling him to make a trade-off between the production cost and the original design concept. The potential of DrAFT in exploring a complex design solution is explained in the next section.

CASE STUDY APPLICATION

In this section, the DrAFT framework is used to develop a conceptual case study: the envelope of a rectangular building with a geometrical pattern that varies parametrically according to aesthetical and performance criteria. Initially, both the building's skin shape and the geometrical pattern were developed by resorting to a set of algorithms of the DrAFT framework. The façade exploration process was based on a conceptual idea of creating an envelope composed of several parametric diamond-shaped elements of different apertures (Fig. 1). The size variation of the apertures should satisfy the need for natural light, while simultaneously matching the aesthetical criteria for the overall design, which aimed at creating a parabola curve shaped effect along the longest façades.

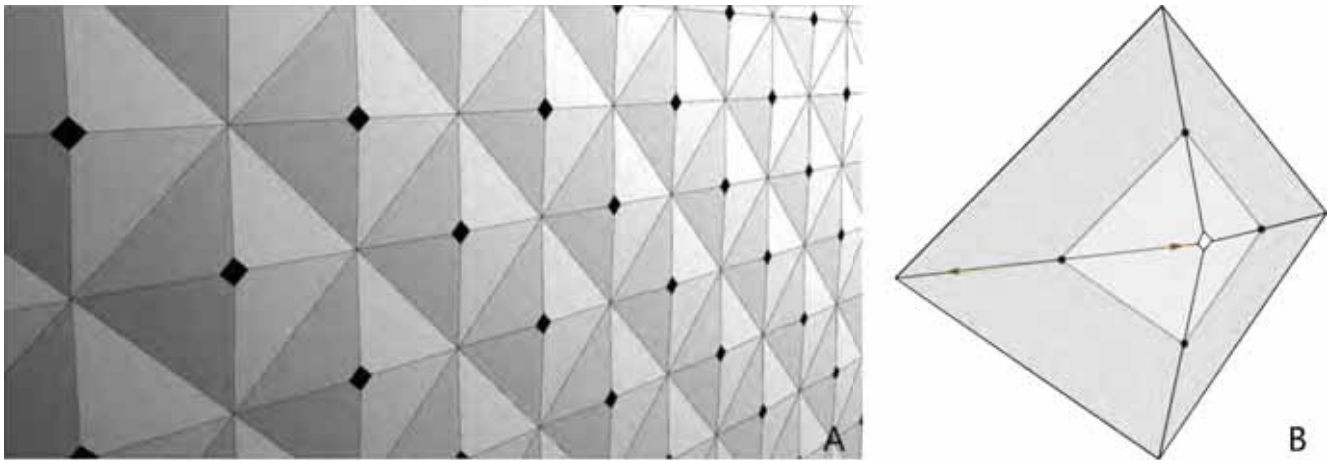


Figure 1: A – Conceptual model of the diamond-shaped façade elements;

B – Conceptual representation of a single façade element, in which the grey line represents its deformation variation.

In practical terms, two algorithms were combined to create the diamond-shaped grid: one from the *Façade Geometry* dimension to shape the surface, and the other from the *Distribution* to produce a grid of points placed in a chess distribution – see Figure 2.A. Then, each grid cell was developed by combining some algorithms from the dimension *Elements*, which were responsible for (1) shaping the units in a diamond-shaped pyramid geometry (Fig. 2.B), and simultaneously (2) applying a deformation to this shape (Fig. 2.C) – i.e., the opening and closing of the pyramidal shape. The parametric variation of each cell depends on the distance between the cell and the attractor curve – Figure 2.D shows the initial geometrical pattern (without deformation), whereas Figure 2.E presents the deformation created by the attractor curve. The use of DrAFT algorithms allowed to iteratively adjust (1) each cell geometric shape, and (2) the applied deformation (i.e. the intensity of the attractor's effect, the geometrical limits of the deformation, etc.) almost instantaneously and without extra effort.

The following stage focused on the optimization of the obtained geometrical pattern, i.e. the search for a solution that, based on the user's design intent and the aesthetical requirements that came from it, was improved in terms of its performance regarding the quality of the building's natural lighting.

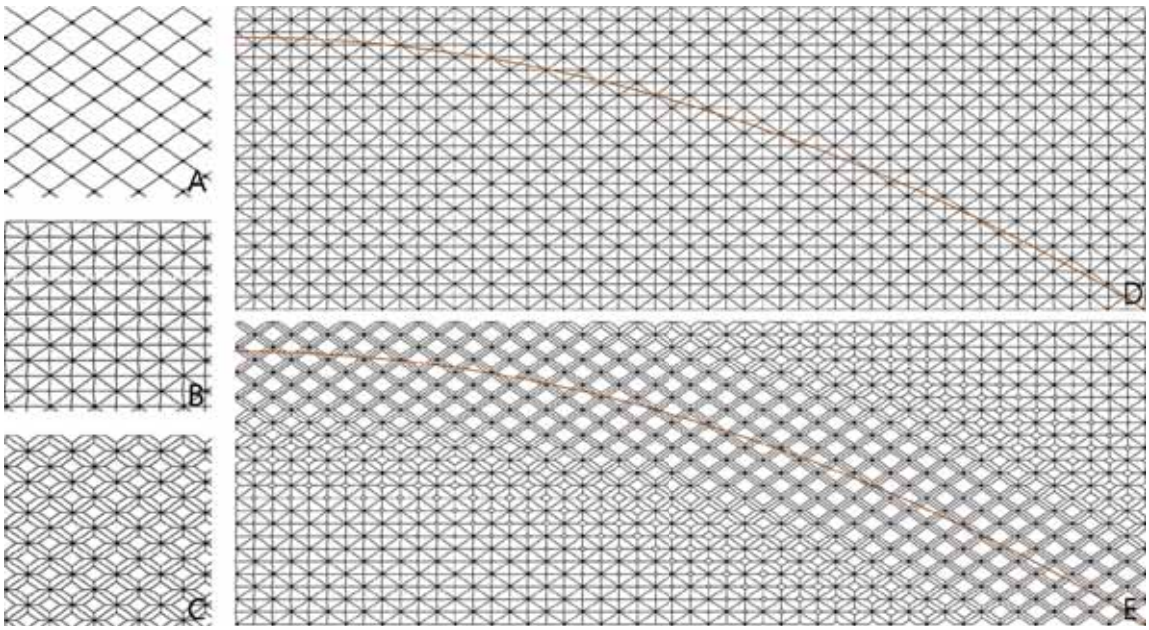


Figure 2: A conceptual representation of the building envelope pattern: A – Creation of the diamond-shape grid; B – The distribution of the pyramidal elements;

C – Deformation of the pyramidal elements (creation of apertures); D – The overall pattern without deformation and the placement of the attractor curve;

E – Control of the elements' deformation according to their distance to the attractor curve.

DESIGN OPTIMIZATION – OPTIMIZATION ALGORITHMS

In this section, one of the optimization algorithms available within DrAFT framework – the Monte Carlo optimization algorithm (Shapiro 2003) – is used to optimize the design solution developed regarding its natural lightning levels. The goal was to improve these levels by geometrically controlling the façade pattern. To simplify the process, only one of the design constraints imposed could be parametrically changed during this process, which, in this case, was the intensity of the deformation caused by the attractor curve, and only one fitness criterion was intended to be achieved – a predetermined lightning level. The optimization algorithm used received as inputs (1) the fitness function, (2) the range of values accepted by the design parameter, and (3) the number of iterations (a higher number of iteration increases the probability of achieving a better solution as it evaluates a larger design space). After the prescribed number of iterations, the algorithm returns the value of the design parameter that corresponds to the best solution found so far, which can then be used to generate the final design. Figure 3 shows an instance of the case study 3D model with its corresponding lightning analysis results.

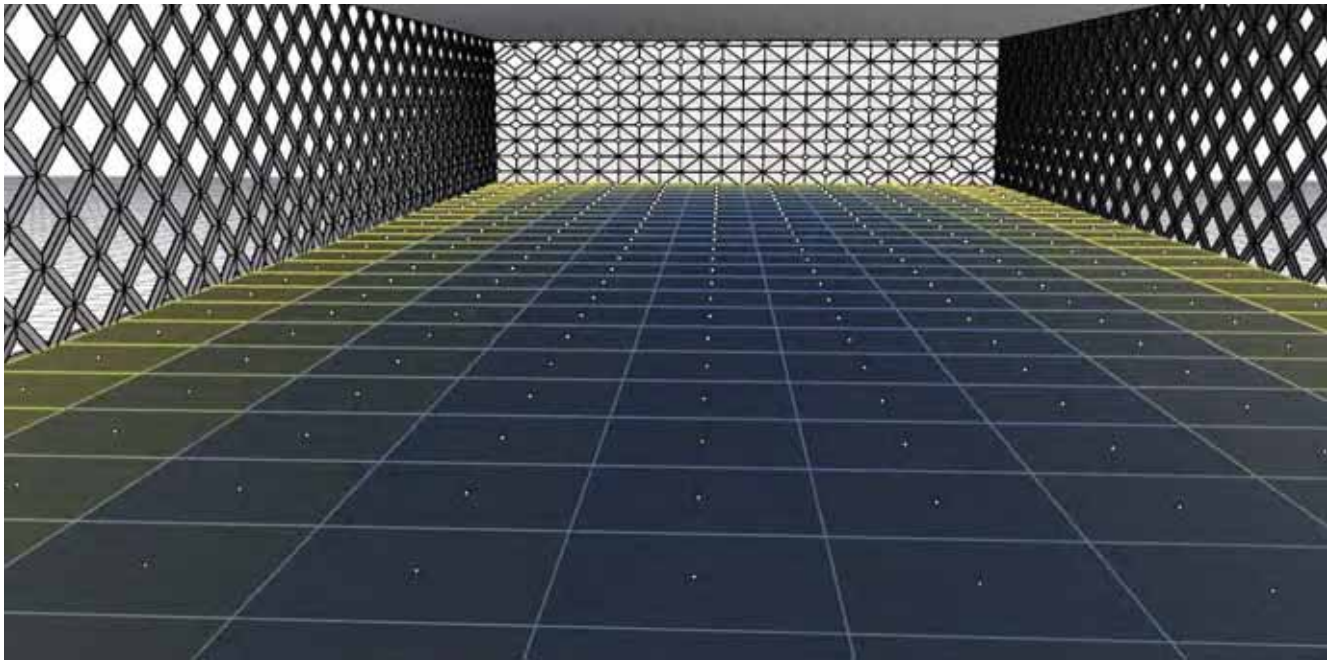


Figure 3: 3D model view of the lightning analysis process.

DESIGN RATIONALIZATION FOR FABRICATION

One of the consequences of the use of algorithmic design methods is the expensive mass-customization they typically entail. In our case study, that is reflected in the large number of different pieces of the obtained façade design. To overcome this problem, the rationalization algorithm available in the DrAFT framework was applied to reduce this number. The initial solution was composed by 2424 different pieces, in a total of 6144, and, as the manufacturing process of these elements required the creation of molds, its fabrication was clearly unsustainable in terms of cost and waste. Using the rationalization algorithm allowed us to significantly reduce the number of different pieces, enlarging the number of identical pieces on each set. Table 1 organizes the values obtained in the different rationalization tests, which includes the number of different types of pieces, the *total of sets*, and the number of times each type is used, the *sets of pieces*. Figure 4 shows each solution's corresponding façade model. After several iterations, the solution that best matched the original idea, and that, simultaneously, had an acceptable manufacturing cost, was the one of discretization $N = 10$.

N		∞	100	60	20	10	5
Set of pieces	A	432	478	478	478	728	1208
	B	1560	1578	1602	1684	1806	2558
	C	2	70	116	254	502	1054
	D	2	36	108	250	488	1324
	E	2	44	108	246	546	
	F	2	52	120	256	578	
	G	2	52	122	254	640	
	H	4	46	118	260	856	
	I	4	60	140	268		
	J	4	42	134	274		
	K	2	54	154	300		
	...	...	...	...	...		
Total of Sets		2424	69	42	15	8	4

Table 1: A table with the number of different sets of pieces and the number of times each set is used. Note the case of N = 5, the façade pattern only uses 4 typologies of sets, meaning that the number of times each type of set appears is by far greater than the other examples.

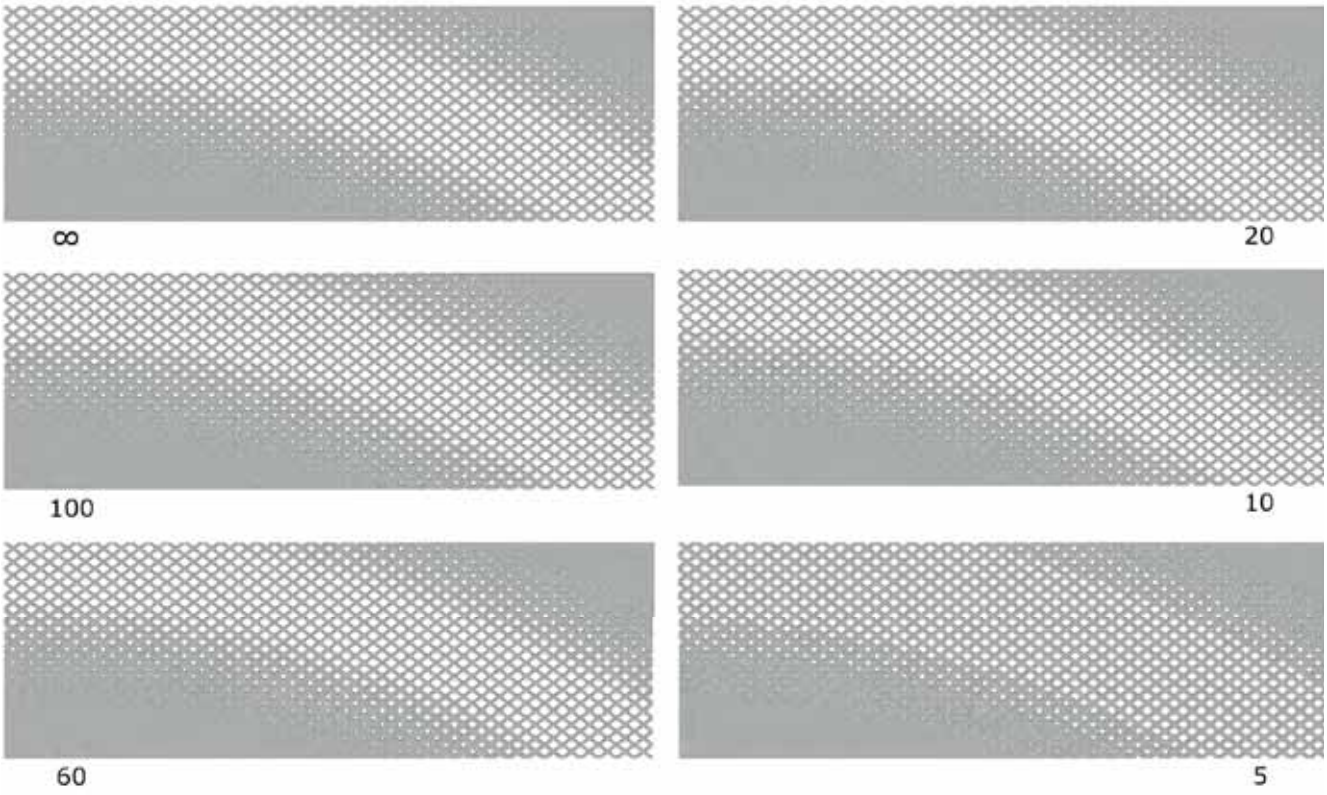


Figure 4: The façade models of the examples presented in Table 1.

EVALUATION

This paper was purposely structured to clearly mark the transition between design stages, with the aim of facilitating the understanding of how the combination and implementation of the different algorithms is done. In practical terms, the design stages are confined in a single two-way workflow. The use of an algorithmic approach allows the user to develop a single script that contains all the geometric information of a design together with algorithms to evaluate and optimize that same design, regarding different performing criteria. Also, it frees the designer from having to create 3D models in different formats to suit the different design and simulation tools, avoiding problems such as loss of information and error propagation, thus potentiating more accurate results in a shorter time.

Figure 5 is a conceptual representation of the design stages considered by the DrAFT framework. The *Design Exploration* stage starts with the initial idea, covering all subsequent processes until a design solution is achieved, which corresponds to the *Design Development* stage. The latter, therefore, embraces the stages explained in the previous sections: 1) the geometric exploration of the design solution, i.e. the *Surface Grid*, *Surface Mapping* and *Façade Cells* development stages; 2) the optimization of the solution regarding a certain fitness criterion, which encompasses the *Design Optimization* stage; and 3) the rationalization of the obtained solution for its subsequent fabrication, the *Design Rationalization* stage. All these five stages are considered in the DrAFT framework, which includes a set of different algorithms suitable for the corresponding design task. The combination of these algorithms therefore allows a (1) greater design flexibility, (2) the visualization of different design scenarios, and (3) the use of more specific and suitable design strategies. Moreover, this algorithmic combination constitutes a single program that is responsible for generating all the design exploration levels, discarding the need of having to create more than one program/model to address each design stage and, therefore, constituting a continuous design workflow.



Figure 5: A temporal diagram representing the design stages embraced by the DrAFT framework.

CONCLUSION AND FUTURE WORK

Currently, we are witnessing an increased concern regarding environmental problems, in which architects play an important role. Architects are more aware of the negative impacts architectural practice has in the environment, and they are now focused on reverting this situation. A design paradigm in which design decisions are based on performance is emerging, named Performance-Based Design. This new design approach is based on the use of computational design methods, which support architects in the search for better performing solutions. Algorithmic approaches, analysis studies, and optimization processes are catalyst for this design trend, but, in turn, require specialized knowledge and specific tools.

Unfortunately, architects are still facing several limitations during this design process: (1) the use of algorithmic approaches requires the mastering of programming languages, a skill for which most of the architects were not trained; (2) the transition between design stages usually means switching between digital tools, which is not only error-prone, but it also forces the production of different models to fit the requirements of different tools; and (3) the current variety of optimization algorithms requires architects not only to master a wide range of tools, but also to know which one is better for a certain design scenario, and also to learn how to correctly apply and interpret each of them.

To support architects in getting better results in viable time, a workflow based on an algorithmic approach must be designed to merge the main design stages – design exploration, analysis, and optimization – into a continuous and flexible process that, not only solves the problem of using multiple tools and digital environments, but also supports the design decision along the design process, actively informing the architect in the selection and application of the most suitable algorithmic patterns and strategies to a specific design scenario. The DrAFT framework presented in this paper was designed precisely for that purpose.

ACKNOWLEDGMENTS

This work was supported by national funds through *Fundação para a Ciência e a Tecnologia* (FCT) with reference UID/CEC/50021/2013, and by the PhD grant under contract of University of Lisbon (UL), Instituto Superior Técnico (IST) and the research unit *Investigação e Inovação em Engenharia Civil para a Sustentabilidade* (CERIS).

REFERENCES

Alexander, C., S. Ishikawa, M. Silverstein, and M. Jacobson. 1977. A Pattern Language: Towns, Buildings, Construction. New York: Oxford University Press.

Alfaris, Anas, and Riccardo Merello. 2008. “The Generative Multi-Performance Design System.” In ACADIA 08 › Silicon + Skin › Biological Processes and Computation, 448–57. http://cumincad.scix.net/cgi-bin/works/Show?acadia08_448.

Andrade, Diego, Mikako Harada, and Kenji Shimada. 2017. “Framework for Automatic Generation of Facades on Free-Form Surfaces.” Frontiers of Architectural Research. Elsevier B.V. doi:10.1016/j.foar.2017.04.003.

Caetano, Inês, and António Leitão. 2016. “Exploring Buildings’ Surface Patterns.” In Architecture In-Play International Conference. Lisbon, Portugal.

Caetano, Inês, Luís Santos, and António Leitão. 2015. “From Idea to Shape , From Algorithm to Design: Algorithmic-Based Processes in Architecture.” In The next City - New Technologies and the Future of the Built Environment [16th International Conference CAAD Futures 2015, 483. São Paulo, Brazil.

Chien, Sheng-fen, Hsiu-pai Su, and Yu-wei Huang. 2015. “PARADE: A Pattern-Based Knowledge Repository for Parametric Designs.” In Emerging Experience in Past, Present and Future of Digital Architecture, Proceedings of the 20th International Conference of the Association for Computer-Aided Architectural Design Research in Asia.

Davis, Daniel, Jane Burry, and Mark Burry. 2011. “Understanding Visual Scripts: Improving Collaboration through Modular Programming.” International Journal of Architectural Computing 9 (4): 361–76. doi:10.1260/1478-0771.9.4.361.

Eigensatz, Michael, Mario Deuss, Alexander Schiftner, Martin Kilian, Niloy Mitra, Helmut Pottmann, and Mark Pauly. 2010. “Case Studies in Cost-Optimized Paneling of Architectural Freeform Surfaces.” In Advances in Architectural Geometry 2010, edited by Cristiano Ceccato, Lars Hesselgren, Mark Pauly, Helmut Pottmann, and Johannes Wallner, 47–72. Springer. doi:10.1007/978-3-7091-0309-8.

Eigensatz, Michael, Martin Kilian, Alexander Schiftner, Niloy Mitra, Helmut Pottmann, and Mark Pauly. 2010. “Paneling Architectural Freeform Surfaces.” ACM Transactions on Graphics 29 (4): 1–10.

Flöry, Simon, and Helmut Pottmann. 2010. “Ruled Surfaces for Rationalization and Design in Architecture.” In ACADIA 2010: Life In:formation, 103–9.

Fu, Chi-wing, and Daniel Cohen-or. 2010. “K-Set Tilable Surfaces.” ACM Transactions on Graphics 29 (4): 1–6. doi:10.1145/1778765.1778781.

Gibson, Ian, David Rosen, and Brent Stucker. 2010. “Development of Additive Manufacturing Technology.” In Additive Manufacturing Technologies: 3D Printing, Rapid Prototyping, and Direct Digital Manufacturing, 19–43. Springer.

Hudson, Roland. 2010. “Strategies for Parametric Design in Architecture: An Application of Practice Led Research.” Ph.D Thesis. University of Bath.

Janssen, Patrick. 2014. “Visual Dataflow Modelling: Some Thoughts on Complexity.” In Fusion - Proceedings of the 32nd eCAADe Conference - Volume 2, Department of Architecture and Built Environment, Faculty of Engineering and Environment, Newcastle upon Tyne, edited by Emine Mine Thompson, 305–14. England, UK.

Khwaja, Salman, and Mohammad Alshayeb. 2013. “Towards Design Pattern Definition Language.” Software - Practice and Experience 43 (7): 747–57. doi:10.1002/spe.1122.

Kolarevic, Branko, ed. 2003. Architecture in the Digital Age: Design and Manufacturing. New York: Spon Press.

Leitão, António, Jose Lopes, and Luis Santos. 2014. “Illustrated Programming.” In Acadia 2014: Design Agency, 291–300.

Leitão, António, Luís Santos, and José Lopes. 2012a. “Programming Languages For Generative Design: A Comparative Study.” International Journal of Architectural Computing 10 (1): 139–62. doi:10.1260/1478-0771.10.1.139.

———. 2012b. “Programming Languages For Generative Design: Visual or Textual?” In RESPECTING FRAGILE PLACES [29th eCAADe Conference Proceedings], University of Ljubljana, Faculty of Architecture (Slovenia), 139–62. Ljubljana. doi:ISBN: 978-9-4912070-1-3.

Mesnil, Romain, Cyril Douthe, Olivier Baverel, Bruno Léger, and Jean-françois Caron. 2015. “Isogonal Moulding Surfaces: A Family of Shapes for High Node Congruence in Free-Form Structures.” Automation in Construction 59. Elsevier B.V.: 38–47. doi:10.1016/j.autcon.2015.07.009.

Moneo, R. 2001. “The Thing Called Architecture.” In Anything, edited by C. Davidson, 120–23. New York: Anyone Corporation.

Qian, Z C, Y V Chen, and Robert Woodbury. 2008. “Developing a Simple Repository to Support Authoring Learning Objects.” International Journal of Advanced Media and Communication 2 (2): 154–73. doi:10.1504/IJAMC.2008.018505.

Qian, Zhenyu Cheryl. 2009. “Design Patterns: Augmenting Design Practice in Parametric CAD Systems.” SIMON FRASER UNIVERSITY.

Shapiro, Alexander. 2003. “Monte Carlo Sampling Methods.” In Handbooks in Operations Research and Management Science, 353–425. Elsevier. doi:10.1016/s0927-0507(03)10006-0.

Son, Seunghyun, Heni Fitriani, Jeong Tai Kim, Seongseok Go, and Sunkuk Kim. 2017. “Mathematical Algorithms of Patterns for Free-Form Panels.” In Proceedings of the 2nd World Congress on Civil, Structural, and Environmental Engineering (CSEE’17), 1–8. doi:10.11159/icsenm17.101.

Su, Hsiu-pai, and Sheng-fen Chien. 2016. “Revealing Patterns: Using Parametric Design Patterns in Building Façade Design Workflow.” In Living Systems and Micro-Utopias: Towards Continuous Designing, Proceedings of the 21st International Conference on Computer-Aided Architectural Design Research in Asia, 167–76.

Terzidis, Kostas. 2004. “Algorithmic Design : A Paradigm Shift in Architecture ?” In Architecture in the Network Society [22nd

eCAADe Conference Proceedings / ISBN 0-9541183-2-4] Copenhagen (Denmark) 15-18 September 2004, Pp. 201-207, 201–7. Warsaw.

Woodbury, Robert. 2010. Elements of Parametric Design. New York: Routledge.

Woodbury, Robert, Robert Aish, and Axel Kilian. 2007. “Some Patterns for Parametric Modeling.” 27th Annual Conference of the Association for Computer Aided Design in Architecture, 222–29. http://moodle.ncku.edu.tw/file.php/2687/assignments/ParametricPatterns.pdf.

Yu, Rongrong, and John S Gero. 2015. “An Empirical Foundation for Design Patterns in Parametric Design.” In Proceedings of the 20th International Conference of the Association for Computer-Aided Architectural Design Research in Asia CAADRIA 2015, edited by Y. Ikeda;, C. M. Herr;, D. Holzer;, S. Kaijima;, M. J. Kim;, and Schnabel ; M, A, 551–560. doi:10.1177/1478077116663351.

Zboinska, Malgorzata A. 2015. “Hybrid CAD/E Platform Supporting Exploratory Architectural Design.” CAD Computer Aided Design 59. Elsevier Ltd: 64–84. doi:10.1016/j.cad.2014.08.029.

EXO-SKINS

Self-actuating, thermally-responsive, laminated bio-composite for retrofit



Nick Braaksma
Bates Masi + Architects (formerly at NDSU)
njbraaksma@gmail.com



Malini Srivastava, AIA
North Dakota State University
malini.srivastava@ndsu.edu



Chad Ulven
North Dakota State University
chad.ulven@ndsu.edu

ABSTRACT

Cost-effective, sustainable, self-actuating, thermally-responsive, bio-composite exo-skins that act like shields or cloaks for existing buildings could reduce the energy demand for existing buildings, achieving the benefits of a retrofit without the complicated and invasive processes of a traditional retrofit procedure.

This paper describes the research to develop an advanced bio-composite to be utilized as an environmental modulating layer for building envelopes in order to reduce energy use. Conceptually and in laboratory tests this material is a laminated, thermally-responsive, self-actuating, advanced bio-composite smart material. Designed in various geometries, this material can be utilized as an applied and independent exterior building layer or exo-skin, responding to environmental conditions in order to create non-invasive retrofitting that can “shield or cloak” existing buildings, in order to modulate heat gains and light, ultimately, improving building energy efficiency. Initial digital modeling and lab-testing, has demonstrated the thermally-responsive dynamic capabilities of the material and the resultant patterns in which it can be designed and deployed as a cloak or shield to achieve energy-use reductions. Laminated smart materials that have been developed thus far are for the large part focused on bimetals or petroleum products. This research is targeted to developing a bio-based smart material alternative from a renewable resource. With a strong agriculture industry, the region in which the authors are located expands the renewable source stream is available on a short and regular cycle.

KEYWORDS

adaptive - kinetic – dynamic, physical testing - mockups, composites, material science, bio-composite, thermally responsive, laminated – bio-composite

INTRODUCTION

Of all sectors, buildings have the largest share of energy use in the United States and therefore a large role to play in efforts to reduce energy use and impact global warming trends. As compared to other uses such as transportation and industrial sectors, residential and commercial buildings together add up to almost 40% of energy use, 70% of all electricity produced (U.S. EIA, 2012). The United States is ranked second in the world for carbon emissions, producing 5,406 million tons in 2014 (US EIA, 2015). Per Raman (2009), estimated population growth will result in a proportionate 40% demand growth for new building stock, and 70% of the existing building stock will still be functional in 2050. According to the US EIA, 46 billion

square feet, or 72% of floor stock, in the U.S. are located in buildings that are over 20 years old (Raman, 2009). Over the lifetime of buildings 80-90% of this energy use is in operations (heating, cooling, lighting, devices) whereas only 10-20% is in embodied energy (manufacturing, demolition) (Ramesh et al, 2010). As a result, investments in reduction of operational energy use of existing buildings can have a large impact on reducing building energy use, global warming trends and resultant climate change. This sector presents a liability for the nation's movement toward a more efficient future. However, traditional retrofitting requires costly processes that restructure the building envelope, improve the comfort or control systems or introduce renewable energy sources. Recent research into smart materials has provided an opportunity to develop climate adaptive building shells (CABs) or adaptive building envelopes (ABEs) without the high costs of high-performance retrofits. Smart materials sense environmental conditions, process that sensory input, and then respond locally with predictable movements.

This research builds on the Climate Adaptive Building Shells (CABs) (Loonen, 2010) or Adaptive Building Envelopes (ABEs) (Erickson, 2013) concepts by proposing a bio-composite smart material as an exo-skin that "cloaks or shields" existing buildings to modulate the exterior environment to reduce energy use. In this way, "cloak or shield" is not reliant upon existing building envelope construction providing a departure and disruption of current and traditional retrofit thinking. Additionally, it is sourced from existing agricultural processes.

BACKGROUND

CLIMATE ADAPTIVE BUILDING SHELLS (CAB)

In recent years, high energy performance architecture has split into two alternative directions: active technologies and passive strategies (Loonen 2010, Loonen et al 2013). Active technologies enhance "the level of sustainability in the built environment via the introduction of innovative technical devices," but are limited by the complexity of the innovative systems (Loonen et al 2013). Passive strategies refer to "buildings where the design of construction and shape of the building itself, as opposed to its servicing, play major roles in capturing, storing, and distributing wind and solar energy, normally with the aim of displacing fossil fuels for space conditioning and lighting" (Loonen et al 2013).

As defined by Loonen (2010), "A climate adaptive building shell (CABS) has the ability to repeatedly and reversibly change its functions, features or behaviour over time in response to changing performance requirements and variable boundary conditions. By doing this, the building shell effectively seeks to improve overall building performance in terms of primary energy consumption while maintaining acceptable thermal and visual comfort". This concept was pioneered by Mike Davies in 1981 with a 'polyvalent wall,'' by controlling the flow of energy from exterior to interior with thin multi-functional layers (Davies, 1981). CABS made possible with the utilization of smart materials capture the complementary aspects of passive design and active technology to provide energy reductions for lighting and space conditioning. Smart materials are a natural extension to CABS, offering an integrated strategy for adaptation without systems reliant on additional energy requirements. Smart materials can be defined as "objects that sense environmental events, process that sensory information," and then act respond to the environment (Loonen et al, 2013). In order to be classified as a smart material it must have the following (Kroschwitz, 1992):

a. Immediacy: immediate response; Transiency: responds to several environmental conditions;
b. Self Actuation: Intelligence is in material itself;
c. Selectivity: response is predictable;
d. Directness: response is local.

Smart materials provide a viable and attractive alternative to active adaptive building systems and take advantage of passive design concepts at the same time. This paper describes the research to develop an advanced bio-composite to be utilized as an environmental modulating layer for building envelopes in order to reduce energy use. Conceptually and in laboratory tests this material is a laminated, thermally-responsive, self-actuating, advanced bio-composite material. Loonen et al (2013) describes the four domains of relevant physics for building envelopes as thermal, optical, air-flow, and electrical. This proposal aims to analyze the optical physics domain B, but as optical performance will certainly influence the thermal domain, the future focus of this research is within the E domain, thermal and optical (Fig. 1).

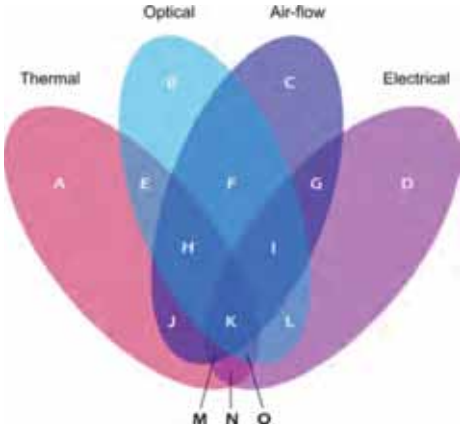


Figure 1: Domains of relevant physics for building envelopes (reproduced from Loonen 2013).

BIO-COMPOSITE LAMINATES BASED ON NATURAL FIBERS

Natural fibers can be produced at 20-40% of the production energy required for synthetic fibers (Faruk et al, 2012) (Dittenber, Gangarao, 2012). Natural fibers possess many different advantages when compared to synthetic or mineral-based fibers such as good specific strength, good specific modulus, low densities, lower cost, and are bio-based. These benefits are most greatly noticed when the applications are in areas where weight is a concern, where natural fibers have approximately a 40% lower fiber density than fiberglass (Joshi et al, 2004). Some of the drawbacks of natural fibers are high moisture absorption, inferior fire resistance, and moderate mechanical properties (Faruk et al, 2012).

There are several factors which can lead to mechanical variability, these are: crop variety, seed density, soil quality, fertilization, field location, fiber location on the plant, climate, weather conditions, harvest timing, fiber handling and extraction methods, and drying processes (Jawaid, Khalil, 2011). In addition to the previously mentioned items, variation in the cross-sectional area along the length of the fiber also leads to mechanical variation (Sherman, 1999; Mohanty, Misra, Drzal, 2001). In order to understand some of the reasons associated with mechanical variability in natural fibers, it is important to understand the structure of the fiber. The flax fiber starts with a stem, which is comprised of bast fiber bundles. These bundles contain groups of elementary fibers which in themselves contain microfibrils. So when working with bast fiber, the term “fiber” is actually used to describe a bundle of elementary fibers which consist of several single fiber divisions (Mohanty, Misra, Hinrichsen, 2000). The breakdown of a bast fiber can be seen in Figure 2.

When discussing elementary fibers, a good way to view them is as a hollow composite. Cellulose fibrils act as the reinforcements, while the hemicelluloses, lignin, pectin, and other amorphous components make up the matrix which holds the cellulose fibrils together. The amounts of these chemical constituents vary by species, strain, and other aspects of a particular plant’s genetics, which leads to varied performance and structure development in different plant fibers (Fuqua, Huo and Ulven 2012).

Natural fibers are broken down into six different groups. The natural fiber groups are as follows: bast fibers (jute, flax, hemp), leaf fibers (sisal and pineapple), seed fibers (coir and cotton), core fibers (kenaf, help, and jute), grass and reed fibers (wheat, corn, and rice), and all other remaining types (wood and roots) (Modin, 2014).

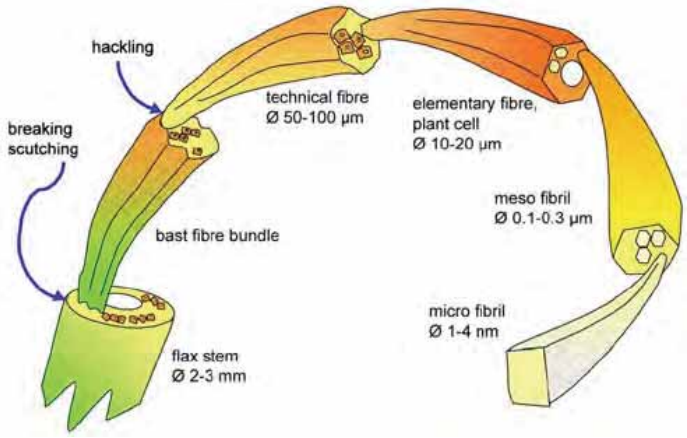


Figure 2. Bast fiber structure (reproduced from Bos, Mussig, van den Oever, 2006).

In this research, Flax fibers are being used as bio-composites due to their high stiffness, tensile strength, and low density. Flax fibers are grown in temperate regions such as: Netherlands, France, Spain, Russia, Belgium, China, India, Argentina, Canada, and the United States (Fuqua, Huo and Ulven, 2012). Flax is also the oldest textile known and is an important standard for the modern textile industry (Fuqua, Huo and Ulven, 2012). The plant can grow between 80 and 150 cm in roughly 80 to 110 days, where after which approximately 75% of the plant's height can be used to produce fiber (Jawaid, Khalil, 2011). Currently about 830,000 tons of flax are produced every year (Fuqua, Huo and Ulven, 2012).

SUSTAINABLE COMPOSITES FOR CONSTRUCTION

Sustainable composites can be constructed using both fibers and polymeric resins that are derived from renewable sources such as plants, particularly those that are annually grown (Jang, 1994) (Lodha, Netravali, 2002). If both fibers and the bio-based resins are biodegradable, the composites are expected to also be biodegradable. As a result, they can easily be composted at the end of their life. A wide variety of plant derived fibers, with different tensile properties, are available around the world. Depending on the mechanical properties of the specific fiber used, the composite properties can be manipulated based on fiber length, orientation, and volume fraction. Several natural fiber types are currently commercially available in many forms, such as loose fibers, yarns, woven and knitted fabrics or nonwoven mats, making it possible to combine them in different layers to design the desired properties for a particular application. Two general types of sustainable composites can be fabricated to be used in construction: i) those that use short natural plant-based fibers and have mechanical properties comparable or better than wood and wood products (normal bio-composites) and ii) those that use long bast fibers that can be oriented and have specific properties comparable to fiberglass composites (advanced bio-composites) (Chabba and A.N. Netravali, 2005) (Netravali, Huang, Mizuta, 2007). In this project, the focus will be on designing and constructing concepts with advanced bio-composites to fully exploit their potential.

METHOD

This research is based on laminating two materials with different coefficients of thermal expansion together to achieve a bending deformation along the length of the strand when heated. In the application of architecture, the lamination strategy has been pioneered by D. Sung to produce thermo-bimetals for an adaptive building envelope (Sung, 2016). Since 2011, Sung had recorded 4 projects testing various thermo-bimetal applications, but notes the need for further testing of smart materials: "The amount of deflection varies depending on the size/shape of the pieces, the air temperature, the position of clamping, and the thickness of the material" (Sung 97). This research, specifically laminates sustainable composites from flax using both fibers that are grown annually and polymeric resins resulting in a compostable bio-composite. Sung (2016) describes the research of self actuating thermobimetals as residing in the gap between "scientific reduction and aesthetic elaboration, between the quantitative knowledge of the environment and its qualitative expression in space" (Sung, 106). This research carries out the investigation of bio-composite material simultaneous its applied architectural geometry. Through the thermobimetal research, D. Sung describes the importance of this integrated approach, "Form, structure and material have to

be developed simultaneously, a simple, comprehensive system will be the resultant with less waste and higher performance" (Sung, 146). The form, movement and corresponding daylighting energy were modeled along with the biocomposite testing. Initially, a broad variety of geometries were tested against their ability to impact day lighting conditions at different rates of expansion. The modeling created thresholds for biocomposite expansion to impact interior conditions, while the architectural form was simplified and informed by the initial biocomposite material expansion testing results. The biocomposite expanded along a single axis, rather than uniformly. The parametric and daylighting modeling allowed testing to determine how much expansion is necessary to impact interior daylight conditions.

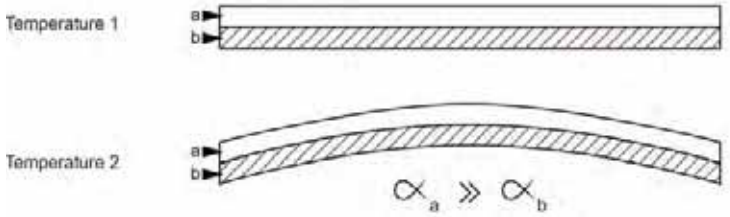
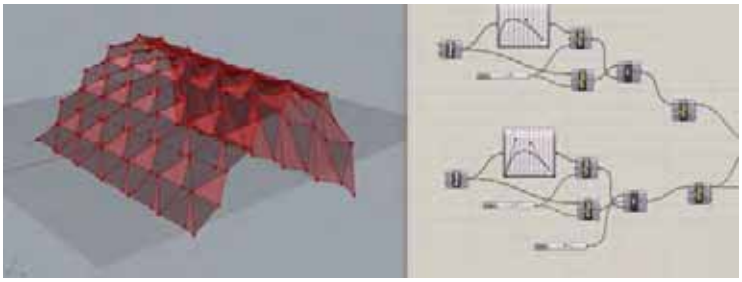
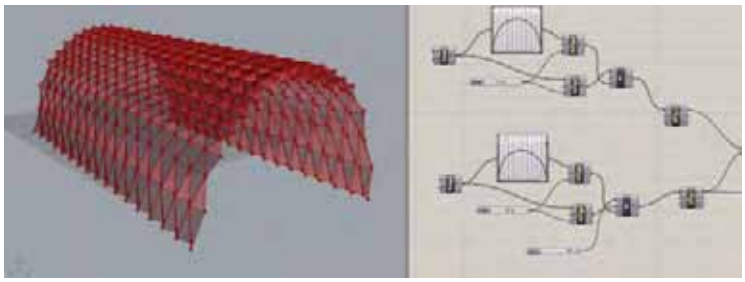
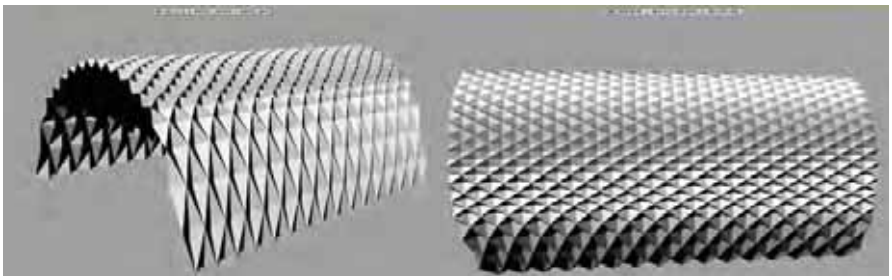


Figure 4. Concept diagram of the laminated bio-composite of two different materials to initiate a thermal response.

Initial geometries for exo-skins were developed digitally to establish a basic design for the thermally-responsive "cloak or shield" concept. Rhinoceros 3d (Rhino) was used as a base 3D modeling tool to develop the design of various iterations. Grasshopper was used to generate the 3D models within Rhino, utilizing the parametric controls to accommodate the movement of dynamic materials. DIVA was used to model daylighting and energy within Rhino, facilitating the analysis of various design iterations performance. The initial studies included folded plates and tensile structures as well as linear louvered systems that spontaneously transformed the shape of component pieces due to thermal response.







Figures 5a-c: Folded plate arches with laminated bio-composite components that respond to thermal stimuli with shape distortions.

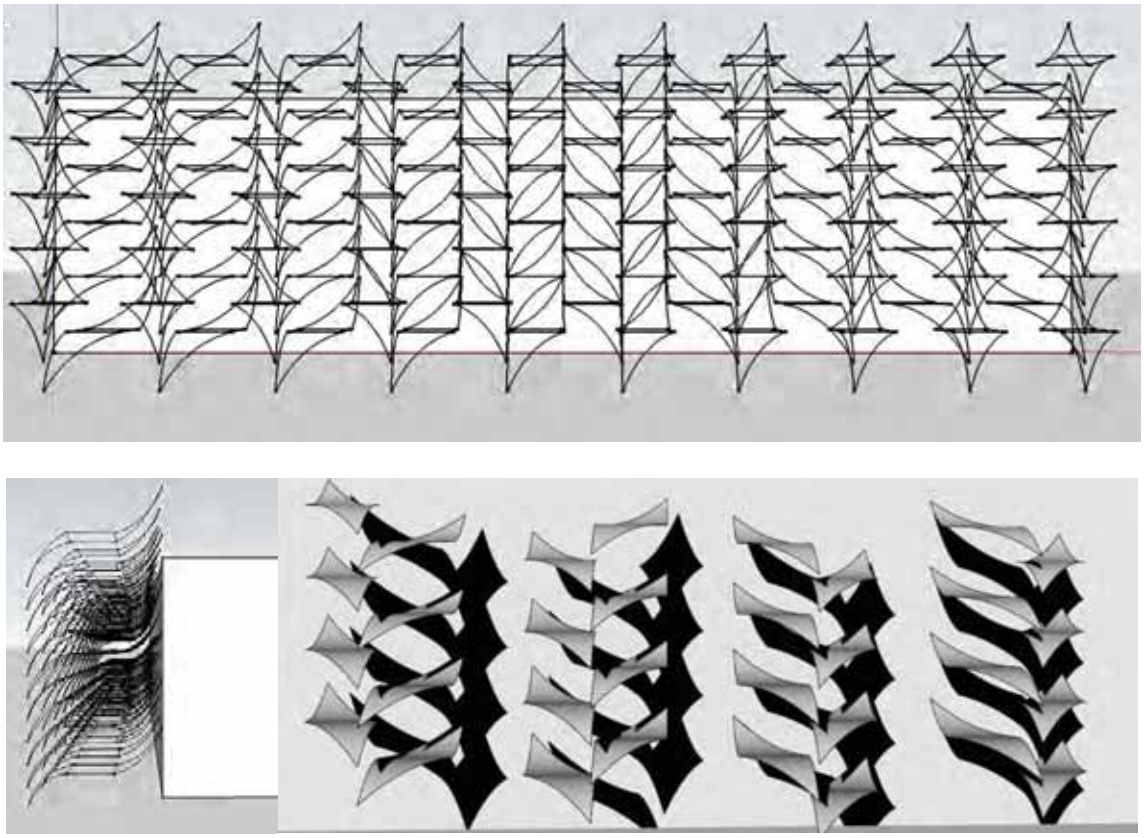


Figure 6a-b: Tensile structure with laminated bio-composite components that respond to thermal stimuli with shape distortions.

The louvered systems were developed in detail as end captured and non-captured repeated modules. The simplest center deflection version was constructed for controlled testing in a laboratory in order to understand the movement patterns of the bio-composites in response to thermal modifications. Initial deflection testing was conducted based on five combinations in order to test the simple pattern outlined in Figure 7a.

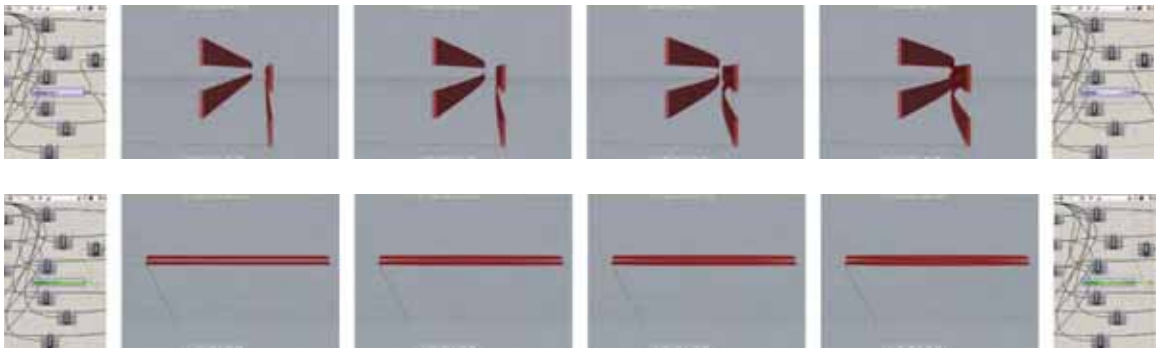


Figure 7a: Simple center deflections.

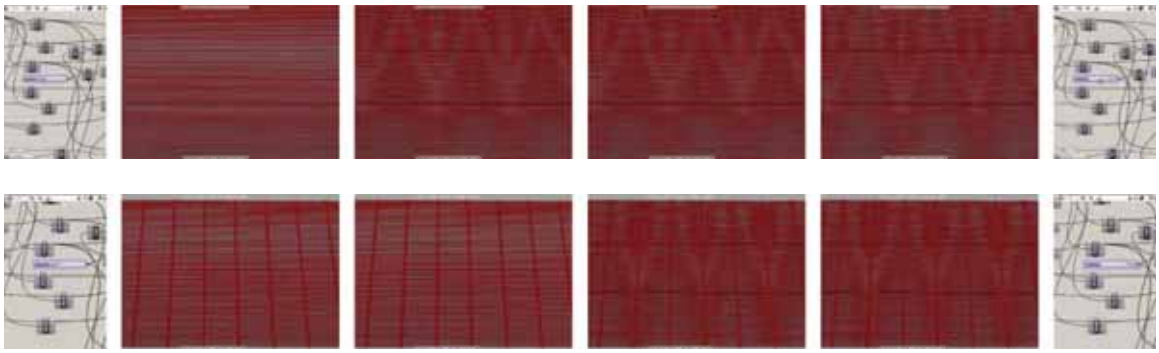


Figure 7b: Simple center deflections to create entire facade self-actuated shading systems with multiple panel geometries.

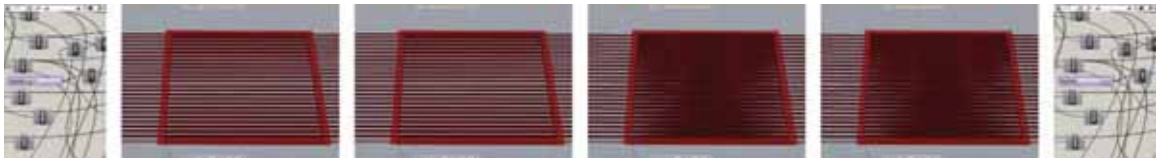


Figure 7c: Combinations of biocomosites to achieve variable responses to thermal stimuli.

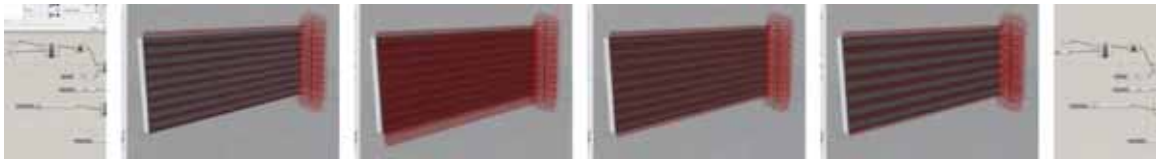


Figure 7d: Louvered structures with laminated bio-composite components that respond to thermal stimuli by edge distortion of individual components.

DIGITAL ENVIRONMENTAL TESTING

In concert with laboratory testing of the louvered systems, initial digital daylight simulations showed the potential of the system to manage daylighting and corresponding heat gain. The simulations were performed in DIVA, software developed by the MIT Sustainable Design Lab (Fig. 8a-b & 9a-b). The simulations assume a conservative range of movement, adopting a design for a potential shading device based on small thermally-responsive movements. The simulations show a potential for controlling the diffuse or ambient natural lighting in the space and reducing heat load to the interior space.

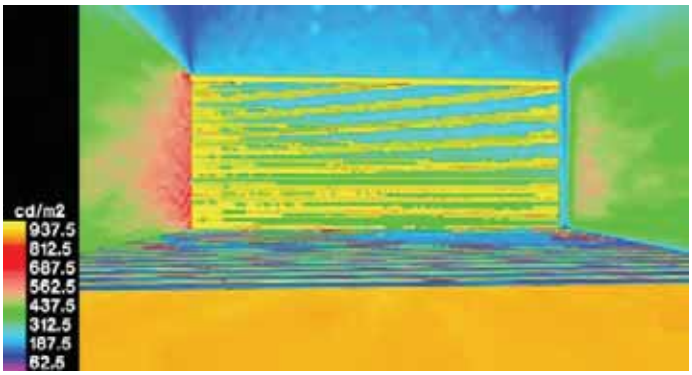


Figure 8a: Luminance, winter solstice, open (DIVA).

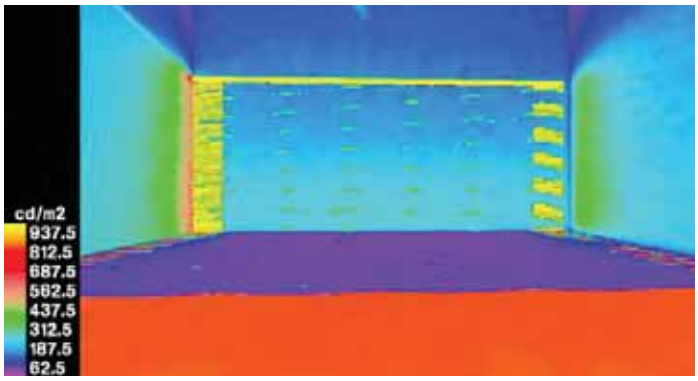


Figure 8b: Luminance, winter solstice, closed (DIVA).

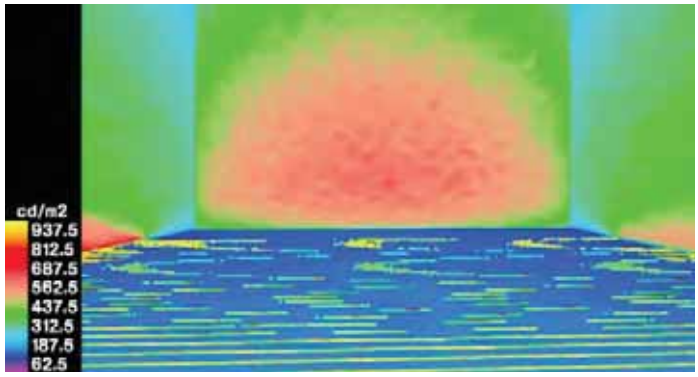


Figure 9a: Luminance, equinox, open (DIVA).

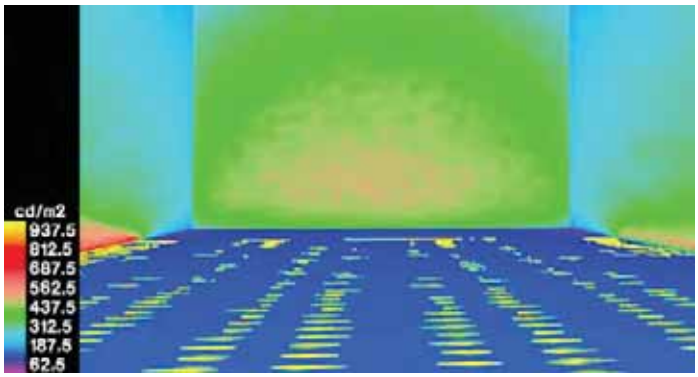


Figure 9b) Luminance, equinox, closed (DIVA).

More extensive and similar simulations are planned for the future for various environmental stimuli such as temperature, moisture and wind in addition to daylighting tests. These will require working simultaneously in Rhino, Grasshopper and softwares like DIVA to understand the potential of laminated, thermally-responsive bio-composites.

DATA

Sourced from Composites Evolution, a worldwide supplier of composite materials based in Chesterfield UK, Biotex Flax is the base material for the five samples that were tested in the laboratory. The Biotex Flax is based on natural fibers, acting as high performance reinforcement textiles designed for fiber-reinforced polymer composite applications. Biotex provides high performance normally associated with glass fiber composites, but with lower weight and environmental impact. The proposed design based on the digital geometry development and testing for the self-actuating composite is a 914.4 mm (36 in) by 50.8 mm (2 in) member that can deflect 12.7 mm (0.5 in) at center upon heating. To find a composite lay-up that will meet this requirement experiment was carried out testing three different composite lay-ups. Due to the size limitations of the oven used for heating, the final dimensions of the composite samples tested were 457.2 mm (18 in) by 50.8 mm (2 in).

Sample 1	Sample 2	Sample 3	Sample 4	Sample 5
$[0_{CF}/90_{CF}]$	$[0_{2FF}/90_{CF}]$	$[0_{2FF}/90_{FFM}]$	$[0_{CF}/90_{CF}]$	$[0_{2FF}/90_{CF}]$

CF = Unidirectional Carbon Fiber, FF = Unidirectional Flax Fiber, FFM = Random Flax Fiber Mat

Table 1: The different composite lay-ups.

All samples were prepared using a vacuum assisted resin transfer molding (VARTM) process with an epoxy resin (Araldine 8604) and an amine hardener (Aradur 8604). Samples 4 and 5 were post cured in an oven at 120ºC for one hour while being compressed flat. A testing apparatus was constructed using wood, cut parallel to the grain, to limit the thermal expansion of the test fixture's effect on the deflection of the materials. The samples were placed into an oven at 65.5 ºC (150 ºF) for one hour. The samples were then removed from the oven and the total deflection of the samples at the center was measured.

RESULTS OF LABORATORY TESTS

The deflection for all the samples tested can be seen in Table 2.

	Sample 1	Sample 2	Sample 3	Sample 4	Sample 5
Deflection	13 mm (0.51 in)	7 mm (0.275 in)	1 mm (0.04 in)	-2 mm (0.079 in)	3.5mm (0.138 in)

Table 2: Deflection of composite after heating.

From the samples tested, Sample 1 showed the largest amount of deflection out of all the samples tested, and at being only half the final length of the proposed full size composite structure could have an even greater deflection to test more geometries and resultant impact on daylighting and resultant thermal control (Fig. 10).



Figure 10: Center deflection position of Sample 1. Before heating (left), after heating (right).

The deflection of Sample 2 is close to half of what is desired for the full size composite structure, and could provide the required amount of deflection need for the full size structure as the digital model (Fig. 11).

The deflection of Sample 3 was almost nonexistent. The random flax fiber mat was too thick causing the structure to be too stiff to allow for much deflection. A thinner mat or pressure molding could be used for future testing.



Figure 11: Center deflection position of Sample 2. Before heating (left), after heating (right).

When allowing the samples to return to room temperature samples 1, 2, and 3 did not return to their original shape, or continue to deform after returning to room temperature 17.8 ºC (64 ºF).

The deflection in the post-cured Sample 4 was in the opposite direction and of less magnitude than what was seen in Sample 1, when removed from the oven. As the sample cooled its direction of deflection became the same as the others, and the total deflection from the starting point can be seen in Table 3.

The deflection in the post-cured Sample 5 was half of the amount of the deflection that was seen in Sample 2 when it was removed from the oven, but upon cooling to room temperature the samples deflection increased another 7 mm (0.275 in). The total deflection for the sample is shown in Table 3.

	Sample 4	Sample 5
Deflection	4 mm (0.156 in)	10.5 mm (0.41 in)

Table 3: Total deflection after heating and then cooling for Samples 4 & 5.

Sample 5 was taken through a second heating and cooling cycle. The sample deflected a total of 10 mm (0.393 in) upon heating and then returned to its starting point. The deflection of the sample during the second cycle can be seen in Figure 12.



Figure 12: Deflection cycle of Sample 5; room temperature 17.7C (left).

EXPLANATION

Some of the results obtained thus far were surprising especially during the cooling cycle. The laminated bio-composites respond differently to heating and cooling cycles. The cooling cycle changes indicate that the laminated bio-composite material's movement in response to thermal stimulation varies greatly based on its fiber structure. In future iterations of the research, the next samples that are prepared the fiber orientation will be switched to [$0_{0°}/90_{90°}$] to attempt for an opposite structural response in the material. For future testing the use of an oven as the heat source will need to be replaced with a directional radiation heat source to better represent actual operating conditions.

Sung (2016) describes the unique importance of design in the development of smart materials, "In the development of responsive materials for building application, geometry plays a significant role on two levels: in the design of the four-dimensional operation and in the alteration of the behavior of smart materials. These issues are specific to designing shape-changing materials and are additional to the standard problems of fabricating, tessellating, pattern making, assembly sequencing, and making building facades performative" (Sung 97).

The preliminary results have shown that the digital design development process and the physical and digital testing process need to be planned in short cycles, quickly responding to the results from one test to another. A rapid cycle of tests that inform design iterations in the search for reliable patterns of self-actuated, thermally responsive movements will be needed.

CONCLUSION AND FUTURE WORK

This testing demonstrates that a thermally activated, self-actuating, laminated bio-composite structure could be made. In a sample size of 457.2 mm (18 in) by 50.8 mm (2 in), as much as 13mm deflection was found in laboratory tests. The results lead to the conclusion that the amount and direction of deflection can be controlled by varying the following factors:

a. fiber type
b. fiber orientation (or lay-up)
c. material thickness and density
d. patterns and geometry

Future directions in research could include design development of exo-skin modularity for repetitions over larger surface areas, sealing the edges of modular geometries in order to create air-tight enevlopes, transparency of material to create ranges of opacity to transparency in the exo-skin. In addition to the simple geometries of the louvered systems, in the future, the folded plate and tensile structures have great potential as exo-skins to act as cloaks or shields due to their self-supporting structural geometries.

ACKNOWLEDGMENTS

This early research was completed with seed funding by Department of Architecture and Landscape Architecture, North Dakota State University. Patrick Simpson (2016 Graduate Research Assistant, Mechanical Engineering) completed the laboratory tests including materials samples.

REFERENCES

Bos, Harriette L., Jörg Müssig, and Martien JA van den Oever. "Mechanical properties of short-flax-fibre reinforced compounds." Composites Part A: Applied Science and Manufacturing 37, no. 10 (2006): 1591-1604.

Chabba, Shitij, and Anil N. Netravali. "'Green'composites part 1: characterization of flax fabric and glutaraldehyde modified soy protein concentrate composites." Journal of Materials Science 40, no. 23 (2005): 6263-6273.

Davies, Mike. "A Wall for all seasons+ Uses for glass in building." Riba Journal-Royal Institute of British Architects 88, no. 2 (1981): 55-57.

Drehobl, Ariel, and Lauren Ross. "Lifting the high energy burden in America's largest cities: How energy efficiency can improve low income and underserved communities." (2016).

Dittenber, David B., and Hota VS GangaRao. "Critical review of recent publications on use of natural composites in infrastructure." Composites Part A: Applied Science and Manufacturing 43, no. 8 (2012): 1419-1429.

Erickson, James. Envelope as Climate Negotiator: Evaluating adaptive building envelope's capacity to moderate indoor climate and energy. Arizona State University, 2013.

Faruk, Omar, Andrzej K. Bledzki, Hans-Peter Fink, and Mohini Sain. "Biocomposites reinforced with natural fibers: 2000–2010." Progress in polymer science 37, no. 11 (2012): 1552-1596.

Fuqua, Michael A., Shanshan Huo, and Chad A. Ulven. "Natural fiber reinforced composites." Polymer Reviews 52, no. 3 (2012): 259-320.

Holbery, James, and Dan Houston. "Natural-fiber-reinforced polymer composites in automotive applications." JOM Journal of the Minerals, Metals and Materials Society 58, no. 11 (2006): 80-86.

Jang, Bor Z. "Advanced polymer composites: principles and applications." ASM International, Materials Park, OH 44073-0002, USA, 1994. 305 (1994).

Jawaid, M. H. P. S., and HPS Abdul Khalil. "Cellulosic/synthetic fibre reinforced polymer hybrid composites: A review." Carbohydrate Polymers 86, no. 1 (2011): 1-18.

Joshi, Satish V., L. T. Drzal, A. K. Mohanty, and S. Arora. "Are natural fiber composites environmentally superior to glass fiber reinforced composites?." Composites Part A: Applied science and manufacturing 35, no. 3 (2004): 371-376.

Kroschwitz, Jacqueline I., and Mary Howe-Grant. "Encyclopedia of chemical technology Kirk-Othmer." Wiley & Sons, New York, USA (1991).

Lodha, Preeti, and Anil N. Netravali. "Characterization of interfacial and mechanical properties of "green" composites with soy protein isolate and ramie fiber." Journal of Materials science 37, no. 17 (2002): 3657-3665.

Loonen, Roel. "CLIMATE AOAPTIVE BUILOING SHELLS: What can we simulate?." (2010). Eindhoven University of Technology.

Loonen, Roel CGM, Marija Trčka, Daniel Cóstola, and J. L. M. Hensen. "Climate adaptive building shells: State-of-the-art and future challenges." Renewable and Sustainable Energy Reviews 25 (2013): 483-493.

Modin, H. A. N. N. A. "Adaptive building envelopes." Chalmers University of Technology (2014): 18-19.

Mohanty, A. K., Manjusri Misra, and Lawrence T. Drzal. "Surface modifications of natural fibers and performance of the resulting biocomposites: an overview." Composite Interfaces8, no. 5 (2001): 313-343.

Mohanty, A. K., M. Misra, and Gi Hinrichsen. "Biofibers, biodegradable polymers and biocomposites: an overview." Macromolecular materials and Engineering 276, no. 1 (2000): 1-24.

Netravali, Anil N., Xiaosong Huang, and Kazuhiro Mizuta. "Advanced'green'composites." Advanced Composite Materials16, no. 4 (2007): 269-282.

Raman, Mahadev. "Mitigating climate change: what America's building industry must do." Design intelligence (2009). Retrieved from http://www.di.net/articles/mitigating-climate-change-what-americas-building-industry-must-do/

Ramesh, T., Ravi Prakash, and K. K. Shukla. "Life cycle energy analysis of buildings: An overview." Energy and buildings 42, no. 10 (2010): 1592-1600.

Sherman, Lilli Manolis. "Natural fibers: the new fashion in automative plastics." Plastics technology45, no. 10 (1999): 62-68. Available: www.ptonline.com. [Accessed 20 2 2013]

Sung, Doris. "Smart Geometries for Smart Materials: Taming Thermobimetals to Behave." Journal of Architectural Education 70, no. 1 (2016): 96-106.

Taylor, C., T. Krosbakken, C. A. Ulven, A. Paramarta, and D. C. Webster. "Structural quality biocomposites of treated flax fiber with epoxidized sucrose soyate resin." In International Conference on Composite Materials. Montreal, Canada. 2013.

U. S. residential and commercial buildings total primary energy consumption (March 2012). Retrieved from United States Energy Information Administration. (2015). Monthly Energy Review 2014. United States Department of Energy.United States Energy Information Administration. (2016). Monthly Energy Review 2015. United States Department of Energy.United States Energy Information Administration. (2015). Monthly Energy Review 2014. United States Department of Energy.

Webster D C, Nelson T J, Paramarta A, Kovash C, Pan X. "High performance, high biocontent thermosets for composites and coatings." 17th Annual Green Chemistry & Engineering Conference, Bethesda, MD, United States, June 18-20, (2013b) GCE-219.

HEAT-ACTUATED AUXETIC FACADES



Amira Abdel-Rahman
Autodesk
amira.a.rahman@alumni.harvard.edu



Elnaz Tafrihi
Steinberg Architects
elnaz.tafrihi@alumni.harvard.edu

ABSTRACT

Highly transformable materials can be used as adaptive exterior shading systems by leveraging the relationship between external stimuli (heat) and reconfigurable facades in order to design new passive kinetic systems. Reversible transformations were explored using materials that exhibit two-way shape memory behavior such as shape memory polymers and shape memory alloys coupled with auxetic patterns. Initial prototypes were made using multi material 3D printing with shape memory polymers. The larger scale prototypes were made with high density foams cut with Robotic water jets.

The preferred geometries selected belong to a family of auxetic patterns that are composed of small units which buckle individually under the influence of external forces that cause porosities throughout the entire structure to open and close gradually. Due to the unique negative Poisson ratio in auxetics, a single applied force is able to actuate a whole grid of cells. The resulting movement of the cells on a facade system offers novel functionality as well as intriguing aesthetics.

Furthermore, the proposed dynamic system can help reduce the total energy consumption of a building while improving its daylight performance and comfort for its inhabitants. In order to test the daylighting performance of the proposed shading system, a dynamic shading system using auxetic pattern was applied to a facade in Cairo, Egypt which was then simulated and optimized using Honeybee in Grasshopper. Based on the results, this system lead to a marked improvement in both daylighting and energy performance compared to a static non-response shading device.

KEYWORDS

adaptive-kinetic-dynamic, polymers, 3D Printing, fabrication prototypes, daylighting-shading, adaptability

INTRODUCTION

Humans have a tendency to value transparency and desire to bring the outdoors and indoors together, while keeping interior spaces comfortable. Dynamic shading systems can satisfy that need and play an important role in creating a comfortable space where indoors and outdoors can feel connected.

Dynamic facades, with their ability to respond to environmental conditions, can help control and redirect the flow of energy. This energy can come in many forms such as heated air-cooled water that can be reused or help with decreasing the need for mechanical systems in buildings.

A primary benefit of dynamic shading systems is the role it can play with reducing solar heat gains. This is especially important in climates where cooling is important and can help improve daylight comfort within the space. Although they can provide a number of benefits, dynamic shading systems have some disadvantages such as a dependency on active systems requiring electricity and high maintenance costs. Active systems such as these are rendered infeasible for small scale projects due to these high construction and maintenance costs. To solve these issue, passive strategies using external stimuli are used in this research, particularly focusing on transformation using heat. In order to implement these passive strategies, this paper explores the use of Auxetic Structures combined with heat responsive materials as a more feasible alternative to active dynamic shading.

BACKGROUND

BACKGROUND - AUXETIC STRUCTURES

Auxetic cellular structures with a Negative Poisson Ratio (NPR) were chosen as a shape morphology to be investigated in this research.

These structures were first reported by Lakes, however the research and applications in such structures was very slow due to the challenges in fabrication of such complex shapes (1987). The recent advances in digital fabrication made the research and implementation of NPR structures in the industry more practical.

Recently, the use of elastic with the property allowing you to change the porosity on demand have numerous applications in many fields including electronics, bioengineering photonics, and robotics (Shim et al. 2013).

In sync with the emerging trend of soft architecture, auxetics have a great advantage that allows them to be used as facade systems in relation to the current state-of the-art dynamic facades as they only require a small force which can cause a dramatic deformation in the system. The absence of complex mechanical joints in these structures gives these systems an edge in terms of ease of fabrication and construction (Overvelde, Shan, and Bertoldi 2012).

BACKGROUND - HEAT RESPONSIVE FACADES

In the recent past, material intelligence and computation has emerged as an alternative to conventional electrical and mechanical systems providing a more compact, reliable, easy to fabricate alternatives. These ‘metamaterials’ have intelligence that is embedded on a material level rather than in the system. Advances in digital fabrication helped a lot in this movement allowing for fast prototyping and proof of concept. These smart materials either have abnormal behavior or are responsive to different stimuli like touch, heat, electric current, light.

As for the architectural applications, the materials were mainly explored in building envelopes as it’s the layer that is directly in contact with the continuous changes in the external environmental factors. In this research, heat is chosen as the external stimuli that is predictable enough to use as a design parameter for the facade system and has a great effect in the built environment. Different smart materials are stimulated by heat such as shape memory alloys polymers, and bimetals that deform when two metals with different thermal expansion are laminated together.

SHAPE MEMORY ALLOYS (SMA) AND POLYMERS (SMP)

Shape Memory alloys and polymers are materials that have the memory of a shape that when deformed and can return to the original shape when heated (Fig. 1).

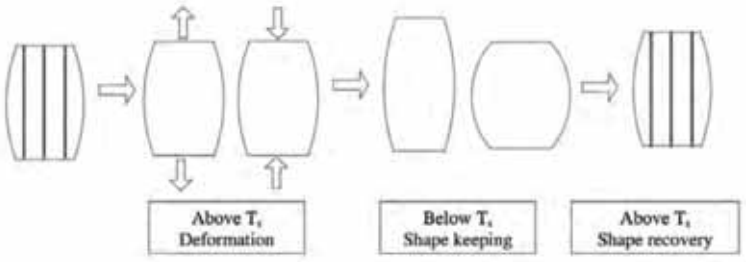


Figure 1: Shape memory effect (Ratna and Karger-Kocsis 2008).

A number of projects that use shape memory alloys in facade systems include the Harvest Screens, AIR flower and Piraeous tower ((Grinham, Blabolil, and Haak 2014; “The Air Flower,” n.d.). Shape memory polymers are now becoming more and more popular due to the popularity of soft materials. In addition, a couple of projects used shape memory polymers in building envelopes (Beites, 2013; Studio Kimii n.d.).

METHOD

In order to investigate the possibility of using heat actuated auxetic structures in a facade system, two research investigations were conducted in parallel. The first investigation is the design and fabrication of auxetic prototypes using digital and rapid fabrication techniques to study the possibility of passive actuation. Second, a full-scale facade system was designed and optimized with a dynamic daylighting simulation to prove the efficiency of using these shapes and structures as shading devices (Fig. 2).



Figure 2: Concept rendering of the auxetic facades.

METHOD - PHYSICAL PROPERTIES

An important aspect of this research is concerned with the production of heat responsive prototypes using novel materials and digital fabrication techniques. A number of different fabrication techniques were explored and evaluated with respect to the ease of fabrication, implementation of passive actuation techniques, mechanical performance, and the scalability of both of fabrication technique and the materials used. The first method used was molding and casting of silicone rubber prototypes (Smooth-on OOMOO 30) using both laser cut and 3d printed molds. These models were used to understand the mechanical behavior of the auxetic structure and to optimize the opening size and form ratio. The second set of prototypes were 3D printed using a multi-material 3D printer (Stratasys Connex 3 Objet500) using flexible and SMP (shape memory polymer) resins. Lastly, a CNC waterjet was used to cut foam as a scalable fabrication technique.

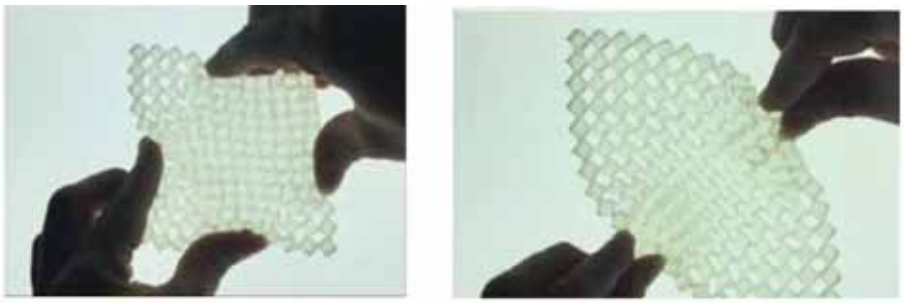


Figure 3: 3D printed flexible prototype.

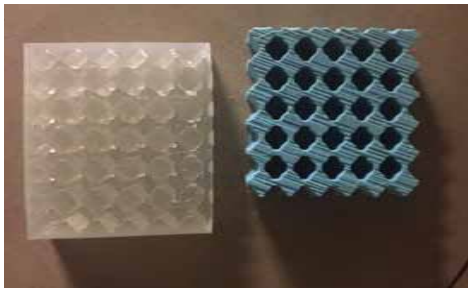


Figure 4: Silicone prototype with 3D printed mold.

METHOD - FACADE DESIGN AND SIMULATION

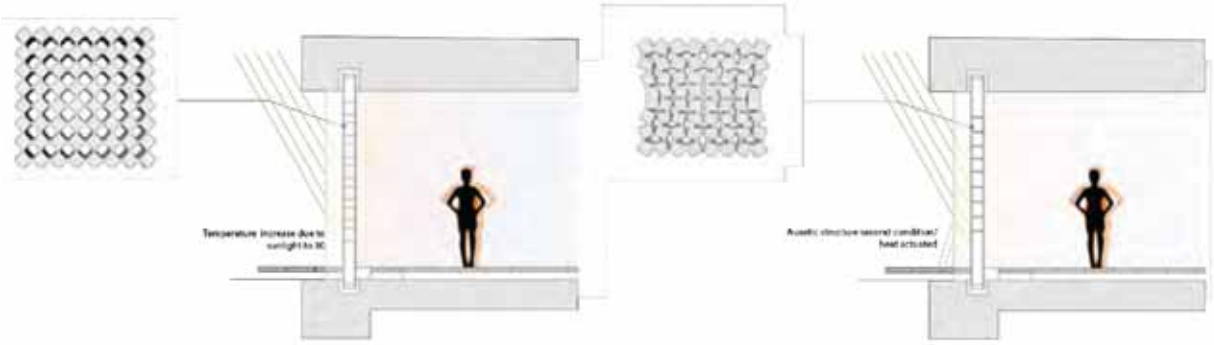


Figure 5: Shoebox simulation concept.

In order to test the efficiency of using passively actuated auxetic shading devices, a shoebox daylighting model was prepared to test the performance of the facade in comparison to two base cases: one without any shading systems and one with horizontal blinds. The design of the shading device was based on a circular grid pattern that closes and open responsively with the temperature and direct solar radiation (Fig. 6). The space simulated is a ground floor 5*10 meters (m) and 3 m high space. The window dimension is 2 m*2 m and 0.3 m from the ground. The simulation was setup in Cairo as a dry hot area that demands highly shaded openings to prevent higher cooling loads and uncomfortable interior spaces. The simulation chosen was a half an hour of point in time illuminance (1m by 1m grid spacing) each in the summer solstice (June 21) to show the effect of dynamic shading in relation to static and no shading condition (Fig. 7).

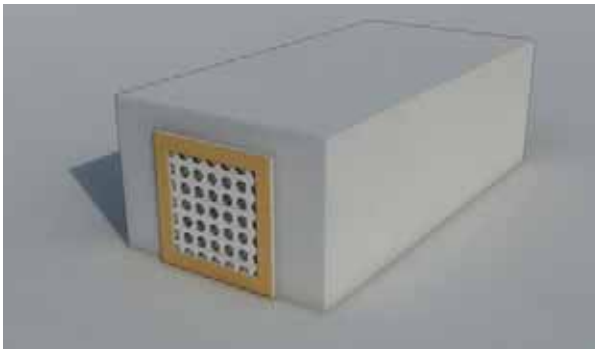


Figure 6: Shoebox model.

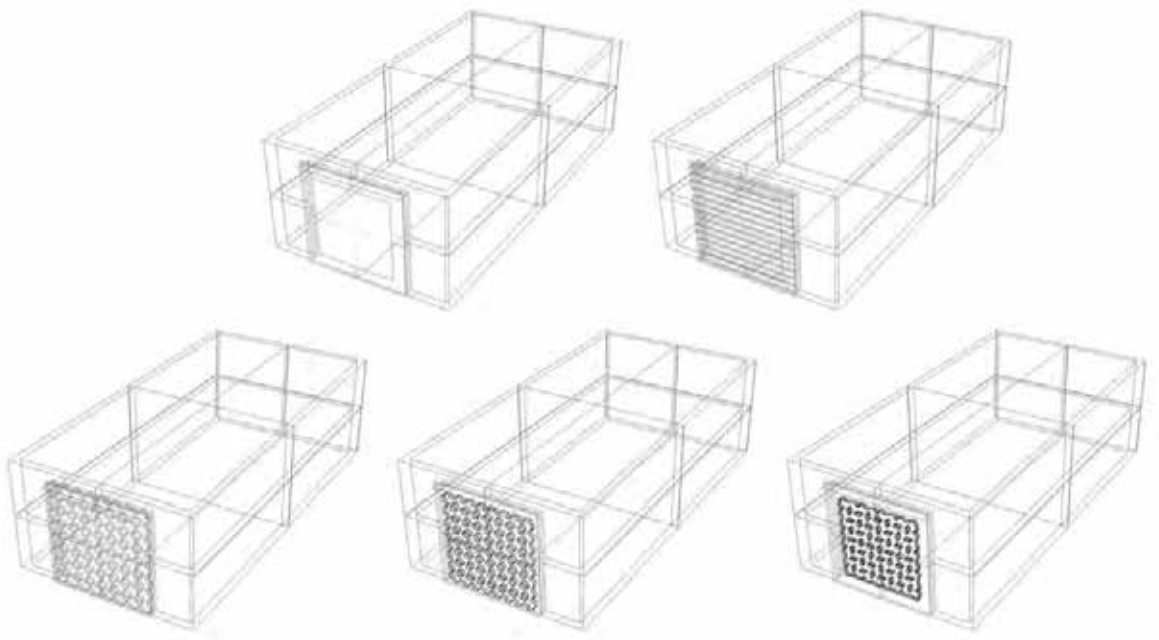


Figure 7: Shading devices simulated.

DATA

DATA - PHYSICAL PROPERTIES

DATA - PHYSICAL PROPERTIES - SHAPE SELECTION

The different geometric properties of the facade have a great effect on the overall behavior the auxetic structures (Johannes, Overvelde and Bertoldi 2014). Among the cast silicone prototypes, a square grid of circle shaped cell openings as well as other opening shapes (Fig. 8) were produced with the annotated relationships between the wall size and grid spacing. It is important to note that the thicker the structures the more lateral stability they will have. If the ratio between the thickness and grid size, this will case out of plane buckling of the structure if the applied external forces aren't perpendicular to the structure. In the intended facade design case each cell will be actuated independently by the shape memory effect. As a result, since there are no external forces applied to the structure, the thickness of the structure is not considered an important parameter in the study.

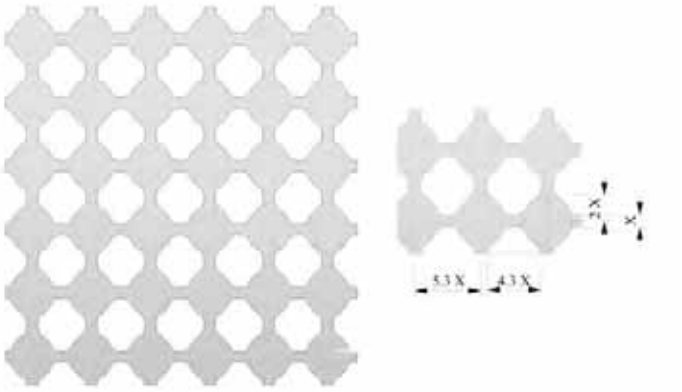


Figure 8: Geometric properties of the auxetic patterns.

DATA - PHYSICAL PROPERTIES - PASSIVE ACTUATION

Different methods of heat induced passive actuation were explored for each of the physical models. For the silicone prototypes, the primary method evaluated was the possibility of using shape memory alloys. The setup was composed of a silicone model between two acrylic panels to prevent lateral buckling with two shape memory alloy springs at each end of the structure (Figure 9).

It is important to note that the amount of heat or force applied to the structure isn't directly proportional to the amount of deformation in the structure. The buckling of the cells isn't proportional with force over time because of the bistable effect of the cell walls which snap when a certain amount force is applied.

If the same mechanism was used for full scale architectural applications, the strength of the shape memory springs should be properly calculated to be strong enough to actuate the auxetic structure while also not flexible enough to be pulled back by a balancing weight or opposing spring pulling the structure to its original opened shape.



Figure 9: Shape memory alloys as an actuation technique.

In order to solve the challenges that come with the above technique, the possibility of fabricating the whole structure from a shape changing material was also explored. Material swelling was previously used as a passive actuation technique where small distributed forces result in actuation (Kang et al. 2013). This is contrary to the previous techniques where a large external force is needed to induce the same actuation. Moreover, this eliminates the need for an extra rigid layer as there is minimal lateral buckling.

Taking these techniques into account, the next set of prototypes were 3D printed using SMP to study the real-world applicability of induced passive actuation and the behavior of the auxetic system. Vero-Blue was chosen as the SMP material due to the fact that it could be 3D printed. In addition, all prototypes were 3D printed in their opened state. The shape training was done by applying an external force at high temperature (~200°C) so that when the structure is at its closed state it could be removed quickly to room temperature (Figure 10).



Figure 10: Shape training the SMP.

Afterwards, when the structure is put under high temperature, it returned to its previously saved opened shape (Fig. 11). It is important to note that the Vero-blue material fatigues quickly and tends to be relatively stiff. Because both the shape training and the process of returning to a closed state require a great force to be exerted, the deformation, to some extent, is irreversible. It should also be noted that in terms of a facade system application, the shape should be 3d printed in the closed state to cause the structure to close when exposed in high temperatures ensuring a decrease in the amount undesirable direct solar radiation inside the building.

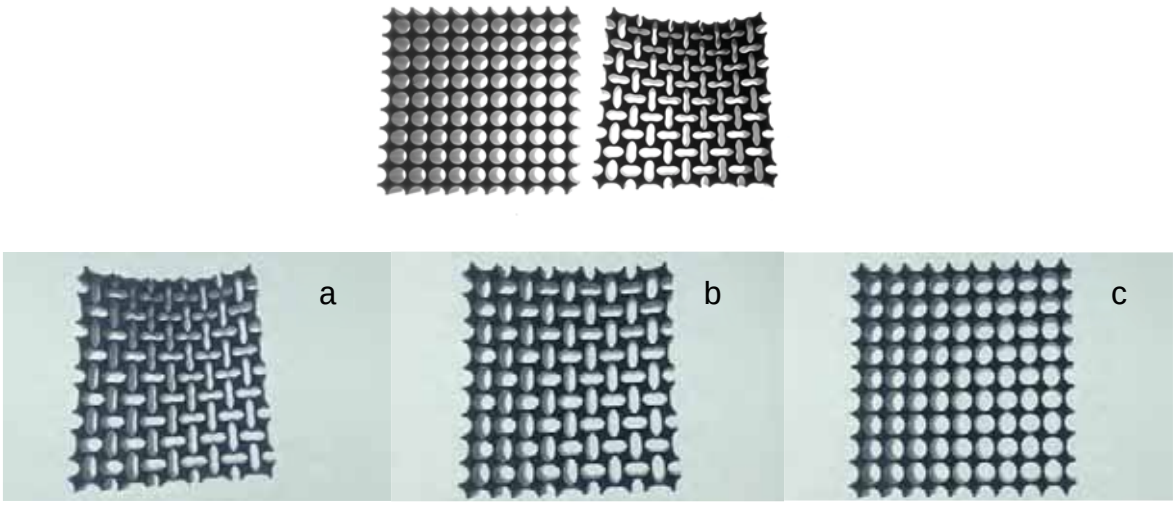


Figure 11: Heat actuation of 3D printed SMP auxetic structure: a) at room temperature, b) at 50°C, c) at 100°C.

The last set of prototypes were fabricated using a waterjet cutting the patterns in a thin sheet of mattress foam. The prototypes were very successful and needed very little force to cause a large amount of deformation (Fig. 12). The time needed to subtractive fabricate these large-scale prototypes was also much faster in comparison to the time needed by additive manufacturing.

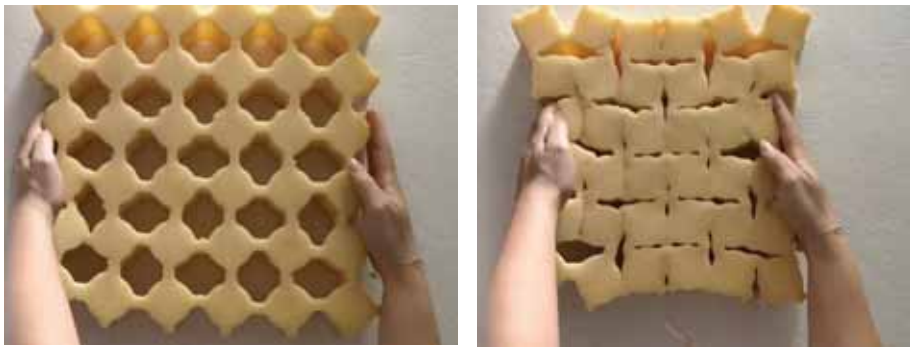


Figure 12: Waterjet-Cut Prototypes.

DATA - FACADE DESIGN AND SIMULATION

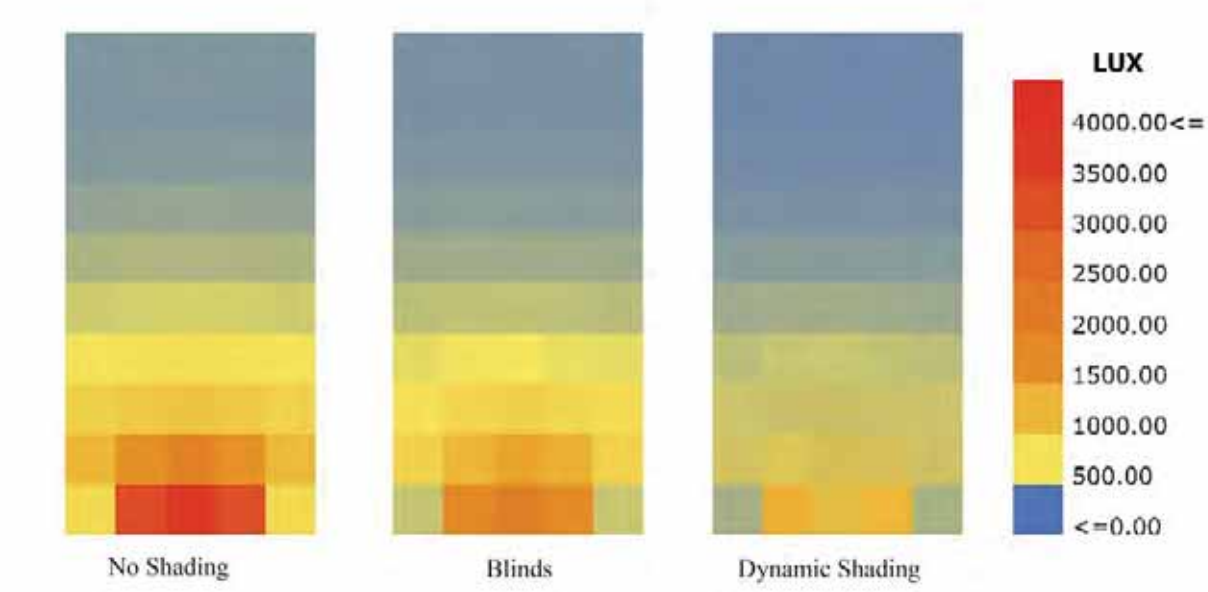


Figure 13: Simulation results.

Due to the complexity of the proposed geometry and its states, in order to simulate a dynamic shading system, 4 sets of annual daylight analyses were done to get the illuminance data of the grids defined within the shoebox model. Simulation 1 included the shading with all holes completely open, Simulation 2 included shading with holes 50% closed, and the final simulation had the holes closed. The hourly results for each node were then analyzed and only June 21st data was selected and averaged as a case to compare the performance of the shading. For hours with highest solar radiation on the facade (10:30 to 13:30), the illuminance data was extracted from closed holes, for hours with less solar radiation (5:30 to 10:30) and (13:30 to 15:30) 50% open holes and the rest of hours the data from open holes on the shading was used.

The explained data of the hourly simulation on each node is averaged and displayed in the above chart (Figure 13). From the daylighting simulation results, there is a noticeable improvement in the daylighting performance when a dynamic heat responsive shading is added. The illuminance result near the windows was decreased from ~4000 lux in the no shading case to ~2000 lux for case with blinds to ~800 lux in the dynamic shading improving the daylighting performance of the space, reducing the probability of glare since there is no great variation in the lux levels. It is important also to note that, since the auxetic structure's openings when contracted aren't 100% closed as there is still some opened slits, the occupants' optical visibility isn't completely obstructed.

EXPLANATION

EXPLANATION - PHYSICAL PROTOTYPES

From the physical prototypes exploratory studies explained earlier, a number of design constraints will have to applied in the design and fabrication of the full scale auxetic facade:

1. A shape morphing material with distributed passive actuation is better than external passive actuation.
2. The fabrication technique should be fast and scalable.
3. The amount of force vs deformation should be minimal to make it easier to design a counter force that will make the shape return to its original form when exposed to low temperature.
4. The material used should be cheap, lightweight and durable.

Therefore, shape memory polyurethane foam or similar shape memory foams is suggested as a material to be used in the future for the implementation of auxetic structures (Lee et al. 2007). With proper fire protection coating, the material is relatively cheap, has high insulative properties and already extensively used in the construction industry. Although most of the research done to explore its shape memory properties were for small scale applications, flexible polyurethane foams are already used in a variety of applications including furniture, packaging and transportation seating (S. M. Kang, Lee, and Kim 2012). Moreover, two-way memory and triple shape effect have been studied in various research initiatives (Hong, Yu, and Youk 2010; Taekwoong Chung, Angel Romo-Uribe, and Patrick T. Mather* 2007; Kim, Park, and Kim 2015).

EXPLANATION - FACADE DESIGN AND SIMULATION

From the simulation data, it is concluded that the dynamic heat actuated facade has a great effect in the improvement of the daylighting performance of the space. From the physical prototype investigations, the use of waterjet cut polyurethane shape memory foam is the best option in the production of a full scale auxetic shading device, and in (Fig. 14), a proposal of facade system assembly is shown below inside an Insulated Glass Unit (IGU).

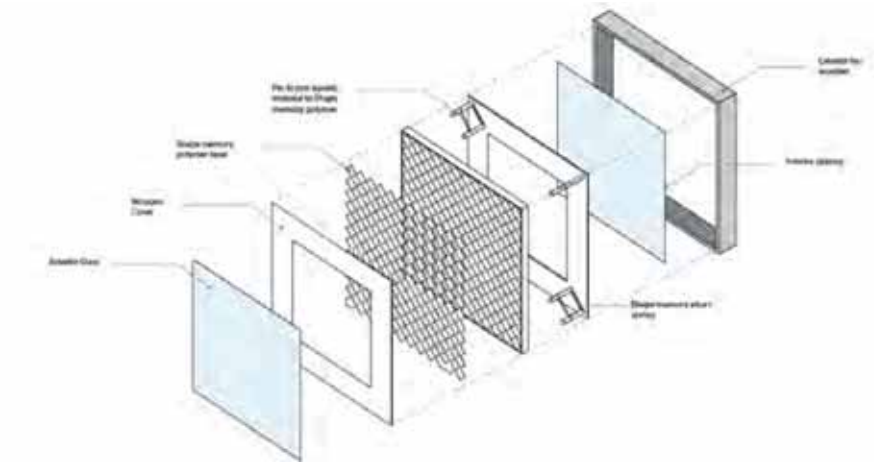


Figure 14: Facade assembly detail.

The facade will not only improve the daylighting performance but the energy performance of the buildings in hot arid climates as well for two main reasons. The first is the prevention of direct solar radiation in the space which will eliminate the necessity of the use of mechanical systems to regulate the system. Second, the polyurethane foam has high insulative characteristics which will increase the U value of the wall assembly improving the energy performance.

CONCLUSION AND FUTURE WORK

In contrary of the conventional classification of buckling and mechanical instabilities as failure modes, auxetic structures prove that these deformations could offer new opportunities in architectural design as well as in construction industry. The rapid advances in material research made the it possible to have durable thermal responsive facade systems using SMP foams that, when implemented in full scale structures, will set a new precedent for the application of soft elements in the building industry.

REFERENCES

Architects, LIFT. n.d. “The Air flower_LIFT Architects.” Accessed October 14, 2017. http://www.liftarchitects.com/air-flower/.

Babaee, Sahab, Jongmin Shim, James C. Weaver, Elizabeth R. Chen, Nikita Patel, and Katia Bertoldi. 2013. “3D Soft Metamaterials with Negative Poisson’s Ratio.” Advanced Materials 25 (36):5044–49. https://doi.org/10.1002/adma.201301986.

Beites, Steven. n.d. “MORPHOLOGICAL BEHAVIOR OF SHAPE MEMORY POLYMERS TOWARD A DEPLOYABLE , ADAPTIVE ARCHITECTURE,” 121–28.

Fortmeyer, Russell Martin, and Charles D. (Charles Dana) Linn. n.d. Kinetic Architecture : Designs for Active Envelopes.

Grinham, Jonathan, Robert Blabolil, and Jeremy Haak. n.d. “HARVEST SHADE SCREENS PROGRAMMING MATERIAL FOR OPTIMAL ENERGY BUILDING SKINS.” Accessed October 14, 2017. http://papers.cumincad.org/data/works/att/acadia14_281.content.pdf.

Hong, Seok Jin, Woong-Ryeol Yu, and Ji Ho Youk. 2010. “Two-Way Shape Memory Behavior of Shape Memory Polyurethanes with a Bias Load.” Smart Materials and Structures 19 (3). IOP Publishing:35022. https://doi.org/10.1088/0964-1726/19/3/035022.

Kang, S. M., S. J. Lee, and B. K. Kim. 2012. “Shape Memory Polyurethane Foams.” Express Polymer Letters 6 (1):63–69. https://doi.org/10.3144/expresspolymlett.2012.7.

Kang, Sung Hoon, Sicong Shan, Wim L. Noorduin, Mughees Khan, Joanna Aizenberg, and Katia Bertoldi. 2013. “Buckling-Induced Reversible Symmetry Breaking and Amplification of Chirality Using Supported Cellular Structures.” Advanced Materials 25 (24):3380–85. https://doi.org/10.1002/adma.201300617.

Kim, YJ, HC Park, and BK Kim. 2015. “Triple Shape-Memory Effect by Silanized Polyurethane/silane-Functionalized Graphene Oxide Nanocomposites Bilayer.” High Performance Polymers 27 (7). SAGE PublicationsSage UK: London, England:886–97. https://doi.org/10.1177/0954008314565398.

LAKES, R. 1987. “Foam Structures with a Negative Poisson’s Ratio.” Science 235 (4792). American Association for the Advancement of Science:1038–40. https://doi.org/10.1126/science.235.4792.1038.

Lee, Sung Ho, Moon Kyoung Jang, Sung Hee Kim, and Byung Kyu Kim. 2007. “Shape Memory Effects of Molded Flexible Polyurethane Foam.” Smart Materials and Structures 16 (6):2486–91. https://doi.org/10.1088/0964-1726/16/6/052.

Overvelde, J. T. B., S. Shan, and K. Bertoldi. 2012. “Compaction Through Buckling in 2D Periodic, Soft and Porous Structures: Effect of Pore Shape.” Advanced Materials 24 (17). WILEY-VCH Verlag:2337–42. https://doi.org/10.1002/adma.201104395.

Overvelde, Johannes T B, and Katia Bertoldi. 2014. “Relating Pore Shape to the Non-Linear Response of Periodic Elastomeric Structures.” Journal of the Mechanics and Physics of Solids 64 (1). Elsevier:351–66. https://doi.org/10.1016/j.jmps.2013.11.014.

Ratna, Debdatta, and J. Karger-Kocsis. 2008. “Recent Advances in Shape Memory Polymers and Composites: A Review.” Journal of Materials Science 43 (1):254–69. https://doi.org/10.1007/s10853-007-2176-7.

Shim, Jongmin, Sicong Shan, Andrej Košmrlj, Sung H. Kang, Elizabeth R. Chen, James C. Weaver, and Katia Bertoldi. 2013. “Harnessing Instabilities for Design of Soft Reconfigurable Auxetic/chiral Materials.” Soft Matter 9 (34):8198. https://doi.org/10.1039/c3sm51148k.

Studio Kimii. n.d. “SHAPE MEMORY POLYMER: RESPONSIVE ARCHITECTURE • Studio Kimiis.” Accessed October 14, 2017. http://studiokimiis.com/shape-memory-polymer-responsive-architecture-2/.

Taekwoong Chung, †, ‡ and Angel Romo-Uribe, and † Patrick T. Mather*. 2007. “Two-Way Reversible Shape Memory in a Semicrystalline Network.” American Chemical Society. https://doi.org/10.1021/MA071517Z.

KINETIC SHADING SYSTEMS

A parametric approach to optimizing daylighting performance



Alireza Jahanara
Texas A& M University
alireza.jahanara@uniroma1.it



Negar Kalantar
Texas A&M University
kalantar@tamu.edu

ABSTRACT

This study focuses on experiments in kinetics and architectural skins. More extensively, it introduces a solution for environmental design issues and daylighting optimizations for kinetic facades. This work explains how dynamic geometry can be inspired from a biomimetic design, as well as the ways in which the selection of appropriate strategies from nature can be used to design dynamic geometries for kinetic façades that reduce the artificial lighting load.

The first step in this research, after creating a dynamic shading geometry, was to develop a research map for understanding the optimization steps for dynamic geometries and ways of determining the variable parameters that affect lighting. This helped us to understand the relationship between the variables in dynamic geometry and daylighting as a design factor. Therefore, this work discusses the way to adjust these variables based on the angle of the sun, in order to receive and absorb the desired daylight reaching workspaces throughout the year.

In this study, dynamic shading was applied to an office building in Houston, Texas, with a fully-glazed steel frame on both the southern and western façades, and dynamic geometry only on the southern facade. The experiment focused on optimizing the daylighting performance by using various integrated software to modify the design and motion of the kinetic façades.

The dynamic geometry simulations were carried out with the Rhinoceros and Grasshopper software packages. The geometry of the dynamic shading device was optimized by adjusting the angle and size of the opening through Galapagos for Grasshopper. Daylight use was measured by DIVA and the sun's radiation was analyzed in Ladybug for Grasshopper. Subsequently, the outcomes were compared to a base case with no shading. The results showed significant improvement in terms of the useful daylight illuminance values. Hence, the main parameters were recognized as the dominant constraints that could affect the daylighting performance of the indoor working space. In the meanwhile, the dynamic geometry of the "opening angle" was one of the parameters effective in creating a balance between the spatial daylight autonomy and the annual sun exposure of the indoor working space.

KEYWORDS

bio-inspired, parametric design, kinetic façade, daylighting opimization

INTRODUCTION

Daylighting devices are important components of any regular climate-responsive façade system. However, the evolution of parametric CAD systems that impact both architectural and regular forms has shifted to a focus on complex geometries. The architectural and engineering integration of daylighting devices in building envelopes with complex geometries pose a challenge in terms of design and performance evaluations (Jang et al., 2017).

Accordingly, simulation tools are effective for testing and evaluating different designs, and even more important, when assessing numerous solutions. It is practical to use optimization simulation tools that can help in finding the optimal results. Consequently, in this study a parametric tool was used to generate a dynamic geometry design. Virtual reality analysis was then used as an output to generate an interactive experience that would provide a higher level of understanding for design analysis and decision-making (Lavin et al., 2017). Integrating daylighting with energy performance to optimize the design process has always been a challenge for designers. Most building environment performance simulation tools require a considerable amount of time and large number of iterations to achieve accurate results. Moreover, combining various daylighting performances has always been an issue, as different software packages are needed to perform detailed calculations. This is why a simplified method for overcoming both of these issues was explored in this research, using recent advances in software integration (Ashouri et al., 2015).

The current study also explains the significance and potential advantages of kinematics with regards to the way geometries can be modeled to optimize surface displacements (Brown, 2016). The proposed dynamic facades focus on generating kinetic geometrical designs that respond to daylight in an office building, using a parametric design method that is based on optimizing daylighting levels in an indoor workspace. In these terms, this exploration of kinetics was developed by achieving different methods of folding the geometric surface (Fig. 1) for the proposed geometric design process.

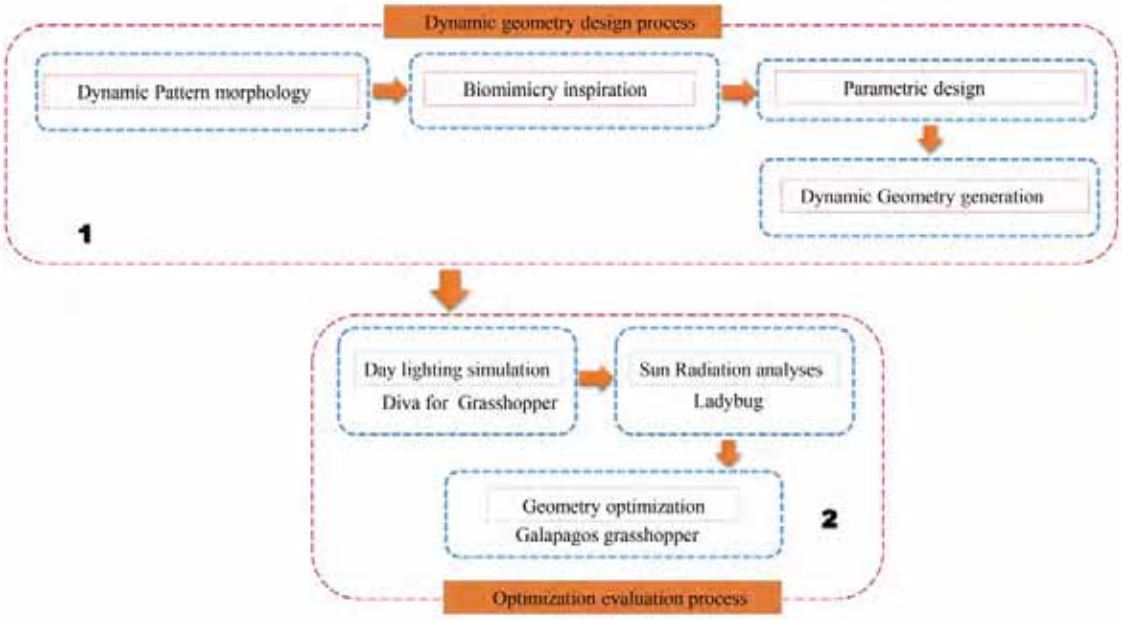


Figure 1: Geometric design exploration and optimization process. Image by the authors.

For the case study, the daylighting optimization of dynamic shading devices was presented for a multistory office space in Houston, Texas. The urban context was not applied in the optimization simulation scheme. A dynamic pattern was generated by integrating performance analysis tools with parametric modelling (i.e., by implementing the Rhino and Grasshopper programs). It was determined that the office workspace conditions should be evaluated by means of a DIVA plug-in as the main tool, given its ability to effectively calculate daylighting metrics; meanwhile, the optimization process was carried out

parametrically to control the dynamic shadings' geometries. This research also proposes the use of Ladybug to analyze the sun's radiation exposure on the façade's skin in order to modify the proposed dynamic geometry and approach maximum daylighting optimization. Finally, it was determined that genetic algorithms (GA) embedded in the evolutionary solver Galapagos were necessary to achieve the optimum results by controlling the parameters.

BACKGROUND

PARAMETRIC DESIGN AND MARGINING VARIABLES

Parametric modeling offers a holistic control for design objects in all processes. The algorithm uses its core method of generation to produce a series of complex forms and structures, based on particular parameters (Schleicher et al., 2015). These parameters consist of two inputs: the static value that is directly connected to actual data, such as a weather profile or solar radiation; and the digital input that is derived from design process data. These contributions are produced in the parametric design formalization, given two reference parameters (Adriaenssens et al., 2016). One is the static value that gives an algorithm reference, and the other is a dynamic parameter that is involved in the architecture design process (Fig. 2).

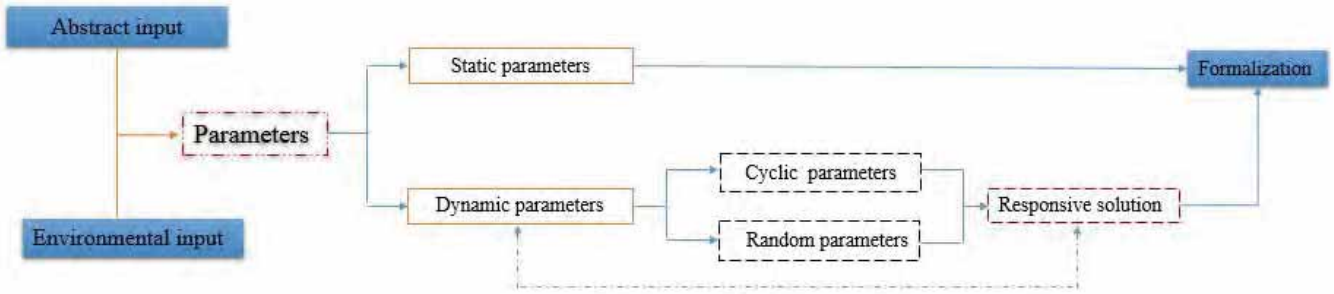


Figure 2: Variable parameter process (https://issuu.com/aveharysakti/docs/parametric_architecture_and_algorit).

These algorithm parameters make available an approach to responsive solutions and scenarios, based on conclusions that change the modeling from static to interactive according to defined algorithms. This produces a parametric modeling that allows the designer to calculate and optimize the suitable design parameters by offering flexibility in the input algorithms. The result is a dramatic sequence of design instruction processes that stem from an evaluation of the logic (Elghazi et al., 2016).

BIOMIMETIC STRATEGY FOR MANAGING LIGHT

While facade designs that focus only on the grade, immovable shading, and solar panels are widespread, increasing research on the structures of kinetic geometries that imitate biometrics have proven that the borders between architecture, biology, and structure can be crossed. Biomimetics have brought about a design approach that applies nature as a guide for innovating technology. Many researchers have focused on the flexible motion of plants blooming and how this process can successfully be transferred to the design of bio-inspired mechanical geometries. However, only a few have addressed the optimization process as a design factor for concepts related to geometric methods. Bio-inspired research has also blurred the boundaries between structure, material, and mechanism by using flexible and elastic constituents (Pesenti et al., 2015).

Following an earlier research line that began by finding a suitable bio-inspired model and describing its blooming motion, the proposed geometry animates the Bird of Paradise plant. This mimicking was key during the design process, defining the deformation of the plant's blooming function and morphology.

Morphological, behavioral, and physiological features all influence the light management efficiency strategy of this design, as well as the plant's ability to manage light intensity. For instance, some plants are able to absorb light because of their intricate structural assembly, while others optimize light by solar tracking and enhancement of the body's exposure (Park et al., 2013). By exploring and learning from such strategies and techniques in nature, a design discipline for a new light management system is emerging, aimed at building skins. The field of biomimetic design continues to be a challenging one for architects, especially with its growing integration with engineering and materials science.

Taking biomimetic living organisms as design solutions for buildings is a unique strategy that facilitates the selection of appropriate strategies from nature. Nevertheless, biomimetics is not about creating an exact replica of nature. Rather, it is about translating its functional biological aspects into architecture on a level of performativity (Park et al., 2013).

In this regard, many experiments were carried out to systematically represent biophysical information in a context similar to that of buildings. In most cases, the design process finds suitable role models for motion, identifying and locating the main elements that cause deformation in the functional and morphological realms. Currently, however, the systematic representation of building applications for light management is limited.

Table 1 includes diagrams of the proposed schematic mapping, which considers daylight to be the key inspirational factor transmitted from the bio-inspiration morphology to the technical kinetic geometry of motion. This mapping targets the enhancement of the indoor workspace environment with saving energy serving as a role engine.

Morphology	Behavior	Physiology
Hazza Bin Zayed Stadium - UAE Project year: 2014	Water Reaction – Royal College of Art Project year: 2015	Pavilion - Germany Project year: 2013
The pattern design of this stadium was inspired by the rotating fractural geometry of date palm fronds as an outer facade. The facade's movement responds to the daily heat to act as a passive cooling device, shading the building during the day and allowing fresh air to flow. Hence, movement depends upon sensors' response to daylighting factors (Archdaily, 2015).	This pattern was inspired by a pinecone that opens and closes naturally to protect its seeds from wet weather and spread them when it is dry. This happens when the outer layer expands beyond the other layer, causing different scales to bend and close the cone. The cone is a tile wherein the outer layer elongates and curves material away when wet (Archdaily, 2015).	The Pavilion is a particularly interesting method within a moisture-driven movement that is observed in spruce cones. This movement takes place through a passive response to changes in humidity, similar to plant movement from cell-pressure metabolism. Hence, movement is independent, with no energy consumption from the plywood sheets' metabolic function (Archdaily, 2013).
		

Table 1: Biomimetic influences on architecture. Image by the authors.

Based on the above schematic diagram, the current research considers and underscores daylighting as an initial factor in the design process, taken as a morphological strategy. Therefore, this work proposes the Bird of Paradise plant as a bio-inspired morphology. The plant has recently been studied by a number of professors who have taken into consideration its construction and mechanical transmission into an architectural structure.

Following their analyses, the proposed research has taken this morphological application to be the core of a kinetic geometry. Hence, order in nature can promote and develop adaptive solutions for building envelopes. Consequently, this work focuses on how the morphological applications of biomimetics can produce an adaptive geometrical pattern that responds to the efficient design factor of daylight.

METHOD

This research presents a method for optimizing a façade design system's devices for controlling daylighting performance in buildings. It is divided into three main sections, as follows:

1. Data input,
2. Process, and
3. Output.

DATA INPUT

There is a need for basic research on this topic, especially that which evaluates the performance of the system. This includes an understanding of the static and dynamic variables and a determination of the best results for daylighting optimization. In this case, this would mean determining the static and dynamic variables, as follows:

1. Façade building properties,
2. Kinetic geometric variable factors,
3. Weather data, and
4. Material properties.

As regards daylighting optimization, the variables are able to include the geometry of the design represented by numbers or indexes on a list. Many authors have mentioned parametric design as a constant within an optimization that can be adjusted for elements of a design vector. Some have also used the term "parameter variable" to describe design constants that are fixed as input references.

PROCESS

Model simulations and daylighting are included here. A parametric model for both indicators is elaborated upon below, based on a realistic representation of the building that considered the physical and optical properties of the materials. The results of these simulations were the input for the desired design optimization process, through:

1. A parametric tool (Grasshopper),
2. Daysim engine (DIVA),
3. Radiation analyses (Ladybug), and
4. Form finding (Galapagos).

Figure 3 illustrates how the research method can provide input variables for parametric designs, and how to adapt and modify these variables throughout the proposed simulation. The suggested flowchart is a target for designing a kinetic geometric response to daylighting optimization so as to maximize the annual envelope's exposure to solar radiation and create a comfortable work zone that consumes electricity. The research method targeted the integration of genetic algorithms with parametric design, in order to achieve optimized solutions in a highly familiar design software environment. The experiment was a combination of the tools mentioned above. The proposed process was tested on a highly recurring design task, merging all of the above information as an optimization process map for understanding the optimization steps necessary for a geometry that responds to the daylight phenomenon.

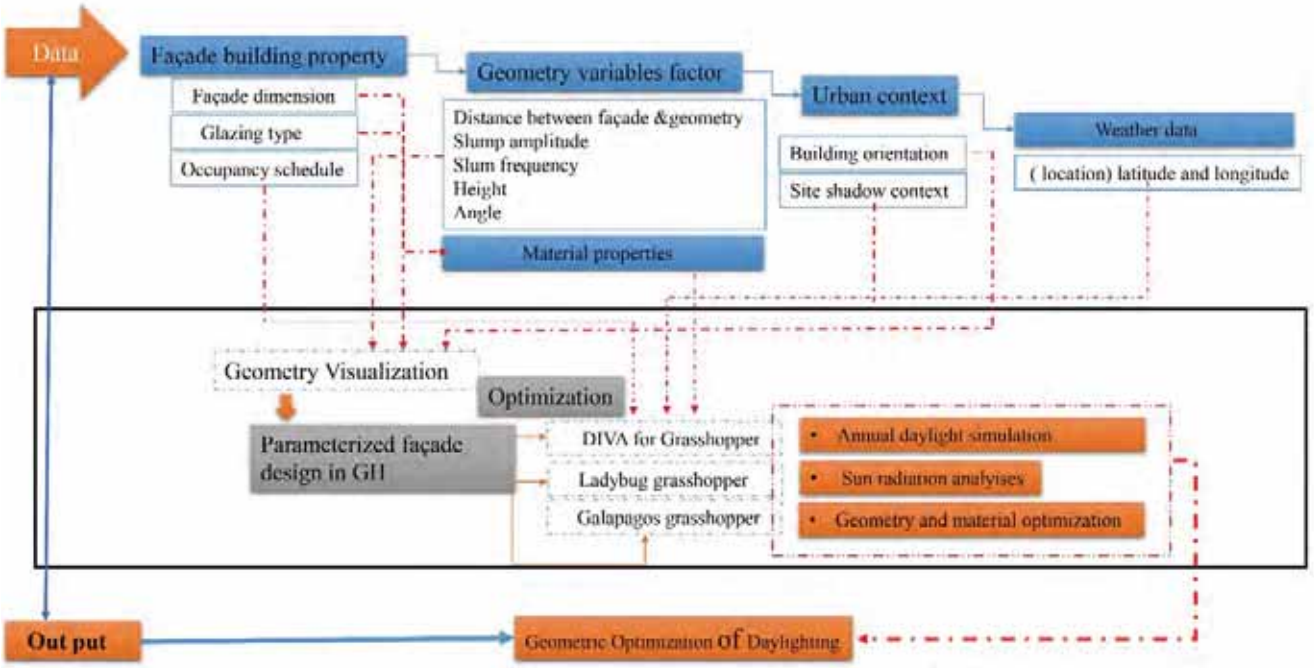


Figure 3: Research plan with the goal of approaching a geometric optimization for daylighting. Image by the authors.

DATA

The case study location was chosen to be Houston, Texas (Fig. 4). The south façade of the office building space was selected for investigating the dynamic geometry. The dynamic geometry was applied to the entire southern façade, but only the fifth floor was chosen for running the optimization simulation plan. The urban context was not analyzed because after a quick observation of the case study, it was obvious that the building had no surroundings that would affect the simulation results, at least in terms of shadow. The space behind the southern façade was a 50.00m wide by 9.00m deep rectangular space, with a 3.20m height (Fig. 4).



Figure 4: Multi-story office building in Houston, Texas, United States.

First, the base case was modeled and its annual daylighting performance observed. Subsequently, a GA was used to optimize the annual daylighting performances of the two parametrically-modeled cases. In the first case, a combination of a redirecting system (light shelf) and shading scheme (solar screen) was added to the base case (Fig. 5).

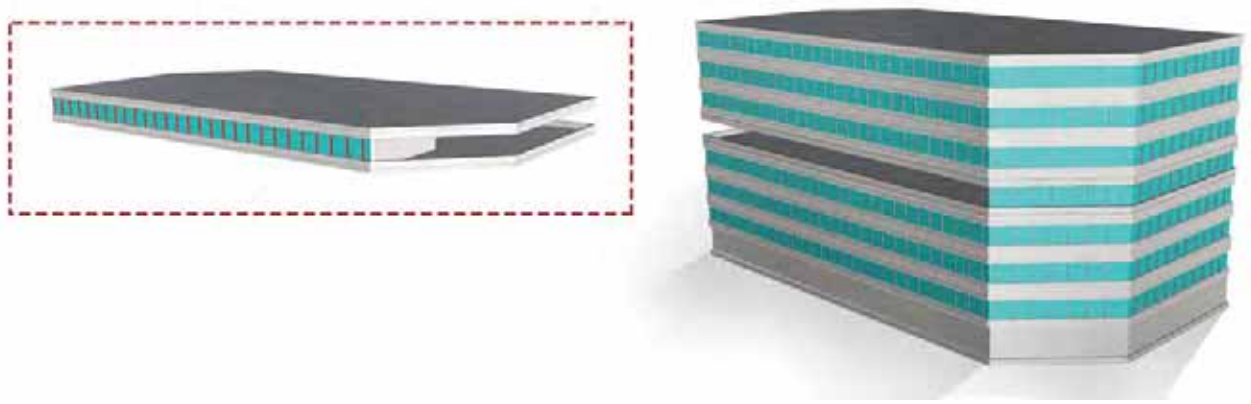


Figure 5: Multi-story office building in Houston, Texas, United States.

DAYLIGHTING SIMULATION METHODOLOGY

The simulation was conducted using the DIVA for Grasshopper plug-in for the Rhinoceros modeling software. The Radiance interface and Daysim were used for the annual simulation and illuminance computations. A simulation was conducted only for the July 21st summer solstice (highest sun path) and December 21st winter solstice (lowest sun path) in Houston, from 8:00am to 4:00pm, and only for the fifth floor (Fig. 6).

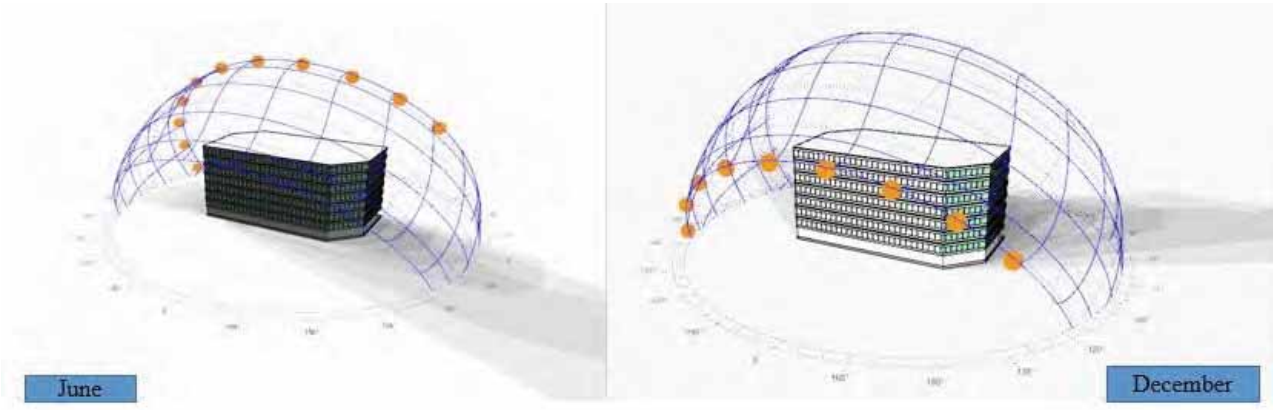


Figure 6: Sun path diagrams for July 21st (left) and December 21st (right) in Houston, Texas, United States. Images by the authors.

The reference plan upon which the daylighting performance was simulated contained 283 measuring points in a grid of 0.1m x 0.1m, and a working plan with a height of 0.7cm. The measurements were found to be equal to or greater than the recommended minimum illuminance values for an office space, 500 Lux; this was considered to be “adequate.” Daylight availability, a dynamic daylighting performance metric, was used for the evaluation. This metric presents three evaluation criteria: “daylit” areas (adequate locations) for spaces that receive sufficient daylight at least half the time (as compared to an outside point); “partially daylit” areas, which are below a useful level of illuminance; and “overly lit” areas that provide warning when an oversupply of daylight (10 times the target illuminance) is reached for at least 5% of the working year.

BASE CASE SIMULATION RESULTS

Daylighting availability was analyzed for the base case’s southern-facing orientations. Overly lit areas reached 44% in July and 57% in December. However, no partially daylit areas were found in the southern-oriented office space, and daylit areas reached 11% in July. In December, 43% of the space was partially daylit (Table 2). The main challenge, therefore, was to eliminate the overly lit areas without significantly increasing the partially daylit spaces. In the simulation described below, 70% of each floor was covered with glass and 30% with aluminum tiles between the glass areas; each sensor’s data scrubbed the illuminance (hourly data). The results indicate the amount of overly lit and daylit areas during specific hours (Table 2).

Description	Source	
Glazing	CIBSE reflectance	Glazing_DoublePane_Low E_80
Interior wall	CIBSE reflectance	GenericInteriorWall_50
Exterior wall	CIBSE reflectance	Outside façade _35
Exterior panel	CIBSE reflectance	Outside façade _35
Celling	CIBSE reflectance	Generic celling _80

Table 2: Material properties of the base cape applied in DIVA.

BASE CASE

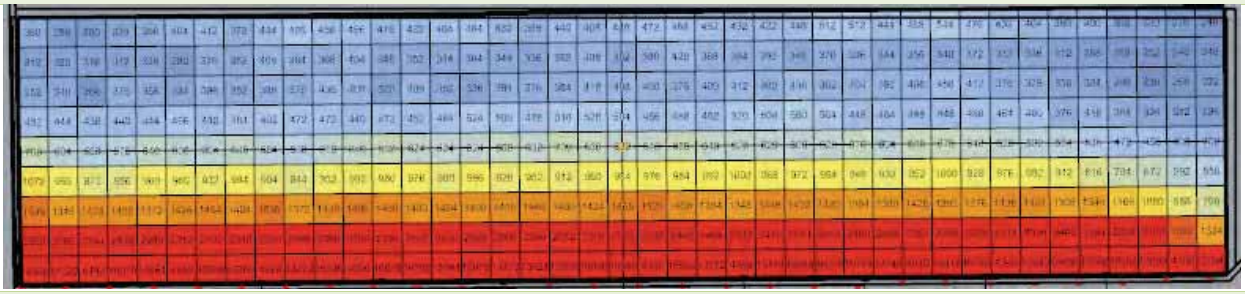
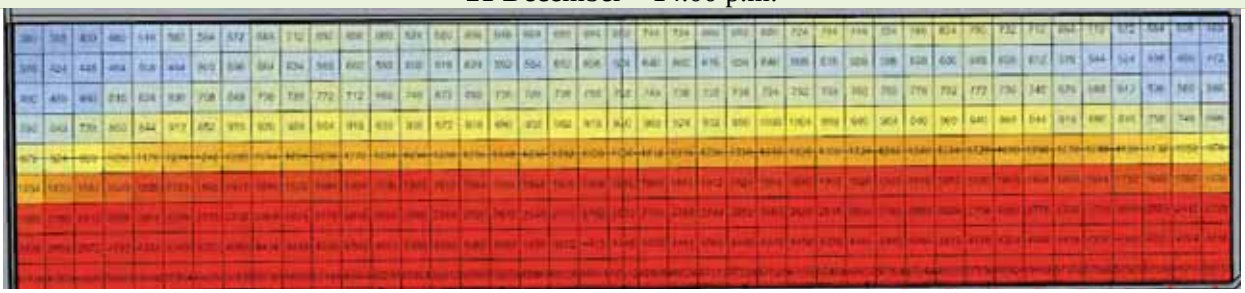
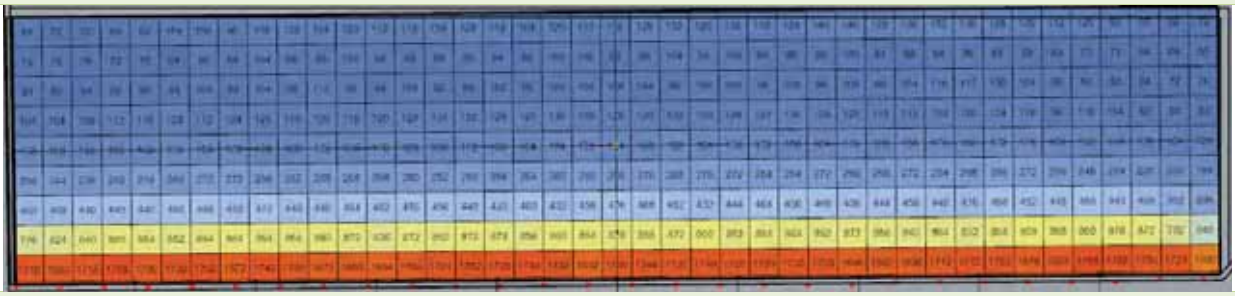
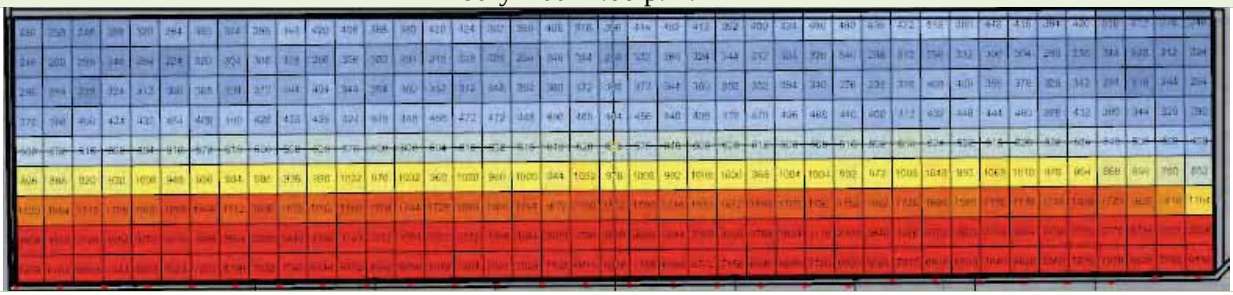
December 21 - at 9.00 a.m.	Daylight result
	Day lit 43%
21 December – 14.00 p.m.	
	Over lit 57%
21 July – at 9.00 a.m.	
	Day lit 11%
21 July – at 11.00 p.m.	
	Over lit 44%

Table 3: Available daylighting distribution for southern-oriented base case offices on the fourth floor.

APPLICATION OF DYNAMIC PARAMETRIC SHADING DEVICES

The concept for the dynamic façade's geometry was influenced by the adaptive morphology of the Carne lily (or Bird of Paradise plant). This flower reacts to the sun by changing from a rectangular shape to a triangular one, maximizing the difference between its extended and folded receptive units to control the daylighting conditions, affecting occupant satisfaction while saving an AC (air conditions) (Fig. 7).

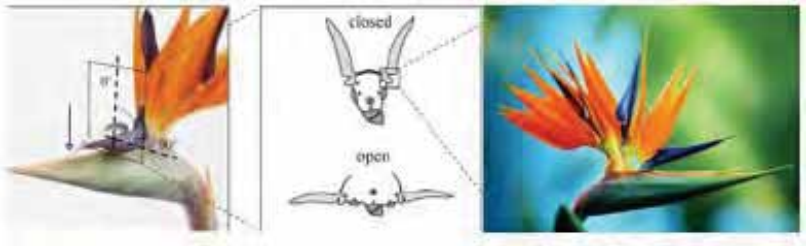


Figure 7: Inspiration for the dynamic geometry.

In this research, a triangular panel was installed on the southern façade to adjust the solar radiation gain. The simulation target demonstrated how the incidence angle could be incorporated with the opening ratio of the complex southern façade, ranging from zero to up to a 90o angle. A 0°-degree incidence angle on a surface meant that the surface was in parallel with the sun's direction, therefore the panel was fully closed. While, an incidence angle equal to or larger than 90°- degree meant that there was no direct solar radiation, and the complex of the kinetic façade is fully open. So, the façade is gradually varied based on the incidence angle of each panel in relation to the solar angle during the working hours (Fig. 8-9).

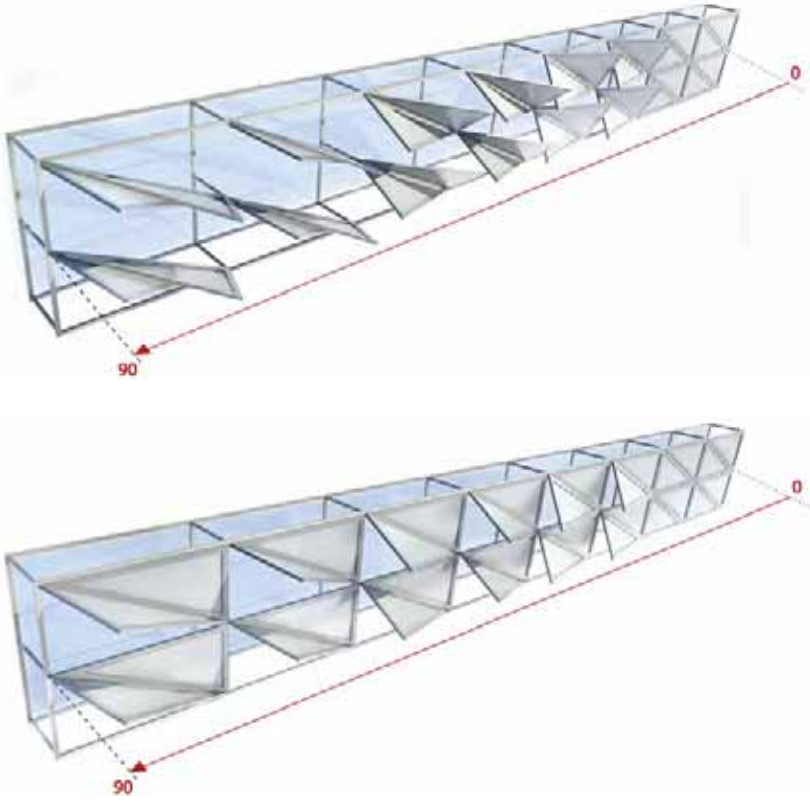
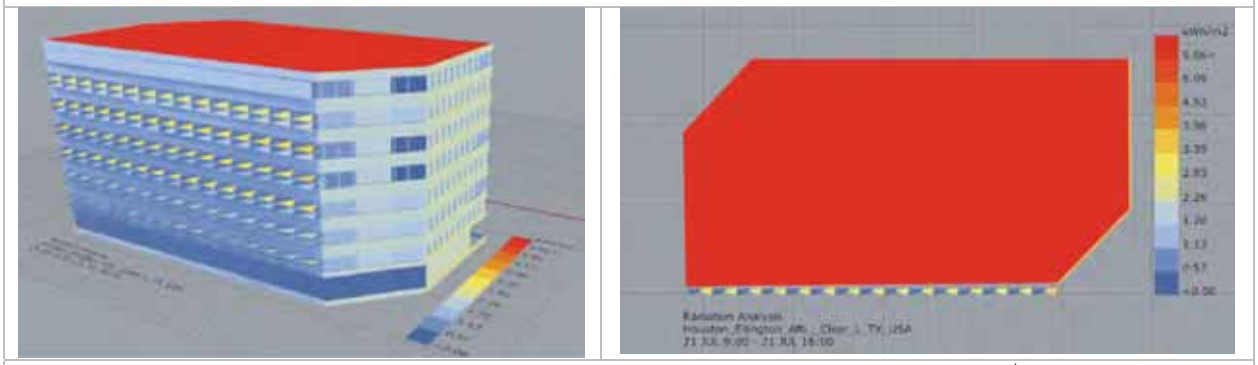


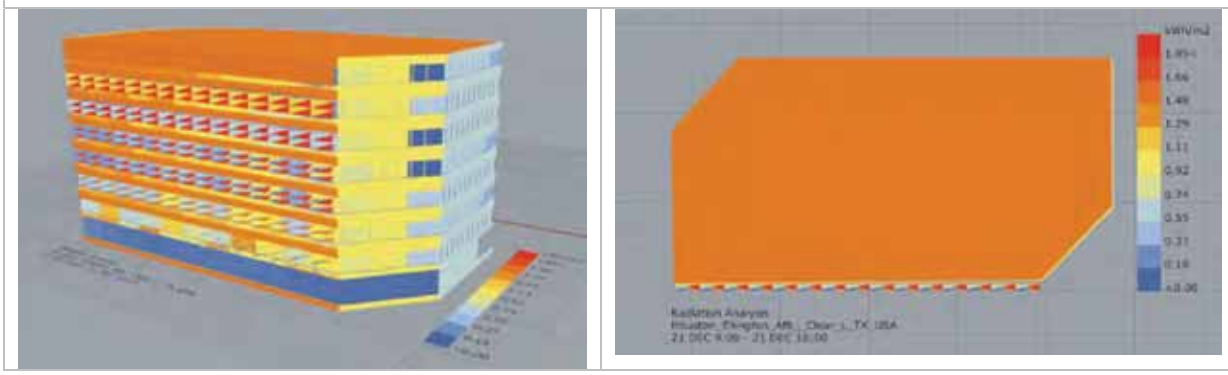
Figure 8-9: Variations in the kinetic façade based on the incidence angle.

RELATIONSHIP BETWEEN THE SUN'S RADIATION AND THE DYNAMIC FAÇADE'S DESIGN

Sun radiation analysis with dynamic shading devices in the south side of façade on July 21st from 9am to 2pm.



Sun radiation analysis with dynamic shading devices in the south side of façade on Dec. 21st from 9am to 2 pm.



The solar radiation Table used in the graphic above was developed to describe both the intensity of the sun's heat and its direction in a single frame. Therefore, the Table can assist us in modifying the proposed dynamic geometry's angle according to the lighting simulation results. For instance, with the southern façade in December, the dynamic geometry absorbed more of the sun's radiation than in July, so the proposed angle at that time was 0◦. This meant that the panels should have been totally closed on the last floor and totally open on the first floor.

EXPLANATION

Based on the design objective, this research using Grasshopper, a plug-in for the Rhinoceros modeling software. Grasshopper allows a designer to parametrically change the model because each design parameter is directly linked to a floating-point slider that determines its value. Galapagos is an evolutionary solver for GA optimization tools that is used within the Grasshopper platform to control and modify the different parameters. During the GA process for this research, a set of initial solutions was randomly generated. Each solution was sent to DIVA for daylighting availability simulations. Then, the results were processed using a fitness function to calculate the daylighting area percentage.

The workflow of searching for an optimized solution with Galapagos is summarized in the following steps:

1. DIVA for Grashopper was run to calculate the initial daylighting, based on the first individual indoor illuminance level of 283 for each sensor. The calculation was done for July 21st and December 21st, from 9:00am to 4:00pm.
2. The maximum and minimum fitness values were assigned.
3. The GA solver Galapagos collected and processed the data, commanding the generation of the next sets of angles for the geometry (Fig.10).

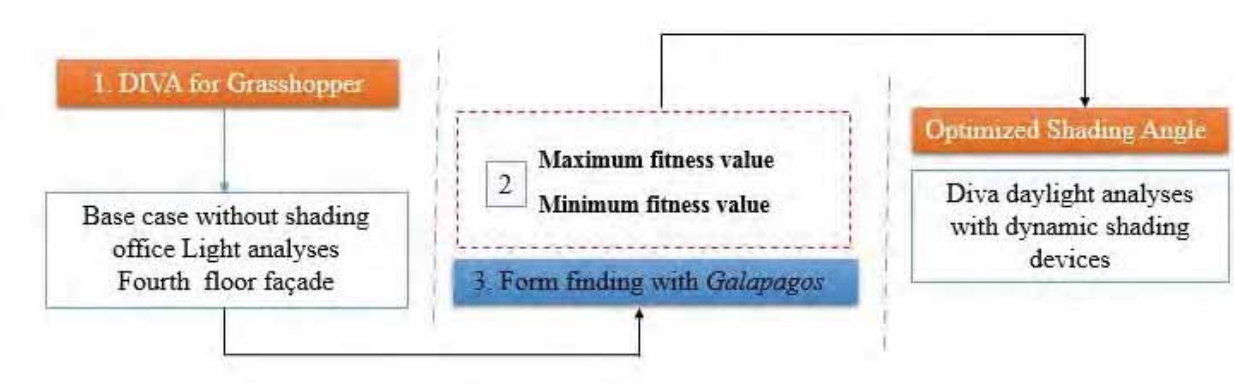


Figure 10: Workflow using DIVA for daylighting and the Galapagos evolutionary solver. Image by the authors.

In this project, the optimization technique used was to find the near-optimum solution based on different criteria for daylighting. Consequently, the main parameters were recognized as the dominant constraints that could affect the daylighting performance of the indoor working space. The dynamic geometry of the "opening angle" was one of the parameters effective in creating a balance between the spatial daylight autonomy and annual sun exposure (Fig. 11).

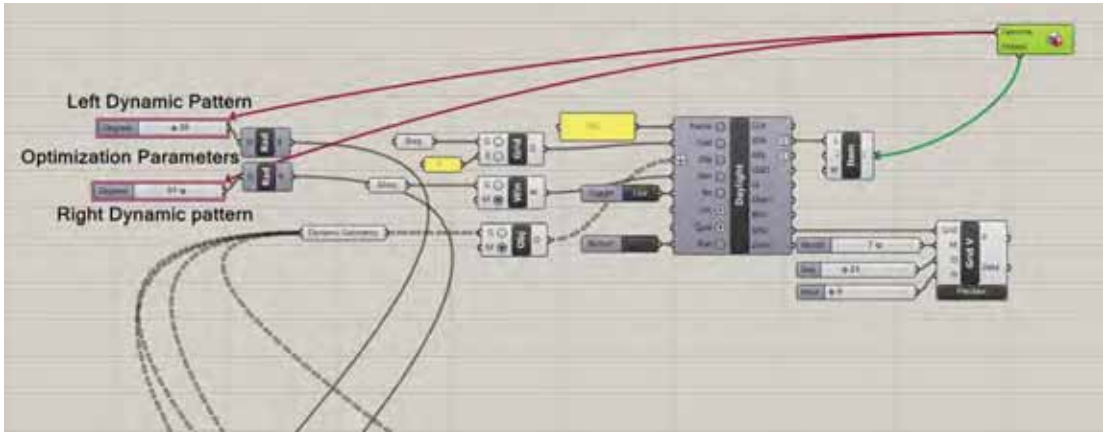
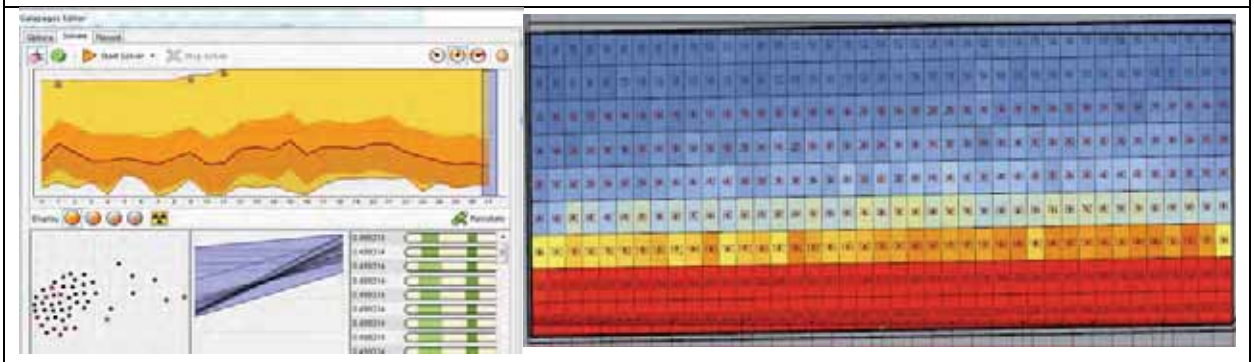
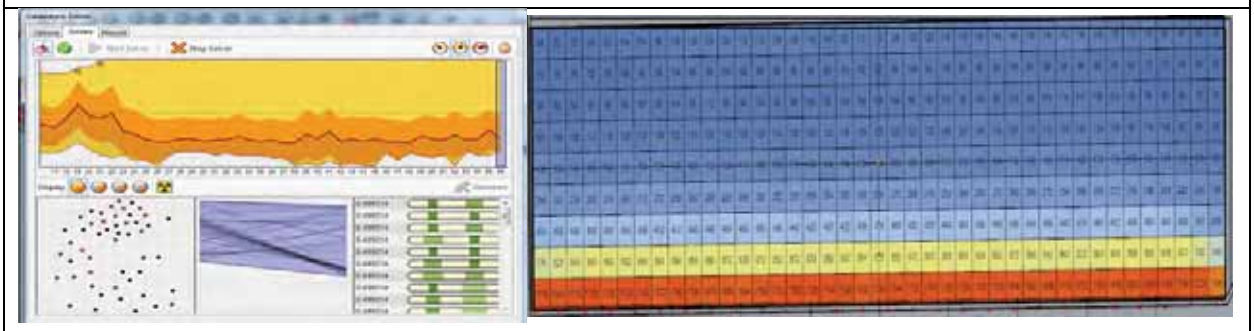


Figure 11: Optimization process angle of the geometry using the GA optimization of Galapagos in Grasshopper. Image by the authors.

Maximum Fitness



Minimum Fitness



Maximum Fitness

Building Parameters Number of panel for each floor	Building Parameters Angle of panel adjust with Galapagos		Spatial Daylight Autonomy sDA
30	Left 86 °	Right 59 °	44.3
Minimum Fitness			
30	Left 25°	Right 38°	32.2

Certain metrics were considered to evaluate the daylighting performance of the building and ensure that the optimization engine accounted for the daylighting availability. One such metric was Spatial Daylight Autonomy (sDA), which was represented as a percentage and used to evaluate the proposed case. The main objective was to maximize the sDA; to accomplish this, Galapagos accepted only one fitness function. Hence, the metrics needed to be combined in order to feed Galapagos a single value.

CONCLUSION AND FUTURE WORK

Combining parametric design with evolutionary optimization is a valid strategy for exploring solutions to the environmental performance problems of buildings. A comprehensive setting for the design problem and further improvement in the simulation tools would help to overcome the main difficulties found in this research. Accordingly, the appearance of new evolutionary optimization tools with 3D modeling software – such as DIVA for Grasshopper – calls for the development of workflows that allow designers to integrate these potential strategies into the various phases of the design process. This integration is especially significant at the early design stage, when the most impactful design decisions are made. The type of simulation performed and the methods used are the most important design development decisions, in this respect.

The combined impact of the proposed geometric design for the southern façade and its opening angle during the day should also be assessed. Hence, a full parametric model of the building is required that can easily be modified according to the information gained from the daylighting simulation results.

To sum up, transitioning from parametric design requires the adoption of adequate metrics to assess the relative merit of each design option. The most relevant area of this research topic is the development of assessment methods for the design alternatives, rather than algorithms or parametric models. This research has furthered the design process for kinetic shading geometry by applying the GA assessment process to enhance daylighting in indoor spaces, targeting electricity consumption with respect to the visual aspect. This highlights the need for designers to be fully aware of the design and performance questions involved in the recent promising evolution in simulations.

REFERENCES

Adriaenssens, Sigrid, and Landolf Rhode-Barbarigos, Kilian A., Baverel O., Charpentier V., Horner M., Buzatu D., “Dialectic Form Finding of Passive and Adaptive Shading Enclosures”, Energies, no.7 (2014), 5201-5220 ISSN 1996-1073

ArchDaily, Dario Goodwin. "Building Elements Come Alive with this Pinecone-Inspired Material that Reacts to Moisture" 08 Jul 2015. Accessed 6 Jun 2017. http://www.archdaily.com/769820/chao-chens-pinecone-inspired-material-reacts-to-water/

ArchDaily, (Accessed 6 Jun 2017), ‘Hazza Bin Zayed Stadium / Pattern Design’.33 http://www.archdaily.com/604755/hazza-bin-zayed-stadium-pattern-design/

ArchDaily, HygroSkin-Meteorosensitive Pavilion / Achim Menges Architect + Oliver David Krieg + Steffen Reichert" 09 Sep 2013. Accessed 6 Jun 2017. http://www.archdaily.com/424911/hygroskin-meteorosensitive-pavilion-achim-menges-architect-in-collaboration-with-oliver-david-krieg-and-steffen-reichert/

Ashour, Yassin, and Branko Kolarevic, “Optimizing creatively in multi-objective optimization”, Spring Sim-SimAUD, Society for Modeling & Simulation International (SCS), 2015, 128-135

Brown, Nathan Collin. "Multi-objective optimization for the conceptual design of structures." PhD diss., Massachusetts Institute of Technology, 2016.

Elghazi, Youmna, and Ayman Mahmoud, “Origami explorations a generative parametric technique for kinetic cellular facade to optimize daylight performance”, shape form and geometry applications, eCCADe, no.34 (2016): 399-408

Gadelhak, Mahmoud, “Integrating computational and building performance simulation techniques for optimized façade designs”, Computation and Performance, eCAADe, no.31 (2016): 1-9

Gadelhak, Mahmoud, and Werner Lang., "Optimization of office building façade to enhance daylighting, thermal comfort and energy use intensity, BSO, P.1116 (2016)

González, Javier, and Francesco Fiorito. "Daylight design of office buildings: optimisation of external solar shadings by using combined simulation methods." Buildings 5, no. 2 (2015): 560-580.

Jang, Do-Jin, and Sung-Ah Kim. "Kinetic Façade Design Using 3D Scanning to Convert Physical Models into Digital Models." World Academy of Science, Engineering and Technology, International Journal of Civil, Environmental, Structural, Construction and Architectural Engineering 11, no. 4 (2017): 458-465.

Lavin, Cristian, and Francesco Fiorito, “Optimization of external perforated screen for improved daylighting and thermal performance of an office space”, International High- Performance Built Environment Conference, Science Direct, no.180 (2017): 571-581

Park, Jong Jin, and Bharat Dave. "Bio-inspired Parametric Design for Adaptive Stadium Façades." In Australasian Journal of Construction Economics and Building-Conference Series, vol. 2, no. 2 (2014): 27-35.

Pesenti, Marco, Gabriele Masera, Francesco Fiorito, and Michele Sauchelli. "Kinetic solar skin: a responsive folding technique." Energy Procedia 70 (2015): 661-672.

PHONGPHETKUL, P. and WANKANAPON, P., 2017. “Daylight and Energy Performance of Automated Shading with Parametric Design: Case Study Bangkok”. DEStech Transactions on Environment, Energy and Earth Science, (eesd).

Rogler, K., 2015. Energy Modeling and Implementation of Complex Building Systems, Pt. 3.

Schleicher, Simon, Julian Lienhard, Simon Poppinga, Thomas Speck, and Jan Knippers. "A methodology for transferring principles of plant movements to elastic systems in architecture." Computer-Aided Design 60 (2015): 105-117.

KINEMATIC STRUCTURAL GLASS

111 Main case study: façade design that accommodates extreme building movements



Lisa Follman, AIA
Skidmore, Owings & Merrill, LLP
lisa.follman@som.com



Gregor Horstmeyer, PE
Eckersley O'Callaghan and Ptrs. LLC
gregor@eocengineers.com

ABSTRACT

The structural glass storefront facade at 111 Main Street in Salt Lake City lends itself as a case study in accommodating large building displacements by utilizing a kinematic assembly of facade elements.

The slender building core that supports all 24 hanging stories of the recently completed tower at 111 Main is set back from the perimeter to allow for an expansive and column-free thirty-five foot tall lobby entrance, and consequently results in significant building movements during seismic events. While all hanging floor plates move together uniformly, a monumental challenge was presented where the lowest hung floor (Level 2) interfaces with the entry façade that is base-supported. This critical interface was identified in the design process and the contractor was engaged early to assist with specialist input to achieve an elegant solution.

As the project architect, SOM was able to work through a collaborative design process with the contractor's engineer of record for the lobby façade system, EOC. Early engagement and open discussions between the design team and contractor allowed for fluid development of a unique but pragmatic system. The team was informed by contributors ranging from designers, architects, engineers, fabricators, and installers, each with specialist knowledge that uniquely informed the final design.

The critical design challenge was to dissect and understand how the building moves during wind storms and seismic events. A study of deflections, rotations, supports, and rigidity was conducted to define a realistic solution that accommodates the imposed building displacements. A kinematic hinge system was developed to accommodate total building vertical movements of nearly 3 feet (91.4 centimeters) with precision linear slide bearings used to absorb lateral building drifts.

Large cantilever structural steel entry portals are designed integrally with the glazed façade system to create feature entrances. Incorporation of architectural timber fins at the entry portals is accomplished with a novel approach to laminate wood veneer into the glass assemblies.

Detailed analysis of global movements, post-failure behavior, gasket and sealant flexibility, are carried out as part of the delegated design requirements to ensure performance through the building's design life.

KEYWORDS

structural glass, storefront façade, structure and seismic, kinematic, extreme movement, timber



Figure 1: 111 South Main Street, Salt Lake City, Utah, United States. Photo © Cesar Rubio.

PROJECT OVERVIEW

111 Main is a 24-story speculative office tower located at the corner of South Main and E 100 South Street in the heart of downtown Salt Lake City, Utah (Figure 1). The project was developed by City Creek Reserve, Inc. (CCRI), the real estate investment portfolio of the Church of Jesus Christ of Latter-day Saints. The building is connected on the ground floor to the Eccles Theatre, a new 2,500 seat performing arts center built concurrently to the 111 Main tower, and is directly across the street from City Creek Center, a 20-acre mixed use development with retail, commercial and residential program completed in 2012.

The 111 Main tower is located on a site previously owned by the Salt Lake City Redevelopment Agency (RDA) and identified as the ideal location for a new performing arts center. A small portion of the site was sold to the 111 Main development team for construction of a new office tower. Because economic feasibility of the office tower required a larger footprint, for the tower project to move forward a 21,000 square-foot (1,950 square-meter) tower floor-plate would need to be constructed on a 15,000 square-foot (1,390 square-meter) site. CCRI obtained air rights to build over the new five-story performing arts center and SOM Architects and Structural Engineers conceived a building with rooftop trusses from which to suspend the tower.

The tower has a rectangular form beginning at Level 5 and continuing up the full height of the building. The tower footprint is 155 feet (47.24 meters) by 135 feet (41.15 meters). Levels 3 and 4 create a 155 foot (47.24 meter) by 87.5 foot (26.67 meter) rectangle, justified to the northern edge of the tower above. Level 2 is a mechanical level enclosed by intake and exhaust louvers, and setback 2.5 feet (0.76 meters) from the property lines along the west and north. The ground floor is 37 feet (11.28 meters) tall and has a footprint of 14,000 square-feet (1,300 square-meters). The northern edge of the building is aligned with the property line along 100 South Street. Above Level 5, the southern edge of the building is suspended approximately 47.5 feet (14.48 meters) over the lot line shared with the performing arts center. The performing arts center encroaches 45 feet (13.72 meters) north into the tower footprint between the ground floor and Level 5.

The building foundation is driven steel HP-piles, reaching depths over 100 feet (30.48 meters) below grade. The HP-piles support a central reinforced concrete core that extends from 18 feet (5.5 meters) below grade up to the mechanical penthouse level (Level 25) at 351 feet (107 meters) above grade. The mechanical penthouse level consists of a two-way steel truss system suspending 18 perimeter columns. The two-way steel truss system at the roof supports 23 suspended levels on the west, north and east, and 20 suspended levels on the south. In order to create a balanced system, on the west, north and east the perimeter columns reach down to Level 2, and on the south the perimeter columns reach down to Level 5. Gravity loads are transferred from the hat trusses to the top of the reinforced concrete core walls using six steel spherical structural bearings. The reinforced concrete core walls are the only connection between the tower and the foundation, and account for the transfer of all gravity, wind, and seismic loads.

Salt Lake City, near the active Salt Lake Segment of the Wasatch Fault Zone, is located in Seismic Design Category D. This means that the building is expected to experience – and is designed to accommodate – severe seismic activity. The building's unique structural design combined with this anticipation of severe seismic activity dictated a column-free ground floor, locating extreme differential movements at the perimeter between Level 1 and Level 2.

LOBBY EXTERIOR ENCLOSURE

Adjacent to the public right of way, there is an all-glass lobby exterior enclosure along the northern and western lengths of the tower's base. The all-glass exterior enclosure was selected for a number of reasons: to express the tower's unique and extraordinary structural system, to display the rare column-free ground floor, and to support CCRI's desire that the L-shaped lobby at the base of the tower be a public, open and active space. The lobby exterior enclosure is constructed primarily of one material – laminated ultra-clear glass. The introduction of additional materials was considered on a case by case basis and limited to only those that were necessary to fulfill specific performance criteria. The use of a limited number of materials, in combination with the oversized module, allowed for each detail to be carefully crafted to express its purpose. Wherever possible, the introduction of a single material is used to resolve multiple criteria.

The lobby exterior enclosure is comprised of twenty five oversized laminated glass face panels. The laminated glass face panels are base-supported for all vertical loads, self-supporting for in-plane loads, and stiffened with transverse laminated glass fins for out-of-plane loads. Laminated glass purlins connect the vertical components and the base of the suspended tower. The laminated glass purlins support laminated glass skylight panels.

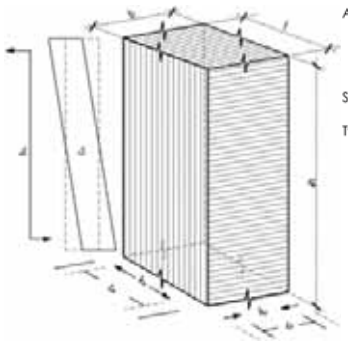
The intersection between the base-supported all-glass lobby exterior enclosure and the lowest floorplate of the tower that hangs above is required to accommodate +14 inches (35.6 centimeters) and -18 inches (45.7 centimeters) of vertical movement, and 3.3 inches (8.4 centimeters) each of parallel and perpendicular movement. In order to avoid the cumbersome and opaque movement joints conventionally associated with extreme building movements, the design and builder teams worked collaboratively to develop an all-glass lobby exterior enclosure where the primary components of the system act as deformable elements.

STABILITY

Each 10 foot (3 meter) wide by 35 foot (10.7 meter) tall laminated glass face panel consists of two 0.5 inch (12 millimeter) sheets of low-iron glass. Each of the laminated glass face panels bears on two pins, 1.4 inches (36 millimeters) in diameter, connected through a hole at either bottom corner. The laminated glass face panels sit on POM setting blocks for installation and dead load support. Following the installation of the laminated glass face panels and pins, the holes are grouted to achieve the required load transfer and bearing on the support pins. With a pin located 12 inches (30.5 centimeters) from each of the bottom edges of the face panel, in-plane stability is achieved through the 8 foot (2.4 meter) offset between pins. In this regard, each face panel is effectively a 10 foot (3 meters) deep by 1 inch (25.4 millimeter) wide beam cantilevered from the ground.

The 1 inch (25.4 millimeter) thickness of the laminated glass face panel results in limited flexural stiffness. Laminated glass fins were introduced at the vertical face panel joints to limit deflections and stress. The laminated glass fins are base supported in a steel shoe that provides translational restraint. In addition to the out-of-plane support, the laminated glass fins stabilize the free edge each laminated glass face panel when subject to in-plane overturning.

The laminated glass face panels are connected to the laminated glass fins through a continuous vertical high modulus structural silicone joint. A black silicone was selected to be visually recessive in elevation and to bring into sharp focus the primary building material: laminated ultra-clear glass. This structural silicone joint has two functions: it is the primary weather barrier, and it transfers the wind loads from the laminated glass face panels to the laminated glass fins. By serving this dual function the structural silicone joint eliminates the need for metal fittings. Incorporation of structural silicone joint geometry into the analysis was imperative to defining accurate stiffness assumptions. A simple 3D unit model was used for determining axial and shear values based on the designed joint sizes (Figure 2).



Axial spring: $k_n = EA/t$ with $A = {}_dh \times b$
${}_dh$ = unit height of silicone joint
b = width of silicone joint (i.e. capture) [refer drawings]
t = thickness of silicone joint

Shear spring : $k_v = GA/t$ with G = shear modulus of structural silicone

Two types of structural silicone are employed on the project:

Dow Corning 121	2 –part silicone	
	E_t = tensile youngs modulus = 1.4 MPa =	**203 psi**
	E_c = compressive young's modulus ≈ 5 x E_t =	1015 psi
	v = 0.5	
	G = shear modulus = 0.47 MPa =	**68 psi**
Dow Corning 795	1 –part silicone	
	E_t = tensile youngs modulus = 0.9 MPa =	**131 psi**
	E_c = compressive young's modulus ≈ 5 x E_t =	653 psi
	v = 0.5	
	G = shear modulus = 0.3 MPa =	**44psi**

Figure 2: Silicone joint unit stiffness model.

Imposed building movements result in out-of-plane movements at the top of both the laminated glass face panels and the laminated glass fins. While the inherent flexibility of the face panel may easily accommodate this displacement, the movement is in opposition to the strong axis of rotation of the laminated glass fin. Forced deflection of the fin would result in overstressing. To avoid this, the movement is accommodated by allowing rotation about the base of the laminated glass fin through the installation of medium modulus bearing blocks. The bearing blocks support the fin horizontally and vertically at the short ends of the base shoe (Figure).

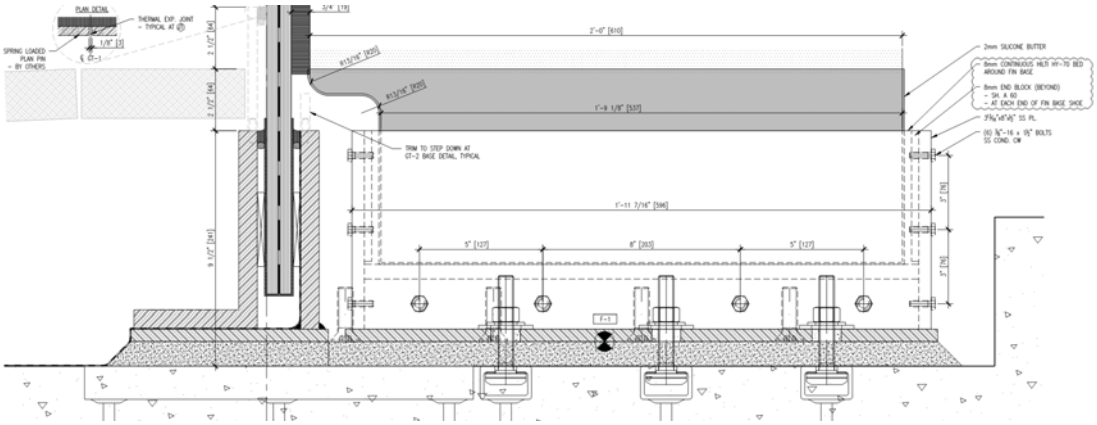


Figure 3: Section detail of laminated glass face panel at the laminated glass fin base.

Heat strengthened glass was used for all laminated glass components of the lobby exterior enclosure. Detailed analysis of high-load areas at bolt holes and fittings is required on any project pursuing assemblies without fully tempered glass to ensure that overstressing does not occur. A study of stress distributions at material boundaries was conducted, with a focus on locations where bearing stress in the (compression-only) bolt hole grout interfaced with the edges of a laminated glass face panel. Rather than extrapolate nodal values between plate elements, we considered each plate elements' Gauss point principal stress values (Figure).

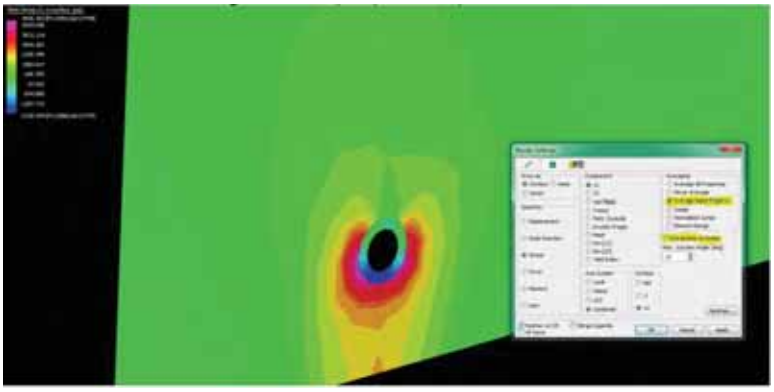


Figure 4: Grout compressive bearing stress and principal glass σ11 stress at hole.

KIENMATIC DEFORMATION

During a seismic event, the size of the tower's concrete core relative to its overall building footprint results in applied lateral loads that develop minor rotations at the concrete core but, in addition to horizontal building drifts, generate significant vertical translations at the perimeter. The rotation of the concrete core and the subsequent tilting of the floors creates a downward movement on one side of the concrete slab at the same time as an upward movement on the opposing side of the concrete slab.

The laminated glass face panels and laminated glass fins are joined to the laminated glass skylight panels and the laminated glass purlins of the lobby exterior enclosure is such a way as to create a kinematic 3-hinge assembly. The bottom of the vertical components are pinned at the ground, the horizontal components are pinned on one end at the top of the vertical

components and on the other end at the concrete slab edge of the tower above. Despite the fact that the concrete slab moves relative to the ground, as it relates to loads applied to the lobby exterior enclosure, the tower is treated as a restrained support. Structural stability and determinacy of the lobby exterior enclosure is defined by its geometric constraints: the vertical and horizontal components of the lobby exterior enclosure have fixed lengths. When the concrete slab of the tower moves, the lobby exterior enclosure components are allowed to move, harmoniously rotating about a series of pinned connections. When the suspended tower and the lobby exterior enclosure experience differential vertical movement, the slope of the skylight panels is altered. When the tower moves up relative to the lobby exterior enclosure, the inclination of the skylight panel becomes steeper and when the tower moves down relative to the lobby exterior enclosure, the inclination of the skylight panel is closer to horizontal (Figure).

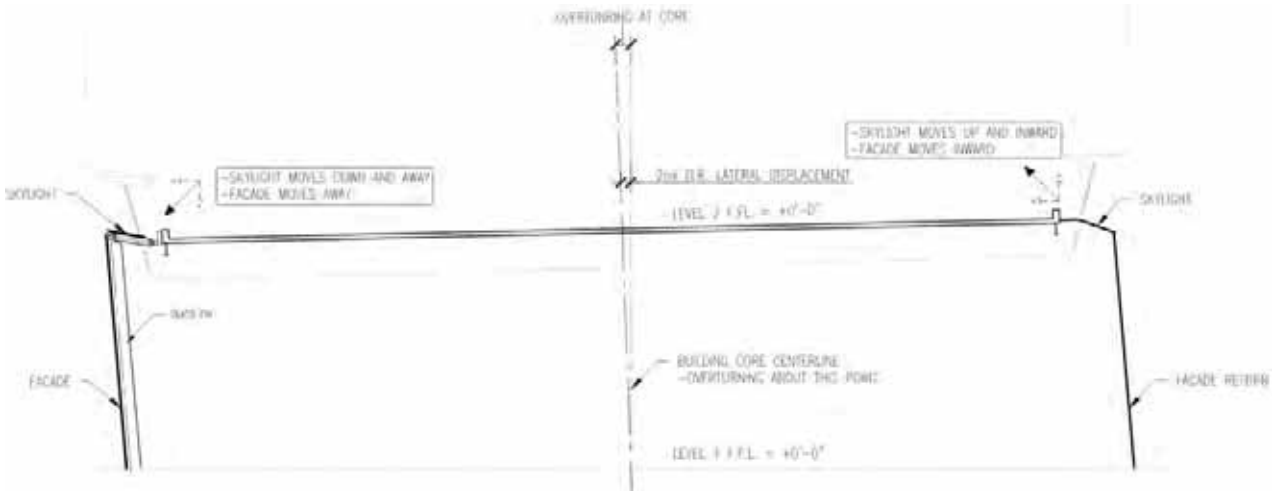


Figure 5: Diagram of building core rotations and kinematic facade movement.

In the three figures below the lobby exterior enclosure movements are illustrated in detail. Consistent with force and displacement theory, upward movement of the concrete slab is accompanied by inward horizontal drift, and downward movement of the concrete slab is accompanied by outward horizontal drift. Figure shows the lobby exterior enclosure when the concrete slab of Level 2 is in its permanent design location. Figure demonstrates movement of the lobby exterior enclosure during maximum positive vertical movement of the Level 2 concrete slab, and Figure demonstrates movement of the lobby exterior enclosure during maximum negative vertical movement of the Level 2 concrete slab. An extruded EPDM gasket runs continuously along the joint between the laminated glass face panel and the laminated glass skylight panel. The black gasket is visually recessive and permits opening and closing of the joint as the lobby exterior enclosure cycles up and down with the load reversals anticipated during a seismic event. The same gasket exhibits inherent stiffness to provide the primary weather barrier under service conditions.

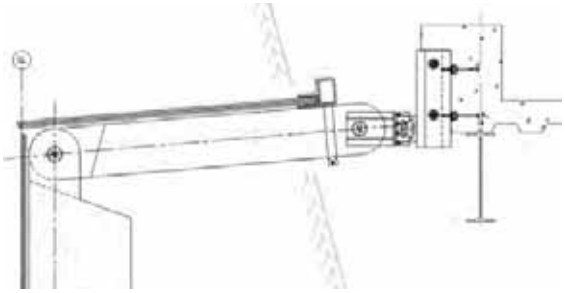


Figure 6: Façade install and service position.

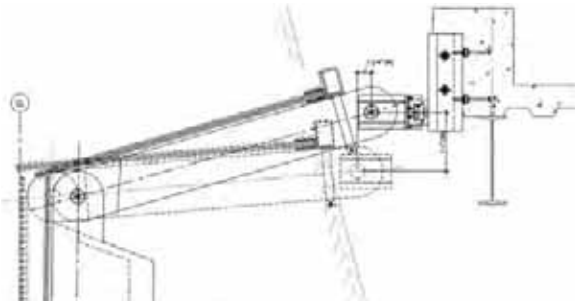


Figure 7: Façade movement during upward movement of the Level 2 slab.

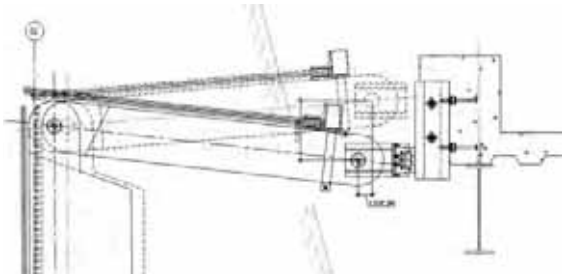


Figure 8: Façade movement during downward movement of the Level 2 slab.

The 10 foot (3 meter) by 6 foot (1.8 meter) laminated skylight panels are supported by laminated glass purlins that are pinned to the lobby exterior enclosure and the base of the suspended tower. As it relates to vertical movement and movement perpendicular to the Level 2 concrete slab edge, the lobby exterior enclosure and the tower are connected. The lobby exterior enclosure, however, was required to be decoupled from tower movement that is parallel to the slab edge.

With respect to the laminated glass face panels, the two pins at the base of each face panel creates a self-supporting system in-plane. Because the ground level does not drift in a seismic event, the lobby exterior enclosure does not drift in-plane when subject to ground accelerations or wind load. Because the base of the suspended tower does drift, it was necessary that the lobby exterior enclosure be permanently released in-plane at its point of attachment to the tower. This was accomplished through the introduction of a Bosch Rexroth linear slide bearing which ensures the lobby exterior enclosure is not over-constrained (Figure).

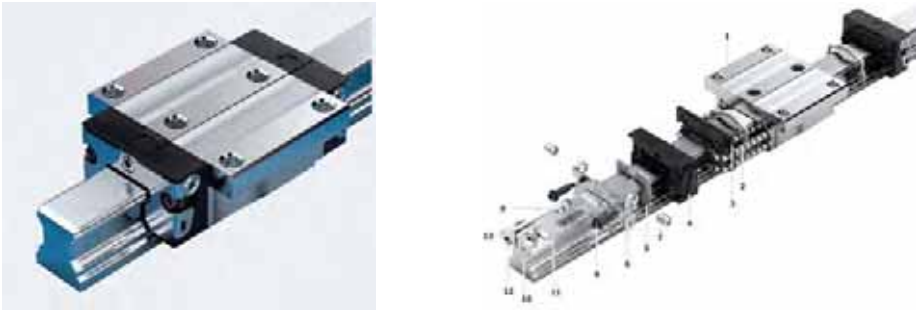


Figure 9: Linear slide bearing and components; Graphics courtesy of Bosch Rexroth.

The bearing system has a high load capacity and a low coefficient of rolling friction which varies minimally as load is applied. Two opposing rows of ball bearings are provided on each side of the travel rail allowing the bearing system to be preloaded onto the rail with internal forces opposing one another. Without applied load on the sliding carriage, the resistance to rolling is present due to the pre-load force. The use and benefit of such a system is that minimal deflection and change to rolling friction characteristics occur when load is applied (Figure). Under various load combinations applied loads in the effective range either unload the top or bottom row of ball bearings. Overall forces on the system remain largely unchanged and as a result the frictional rolling resistance and permissible carriage accelerations remain constant.

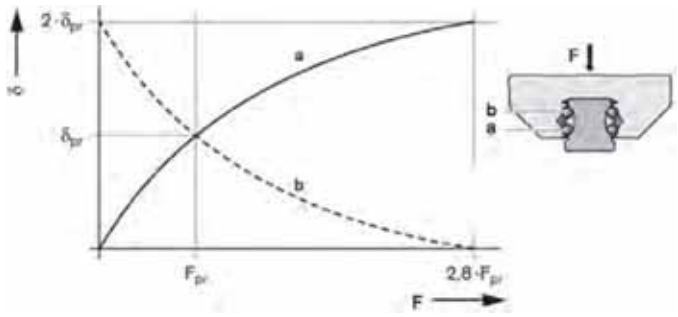


Figure 10: Linear slide loading and deflection characteristics; Graphics courtesy of Bosch Rexroth.

CORNERS

The lobby exterior enclosure has three all-glass corners, one at the main building corner and two where the lobby exterior enclosure returns to meet the base of the tower. The laminated glass corner face panels are mitered, eliminating the need for a laminated glass fin or additional metal fittings at the corner. Elimination of these additional supports is achieved by providing an appropriately sized structural silicone joint. Because the lobby exterior enclosure is decoupled from the suspended tower and self-supporting, there is no out-of-plane movement at the corner. At the free panel edge – the vertical edge of the laminated glass corner face panel located 10 feet (3 meters) away from the corner – the anticipated out-of-plane movement is 3.3 inches (8.4 centimeters). When differential out-of-plane movement is imposed, it is accommodated at the by allowing the laminated glass corner face panel to warp. The mitered edge of the laminated glass corner face panel is restrained while the laminated glass purlin pushes and pulls the free edge of the corner face panel.

The 20 foot (6.1 meter) by 6 foot (1.8 meter) laminated glass corner skylight panels are trapezoidal in shape. The corner skylight panels are parallel and orthogonal to the building at the front and back edges, and at the laminated glass fins located 20 feet (6.1 meters) away from the corner. At the corner, panels are cut back towards the tower at a 45° angle. Each of the corner skylight panels cantilevers over the top of the glass purlin closest to the corner. Coplanar movement between the corner skylight panels is achieved with a sliding-pop interface at the corner – the corner skylight panels slide up and over one another in a seismic event. The cantilevered free end of the corner skylight panel offers enough flexibility to let the cantilever elements interface without overstressing the glass. To ensure smooth operation of the sliding-pop detail, a 30° miter on the free edge of laminated glass corner skylight panels is required. Because available glass processing technology is limited to a 45° edge miter, a low-friction block was bonded to mitered edge of each corner skylight panel in the form of a custom stainless steel shape. This stainless steel shape was designed to transition the 45° angle of the laminated glass skylight corner panel to the required 30° angle and carefully crafted such that the exposed portion of the cast stainless steel shape is approximately 0.75 inch (1.9 millimeter) wide, and is aligned with the vertical 0.75 inch (1.9 millimeter) silicone joint at the corner face panels. There are thin black silicone lines on either side of the exposed portion of the cast stainless steel shape. A sheet gasket is bonded to the top of the skylight panels, sealing the joint and providing a weather barrier that can easily accommodate cyclic movement, while the bottom is treated with silicone weather sealant to provide a double seal. (Figure 2)

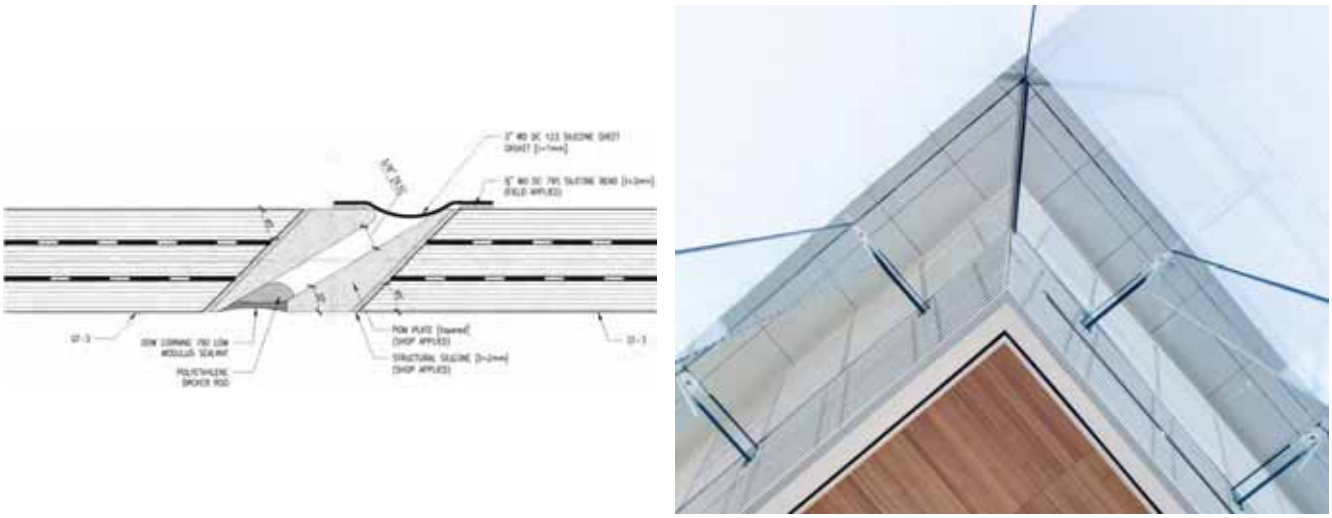


Figure 2: Section detail at corner skylight sliding-pop intersection (left). View of skylight corner from the ground (right). Photo © Paul Richer.

At the southeast and northeast corners of the lobby exterior enclosure, a single laminated glass face panel returns and ties the lobby exterior enclosure back to the tower structure. At these locations, the corner conditions are more challenging to solve because the differential movements are large and the return face panel acts as an undesired stiffening element. As such, the return face panels are treated as a transverse fin, not as a face panel. A single pin is employed at the base of the return face panel to permit in-plane rotation. Where the return face panel meets the base of the tower, a vertically oriented linear slide is employed to accommodate the +18"/-14" building movement (
Figure 3). Warping at the skylight panel is rigorously checked with localized analysis models and ultimately accommodated with a series of hinges and silicone joints.

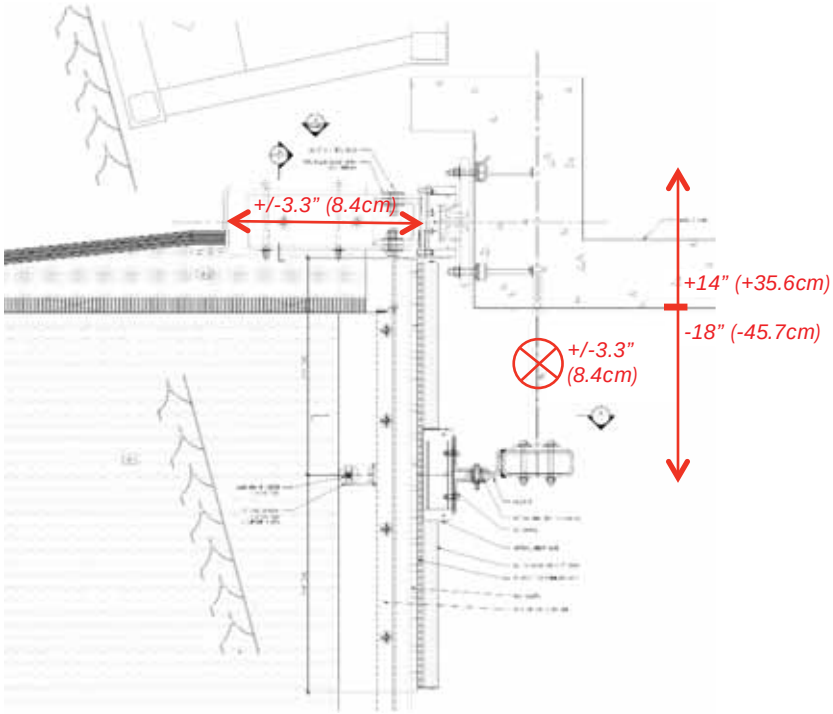


Figure 3: Section detail at return panel, including anticipated movements at return panel connection to tower base.

PIVOT JOINTS

The laminated glass skylight panels and laminated glass purlins act as a hinge to accommodate the differential vertical movement between the lobby exterior enclosure and the suspended tower with a hinging motion through a pinned-pinned

connection. One end of the purlin is pinned at the head of the laminated glass fin and the other end at the edge of the Level 2 concrete slab. The purlin and the fin are each comprised of four 0.5 inch (12 millimeter) sheets of ultra-clear low iron glass of heat-strengthened glass. To create the pinned connection, the inner two lites of the fin stop short while the outer two lites of the purlin stop short, forming a mortise and tenon connection. The form of the connection traces the rotations and required movement clearances (Figure 4).

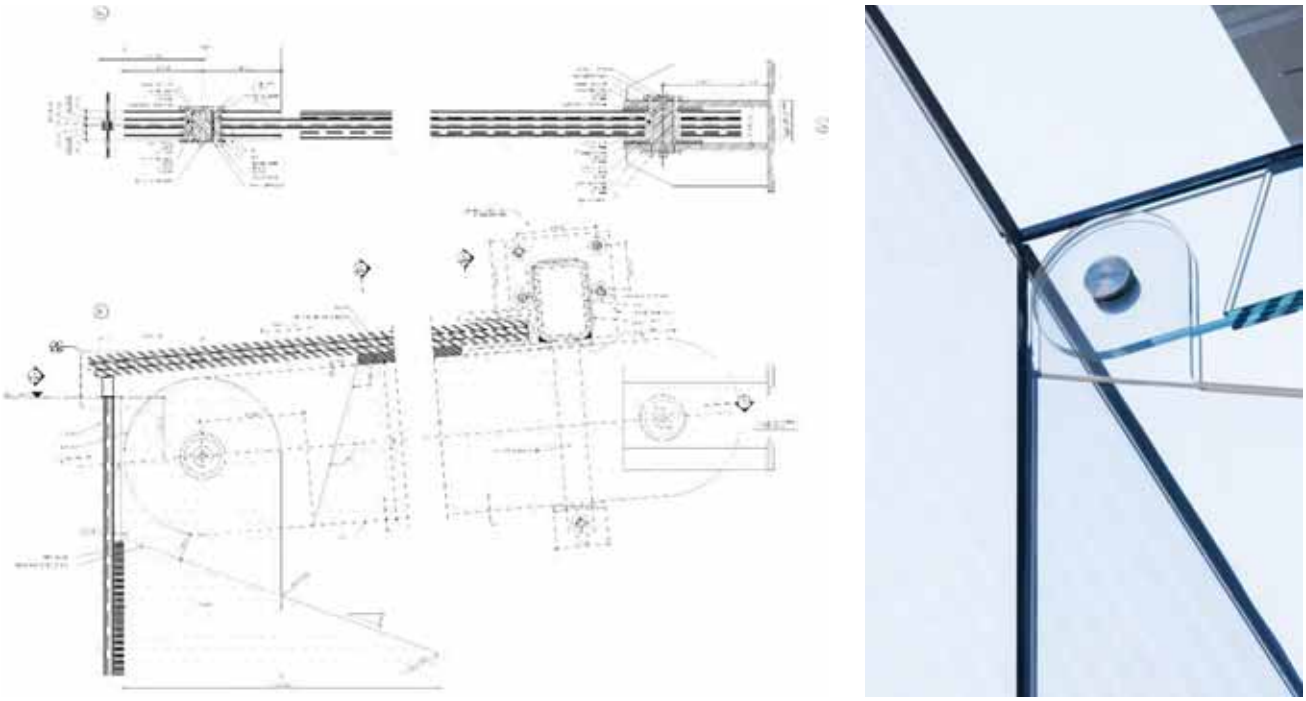


Figure 4: Plan and section details at laminated glass fin (left). View of hinged connection (right). Photo© Paul Richer.

At both ends of the laminated glass purlin, all forces are transferred between elements through a metal pin. Glass offset fabrication and post-lamination tolerances are accommodated with injectable cementitious grout. It is critical to ensure free-rotation of the purlin element and pinned connection to prevent generation of unexpected stresses at the holes. Grout interlock between the fixed and rotating elements is prevented through a series high-elasticity low-friction bearing pads and stepwise installation methodology.

TIMBER FIN INTEGRATION + EMBDEDDED LAMINATION

The two public lobby entrances, one on 100 South Street and one on Main Street, are constructed of glass, steel and wood. Two modules wide, a structural steel frame was designed to support two of the laminated glass face panels and the three laminated glass fins supporting them. The steel frame, laminated glass side panels and laminated glass lintel panels serve to define the 20 foot (6.1 meter) wide by 20 foot (6.1 meter) tall by 7.5 foot (2.29 meter) deep lobby entrance. Given the transparent nature of the all-glass lobby exterior enclosure, bringing prominence to the building entrances was imperative. It was the introduction of wood, a quarter sliced California Eucalyptus, which served to set the entrances apart from the adjacent all-glass lobby exterior enclosure.

A series of 2.5 inch (6.35 centimeter) by 6 inch (15.24 centimeter) solid kiln-dried eucalyptus fins are attached to the laminated glass side panels and laminated glass lintel panels that frame the entrances. Each of the eucalyptus fins are mechanically fastened to continuous concealed stainless steel hardware. The out-of-plane stability of the eucalyptus fins is achieved through a continuous 2 inch (5.1 centimeter) wide bead of structural silicone between the timber fin and the glass panel. At the laminated glass lintel panels, vertical loads are transferred through a series of embedded metal plates. The metal plates are attached to the lintel panels with internally threaded laminated titanium fittings (

Figure 5).

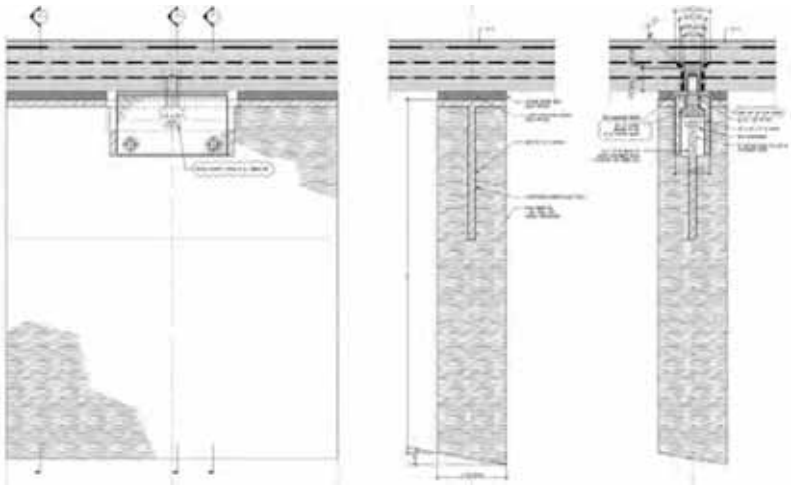


Figure 5: Section details at titanium insert and concealed timber fin support.

To eliminate visibility of the 2 inch (5.1 centimeter) wide structural silicone lines used to adhere the stainless steel hardware to the laminated glass from the outside of the entrances, and to achieve the appearance of solid wood on all sides, a natural wood veneer was captured inside of the laminated glass side and lintel panels. Because this had not been done before, a series of tests and fabrication samples were created. The team was able to determine that, although the outer lite of the glass panel is structurally compromised because of the reduced composite behavior experienced with inclusion of the timber veneer strips, dried timber veneer could be laminated into the glass panels. The final design gives appearance of an entrance constructed of only glass and timber (Figure 15).



Figure 6: View of the lobby entrance. Photo © Cesar Rubio.

SUMMARY

At 111 Main, a unique collection of site complexities combined with significant seismic activity resulted in extreme differential movements between the tower and the lobby exterior enclosure. Engagement by the project development team of design and construction professionals early in the process led to a collaboration resulting in the novel use of a kinematic system to accommodate the extreme building movements anticipated from overturning of the tower's slender concrete core. Elements of the lobby exterior enclosure are engaged as a hinge, eliminating the need for conventional opaque movement joints. A highly customized series of pivots, releases, and flexible joints is used strategically across the lobby exterior enclosure, and rigorously checked for clearances and clashes by studying and understanding the imposed movements. By working collaboratively, the design team, contractors, engineers, and fabricators were able to develop details and engineering approaches to address each of unique design challenges encountered in developing an innovative solution. The result is a structural glass lobby exterior enclosure that does not rely on opaque structural elements or materials to accommodate movement, and one that fully achieves the desired aesthetics.

ACKNOWLEDGMENTS

The authors would like to thank those who made significant contributions to the design and construction of the 111 Main lobby exterior enclosure, including but not limited to:

- City Creek Reserve, Inc.
- Okland Construction, Inc.
- Steel Encounters, Inc.
- Sedak GmbH & Co.
- TriPyramid Structures, Inc.

KINETICS IN BUILDING FACADES

Development of taxonomy of kinetics in climatic building envelopes



Sean Cullen
Queen's University Belfast
scullen05@qub.ac.uk



Professor Greg Keeffe
Queen's University Belfast
g.keeffe@qub.ac.uk

ABSTRACT

The prominence of climatically responsive building facades through the use of kinetics has proliferated in recent years due to a concern for the reduction in building energy demand and increasing user comfort. However, no resource provides an extensive catalogue of knowledge around how kinetics in the building façade are used, what they aim to achieve and where they exist. Consequently, the taxonomy acts as a useful tool to organize and better understand a body of knowledge that will become increasingly important for architects, engineers and clients in years to come.

Through a grounded theory approach, a database of existing projects is analyzed through categorizing and coding their kinetics as well as their 'type'. Kinetics are coded: rotate (vertically or horizontally); linear (vertically or horizontally); flex; fold (point or linear); translate; and, scale. Each project is given an order of complexity, up to three, depending on the number of kinetic mechanics within the façade system. It results in 729 potential sequences, a vast number of which are still to be explored. 'Type' refers to: light (L); thermal (T); airflow (A); generator (G); and, a combination of each (TL, AT, AL, LG, TG, AG). These are cross-referenced with climatic indicators and date of completion.

The taxonomy allows for an understanding of how 'type' interconnects with climate conditions and how complexity of kinetics has increased over time. Similarly, it indicates the role of kinetic façade systems in managing lighting conditions, which historically lies beyond the remit of mechanical services – the environmental management system of choice in the last century. It also highlights how other types, like generator systems, are becoming more prevalent.

KEYWORDS

adaptive - kinetic – dynamic, innovative or unique, intelligent, taxonomy, history of facades, façade theory or philosophy, future trends

INTRODUCTION

In recent years, there has been a shift in the way environmental management systems improve user comfort and energy efficiency within buildings. As Banham (1967) explored in *The Architecture of the Well-Tempered Environment*, mechanical services became the default means through which buildings managed humidity, airflow and temperature. Passive, preventative techniques managed by the building façade have become commonplace through kinetic systems which are responsive to climate and weather. Like Banham, this paper is interested in 'mosts, not firsts' (1967). Its aims to better understand commonalities and trends that prevail in design, purpose/aim and technique employed. The application of kinetics within contemporary building envelopes is an endeavor to develop facades that respond to climatic conditions with the aim of increasing building performance and reducing energy consumption. The increasing importance of kinetic techniques within façade design and manufacturing requires further analysis, investigation and understanding. Currently, no

extensive catalogue or database of kinetic building facades exists. A taxonomy will provide a clear knowledge base of precedents identifiable through 'type', purpose/aim, technique and date. It aims to understand commonalities and trends for the benefit of architects, engineers and clients. Previous work (Cullen, Keeffe & Kinnane, 2016) analyzed responsive facades as establish material culture artefacts, evaluating their evolution and exposing concepts that prevail in practice. Reasons for 'selection' and conservatism include social learning mechanisms, limitations to manufacturing as well as architectural project limitations – including budget, schedule and maintenance costs. With these prevalent trends, it is critical to understand how designers have shaped the building façade according to climatic conditions, what role it intends to fulfil and what kinetic movement patterns adopted.

IMPORTANCE OF TAXONOMIES

The importance of developing a taxonomy lies in the ability to remove oneself from a close working relationship with a specific field and analyze it from the perspective of the author. As Glass and Vessey (1995) state, "taxonomies organize a body of knowledge that constitutes a field." It is important because it allows researchers and practitioners to generalize, communicate and apply research findings through it – as Knaack (2011) demonstrates through the development of a roadmap for the future of the façade. For this to be possible, the field must be at a point of development whereby "scholars attempt to characterize their own limited areas of interest with respect to the whole field" (Glass and Vessey, 1995). The importance of taxonomies is twofold. Firstly, it provides structure to bodies of knowledge in a way which is accessible and easily understood. It defines critical and important aspects clearly and coherently. Secondly, taxonomies predict the development and evolution of the field. To provide an example of this consider the periodic table. The prediction of some elements took place long before they were isolated or identified. George Wheaton (1973) describes the development of taxonomies as a process and product: "On the one hand, classification is the act or process of systematically arranging some subject matter into groups or categories according to selected criteria. On the other hand, classification is the more or less formally structured set of classes or categories which emerge." Developing taxonomies is a process that evolves and transforms over time rather than acting as an end in itself. Glass and Vessey (1995) refer to taxonomies as dealing with the problem area versus the solution area. Consequently, it makes them an ideal tool to root out approaches to problem solving taken by others. Understanding these concepts, which initially emerged in computer programming fields, can be translated to architectural practice. Blum (1989) "conceptualizes the application domain as consisting of conceptual models of the problem to be solved, and the implementation domain as consisting of formal models used in a solution to the problem." The separation between the problem area and the solution area is important to maintain when developing taxonomies. However, the formal models of the solution area are vital because architecture must be constructed, limited by the exigencies of manufacturing, tooling and materials, as well as costs and schedules, as will be discussed later.

DATABASE

Grounded theory uses a qualitative, inductive method of research that combines the process of data collection and analysis in a continual, cyclical nature. It allows highly contextualized theories to emerge from data analyses using basic tools – categories and coding (Willig, 2013). This process creates a catalogue or database of existing projects and precedents relevant for the establishment of a kinetic taxonomy. Similarly, the practice of information architecture offers an interesting insight into organizing and the storing of information in order to enhance usability. The Dewey Decimal System offered an effective way to categorize books within a library under themes as the number of books greatly increased. This research applies a similar method to the database sample of 45 projects for: a) kinetic movement; and, (b) 'type'. Rosenfeld and Moreville (2007) state, "A major way that libraries and librarians add value to the printed materials is by placing them within the framework of an information architecture that facilitates access to those materials." According to Rosenfeld and Moreville (2007), the coding of the data acts as 'findability engineers'. It is vital that this coding is clear and coherent in order for the information to be accessed and understood for potential users.

A TAXONOMY OF KINETICS

The kinetic movement of each precedent in the database was determined and coded. As a result, the following kinetic motions were established: rotate (vertically or horizontally); linear (vertically or horizontally); flex; fold (point or linear); translate; and, scale (Fig. 1). Some are based on examples of Moloney's (2011) identified kinetic patterns – rotation, translation and scaling. However, a notable difference emerged between the final kinetic patterns and the mechanical kinetics which informed the observable movement. An example of such degrees of complexity are highlighted in the mechanics of the windscreen wiper. It requires three kinetics motions to enable the rotation of the wiper on the windscreen – rotational (vertical), linear (horizontal) and, finally, rotational (vertical). Therefore, when determining the kinetic pattern, it was not simply the final, visible motion identified and coded, but all kinetic inputs required. Consequently, it established orders of complexities in each of the precedents, ranging from only one step to three steps.

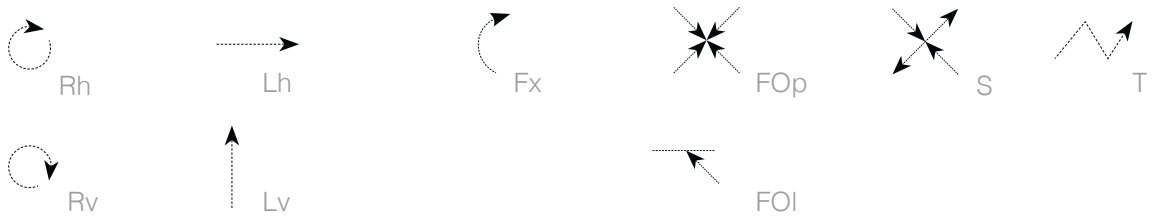


Figure 1: Kinetic principles for the development of a taxonomy.

The process of coding each precedent within the database led to the development of a kinetic taxonomy (Fig. 2). For each kinetic pattern in the system, the prefix donates the order of complexity, from Order 1 to Order 3. The codes, on the far right hand side, donate the observational kinetic movement of the façade while the center codes annotate unobservable kinetics required to move the facade. The variations result in a vast number of potential variations – 729 different kinetic categories in total. When determining the taxonomy, the sequence of the kinetic pattern is critical, and the reason for so many various combinations.

A significant potential of unexplored opportunities within climatically responsive facades is noticeable through this process. These systems are possible but lie beyond the scope of designers and manufacturers for now. Future kinetic systems will begin to populate this taxonomy, indicating where previous works have deployed similar kinetic systems but also offering new examples of ones untested. However, it is likely that façade designs will focus on proven kinetic sequences. This is because the exigencies of manufacturing and architecture rely on economics, schedules, costs and reliability. However, variations and testing of the new will eventually become acceptable and applicable due to improvements in manufacturing, cost effectiveness of production and application as well as management of complex systems. It is notable that the most complex kinetic systems emerge from experimental research with limited commercial applications.

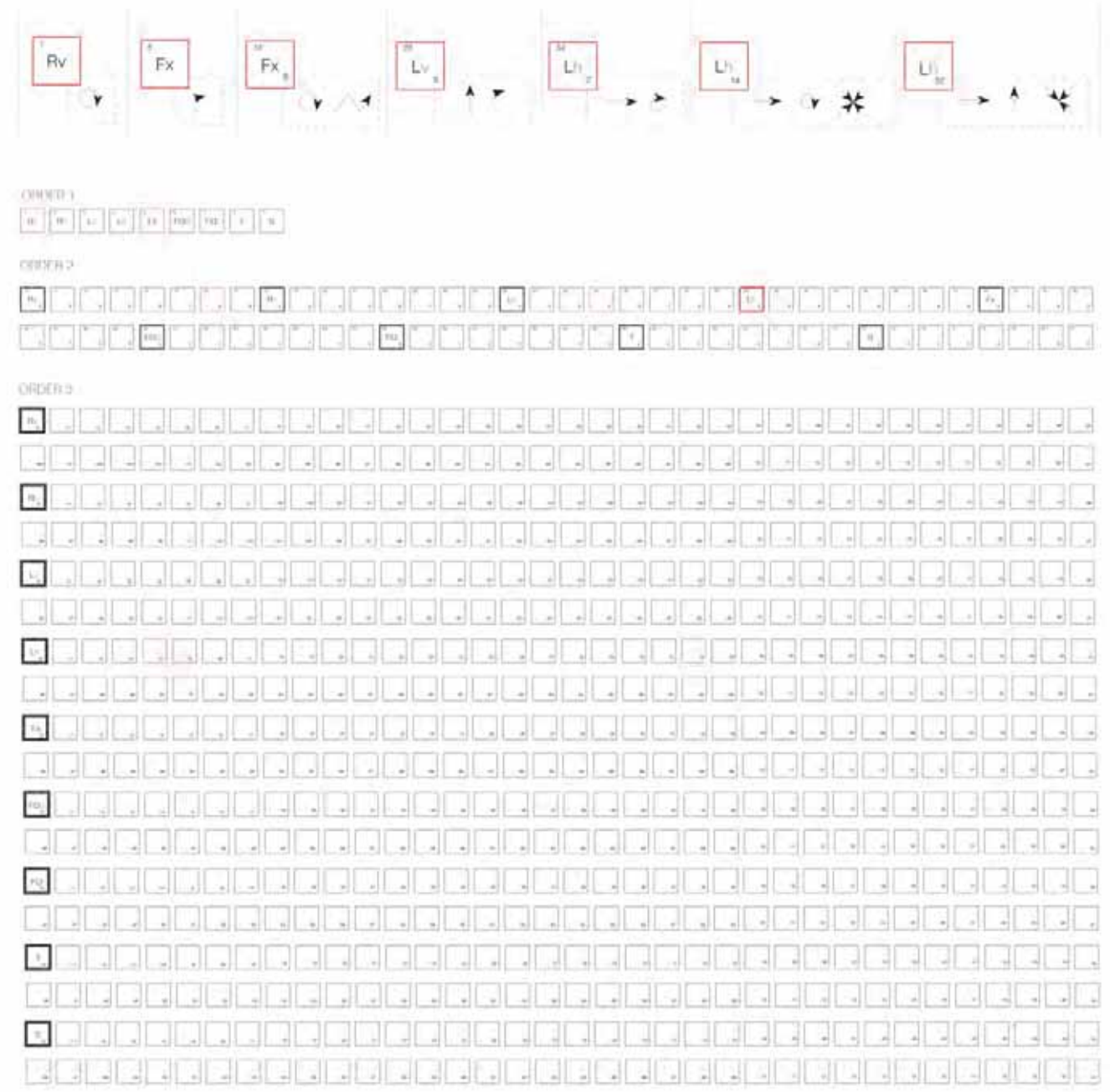


Figure 2: A taxonomy of kinetics in climatically responsive building facades - the highlighted examples below are from the database of project indicating how they would be referenced according to the mechanisms employed and where they would sit within the taxonomy depending on order of complexity.

TYPOLOGIES IN CLIMATE CONTROL

Despite the use of developing a taxonomy of kinetic sequencing within responsive building facades, an understanding of how they are used and in what climate they are located is equally as crucial. For this reason, a second level of coding to the taxonomy adds increased functionality and knowledge for façade designers. The same precedent database was then coded according to ‘type’. The basis for ‘type’ was founded on the framework developed by Loonen et al (2016) in identifying multi-domain integration for adaptive building envelopes when modelled in building performance simulation (BPS) tools. One has been added – generator - and one removed – building services – as this ware not applicable to climatically responsive building envelopes. The final categories included: light (L); thermal (T); airflow (A); generator (G); and, a combination of each (TL, AT, AL, LG, TG, AG). Detailed data for each precedent was layered on top of this, including the climate classification of each projects location and the date of construction. The Koppen-Geiger climate classification determined the primary

conditions to which the kinetic systems react. It aims to evaluate whether certain typologies proliferate in specific climates; whether certain ‘types’ are more frequent than others and how, over time, there is any shift in prominence, if any. The resultant Sankey diagram was developed (Fig. 3). It was formatted in this way to demonstrate flows of information and knowledge in an easily understandable format. The far left indicated climate, the center indicates ‘type’ – in the order mentioned above, bottom to top – and, the far right is an indicative timeline of deployment – top being most recent.

FINDINGS

The result of this process exposed a number of key insights. The first is the limited number of climates represented through the process. This could be for a number of reasons. Firstly, the zones not represented are of extreme weather conditions and, as a result, would be sparely populated and most likely underdeveloped. Importantly, they would also be least likely to have varying climatic conditions worthy of employing a responsive system. The possible exception to this is Dubai – BWh on Koppen-Geiger scale. Secondly, the climates are not significant ones in Europe and North America, the location of most of the identified precedents. It is for this reason that two climates are most represented – Cfa and Cfb. These are also climates which are temperate, and, consequently, easier to manage climatic conditions. It also presents less risk and adverse effect if an implemented design does not function as desired. Lastly, the small sample size might be a reason for the limited climate locations.

There is a clear dominance of certain ‘types’. Singular ‘types’ are far more frequent than those which adopt multiple functions – 32 singular, 13 multiple. The mediation of light is the most frequent ‘type’, as the easiest form of system to implement. The inability for mechanical systems to account for and manage lighting conditions hints at the prominence of this type within the system – other conditions are managed easier with greater historical precedent through mechanical environmental management systems. However, in more recent times, there is a shift to building façade systems to perform more complex tasks which historically mechanical systems would manage for comfortable internal environments. This is why, over time, the more complex, multiple ‘types’ are more prevelant, along with simply greater numbers. Interestingly, one ‘type’ was not identified in the sample set – AirflowGenerator (AG). The climatic conditions Cfa and Cfb are made up of many varying approaches to climatic systems. As mentioned earlier, this may be the result of limited risk in temperate climates to implement varying systems. Of the 11 climates represented, over half – six – utilize a single façade ‘type’. This would indicate that the systems in these climates are relatively immature and there is a dominant climatic condition which it must deal with.

DISCUSSION

As a result of the taxonomy, manufacturers, designers and clients can utilize it to reference desired outcomes for kinetic, climatically responsive facades. It has established clear links between ‘types’ and climates as well as highlighted climates where many or none exist. The importance in understanding these patterns is vital to structuring knowledge and application of climatically responsive facades. Creating a framework tool increases uptake and reduces risk because of the clarity and coherence offered in terms of what others have implemented. It develops the understanding of ‘selectionism’ within a system and enhances social learning mechanisms to refine focus areas. Employing resources to the exploration into the entirety of the taxonomy is beyond the realms of marketplace economics and architectural practices but it offers unique understanding as to the potentials beyond these forces.

Consequently, in order to explore the potentials of a territory unaffected by the forces of the marketplace, finance, timescale and logistics must be considered. Early years of the 1960s the idea prevailed of enabling the exploration of the abstraction into territories beyond these limitations (Frampton, 2007). Archigram were pioneers of such thinking, pushing definitions and understanding towards a future ‘terra’ which lies between the deterritorialized and the reterritorialized of speculative design (Negri, 2014). Between the world of ‘techno-nilhism’ and speculative fiction, rests ideas and provocations that do not attempt to predict the future. Instead, they act as critiques of current cultural, social, economic and environmental values. The façade acts as an artefact indicative of these characteristics of a given place and time. Its ability to represent these through built form makes it an emblem for development, not only of built form, but also of systems of production and labor. In adopting the building façade as a mechanism to explore these abstracted landscapes, void of any built environment as Noys (2015) believes, it defines our understanding of the ‘environmental package’ in the context of globalization and financialisation of construction.

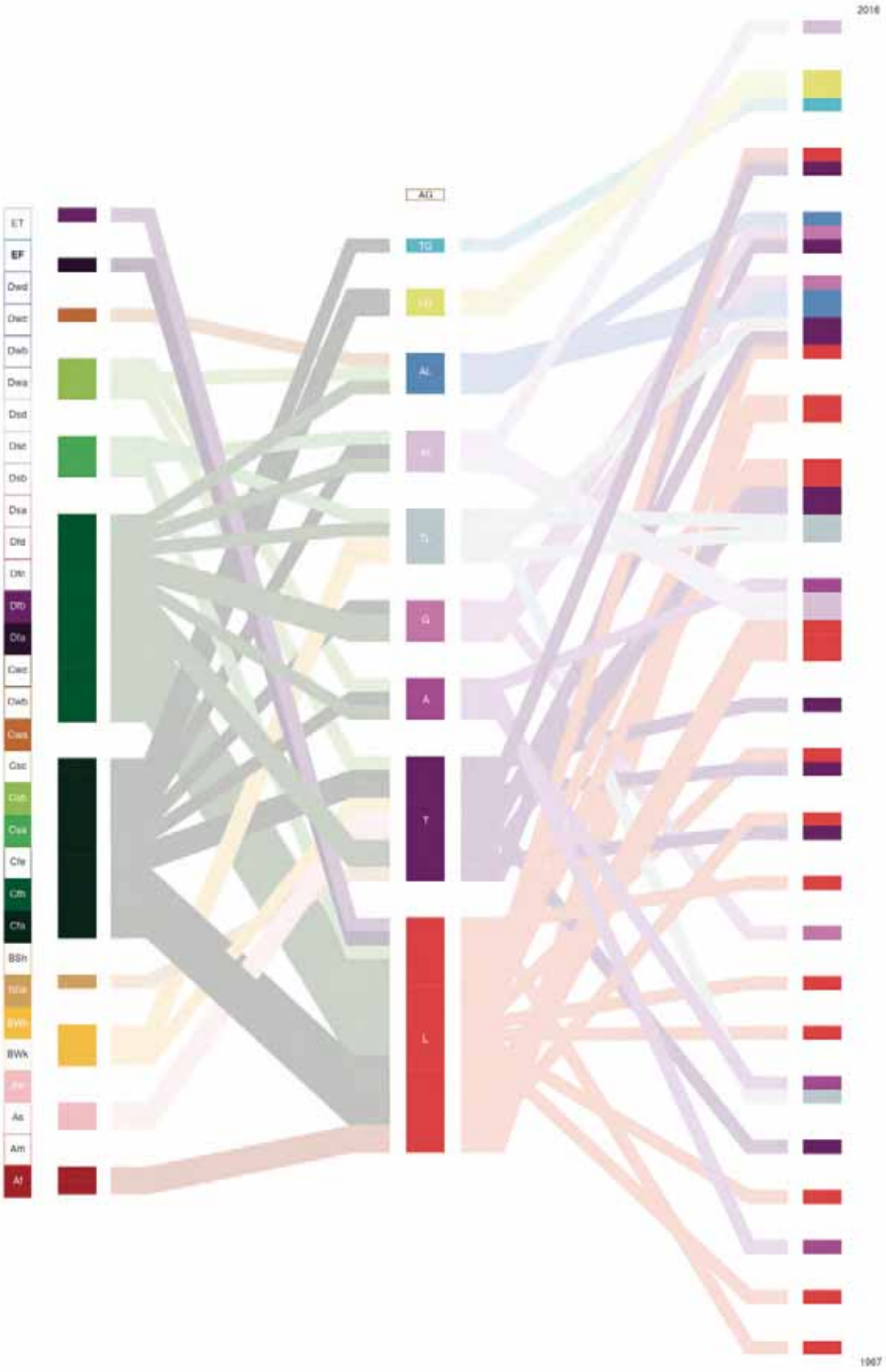


Figure 3: Sankey diagram indicating from left to right: climate; 'type'; and, over time – top most recent.

FUTURE WORK AND CONCLUSION

The grounded theory approach to this work acknowledges the cyclical nature of the research methodology. For this reason, new precedents will continually be added to the database in order to support, shape and refine the taxonomy while improving usability through developing a digital interface for use. Similarly, it will look more closely at the relationship between kinetics and 'types'. This will determine whether there is a clear relationship between kinetic systems and function. If there is, the potential for the taxonomy to function as a design tool for architects and engineers becomes significant. It will also identify frequency of kinetic sequences, determining whether the proliferation or focus exists in certain areas. It will demonstrate current areas of development. Likewise, the work will establish links between climate and kinetic sequencing to understand the relationship between the two. If specific kinetic patterns occur in similar locations, it will determine whether this is a result of climate or proximity to manufacturers who continually produce similar products. It will continue to investigate the connection between orders of complexity, costs of application and maintenance requirements to provide a more holistic understanding to a user of the database or taxonomy. Similarly, investigating the tie of predominant systems to geographic location and climates will provide insight into the clustering, if any, of 'types' of systems. It must be noted that when it comes to information architecture, "everyone (including the authors) is biased by their disciplinary perspective" (Rosenfeld and Moreville, 2007). The understanding of the author is unique but one which provides a platform the others to develop and expand upon as well.

Finally, an explorative, speculative body of work will seek to begin to inhabit the scope of the taxonomy unexplored. It will come in the form of design vignettes with the purpose of exposing ideas regarding social, economic and environmental values prevailing today. It is only through this form of deterritorialisation and abstraction where a cultural critique of value, capital and aesthetics can be explored. The consideration of capital and human will is significant in the age of globalized labor, supply chains and markets. As an 'entity' rather than an individual, the shaping of the built environment has less consideration because of the detachment between building, client and architect. The systems that produce buildings – not necessarily architecture – are done at scales beyond the controls of individual will, critique and desire. Capital forces, which deal with diverse stakeholders, dilutes will at the expense of productivity and 'value for money'.

REFERENCES

Banham, Reyner. 1969. *The Architecture of the Well-Tempered Environment*. London: Architectural Press.

Blum, B. 1989. "A Paradigm for the 1990s Validated in the 1980s." *American Institute of Aeronautics and Astronautics*: 502-511.

Cullen, S., Keeffe, G., & Kinnane, O. (2016). Mapping Responsive Envelopes: Material culture evolution and climatically responsive building facades. In D. Noble, K. Kensek, & S. Das (Eds.), Face Time: The Emergence of the Facade as the Integrative Factor in Holistic Building Design (Vol. 2, pp. 201-207). Los Angeles: Tectonic Press.

Frampton, Kenneth. 2007. *Modern Architecture: A Critical History*. World of Art. 4th ed. London: Thames & Hudson.

Glass, Robert and Iris Vessey. 1995. "Contemporary Application - Domain Taxonomies." *IEEE Software* (July): 63-76.

Knaack, Ulrich. (2011, March). About innovation. Paper presented at the Conference of Adaptive Architecture at The Building Centre, London, United Kingdom.

Loonen, Roel, Fabio Favoino, Jan Hensen, and Mauro Overend. 2016. "Review of Current Status, Requirements and Opportunities for Building Performance Simulation of Adaptive Facades." *Journal of Building Performance Simulation* 1493 (April).

Moloney, Jules. 2011. *Designing Kinetics for Architectural Facades: State Change*. Abingdon; 4: Routledge.

Morville, Peter and Louis Rosenfeld. 2007. *Information Architecture for the World Wide Web*. Beijing; Cambridge: O'Reilly.

Negri, Antonio (2014) 'Reflections on the Manifesto' *#Accelerate*, pp.363–378.

Noys, Benjamin. 2015. "Architectures of Accelerationism." In *History and Critical Thinking Debates: Locating the Politics of Architecture Series*, pp.1–21. London: Architectural Association School of Architecture.

Wheaton, GR. 1973. *Development of a Taxonomy of Human Performance: A Review of Classificatory Systems Relating to Tasks and Performance*. Washington DC: American Institute for Research.

Willig, C. 2013. *Intorducing Qualitative Resrach in Psychology*. New York: Open University Press.

PATCHWORK

How textile techniques generated the first enclosures, coded complex machines, and influence space, form, and structure in the digital age



Alexander G. Worden, AIA
Studio NYL
aworden@studionyl.com

ABSTRACT

It may be difficult for modern man to believe that what is known as handicraft was once the advanced manufacturing of the day. These techniques were used to create the first garments and portable shelters. There is much speculation as to their origin. However, the common thread in early enclosures is skin. Whether hides or woven surfaces, this cladding adorned the human form for warmth and then evolved into the first to enclose space and delineate interior from exterior. From these noble beginnings, the built environment of today is a global village of brick, glass, and metal. However, all methods of construction are steeped in these early traditions of fabrication.

Many of the advancements of the world today trace back to the textile techniques of early man. Beyond the realm of handicrafts and pastimes, fiber techniques continue to generate complex concepts and forms. From the punch cards of the jacquard loom to the first read-only memory used in the Apollo space missions, the sheer breadth and variety of these examples express textiles' deep influence in process and result.

With the increase in digital technologies and the rapid manufacturing of modern autonomous machines, traditional indigenous structures and fabrication techniques can easily be seen as outdated in comparison. However, simply because these digital tools and techniques exist, does not mean that traditional techniques cannot be used in new ways to aid or influence the design, development and fabrication of the built environment. In fact, it should be just the opposite.

Throughout history, designers have seen the benefits of exploring and playing with these early fabrication techniques previously seen as pastimes of folk art. However, by leveraging these handicraft methodologies, it enables a seamless balance of old and new technologies to augment each other, effectively marrying early fabrication techniques with those of the digital era. From fibrous loops to weaving of walls, these fabrication techniques have heavily influenced many facets of the built environment in the 21st century.

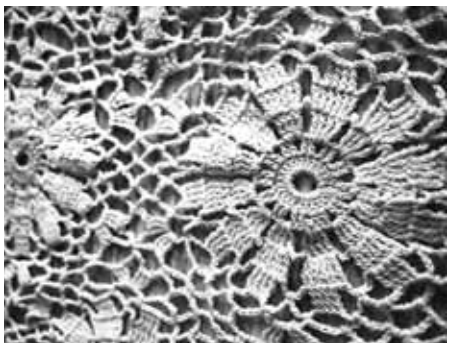


Figure 1: Ornamental crochet table runner.



Figure 2: Rose Window Cathedral of Assisi, Italy. By Stefan Kühn - CC BY-SA 3.0.

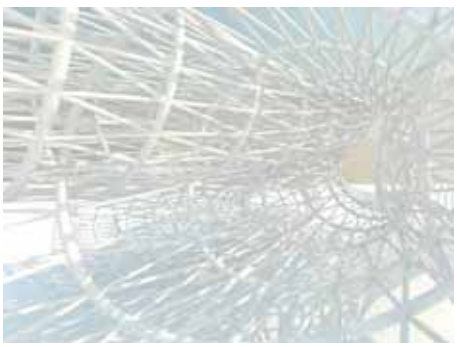


Figure 3: Digital translation of crochet structure.

KEYWORDS

design processes, facade theory or philosophy, history of facades, generative design, computational design



Figure 4: Diagrid skylight canopy at the British Museum in London. This triangulated grid pattern has been found naturally in plants and animals and in the textiles of the early humans.

INTRODUCTION

“We shape our tools and our tools shape us.” – Marshal McLuhan

In the 21st century, humanity finds itself split between two environments — the physical reality described by our senses and the digital realm where the laws of physics are suspended and materiality consists of zeros and ones. This paradigm is no different from that of any other new technology. Upon its advent and integration into the rigors of everyday life, the exploitation of new tools is without restraint or justification; it is progress for the sake of progress. However, as new technologies become more commonplace, novelty cools and a shift occurs. Questions arise — how does this tool help? When does one utilize it? Moreover, what is its effect? It is critical to attempt to understand how any tool is most efficiently utilized while understanding the feedback loop effect on the human mind and society as a whole.

It is difficult to imagine that this pattern occurs with any technology, even the primitive techniques of early humans. Ultimately, any technological addition changes the group and the overall environment. Early techniques in pottery, carpentry, but specifically textiles are perfect examples of how even the simplest of techniques radically change the course of a people. These early methods of shaping material gave rise to clothing, nets, animal pens, and ultimately the first structures. As there are no records of how these all came to be, many have hypothesized their origins. But the most notable are those proposed by Gottfried Semper. His theories in textiles are still prominent to this day due to their deep insights into how man perceives nature and how he manipulates materials into functional and artistic products.

From the hearth and mound to the roof and enclosure, the process of developing structures, at its core, has remained relatively unchanged, and it could be argued that today’s buildings are, elementally, no different from that of early peoples’. Regardless of the tools of the day, it is material and method that generate the essential elements of the built environment. However, beyond the function and aesthetic, there must be a desire to understand the importance of when to use a tool, how it affects the process, and when it is to be implemented. There is no better tool or technique than that of textiles as it predates history and has continued to evolve alongside man throughout the ages.

These surfaces of woven, knotted, looped threads create some of the most intricate works that are as aesthetically pleasing as they are functional. From early fishing nets and loincloths, to the complex textile machines of the industrial revolution and the development of early computing, these base textile techniques have been behind the creation of many historical achievements. Because of this continuity, textiles are the perfect vehicle to better approach and understand the burgeoning digital environment and its machines. By blending materiality and process of rule-based production, these pliant modes of fabrication can aid in the play between the digital and physical environments, forms, surfaces, and structures before man is lost within them.

BACKGROUND: BRIEF HISTORY OF TEXTILE

The origin of textiles is unknown. However, over the centuries, thousands of samples have been excavated from all over the world, the oldest being that of the Gravettians, an early culture of the Paleolithic period, dating back approximately to 33,000 BCE. These sites uncovered the earliest preserved textiles and other fibrous works that over the millennia had been ossified and fossilized into stone. Regardless of their beginnings, in studying the various fabrication methods used in the creation of the early textiles, they share a common theme — that of knotting, looping and braiding, resulting in products of spectacular variety and complexity.



Figure 5: Stone carving with embellished braids.

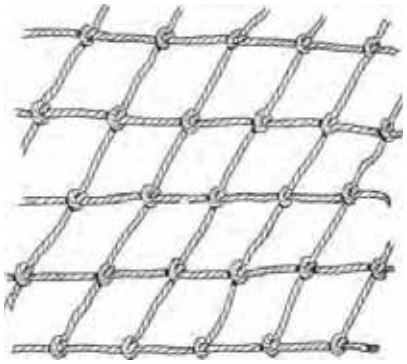


Figure 6: Sketch of early knotted netting.



Figure 7: Imprinted textiles on potash and clay.

In the earliest textiles discovered, a form of knotless netting was used. This technique, Naalebinding, uses a needle to loop fiber back on itself. A single open knot is stitched and subsequent loops are threaded through the previous stitch. Naalebinding is the earliest known textile technique upon which all other textile procedures are based. This process establishes a set of steps or rules that guide its fabrication. Those skilled in these methods know these instructions as a textile pattern. By employing the simplest of loops, the variety of different fabrication sub-techniques is staggering, even in the oldest of textiles discovered. These looped fabrics were typically used for nettings and garments, primarily due to the fact that the looping technique imbues the fibers with an elasticity that did not previously exist in the unprocessed threads.

From these knotless netting techniques, similar to that of crochet, larger swaths of textiles most likely gave rise to the creation of loomed weaving. Unlike the looping of threads, weaving uses a crossing of threads in a bidirectional manner called warp and weft. This crossing pattern promotes an efficient use of material and effort resulting in a much larger and tighter finished product and one that is more resistant to rain and wind. Because of the nature of the woven textile, it is likely that the large textiles used in the first huts and shelters utilized this technique. However, due to the looping process, the warp threads must be tied off. Here, the looping and knotting techniques are reintroduced at the fringes. As a result, these techniques work in tandem and each textile procedure is used for the expressed purpose while maintaining an artful approach to the end product.



Figure 8. Naalebinding using manila rope.



Figure 9. Naalebinding using sisal.

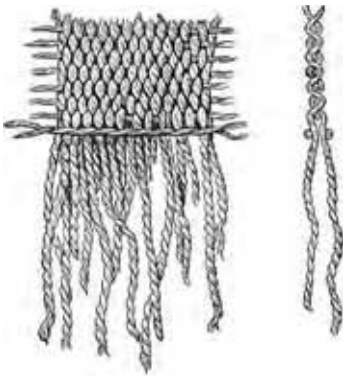
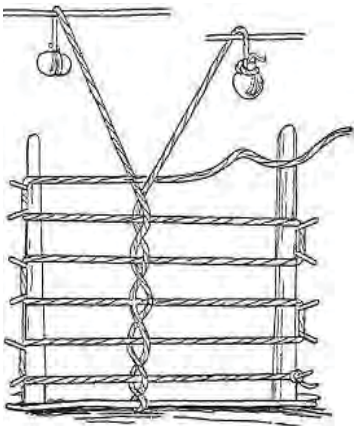


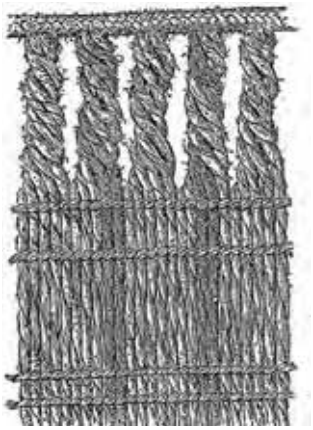
Figure 10. Untied fringe from a woven textile.

As peoples, tribes, and cultures began to develop, the nomadic hunters and gatherers settled into an agrarian lifestyle. The use for textiles as shelters shifted. No longer did the shelter have to travel with them. Instead, their lodgings became more permanent. Alongside this radical shift of living was the development of certain machines to aid in the daily chores. As with all invention, the introduction of new tools shaped and influenced man's environment and, ultimately, his thinking. As soon as inventions began to supplement a laborious task, these early peoples adopted it in order to apply energies to other areas of life. This is where technology finds its place — alongside the endeavors of man, and a simultaneous evolution born out of necessity. This wedding of tool to augment activity is found in the early needles of the Naalebinding. But with an increased complexity in the processes of weaving, comes the creation of the manual loom. This relatively innocuous device, steeped in a tradition of textile fabrication, is at the heart of great tapestries, fine silks, and more unexpectedly, that of a digital revolution.

DOMAINS: FROM ANALOG TO DIGITAL

All textile fabrication, regardless of its style, uses a set of rules in order to execute the specific works. Although many use the terms like Weaving, Naalebinding, Crochet, and Knitting interchangeably, they are all very different in both procedure and execution. The latter three are primarily hand techniques using simple hooks or needles, whereas weaving uses many threads and requires a jig and, for larger textiles, a laydown space. This looming process is systematic and follows a distinct set of procedures in order to achieve the final woven product.





Figures 11 and 12: Examples of early loom for twisted weaving prior to weaving shuttle.



Figure 13: Ground loom operation by woman.

In the first incarnations, these hand and ground looms were used to weave fabrics for rugs and tented enclosures. As cultures and societies developed into large civilizations, the demands for textiles grew. With this evolution in human ecology, people continued to invent new contraptions for various things, including more robust textile machinery. As the weaving looms evolved, so did the complexity of the patterns. With the onset of these complex new patterns and high demand of the population, weavers became overburdened, resulting in mistakes and delayed product. As a result, the need for a new approach to this process was essential, and in the late 18th century, the first semi-automatic pattern-generating loom was created.

The inventor of this complex loom, Basile Bouchon, was a textile entrepreneur and the son of an organ player. His machine created detailed arrangements by employing a long scroll of perforated paper, borrowing the concept from brailed music boxes. The holes in the paper held needles in place as the weaving shuttle moved back and forth, resulting in the development of a pattern that was extraordinarily difficult to achieve by hand. As with many inventions, the problems solved gave rise to new demands, which pushed the loom to evolve. Jean Baptiste Falcone, Bouchon's assistant, replaced the perforated rolls with solid punch cards to eliminate errors produced by the tearing of the paper. Innovation continued at the hands of Jacques Vaucanson, who attempted to automate the process, an effort that remained unsuccessful until Joseph-Marie Jacquard.



Figure 14: Bouchon Loom. Image by Dogcow, CC BY-SA 3.



Figure 15: Punch cards in operation



Figure 16: Jacquard Loom By David Monniaux, CC BY-SA 3.0.

Known today as the Jacquard loom, this machine was the first to autonomously compute and execute a pattern using punch cards arranged in a long band. This series of solid cards enabled the binary rules of over and under to be executed without the need for any human intervention. Through the years, textile machines became more efficient and even more complex. With the push for mechanized automation, along with the application of binary logic, these procedures, steeped in the making of textiles, were appropriated to program the first complex calculators.

Originally the size of entire rooms, these enormous computers could do highly advanced calculations using punch cards—the very same technology stemming from the perforated paper used by Bouchon. During early stages of the Apollo missions, there was an issue in guiding the lunar modules on the dark side of the moon. Engineers at Raytheon, along with mathematicians at MIT, developed a concept for coding programs that would automatically guide the craft, which became known as the Apollo Guidance Computer.

This array of modules stored programs of Read-Only Memory (core rope memory), which was created by the threading of copper wire either through or around a magnetic transistor in order to code the program. When the copper wire is threaded through the transistor, the code is read as a one (1), but if around the transistor, a zero (0). In order to fabricate these modules with the required consistency and precision, workers experienced in fine weaving and lace were hired to weave these complex programs. This technology was called LOL memory, an acronym which stood for Little Old Lady. Regardless of the name, the fabricators of these modules are celebrated for their works not only in textiles, but in the advancement of digital technology.



Figure 16. A textile worker weaving the core rope memory. Aka "Little Old Lady" Memory.

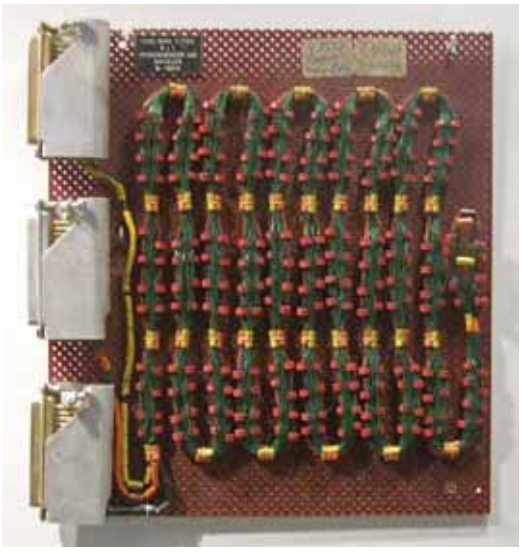


Figure 17: Example of core rope memory module completed.

Ultimately, LOL and core rope memory were the foundation of the digital revolution. The lineage of today's ubiquitous smart phones and micro-circuitry can be traced back to the beginnings of a rule-based fabrication of the earliest textile techniques — over and under, yes and no, zero and one. It is with the aid of the machine, in augmenting effort, not replacing it, that man has been able to prosper. Without the textile to define the set logic and process, the development of such advancements would not have been possible. So what can be learned from this? In a world seemingly split between a physical and digital environment, perhaps we should look into what the textile can teach us relative to the virtual world it helped create.

A CONSEQUENCE OF INNOVATION

As mentioned previously, the introduction of any new paradigm demands the attention and full involvement of its creators. The digital revolution is no exception. However, unlike previous technological advancements, this new digital environment has the ability to draw one in so deeply that the physical experiences and haptic nature of the material world are transformed into novelty — a secondary stage in which virtual experiences operate. With digital technology developing at light speed, its influence on the evolution of the built environment is astonishing. With this comes risk, as Semper described shortly after the industrial revolution: "Innovation and implementation of new technologies would enable us to rise above our past. It is imperative that these means and techniques be used to their fullest extent. Failure to understand and master new technologies, while applying critical judgment to the result, will only lead to the rapid regression of our culture." With the unchecked usage of the digital tools in conceptualization, design, and development of architecture, these concerns are just as apt today. Regardless of the digital domain, the built environment consists of real materials and exists as manifestations of physical reality. Therefore, a balance of play must be found between both the physical and digital environs.

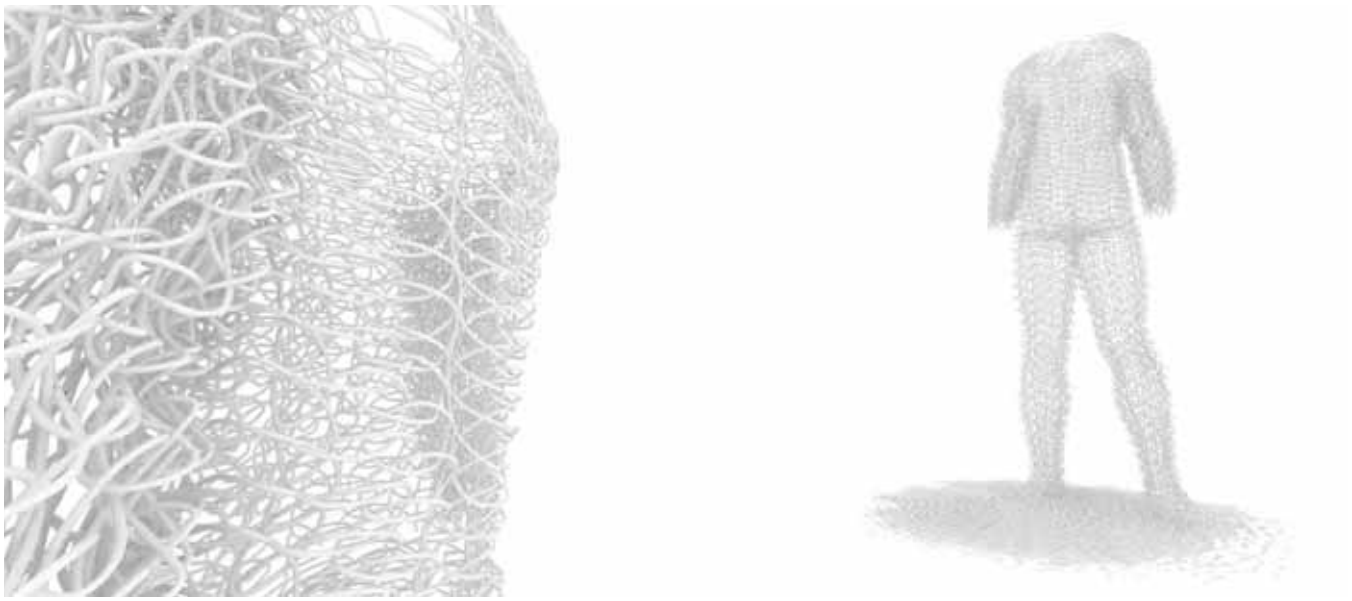


Figure 18. Exploration of digital crochet wrapping over the form of a human male using Rhino 3d/ Grasshopper. Once the parametric model is "baked," it is no longer parametrically pliable.

EXPERIMENTATION: AUGMENTING TEXTILE AND PROCESS

In the encouragement of the virtual, there has been a push, as with all new technology, for its immediate and prolific application, especially in architecture, where digital programs are used to generate form and document the construction methods. Due to the immateriality of simulations, along with the ability to suspend the laws of physics, this new territory of digital exploration encourages the development of wild, implausible, self-intersecting forms. However, to heed the warnings of those before, it is critical to approach the use with feet grounded in physical reality. By doing so, a playful game between the analog and digital begins. The analog, specifically that of textile modeling techniques, can aid designers in the conceptualization of form and surface, while the role of the digital tool is utilized to augment the result. Here, the textile is established as the generator of form and concept, steeped in a deep history of materiality and technique.

By tracing the lineage and history of fiber techniques, it is clear that the exploration of these textile techniques is limitless and can lead to new and astonishing innovations. Similar to the Apollo missions, it is important to actively explore all domains in order to arrive at a method that engages the capabilities of the software and the techniques so that the two work in concert. In studying the lineage of the built environment, it is a small leap to apply these early techniques in the definition of space, form, and enclosure.

Due to the varying styles, there are many textile techniques that can be utilized, but it is important to understand how the elemental concept of looping fibers can lead to a new application of modeling in architecture. With that, one can look to Naalebinding and its cousin, crochet. Often seen as a handicraft and deemed to be a simple pastime or folk art, in recent decades, crocheting has become a powerhouse of exploration in advanced modeling of complex mathematics and geometries. In 1997, Daina Taimina, a Professor of Mathematics at Cornell University, was the first to realize crochet's unique capacity for fabricating complex geometries, specifically the negative curvature of hyperbolic surfaces. She realized that the mathematical formulas for these surfaces could be translated into a crochet pattern. This was achieved by looping a stitch into the same space twice in an exponential pattern, resulting in a pliant hyperbolic surface.



Figure 19 and 20: Generative techniques in crochet enable the fabrication of hyperbolic geometries. Figure 21: White threads are actually parallel on the hyperbolic plane.

From there, this technique of using computational formulations and translating them into crochet patterns took off in the fiber arts and mathematics communities. From these explorations in hyperbolic geometries, others have exploded how digital models can be transformed into a pattern or code and crocheted by hand. As a result, this augmented process creates a dialog between the digital script and analog fabrication. It is not solely a top-down or a bottom-up process, but rather recursive middle play where technique drives the digital pattern, and the pattern results in the physical model.

From these interesting crocheted forms, the jump to large structures and spatial architecture is no different than that of any modeling method using basswood and foam block models. Unlike these typically static model-making techniques, crocheting and other textile techniques like knitting, knotting, braiding, and weaving, find a balance between the analog models and the digital programs. They metabolize the pliant fiber models into defined architecture. Within both the physical reality and digital environments, there are two distinct categories of operation that can be utilized for experimentation—Generative and Transformational techniques (Rahim, 2007). Though these techniques were first defined within the realm of the digital, they apply to the pliant fabrication techniques of the material world as well.

Generative techniques are the coded, rule-based applications that inform the development of the structure. An example of this is the looping, weaving, knotting, or braiding of fibers, which result in the creation of a product that is inseparable from the technique used to create it, such as the crocheted hyperbolic surfaces. In action, a square, triangle, and circle evolve through the application of exponential loops into hyperbolic versions where the base geometry is coded into the final product.



Figure 22. Examples of generative process in crochet. The base forms are transfigured into hyperbolic versions. Figure 23: Hyperbolic Enneper surface in Rhino/ Grasshopper3d.

Transformational techniques are quite different and are the geometric or force manipulations acting on a defined form. This process is applied to an object and is an external operation. Some examples are stretching and pleating. Here, the forces applied to the specimen are bound by the generative process but have the ability to force the reconfiguration of the material and its base code. A prime example of this is observed in the overstretching of a crocheted tube. In the overstretching, the slipstitched loops reconfigure themselves, giving rise to a new pattern and optimized structure, that of a triangulated diagrid

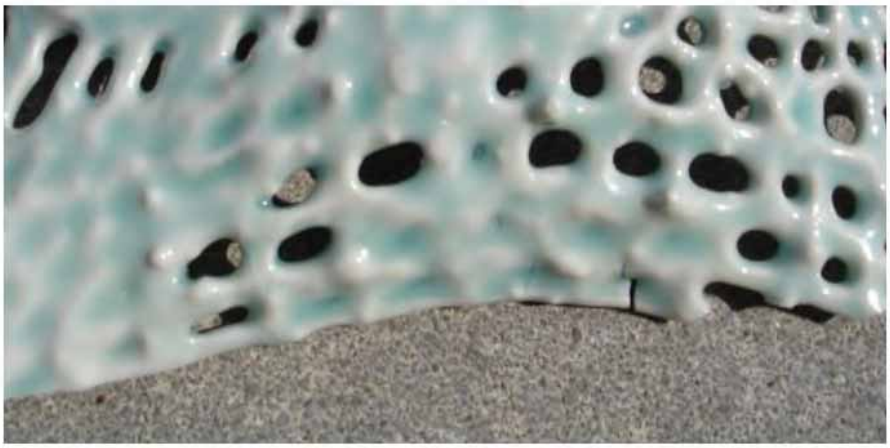
arrangement. This transformation of pattern and its overall result enables the designer's decisions to be steeped in a material intelligence rather than the superimposition of a gridded configuration on a form.



Figure 24: Stretching experiments (over rolling pin) using a slipstitch crochet in acrylic thread results in a reorganization of the crochet structure similar to that of a triangulated grid.

Using these methods promotes a playful approach to material and technique while operating in the tactile domain of physical space. However, other notable techniques use the application of a liquid agent to aid in the development and exploration of form and structure. An illustrative example is that of Frei Otto's wool thread experiments, by which a kaleidoscopic grid of threads are bound by a ring, loosened then dipped in water. The surface tension of the water pulled the threads to one another, creating a natural result, one that can only be achieved by allowing the playful interaction of the frame, threads, and liquid.

Another way of using fibers and liquid agents to explore more practical applications is by the immersion of a textile system into a hardening substance like lacquer, plaster, or porcelain. By doing this, the pliant textile is embedded with new information from the liquid agent. In lacquer, the liquid hardens the threads together resulting in a still flexible surface, but it has a memory of the form in which it cured. The plaster example hardens completely, but similar to fiberglass, has an increased strength due to the wedding of the two materials. Finally, the porcelain agent, when dipped multiple times, results in a porous structure that only references the basic pattern of the original textile. Similar to the nomenclature of the digital tools, when baked, the fibers surrounded by the hardened porcelain are burned out, resulting in a hardened ceramic structure. Though it has lost the pliable nature of the textile, the overall form and effect are informed by the original.











Figures 25-27: Experiments in hardening of crochet textiles using porcelain slip and plaster of paris. Figures 28 and 29: Lacquer agent used results in embedded memory of crochet threads.

These experimentations are the embodiment of Semper's Theory of Stoffwechselthese or Transmaterialization, where, through processing, the concept or manifestation of one material, specifically textile, is appropriated by that of another. Through this metabolic process, Semper stated that "all operations in textile seek to transform raw materials with the appropriate properties into products, whose common features are great pliancy and considerable strength, used as pliant surface to cover, to hold, to dress, [and] to enclose..." In today's digital age, this application of exploration occurs in both realms of the virtual and physical realities, and the processes used in the fabrication of the built environment have the opportunity to oscillate between these two realms. The results of this interactive play from handicraft techniques, augmented through the application of the digital proxies and tools, lead to fantastical textures, forms, and spaces.

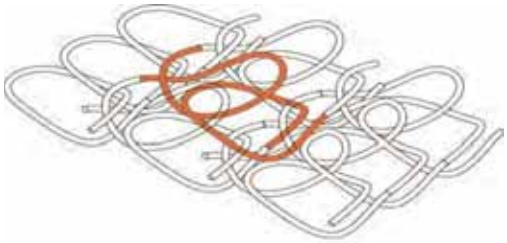


Figure 30: Diagram of slip stitch and base module used in the digital array.

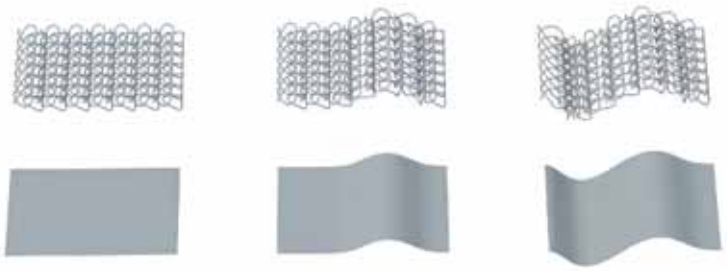


Figure 31: Mapping of modular array to undulating surfaces in Rhino/ Grasshopper.

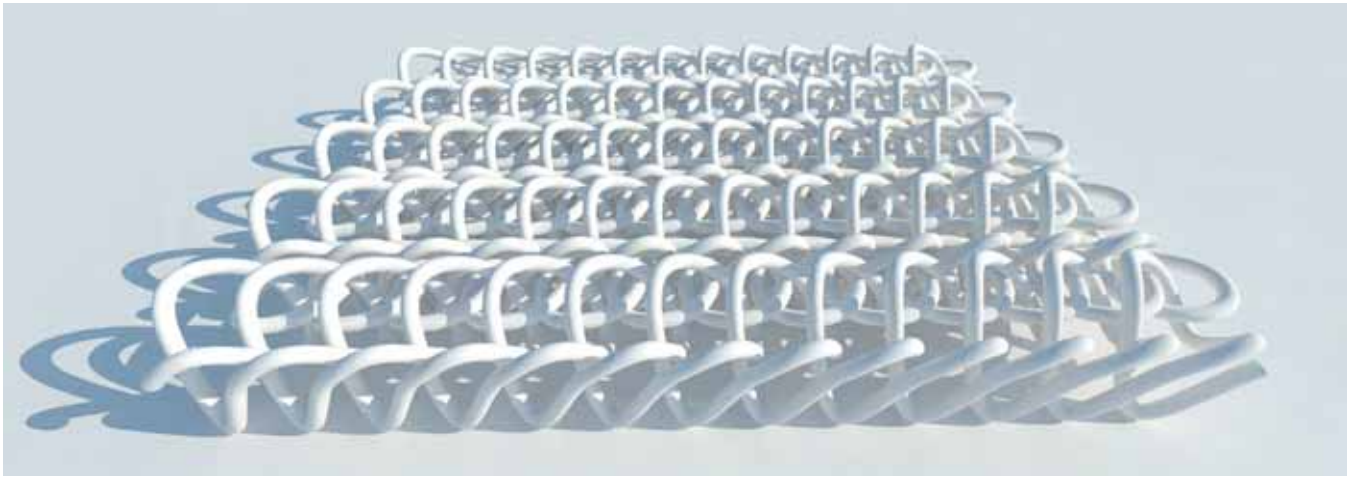
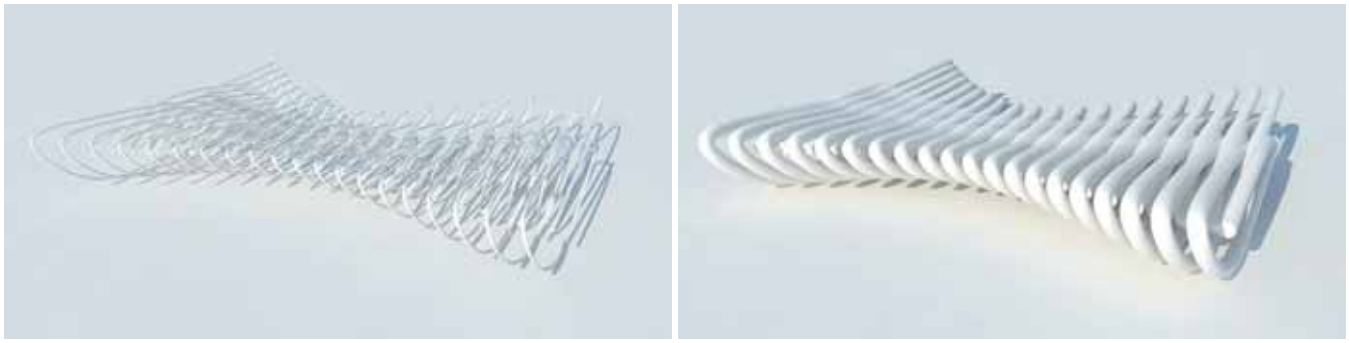


Figure 31: A digital simulacra of a crocheted slip stitch arrayed in Rhino/ Grasshopper.



Figures 32 and 33: Experiments in scalability based on point attractors.

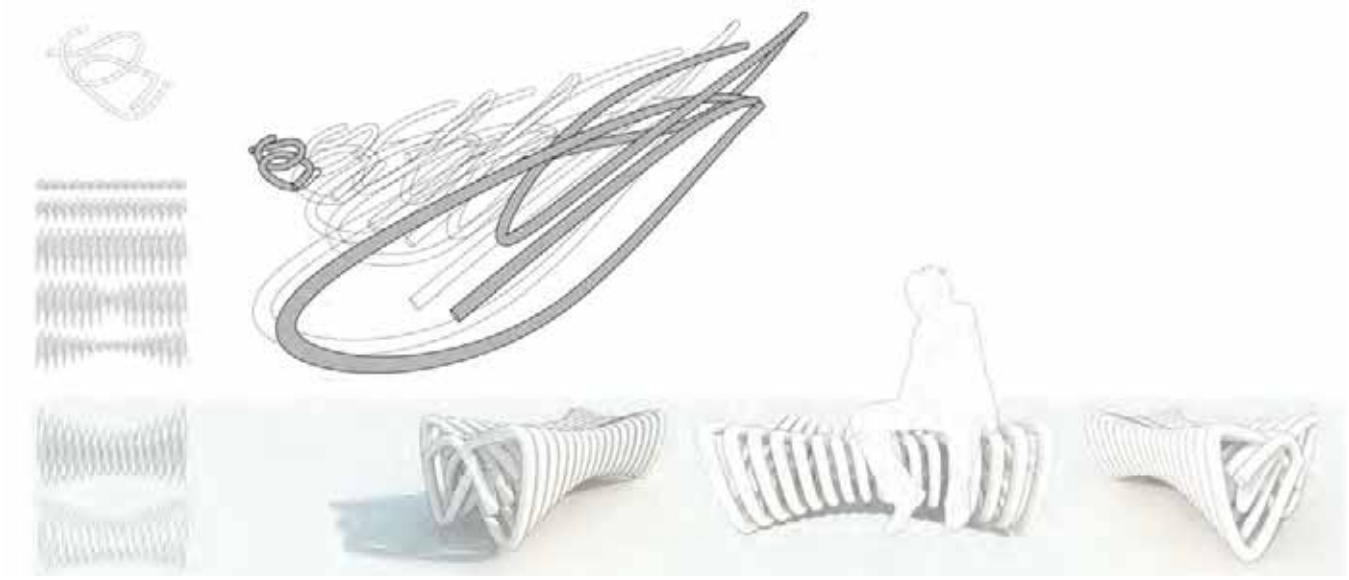


Figure 34: A practical example of how the digital crochet experimentation can inform the design and development of an outdoor bench. Though the fabrication methods in constructing the final bench may not utilize crochet, the form, structure, and overall deep decoration of the bench is steeped in the textile process.

Similar to the acting liquid agents, the fluid and parametric properties of this digital domain enables an exploration of a new type of textile. By using a textile technique and material, the digital model is steeped in a material intelligence rather than just being at the whim of the programmatic constraints. The digital setting does enable something that the analog model is not easily capable of — the scalability and suspension of physical properties. Just as Semper suggests, man transmaterialized textile into carved stone, and the Gravettian garments fossilized.



Figure 35-37: Analog experiments in creating new forms and spaces using a jig or formwork to engage the textile and enable the manipulation of the pliant model. In setting these rules, the textile model can be opened, closed, anchored, or stretched. The possibilities are only bound by the designer.

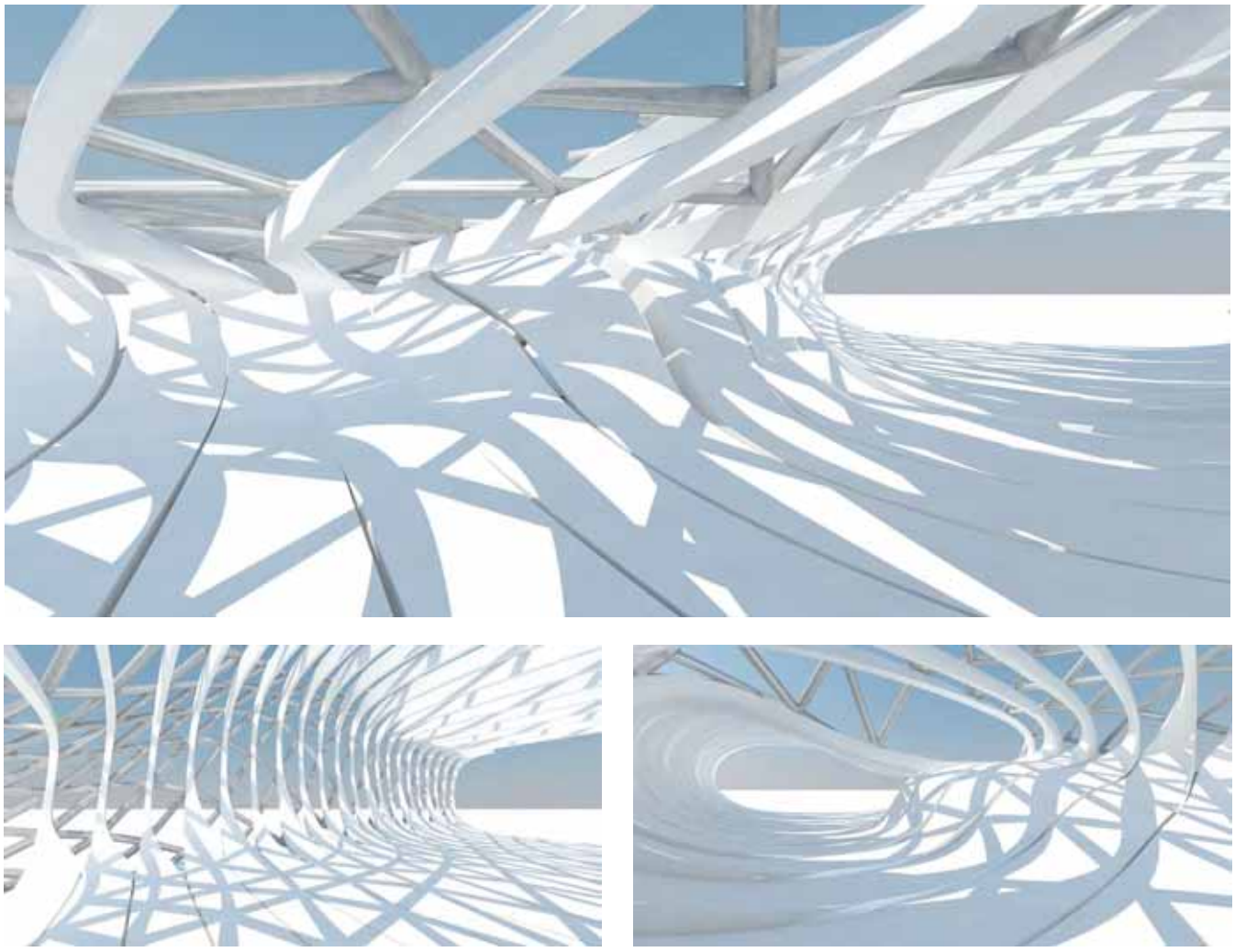


Figure 38-40: Digitized versions of analog experiments similar to those figures above. Using the digital, one can play with testing and visualizing a structure derived from a textile model.

The process of applying a likeness, a relational framing from one material to another, occurs similarly in the digital translation. Dennis Dollens states: “Virtual Space becomes an arena for speculation and contemplation, for testing, turning, warping, morphing and animating spatial sequences that otherwise would remain static graphic images. (The) digital space becomes a contributor to the development of ideas and forms, not merely a passive host to preconceived shapes or prescribed software formats and output (Dollens, D. 2001).”

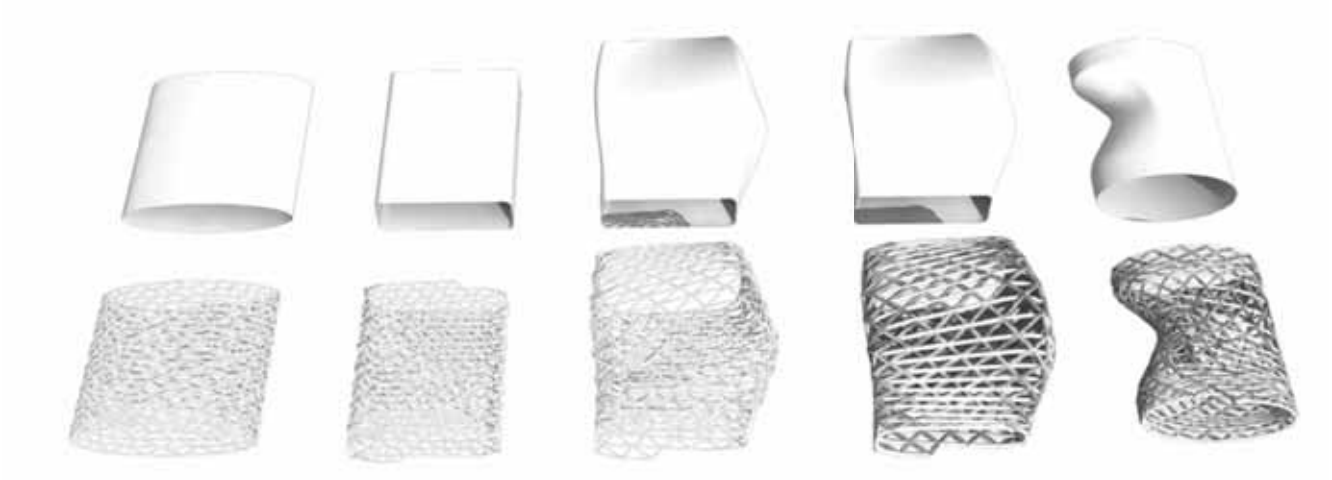
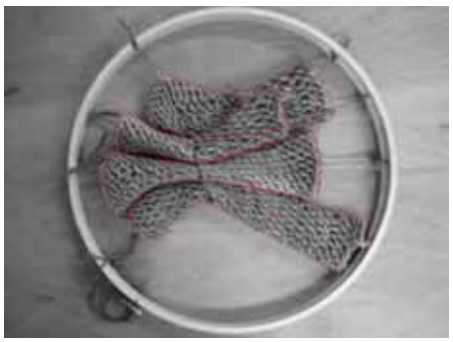
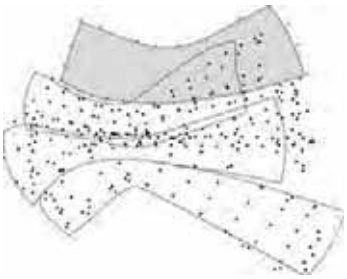


Figure 41: Application of Grasshopper script using the reorganized diagrid from the stretched crochet model.







Figures 42-44: A bundle of organized crochet tubes in a jig are digitized using both photography and point digitizers along with the digital modeling software to develop a virtual version of the analog crochet model.

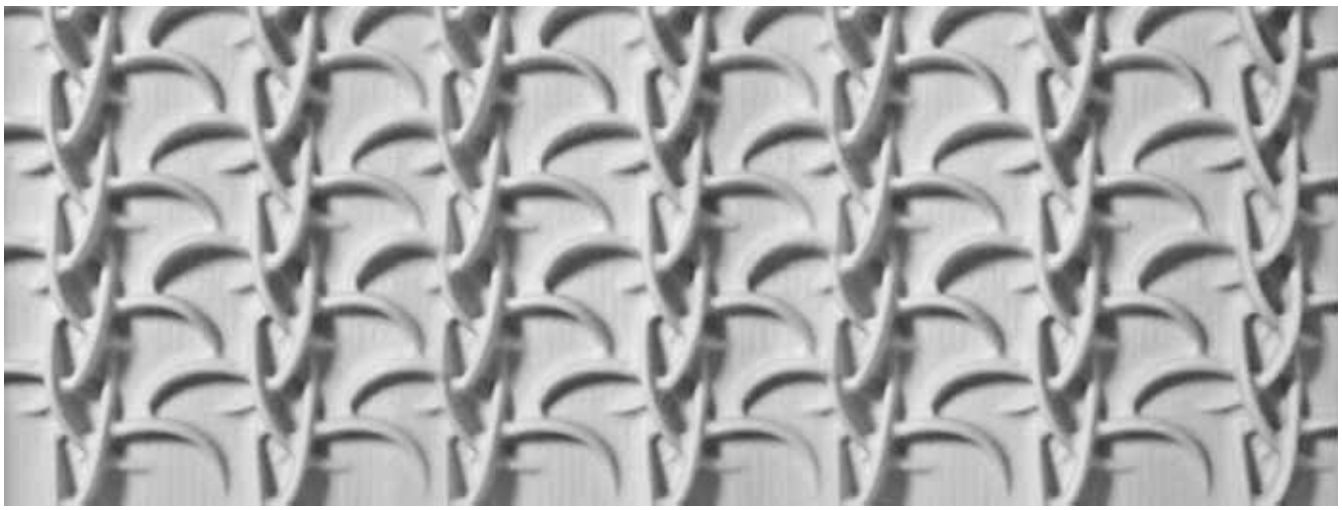
It is important to realize that once digitized, these complex models and structures are at the whim of the capabilities of current fabrication technologies. Scale from model into architecture finds itself with the same problem early peoples did with larger woven textiles. The new inventions create new demand, which results in new machines. With the continual evolution of digital fabrication technologies and parametric tools, designers may find that these textile techniques and handicraft pastimes may not only aid in the conceptualization of their ideas but may be the next evolution in digital fabrication. The key is in the understanding that new inventions are to be used to augment human efforts but not supplement human judgment or intervention. Allowing the rigors of involvement of the human spirit to be sublimated by the autonomic process of the machine or digital environment could quickly lead to what Semper feared — a rapid regression of man and his culture.



EXPERIMENTATION: CONCEPTUAL APPLICATION







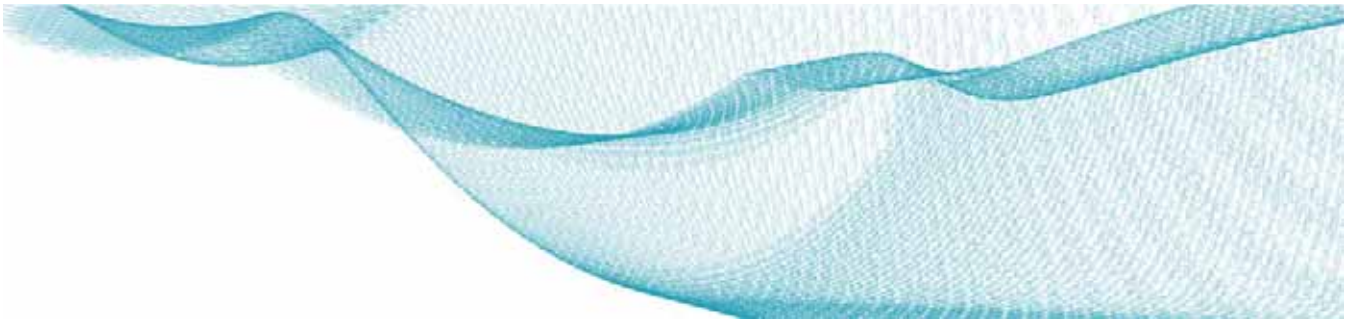
Figures 45-47: Experiments in the use of 3D printing and CNC milling of the digital crochet model. Semper's theory of Transmaterilization in action.







Figure 48-50: Explorations in macrotextiles. Crocheted using various diameters of polyethylene rod. The digital model is not the only platform that enables the scalability but material itself.



THE REAR VIEW MIRROR: A POTENTIAL IN TEXTILES

As man evolves, it is likely that more problems will arise in both the physical and digital environments. With these new tools, it is important to understand their place in the world and understand the history behind them. It's interesting to think that at the beginnings of this digital age, there is a textile machine that derived patterns based on punch cards. When it comes to architecture, it is important to know how to use a tool and the history behind it. There are many things to be learned by taking up sewing, crocheting, weaving, or pottery, beyond the benefits of doing something for the sheer joy of it. These pastimes and handicrafts can aid in the generation of ideas and insights beyond that of design studio. Marshal McLuhan said, "There is absolutely no inevitability so long as there is a willingness to contemplate what is happening." So long as there is continued experimentation, play, and participation in the processes of the physical environment, the door is open to unexpected inspiration and beauty. Some may believe that there is nothing new under the sun. However, man's ability to artfully explore material and his environment has no bounds.

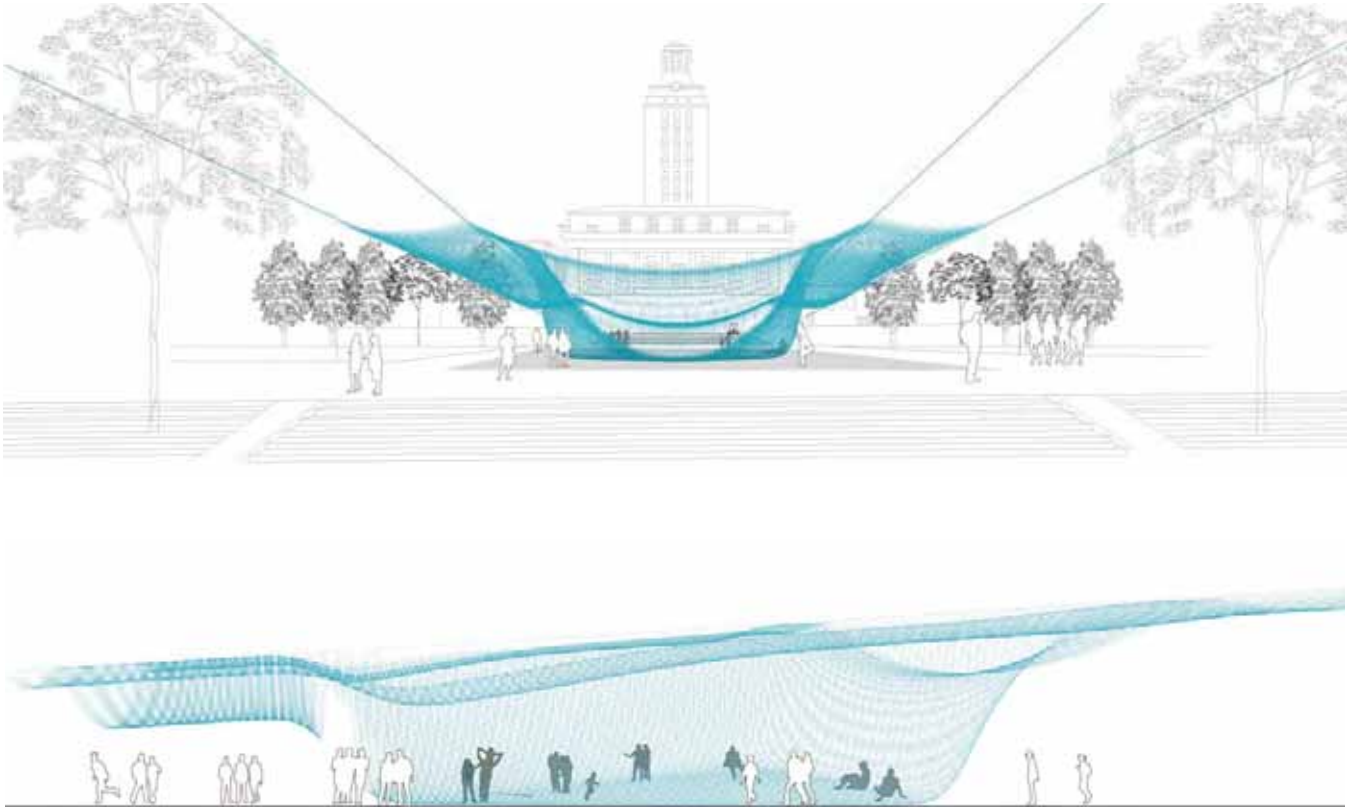


Figure 51-53: Macrotextile installation on a University campus used to promote shade and a gathering place during the spring and summer months.

ACKNOWLEDGMENTS

I would like to thank all those who have supported the application of analog modeling and textiles in the field of architecture and to all who mindfully approach new technologies. This paper is dedicated to Elenora Lahoda, thank you for teaching me how to crochet.

REFERENCES

Dollens, Dennis. *D2a, Digital to Analog*. Santa Fe: SITES, 2001.
Holmes, William Henry. *Prehistoric Textile Fabrics Of The United States*. Smithsonian Institution, 1881
McLuhan, Marshall. *Understanding media: the extensions of man*. Cambridge (Mass.): The MIT Press, 1965.
Potter, Annie. *A living mystery: the international art & history of crochet*. United States: A.J. Publishing International, 1990.
Rahim, Ali. Catalytic formations: architecture and digital design. London: Taylor & Francis, 2007.
Semper, Gottfried. *The Four Elements of Architecture and Other Writings*. Cambridge University Press, 1989.
Taimiņa, Daina. *Crocheting adventures with hyperbolic planes*. Wellesley, MA: A.K. Peters, 2009.

ADDITIONAL READINGS

Ettlinger, Or, Peter Krečič, and Fedja Košir. The architecture of virtual space. Ljubljana: Faculty of Architecture, 2008.
Otto, Frei. IL25: Form Force Mass. Institute for Lightweight Structures, 1990.
Otto, Frei. IL14: Adaptable Architecture. Institute for Lightweight Structures, 1975.
Spuybroek, Lars. The Architecture of Continuity: Essays and Conversations. Rotterdam: V2 Pub. 2008.

FIGURES

All figures are public domain or work of the author unless otherwise credited.

STRUCTURING SKIN

Patterns of integrating cladding and structure



John Neary
Senior Associate, HOK NY
john.neary@hok.com

ABSTRACT

Curtain wall is the prevailing type of enclosure on modern buildings because of its economy, its independence from structure that allows flexibility in design, its thinness that allows maximum usable floor space, and its speed of erection—in short, its expedience. But ever since the appearance of the steel and concrete frame and the curtain wall in the late 19th century, architects have continued to consistently, insistently, render structure, or apparent structure, on the non-load-bearing surfaces of some of the most influential works of modern architecture. Many high-profile contemporary projects have enclosures that appear to be structural shells of some sort, but are really curtain wall on a concealed frame. There are some significant modern buildings that employ structural enclosure systems, most built prior to the end of the 20th century, but they have been outside the mainstream and with limited influence on the conventions of modern construction. Still, their motives and success in integrating structure and skin are worth studying as examples of doing more with the material we incorporate in buildings, as a basis for developing more integrated and sustainable ways of building in the future.

The growing realization of the need for more sustainable ways of building makes the possibility of the curtain wall doing more, as a genuine structural enclosure, something we should explore from functional and formal perspectives.

This study presents modeling of different patterns of full-bay braced panels of a prototype structural enclosure system on a high-rise steel frame tower, showing a significant contribution to serviceability-level wind stiffness. This builds on previous studies of stick-framed steel mullion systems that tested infill spandrel panels and then bracing rods for in-plane stiffness. A variety of bracing and non-bracing panel configurations were modeled to test efficiency and demonstrate effectiveness in various arrangements that imply adaptability to different design constraints and intentions.

The results provide preliminary metrics for integrating cladding and primary structure to economize on steel in the primary frame and on aluminum in the cladding, with roughly 20% improvement in life cycle cost and embodied carbon in the primary structure and the enclosure compared to a conventional base case. At the same time, the structural details and mix of structural and non-structural panel types creates an animated façade, expressing function in form and speaking to our evident desire to see structure revealed.

In sum, building skin represents a significant amount of material that should, and can, be utilized as part of the structure.

KEYWORDS

structural skin, integration, embodied carbon, steel facades, unitized curtainwall, megapanel, history of facades

INTRODUCTION

“A skin always remains a skin...Whatever its virtues may be, it can never assume the natural primacy of structure. Structure is obvious, basic, and irreducible. It is the perennial source of strength, the spring of clarity. Even when it may seem ugly, it is never false (Cossutta, 1966).”
A. Cossutta

“If we do more with less, our response will be adequate to take care of everybody (Fuller, 1971).”
R. Buckminster Fuller

INTRODUCTION: INTEGRATING SKIN AND STRUCTURE

With the exception of the intentionally neutral gridded glass skins of the International Style of the 1950’s and 60’s, which provoked the Post-Modern historicist movement and the sculptural experiments of Brutalism in reaction to their monotony, modern architecture has often included an effort to express or to represent structure, and its modulation and scale, on what is really the non-load-bearing surface of the curtain wall. Curtain wall, made up of lightweight, usually aluminum mullions spanning floor-to-floor, infilled with transoms of aluminum supporting vision lites and spandrel panels of opaque glass or metal, is the defining exterior enclosure of the modern era. It developed in the early 20th century, following the advent of the steel frame with its economical spans of 30 or more feet. This scale supersedes the individual window or room-size, and the manageable size of individual lites of glass, resulting in the enclosure having a different modulation than the building structure.

We have always, throughout history, seen evidence of the inner structure of buildings on their facades, and we are engaged by this evidence of material substance. This at least partly explains the persistence of the structurally active exterior wall in the modern era, despite the predominance of the curtain wall. The potential of the structural building skin suggested by the model of the airplane fuselage-- an inspiration to early modern architects, especially Corbusier-- has remained unrealized, but it seems to still have a hold on the imagination of prominent architects designing buildings with apparently structural forms and surfaces. We frequently see examples of exterior skins that suggest exposure of the working frame and the taught surface of the shell, the implication of exposed working structure providing the common source of attraction.

This study sets out to intentionally integrate the economic advantages of curtain wall with the potential to economize on material by utilizing its structural capacity-- both to reduce material and embodied energy and to achieve the aesthetic effect of structure that we find so compelling in so many modern buildings that express or expose structure on the exterior.

The investigation presented here shows analysis of a full-bay structural enclosure panel (developed in an earlier study to contribute wind-stiffness to a braced core building frame) in an array of optimization scenarios involving different patterns of structural and non-structural cladding bays on the tower surface (Structural eXterior Enclosure, 2017) (Fig. 1).

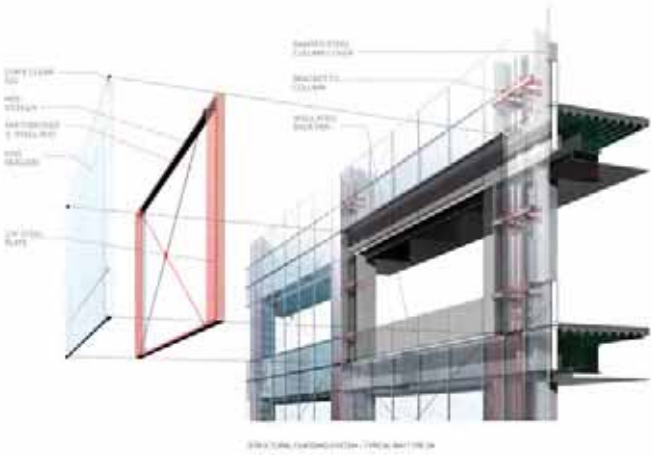


Figure 1: Previous structural bay study, exploded perspective view. Image by HOK.

Different arrangements of structural and non-structural bays are tested to optimize the weight and complexity of the enclosure. The benefits in terms of savings in tonnage of the primary frame and the amount of aluminum in the cladding are measured against a conventional base case (Structural eXterior Enclosure, 2017) (Fig. 2).

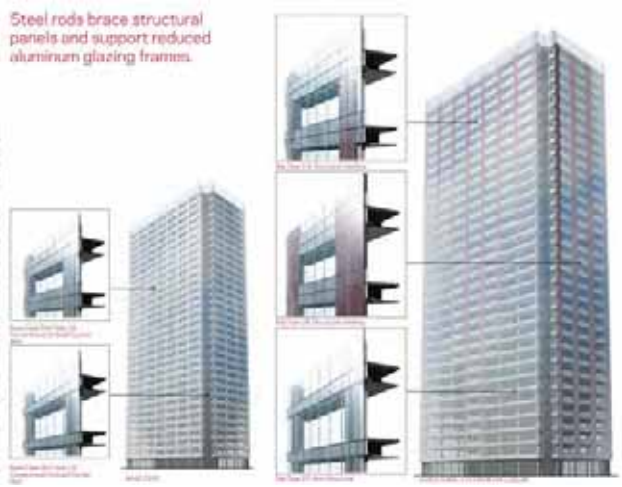


Figure 2: Tower renderings from Structural eXterior Enclosure. Base Case Tower, left. Structural Enclosure Tower, right, with three types of mega-panel. Image by HOK.

The braced mega-panel is a sequel itself to a previous investigation of a steel-mullion and infill bracing system, which showed significant potential for a cladding system to make a significant contribution to serviceability wind bracing on a high rise structure (Structural Skin, 2016) (Fig. 3).

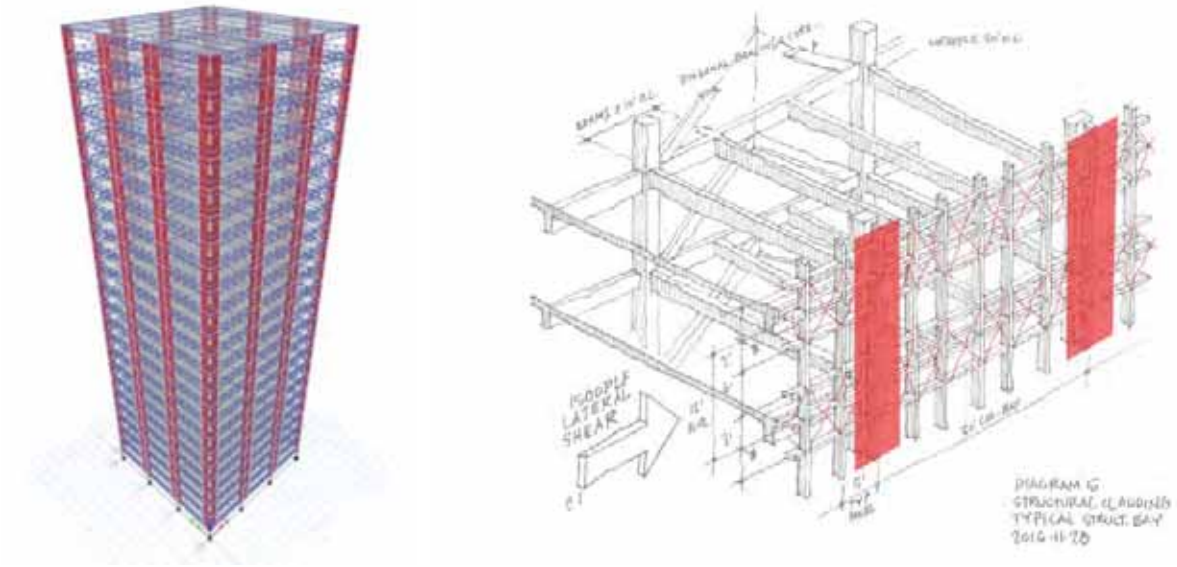


Figure 3: Structural skin stick framed system structural model and typical bays sketch. Image by HOK.

The braced mega panel achieves much greater efficiency, showing promise of developing into an approach with real-world application that could realize improvements over conventional cladding in terms of thermal performance, and in terms of embodied energy of the cladding and the primary structural frame of mid- to high-rise towers. The panel details are based on simple steel HSS frames attached to the slab edges and the columns (Fig. 4).

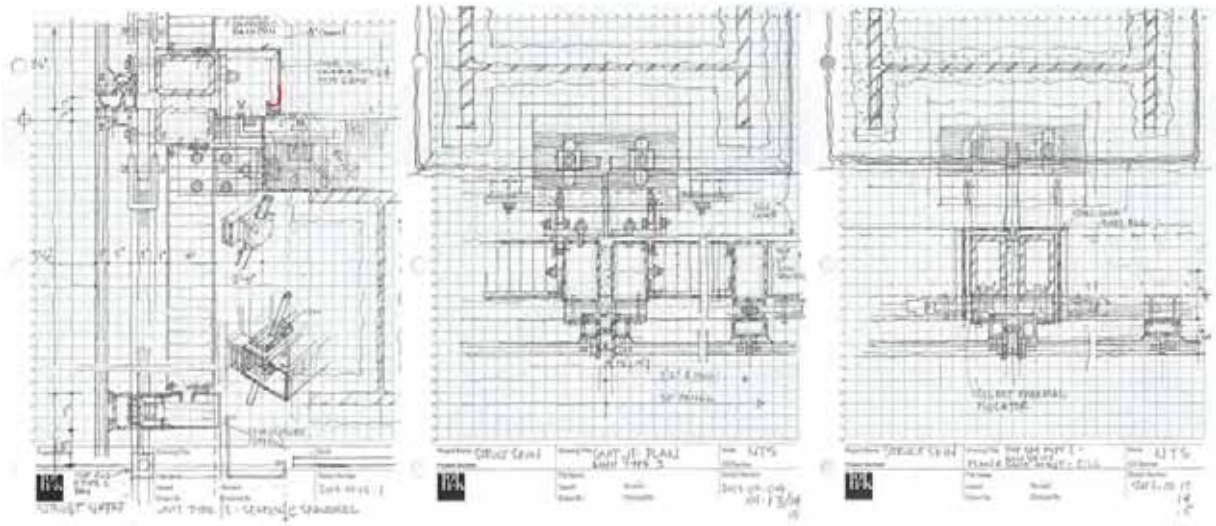


Figure 4: Structural bay section and plan preliminary details; non-structural bay plan preliminary detail.

Studies of the panel connections for the original mega-panel scheme were based on using conventional embed anchors augmented by attachments to the columns along the panel jambs, and standard unit joints in the veneer glazing system (Fig. 5).

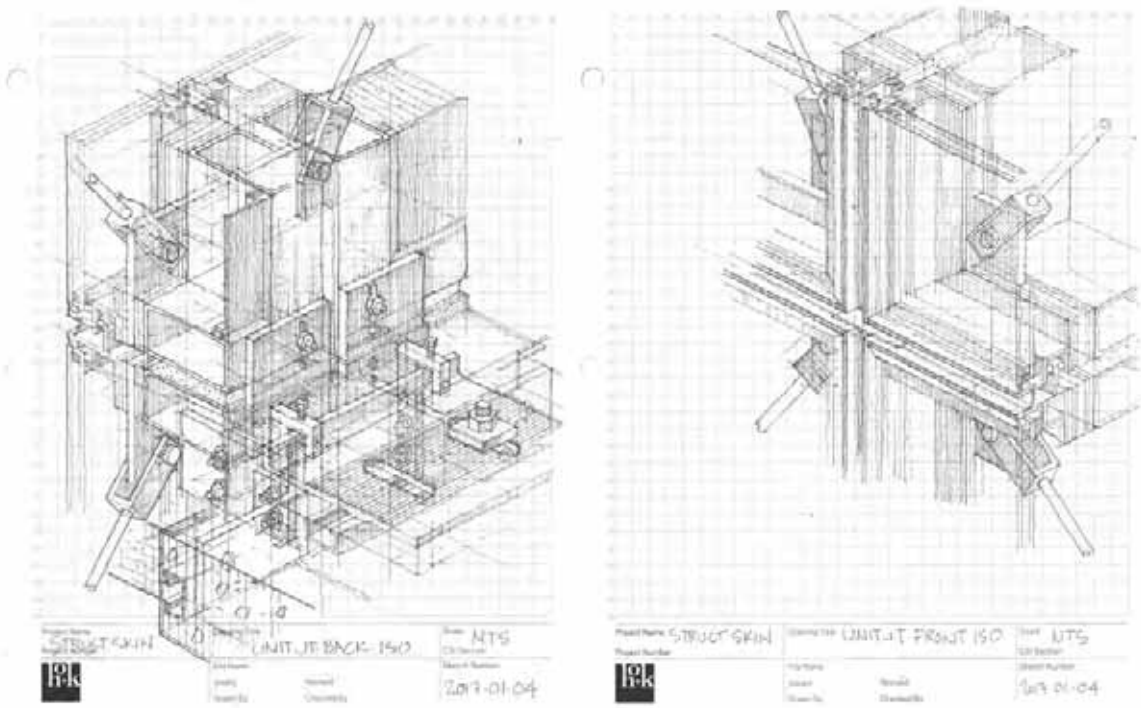


Figure 5: Structural bay connection at slab, axonometrics from interior, exterior. Images by HOK.

BACKGROUND: CURTAIN WALL AND THE RECURRING THEME OF STRUCTURAL ENCLOSURE

Notable examples of modern-period buildings with exposed structure incorporated into the exterior provide a source of practical lessons in what actually works, what has had some problems, and also evidence of the powerful aesthetic motivation to make structure evident.

Louis Sullivan created a reading in the Wainwright Building-- perhaps the first tall building with the quality of real architecture-- of vertical piers to express the vertical 'function' of the form, which doubled the actual number of columns in the underlying steel frame. Neither this apparent structural falsehood, nor the ornate terracotta tracery suggesting the vital force of plant growth as symbol of life itself in figural ornament, seemed to violate Sullivan's notably high sense of principle in expressing the natural function of form. It was not utilitarian minimalism that he advocated, but a purposefulness that suggested, perhaps figuratively, the functional basis of structures in nature. For Sullivan, the creative impulse to create order was a legitimate structural function to express in the geometry of the façade. So was the underlying energy of the designing mind, which Sullivan made analogous to the energy in a seed that grows into the flowering plant (Fig. 6).

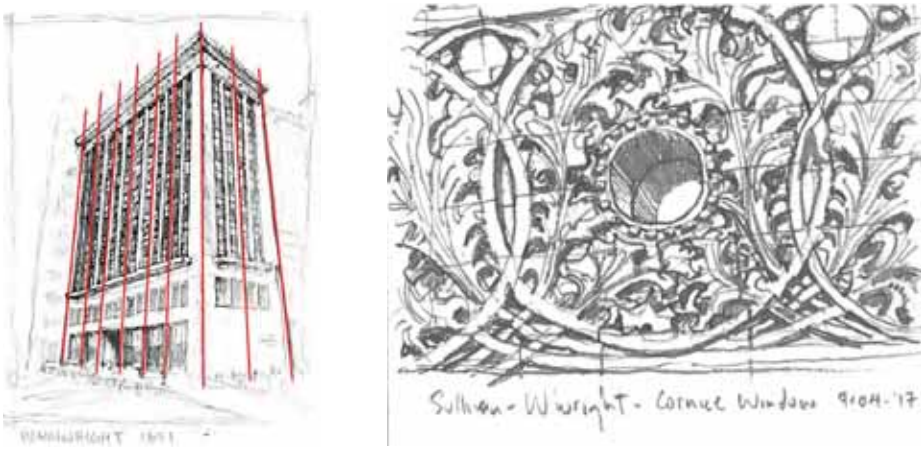


Figure 6: Sullivan-Wainwright view and detail sketch. Red lines indicate structural column bays.

The impulse to deviate from the economy and convenience of the curtain wall persisted throughout the modern period in work such as the stressed skin house prototypes of Buckminster Fuller and the steel-framed facades of Mies van der Rohe's buildings such as 860-880 Lake Shore Drive, Crown Hall and the Chicago Federal Center. Students of Mies, including Jacques Brownson of IIT and CF Murphy, created a body of work in the 1960's known as the Second Chicago School, which influenced real and simulated structural enclosures on tall buildings through the 1970's. The most fully realized example is Brownson's Daley Center in Chicago, which has a stressed skin exterior of Cor-Ten steel incorporating plate glass fenestration that infills between the massive columns and spandrels (Fig. 7).

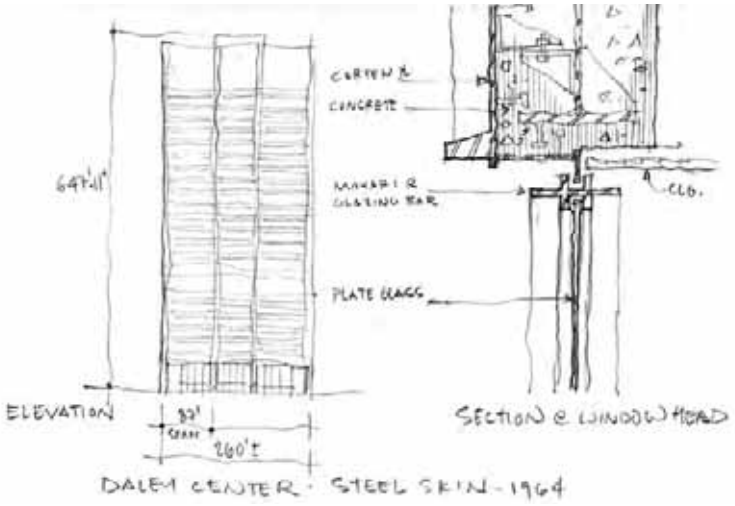


Figure 7: Brownson-Daly Center elevation and detail sketch.

The other side of the coin is the Liberty Plaza in New York by SOM, which mimics the monumental steel frame expression of the Daly Center and has an exposed painted steel spandrel beam protected from fire by a flame shield at the bottom flange—not structural skin, really, but structure as skin, with some extras added. The exterior painted surface is structural, mostly, but lacking the conceptual clarity of its source.

At around the same time the Chicago buildings were exploring exterior enclosures that were not just curtain wall, the influence of Corbusier's massive concrete facades of the preceding few years produced a body of work that included precedent for the framed-tube exteriors which appeared after 1963. The Skilling engineering firm of Seattle, working with architect M. Yamasaki, conceived of the steel tube for the World Trade Center around the same time the Dewitt-Chestnut tower, a perforated concrete tube, was being designed by F. Khan at Skidmore Owings & Merrell. The egg-crate exterior of the marble-veneered concrete box, evoking the Corbusier facades, spoke to the intrinsic aesthetic appeal of integrated structure and enclosure, as expressed by I.M. Pei's design partner Aldo Cossutta. Pei and Cossutta pioneered the exposed concrete bearing wall façade in high-rise buildings in the United States in the 1950's and 1960's.

These buildings were predecessors of the High-Tech school that came of age with the Beaubourg museum, with its exposed trusses and pipe columns filled with water for protection from fire (Fig. 8).

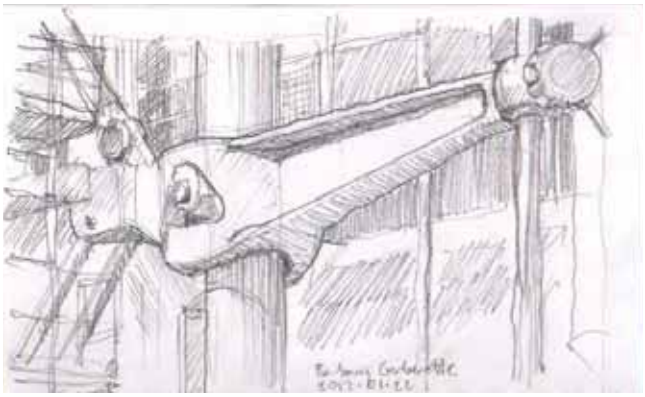


Figure 8: Piano, Rogers and Rice, Beaubourg Gerberette sketch.

High-Tech owed a debt to the ideas of Fuller and Mies, and manifested a romantic interest in the 19th-century industrial constructions of Eiffel and Brunel. High-Tech also saw the reality of structure as an alternative to the monotonous commercial facadism of International Style modernism. But it was expensive and idiosyncratic, if not outright affected in its at-all-cost expression of structure. The steel mullions of Mies' and Brownson's architecture would be enormously expensive to build today, as well as being expensive to maintain compared to conventional aluminum curtain wall. The perimeter tube structure that followed from the 'structural mullions' of Mies had dense, largely opaque exterior surfaces, a drawback avoided in the braced tube and braced core tower concepts that became the most common structural types for tall buildings later.

The structural exterior conceived as a perforated shell—perforated to allow light if not air into the building—underlies the framed tube concept of the 1960's, which developed into the braced tube. It is the conceptual underpinning of other, more bio-morphic building concepts that appear to be shells but usually are not, such as the precast concrete shroud, or 'veil,' of the Broad Museum (Fig. 9).

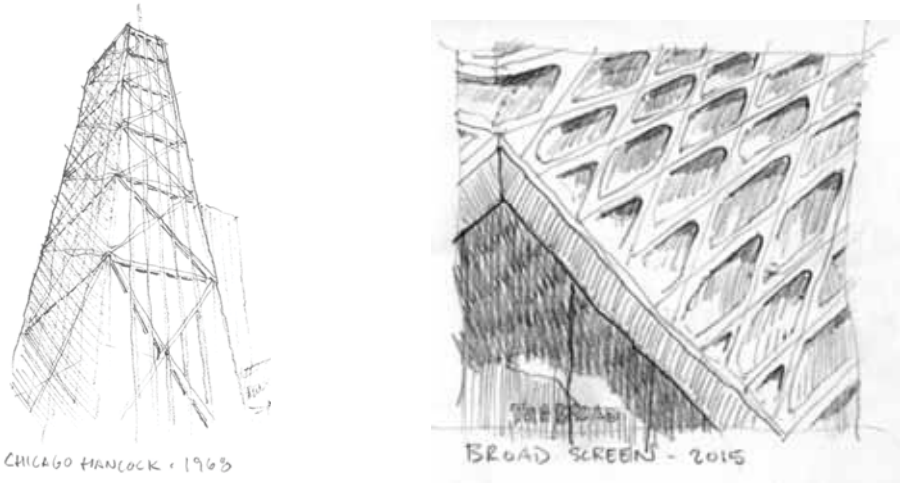


Figure 9: Hancock Chicago, braced tube; Broad Museum detail of GFRC veil.

The pod conceived by Buckminster Fuller as the Dymaxion House in 1930 is an example of a true stressed skin, inspired by grain bins and airplane fuselage monocoque construction. But shells are not robust structures in bending and shear, the forces most encountered by buildings, and the stressed skin has remained a fringe interest in large-scale architecture (Structures, J.E. Gordon, Pg. 312). Despite seeming quintessentially modern in some sense, the streamlined membrane aesthetic is almost exclusively an affectation in architecture. The exposure of structure generally can be seen in that light, defying the economics of the curtain wall by requiring extra coordination, raising issues of fire-safing and thermal bridging, involving expensive finishing of intrinsically heavy and low-tolerance elements. But the underlying motivations, which were sidelined following the eclipse of mainstream modernism by the aesthetic and theoretical interests of Post Modernism in the 1980's, remain with us—difficult-to-articulate reasons we are attracted to seeing structure. Understanding them could provide answers to the problems of creating aesthetically compelling and environmentally sustainable buildings.

The most obvious possible reason, from something like an evolutionary perspective, is that we are attracted to evident structure because it suggests strength, and durability. Durability is the foremost measure of long-term value or economy in construction, despite the modern preoccupation with first-cost and rapid amortization. Exposing structure costs more initially and takes more effort and skill than wrapping a building with curtain wall, but the older buildings in the world usually feature some kind of exposed structure, either mass bearing walls of masonry or timber half-frames. They require maintenance to survive, which means people must care about them, so they must be attractive in some sense—a circular logic of historical survival.

As net-zero operating emissions becomes reality, embodied CO2 equivalents and lifespan will become the primary measures of environmental sustainability in architecture. The integration of structure and enclosure is a way of addressing the significant mass of material in the conventional enclosure that could be put to work to make the core and shell 'do more with less,' in the words of Buckminster Fuller (*Nine Chains to the Moon*, 1938, 1971)—as Fuller tried to do in the Dymaxion. With refinement, this approach could work to fundamentally improve the sustainability of the way we enclose the large and tall building.

The structural enclosure system explored here preserves some of the functional and aesthetic advantages of the frame and the modern curtain wall (in terms of performance and economy) but also engages the skin with the structure to achieve greater material efficiency than is the current norm. Simple and robust surface details would ensure long life-cycle.

STRUCTURAL SKIN

The wall system proposed here is for a high-rise steel-framed office tower (Fig. 10).

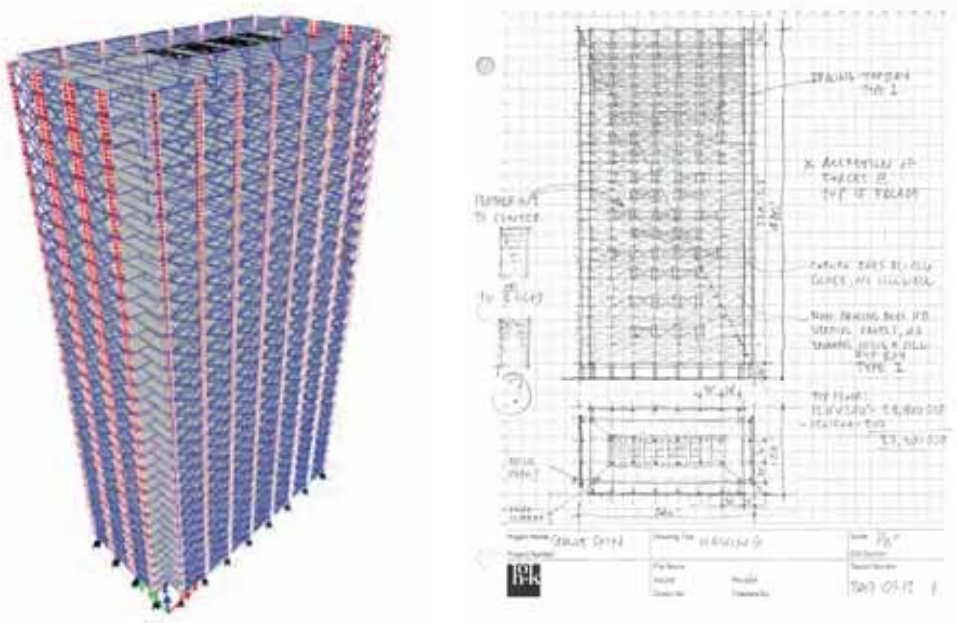


Figure 10: Tower massing with initial full array of bracing, study for optimized bracing pattern. Image by HOK.

The structural skin, maintaining a nominal 8” depth, only provides stiffness to the primary frame in tension. The braced portions of the faces of the tower act as tension membranes, in-plane. The corners of the mass are cut away to emphasize the separate structural action of each planar face. The design exercise began with bracing in every bay of the four facades, then examined subtracting different patterns of bracing to balance strength, stiffness and weight (Fig. 11).



Figure 11: Tower View, speculative urban site at Bryant Park in New York City. Image by HOK.

Working in conjunction with the braced core, the braced skin contributes significantly to the tower's over all stiffness, to limit serviceability level wind deflection (Fig.12).

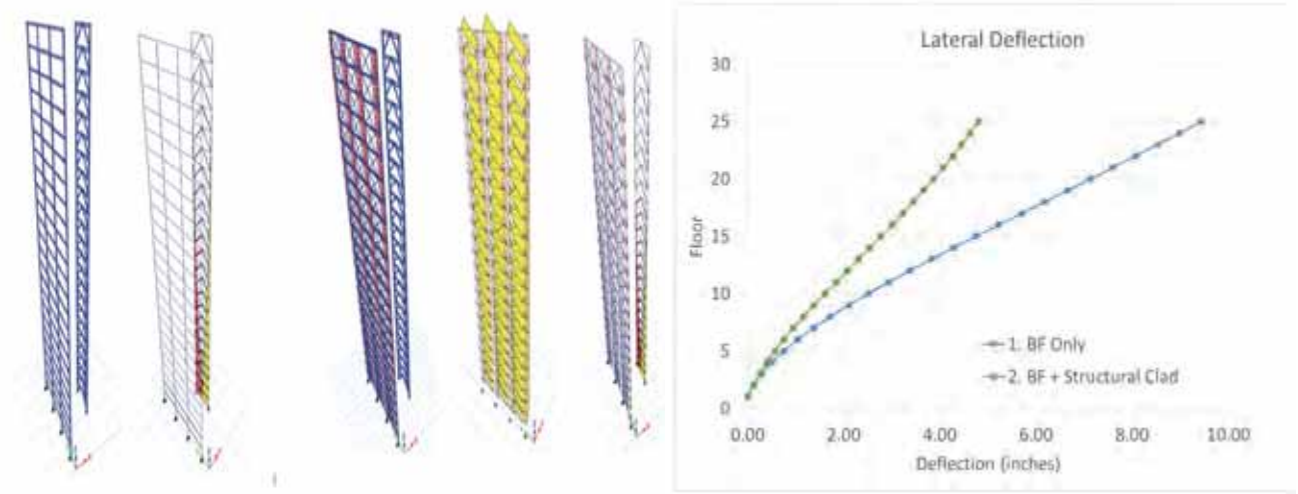


Figure 12: Load distribution diagrams for braced frame and braced frame with structural cladding. Image by HOK.

This study examines a 25-story building with one-bay steel concentric-braced frames and multi-bay structural braced skin. The steel braced frame is 30' wide x 30' deep, located in the center bay of the core. The structural braced skin is arranged in 30' bays on the perimeter. All columns, beams and braces in the primary frame are various W sections. The structural skin framing is composed of horizontal and vertical HSS sections reinforced with steel plate and diagonal rods.

The structural steel braced frame was sized per IBC, ASCE and AISC LFRD specification for strength requirements to resist gravity, wind and seismic loads. The structural skin was introduced only for serviceability and comfort-related purposes, adding supplemental lateral stiffness to resist wind. This means the skin elements do not need to be fireproofed

Linear and nonlinear static analysis was conducted for the braced frame alone and for the braced frame with structural skin to determine load distribution and lateral deflection. The steel braced frame resists over-turning moment by itself, deflecting 9.44 inches at the top floor, while the braced frame with the structural skin work interactively, deflecting 4.88 inches at the top (Fig. 12).

A key advantage of the structural skin approach is the flexibility afforded by the location on the perimeter. The braced frame located in the core is constrained by the limited locations available for bracing dictated by access requirements for stairs and elevators and service spaces. The bracing on the exterior of the tower can create large and efficient expanses of bracing diaphragm.

The multi-bay distributed structural skin bracing increases overall structural stiffness by a factor of 2 by increasing the moment arm of the lateral-resistant structure.

The structural skin is based on a full-bay ‘mega panel’ with a steel HSS frame incorporating shear panels at the jambs that attach to the floor diaphragms and the primary frame columns. A study of efficiency of different configurations of individual panels sized as conventional curtain wall units led up to the full-bay structural mega-panel (Fig 13).

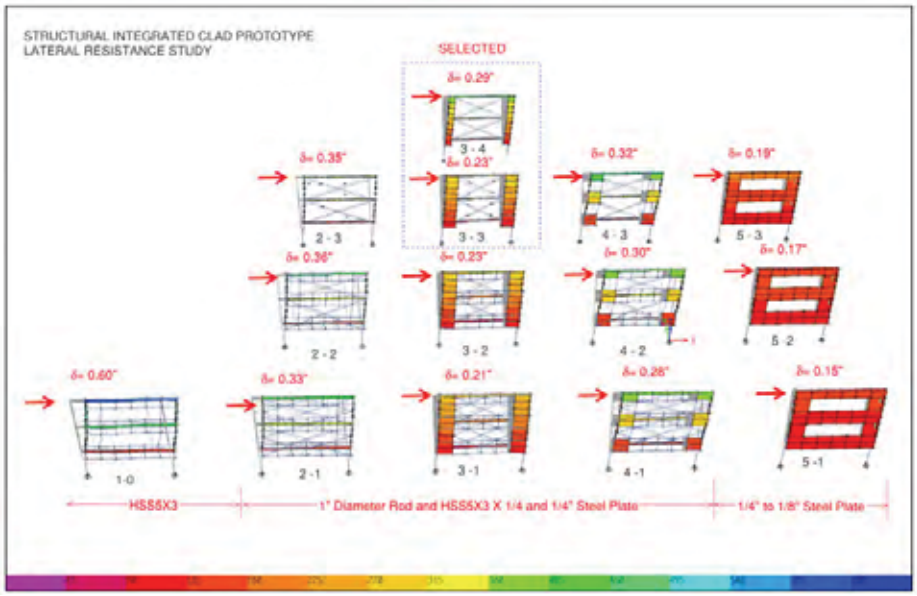


Figure 13: Structural panel prototypes and lateral resistance comparison. Image by HOK.

The top and bottom of the frame attach to the structural slab in a way similar to a normal curtain wall for bracing, but wind load stiffness contributed by the steel panel frame and the 1” diameter cross-bracing is transmitted through the anchors at the corners to the columns by distribution through the shear panels. The cladding system only works in tension so buckling of the thin plate it represents is avoided. (Fig.14).

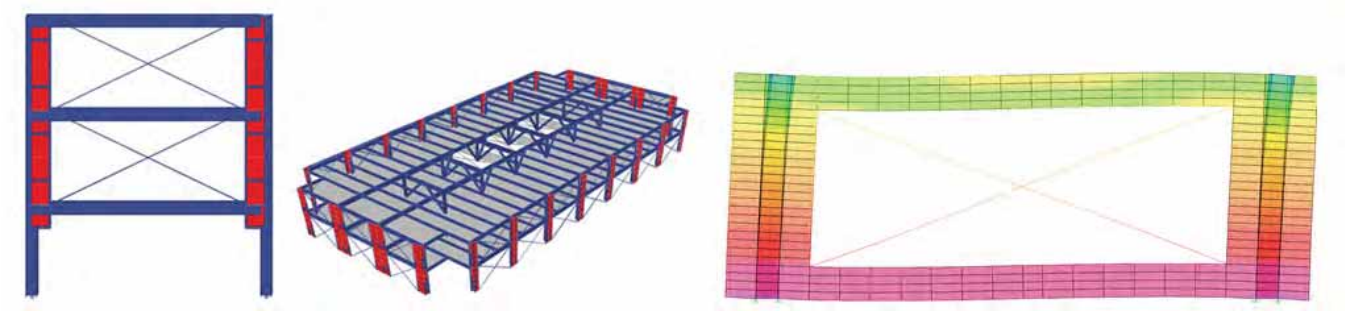


Figure 14: Typical panels, left. Typical tower floor, center. Stress and strain diagram of braced panel, right. Images by HOK.

The quantity of aluminum in the proposed enclosure system is minimized by replacing conventional mullions spanning floor-to-floor with shallow framing braced for wind by the structural enclosure panel cross-bracing.

The structural skin bay is distinguished by the X-brace of high-strength pre-stressed rods that take the lateral force into the anchorages at the columns. The non-structural bays, (resulting from optimization analysis showing that the skin’s benefit in terms of stiffness is offset by its added material at a point below the full-clad threshold), are defined with curved units 10’ wide, that are clearly not participating in the shear-plane of the braced units. While they are not contributing to the primary structural system performance, the curved single-lite units nonetheless have a unique structural character compared with conventional curtain wall, which has mullions span floor-to-floor taking the wind load on the glass. The curvature of the glass

in this proposal would create a natural beam allowing for the shallow mullions to match those braced by the cross-rods in the structural bays (Fig. 15-18).

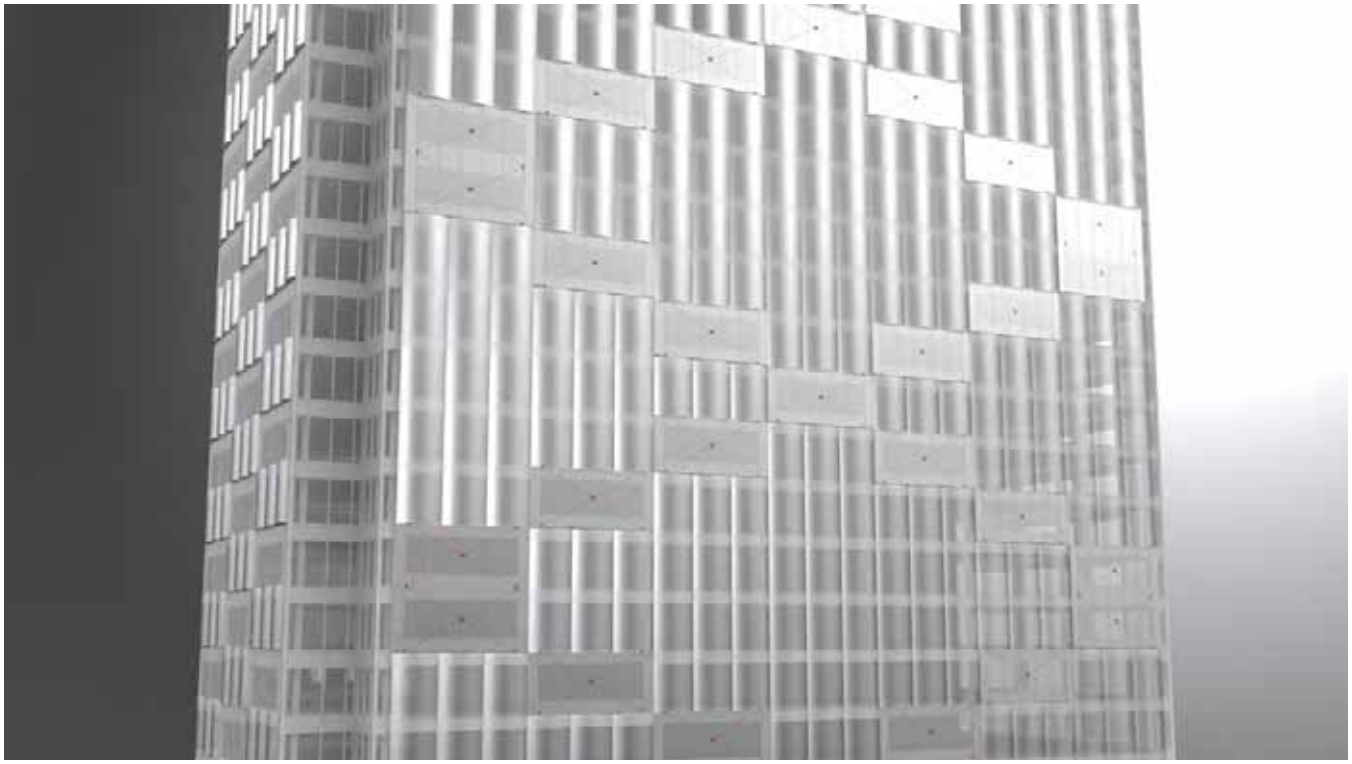


Figure 15: Typical panels, structural with X-bracing, non-structural with bay-window glass. Image by HOK.

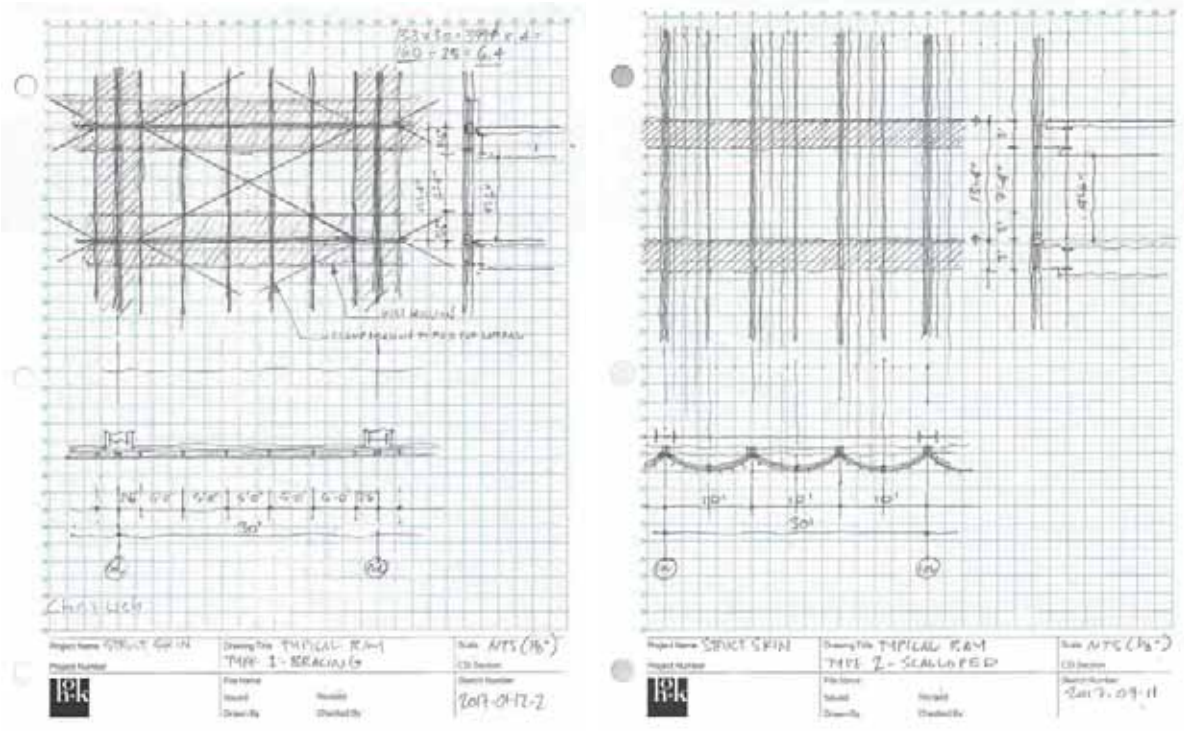


Figure 16: Typical panels plan, section, elevation. Images by HOK.

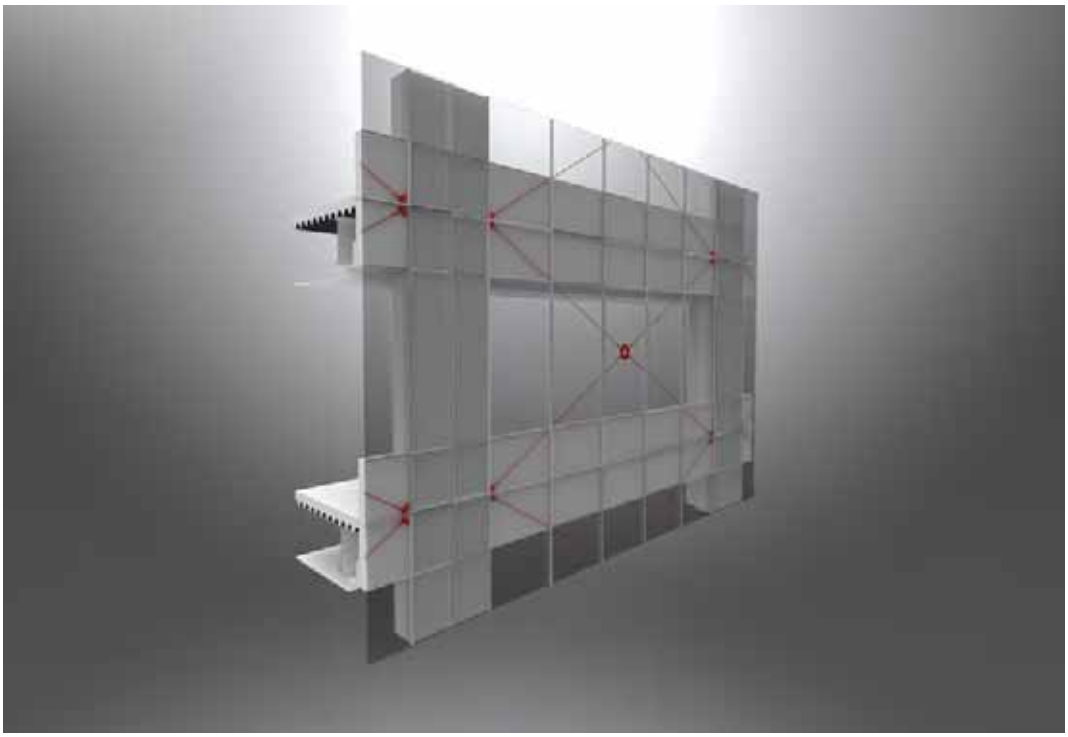


Figure 17: Typical structural panel. Image by HOK.

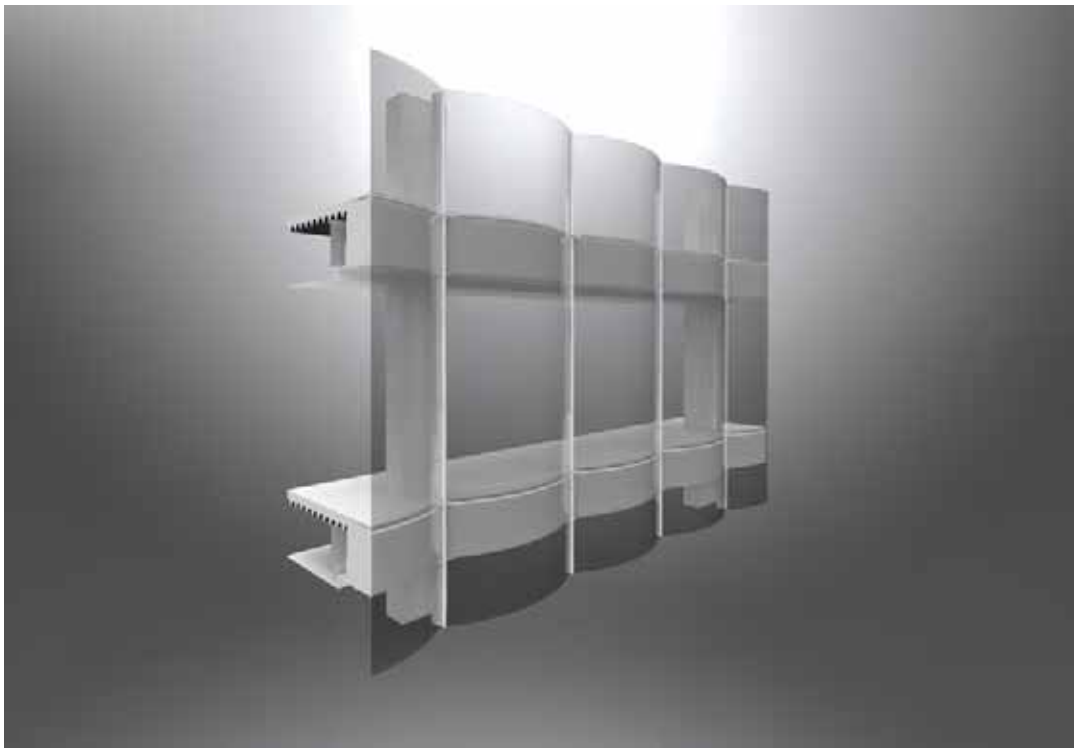


Figure 18: Typical non-structural units. Image by HOK.

Details of the panel glazing and framing, and connections of panels to the primary structure illustrate how structure is displayed through the glazing, keeping thermal bridging to a minimum (Fig. 19).

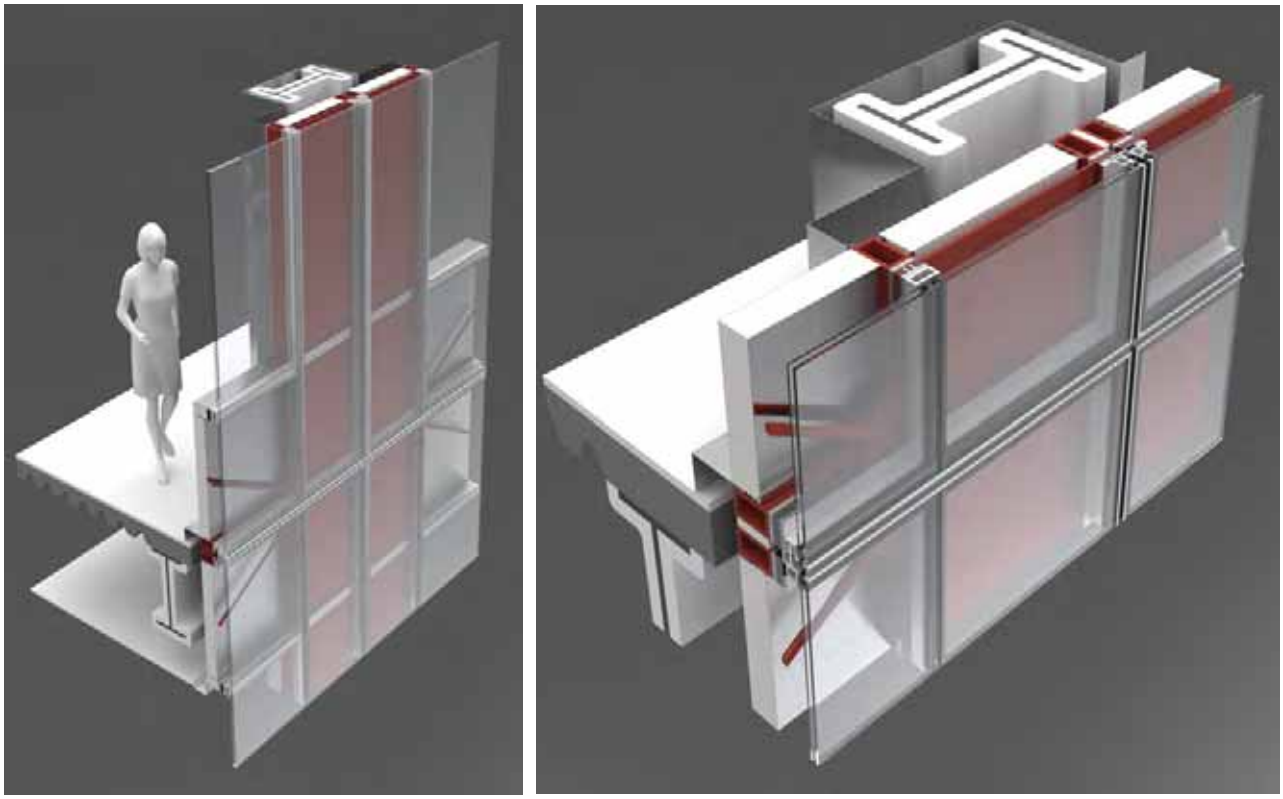


Figure 19: Structural bay connection study. Structural components (steel) are in red. Image by HOK.

COMPARATIVE ANALYSIS OF CLADDING PATTERNS

With an assumed limit on the contribution of the skin to the stiffness of the frame-- so that it does not ever take load required to be handled by fire-proofed primary structure-- the structural bays are only needed in a percentage of the cladding. Disposition of the braced panels is checked for efficiency by analysis of tower stiffness and weight. Structural modeling of a series of different patterns on the elevations of a 30-story prototype commercial office building shows the impact of trading off structural and non-structural panels, with some shifting of material between the enclosure and the primary frame.

The building serviceability limit was set as H/400. Deflections from all systems were summarized for the lateral serviceability performance check. As the building has sufficient braced frames and structural clad frame in longitudinal direction all seven systems showed the satisfactory lateral performance under the corresponding wind load with minor variation. However, in transverse direction the braced frame alone is not sufficient enough to meet the H/400 criteria. It is shown that the structural clad frames with the braced frame provide their lateral contribution to overall performance.

The schemes are modeled in ETABS structural design software. Unlike the original study, a new approach to defining how the skin and frame interact has resulted in an inversion of the accumulation of force in the skin, with higher stresses now appearing as the floors descend rather than, as in the previous study, as they rise.

Mixing structural and non-structural panels can create animated aesthetic effects on the building surface while improving sustainability. The stiffness of the overall structure is determined based on the global layout of the braced panels, as well as the individual panel stiffness, which is driven by the size of the rods. Elevation stress diagrams show the accumulation of forces in the surface structure in the different arrangements tested (Fig. 20).

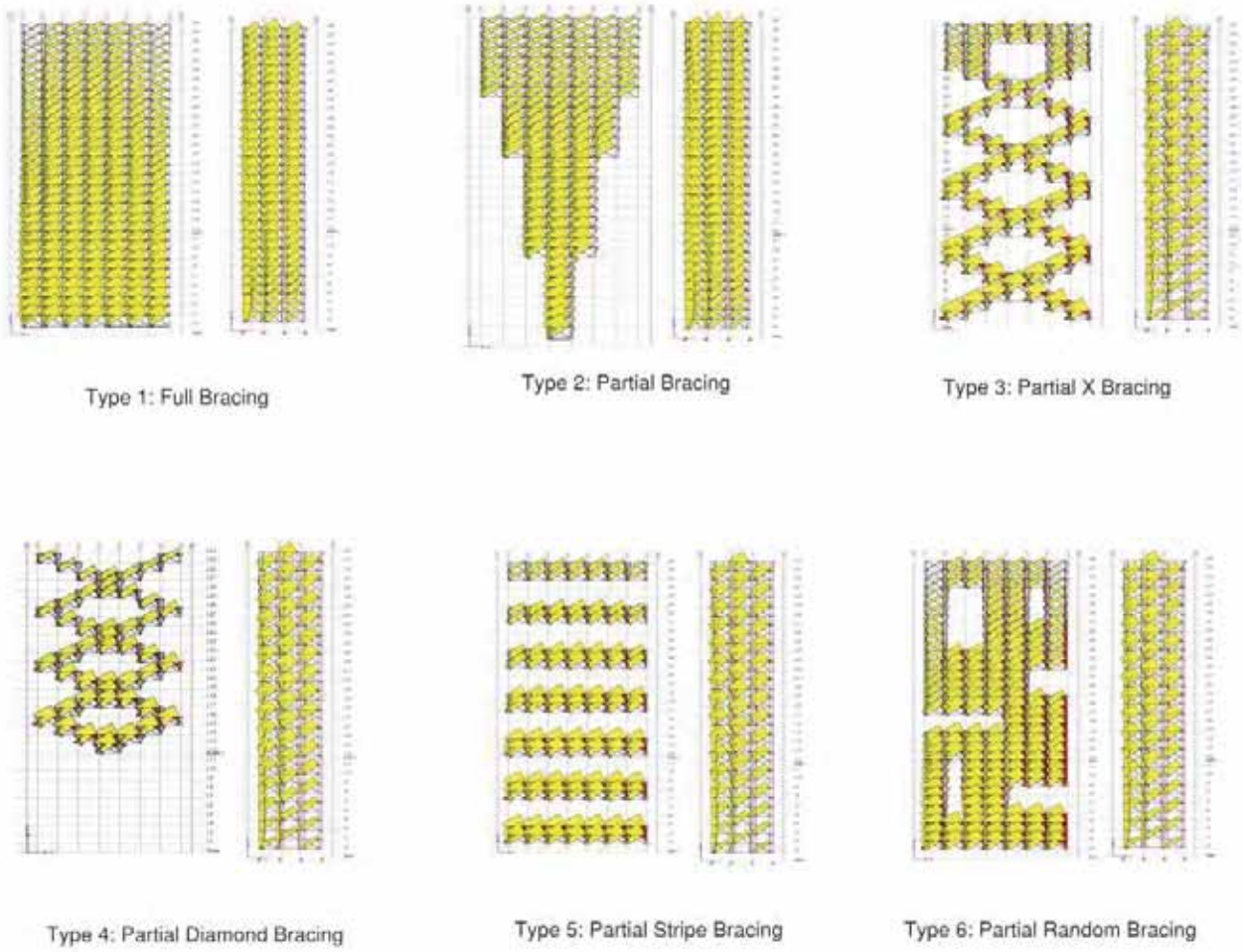


Figure 20: Structural skin pattern studies.

The contribution to tower stiffness and the overall steel tonnage of the primary frame and structural skin were measured using the structural analysis models (Fig. 21).

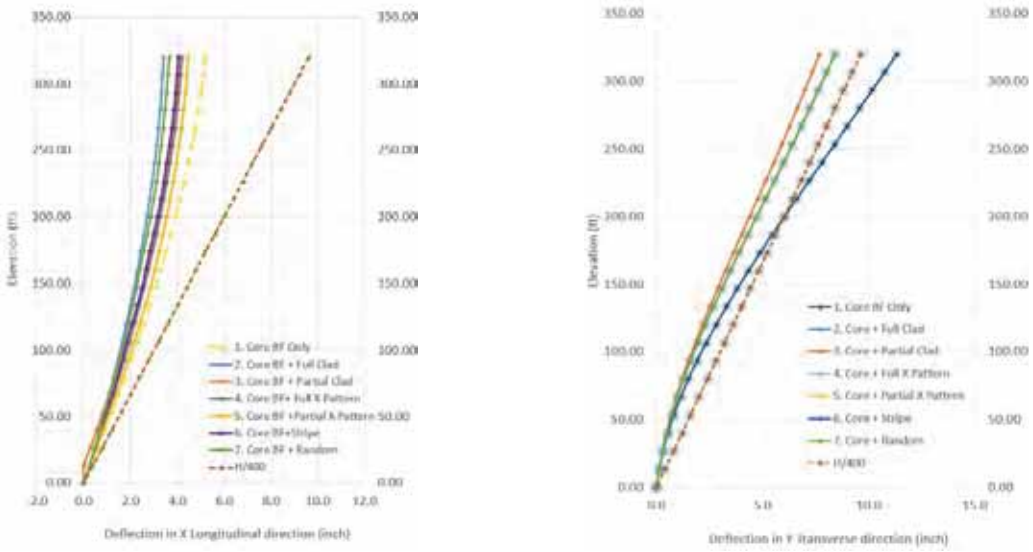


Figure 21: Stiffness comparison graph.

Comparison of the overall tower deflection under a 50-year wind for the different schemes, along with tonnage of steel in the different versions shows correlation of efficiency and symmetrical geometry. A random aperture version of the full-clad scheme was examined for reference relative to common architectural requirements for program-driven arrangements of windows or of massing, just for comparison to the symmetrical, more generic, and more efficient versions.

A partial X pattern is the most effective, though the repetition of the overall X could offset the benefit of the less regular skin pattern. The legible X bracing has a simplicity that makes it attractive in terms of presenting a legible, figural form (Fig. 22).

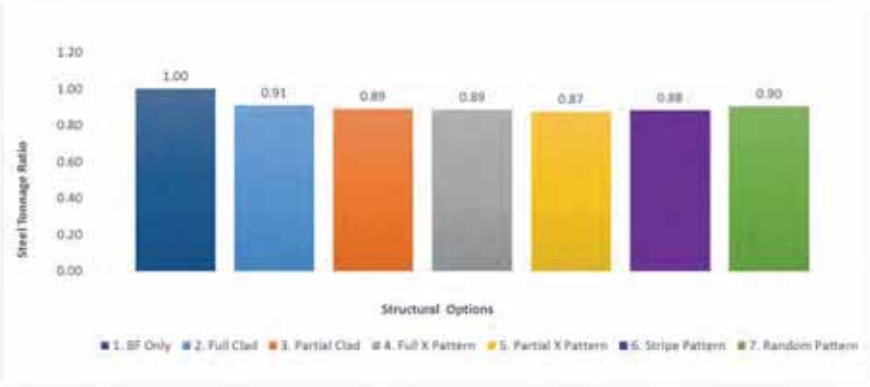
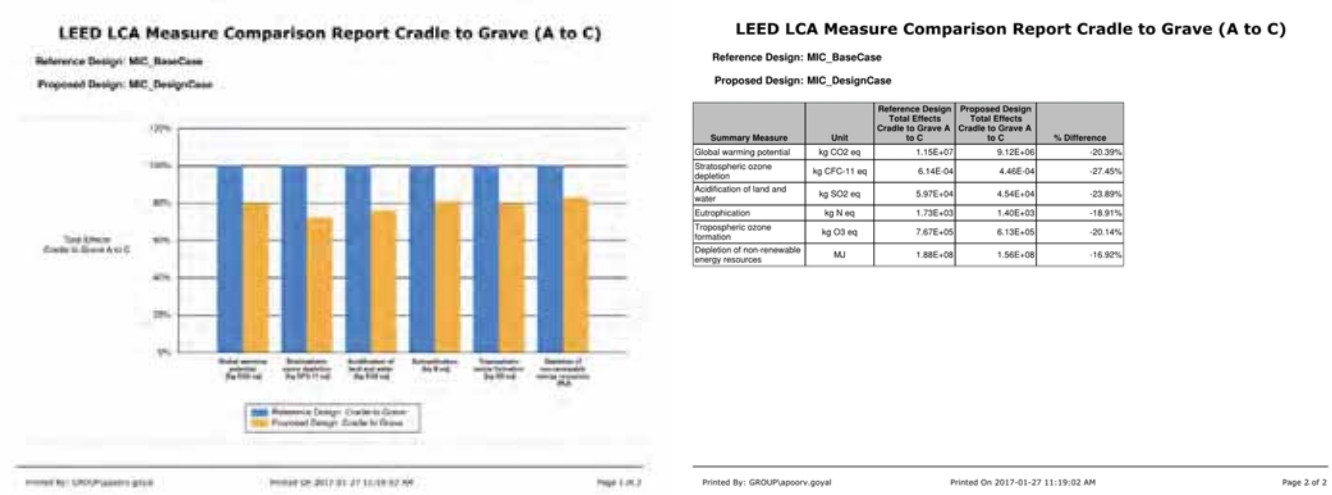


Figure 22: Tonnage ratio comparison chart.

Life Cycle Analysis can be extrapolated from the previous study, which translated tonnages of aluminum and steel in the frame and skin into estimates of embodied energy using the Athena program used for LEED certification. Compared to the conventional base case, the proposal eliminates nominally 2” x 6”x ¼” aluminum mullions at each vertical module. At approximately 5plf that equates to 13.3’ x 5plf x 5= 133 lbs. per bay. 133 divided by the 399 sf area of the bay= .83 psf. With approximately 288k sf of skin, the total aluminum saved = 240k pounds, or 120 tons. The net result is a 20% reduction in embodied CO2 and life-cycle cost for the frame and enclosure, and a 25% reduction of overall effective U-value of the

façade, at net 0.31, due to reduction of the mass of the aluminum mullions required, relative to a conventional baseline case (Structural eXterior Enclosure, 2017) (Fig. 23).



LEED LCA Measure Comparison Report Cradle to Grave (A to C)

Reference Design: MIC_BaseCase

Proposed Design: MIC_DesignCase

Summary Measure	Unit	Reference Design Total Effects Cradle to Grave A to C	Proposed Design Total Effects Cradle to Grave A to C	% Difference
Global warming potential	kg CO2 eq	1.15E+07	9.12E+06	-20.39%
Stratospheric ozone depletion	kg CFC-11 eq	6.14E-04	4.46E-04	-27.45%
Acidification of land and water	kg SO2 eq	5.97E+04	4.54E+04	-23.89%
Eutrophication	kg N eq	1.73E+03	1.40E+03	-18.91%
Tropospheric ozone formation	kg O3 eq	7.67E+05	6.13E+05	-20.14%
Depletion of non-renewable energy resources	MJ	1.88E+08	1.56E+08	-16.92%

Printed By: GROUP\apoorv.goyal Printed On 2017-01-27 11:19:02 AM Page 2 of 2

Figure 23: Lifecycle Cost Analysis.

METHOD: COMPARATIVE ANALYSES

A series of schemes was developed, each one analyzed for strength and stiffness with structural skin and a braced-core steel frame. 25-story, three-dimensional buildings were used as a basic model with the centralized concentric and eccentric braced frames in longitudinal and transverse directions. The braced frames were designed for the strength requirement only.

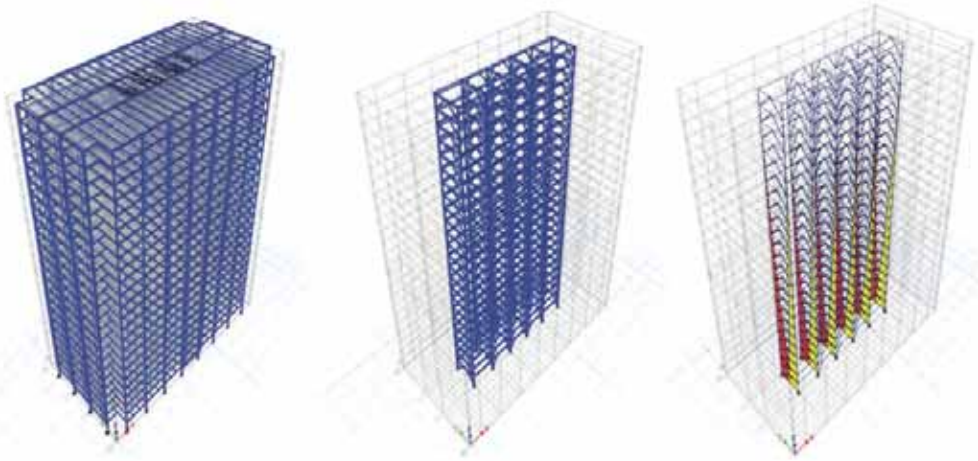
The seven schemes analyzed were:

A Base Case and six schemes were proposed with distinctive structural cladding on each face of the building to enhance structural serviceability-- Core Braced Frame Only, Core BF with full structural clad, Core BF with Partial clad, Core BF with Full X pattern, Core BF with upper Partial X pattern, Core BF with stripe pattern, Core BF with random pattern.

Nonlinear static analysis was conducted to estimate the overall lateral deflection under the wind load. Lateral load path for each scheme is illustrated as follows:

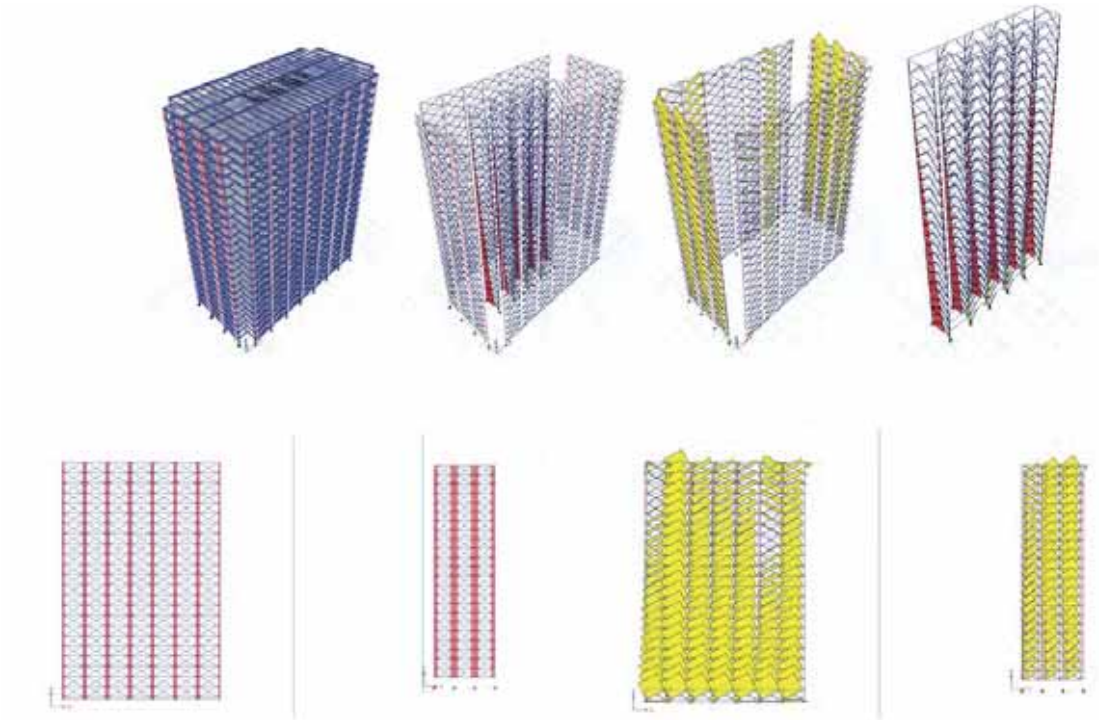
1. Core-Braced Frame only, as a baseline. Steel Tons= 1.0 (Baseline)
2. Core-Braced Frame with Full Structural Clad. Steel Tons = 0.91.
3. Core-Braced Frame with Partial Clad. Steel Tons = 0.89.
4. Core-Braced Frame with full X-pattern Partial Clad. Steel Tons = 0.89.
5. Core-Braced Frame with partial X-pattern Partial Clad. Steel Tons = 0.87.
6. Core-Braced Frame with stripe pattern Partial Clad. Steel Tons = 0.88.
7. Core-Braced Frame with random pattern Partial Clad. Steel Tons = 0.90.

Non-linear static analyses were conducted to estimate the overall lateral deflection under 50-year wind load. Lateral load path for each scheme subjected to transverse wind force is illustrated as follows (Fig. 24-30).



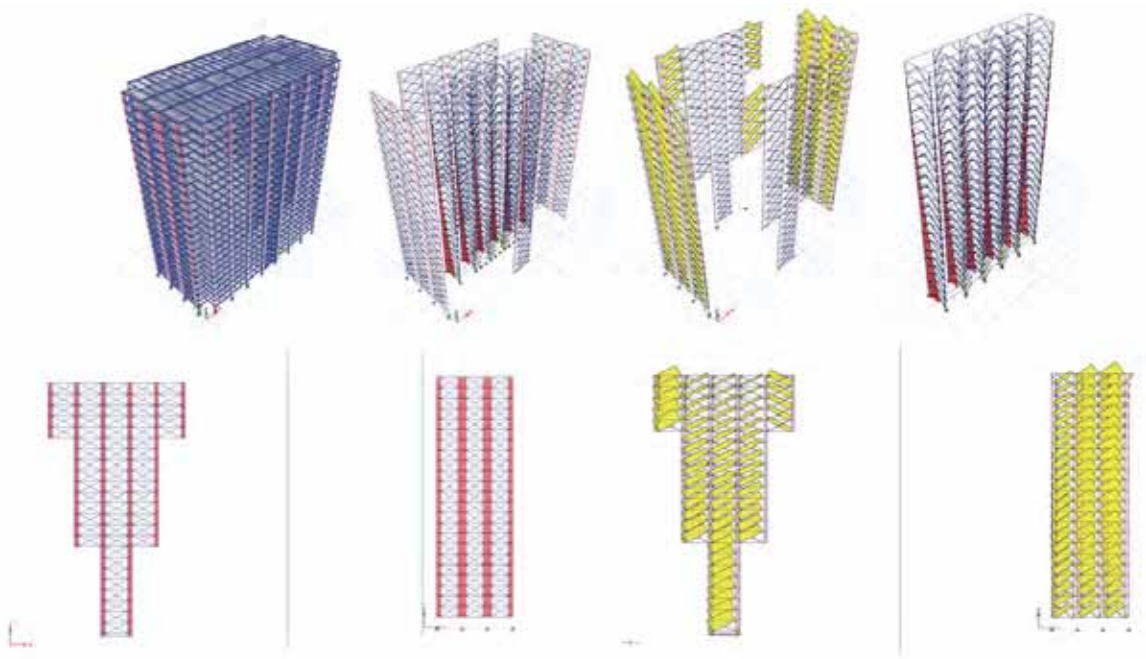
1. Steel Tons = 1.0 (Baseline)

Figure 24: Scheme 1 CB frame only, baseline. Image by HOK.



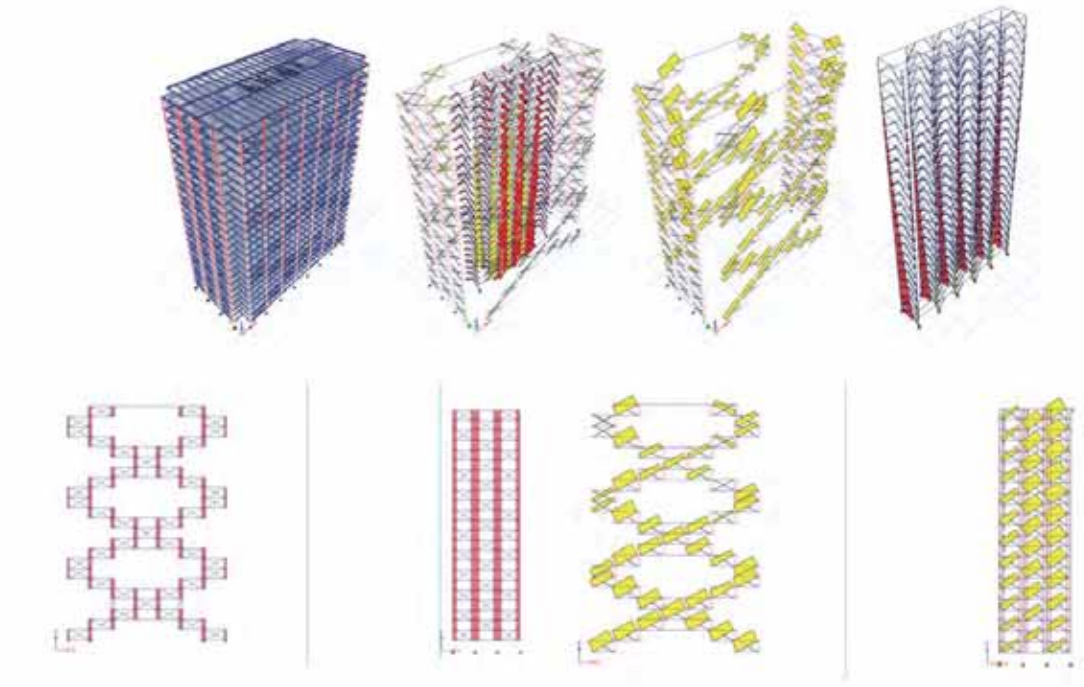
2. Steel Tons = 0.91

Figure 25: Scheme 2 full CB frame with full structural clad. Image by HOK.



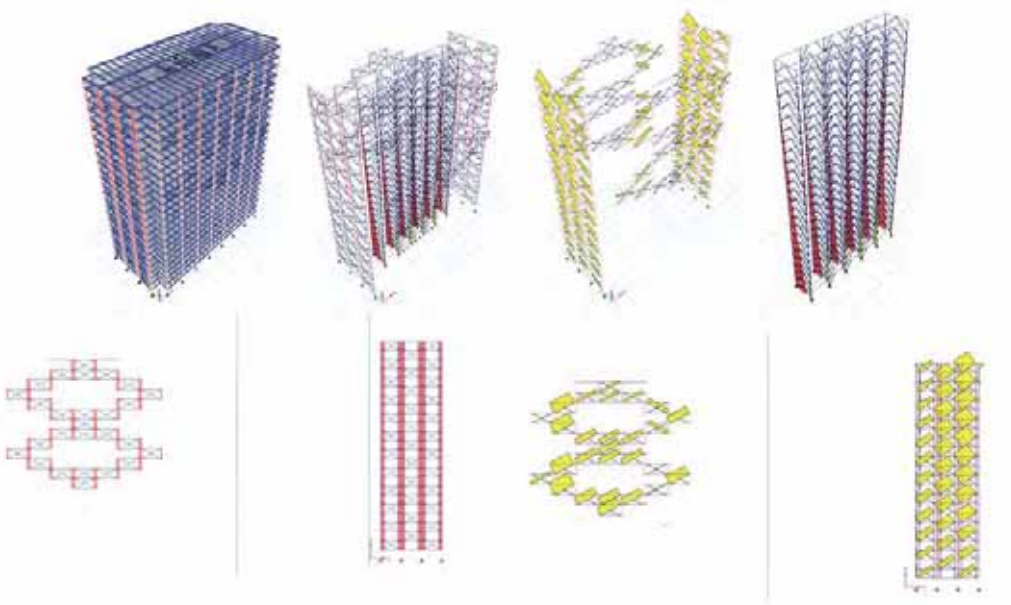
3. Steel Tons = 0.89

Figure 26: Scheme 3 full CB frame with partial clad. Image by HOK.



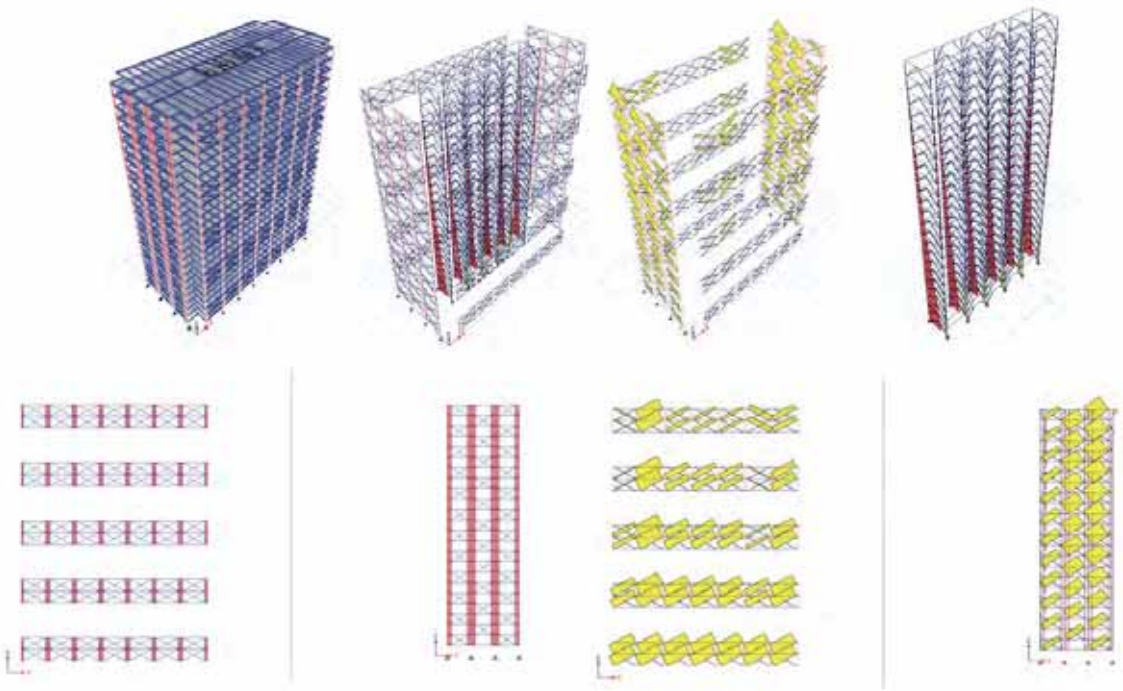
4. Steel Tons = 0.89

Figure 27: Scheme 4 full CB frame with full X partial clad. Image by HOK.



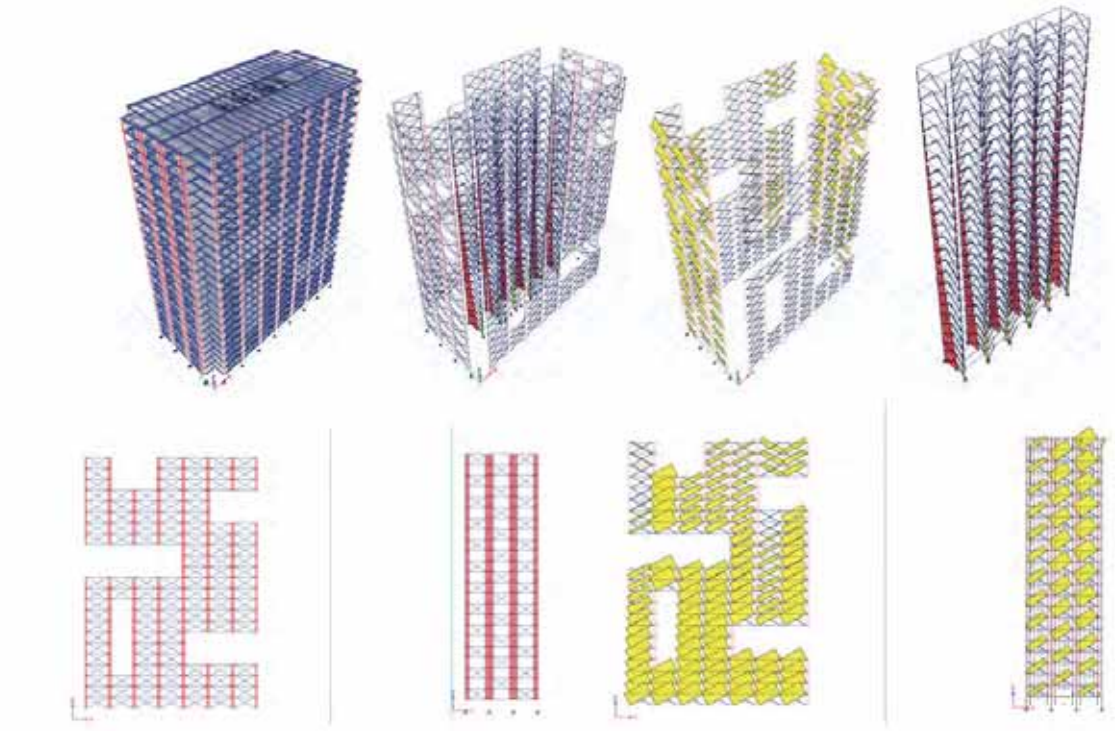
5. Steel Tons = 0.87

Figure 28: Scheme 5 full CB frame with partial X partial clad. Image by HOK.



6. Steel Tons = 0.88

Figure 29: Scheme 6 full CB frame with stripe pattern partial clad. Image by HOK.



7. Steel Tons = 0.90

Figure 30: Scheme 7 full CB frame with random pattern partial clad. Image by HOK.

EXPLANATION & CONCLUSION

The evolution from stick-framed steel HSS mullions with infill shear panels, to steel mullions braced with rods, to a full-bay structural mega-panel shows the possible beginning of a fundamental change in the approach to enclosing large buildings, moving away from the single-lite, nominally 5'-wide curtain wall units which are the default building block of the modern façade. Two-story high and multi-lite-wide units were used in the 1950's, when the aluminum curtain wall was just becoming the prevalent enclosure, but the economics of fabrication and installation somehow saw their disappearance. Likewise, the popularity of precast concrete in the 1960's and 70's drove column-to-column scale of pre-fab panels, but the weight of the material and the difficulty of shipping and installing it, (along with the growing desire for maximizing the transparency of the façade), led to its relative obscurity compared to the aluminum single-lite unit. The savings in number of pieces lifted into place, coupled with the potential elimination of deep mullions by using the panel frame diagonals to brace glazing against wind, are two reasons to look again at the large scale enclosure panel. Savings of primary structure is added incentive.

The growing realization that our buildings must become more sustainable in their conception, construction and operation is bringing us down to earth with respect to maximum transparency which has been the fashion lately. The energy used to air-condition buildings with more than 30% window-to-wall ratio is unjustifiable. Likewise, to use large quantities of aluminum, which represents by weight approximately three times the embodied energy of steel, according to industry-published metrics, is impossible to justify today ("Structural Skin," 2016). More efficient production, shipping and installation, according to the principles that have made prefabrication a subject of architectural interest since the beginning of the modern era, must become reality.

The goals of material efficiency that were so intellectually appealing in the speculations of Buckminster Fuller and other modernists who explored structural skin should now be achievable with developments in digital design and construction technology, and with the growing impetus to-- as Fuller urged us-- "do more with less." Making the enclosure structurally active, rather than dead weight, is something we need to do.

The next step in the evolution of this study will be to build real prototypes and test them for economical manufacture and actual installation. The different patterns of effective structural cladding illustrated in this study provides a basis for an expectation that the approach will be applicable to a range of building types and will be flexible, affording freedom in support of the designer's particular intentions and desires.

ACKNOWLEDGMENTS

Structural design and analysis for the three studies represented here by Simon Shim, PE, Senior Associate at HOK, NY.

Architectural design and renderings for the latest Structural Skin study by Michael Miller, designer at HOK, NY.

Architectural design and renderings for the Structural eXterior Enclosure entry to the Metals In Construction 2017 competition by Michael Miller, Zifan Liu, and Zhenhuan Xu, designers at HOK, NY. LEED analysis and thermal modeling by Apoorv Goyal, Sustainability Specialist at HOK, NY.

Support for the three studies represented here was generously provided by Matt Breidenthal, Regional Leader of Engineering, HOK.

REFERENCES

Cossutta, Aldo. "From Precast Concrete to Integral Architecture". Progressive Architecture, October 1966.
Fuller, Buckminster. *Nine Chains to the Moon*. Anchor Books. 1971. (Orig. 1938).
Gordon, J. E. *Structures, or Why Things Don't Fall Down.* Penguin Books. 1978.
Neary, John. "Structural Skin: Integrating Structure and Cladding," Façade Tectonics Institute, October 2016.
Neary, John and HOK team, "Structural eXterior Enclosure," Finalist, Metals In Construction 2017 "Reimagine Structure" competition. Metals In Construction Magazine, Spring 2017.

UNITIZED CURTAIN WALL

Case studies in performance optimization and design variation



Brian Masuda
Ennead Architects
bmasuda@ennead.com



Kathleen Kulpa
Ennead Architects
kkulpa@ennead.com



Margaret Tyrpa
Ennead Architects
mtyrpa@ennead.com

ABSTRACT

Unitized curtain wall has become ubiquitous in contemporary façade design and construction due to advantages associated with speed of erection, lower installation cost and improved quality control. The degree to which these benefits are realized is directly proportional to the ability of the designer to maximize repetitive detailing and minimize the number of unit types. These two factors often contribute to design solutions that are characterized by a uniform appearance.

With the ever-increasing performance requirements of building facades, the ability for unitized curtain wall systems to transcend their innate uniformity by accommodating variability in configuration and material infill is becoming compulsory. There is an increasing need for exterior wall systems that can accommodate variation within an efficient framework in order to respond to unique and specific environmental, programmatic and aesthetic parameters.

The David H. Koch Cancer Center Memorial Sloan Kettering in New York City and The Beus Center for Law and Society in Phoenix, Arizona are two case studies that explore the potential variability in unitized wall systems as a way to optimize performance. Key points to be covered include: designing flexibility into the module to create a more adaptable response to specific solar conditions, context, program, and aesthetic considerations; the integration of opaque infill panels into a unitized wall system adopting properties of a rainscreen to optimize thermal values; and the ability of a unitized wall system to support self-shading geometry and depth as a strategy to control solar heat gain without additional layers which often result in thermal bridging. The similarities and differences between the two facades designs as a response to their distinct climates will be highlighted for each of the above topics.

KEYWORDS

unitized curtainwall, rainscreen, design optimization, performance, case study

INTRODUCTION

When first introduced, unitized curtain wall systems were mainly reserved for large scale urban buildings with great expanses of repetitive glass and metal facades. Projects with these characteristics were able to best capitalize on the economic and technical benefits of unitization including greater quality control during fabrication as well as ease and speed of installation on site. The technical benefits of unitized system include an integral pressure equalized chamber within the depth of the wall and a dual seal system with integral gutters at stack joints to better control air and water infiltration. Aligning the vertical mullions and horizontals at the perimeter of each unit is the basis of a unitized system but most often results in a repetitive gridded façade.

The unitized wall was embraced by the design and construction industries but became synonymous with unarticulated, gridded, glass facades. As unitized curtain wall assemblies become more affordable and commonplace, the type and scale of projects incorporating unitized wall systems continues to expand. With this diversification grows a need for customization within a system based on repetition. In order to address the multitude of design criteria in every project, architects are searching for methods to provide flexibility within unitized wall systems that allow for nuanced solutions able to better address specific programmatic, aesthetic, and performance requirements.

Parallel to the heightened demand for greater design flexibility, unitized wall systems need to be able to respond to the increasingly stringent environmental performance requirements for building envelopes. The demand for unitized systems to accommodate opaque panels with enhanced insulation and shading strategies continues to grow. Unitized curtain walls have many benefits over stick-built systems and are truly optimized when they possess the ability to accommodate variation within a repetitive system.

BACKGROUND

MSK + CUNY

The MSK+CUNY project, located on the Upper East Side of New York City, was a joint venture between two institutions, Memorial Sloan Kettering Cancer Center and The City University of New York / Hunter College, to build a co-joined building on one site. The projects have a combined square footage of over 1 million square feet; MSK with 24 floors and CUNY with 17. The design challenge was to create a unified single development which was formally balanced but met the specific requirements the two building types; one being an out-patient cancer care center and the other, a university teaching laboratory building. A series of shifted volumes was developed to respond to programmatic requirements and to break-down the overall bulk of the building within the context of the neighborhood (Fig. 1a). These shifted volumes mask a shared party wall by overlapping the property line between the buildings. The volumes also create a series of exterior terraces for each of the buildings to maximize access to views and natural light (Fig. 1b).

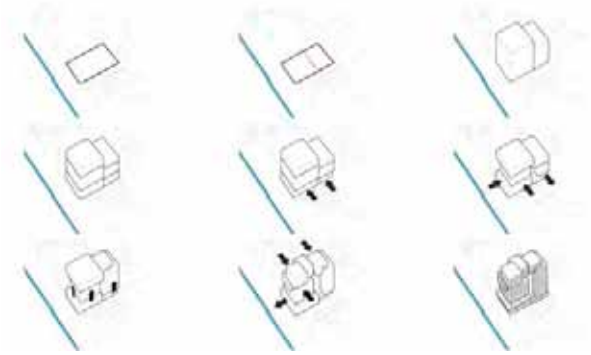


Figure 1a: MSK + CUNY morphology diagrams. Diagram courtesy of Ennead Architects.

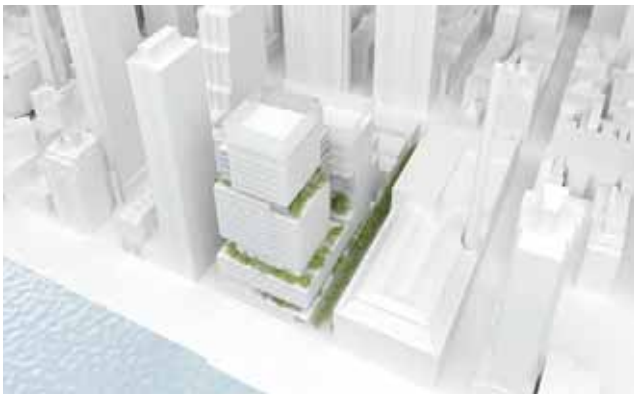


Figure 1b: MSK + CUNY aerial view rendering. Image courtesy of Ennead Architects.

BEUS CENTER FOR LAW & SOCIETY

The Beus Center for Law and Society (BCLS), the new home to the Sandra Day O'Connor College of Law at Arizona State University, is a six-story, 280,000-square-foot building located at the heart of ASU's Downtown Phoenix Campus. The design of the facility re-imagines the traditional law school as a public building, signifying a transformative approach to legal education and greater transparency into the legal system in America. The permeable courtyard massing with a north-south pedestrian slice through its social core invites the City of Phoenix into the heart of the institution, exposing the public to its three grand double-height communal spaces: the Great Hall, the Law Library and the Law Courtyard and creates a unique urban environment aimed at encouraging vibrant connections between ASU, the College of Law, practicing legal professional, and the local downtown Phoenix community (Fig. 2).



Figure 2: BCLS morphology diagrams. Diagram courtesy of Ennead Architects.

ANALYSIS & RESPONSE

MSK + CUNY



Figure 3: MSK + CUNY exterior wall rendering. Image courtesy of Ennead Architects.

The development of an exterior skin that satisfied both buildings had inherent design challenges. The two buildings did not share floor to floor heights, nor a common structural module, both which were determined by the building type. The programmatic layout including areas of public and mechanical spaces also had no relationship between the two buildings and yet required different expressions at the exterior wall. In order to create a unified exterior enclosure, the exterior wall had to incorporate a flexible module that could tailor to both building types and the many different programmatic conditions.

STACKING & MODULATION

The wall was designed to be a unitized curtain wall which is typical of New York City high rises, given the constricted sites and high cost of site labor. A typical unitized wall, however, is repetitive and modular which would highlight the two buildings' differences. Additionally, a typical horizontal arrangement of vision and spandrel zones would not address the treatment rooms and laboratories spaces which were located at the building perimeter and needed equipment and millwork along the exterior wall without resulting in treating much of the vision area as additional spandrel.

Each building had a structural bay dictated by the building type, 34'-6" for MSK based on efficient clinical room layout, and 21'-0" for CUNY, based on an efficient lab module. Each structural bay was divided into corresponding planning modules. MSK's grid of 34'-6" divided into (3) 11'-6" modules and CUNY 21'-0" divided into (2) 10'-6" modules. From that, each was divided into an asymmetrical pair of the 11'-6" and 10'-6". (4'-11"/6'-7" and 4'-6"/ 6'-0"). The unit pairs (11'-6" and 10'-6") tracked vertically from floor to floor, but within that larger grid the asymmetry of the pair division allowed for more variance and aided in satisfying the different programs. The offset verticals are not common in unitized wall, but due to a continuous gutter at each stack joint, were possible to incorporate without sacrificing system performance or constructability.

These divisions became the façade unit modules for each building. The modules were then further divided into patterns of opaque and glazing with calculated percentages of vision glass. This allowed for varied levels of opacity which could respond to the program requirements across the facade. Levels of transparency were linked to the programmatic spaces at the perimeter of each building and mapped onto the building façade (Fig. 4).

Four distinct patterns of modules were developed to achieve the varying levels of transparency (Fig. 5a). The module repeat shifted a bay at each level to create variability in the pattern (Fig. 5b).

A strict application of the resulting module pattern over the entirety of the façade would have resulted in visually distracting distinct areas of each, and not the desired continuous texture. But since the module pairs were interchangeable, the team could switch out units for a more acceptable blending of the patterns as well as flexibility in addressing coordination anomalies at local conditions of the building perimeter (Fig. 6).

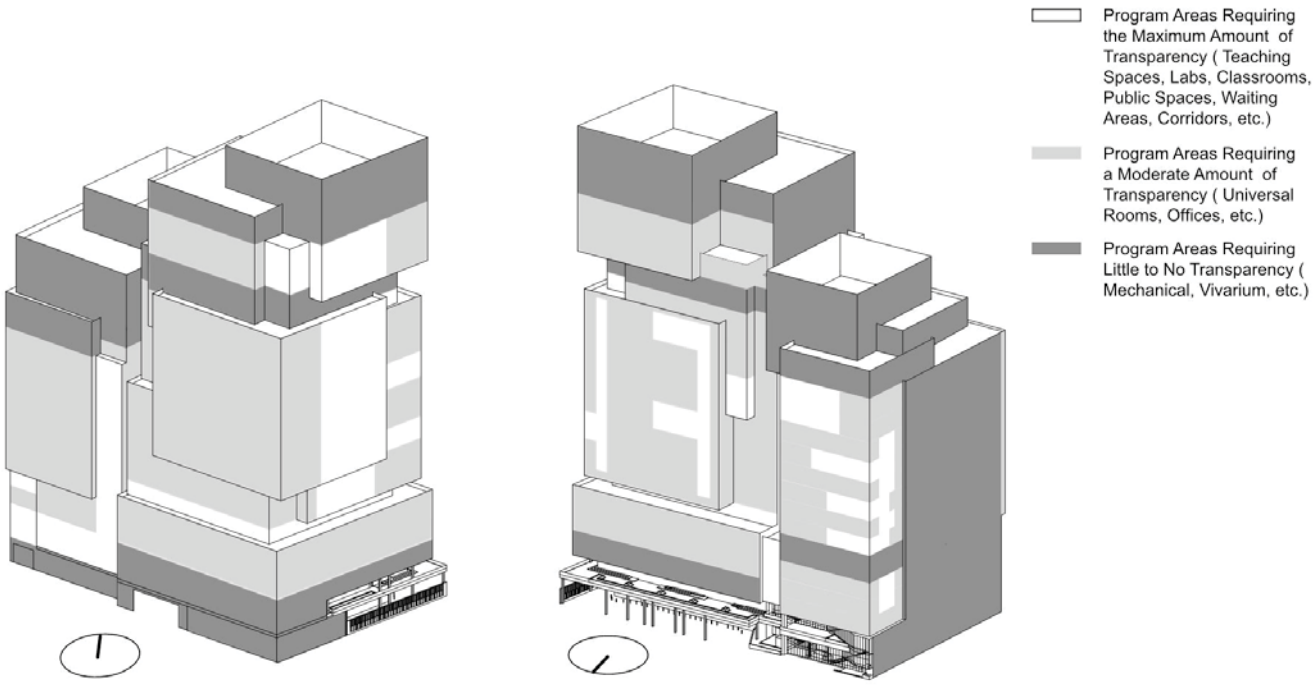


Figure 4: MSK + CUNY transparency levels based on programmatic zoning. Diagram courtesy of Ennead Architects.

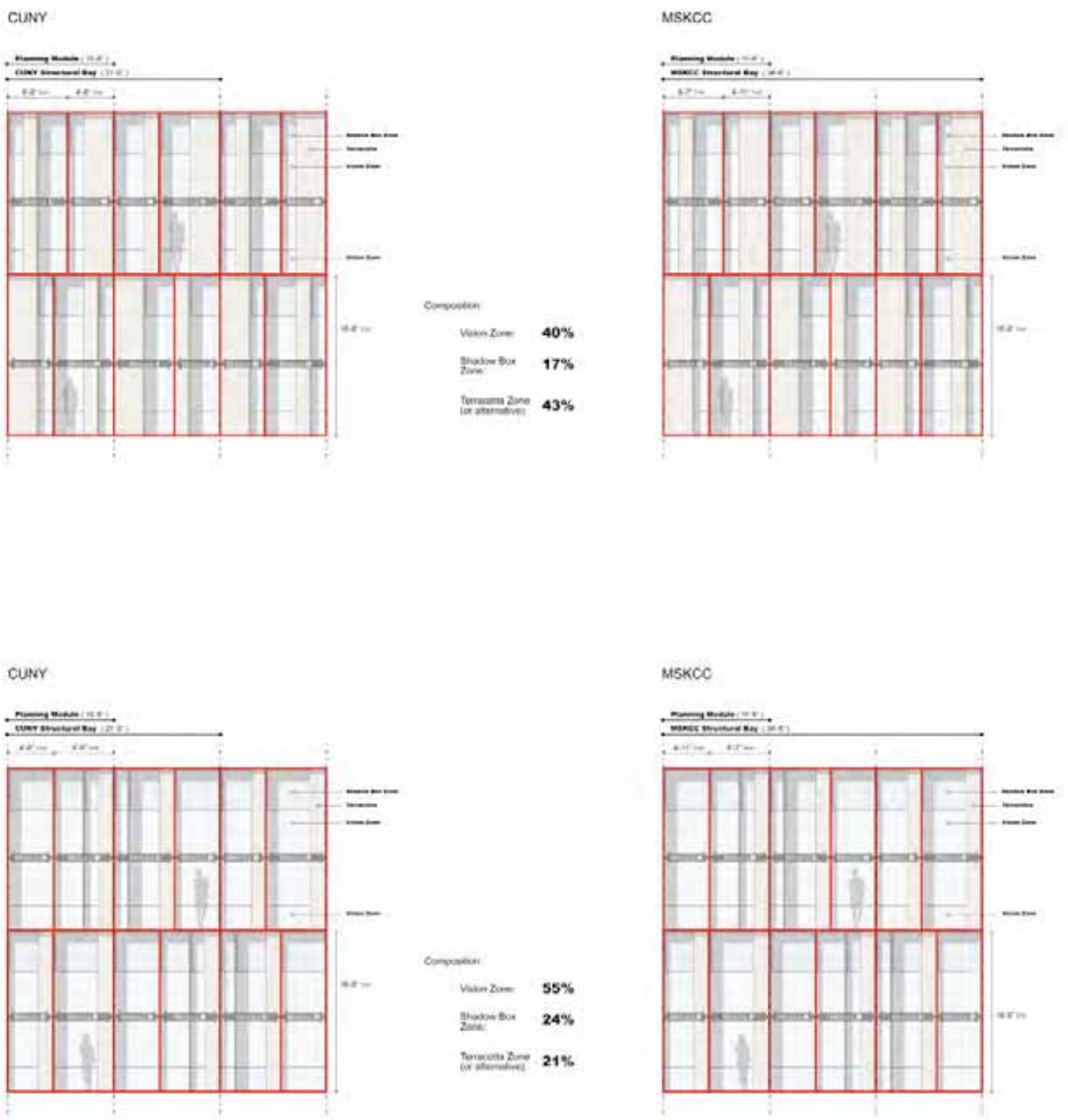


Figure 5a: MSK + CUNY facade patterns at different levels of transparency. Diagram courtesy of Ennead Architects.



Figure 5b: MSK + CUNY façade patterns stacking diagram. Diagram courtesy of Ennead Architects.

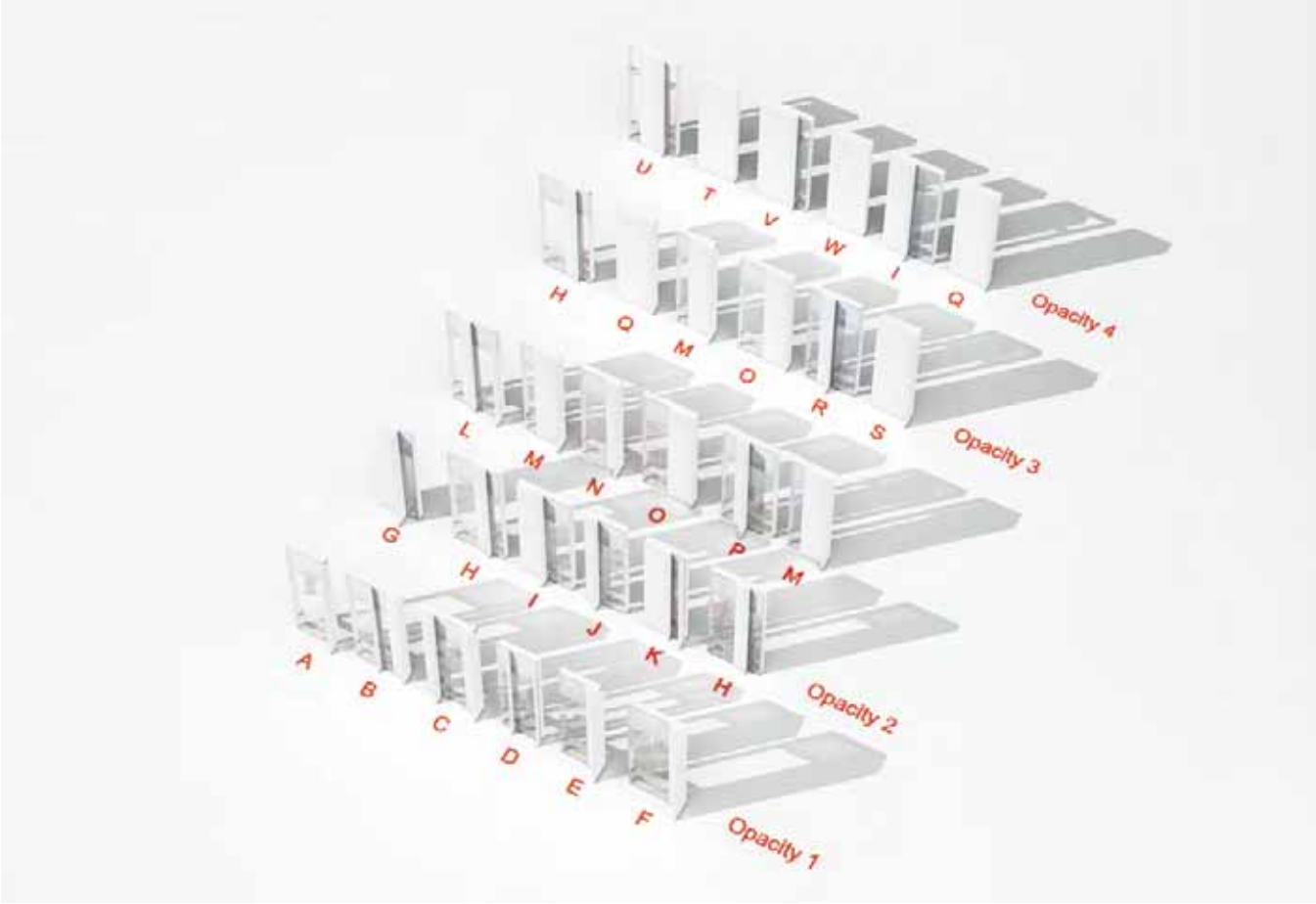


Figure 6: MSK + CUNY modules used for each transparency level. Diagram courtesy of Ennead Architects.

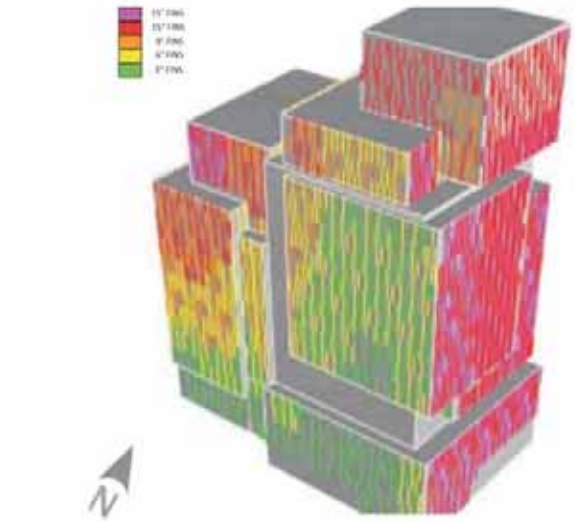
GEOMETRY & SOLAR CONTROL

The MSK client specifically requested maximizing the views for the patients receiving treatment, ideally vision glazing which did not require exterior or interior shading devices, even during peak hours of sun exposure. The majority of clinical rooms in the MSK building are located along the north, south and east perimeter walls. The exterior wall design needed to maximize the views while keeping the window to wall ratio quite low while providing adequate solar control without shades or screens. The opaque portions of each module were offset from the face of glass by 4-1/2" which adds a depth to the wall and provides some solar shading due to the vertical orientation of the openings. A vertical fin was introduced to the left side of the opening to provide additional solar control. The fins were developed in 4 different depths, 6", 9" 10" and 14", to coincide with the width of the adjacent opening (Fig. 7). When the exterior wall modules were mapped onto the elevation, an analysis using grasshopper further calibrated the fin depths based on the solar control needed at specific locations on the building (Fig. 8).

Glass selection was also incredibly important to minimize solar heat gain and glare during peak sun exposure hours. A family of Low-E coatings from AGC Interpane was selected which ranged in Visual Light Transmittance from 50% to 80% (50, 60, 70, and 80). This allowed the team to use glass types based on the specific performance data required for each elevation. The triple silver, the highest performing glass, was reserved for the east elevation which receives direct sunlight for much of the day but also offers the most stunning views of the East River and beyond.



Figure 7: MSK + CUNY vertical fin depth related to opening width. Diagram courtesy of Ennead Architects.



Incident Solar in kWh/m2	Option 4 1'-6" Panels	3'-0" Panels	4'-6" Panels
>900	12	15	15
750-900	9	12	12
600-750	6	9	9
450-600	3	6	6
<450	0	3	3

Figure 8: MSK + CUNY grasshopper analysis to further calibrate fin depth. Diagram courtesy of Ennead Architects.

INTEGRATION OF OPAQUE WALLS & THERMAL PERFORMACE

The design team evaluated material options for the opaque portions of the unitized curtain wall and chose terra cotta for its design properties and opportunities and for texture and depth. This allowed for continuous insulation outboard of the framing which greatly increased the R value of the overall system. Venting the zone outboard of the weather barrier panel, which was coplanar with the glazing, created a pressure equalized zone at all of the opaque panels further enhancing the wall performance.

ANALYSIS & RESPONSE

BEUS CENTER FOR LAW & SOCIETY





Figure 9a: BCLS exterior sandstone and glass façade. Image courtesy of Ennead Architects.

Figure 9b: BCLS outward-facing unitized façade location. Diagram courtesy of Ennead Architects.

Sited in the Sonoran Desert, sustainability was a key driver throughout the design process and integral to the conception and development of the building's massing and in particular its envelope. The overall courtyard massing is self-shading by nature by reducing the amount of direct sunlight that hits its internal, more transparent, vertical surfaces and north-south "canyon" while also promoting air movement through the ground level pedestrian way.

The outward-facing facades with a high exposure to direct sunlight consist of a unitized self-shading, saw-toothed design that seamlessly integrate glazing and opaque panels into an undulating array that serves as a key identifiable feature of the building (Fig. 9a and 9b). The modular units are comprised of Arizona sandstone with aluminum and glass windows whose geometry changes in response to solar orientation and programmatic requirements (Fig. 10). Aluminum vertical fins project out of the façade at a 1:2 ratio relative to the varying width of adjacent windows (Fig. 11). The 1:2 depth to width ratio was established through solar and daylight analysis in order to strike the right balance between daylighting, glare, and solar shading (Fig. 14). The façade units were assembled off-site in a factory and shipped to the building site to assure quality of fabrication, erection speed, and to meet the high thermal performance standards demanded by Arizona State University's Sustainable Design Advisory Committee. Working diligently with the wall fabricator and installer, the innovative wall system incorporates prefabricated insulated back-up panels behind its opaque surfaces, a thermally broken panel support system, as well as an additional layer of continuous interior insulation directly attached to the back of curtain wall assembly. All of these factors contributed to a final façade design that achieved a high level of thermal efficiency and visual variation that exceeded initial expectations (Fig. 13).

STACKING & MODULATION

During the design process, digital tools were used to analyze a range of solar-related issues including building configuration, facade orientation, glare and daylighting, shading, and heat gain. This analysis informed everything from early massing decisions and program distribution to the refinement of the building's façade design (Fig. 12).

A diverse program, high thermal performance requirements, a modest budget, coupled with a repetitive structural grid, demanded an economical unitized façade solution that would allow for variation in geometry and fenestration without sacrificing thermal performance and a unified aesthetic.

At the perimeter of the building, a 24'-0" x 34'-6" structural grid was established to satisfy planning requirements for smaller office and meeting spaces along with larger program areas such as classrooms and collaborative spaces (Fig. 10). Module widths were set at either 5'-9" or 6'-0" depending on the façade. Each module was then bisected in varied widths of glass and stone in proportions that responded to different window wall ratio requirements as determined by building programming, thermal analysis, as well as daylighting needs. All units tracked vertically from floor to floor, with the intermittent vertical mullion location responding to the structural grid and interior layouts (Fig. 11).

Four basic curtain wall module types with a vision to spandrel ratio that ranged from 24% to 74%. Through mirroring these units, additional variation within the unit array was achieved. Further variation was introduced into the system in order to respond to the higher floor-to-floor height at ground floor with the sandstone panels subdivided into five or six horizontal bands as required.

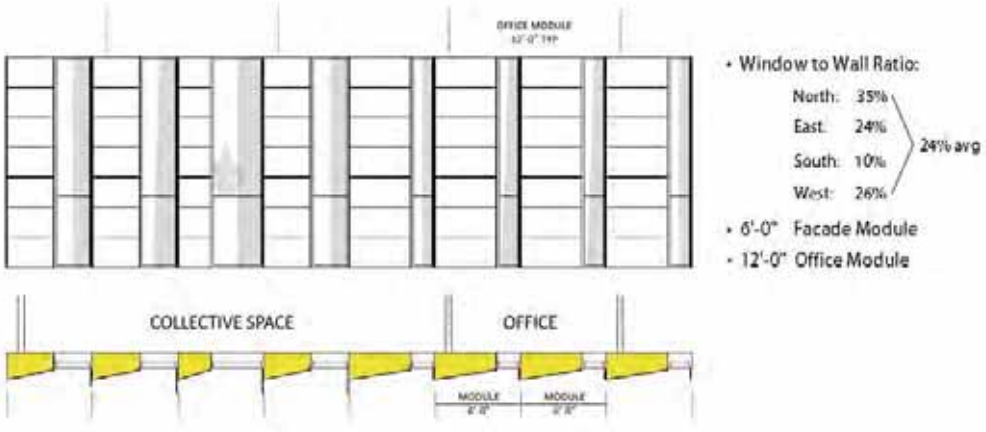


Figure 10: BCLS window to wall ratio diagrams based on program type and solar orientation. Diagram courtesy of Ennead Architects.

GEOMETRY & SOLAR CONTROL

Vertical, strip glazing units at various widths were captured between sandstone-clad spandrel panels in a saw-toothed configuration achieving self-shading through window recess with an extended jamb return. A projection of uniform depth was established for all extended jamb returns. The angle of the sandstone panels changed as the opaque module width varied. In addition to the self-shading plan profile of the units, vertical fins were added to the east and west modules to help mitigate direct solar gain as well as reduce glare within the interior spaces (Fig. 11a). The depth of the vertical fins was directly proportional to width of the glazing module which responded to the interior program type. Larger window openings were reserved for communal spaces such as meeting rooms and open study areas while more modest openings were applied to private offices (Fig. 11b).

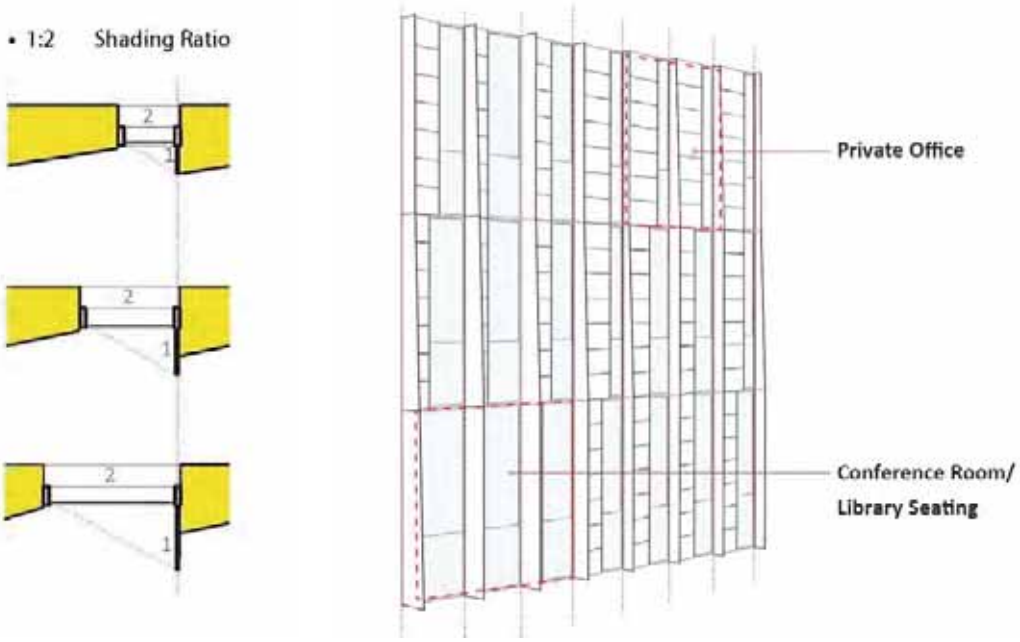


Figure 11a: BCLS vertical fin projection diagrams relative to window opening. Diagram courtesy of Ennead Architects.

Figure 11b: BCLS window to wall ratio diagram based on program type. Diagram courtesy of Ennead Architects.

INTEGRATION OF OPAQUE WALLS & THERMAL PERFORMANCE

Parametric studies were used to evaluate different patterns and rhythms of the modular array to calibrate window-to-wall ratios in order to keep internal cooling loads within specific low targets. Lower cooling loads allowed for the implementation of an energy efficient chilled beam system which improved interior thermal comfort, while still providing appropriate daylighting levels and views outward. Specific hotspots on the façade were identified and the balance of glazing to opaque surfaces of individual units were adjusted to achieve desired performance values (Fig. 14).

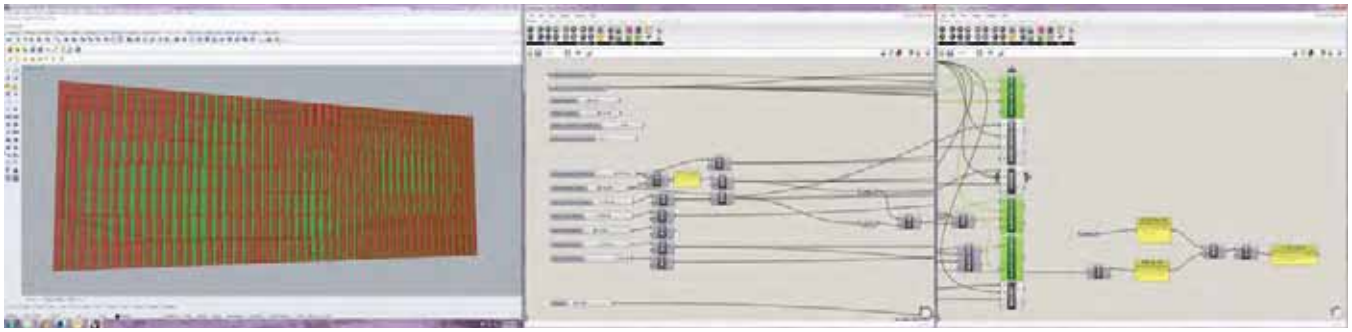


Figure 12: BCLS grasshopper analysis to study unit geometry. Diagram courtesy of Ennead Architects.



Figure 13: BCLS west façade. Photo courtesy of Bill Timmerman.

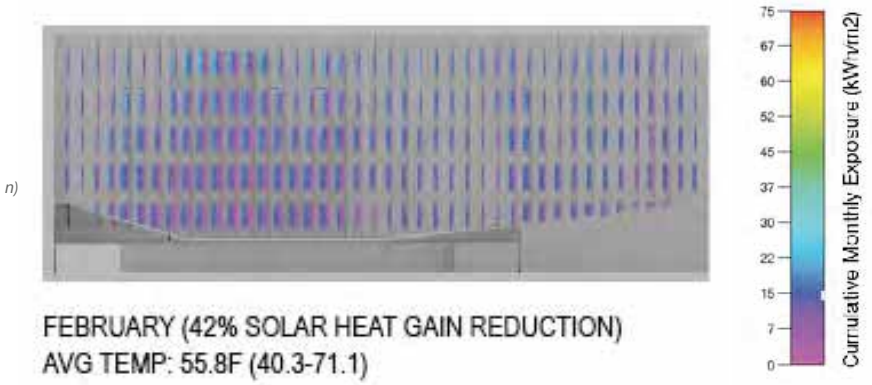
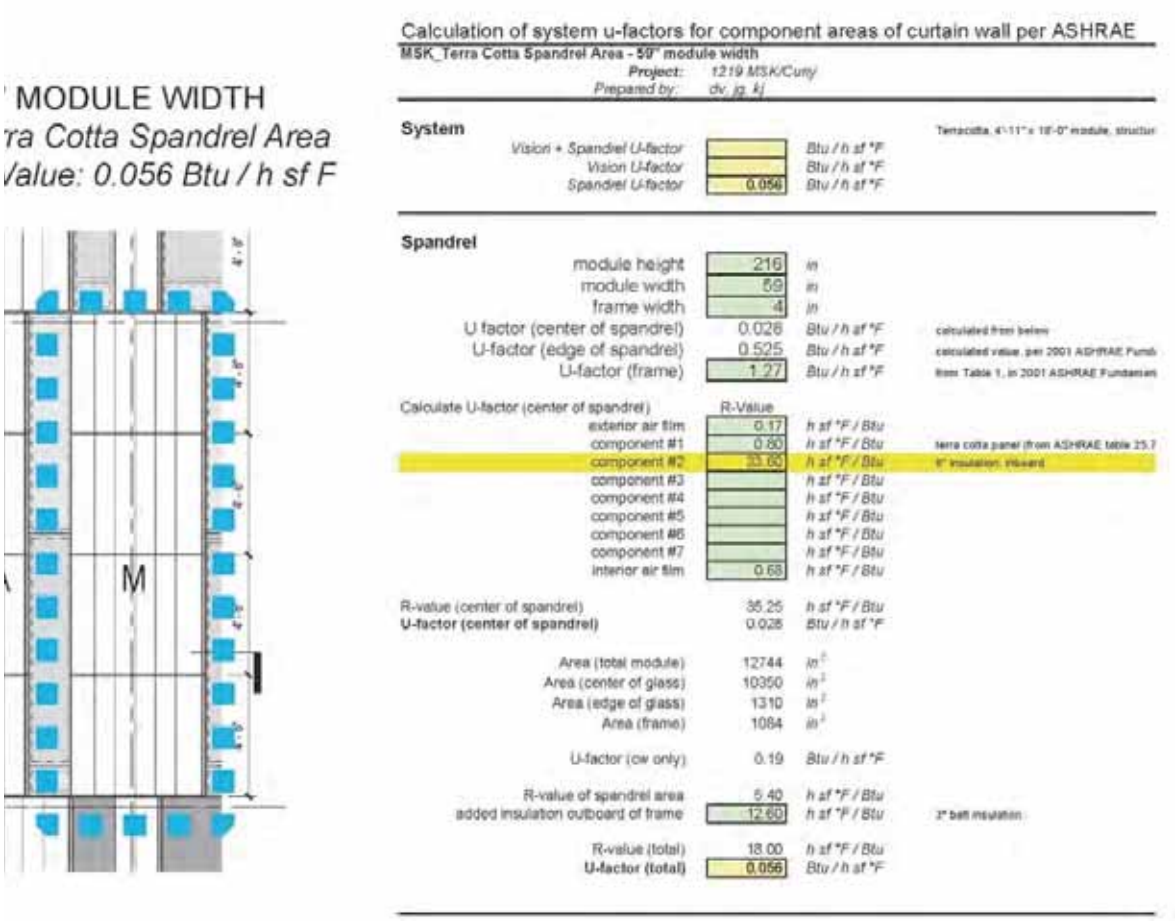


Figure 14: BCLS solar heat gain analysis of west façade. Diagram courtesy of Buro Happold Engineers.

DETAIL DEVELOPMENT

MSK + CUNY

The MSK+CUNY curtain wall design was based on the principals of unitized system; split vertical mullions, continuous gutters at the stack joint, and a continuous air barrier at the inside face of the wall. The weather barrier and glazing line were consistent across the system. The terra cotta was selected as the opaque wall material and was offset from the glass/ weather barrier by the 4-1/2" which allowed for an additional 3" of continuous semi-rigid insulation outboard of the framing. increased the R value of the opaque wall to an average 12.6 (Fig. 15). Additional insulation was added to the interior of the wall as mullion wrap at all of the non-vision areas to raise the overall R value to over 20. The average R value at areas of spandrel glazing is 5.4.



Calculation of system u-factors for component areas of curtain wall per ASHRAE

MSK_Terra Cotta Spandrel Area - 59" module width

Project: 1219 MSK/Cuny
Prepared by: dv, jg, kj

System

Vision + Spandrel U-factor		Btu / h sf °F	Terracotta, 4'-11" x 10'-0" module, structur
Vision U-factor		Btu / h sf °F	
Spandrel U-factor	0.056	Btu / h sf °F	

Spandrel

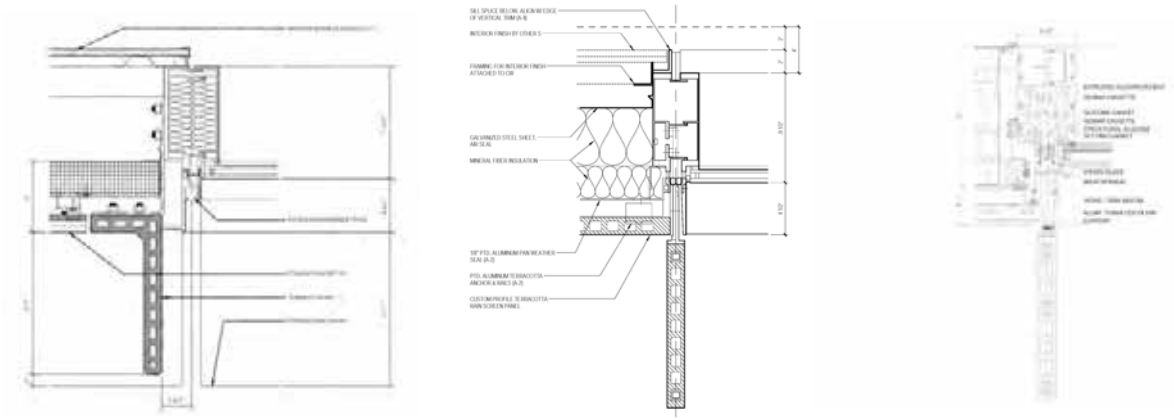
module height	216	in	
module width	59	in	
frame width	4	in	
U factor (center of spandrel)	0.028	Btu / h sf °F	calculated from below
U-factor (edge of spandrel)	0.525	Btu / h sf °F	calculated value, per 2001 ASHRAE Fund
U-factor (frame)	1.27	Btu / h sf °F	from Table 1, in 2001 ASHRAE Fundamen

Calculate U-factor (center of spandrel)	R-Value		
exterior air film	0.17	h sf °F / Btu	
component #1	0.80	h sf °F / Btu	terra cotta panel (from ASHRAE table 25.7
component #2	35.60	h sf °F / Btu	6" insulation, inboard
component #3		h sf °F / Btu	
component #4		h sf °F / Btu	
component #5		h sf °F / Btu	
component #6		h sf °F / Btu	
component #7		h sf °F / Btu	
interior air film	0.68	h sf °F / Btu	
R-value (center of spandrel)	35.25	h sf °F / Btu	
U-factor (center of spandrel)	0.028	Btu / h sf °F	

Area (total module)	12744	in^2	
Area (center of glass)	10350	in^2	
Area (edge of glass)	1310	in^2	
Area (frame)	1084	in^2	
U-factor (cw only)	0.19	Btu / h sf °F	
R-value of spandrel area	5.40	h sf °F / Btu	
added insulation outboard of frame	12.60	h sf °F / Btu	3" batt insulation
R-value (total)	18.00	h sf °F / Btu	
U-factor (total)	0.056	Btu / h sf °F	

Figure 15: MSK + CUNY R-value calculation for terracotta panels. Diagram courtesy of Heintges & Associates.

Early detailing for the terra cotta included an integral ‘L’ shaped vertical fin (Fig. 16, Concept detail). Preliminary discussions with the terra cotta manufacturers revealed that the fin needed to be constructed and supported differently than the adjacent flat tile areas. The L shaped panel was also difficult to fabricate in the depths required, up to 14”. In the bid set details, the fin was moved to the mullion centerline and developed as a baguette with integral aluminum framing within the baguette voids (the window washing track was relocated to mullions without a terra cotta fin) (Fig. 16, Bid Set Detail). The fin bracket developed to support the fin was then able to attach at the split verticals. Brackets lengths were minimized, and thermal isolators were introduced to limit the thermal bridging.



CONCEPT TYPICAL MULLION DETAIL *BID SET TYPICAL MULLION DETAIL* *CONTRACTOR’S TYPICAL MULLION DETAIL*

Figure 16: MSK + CUNY detail progression of typical mullion and terra cotta fin detail. Diagrams courtesy of Ennead Architects and Benson Industries.

The module infill was developed as a structurally glazed insulated glass unit, aluminum panel or louver as required to meet the building’s needs (Fig. 17). This allowed the overall pattern to be consistent at mechanical spaces or areas that did not require or could not have glass. The detailing for the modules was consistent for all types and was only described by letter and infill type. The module infill could be revised throughout the design process for maximum flexibility and coordination at anomalous conditions.

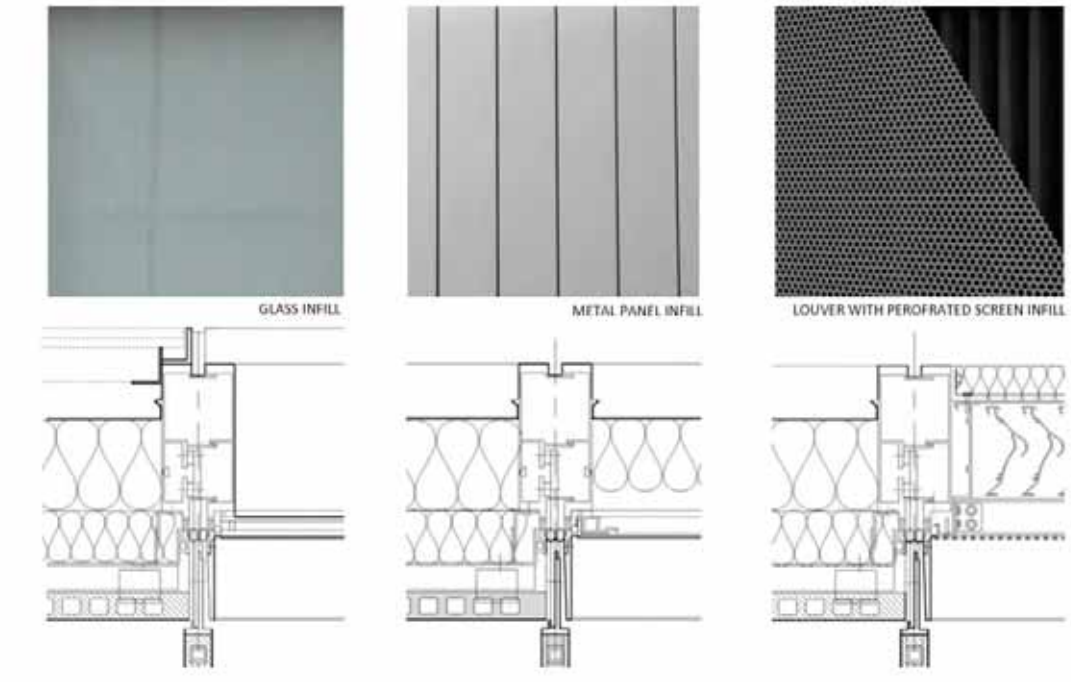


Figure 17: MSK + CUNY interchangeable infill materials. Diagram courtesy of Ennead Architects.

DETAIL DEVELOPMENT

BEUS CENTER FOR LAW & SOCIETY

The opaque portions of the BCLS's unitized wall system were developed as a spandrel back pan assembly and rainscreen stone panel system utilizing locally sourced sandstone. Given tight budget constraints but high thermal insulation requirements, the industry standard back pan assembly, consisting of galvanized sheet metal and insulation, was replaced during design development with exterior sheathing and 6" thick mineral wool insulation inserted into a typical unitized curtain wall framing system (Fig. 18).

In a desert climate, where the exterior air temperature is higher than interior air temperature for much of the year and prolonged freezing conditions are not likely, it was determined that the air and vapor barrier be placed on the exterior side of the assembly. The air and vapor barrier membrane was detailed to be adhered to the exterior of the unit and sealed to the frames, creating a consistent weather barrier.

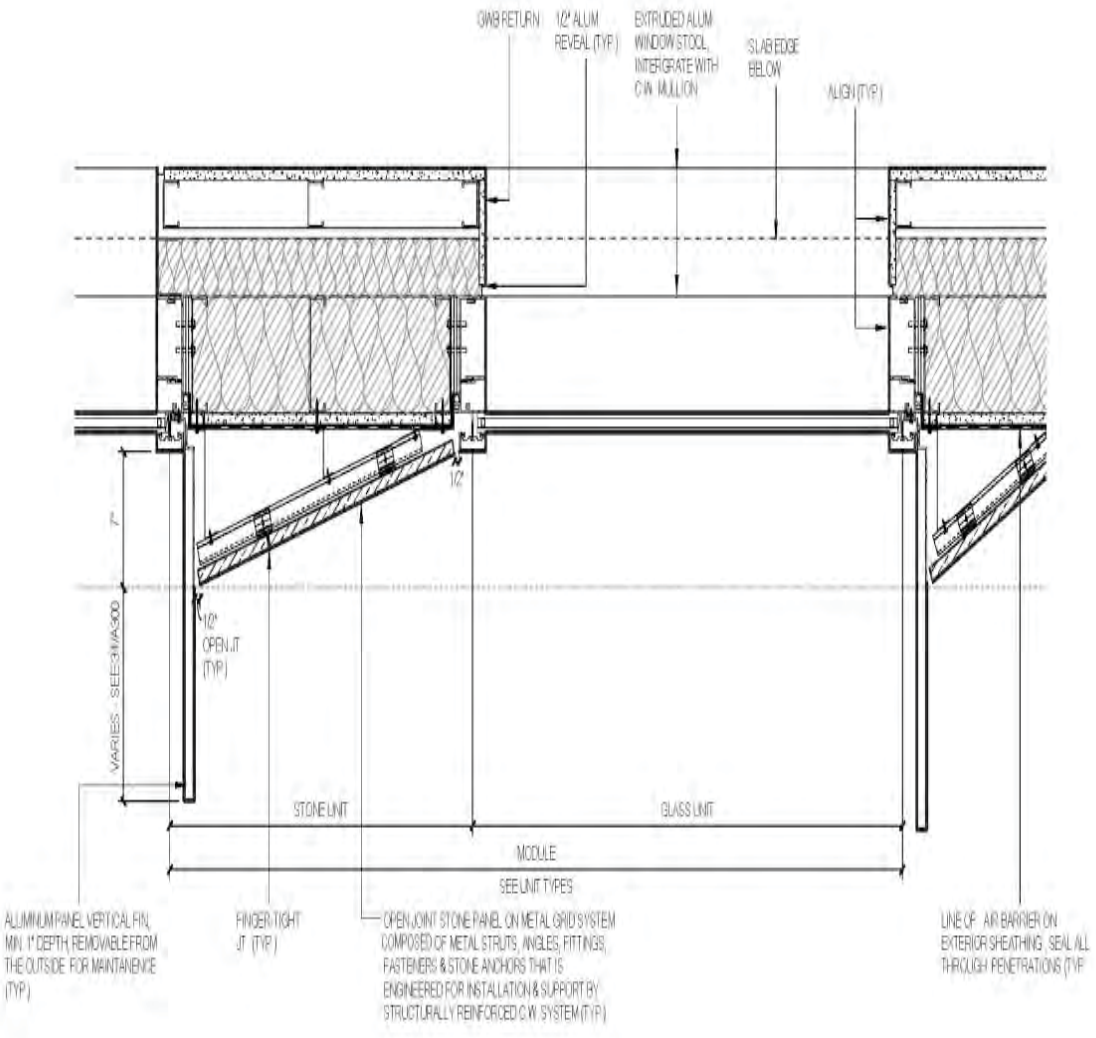


Figure 18: BCLS unit plan detail - construction documents. Diagram courtesy of Ennead Architects.

During the bid and shop drawing process, the proposed back pan assembly at the opaque wall conditions was replaced with readily available, prefabricated exterior insulated metal panel. This simplified the system and lowered the cost without sacrificing the thermal performance of the wall. 3" foam panels clad on both sides with 26-gauge UV resistant coated steel sheets minimized thermal movement and allowed for the stone cladding to have minimal 1/8" open joints. The foam panels also provided an R-value of 22.5 for the opaque portions of the wall. 3" thick mineral wool insulation was applied to the back of spandrel panels and curtain wall framing (mullion wrap) to further increase thermal performance of the wall (Fig. 19 and 20).

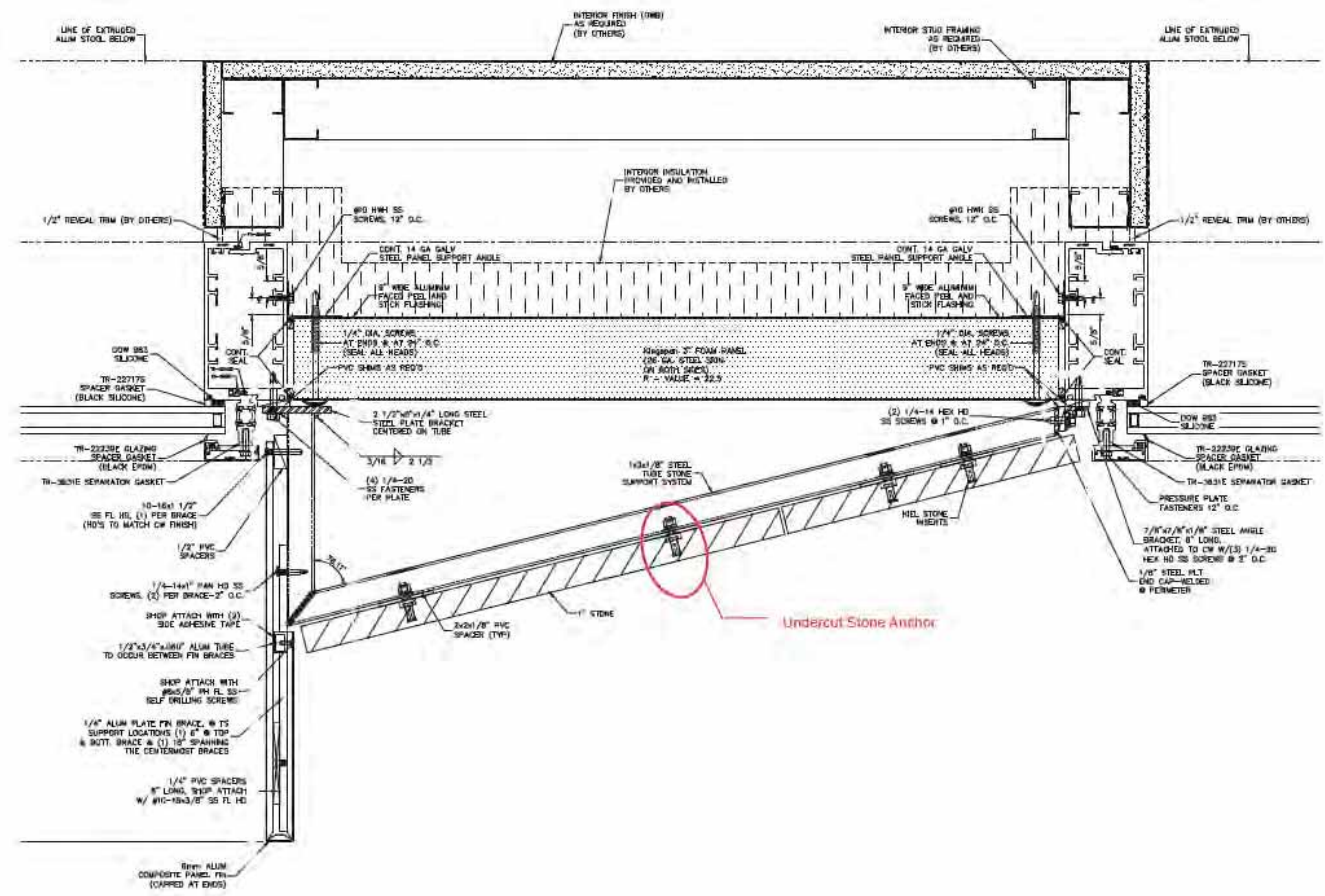


Figure 19: BCLS curtain wall unit plan detail – shop drawing. Diagram by Kovach Building Enclosures.

The stone panel framing brackets were designed at varying angles to achieve the saw tooth wall profile. Thin cut 1 ¼" stone panels were selected to reduce the weight of individual façade units. Conventional pin and kerf anchors were not an option for the thinner stone panels, instead a "back-drilled" undercut anchor system was utilized. The undercut anchor profile was fabricated to eliminate points of compression stress that could result in cracking. The individual anchors were mounted on custom horizontal aluminum channel framing brackets.

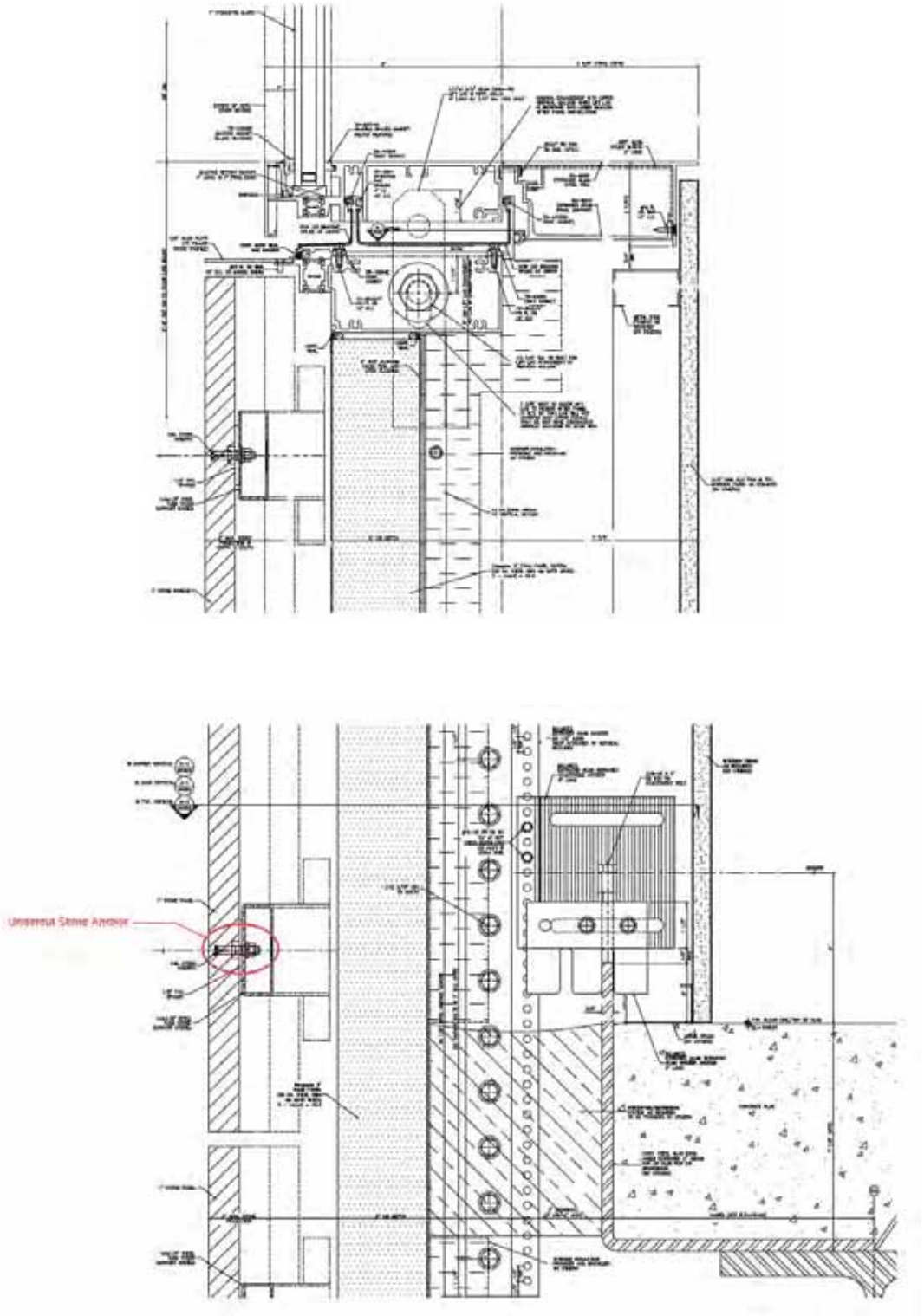


Figure 20: BCLS curtain wall unit section detail - shop drawing. Diagram by Kovach Building Enclosures.

CONCLUSIONS

Unitizing curtainwall meets many of the demands of the current building industry: factory quality construction and a fast and cost-effective installation. Traditional unitized wall systems would benefit from improved overall performance and system variability. The two case studies above highlight innovative strategies for incorporating added performance and flexibility into the design of unitized facades in order to exceed code required performance criteria and to respond to specific site and programmatic parameters. By combining the thermal properties of rainscreen assemblies into the opaque areas of the unitized wall systems, each case study project was able to achieve performance values that far exceed the typical curtainwall spandrel. Through analysis and design iteration, the glazing application in each of the two projects was optimized for daylighting and views. This optimization resulted in low overall window to wall ratios, increased thermal performance and a significant energy savings. Furthermore, the geometry and depth in both façade designs achieved self-shading properties which were then modulated and fine-tuned based on the solar orientation. Allowing the curtain wall to aid in solar control eliminated the need for exterior screens which often compromises the façade's thermal performance with penetrations back to building structure. And last, but not least, the design team was able to achieve aesthetic variation within a single wall system design; one that could to meet diverse programmatic needs within the building and add to the visual elegance of the projects.

Multi-Layer <> Facades

A COMPACT, UNITIZED DOUBLE SKIN FACADE

Thermal performance comparison in US climates



Alex Cox, LEED AP
Permasteelisa North America
alex.cox@permasteelisagroup.com



James Hock, LEED AP BD+C
Permasteelisa North America
j.hock@permasteelisagroup.com



Laura Ziegler
Permasteelisa North America
l.ziegler@permasteelisagroup.com



Karin Lamberts
Scheldebouw B.V.
k.lamberts@permasteelisagroup.com

ABSTRACT

Driven by an increasing demand for high thermal and acoustic performance, transparency, and low maintenance costs, a number of facade innovations have been developed over the past 50 years. These advancements, collectively part of the emerging market of dynamic, adaptive facades, give designers the freedom to control energy loads and glare through the building envelope using building management software. Integrated, intelligent control systems are being developed to optimize energy performance and meet sustainability goals with minimal compromise to aesthetics and transparency.

Double skin facades, which feature two distinct glazed wall assemblies separated by an air cavity and typically include a shading device in the cavity, have been successfully used on a number of projects in Europe for the past 20 years, as well as a few in the US. More recently, the compact double skin facade known as MFreeS, which is a unitized cavity wall with integral blinds, has been developed by Permasteelisa Group and its research partners. To date, there are fewer applications of these double skin facades in the US market, due primarily to the lower cost of energy and less-stringent building codes.

This study uses whole-building simulation software to compare annual energy consumption of conventional, double-skin, and MFreeS facades in various US cities in a hypothetical south-facing office room, for the purpose of quantifying performance of the various systems.

The results show that overall building energy consumption can be significantly reduced by the use of double-skin and *mfree-S*℠ facades - by as much as 20% in most climates – relative to the baseline single skin façade. It is also seen that the conventional steady-state measures of thermal attributes, such as U-value and solar heat gain coefficient, are poor predictors of actual energy use for buildings with dynamic facades. The use of whole-building simulation tools has the potential to save more energy on a yearly basis in the US market.

KEYWORDS

Unitized curtainwall, double-skin, closed-cavity façade, adaptive, dynamic, innovative, ventilated, energy efficiency, acoustic, holistic, sustainability, condensation

INTRODUCTION

Facade design in the last 50 years has seen tremendous innovation in the area of thermal performance. Some notable developments include insulated glazing units, which became commercially viable in the 1960's and significantly improved the u-value of glazed wall systems. Shortly thereafter, in the 1970's, the concept of pressure-equalization in curtain wall design brought significant improvements in water management and reliability (WBDG, 2017). During the energy crisis of the 1970s, low-emissivity coatings were developed by DOE-funded research at LBNL and Suntek Research Associates. This technology was a significant advance in thermal performance, saving an estimated 1.5 quadrillion BTUs annually in the US market alone (EERE, 2017). These innovations were widely adopted and today form the basis of most curtain wall systems.



Figure 1: Post Tower (2003) by Helmut Jahn in Bonn, Germany features a double skin façade.

Left image © Daniele Domenicali. Right image by Wolkenkratzer (https://commons.wikimedia.org/w/index.php?curid=25687313).

Today, double-skin facades are more prevalent in Europe than in the US market, due to several factors. These include 1) the higher cost of energy in the EU market (requiring better thermal performance), 2) familiarity of tradespeople with the systems (resulting in faster installation and lower cost), and 3) more stringent building code requirements for energy performance.

Based on feedback from clients and consultants, the Permasteelisa Group has identified several specific factors which limit the implementation of DSFs in world markets:

1. The need to clean and maintain four glass surfaces, instead of two in the typical single skin façade (SSF).
2. The reduction in effective useable area of the floor plate, due to the cavity depth (typically one meter) or opening door for maintenance.
3. The need for access to the cavity for maintenance requires opening the inner skin, which prevents full utilization of the areas at the perimeter, which are typically the most desirable spaces in the building.
4. The risk of condensation on the interstitial glass surfaces between the two skins.
5. The added cost and construction time of building two discrete wall systems.

To address these factors, the Permasteelisa Group and our research partners have developed a new dynamic facade system, known as ***mfree*-S**[ccr]. Components of the system are shown in the exploded axonometric (Fig. 2). The system is comprised of unitized panels with a depth of 6 to 8 inches, similar to a standard double-glazed unit (DGU). Blinds are protected in the cavity, and a low-pressure supply of dry, clean air prevents condensation and dust. This provides the thermal advantage of an exterior operable shading device without the high maintenance costs. Because the system is completely closed, it can be installed in the same manner as SSF. The shading controls are programmed by the blind control management software, which has several benefits: the facade can communicate with the HVAC system, the panels can be reprogrammed to account for changes in shading conditions (i.e. a new building adjacent), and one wall type can be used for all elevations and exposures.

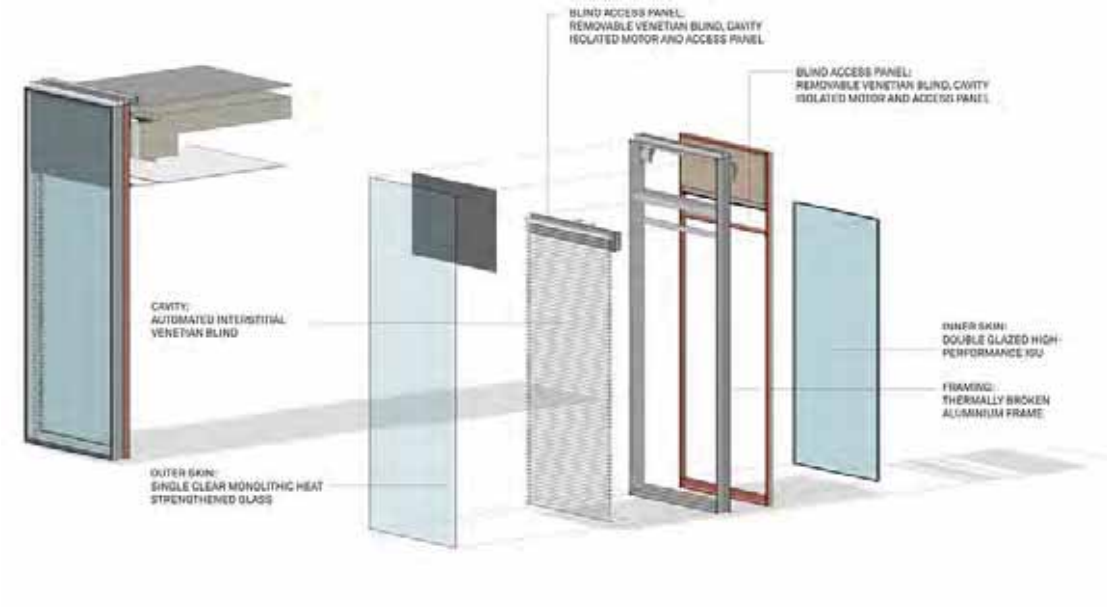


Figure 2: Exploded diagram of MFreeS system. Image by AECOM.

All blinds integrated in the blind cavity are thoroughly tested at full scale and at project specific cavity conditions. Cost-effective premium blinds will be made to have life-expectancy and durability of the integrated blinds to match durability of double glass. Moreover if early failure of a blind would occur, a maintenance hatch allows access for repair/replacement of the blinds and motors are always direct accessible the inside of the building.

To evaluate the airflow required to offset condensation with overly pressurizing the cavity, Permasteelisa Group developed a detailed analysis software tool, known as DSCAT (Laverge et al, 2010). This allows the airflow system to be designed case by case, for projects with various unit sizes and climatic conditions.

A comparison between traditional facades, including SSF and DSF typologies, and ***mfree*-S**[ccr] technology is needed to relate their performance requirements, such as energy impact, thermal comfort, acoustic comfort, condensation risk, cleaning and maintenance cost, overall project cost, etc. Software analysis tools have been developed for quantitative performance assessments such as energy consumption, thermal comfort, and acoustic performance. Qualitative evaluation is also provided for the other facade behaviors.

OVERVIEW OF FAÇADE TYPES EVALUATED

In this study, the thermal performance parameters of the following five facade types are evaluated and compared in several cities in the US market (Fig. 3):

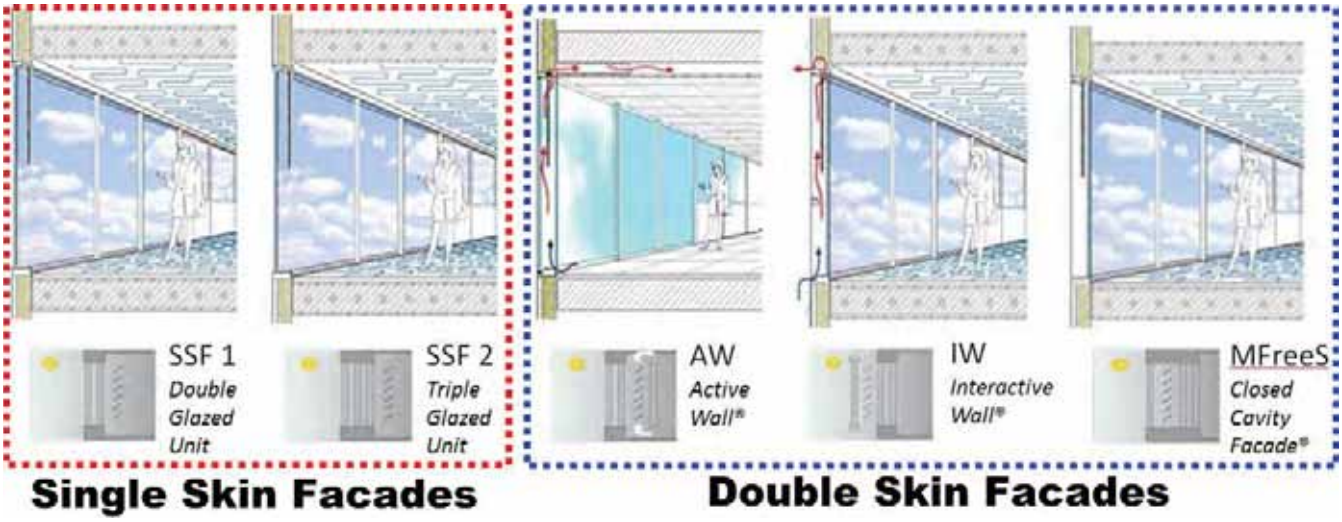


Figure 3: Typologies studied. Image by Permasteelisa Group.

1. Single-skin facade 1 - A double-glazed unit (DGU) with internal blinds in the room and a high performance low-E coating on surface #2. This is considered standard practice in most US cities today and serves as a baseline.
2. Single-skin facade 2 - A triple-glazed unit (TGU) with internal blinds in the room and low-E coatings on surface #2 and surface #5. This is an improvement to Facade 1 which clients sometimes ask us to consider, for thermal and acoustic reasons.
3. Active Wall® (AW) - A DSF consisting of a DGU on the outside and single glazing on the inside, creating a ventilated cavity where blinds can be integrated and indoor return air passing through the cavity of the DSF is ducted to the mechanical system.
4. Interactive Wall® (IW) - A DSF consisting of single glazing on the outside and a DGU on the inside, creating a ventilated cavity where blinds can be integrated and air flowing from outdoors through the cavity returning back to the outdoors via stack and/or wind effects.
5. Permasteelisa moisture-maintenance free Sustainability Closed Cavity Facade (***mfree-S***℠) - a fully sealed cavity with the same glazing and blind configuration as Facade 4 (IW), with a very low volume of clean, dry air supplied to the cavity to prevent condensation and dust with the cavity at all times. A detailed analysis software tool, called DSCAT, was developed to design the air supply system in order to optimally condition the cavity (Laverge et al, 2010).

METHOD

In order to obtain reliable predicted energy performance for office buildings with dynamic DSF systems and cavity ventilation, it is necessary to use whole building simulation tools. For this purpose, a software program called “CAPSOL-Excellent” was developed as part of a Permasteelisa research program based on collaboration with research partner Physibel (De Bleecker et al, 2007). This software program was used in this comparative study. The base engine of the software is “CAPSOL” which was validated against numerous international standards (Physibel, 2002). In a dedicated research program known as “Active Facade project” (BBRI, 2002), evidence was given that reliable assessments can be made when using such detailed dynamic whole building simulation methods. An example from this research is shown in Figure 4, where the temperature profile of an Active Wall® is measured and recorded in a Paslink test cell, as well as several different software tools. The CAPSOL-Excellent prediction was in very good agreement with measured results.

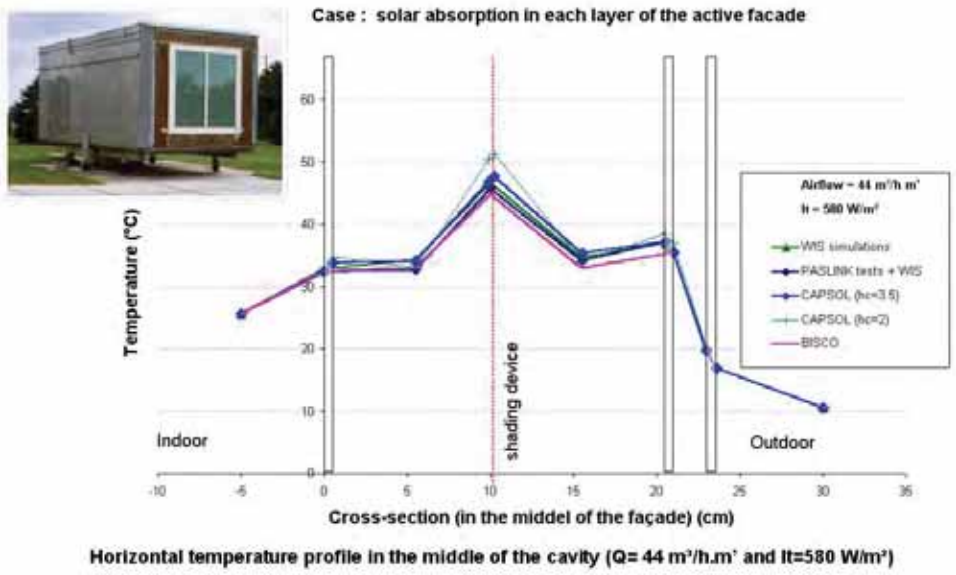


Figure 4. Validation of software engines. Image by BBRI.

For the evaluation of the five facade types shown in Figure 3, a south-facing office room was modeled, with the following inputs and assumptions:

Assumptions	
Room Dimensions	16’-4” (5m) deep x 9’-10” (3m) wide (curtain wall full width)
Floor to Floor height	12’-4” (3.75m)
Vision/Spandrel Ratio	65% vision / 35% spandrel
Internal Wall Type	Drywall with 2” mineral wool
Facade Orientation	South
Sun Sensor Level to Close Blinds	63.4 BTU/hr/ft^2 (200 W/m^2)
Ventilation through Cavity	2119 ft^3/hr (60 m^3/hr)
Outdoor Air Rate	2384 ft^3/hr (67.5 m^3/hr)
Comfort Hours	8am - 5 pm, Monday - Friday
Heat Exchanger Efficiency	67%
Heating System Efficiency	85%
Cooling System COP	3
Low-E coatings	High Performance (HP): VNE-63 by Viracon Low-E: iPlusE by Interpane
Glass substrate (coated & uncoated)	¼” Clear (6mm)
DGU/TGU Cavities	½” Air (12mm)
Ventilated Cavities	7-⅞” (200mm)

Sample weather data was used as input in CAPSOL-Excellent for each city is shown in Figure 5 (Meteonorm v6.1). For each climate and facade type, the heating and cooling power is varied in the simulation to optimize thermal comfort. The cooling or heating power is varied to minimize or 'zero out' yearly transgression hours, defined as hours where the interior temperature exceeds 77 °F or falls below 70 °F. By measuring the energy required to reach this target for each facade type, we can compare them on a level playing field. Note: for glare control, the blinds are included in this analysis for all facade types, including the SSF's. The blinds are automatically lowered when a threshold solar intensity (W/m^2) is reached.

For Façade type 5, ***mfree-S***^{vcr}, the blinds are modeled in two settings: blinds fully up, and blinds fully down and closed. As noted in the table above, the sun sensor level to close the blinds is set to 200 W/m^2. Although this simple setting was chosen for ease of comparison between the different façade systems, the ***mfree-S***^{vcr} control system can handle very detailed blind control settings including many in-between angle changes for glare and energy optimization.

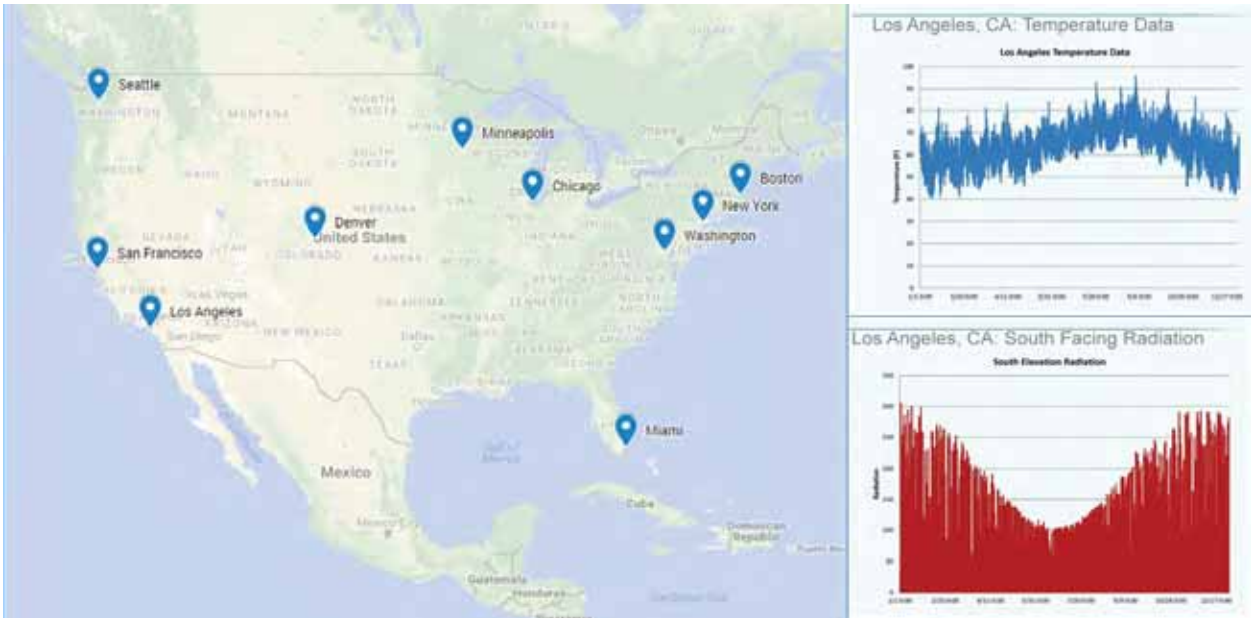


Figure 5: Map of climates studied, example weather data. Map data © 2017 Google Maps, graphs by Permasteelisa Group.

To get a wide range of climate types and responses, 10 locations were studied:

- Boston, MA
- Chicago, IL
- Denver, CO
- Los Angeles, CA
- Miami, FL
- Minneapolis, MN
- New York, NY
- San Francisco, CA
- Seattle, WA
- Washington, D.C.

DATA

Figures 6 through 15 show the thermal and energy results of the subject room for each city. In these graphs, the five facade types are shown on the top as input. The following results are presented:

- The conventional steady state performance parameters of the glazed system in accordance with ISO 15099 (2003): U-value, solar heat gain coefficient (SHGC), and visible light transmittance (VT);
- The yearly total primary energy consumption of the office spaces by means of a detailed, dynamic whole building simulation (CAPSOL-Excellent): heating (RED), cooling (BLUE), and total energy consumption (GREEN) on a yearly basis per square meter of office floor. Notes: 1) these values should be used only for comparison of the variable facade types; for an actual building, this analysis is redone with specific facade and building properties, such as blind color and reflectivity, glass make-ups, etc. 2) The potential energy savings by provision of daylight by dynamic facades is not included in this study.

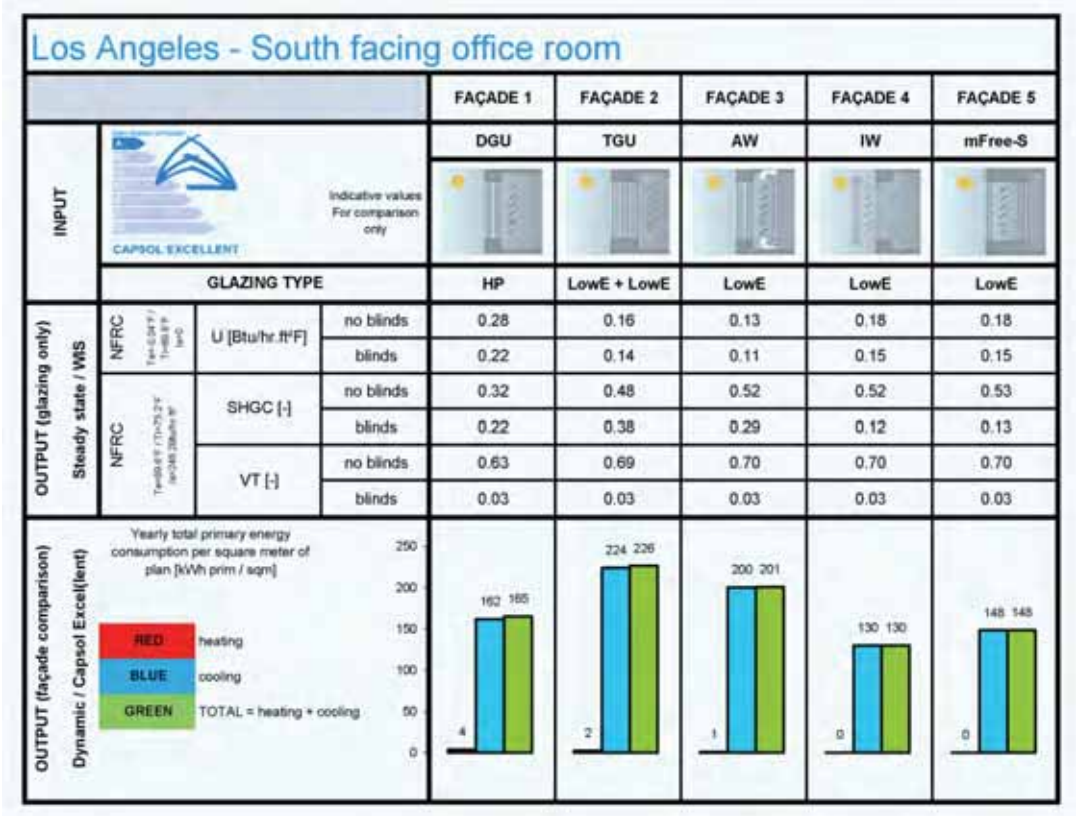


Figure 6: Los Angeles. Diagram by Permasteelisa Group.

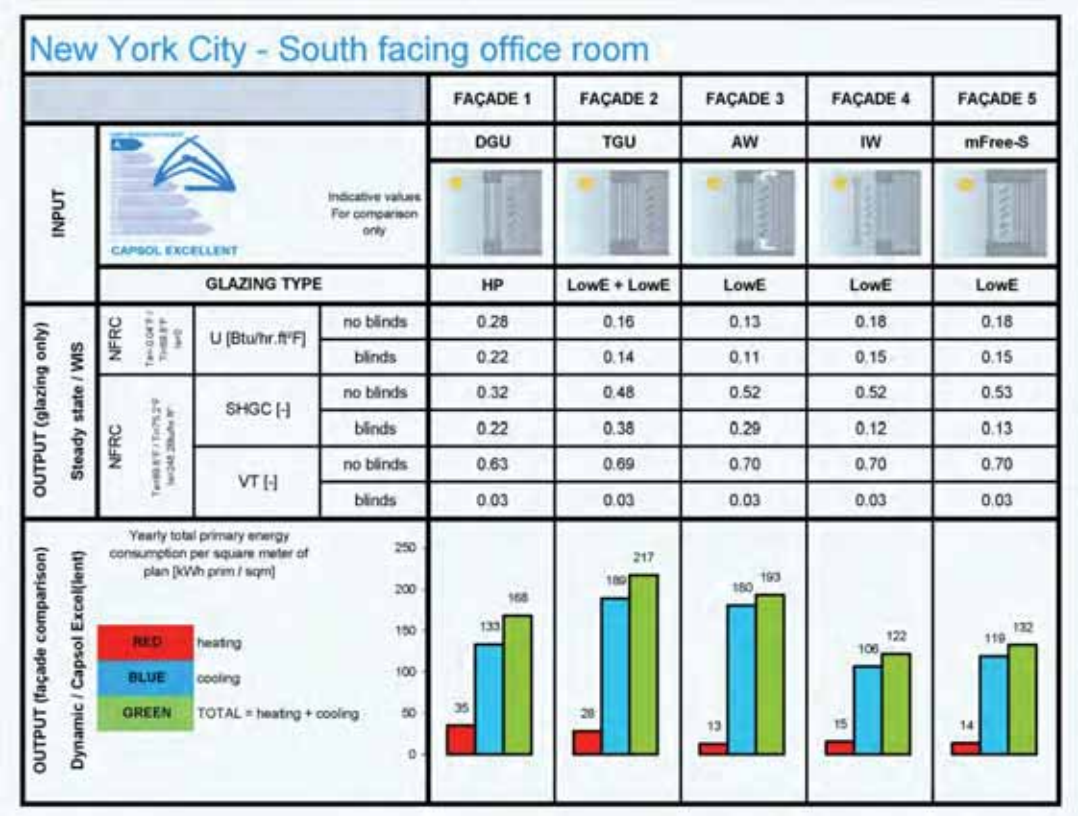


Figure 7: New York City. Diagram by Permasteelisa Group.

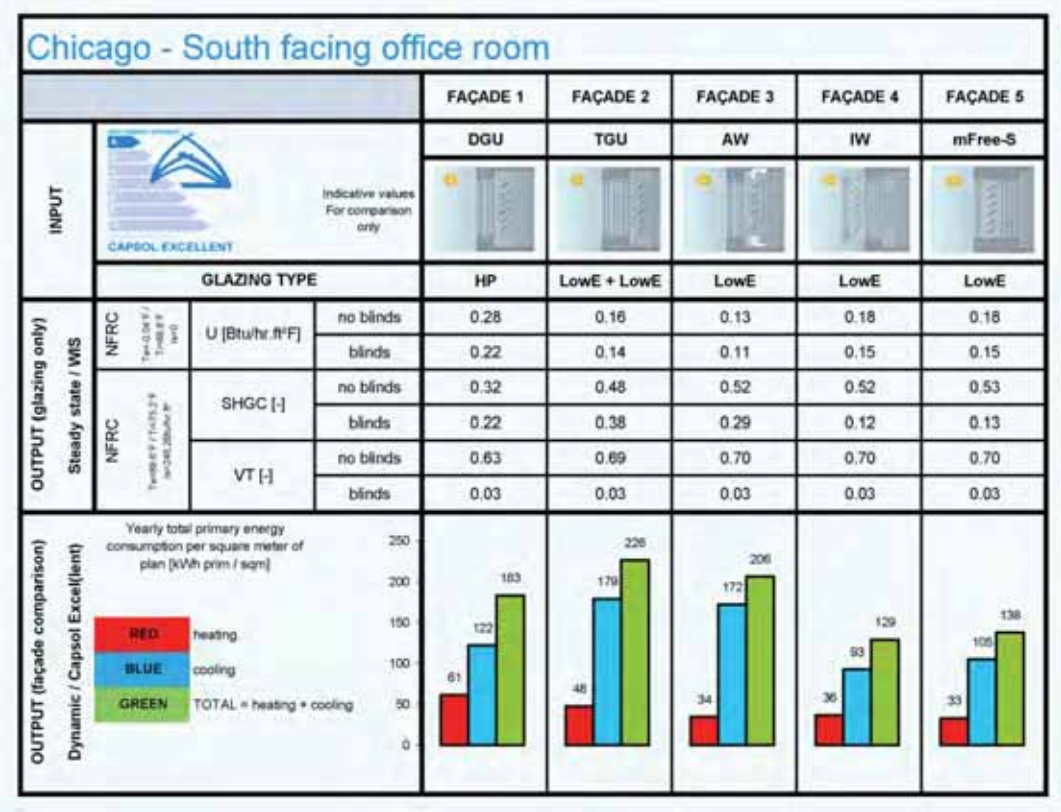


Figure 8: Chicago. Diagram by Permasteelisa Group.

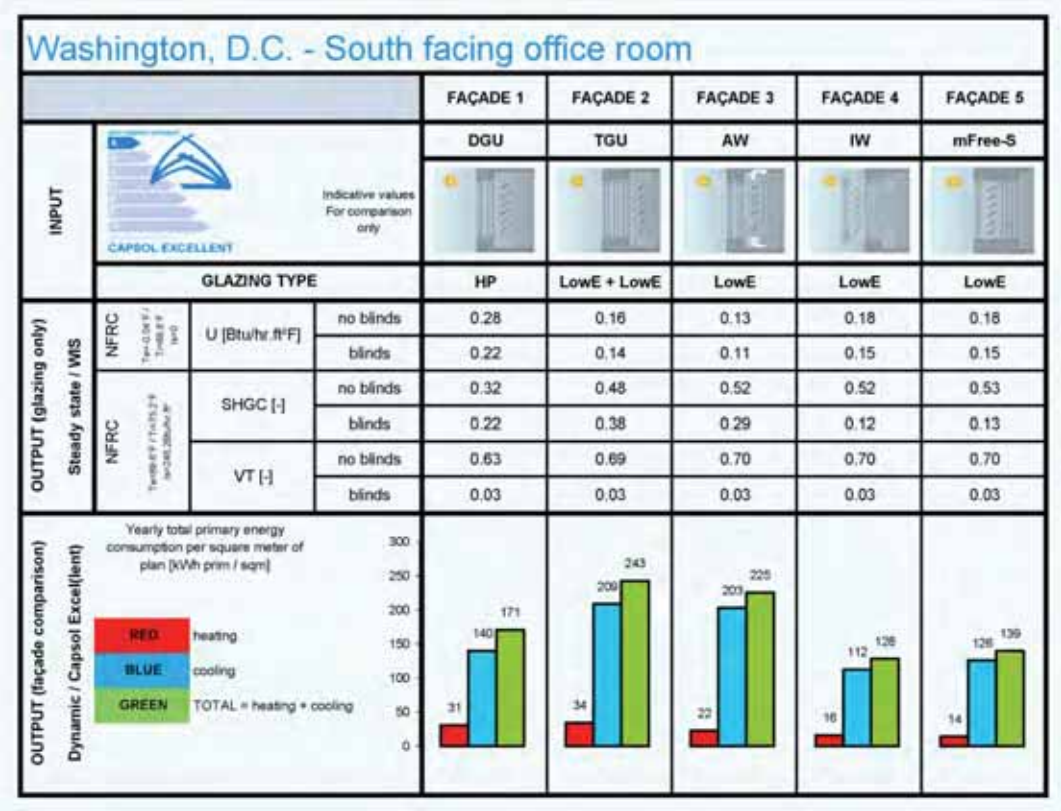


Figure 9: Washington, D.C. Diagram by Permasteelisa Group.

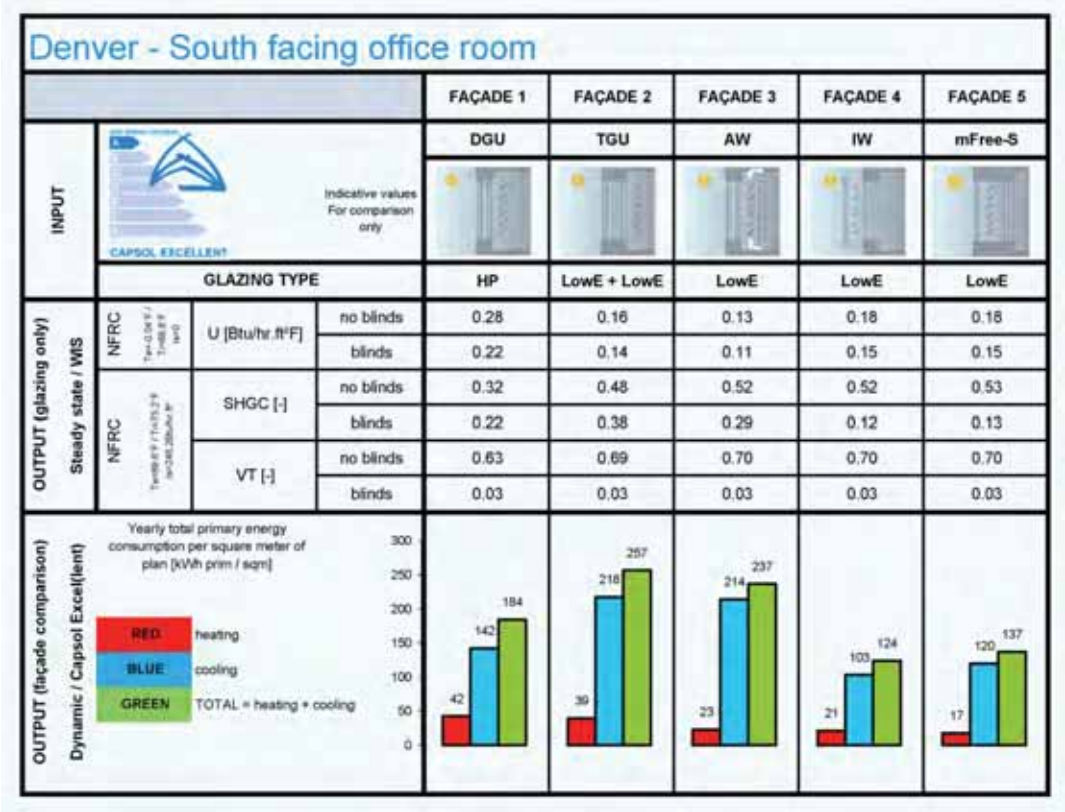


Figure 10: Denver. Diagram by Permasteelisa Group.

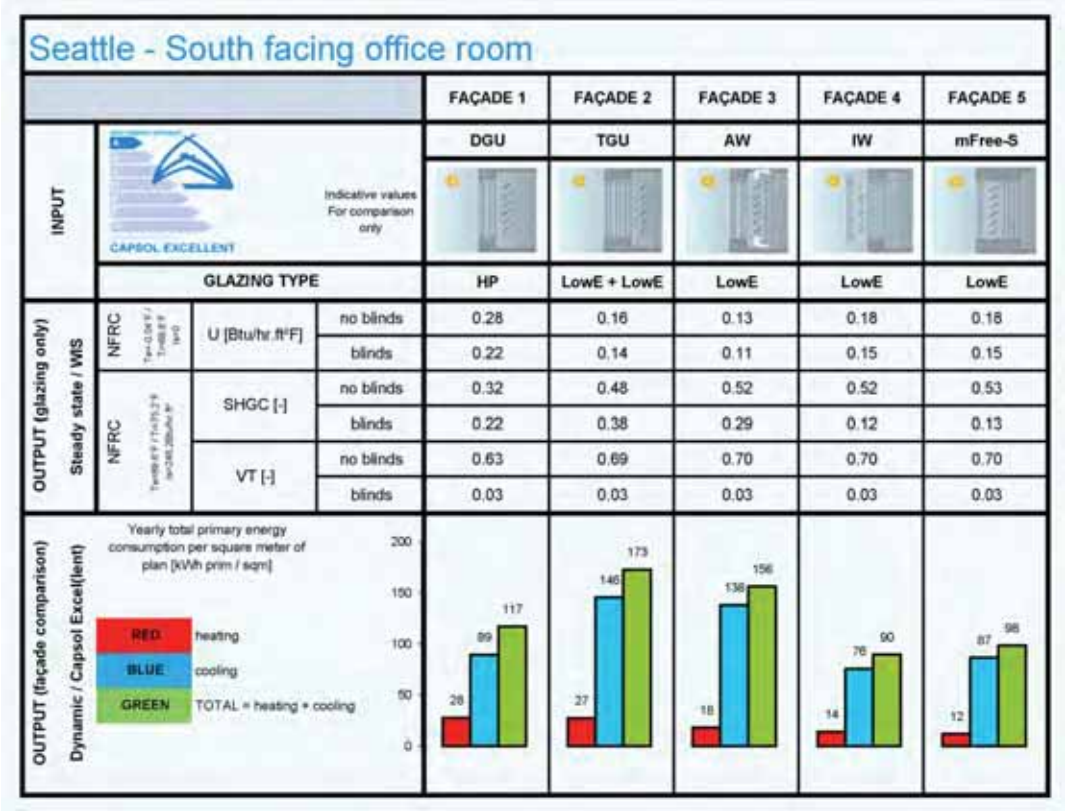


Figure 11: Seattle. Diagram by Permasteelisa Group.

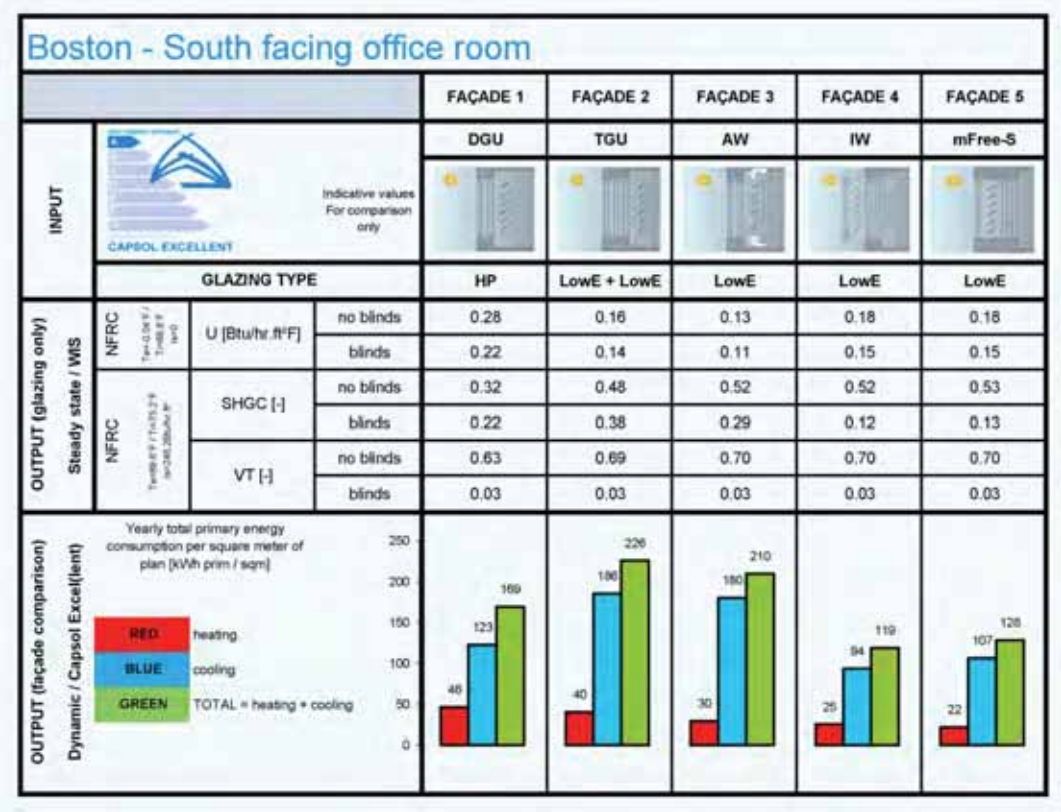


Figure 12: Boston. Diagram by Permasteelisa Group.

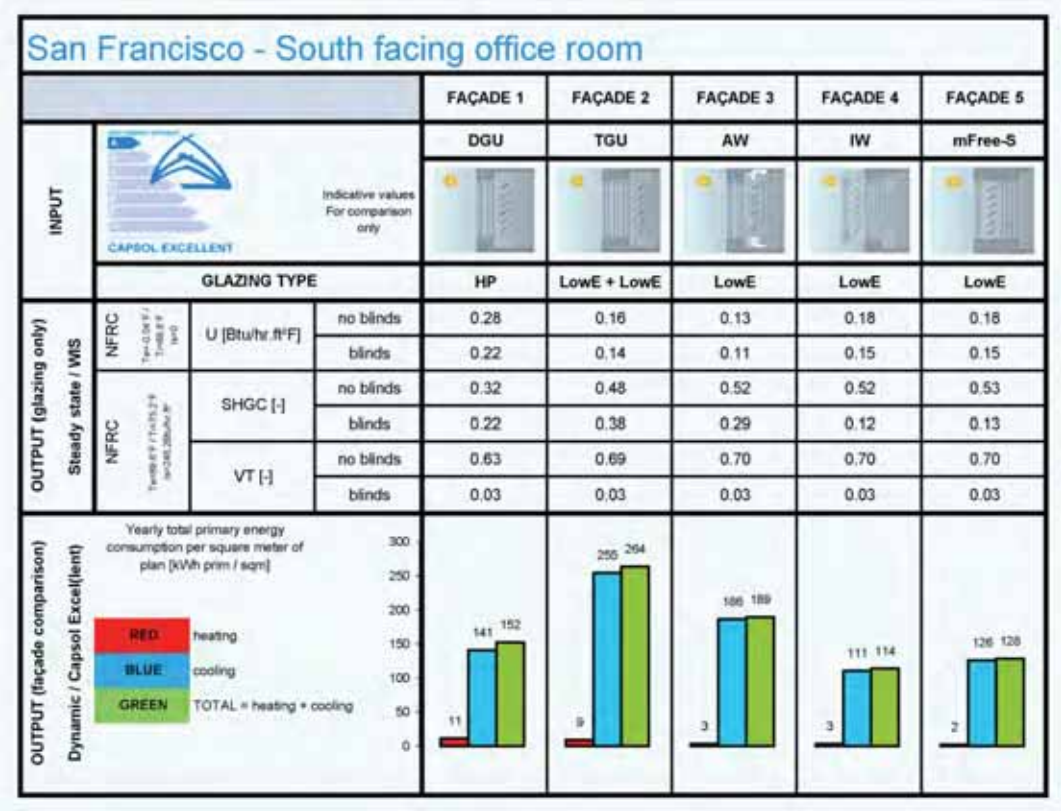


Figure 13: San Francisco. Diagram by Permasteelisa Group.

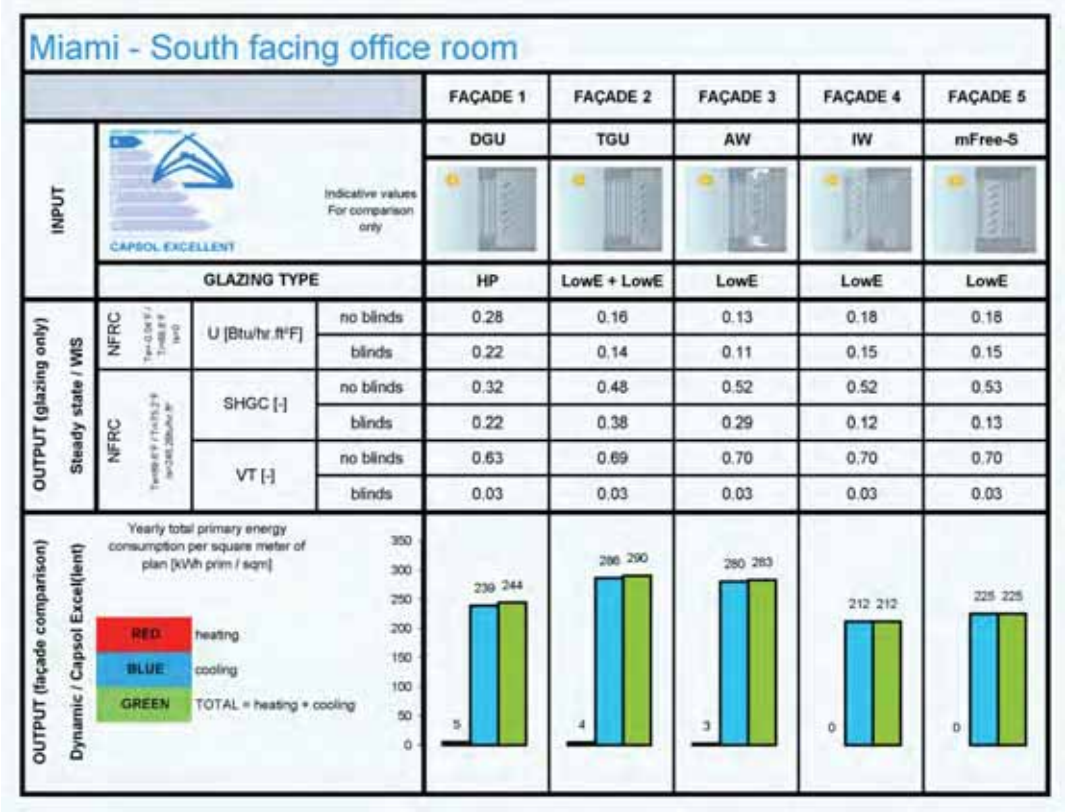


Figure 14: Miami. Diagram by Permasteelisa Group.

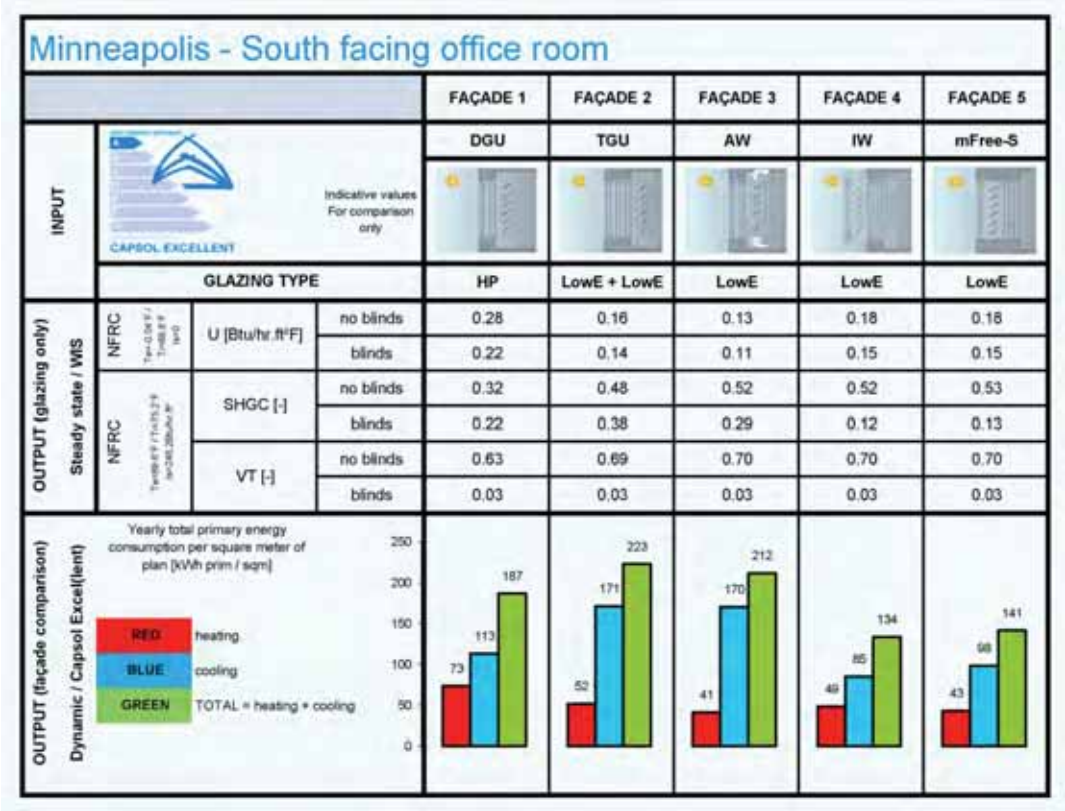


Figure 15: Minneapolis. Diagram by Permasteelisa Group.

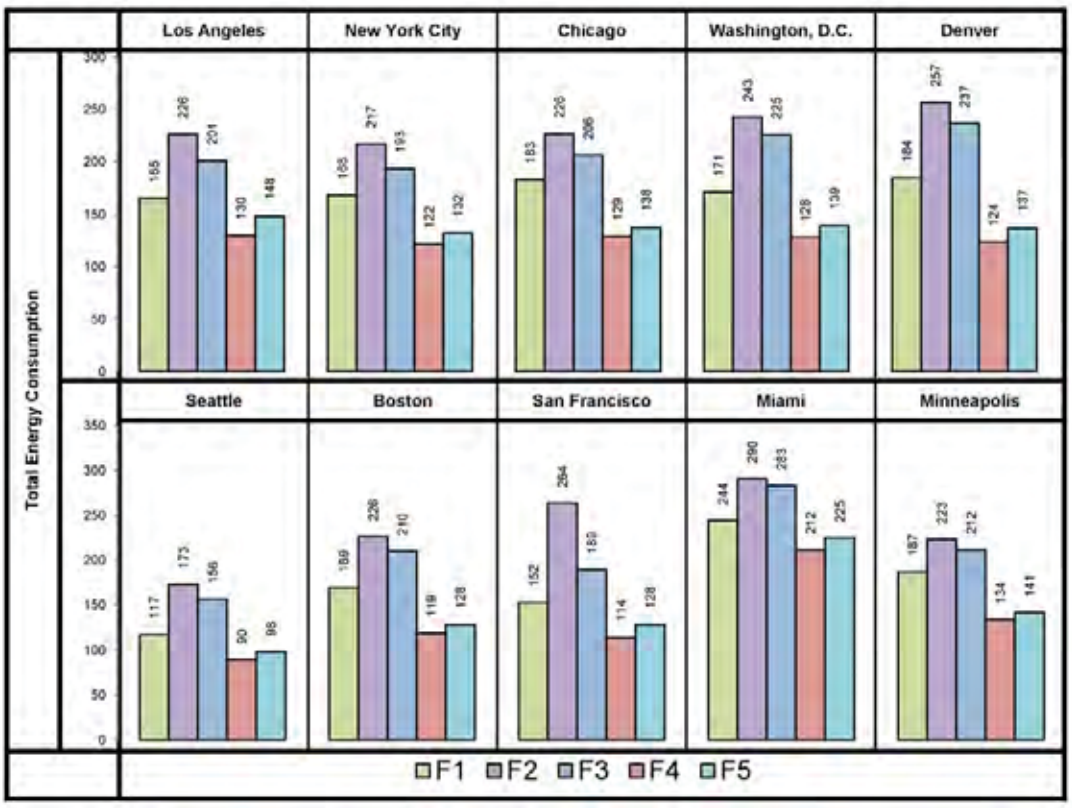


Figure 16: Summary of total energy consumption for all cities studied.

ANALYSIS & OBSERVATIONS

The results from the dynamic whole building simulation show that:

1. In all climates, the use of DSF and ***mfree-S***[cc] results in lower total energy consumption than SSF (most notably in cooling energy).
2. Cooling uses more energy than heating in all climates studies, suggesting that solar control in office buildings is important, and U-value is probably less important than SHGC.
3. On energy performance the ***mfree-S***[cc] Closed-Cavity Facade performs nearly as well as Interactive Wall in all locations while providing other specific requests from clients and architects (maintenance, acoustics, durability).

Facade 1 can be said to represent a baseline for US commercial buildings: a DGU with internal blinds. The high performance coating is VNE-63 by Viracon, with a visual light transmittance of 0.63, and a visible light/solar heat gain ratio of 2.

Facade 2 with triple glazing (only thermal coatings) provides better insulation than the baseline double-glazed unit (solar coating) and is also slightly more transparent. We can see a reduction in one-dimensional, center-of-glazing U-value from 0.28 to 0.16, and a corresponding reduction in heating consumption (e.g. 21% in Chicago climate). However, we notice in all climates that the total energy consumption goes up, due to higher cooling loads. For example, in Washington D.C., the total energy increases 42%.

We can observe a trend of significantly lower cooling energy demand with the IW and ***mfree-S***[cc] (facades 4 and 5) than the SSFs (facades 1 and 2). However, reviewing only the steady state characteristics does not anticipate this performance. For example, comparing Facade 2 (TGU) with Facade 4 (IW): the TGU has a slightly lower U-value and SHGC (when blinds are up), but the annual energy costs are higher in all cities, with the difference greater than 40% in NYC and Boston. The strong variable differences in performance parameters for DSFs and ***mfree-S***[cc] (U-value and SHGC in function of the blind settings and ventilation flow) are the cause of their lower cooling energy consumption. Other researchers have found similar results in dynamic glazing systems such as electrochromic glazing (ref. Window Systems for High Performance Buildings, LBNL,

2004). Regulations and building codes which allow for dynamic modeling in lieu of steady state parameters will allow for more sustainable building skins.

Both Facades 1 and 2 suffer from the 'greenhouse effect': since the shading device is on the room side, incident radiation has to be managed in the form of heat build-up in the room. Facades 3, 4 and 5 feature the shading device in the cavity, so radiation is managed more in the cavity itself and this greenhouse effect in the office is mitigated, with a corresponding decrease in energy use in both hot and cold climates. We can also note these dynamic facades are more transparent (VLT = 0.70), so it is possible to achieve relatively high transparency with low energy use.

Comparing Facade 3 (Active Wall) to Facade 4 (Interactive Wall), we see the effect of moving the blinds further toward the exterior: SHGC with the blinds deployed is reduced by a factor of 2 (when the blinds are down), and there is corresponding drop in cooling energy.

CONCLUSION AND FUTURE WORK

From the standpoint of energy consumption in this study, Facade 4 (Interactive Wall) performs the best in all climates. Some notable examples of this DSF system in use include the Shard in London by Renzo Piano Building Workshop in 2012, and the Tower at PNC Plaza by Gensler in 2015 (Fig. 17).



Figure 17: The Tower at PNC Plaza. Diagram by Permasteelisa Group, image by Connie Zhou.

However, the ***mfree-S*** facade performs nearly as well as the Interactive Wall DSF and offers many advantages, including lower maintenance (no cavity to clean and no damage to the blinds), elimination of condensation in the cavity, more useable floor area, and faster installation. Since its development between the years of 2000 to 2005 by the Permasteelisa Group, this system has been used in over 15 projects in Europe, Asia and Australia. Some recent examples include Roche Building 1 (Fig. 18) and 200 George Street in Sydney, Australia (Fig. 19).



Figure 18: Roche Building 1, Basel, Switzerland. mfree-S *example. Right image © Johannes Marburg Photography.*



Figure 19: 200 George Street, Sydney, Australia. mfree-S *example, with wooden blinds. Left image © Matthew Longden, right image © Alexander Mayes and McKenna Morozer.*

In addition to the five facade typologies chosen for this study, there are a number of other combinations and options that are common in the glazing market today. For example, electrochromic glazing, high performance low E coatings, DGUs with low E coatings on surface #2 and #4 (room-side low E), TGUs with low E coatings on surface #2 and #4, blind color and reflectivity, and other combinations.

Added to these quantitative comparisons, a study is needed which includes all aspects of energy use and cost, considering the lifespan of the building. Ideally this would consider maintenance and cleaning costs, acoustic performance, daylighting, glare control and user comfort, upfront material costs, energy use, durability, life expectancy and embodied energy during production and construction.

Today, dynamic facades with “intelligent” control systems which continually adapt to changing environmental conditions and user’s needs have the potential reduce energy consumption significantly over conventional facade types. Future developments in these systems may include smart grid integration, to control and predict building energy consumption on a neighborhood or regional level.

ACKNOWLEDGMENTS

The authors would like to thank their software and university research partners for their contributions during the developments of the innovative façade solutions.

REFERENCES

Aksamija, Ajla. Sustainable Facades: Design Methods for High Performance Building Envelopes. John Wiley & Sons, 2013.

BBRI(2002), Prediction of thermal comfort and energetic behavior of active facades.

Carmody, J., Selkowitz, S., Lee, E.S., Arasteh, D. & Willmert, T. Window Systems for High-Performance Buildings, New York, Norton & Co. (2004).

De Bleecker, H., Berckmoes, M., Standaert, Piet, Aye, Lu.(2012). MFREE-S Closed Cavity Façade: Cost-Effective, Clean, Environmental. CTBUH Proceedings, Shanghai, 2012.

De Bleecker, H., Berckmoes, M., Van de Linde, L.W., Standaert, P., Blasco, M.(2007). EPBD, Energy Performance of Building Directive. IWT 060756, January.

ISO 15099 (2003) Thermal performance of windows, doors and shading devices – Detailed calculations.

Laverge, J., Janssens, A. Schouwenaars, S. & Steeman, M. (2010). Condensation in a closed cavity double skin façade: a model for risk assessment. Proceedings of ICBEST 2010, Vancouver, British Columbia, June.

National Institute of Building Sciences, “Whole Building Design Guide (WBDG).” https://www.wbdg.org/guides-specifications/building-envelope-design-guide/fenestration-systems/curtain-walls#details (accessed September 12, 2017).

PHYSIBEL, (2002). Capsol v4.0 Manual.

US Office of Energy Efficiency and Renewable Energy, “EERE Success Story.” https://energy.gov/eere/success-stories/articles/eere-success-story-energy-efficient-windows-are-saving-americans (accessed September 26, 2017).

DIFFERENTIATED BUILDING SKIN

An Experimental Case for AM Structural Components



James Warton
HKS LINE
jwarton@hksinc.com

ABSTRACT

The Los Angeles Stadium's doubly curved skin is composed of over 35,000 unique triangular panels covering 296,502 square feet of surface area. The panels are uniquely articulated and cut to specification using a 3-axis CNC die-punch machine and fabricated from 0.125" thick anodized aluminum. The connections supporting these panels require a unique configuration for fixation at each juncture and present a foreseeable entry-point application for additively manufactured (AM) metal components.

An experimental connection prototype has been developed to address challenges unique to its differentiated geometry, fabrication process, and performance criteria. The design-to-fabrication workflow developed for the skin demonstrates improved efficacy at various stages between design development and fabrication, and is being extended for use on 3D printed metal components. Localized topology optimization yields reduced loading over commonly accepted approaches that employ standardization for a worst-case condition. In addition, the proposed node is discretized into an assembly to accommodate limited build volume commonly associated to AM systems currently on the market. The proposed approach suggests improved production time over experimental alternatives. Potential for 3D printing as a fabrication method at this scale of execution is evident. However, software developments and availability of manufacturing facilities must be realized to achieve feasibility.

KEYWORDS

computational design, design optimization, metal, fabrication automation, direct-to-fabrication, additive manufacturing, topology optimization

INTRODUCTION

The case study presented leverages experiences and lessons learned during the design and development of a cladding system for an NFL football stadium and future home to the Los Angeles Rams designed by HKS Architects. Located in Inglewood, California the project was awarded to Turner Construction Company, with completion scheduled for late summer of 2020. Crown Corr was awarded contracts to assemble and install the 296,502 square feet of stadium cladding and supporting spaceframe. Zahner will perform fabrication for over 35,000 uniquely articulated panels comprising the stadium's aluminum skin and were instrumental in design-assist services necessary to develop this cladding.

These large-scale sports and entertainment venues often challenge traditional means of documentation and necessitate alternative approaches to design development and project deliverables. A promising characteristic of AM is the ability to fabricate complex components directly from a meshed boundary representation. The magnitude of scope and degree of geometric complexity common among large stadium envelopes contribute to this typology's effectiveness for the exploration of additively manufactured structural components. Previous research projects have explored various applications for metal building components using AM. The design methodology described by researchers at Arup are particularly relevant to this exploration (Galjaard et. al., 2015). The abundance of unique geometric conditions and components existing in projects of this scale; however, challenge the feasibility of workflows requiring the use of software where automated interoperability is lacking. Currently, Altair's OptiStruct doesn't provide an API that would enable seamless integration and interoperability between Rhino/Grasshopper. The level of automation to provide discrete optimization is not yet feasible; however, discussion is underway to bridge these labor-intensive gaps.

A geometric framework written by the authors in C++ was utilized for improved computational efficiency over workflows commonly using Rhino/Grasshopper, and was deployed for design development and documentation of the stadiums perforated panels (Warton, J., Dwivedi et. al., 2014). Since the panels are fabricated using a 3-axis CNC die-punch machine, the format for documenting each panel's unique size, shape, and perforation could be provided through discrete text files enabling a more effective file-to-fabrication execution. These panels are fabricated from 0.125" thick aluminum the anodized for a titanium white finish. The perforation pattern consists of up to six hole sizes ranging from 0.375" to 1" at 0.125" increments. The size of each coined die-punched hole corresponds to a global grayscale image mapped to the domain of the stadium skin's parent design surface.

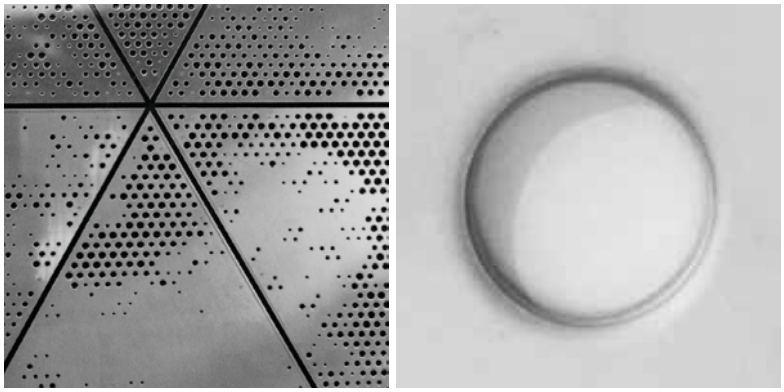


Figure 1: Titanium anodized aluminum panels with coined die-punch perforation pattern and 0.375" open joint and close up showing coined die-punch perforation. Photos courtesy of James Warton.

The structural nodes connecting these panels were selected for the investigation of metal components fabricated using AM with the promise of implementing local optimization rather than a one-size-fits-all approach. While several AM technologies are available for production of parts this size (Sanderson et. al., 2016), a system using powder supported laser sintering was selected. These nodes provide the fixation between up to six adjacent panels and a supporting standoff extending from the spaceframe substructure. Like the panels, no two nodes are the same. This is a factor of the non-uniform curvature of the exterior skin and the underlying structural grid that is projected onto the surface. The typical configuration of each node is a central hub with six elements extending toward the panel's uniquely oriented fastener location.



Figure 2: Additively manufactured node prototype subdivided into separate branching elements. Photo courtesy of James Warton.

Key challenges for this research project stem from lacking availability of workflows that can effectively be scaled to problems of scope reaching in the magnitude of thousands, tens of thousands, or higher. Topology optimization is computationally intensive and the setup time for even one component can be laborious. Modelling efforts required to translate the topology into a functional component are even more involved, requiring hours of meticulous manual operations. Once properly modelled, additional analysis must be performed to validate structural compliance of the part, and may lead to further modelling efforts if stresses exceed acceptable levels. Interoperability between design, optimization, and analysis software limit fluid and efficient execution at the scope required for projects like the stadium in Los Angeles.

Once a satisfactory design is achieved, manufacturing and fabrication constraints often present another set of criteria limiting the viability or efficacy of components. Cost and build time constraints common among most AM systems privilege compact part arrangements that maximize the ratio of part volume to build height and build volume. Nesting of components within the available build volume may improve this ratio; however, further gains can be achieved through strategic discretization of parts into assemblies. Methodologies for this discretization require further investigation, and the effective integration of this step within an automated workflow requires development to be implemented at scale. To capitalize on the potential gains of local optimization and direct-to-fabrication the roadmap for a fully automated workflow must be understood. The objective for this ongoing research is the development of a platform that supports this workflow.

METHOD

Computational overhead associated to the abundance of panels and nodes existing within the stadium's skin present significant challenges for design-to-fabrication automation. To address these challenges, a framework was developed in C++ that would allow for multi-threading on the CPU as well as access to the GPU for intensive matrix calculations. Implementation was tested on the panel geometry prior to beginning work on the supporting nodes. To improve computational performance, the C++ framework developed by the authors leverages multithreaded functions and implements open source libraries such as Armadillo v5.600.2 (Yalamanchili et. al., 2015) and ArrayFire v3.2.2 (Levelle et. al., 2016) for GPU based matrix operations and image processing functionality. OpenGL is also implemented for visualization purposes.

A design surface modelled in Rhinoceros was shared among consultants as a working input for coordination on the stadium's skin during initial stages of development. The final record documents included both design surface as well as the generic tessellated panels, but a more discrete method was developed to describe the individual panels for fabrication. During pre-design coordination between HKS, Studio NYL, Walter P. Moore, and Zahner, Zahner's team communicated that one of the primary bottlenecks for fabrication was associated to setup and translation of CAD files, such as .DXF or .DWG into machine instruction. For this reason, the authors proposed a text based file format containing all dimensional criteria as the method for documentation and delivery. This would enable the fabricator to automate the translation of these files directly into machine instruction and minimize file conversion time required for setup on each panel. Once the doubly-curved surface was tessellated into panels for production, the node center points were extracted using Grasshopper and formatted into a single text file. The point data and corresponding UV parameters extracted from the design model was formatted into eight lines of instruction per panel.

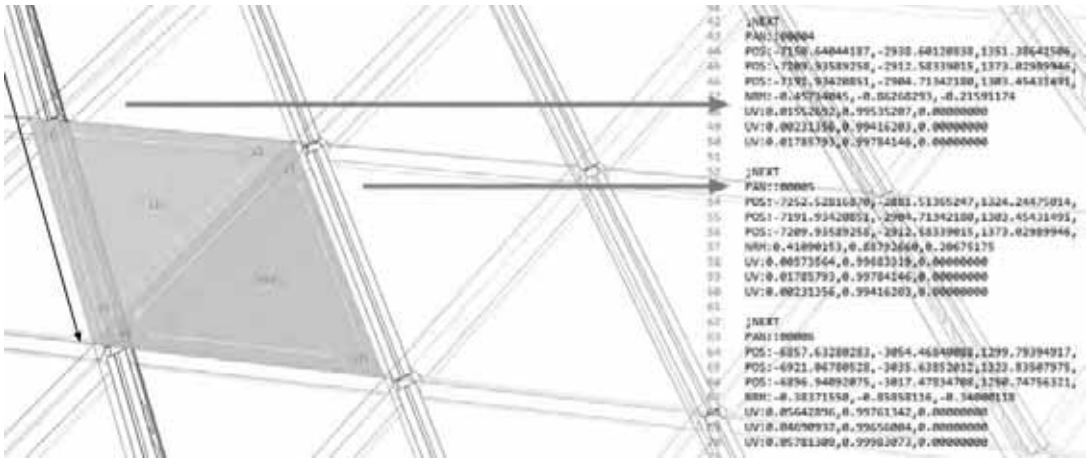


Figure 3: Panels in world coordinate system and associated UV parameters corresponding to parent design surface. Diagram courtesy of James Warton.

As the panel identification and its node positions are read using the C++ application described previously, this data is stored and a new panel object is defined. The application calculates the transformation from 3D world coordinates into 2D machine space and stores instances of each becoming part of the panel objects properties. After being described according to a local coordinate system, the panel corner positions and edges are defined according to a predetermined edge offset parameter, the panel is subdivided with a perforation grid unique to each panel's geometry, then the fastener positions are located to coordinate with this grid. A separate routine is then performed to map pixel values from the global design image into the panel's perforation grid. Grayscale values from the design image ranging between 0-255 are then remapped to correlate with hole sizes corresponding to one of six die punch tools used during the fabrication process. Once a panel's fabrication data is fully defined, a text file is generated containing a comprehensive geometric description of the panel.

Proper coordination was ensured through an agreed set of file formatting conventions such as feature tokenization and panel nomenclature. Each panel was described in both world/project and local coordinate systems. Node center point positions, corner positions, and panel orientation vectors were provided in the world coordinate space for validation against the three-dimensional model file. For fabrication, node positions, finished corner positions, fastener positions, and perforation center point positions with their specified diameter were provided within local coordinate space using a consistent counter-clockwise winding order. These local coordinates were established based on an origin point and x-axis coincident with the first node position and first panel edge respectively. Panels were also designated as right handed or left hand to ensure consistent directionality of material grain defined by the rolling direction or coil orientation prior to cutting and forming. This also allowed for positioning of panels to minimize sheet waste during the fabrication process.

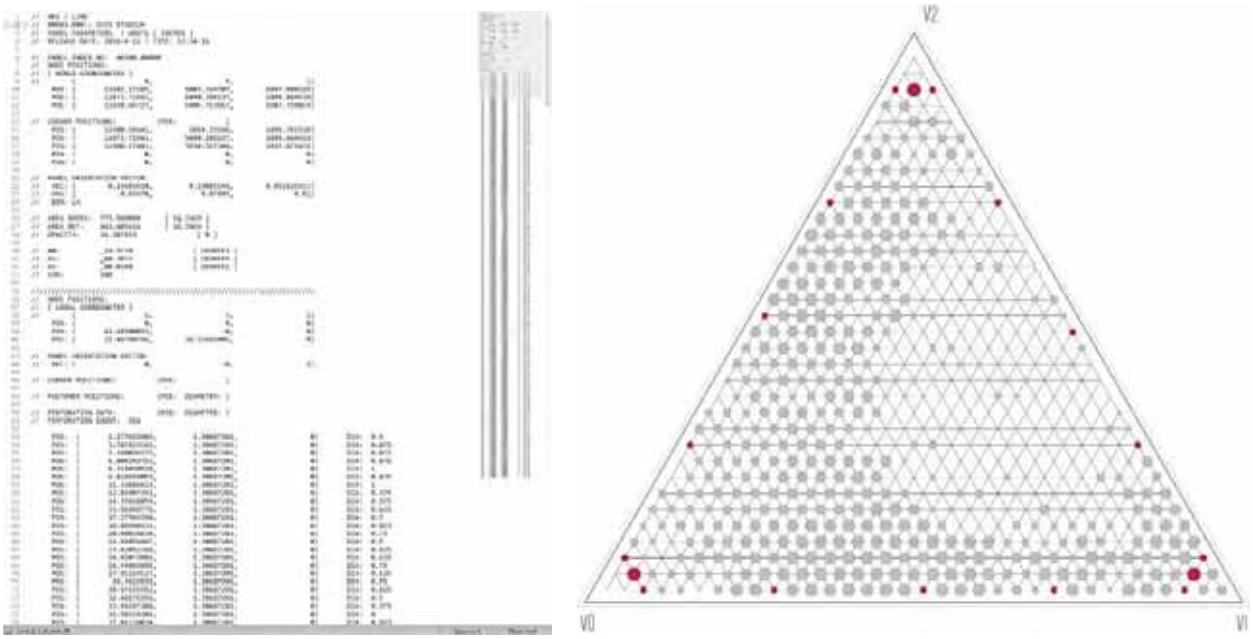


Figure 4: Discreet text file containing description of panel geometry in machine coordinate space, and graphic visualization of panel. Diagrams courtesy of James Warton.

A graphic interface provides a searchable visual display of all the panels within the currently processed batch alongside a global view of the stadium indicating the active panel's location. Various display states are also available describing overall system mappings of area deviation, angle deviation, and panel opacity. The average file size is 47KB and file sizes range between 4-145KB dependent upon quantity of perforations specified for each panel.

The C++ library used for developing these perforated panels has since been extended to address the additional geometric complexity required to describe the design volume, fixation points, and loading conditions used for the initial stage of topology optimization. The node construction process begins with the theoretical vertex shared among adjacent panels. The upstand vector and interior offset is calculated based on the vertex normal and establishes the base element for the node's tree structure. The panels associated to each node and the respective fastener are then used to locate each fixation position and orientation vector. These vectors provide the outermost elements for the node's tree. The connecting elements between fixations at panel and upstand complete the tree and a volumetric bounding condition is defined. The bounding conditions represent the maximum design volume and can be used as an input for the topology optimization process. While

this framework successfully automates the geometric conditions and data structures for the full scope of node conditions supporting the stadium's skin, interoperability between optimization solvers are still being explored.



Figure 5: Discreet text file containing description of panel geometry in machine coordinate space, and graphic visualization of panel. Diagram courtesy of James Warton.

Once the branching structure is described as an assembly of linear elements, the initial FEA can be performed to establish the baseline part volume. Ultimately each member of these baseline branching volumes will be size optimized through multiple iterations of FEA using a procedurally defined load case specific to each node. The FEA solvers developed for this framework have been validated against proprietary solvers; however, have not at present been integrated into a fully automated process. The resulting volume or boundary representations serve as an initial design space and are provided as an input for topology optimization. To test this approach alongside fabrication process constraints, a generic node was generated and the topology optimization process was performed using Altair's SolidThinking Inspire. The topology mesh generated from this process was analyzed to ensure compliance and subsequently reduced in density until failure. After the minimum compliant material density is achieved and a corresponding volumetric mesh topology generated, the part geometry was modelled with further refinement. The appropriate fixation and design features necessary for a fully functional part were then added. The part was analyzed to ensure validation against the initial load cases. The resulting part constituents are then reoriented to fit comfortably within the 800 x 400 x 500mm (x, y, z) build volume of Concept Laser's X line 2000R; however, it became clear that the estimated 50-hour build time and cost could be greatly improved upon. Dividing the node into discrete linear armatures allowed for a more compact arrangement where two nodes could be packed within an even smaller build volume.

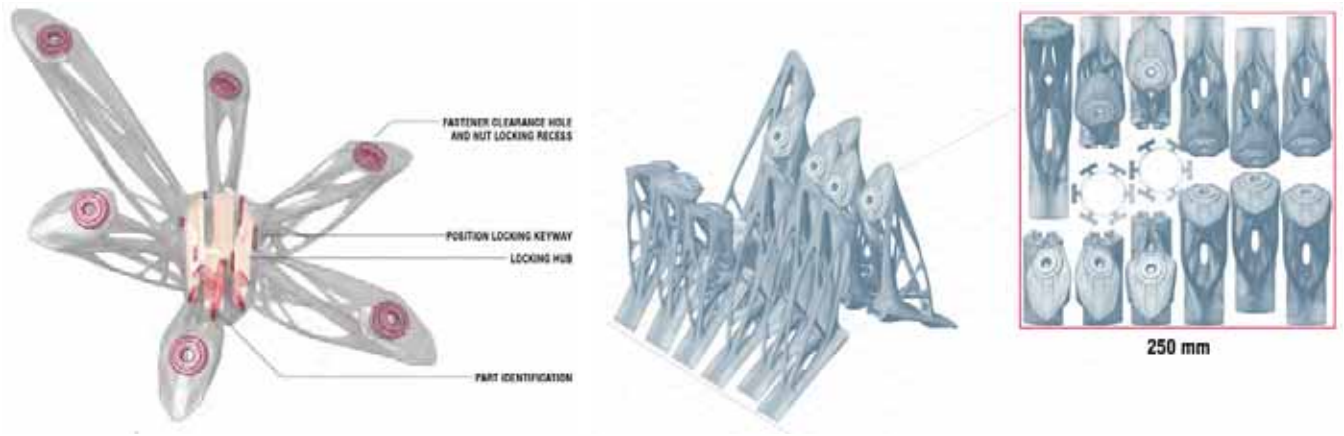


Figure 6: Once the node is separated into individual branching elements, these parts can be consolidated on a more compact build plate. Diagrams courtesy of James Warton.

This allowed the use of Concept Laser's smaller M2 cusing system. This machine features a 250 x 250 x 280mm (x, y, z) build volume. Several iterations of this design approach were conducted ultimately reducing the cost per node by almost 60% while maintaining an equivalent build time. The initial design was quoted at approximately $11,000. Incorporating the assembly strategy and organizing the components to maximize the available build volume reduced the cost to $3,750 per assembly. Because the development of this theoretical node was performed in parallel to the design development of the

actual for-construction systems a true equivalent comparison was not possible at the time this paper was prepared. The skin, supporting substructures and primary framing went through numerous options and were fundamentally altered after the theoretical node development was nearing fabrication. Due to this situation performance concerns have been focused on workflow and prototyping constraints that would inform future research and development of a computational design tools that automates many of these labor-intensive operations.



Figure 7: Additively manufactured node prototype subdivided into separate branching elements. Each branch is indexed per its position relative to the building envelope. A unique locking key prevents each component from being improperly assembled or out of sequence. Photo courtesy of James Warton.

Subdivision approaches such as this may prove advantageous for production; however, this decision would have inevitable impacts on production time and coordination due to the additional assembly. It is likely that the assembly could be performed concurrently with subsequent print processes.

DATA AND EVALUATION

While it is generally accepted that lower-level programming languages such as C++ outperform higher-level programming languages, a benchmarking trial was established to observe this in quantifiable terms. Grasshopper offers limited ability to profile its performance, so a precise measure of time required to complete computation for each function is not available. Because of this limitation, this trial was conducted recording overall calculation times rather than conducting a piece-wise process comparison. The two most computationally intensive functions within the panel construction process were calculating the subdivision grid for perforation positions and the evaluation of perforation size. These functions were implemented within Grasshopper to benchmark against code written in C++. These outcomes were then compared to implementation written in C++ using both single-threaded and multi-threaded programs executing the entire procedure required to define and document the perforated panel system. To further simplify the comparison, the input data describing each panel's world coordinates was internalized within the .gh definition, rather than read from an external source file. Each trial was conducted five times, with the resulting averages recorded on the following graphs.

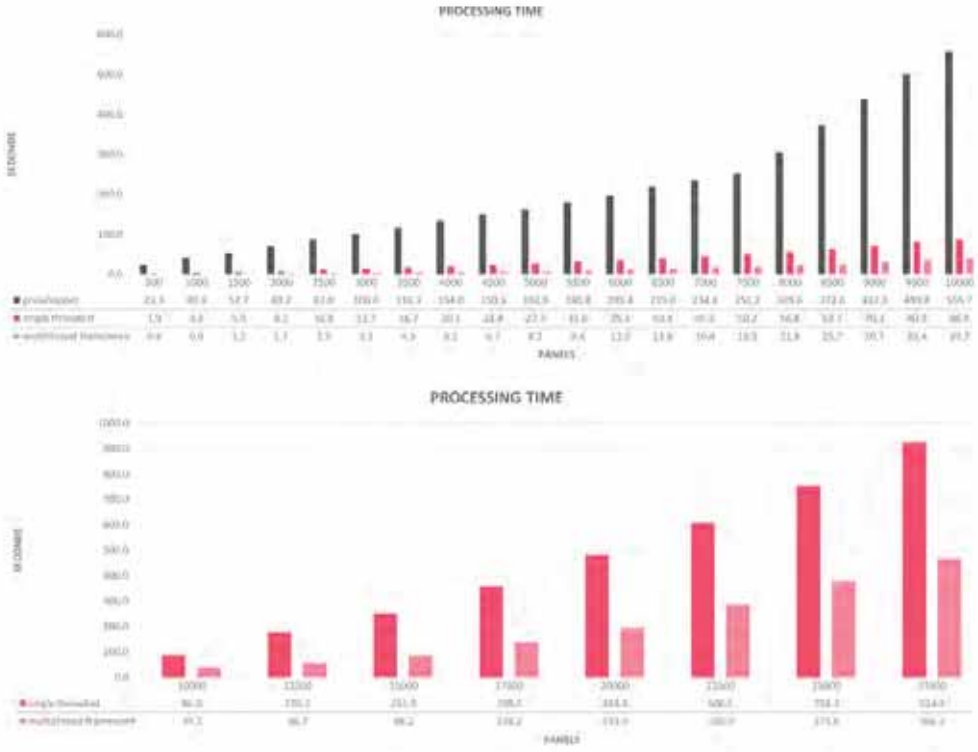


Figure 8: Performance comparison showing computation speed for Grasshopper and customized code written in C++.

Comparison showing single threaded vs. multi-threaded performance of customized code written in C++. Diagrams courtesy of James Warton.

Computational performance improvements are noted using the methods developed for this project; however, they have not been fully validated for the scope of operations required for locally optimized structural components designed for AM. Localized topology optimization and FEM validation of on a large scale is inefficient due to the workflow connectivity and interoperability gaps between architectural design tools and engineering applications. The programs that are effectively appropriate for this task on a small scale are not currently suited for automation.

CONCLUSION

The implementation of AM building components represents a foreseeable area of innovation. This technology promises the ability to produce architectural and structural components with specificity and complexity that are restricted by other manufacturing processes. While this opens the possibility for improved structural performance by reducing weight and material associated to designing each part for a worst-case condition, the ability to execute at scale optimization is not currently feasible (Pottman et. al., 2015). The workflow being developed demonstrates foreseeable performance improvements over the widely accepted alternative. Additional work is required to bridge interoperability between design and engineering platforms, but the development of a fully automated workflow is needed to effectively realize the potential of additive manufactured structural components. The release of an API for Altair's OptiStruct and/or Inspire would greatly aid interoperability and access directly to the backend topology optimization and FEM solvers. This would allow further validation of the proposed processes. In the absence of this connection collaboration with Altair is among the next steps toward bridging this gap.

Components designed to maximize compact build volume utilization demonstrate improved production cost, but the time required using workflows currently available can be restrictive for situations with an abundance of non-standard parts. If an understanding of these fabrication constraints can be incorporated into the design process this could lead to improved cost feasibility for AM applications. The workflows developed for AM should address these constraints and allow for solutions that automate or minimize time required to accommodate these conditions. Additional advantages may arise from the direct-to-fabrication processes used for describing AM components and free up time typically associated with formatting and documentation.

The experimental connection prototype presented addresses many of the challenges associated with differentiated geometry, fabrication process, and performance criteria; however, the process employed during design was not ideal. Software developments must be realized before implementation at scale can be obtained.

ACKNOWLEDGMENTS

The research for the paper was financially supported by HKS Architects. Without the influence and encouragement of Dan Noble and Heath May this research would not have been possible. I am also grateful to the various members of the design team participating on the Los Angeles Stadium. The intelligence and collaborative spirit among this group was inspiring and provided valuable insight. Involvement on this project was essential to the foundation of this ongoing research.

REFERENCES

Galjaard, S., Hofman, S., Perry, N., Ren, S. “Optimizing Structural Building Elements in Metal by Using Additive Manufacturing.” Proceedings of the International Association for Shell and Spatial Structures (2015).

Galjaard, S., Hofman, S. and Ren S. “New Opportunities to Optimize Structural Designs in Metal by Using Additive Manufacturing.” Advances in Architectural Geometry. (2014): 79-93.

Levelle, E., Heijden, R., Riese, M., and Ra, N. “Data and Order, The Making of Complex Architecture.” Façade Tectonics 2016 Conference Proceedings, Vol. 2 (2016): 335-344.

Pottman, H., Eigensatz, M., Vaxman, A., and Wallner, J. “Architectural Geometry.” Computer and Graphics, Vol. 47 Issues C, Pergamon Press, Inc. Elmsford, New York, (2015): 145-164.

Sanderson C. and Curtin, R. “Armadillo: a template-based C++ library for linear algebra.” Journal of Open Source Software, Vol. 1, (2016): 26.

Warton, J., Dwivedi, R., and Kovacevic, R. “Additive Manufacturing of Metallic Alloys: An Architectural Case.” Robotic Fabrication in Architecture and Design. (2014): 147-161.

Warton, J. and Kovacevic, R. “Additive Manufacturing, Abstract Assemblage, and Material Agencies.” 2014 TxA Emerging Design + Technology Conference Proceedings. (2014): 7-17.

Yalamanchili, P., Arshad, U., Mohammed, Z., Garigipati, P., Entschev, P., Kloppenborg, B., Malcolm, J and Melonakos, J. “ArrayFire - A high performance software library for parallel computing with an easy-to-use API.” Atlanta: AccelerEyes. (2015).

THE DOUBLE SKIN FAÇADE

Enhancing air quality in urban canyons



Lee A. Fithian, AIA, AICP, NCARB, LEED AP
University of Oklahoma
leefithian@ou.edu

ABSTRACT

The largest source of air pollution in North America is the atmospheric boundary layer of a city caused by its urban canyons with pollutants produced primarily by automobiles. The pollution mix is dominated by CO, CO2, NO2, Hc and small particulates. When sufficient sunlight is available, this leads to the development of photochemical smog and secondary pollutants such as VOCs. The removal of air pollutants at the street level is normally dependent upon air temperature stratification. Free flow of the air is important to diffusing the pollution into a larger volume. “The worst conditions for dispersion occur where there is a temperature inversion and the boundary layer is stable. Turbulence is then suppressed and upward motion is effectively eliminated”(Oke 1992). The Double Skin Façade (DSF) is a façade system technology that can not only meet the needs of the building occupants for natural ventilation, thermal efficiencies, and daylighting, but also the DSF can interact with street level ventilation. Computational Fluid Dynamics (CFD) can illustrate the velocity profile for a building without a DSF and with recirculating flow at the street level simulating the boundary layer condition (Fig. 1, left). CFD was used to illustrate the velocity profile for a building with a DSF showing the flow entering through the bottom of the DSF and exiting at building roof level approximately 60 feet (Fig. 1, right).

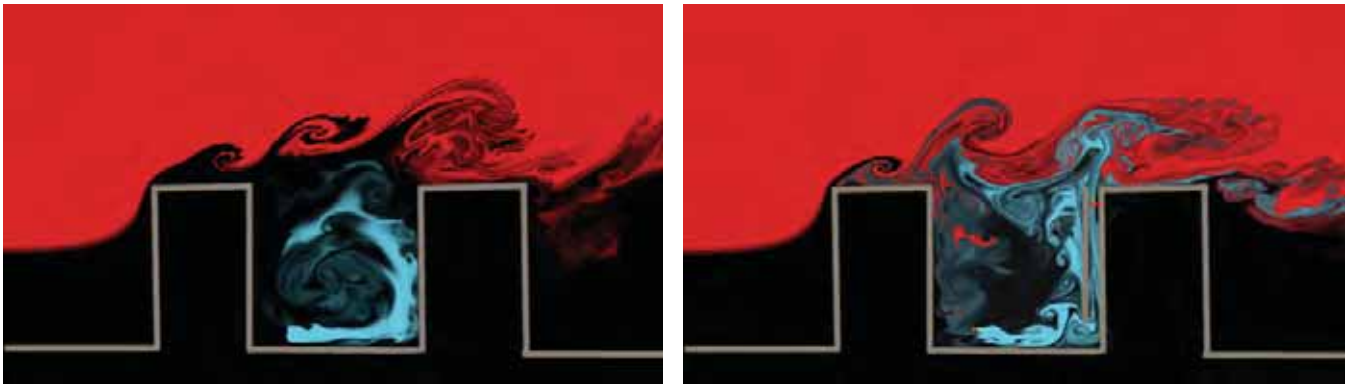


Figure 1: Urban canyon showing sequestered air pollutants (left) and with DSF showing potential mixing and removal of air pollutants (right).

The double skin façade can increase flow at the street level and enhance mixing at the urban boundary layer, which will assist in the evacuation of criteria air pollutants from urban canyons. This interdisciplinary approach yields the promise and expression of a building façade that serves a functional purpose beyond aesthetics, natural ventilation, daylighting, and thermal efficiency, which presents a transformative approach to building design.

KEYWORDS

double-skin, innovative, ventilated, computational fluid dynamics (CFD), urban habitat and the building façade, ventilation, health

INTRODUCTION

Human health stands to benefit at the intersection of urban climatology, urban design, and architecture. Urban designers are working to great effect to create a “sense of place,” reduce traffic and increase walkability. Architects develop great buildings to enhance the streetscape and “activate” communities along the streets, but in many cases urban climatology is taken into account only as wind loads or to identify a need for building energy efficiencies. The existing inventory of buildings and streets are slowly being redesigned to accommodate more foot traffic, new towns are being designed to counter sprawl and increase walkability, but the air pollution issues caused by their morphology, and street proportions are little understood and frequently overlooked. It is necessary to identify strategies to mitigate urban criteria air pollutants within the urban canyons. One method is to utilize buildings as effective contributors to urban streetscape and infrastructure to mitigate air pollutants.

If we are trying to make streets more walkable to boost economies and help people live healthier lifestyles, it is important to take into account that street plantings are insufficient to mitigate air pollution in a variety of urban configurations. Planners, Urban Designers and Architects must become familiar with the ramifications of street configurations and urban form as they relate to the potential of trapped criteria air pollutants. Architects can effectively create design interventions within their building façades that can mitigate some of the criteria air pollutants that are found in these urban street configurations.

BACKGROUND

As urbanization and densification increases, the microclimates of urban/higher density suburban areas change. Oke explains in *Boundary Layer Climates* that the largest source of air pollution in North America is the atmospheric boundary layer of a city caused by its morphology with pollutants produced primarily by automobiles. The pollution mix is dominated by CO, CO_2, NO_x, Hc and small particulates. When sufficient sunlight is available, this leads to the development of photochemical smog and secondary pollutants such as VOCs *(Oke 1992)*.

The removal of air pollutants at the street level is dependent upon air temperature stratification. Free flow of the air is important to diffusing the pollution into a larger volume. Dispersion is best when there is strong instability and deep mixing characteristics during sunny summer time conditions. “Conversely, the worst conditions for dispersion occur where there is a temperature inversion and the boundary layer is stable. Turbulence is then suppressed**,** and upward motion is effectively eliminated. Wind and turbulence are vital to the dispersion of air pollutants. In areas characterized by low buildings, the exchange between street-level where car pollutants are emitted, and above roof-level depends upon the height to width ratio. If the streets are narrow (< 1:1 height to width ratio) air exchange is restricted compared with that in a more open arrangement (>1:1.5) where the vortex circulation aids street-level flushing”*(Oke 1992).*

The World Health Organization (WHO) establishes the air quality guidelines which provide an assessment of health effects of air pollution and a threshold for health-harmful pollution levels. The 2005 WHO Air quality guidelines offered global guidance on thresholds and limits for key air pollutants that pose health risks. The guidelines are based on the evaluation of scientific evidence for particulate matter (PM), ozone (O_3), nitrogen dioxide (NO_2) and sulfur dioxide (SO_2). While there are various sources of the air pollutants, in particular, particulate matter (PM) and Ozone (O_3) have a profound association with urban areas. Excessive ozone – at the ground level is not to be confused with the ozone layer in the upper atmosphere – ground level ozone in the air can have a marked effect on human health. It can cause breathing problems, trigger asthma, reduce lung function and cause lung diseases.

THE DESIGN GUIDES FOR URBAN CORES AND TOWN CENTERS

Increasing urbanization has led to the development of planning guidelines to establish parameters that lead to successful developments, account for social equity issues, and promote smart growth and densification. These planning guidelines are called Form Based Codes (FBC) because they apply requirements for streetscapes, building facades, setbacks, typologies and a host of other urban design principles. In association with the Congress for New Urbanism (CNU), the National Association of City Transportation Officials (NACTO) has created a compendium of principles and practices for Complete Streets based on the Transect – a density classification system - which includes the design capacity for safe interaction of automobiles, pedestrians, bikers, multi-modal transit, and urban infrastructure *(“Urban Street Design Guide” 2017)*. The sidewalk is the area where people interface with one another, with businesses, and within the streetscape which is directly within the urban canyon.

While a FBC provides guidelines for buildings in urban cores and the establishment of new town centers, their requirements for height to width ratios also shape the relationship between the building and street. This can result in an urban morphology that creates a form called an urban canyon. The movement of traffic, pedestrians, and bikers governs the width ratio based upon activity within the right-of-way between buildings. The problem becomes one where we are intentionally creating places which are unwittingly unhealthy. When we consider most New Towns are 4-6 stories (approximately 62'-74') and the predominant width of the ROW (approximately 64'-72') the morphology of the urban canyon creates the <1:1 height to width ratio where meteorological influences including wind speed and direction create boundary layer inversions beneath the urban canopy layer. At these ratios, air pollution can become sequestered within the urban boundary layer. Green Infrastructure is assumed to offset some of the air pollution but in actuality street plantings serve only as surfaces for deposition of PM and minor conversion of CO_2, they do not actually mitigate VOCs *(Pugh et al. 2012)*. Our place making**,** and urban streets designed for walkability are placing more people within the streetscape without effectively dealing with air pollution issues.

THE USE OF THE DOUBLE SKIN FACADE

The double skin façade (DSF) is a technology that can meet the needs of the building occupants for natural ventilation, thermal efficiencies, and daylighting. The methodology was developed utilizing Computation Fluid Dynamic software (FLUENT) to evaluate the double skin façade for thermal properties, proper spacing of the façade glazing and velocity flow profiles. A consequence of this research was the work showed that the velocity profile for a building with a DSF can interact with street level ventilation. The velocity profile for a building without a DSF shows recirculating flow at street level (Fig**.** 2, left). The velocity profile for a building with a DSF shows the flow entering through the bottom of the DSF and exiting at building roof level (approximately 60 feet) enhancing the opportunity of turbulence and mixing (Fig**.** 2, right). The findings from this study were published and presented at conference *(Abou-Nassar, Siddique, and Fithian 2012)*.

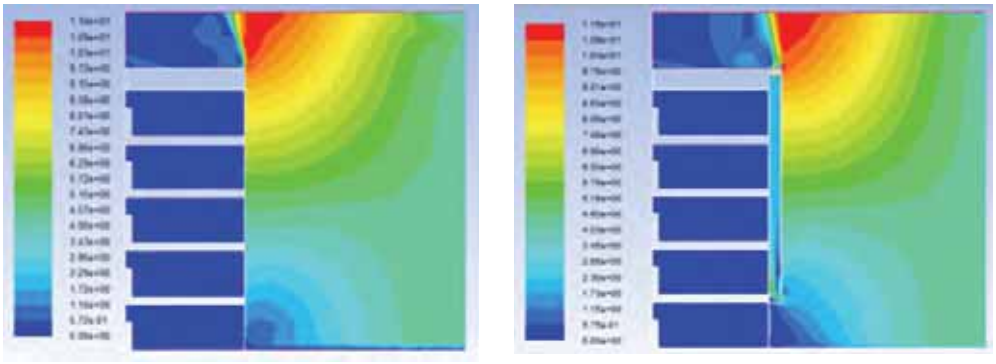


Figure 2: Velocity profile for a building without DSF (left) and velocity profile for a building with a DSF (right).

Biological systems can be used as an inspiration to transform our perception of building science and technology by identifying and developing regenerative building envelopes. Form Based Codes are already setting dictates as to massing, materials, transparencies and floor-to-floor heights, it is not a great leap to ask the façade technologies to do a bit more. The use of a building to remediate environmental pollutants beyond the building perimeter represents a fundamental paradigm shift as to the nature of buildings in the urban and suburban environment. It can be assumed that urban buildings and suburban/urban developments can ameliorate air pollution levels to the benefit of the health and welfare of the people within their area of influence. Indeed, when we look at urban infrastructure and resiliency issues, buildings and their systems are already being used to offset water needs and provide resources during and after extreme climate events *(Fithian 2015; Fithian, Siddique, and Wang 2017)*.

METHOD

DOUBLE SKIN FACADES – EVALUATION AND SELECTION

While the understanding of the capacity of the DSF to evacuate air at the street level within the zone of influence was fundamental, identifying the configuration of DSF that was best suited for supporting mixing, biofilter integration (future research intended to mitigate criteria air pollutants), and maintenance was necessary. The various definitions of DSF are characterized and described in the Belgian Building Research Institute publication "Ventilated Double Facades"*("Innovative Building Skins: Double Glass Wall Ventilated Facade" 2015)*. The classification takes into account the modes of how the façades work and introduces three criteria which are independent of one another: 1) the type of ventilation (natural,

mechanical, and hybrid ventilation); 2) the partitioning of the façade; and 3) the modes of ventilation of the cavity. The types of partitioning of the façade are listed below with pros and cons regarding their efficacy for interfacing with the street level and potential for providing natural ventilation (Table 1):

Description	Pros	Cons
Ventilated double façade partitioned by story with juxtaposed modules	Allows partitions to isolate horizontally	Vertical partitions limit efficacy of evacuating street level to one story
Multi-story ventilated double façade	Cavity is wide enough to permit access for service. Supports natural and mechanical ventilation	Difficulty of access limits maintenance of each story
Multi-story louver naturally ventilated facade	Louvered metal floors are installed at the level of each story in order to allow access and maintenance	none

Table 1: Evaluation and selection of DSF technology.

There are numerous ventilations systems associated with DSF and this research isolated one for study due to how the airflow interacted at the streetscape level. Two classification systems were identified, British and North American. In the British system there are five primary types based on commonality of façade (Boake 2008):

- Category A: Sealed Inner Skin: subdivided into mechanically ventilated cavity with controlled flue intake versus a ventilated and serviced thermal flue.
- Category B: Openable Inner and Outer Skins: subdivided into single story cavity height versus full building cavity height.
- Category C: Openable Inner Skin with mechanically ventilated cavity with controlled flue intake
- Category D: Sealed Cavity, either zoned floor by floor or with a full height cavity.
- Category E: Acoustic Barrier with either a massive exterior envelope or a lightweight exterior envelope.

In the American system there are three basic system types: Buffer System, Extract Air System and Twin Face System. It is important to note that future research will include integrated biofilters to remove criteria pollutants. At this time, systems were selected that did not utilize outside air that also provided interior ventilation for the building occupants. Consequently, the system selected as part of this paper is a Hybrid system that has a sealed inner skin with a mechanically ventilated serviced cavity.

DATA

For purposes of this research, it was necessary to model double skin façade airflow perpendicular to the urban canyon as this was the most extreme system exhibiting the least amount of mixing. The model included windward and leeward applications of the system, in order to determine airflow ventilation. When decoupled from the building environmental volumes and buoyancy effects, it was established that mechanically assisted ventilation was necessary.

Preliminary studies are utilizing a very simplistic wind tunnel application (Algorizk, Wind Tunnel) that simulates Computation Fluid Dynamics (CFD) assuming an incompressible and homogeneous fluid with Navier Stokes equations with a very simple velocity field in a 120x180 grid. CFD modeling includes attributes that can combine urban canyon morphology, façade integrated DSF geometry and wind speed necessary to identify mixing. The data generated yielded preliminary results that determined the technology is sufficient to producing mixing and evacuation at the streetscape level.

Condition 1 Urban Canyon with no DSF	
Condition 2 Urban Canyon with no DSF and Boundary Layer Condition Showing Sequestered Air Pollutants	
Condition 3 Urban Canyon with DSF Leeward and Boundary Layer Condition Showing Mixing and Evacuation of Air Pollutants	
Condition 4 Urban Canyon with DSF Windward and Boundary Layer Condition Showing Mixing and Evacuation of Air Pollutants	

Table 2: Results of CFD modeling of airflow in urban canyons with and without DSF.

EXPLANATION

Table 2 illustrates the summary conditions of the relationship between the urban canyon and the perpendicular airflow. In Condition 1 we see the skimming flow regime that occurs over urban canyons and is demonstrated by the visualization of the airflow and simple urban forms with streetscape in the CFD application. Condition 2 illustrates the sequestered condition that occurs in the urban canyon as the skimming regime that creates the boundary layer and does not interact with the streetscape air source. Condition 3 illustrates the introduction of a leeward side DSF with mechanical ventilation assist, demonstrating mixing of the boundary air and evacuation of the streetscape air source. Finally, Condition 4 illustrates the introduction of a windward side DSF with mechanical ventilation assist, demonstrating mixing of the boundary air and evacuation of the streetscape air source.

CONCLUSION AND FUTURE WORK

This research has demonstrated that the Double Skin Façade can interact with the streetscape level air and enhance mixing at the urban boundary layer, which will assist in the evacuation of criteria air pollutants from urban canyons. This façade technology-based approach yields the promise and expression of a building DSF that serves a functional purpose beyond natural ventilation, daylighting, and thermal efficiency. This presents a transformative approach to building design allowing the façade to enhance adjacent airspace, effectively creating a design intervention with the building façade that can remove some of the criteria air pollutants found in these urban street configurations.

Further research will model double skin facades with an integrated biofilter in a selection of climates and orientations, including windward and leeward applications of the system, in order to determine airflow ventilation and mixing rates. When coupled with the urban canyon environmental volumes and buoyancy effects, it should be possible to establish if there is enough capacity to ventilate street level air pollution as well as mitigate the criteria air pollutants through the use of the integrated biofilter. Preliminary studies utilizing the wind tunnel simulation software have indicated that additional modeling should utilize more robust CFD software. The CFD modeling should include airflow buoyancy attributes that can combine urban canyon morphology, façade integrated DSF geometry and the pressure drop coefficients created by an integrated biofilter. The data generated will yield results that will determine whether the technology is sufficient to ameliorate the criteria air pollutants.

ACKNOWLEDGMENTS

I would like to gratefully acknowledge the support of my Ph.D. Chair Zahed Siddique, PhD.

REFERENCES

Abou-Nassar, Guy, Zahed Siddique, and Lee Fithian. 2012. “Computational Analysis to Design Energy Efficient Built Environments.” In *ASME 2012 International Design Engineering Technical Conferences and Computers and Information in Engineering Conference*, 177–186. American Society of Mechanical Engineers. http://proceedings.asmedigitalcollection.asme.org/proceeding.aspx?articleid=1736102.

Boake, Terri Meyer. 2008. “The Tectonics of the Double Skin.” *Waterloo: School of Architecture*. http://www.academia.edu/download/31978126/tectcase.pdf.

Fithian, Lee. 2015. “How Advanced Building Systems Can Offset Water Infrastructure Needs.” *52nd International Making Cities Livable* eReport.

Fithian, Lee, Zahed Siddique, and Naiyu Wang. 2017. “Investing in Sustainable Buildings to Enhance Community Resilience.” *ASCE Architectural Engineering Institute Conference Proceedings*.

“Innovative Building Skins: Double Glass Wall Ventilated Facade.” 2015. http://www.academia.edu/180367/Innovative_Building_Skins_Double_Glass_Wall_Ventilated_Facade (accessed March 11).

Oke, T. R. 1992. *Boundary Layer Climates*. London; New York: Routledge.

Pugh, Thomas A. M., A. Robert MacKenzie, J. Duncan Whyatt, and C. Nicholas Hewitt. 2012. “Effectiveness of Green Infrastructure for Improvement of Air Quality in Urban Street Canyons.” *Environmental Science & Technology* 46 (14): 7692–99. doi:10.1021/es300826w.

“Urban Street Design Guide.” 2017. *National Association of City Transportation Officials*. http://nacto.org/publication/urban-street-design-guide/ (accessed March 10).

MULTILAYER DESIGN TECHNIQUE IN THE METAL FAÇADES

Using sheet metal fabrication in the prefabricated metal facade



Soleyman Arebi, Ph.D.
Arvin Uzman
s.arebi@yahoo.com



Kianoosh Farhang Djavid
Arvin Uzman
kian@westelite.ca



Naser Paryab
Arvin Uzman
paryab@arvin-uzman.com



Bahram Allahyari emadi
Arvin Uzman
allahyari@arvin-uzman.com



Mohammad Manafazadeh
Arvin Uzman
manafzadeh@arvin-uzman.com



Hossein Mahmoudi
Baran Office
Office.baran@yahoo.com

ABSTRACT

Multilayer design technique in metal façades is introduced in this paper. Generally, in this technique, a metal façade is designed in the fourth layer. Base element, support bracket, vertical/horizontal substructure and final decorative panels are forth layers in this technique. The first layer is the base element of the metal façade that is attached to the main structure by the on-site welding process. The second layer is a support bracket that is composed of sheet metal with I-Shape geometry. The third layer is vertical/horizontal substructure that is manufactured by sheet metal process with the T-shape and U-shape geometry. Finally, the last layer is the decorative panel that mostly is a sheet metal folded panel with laser cut texture. All layers are connected together in the site with the standard stainless steel bolts and nuts. Some criteria for the geometry and cross section design in these layers are; minimization of the raw material, ergonomic installation, to be modular, coating all surface, fast installation, able to CNC based manufacture, adjustable for sharp installation, easily replaceable, weight minimization, omitting the storage limitation and the complex shape metal façade limitation. Analysis of the results in the several installed projects proofs that using this technique reduces the runtime and final project cost. Also, final geometrical quality and durability of the installed metal façade are increased.

KEYWORDS

metal façade, multilayer structure, modular prefabrication design, optimal configuration, final project cost

INTRODUCTION AND BACKGROUND

INTRODUCTION-METAL FAÇADE ADVANTAGES

Metal facade panels can be used to dramatically enhance the outdoor appearance of many different types of buildings. Metal building facades can reduce energy usage and provide aesthetic appeal to the exterior of the building (Harris P, 2006). The façade is the filter between the climate outside and the conditioned space inside. By balancing light & ventilation, metal façade can allow architects to manage interior heat build-up from the sun (Aksamija A, 2016). By deflecting heat, less energy output is required from HVAC systems, providing a more consistent interior temperature (Jesús M et. al., 2014). As a screening element, metal façade decreases the amount of indoor lighting required. Due to its potential for permeability to natural daylight, a metal facade can reduce the amount of artificial light needed (Brandl, D et. al., 2014). Also, the main features of the façade are: symbol of a city culture, helps to maintain durability and building life, important role in sound transmission in the building, low cost maintenance, flexibility in the complex architect geometry, completely prefabricated production at the factory, high accuracy and speed in the production and final installation, resistance and durability against various environmental conditions, lightweight, variety in materials and texture, easy storage and transfer, can be installed on various structures such as glass curtain wall. Also, another major feature is pressure equalization subjected to variable wind loading (Michael J et. al., 2016). Materials which are used for metal facade are versatile. Easily bent and configured to design, it can be used as a lightweight decorative element or as a structural component in buildings. Metal has a structural strength many other materials do not have. They can withstand harsh weather environments, with the ability to control or equalize pressure due to its high strength-to-weight ratio. The metal perforations also decrease the weight needed to be supported by the building's framework (John N, 2016). Comparing with the metal facades, concrete, stucco, brick, block and other masonry facades can look great and are extremely long lasting and durable, but they are also expensive, heavy and labor intensive to install. Also, the installation is often a slow process, especially if bad weather causes delays (Christoph P, 2016). As a result, masonry facades tend to be bland and simple, with little variation and few eye-catching details (Gökhan K, 2016). Another material that is often used for the architectural façade is composite panels. The low price is the main reason for using these panels. Most important advantages of a metal facade than a composite are the fire resistance (for example Grenfell Tower fire disaster 2017), texture cutting diversity and final durability. This paper introduces the sheet metal process for metal façade production. In this process, flat metal sheets become folded parts. With the help of this method, it is possible to can create various metal enclosures such as machine body and metal industrial boxes. This process is summarized as follows: The first step is product engineering design with 3D modeling software such as AutoCAD, Solid Works, and CATIA. Then, the flattened shape of parts is sheared by CNC laser cut machine. The next stage is folding the sheared parts by bending cell machine. The next stage is grid blast and final electrostatic coating. Due to the importance of color in metal parts in order to prevent rust and corrosion, as well as the appearance of the final product, this section is especially important. To do this, the grit blasting of the metal parts before the paint spraying is carried out on the piece, while removing the layer of oil in the sheet, the surface of the sheet is thoroughly coated to allow the paint to be applied. The metal parts are guided by sandblasting and spraying with special rails to the colored furnace and cooked up to 230 ° C for a specified period. All parts are shipped to the site after being manufactured at the factory. At this stage, the components are based on a predetermined sequence and according to the timetable on the structure. At each stage, the parts are connected with the bolts and nuts. After the final installation of all the parts and final settings, the bolts are tightened as much as necessary with the help of the torque meter. As a result of this method, the installed faces will be completely smooth. After installation, all parts and fittings are inspected. Finally, the facade is cleaned up.

METHOD

METHOD-MULTILAYER TECHNIQUE INTRODUCTION

Generally, in the multi-layered technique, a metal façade is designed in the fourth layer. Base element, support bracket, vertical/horizontal substructure and final decorative panels are four layers in this technique (Fig.1). The first layer is the base element of the metal façade that is attached to the main structure by the welding process. The second layer is a support bracket that is composed of sheet metal process with I-Shape geometry. The third layer is vertical/horizontal substructure that is manufactured by sheet metal process with the T-shape and U-shape geometry. Finally, the last layer is the decorative panel that mostly is a sheet metal bent panel with laser cut texture. All layers are connected together in the site with the standard stainless steel bolts and nuts.

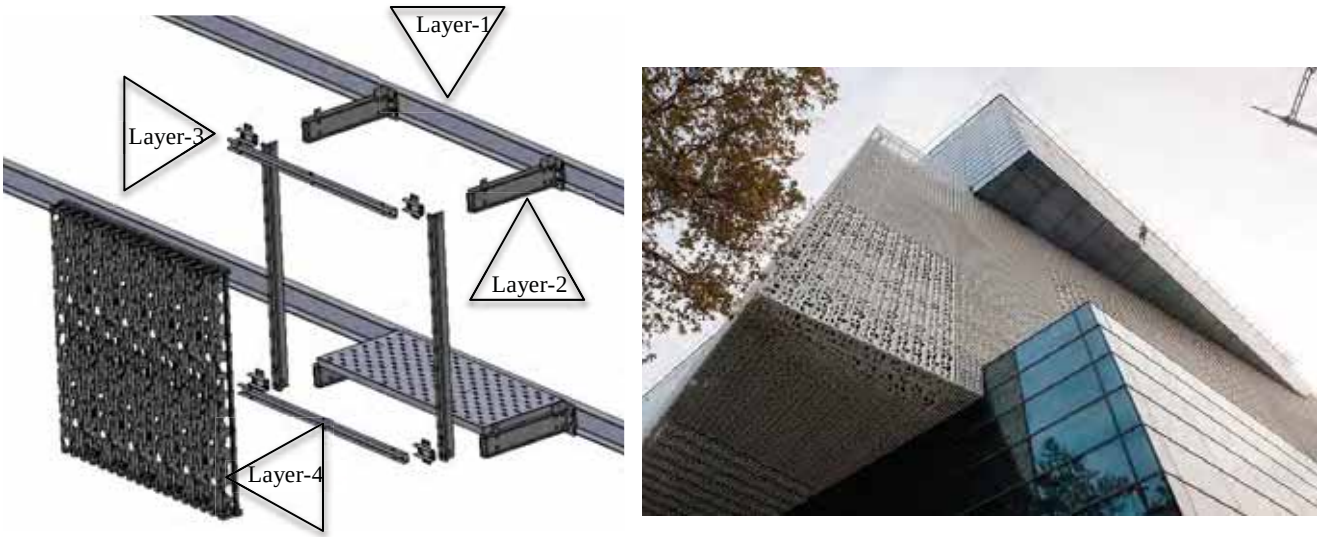


Figure 1: Layers of the proposed multilayer technique and reference installed project (Charsoo Center, Tehran, 2014).

METHOD-LAYER 1: BASE ELEMENT

The first layer is the base element of the metal façade that is attached to the main structure by the welding process. First, the standard U channel is sheared with high precision. Finally, it is installed on each level of the floors. In metal buildings, the connection of this layer is done with the aid of a special bracket. It is used in concrete buildings with the help of an intermediate plate connected with the bullet to the level of the building. At this stage, before the final welding of the connection plate to the profile, the necessary measurements are made.

Details of base installation are shown in Figure 2.



Figure 2: First layer, base element, isometric and side view.

As it is shown in the Figure 2, this layer is composed of three parts: Initial bracket, U channel, and support bracket base. The initial bracket is made of steel sheet with 8-10 mm thickness (according to façade weight). Also, support bracket base is laser cut sheet metal with holes for connecting the support bracket to it. Also, there are some welded nuts on the support bracket

base for connecting the spandrel clad in the second layer. The support bracket base is coated with hot-deep galvanized. Main Specifications of this technique are described as following:

- High-speed installation.
- Lower cost due to the use of U channel profile.
- The ability to adjust the base layer and compensate errors from the structure misalignment.
- Scalable for various façade type (for each facade with different weights, only sizes are designed and changed).
- Can be installed without scaffolding (climber is enough).
- The ability to spray fireproof material on it.
- Access to bolt and nut connection between support bracket and its bracket base (due to use U channel profile).

METHOD-LAYER 1: SUPPORT BRACKET

This layer is pre-fabricated I-shape that is made using the sheet metal process. At first, roll sheet is sheared by laser cutting machine. Then I-shape is generated by bending machine. Finally, electrostatic powder coating or hot-deep galvanized are used for final coating. Stainless steel nuts and bolts are used for final assembling in the factory and site. The walkway is installed on this support bracket. The walkway is made using the sheet metal process. For manufacturing this part, galvanized sheet metal is punched and forming tool is used to create brush surface. Details of support bracket are shown in Figure 3.

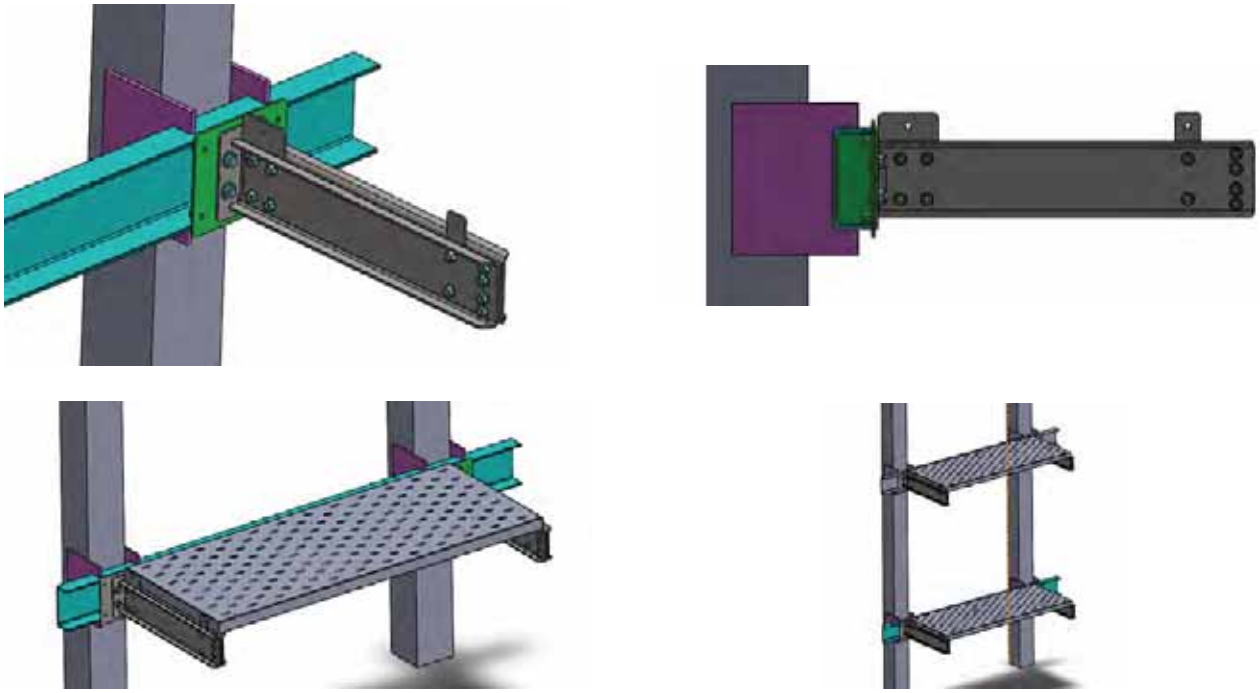


Figure 3: Details of support bracket.

METHOD-LAYER 3: VERTICAL/HORIZONTAL SUBSTRUCTURE

This layer consists of T-shape vertical and U-shape horizontal brackets. Both brackets are produced using a sheet metal process. These parts are produced at the factory and then shipped to the site. Finally, the support bracket is connected to bolts and nuts. At this stage, after the final connection, the position of the parts is checked in all three horizontal and vertical and depth directions and it is corrected if necessary. Details of this layer are shown in Figure 4.



Figure 4: Details of the vertical/horizontal substructure.

METHOD-LAYER 4: FINAL DECORATIVE PANELS

The final layer contains the main façade, which includes decorative panels. These panels are made of the sheet metal process. A laser cutting machine is used for creating custom texture. Then, a CNC bending machine is used for folding the texturized panel. Final coating mostly is powder coating with customized code. On-site, panels are installed to the previous layer with stainless steel nuts and bolts. Details of this layer are shown in Figure 5.

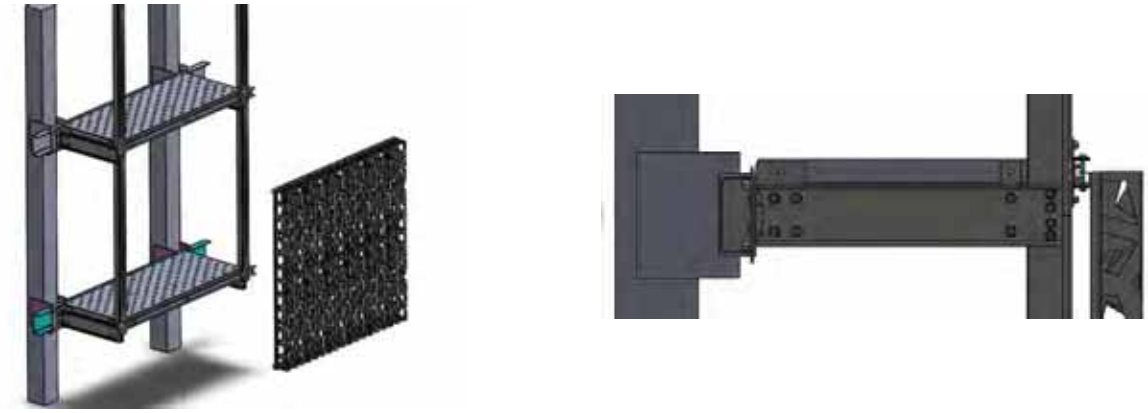


Figure 5: Final decorative metal façade.

RESULTS FOR STRUCTURAL ANALYSIS AND DIMENSIONS

To design the exact dimensions of the layers elements in each metal façade, structural analysis is performed. Wind force and earthquake forces are considered in the calculations. According to allowable deflection and vibration frequency, the thickness of the sheet metal parts is identified. For example, results for typical metal façade with the Iranian Gerehkari texture are shown in Figure 6.

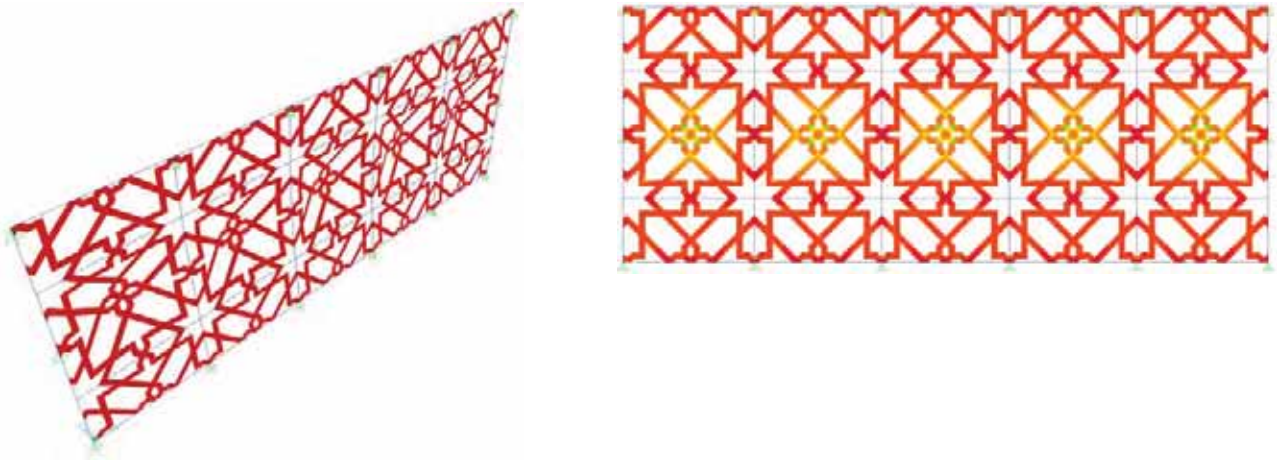
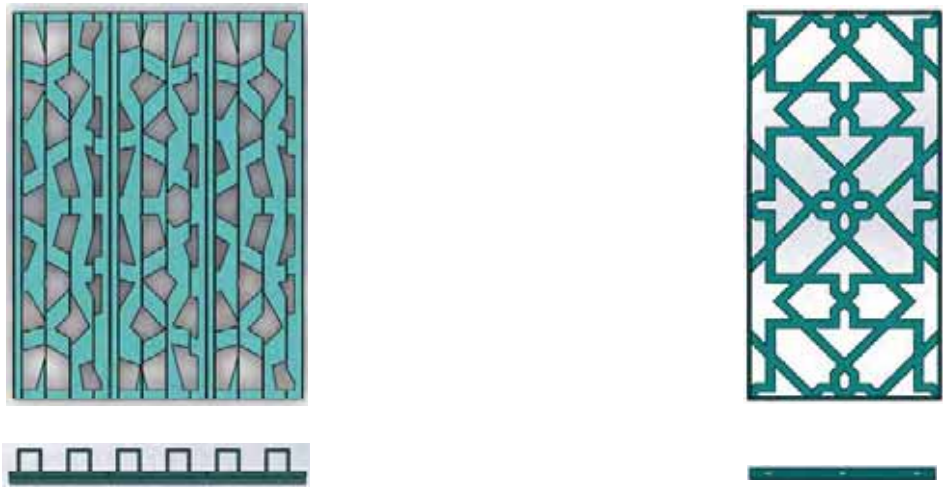


Figure 6: Deflection results for typical metal façade with the Iranian Gerehkari texture.

Size of this panel is 9m×3.8m. The maximum deflection in this metal façade is 53 mm and period of oscillation is 0.163 second. Based on the structural analysis results, the thickness of sheet metal parts in layers 1-4 is designed. The results for the metal facades in the common size (2m×2m panel size) are reported in the next sections.

RESULTS- LAYER 4

For the common size, steel, galvanized steel or 6030 aluminum alloy sheets with the 2 - 4 mm in thickness are used. For common texture with 62 percent minus area, a steel sheet with the 4 mm thickness is used. Two types of the façade panels are shown in Figure 7.



A sample of the folded façade panel.

A sample of the unfolded façade panel.

Figure 7: Two types of the decorative façade panels.

RESULTS- LAYER 3

Vertical and horizontal substructures are folded sheets with T and U-shape brackets. For the common size of façade panels, steel sheet with 2mm thickness is used for this layer. In this layer all parts connected with the stainless steel bolts and nuts. In the connection nodes, bolts are installed in the oval hole to allow adjustment of the substructure in three directions. Also, the final formed grid of horizontal and vertical brackets forms a stable structure. Details are shown in Figure 8.



T shape vertical bracket.

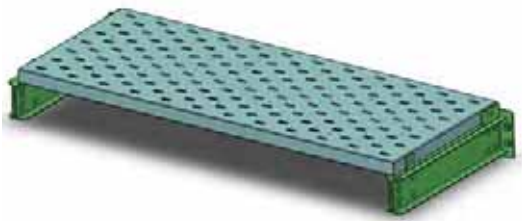


U shape horizontal bracket.

Figure 8: T and U shape of vertical and horizontal brackets.

RESULTS- LAYER 2

The support bracket is an I-shaped bracket that is assembled with bolt and nuts. For the common size of façade panels, Steel sheet with 5mm thickness is used for this layer. This I-shaped has been designed for bending capacity, walkway base and fasteners installation. The walkway is designed for tolerating a 150 kg person. The walkway is 2 mm galvanized sheet with 60 cm width. Details are shown in Figure 9.



The support bracket and walkway in layer 2.



I-shape of support bracket.

Figure 9: The support bracket and walkway.

RESULTS-LAYER 1

The weight of the entire facade is tolerated by this layer. According to the structural point of view, the critical point is the support plate. For the common size of façade panels, the total weight of layers 2 - 4 is 50 $kg/\,\mathrm{m}^2$. Wind force and weight of layers 2-4 are tolerated by this layer.

EXPLANATION

EXPLANATION-TOTAL DURATION OF THE REFERENCE PROJECTS

For evaluation of the proposed technique, the total time duration of the selected reference projects is reported in Table.1.

Arvin Uzman Projects	View	Finish Date	Duration (Month)	Area (m^2)	Manufacturer ratio	Installation Ratio	Total Ratio
Charsoo Outer		20/11/2014	16	4300	11 m^2/day	50 m^2/day	30 m^2/day
Charsoo Interior		1/2/2015	9	4600	20 m^2/day	80 m^2/day	50 m^2/day
Ferdowsi		23/1/2016	2	1100	22 m^2/day	60 m^2/day	41 m^2/day
Nafis		20/12/2015	2	1500	25 m^2/day	90 m^2/day	58 m^2/day
Soheil		1/11/2016	1	600	25 m^2/day	30 m^2/day	28 m^2/day
Didar		17/7/2017	2	1500	25 m^2/day	25 m^2/day	25 m^2/day

Table 1: The total time duration for selected reference projects.

Also, manufacture, installation and total ration are reported here. Results show that the average total ration for various projects is 30 m^2/day. Comparing to the other techniques that are used in Iran, this speed is three times faster. In addition to other advantages mentioned, the total cost of this method is also lower compared with the other methods. The following is a graphic illustration of the selected reference projects.





Figure 10: Reference project: Nafis Center, 2015.





Figure 11: Reference project: Charsoo Center, 2014.





Figure 12: Reference project: Didar Center, 2016.

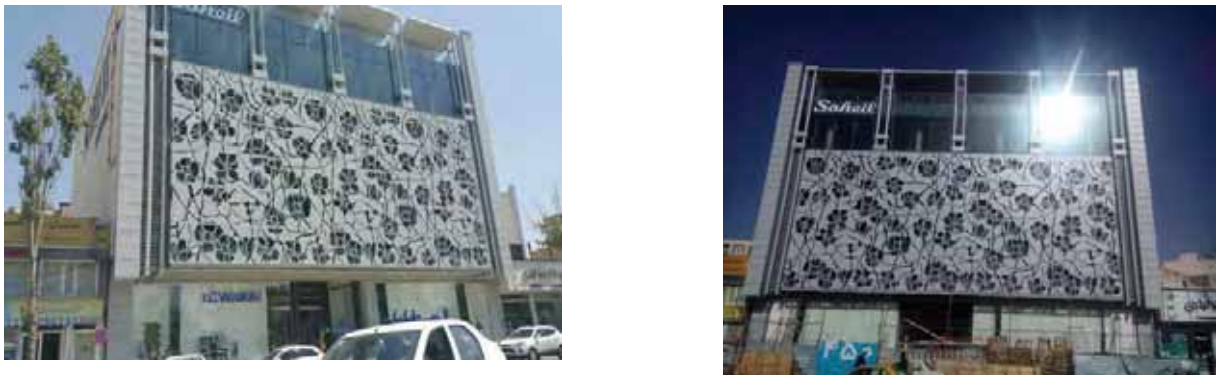


Figure 13: Reference project: Soheil Center, 2016.

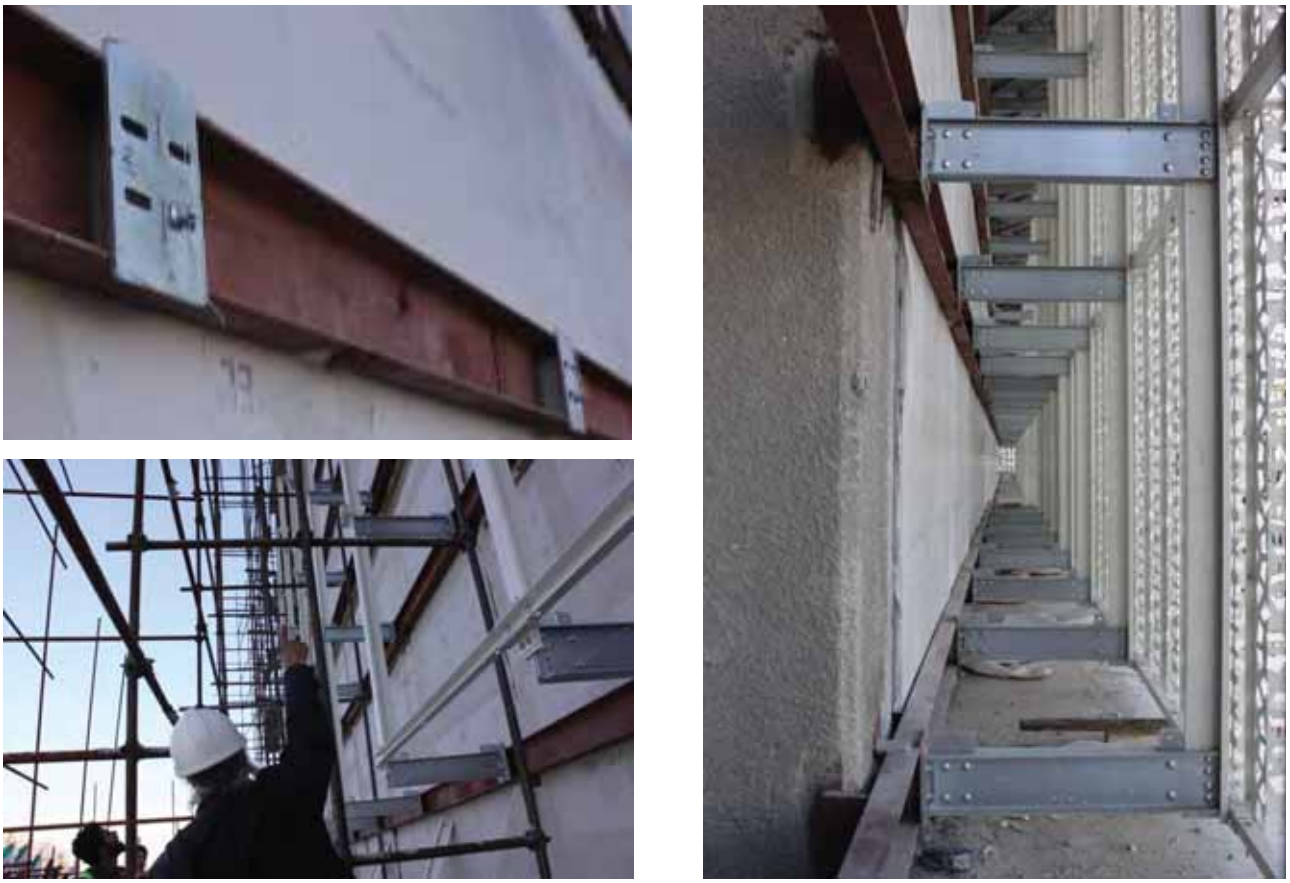


Figure 14: Layers in façade reference installed project (Charsoo Center, Tehran, 2014).

CONCLUSION AND FUTURE WORK

The multilayer technique in the architectural metal façade design is introduced in this paper. At the first, four layers of design technique are introduced. Sheet metal process is introduced as an optimal production method for the metal façade cladding. The detailed design of each layer is discussed. The results were presented for structural analysis of the metal façade for all parts of the layers. Thickness, materials and cross-section of the parts are designed for each layer. Also, the total duration of the selected reference project is shown. Results show that using multilayer technique and sheet metal process for metal façade cladding reduce the total duration of the architectural metal façade projects. Also, there are many advantages to using this technique. The durability of the façade parts, minimization of the raw material, ergonomic installation, to be modular, coating all surface, ability to be manufactured by a CNC-based process, adjustable for precise installation, easily

replaceable, weight minimization, easy storage and application for complex façade main aspects of using this technique. Finally, a graphic illustration of the sheet metal process and selected reference project is presented.

ACKNOWLEDGMENTS

The reference projects could not be realized without the efforts of the workers in the factory and site. Thanks to the Arvin Uzman Company workers (Authors Company) in the factory and installation site.

REFERENCES

Ajla Aksamija, “Thermal and energy performance in different climate types”, Facade Tectonics world congress, (2016), Los Angeles.

Brandl, D., T. Mach, M. Grobbauer, and C. Hochenauer. “Analysis of Ventilation Effects and the Thermal Behavior of Multifunctional Facade Elements with 3D CFD models.” Energy and Buildings 85 (2014): 305–320.

Christoph Paech, Structural membranes used in modern building facades, Procedia Engineering 155 (2016) 61 – 70.

Gökhan Karakuş, Doha Tower, 2016, On Site Review Report.

Harris Poirazis, Double Skin Façades, A Literature Review, A report of IEA SHC Task 34 ECBCS Annex 43, 2006.

Jesús M. Blanco, Pedro Arriaga, Eduardo Rojí, Jesús Cuadrado, Investigating the thermal behavior of double-skin perforated. sheet façades: Part A: Model characterization and validation procedure, Building and Environment 82 (2014)

John Neary**,** "Integrating structure and cladding" Facade Tectonics world congress, (2016), Los Angeles.

Michael Johann Paar, Alexander Petutschnig, Biomimetic inspired, natural ventilated facade – A conceptual study, Journal of Facade Design and Engineering 4 (2016) 131–142.

MULTI LAYER FACADES

A modern take on the challenges and balances

Robert Moisy
Surface Design Consulting Pty Ltd
r.moisy@surfacedesign.com.au

ABSTRACT

The history of high performance façades and glazing has been a tale of attempting to manage the conflicting requirements of, on one hand inviting connection with the environment through providing access to daylight and views, while restricting or rejecting other aspects of the natural external environment namely heat, cold, rain and wind as well as human caused attributes such as noise, dust, pollution and security risks.

The development of various products and façade systems have been strongly influenced by the climate but also the economic fortunes of the countries of the products origin. To an extent these have been driven by the technologies and materials available at the time.

Invariably single skin/single layer products and systems have prevailed but for various reasons have not fully been able to satisfy the balancing act and as a response over time various multilayer approaches have come and gone in an attempt to find a way to manage the various conflicting requirements.

The transformation of façade systems from “exclosure” (keeping the wind and rain out) to that of a filter (admitting light not energy) are well known. Multi-layer façade systems allow designers to integrate measures that meet both the environmental filter and the metaphoric transparency that modern designs set for corporate and intuitional buildings.

This paper looks at the current trends in the construction of modern multi layered façades and façade products that integrate both static and variable interstitial elements to provide a dynamic response to their environment and how these interact with the buildings system they support and drive.

We explore a brief history of the development of multi layered façades and glazing to acknowledge their contribution as forerunners to today’s high performing multilayered façade systems and how each of the impact on the building mechanical and lighting systems. We explore this relationship with respect to the external environment, the thin and thick facade and how they affect building use.

We will present the challenges, processes, performance and testing required and undertaken to deliver several leading-edge projects that have adopted multi-layered facades to respond to their particular performance briefs.

KEYWORDS

multi-layer facades, closed cavity, interstitial shades

INTRODUCTION

The façade is a complex set of material layers that protect the users of a space from nuisance environmental parameters. The modern façade is also expected to provide connection to valuable external environmental parameters such as daylight and views. It is the intent that the façade creates the barrier from severe heat and cold, maintaining energy efficiency (reduce heating and cooling energy requirements), promoting sustainability, wellbeing and health while reducing the carbon footprint. The façade, if delivered appropriately, provides positive results to the people within the space as well as financial gains of the tenant and the owner.

During design, performance requirements are identified, however, there is usually no clear hierarchy of these performance expectations. When these are coupled with the costs, and procurement limitations the complexities increase. The designer is expected to make judgements and often required to negotiate and sacrifice one performance requirement for another. Being multifaceted and multidiscipline in nature of the façade design requires input from many stakeholders including the design team (architect, façade engineer, structural engineer, mechanical and services engineers, acoustics and fire engineers) and the client (as the façade is often the image and brand of the building), as well as community authorities and urban planners that must confirm compliance to local standards.

The façade engineer and architect are armed with many options of façade typologies, from single to multi skin facades, technology and geometrical options, and various levels of transparency both in and out. The designers must weigh up these options to deliver the best outcome for the project. As a designer, we must live by these decisions, they must be rationale and considerate. Traceability and transparency in these decisions is key for future learning and promotion of advancement of the understanding of various designs. Designers are expected to make decisions that consider all relevant options, dismiss those that are undesirable, be aware of confirmation bias's often influencing judgements (particularly contractors and clients), solve the multiple equations, be creative and open minded.

We will investigate the expectations and performance requirements and the challenge of balancing the conflicting parameters, present the modern façade, discuss various typologies and their benefits and shortcomings and present a methodology for comparative assessment that allows project specific considerations, holistic approach and client outcomes.

THE ENVIRONMENT

Buildings from all over world experience various temperature extremes and wind and storm events. The focus of this paper is to provide comparative performance requirements, methods and outcomes and applicable to any location. We have chosen Sydney Australia as the base case for discussion. Sydney experiences a moderate temperature range with hot summers and cool moderate winters. In summer Sydney experiences, acute storms and occasionally high wind speeds. This relatively intense summer weather requires design for both high levels of glare and heat at the perimeter. Sydney is a harbour city, which impacts durability requirements.

The beautification of the city makes it a desirable city for views. With substantial daylight and views available these typically become key drivers in architectural and sustainability aspirations.

As a moderate winter environment with hot intense summer weather and substantial views and daylight available designers must balance these parameters at the façade.

HISTORY/BACKGROUND

Modern Sydney has developed with most of the worlds technical façade solutions in mind and therefore provides a suitable example to showcase many of the facade typologies. The moderate winters do not require highly insulated facades, this opens up the amount of glazing possible within a building, it is often the aspiration to achieve floor to ceiling glazing in the modern Sydney market.

Designers in Sydney are generally familiar with the international market and available products, many applications have a delay period from European (or US) examples.

FAÇADE CONSTRUCTION TYPES

For the purposes of this paper we have limited our discussion to the following main façade families used for modern offices, we have focused on predominantly glass facades, being a single skin (curtain wall or otherwise), traditional double skin façade (large air cavity of say 600mm – 900mm), small cavity façade (with air cavity of nominally 100-200mm) with the closed cavity façade as a subset of the small cavity facade. In all cases various percentage area of spandrels have been considered along with various glass technologies and we have discussed the types of shading devices both fixed shades and automatic or dynamic shading elements.

SINGLE SKIN FACADE

The single skin façade refers to unitized curtain wall, window wall or stick systems. The first single skin curtain wall in Australia was the Berger House building (82 Elizabeth Street) in the mid 1950's (reference CHSLEP2000 Listing Review).

Modern single skin facades in Sydney generally adopt high performance clear or light grey double-glazed units achieving a visual light transmission of a range of 40-60% and a solar heat gain coefficient of 0.2-0.35 respectively. When these high performance single skin facades are combined with a blind and/or shading element a best case solar heat gain coefficient in the order of 0.15 is achieved, with an effective Visual light transmission in the order of 5-15% (however note the use of slat or perforated screen type or integrated mesh type shading devices allow views between slats or mesh with high VLT, the obtrusiveness of the blind or mesh is a subjective issue).

U values of these systems range in the order of 2.4-3.4, with thermal breaks and/or argon filled cavity DGU occasionally adopted to assist.

The single skin façade remains the prominent façade in Sydney and Australia, when coupled with modern glass products, fixed sunshades, or dynamic sun shading systems, these generally perform suitably for Sydney conditions.

DOUBLE SKIN FACADE

The double skin façade such as that at Sydney University Law School (completed 2006) and 1 Bligh Street Sydney (completed 2008) are rare in the modern market. They provide superior thermal performance (both in terms of insulation and shading performance when coupled with an integrated shading device). The shading device in both the examples is automated and dynamic, it is semi protected from the external environment by the external glass skin, and it shades the internal glass skin and in turn the perimeter zone. The cavities in both instances are ventilated to the outside. The additional skins and wide cavities require spatial depth, maintenance however in both instances they create an architecture unachievable in a single skin. These facades are generally costly in comparison to a single skin façade. The performance of these facades is typically in the order of a VLT of 50-60% with a best case SHGC of 0.1 (with blinds or shades fully closed). The U-value of these facades reaches in the order of 1.1. The acoustic performance of these facades varies on the details however generally perform better than their single skin cousins.

SMALL CAVITY DOUBLE SKIN FACADES

The small cavity DSF refers to a modified single skin façade where an internal operable sash is installed, the blind can be installed within the cavity, these are common and seen also as retrofits. These facades achieve good shading while maintain the ability for high VLT when the blinds are not deployed. The extra layer also assists in acoustic performance and the air gap is particularly effective for low frequency noise attenuation. The internal sash is operable to allow cleaning access to the cavity formed. Access to this internal sash can limit the use of the adjacent perimeter behind the façade.

These facades are common in hospital buildings where infection control is a key parameter as the internal sash allows a clean surface and a protective layer too the blind, the added acoustic performance also assists performance for recovery spaces and the like. We also see these façade types in airports, lecture theatres, recital halls, hotels, bedrooms and other facilities where superior acoustic performance is required.

MODERN VARIATION ON SMALL CAVITY FACADES - CLOSED CAVITY FAÇADE

The closed cavity façade was introduced to the Australian market by Permasteelisa in 2011 on the 200 George Street project. Having been researched and developed for the European and Middle East market, the 200 George Street is the largest CCF project in the world and the only one with timber blinds. The CCF model has been rolled out across other projects in Sydney including 100 Mount Street and UTS Central. In all of these projects automatic blinds are installed as part of the system providing dynamic solar shading and glare control.

While the traditional small cavity façade requires maintenance to the cavity, whether it be from insect intrusion, dust or condensation the CCF avoids this problem through the use of clean and dry air that is pumped into the cavity to keep it both clean and dry.

The CCF achieves U values of nominally 1.8 (system), VLT up to 60% and SHGC of 0.1-0.3. With the added acoustic performance of the extra layer of glass these facades appear to outperform the traditional versions.

GLASS TECHNOLOGY

The Sydney market is exposed to all glass technology including Low e coated glass (soft and hard coatings, with modern triple silver coatings common, Coloured substrates (Crystal Grey and Greys are relatively common), High performance DGU, Integral shading devices (meshes, etc). Switchglass is yet to see exposure on any significant projects in Sydney or Australia.

SEALED BOXES

The performance expectations of a façade typically include the need for a sealed facade to the building, this aspect is often non-negotiable for modern city offices. This provides weatherproofing from rain and wind and along with a sealed membrane comes sound attenuation, the level of sound attenuation depends on the makeup of the layers of the membrane, these layers are also attributable to thermal insulation. Sealing a building and paired with the relevant air conditioning system allows control of the air quality within the building including humidity, air pollution, CO2, pollution, airborne dust, pollen, insects and vermin. Sealing the building via the façade creates a controllable compartment for human safety events such as fire. Buildings are usually broken down internally with sealed floor slabs, and partitions to compartmentalize and in turn isolating spaces in the event of a fire.

The move to hermetic sealing of buildings is rather new as natural ventilation predates the modern concept of the sealed membrane. Natural ventilation is generally not encouraged in modern offices or institution building with modern mechanical engineering pushing for controllable air flow and quality to the working spaces which is easier to do with a sealed box. Introducing openable windows is typically a romantic aspiration in most offices, with clients and tenants generally preferring a sealed box with natural ventilation perhaps best left to apartment buildings.

THE BATTLE OF LIGHT VERSUS SHADE AND THE ROLE OF THE DYNAMIC SHADING DEVICE

One of the most highly fought battles in any design process is the one for light and shade. With light comes a connection to nature and positive biological response among most humans, however it also brings heat that can be uncomfortable in peak conditions. Design teams are often caught in this paradox. We must limit heat energy through the façade under peak summer conditions while creating suitable connection to daylight and views.

The amount of heat one can allow through the façade and to the perimeter zone are governed by the mechanical systems and the energy efficiency targets of the building. The perimeter zone (usually defined as the first four metres around the perimeter by the mechanical engineers, although this may vary depending on the project details and the mechanical engineer) must be designed with the mechanical system to achieve the relevant comfort levels expected for the space. As a comparative assessment, an active chilled beam mechanical system may accept approximately 85W/m2 at the perimeter whereas the more efficient and best quality for comfort mechanical system such as an underfloor air supply with overhead passive chilled beams will only allow in the order of 65W/m2. These performance requirements drive the performance of the façade system shading performance and could be in the order of 0.16 SHGC for 85W/m2 versus 0.12 SHGC for 65/m2. This is a 50% better performing façade in terms of shading and results in a different appearance façade, it could also be the difference between a design using a single skin façade and a double skin façade or a small cavity façade. This potential phase change of façade types driven by the energy requirements is a key consideration in selection of a suitable façade system.

Fixed shading devices and dark (low solar heat gain coefficient) glass, combined with an internal blind may be suitable in terms of SHGC, while at the same time providing low VLT all the time. The adoption of dynamic shading elements such as blinds can allow a façade to vary its performance throughout the day to deal with the heat loads, providing overall better access to daylight and better access to views. Further by using dynamic shading devices that allow views through, such as fabrics, or slatted blinds, perforated materials and even perforated blind slats can improve the overall performance of a façade in regard to both its heat rejection performance and its ability to provide higher VLT’s and access to external views.

PERFORMANCE COMPARISON TABLE

The following Performance Comparison Table is a summary of the various multilayered façade typologies for direct comparison. From this table, we are able have informed discussions and understand the limitation and consequences of these designs in regards to the overall performance, the architecture, construction and cost:



Figure 1: Performance comparison table.

COST VERSUS PERFORMANCE/THE VALUE PROPOSITION

In addition to the PCT we have provided the following graphic as to serve as a value proposition of Cost Versus Performance. This chart allows further assessment of the benefits and limitations of the various designs, to assist decision making and option studies for your building.

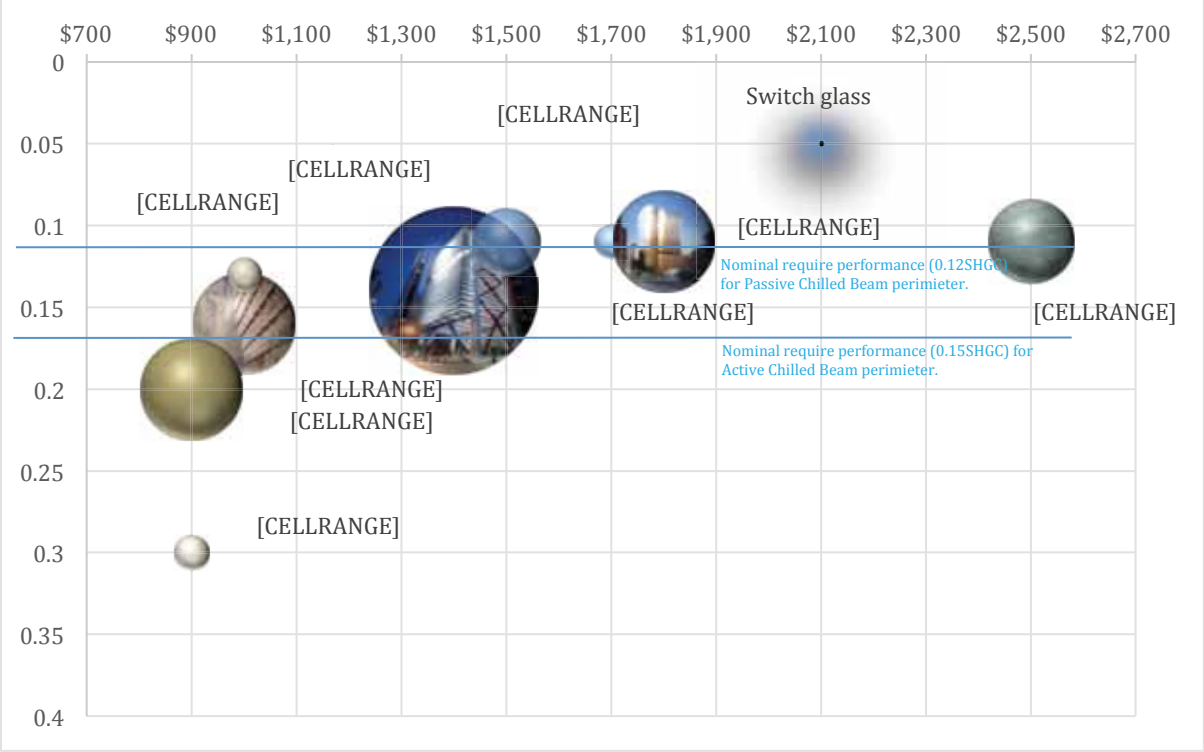


Figure 2: Cost versus performance chart. The vertical axis shows nominal SHGC for each façade typology, the horizontal axis shows nominal cost per square metre of façade. The size of the bubble indicates the (nominal) prolificacy of each type in Sydney Australia in Modern Buildings. Note the nominal cut off for performance of SHGC in comparison to two high end mechanical systems at the perimeter of the building of Active Chilled Beam (SHGC 0.15) and Passive Chilled Beams (SHGC 0.12). These figured will vary from project to project.

CONCLUSION

Cities provide vibrant and exciting social environments however the city's streets will never achieve performance expected within a building, and nor should they. The cities buildings contain offices, schools and living quarters. The modern building aims to tame the environment and maximize efficiency and human comfort. Comfort within a building is judged on the façade to provide a sense of security, keeping the space dry and clean, thermally comfortable, quiet and calm as well as the subtler effects such as a connection to natural light and nature. The façades role in this respect is more than just a wind break, an umbrella or a parasol, rather it is the skin, filter and the barrier to the harsh external environment and in this paper, we have discussed the conflicting performance aspirations and provided guidance and tools to assist the balancing effect required by the designers to make decisions and measure the various outcomes and paradox.

THE THERMAL BLANKET CONCEPT

An active double skin façade at the Manhattan Beach Library



Bharat Patel, PE, CEM, LEED AP
Harley Ellis Devereaux
bpatel@hed.design



Michael Bulander, AIA, LEED AP
Harley Ellis Devereaux
mbulander@hed.design

ABSTRACT

This paper tells the story of a Double Skin Façade (DSF), where high performance and multi-disciplinary collaboration saves a library concept of openness, transparency and aesthetic delight. At the recently constructed Manhattan Beach Library the integrated design approach between architects, building scientists, and mechanical engineers saved an aesthetically stunning double glass façade from cost cutting measures by making it an integrated part of the building systems. The multi discipline design team developed a performance concept that gave the active double skin façade (ADSF) a functional justification. A first concept aimed to reclaim the conditioned air generated in the air space between the glass layers into to cool and heat the building interiors. This approach required an intake at the bottom which was detrimental to the main design vision of openness and transparency. Therefore, the design team developed a second concept where the idea of a 'thermal blanket' is employed. This is a solution where the double glass façade can be considered a 'transparent insolation'. A post occupancy evaluation (POE) identified areas where the building was not performing as modeled, which were then subsequently eliminated. The Manhattan Beach Library highlights the importance of collaboration between multiple disciplines adding real value to this building component and resulting in a stunning award-winning high-performance library that stands to serve the community.

The Double Glass Façade at the Manhattan Beach Library is of interest to an international interdisciplinary audience because it is a pioneering design that uses an active double façade that responds to climate conditions. This leads to the development of a new approach to the double skin façade; the *'Active Double Skin Façade' (ADSF).* This pioneering concept can be a model for other climate zones and make the architectural element of the double skin façade more important in the future.

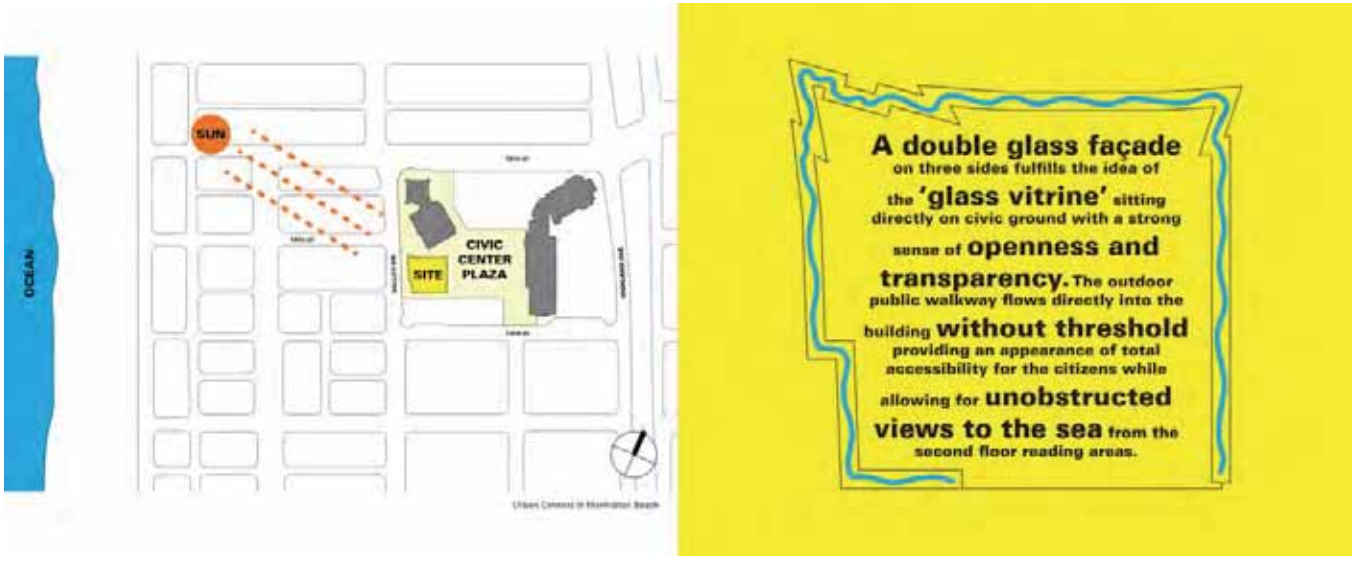


Figure 1: Site Diagram showing solar orientation and Civic Center adjacency. Located on a prominent site, the award-winning Manhattan Beach Library captures views of the Pacific Ocean and provides a welcoming enhancement to the local community. Photo courtesy of Eric Staudenmaier. Diagram courtesy of the author.

KEYWORDS

double-skin, energy efficiency, computational fluid dynamics (CFD), finite element analysis (FEA), design-build

INTRODUCTION

The Manhattan Beach Public Library is located within the Manhattan Beach civic center lot, two blocks away from the coastline with dramatic views over the ocean. Due to its location in the view corridor of surrounding residential houses the roof is developed as a 5th façade with no HVAC equipment sitting atop. It's 15,000 sf area is distributed over two stories which are surrounded by a double skin façade on three sides. This glass façade fulfills the idea of the 'glass vitrine' sitting directly on civic ground with a strong sense of openness and transparency. The outdoor public walkway flows directly into the building without threshold providing an appearance of total accessibility for the citizens while allowing for unobstructed views to the sea from the second floor reading areas. The library achieved a LEED Gold rating.

In the initial design the DSF was designed as an open joint rainscreen system (Design Architect: Johnson Favaro). Through the design-build (DB) project delivery method, HED was able to turn the DSF into an important element of the building's HVAC system. Since HED is an integrated studio where architects, engineers and building scientists closely collaborate, the final design reconciles, through several iterations, engineering requirements with the aspirations for an open civic presence.

The rainscreen system as originally designed resulted in many technical problems that became costly to mitigate. High maintenance with a constant need for cleaning due to dirt and salt deposits on the one hand and high solar heat gain with glare issues on the other had an impact on the budget making the DSF a prime target for value engineering efforts. HED devised the DSF as a closed system. The first design concept was to capture heat and release it where it was needed. For example, in the morning the sun heats the east facing façade while the west, north and south has a heating demand. The team utilized optimum fluid dynamics design to move the heat from one side of the building to the other side thus reducing the HVAC energy demand. Since natural buoyancy was the passive engine to move the air, a vent at the bottom of the façade was required. After evaluating the visual impact of this solution, the team decided that it would impair the sense of continuity from the outside to the inside. Subsequently a second and final concept was developed where the sealed space between the glass layers becomes a thermal blanket essentially creating a transparent insulation.

This is of interest to an international interdisciplinary audience because it is a pioneering design that uses an active double façade that responds to climate conditions. This leads to the development of a new approach to the double skin façade; the "Active Double Skin Façade" (ADSF). This concept pioneered on the Manhattan Beach Library can be a model for other climate zones and make the architectural element of the double skin façade more important in the future.

Design Concept 1 – Reclaim Heat from Double Façade: The design utilized optimum fluid dynamics design to reclaim heat from one side of the double façade and use it where it is required, and thus reducing the HVAC energy demand.

Design Concept 2 – Provide a thermal blanket between the double façade therefore minimizing heat transfer for both heating and cooling.

It was important to understand the performance of the building during occupancy. Therefore, after the first year of occupancy a post occupancy evaluation (POE) was conducted. The measured data confirmed that the system is performing as designed after a few minor modifications.

BACKGROUND

The University of Southern California's Keck School of Medicine Eli and Edythe Broad CIRM Center for Regenerative Medicine and Stem Cell Research building provided an example where one side incorporates a double façade skin system.

The double façade consists of three functional layers, the outer glazing, the inner glazing, which is part of the building skin, and the air gap that separates the glazing systems. Typically, the exterior façade layer is made up of single glazing and the separation gap varies depending on the intent of the design, in this case the separation is two feet continuously along the three sides of the façade, the fourth side consists of a wooden louver type of appearance. The overall exposed glass surface area is approximately 11,000 square feet.

During the day the solar radiation falling on the outer façades partially provides protection to the building from direct solar radiation. Some of this heat passes through the single glazing and heats the air. The original design was a rain screen with gaps between the tiles that allowed the air to escape immediately to the outside. The proposed design seals the outer façade thus allowing the air to be heated, this created a ventilated double façade which allows hot air to rise due to buoyancy, similar to chimney effect to the top of the building. Climatic analysis based on California Energy Code shows heating is required for most of the year therefore if any heat that can be reclaimed would be a benefit to the project. To understand the performance of the double façade it was necessary to perform a detailed analysis of the system and the relationship to weather conditions.

For the second design concept another study was performed that required to seal the bottom of the façade to the ground floor slab, resulting in a totally sealed façade structure without any air intake vents A much better design emerged where exhaust air that would normally be expelled from the building was being circulated within the double façade. This would provide a thermal blanket of 75F around the building. The fan is configured as a variable speed fan and will be controlled by thermostats at each of the façades within the cavity increasing or decreasing in speed depending on the air temperature. In order to understand the behavior of the air movement with the double façade Computational Fluid Dynamics was performed. Results confirmed the benefits of this design to reduce the energy loads of the building. It also reduced maintenance costs when compared to the original rain screen design.

METHOD

DESIGN CONCEPT 1

The analysis was based on a number of software applications these included Energy Plus engine with an interface of Design Builder. When assessing the feasibility of heat recovery, the following parameters were examined, orientation, buoyancy, air temperature, airflow, and material effects. The initial analysis examined the temperature difference at the inlet air temperature between the facades and compared to the outlet air temperature, this varied depending on solar radiation at a particular time, day and month. The climatic data used for this analysis was obtained from DOE Energy Plus website weather file for Climate Zone 6.

To minimize operational costs, the design incorporates two economizer systems. One economizer is used to operate in heating mode and the other operates in the cooling mode. Both uses the natural systems to maximize energy savings. During the heating mode heat is reclaimed from double façade to preheat the air entering the HVAC system. The free heating system would provide heating on most days of the year, the heating system only turns on during very cold conditions it is intended to supplement the recovery system.

During the cooling economizer mode, the heated air generated by the double façade would be bypassed and released back into the ambient air. The cooler ambient air being drawn into the fresh air air-conditioning unit located in the mechanical room will provide free cooling.

Calculated Values	
Total solar transmission (SHGC)	0.24
Direct solar transmission	0.19
Light transmission	0.309
U-value (ISO 10292/ EN 673) (Btu/h-ft2-F)	0.569
U-Value (Btu/h-ft2-F)	**0.574**

Calculated Values	
Total solar transmission (SHGC)	0.819
Direct solar transmission	0.775
Light transmission	0.881
U-value (ISO 10292/ EN 673) (Btu/h-ft2-F)	1.007
U-Value (Btu/h-ft2-F)	**1.018**

Figure 2: The diagram on the left shows internal glazing high performance low-e. The diagram on the left shows clear external glazing. Diagram courtesy of the author.

The principles in reclaiming heat from the double façade is one of maximizing temperature difference that is energy it also provides the motive force which is buoyancy to move the air, this is measured in cubic feet per minute (CFM). It was modeled with the revised design with 6” vent at bottom and 1’ on the top.

The following case study considers the effect of buoyancy and impact of wind.

The heat recovery from three façades were studied for all 12 months of the year. An average hourly CFM and Delta-T was analyzed for all months, which enabled us to calculate heat recovery from these façades.

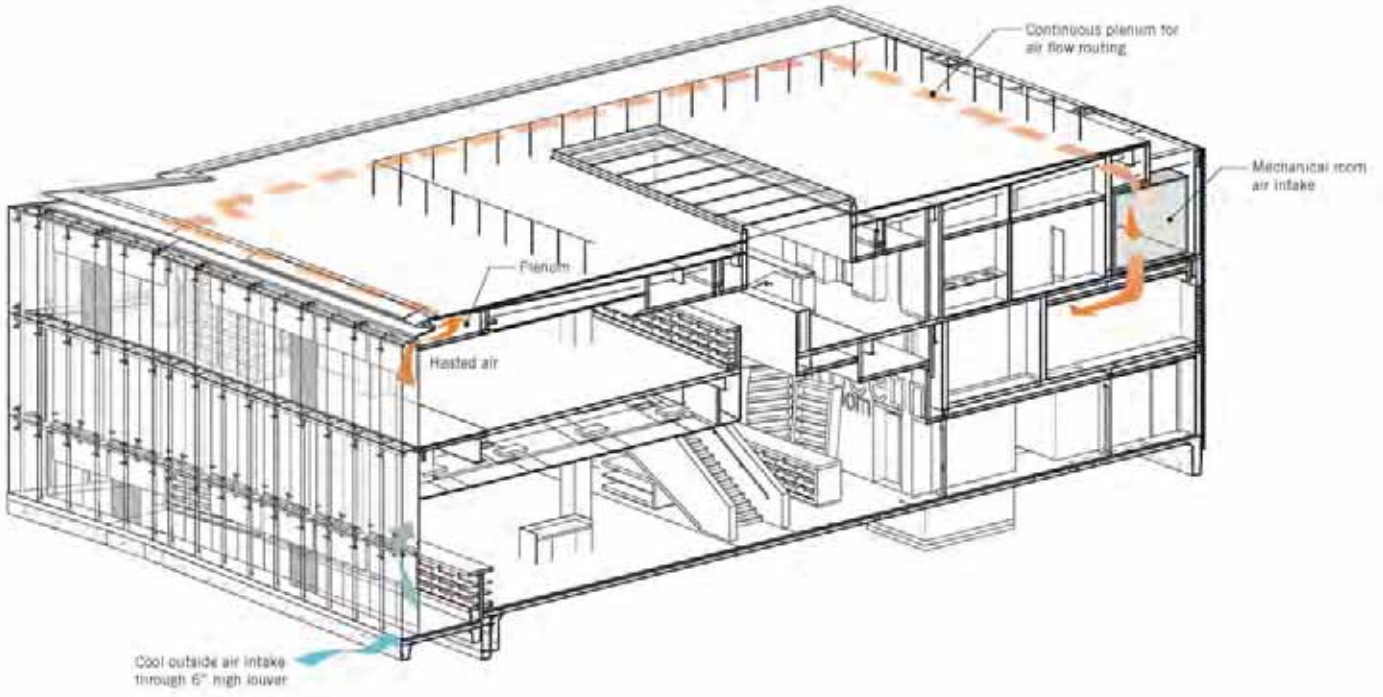


Figure 3: This sketch shows the airflow through the double façade and the heat reclamation process.

The cool air outside enters at the bottom of the façade and is heated via solar radiation. Diagram courtesy of the author.

DESIGN CONCEPT 2

The design was based on the California Energy Code – Title 24 weather files, however the weather data is based on historic data, it does not take into consideration climate change. According to the Intergovernmental Panel on Climate Change, temperatures will rise in the future 2.5 and 10 degrees Fahrenheit over the next century. This was one of the compelling augments that was discussed as part of the design. Another important design parameter was to provide an inviting and

openness of the building from the outside. Therefore, by sealing the façade at the bottom instead of either a vertical or horizontal grille for air intake as described in the first design concept provided this barrier free appearance.

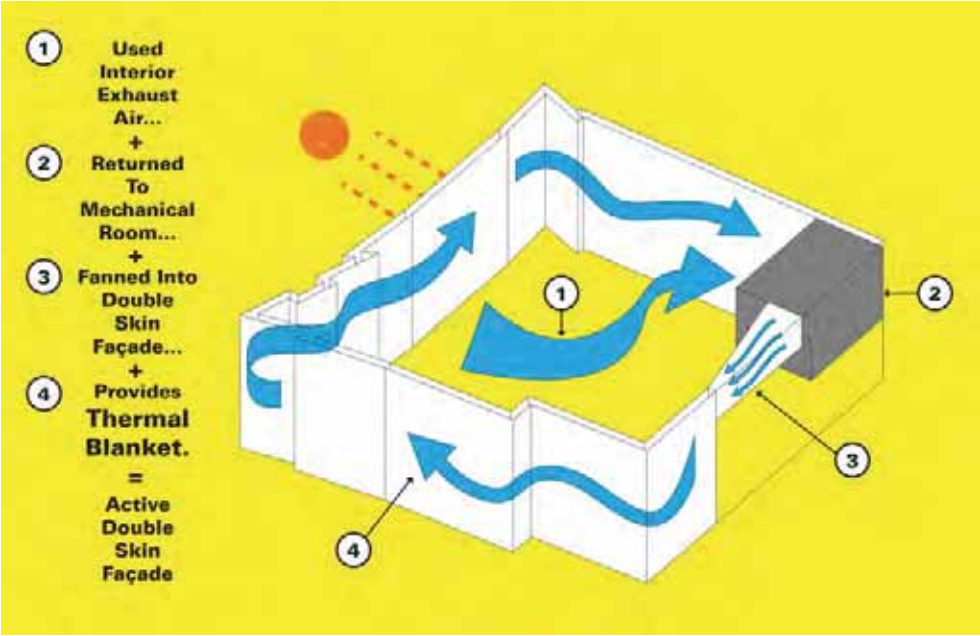


Figure 4: Air circulation and the heat reclamation process. Diagram courtesy of the author.

DATA

DESIGN CONCEPT 1

(TYPICAL ANALYSIS OF TOP AND BOTTOM VENTS OF FAÇADES)

All three double glazed façades were analyzed for the rise in temperature rise (delta-t) and airflow (cfm) of the air between the two facades for all months of the year. An average delta-t and cfm were then used to analyze the magnitude of heat recovery. Below is a typical example for the month of August.

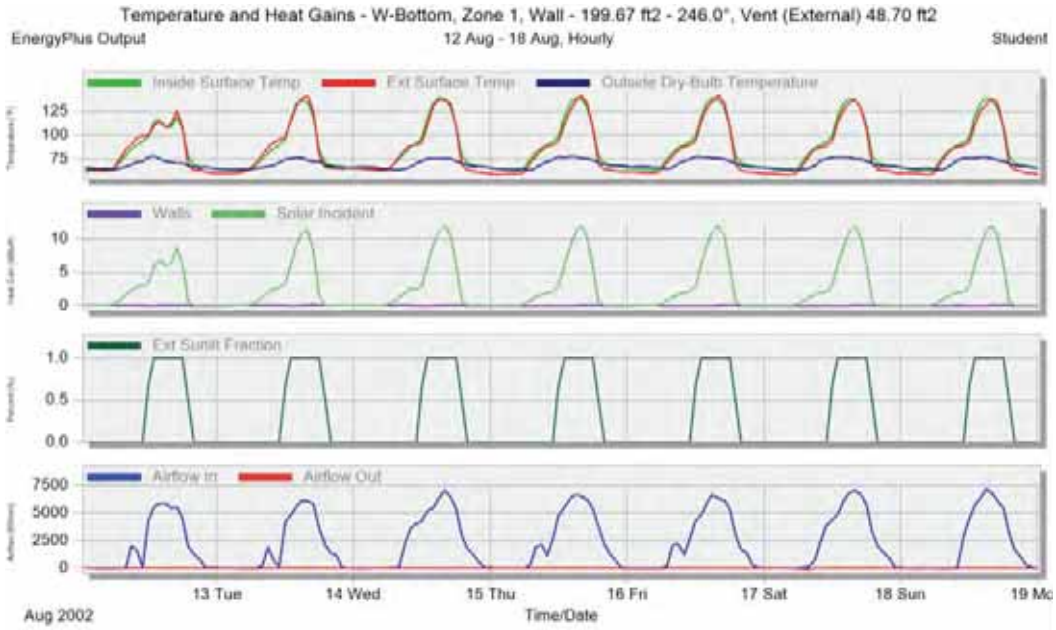


Figure 5: Buoyancy driven airflow pattern vent of southwest facade. Diagram courtesy of the author.

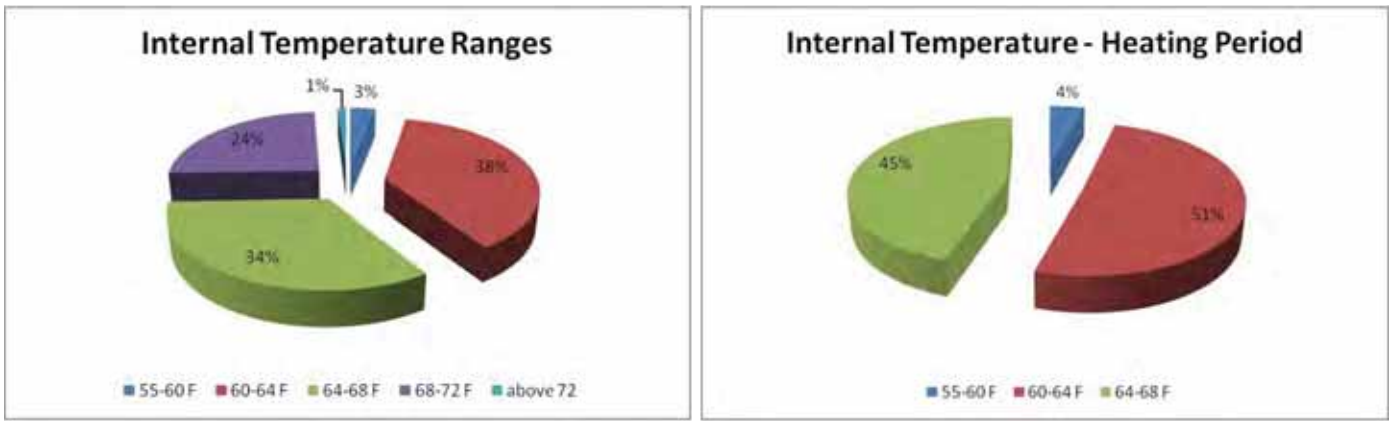


Figure 6: The diagram on the left shows how heating dominates at this location with 74% of time requiring heating. The diagram on the right shows how the heat recovery system should be effective 96% of the time when heating is required. Diagram courtesy of the author.

DESIGN CONCEPT 2

The velocity distribution of air moving for all three axis i.e. X, Y, and Z between the double façade was studied. Additional CFD analysis was performed to understand the temperature profile as the air moves around the perimeter of the building.

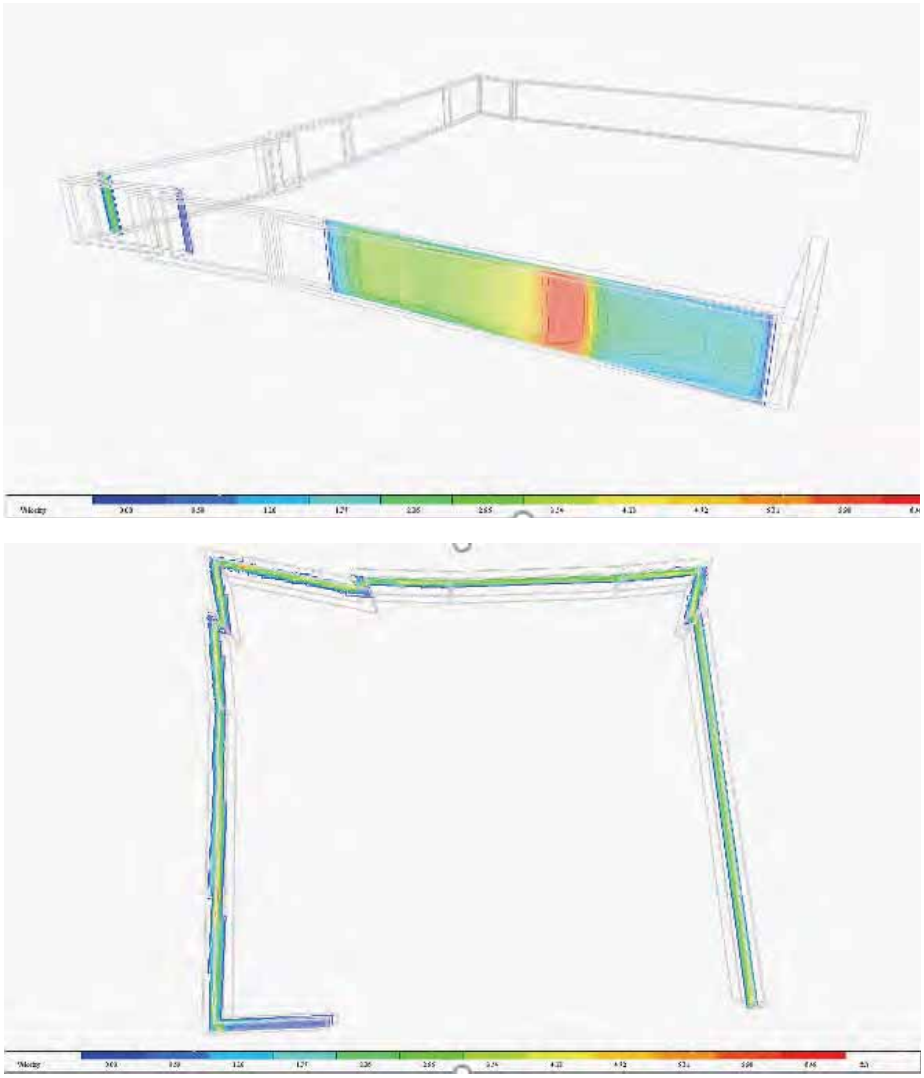


Figure 7: The diagram at the top shows the X-Axis. The bottom diagram shows the Y-Axis. Diagram courtesy of the author.

EXPLANATION

An active ventilated double façade system would result in the reduction in both maintenance and operational costs. Essentially, because the frequency of cleaning two sides of the double façade would be reduced, compared to a rain screen design and both heating and cooling loads would be reduced. Another benefit is that it allowed the perimeter-heating system be eliminated, which results in a reduction of capital, operational and maintenance costs. The simple payback of incorporating an active double façade system is approximately 9 years.

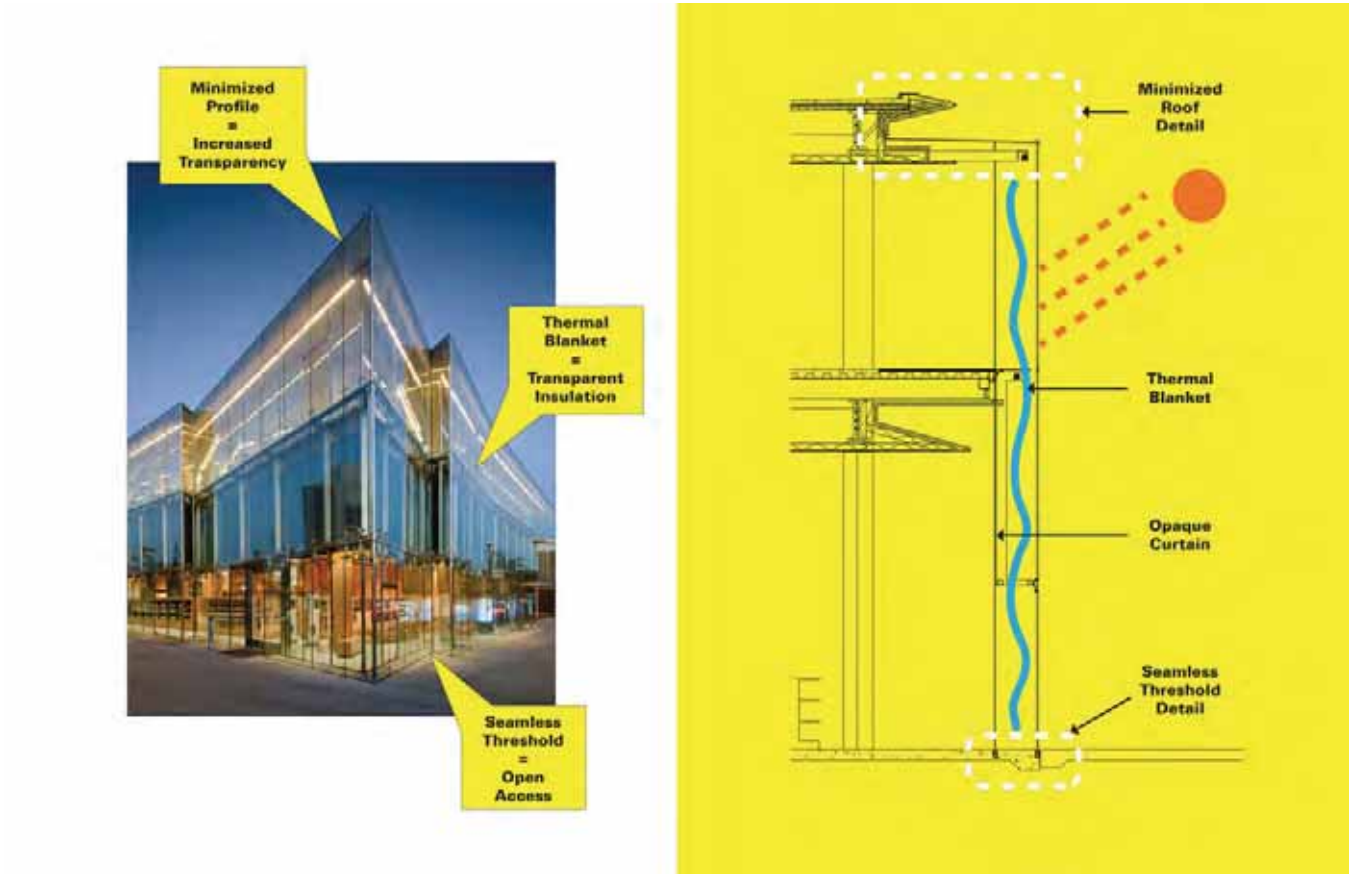


Figure 8: System section diagram and associated built photo location. Photo courtesy of Eric Staudenmaier. Diagram courtesy of the author.

POST OCCUPANCY

In conclusion the active double façade system with an exhaust air circulating around the building provides a thermal blanket and has proved to be energy efficient. The actual performance of the system has been fine-tuned and is functioning as modeled.

POST OCCUPANCY

During two of the summer months the library experienced high indoor temperature. The design team used the building management system to analyze the data to understand the buildings performance. Based on the data the possible causes of the higher indoor temperature are described below with recommendations:

DATA

The weather data used was based on the nearest weather station, Los Angeles International Airport (23174/LAX). Hourly data of outdoor temperature (DB/WB), wind speed, and sky conditions in the period August 2015 to February 2016 was used in this analysis. The Building management system provided indoor temperature of different zones served by each fan coil unit, the inlet air fans. The data provided was from August 2015 to February 2016. Mechanical floor plans, schedules, specifications, design criteria, and sequence of operation were reviewed.

FINDINGS

The analysis examined and compared measured indoor temperature, designed temperature, equipment operation, outdoor weather condition and actual indoor air temperature. Key findings associated with high temperature issue are listed below:

a. Outdoor Temperature

Manhattan Beach was designed in accordance with the California Energy code: Climate zone 6; ASHRAE 0.5% design outdoor dry bulb temperature is 84 °F. However, the outdoor temperature trend data shows that, there are 84 hours in summer 2015 (August to October) that exceeds 84 °F (See Table 1 & Fig. 1). Therefore 1% of year the temperature exceeded 84 °F (84 divided by 8760 hours) which is greater than the designed 0.5% as stated by ASHRAE. In September 2015, there were 33 hours exceeds 84 °F, therefore as a percentage of a typical 8-hour day, exceed the indoor temperature by 13.7% i.e. (10am-6pm), 33/ (8x30) = 13.75%. However, from the indoor temperature readings we see that 10% of hours exceeded the temperature indoor set point.

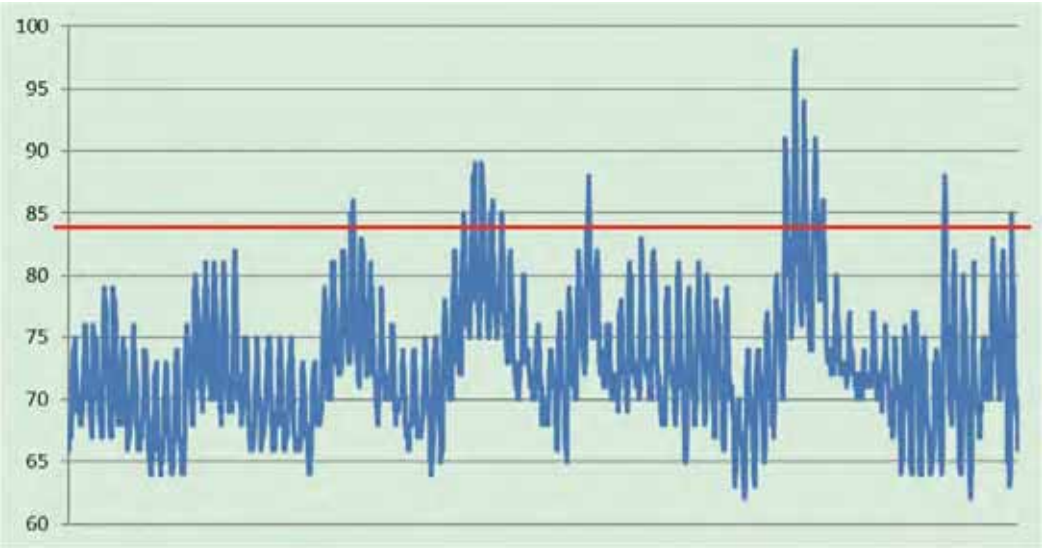


Figure 9: Outdoor temperature profile in summer 2015. Diagram courtesy of the author.

b. Indoor Temperature

Taking September 2015 as a sample month (hottest month), hourly indoor temperature data of each fan coil units were analyzed (Fig. 2). The designed indoor temperature from the T24 calculations is 74 °F with a ± 2°F range, so the highest temperature acceptable is 76 °F and 10.43 % hourly data point exceeds 76 °F. (Table 3). So most indoor space stays within designed temperature range, and these hours that out of range has encounter extremely high outdoor temperature as discussed previously.

However, the space served by FC-6 has high indoor temperature at late afternoon for most of the days in this month. It was this space experiencing high temperature as alarmed by the building management system. Further investigations were conducted to understand why this was occurring.

c. Analysis of FC-6 and its Serving Space

FC-6 serves the main entrance (west); its thermostat (T-6) is located on the column close to the entrance. The adjacent space -Popular Library- is served by FC-5, and T-5 is located on another column near T-6. The temperature profiles of FC-5&6 are plotted below for comparison. Hourly data in hottest days of October 2015 (Oct 10-Oct 14) were selected as sample data.

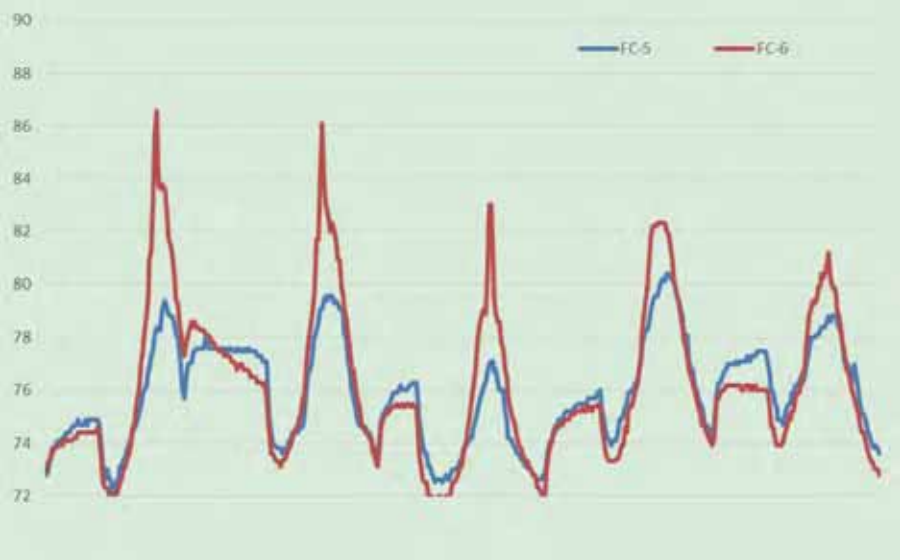


Figure 10: Diagram showing comparison of temperature profile of FC-5. FC-6. Diagram courtesy of the author.

Fan Coil unit 5 and 6 serve the same space and are located near each other so one would expect a similar behavior from readings of their respective thermostats. The temperature profile from both FC-5 and FC-6 have similar indoor temperature profiles from mid-night to around 2:00pm each day. However, after 2:00pm FC-6 experiences a steep rise and reaches a high maximum temperature compared to FC-5. Possible causes for this maybe:

- Thermostat serving FC-6 is located near the entrance door, therefore having the door constantly opened and closed may contribute to false readings.
- From site investigation T-6 is located on the unshaded side of column, facing south (see below). This is an inappropriate installation because of the thermostat is exposed to direct sunlight exposure in the afternoon, also street reflection of the solar gain even when the blinds are partially drawn.

In conclusion, the active double façade system works well, and the space stays within designed temperature range under normal weather conditions.

OPERATION RECOMMENDATIONS BASED ON ONE YEAR AFTER POE

The operation recommendations are proposed for extreme hot hours only, late afternoon during summer hot days.

- Relocated thermostat of FC-6 (T-6) to the shaded side of column. FC-7 could be better controlled by disconnecting it from T-C7 and taking a signal from T-5. Therefore T-5 will be controlling TC-5 and TC-7.
- During extreme hot hours, roll down the blinds all the way down at southwest corner of first floor, preventing direct or indirect solar heat gain, which contributes to the largest portion of cooling load.



Figure 11: The photo on the left shows the Thermostat installation on the unshaded side. The photo on the right highlights the need to extend the blinds all the way down in order to reduce the direct or indirect solar heat gain. Photos courtesy of the author.

CONCLUSION

In conclusion, the active double façade system with exhaust air circulating around the building providing a thermal blanket has proved to be energy efficient. The actual performance of the system has been fine-tuned and is functioning as modeled. This design concept can therefore serve as a model for other double skin facades where transparency and openness are key elements of the architectural vision.

ACKNOWLEDGMENTS

Harley Ellis Devereaux (HED), Architect of Record | MEP
Johnson Facaro, Design Architect



Figure 12: The Manhattan Beach Library, view from Valley Drive showing the West facing elevation. The Active Double Skin Façade creates a seamless transition that blends with the micro-climate and creates a dynamic visual quality that responds dramatically to changes in light. Photo courtesy of Eric Staudenmaier.

Process <> Design

EMULATING NATURE'S STRUCTURED RANDOMNESS IN FAÇADE DESIGN

Using parametric modeling tools to develop rich façade modulation



Ned S. Kirschbaum FAIA, CCCA, LEED AP BD+C
Fentress Architects
kirschbaum@fentressarchitects.com

ABSTRACT

The wonder of nature is the abundance of unique forms she creates based on a few simple physical principles or laws. No two snowflakes are alike. Even identical twins are not identical. Nature creates random and unique patterns or structures to suit their environment based on invariable physical laws interacting with chance—but specific—environmental conditions. The result is a magnificent biodiversity of form with a common familial relationship. How can one use this model to design facades that are unique in form or pattern while at the same time respond to formal criteria? The now relatively common availability of significant computing power coupled with the development of parametric modeling tools provides us the opportunity to do just that.

The feature skylight for the Orlando International Airport South Terminal Expansion and the landside glazed curtain wall for the Portland International Airport Concourse E Extension are two examples of naturally inspired façade structures. Both the feature skylight and the curtain wall comprise a limited set of relatively simple rectilinear parts organized to respond to functional requirements including daylighting, acoustics, and space usage combined in complex and random patterns that result in a natural richness of texture and form. For each of these façade elements a set of form-generating parameters were established by the Lead Designer. The design team developed Grasshopper scripts that generated formal "solutions" in Rhino that were reviewed by the Lead Designer and iteratively adjusted and refined until the technical and aesthetic design goals were achieved. Using Grasshopper, Excel, and Dynamo, the resulting Rhino geometry was migrated to Revit for construction documentation using adaptive components. The resulting richness of expression would not have been achievable without the use of these tools.

KEYWORDS

parametric workflows, computational design, Rhino/Grasshopper, Revit/Dynamo, Building Information Modeling (BIM)

INTRODUCTION AND BACKGROUND

The façade elements for Portland and Orlando take their inspiration from the natural environment. In both cases the challenge was to develop a system of regular elements that gives the impression of the underlying structure and the randomness found in the natural world.

PORTLAND INTERNATIONAL AIRPORT CONCOURSE E

In initial meetings with the client, it was evident that the Port desired the design of Concourse E to draw its inspiration from the majestic forests, waterfalls, and canyons of the Pacific Northwest region (Fig. 1). The airport approach road is envisioned as a canyon between the existing administration building on the left and the new concourse extension on the right (Fig. 2). The south wall of Concourse E is conceptualized as the forest edge. A hierarchy and filigree of elements was initially

diagrammed to establish the design intent (Fig. 3). This framework is further enriched by using three types of glazing joint treatments: butt glazed, conventional 1-inch-deep captured, and 8-inch-deep fin to simulate the richness of the forest edge (See Figure 4).



Figure 1: Regional inspiration images for the design of Portland International Airport Concourse E. Image courtesy of Fentress Architects.



Figure 2: Portland International Airport Concourse E Extension – landside view. Image courtesy of Fentress Architects.

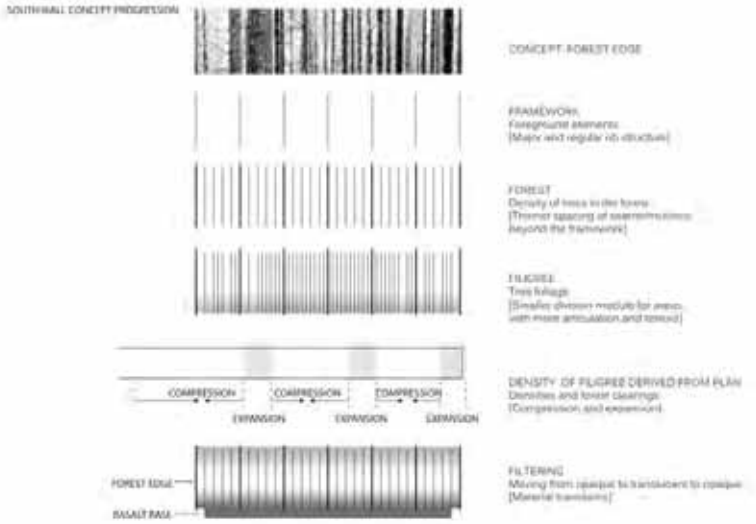


Figure 3: Forest edge framework. Image courtesy of Fentress Architects.

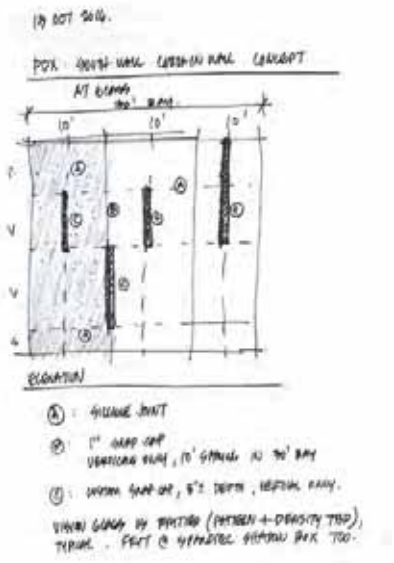


Figure 4: Glazing joint treatments. Image courtesy of Fentress Architects.

ORLANDO INTERNATIONAL AIRPORT SOUTH TERMINAL

In the initial solicitation for Master Architect Design Services the Greater Orlando Aviation Authority (GOAA) made it clear that, as a gateway to the area, the new airport terminal should introduce visitors to what the Chamber of Commerce has trademarked *The Orlando Experience*™. Rather than focus on the area's theme parks, *The Orlando Experience*™ is characterized by the unique and lush tropical environment of Central Florida, specifically the natural elements of water, trees, and sky. To orient the passenger and make wayfinding intuitive, the floor plan is organized along a single circulation spine called "The Boulevard" that is marked by water features, lined with palm trees, and illuminated with a monumental skylight (Fig. 5). In response to environmental consideration the skylight is composed of opaque, fritted, and clear glass panels (Fig. 6). Direct sunlight is further moderated by a series of baffles below the skylight that also provide acoustic absorption. The skylight panels and baffles are arranged to provide a hierarchy of filtered and direct light (porosity) that relates to the civic nodes in the plan below and emulates the filtered light in a tropical jungle (Fig. 7).





Figure 5: Orlando International Airport "Boulevard" skylight renderings. Image courtesy of Fentress Architects.



Figure 6: Opaque, fritted, and transparent panels along "Boulevard" skylight. Image courtesy of Fentress Architects.

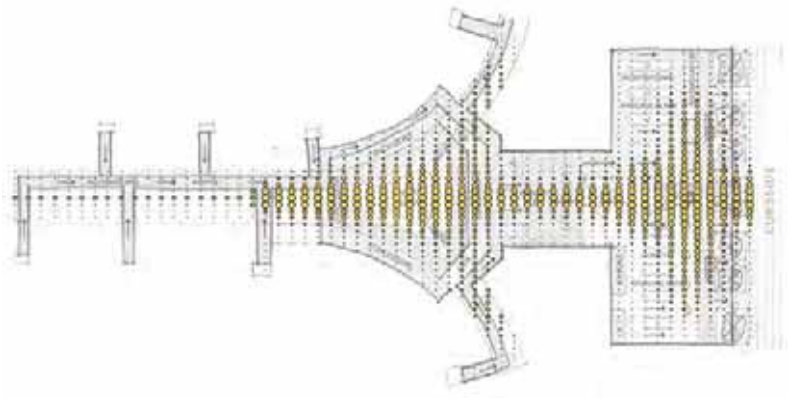


Figure 7: Relationship skylight porosity with civic spaces along the "Boulevard." Image courtesy of Fentress Architects.

METHOD

The goal for both projects was to create a design composed of simple geometric elements combined to create a varied, random and organic feel. To achieve this, custom parametrically-driven design tools were developed to permit fast study of alternative designs that respond to objective criteria such as acoustical needs, light levels and space function, as well as qualitative objective inputs such as light quality, balance, composition and proportion.

FORM-GENERATING SCRIPTS – PORTLAND INTERNATIONAL AIRPORT CONCOURSE E

The design team began with a conventional curtain wall layout. Mullions are spaced at 5 feet on center and centered in each of 28 bays. The panels are divided vertically at 11.75 feet and again at 17.75 feet above the sill (Fig. 8). In the script, this layout is parametrically driven; however, the location value for each mullion is set as a constant and was not altered as part of the design studies. A secondary overlay grid, offset 2.5 feet from the mullions, is introduced in the middle four panels (Fig. 9). The design uses this regular grid as a framework or skeletal structure onto which is layered a variety of components that create an unpredictable, complex, natural rhythm on the façade emulating the variation in size and spacing of trees in a forest.

As noted above, there are three glazing joint treatments: butt glazed, conventional 1-inch-deep captured, and 8-inch-deep fins. There are also three glass types that occur as vision glass at the concourse and as opaque wall at the retail/bathroom cores by employing shadow boxes. Using these few building blocks, the script shuffles them as described below to create a richly varied and harmonious façade composition.

The first step in the randomization process begins with culling the number and location of the 2.5-foot offset grids. The script removes either two or three of these grids per bay and then, using the "Jitter" function in Grasshopper, shuffles the resulting bay layouts based on a decimal shuffle strength parameter between 0 and 1 and a randomization integer seed between 0

and 10. The designer had predetermined that these locations would receive deep fins and that they would be either 11.75 feet tall spanning the bottom panel or 17.75 feet tall spanning the bottom two panels. By creating an alternating list of these two values (11.75 and 17.75) with the list length equal to the previously determined number of locations of 2.5-foot grids and then shuffling their order with the “Jitter” function, each location is assigned a fin height (Fig. 10 and 11).

Glazing joint treatment (or Exterior Application Type as it is called in the script) is then determined for each interior vertical mullion location. Each mullion is divided into three segments. Six joint permutations are considered and coded with the following binary sequences: 0,0,0; 1,0,0; 0,1,0; 1,1,0 (two types); and 0,1,1. A zero (0) represents a butt joint; a one (1) represents a cap or fin (Fig. 12). When a cap is indicated, it may be either a 1-inch-deep cap or an 8-inch-deep fin depicted in Figure 12 by two colors. The coding for this portion of the script is too complex to describe here; however, using a series of binary lists that are created, shuffled and reconstituted through the “Jitter” and “Random Reduce” functions, each of the approximately 140 x 3 mullion locations is assigned a glazing joint treatment type. The degree of randomness is controlled by a shuffle strength input parameter.

Finally, a sub-routine in the script randomly locates each of the three types of glazing with each bay. Both individual and group randomization were considered and visually tested. The first case takes all panels as discrete entities and using similar strategies to those discussed above controlled by a randomization strength parameter, assigns one of the three glass types to each panel (Fig. 13). The latter case takes vertical groupings of panels for global randomization. The design team selected the former strategy as more visually consistent with the design intent and tested four randomization strengths (Fig. 14) selecting a value of 0.4 random. It was also necessary to distinguish vision glass panels from opaque (spandrel) panels. This was accomplished by inputs from Rhino to Grasshopper, and dividing the base surface into bounding boxes representing the extents of each panel type. The three types of glazing panels were then cross-referenced against the bounding boxes using Boolean tests to classify and separate the panels into distinct vision or spandrel sets, turning 3 sets into 6 sets (Fig. 15).

The Grasshopper script includes a control panel that gives the designers a user-friendly interface from which to control the various controlling parameters without needing to understand the complex script. The final design concept was then migrated to Revit for construction documentation as described below.

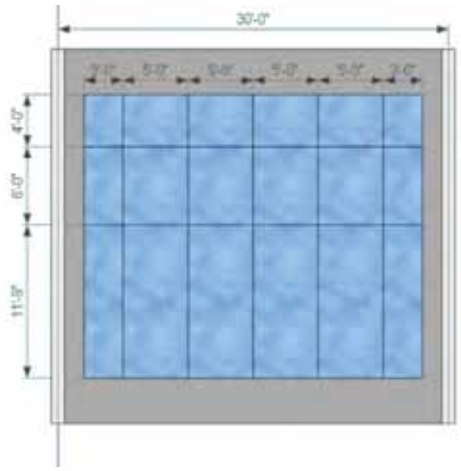


Figure 8: Basic bay geometry. Image courtesy of Fentress Architects.

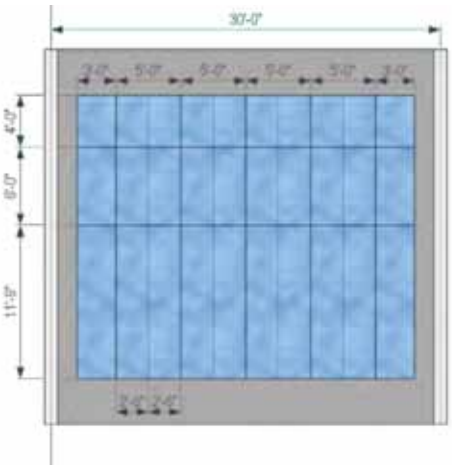


Figure 9: Secondary vertical cap spacing. Image courtesy of Fentress Architects.

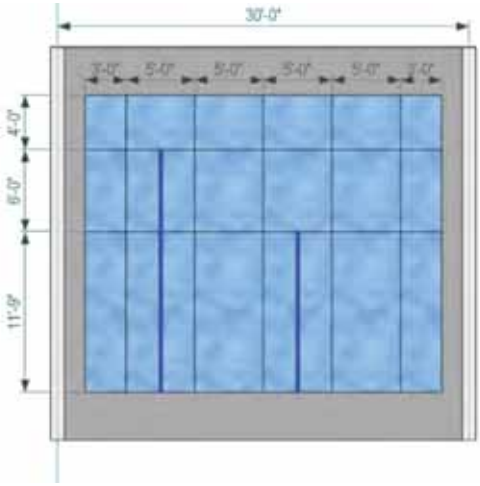


Figure 10: Possible intermediate fin layout. Image courtesy of Fentress Architects.

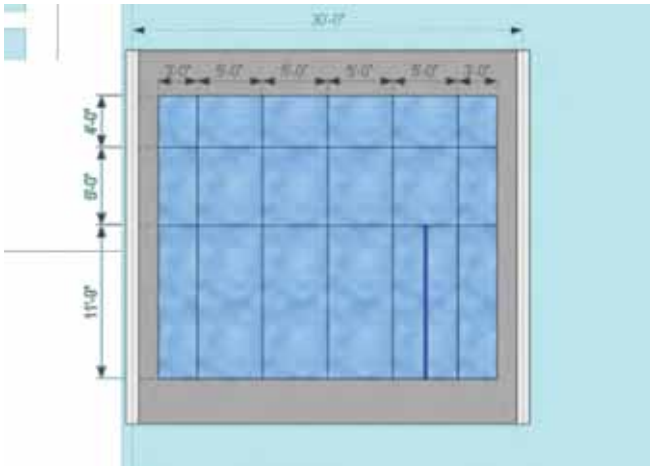


Figure 11: Possible intermediate fin layout. Image courtesy of Fentress Architects.

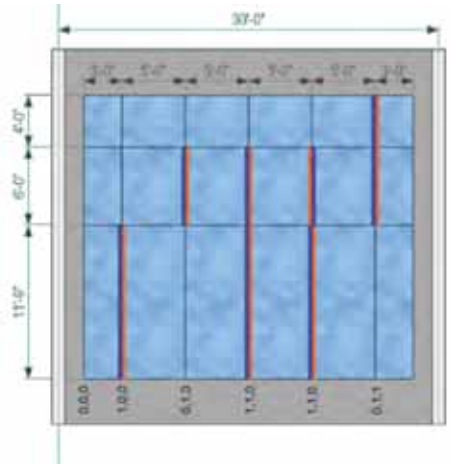


Figure 12: Joint permutations with binary coding. Image courtesy of Fentress Architects.

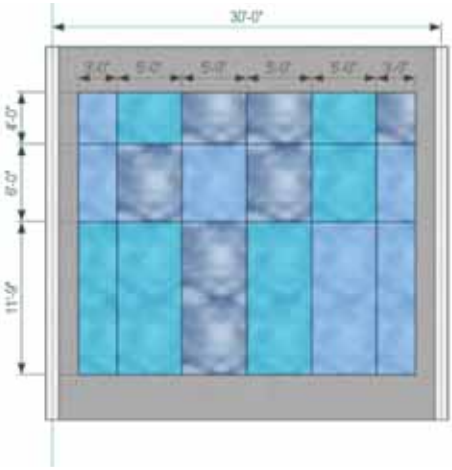


Figure 13: Random glass permutation. Image courtesy of Fentress Architects.



Figure 14: Grasshopper-generated wall patterns with variable glazing type randomness. Image courtesy of Fentress Architects.

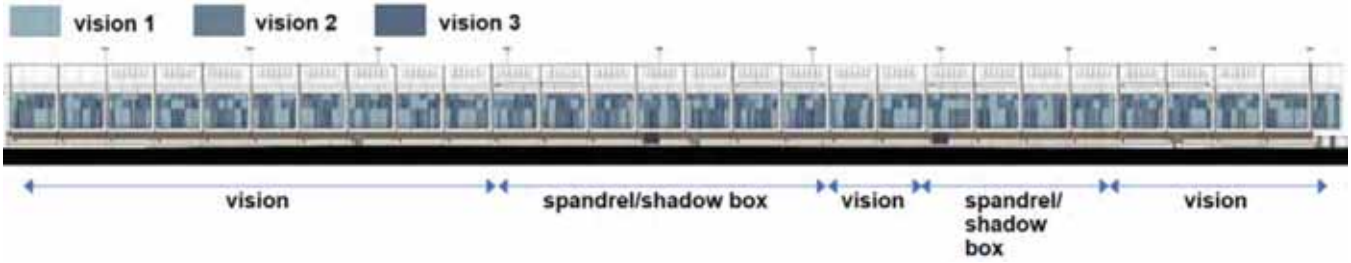


Figure 15: Final glazing panel randomization. Image courtesy of Fentress Architects.

FORM-GENERATING SCRIPTS – ORLANDO INTERNATIONAL AIRPORT SOUTH TERMINAL

There are many interactive variables driving the geometry and design of the skylight system at the Orlando International Airport South Terminal (Fig. 16). The form-generating Grasshopper script needed to consider the following:

- Pitch or cross slope of the gable
- Longitudinal slope of the skylight
- Skylight panel module—width and length
- Longitudinal plan location of slope inflection points along the length of the skylight
- Kingpost truss locations
- Purlin spacing
- Density and location of opaque and transparent skylight panels
- Baffle row spacing
- Baffle width and gap spacing
- Baffle rail longitudinal undulation profile

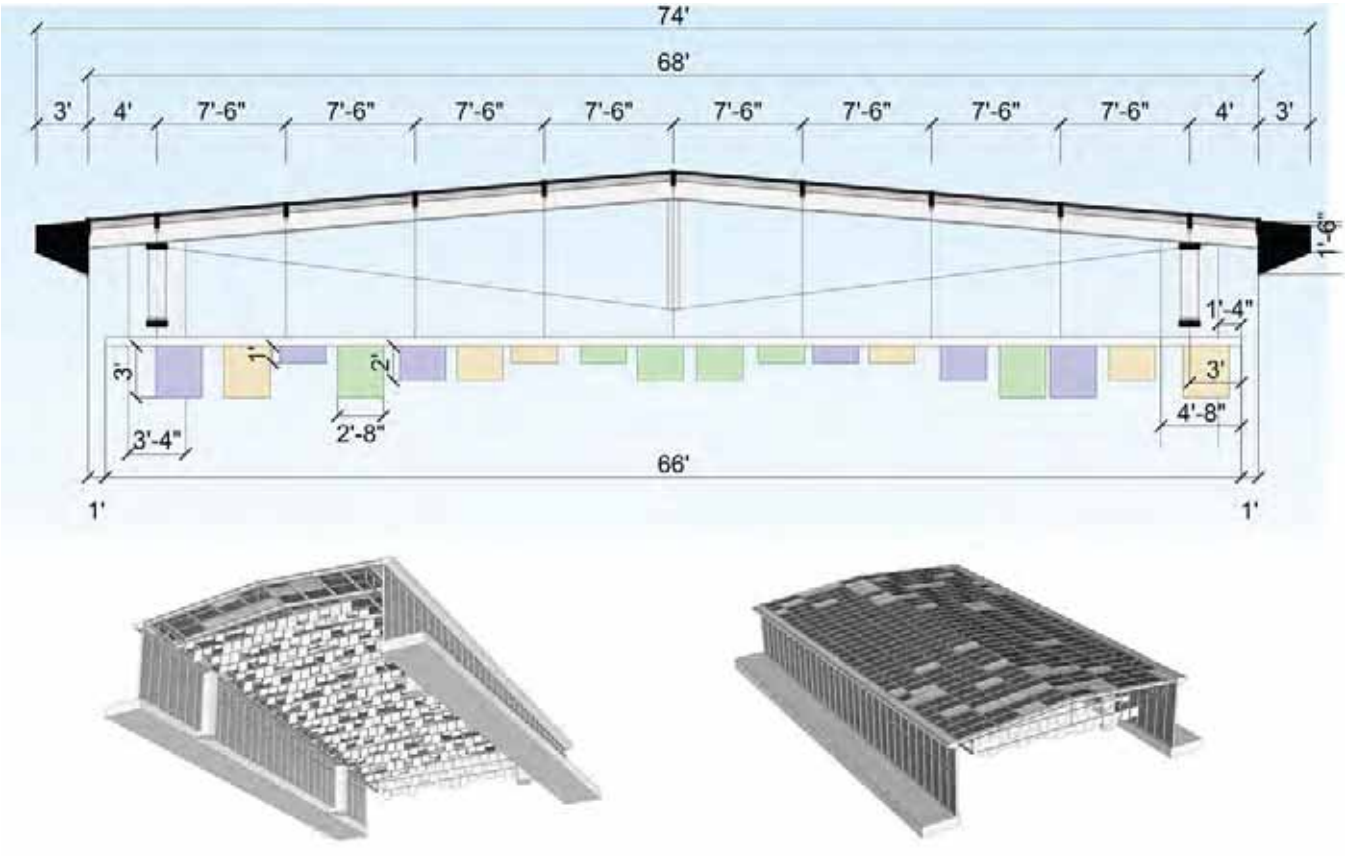


Figure 16: Cross-sectional geometry of skylight, kingpost truss and baffles. Image courtesy of Fentress Architects.

Basic Geometry: The first part of the script parametrically establishes the basic modular geometric framework of the skylight itself which, due to the longitudinal slope, requires a rather complex set of calculations. This permitted the design team to quickly study, coordinate and optimize the first six variables noted in the list above. Considerations included the size of glass lite, structural bay size, skylight member span capacity, and alignment with the vertical curtain wall module. While not groundbreaking, this level of parametric design nevertheless saved hours of remodeling the skylight for each of the many possible permutations the design team considered. The final design settled on the following:

- Pitch or cross slope of the gable: 1 inch per foot
- Longitudinal slope of the skylight: 1/4 inch per foot for some segments and 1/2 inch per foot for others
- Skylight panel module: 4-feet-wide by 7.5-feet-long
- Inflection point locations are fixed as a multiple of the 4-foot width module
- Kingpost truss locations are fixed as a multiple of the 4-foot width module but are not uniformly spaced
- Purlins are set to align with skylight panel length

Opaque and Transparent Roof Panel Placement: This portion of the script was written to address two design goals: 1) create a purposeful hierarchy of light to signify important civic spaces, reinforce wayfinding, and enliven retail/food and beverage hubs, and 2) produce an organic, varied, dappled light effect while supporting the first goal. The script employs a tool that was named the “roof pattern line” (Fig. 17). The roof pattern line graphically depicts the relative density of transparent panels at any given longitudinal location. It can be manipulated by the designer with the results seen in real time.

Grasshopper uses the roof pattern line as a variable input to the script and calculates the ratio of transparent to opaque panels in each row of the skylight. The skylight row is 100 percent transparent at the maximum amplitude of the roof pattern line and 100 percent opaque at the minimum amplitude. Intermediate densities of transparent panels are calculated as a ratio of the roof pattern line amplitude in that location to the maximum amplitude. The number of transparent panels is determined based on this percentage rounded to the nearest integer. However, the resultant pattern stacks all the transparent panels to one side and all the opaque panels to the other.

The Grasshopper script then employs the “Jitter” function to randomize the location of opaque panels in each row. The inputs to the “Jitter” function include a seed list uniquely identifying each row and a jitter strength value from 0 to 1. The jitter strength value is then adjusted so that the designer can, in real time, select the degree of randomness most aesthetically appealing.

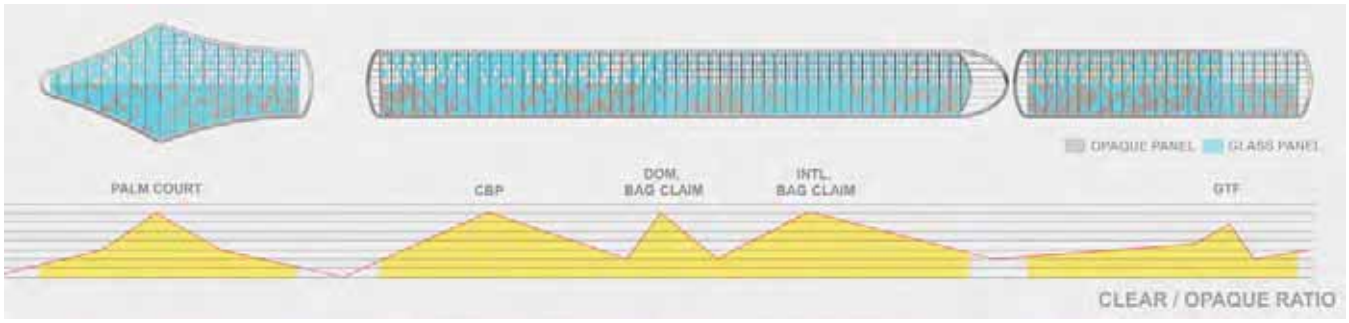


Figure 17: The roof pattern line controlling the clear-to-opaque skylight panel ratio. Image courtesy of Fentress Architects.

Baffle Size and Spacing: As indicated above, the design introduces another level of visual complexity by adding a layer of shading baffles hung from rails below the skylight. The baffles create an even more complex dappling of the light and moderate glare from the overhead glazing. The baffle row spacing, height, width and gap between adjacent baffles are parametrically driven which allowed for real-time study of the visual result of varying each one. Each row is composed of an equal number of 1-foot-tall, 2-foot-tall and 3-foot-tall baffles. After a series of studies varying the baffle width and gap width between baffles, the baffle width was set at 2 feet 8 inches wide with 18 evenly spaced baffles per row. Baffle rail spacing is initially set one-half module off the skylight mullion module above with one row of baffles per row of skylight panels. This is considered 100 percent density in the script and can be modified. After studying alternatives, the final design employs a 67 percent density, locating the rails at 6 feet on center, shifted one foot off the skylight module above.

Baffle Placement Location: Like the opaque skylight panel location discussed above, the script initially stacks all baffles in the same size order for each row. Also, because they are all the same width and evenly spaced they form regular longitudinal rows as well. Neither of these results is consistent with the organic design intent, so additional modules in the script were developed to scatter the baffles in a more natural arrangement. Three techniques were employed. First, like the opaque/transparent skylight panels above, the Grasshopper “Jitter” function was employed to randomly relocate the panels in each row. Second, the Grasshopper “Random” function was used to vary the gap between adjacent panels in a row by inputting a variable range, e.g. +/- 2 inches, and allowing the “Random” function to randomly shift the panels within the specified range. Even after employing both techniques the design team was not satisfied with the aesthetic effect. So, a third and final modification to the script shifted alternating rows by one half of the center-to-center baffle spacing.

Baffle Row Undulation: The final design strategy used to create an organic feeling was to add an undulation to the rail heights for each row, varying the distance between the bottom of the baffle rail and the floor. The undulation is driven parametrically from a vertical curve drawn in Rhino and controlled by the designer (Fig. 18). The height above the floor is increased at both major and minor feature spaces below and lowered in between. Curve-smoothing routines within the script translate the amplitude of the control curve into the final positions for the baffle rails.

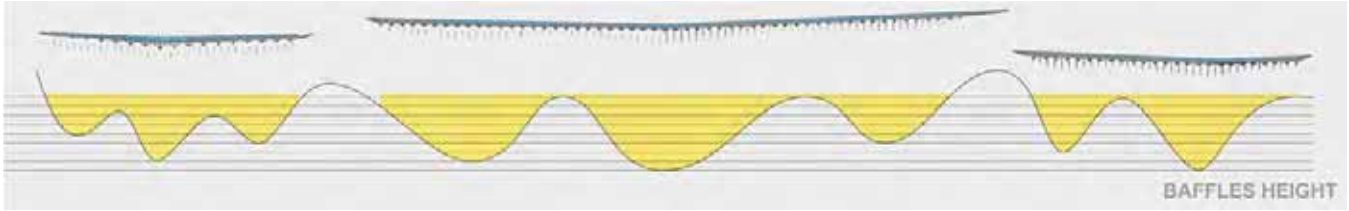


Figure 18: The baffle undulation line controlling the height above the floor to the baffle hanging bar. Image courtesy of Fentress Architects.

Like in nature the resulting forms respond to external forces (in this case the Roof Pattern Line and the Baffle Undulation Line) using predictable rules that result in a rich and unpredictable expression. The resultant organic design recreates the impression of light through a forest canopy interpreting the Client's stated objective to have the architecture reflect *The Orlando Experience*™.

DATA MIGRATION FROM GRASSHOPPER SCRIPTS TO REVIT DOCUMENTATION

Interoperability among design software tools is the holy grail of the design profession. While theoretically embraced by the software development community, it does not really exist. Instead, migration tools need to be specifically developed for each project to permit geometry generated in parametrically-driven design software like Grasshopper to be used in Building Information Modeling documentation software like Revit. For both projects discussed such tools were developed to permit automation in updating the Building Information Model as modifications were made in the design model. Utilizing Grasshopper, component geometric data was "deconstructed" to fundamental point data (x,y,z coordinates) and exported from Rhino to an Excel file with separate data sheets for each type of element to be reconstructed. The Excel spreadsheet data was used by Dynamo to construct comparable geometry in Revit using adaptive component families built in Revit for this purpose (Fig. 19).

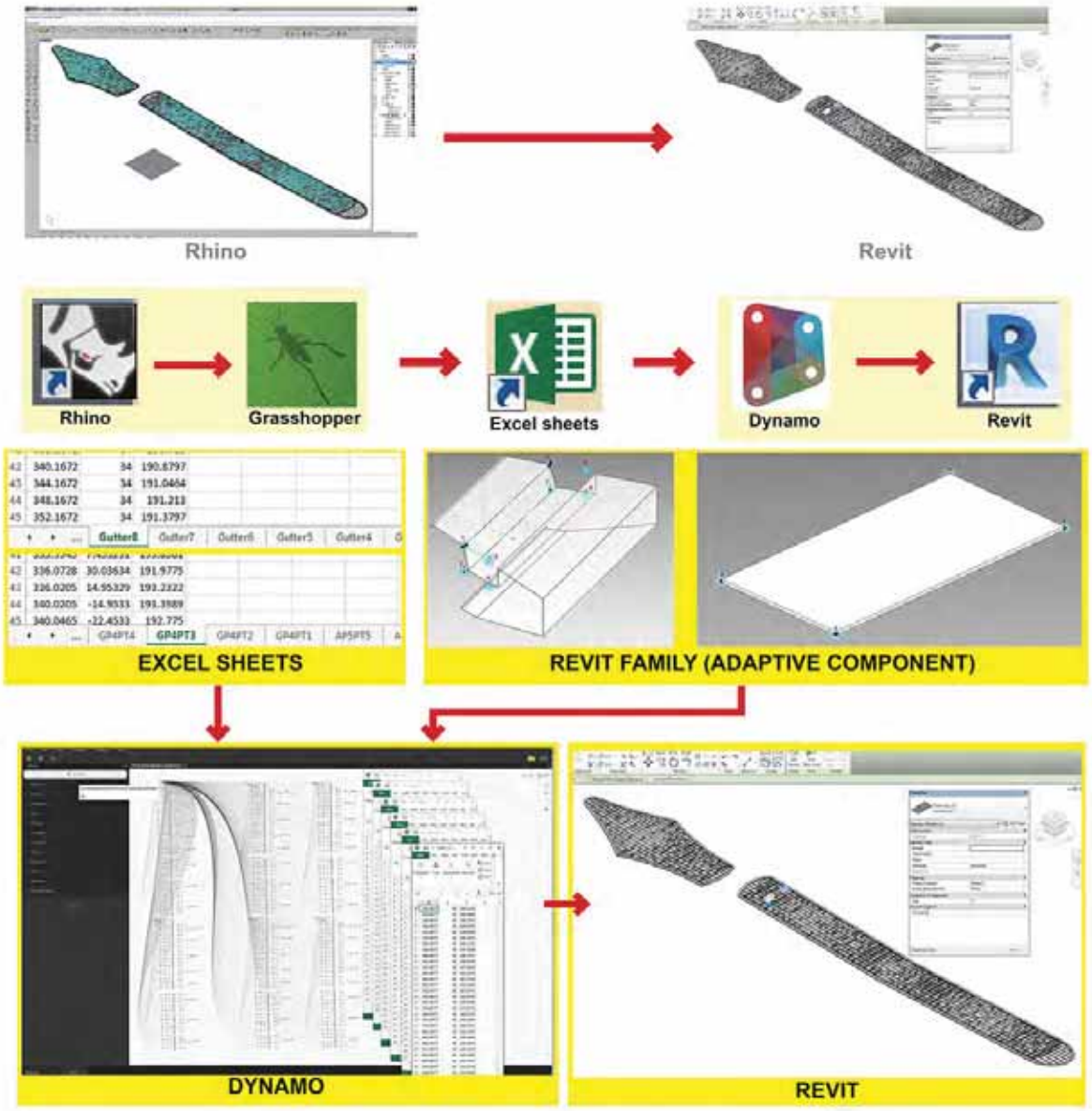


Figure 19: Data migration schematic. Image courtesy of Fentress Architects.

Creating the migration tools described above was a complex process that required iterative development and testing to ensure reliable results; however, once the scripts were written and adaptive components built, the one-way data migration from the design model in Rhino to the production model in Revit was a relatively smooth and efficient process. From a productivity and work-flow perspective it is unfortunate that two concurrent models needed to be maintained. While others in the design profession have reported success in creating proprietary tools to link the two models in a “round trip” manner so a modification to either model is reflected in the other, in the timeframe available we were unable to develop such a seamless tool. We continue to work toward this end and have recently implemented Flux software as a “neutral” data repository that can be accessed by either model and create mirrored geometry in both.

CONCLUSIONS

Parametric design with extensive scripting is usually associated with design and documentation of freeform, curved, non-linear (singly and doubly curved), complex geometrical surfaces. This study shows that the tool is equally valuable and important in developing and enhancing design studies of elements that are predominantly composed of linear and planar elements. Considering the complex interrelationships of the various elements in the two cases described, the number of studies required to arrive at a suitable design would not have been possible using traditional design methodology.

In the case of Portland International Airport Concourse E, a visual framework representing the structure of the forest edge created the underpinning on which the scripting parameters were built. For the Orlando International Airport skylight, the framework was driven by functional nodes in the floor plan below and the desire to vary natural daylight levels to highlight them. Scripts for both projects relied heavily of randomness tools available in the design software to create the design results which were iteratively tested against performative criteria like lighting levels and acoustical absorption. Ultimately, however, the final choice of an appropriate seed list and randomization strength was based on the subjective input and direction of the project’s Lead Designer.

ACKNOWLEDGMENTS

The design team for these projects included Mark Outman, FAIA, Hengchen Liu, Ana Maria Drughi and Ron Shvartsman, without whose assistance this paper would not have been possible.

PERFORMANCE CRITERIA FOR MUSEUM ENCLOSURE DESIGN



Karen Brandt
Heintges
kbrandt@heintges.com

ABSTRACT

This paper develops a framework of considerations for the development of project specific performance criteria for the design of art museums and art-viewing facilities. Three areas of performance are addressed: light control, interior environmental conditions, and condensation resistance. Also discussed are challenges related to integrating these criteria with wider institutional goals such as access to artwork and resources and responsible energy use.

KEYWORDS

museums and art-viewing facilities, performance criteria, curtain wall, condensation, operations, design processes

INTRODUCTION

Within the larger field of custom facade design, building envelopes for museums and art-viewing facilities are a sub-category with unique and complex performance requirements for which a general overview is useful, but may be difficult to find, as the relevant criteria falls across multiple disciplines, including museum conservation, mechanical system design, and building enclosure best practices. This paper will focus on three areas of envelope performance that are particular to new construction for museums and art-viewing facilities or are more stringent than typical, and does not constitute a general summary of all building enclosure performance criteria. The three areas are:

- Natural light control.
- Interior environmental conditions.
- Condensation resistance and mitigation.

NATURAL LIGHT CONTROL

Illumination using full spectrum light, such as daylight, is generally considered the highest quality experience for viewing artwork not only for perception of color, but for the psychological effects and dynamic viewing experience that daylight provides. Nevertheless, direct solar penetration into art-viewing spaces should generally be avoided to avoid photochemical damage to artwork and collections.

There are numerous approaches to controlling natural light in museums and art viewing facilities, but most fall within two general categories: approaches which use of daylight as a primary source of light throughout, and second, approaches which exclusively use artificial lighting in gallery spaces, limiting daylight to other programs where sensitive artwork is not displayed such as lounges, offices, entry and circulation, and cafes.

The first approach typically incorporates a multi-layer system for light control informed by complex solar shading analysis: windows and skylights with innovative building geometry (such as light scoops, monitors, or exterior arrays of shading screens) are designed to block direct solar penetration, a middle layer of diffusing material is used to modulate light levels and reflections, and a third interior layer of shades or curtains is used for glare and blackout control. Systems may also incorporate motorized louvers to block and redirect light levels based on weather conditions, gallery requirements, and changing urban conditions.



Figure 1: An example of a multi-layer clerestory glazing and monitor system at the special exhibitions gallery of the Whitney Museum of American Art.

Shades may either be incorporated within the building enclosure to achieve maximum integration of systems or be part of the interior fit out. When motorized components are positioned within the depth of the façade, power supply and controls may be integrated into framing (mullions and transoms) to conceal wires, necessitating coordination between different trades. Shades and blinds should also be coordinated with perimeter HVAC systems as they may block heat, lowering the interior surface temperature of façade components and reducing condensation resistance performance. Roller shades and stretched ceilings may contain off-gassing components known to be detrimental to human health, and which in some cases may be agents of deterioration for artwork.

The second approach requires less complex solar shading analysis, but is more challenging when visual connection to the exterior is integral to the gallery experience and the building is intended to dynamically interact with the surrounding environment, a current trend in urban museums. Glare between zones may also be an issue. Lack of daylighting in galleries may be perceived to contradict green energy goals, in which use of natural light often plays a prominent role.

The following enclosure design considerations are general good practice:

- Color Rendering Index: glazing design to achieve a color rendering index of 97 or greater in transmission.
- UV Transmission: glazing design to minimize UV transmission.
- Light levels: limit direct penetration of solar radiation and manage light exposure cumulatively.

COLOR RENDERING INDEX: GLAZING DESIGN CONSIDERATIONS

The most familiar metric used to measure the accuracy of color rendition through glazing is Color Rendering Index (CRI), identified as R_a. Glazing products should maintain the full color spectrum of daylight as a neutral illuminant for artwork to the maximum extent possible. The higher the R_a value, the more accurate the transmission of light in the visible spectrum compared to the energy distribution in daylight.

The R_a value was developed by CIE (the International Commission on Illumination) for the evaluation and comparison of lighting products and types of illumination, and has only secondarily been adapted as a metric for glazing products. R_a compares the color of an object under light from a specific source in comparison with a reference light source of comparable color temperature. It is worth noting that the light source is unspecific in the CIE definition, although daylight is often used. R_a as a metric for glazing is different, both in that it is light source specific and because it measures the color shift between a reference object under daylight compared with the same object in daylight transmitted through a particular glazing product. Not all glass suppliers identify R_a in published performance data; however, for many glass compositions, data from LBNL's IGDB (Lawrence Berkeley National Laboratory, International Glass Database) may be used to calculate R_a in transmission in LBNL's Optic software. It is worth noting that R_a measures color fidelity in transmission for incident light perpendicular to the glass surface, and at more oblique angles of incidence R_a will decrease, particularly for coated glass products.



Figure 2: To achieve the highest quality of transmitted light, uncoated low-iron glass is used in insulating glass units facing the MoMA Sculpture Garden.

R_a of 97 or better in transmission is recommended for museums and art-viewing spaces. To achieve R_a 97, use of low-iron glass is generally required and coatings in particular should be evaluated for color neutrality (for comparison, the color rendering index ¼ inch clear float glass alone is about 98, with variation between different glass suppliers). Other glass processes and decorative treatments, such as colored interlayers, ceramic frits, and acid-etching should also be analyzed for their impact on color rendition. Project glass specimens should at minimum be physically tested to confirm spectral transmission at the commencement of project glass production.



Figure 3: Low-iron channel glass was developed for the Nelson-Atkins Museum of Art for optical characteristics and high R_a

ULTRAVIOLET (UV) TRANSMISSION AND PHOTOCHEMICAL DAMAGE

When natural light is used for illumination in galleries and art-viewing spaces, vision and translucent spandrel glazing should be designed to minimize damage by filtering ultraviolet (UV) radiation. Although all wavelengths of light cause irreversible damage, shorter wave UV radiation (typically identified as wavelengths below 380 nm) is more damaging to organic materials due to its higher energy level compared with visible light and long wave radiation. That said, even light in the visible spectrum (approximately 380-720 nm) causes damage despite its lower intensity. All light sources should be evaluated for damage potential relative to luminous intensity and spectral power distribution. A general recommendation for maximum UV exposure from all light sources (sunlight and artificial light) is less than 75 µW/lumen (microwatts/lumen) (*Environmental Conditions*, 2001), with more conservative guidelines for sensitive materials, such as from NARA (National Archives) limiting exposure to no more than 10 µW/lumen (*Technical Guidelines*).

A frequent requirement included in museum facade specifications is to filter solar radiation so that transmission at 400 nm is half or less than that transmitted at 550 nm, and transmission at 320 nm and at 380 nm should be limited to less than 1% of UV light transmitted at 550 nm.

Monolithic glass itself filters most UV below 320 nm. Use of laminated glass further reduces UV radiation and also provides enhanced acoustic performance. Glass laminated with polyvinyl butyral (PVB), the most common interlayer in architectural laminated glass, reduces approximately 99% of UV radiation, although not all PVB products meet the criteria above. Ionoplasts, another category of interlayers, also provide UV protection in typical formulations. During design phases spectral data for all project glass compositions, as well as blind and shade materials should be provided in in 5-10 nm increments to confirm compliance with specifications. Samples of project glazing and shade materials should also be physically tested at the beginning of project glass production to verify performance.

LIGHT LEVELS

For the most damaging wavelengths, filtering daylight through the building enclosure is only one component of a comprehensive strategy to meet conservation goals. Whereas older guidelines focused on absolute levels of illuminance for different media (works on paper 5 foot candles, oil paintings 15-20 fc) (Garry, 1986) and did not take into account time, contemporary guidelines recommend monitoring both exposure intensity and duration, measuring cumulative exposure in foot candle-hours. Both time and energy intensity can be tracked for individual objects, important for artwork situated near glazing where actual exposure may vary from historical averages. Blinds or shades may be programmed to open and close based on exterior light levels and hours of operation, with a threshold established based on gallery type and corresponding interior light level, such as 100 fc. For comparison, light intensity through clear, uncoated glass on a sunny day may reach over 1000 fc and direct sunlight can achieve an intensity of up to 10,000 fc.

On museum and art-viewing institution facades with a mix of complex multi-floor glazing and rainscreen cladding, curtain wall systems (rather than punched windows in metal framed backup wall construction) are often used to meet both performance and architectural requirements. This system type allows for incorporation of a factory fabricated, continuous metal (galvanized steel sheet or aluminum) vapor barrier at the interior, a significant advantage compared with taped metal film in cold climates. Nevertheless, two challenges in particular are worth mentioning for curtain wall systems in museums, where low window-to-wall ratios are typical for daylight control. The first is condensation resistance, the second challenge is energy code compliance.

Despite improvements in thermal performance in building enclosures, exterior wall energy code compliance has become more challenging over time due to increasingly stringent code requirements. In many jurisdictions, as well as in the ICC model energy code, curtain wall is not recognized as a distinct exterior wall type with respect to u-factor—California being a notable exception. Opaque curtain wall systems are, in the absence of a more appropriate category, categorized as metal framed assemblies and accordingly assigned an extremely low prescriptive u-factor target, significantly lower than industry standard performance. Although u-factors below 0.07 Btu/hr-ft2-F can be achieved with curtain wall, advanced system enhancements are needed and should be considered in early system design.

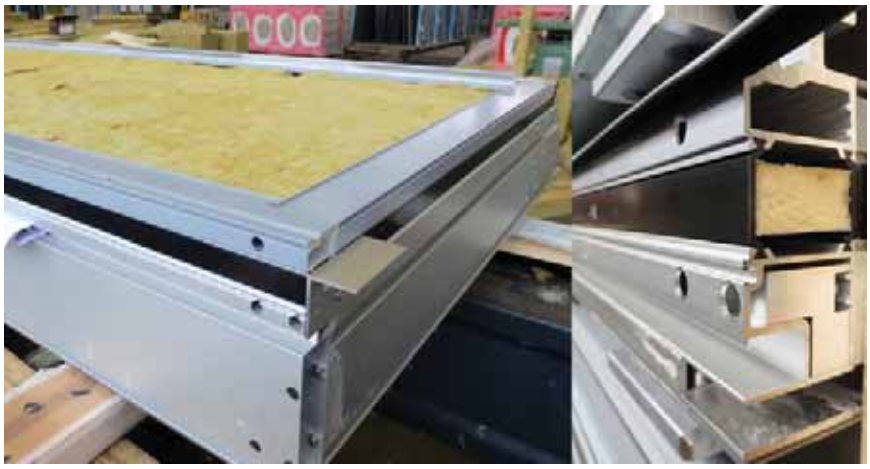


Figure 4: Example of thermal enhancements in a curtain wall system designed to achieve a system u-value below 0.07 Btu/hr-ft2-F. *Note, exterior aluminum sheet not yet installed in photo.*

INTERIOR ENVIRONMENTAL CONDITIONS

Temperature and relative humidity (RH) are the two primary mechanical system considerations for museum and art-viewing facility enclosure design and attention to these criteria are hallmarks of most, if not all, conservation strategies.

HISTORICAL BACKGROUND

Experimentation and early steps toward precise interior environmental control were enacted by a small number of museums and institutions in the first half of the twentieth century, including the introduction of active humidification at the Boston Museum of Fine Arts in the early 1900's. By the late 1930's–early 1940's a general consensus around 60°F and 60% RH as optimal interior environmental conditions had emerged. Implementation of more precise temperature and RH targets by means of active mechanical control increased significantly after WWII, enabled by the growing availability and lower cost of air conditioning and related environmental controls technology. The benefits of a static, low temperature-high relative humidity environment were advocated using the example of artwork moved for protection during WWII. Artwork which had been stored in caves and quarries—extremely controlled environments for temperature and humidity—were observed to have remained in excellent condition during storage, but deteriorated rapidly when returned to museum environments with significant fluctuations in humidity and temperature (J. P. Brown et. al., 1996). It is now generally acknowledged that these early targets were as much derived from tolerances of available mechanical system technology and individual institutions' particular circumstances as from scientific experimentation regarding the physical stability of any particular type of artwork.

Acceptable range for temperature and RH continues to be the subject of considerable debate, but by and large the narrow prescriptive parameters of 70°F ± 2°F and 50% RH ± 5% established in the late 1970's have been revisited in light of scientific research and improved material science (with the notable exception of loan agreements tied to older requirements). Lower ambient temperature and RH targets are now recommended, and 65°F and 45% RH are cited in current ASHRAE guidelines, as is greater latitude in range: ± 4°F and ± 10% RH for short fluctuations, ± 9°F for seasonal adjustment of the temperature set point (2015 ASRHRAE Handbook, 2012). These expanded guidelines are better able to take into consideration an institutions' specific needs, including climate, building stock, and types of artwork. As another example, the current general guidelines for exhibition and storage spaces at the Smithsonian, which encompass a wide range of collections and structures in different climates, are 70°F +/- 3°F and 45% RH +/- 8% RH (*Smithsonian Institution Facilities Design Standards,* 2012).

With this new flexibility, local climate is increasingly able to be taken into consideration, for example, specification of separate warm and cold season setpoints and gradually reduction of RH in extreme cold weather for condensation resistance performance. This shift toward allowing wider, gradual, short-term fluctuations and seasonal setpoints correlated to local climate is aligned with responsible energy use.

AMBIENT TEMPERATURE AND RH TARGETS: ENCLOSURE DESIGN CONSIDERATIONS

Surface temperatures of interior-facing surfaces of the building envelope should be controlled to limit excessive air movement near artwork and collections, such as may be caused by downdrafts from large expanses of poorly performing glazing. Increased air turbulence not only creates fluctuations in RH, but can lead to higher rates of airborne particulates deposited on artwork, an issue for maintenance issue as well as potential chemical damage (William, 1993).

Broadly speaking, most materials are less sensitive to fluctuations in temperature than RH relative to the potential for irreversible damage, although room temperatures which are too low or too high can lead to accelerated rates of microbial deterioration or chemical deterioration, respectively. People are generally the opposite, more sensitive to temperature than relative humidity. Unfortunately ideal temperatures for conservation of most artwork, photographs in particular, are cooler than for human thermal comfort. To encourage museum attendance and access, the ambient air temperature in most museums and art-viewing institutions is maintained for human comfort, whereas RH is established for object conservation. This may drive the absolute moisture content in the air higher than required, increasing the risk of condensation in cold climates (Lukasz).

Relative humidity which is too low can lead to desiccation. RH which is too high can lead to corrosion, mold, or accelerated rates of fading due to light exposure (Stefan, 2007). Rapid fluctuations in temperature and RH may cause stresses due to swelling and thermal movement of materials beyond their elastic limit, and composite objects may delaminate or crack when different adjacent materials expand and contract at different rates (Marion, 2007). Contemporary research indicates that the

majority of damage to objects occurs below 25% RH and above 70% RH, a much wider range than previously thought. This points to rate of change, rather than narrow range, as potentially the more significant factor for conservation (Jonathan, 2004). Allowable variation in RH of ± 20% RH over 4 months, or even 40% ± 10% over 24 hours, are examples of currently proposed approaches to RH set-point and tolerance with significant implications for the design of the building envelope, particularly condensation resistance performance.

CONDENSATION RESISTANCE AND MITIGATION WITHIN THE BUILDING ENVELOPE

In climates with cold seasons, the elevated interior relative humidity specified for museums and most art-viewing facilities makes condensation mitigation more challenging than most other building types. Condensation is a concern due to both direct damage from water and indirect damage from mold or deterioration related to excessive relative humidity. Hidden condensation is often the greatest concern for the building envelope, as it may remain undetected for long periods of time after pervasive damage has occurred. Visible condensation may ultimately be less damaging as it can be identified and addressed swiftly. The design and specification of the building envelope should prohibit condensation on visible and non-visible interior surfaces of the building envelope and require envelope components inboard of the vapor barrier to remain above the dewpoint temperature. Condensation studies should use location specific, extreme environmental conditions as the basis for analysis, such as the ASHRAE 99.6 % heating dry bulb temperature and mean wind speed for regions with cold seasons.

Avoidance of potentially damaging microclimates at the building perimeter should be addressed during early design phases through coordination with perimeter mechanical systems with appropriate zoning. Realistic tolerances for air temperature and relative humidity should be established and maintained. Even with this effort, pockets of heterogeneous temperature adjacent to the facade may be created by factors outside the mechanical system design such as permanent or temporary exhibit walls blocking heat transfer to the perimeter, still air trapped by shading devices, and abrupt fluctuations in temperature from exterior doors (designed without vestibules to maximize connections to adjacent exterior spaces).

The specific ambient temperature range or gradient anticipated at the building perimeter should be used in condensation resistance analysis, not overall interior or gallery averages which may be warmer than at the perimeter. CFD analysis may be required to develop accurate ambient air temperature data during design phases. This is of particular concern for building envelopes with complex geometry, which may not be adequately conditioned using standard mechanical system approaches, and which may be more susceptible to formation of pockets of stagnant air or turbulent air such as in corners with sharp angles or adjacent to sloped facade surfaces. In addition, low velocity displacement ventilation systems, which may be proposed for energy efficiency or aesthetics, should be carefully evaluated for anomalies in temperature stratification at the building perimeter impacting condensation resistance performance.

PASSIVE AND ACTIVE STRATEGIES

Envelope design approaches to mitigate condensation may be divided into two general categories, passive and active. Passive approaches may be defined as those which function without supplemental electrical energy, and include basic detailing recommendations such as maintaining continuity of the vapor barrier, reducing thermal bridges, and adding insulation within the building envelope (even seemingly straightforward thermal enhancements such as increasing insulation in exterior walls can become a complex endeavor in historical buildings, where adding insulation without careful moisture migration analysis can result in loss of stasis and deterioration of enclosure components previously protected by heat loss from the interior, notably masonry). Improved thermal performance can also be achieved through use of composite thermal breaks, triple glazing, as well as highly insulating materials such as nanogel insulation and vacuum panels.

Additional passive tools include separation of high RH spaces away from acute areas of the building envelope, such as exterior doors and operable glazed walls, and use of thermal mass and sorptive materials to buffer abrupt changes in temperature and RH. Increasingly accurate and comprehensive simulation tools are essential tools of passive mitigation approaches. Condensation resistance calculations may be approached through both steady state and dynamic (transient) analysis. Dynamic analysis is more time and resource intensive and generally provides more accurate results, whereas steady state analysis is faster, but more conservative as it does not consider durations of extreme weather conditions or the regulating influence of thermal mass.

Active approaches to condensation mitigation includes seasonal adjustment of building mechanical systems, gradual reduction of the RH setpoint in cold weather, raising blinds and shades to improve heat flow to the building enclosure in

extreme cold conditions (night and limited daylight conditions), positive pressurization of spaces to control the direction of air infiltration, and where absolutely necessary, supplementary dedicated perimeter heating such as finned tube radiation and electric heat trace cabling. It is worth noting that many active approaches have drawbacks including increased capital and maintenance costs, energy consumption, human error, and risk of abrupt changes in temperature and RH in emergencies or system failures when a backup system is not in place. In addition, active, local HVAC supplementation at the perimeter may result in rapid fluctuations in temperature and relative humidity at the point of delivery, such as perimeter overhead diffusers. As an example, when humidified supply air is used to rebalance RH, the supply air may have a relative humidity as high as 85% to have a rapid, appreciable impact on the volume of air in the room. This can create a risk of potential condensation formation in cold weather if devices supplying undiluted humidified air are pointed at, or in close proximity to, building enclosure components engineered for condensation resistance performance at a lower RH.

CONCLUSION

Design of the building envelope for museums and art-viewing facilities requires thoughtful attention of numerous unique considerations and institutional goals. Based on new science and material research, conservation requirements for the building envelope are becoming more nuanced, contributing to more accurate risk assessment related to the design of the building enclosure and allowing for a more flexible range of acceptable temperature and RH criteria. This flexibility can contribute to achieving goals previously assumed to be mutually exclusive, such as use of monumental glazing and use of daylighting in galleries, maximizing public accessibility to artwork, and responsible stewardship of collections. Although flexibility may require additional effort on the part of the project team to develop consensus regarding performance criteria, in comparison to rigid, but clear, older prescriptive guidelines, the effort is valuable as performance criteria tailored to an institution's particular needs can result in facade designs achieving responsible energy use, fulfillment of conservation goals, and architectural excellence in new and innovative ways.

REFERENCES

2015 ASRHRAE Handbook—HVAC Applications and Equipment, Chapter 23: Museums, Galleries, Archives, and Libraries, part 23.3.

Environmental Conditions for Exhibiting Library and Archival Materials, ANSI/NISO Standard Z39.79-2001. 3.5.1 Ultraviolet Light.

Garry Thomson, The Museum Environment. "Light" Part 1 (London, Butterworth-Heinemann, 1986).

J. P. Brown and William B. Rose, "Humidity and Moisture in Historic Buildings: The Origins of Building and Object Conservation," APT Bulletin: The Journal of Preservation Technology, Vol. 27, No. 3, Museums in Historic Buildings (1996).

Jonathan Ashley-Smith, Richard Kerschner, Sarah Staniforth, with James Druzik and Jeffrey Levin, "Sustainable Access: A Discussion About Implementing Preventive Conservation," The Getty Conservation Institute, Newsletter 19.1 (Spring 2004).

Lukasz Bratasz, "Allowable microclimatic variations in museums and historic buildings: reviewing the guidelines," Climate for Collections, Doerner Institute.

Marion Mecklenberg, "Determining the Acceptable Ranges of Relative Humidity And Temperature in Museums and Galleries, Part 1, Structural Response to Relative Humidity," 2007, https://repository.si.edu/handle/10088/7056.

Smithsonian Institution Facilities Design Standards, Smithsonian Institution, Office of Engineering Design and Construction, January 2012, 23.5. (http://www.sifacilities.si.edu/ae_center/pdf/SI%20Standards_Jan2012.pdf).

Stefan Michalski, "The Ideal Climate, Risk Management, the ASHRAE Chapter, Proofed Fluctuations, and Toward a Full Risk Analysis Model," Experts' Roundtable on Sustainable Climate Management Strategies, Tenerife 2007, GCI.

Technical Guidelines, National Archives (https://www.archives.gov/exhibits/borrowing/technical-guidelines.html).

William Nazaroff, *Airborne Particles in Museums*. Research in Conservation 6. Marina del Rey, CA: Getty Conservation Institute, 1993.

Safety <> Structure

BALLISTIC AND BLAST INTEGRATED DESIGN



James Hock, LEED AP BD+C
Permasteelisa North America
j.hock@permasteelisagroup.com



Marc Zobec
Permasteelisa Group
marc.zobec@permasteelisagroup.com



Alberto Franceschet
Permasteelisa North America
a.franceschet@permasteelisagroup.com



Guido Lori
Permasteelisa Group
g.lori@permasteelisagroup.com

ABSTRACT

Increased security needs have led to a demand in enhanced curtain wall façade performance. In addition to thermal, acoustic, and structural requirements, the building envelope has to be designed to dissipate blast loads and protect against ballistics. The purpose is to minimize injuries, loss of lives, and reduce the risk of a global building collapse. These additional security considerations will have further impacts on pricing, design, engineering, testing, and other business functions.

Since ballistic glazing products are already “rated” when purchased from a manufacturer, the facade engineer is responsible for understanding the mechanics of projectile penetration. In terms of resisting projectile penetration, the measure of success is for the product to have a ballistic limit velocity greater than the impact velocity of the projectile. Therefore ballistic design aims to achieve local penetration resistance and as such greatly stiffens the overall glass and other facade components, thus negating the principle of a dissipative system.

On the contrary, to accomplish blast requirements, the designer will increase the façade ductility by accounting for elasto-plastic deformations. This approach considers global dynamic interaction between the major components of the façade. The key elements within a blast façade include, but are not limited to, laminated glass, structural silicone, catenary clips, shear blocks and thoughtfully designed framing members. Therefore a blast enhanced dissipative façade compared to a façade providing ballistic resistance results in somewhat of a design paradox.

This paper will focus on integrated ballistic and blast design, showing the possible shortcomings and design solutions to mitigate them.

KEYWORDS

unitized curtainwall, laminated glass, interlayers, blast, ballistics, security, dissipative

INTRODUCTION

A glass curtainwall serves many functions including structural integrity (wind, dead, snow, seismic, fire, live loads), accommodating building and tolerance movements (slab deflections, sway, shortening, creep) and acting as an environmental filter for solar, moisture, thermal and acoustic transmission. Figure 1 shows a basic schematic of a unitized curtainwall. In its most fundamental form, curtainwall consists of extruded aluminum framing profiles mechanically fixed together with infill elements including glass, metal panels, natural stone, ceramic, etc.

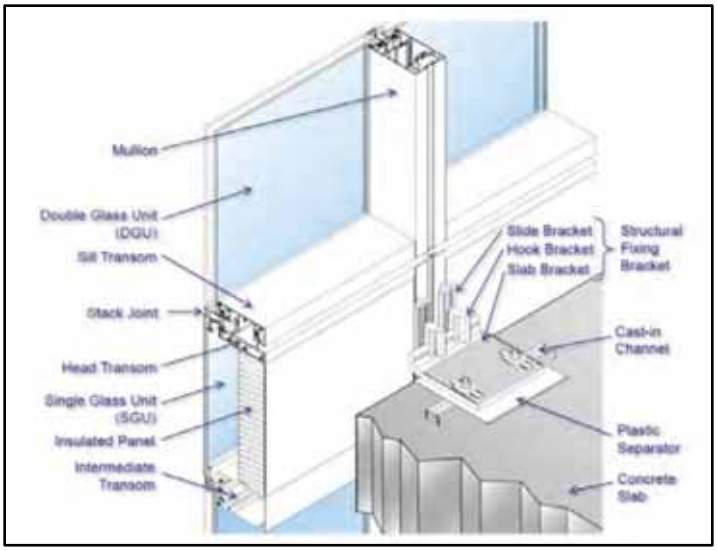


Figure 1: Basic curtainwall schematic.

Throughout the last few years, embassy and federal office buildings have increased the demand for curtain wall security performance. These types of projects usually request simultaneous resistance against blast, ballistic and burglary attacks. The main purpose of blast resistant facades is to minimize injuries and loss of life. This can be satisfied if the facade remains sealed against the external blast overpressure and if the primary building structure and cladding system resists the blast without major collapse. The risk of injuries to the occupants due to flying glass splinters must also be mitigated (Norville et. al., 1999). Usually these objectives are achieved by accepting permanent deformations of the façade elements. Assuming the façade is sacrificial and replaceable after the blast event, results in a more sustainable and economical design (Zobec 2014).

Ballistic performance is often specified in conjunction with blast enhancement. The energy of projectile penetration is a function of the velocity, shape, mass, and material properties of the projectile. The thickness and material properties of the target also affect the ballistic performance. In ductile materials, projectile impact and penetration causes a permanent, localized deformation of the target. When designing ballistic resistant facades, the time, distance, velocity, and varying nature of the inputs make it very complex. The major element of the façade, the glazing, is in general certified by the supplier for ballistic protection through range testing, and the façade engineer must only identify from the project specifications the level of attack and performance required. Ballistic glass usually consists of thick multilayers of HS or FT glass, alternately laminated using stiff interlayer materials such as ionoplast or polycarbonate. The scope is to create a projectile barrier, with hardened layers resistant to the initial penetration toward the outer surface and more flexible internal layers, capable of appreciable deformation and hence minimizing the risk of spall. In order to avoid complete spall, often a spall shield film is attached to the inner surface of the glazing.

It is clear that blast and ballistic performance have opposing design approaches especially in terms of glazing selection criteria. In this way blast design will be governed by the glazing selected to comply with the ballistic protection, and higher glazing stiffness will result in an overall (balanced) stiffer system. The design challenge is to provide adequate ballistic protection without compromising an economically safe and sustainable true balanced blast enhanced solution.

BALLISTIC DESIGN

Two principal standards are used in North America to rate the performance of bullet resisting equipment [13; 2].
At projectile impact, two longitudinal waves (plastic and elastic) are formed in the target. Permanent deformation propagates from the point of impact through a target in a plastic wave. This wave is preceded by an elastic compression wave which propagates in a hemispherical pattern.

The shape of a projectile has a significant effect on its ability to penetrate a target. At low velocities, a projectile may not have sufficient energy to perforate a target. When this happens, the target either experiences partial penetration or the projectile dissipates its energy by displacing the target. With thin targets, displacement coincides with plastic deformation because the target conforms to the shape of the projectile. In the usual case, the projectile will deform. Asymmetrical deformation will alter the path of the projectile as it traverses the target. Low velocity impact and incomplete penetration may cause significant damage because the inherent energy in the collision causes an elastic or plastic displacement of the target. With thick or brittle materials, like glass, stresses can exceed capacity for the target material causing failure on the distal side. Most of the major glazing manufacturers offer products which provide ballistic or forced entry/physical attack resistance to a varying degree as per national and international standards. In glazing, the layers are usually comprised of some combination of tempered or heat strengthened glass, polyvinyl butyral (PVB), thermoplastic urethane (TPU), and sometimes special plastics. The idea is for successive toughened glass layers to shatter on impact, and in doing so, flatten the bullet to reduce its ability to penetrate the layers that follow. The PVB bonds the glass layers together, and absorbs the impact energy. The glazing therefore has to be designed as stiff as possible, including the interlayer.

For frame sections, section properties may be sufficient structurally, but result in effective thicknesses that are insufficient to resist projectile penetration. The two easiest methods to solve this issue are to increase section element thicknesses beyond structural requirements or to add armor in critical areas. The best place to add aluminum is at the face nearest the threat. In curtain wall framing this usually means making the front flanges of the framing elements thicker. Unfortunately, cost considerations, geometry, undesirable weight, and the technical limitations of the extrusion process limit the relative dimensions of a die shape.

BLAST DESIGN

Blast load classes and hazard level specifications are based on performance conditions laid out in the General Services Administration Standard Test Method for Glazing and Window Systems Subject to Dynamic Overpressure Loadings (GSA Security Criteria 1997) and ISO standards (ISO 16933:2007).

An explosion is a very rapid release of chemical energy. After the explosion, the blast overpressure wave travels in the surrounding air in a hemispherical shape. The second phase of the blast is commonly called the shock front. This contains the greatest part of the explosive energy. The velocity of propagation is greater than the speed of sound in air (1500-9000 m/s). One surface impinged by the blast wave experiences a pressure time history like shown in Figure 2. After the first phase of positive pressure, which decays in few milliseconds, a negative phase occurs, due to the over-expansion of the shocked air: in a fixed position of the space any surface experiences the suction blast wind, moving air particles back to the center of the explosion.

The most common approach in achieving blast enhancement is to sufficiently increase the resistance and stiffness of the facade in order to primarily resist the energy transferred by the blast through small, elastic deformations. The alternate, and preferred, approach is to increase the maximum allowable deformations of the system (ductility) by absorbing and dissipating the blast energy transferred through large, elastoplastic deformations (Zobec 2013).

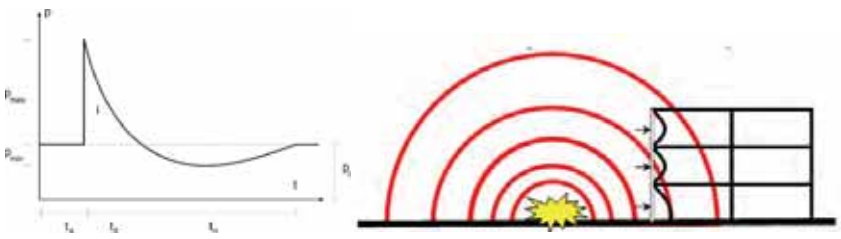


Figure 2: Blast wave impinging a building (right) blast reflected pressure time history and impulse (left).

The first requirement of a blast enhanced façade is the use of laminated glass for the innermost glass leaf. This ensures retention of glass fragments, and allows energy dissipation of the blast wave by means of its' post-breakage behavior shown in Figure 3. Outer laminated glazing can be also considered in order to avoid airborne glass splinter towards the external of the building, limiting the risk of secondary fragment injuries for the people, reducing the risk for the rescue teams just after the blast event and the effort to restore the building activities. The 4 phases of the laminated glass behavior are characterized as: intact phase, one glass layer intact, interlayer elastic phase and interlayer "plastic-like" behavior. Interlayer failure usually occurs as a result of the glass fragments at the frame edge shearing the PVB due to excessive edge rotations. For this reason, no less than 4 PVB layers should be used, with research and testing showing an allowable a maximum displacement of 27.8% of the short span with a 90% confidence level (Morison 2007). In contrast with ballistic design, low flexurally resistant glazing and a tough yet appreciably flexible interlayer should be used. This type of glazing minimizes edge reaction load transfer to the supporting framing members and hence reduces the size of framing components and connections.

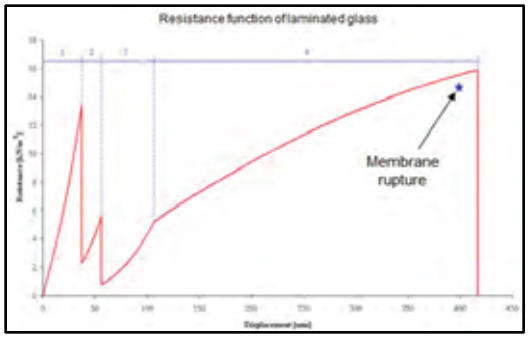


Figure 3: Resistance function for laminated glass (resistance vs. displacement).

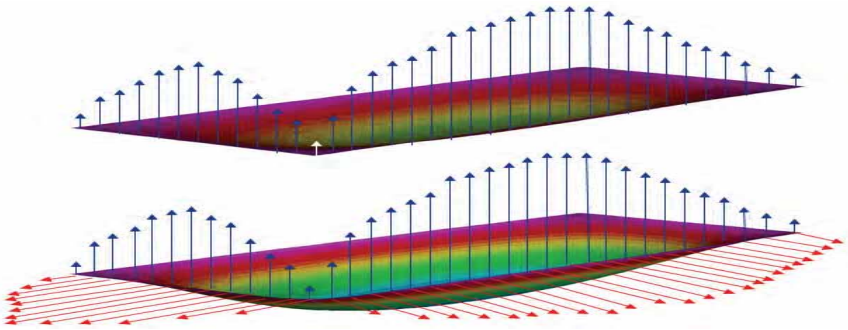


Figure 4: Small deformations (top) large deformations PVB (bottom).

The structural silicone joint (as per the system shown in Figure 1 is the preferable design to transfer the load from the glazing to the frame, as in this way the full glazing capacity is utilized. However, by means of silicone joints, the load transfer will be modified in comparison to mechanically retained glass and by deep rebates, as a force component in the plane of the glazing appears. In Figure 4, the large deformations include out of plane reactions and an additional in-plane reaction components or what are known as splitting forces. For insulated glass units (IGU), the air cavity acts as an adiabatic gas-spring driving load transfer between the external (blast) loaded pane and unloaded internal pane. When the outer glass pane of an IGU is loaded by blast overpressure, it displaces towards the inner glass pane resulting in a volumetric and pressure variations with time in the IGU cavity. The structural silicone must also be capable of transferring blast loads safely from the glass to the supporting members. Tests of structural silicone under high strain rates exhibited tensile sealant strengths with 60% greater resistance than under quasi-static loads, and elongation at break exceeding 350%. In-plane PVB membrane reactions to the structural silicone result in horizontal splitting forces causing the male and female mullions to separate resulting in flexural and torsional instability. As the blast design goal is to effectively dissipate energy, the design includes anti-buckling (catenary) clips, Figure 5, that allows the male/female mullions to rotate prior to fully engaging. This permits further deformations, reducing peak reactions on the structural silicone and PVB interlayer.

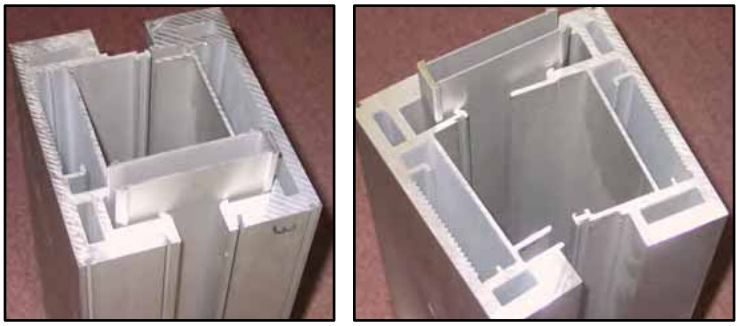


Figure 5: Anti-buckling (catenary) clips.

In order to reduce the load transferred to the main structure of the building, the frame should also be ductile; undergoing plastic deformations in turn resulting in further energy dissipation. In the design of blast resistant façades permanent deformations are allowed (PSDB 2004). Frame sections should be compact; forming stable plastic hinges while minimizing local buckling instability. Due to permanent mullion deformations, effective elastic shorting of the mullion also results in vertical splitting forces that can cause stack joint disengagement, in turn compromising safety and structural stability of the system. Vertical splices maintain panel engagement at the horizontal joint; allow shortening movement, and transfer shear between mullions. Facade brackets are primarily designed to resist wind, self-weight and seismic loads. In order to resist blast loads, they require additional enhancements. The use of dissipative materials within the bracket design allows for greater mobilization of the façade inertial mass. The design results in significant decreases of overall facade reactions transferred to the main structure, lowering glazing stresses, and thus allowing a reduction in the overall glass thickness.

Numerical simulations of the design should be undertaken considering all the major façade components interacting simultaneously in order to take into account relevant dynamic interactions. Multiple Degree of Freedom (MDOF) models are preferable to FEM-FSI models because of their effective representation of the façade behavior (Lori et. al., 2009). However component properties such as post-elastic behavior and high strain rate loading should be accurately assessed. Whilst they may be considered an approximate method, considering uncertainties in loading and material properties, MDOF models provide sufficiently accurate results, whilst FEA calculations usually require excessive calculation times and significant expertise in modeling material behavior such as post-breakage laminated glass response, air cavity resistance, and aero-elastic damping mechanisms (Newmark 1956). Sequential methods are very often the reference method but they should be used with care since, under certain conditions, they underestimate some important constraints resulting in oversized members since the glazing is assumed to have rigidly supported edge conditions as well as neglecting the important contribution of frame deformability. By considering the interactive response of the glazing and frame, a true balanced design can be carried out (Le Gall – Zobec 2016). In contrast to the sequential Single Degree of Freedom (SDOF) approach, an initial true balanced design approach is undertaken by initially analyzing the minimum acceptable glazing required to satisfy wind and live load requirements (Applied Research Associates 2005). If a suitable mullion can be found, which ensures the glazing-mullion system complies with the specified performance, then that glazing is deemed to be structurally adequate. An iterative process is conducted in order to ascertain the most economical combination of glazing and other façade components necessary to satisfy specification requirements.

One important concept that effectively describes blast performance is the Isodamage curve (P-I chart) shown below. Any point on the Pressure-Impulse chart is representative of one possible blast load and can be expressed in terms of explosive mass (TNT) and standoff distance from the target (stand-off). All the possible threats to the left and below the curve denote an undamaged condition whilst threat combinations to the right and above the curve in exceed the defined damage limits. Iso-damage curves are effective ways to represent the performance of facade components for all ranges of possible blast loads.

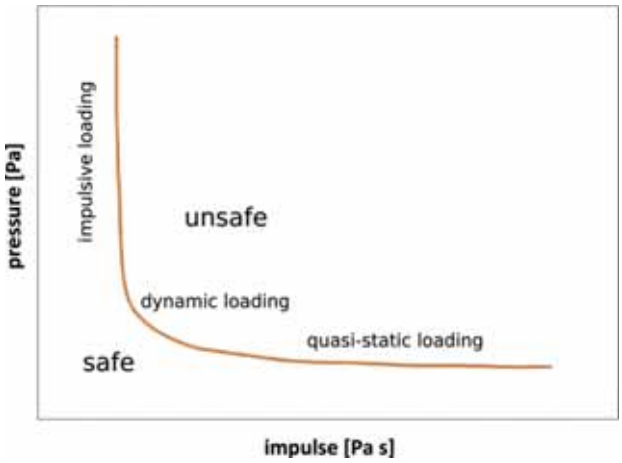


Figure 6: Isodamage curve (P-I Chart).

SHORTCOMINGS OF THE CLASSIC INTEGRATED BALLISTIC/BLAST DESIGN

When façade project specifications contain both ballistic and blast requirements, the starting point of the design is the ballistic glazing. In general the glazing necessary to achieve ballistic requirements will be significantly overdesigned with respect to the minimum glazing necessary to achieve the required blast performance. This means that it will be difficult to maximize the energy absorbing capacity of the glazing. Thus, frequently the glazing selected for ballistic requirements remains intact under the design blast load, coincidentally resulting in the maximum protection level (GSA 1 or ISO A). The most critical scenario for the blast design occurs when glazing breakage under blast design loads is uncertain and within glass strength uncertainties.

Glazing breakage initiates the transition to post-breakage membrane behavior; characterized by large interlayer deformations, resulting in a sudden change in the load transfer mechanism and hence subsequent splitting forces. In particular, unitized systems with structurally sealed glazing, splitting forces can be a serious design constraint. A proper silicone bite must be provided, capable to resist the maximum splitting forces. When a ballistic glazing with SentryGlass® is adopted, minimum bite requirements can reach values of around 2-3 inches!

Figure 7 represents the Isodamage curves calculated for a 5’x13’9’’ façade unit with glazing:

- Outer Glass: 3/8” HS,
- Cavity: ½”,
- Inner Laminated Glass: 3x3/8” HS with 2x0.09” of SentryGlass® interlayer.

The blue curve denotes the initial glass breakage limit, GSA 1 condition, based on a static 750/1000 probability of breakage. It must be considered that this design strength; 15.52ksi for HS glass, corresponds to a lower bound probability of breakage under high strain rate conditions (due to Dynamic Increase Factor effect). In the absence of extensive statistical data, intrinsic calculations indicate that this corresponds to a 2% probability of breakage for HS glass. If a 50% probability of breakage strength is adopted (23.2ksi), the red curve is obtained. This represents the same first breakage Iso-damage curve but occurs for at least 50% of the samples. As an example, designing for a GSA D blast threat, a large majority of the façade the glazing would remain intact even though the calculations based on the design strength denotes that it would break.

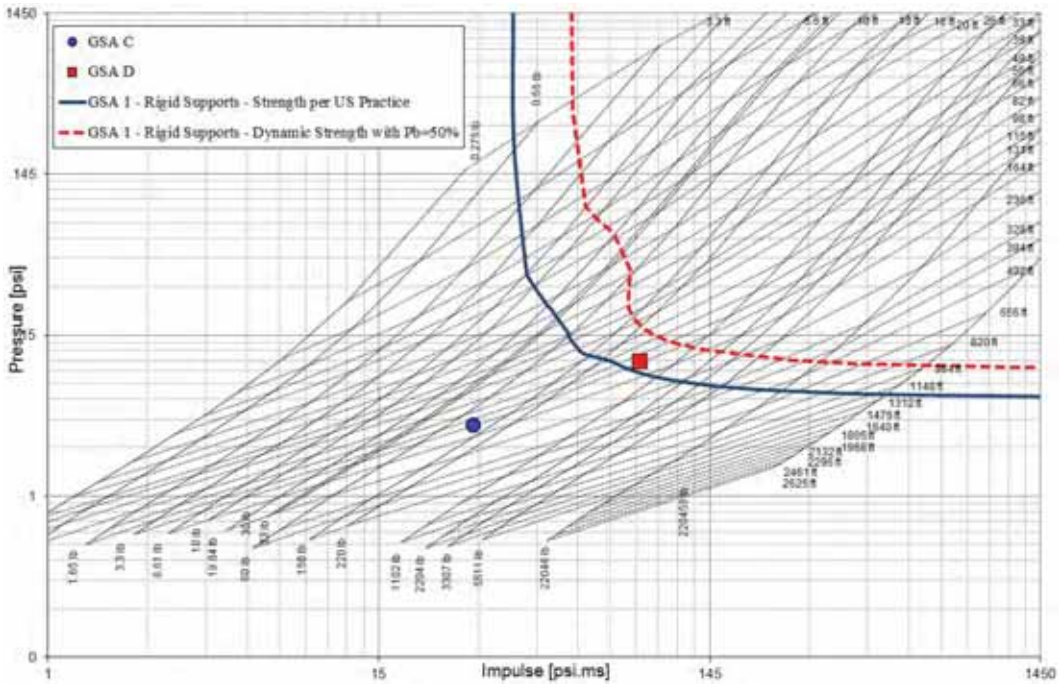


Figure 7: Isodamage curves for glazing first breakage: variation with the glass strength.

If the sequential approach is adopted, in order to design a mullion cross section for the glazing in the previous exercise, a mullion depth of 7.87'' with a cross sectional area of 7.8in2 (male & female), inertia of 53.33in4, an elastic modulus of 12.35in3, and a plastic modulus of 17.82in3 would be required based on a mid-span displacement criteria of H/20 (or 6° of end rotation). However, once the coupled glazing and mullion behavior is analyzed, the red Isodamage curve in Figure 8 is derived. This denotes that under the design load GSA D the glazing would remain intact: the flexibility of the mullion will have a similar effect of increasing the design strength. Note that glazing breakage would occur due to the one-way spanning deformation shape, whilst the stress the glass due to the two-way spanning behavior is significantly lower than the design strength, with the exception of the high impulse region where the behavior will be dominated due to impacts between the outer and inner glass. It is also interesting to note that enhancing the mullion cross section and using a double hollow cross section, with depth still 7.87", cross section area 10.66in2, inertia 73.5in4, elastic modulus 18.67in3 and plastic modulus 24.65in3, the threat with intact glazing will increase, as the one-way spanning breakage mechanism will still dominate. Only by providing a mullion with an elastic modulus an order of magnitude higher, the Isodamage curve will get closer to the ideal curve on rigid supports: the figure shows the curve for a double hollow rectangular section with depth 15.75", cross section area 52in2, inertia 1163in4, elastic modulus 147.7in3 and plastic modulus 213.6in3.

It can be concluded that when thick ballistic glazing is adopted, the rigid support hypothesis is far from the actual coupled glazing-mullion behavior. This can't always be considered a safe design, as several components can be affected due to the incorrect estimation of the final glazing.

Probably the most critical outcome under this perspective is the bracket reaction to outward loading. This output is typically underestimated when glazing is expected to break adopting a sequential approach, however, it doesn't break due to the flexibility of the mullion. This is also amplified by the fact that negative blast phase effects are typically not considered in calculations. For instance, Figure 9 shows the expected peak inward and outward reactions when the glazing and mullion are modelled to behave interactively under GSA D design load. Considering that the application of the sequential method has resulted in an inward reaction of 54,406lbf and an outward reaction of 24,280lb, it can be seen that the inward reaction is adequate even if the sequential method has predicted the glazing to be broken. On the contrary the outward reaction starts to be exceeded for threats lower than the design threat. It can be concluded that under these conditions, applying the sequential method and neglecting the negative blast phase, results in a façade system that would be inadequate to resist significantly lower threats than the actual design threat. This results in a critical lack of robustness for the blast design. Considering maximum capacity loading would give a larger inward reaction, the large plastic inward deformation would likely

not excite significant rebound actions. Only an efficient sensitivity analysis with respect to the design strength, and taking into account the blast loading negative phase, can detect the outward peak reaction.

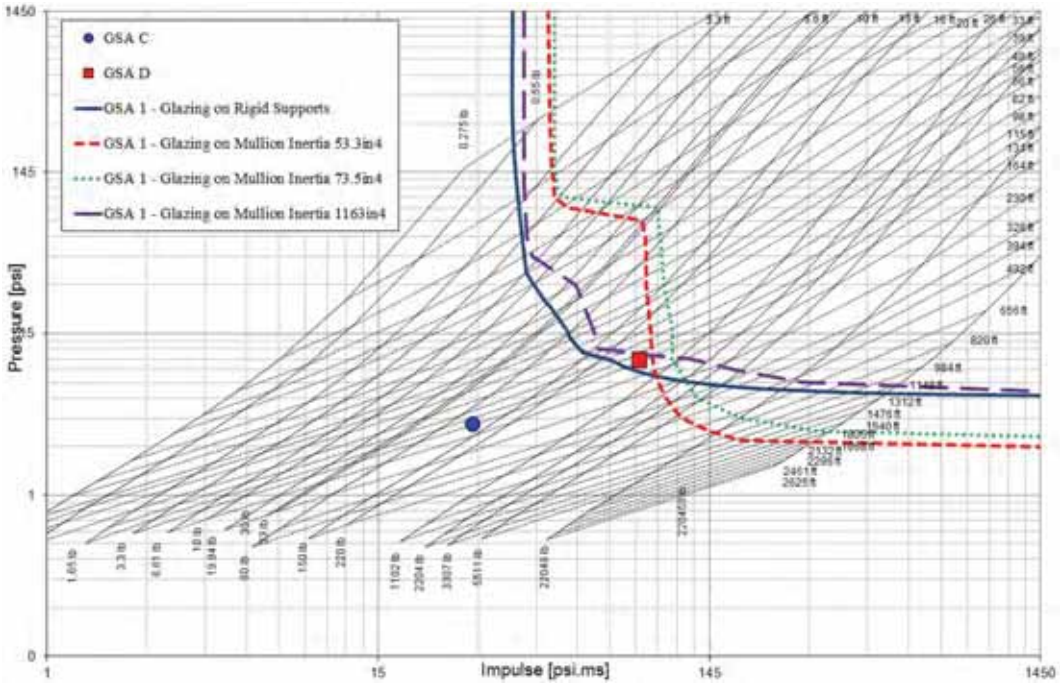


Figure 8: Isodamage curves for glazing first breakage: variation with the mullion deformability.

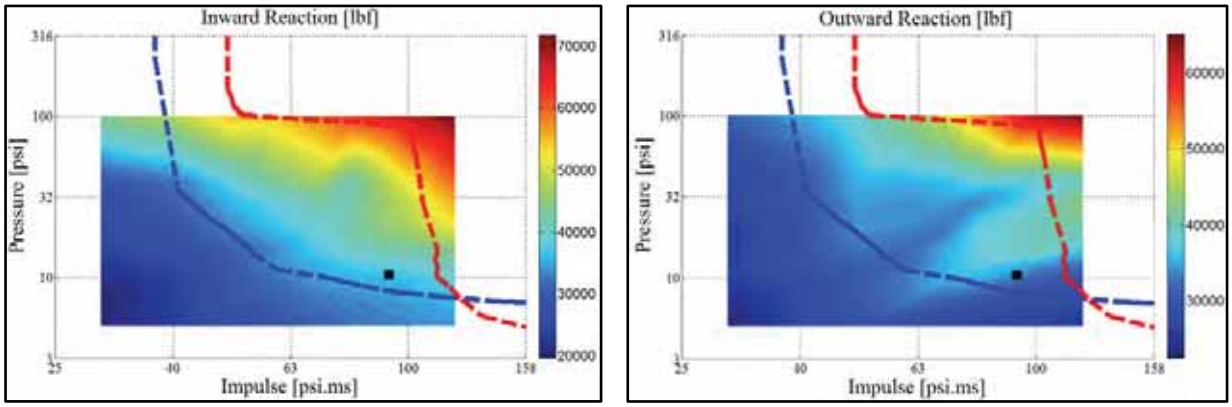


Figure 9: Peak reaction inward and outward for threats in the surroundings of the design threat: lack of robustness for the outward reaction.

Black square represents the GSA D Blast Standard Load.

BENEFITS OF A DISSIPATIVE BRACKET

The integrated ballistic-blast design can be affected due to the relatively large glazing stiffness. One possible solution to overcome this shortcoming is by the use of a dissipative bracket. The dissipative bracket is a deformable support that behaves in a rigid way under the wind design loads, whilst deforming under the blast design load; allowing the full façade mass to translate (Figure 10). The bracket resistance function is represented in Figure 10. Beyond the activation force, the resistance offered by the bracket remains constant within a suitable range of displacement, while the ensuing hardening zone governs a second rigid behavior at the end of the dissipative region.

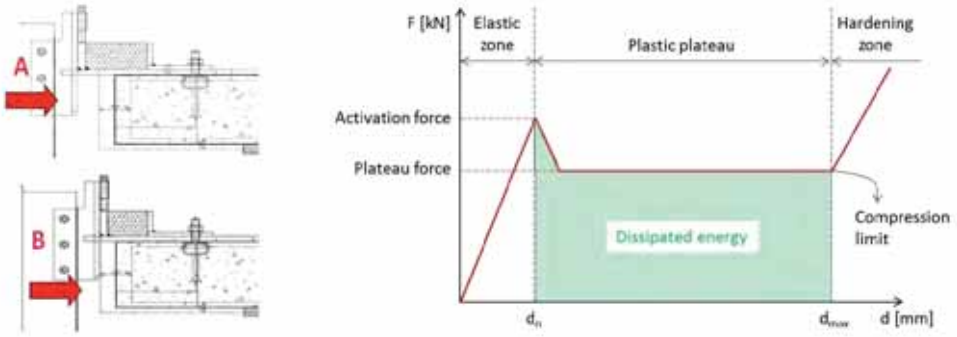


Figure 10: Dissipative bracket mechanism (left), typical resistance function (right).

The dissipative behavior should be applied for both inward and outward loading directions. The target resistance function is achieved by means of adopting crash absorbing materials and the components can be assembled in series or parallel. Resistance to wind loading is achieved by adopting rigid pins calibrated to shear at a prescribed activation force. A small drop of force is noted to occur between the activation force (failure of the pin) and the plateau sum of the dissipative component reactions. The target bracket behavior should be verified and calibrated by means of a quasi-static or high speed loading test when dynamic effects have been assumed for the assembly of the resistance functions. The testing results for one sample under inward loading are shown in Figure 11. The graph includes the velocity time history (target velocity 6.7ft/s), deformation range (2.4'') and the plateau resistance (around 20,000lbf).

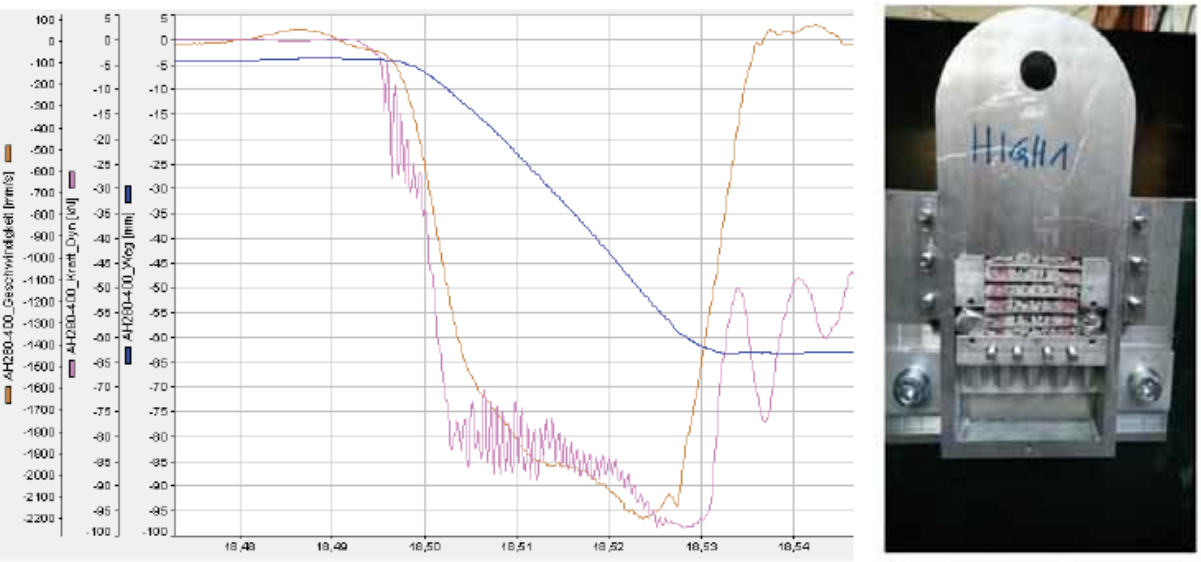


Figure 11: Dissipative bracket experimental test results (velocity, deformation, and reaction vs. time).

The benefits are:

- The load transfer to the building can be mitigated for both inward and outward directions, reducing the peak value of the rigid reactions by about 30-40%.
- Stresses on the façade components are reduced compared with using the rigid bracket. As the dissipative bracket is activated, inertial forces of the overall façade mass are the major force to counter-balance the blast wave loading.

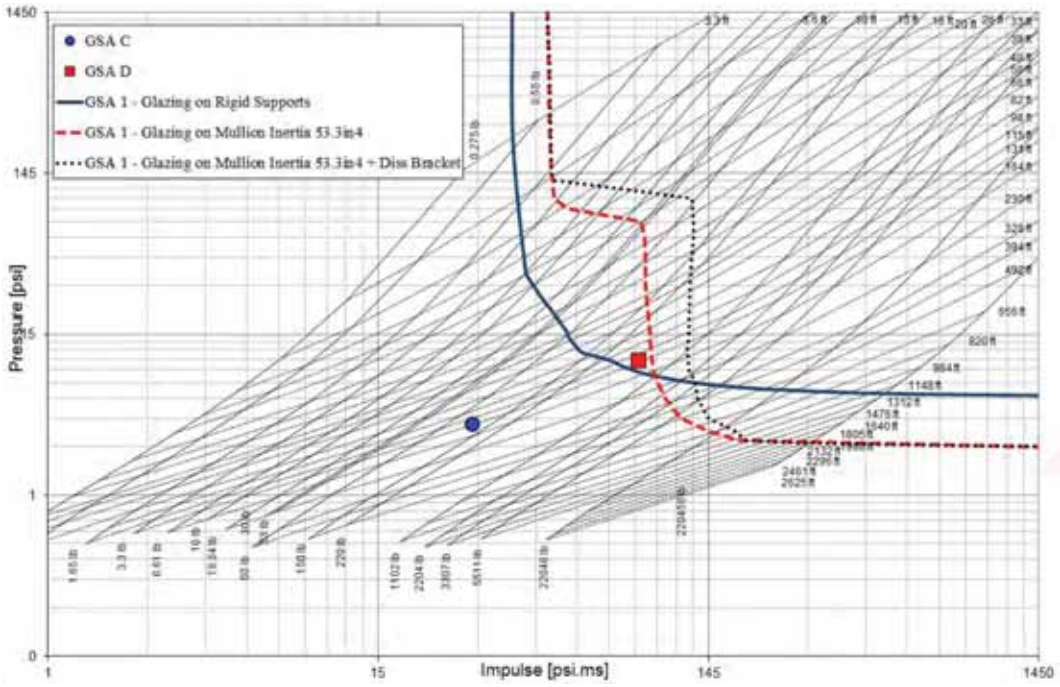


Figure 12: Isodamage curves for glazing first breakage when dissipative bracket is adopted.

When a dissipative bracket with plateau in both inward and outward direction of 20000lbf is integrated in the system discussed above, the first break Iso-damage curve shifts toward the black curve shown in Figure 12. A threat area is still gained with respect to the red curve. This gain results in a decisive step ensuring that the glazing remains intact. This, in turn, relaxes the need for a large silicone bite. At the same time the bracket would limit the peak outward reaction avoiding the issue previously described. Further optimization could be then conducted on the mullion design, as the bracket would also reduce mullion deflection and allow for a reduction of the cross sectional properties. This process could be iterated, aiming for a dissipative bracket with lower plateau, and thus a less stiff glazing-mullion system. The final outcome would be a system with economical framing members and improved overall safety under blast loads.

CONCLUSION AND FUTURE WORK

- Blast and ballistics overall design approaches are generally in contrast with one another.
- A true balanced design is required taking into account each individual component and their interaction
- Extensive testing is necessary in order to understand actual performance
- Blast energy dissipation may be effectively achieved by the use of a dissipative bracket thus enabling the use of thicker glazing that satisfies ballistic projectile resistance.
- Although, component sizes may be enhanced to satisfy resistance to projectile penetration, dissipative brackets will in any event effectively reduce façade reactions to the main structure.
- A dissipative bracket will effectively dissipate energy by mobilizing the full façade mass and hence inertia.
- The use of a dissipative bracket can offset the need for further blast design enhancements. This would reduce costs without compromising security

ACKNOWLEDGMENTS

A special thanks to the entire Permasteelisa Group team.

REFERENCES

Applied Research Associates Inc. *Window glazing analysis response & design – WINGARD – Technical manual*, ARA-TR-05-16462-2, US General Services Administration, Washington DC, July 2005.

BS EN 1063 2000, *Glass in Building. Security Glazing. Testing and Classifications of Resistance Against Bullet Attack*

Charles N. Kingery and Gerald Bulmash. *Airblast parameters from TNT spherical air burst and hemispherical surface burst.* Technical report, Defence Technical Information Center, Ballistic Research Laboratory, Aberdeen Proving Ground, Maryland, 1984.

GSA Security Criteria, Building Technologies Division Office of Property Development Public Building Service Administration,

1997.
ISO 16933:2007, Glass in Building - Explosion Resistant Security Glazing. Test And Classification For Arena Air-Blast Loading.
Le Gall – Zobec, A. *Balanced Design of Blast Enhanced Glass Curtain Wall Facades*. June 2016.
Lori G., Zobec M., Franceschet A., Manara G., "The behavior of facades due to blast loads – A single degree of freedom performance evaluation approach", Glass Processing Days, 2009.
Morison, C., Zobec, M., Franceschet, A.: "The measurement of PVB properties at high strain rates and their application in the design of laminated glass under bomb blast", International Symposium on the Interaction of the Effects of munitions with structures, 2007.
Newmark N M. "An engineering approach to blast resistant design", American Society of Civil Engineers Transactions, Paper No 2786, Vol 121 p45, 1956. (Noted as published "essentially as printed here" as proceedings –Separate No 506, October 1953.)
Norville, H.S., Harville, N., Conrath, E.J., Shariat, S., and Mallone, S.: "Glass-Related Injuries in Oklahoma City Bombing", Journal of Performance of Constructed Facilities 13(2), 1999.
PSDB *Notes on Design for Glazing Protection*, Current UK Design Philosophy. Home Office, Police Scientific Development Branch, 2004.
DoD, UFC 3-340-02 Structures to resist the effects of accidental explosions, US Army Corps of Engineers/Naval Facilities Engineering Command/ Air Force Civil Engineer Support Agency, 2014.
UL 752 Underwriters Laboratories, Inc. Standard for Safety, *Bullet-Resisting Equipment and the U.S. Department of Justice Standard for Ballistic Resistant Protective Materials* (NIJ Standard 0108.01).
Zobec, M. "Blast Enhanced Glass Facades: an integrated and holistic design approach", PhD Thesis at University of Technology, Sydney, 2013.
Zobec, M., Lori, G., Lumantarna, R., Ngo, T., Nguyen, C. (2014) "Innovative design tool for optimization of blast enhanced facades", Journal for Façade Design & Engineering.

BLAST PERFORMANCE OF TSSA

Testing of point fixed assemblies



Jon H. Kimberlain
Dow Chemical Company
jon.kimberlain@dowcorning.com



Lawrence D. Carbary
Dow Chemical Company
l.carbary@dowcorning.com

ABSTRACT

Architectural preferences for commercial building continue towards increased transparency resulting in large lites of glass with minimal visual obstruction. Point fixed glazing systems meeting this architectural desire are popular especially in entry or common areas at ground level. Recent technology advances have allowed the use of super high strength adhesives to attach these large lites to fittings without the requirement of drilling through glass.

The typical ground floor location increases the probability that the system must function as a protective layer for occupants of the building above and beyond the typical code required exposures such as wind loading. Some blast performance testing has been published on drilled point fixing systems but not on the adhesive method.

The purpose of this paper is to document mock-up testing using a shock tube with an explosive charge to simulate blast loads onto adhesively bonding transparent assemblies. The variables include pre-defined blast loads from ASTM F2912-17 performed on lites laminated with SGP ionomer interlayer.

The study, a first of its kind, enables the ability to quantify potential blast performance for use in large scale testing and building design. Four 2.36” diameter TSSA fittings were attached to lites 60” x 60”. Four assemblies loaded to 7 psi or less showed no breakage or effect on TSSA and glazing. Five assemblies were loaded above 9 psi, and four of the five showed glass breakage resulting in glazing displaced from the opening. In all cases, TSSA remained attached to the metal fittings and no failure, adhesive or cohesive, was noted. The testing shows that this tested TSSA design is capable of an effective safe system, according to AAMA 510-14, at loads of 7 psi or less. The data generated here can be used for engineering the system of TSSA to meet specified loads.

KEYWORDS

innovative or unique, blast performance, physical testing – mockups, resilience, component performance, adhesives, means and methods

INTRODUCTION

Structural silicone attachment of glass panels has been used for nearly 50 years to enhance the aesthetics and performance of modern architecture (Hilliard, 1977; Zarghamee, 1996, Carbary 2007, Schmidt, 1989, et. al). The attachment method allow smooth uninterrupted facades with a great deal of transparency. Architectural desires for increased transparency has resulted in the development and use of cable net walls and bolted point supported facades. Architecturally challenging iconic buildings will include the modern technology of the day and must meet the local codes and standards for construction and safety.

Transparent Structural Silicone Adhesive (TSSA) was studied and presented as an alternative to drilled bolted fittings to support glass (Wolf, 2011; Clift, 2011, et. al.). The crystal clear adhesive technology with strength, adhesion and durability has a set of physical properties that allow façade designers to engineer attachment systems in unique and novel ways. Circular, rectangular, and triangular fittings to meet aesthetics and structural performance are easily engineered. TSSA is cured in an autoclave alongside of laminated glass being processed. When the material is removed from the autoclave cycle, 100% proof testing can be completed. This quality assurance benefit is unique to TSSA as it provides immediate feedback on the structural integrity of the assembled pieces.

Conventional Structural Silicone materials have been studied for impact resistance and blast mitigation (Clift, 2015 and Yarosh 2010). Wolf et al provided data generated at the university of Stuttgart that showed increased tensile and elongation of structural silicone materials under extreme strain rates of 197in/s when compared to the quasi-static strain rates specified in ASTM C1135-17 to indicate a strain dependent relationship on physical properties. As TSSA is a highly elastic material, with higher modulus and strength compared to structural silicone, it is expected to follow the same general behavior. Although lab testing at high strain rates was not conducted, it was expected that the high strain rates in a blast would not affect the strength.

Bolted glass connections have been tested to blast mitigation standards (Morgan, 2013) and presented at Glass Performance Days in 2013. The visual results clearly showed the advantage of mechanical retention of the glazing after glass breakage. This will be a challenge for a purely adhesively attached system.

TEST SPECIMENS: FABRICATION AND QUALITY ASSURANCE

Frames were fabricated from American Standard Steel Channels of dimension 6” x 1.92” x 0.20” web thickness commonly referred to as a C 6” x 8.2# channel. The C Channels were welded together at the corners and a 0.375” thick triangular section was welded in the corners, set back from the face of the frame. An 0.71” hole was drilled in the plate so that a 0.55” diameter bolt could be easily inserted into it.

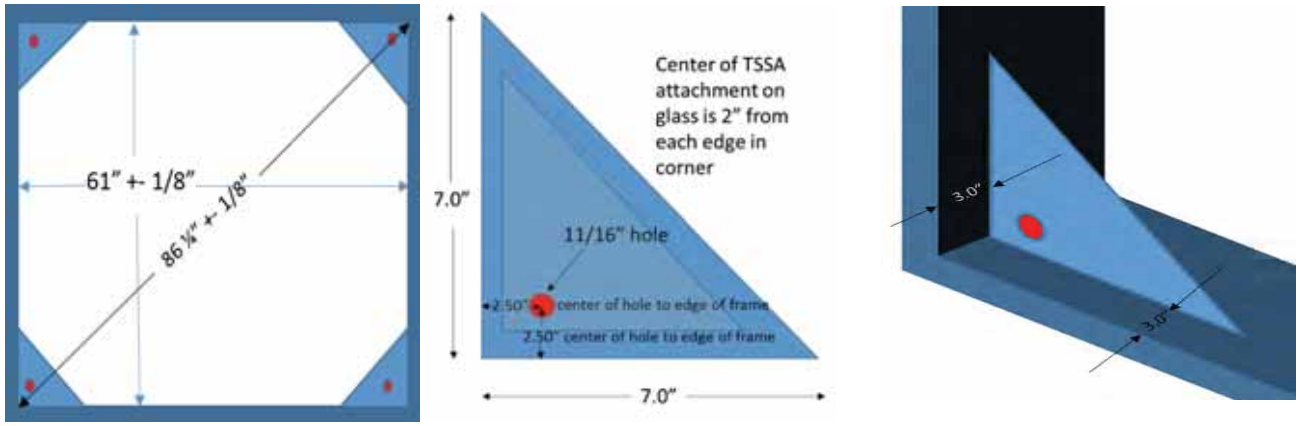


Figure 1A-C: Steel frame elevation and dimensions.



Figure 2: Glass with TSSA attachment set into frame. Exterior face shown with fittings attached to the interior side of glass.

The 2.36” diameter TSSA metal fittings were placed 2” from each corner. Four fittings were applied to each piece of glass to make everything symmetrical. A unique feature of TSSA is the fixture can be placed close to the edge of glass. Drilled fittings into glass for mechanical retention have specific dimensions from the edge that have to be incorporated into the design and the holes must be drilled before tempering.

The glass chosen for the project was two layers of 1/4” tempered clear 5’ x 5’ laminated with Sentry Glass Plus (SGP) ionomer interlayer 0.060”.

TSSA discs 0.040” thick were applied to a primed stainless steel fittings 2.36” in diameter. The primer is designed to enhance the adhesion durability to stainless steel and is a combination of silane and titanate in solvent. The metal discs were pressed onto the glass with a measured force of 100 psi for one minute to provide wetout and contact.

The assembly was put into an autoclave that reached 175 psi and 272°F so that the TSSA would achieve a 30 minute soak time in the autoclave required for cure and adhesion.

After the autoclave was finished and cooled, each TSSA fitting was inspected, and then torqued to 40.6 ft-lb to demonstrate a proof load of 190 psi.

The fittings used for the TSSA were supplied by Sadev and identified as R1006 TSSA fittings. Fittings for TSSA are comprised of a ball and socket swivel connection to allow nominal rotation under windload to mitigate cantilever forces on the adhesive connection.

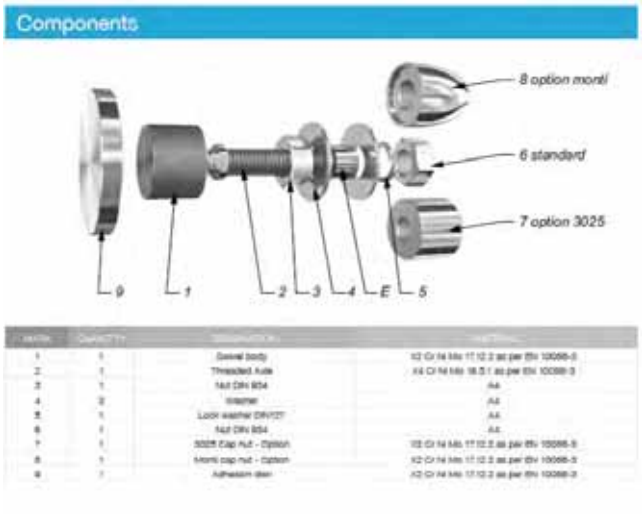


Figure 3: Exploded details of R1006 TSSA fitting by Sadev.

The body of the fittings were assembled onto the cured pucks on the glass and the assembly was lowered into the steel frame. The nuts on the bolts were adjusted and secured so that the exterior glazing was flush with the exterior of the steel frame. The ½" x ½" joint about the perimeter of the glass was sealed with two part structural silicone so that testing to pressure loading could commence the next day.

Testing was conducted utilizing a shock tube at the University of Kentucky Explosives Research Laboratory. The shock tube consists of a reinforced steel body with capability to install up to 12' by 12' glazing units on the face. The shock tube is driven by the use of explosives placed along the length the tube to simulate both the positive and negative phase of a blast event (Wedding, 2012). The entire glass and steel frame assembly were placed into the shock tube for testing as shown in Figure 4.



Figure 4: Frame and glazing installed into the shock tube.

Four pressure sensors were mounted inside the shock tube so that the pressure and impulse could be accurately measured. Two digital video camcorders and a digital SLR camera were used to document the test. A MREL Ranger HR high speed camera located adjacent to the window outside the shock tube captured the test at 500 frames per second. A deflection laser recording at 20 kHz was set adjacent to the window to measure deflection at the center of the window.

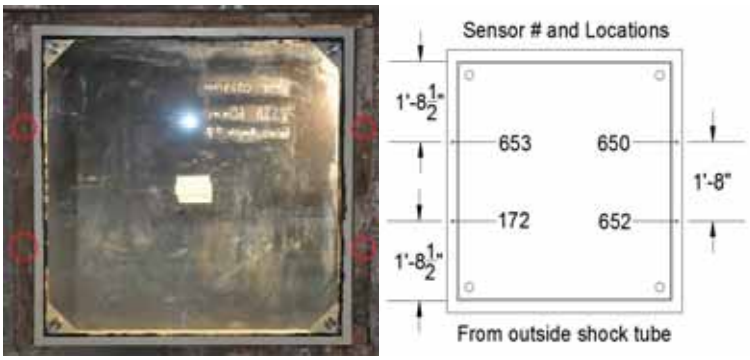


Figure 5A-B: Pressure sensors location inside the shock tube.

Four frame assemblies were tested a total of nine times. If the glass did not leave the opening, the assembly was retested at a higher pressure and impulse. The target pressure and impulse is recorded along with the glass deflection data in each case. Each test was then also given a rating based on the Voluntary Guide Specifications for Blast Hazard Mitigation for Fenestration Systems, AAMA 510-14.

RESULTS AND DISCUSSION

As mentioned above four frame assemblies were tested till the glass was removed from the opening from the blast.

The first test was targeted to reach 10 psi A 89 psi-msec impulse. Under the applied load, the glazing shattered and released from the frame. Deflection at the center of glass was greatest during the loading event with the appearance of stiffening within the glass plane due to less deflection at the connection point of the fittings. The shattering pattern was consistent of tempered glass during observation with rapid development of small shards during the fracturing process. The Sadev point fittings had TSSA adhered to the broken tempered glass. The glass shards in the adhesive layer were from the exterior glass connection. No exposure or damage was present to the underlying laminate or adhesive. No damage or deformation was observed within the hardware of the fitting which also carried through each subsequent test.

The glazing left the opening after it had roughly 4” of deflection as the tempered glass shattered.

Frame #1					
Test #1					
	Pressure (psi)	**Impulse (psi-ms)**	**Deflection**	**AAMA 501-14 Ratings**	
1	9.289	75.824		ISC Performance	**5**
2	10.070	84.527		ISC Protection	**Low**
3	10.723	78.527		ISC Hazard	**High**
4	11.559	79.355		UFC Protection	**Below AT Standards**
AVE	**10.41**	**79.355**	**-4”**	ASTM F 1642	**High Hazard (N/A)**
Target	10	89	**glass fail**		

Table 1: Frame 1 results.



Figure 6: Glass breakage at ~4" of deflection, Frame 1, Test1.



Figure 7: Glass shards adhered to the TSSA and weatherseal.

Frame 2 was tested three times with increased consecutive loading. The results showed no failures till the pressure approached 10 psi. Measured pressures of 6.42 psi and 6.59 psi did not affect the integrity of the assembly. At the measured pressure of 9 psi the deflection of the glass caused breakage and the glazing left the opening. All TSSA fittings had broken tempered glass attached to the adhesive layer as identical to Figure 7.

Frame #2					
Test #2					
	Pressure (psi)	**Impulse (psi-ms)**	**Deflection**	**AAMA 501-14 Ratings**	
1	5.956	21.240		ISC Performance	**1**
2	6.525	28.173		ISC Protection	**Safe**
3	6.431	22.458		ISC Hazard	**None**
4	6.764	22.174		UFC Protection	**High**
AVE	**6.419**	**23.511**	**-2" + 1"**	ASTM F 1642	**No Break (H1)**
Target	4	28	**glass intact**		
Frame #2					
Test #3					
	Pressure (psi)	**Impulse (psi-ms)**	**Deflection**	**AAMA 501-14 Ratings**	
1	6.082	38.408		ISC Performance	**1**
2	6.586	45.878		ISC Protection	**Safe**
3	6.624	42.983		ISC Hazard	**None**
4	7.082	40.087		UFC Protection	**High**
AVE	**6.593**	**41.839**	**-2.2" + 0.8"**	ASTM F 1642	**No Break (H1)**
Target	6	42	**glass intact**		
Frame #2					
Test #4					
	Pressure (psi)	**Impulse (psi-ms)**	**Deflection**	**AAMA 501-14 Ratings**	
1	8.265	72.881		ISC Performance	**5**
2	8.530	74.882		ISC Protection	**Low**
3	9.386	80.961		ISC Hazard	**High**
4	9.948	74.201		UFC Protection	**Below AT Standards**
AVE	**9.032**	**75.731**	**-4"**	ASTM F 1642	**High Hazard (N/A)**
Target	10	89	**glass fail**		

Table 2: Results of Frame 2 - tests 2, 3 and 4.

Frame 3 was tested two times with increased consecutive loading. The results showed no failure till the pressure approached the targeted 10 psi. Measured pressures of 7.03 psi did not affect the integrity of the assembly. A data acquisition failure did not allow deflection to be taken, however visual observations from video suggest that that Frame 2 test #3 and Frame 4 Test #7 are similar in deflection. At the measured pressure of 9.28 psi the deflection of the glass measured at 7.5" caused breakage and the glazing left the opening. All TSSA fittings had broken tempered glass attached to the adhesive layer as identical to Figure 7.

Frame #3					
Test #5					
	Pressure (psi)	**Impulse (psi-ms)**	**Deflection**	**AAMA 501-14 Ratings**	
1	6.196	39.838		ISC Performance	**1**
2	6.703	43.912		ISC Protection	**Safe**
3	7.111	41.954		ISC Hazard	**None**
4	8.099	40.813		UFC Protection	**High**
AVE	**7.027**	**41.539**	**NO Data**	ASTM F 1642	**No Break (H1)**
Target	6	42	**glass intact**		

Frame #3					
Test #6					
	Pressure (psi)	**Impulse (psi-ms)**	**Deflection**	**AAMA 501-14 Ratings**	
1	8.265	79.063		ISC Performance	**5**
2	8.692	78.275		ISC Protection	**Low**
3	9.539	80.141		ISC Hazard	**High**
4	10.625	79.391		UFC Protection	**Below AT Standards**
AVE	**9.280**	**79.218**	**-7.5”**	ASTM F 1642	**High Hazard (N/A)**
Target	10	89	**glass fail**		

Table 3: Results of Frame 3 - tests 5 and 6.

Frame 4 was tested three times with increased consecutive loading. The results showed no failure till the pressure approached the targeted 10 psi the second time. Measured pressures of 6.79 and 9.42 psi did not affect the integrity of the assembly. The glass was measured to deflect 4” during test #8. It was anticipated that this loading would cause the glass to break, however an additional data point was able to be taken. During test #9, the measured pressure of 9.56 psi deflected the glass 7.5” and caused breakage and the glazing left the opening. All TSSA fittings had broken tempered glass attached to the adhesive layer as identical to Figure 7. The fittings were easily removed from the steel frame without any apparent damage in all test cases.

Frame #4					
Test #7					
	Pressure (psi)	**Impulse (psi-ms)**	**Deflection**	**AAMA 501-14 Ratings**	
1	6.381	39.1		ISC Performance	**1**
2	6.787	38.175		ISC Protection	**Safe**
3	6.924	40.645		ISC Hazard	**None**
4	7.423	39.463		UFC Protection	**High**
AVE	**6.879**	**39.346**	**-3" + 1.5"**	ASTM F 1642	**No Break (H1)**
Target	6	42	**glass intact**		

Frame #4					
Test #8					
	Pressure (psi)	**Impulse (psi-ms)**	**Deflection**	**AAMA 501-14 Ratings**	
1	8.481	79.567		ISC Performance	**1**
2	8.747	72.137		ISC Protection	**Safe**
3	9.345	78.396		ISC Hazard	**None**
4	11.116	82.147		UFC Protection	**High**
AVE	**9.422**	**78.062**	**-4" + 1.5"**	ASTM F 1642	**No Break (H1)**
Target	10	89	**glass intact**		

Frame #4					
Test #9					
	Pressure (psi)	**Impulse (psi-ms)**	**Deflection**	**AAMA 501-14 Ratings**	
1	8.708	80.219		ISC Performance	**5**
2	9.066	76.767		ISC Protection	**Low**
3	9.937	81.742		ISC Hazard	**High**
4	10.520	80.265		UFC Protection	**Below AT Standards**
AVE	**9.558**	**79.748**	**-7.5"**	ASTM F 1642	**High Hazard (N/A)**
Target	10	89	**glass fail**		

Table 4: Results of Frame #4.

The TSSA remained intact for each loading test indicated by no damage to the layer or hardware even under glass failure. When the glass remained intact, the there was no visual change in the TSSA after the testing concluded. The High speed video showed the glass breaking at the mid points of the span, and then leaving the opening.



Figure 8A-C: Glass Failure at test 4, 6, and 9.



Figure 9: Glass at max deflection at test 8.

From the figures 8 and 9 comparing glass failure to none, it is interesting to note that the pattern of fracture in the glass occurs in sections away from the adhesive point of attachment indicating that the unbound sections of glass is reaching a bending point that has rapidly approached the embrittlement yield point in the glass versus the sections that are held adhesively. This suggests that the broken plate in these sections is likely moving mostly in shear during the testing as the adhesive connection to the fitting constrained outward deflection versus observed in the center of glass. In combination with this principle and the observation that the failure mode appears to be embrittlement in the glass thickness at the interface of the adhesive, the control of the deflection by increased glass thickness or other means should improve the performance as stated design loads are increased.

Frame 4 Test #8 was a pleasant surprise at the test facility. While the nonbreaking of the glass allowed the frame to be tested again, this large load was held intact by the TSSA and the perimeter weatherseal. The design windload for this TSSA system using 2.36” diameter attachments supporting the glazing is 50 psf. This is a moderate design with desirable architectural transparency that exhibited extreme loading and the TSSA remained intact.

CONCLUSIONS AND RECOMMENDATIONS

This study was undertaken to determine if adhesive attachment of glazing systems has some sort of inherent danger or flaw in low level specified blast performance requirements. It is clearly evident that the simple system of 2.36” TSSA fittings applied close to the edge of the glazing has performance up to the breakage of the glass.

When glass is designed to resist breakage, TSSA is a viable method of attachment to provide a level of protection while maintaining the architectural desire for transparency and openness.

Based upon the standard, ASTM F2912-17, the window assembly tested meets a hazard level of H1 at a specification level of C1.

The fittings used in the study, Sadev R1006, were unaffected after all tests with no evidence of damage or deformation. (see Figure 7)

Previous research by Morgan with blast testing of drilled assemblies were approximately 4" on drilled center of from the edges of glass. The adhesive attachment method utilized in the study which was approximately 2" from center of connection from the edges of glass resulted in additional transparency of the assembly by keeping the hardware closer to the edges.

Tempered glass used in this study was the "weak link" in the system. Once the glass broke, the TSSA and the perimeter weatherseal were unable to retain the bulk of the glazing because small shards of glass remained on the silicone adhesive.

From perspective of design and performance, TSSA adhesive systems have now been demonstrated to provide protection in blast rated façade assemblies in the initial levels of blast performance specification as noted by widely accepted industry standards. The tested façade indicates a clear performance difference in hazard classification for loads between blast loads of 6 psi and 10 psi. Of importance, though, is that the difference in hazard classification is not attributed to a failure in the adhesive. Based on observations, properly sizing the glass to minimize deflection to prevent embrittlement due to bending and increased shear response at the interface of attachment appears to be a critical factor in performance. Future designs may be able to incorporate reduced hazard levels at higher loadings through increased glass thickness, location of the point fixation relative to edge and/or increased contact diameter of the adhesive.

REFERENCES

Hilliard, J. R., Parise, C. J., and Peterson, C. O., Jr., Structural Sealant Glazing, Sealant Technology in Glazing Systems, ASTM STP 638, ASTM International, West Conshohocken, PA, 1977, pp. 67–99.

Zarghamee, M. S., Schwartz, T. A., and Gladstone, M., "Seismic Behavior of Structural Silicone Glazing," Science and Technology of Building Seals, Sealants, Glazing and Waterproofing, Vol. 6, ASTM STP 1286, J. C. Myers, Ed., ASTM International, West Conshohocken, PA, 1996, pp. 46–59.

Carbary, L. D., A Review of the Durability and Performance of Silicone Structural Glazing Systems, Glass Performance Days, Tampere Finland, June 2007 conference proceedings pp. 190-193

Schmidt, C. M., Schoenherr, W. J., Carbary L. D., and Takish, M. S., "Performance Properties of Silicone Structural Adhesives," Science and Technology of Glazing Systems, ASTM STP1054, C. J. Parise, Ed., American Society for Testing and Materials, Philadelphia 1989, pp. 22-45

Wolf, A.T, Sitte, S., Brasseur, M., J., and Carbary L. D, "Preliminary Evaluation of the Mechanical Properties and Durability of Transparent Structural Silicone Adhesive (TSSA) for Point-Fixing in Glazing" Fourth International Symposium on Durability of Building and Construction Sealants and Adhesives, Journal of ASTM International, published online August 2011, Volume 8, Issue 10 (November 2011), JAI 104084, available at www.astm.org/DIGITAL_LIBRARY/JOURNALS/JAI/PAGES/JAI104084.htm.

Clift, C., Hutley, P., Carbary, L.D., Transparent Structural Silicone Adhesive, Glass Performance Days, Tampere, Finland, June 2011, conference proceedings pp. 650-653

Clift, C., Carbary, L.D., Hutley, P., Kimberlain, J., "Next Generation Structural Silicone Glazing" Journal of Facade Design and Engineering 2 (2014) 137–161, DOI 10.3233/FDE-150020

Kenneth Yarosh, Andreas T. Wolf, and Sigurd Sitte "Evaluation of Silicone Sealants at High Movement Rates Relevant to Bomb Mitigating Window and Curtainwall Design" Journal of ASTM International, Vol. 6, No. 2 Paper ID JAI101953

Morgan, T., Advances in Explosion Resistant Bolt Fixed Glazing, Glass Performance Days, June 2103, Conference proceedings pp 181-182

Wedding, William Chad, and Braden T. Lusk. "Novel method to determine blast resistant glazing system response to explosive loading." *Measurement* 45.6 (2012): 1471-1479.

FIRE SAFETY IN HIGH RISE EXTERIOR FACADES

Mineral wool design strategies for ASTM E 2307 and NFPA 285 compliance



Angela M. Ogino
Owens Corning Thermafiber
ANGELA.OGINO@OWENSCORNING.COM

ABSTRACT

One of the most complex yet least understood areas where fire can spread is at the perimeter of a building. Fire can not only spread from floor-to-floor via the edge-of-slab/curtainwall intersections but also along the exterior of the building enclosure. This is a rapidly growing concern for AEC professionals. As energy standards and building codes continue to evolve, the process of designing buildings (while also addressing energy efficiency) has become increasingly challenging. For example, to enhance energy efficiency, codes are prescribing air barriers and increasing amounts of continuous insulation in every climate zone. These components are often combustible and sometimes seem at odds with the building code. Moreover, there is a proliferation of exterior claddings (also often combustible) which designers can choose from. The objective of this white paper is to explore design and construction best practices, which are based on decades of full-scale fire testing and wall assembly performance during actual building fires.

Readers will:

- Gain a stronger understanding of the vertical spread of fire in high rise buildings and why fire containment is important for occupants in the building as well as emergency responders.
- Learn how to identify proper wall design techniques that will help provide fire safety in multi-story wall applications.
- Learn how common building materials, used in wall construction, behave when exposed to the rigors of fire per NFPA 285, ASTM E 2307 and ASTM E 119 fire tests.
- Be provided with the tools needed to design code compliant assemblies so that the fire can be contained to the floor of origin, allowing more time for occupants to evacuate the building.
- This white paper also provides an understanding of what design criteria are required for a rated assembly and assembly performance.

KEYWORDS

Curtainwall, codes - standards - rating systems; design processes; component performance; perimeter fire containment; continuous insulation; wall system assembly

INTRODUCTION

Recent international news headlines reporting catastrophic fires in high-rise buildings have brought renewed attention to the importance of perimeter and exterior wall fire performance. Now more than ever, commercial building professionals have a

responsibility to understand how to optimally design and specify fire containment systems that incorporate components with proven compatibility, code compliance and performance.

With no room for error when designing and building commercial buildings, today's commercial architects and specifiers use a rule of three in fire prevention and containment design strategy: detective, active and passive safety-systems.

This balanced approach to fire safety begins with the detective systems that include smoke alarms and heat detectors in buildings. The second line of defense centers on active fire containment systems that include the installation of automatic sprinklers. In the event of a catastrophic fire, the passive containment safety-system will help confine the fire to the room of origin by maintaining the integrity of the wall and the floor juncture for the time period designated by codes.

When activated, these three fire safety components will extend the crucial window of time for building occupants to evacuate the structure and fire personnel to access and extinguish the blaze. However, the perimeter is one of the most complex and vulnerable areas where fire can spread in a commercial structure. This fire sensitivity, especially in curtain wall construction, is due to heat from fire causing disintegration of the wall after the aluminum framing and aluminum anchors that hold up the exterior wall begin to melt.

There are several specific test methods developed to measure construction assembly designs for fire containment, including:

- ASTM E2307 (perimeter fire containment)
- NFPA 285 (spread of fire along building exterior)
- ASTM E1966 (for fire resistive joint systems)

In the wake of energy codes ushering in ASHRAE 90.1 criteria for continuous insulation(ci) and air/water resistive barriers that are often combustible, architects and specifiers now face added complexities when designing the building façade. The adoption of ASHRAE 90.1 was also responsible for triggering the requirement for NFPA 285 testing to measure what happens during a fire when a non-combustible building is wrapped in combustible materials.

Fortunately, recent advancements in perimeter and exterior wall fire performance solutions along with available educational resources are providing an arsenal of new tools to help architects and specifiers improve accuracy and code compliance while streamlining design and installation.

BACKGROUND

FIRE SPREAD AT AN EXTERIOR CURTAIN WALL ASSEMBLY

The foundation to specifying code compliant perimeter fire containment begins with understanding the three primary paths of fire propagation in a commercial building.

The first fire path is straightforward and results from an unprotected void between the floor slab and the exterior curtain wall. Flame and hot gasses will propagate through the joint between the wall and the slab edge.

The second fire path occurs if the spandrel panel is not properly protected and the fire can break through the spandrel or spandrel framing and compromise the wall via the exterior and burn through the interior wall.

The third fire path is called Leapfrog and is a more complicated progression path. This is where the fire breaks through the vision glass on the floor of origin, allowing flame and hot gasses to escape outside the building and up the exterior face of the curtain wall, breaking through the vision glass on the floor above. Although containment against fire spread via leapfrog is currently not a requirement for the perimeter curtain wall condition per the building codes, it still provides a viable path for fire to spread quickly in a high rise structure and needs to be evaluated for building occupant safety.

These fire paths have been studied and tested to identify failures and apply those learnings to develop more effective perimeter fire containment assembly solutions.

It was previously assumed that filling that void created between the floor slab and exterior wall would prevent fire and smoke from propagating to the floor above. However, when that void is filled with mineral wool safing insulation only, without protecting a portion of the spandrel area, the curtain wall will fail and allow the mineral wool to fall out of the void.

Testing that followed in the 1990s in both the United States and United Kingdom continued to help highlight key learnings surrounding curtain wall failings.

As the cross-section drawing illustrates, a test in 1999 by the Loss Prevention Council in the United Kingdom installed mineral wool between the glass and face of the floor slab (Fig. 1).

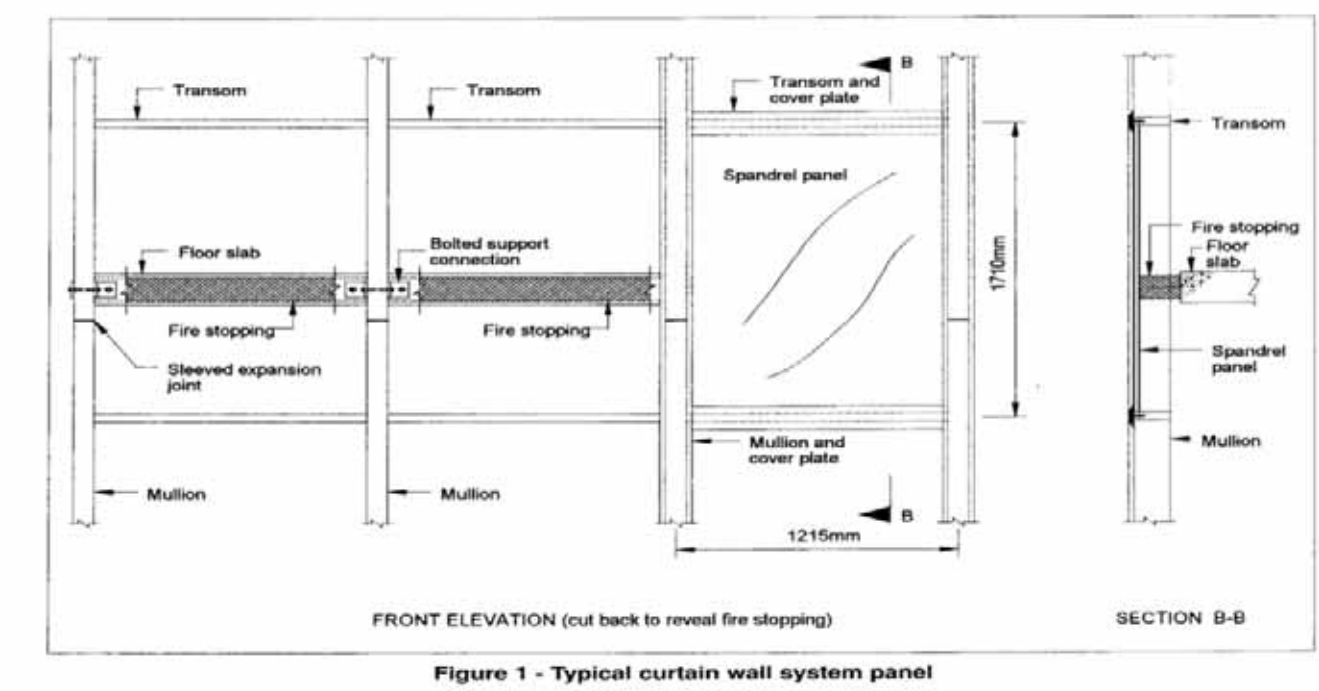


Figure 1: Typical curtain wall system panel.

Within the first 10 minutes of the fire, the glass broke out and the safing fell out of the void allowing fire to propagate to the next floor. In depth testing conducted by Underwriters Laboratories (UL) lead to the development of a test standard that ultimately became ASTM E2307, Standard Test Method for Determining Fire Resistance of Perimeter Fire Barriers Using Intermediate-Scale, Multi-story Test Apparatus (Fig. 2).

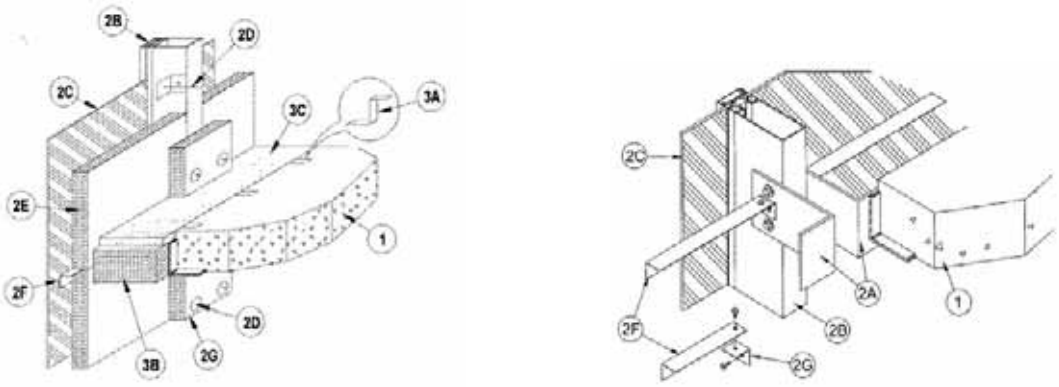


Figure 2: UL's first published curtain wall assembly: CW-S-2001, issued: 4/14/97.

Following more than 20 years of various code requirements for the floor-to-floor fire containment in the curtain wall condition, ASTM E-2307 was published as the definitive test method for evaluating the performance of perimeter fire containment assemblies and was quickly adopted in the 2006 edition of the International Building Code (IBC).

CONTINUOUS INSULATION SYSTEMS AND NFPA 285

The wide spread adoption of the IBC and the rise of continuous insulation (CI) in energy standards such as ASHRAE 90.1 and the IECC happened to coincide in the 2000's. During this time, it was more common for walls required by the IBC to be made of noncombustible components. Moreover, the energy standards began to prescribe increased amounts of continuous insulation (ci) in exterior walls to enhance thermal efficiency, which is often, not always, a combustible foam plastic. More recently, energy standards have begun requiring air barriers, which are also, often times, combustible. In other words, new buildings were often required to be of non-combustible construction, yet also required to be wrapped in combustible materials.

It wasn't until this rise of CI that NFPA 285 became a widely enforced test requirement. That is why many architects during the 2008 – 2010-time frame were unaware that their new designs including CI needed to be NFPA 285 compliant.

CODE REQUIREMENTS FOR NFPA 285 COMPLIANCE

NFPA 285 is typically required when combustible air/water barriers are used or when foam plastic insulation is used in the exterior walls of construction types I, II, III or IV. These construction types, by code definition, have exterior walls constructed of non-combustible materials.

NFPA 285 is a fire test standard that measures the likelihood that a wall system assembly containing combustible components may be ignited by a fire plume emitting from a window opening, and then propagate the fire away from the point of origin either on the surface of the wall or through its core and cavities. Although it was never intended to be a test exclusively for exterior insulation finish systems (EIFS), NFPA 285 was largely viewed as an EIFS test, and was not initially utilized to evaluate other types of cladding or construction.

Today's IBC codes are now very specific about addressing the protection requirement for the intersection of the floor assembly and exterior curtain wall. The NFPA 285 test is now used when the IBC requires non-combustible wall construction; and the energy code requires the building to be wrapped in air/water resistive barriers, often combustible; and/or continuous insulation, often combustible; and/or combustible exterior cladding is used.

This requirement is referenced in many sections of the IBC, including 1403.5 for water resistive barriers and 2603.5.5 for foam plastic insulation. The 2015 IBC added 2603 5.5 vertical and lateral fire propagation which requires NFPA 285, except if 1 story, sprinklered and covered with metal OR, if covered on EACH FACE with min 1" masonry or concrete, AND there is no air space, OR, foam plastic has flame spread ≤ 25 and air space is 1" max.

The 2015 IBC code also added 1403.5 vertical and lateral fire propagation requirements that… "exterior walls on buildings of Type I, II, III, or IV construction that are greater than 40' in height above grade plane and contain a combustible water-resistive barrier shall be tested in accordance with and comply with the acceptance criteria of NFPA 285."

CODE REQUIREMENTS FOR PERIMETER FIRE CONTAINMENT ASSEMBLIES

The IBC code references section 705.8.5. Section 705.8.5 refers to the 3' spandrel height and is always being questioned because it is interpreted as a spandrel height is not needed or only safing is necessary to meet the extension of the rating of the floor slab.

This code section has three exceptions that specifically state that the section does not apply if the building is three stories or less in height, if an automatic sprinkler system is installed or if it is an open parking garage. However, there is nothing in this section or any other section of the code that states the Exterior Curtain Wall/Floor intersection (715.4) can be ignored.

Section 715.4 states “Where fire resistance-rated floor or floor/ceiling assemblies are required, voids created at the intersection of the exterior curtain wall assemblies and such floor assemblies shall be sealed with an approved system to prevent the interior spread of fire. Such systems shall be securely installed and tested in accordance with ASTM E2307 to provide an F rating for a time period not less than the fire- resistance rating of the floor assembly. Height and fire-resistance requirements for curtain wall spandrels shall comply with Section 705.8.5.

There is an exception within the code language that states that voids created at the intersection of the exterior curtain wall assemblies and such floor assemblies where the vision glass extends to the finished floor level shall be permitted to be sealed with an approved material to prevent the interior spread of fire.

Such material shall be securely installed and capable of preventing the passage of flame and hot gases sufficient to ignite cotton waste where subjected to ASTM E 119 time-temperature fire conditions under a minimum positive pressure differential of 0.01 inch (0.254 mm) of water column (2.5 Pa) for the time period equal to the fire-resistance rating of the floor assembly.

It should be noted that the exception was written in the codes when there were no tested assemblies per ASTM E2307 for addressing vision glass extending to a finished floor. However, there are existing systems in the UL Fire Resistance Directory, tested to ASTM E 2307 that are now available for these conditions.

Therefore, section 715.4 is very specific and strictly enforces the requirement that the fire resistance rating of the floor assembly be maintained. There are no exceptions.

In 2006, to try and eliminate the confusion over section 705.8.5, a new section was added. Section 715.5 Spandrel Walls states that where Section 705.8.5 does not require a fire-resistance rated spandrel wall, the requirements of Section 715.4 shall still apply to the intersection between the spandrel wall and the floor.

METHOD

DYANMICS OF VERTICAL FIRE SPREAD

To explore the dynamics of vertical fire spread at the building perimeter, it is important to understand how curtain wall materials perform in commercial fire exposure. The ASTM E 119 test method is the standard used to evaluate the duration of which various types of building elements either contain a fire, retain their structural integrity, or exhibit both properties during a predetermined test exposure.

The test exposes a material to a standard controlled fire to achieve specified temperatures throughout a specified time period. This follows a curve known as the ASTM E 119 Time- Temperature Curve (Fig. 3). The time is shown in hours across the bottom and the temperature in °F is shown on the vertical line. The thick red line illustrates the exposure at the beginning of the test which takes place quickly, with temperatures growing very rapidly. The important callouts from this diagram include:

- The temperature of 1,050° F occurs six minutes into the E 119 fire test. At this temperature material like Spray Foam, Zinc, and Glass Fiber insulation used in an exterior curtain wall system have been compromised and will melt. Low melt point insulations used in perimeter fire barrier systems will not effectively provide protection and prevent the propagation of fire at the exterior curtain wall/floor joint location. If insulation such as glass fiber is installed to provide protection against fire or even for thermal performance, the temperatures that occur very early into a fire exposure will cause the material to melt or fall out of place thus compromising the protection of the spandrel area.
- The temperature of 1,220 degrees F takes place at nine minutes into a fire. It is at this time and temperature that any type of aluminum framing members or unprotected curtain wall anchors will begin to melt. Preserving the spandrel area of a perimeter fire containment assembly is critical for maintaining a tight seal where the mineral wool is installed between the exterior curtain wall and the concrete floor assembly. This detail is critical for code compliance for maintaining a barrier to flame and hot gases at the interior joint. If the aluminum framing and the components that support the exterior wall are not properly protected, the assembly will fail as early as 9 minutes, allowing fire to spread vertically to the floors above.
- The third point on the curve is the temperature of 1,510°F, which occurs 25 minutes into the fire test. It is at this time and temperature that plate glass melts. However, as shown in perimeter fire containment testing, the glass whether

it is vision or spandrel glass, breaks out as early as 5 minutes into a fire. This is cause for concern as documented by the research conducted by the Loss Prevention Council in conditions where mineral wool was installed at the interior joint between the glass and the concrete floor slab. The glass failed as early as 10 minutes into the fire allowing the mineral wool to dislodge and fire to propagate to the next level.

- The temperature of 2,080 degrees F which occurs at five hours into a fire is the time and temperature that mineral wool insulation was exposed. The test was terminated after five hours with the mineral wool remaining fully intact. Demonstrating that mineral wool is the only tested and proven material for protecting the low melt point components of a curtain wall assembly.

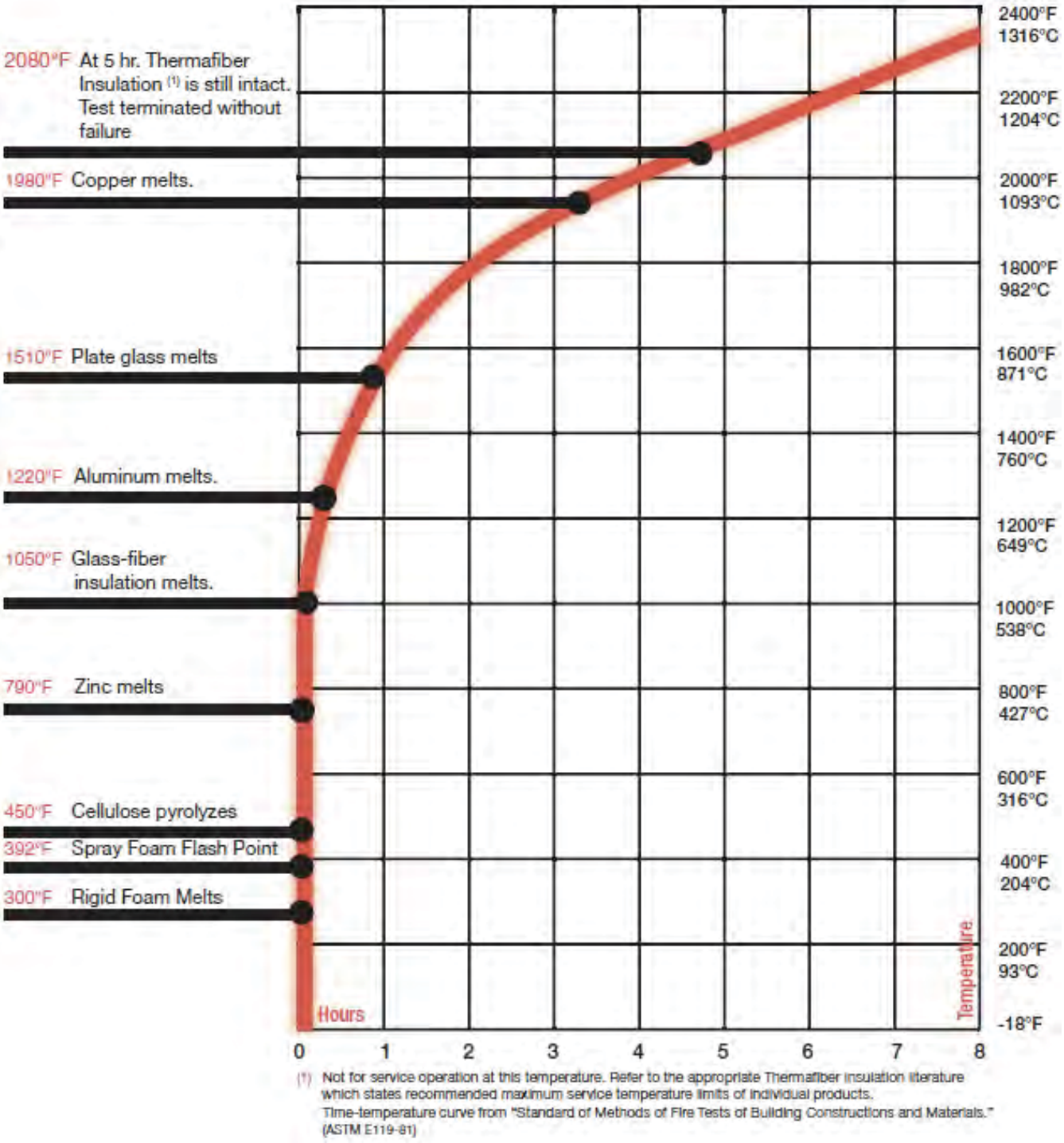


Figure 3: ASTM E 119 time-temperature curve diagram.

NFPA 285 ASSEMBLY TESTING

A second baseline fire test used to help inform designers on the fire performance of exterior enclosures/facades is the NFPA 285 assembly test. Per the 2012 IBC, NFPA 285 is required when combustible elements such as cladding panels, air and water resistive barriers or foam plastic insulation are in Types I, II, III and IV construction that have non-combustible walls.

The 30-minute test is conducted on a full scale two story wall assembly, built as it would be in the field, on the front side of a three sided test structure (Fig. 4).

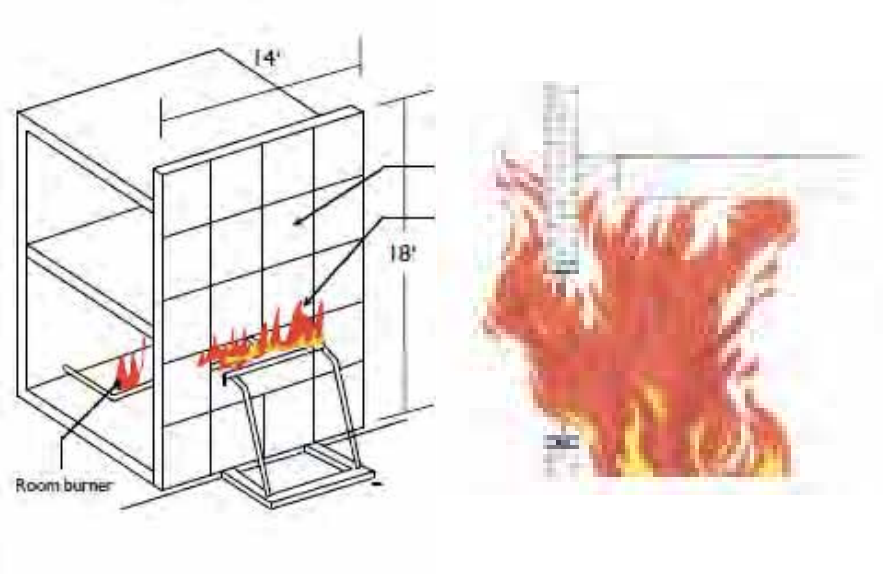


Figure 4: NFPA 285 assembly test.

The test wall, has a window in the center of the lower floor. The test scenario is that a flashover fire, unrelated to the combustibles in the wall, has occurred in the lower story room emitting a fire plume through the window and out of the room of origin. Early in the 30-minute exposure the fire plume wraps around the window head, extending up the exterior surface of the wall. To pass, the wall assembly must limit fire spread vertically and horizontally away from the window. The extent of fire spread is determined visually, measured in feet, and by temperature that is measured by thermocouples placed throughout the wall assembly (Fig. 5).

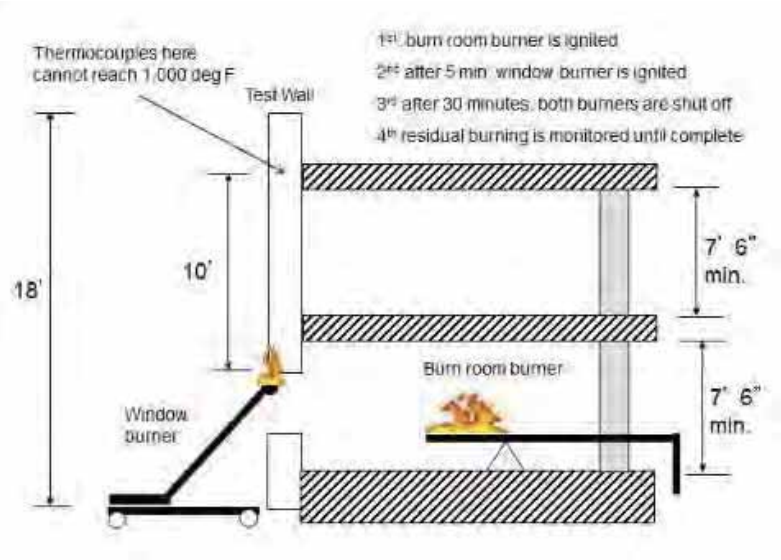


Figure 5: NFPA 285 assembly test measured by thermocouples in wall assembly.

NFPA 285 tests a two-story simulation of a fire where in:

- Room burner is ignited
- 5 Minutes – Window burner ignited
- 30 Minutes –Fire is terminated
- Monitor distance fire spreads visually
- Monitor internal wall temperatures

The images below (Figs. 6 and 7) illustrate that this particular assembly passes NFPA 285. The following visual observations can be made by removing the brick veneer.

- Flame exposure on the exterior face of the wall shows less than 10 feet above the window opening.
- Also, visual observation shows that flame did not extend greater than 5 feet from the centerline of the window opening.
- It should also be noted that limiting temperature rise on both the exterior and interior of the wall cavity are requirements for passing NFPA 285.
- Also, flame should not be visually observed within the 2nd story of the Intermediate-scale multistory test apparatus (ISMA) apparatus.



Figure 6: Fire plume exiting 1st story window.



Figure 7: Wall showing limited fire spread after brick veneer has been stripped.

It is important to understand the distinction between the ASTM E119 and NFPA 285 tests.

ASTM E119 is a structural fire resistance and system integrity test, measured in time, typically hours per the 2012 IBC section 703.2. Where as NFPA 285 tests limiting fire spread and growth via surface and inside wall cavities in 30-minute duration as is referenced in multiple sections of the 2012 IBC.

Under section 2603.5 “exterior walls of buildings of any height”, NFPA 285 represents only a single test is separate from other code requirements. Other important requirements include:

- NFPA 275: Provide thermal barrier separation from interior
- NFPA 259: Potential heat limit
- ASTM E84: Flame spread maximum 25
- NFPA 268: Ignition resistance

ASTM E 2307 TESTING

ASTM E 2307 also utilizes the intermediate multi-story test apparatus, same as NFPA 285. However, there are unique differences between the two standards. ASTM E 2307 represents the standard test method for determining fire resistance of perimeter fire barrier systems. It evaluates the interior joint beginning at the face of the floor slab to the interior face of the exterior curtain wall. The primary pass/fail criteria is the ability to resist the passage of flame and hot gasses through the interior joint. The protection needs to prevent flame through and passage of gases significant enough to ignite cotton waste. The interior joint must remain securely in place for the time duration equal to the fire resistance rating of the floor assembly (typically 2 to 3 hours).

The apparatus consists of a burner room on the first floor and an observation room located on the second floor directly above the burner room. The basic principle is to engulf the first floor room with flame and hot gasses to simulate a room fire which starts the test with ignition of the room burner.

The vision glass on the first floor breaks out approximately five minutes into a fire. The window burner is then ignited at the five-minute mark to simulate the fire exposure on the outside of the building causing flame and hot gasses to lick up the face of the exterior wall. The objective is to prevent flame and hot gasses from entering into the room above through the interior joint opening.

These are photos of an actual test per ASTM E 2307 (Fig. 8). The first picture shows the assembly as the fire begins with ignition of the room burner. To simulate the vision glass breaking out, at 5 minutes into the fire test, the exterior window burner is ignited exposing the exterior of the wall assembly to direct fire impingement.



Figure 8: ASTM E 2307 fire test begins with ignition of room burner (left). Ignition of the exterior window burner at 5 minutes into the fire test (right).

The aftermath of the fire shows the destruction caused by the flame and hot gases, including the loss of the transom and mullions (Fig. 9).



Figure 9: Destruction following ASTM E 2307 fire test.

DATA

The data from the full-scale fire testing and wall assembly performance during actual building fires illustrates design and specification best practices for preventing fire spread at the perimeter of the building per ASTM E 2307. The results also reinforce that the choice of the cladding, insulation, and the details around openings, are critical in accomplishing an assembly that is NFPA 285 compliant.

With CI and NFPA 285 now a “standard method and material” practice, multiple assemblies have been tested or have been accepted through engineering judgments. ASHRAE 90.1 criteria for continuous insulation(ci) also includes prescriptive requirements for often combustible continuous insulation “ci” over steel stud framing and air and water resistive barriers, also often combustible.

CLADDING CONSIDERATIONS

There are many types of cladding used on walls requiring NFPA 285 compliance. Common cladding materials include masonry veneers (brick, CMU, and stone both natural and manufactured), precast concrete and insulated precast concrete, terra-cotta, composites, laminates, architectural metal panels (both single skin and ACM, aluminum composite material, or MCM, metal composite materials). Masonry and concrete are themselves highly fire resistant and provide quite substantial protection for the potentially combustible layers of CI and/or the air/water resistive barrier inside the wall system. Other materials such as ACM’s provide very little fire resistance, and may themselves contribute to fire spread and require NFPA 285 testing even when used alone with no other combustibles in the wall system.

As demonstrated in the ASTM E 119 Time- Temperature Curve diagram, mineral wool is non-combustible and highly fire resistant. As a result, it delivers optimal performance in any continuous insulation open joint systems that may be exposed to fire, and in non-masonry systems that provide little fire resistance such as behind ACM/MCM panels. Mineral wool can be used behind virtually any type of cladding systems, including: floor line and detailing; steel ledge, shelf angle, detailing; and transitions from wall to roof.

NFPA 285 COMPLIANT WALL ASSEMBLIES

Many manufacturers of insulation, air and water barriers and exterior cladding materials have published design aids to guide the specification of NFPA 285 compliant wall assemblies. This is important given the range of combustible materials used in non-combustible wall construction that are subject to the NFPA 285 test. This list includes foam plastics, a growing number

of ci and AWB materials, and cladding such as high-pressure laminates, metal composites, and fiber-reinforced polymer panels.

The best practices for NFPA 285 design compliance address options for a variety of wall types and the materials, including:

Base wall system. Base wall may be steel stud, concrete or CMU “ci” direct to framing or, over exterior gypsum sheathing stud cavity insulation. The stud cavity can be empty, or, it may have fiber glass, spray foam, or mineral wool or any non-combustible insulation. It is important to consult the guide specifications of the material manufacturers to insure that wall system designs are consistent with their recommendations and with the NFPA 285 test data in their portfolio since not all combinations have been tested.

Air and water resistive barriers. Air/water resistive barriers must be included in the assembly spray membrane, roll or sheet applied over gypsum sheathing under foam “ci” or, over foam “ci.”

Opening head details at brick steel stud cavity walls. One of the most important details in the NFPA 285 test is the opening head detail. Sill and jamb details are important, but not as critical as the head. The opening head receives the most intense fire exposure of any part of the wall assembly as the fire exits the room of origin and rolls around the opening head. Examples of fire stopping at head detail: A continuous steel bearing angle that completely closes the opening head is a very effective fire stop detail. In a situation where the continuous steel angle is not placed directly over the window head but rather at the floor line, there will be a loose steel lintel over the openings. Wood blocking, or wood nailing bucks, fit tightly to the steel are also a simple and effective closure of the head cavity. The NFPA 285 test is conducted without a window unit in place. So, if the head and jamb closure details are specified correctly to prevent fire penetration, then any type of window may be in the opening because it has no impact on passing the test.

Opening jamb & sill details at brick steel stud cavity walls. Examples of firestopping at jambs include mineral wool fire safing compressed between the back of the brick veneer and the face of the gypsum sheathing, continuous insulation is maintained between the foam plastic and the mineral wool, while effectively fire stopping the opening. An excellent fire resistant detail is created by simply putting mineral wool in the jambs. Another jamb detail includes the use of full masonry returns at the opening. Although not as thermally efficient as using mineral wool, it is a very effective fire stop detail that closes the jamb opening.

Precast concrete head conditions. The complexity of the head opening detail varies with the type of construction. A precast sandwich panel successfully passes NFPA 285 with a simple wood nailer that also serves as a fire block surrounding the opening. The steel stud wall uses a stand-off steel shelf angle that is packed with compressed mineral wool fire safing. Each detail is an effective technique to close the head opening and contribute to a passing NFPA 285 wall assembly. Actual window frames are usually not included in the NFPA 285 test because they are often made of aluminum and melt out so quickly. They have negligible impact on passing or failing the test.

Cladding. The cladding you choose impacts Continuous Insulation options. Rule of thumb: Generally, thermoplastic insulation like expanded polystyrene or extruded polystyrene, and can only be used under masonry claddings. Polystyrene cannot be used under metal cladding. Polystyrene needs more fire protection than metal cladding provides. Fire enhanced thermoset polyisocyanurate, not just polyisocyanurate, but a fire-enhanced polyiso, is required when used under metal cladding. Some varieties of polyiso have proprietary formulations that make them more fire resistant than standard polyiso. Generally, those enhanced products must be used under metal cladding to pass NFPA 285.

Given the sheer volume and complexity of designing a wall assembly that addresses each of these NFPA 285 compliance standards, architects are increasingly specifying tested, compliant wall systems. This approach addresses the fact that NFPA 285 is an assembly test and not a test of individual components.

EXPLANATION

In the event of a multi-story building fire, the first line of defense for the occupants is the integrity of the building design. Through trial and error of perimeter fire containment tests, six basic design principles have been proven to provide successful fire containment at the perimeter of the building and compliance with ASTM E 2307 (Fig. 10).

While commercial building is not a one-size-fits-all proposition, here is a checklist for the six components for any listed perimeter fire containment system assembly:

1. **Install mineral wool as the insulation for the perimeter fire containment barrier** (both within the curtain wall spandrel and the interior joint). Mineral wool insulation, at the required densities and thickness, is the only tested and proven material that will provide protection to the spandrel and interior joint.

2. **Mechanical attachment of mineral wool curtain wall insulation.** There are no one size fits all when it comes to mechanical fasteners. Specific mechanical fastening methods, as per the tested assembly, must be installed to assure that the system operates as designed under the duress of fire, thermal and structural movement consequential to the rigorous exposure of ASTM E 2307.

3. **Provide backer reinforcement at the safe-off line.** Most listed systems reference either a 20-gauge, galvanized steel T-Bar, L-Angle or hat channel. Other systems utilize other components that withstand the exposure of an ASTM E 2307 fire to provide the required reinforcement of the curtain wall insulation. This detail is critical to prevent the spandrel insulation from bowing due to the force of compression at the safing joint. Again, the common factor is that all systems require some form of reinforcement behind the mineral wool spandrel insulation at the safe-off line. This is also critical for providing a tight seal at the interior joint. The lack of reinforcement causes the spandrel insulation to flex, creating even the smallest of gaps or seams which allows flame and hot gases to penetrate the safe-off opening and potentially engage combustibles on the floor above. There is another common misconception that metal panels, such as aluminum or steel back pans, will provide the necessary reinforcement. Regardless of whether they are steel or aluminum, testing has proven these panels to be a failure point at the safing line if not properly reinforced.

4. **Compression-fit mineral wool safing insulation** within the void between the floor slab and the exterior curtain wall insulation. The correct density, orientation, and compression are required to establish the proper seal at the interior joint.

5. **Protect exposed vertical aluminum framing with mineral wool insulation mullion covers.** This a detail that is often removed from the system as it is perceived to be a minor contributor to the performance of the assembly. Particularly when it obstructs interior finishes or window shade pockets. Again, another common error in design is to eliminate the element that covers and protects the mechanical fasteners that keep the spandrel insulation in place as well as help to retain the exterior wall in position so that the safing joint mineral wool insulation continues to block fire and smoke. Elimination of this component results in a shorter fail rate of the exterior curtain wall element.

6. Apply a Smoke Barrier System for Smoke Containment. Because smoke inhalation is responsible for the majority of fire-related deaths, all perimeter fire containment systems are tested and listed with a smoke barrier applied over the top of the safing mineral wool insulation. Application of an approved smoke barrier, typically spray, is applied over the safing mineral wool insulation.

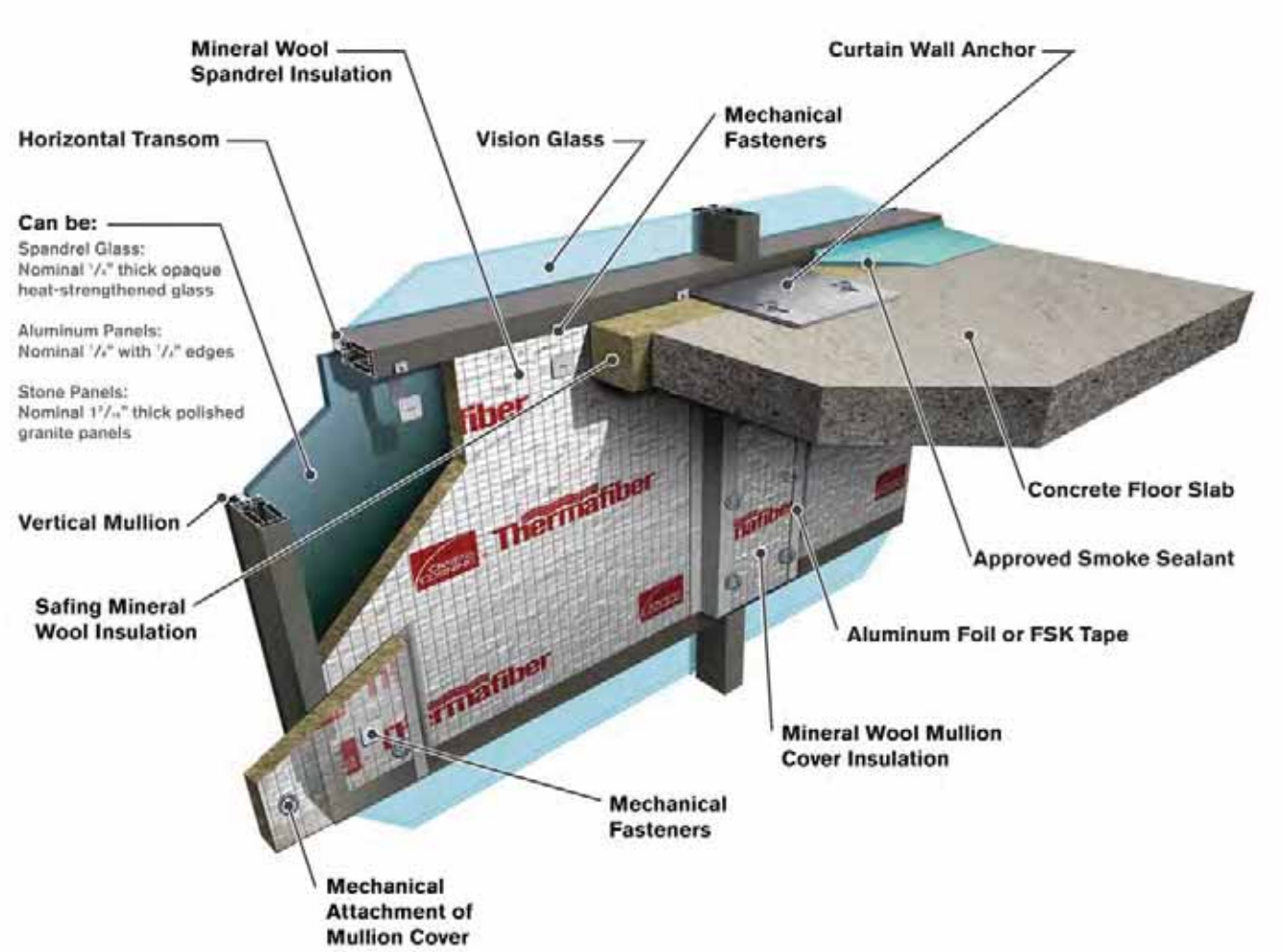


Figure 10: Six basic design principles for fire containment at the perimeter of the building and compliance with ASTM E 2307.

Leading manufacturers have also evaluated special conditions, such as wider spandrels, back pans, shorter spandrel heights, to create tailored solutions that address performance and safety considerations.

CONCLUSION AND FUTURE WORK

In this high stakes design scenario where commercial building occupants depend on architects and specifiers for their safety, perimeter fire containment and continuous insulation system solutions can help alleviate the pressure building designers face to get it right.

In addition to sharing testing results, many manufacturers and third parties also provide additional resources to collaborate with commercial building professionals to help manage insulation details at every step by offering expert engineering judgments, recommendations for specific products, CAD drawings and consultation on good design practices. This is particularly helpful if there are no tested assemblies that match the construction design.

Ultimately, it is imperative for architects and specifiers to remain educated on where and how to incorporate code-compliant specifications and tested assemblies into commercial buildings to allow more time for occupants to evacuate.

ACKNOWLEDGMENTS

The author wishes to acknowledge the following organizations: International Firestop Council (IFC), UL® Laboratories, Loss Prevention Council, Drew Clausen, Herbert Slone.

REFERENCES

ASTM E2307 Standard https://www.astm.org/Standards/E2307.htm.

Commercial Architecture podcast on Perimeter Fire Containment. http://www.commercialarchitecturemagazine.com/high-sky-safety/.

International Code Council- International Building Code, Chapter 7 Fire and Smoke Protection Features, Section 715.4 Exterior curtain wall/floor intersection. https://codes.iccsafe.org/public/document/IBC2015/chapter-7-fire-and-smoke-protection-features.

International Firestop Council. http://www.firestop.org/.

Morris, Brian. *Fire Spread in Multi-story Buildings with Glazed Curtain Wall Facades*.Loss Prevention Council, 1999.

NFPA 285 Standard http://www.nfpa.org/codes-and-standards/all-codes-and-standards/list-of-codes-and-standards/detail?code=285.

Owens Corning NFPA Design Guide. http://www.owenscorning.com/NetworkShare/EIS/Owens-Corning-Enclosure-Solutions-NFPA-285-Design-Guide.pdf.

Slone, Herbert. “The Evolution of Continuous Insulation.” BDC University. https://www.bdcuniversity.com/evolution-continuous-insulation.

Thermafiber Technical Library, Technical Papers. https://www.thermafiber.com/technicallibrary/technicalpapers/.

UL Firefighter Safety Research Institute (FSRI). https://ulfirefightersafety.org.

Video on perimeter fire containment. https://youtu.be/2THHBs-50Nw.

HARDENED FAÇADES EFFECTS ON STRUCTURAL SYSTEMS

Analytical study and test of blast-resistant façades effects on structural braced frames



Aldo E. McKay, PE
Protection Engineering Consultants
amckay@protection-consultants.com



Cliff A. Jones, SE, PE, PSP
Protection Engineering Consultants
cjones@protection-consultants.com



Phillip Benshoof, PE
United States Department of State Bureau of Diplomatic Security
BenshoofPC@state.gov

ABSTRACT

To ensure the safety of U.S diplomatic personnel overseas, the U.S Department of State (DoS) has developed façade retrofits capable of resisting high blast loads. Historically, these hardened façades have been primarily used in reinforced concrete frame structures that are perceived to perform better against high lateral forces generated by these façades. As the DoS builds and renovates existing steel-framed buildings, it is vital to understand the effects of hardened façades on steel structures to avoid potential collapse situations that would pose a threat to the building occupants.

An analytical study evaluated the global lateral response of steel frames representative of typical diplomatic facilities using hardened and conventional façades against high blast loads. Conventionally-designed steel frame buildings when used in conjunction with blast-resistant façades could be susceptible to failure due to the high blast reactions transferred to the Lateral-Force-Resisting-System (LFRS). However, when used with conventional façades, the rapid failure of the façade significantly reduces the loads on the LFRS. A test program was initiated to validate the findings from the study. Two tests have been planned using a full-scale, conventionally designed three-story steel braced frame. Test 1, in which a conventional curtainwall was installed on the steel frame structure has been conducted and the results validated the initial findings that conventional façades do not generate significant lateral loads in the LFRS. Test 2 which is in progress, will use a hardened façade and is expected to be performed in the fall of 2018. A review of the research program findings along with a brief discussion of new tools and methods to reduce blast reactions transferred to the LFRS are presented.

KEYWORDS

blast, hardened façade, physical testing, curtainwall, security, precast, precast façade

INTRODUCTION

The U.S. State Department owns buildings and leases space in buildings for diplomatic purposes worldwide. Many of these buildings were not built considering any blast-resistant requirements, are not on an embassy compound that provides standoff, nor were they purpose built with all of the most recent physical security requirements and standards to ensure the safety of overseas State Department employees. As a result, oftentimes the exterior envelope of these buildings must be upgraded using hardened façades to provide blast, ballistic and forced-entry protection. These hardened façades typically consist of thick and heavily reinforced concrete or CMU walls, structural steel backup frames for curtainwalls, and thick-laminated or polycarbonate glazing systems. When exposed to high blast loads, these hardened façade systems can transfer high lateral reactions to the supporting lateral-force-resisting-system (LFRS). The State Department, historically, has preferred reinforced concrete (RC) frame structures when purchasing or leasing existing space in office buildings. One reason for selecting RC frames over other types of structures is that RC frames are generally heavy structures built as rigid frames with monolithic joints. Thus, when properly detailed, RC frames provide very good lateral resistance to blast loads. Another reason is the lack of blast data for other types of structures' (e.g. conventional steel frames) inherent resistance to blast loads. The preference for RC frame structures can influence the decision to avoid a particular building that has the potential to provide a better investment, a more secure site and perimeter, or one that offers more standoff to existing roadways and parking. Recognizing this lack of data, the State Department's Bureau of Diplomatic Security Research and Development branch initiated a research and test effort to study the resistance of steel frame buildings to extreme lateral blast loads.

BACKGROUND

Beginning in late 2010, an analytical study (McKay et. al., 2011) evaluated the global lateral response of different types steel frames representative of typical diplomatic facilities using hardened and conventional façades against high blast loads. The objective was to identify and quantify the effects of blast-resistant façade systems on the lateral response of steel frame structures under relatively high blast load environments. One of the guiding principles of the study was to make use of conventional structural analysis tools and methodologies that align with established consensus criteria so that the findings of the study could be widely usable. The lateral response of different types of typical mid-rise steel frame structures, including moment frames and braced frames, was investigated through nonlinear dynamic (NLD) analysis using general purpose structural analysis software. Two of the more important conclusions from the initial study were:

1. Conventional façade systems, when exposed to high blast loads fail very early in the response, transfer minimal loads to the structure, and do not cause significant response of the (LFRS).
2. Hardened façade systems transfer large dynamic reactions into the structure and may induce significant deformation in conventionally-designed (non-seismic) steel braced frames of three-stories or fewer as shown in Figure 1 (Left hand side).

Following the analytical study, a test program (McKay et. al., 2013) was initiated to validate the findings from the study. Two tests have been planned using a full-scale, conventionally designed three-story steel braced frame. The frame was designed in accordance with ASCE7-10. Test 1, in which a conventional curtainwall was installed on the steel frame structure was conducted in 2014 and the results validated the initial findings that conventional façades do not generate significant lateral loads on the LFRS as shown in Figure 1 (Right image). Test 2 which is in progress, will use a hardened façade. The data collected from Test 2 will be used to verify the findings from the analytical study and to improve modeling methods for the lateral response of steel braced frames in high blast load environments.

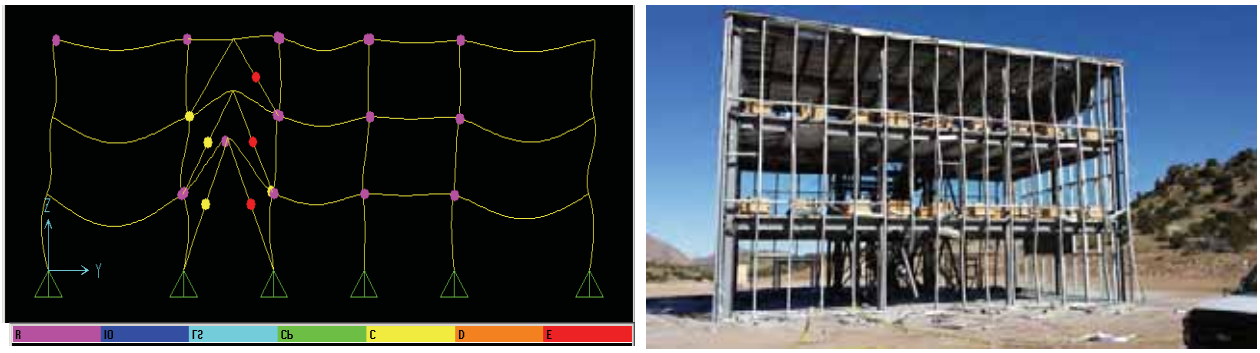


Figure 1 Chevron brace frame collapse mechanism resulting from blast analysis with hardened façade (left, magnified deformation for visualization), and failed conventional glazed curtainwall after blast test (right).

RESEARCH METHOD

First, an analytical study (McKay et. al., 2011) was performed to that included an extensive literature review and simple analytical modeling of a variety of typical steel building types. The primary purpose of this study was to evaluate the effects of different façade types on the lateral response of blast-loaded structures using general purpose structural analysis software and consensus guidelines used for nonlinear dynamic analysis (NLD) of steel frame buildings. The analytical study was followed by a test series intended to verify analytical findings and to generate experimental data for improving modeling approaches.

ANALYTICAL STUDY

In this study uncoupled analysis approaches were used where reactions from the façade systems are generated considering rigid supports, neglecting deformation of the structure. These reactions were then applied as loads to a separate model of the supporting frame structure. The supported façade components (curtain and infill walls) tend to have relatively short natural periods compared to the longer natural period of the supporting frame structure (generally due to the mass of the building). Therefore, the interaction between façade components and the supporting structure will be minimal, and the assumption that the building provides rigid support during façade response, and the response of the frame and façade system are effectively out-of-phase (for the frame structure analysis purposes), is adequate.

Analysis Cases - Steel frames can be designed to resist lateral loads as Moment Frames (MF), Braced Frames (BF), Shear Walls (SW) or a combination of these systems. In non-seismic regions, braced frames are the most popular for low and mid-rise buildings because they are often the most economical method to resist conventional wind loads. Different configurations of bracing systems can be used depending on the specifics of each building. The most commonly used brace frame types are: Chevron, Diagonal, and X-braces. Steel Moment Frames and Shear Walls are less popular for conventional design but are particularly common in seismic and progressive collapse applications. Seven different steel frame systems, representative of the most commonly used Lateral Force Resisting Systems (LFRS) for steel buildings, were selected to perform three-dimensional non-linear dynamic analysis. All systems were designed as six-story buildings. The Chevron and X-Brace systems were also designed in 3- and 12-story configurations to investigate the effects of building height. The selected systems considered in this analytical study are listed in Table 1.

Lateral Force Resisting System (LFRS)	Controlling Lateral Load	Building Heights Investigated
BF: Chevron	Wind	3 story, 6 story, 12 story
BF: X - Bracing	Wind	3 story, 6 story, 12 story
BF: 2 Story X - Bracing	Wind	6 story
BF: Diagonal Bracing (inbound brace in tension)	Wind	6 story
BF: Diagonal Bracing (inbound brace in compression)	Wind	6 story
BF: Eccentrically Braced (EBF)	Seismic	6 story
MF: Moment Frame	Wind	6 story

Table 1. Steel frame cases.

There are several parameters, in addition to the type LFRS, that can affect the final configuration, and consequently the response, of steel frame structures subjected to large dynamic lateral loads. Some of these parameters are: building layout, story height, plan shape, location and number of LFRS lines, and design criteria. Extensive research would be required to thoroughly investigate the effects of each these parameters on the lateral response of frame structures. In order to compare the performance of each of the LFRS to each other, effects caused by the other parameters must be controlled. Therefore, the frame structures for all analysis cases were designed based on the same plan geometry. The baseline floor plan used for the design of all analyzed buildings was developed considering the geometry and characteristics of a typical office buildings. The baseline floor plan was designed with 30-ft exterior bays all the way around the building and interior bays ranging from 20- to 22.5-ft, as shown in Figure 2. Floor to floor height was 13.5-ft. Each building type was designed to satisfy the strength and serviceability limits of ASCE 7-10, based on typical dead and live loads for office buildings. In addition, to ensure that the baseline lateral stiffness and strength of all the systems were comparable, all buildings were designed for a basic wind speed of 115-mph for strength and 90-mph (50-year wind) for serviceability, per ASCE 7-10, and an interstory drift limit of $h/400$. Steel frame components were designed following conventional design approaches per the AISC Steel Construction Manual.

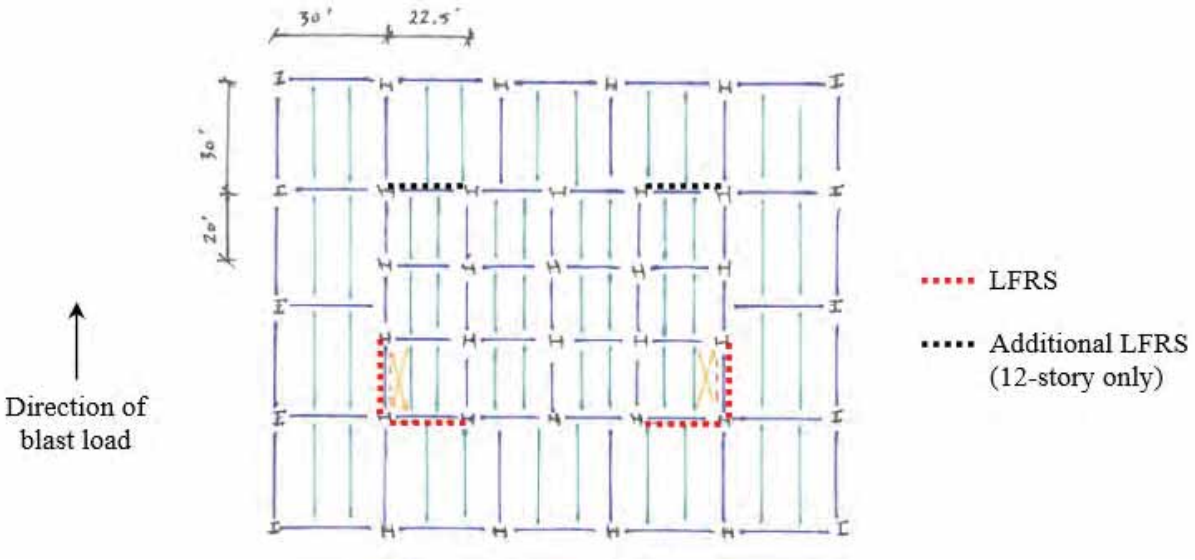


Figure 2 Baseline floor plan for analytical models.

Blast Resistant and Conventional Façade Design - Two façade types were considered in this study: conventional (non-hardened) and blast-resistant (hardened). The non-hardened façade consisted of 8-inch deep cold formed steel stud (CFSS) slab-bypass (balloon construction) wall system designed for conventional loads only (e.g. gravity, wind, seismic, etc.) per ASCE7. The hardened façade consisted of rectangular steel HSS tubes, spaced at 4-ft on center, with brick veneer wall and/or metal plate (see
Figure 3). In addition to conventional loads, the hardened façade, was designed to resist a specified design blast load using the single-degree-of-freedom (SDOF) methodology.

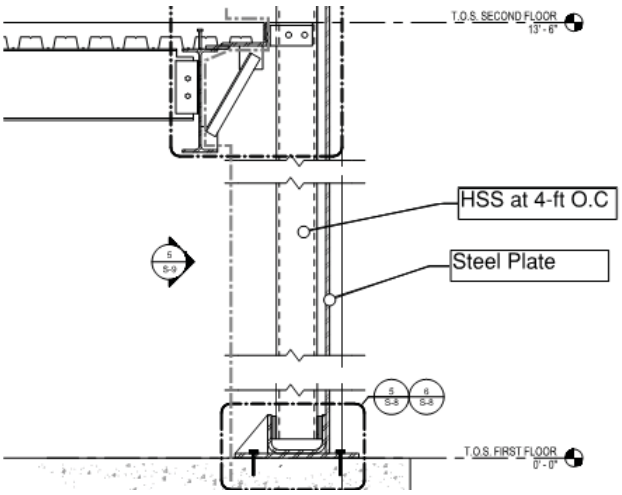


Figure 3 Partial section of hardened façade made with HSS tubes and metal plate.

Nonlinear Dynamic (NLD) Analysis - As the first step of the uncoupled analysis approach, the dynamic reactions from the façade components due to the design blast load were determined by SDOF analysis, using the SDOF Blast Effect Design Spreadsheet (SBEDS). The CFS and HSS studs of the non-hardened and hardened façade systems, respectively, were analyzed as simply-supported beams, subjected to uniform lateral blast loads. Dynamic reactions from these SDOF analysis (example in in Figure 4) were imported into structural analysis and design software and applied to the structural frame as load time-history functions for each of the analysis cases shown in Table 1. The dynamic reactions from the façade were applied as lateral point loads on the floor diaphragms on the blast loaded side of the building, as depicted in Figure 4.

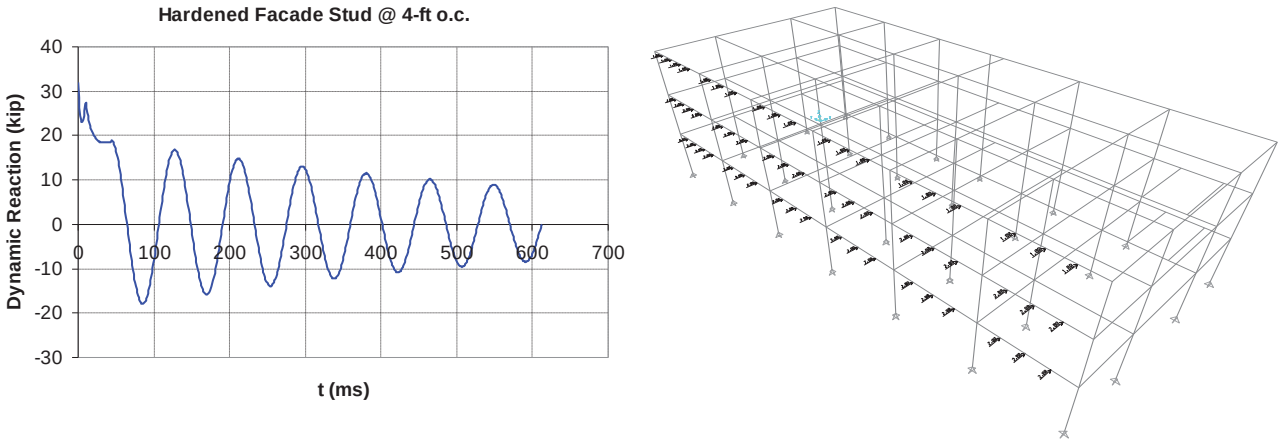


Figure 4. *Hardened façade dynamic blast reaction from SDOF model (left), and façade reactions applied to building model (right).*

For the three and six-story buildings, a uniform façade system was used assumed around the building perimeter and the maximum blast load at ground level was applied uniformly over the reflected face of the building. For the 12-story building, however, dynamic reactions were determined considering the variations in the standoff and the angle of incidence of the blast load over the height of the building, which resulted in decreasing blast pressures at the higher stories.

Nonlinear Model - Material nonlinearity was incorporated into the analyses by using the discrete plastic hinge approach per Chapter 5 of ASCE 41 for NLD analysis of steel frames. ASCE 41 provides modeling parameters in the form of “Hinge Definitions” which define resistance deflection curves that approximate the non-linear response of numerous types of components such as connections, beams, columns, slabs, and braces.

TEST SERIES

A test program was initiated to perform a series full-scale blast tests on a typical three-story steel Conventional Braced Fame (BF); Test 1 with a conventional façade and Test 2 with a blast-hardened façade. The main goal of the test series is to obtain a better understanding of the lateral response to blast loads and adequacy of steel buildings for State Department occupancy. The data obtained from the tests will be used to validate and update the findings of the analytical study, and possibly to improve non-linear modeling parameters for plastic hinges specifically for lateral response to blast loading. Test 1 was performed in the fall of 2014 at the Energetic Materials Research Testing Center (EMRTC). The main goal of this test was to investigate and validate the findings of the analytical study that indicate that conventional façades exposed to blast loads (of the magnitude used in this study), fail very quickly, and therefore, do not transfer significant reactions to the LFRS.

Test Specimen - The test structure consists of a 3-story conventional steel BF with 3-bays in the long direction and 2-bays in the short direction as shown in
Figure 5. The typical floors consist of reinforced concrete (RC) composite metal decks supported on steel beams. The roof consists of corrugated metal deck supported on open-web steel joists (OWSJ). The floor-to-floor height of the structure is 13.5-ft and the bay spacing is 20-ft. The LFRS consists of chevron braced frames and the façade system is a conventionally designed and detailed full-height glass curtainwall. The entire structure and façade was designed for conventional wind and gravity loads only. The façade glazing system consisted 7.5 inches deep aluminum mullions with 1 inch (nominal thickness) Insulated Glass Units (IGU) with non-laminated Tempered Glass.
Figure 6 shows a picture of the test specimen prior to the test indicates the location of braced frames and shows the direction of travel for the applied blast load.

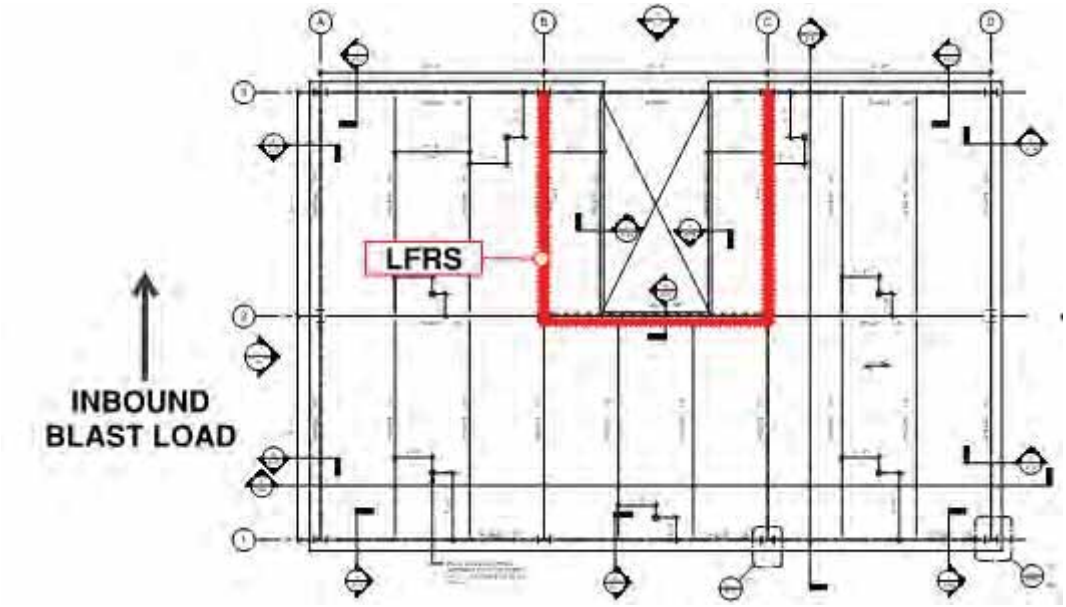


Figure 5 Test structure – floor plan.



Figure 6: Test structure and instrumentation tower.

Instrumentation – The test structure was instrumented with a combination of pressure, strain and deflection gauges, specifically set up to measure the following aspects of the lateral response of the structure: (1) applied blast load, (2) frame lateral displacement in time at each floor level and the roof (drift), (3) local damage of critical elements, and (4) Load transfer between the façade and the structural frame.

Twenty-one (21) pressure gauges were installed on and within the structure to measure exterior reflected and incident blast pressures, as well as internal pressures. Eleven (11) reflected pressure (RP) gauges were placed on the directly-loaded face of the building as shown in
Figure 7 to determine the reflective blast load time-histories at each floor. Two (2) of the 11 pressure gauges were placed at column lines B and C at mid-height between the 3rd floor and the roof to try to quantify any clearing effects. Sixty-three (63) strain gauges (60 full-bridge strain gauges and 3 strain rosettes) were used to measure reactions and internal forces for various components and connections of the main LFRS.

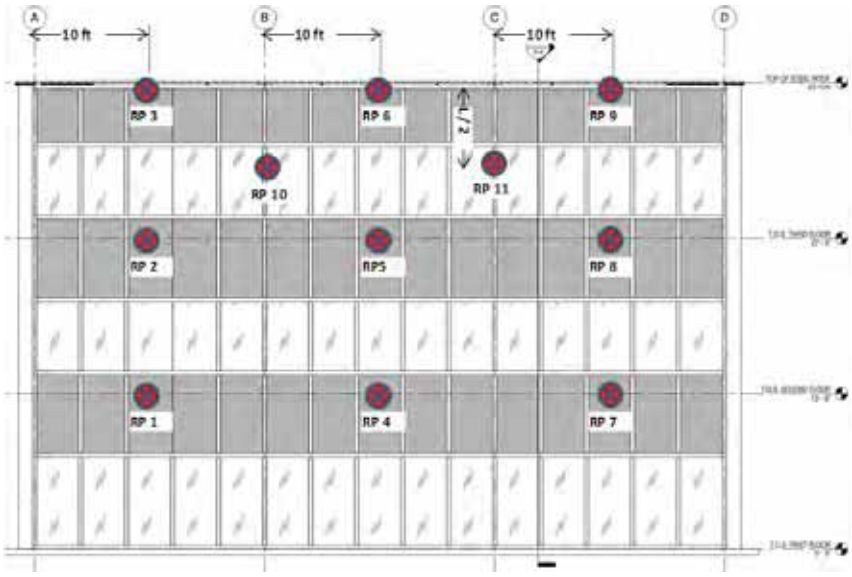


Figure 7: Location of reflected pressure gauges on south elevation.

Nine (9) displacement gauges were used to measure the lateral (drift) displacement of the structure. The displacement gauges were located on the backside (opposite the blast location) of the test structure as shown in

Figure 8. Since the lateral displacement of the structure is one of the critical measurements for this test, a combination of digital laser gauges, scratch gauges and string potentiometers were used on both sides of the structure centerline to provide redundancy and verification. In addition, by utilizing two lines of gauges, any torsion during the test could also be measured.

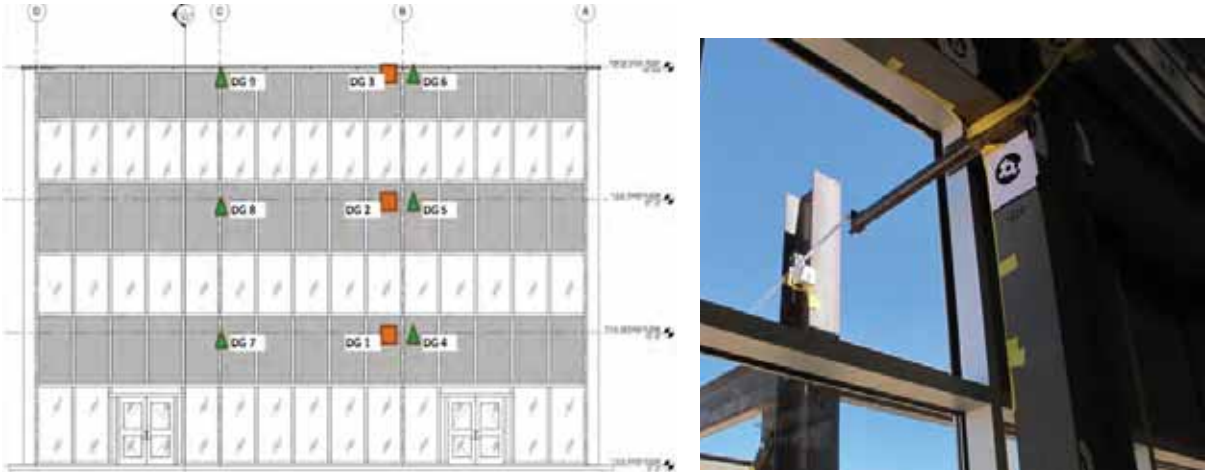


Figure 8: Location of displacement gauges on north side of structure (left), installation of scratch gauge (right).

Finally, load cells were placed at the connections of two (2) curtainwall mullions on the reflected face at the 2nd floor level to measure the lateral dynamic blast reactions transferred from the glass curtainwall to the structure.
Figure 9 shows the location and installation of one of the load cells.

ANALYSIS DATA

In order to be consistent in the evaluation of the different LRFS and to be able to relate their performance to existing consensus documents, PEC used the Structural Performance Levels given in ASCE 41 to evaluate the performance of the LFRS. The structural performance levels in ASCE 41 are defined in terms of damage description of the components of the LFRS along with recommended drift limits for seismic response of buildings. S-1 is the best possible performance and

represents a structural condition after the event where Immediate Occupancy (IO) is possible (no damage). S-5 is the least acceptable performance and represents a structural condition after the event where collapse is prevented (Collapse Prevention (CP)), but is heavily damaged, such that the structure can be evacuated, but occupancy and re-use is unlikely without extensive and substantial repairs. A summary of the predicted analytical results for the range of structural systems with hardened façades considered in this study is provided in Table 2, below, followed by detailed results for select analysis cases. Analyses with conventionally designed façades are omitted as they all resulted in no damage to the LFRS.

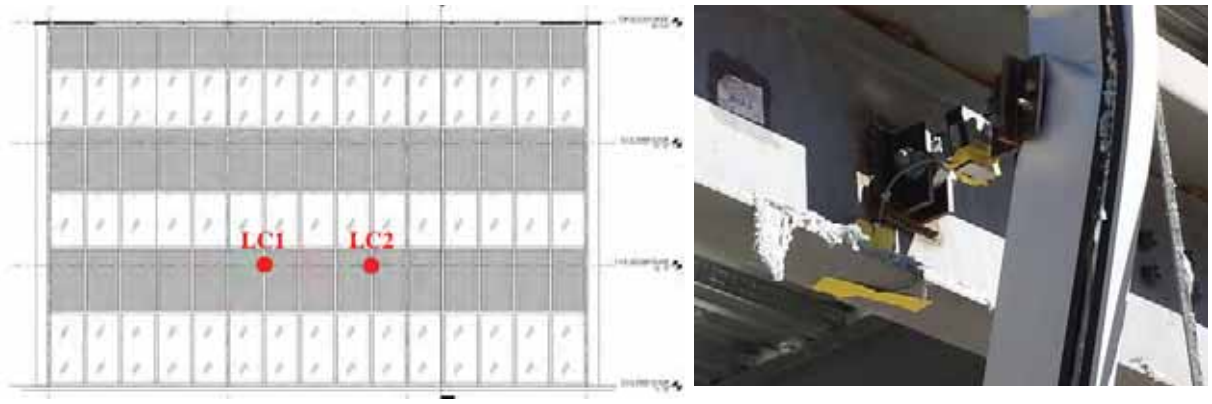


Figure 9: Location (left) and installation (right) of load cells to measure curtainwall blast reactions.

LFRS	Structural Performance	LFRS Damage Notes
3-Story Chevron	● > S-5	Complete damage, failure of braces and beam connections at bracing locations
6-Story Chevron	● S-4	Partial damage, failure of upper floors bracing components, moderate axial Loads in adjacent column
12-Story Chevron	● S-1	No damage
3-Story X-Braced	● > S-5	Complete damage, failure of braces and beam, high axial Load demands in adjacent columns
6-Story X-Braced	● S-4	Partial damage, failure of upper floors bracing components, high axial load demands in adjacent columns
12-Story X-Braced	● S-2	Little Damage, failure of braces in upper two stories, moderate to low axial demands on adjacent columns
6-Story Diagonal-Comp	● S-4	Partial damage, failure of one bracing component at 5ht floor, high axial loads in remaining bracing elements, moderate axial loads in adjacent columns
6-Story Diagonal-Ten	● S-4	Partial Damage, failure of bracing component at upper floors, moderate to high axial loads in adjacent columns
6-Story X-Braced (2story)	● S-2	No damage, moderate to high axial demand on bracing components and adjacent columns
6-Story MF	● S-1	No damage, low flexural demands in moment connections, low axial demands on columns
6-Story EBF	● S-3	Little Damage, shear failure of link beams at middle floors, high axial demand in some bracing components, and in lower adjacent columns

Table 2 Summary of results – analytical study for blast frame response using hardened façades.

The three-story X-Braced frame analysis predicted in significant damage of the LFRS for the case with a blast-hardened façade. Based on the performance levels in ASCE 41, this building would be considered greater than category S-5 and would have a high potential for collapse. The failure predicted failure progression begins with compression failure of the bracing components during inbound response and compression failure of the remaining bracing elements during rebound. After the braces exceed the allowable limits, the columns and gravity beams become the main contributor to lateral strength, acting, effectively, as a moment frame. As a result, some of the weaker (perimeter) columns experience axial demands estimated at

62% of their capacity. The peak sway drift was 2.1-in., measured at the roof level. Figure 10 shows the final stage at failure.

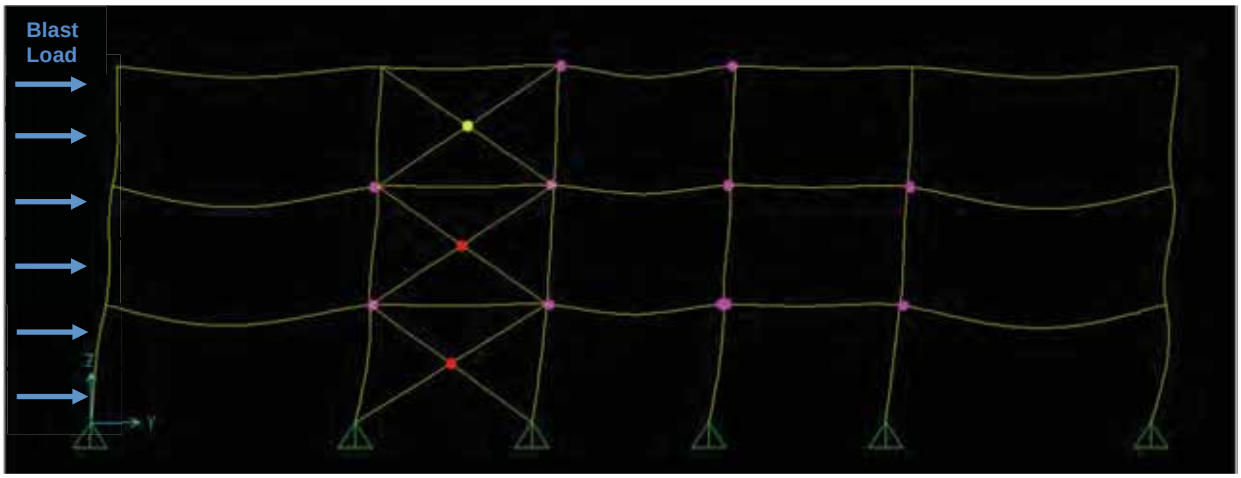


Figure 10: X-brace 3-story frame final stage, red and yellow dots represent potential location of failure (plastic hinges).

The 6-Story X-Braced frame resulted in partial damage of the LFRS. This structure showed damage of the bracing components in the upper floors but that damage should not be enough to compromise the ability to carry gravity loads. In addition, the system was able to resist subsequent cycles of response after the bracing elements in the upper floors reached their failure limit. Figure 11 shows the final stage at failure. The peak sway deflection was 4.3 inches measured at the roof level.

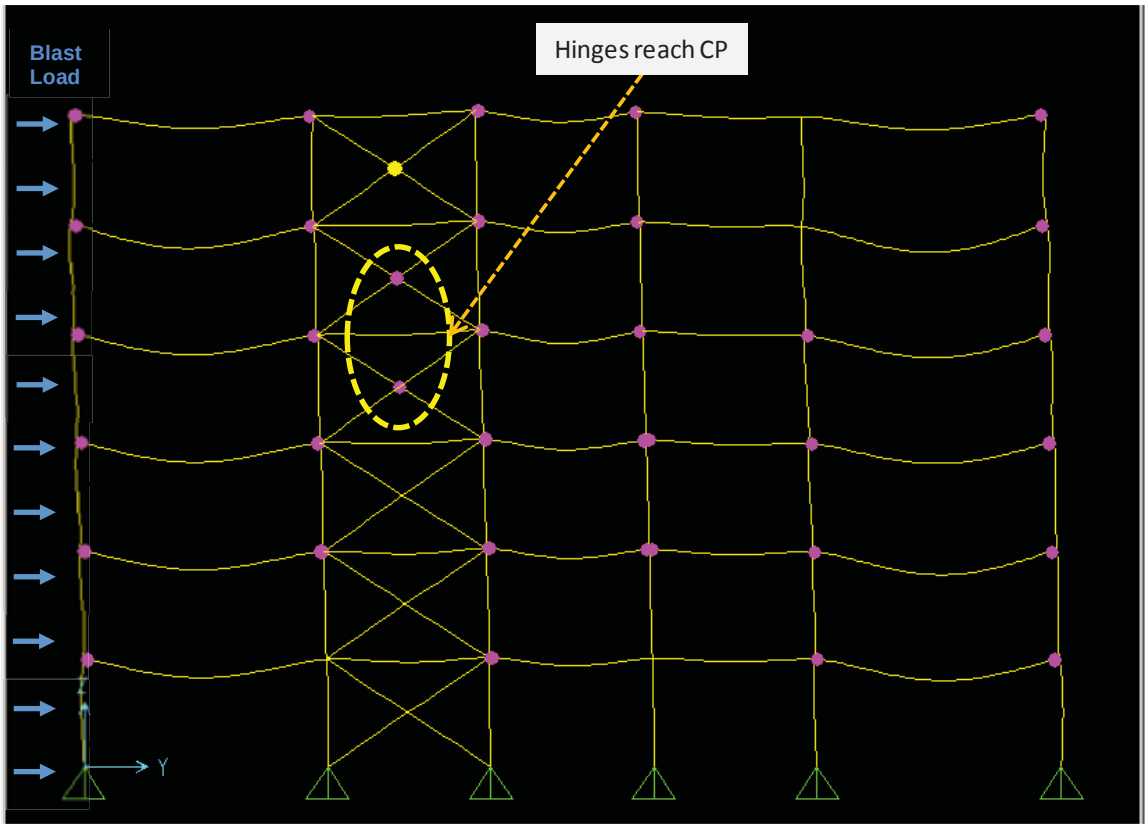


Figure 11: X-braced 6-story frame final stage – CP = Collapse Prevention Limit.

TEST 1 DATA

Drift Displacement Response: Nine (9) displacement gauges consisting of string potentiometers and scratch gauges were used to measure the lateral (drift) displacement vs. time of the structure (as shown in

Figure 8). A summary of the measured peak drift displacements resulting from the blast response is provided in Table 3. Figure 12 illustrates the measured displacement histories at the roof level.

Gauge	Type	Floor	Peak Inbound Drift	
			Displacement [in]	Time [msec]
DG1	String Potentiometers	2nd	0.4	127.7
DG2	String Potentiometers	3rd	0.9	121.3
DG3	String Potentiometers	Roof	1.3	116.2
DG4	Digital Scratch Gauges	2nd	0.6	140.9
DG5	Digital Scratch Gauges	3rd	0.9	120.6
DG6	Digital Scratch Gauges	Roof	1.3	115.1
DG7	Digital Scratch Gauges	2nd	0.6	140.1
DG8	Digital Scratch Gauges	3rd	0.8	141.4
DG9	Digital Scratch Gauges	Roof	1.3	126.3

Table 3: Measured sway displacements.

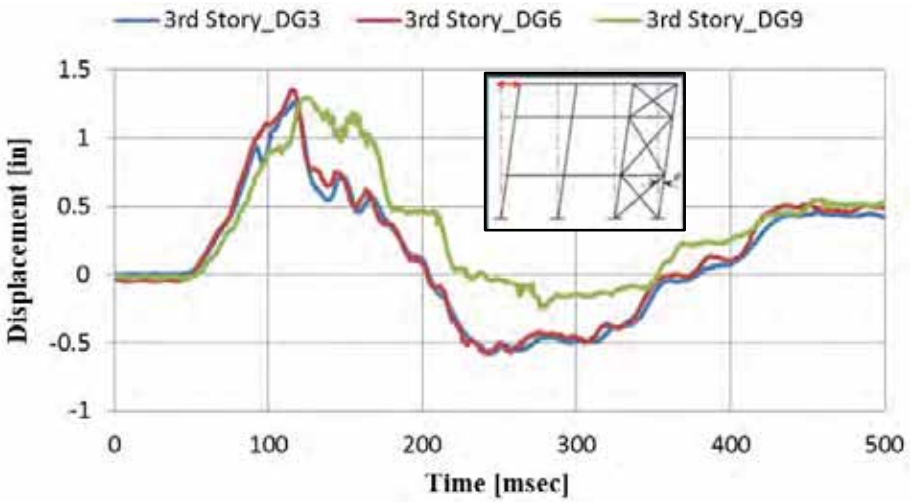


Figure 12: Lateral displacement history – 3rd story (roof).

Building Envelope Damage: As expected, the exterior curtainwall failed shortly after arrival of the blast load. Figure 13 illustrates the post-test condition for the directly-loaded face of the building. The roof system was also noticeably damaged but remained in place. In general, bridging members between roof joists were severely damaged and, in many cases, completely failed. Several joists experienced buckling of web struts and bottom chords members (see Figure 14) and the seated connections were damaged in several locations. Finally, the façade elements showed a variety of failure modes including both local and global (lateral torsional) buckling, tension rupture, block shear rupture at connections, and failure of stack joints. In addition, several members failed completely, detaching from the structure and landing in the space around the test structure. Figure 15 illustrates the post-test condition of the façade elements and connections.



Figure 13: Post-test condition of reflected face (south elevation).

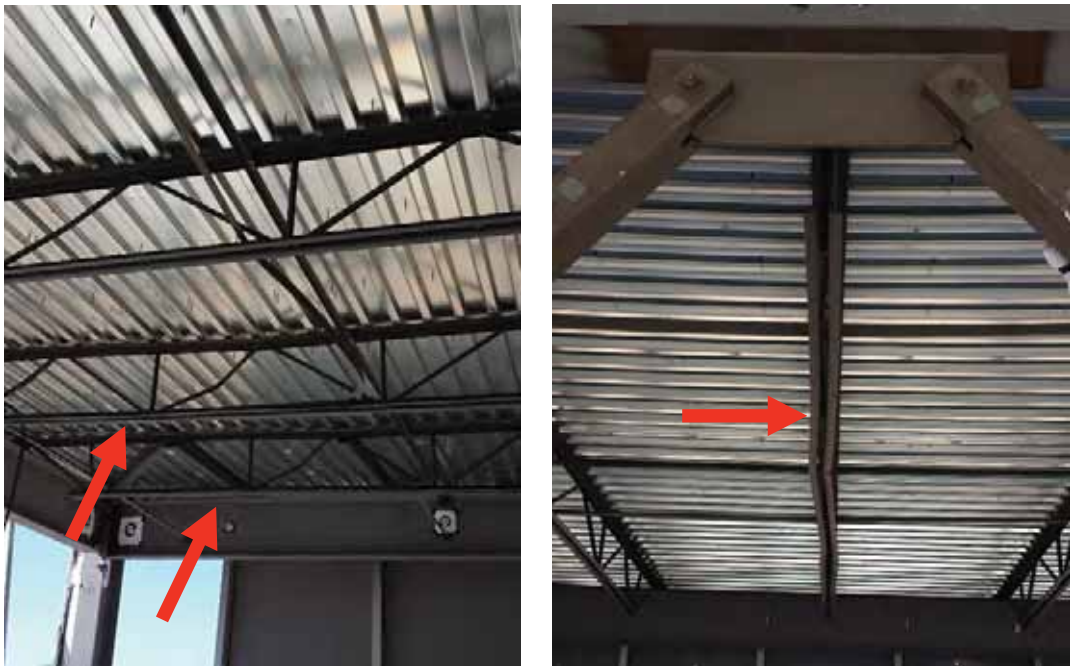


Figure 14: Post-test roof joist condition buckling of web members (left) and buckling of bottom chord (right).



Figure 15: Post-test façade condition.

Load Cell Reactions: The average peak force measured by the load cells was approximately 17-kip. Complete reaction histories are provided in Figure 16.

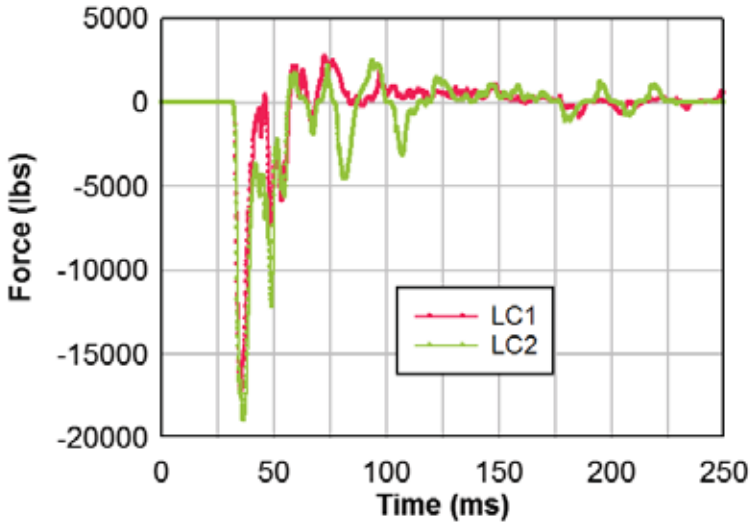


Figure 16: Measured dynamic façade reactions at load cells.

Lateral Force Resisting System (LFRS): There was no damage observed on components of the LFRS (connections, braces, columns, welds, etc.). Figure 17 shows the post-test condition of the apex connection at a 3rd floor brace. This photo represents the typical post-test condition of the braces throughout the structure.

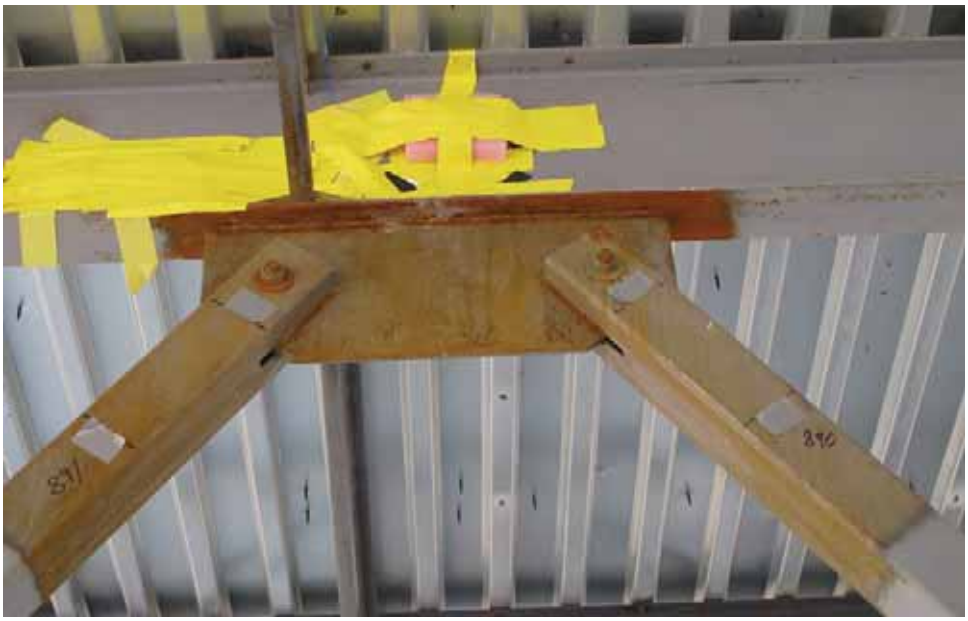


Figure 17: 3rd floor brace – apex connection.

DISCUSSION OF RESULTS FROM ANALYTICAL STUDY AND TEST 1

Effects of Blast-Resistant (Hardened) vs. Conventional (Non-Hardened) Façade Systems – In the analytical study, all three and six-story buildings, shown in Table 2, were analyzed dynamically for reactions transferred from blast-loaded hardened and conventional façade systems. The results of SDOF analyses of the façade components showed that the blast-loaded conventional façade components fail very quickly. As a result, the dynamic reactions transferred to the supporting structure are minimal and do not cause significant response of the LFRS. The hardened façade system, designed to resist the design blast load without failure, absorbs and transfers a significant amount of energy from the directly applied blast loads to the supporting frame structure. Consequently, the LFRS is subjected to high dynamic reactions that induced significant lateral response (drift and component damage).

Test 1 showed that the response of the LFRS in a typical office building with a conventional glass façade results in very low lateral drift values (per ASCE 41) and no apparent damage of the structural components when exposed to blast loads in the range used for this test. This confirms the findings from the analytical study that conventional façade systems fail very early in the response, reducing the dynamic reactions transferred to the structure. Furthermore, the dynamic reaction histories measured with the load cells (see
Figure 9) at the mullion connections were used to calculate the impulse transferred to the structure by the glass façade. Since the diaphragm-level connections between the curtainwall and the structure are the only connection points from façade to structure, this is a direct representation of the load transferred by the façade. As shown in Figure 18, the measured impulse calculated from the dynamic reactions is approximately 17-psi-msec, which is significantly less (by an order of magnitude) than the reflected blast impulse measured on the directly-loaded face of the structure.

Effectiveness of Method of Analysis – The lateral displacements measured from the test (Figure 12) were compared to pre-test analyses of the test structure performed using the analytical approach described above. The average peak inbound lateral (drift) displacements measured with string potentiometers and scratch gauges are provided in **Error! Reference source not found.**. The inbound lateral (drift) displacements measurements were very similar to the upper bound values of the expected range of performance based on pre-test analytical predictions (see **Error! Reference source not found.**).

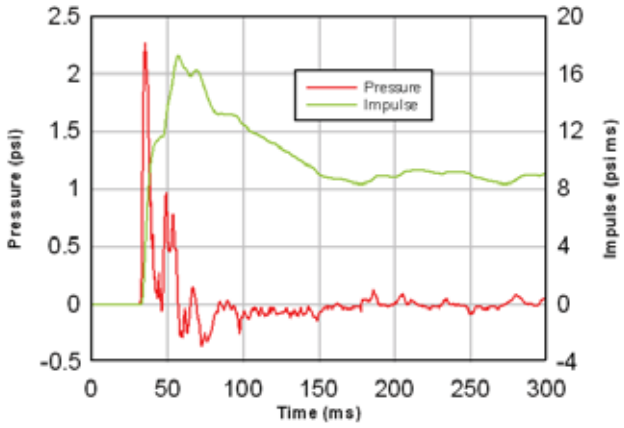


Figure 18: Calculated impulse transferred by façade to structure.

Floor	Post-Test Measurement
	Peak Displacement [in]
Roof	1.3
3rd	0.9
2nd	0.5

Table 4: Average of measured peak inbound frame lateral displacements.

Floor	Pre-Test Calculation
	Peak Displacement [in]
Roof	0.12 to 1.20
3rd	0.11 to 1.11
2nd	0.06 to 0.50

Table 5: Pre-test inbound frame lateral displacements – range of response.

In **Error! Reference source not found.**, the upper bound values of the pre-test predictions were based on a load case that included direct blast loading of the exposed faces of structural elements after the rapid failure of the façade in addition to the dynamic reactions from the façade. The lower bound values were based on loading that included only the dynamic reactions of the façade, without the direct load on exposed elements. Based on the similarity of the measured frame lateral displacements with the upper bound pre-test values, and the low measured impulse transferred from the façade into the structure (see Figure 18), it appears that a significant portion of the load that caused the drift response of the structure was due to direct loading from the blast after rapid failure of the façade (Conventionally designed non-laminated IGU panes).

In addition, the comparisons of test results and pre-test analyses showed that the lateral stiffness of the LFRS can be captured reasonably accurately with standard structural design software and analysis assumptions as demonstrated by the results of the pre-test analyses. For example, the natural period of the lateral response measured during the test was approximately 380-msec (see Figure 19) which is only 5% different from the calculated value of 400-msec in the pre-test analysis. Since the mass or weight of the test structure was carefully controlled and accurately captured in the pre-test model, the similarity in natural periods (test vs. pre-test calculations) is an indication that the lateral stiffness of the LFRS calculated with the pre-test analysis is comparable to the tested structure.

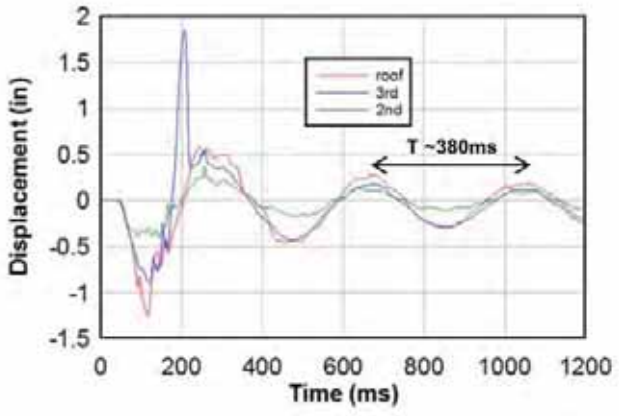


Figure 19: Measured natural period of response.

CONCLUSION AND FUTURE WORK

An analytical study, performed using conventional structural analysis methods and tools, evaluated the lateral response of typical steel LFRS against the effects of blast loads using conventional and blast-hardened façade systems. The results showed that conventionally designed blast-loaded façades fail almost instantaneously and do not impose significant demands or cause significant damage to the LFRS. Analyses also showed that conventionally-designed (i.e. non-seismic) steel braced frames of three-stories with hardened façades could be vulnerable to collapse when exposed to blast loads with impulses between 300 and 350 psi ms, which are typical of State Department for overseas buildings. The State Department for overseas buildings blast impulse in general can be two or three times higher than typical blast impulse loads used in the design of Federal and Military facilities.

Test 1 verified the findings from the analytical study that conventional façades fail rapidly under blast loads and, as a result, do not transfer high lateral reactions to the LFRS. It is important to point out that the catastrophic failure of the conventional façade system would produce blowout of the façade components into the interior space of the building resulting in high levels of injury and lethality for the building occupants creating an unacceptable environment and providing an inadequate level of protection. However, since the focus of this study is on the effects of blast-loaded façades on the LFRS, this test was important as it defines the baseline structural response to blast loading for the case where a conventional façade is used. In addition, the displacement data obtained from Test 1 also demonstrates that the simplified method of analysis used for the analytical study reasonably captures the response of the building frame.

Preparation for Test 2 is in progress. The three-story structure used in the first test will eventually be retrofitted with a blast-resistant (hardened) façade, capable of resisting the blast threat used in this test program. The main goal of Test 2 will be to investigate the findings of the analytical study that indicate that blast-resistant building façades designed to fully resist the blast loads used in this effort can transfer significant reactions to the LFRS that may cause failure of critical components in conventionally-designed steel braced frame structures of three-stories or fewer. The planned blast-resistant façade for Test 2 will consist of a heavy glazed-aluminum curtainwall system on the directly loaded (reflected) face of the building, and heavy steel frame with metal panels on all other faces. To replicate typical requirements of U.S. diplomatic buildings, forced-entry (FE) requirements will also be incorporated on the first story. Figure 20 provides an illustration of the planned concept for Test 2.



Figure 20: Rendering of test structure for upcoming Test 2 using a hardened façade.

ACKNOWLEDGMENTS

We would like to acknowledge State Department's Bureau of Diplomatic Security Research and Development branch, and The Energetic Materials Research and Testing Center (EMRTC) for their contributions to this effort.

REFERENCES

American Institute of Steel Construction (AISC), 2010, Seismic Provisions for Structural Steel Buildings, AISC.

American Institute of Steel Construction (AISC), 2011, Steel Construction Manual, 14th Edition, AISC.

American Society of Civil Engineers (ASCE), 2010, Minimum Design Loads for Buildings and Other Structures, ASCE 7, ASCE.

American Society of Civil Engineers (ASCE), 2007, Seismic Rehabilitation of Buildings, ASCE 41, ASCE.

Department of Defense (DoD), 2014, "Unified Facilities Criteria (UFC) 3-340-02: Structures to Resist the Effects of Accidental Explosions," DoD.

Federal Emergency Management Agency (FEMA), 2000, Prestandard and Commentary for the Seismic Rehabilitation of Buildings, FEMA 356, FEMA/ASCE.

McKay, A., Bazan, M., Gomez, M., Marchand, K., Steel Frame Structure Performance in Blast Environments, Task 2 Analysis and Final Reporting, San Antonio, Texas, USA, December 2011.

McKay, A., Jones, C., Bewick, B., Test Plan Report for: Full Scale Test of Steel Braced Frame Structure, San Antonio, Texas, USA, March 2013.

McKay, A., Jones, C., Test Results Report for: Full Scale Test of Steel Braced Frame Structure, San Antonio, Texas, USA, March 2015.

McKay, A., Jones, C., and P. Benshoof, Investigation of Conventionally Designed Steel Frame Structures' Inherent Resistance to Lateral Blast Loading, Test 1 Results. Paper presented at the Military Aspects of Blast and Shock Symposium (MABS 24), Halifax, Nova Scotia, Canada, September 2016.

U.S Army Corps of Engineers Protective Design Center (PDC), 2008, Methodology Manual for the Single-Degree-of-Freedom Blast Effects Design Spreadsheets (SBEDS), TR-06-01 Rev 1.

U.S Army Corps of Engineers Protective Design Center (PDC), 2008, Single Degree of Freedom Structural Response Limits for Antiterrorism Design), TR-06-08 Rev 1.

LIGHTNING PROTECTION AS BUILDING ENVELOPE



Jennifer Morgan
East Coast Lightning Equipment, Inc.
jen@ecle.biz



Michael Chusid, RA FCSI CCS
Building Product Consultant
michael@chusid.com

ABSTRACT

A building's envelope mitigates the effects of meteorological phenomena – including lightning – upon the structure and its occupants and contents. The risk of lightning damage is increasing due to climate change and our growing dependence on electronic devices that can be destroyed by electrical surges. New and underutilized techniques offer improvements to lightning protection systems (LPS) and advance best industry practices. These include risk assessment protocols, use of creative and decorative strike termination devices instead of standard air terminals (lightning rods), compliance with sustainability and resilience standards, lightning monitoring and surveillance systems, testing with triggered lightning, and risks associated with unconventional lightning protection devices. The authors urge design and construction professionals to take proactive measures to improve lightning protection of the built environment.

KEYWORDS

aesthetics, climate change, codes - standards - rating systems, extreme environments, professional standard of care, resilience, risk assessment

INTRODUCTION

Critical analysis of lightning protection is missing from most discussions about building facades. This is a dereliction of the design community's professional responsibility as lightning endangers public health, safety, and welfare (HSW). The magnitude of destruction caused by lightning is often overlooked because lightning strikes typically occur one at a time and in scattered locations; they command fewer headlines than do disasters such as earthquakes, floods, and hurricanes that effect many people and buildings in single events (Fig. 01). Yet lightning is a worldwide scourge (Fig. 02); lightning strikes 25 million times a year in the United States alone and causes damage in excess of five billion dollars (US) annually.

This destruction is likely to increase due to two trends:

- **Climate Change:** Global warming has been shown to increase lightning frequency and intensity. Recent hurricanes provide a dramatic illustration of this; Hurricane Harvey, for example, made landfall with "non-stop lightning" (*Washington Post*) (Fig. 12).
- **Vulnerability of Electronically-Controlled Systems and Digital Devices:** Buildings are increasingly dependent upon systems and devices that can be damaged by electrical surges from lightning (Fig. 3). The grounding systems installed as part of the electrical power systems in buildings are insufficient to prevent lightning damage.

Recognizing lightning protection is within province of facade tectonics enables architects to influence layout of LPS for compatibility with aesthetic intent, take advantage of new and underutilized techniques, and meet industry's standard of care.

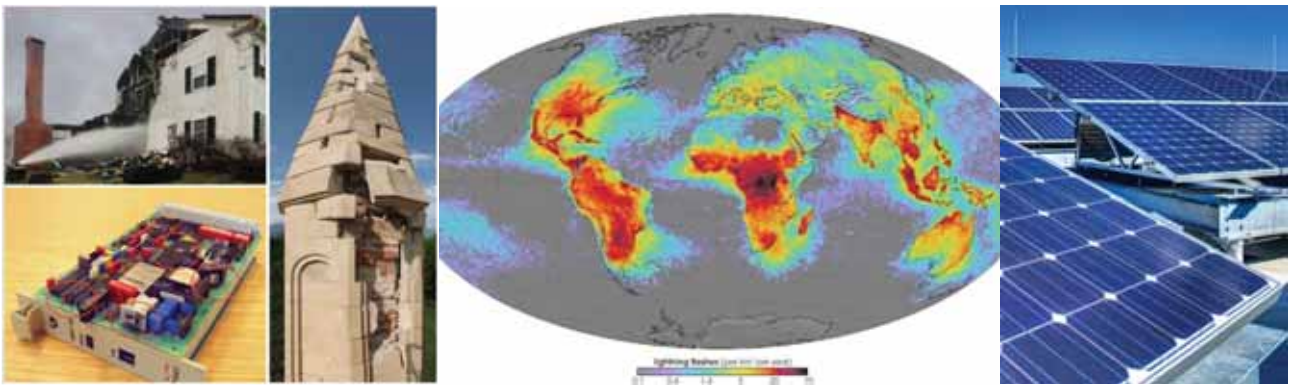


Figure 1 (Left): Lightning damage includes building fires, structural damage, and damage to electronic devices. It also causes wild fires, damage to trees and infrastructure, injuries, and death. Figure 2 (Center): Map shows global distribution and density of lightning strikes (NASA). Figure 3 (Right): Rooftop equipment, including solar collectors, must be protected.

BACKGROUND

The basis for reliable and economic LPSs was established in the 18th Century by Ben Franklin and others; since then it has been vetted, refined, and codified. Accepted North American standards applicable to buildings include:

- Canadian Standards Association / National Standard of Canada: CAN/CSA-B72-M87 – *Installation Code for Lightning Protection Systems*.
- Lightning Protection Institute: LPI 175 – *Standard of Practice for the Design – Installation – Inspection of Lightning Protection Systems*.
- National Fire Protection Association: NFPA 780 – *Standard for the Installation of Lightning Protection Systems*.
- UL, LLC: UL 96 – *Standard for Lightning Protection Components* and UL 96A – *Installation Requirements for Lightning Protection Systems*.

Lightning leaps through the atmosphere in step leaders about 150 feet long, then zig-zags to follow the electrical path of least resistance. This is modeled as a 300-foot diameter sphere rolling across surface of building; lightning can attach at any location where sphere touches a structure. Air terminals (colloquially known as “lightning rods”) are located in locations and at sufficiently close spacings to assure rolling sphere encounters LPS before sphere contacts building. LPS then provides highly conductive path to divert lightning into grounding electrodes. Other essential components of LPS include bonding to plumbing, structural system, and other metal bodies in structure and surge protective devices on power and communication lines entering building (Fig. 03 and 05).

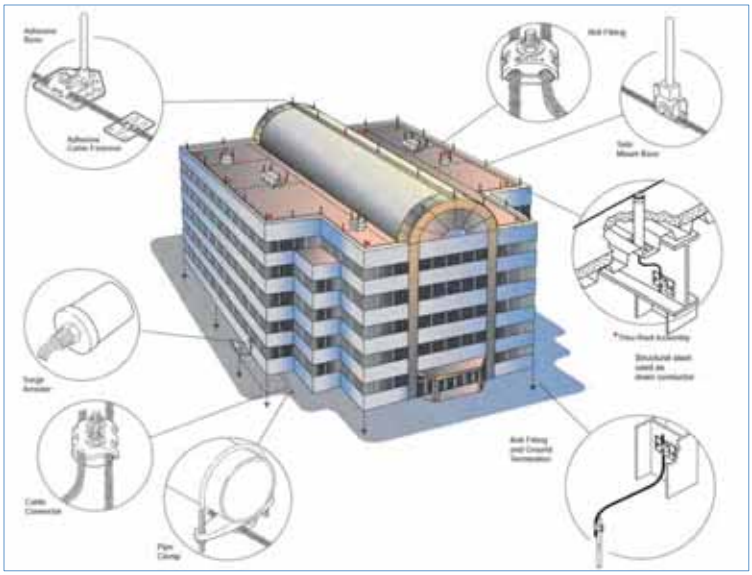
Lightning Protection Institute Inspection Program (LPI-IP) and UL each offer programs to certify or list qualified lightning protection designers and installers. They also offer building inspection services that can be incorporated into building commissioning to assure an installation complies with specified requirements.

By relying on the triad of standards - qualified specialists - and commissioning, most project specifications can reliably delegate LPS design to certified lightning protection specialists (http://www.constructionspecifier.com/wp-content/uploads/2015/08/264100-LightningProtection-guidespec.doc for non-proprietary guide specification).

Major model building and electrical codes *do not* require lightning protection systems. Model codes have requirements with respect to wind, rain, snow, temperature, humidity, and other weather phenomena, so it is difficult to understand lack of lightning-related code requirements.

A growing number of institutions and authorities having jurisdiction, however, do have LPS requirements. Examples include:

- Florida Building Code
- Illinois Capital Development Board
- New York School Construction Authority
- Port Authority of New York and New Jersey
- U.S. Department of Defense
- U.S. General Services Administration
- University of Virginia



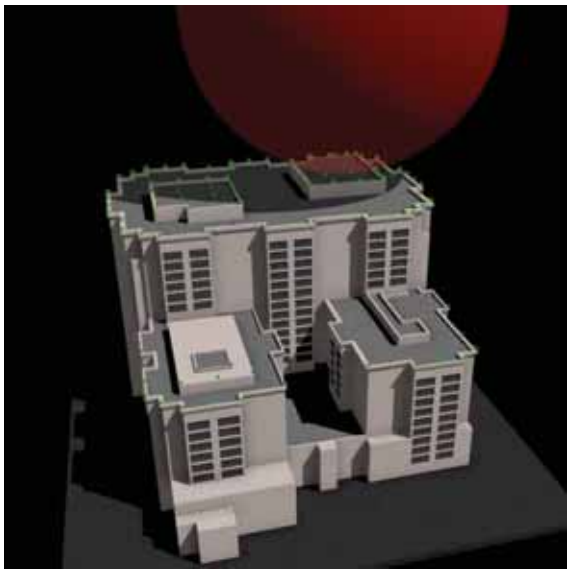


Figure 4 (Left): Drawing shows typical components of a lightning protection system. Components must comply with lightning protection standards; devices intended for ordinary electrical wiring are not sufficient for lightning. Illustration demonstrates how structural steel framing members can be used as down conductors between air terminals and ground electrodes (East Coast Lightning Equipment, Inc.). Figure 5 (Right): Rolling sphere method is used to model how lightning attaches to structure. Air terminals, shown in green, must be located to prevent 300-foot diameter sphere from making contact with structure (Lightning Safety Alliance).

An absence of code requirements does not alleviate design professional's responsibility to consider lightning when designing buildings. Codes establish *minimum* levels of performance; licensed professionals have obligation to go beyond code requirements when required for HSW.

This mandate is also written into the professions instruments of service. For example, American Institute of Architects (AIA) D200 - *Project Checklist* that says architects are to, "obtain seasonal climate and microclimate data from the weather service," as part of site analysis. Knowing a site's ceraunic characteristics obligates designer to respond appropriately.

AIA B101 - *Standard Form of Agreement Between Owner and Architect* says, "architect's basic services consists of… electrical engineering services." If an architect expects electrical engineering consultants to take responsibility for lightning protection, clear instructions should be given and expectations documented. Electrical engineers may feel they have met requirements by adherence to the National Electrical Code (NEC), but the NEC grounding requirements are insufficient for the tens of thousands of amps that surge through a lightning strike in microseconds. As stated in the International Association of Electrical Inspectors (IAEI) handbook *Soares Book on Grounding and Bonding*, the "…installation of a lightning protection system is much different from the installation of electrical service wiring." Furthermore, "…specialized material and installation methods such as that specified in NFPA 780 and UL 96 are required and the system should only be installed by qualified personnel trained and certified in the installation of lightning protection systems."

Some people assume lightning protection should be electrical engineers' responsibility because it relates to electricity. This is akin to arguing that roofing is plumbing engineer's responsibility because it relates to water. LPSs and electrical power systems need common grounds, but are typically designed, installed, and function as separate entities.

RISK ASSESSMENT

The standard of care is utilization of NFPA 780's Annex L – "Lightning Risk Assessment." It recommends an LPS when a structure's vulnerability to lightning is greater than its tolerable risk. Vulnerability is determined by lightning density maps and structure's area, height, topography, and proximity to taller structures or trees. Risk is affected by conductivity and combustibility of roof and structural system, value and combustibility of building content, ease of evacuation, required continuity of operations, and environmental consequences of lightning strike.

Regardless of lightning risk assessment results, NFPA recommends LPS if any of following conditions apply:

- Large crowds
- Continuity of critical services
- High lightning flash frequency
- Tall isolated structures
- Explosive or flammable content
- Irreplaceable cultural heritage

Calculations for NFPA's "Simplified Risk Assessment" can be performed manually or with a simple spreadsheet. Alternatively, online calculators are available that allow project data to be entered, calculations performed, and a written report downloaded in a matter of a few minutes (Fig. 06).

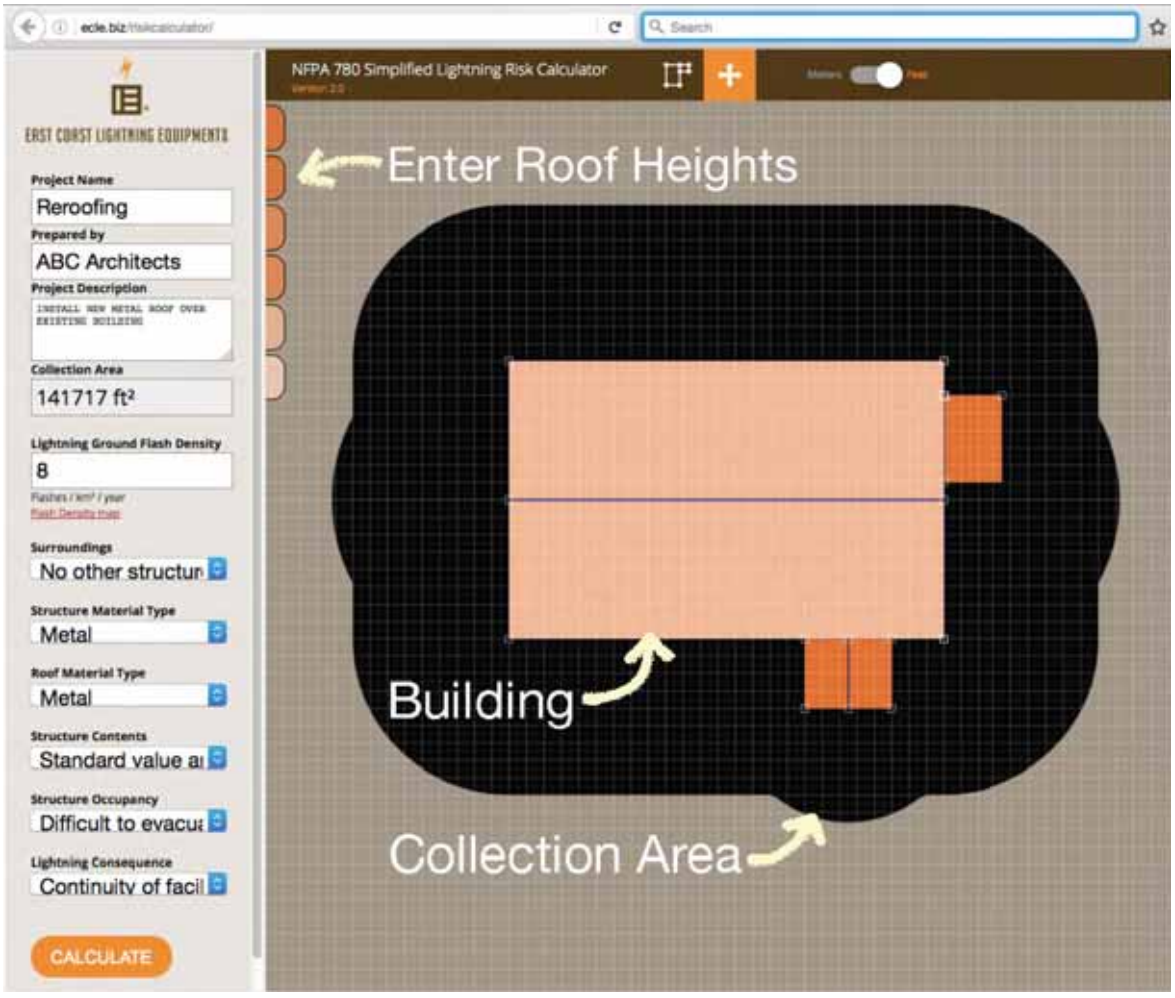


Figure 6: Screenshot shows data inputs required for NFPA 780 Simplified Risk Assessment. Entering project plan and roof heights enable app to calculate "collection area" in which lightning strikes can affect structure. Lightning ground flash density is read from maps. Appropriate descriptions are selected from drop-down lists to describe surroundings, structure and roof material types, relative value of contents, occupancy considerations such as ease of evacuation, the consequences of a lightning strike such as need for continuity of service or potential environmental hazards (East Coast Lightning Equipment, Inc.).

If NFPA algorithms indicate LPS is optional, report can be filed as evidence that designer has performed reasonable due diligence. If report indicates LPS is required, designer should discuss this with building owner and take appropriate actions.

Failure to observe best industry practices can expose design professionals to negligence claims due to personal or property injuries caused by lightning. Data on frequency of such claims is not available as most are settled out of court.

AESTHETICS

One reason architects cite for not using LPS is that air terminals and conductors cables detract from designers' aesthetic intent for buildings. Claiming LPS is ugly is, itself, an unattractive defense to negligence suits.

We have all seen poorly designed and carelessly installed LPSs, so perhaps should empathize with designers. In reality, most LPS installations detract only minimally or not at all from visual aesthetics. Air terminals are as thin as 3/8-inch diameter and as short as 10 inches tall; they fade to invisibility when seen at normal viewing distances. They can be set 24 inches back from roof perimeter, effectively hiding them from view as one approaches buildings. With modest attention to layout, they can be easily integrated into any design (Fig. 07 and 08).

Conductors can usually be installed within building walls; the braided cables are about as thick as fingers and allow lightning to pass without enough resistance to generate heat or ignite fire. If conductors must be exposed to view, they can usually be located to inconspicuously follow building lines, and a metal or finish used to harmonize with other building materials.

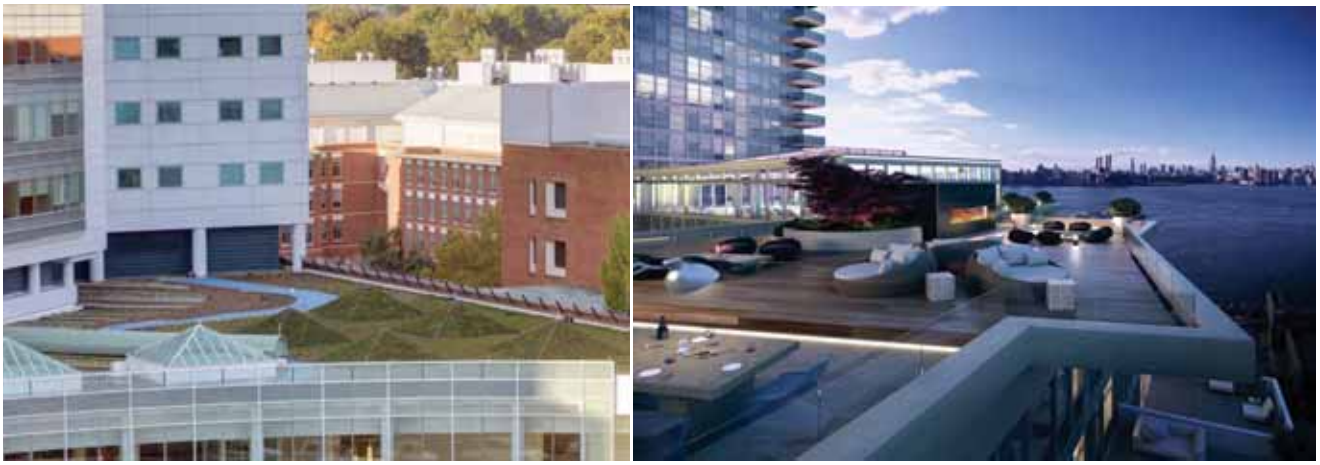


Figure 7 (Left): University of Virginia Hospital shows thoughtful integration of LPS into variety of building materials and conditions. Conventional air terminals are installed on parapet of glazed curtainwall. Air terminals on pyramidal skylights and planted features are taller than required by LPS standards to better suit visual scale of project. Rooftop conductors are installed underneath vegetated roof. The black, steel handrails at far side of green roof is used as strike termination device; its individual segments are electrically interconnected and made part of LPS without requiring surmounted air terminals. Conventional air terminals on building's upper roof are similar to those shown on background buildings (Photo Andrew Shurtleff). Figure 8 (Right): The LPS on rooftop terraces and gardens at 2 North 6nd Place, Brooklyn, NY is concealed in plain sight. Metal caps on glass balustrade segments are electrically interconnected and attached via slender metal balusters to LPS conductors installed underneath the roof paving (Architect: Stephen B. Jacobs Group).

An underutilized technique can make it unnecessary to install air terminals at all. Recognized lightning protection standards allow metal elements of buildings to be used as strike termination devices in place of air terminals as follows:

- "Metal parts of a structure that are exposed to direct lightning flashes and that have a metal thickness of 3/16 in. or greater shall only require connection to the lightning protection system…" NFPA 780 §4.6.1.4.
- "Metal handrails or guardrails, including metal cables, outside a zone of protection that are 1/8" thick or more shall not require air terminals..." UL96A §8.8.1.
- The strike termination devices have to be positioned where air terminals would have been required, made electrically continuous, and connected to the rest of LPS.

Strike termination devices can find suitable expression as a visually prominent crucifix mounted atop a church, brise-soleil that extends above eave line, rooftop handrails, helicopter landing pads, and other metal structures. Many of applications reduce construction costs by providing double-duty. Sculptures and decorative features can also serve as part of LPS (ecle.biz/products/decorative-sculpture-and-custom).

At 220 Central Park South, New York City, designed by Robert A.M. Stern, zoning limited building height to 950 feet and intense political pressure prevented issuance of variance for air terminals. Specially formed 3/16-inch thick metal copings will be used as strike termination devices to maximize usable building volume.

Rooftops in urban areas are being transformed into tenant amenities such as gardens, pools, and terraces. Railings, parapets, and balustrades surrounding these roofs are usually in locations that require air terminals. While this need can be tastefully satisfied by custom-designed air terminals (Fig. 09), other developers want to eliminate even these intrusions into their multi-million dollar views. At 2 North 6th Place, Brooklyn, NY, custom-fabricated metal caps on top of glass wind screens serve as inconspicuous strike termination devices (Fig. 08).

Rather than hiding or camouflaging air terminals, some designers use them for creative expression or insert them boldly and confidently into their designs (Figs. 10 and 11).







Figure 9 (Left): Custom designed air terminal is integrated into a glass balustrade and parapet (Photo Warren Lightning Rod Co.). Figure 10 (Center): Employing "Harry Potter Gothic" motifs, this private residence has custom fabricated strike termination devices repeating the zig-zag motif used throughout the house (Priestley Lightning Protection, LLC). Figure 11 (Right): Zaha Hadid inserted air terminals with unrestrained delight into the design of King Abdullah Petroleum Studies and Research Center, in Riyadh, Saudi Arabia (East Coast Lightning Equipment, Inc.).

SUSTAINABILITY AND RESILIENCE

The essence of the linked issues of sustainability and resilience is to assure structures and communities provide sustained serviceability. Thus defined, lightning protection is a core practice in holistic approaches to sustainable and resilient architecture.

Lightning protection is not mentioned directly as basis for credit under U.S. Green Building Council's (USGBC) Leadership in Energy and Environmental Design (LEED) program. Project teams can, however, pursue innovation credits given for strategies that go beyond code requirements and, "may not be addressed by any LEED prerequisite or credit but warrant consideration for their sustainability benefits."

Lightning protection also deserves consideration under LEED pilot credits:

- **Credit IPpc98 —Assessment and Planning for Resilience**, which requires project teams to "identify the potential high risks associated with natural hazards affecting the project site(s) and building function."
- **Credit IPpc99 — Design for Enhanced Resilience**, which states intent to "design and construct buildings that can resist, with minimal damage, reasonably expected natural disasters and weather events..."
- **Credit IPpc100 — Passive Survivability and Functionality During Emergencies**, which has options requiring back-up generators or photovoltaic collectors — systems vulnerable to lightning unless protected (Fig. 03).

Lightning accompanying hurricanes, tornados, blizzards, and other severe storms interferes with emergency response and recovery operations by disrupting communications and infrastructure, endangering first responders, and causing fires and injuries (Figs. 12 and 13). Programs promoting resilience also underscore the importance of lightning protection, including:

- **FORTIFIED for Safer Business Standard**, published by Insurance Institute For Business & Home Safety, recommends lightning protection risk assessment. The FORTIFIED program (disastersafety.org/fortified) is incorporated into LEED Credit IPpc99 and RELi, the resilient design component of the C3 Living Design Project (c3livingdesign.org).
- **Performance Excellence in Electricity Renewal (PEER) Rating System** Version 2, administered by Green Business Certification, Inc. (GBCI), offers credits for conducting "a comprehensive risk assessment for critical assets within the project boundary" and undertaking measures "that improve project reliability and power quality by protecting infrastructure from common external threats that may cause equipment damage, malfunctioning or service interruption" (peer.gbci.org).



Lightning added to damage associated with Hurricane Harvey in August 2017. Figure 12 (Left): Dots represent lightning activity during 24 hours on 2017-Aug-27; the orange and red indicate higher levels of activity (LightningMaps.org). Figure 13 (Right): One of the Houston-area building fires ignited by lightning during storm (kfdm.com).

LPSs also have outstanding life-cycle performance since most components last indefinitely and can be reused or recycled without loss of metallic value.

LIGHTNING MONITORING AND SURVEILANCE

Scientific investigation of lightning is advancing on many fronts and having impact on architecture and facility management.

For example, monitoring of lightning activity has improved dramatically. During 2017 hurricane season, National Geostationary Operational Environmental Satellite System (GOES-16) operated by National Oceanic and Atmospheric Administration (NOAA) provided unprecedented views inside storm to show propagation of lightning (Fig. 14). Other lightning monitoring systems provide near simultaneous documentation of the generalized location and intensity of lightning. As this is being written, National Weather Service is reporting that San Francisco Bay Area – a region of relatively low lightning activity – received an astonishing 7,000 lightning strikes (1,200 cloud-to-ground strikes and 5,800 in-cloud strikes) in a single night.

These monitoring techniques provide only generalized locations for lightning strikes. Other techniques can pinpoint lightning strikes to within several meters and report the information in close to real time. Optical lightning monitoring systems, for example, use high speed, zero dead time cameras to detect and record 100% of strikes within a specified surveillance area. The solar powered systems use robust components and are readily deployable; they provide near-immediate reports that allow timely responses. This precision and speed that can be invaluable for any organization with mission critical assets spread across a large campus or field of operations. At wind farms, for example, monitors can determine if a particular wind turbine has been struck so the damaged turbine can be safely shut down before a damaged blade causes a catastrophic failure. Other early adopters include airports and other transportation hubs, refineries and large industrial complexes, military bases, and governmental and research campuses (Fig.15).

As true scope of lightning activity is better understood, it will demand increased attention from architectural community, leading to reevaluation of programming, design, construction, and operational decisions. Already, for example:

- Designers of outdoor stadia must consider whether and to where attendees should be evacuated when lightning threatens or if attendees are safer hunkered down in their seats under LPS mounted over the stands?
- Golf courses and other outdoor recreational facilities are increasingly building lightning protected enclosed sanctuaries where players can take refuge when thunder is heard.
- Schools are advised, “It may be best to hold classes beyond regular dismissal time until the severe weather threat has passed. Likewise, at the end of the school day, students may need to be held from boarding buses until the danger has passed.” according to “A Guide to Developing a Severe Weather Emergency Plan for Schools” by the National Weather Service.
- Should temporary LPS be required during construction to provide refuge to people working on site and to protect building equipment and systems that are in place prior to permanent LPS installation? This may be required under OSHA’s General Duty Clause (www.weather.gov/media/owlie/OSHA_FS-3863_Lightning_Safety_05-2016.pdf).

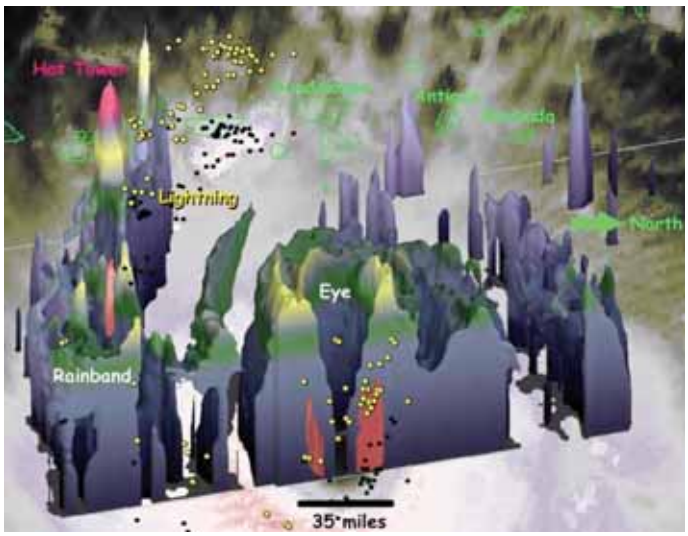




Figure 14 (Left): Satellite data from Hurricane Irma allowed computerized generation of 3-D images showing origins of lightning strikes within storm. As hurricanes form, moist air rising from sea causes water molecules to collide with airborne ice crystals and generate static electricity due to friction. When charges build sufficiently, they discharge as lightning (NOAA). Figure 15 (Right): Optical monitoring systems provide accurate and timely information about lightning strike. This enables facility and operation managers, such as those at this spaceport, to respond quickly and appropriately to minimize damage or interruptions to critical infrastructure (Scientific Lightning Solutions, LLC).

TESTING WITH TRIGGERED LIGHTNING

Seismic-resistant design improved when it became possible to test full-size structures on shake tables instead of via small scale simulations. A similar advance is now available for lightning safety engineering.

University of Florida’s International Center for Lightning Research and Testing (ICLRT) at Camp Blanding, FL, for example, launches small rockets toward thunderclouds. The rockets trail thin wires that provide conductive paths for actual lightning currents to follow to ground where tests can be conducted. Triggered lightning provides much more realistic testing conditions than can be achieved using even the largest laboratory spark generators. Laboratory spark generators mimic either high voltage or high current, but fail to reproduce both quantities simultaneously as they occur in real lightning.

- Testing has been used to improve the design of lightning protection components. For example, Franklin advocated air terminals with tapered points; recent research with actual lightning has demonstrated that blunt air terminals are more effective. (See Moore et al, Geophysical Research Letter, May 15, 2000)
- Manufacturers of electronic devices can test hardware for its robustness.
- Triggered lightning can test complete buildings, building systems, and modules. Little is known, for example, about how cross laminated timber (CLT) framing systems will fare in lightning strikes; testing may reveal valuable insights leading to improved safety or greater confidence.

DARK CLOUD INSIDE SILVER LINING

While lightning protection is advancing on many fronts, designers must remain skeptical about exaggerated claims made for some lightning protection devices. The standards referenced in the Background section of this paper have been thoroughly examined by independent academic, governmental, military, and public safety organizations and found to be highly reliable.

The same cannot be said about claims made for certain non-conventional air terminals.

Early streamer emission (ESE) air terminals have proprietary configurations or contain electrical charging capacitors. These so-called enhancements are advertised as providing larger zones of protection than that of conventional air terminals and permitting use of fewer air terminals, bonds, and grounds. Manufacturers claim that a single mast-mounted ESE device can protect even large buildings and open areas. They use questionable mathematics to extrapolate data from laboratory tests to natural lightning, but static electric discharges made with manmade apparatuses do not scale to actual lightning strikes that can travel many miles before striking buildings. Lab tests also fail to account for surrounding objects, weather and other external conditions.

A U.S. District Court ordered two ESE device manufacturers to stop making false advertising claims about radii of protection provided by their products. The Court found unrefuted evidence that “tests on which [ESE manufacturers] base their advertising claims are not sufficiently reliable to establish that [their] air terminal products provide an enhanced zone of protection” (Heary Bros. Lightning Protection Co, Inc. et al v. National Fire Protection Association, Inc. et al; US District Court for District of Arizona).

To avoid the stigma attached to ESE, one company promotes a “collection volume method” for placement of its devices. Despite new terminology, the lack of results appears to be the same. Adding to confusion, ESE devices are now included in French and Spanish standards that are premised upon evidence that has been repeatedly rejected by NFPA and other standards-development organizations.

Charge transfer systems (CTS) are another non-conventional approach to lightning protection. Instead of providing a path to safely conduct lightning into ground, CTSs are purported to prevent lightning from even occurring in vicinity of structure equipped with them.

Some look like umbrellas wrapped with barbed wire and others like dandelions or sea urchins with fine wires radiating from a hub. The metal points are said to leak ions from the earth into the atmosphere, thereby creating a corona that inhibits lightning.

Corona effects can be demonstrated in labs but do not protect structures from forces acting under actual meteorological conditions. As one lightning protection professional says “after travelling for miles looking for a place to attach to ground, lightning isn’t going to let a few meters of corona get in its way.”

The Federal Aviation Administration, Kennedy Space Center, U.S. Air Force and other authoritative sources have documented CTS failure. Studies comparing similar buildings with and without CTS devices have found no significant difference in the frequency of lightning strikes. NFPA has repeatedly reviewed and rejected requests from CTS manufacturers to write standards for these products.

CONCLUSION AND FUTURE WORK

Lightning is a threat to HSW and causes a significant and growing amount of damage. Techniques to protect buildings against lightning are proven, readily available, and economical. Yet in U.S. and based on NFPA criteria, it is estimated that less than 10 percent of buildings requiring LPS are protected.

It has been said that only a highly visible tragedy will motivate society to embrace more stringent safety measures. Lightning ignites more than 6,000 fires in residences annually, and we accept this with barely a note. What sort of epochal disaster will it take to shock us into action?

Instead of waiting, we encourage proactive measures:

- **Design and Construction Practitioners:** Create protocols within your practices to assure that NFPA 780 lightning risk assessment is conducted on every design, building, and remodeling project undertaken.
- **Academics:** Make NFPA 780 lightning risk assessment part of your schools' building sciences curriculum. In design studios, require risk assessment as part of site analysis, sustainability analysis, and design documentation.
- **Advocates:** Insist lightning protection be specifically identified as part of green and resilient building design initiatives. Work to make lightning safety part of your local building codes and community resiliency guidelines.
- **Building Science Researchers:** Consider how rocket triggered lightning and new lightning monitoring technologies can be used to advance understanding of how electrical storms interact with building systems and components and to develop better ways to build.
- **Continuing Education:** Lightning Safety Alliance offers AIA/CES-approved continuing education programs and will send qualified presenters to your office, school, work place, community organization, or professional society.
- **Personal Safety:** "When Thunder Roars, Go Indoors." This advice, from the National Weather Service, can save your life, especially if you can go into a building with a lightning protection system (Fig. 16).

ACKNOWLEDGMENTS

The authors acknowledge support of East Coast Lightning Equipment, Inc.; Scientific Lightning Solutions, LLC; Lightning Protection Institute; Lightning Protection Institute Inspection Program, Lightning Safety Alliance; and lightning protection designers, installers, and researchers throughout North America who have shared their expertise, photos, and case studies.

REFERENCES

1. Lightning protection in the context of architecture, building, and design.

Chusid, Michael.
--- "Lightning Protection: The Architect's Standard of Care." Architectural Products (March 2016).
--- "Lightning Protection is a Work of Art." Building Enclosure (Fall 2016).
--- "Lightning Protection: Tried and True Versus Non-Standard and Non-Accepted." Electrical Business (September 2016).
--- "Preventative Care for Medical Buildings." Medical Construction & Design (July/August 2015).

Morgan, Jennifer and Chusid, Michael.
--- "Reroofing and Lightning Protection." Construction Specifier (May 2017).
--- "When Lightning Strikes." Modern Steel Construction (October 2016).
--- "Lightning Protection and the Building Envelope." Construction Specifier (August 2015).
--- "Lightning Protection, Roofing and Weather." Architectural Roofing & Waterproofing (Winter 2016).
--- "Lightning Protection: Five Concepts you Need to Understand." Construction Canada (March 2016).
--- "Lightning Protection and the Building Envelope." Journal of the National Institute of Building Sciences (August 2016).
--- "Understanding Lightning Protection Systems." Consulting-Specifying Engineer (May 2017).

2. General References
--- Lightning Protection Institute, www.lightning.com.
--- Rakov, V, and Uman, M. Lightning: Physics and Effects, Cambridge University Press, 2003.
--- Uman, M., The Art and Science of Lightning Protection, Cambridge University Press, 2008.



Figure 15: Most lightning fatalities occur during outdoor activities where victims are most directly exposed to lightning strikes. Yet this advice from the National Weather Service and National Oceanic and Atmospheric Administration should also be a reminder that indoor spaces must be designed and constructed to provide lightning protection.

WHEN FAÇADES KILL

A problem of extreme flammability



Terri Meyer Boake
University of Waterloo
tboake@uwaterloo.ca

ABSTRACT

The tragic fire of June 14, 2017 at the Grenfell Tower in London, England has brought to a very public global forum issues related to the impact of façade choices to the fire safety of a building, its occupants, neighbors and the fire-fighting crew. Such fires are becoming increasingly common as flammable Aluminum Composite Panel products have been used on thousands of projects prior to their used being banned in multiple jurisdictions only as distantly as 2012.

Façade systems have been developed for new buildings as well as to retrofit existing modern projects to increase energy performance and provide a facelift to banal or brutalist projects. Lighter weight façade materials have been favored over traditional non-combustible materials such as brick, concrete and stone, as a means to keep loading within the capabilities of existing structures. These lighter materials as well as many newer insulation types tend use petroleum based materials, making them highly flammable rather than simply combustible.

This paper looks at issues of product confusion regarding the specification of a range of available Aluminum Composite Panel (ACP) products that have contributed to the widespread use of a now partially banned product on many high rise towers. Vague building codes that lack robust fire testing and that vary by jurisdiction will also be seen to have contributed to these failures. The building height of 15 to 18m will be discussed as an appropriate measure of the acceptability of the use of a flammable façade. Practices surrounding the improper detailing of the rainscreen wall system associated with accelerating the Grenfell Tower fire will also be discussed.

Finally a series of recommendations will be made regarding appropriate building heights and the impact of exterior wall design for openings and balconies, for the use of flammable cladding.

KEYWORDS

fire, flammable cladding, rainscreen, codes and standards, aluminum composite panels

INTRODUCTION

The tragic fire of June 14, 2017 at the Grenfell Tower in London, England, has brought to a very public global forum, issues related to the impact of façade choices to the fire safety of a building and its occupants. Reactions to the event ranged from sheer horror that a façade could possibly be that combustible, to head shaking that such a façade system could have been installed in spite of a growing body of evidence that would suggest the inevitability of such a fire. Unlike previous façade fires, the death toll at Grenfell was extreme, making the detailed investigation into the causes of the fire impossible to avoid, and future prevention, urgent.

Approaches to contemporary façade design are experiencing an increased level of experimentation through the use of innovation that explores unique geometries and new, lighter materials. Façades have become “the architecture” on many projects whose floor plate and structural materiality are often governed by quite pragmatic concerns. Façade systems have also been developed to retrofit existing modern projects to increase energy performance and provide a facelift to banal or brutalist projects. In the case of Grenfell Tower, the retrofit façade had the dual purpose of increasing energy efficiency as well as improving the dull aesthetic of the block. Lighter weight façade materials can be favored as a means to keep loading

within the capabilities of existing structures as they can be installed directly over existing exterior systems, allowing residents to stay in place during construction. These lighter materials which often incorporate thermoplastic insulation which is petroleum based, makes them highly flammable. So in direct contrast to traditional non-combustible materials, ACP provide fuel for a fire.

A DEVIATION FROM THE PERFORMANCE EXPECTATIONS OF TRADITIONAL MATERIALS

The high death toll at Grenfell can be in part attributed to the directive from the fire department to "shelter in place" rather than undertake the risk of evacuation through smoke filled corridors and the single stairwell.[1] A high number of tower fire deaths can be attributed to smoke inhalation rather than death by the fire itself. Many of these deaths occur in corridors and stairwells. The "shelter in place" directive reveals the ignorance of the fire department regarding the unusual nature and potential behavior of the cladding system on the tower. In normal circumstances, and indeed considering the materiality of the un-renovated tower, this advice may have been as prudent as it is common. Even while the fire skipped rapidly up the face of the building, the fire-fighting team seemed not to quickly change these tactics that presupposed a non-flammable cladding system.

Traditional modern cladding materials such as brick, concrete and stone are inherently fire resistant and classed as non-combustible ("Fire Ratings for Construction Materials" 2013). Traditional insulation materials such as fiberglass and rock wool are also fire resistant. Even aluminum frame curtain wall systems have incorporated the practice of providing fire stopping between floors, on the interior of the façade for many decades. Although these façade systems will eventually fail in a severe fire event, they do not provide fuel for the fire nor do they channel its flow, hidden, within the wall itself.

Many of the insulation components of the newer façade systems use thermoplastic insulation, which is highly flammable. So in direct contrast, these materials provide an *accelerant type fuel* for a fire. So in the case of Grenfell, while the interior structure was constructed of traditional non-combustible materials with a normal fire load established by the contents, the cladding was not and so posed an extreme risk where the fire was unconventionally spreading from the exterior to the interior of the building. This accelerated the speed of spread and actually required more rapid evacuation than for a traditional fire.

DOCUMENTATION AND EVIDENCE

What makes the case of Grenfell even more tragic is that it was not an isolated incident but one in a series of major cladding fires. This is a critical fact as the previous fires should have put architects and material manufacturers on the alert for safety issues when utilizing this type of cladding system. Legally there may be limitations regarding what architects are required to know or be aware of, if incidents happen outside of the local or national jurisdiction. However, although not in the UK, the New Year's Eve fire at The Address in Dubai was highly covered in the UK news media, as were the repeat fires at The Torch in Marina Bay. Architecture is a global practice and so the incident in Melbourne should also have been noteworthy.

LIST OF SIGNIFICANT FAÇADE FIRES DISCUSSED

• February 12, 2012	Tamweel Tower, Dubai	("Fire Breaks Out at Tamweel Tower" 2012)
• November 25, 2014	Lacosse Apartments, Melbourne	(The Australian Business Review 2015)
• February 21, 2015	The Torch, Dubai	("Hundreds Evacuated after Fire" 2015)
• December 31, 2015	The Address, Dubai	("Massive Fire at Dubai Skyscraper…" 2016)
• July 20, 2016	Sulafa Tower, Dubai	("Dubai Sulafa Tower Fire" 2016)
• August 4, 2017	The Torch, Dubai	(BBC News 2017)

As the Grenfell Tower case is presently in the courts, the evidence used in the preparation of this paper is derived from a plethora of online articles. The references in this paper represent an abbreviated list as the full list is as long as the word limit of the paper. Research into the online coverage of the incident can be clearly divided into articles that reflect reports that are addressed at public perception and education versus those quite technical in nature and targeted at the architectural and engineering community. The most telling caption from *The Sun* UK is "DEATHTRAP DÉCOR What is cladding, why was it

[1] *The internal issues of the tower, including dependence on a single stairwell and a lack of sprinklers will not be addressed in this paper.*

used on Grenfell Tower and how many other tower blocks have failed latest fire tests (“Deathtrap Décor” 2017)? The public is outraged and needs answers.

Although the majority of the articles have not been written by building experts, there are adequate common facts as well as credible details regarding the construction method and material nature of the buildings (The Guardian 2017). It is not the purpose of this paper to necessarily cast blame, but rather look from a higher, albeit morality-based perspective, as to the role of the architect when it comes to material selection and detailing of the façade within a constantly changing world of materials. It is also important to frame flammability as a general issue that must be addressed for all façade design experimentation, regardless of height, building use, budget or location.

CONFUSION AFTER THE GRENFELL FIRE

Immediately following the Grenfell Tower fire, numerous agencies made statements regarding the status of approvals for the cladding used, in rather obvious attempts to shift the blame. It was noted that the fire-resistant type of ACP had been originally specified but the cheaper flammable type substituted to achieve cost savings (“Cladding Cost Cutting” 2017). Preliminary admissions were that the cladding may have been a factor in spreading the blaze. The cladding was identified as being manufactured by *Arconic*. *Arconic* makes a fire resistant brand of cladding called *Reynobond FR*, as well as a completely non-combustible version, but these weren't used on the recent retrofit of Grenfell Tower. The type used was identified as *Reynobond PE* which consists of two aluminum composite panels that are filled with insulation that can often include polyethylene plastic. If improperly installed, it is at risk of becoming flammable. Articles noted this as the reason why the U.S., Germany and several other countries have banned its use on high-rise buildings (“Grenfell Tower Fire Started In Fridge Freezer” 2017) while noting that the material is considered acceptable on buildings in the UK shorter than 18m.

However, even this type of cladding - when properly fitted and with its polyethylene insulation expertly encapsulated - should resist fire, the Fire Protection Association (FPA), the UK's national fire safety organisation, said (“London Fire” 2017).

A spokesman for the Department for Communities and Local Government told CNN that the use of a composite aluminum panel with a polyethylene core would breach current UK building regulations guidance, which says this material should not be used as cladding on buildings over 18 meters (59 feet) in height (“UK Chancellor” 2017).

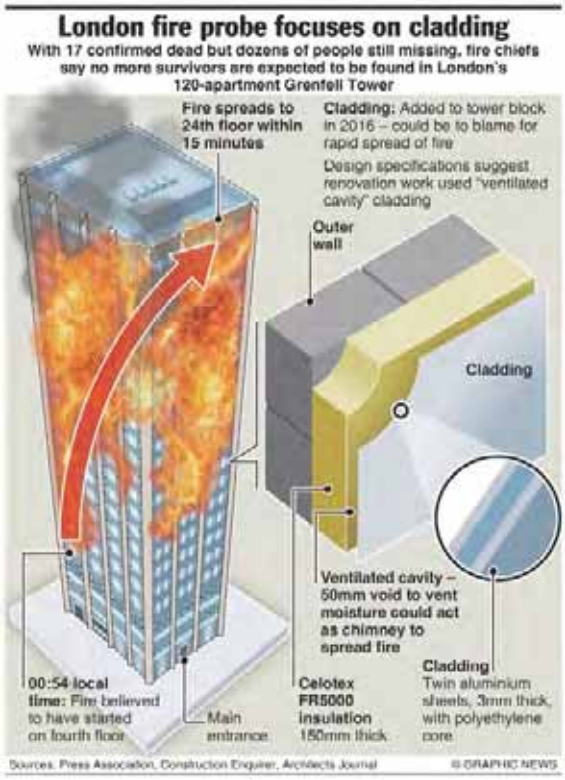


Figure 1: Details of the façade construction at Grenfell Tower from one of a number of articles written to explain the problem to the public (“Grenfell Tower Fire Raises Fears” 2017).

The RIBA issued a statement following the fire that outlined both required and suggested improvements to current UK building standards that seem to be caught in delayed review for several years (Architect Magazine 2017). Sadly it would seem that architects are not included in the post fire expert panel review in the UK, which is a frustration to UK architects who seem to have lost their position in the overall process, while retaining responsibility for faults (Architect Magazine 2017). However, as building codes and bylaws are typically minimum performance requirements, there is opportunity for architects to show knowledge and leadership when it comes to façade design.

Extensive fire tests were conducted (according to the police) immediately after the fire on the remaining unaffected parts of the tower cladding. According to the report,

Police said both the insulation and tiles used in cladding at the 24-storey Grenfell Tower block failed all post-fire safety tests. “Preliminary tests show the insulation samples collected from Grenfell Tower combusted soon after the test started," McCormack said. Such were their concerns after the tests that the information was immediately shared with government to disseminate more widely (“Grenfell Tower Fire Started In Fridge Freezer” 2017).

Details of the precise nature of the fire tests was not included in the above article to validate the methods, but the results suggest that the failure of the materials was not in any doubt. The division between the fire load from the cladding versus the added cavity insulation was not disclosed.

INCONSISTENCY OF SPECIFICATIONS AND GLOBAL FIRE TEST METHODS

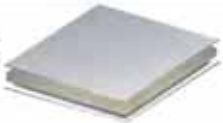
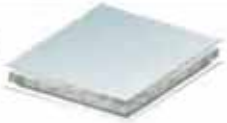
Many of these new materials and innovative approaches to façade design and refurbishment have not been rigorously fire tested in advance of construction. Fire test standards vary around the globe, and the inconsistency in performance expectations has contributed to the extent of the façade fires. The ultimate test is of course a real fire. Bad results are exacerbated when the failure is associated with a tall building.

Where the field of architecture and engineering has become increasingly global, meaning that the transfer of design ideas and their related materials is no longer regionally limited, the area of building regulations has remained highly jurisdictional. Where ideas, materials and façade design trends are copied around the globe at lightning speed, building regulations seem to change at a snail’s pace. Although numerous façade fires had taken place using similar materials and systems in countries outside of the United Kingdom, there was resistance and reluctance to incorporate such information into the British fire codes for tall buildings. Post fire banter exhibited wide confusion regarding the legality of the use of the flammable cladding and additional polyethylene insulation as the cladding material was said to be acceptable on low rise buildings. It was substituted on the tower block to achieve a cost savings. Indeed in the case of Grenfell its status as a council property had injected numerous others into the approval process for material selection, well beyond when the drawings left the architect’s office.

Shortly after the Grenfell fire, *Arconic*, the cladding manufacturer of the implicated *Reynobond PE* panels announced that their manufacture would cease.

> "We believe this is the right decision because of the inconsistency of building codes across the world and issues that have arisen in the wake of the Grenfell Tower," *Arconic* said in a statement. "We will continue to fully support the authorities as they investigate this” (“Grenfell Tower Cladding Maker” 2017).

Table 1 ALUCOBOND composite panels

Characteristic	Panel type		
	Standard ALUCOBOND	ALUCOBOND plus	ALUCOBOND A2
			
Core	Low-density polyethylene (LDPE)	Thermoplastically bonded aluminium hydroxide	Inorganic filler materials with thermoplastic binder
Length (mm)(1)	3200,4000	3200,4000	3200,4000
Width (mm)	1000,1250,1500(2)	1000,1250,1500(2)	1250,1500(3)
Thickness (mm)	3, 4 and 6	3 and 4	3 and 4
Density (kg m⁻²)	900-940	1600-1800	1600-1800
Core colour	Black	Grey	Grey/white

(1) Lengths up to 8000 mm available on request.
(2) 1750 mm width available on request.
(3) 1650 mm width available on request.

Figure 2: The three varieties of Alucobond panels are pictured above. Their specific fire ratings vary as a function of jurisdiction and also, according to their website, by the colour of the panel. At the present time only Alucobond A2 is recommended for buildings over 18m. Image from 3A Composites Gmbh website.

Of critical interest is their acknowledgment of the inconsistency of global codes. Where the *Arconic* distributed *Reynobond PE* product will no longer be available in Europe or elsewhere, whether permitted by codes or not, the distribution of *Alucobest*, the product implicated in the Melbourne tower fire, continues to be available in the Asian and Australian markets. The marketing information on *Alucobest* makes no reference at all to its shortcomings with respect to fire resistance, or to suggest any limitations on its applicability. To the contrary it is marketed through “Trust Technology” under that catch phrase “the way to trust is to test”, with a product endorsement at the recipient of the BCI Asia Architects’ Choice Awards 2014.



Figure 3. Alucobest is still being promoted in Asia in spite of its involvement in a number of fires and its chemical similarity with other panels. Image from Alucobest website (http://www.huayuanfu.com/e/faq.htm).

Material substitutions associated with value engineering can be blamed in many cases where the more fire resistant panel was specified but the less expensive flammable panel used as the result of cost cutting. The fire protective designation of the paneling is backgrounded to cost. In the case of Grenfell the shift was from a zinc clad panel to an aluminum one as a cost saving measure. It was not highlighted when the selection was made that the lower cost panel had a different core as well as a different metal.

> “The email suggested ways to bring the price down of the cladding such as using aluminium panels rather than zinc which would save £293,368. Zinc panels would have been fireproof, whereas the aluminium panels that were eventually used contained a flammable polyethylene core” (“Cladding Cost Cutting” 2017).

A similar situation is felt in Australia, where Australian made products are in continual competition with Chinese made products. The Quality Control measures on Chinese products are often questioned.

> "The aluminium composite panel cladding, called *Alucobest*, commonly used in high-rise apartment buildings in the past 10 years, is imported from China and is significantly cheaper than the more fire-retardant and non-combustible Australian-made *Alucobond*, which complies with safety and fire standards. Testing of the Alucobest cladding from the Lacrosse building found it was in breach of the combustibility requirements under the Building Code of Australia. Industry experts claim only an invasive test can reveal the difference between the cheaper Alucobest and Alucobond cladding because they look, feel and smell exactly the same" (The Australian Business Review 2015).

The article reference to the Australian version of *Alucobond* might be seen to imply that there was not the variety of choice of that product as per the *Alucobond* website, although citing that it was fire-retardant and non-combustible. To be correct it would be necessary to be much more specific as to its sub-type. Hence the article adds to the confusion already present between the similarly named products.

3A Composites Gmbh, the company that manufactures *Alucobond*, which has also been implicated in fires, while noting that its product was not used on the Grenfell Tower, makes this statement on its website regarding its safe use under current (2017) British codes:

> "BR 135 – up-date: In the light of recent events in the UK as well as ongoing tests and expected changing building regulations, *3A Composites GmbH* has decided to publish a general recommendation for the use of *ALUCOBOND® A2* material on towers over 18m, mainly because of the lack of influence *3A Composites* can have on the whole wall build-up and the final decision over the product taken by others. Meanwhile, commissioned by DCLG, additional tests to our BS8414-1&2 tests have been conducted which also met the performance criteria set in BR 135: 2013. This is proof that respecting the specified wall build-up therein (including the type of insulation, the installation and necessary cavity barriers), our *ALUCOBOND® PLUS* (classified B-s1,d0 according to EN 13501-1 with a calorific value of 12.8 MJ/kg) is compliant with current Building Regulations and therefore acceptable for buildings over 18m" (Alucobond News and Press Office 2017).

One phrase sticks out "mainly because of the lack of influence *3A Composites Gmbh* can have on the whole wall build-up and the final decision over the product taken by others" as being particularly unclear in terms of this recommendation. It may refer to complications in overall wall design such as at Grenfell Tower where the combined use of the exterior metal panel with the cavity insulation exacerbated the problem. It is extremely unclear as to the final suitability of the products for safe use given the number of conditions and mysterious compliance tests cited.

7 Behaviour in relation to fire

7.1 When tested to BS 476-6 : 1989, ALUCOBOND panel achieved a fire propagation index (I) of 0 with sub-indices (i_1), (i_2) and (i_3) also of 0 and when tested to BS 476-7 : 1997, the product achieved a Class 1 surface spread of flame.

7.2 When tested in accordance with BS EN 13501-1 : 2007, the ALUCOBOND plus panel,with outer aluminium sheet coated with primer and a two-layered finish coat, when tested for reaction to fire, achieved a classification of B-s1, d0.

7.3 When tested in accordance with BS EN 13501-1 : 2007, the ALUCOBOND A2 panel when tested for reaction to fire, achieved a classification of A2-s1, d0.

7.4 The panels are capable of achieving Class 0 surface or a 'low risk' material in relation to the national Building Regulations.

7.5 These performances may not be achieved by all colours of the panel and the designations of a particular colour should be confirmed by:

England and Wales — test or assessment in accordance with Approved Document B, Appendix A, Clause 1

Scotland — test to conform with Regulation 9, Annex 2C[1], Table, or Annex 2E[2]

Northern Ireland — test or assessment by a UKAS accredited laboratory or an independent consultant with appropriate experience.

(1) Technical Handbook (Domestic).
(2) Technical Handbook (Non-Domestic).

7.6 The fixing gasket is present in such small quantity as to have negligible effect on the overall fire performance of the cladding.

7.7 For resistance to fire, the performance of a wall incorporating the system can only be determined by tests from a suitably accredited laboratory and has not been assessed as part of this Certificate.

7.8 Cavity barriers should be incorporated behind the cladding, as required by the national Building Regulations, but should not block essential ventilation pathways. Particular attention should be paid to preventing the spread of fire from within a building breaching the cladding system through window and door openings.

Figure 4: Alucobond specification materials noting the behavior of the material in a fire based on UK Code requirements (http://www.alucobond.com).

The UK targeted specification for *Alucobond* makes note of three significant potential detailing issues in the use of their product under items 7.6, 7.7 and 7.8. The sealing gaskets are not included in standard testing and these may be seen to protect the insulation core from fire exposure. The panels are tested in isolation, so not tested in conjunction with the back-up wall, its additional cavity insulation and materials. And note is made to prevent the spread of fire from within the building to the cavity. All three of these conditions exacerbated the spread of fire at Grenfell Tower.

Mulk Holdings International/Eurocon, the producer of the flammable panels involved in the New Year's Eve fire at The Address in Dubai has ceased production of the panels and it clearly states on the company website that they are producing "fire-rated" metal composites, although the specific test method currently used is not noted. In reference to the panels used on The Address, sources note that the panels had been tested and conformed to ASTM E119 - 16a: Standard Test Methods for Fire Tests of Building Construction and Materials ("Most Dubai Towers Built Before 2012" 2016). It was noted that the test did not include the gaskets and sealants used between the panels. The test is also noted as excluding:

- 4.4.2 Evaluation of the degree by which the test specimen contributes to the fire hazard by generation of smoke, toxic gases, or other products of combustion
- .4.4.3 Measurement of the degree of control or limitation of the passage of smoke or products of combustion through the test specimen.
- 4.4.4 Simulation of the fire behavior of joints between building elements such as floor-wall or wall-wall, etc., connections.
- 4.4.5 Measurement of flame spread over the surface of test specimens (ASTM E119).

All of the above exacerbated the extreme failure of the panels during the fire.

Fire test methods in addition to not being globally uniform seem to rely on very limited material tests, typically not in combination with a variety of back up walls. For example in the United Kingdom it is noted, "For the past three decades fire

safety experts have warned that the ‘Class O’ designation was based on small-scale tests conducted in laboratory conditions and did not properly evaluate cladding in a live fire” (“Eight Failures” 2017).

The basic nature of manufacturing in China and the proliferation of “knock off” and alternate materials, as well as the substitution of materials that is dominant in their manufacturing system makes it virtually impossible to be certain about products in general. As mentioned for the *Alucobest* product, no fire rating information was available on the product website. General safety concerns are less stringent in their construction industry.

THE LARGER FAÇADE DESIGN ISSUES ARISING

The cases of these high profile cladding fires must be seen as central to the requirement for new regulations and best practices in design for all façades. Even where code leadership is absent, fire tests limited and regulations are insufficient, the design community needs to address the problem. It is about life and death, not just capital cost and insurance dollars. The solutions to the problem can be globally applied as the conditions are universally the same. And much of this is quite logical.

COMBUSTIBLE VERSUS FLAMMABLE:

Materials are typically designated as either falling into a combustible versus a non-combustible category. Traditional combustible materials that have been used as cladding would include wood and vinyl. The flame spread rating of different types of wood ranges from 25 to 200 according to ASTM Test Method E-84. Traditional non-combustible cladding materials would include brick, concrete, stone and stucco whose flame spread rating is zero (Flame Spread Ratings). Combustible materials burn and spread fire and contribute to the fire load and hence have been limited to use on low rise buildings (definition of low rise varies by jurisdiction) with a sufficient set back from adjacent properties. Again the setback requirements vary by jurisdiction, but in dense North American urban locations all combustible cladding is often banned where the distance to the property line is generally less than 1.2m.

The flame spread ratings of the various “poly” based insulation materials varies greatly by product, by manufacturer, and by the jurisdictional testing facility. Given the global nature of the building industry it makes the specification of these materials more difficult than for traditional non-combustible materials as the suggested code limits for their flame spread ratings is also dependent on the detailing of the wall assembly and additional materials used to prevent the spread of fire to the interior. Adding to the specification confusion here is the plethora of types: polyisocyanurate, polyethylene, polyurethane – most of which come in both board types as well as with a spray application.

Aluminum Composite Panels, where using a thermoplastic core, and particularly when combined with additional unprotected polyethylene insulation in the cavity, have succeeded in creating a new danger class of cladding that should properly be labeled *flammable* rather than simply combustible. This new type not only burns, as well as contributes to the fire load, but also acts as an accelerant to the fire. As such it is perhaps not suitable for use as a cladding material at all. Some manufacturers have already ceased production of the panels and a complete boycott of the use of those products that still remain on the market may help to ensure that they too will cease production.

However more problematic is the role of the additional polyethylene insulation that was installed in the cavity to increase the energy efficiency of the wall. This is an important building material and very safe to use in many circumstances where it is normally adequately protected, such as around foundation walls and in roof assemblies. If it is not possible to properly detail a sealed poly-type insulation in the cavity, then it should not be used in that location and an alternate fire retardant insulation needs to be specified. What is not clear at present is the division of the contribution of the Aluminum Composite Panels versus the cavity insulation in the Grenfell Tower fire.

HEIGHT VERSUS FLAMMABILITY:

Also at variance across the globe is the question of a suitable height for the use of combustible cladding, a measure that is often influenced by building typology as well as urban site situation, fire-fighting access and setbacks. In North America multi-family dwellings that are deemed to be low-rise (typically under 6 storeys) have tended to allow for the use of some combustible materials and indeed the type of panels that were used on the Grenfell Tower. This has been linked to the potential ease of evacuation as well as to the typical reach of the ladder on fire-fighting equipment.

Eighteen meters has been cited as the break off point for the use of the flammable cladding in the UK, fifteen meters in the UAE. Interestingly the flammable product produced by *Arconic* that was used on Grenfell Tower, had a disclaimer that it should not be used in buildings over 10m in height. The pending legal action for Grenfell is looking at the liability of the manufacturer in knowingly providing material for a project that clearly exceeded this limiting height.

As the Grenfell incident revealed, ladder reaches vary widely. And so for designers to be ensured of the availability of a long reach ladder in order to use a flammable cladding seems ill advised. Reports after the Grenfell Tower fire blasted the fire department for having such low reach ladders, citing other jurisdictions with further reach ("Ladders Came Up Short" 2017). This specificity of fire-fighting equipment as a deciding factor in cladding specification would not seem a sensible strategy as such could easily change over the years. Is there indeed any safe height that could allow the use of highly flammable cladding? To look at the question with brutal honesty, is a fully engulfed in flames 6 storey building much superior to a 24 or 70 storey building engulfed in flames?

TOXIC GASES

The generation of toxic gases was noted at the Grenfell Tower fire as being a contributing factor to the number of deaths. The additional cavity insulation used in the Grenfell Tower, Polyisocyanurate, is said to have released hydrogen cyanide gas when burned.

> "It's widely known that the inhalation of toxic gas within smoke accounts for most deaths and injuries within fire, and yet fire toxicity in construction materials is completely under-regulated. "Unlike ships, trains or aircraft, where fire toxicity is regulated because it is accepted that escape may not be possible, the UK and most of Europe have no regulations on the toxicity of fire smoke from construction products, even though escape from a high-rise building may be equally impossible" ("Grenfell Tower Victims 'Poisoned By Cyanide'" 2017).

The added problems associated with many thermoplastics lay in the toxins that they create when burned. The residents of Grenfell Tower suffered cyanide gas poisoning as the burning of the cladding and cavity insulation ("Grenfell Tower Victims 'Poisoned By Cyanide'" 2017). Where this might not pose an immediate health risk to occupants in a sealed office tower during a fire event, the nature of operable windows on residential towers allows both the fire and the associated toxic gases to enter the interior space. This might suggest a more differentiated approach to the specification of insulation on sealed buildings versus those with operable windows. However with a push to more sustainable buildings that include natural ventilation, this differentiation would have to be clearly set out via a detailed façade analysis and not simply by building type (commercial versus residential, for instance).

Regardless of the occupants or building use type, fire-fighters should not also be subjected to breathing excessive toxic gases during a fire event. Where there can be little control of the interior fire load given the nature of contents, there should be adequate control over the chemical nature of cladding and insulation materials. Again traditional materials such as fiberglass and rockwool have not posed this problem and fire-fighting techniques and practices are based upon this assumed state of construction.

THE ROLE OF THE AIR SPACE:

The use of an air space behind the cladding system for the purpose of air pressure equalization is a long standing practice in Canada and numerous other cold climate countries. The Canadian codes recognize that such spaces *may not* be continuous up and around the façade, for reasons of fire spread as well as for control of unwanted channeled winds that will encourage water penetration during rain/wind events.

The continuity of the air space behind the Grenfell Tower aluminum façade has been cited as one of the main causes for the near instantaneous spread of the fire up the building – a chimney effect. The cavity is said to have been 50mm in width, which is larger than many Canadian rain screen systems where 25mm is a more common dimension ("Grenfell Tower Refurbishers" 2017). Investigation into the extreme nature of the fire seemed to think that even some discontinuities, which were in fact required by code, would have helped little to prevent the spread of the fire due to the high fuel load. Beyond the highly flammable core in the panel, which was only several mms thick (designed more to stiffen the panel than to provide a high level of insulation), the exposed 150mm polyethylene primary cavity insulation provided an excessive amount of load. There has been criticism of the project in the excessive levels of insulation used.

Manufacturers of the types of polyethylene based insulation used in Grenfell Tower, be they board type of spray installed, indicate in their specifications that a high level of containment is necessary to use the product in wall cavities. This would include encasement in a more fire resistant material such as gypsum board. Specifically mentioned is the use of a thermal barrier between the insulation and the interior of the building, to prevent ignition by temperature from interior fires. Most manufacturers do not suggest guidelines to protect from ignition from the exterior or from within the cavity (Technical Bulletin 405). These guidelines vary as well based on the home country of the manufacturer, but do indicate that the fire risk for the use of the material in a well ventilated cavity is known.

Fighting Grenfell Tower fire was made more difficult by the combination of the metal cladding panels and the cavity insulation. The metal panels provide a barrier to dousing, at least until the aluminum achieves its melting point of 600C, allowing the water to enter behind the panels. Given the accelerated spread of the fire in the cavity, access for fire-fighting was achieved far too late to be of any use (CBC News 2017).

ADJACENCY ELEVATES RISK:

Low rise residential codes have long incorporated minimum setbacks as a means of preventing the spread of fire from building to building, controlling combustible cladding materials as well as the percentages of unprotected openings. Where the Grenfell Tower was located at a significant distance from other buildings, thereby removing the risk of the spread of fire to other properties, The Torch and Sulafa Tower fires were at high risk of spreading to adjacent towers. The spaces between towers in Dubai are extremely tight, and wind could easily cause drift into falling enflamed cladding pieces, that could light nearby buildings. Adjacent balconies could easily trap falling debris.

It would be prudent to suggest that combustible cladding also be prohibited from use on tower projects based on the proximity of adjacent buildings. This would include not only the cladding itself, but pending further investigations, the use of flammable insulation in the cavity, if not properly detailed for protection from fire and excess heat.

FAÇADE OPENINGS AND BALCONIES:

The Torch Tower and Lacosse Apartment fires were both residential high rises with balconies, and both fires found to have been started by cigarettes left burning in a balcony planter that subsequently caught fire and spread to the cladding. The fire at The Address was initiated by an electrical fault from an exterior spotlight (“Electrical Fault Caused” 2017). Grenfell Tower’s windows were largely open given that it was a warm evening and most occupants did not have air conditioning. This also allowed the fire to rapidly skip from floor to floor.

Where it might seem obvious to preclude the use of BBQs on balconies, the increasing ban on interior tobacco smoking is driving smokers to their balconies. So even a low rise building will have an increased risk of a façade fire due to smoking. And the increased use of exterior decorative lighting on many towers increases the risk from an electrical short.

To reduce the risk from a flammable and even a traditional combustible cladding material, they should not be used where there are operable windows or balconies. Given the issues that have arisen in the fires in the Marina Bay district in Dubai, consideration is due to the nature of the façades on adjacent structures in terms of the presence of balconies and operable windows, even if the subject building under design has a sealed envelope that might pose less self-risk. Occupancies that stack uses may also have variations in the inclusion of openings that also might create varied risk over the height of the façade.



Figure 5. The Sulafa Tower (left) sits extremely near to adjacent towers. Photo by author, taken in February 2016 prior to the fire.

ASSUMPTION OF RESPONSIBILITY:

As in the case of a catastrophic building disaster, nobody truly wishes to assume primary responsibility for the life and economic losses. Yet as professionals, architects must assume a role. The profession by its nature and education has not been trained to design to the lowest passable criteria, and most appreciate that Building Codes tend to define a minimum set of requirements versus a laudable performance target.

The projects that have suffered these catastrophes were not all designed for low cost solutions, as has been blamed on the Councils that decided in favour of the lower cost solution for Grenfell Tower, in spite of apparently understanding the risk. The multitude of towers in the UAE that are still clad in this problem material were designed and built for relatively high end tenants.

Should architects simply design to building regulations, however flawed? Should the façade design community take a leadership role in promoting safe façade design? This may include lobbying for the ultimate banning of certain questionable materials given the obvious inability of constructors and developers to properly understand the ramifications of the substitution of less expensive materials – as was the motivation in Grenfell – that are presently legal to use in low to mid rise buildings. Why is such a material even deemed safe at all?

In the case of many tall buildings, the façade can be the last hold onto “design” that the profession of architecture has on the building. Its detailing, materiality, and determination of performance are for the most part under the direction of the architect. Yet in the case of the committee recently struck to examine the upgrade of fire codes for tall buildings in the UK, no architects were invited to participate in the revisions. Why? Is this a UK problem? *How can this façade design community engage this process?*



Figure 6: Copycat product naming only makes specifications more difficult. Inage from The National (The National 2017).

Material vendors may eventually be held partially at fault, pending the outcome of the UK investigation which is said to be looking at "corporate manslaughter". Should the material vendors be aware of the location of installation of a product that is understood to have limited legal applicability?

HUNDREDS OF TOWERS WITH THE SAME CLADDING

Where it may be clear that such flammable cladding systems should not be used on any future buildings, there have been identified well over 1,000 towers in the UK, UAE and Melbourne alone that used the dangerous material (The Australian 2017). A study done after The Address fire cited that most buildings constructed in Dubai prior to 2012 used the cheaper more flammable cladding ("Most Dubai Towers Built Before 2012" 2016).

Many towers that were built in the 1960s and 70s had been re-clad in the interest of adding extra insulation for energy savings, which is beneficial. Widespread testing is being conducted in the UK and over 600 towers have been identified with similar cladding issues ("London Fire" 2017). Several towers have been evacuated as a precautionary measure while the cladding system is removed and replaced. The sheer numbers of suddenly displaced occupants are proving difficult to accommodate, however replacement prior to a fire will be more expedient than post fire due to the implications of fire damage.

Where it seems to be the correct action to replace this cladding system, the costs will be high to bear. In the UAE there was a move to ask the occupants of Tamweel Tower to bear part of the costs of the 5 year repair project (The National 2017). One of the major costs being the displacement and re-accommodation of the tenants for an extended period of time. Excluded from the current work at Tamweel is the raising of the height of balcony railings to further restrict fire spread.

Emaar Properties, the owner of The Address has received a DH1.22 billion insurance claim for its fire ("Emaar to Receive Dh1.22 Billion" 2017). This is likely to set a precedent given the high profile nature of the fire.

The UAE issued a new very strict fire code in January 2017 and as of September 2017 has charged building owners to replace all paneling on existing buildings that contravenes the new fire code ("Dubai Starts Replacing Skyscraper Facades" 2017). Design professionals in the UAE will be carefully monitored as the new codes are enforced, with steep financial penalties for failing to comply. It is still not clear who will bear the cost of the cladding replacement or whether the work will be done while the tenants stay in place.

CONCLUSION

What has been outlined in this paper is at its best, a confusing situation. The root of the problem lies in the main with the production of a flammable cladding type, in combination with a flammable cavity insulation, that was deemed to be safe (enough) for buildings under 15 to 18 meters in height. With so many products that look similar as well as having similar names, with their actual fire resistance relatively untested and not adequately flagged, it is not surprising that improper substitutions were made. The nature of an industry bent on cost-cutting seemed incapable of understanding all of the facts when switching out for a cheaper solution.

This paper has not addressed issues within Grenfell Tower regarding the acceptability of a single stair as a means of egress in a 24 storey tower, the absence of a sprinker system nor other problematic aspects of the project.

Although the post mortem on the failure of Grenfell is still in process, an interim report released in December 2017 indicates that the UK Building Regulations are "not fit for purpose" and some significant changes are forthcoming ("Fire Safety Review" 2017). A committee has been struck at the Council on Tall Buildings and Urban Habitat to debate and make best practice recommendations to the global design community.

Should highly flammable cladding be permitted on any building? No. Because façades should be designed to inspire and protect, not to kill.

REFERENCES

Alucobond News and Press Office. August 22, 2017. http://www.alucobond.com/news1.html?&no_cache=1&mode=single&postid=164475860951.

Architect Magazine. "RIBA Releases Statement on Fire-Safety Design Following Grenfell Tower Tragedy." June 29, 2017.

ASTM E119 - 16a - Standard Test Methods for Fire Tests of Building Construction and Materials. https://www.astm.org/Standards/E119.

BBC News. "Dubai's Torch Tower Catches Fire For Second Time In Two Years." August 4, 2017.

CBC News. Why Grenfell Tower became a raging, wind tunnel of a fire, June 16, 2017. http://www.cbc.ca/news/world/london-fire-grenfell-tarling-expert-1.4163560

"Cladding Cost Cutting: Grenfell Tower Cladding 'Was Downgraded From The Fireproof Version To Save The Council £293,000'." June 30, 2017. https://www.thesun.co.uk/news/3915686/grenfell-tower-cladding-was-downgraded-from-the-fireproof-version-to-save-the-council-293000/.

Cladding 'Makes 30 Buildings In Melbourne Fire Risks.' June 19, 2017.

"Deathtrap Décor: What Is Cladding, Why Was It Used On Grenfell Tower And How Many Other Tower Blocks Have Failed Latest Fire Tests?" August 3, 2017.

"Dubai Starts Replacing Skyscraper Facades After Series Of Fires." September 24, 2017.

"Dubai Sulafa Tower Fire: Terrifying Scenes As Hundreds Evacuated After Blaze Rips Through Luxury Marina Apartments." July 20, 2016. http://www.mirror.co.uk/news/world-news/dubai-sulafa-tower-fire-massive-8455408.

"Eight Failures That Left People Of Grenfell Tower At Mercy Of The Inferno." June 16, 2017. http://www.telegraph.co.uk/news/2017/06/15/eight-failures-left-people-grenfell-tower-mercy-inferno/.

"Electrical Fault Caused The Address Downtown Dubai Hotel Fire." January 20, 2016. https://www.thenational.ae/uae/electrical-fault-caused-the-address-downtown-dubai-hotel-fire-1.201694.

"Emaar to Receive Dh1.22 Billion Insurance Claim on Address Downtown Hotel Fire." February 6, 2017. https://www.thenational.ae/business/property/emaar-to-receive-dh1-22-billion-insurance-claim-on-address-downtown-hotel-fire-1.3434.

"Fire Breaks Out at Tamweel Tower." November 18. 2012.

"Fire Ratings for Construction Materials" http://articles.extension.org/pages/31039/fire-ratings-for-construction-materials. 2013.

"Fire Safety Review: Building Regulations are 'Not Fit For Purpose.'" December 18, 2017. https://www.architectsjournal.co.uk/news/fire-safety-review-building-regulations-are-not-fit-for-purpose/10026395.article#commentsubmitted.

Flame Spread Ratings. http://sfm.dps.louisiana.gov/doc_flamespread.html.

"Grenfell Tower Cladding Maker Arconic Stops Selling Non Fire-Resistant Version." June 27, 2017. http://www.cbc.ca/news/world/cladding-arconic-alcoa-grenfell-fire-1.4178157.

"Grenfell Tower Fire Raises Fears Over Lax Building Regulations." June 15, 2017. https://eandt.theiet.org/content/articles/2017/06/grenfell-tower-fire-raises-fears-over-lax-building-regulations/

"Grenfell Tower Fire Started In Fridge Freezer, Criminal Charges Being Considered." June 23, 2017. http://www.cbc.ca/news/world/cladding-arconic-alcoa-grenfell-fire-1.4178157

"Grenfell Tower Refurbishers Over Insulated Building To Avoid Repeat Job." June 18, 2017.

http://www.express.co.uk/news/uk/818321/Grenfell-tower-fire-over-insulated-avoid-repeat-job-cladding.
"Grenfell Tower Victims 'Poisoned By Cyanide' After Insulation 'Released Highly Toxic Gas'." June 22, 2017. http://www.telegraph.co.uk/news/2017/06/22/grenfell-tower-victims-poisoned-cyanide-insulation-released/.
http://www.architectmagazine.com/practice/riba-releases-statement-on-fire-safety-design-following-grenfell-tower-tragedy_o
http://www.bbc.com/news/world-middle-east-40822269.
http://gulfnews.com/news/uae/emergencies/fire-breaks-out-at-tamweel-tower-in-jumeirah-lake-towers-1.1106387.
http://www.alucobond.com. Retrieved 30 September 2017.
https://www.japantimes.co.jp/news/2017/09/24/world/dubai-starts-replacing-skyscraper-facades-series-fires/#.WdJoTNFyOUk.
http://www.huayuanfu.com/e/faq.htm.
https://www.thesun.co.uk/news/3804113/grenfell-london-tower-fire-cladding-fire-tests-latest-updates/.
http://www.theaustralian.com.au/business/property/docklands-tower-blaze-exposes-dirty-secret-of-cheap-cladding/news-story/bdfe1856c4955b3da453bbea543cfd2b.
http://www.theaustralian.com.au/news/nation/cladding-makes-30-buildings-in-melbourne-fire-risks/news-story/9c12c1c973bb508242d7b5579dde2fdf
https://www.theguardian.com/world/2015/feb/21/fire-dubai-skyscraper-evacuation.
https://www.theguardian.com/world/2015/dec/31/dubai-skyscraper-fire-ablaze-new-years-eve-fireworks.
https://www.theguardian.com/uk-news/2017/jun/14/what-happened-at-grenfell-tower-london-fire-visual-guide.
"Hundreds Evacuated after Fire in Dubai Skyscraper." February 21, 2015.
"Ladders Came Up Short and Cost Lives in London Blaze, Firefighters Say." July 8, 2017. https://mobile.nytimes.com/2017/07/08/world/europe/grenfell-fire-london-ladder.html.
"London Fire: 600 High-Rises Have Grenfell Tower-Style Cladding." June 22, 2017. https://www.nbcnews.com/news/world/london-fire-600-high-rises-have-grenfell-tower-style-cladding-n775401.
"London Fire: A Visual Guide To What Happened At Grenfell Tower." August 4, 2017. http://www.bbc.com/news/uk-40301289
"Massive Fire at Dubai Skyscraper Interrupts New Year's Eve Fireworks." January 1, 2016.
"Most Dubai Towers Built Before 2012 'Have Non Fire-Rated Exterior Panels'." January 4, 2016. https://www.thenational.ae/business/property/most-dubai-towers-built-before-2012-have-non-fire-rated-exterior-panels-1.187389.
Technical Bulletin 405: Fire Resistance Properties of Polyiso Foam Plastic Insulation Used in Wall Assemblies - Facts and Comparisons.
The Australian Business Review. "Docklands Tower Blaze Exposes 'Dirty Secret' Of Cheap Cladding." April 29, 2015. http://www.theaustralian.com.au/business/property/docklands-tower-blaze-exposes-dirty-secret-of-cheap-cladding/news-story/bdfe1856c4955b3da453bbea543cfd2b.
The Guardian. "What Happened at Grenfell Tower." June 14, 2017.
The National. "Mixed Emotions As Tamweel Tower Residents Wait To Go Home." February 22, 2017. https://www.thenational.ae/uae/environment/mixed-emotions-as-tamweel-tower-residents-wait-to-go-home-1.14056.
"UK Chancellor: Cladding on Grenfell Tower 'Banned on High-Rises'." June 18, 2017. http://www.cnn.com/2017/06/18/europe/grenfell-tower-fire/index.html.

Facade Tectonics 2018 World Congress
Sponsors

SCHÜCO

trosifol™
world of interlayers

POHL
Competence from Tradition since 1856

AIA Los Angeles

NACC
Architectural Glass and Metal Technician
AGMT Certification Program
North American Contractor Certification

Boston Valley Terra Cotta

CLARK PACIFIC

GIROUX GLASS™ INCORPORATED

PCI WEST

Pilkington Planar™
by W&W Glass, LLC

Roschmann GROUP

Southern California Glass Management Association

TECHNOFORM GROUP

TECHNO FORM

USC School of Architecture

USGlass Metal & Glazing
Devoted exclusively to the architectural glass industry

VIDARIS

WALTER P MOORE

wsp

Facade Tectonics Organizational Members

INNER CIRCLE

Schüco USA
University of Southern California

PARTNERS

Enclos
POHL

PATRONS

Clark Construction Group
MATT Construction
TriPyramid Structures

DONORS

Boston Valley Terra Cotta, CO Architects, Derix Art Glass Consultants, Eckersley O'Callaghan, HOK, Kuraray, Roschmann Steel & Glass Constructions, SHoP Architects, Technoform, WRNS Studio, YKK AP America

CONTRIBUTORS

AkzoNobel, AZA INT, Dean J. Vlahos FAIA & Associates, Front, Giroux Glass, HDR Architecture, Mark H. Savel Architects, The Ornamental Metal Institute of New York, W&W Glass, Walter P Moore, Wheaton & Sprague, YKK AP Facade

SUPPORTERS

altPOWER, Architectural Glass Institute, Architectural Windows and Glass, Atelier Ten, Benson Industries, Bostik, Building Blocks Inc., Cambridge Architectural Mesh, Carnevale & Lohr, cl-talon, CLEB Labratory Inc., Coreslab, ENAR Envolventes Arquitectonicas, Facades+, Fairview Architectural, FreMarq Innovations, Gensler, Hathaway Dinwiddie, Heintges & Associates, HGA Architects and Engineers, KEPCO+, Kreysler & Associates, Larson Engineering, LMCI Painters and Allied Trades, MG2 Corporation, Mitchell | Giurgola Architects, Morrison Hershfield, NACC and AGMT Certification Programs for Glazing Installers, Northern California Allied Trades, Owens Corning, ParexUSA, Perkins+Will, Pioneer Cladding & Glazing Systems, PPG Industries, Reynaers,
Sage Glass, SAPA Group, Serge Ferrari North America, Southern California Glass Management Association, Staticus, STUTZKI Engineering, Thornton Thomasetti, Veneklasen Associates, Vidaris, Viracon, Walters & Wolf, Zahner

ACADEMICS / NONPROFITS

Finishing Contractor's Association, Lawrence Berkeley National Lab, Thomas Jefferson University, University of Southern Denmark, Woodbury School of Architecture

Facade Tectonics 2018 World Congress
Scientific Review Committee

Rebecca Abano City of Los Angeles Dept of Public Works • **Achilles Ahimbisibwe** Uganda Martyrs University • **Edwin Akins** Kennesaw State University • **Nihal Saif** Abu Dhabi University, College of Engineering & Computer Science • **Kais Al-Rawi** Walter P Moore • **Mohamed Aly** American University in Cairo • **Brian Ambroziak** The University of Tennessee Knoxville, College of Architecture + Design • **Eleni Antonelli** Neumann Sloat Arnold Architects, Inc. • **Phillip Anzalone** New York City College of Technology • **Basilio Baffi** • **Anton Bakerjian** Gensler • **Ron Bertoli** Inhabit Group • **Pravin Bhiwapurkar** University of Cincinnati, School of Architecture and Interior Design • **Ahmet Biler** Istanbul Technical University, Institute of Energy • **Kenneth Black** Virginia Tech, School of Architecture + Design • **Keith Blaine** California State University, Northridge • **Valerie Block** Kuraray • **Terri Meyer Boake** University of Waterloo, School of Architecture • **Robert Bombino** RDH Building Science • **Sumit Brahmbhatt** Brahmbhatt Architects, Inc. • **Dale Brentrup** UNC Charlotte, School of Architecture • **Timothy Brown** Clemson School of Architecture • **Gerardo Brown-Manrique** Miami University, Department of Architecture + Interior Design • **Paul Burch** Burch-Enterprises • **Patricia Edith Camporeale** Universidad Nacional De La Plata, Facultad De Arquitectura Y Urbanismo • **Lawrence Carbary** Dow Corning • **Paul Carew** PJ Carew Consulting • **Bruce Carriere** AkzoNobel • **Stan Carroll** Oklahoma State University, School of Architecture • **Juliana Portela Vilar de Carvalho** Federal University of Rio Grande do Norte • **Paulo Lago de Carvalho** University of Minho, Architecture and Product Design • **James Casper** Enclos • **Mina Chow** USC School of Architecture • **Mike Christenson** North Dakota State University • **Charles Clift** Curtainwall Design Consulting • **Angela Clua Longas** École Polytechnique Fédérale de Lausanne, Laboratory of Architecture and Sustainable Technologies • **Cristobal Correa** BuroHappold Engineering • **Rolando Arturo Cubillos-González** Universidad Católica de Colombia • **Thanh Dang** University of Huddersfield • **Ryan Danks** RWDI • **Shreya Das** HMC Architects • **Russell H. Davies** AVRO Consult-Engineering, P.C. • **Carrie Davis** Protection Engineering Consultants • **Chris DeHaven** McCarthy • **Stephen D. Dent** University of New Mexico, School of Architecture and Planning • **Florian Doebbel** Sika Group • **James Doerfler** Philadelphia University, College of Architecture and the Built Environment • **Christopher Domin** University of Arizona, College of Architecture • **James Donaldson** Johnson Fain • **Brenda Milhomem Dourado** Universidade De Brasilia, Faculdade De Arquitetura E Urbanismo • **Bronne Dytoc** Kennesaw State University • **Michael Elstner** Interpane Glass Industries AG • **Salim Elwazani** Bowling Green State University, College of Technology Architecture and Applied Engineering • **James Erickson** Arizona State University • **Dr. Carlos Esparza-López** Universidad de Colima • **Gustav Fagerström** Walter P Moore • **Lisa G. Follman** Skidmore, Owings & Merrill, LLP • **Chris Fronsoe** ICD High Performance Coatings • **Robert Garlipp** Gensler • **Laura B. Garofalo-Khan** University at Buffalo, School of Architecture and Planning • **Pedro Lima Gaspar** Technical University of Lisbon, Department of Architecture • **Dorothy J. Gerring** Penn College, Architectural Technology •

Marjan Ghobad PJ Carew Consulting • **Glenn Goldman** New Jersey Institute of Technology, College of Architecture and Design • **Isik Goren** Istanbul Technical University, Department of Architecture • **Jill Guerrero** Kollin Altomare Architects • **Jeff Haber** W&W Glass • **Bruce Haglund** University of Idaho College of Art and Architecture • **Syma Haque Trisha** Bangladesh University of Engineering and Technology, Department of Architecture • **Navid Hatefnia** PJ Carew Consulting • **Brian Herman** Benson Industries • **Alfonso E. Hernandez** Kirksey Architecture • **Glenn E. Hill** Texas Tech University, College of Architecture • **James Hock** Permasteelisa Group • **Jeanne Homer** Oklahoma State University, School of Architecture • **Stacey Hooper** NBBJ Design • **Hormoz Houshmand** BuroHappold Engineering • **Endrit Hoxha** École Polytechnique Fédérale de Lausanne, Laboratory of Architecture and Sustainable Technologies • **Jianhui Huang** Tianjin University, School of Science • **Guadalupe Huelsz Lesbros** Unidad De Communicación De La Ciencia • **Mark Hulme** Marx/Okubo • **Giuliana Iannaccone** Politecnico Di Milano Dipartimento di Architettura • **Dr. Walaa Salah Eldeen Ismaeel** The British University in Egypt, Department of Architecture • **Stephen Katz** Gensler • **Gene Keeton** KDENT, Inc. • **Ted Kesik** University of Toronto, Architecture, Landscape and Design • **Iman Khajehzadeh** The Open Polytechnic, School of Science, Technology and Engineering • **Jihun Kim** New York City College of Technology • **Jasha Kistler** The Façade Group • **Prof. Dr. Ing. Ulrich Knaack** TU Delft, Department of Architectural Engineering + Technology • **Kyle Konis** USC School of Architecture • **Debjit Kundu** USC School of Architecture • **Mili Kyropoulou** HKS | LINE • **Caroline Lama** Vidaris, Inc. • **Andy Lang** Morrison Hershfield • **Yahya Lavafpour** University of Liverpool, School of Architecture • **Sarah Le Clerc** Open Mode Design • **Geok Ser Lee** U.S. Green Building Council • **Evan Levelle** Front, Inc. • **Vikki Lew** U.S. Green Building Council • **Martina Lind Roschmann** Steel & Glass Constructions Inc. • **Ahoo Malekafzali Ardakan** North Carolina State University • **Khaled Mansy** Oklahoma State University, School of Architecture • **Marcin March** Eckersley O'Callaghan • **Kirk Marchand** Protection Engineering Consultants • **Andrea Martinez** USC School of Architecture • **Heath May** HKS | LINE • **Justin Miller** Auburn University, College of Architecture, Design and Construction • **Seokim Min** Gensler • **Manzer Mirkar** U.S. Green Building Council • **Robert Moisy** Surface Design • **Sameh Mona** An-Najah National University • **Stephen M. Morse** Texas Tech Univeristy, National Wind Institute • **Michael Mulhern** TriPyramid Structures • **Scott Murray** The Illinois School of Architecture • **Nick Novelli** HeliOptix LLC • **Erik Olsen** Transsolar • **Emeka Efe Osaji** Leeds Sustainability Institute • **Maria Federica Ottone** University of Camerino, School of Architecture and Design • **Charles Ou-Yang** Ball AIA Architecture • **Zuhal Ozgul** Metal Yapi • **Vera Parlac** University of Calgary, Department of Environmental Design • **Luisa Pastore** École Polytechnique Fédérale de Lausanne, Laboratory for Integrated Performance Design • **Mic Patterson** Schüco USA • **Michael Pedersen** Gensler • **Sophie Pennetier** Arup • **Francesca Perazzelli** • **Troy Peters** Wentworth Institute of Technology • **Pina Petricone** Giannone Petricone Associates Architects • **Michael Plewacki** Morrison Hershfield • **Jeff Ponitz** Cal Poly, College of Architecture and Environmental Design • **Henry Richardson** Atelier Ten • **Satwant Rihal** Cal Poly, Architectural Engineering • **Awilda Rodriguez Carrion** Oklahoma State University, School of Architecture • **Rosa Romano** University of Florence, Department of Architecture • **Eduardo Rosa** Interpane Glass Industries AG • **Roy Kim** USC School of Architecture • **Helen Sanders** Technoform •

Daniele Santucci Technische Universität München, Faculty of Architecture • **Paolo Sanza** Oklahoma State University, School of Architecture • **Nikhita Sapuram** Ficus Landscape • **Vaughn Schauss** Kuraray • **Jefferson Schierbeek** Addison Schierbeek • **Marc Schiler** USC School of Architecture • **Larry Schlossberg** Gruen Associates • **Marc Schulitz** Cal Poly Pomona, College of Environmental Design • **Dirk Schulte** Tianjin North Glass • **Jerome D. Scott** Great Scott! Visuals • **Daniel Caserta Segraves** Thornton Tomasetti • **Feride Sener Yılmaz** Istanbul Technical University • **Greg Sheldon** BNIM • **Will Sheppird** Sheppird Associates • **Peter Simmonds** Building and Systems Analytics LLC • **Karl Singporewala** Ian Ritchie Architects • **Sarah A. Sinusas** WJE • **Jin Young Song** DIOINNO Architecture PLLC • **Matt Staublin** HOK • **Josephine Stoddard** Taupo Plan Service • **Ashley Stoner** Perkins+Will • **Jim Stringfellow** The G.James Group of Companies • **Melissa Szotkowskie** Oldcastle BuildingEnvelope • **Abel Tablada de la Torre** NUS Architecture • **Grace Tan** • **Farimah Tehrani** Dadras Architects INC. • **Katrin Terstegen** Cal Poly Pomona, College of Environmental Design • **Francesca Thiebat** Polytechnic University of Turin • **Santiago Torres** Arup • **Patrick J Tripeny** The University of Utah, School of Architecture • **Angela P. Vargas** Apavardi • **Jose Vargas** Vesselcrossing Architecture • **Denis Vitoreli** Huitt-Zollars, Inc. • **Hamid Vossoughi** WSP • **Maria Carolina Waldheim** School of Architecture, Urbanism and Design of the National University of Cordoba • **Wayne M. Walker** Gensler • **Felix Weber** Arup • **Anne Whitacre** HOK • **Marie Wilson** In2itive Architecture • **Allyne Winderman** Cal Poly Pomona, College of Environmental Design • **Edwin Woll** Tomko Woll Group Architects Inc. • **Audrey Wu** Gensler • **Shuyi Wu** University of Southern California • **Donald Yamami** Moore Ruble Yudell Architects & Planners • **Zhan Yang** University of Southern California • **Joshua Zabel** Kreysler & Associates • **Kimberly Elman Zarecor** Iowa State University, Department of Architecture • **Babak Zareiyan** USC Department of Civil and Environmental Engineering • **Zhou Mingming** • **Tatyana Zhukova** Interior AT Design Inc.



TECTONIC
PRESS

ISBN 978-1882352463

Facade Tectonics